Δελτίο της Ελληνικής Γεωλογικής Εταιρίας
Bulletin of the Geological Society of Greece

Τόμος XLVII, No2

Volume XLVII, No2

13° Διεθνές Συνέδριο της Ελληνικής Γεωλογικής Εταιρίας
Έρευνα και Εκμετάλλευση Ορυκτών Πόρων

13th International Congress of the Geological Society of Greece
September 5-8 2013, Chania, Crete, Greece

13th International Congress of the Geological Society of Greece
Exploration and Exploitation of Mineral Resources

Χανιά/Chania
2013

ΔΕΛΤΙΟ ΤΗΣ ΕΛΛΗΝΙΚΗΣ ΓΕΩΛΟΓΙΚΗΣ ΕΤΑΙΡΙΑΣ

Τόμος XLVII, No 2

BULLETIN OF THE GEOLOGICAL SOCIETY OF GREECE

Volume XLVII, No 2

13ο Διεθνές Συνέδριο της Ελληνικής Γεωλογικής Εταιρίας

Έρευνα και Εκμετάλλευση Ορυκτών Πόρων

13th International Congress of the Geological Society of Greece

Exploration and Exploitation of Mineral Resources

13th International Congress of the Geological Society of Greece
September 5-8 2013, Chania, Crete, Greece

ΕΠΙΜΕΛΕΙΑ ΕΚΔΟΣΗΣ

ΜΑΝΟΥΤΣΟΓΛΟΥ ΕΜΜΑΝΟΥΗΛ

ΠΥΛΙΩΤΗΣ ΙΩΑΝΝΗΣ

Πολυτεχνείο Κρήτης

EDITORS

MANOUTSOGLOU EMMANOUIL

PYLIOTIS IOANNIS

Technical University of Crete

Χανιά/Chania 2013

ΔΟΜΗ ΤΩΝ ΠΡΑΚΤΙΚΩΝ / SCHEME OF THE PROCEEDINGS

ΤΟΜΟΣ 1 / VOLUME 1

Εναρκτήριες Ομιλίες/Opening Lectures

Παλαιοντολογία, Στρωματογραφία και Ιζηματολογία/Palaeontology, Stratigraphy and Sedimentology

Γεωμορφολογία/Geomorphology

Πετρολογία και Ορυκτολογία/Petrology and Mineralogy/

ΤΟΜΟΣ 2 / VOLUME 2

Τεκτονική και Γεωδυναμική/Tectonics and Geodynamics

Υδρολογία και Υδρογεωλογία/Hydrology and Hydrogeology

Γεωχημεία και Βιογεωχημεία/Geochemistry and Biogeochemistry

Περιβαλλοντική Γεωλογία/Environmental Geology

Γεωεπιστήμες στην Εκπαίδευση και Γεώτοποι/Geosciences in Education and Geosites

ΤΟΜΟΣ 3 / VOLUME 3

Γεωφυσική και Σεισμολογία/Geophysics and Seismology

Φυσικές Καταστροφές Natural Hazards

Τηλεπισκόπηση και ΓΣΠ/Remote Sensing and GIS

Θαλάσσια Γεωλογία/Marine Geology

ΤΟΜΟΣ 4 / VOLUME 4

Κοιτασματολογία, Μεταλλευτική Τεχνολογία και Οικονομική Γεωλογία/Ore Geology, Mining Technology and Economic Geology

Τεχνική Γεωλογία και Γεωτεχνική Μηχανική/Engineering Geology and Geotechnical Engineering

Γεωθερμία/Geothermics

Έρευνα και Εκμετάλλευση Ορυκτών Πόρων/Exploration and Exploitation of Mineral Resources

Βιομηχανικά Ορυκτά και Πετρώματα/Industrial Minerals and Rocks

Ενεργειακές Πρώτες Ύλες/Energy Resources

ΠΕΡΙΕΧΟΜΕΝΑ/CONTENTS

ΤΟΜΟΣ 1 / VOLUME 1

Εναρκτήριες Ομιλίες
Opening Lectures

Παλαιοντολογία, Στρωματογραφία και Ιζηματολογία
Palaeontology, Stratigraphy and Sedimentology

Γεωμορφολογία

Geomorphology

Πετρολογία και Ορυκτολογία
Petrology and Mineralogy

ΤΟΜΟΣ 2 / VOLUME 2

Tectonics and Geodynamics/Τεκτονική και Γεωδυναμική

Hydrology and Hydrogeology/Υδρολογία και Υδρογεωλογία

Geochemistry and Biogeochemistry/Γεωχημεία και Βιογεωχημεία

Environmental Geology/Περιβαλλοντική Γεωλογία

Geosciences in Education and Geosites/Γεωεπιστήμες στην Εκπαίδευση και Γεώτοποι

Τεκτονική και Γεωδυναμική
Tectonics and Geodynamics

Υδρολογία και Υδρογεωλογία
Hydrology and Hydrogeology

Γεωχημεία και Βιογεωχημεία
Geochemistry and Biogeochemistry

Περιβαλλοντική Γεωλογία
Environmental Geology

Γεωεπιστήμες στην Εκπαίδευση και Γεώτοποι
Geosciences in Education and Geosites

ΤΟΜΟΣ 3 / VOLUME 3

Geophysics and Seismology/Γεωφυσική και Σεισμολογία

Natural Hazards/Φυσικές Καταστροφές

Remote Sensing and GIS/Τηλεπισκόπηση και ΓΣΠ

Marine Geology/Θαλάσσια Γεωλογία

Γεωφυσική και Σεισμολογία
Geophysics and Seismology

Φυσικές Καταστροφές
Natural Hazards

Τηλεπισκόπηση και ΓΣΠ
Remote Sensing and GIS

Θαλάσσια Γεωλογία
Marine Geology

ΤΟΜΟΣ 4 / VOLUME 4

Κοιτασματολογία, Μεταλλευτική Τεχνολογία και Οικονομική Γεωλογία
Ore Geology, Mining Technology and Economic Geology

Τεχνική Γεωλογία και Γεωτεχνική Μηχανική
Engineering Geology and Geotechnical Engineering

Γεωθερμία
Geothermics

Έρευνα και Εκμετάλλευση Ορυκτών Πόρων
Exploration and Exploitation of Mineral Resources

Βιομηχανικά Ορυκτά και Πετρώματα
Industrial Minerals and Rocks

Ενεργειακές Πρώτες Ύλες
Energy Resources

Δελτίο της Ελληνικής Γεωλογικής Εταιρίας, τομ. XLVII , 2013
Πρακτικά 13ου Διεθνούς Συνεδρίου, Χανιά, Σεπτ. 2013

Bulletin of the Geological Society of Greece, vol. XLVII 2013
Proceedings of the 13th International Congress, Chania, Sept. 2013

TIME SERIES ANALYSIS OF THE NOANET CGPS STATIONS

Chousianitis K.[1], Ganas A.[1], Papanikolaou M.[1], Argyrakis P.[1], Drakatos G.[1] and Makropoulos K.[1]

[1] Institute of Geodynamics, National Observatory of Athens, chousianitis@noa.gr, aganas@noa.gr, g.drakat@noa.gr, papanikolaou@geol.uoa.gr,pargyrak@geol.uoa.gr, kmacrop@geol.uoa.gr

Abstract

The National Observatory of Athens has begun installing permanent GPS stations on February 2006 including a EUREF permanent station in Attica, NOA1. Currently the National Observatory of Athens operates 20 continuous GPS stations around Greece all sampling at 1-s and transmitting real-time data to Athens. Several stations also sample at 0.2-s (5 Hz) and record the data in the ring buffer for a period of 1-2 days. Their location is carefully selected so that both geological and seismotectonic criteria are fulfilled. All stations are situated close to major seismogenic structures of Greece such as the Cephalonia Transform Fault (CTF) in the Ionian Sea (VLSM, PONT, SPAN, KIPO), and the two North Anatolian Fault branches in the North Aegean Sea (PRKV, LEMN). We describe the CGPS data archiving and processing procedures, used to combine into a uniform velocity solution the observations of all the NOANET stations, accounting for the seasonal (annual and semi-annual) signals, and considering the off-sets in the coordinate time-series.
Key words: *Geodesy, Geodynamics, Time series analysis, Greece.*

Περίληψη

Το Γεωδυναμικό Ινστιτούτο του ΕΑΑ ξεκίνησε γεωδαιτικές παρατηρήσεις το έτος 2006 με την ίδρυση και λειτουργία του μονίμου σταθμού αναφοράς NOA1. Σήμερα το δίκτυο NOANET αριθμεί 20 μόνιμους σταθμούς (σε συνεργασία με τρίτους φορείς) με βήμα δειγματοληψίας το 1-s και σε σύνδεση πραγματικού χρόνου με το κέντρο συλλογής και αποθήκευσης των δεδομένων (Αθήνα, Θησείο). Αυτή η εργασία παρουσιάζει την διαδικασία συλλογής και επεξεργασίας των δεδομένων GPS, λαμβάνοντας υπόψη τα περιοδικά σήματα (ετήσια και ημιετήσια) που υπεισέρχονται στις χρονοσειρές και δίνοντας σφάλματα στις εκτιμήσεις των ταχυτήτων με ανάλυση ενός μοντέλου θορύβου. Τέλος, παρουσιάζονται αποτελέσματα στο ITRF2005 για τους σταθμούς εκείνους των οποίων η διάρκεια καταγραφής έχει ξεπεράσει τα τρία χρόνια, γεγονός που εξασφαλίζει αξιόπιστες τιμές ταχυτήτων.
Λέξεις κλειδιά: *Γεωδαισία, Γεωδυναμική, Ανάλυση χρονοσειρών, Ελλάδα.*

1. Introduction

Greece is located at a complex seismotectonic regime dominated by the convergence of Mediterranean and Eurasian plates and their collision along the Hellenic Arc. As a result the area exhibits high seismicity. Relative motion of these plates accumulates stress in the lithosphere,

causing observable crustal deformation (McClusky et al., 2000; Ganas and Parsons, 2009; Floyd et al., 2010). Earthquake activity occurs due to tectonic stress release along both, the crustal faults and the Mediterranean-Eurasia plates' interface, a fact that makes the study of crustal deformation an interesting and essential issue. In southern Greece, earthquakes are caused primarily by interaction between the relatively small Aegean Sea and the larger Africa (Nubia) plates. In northern Greece the main seismic hazard comes from the two branches of the north Anatolian Fault that terminate inside the Aegean Sea. In western Greece there are two large faults, both offshore, the Cephalonia Transform and the Appulian thrust. The largest 20th earthquakes to have occurred near Greece's plate boundaries had magnitudes of about 7.2-7.3. However, globally, convergent-plate tectonic environments similar to that of the Hellenic arc commonly produce M>8 earthquakes.

Geodetic investigation of the kinematics of Greece via campaign GPS observations started in the late 1980s – early 1990s following the documentation of large-scale continental extension across the Gulf of Corinth (~1 cm/yr; Billiris et al., 1991). It was soon realized that the kinematics of deformation involved a combination of westerly motion of Anatolia and south-westerly motion of the central and south Aegean, relative to Eurasia, in tandem with N-S convergence across the Hellenic Arc (Le Pichon et al., 1995; McClusky et al., 2000; Kahle et al., 2000). It is also evident that there is a progressive increase in GPS velocities southward in northern Greece (Macedonia – Thrace) toward the North Aegean Trough, across which the velocities increase and change direction dramatically. During the last decade, a number of groups conducted research on the fragmentation of the upper crust in microplates or continental blocks (e.g. Avallone et al., 2004; Nyst and Thatcher, 2004; Reilinger et al., 2006; Floyd et al., 2010) and on mapping crustal motions and interseismic velocities in the central part of the country (e.g. Briole et al., 2000; Bernard et al., 2006; Hollenstein et al., 2008). Most of above studies show that present-day Aegean deformation is typically focused in narrow deforming zones (rift axes or transcurrent faults) that are surrounded by rigid, less active blocks. The Institute of Geodynamics of the National Observatory of Athens, in order to monitor the ongoing deformation across major fault zones in Greece and to correlate the rate of strain accumulation with the occurrence of major earthquakes, has began the installation since 2006 of NOANET, a real-time, high-rate GNSS network. This paper describes the instrumental set-up, the data-logging strategy and the processing procedures used to combine into a uniform velocity solution the observations of the NOANET continuous GPS (CGPS) network.

2. Instrumentation and Data Archiving

The NOANET network currently comprises 20 stations (Figure 1) and has been operating since February 2006 following the EUREF (Regional Reference Frame Sub-Commission for Europe) Permanent Network standards. The aim of this network is to monitor and quantify crustal deformation in Greece, so the location of each station was carefully selected in order that both geological and seismotectonic criteria are fulfilled. Most stations are located close to major seismogenic structures of Greece in order to optimally measure tectonic motions. The stability of points was an important issue during the network design. All stations are installed on bedrock (Table 1).

The NOANET stations are connected to the main server in Athens via the Internet or via leased telephone lines and have 1-week power autonomy. All stations are equipped with dual-frequency GPS receivers. Our stations collect data every 1 s and transmit them to Athens on the hour (hourly files). 5 Hz (0.2 s) data are also collected on the ring buffer and remain available for manual download for a period of 48 hours. Data archiving is performed in two modes: a) 1-s raw data of each station are archived in hourly intervals and b) daily data for each station are archived in 30-s sampling rates. Two diagrams showing 30-s data completeness for NOANET stations since 2006 are presented in Figure 2.

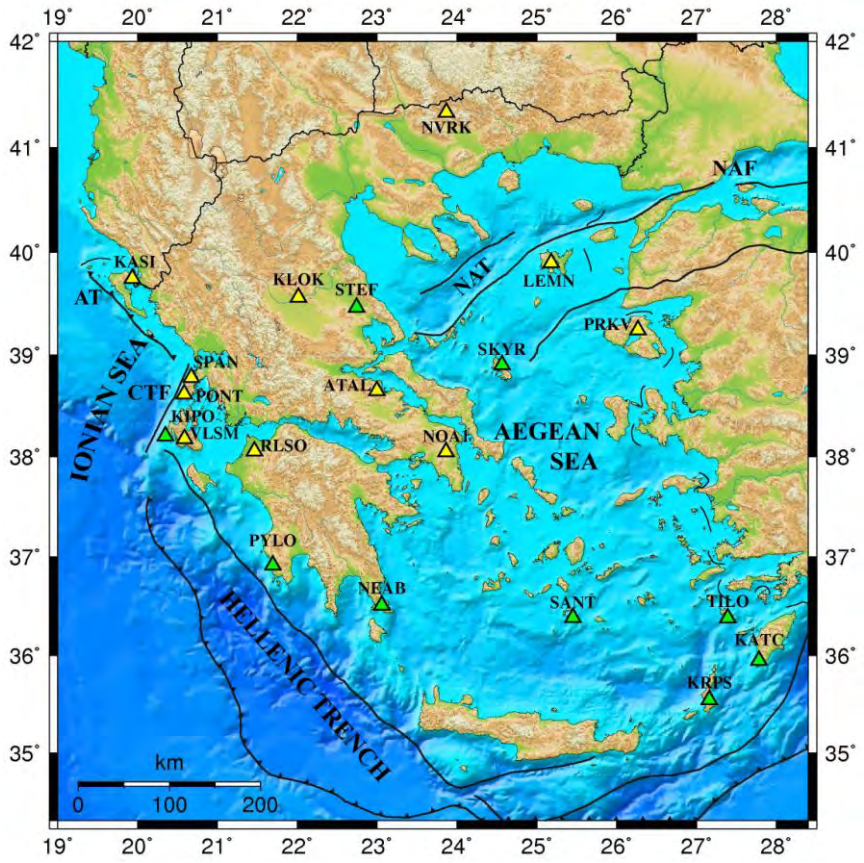

Figure 1 – Relief map showing the locations of the CGPS stations archived at NOA. Yellow triangles denote stations installed prior to 2011. Abbreviations: AT, Apulian Thrust; CTF, Cephalonia Transform Fault; NAT, North Aegean Trough; NAF, North Anatolian Fault.

The network server in Athens is collecting data in automatic mode. The in-house software consists of the LEICA SPIDER sofware version 4.1.1 which is used to manage check and control the reference stations as stand alone stations and as a network. A daily file is created at midnight by sub-sampling the hourly observations every 30-s intervals. This file is converted to RINEX format and delivered to the NOA Web Server where it is available for immediate download (http://www.gein.noa.gr/services/GPS/GPS_DATA/). We currently use a real-time quality processing of four reference stations using the LEICA SpiderQC v.4.1 software.

Table 1 - NOANET station coordinates and monumentation.

Code	Lat.	Long.	Date	Monumentation	Lithology
VLSM	38.177	20.588	2/14/2006	Roof	Limestone
NOA1	38.047	23.864	3/13/2006	Roof	Marble
RLSO	38.056	21.465	7/29/2006	Roof	Sandstone
PONT	38.619	20.585	2/15/2007	Roof	Limestone
KASI	39.746	19.935	4/1/2007	Roof	Limestone
SPAN	38.781	20.673	5/22/2007	Roof	Schist

Code	Lat.	Long.	Date	Monumentation	Lithology
LEMN	39.897	25.181	6/16/2007	Roof	Andesite
PRKV	39.246	26.265	6/30/2007	Exposed Rock	Andesite
NVRK	41.337	23.870	7/12/2007	Roof	Sandstone
KLOK	39.565	22.014	7/17/2008	Exposed Rock	Marble
ATAL	38.653	22.999	3/27/2009	Roof	Alluvium
KIPO	38.203	20.348	8/31/2010	Roof	Limestone
PYLO	36.914	21.695	8/24/2011	Roof	Limestone
NEAB	36.509	23.060	6/27/2012	Roof	Sandstone
KPRS	35.547	27.162	8/14/2012	Roof	Sandstone
SANT	36.385	25.452	8/17/2012	Roof	Volcanic Rocks
KATC	35.951	27.781	10/05/2005	Steel mast	Marl
STEF	39.464	22.742	9/7/2012	Roof	Conglomerate
SKYR	38.904	24.565	11/27/2012	Roof	Schist
TILO	36.380	27.394	07/01/2005	Exposed Rock	Limestone

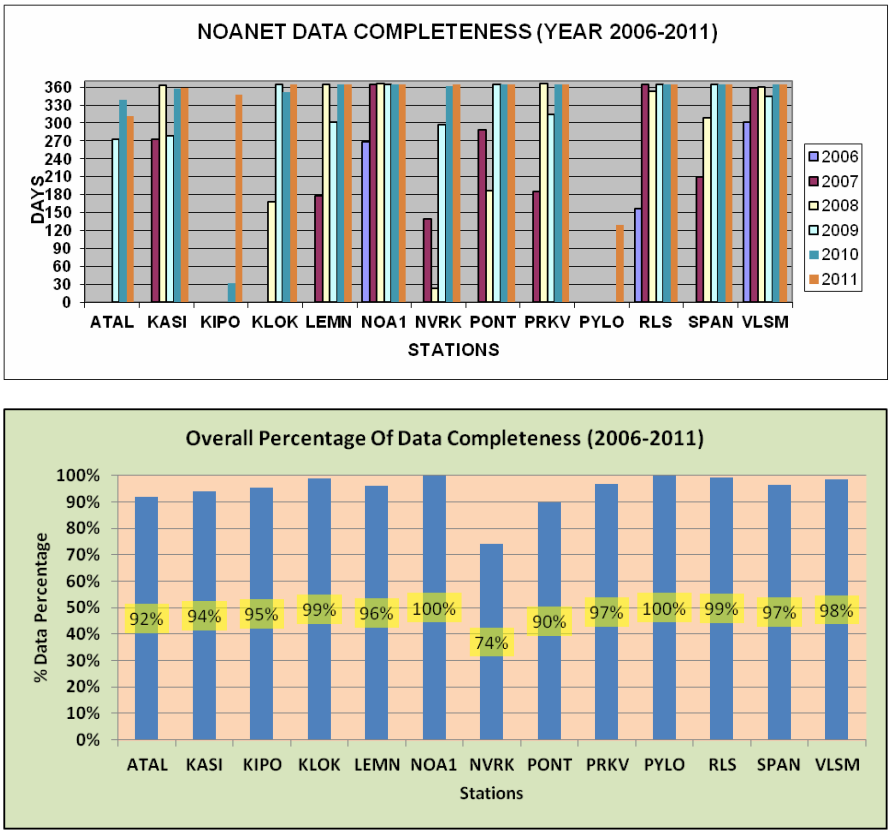

Figure 2 - Diagrams of NOANET data completeness from 2006 until 2011.

3. Processing of CGPS Data

All data are processed in 24-h sessions using the GAMIT/GLOBK software package (Version 10.4; Herring et al., 2010) in a three step distributed processing approach, which is based on the «quasi-observation» theory and the reference frame is not defined until the last step of the analysis (Feigl et al., 1993; Dong et al., 1998). In the first step we apply loose a priori constraints to all of the parameters, choosing the ionosphere-free linear combination, and fixing the ambiguities to integer values to obtain daily estimates of station coordinates, satellite state vectors, the tropospheric zenithal path delay at each station every 2 hr, and the orbital and Earth Orientation parameters (EOP). We use precise orbits from the International GNSS Service (IGS). The effect of solid-earth tides, polar motion and oceanic loading is taken into account according to the IERS/IGS standard 2003 model (McCarthy and Petit, 2004). We apply the ocean-loading model FES2004 (e.g. Lyard et al., 2006) and use IGS absolute elevation and azimuth dependent tables for modeling the effective phase center of the receiver and satellites antennas. Data from 21 well performing fiducial stations of IGS are included in the analysis to tie our regional measurements to an external global reference frame and to improve the ambiguity resolution by putting tight constraints (3 to 5 mm on the horizontal and 5 to 10 mm on the vertical) on these sites from their a priori coordinate values in the ITRF05 Reference Frame (Altamimi et al., 2007). The coordinates of the Greek permanent stations are allowed to vary freely by way of very loose constraints (50 metres). An automatic cleaning algorithm is applied to post-fit residuals in order to repair cycle slips and to remove outliers. For each session, we obtain two solutions based on phase ambiguity resolution, one bias-free and one bias-fixed, along with the associated variance-covariance matrices.

In the second step, we combine our loosely constrained bias-fixed solutions of our regional network with analyzed global and regional solutions provided by SOPAC (http://sopac.ucsd.edu) into single day unconstrained solutions. In the final third step we obtain station position time series in a common reference frame by considering the daily loosely constrained estimates of station coordinates, orbits and EOP and their associated variance-covariance matrices as quasi-observations and passing them to GLOBK which employs the Kalman filtering approach. The reference frame during the formation of these combined network solutions is again loosely defined until the last processing step, where we realize a common reference frame applying generalized constraints (Dong et al., 1998; 2002) while estimating a seven-parameter Helmert transformation (three network rotations, three network translations and one scaling parameter), aligning each individual daily solution to the 2008 realization of the International Terrestrial Reference Frame. The reference frame is defined by minimizing, in the least-square sense, the departure from the prior values determined in the ITRF05-NNR frame of the 21 IGS stations incorporated in the GAMIT processing part. Five iterations are used to eliminate bad sites and to compute station weights for the reference frame stabilization.

3.1. First-order Features of Time Series

After deriving the position time series, we perform an analysis with the aim of modeling the constant velocity for each component of each station, together with the annual and semi-annual signals and the offsets observed in the series using TSVIEW software (Herring, 2003). The successful modeling of these first-order features observed in time series leads to accurate and realistic determination of geodetic velocities. They have been identified in several studies of continuous GPS time series and include seasonal signals and epoch offsets. Seasonal signals may be related to a) gravitational excitation, such as solid Earth tides, ocean tides, and atmospheric tides, b) to thermal origin coupled with hydrodynamics, such as ground water change in both liquid and solid form, and bedrock expansion, and c) to sources that are indirect due to geophysical processes, or of instrument, or modeling deficiency, such as incomplete removal of atmospheric effects and thermal effects of antenna and monument (Blewitt et al., 2001; Van Dam et al., 2001; Blewitt and Lavallee, 2002; Dong et al., 2002). These signals are commonly modeled as a

combination of sinusoids with a fundamental period of one year plus first harmonic mode of six-month period. The epoch offsets in the time series are in general caused either by nearby earthquakes that affect the GPS station, or by antenna changes. The latter can occur when these changes are not well-modeled in the processing software due to erroneous references during the installation time, or when the antenna model does not adequately describe the measurements (Nikolaidis, 2002). The mathematical expression that describes the geodetic time series accounting for first-order features may be written (Langbein, 2004) as:

Equation 1 – Expression for First-order Features Modeling of Time Series

$$d_i = a + bt_i + \sum_{k=1}^{k_0} v_k (t_i - T_k) H(t_i - T_k) + \sum_{j=1}^{j_0} o_j H(t_i - T_j) + \\ + \sum_{m=1}^{m_0} \left[a_m \sin\left(\frac{2\pi t_i}{T_m} \right) + b_m \cos\left(\frac{2\pi t_i}{T_m} \right) \right] + e_i$$

where d_i is the measurement at time t_i; α is the site position; b is the linear rate; v_k are rate changes starting at $t_i=T_k$; $H(t_i-T_j)$ is the Heaviside step function which equals 1 for $t_i \geq T_j$ and 0 otherwise; o_j are offsets in the time series at $t_i=T_j$; α_m and b_m are sine and cosine amplitudes at period T_m and e_i denotes noise.

Moreover, because of the existence of abnormal outliers in daily solutions, we perform editing in order to remove erroneous samples from contaminating the velocity solutions, and to retrieve clean time series. We use an automatic outlier function with a 5 sigma rejection level. As an example, we present the north, east and up raw and detrended position time series, with annual and semi-annual signals and offsets for two NOANET stations in Figure 3a and 3b, respectively. In some time series we detect offsets, which we model as step functions. All these offsets are identified by inspecting the data residuals in combination with the knowledge of each site history and nearby earthquakes. So far, all of the observed offsets in the time series can be attributed to hardware changes within the time span of the processed data apart from the offsets mainly in the North and Up components of RLSO which can be attributed to co-seismic deformation generated by the nearby 2008 Achaia earthquake (Figure 3a; Ganas et al., 2009).

3.2. Error Estimates of Station Velocities

Analyses of continuous GPS data have showed that there is a significant amount of coloured noise content within geodetic time series (e.g. Bock et al., 1997; Zhang et al., 1997). Thus, the white noise assumption that measurement errors are random and uncorrelated from one epoch to its next is not the case for GPS data (e.g. Johnson and Agnew, 1995; Williams et al., 2004) and if a pure white-noise model is used, it may result in unrealistically low velocity uncertainties, especially for continuous data, that can be underestimated by a factor of 5 or more (e.g. Mao et al., 1999). To account for time-correlated errors in our processed time series, we model them using a first-order Gauss-Markov process. For each coordinate component we estimate the increase in the normalized χ^2 (chi-squared per degree of freedom) of successively longer time averages. For a white noise error model, the normalized χ^2 would not depend on averaging time, but for non-white noise spectra, the normalized χ^2 increases with successively increasing averaging time. Next, the time-averaged values of the normalized χ^2 are fitted to the exponential function expected for a first-order Gauss-Markov process so as to estimate a correlation time and the long-term variance. This model is used to predict site velocity uncertainties based on the span of the time series. Since GLOBK is a Kalman filter that is able to realize random walk noise model, which is a first-order Gauss-Markov model with infinite averaging time, we calculate the random walk model values

that would predict the same velocity uncertainties as the first-order Gauss-Markov model for the time series using the following equation:

Equation 2 - Magnitude of Random Walk Noise Component

$$b^2 = \sigma_{RW} T$$

where b is the magnitude of the random walk noise, σ_{RW} is the velocity uncertainty estimates and T is the time span of the time series (Zhang et al., 1997). These values are used as input to GLOBK in order to add random walk to the error model and calculate ‘‘realistic’’ uncertainties for the velocity estimates. After the above time series analysis, our final velocity solution accounting for seasonal signals, offsets and time-correlated noise content is produced by combining the individual epoch-by-epoch solutions into one “stacked” solution by means of the GLOBK's Kalman filter.

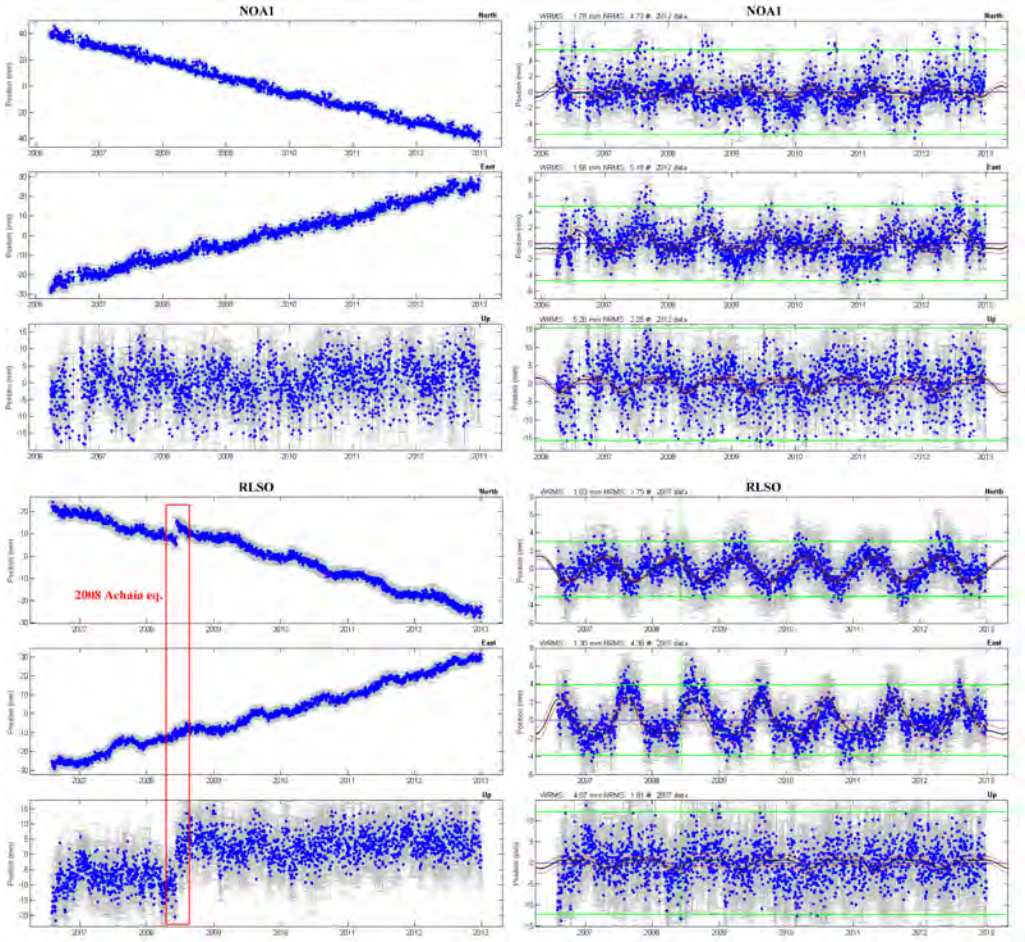

Figure 3 – a) Raw time series plots of daily position estimates of stations NOA1 and RLSO referred to the ITRF2005 reference frame (N, E, U). The error bars represent 1-σ uncertainties obtained from the analysis. b) Detrended time series plots of daily position estimates of stations NOA1 and RLSO referred to the ITRF2005 reference frame (n,e,u). The error bars represent 1-σ uncertainties obtained from the analysis. The black solid lines represent the annual and semi-annual signals along with their uncertainties (red lines, placed plus and minus 1-σ), while the vertical green lines show epochs of detected offsets.

Table 2 - ITRF2005 positions together with velocities and 1-σ uncertainties.

	Position				ITRF2005 Velocity (mm/yr)			White noise/Random Walk Uncertainty (mm/yr)		
Station	**X**	**Y**	**Z**	**Epoch**	**Ve**	**Vn**	**Vu**	**σVe**	**σVn**	**σVu**
NOA1	4599643.3188	2034827.9763	3909890.7492	2011.210	7.16	-11.94	0.82	0.03/0.14	0.03/0.11	0.09/0.24
VLSM	4699991.6109	1765547.7167	3921162.2145	2010.338	17.20	3.67	-0.44	0.03/0.13	0.03/0.16	0.10/0.27
RLSO	4679938.9937	1840151.1569	3910407.7025	2010.391	8.86	-8.58	0.56	0.05/0.41	0.04/0.20	0.16/0.55
LEMN	4434466.0760	2084864.3739	4069305.4627	2009.809	6.56	-1.37	0.86	0.03/0.18	0.04/0.41	0.10/0.26
KASI	4616572.5823	1674415.5562	4056441.2931	2009.664	19.49	14.10	-1.12	0.04/0.08	0.03/0.10	0.12/0.24
KLOK	4564747.0219	1845610.7736	4040935.1159	2009.710	20.74	5.78	-1.07	0.05/0.18	0.04/0.08	0.15/0.41
SPAN	4658312.2345	1757780.6697	3973702.5878	2009.796	20.69	4.01	-0.31	0.04/0.22	0.04/0.30	0.11/0.25
PONT	4671272.6580	1754437.0593	3959389.3952	2009.116	19.53	7.65	-2.78	0.05/0.17	0.03/0.08	0.14/0.51
ATAL	4591113.8365	1948751.1665	3962396.6812	2010.081	12.06	-5.29	0.73	0.10/0.18	0.09/0.23	0.41/1.59
PRKV	4435581.3060	2188830.4885	4013585.9082	2009.732	4.64	-0.14	-0.92	0.10/0.22	0.09/0.25	0.31/0.87

4. Conclusions

In this paper we present the NOANET, a permanent GPS network for regional studies in seismology and geodynamics in Greece. We described the procedures routinely used to download, store and analyze data from NOANET, with the goal of deriving a self-consistent three dimensional velocity field that can be used for further geodynamics and geo-kinematics applications, such as to measure coseismic, postseismic, and interseismic deformation across major fault zones; plate motion and crustal deformation at plate boundaries in the eastern Mediterranean; volcano deformation along the south Aegean Volcanic Arc; and the deformation associated with glacio-eustatic motions and its application to sea-level studies. We produce daily bias-free and bias-fixed solutions of the geodetic parameters along with the associated variance-covariance matrices. We process IGS stations together with the Greek stations in order to optimize the network internal constraints. The daily solutions derived from the processing are characterized by a very high percentage of fixed narrow-lane phase ambiguities up to 95%. Prior to producing the velocity solution, we analyze the time series for periodic signals, offsets, and accounting for time-correlated noise content, because each of these factors affects the velocity estimate and the associated errors (Table 2).

5. Acknowledgments

We thank our colleagues Marco Anzidei, Enrico Serpelloni, Pierre Briole, Bob King, Kirill Palamarchuk and Ivan Georgiev for useful discussions on network operation and data processing. NOANET was funded by EU (FP6 and FP7), regional programmes and Greek Government funds.

6. References

Altamimi Z., Collilieux X., Legrand J., Garayt B. and Boucher C. 2007. ITRF2005: a new release of the International Terrestrial Frame on the time series of station positions and Earth orientation parameters, *J. Geophys. Res.,* 112(B09401), doi:10.1029/2007JB004949.

Avallone A., Briole P., Agatza-Balodimou A.M., Billiris H., Charade O., Mitsakaki C., Nercessian A., Papazissi K., Paradissis D. and Veis G. 2004. Analysis of eleven years of deformation measured by GPS in the Corinth Rift Laboratory area, *C.R. Geoscience*, 336, 301–312.

Bernard P., Lyon-Caen H., Briole P., Deschamps A., Boudin F., Makropoulos K., Papadimitriou

P., Lemeille F., Patau G., Billiris H., Paradissis D., Papazissi K., Castarede H., Charade O., Nercessian A., Avallone A., Pacchiani F., Zahradnik J., Sacks S. and Linde A. 2006. Seismicity, deformation and seismic hazard in the western rift of Corinth: New insights from the Corinth Rift Laboratory (CRL), *Tectonophysics*, 426(1-2), 7–30.

Billiris H., Paradissis D., Veis G., England P., Featherstone W., Parsons B., Cross P., Rands P., Rayson M., Sellers P., Ashkenazi V., Davison M., Jackson J. and Ambraseys N. 1991. Geodetic determination of tectonic deformation in central Greece from 1900 to 1988, *Nature*, 350, 124–129.

Blewitt G., Lavallee D., Clark P. and Nurutdinov K. 2001. A new global mode of Earth deformation: Seasonal cycle detected, *Science*, 294, 2342– 2345.

Blewitt G. and Lavallee D. 2002. Effect of annual signals on geodetic velocity, *J. Geophys. Res.*, 107(B7), 2145, doi:10.1029/2001JB000570.

Bock Y., Wdowinski S., Fang P., Zhang J., Williams S., Johnson H., Behr J., Genrich J., Dean J., Van Domselaar M., Agnew D., Wyatt F., Stark K., Oral B., Hudnut K., King R.W., Herring T.A., Dinardo S., Young W., Jackson D. and Gurtner W. 1997. Southern California permanent GPS geodetic array: Continuous measurements of crustal deformation between the 1992 Landers and 1994 Northridge earthquakes, *J. Geophys. Res.*, 102, 18013–18033.

Briole P., Rigo A., Lyon-Caen H., Ruegg J.C., Papazissi K., Mitsakaki C., Balodimou A., Veis G., Hatzfeld D. and Deschamps A. 2000. Active deformation of the Corinth rift, Greece: Results from repeated Global Positioning System surveys between 1990 and 1995, *J. Geophys. Res.*, 105(B11), doi:10.1029/2000 JB900148.

Dong D.N., Herring T.A. and King R.W. 1998. Estimating regional deformation from a combination of space and terrestrial geodetic data, *J. of Geod.*, 72, 200–214.

Dong D.N., Fang P., Bock Y., Cheng M.K. and Miyazaki S. 2002. Anatomy of apparent seasonal variations from GPS-derived site position time series, *J. Geophys. Res.*, 107(B4), 2075, doi:10.1029/2001JB000573.

Feigl K.L., Agnew D.C., Bock Y., Dong D.N., Donnellan A., Hager B.H., Herring T.A., Jackson D.D., King R.W., Larsen S.K., Larson K.M., Murray M.H. and Shen Z.K. 1993. Measurement of the velocity field in central and southern California, *J. Geophys. Res.*, 98, 21667–21712.

Floyd M.A., Billiris H., Paradissis D., Veis G., Avallone A., Briole P., McClusky S., Nocquet J-M., Palamartchouk K., Parsons B. and England P.C. 2010. A new velocity field for Greece: Implications for the kinematics and dynamics of the Aegean, *J. Geophys. Res.*, 115(B10403), doi:10.1029/2009JB007040.

Ganas A. and Parsons T. 2009. Three-dimensional model of Hellenic Arc deformation and origin of the Cretan uplift, *J. Geophys. Res.*, 114(B06404), doi: 10.1029/2008JB005599.

Ganas A., Serpelloni E., Drakatos G., Kolligri M., Adamis I., Tsimi C. and Batsi E. 2009. The Mw 6.4 SW-Achaia (western Greece) earthquake of 8 June 2008: Seismological, field, GPS observations and stress modeling, *J. Earthquake Eng.*, 13, 1101–1124.

Herring T.A. 2003. MATLAB Tools for viewing GPS velocities and time series, *GPS Solut.*, 7(3), 194–199.

Herring T.A., King, R.W. and McClusky S. 2010. *Documentation for the GAMIT/GLOBK GPS processing software release 10.4.*, Mass. Inst. of Technol., Cambridge.

Hollenstein, C., Müller, M.D., Geiger, A.and Kahle H.G. 2008. Crustal motion and deformation in Greece from a decade of GPS measurements, 1993–2003, *Tectonophysics*, 449, 17–40.

Johnson H. and Agnew D. 1995. Monument motion and measurements of crustal velocities, *Geophys. Res. Lett.*, 22, 2905–2908.

Kahle H-G., Cocard M., Peter Y., Geiger A., Reilinger R., Barka A.and Veis G. 2000. GPS-derived strain rate field within the boundary zones of the Eurasian, African, and Arabian Plates, *J. Geophys. Res.*, 105(B10), 23353–23370.

Langbein J. 2004. Noise in two-color electronic distance meter measurements revisited, *J. Geophys. Res.*, 109(B4), B04406, doi:10.1029/2003JB002819.

Le Pichon X., Chamot-Rooke N., Lallemant S., Noomen R. and Veis G. 1995. Geodetic determination of the kinematics of central Greece with respect to Europe: implications for eastern Mediterranean tectonics, *J. Geophys. Res.*, 100(B7), 12675–12690.

Lyard F., Lefevre F., Letellier T. and Francis O. 2006. Modeling the global ocean tides: modern insights from FES2004, *Ocean Dyn.*, 56(5-6), 394–415, doi:10.1007/s10236-006-0086-x.

Mao A., Harrison C.G.A. and Dixon T.H. 1999. Noise in GPS coordinate time series, *J. Geophys. Res.*, 104, 2797–2816.

McCarthy D.D. and Petit G. 2004. IERS Conventions 2003*, IERS Technical Note*, 32, Verlag des Budesamts fuer Kartographie und Geodasie, Frankfurt.

McClusky S., Balassanian S., Barka A., Demir C., Ergintav S., Georgiev I., Gurkan O., Hamburger M., Hurst, K., Kahle H., Kastens K., Kekelidze G., King R., Kotzev V., Lenk O., Mahmoud S., Mishin A., Nadariya M., Ouzounis A., Paradissis D., Peter Y., Prilepin M., Reilinger R., Sanli I., Seeger H., Tealeb A., Toksoz M.N. and Veis G. 2000. Global Positioning System constraints on plate kinematics and dynamics in the eastern Mediterranean and Caucasus, *J. Geophys. Res.*, 105(B3), 5695–5719.

Nikolaidis R. 2002. Observation of geodetic and seismic deformation with the Global Positioning System, *Dissertation*, University of California, San Diego.

Nyst M. and Thatcher W. 2004. New constraints on the active tectonic deformation of the Aegean, *J. Geophys. Res.*, 109(B11406), doi:10.1029/2003JB002830.

Reilinger R., McClusky S., Vernant P., Lawrence S., Ergintav S., Cakmak R., Ozener H., Kadirov F., Guliev I., Stepanyan R., Nadariya M., Hahubia G., Mahmoud S., Sakr K., ArRajehi A., Paradissis D., Al-Aydrus A., Prilepin M., Guseva T., Evren E., Dmitrotsa A., Filikov S.V., Gomez F., Al-Ghazzi R.and Karam G. 2006. GPS constraints on continental deformation in the Africa-Arabia-Eurasia continental collision zone and implications for the dynamics of plate interactions, *J. Geophys. Res.*, 111(B05411), doi:10.1029/2005JB004051.

Van Dam T., Wahr J., Milly P.C.D., Shmakin A.B., Blewitt G., Lavallee D. and Larson K.M. 2001. Crustal displacements due to continental water loading, *Geophys. Res. Lett.*, 28, 651–654.

Williams S.D.P., Bock Y., Fang P., Jamason P., Nikolaidis R., Prawirodirdjo L., Miller M. and Johnson D.J. 2004. Error analysis of continuous GPS position time series, *J. Geophys. Res.*, 109(B03412), doi:10.1029/2003JB002741.

Zhang J., Bock Y., Johnson H., Fang P., Williams S., Genrich J., Wdowinski S. and Behr J. 1997. Southern California permanent GPS geodetic array: error analysis of daily position estimates and site velocities, *J. Geophys. Res.*, 102, 18035–18055.

Δελτίο της Ελληνικής Γεωλογικής Εταιρίας, τομ. XLVII , 2013
Πρακτικά 13ου Διεθνούς Συνεδρίου, Χανιά, Σεπτ. 2013

Bulletin of the Geological Society of Greece, vol. XLVII 2013
Proceedings of the 13th International Congress, Chania, Sept. 2013

NOAFAULTS: A DIGITAL DATABASE FOR ACTIVE FAULTS IN GREECE

Ganas A.[1], Oikonomou I. A. [1] and Tsimi C.[1]

[1] *1Institute of Geodynamics, National Observatory of Athens, Lofos Nymfon, Thission 11810 Athens, Greece, aganas@noa.gr athanoik@gmail.com christinant@gmail.com*

Abstract

This paper documents the approach to compiling a digital database of fault geometry and additional attributes primarily to support seismicity monitoring at the National Observatory of Athens (NOA). A database for Greek active faults has been constructed from published fault maps in peer-reviewed journals since 1972. The standard commercial software ARC GIS has been used to design and populate the database. The fault layer was produced by on-screen digitization and is available to the scientific community in ESRI shapefile (SHP) and TXT formats in WGS84 projection. A KML file is also available to display the fault data in an Earth browser such as Google Earth. In this version of the database, we focus our attention to the active faults of the upper (Aegean + Eurasian) plate and the back-arc region of the Hellenic Arc, in general. 963 faults are included. The database is freely accessible from the Internet.

Key words: *Active faults, GIS, Hellenic Arc.*

Περίληψη

Στην εργασία παρουσιάζεται η μεθοδολογία ανάπτυξης της ψηφιακής βάσης δεδομένων για τα ενεργά ρήγματα της Ελλάδος. Τα ρήγματα προέρχονται από χάρτες δημοσιευμένους σε περιοδικά με κριτές από το 1972. Όλα τα ρήγματα ψηφιοποιήθηκαν σε περιβάλλον ArcGIS και σχηματίστηκε βάση δεδομένων με τα χαρακτηριστικά της γεωμετρίας τους, ρυθμού ολίσθησης και σεισμικής συμπεριφοράς (τελευταίο σεισμικό γεγονός, άλμα κλπ) για όσα ρήγματα βρέθηκαν στοιχεία. Συνολικά περιλαμβάνονται 963 ενεργά ρήγματα. Η βάση διατίθεται ελεύθερα στην επιστημονική κοινότητα.

Λέξεις κλειδιά: *Ενεργά Ρήγματα, GIS, Ελληνικό τόξο.*

1. Introduction

Greece is well known in the geosciences for its active tectonics and accompanying seismicity (e.g. Skouphos, 1894; Maravelakis, 1943; Papazachos and Delibasis, 1969; McKenzie, 1978; Delibasis et al., 1981; Mariolakos et al., 1981; Mercier et al., 1983; Pavlides and Mountrakis, 1987; Mariolakos et al., 1989; Ambraseys and Jackson, 1990; Roberts and Jackson, 1991; Taymaz et al., 1991; Doutsos and Poulimenos, 1992; Armijo et al., 1992; Caputo and Pavlides, 1993; Jackson, 1994; Roberts and Ganas, 2000; Lekkas, 2001; Goldsworthy et al., 2002; Caputo et al., 2010; Figure 1). A search on the ISI Web of knowledge database (during March 2013) for Greece AND active faults produced 458 papers for the period 1970-present. Almost every single paper refers to

an active fault, providing some information on its geometry, kinematics and/or earthquake potential. Yet, a complete active fault database in digital form is missing for this country.

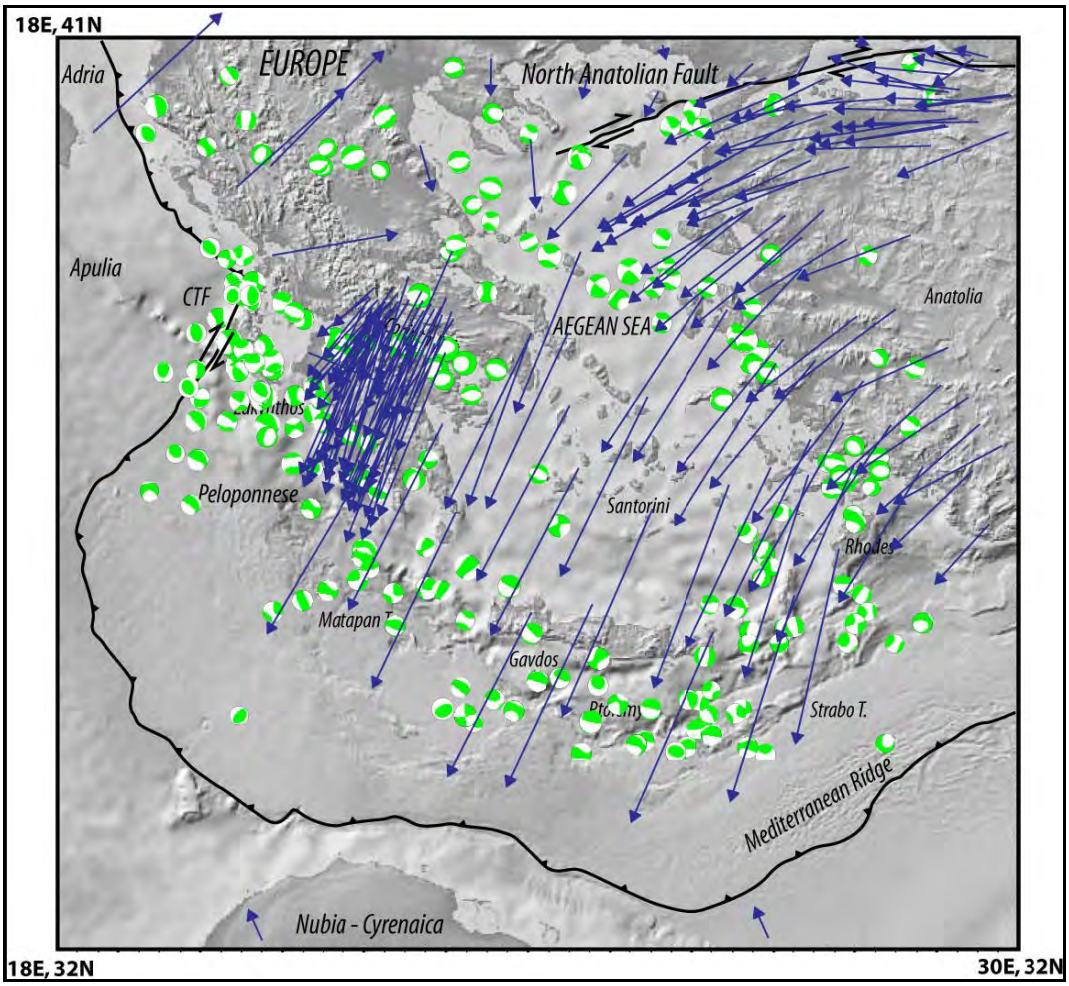

Figure 1 - Relief map of the Hellenic Arc and the Aegean Sea. The surface trace of the Hellenic Arc is shown as adapted after Kreemer and Chamot-Rooke (2004). Also shown are large faults – plate boundaries (North Anatolian Fault - CTF stands for Cephalonia Transform Fault), GPS vectors and selected earthquake focal mechanisms from the Global CMT database http://www.globalcmt.org / (compressional quadrants are shown in green). Image after Ganas and Parsons (2009).

We present first results of a project which stems from the everlasting need to construct seismicity maps containing accurate traces of faults (neotectonic and/or active) for routine seismic monitoring at NOA. During co-seismic and early post-seismic phase (24 hrs) there is a growing pressure by scientists, engineers, politicians and the media to associate earthquake epicentres with faults or faultlines. This is because we have identified two main hazards associated with active faults: ground rupture and ground shaking associated with the rupture. While ground rupture affects only the area in the immediate vicinity of the fault, the ground shaking will impact a much larger area. Existing maps in Greece (e.g. Delibasis et al, 1981; IGME, 1989; Papazachos et al., 2001) can be used for synoptic views because of their small scale (1:275000 or smaller). The Earthquake Planning and Protection Organisation of Greece (EPPO; www.oasp.gr) has published a series of 1:100000 neotectonic map sheets (ten sheets as of June 2013), only in hard copy. The

Greek Database of Seismogenic Sources (Gre.Da.S.S.) was presented by Pavlides et al., (2008) and Pavlides et al., (2010), focused on the North Aegean region and by Caputo et al., (2012) and Sboras (2012) on northern Greece.

Recently, large-scale (equal to or greater than 1:50000) maps of active faults are required by the Greek Ministries of Environment and Infrastructure in order for city plan expansion to be approved (e.g. Ganas et al., 2010). Most major cities of Greece like Athens, Thessaloniki, Patras and Heraklion host large ports and airports, refineries, large industrial plants, gas pipelines etc which are infrastructures of high economic importance. According to the current Building Code of Greece (EAK, 2000) and to Eurocode 8 regulations (EC-8, 2002) active faults need to be taken seriously in consideration in city planning and infrastructure projects. For the purposes of this study we consider faults as active if they show geologic evidence for slip during the last 125000-130000 years. As geologic evidence we consider published maps or reports or cross-sections documenting displacement of Holocene – late Pleistocene deposits and/or landforms. A longer time period than the Holocene is more appropriate, especially since most earthquake recurrence intervals along intra-plate faults are thousands to tens of thousands of years (see Crone et al., 1997, and Machette, 2000 for the paleoseismic perspective). Also, this age limit is followed by many countries (USA – WSSPC 1997, AIST Japan, New Zealand etc; see reference section for government sources). We also include offshore faults with seismological evidence for their activity during instrumental times (e.g. the 2001 Skyros earthquake fault, Benetatos et al., 2002).

In terms of active tectonics in Greek territory and its boundaries we may distinguish two major settings: the Hellenic Arc and the Greek mainland including the Aegean Sea and parts of western Anatolia (Figure 1). The Hellenic Arc defines a plate boundary between Eurasia and Africa lithospheric plates (Nubia; Ganas and Parsons, 2009 and references there in). We will not consider faults or fault segments along the plate interface as no consensus neither exist on the extent of past ruptures or on the degree of seismic coupling (see papers by Laigle et al., 2002, 2004; Ganas et al., 2009; Shaw and Jackson, 2010) along the arc. Therefore, we focus this first version of the database to the upper plate. The upper plate comprises the provinces of Central Greece, Macedonia, Thrace, Epirus, Peloponnese, Cyclades, Crete and Dodecanese. The latter two lie in a prominent position in the fore-arc of the Hellenic Subduction Zone where large, shallow earthquakes are most likely to occur by normal and strike-slip faulting (e.g. Delibasis et al., 1981; Armijo et al., 1992; Ganas and Parsons, 2009; Caputo et al., 2010). The upper crust of the fore-arc region displays numerous evidence of extensional deformation along both arc-parallel, high-angle, E-W striking faults and along arc-normal, high-angle pure-normal and oblique-normal faults that strike on average N-S. Other sets of normal faults striking NW-SE and NE-SW occur as well. The Greek mainland also deforms by normal faulting (e.g. Ambraseys and Jackson, 1990; Roberts and Jackson, 1991; Doutsos and Poulimenos, 1992; Piccardi, 2000; Kokkalas et al., 2007) while strike-slip tectonics prevail in the central and north Aegean Sea (Taymaz et al., 1991; Koukouvelas and Aydin, 2002).

2. Material and Methods

2.1. Identification of Faults

The digitized faults were identified and selected from literature sources, mainly published papers in peer-review journals. These papers were published during the period 1970-2010 and contain fault maps of active faults at a variety of scales. The majority of faults show normal-slip kinematics. The parameterization of the faults includes typical elements such as geometry, kinematics, evidence for activity etc (Table 1). The geological setting of the fault was determined according to Papanikolaou (1989) in most cases. The fault attributes were inserted into an Excel spreadsheet containing the main characteristics of each structure (geometry, kinematics) and were imported to the ARCGIS v 9.3. Number of active faults included in the database: 963.

To design and parameterize the fault database we followed the template produced under the EU project COST 625 (2000-2006; http://fir.seismology.hu/cost625/index.html)

2.2. Method of Work

The working method comprises the following stages: a) scanning of the fault map included in the selected publication in TIFF format (e.g. Figure 2 showing fault traces in north Parnitha region, central Greece; Figure 3 shows a field photograph of the fault surface) b) georeferencing of the scanned raster (TIFF) image using ArcGIS v9.3 software c) digitization of the fault traces as ESRI shapefiles (SHP) d) editing of the attribute table using published information such as fault length, dip direction, dip angle, slip rate etc (Figure 4).

Table 1 - Fault attributes contained in the NOAFaults database.

Parameter	Type	Description
Fault code	Number	Fault number
Fault name	Text	Name of structure
Kinematics	Text	Normal/Reverse/Strike slip sinistral /Strike slip dextral
Geological Setting	Text	Isopic zone of the Hellenides
Location Reliability	Text	At mapping scale: (1:50000 and above) is precise. (1:50000<scale<1:250000) is approximate. (1: 250000 and below) or map scale taken from seismological data is inferred.
Monitoring	Text	Description of possible monitoring networks.
Paleoseismology	Text	Description of possible paleoseismological studies.
Creep	Text	Yes/No
Co-seismic slip (m)	Text	Yes/No
Notes	Text	If necessary
Activity reliability	Text	Proven (from trench or seismic rupture) / Very Likely (from geomorphological criteria, or microseismic activity) / Possible (from orientation of structure with respect to the current stress field).
Slip rate (mm/yr)	Number	If known
Instrumental Seismicity	Text	Yes/No
Historical Seismicity	Number	Yes/No
Seismic Events	Text	List of earthquakes attributed to this fault
Max Magnitude	Number	Maximum recorded magnitude (Ms or Mw)
Risk level	Text	Crossing or in the vicinity (5 km) of towns - hazardous facilities (refineries etc). Low if fault length is less than 1 km. Medium if 1km <fault length <5km. High if fault length is more than 5 km.
Study quality	Text	Detailed/To be improved
Notes	Text	If necessary
Figure	Number	Figure with digitized faults (from original paper)
References	Text	Author(s) and title of paper(s)
Compiler	Text	Name of the compilers

The following control layers were used i) a vector (SHP format; standard industry format) file of the coastline of Greece at the scale of 1:250000 and ii) the longitude-latitude coordinates provided by the original fault map itself, as published in the literature. The coastline layer had the Greek national projection (Photogrammetric Engineering and Remote Sensing, 2002). All maps based on the coastline control layer were re-projected to geographic coordinates in WGS84. In the second case (based on the original map), we assumed that their geographic coordinates represent tick points under the WGS 1984 ellipsoid. The error of the georeferencing is a function of 1) the poly nomial used in the rectification of each map 2) the original map scale and 3) the quality of the con-

trol layer. Depending on the scale of the original map we calculated registration errors at the range 12-450 m (the latter error refers to offshore faults).

The digitization of faults took place on-screen using appropriate zooming, paying attention to all fault geometry details provided by the authors. Each fault segment is represented by a vector feature of the database. Then, characteristics of the fault segment such as fault strike, dip, rake, length, slip rate, co-seismic displacement etc were added to the appropriate fields in the database. Individual SHP files were converted to TXT (ASCII) files and then were grouped in 1 set to facilitate further processing.

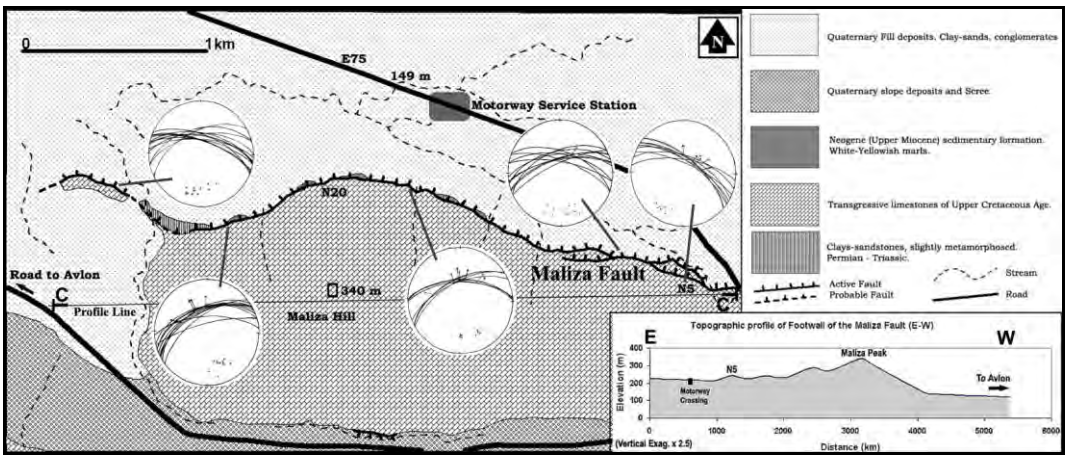

Figure 2 - Geological map showing the Maliza active fault in central Greece (after Ganas et al., 2004). Stereonets show results from slip data collection localities.

Figure 3 - Field photograph of the Maliza active fault (locality N5 on the map in Fig. 2). View to the south.

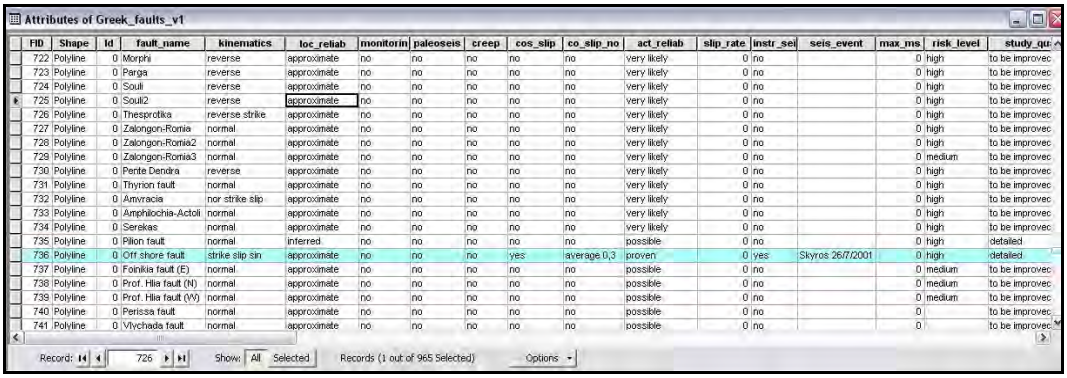

Figure 4 - Attribute table of the NOAFaults database. The seismic fault that ruptured during the Skyros 26 July 2001, shallow earthquake (Benetatos et al., 2002) is highlighted.

The database contains no information on the 3-D shape of faults. All faults are shown in 2-D as lines (Figure 5). We assume that the finite shape of normal and reverse faults is elliptical and that of strike-slip faults is rectangular, however, the user of the database should not make any assumption on the fault shape of the feature in study. Details on fault geometry and kinematics should be looked at original papers.

The SHP files were also converted to TXT format so that GMT software users (Wessel and Smith, 1995) could access the dataset and plot it on their maps. In this case, each fault is represented by one TXT file containing the geographic coordinates of start-end and intermediate vertices. No fault attributes are included. A KML file is also available to display the fault data in an Earth browser such as Google Earth http://earth.google.com / (Figure 6). All three file formats are available from www.gein.noa.gr

3. Discussion

3.1. Ambiguity of Fault Location on Fault Maps

In Greece, topographic maps for general use are available at 1:50000 and 1:100000 scales from the Hellenic Military Geographical Service (HMGS). They use a national projection system called EGSA'87 (Photogrammetric Engineering and Remote Sensing, 2002), which is a Transverse Mercator Projection, mapping Greece in one zone. A few areas are also available at 1:25000 scale. Most geologists use such maps as cartographic background to draw their faults. Following this reality, we introduced the following criteria to differentiate among fault location reliability.

Precise fault trace: the map from which the fault was digitized is 1:50000 scale or larger (e.g. Papanikolaou et al., 1998; Morewood and Roberts, 1999, 2001, 2002; Ganas et al., 2004). For Greece, the 1:50000 maps carry an accuracy of 15 m in the horizontal and 5 m on the vertical.

Approximate fault trace: the map from which the fault was digitized is 1:50000 scale or smaller (up to 1:250000; e.g. Jenkins, 1972; Mettos et al., 1991; King et al., 1993; Galanakis et al., 1998). Also, in case of no surface expression the location can be approximated by good-quality seismological data where epicentre planimetric accuracy is better than 2 km (e.g. seismic fault of the 2001 earthquake, offshore Skyros, Benetatos et al., 2002, Figure 4; seismic fault of the 8 June 2008 earthquake in NW Peloponnese; Ganas et al., 2009).

Inferred fault trace: the location of the fault is based on published seismological data (epicentres of aftershocks) of regional networks or seen in offshore seismic profiles (e.g. Laigle et al., 2000; Stefatos et al., 2002; Ganas et al., 2013).

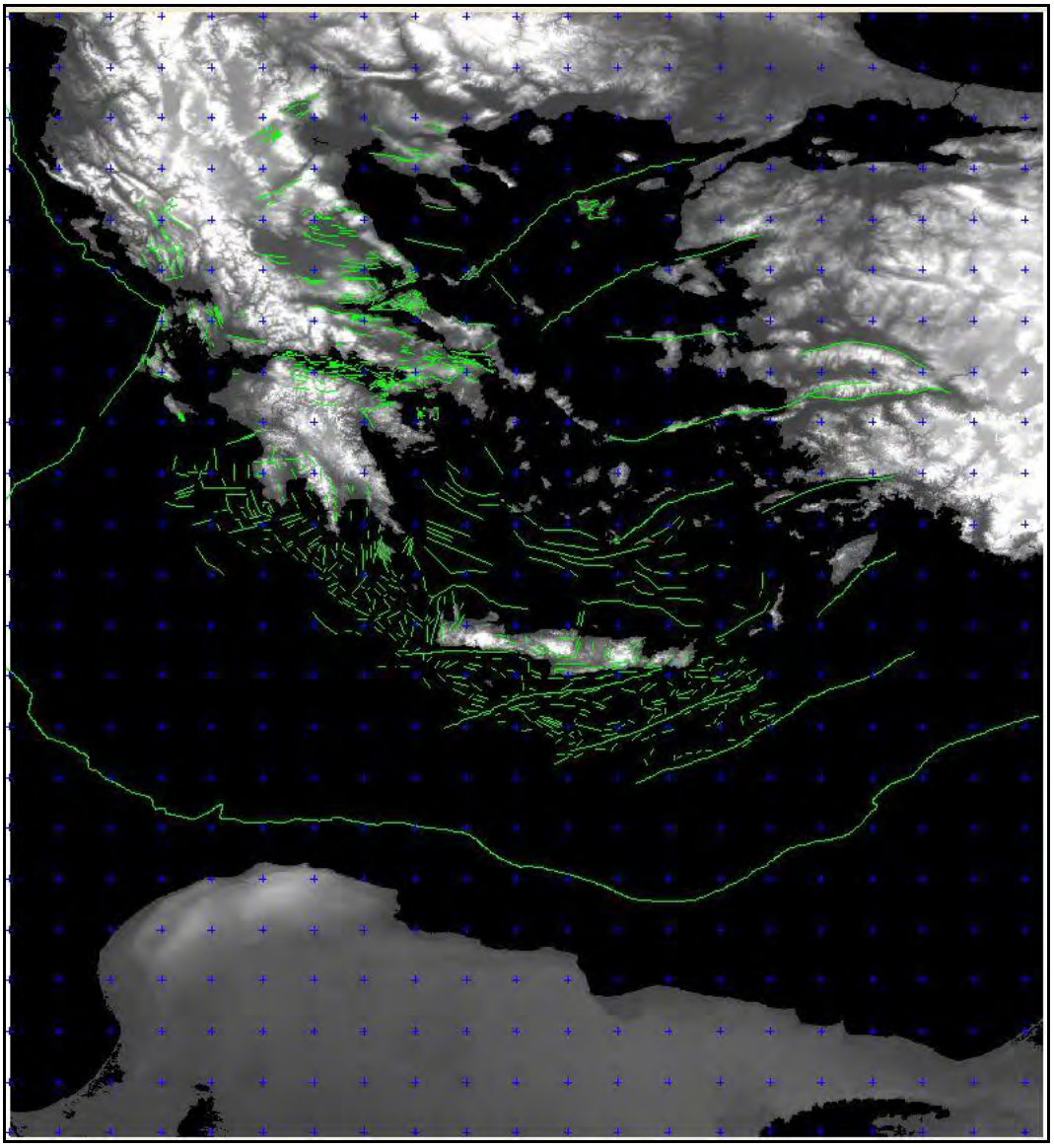

Figure 5 - Map of active faults of Greece (green lines) contained in NOAFaults database over a raster DEM (ETOPO2, 2004) in geographic projection. Faults are shown without kinematic information. Higher elevations are shown in bright tones of grey. Blue crosses are half-degree ticks.

3.2. Ambiguity on Fault Activity Reliability

We introduced the following criteria to differentiate among fault activity reliability:

Proven activity as demonstrated by reported co-seismic displacement along the fault trace during large earthquakes (e.g. Pavlides and Tranos, 1991; Pavlides et al., 1995; Ambraseys and Jackson, 1998), including the age of last motion measured in paleoseismological trenches (e.g. Heliki fault in Peloponnese, Koukouvelas et al., 2001; Atalanti fault in central Greece; Pantosti et al., 2004; Kaparelli and Mygdonia faults in Chatzipetros et al., 2005). Other evidence of present activity includes displacement of Holocene-Late Pleistocene sedimentary deposits and/or Middle-Late

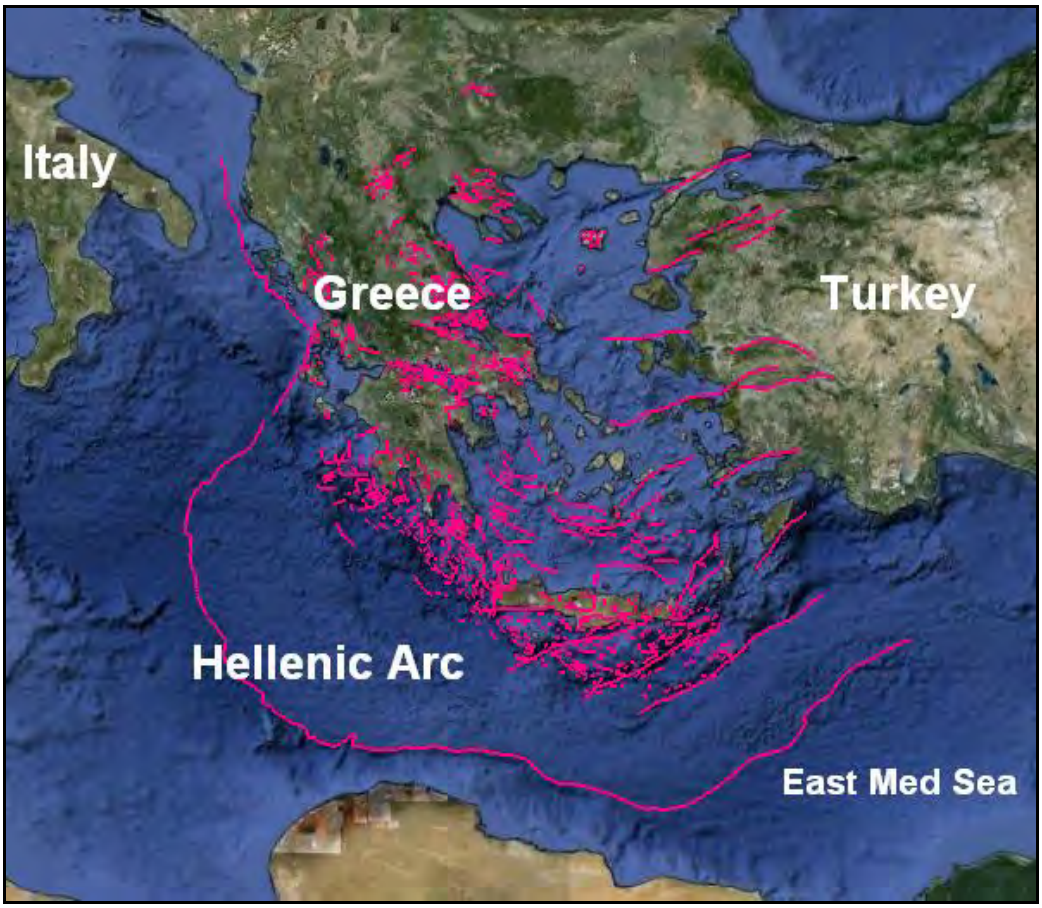

Figure 6 - Google Earth Image (September 2011 version) showing traces of active faults (purple lines). Faults shown are those of the upper (Aegean) plate.

Pleistocene sedimentary deposits (e.g. Caputo, 1996; Ganas, 1997; Maroukian et al., 2000; Goldsworthy and Jackson, 2001).

Activity Very likely as demonstrated by a) microseismic activity aligned for several kilometres for half- to two fault lengths as seen on seismicity maps (e.g. Louvari et al., 1999; Ganas et al., 2009), b) geological indicators (bean-shaped basins filled with Neogene syn-rift etc; e.g. Roberts and Ganas, 2000) and c) geomorphologic indicators (systematically displaced streams and erosion surfaces, existence of triangular facets along mountain fronts, etc; Papanikolaou et al., 1988; Ganas, 1997; Goldsworthy and Jackson, 2000).

Activity Possible as demonstrated by the orientation (strike) of fault with respect to the current stress field (e.g. offshore faults along the Hellenic Arc; Mascle et al., 1982; Hatzfeld et al., 1990), and/or by faults located near sharp discontinuities on GPS profiles (e.g. faults reported by Underhill, 1988, onshore Zakynthos where a GPS profile discontinuity exists in Hollenstein et al., 2008).

3.3. Overlapping Sources of Information

Many active faults are included in overlapping maps of the same area by different authors. For example the ISI Web of Knowledge database contains 149 papers on active faults AND Gulf of Corinth (June 2013 search). In such cases, we proceeded with a careful selection of those papers that contain the original fault maps, both onshore and offshore. It is possible that we missed a few

papers in this research as we could not trace back in literature all published papers. We ask for the understanding of those authors that see their work not mentioned in this database. As we present this product in its preliminary version, we aim to integrate this knowledge in future editions of this database. If possible, we also ask for their inputs by sending original material to the first author in Athens.

3.4. Lack of Consensus

There were cases where the fault trace is debatable among various authors, so as a decision had to be made by us. For example, old maps of the Atalanti fault in central Greece (IGME, 1989) show this active fault to reach the town of Agios Konstantinos (about 15 km to the northwest of Atalanti) while newer maps (Ganas, 1997; Ganas et al., 1998; Cundy et al., 2000) show it to terminate near the town of Atalanti. It is unfortunate that this version of the database cannot present all published versions of Greek active faults. Therefore, a disclaimer has been added at the end of this paper cautioning users to probable errors and omissions of this product.

3.5. Future Steps

We plan to update the database at regular intervals. Future add-ons may include details on fault geometry (strike, dip angle and dip direction) and kinematics (rake angle, sense of displacement), field photographs of selected fault planes known for hosting large earthquakes, GPS measurements from permanent stations close to major faults, links to on-line sources (libraries, etc), historical seismicity data etc.

We also anticipate that the database may be used in seismic hazard assessments (assuming the active faults as seismic sources) and as a tool for earthquake risk assessment in various parts of Greece. The database is more complete in the regions of central Greece (including Thessaly and Peloponnese), in west and central Macedonia and along the Hellenic Arc. The Hellenic Arc is prone to tsunamis (e.g. Lorito et al., 2008) so the database may be used in tsunami early warning applications. We could not retrieve lots of literature pieces for eastern Macedonia, Thrace and the Aegean Sea, so these areas will become targets for future updates of the database.

4. Conclusions

This paper documents the approach to compiling a digital database of fault geometry and additional attributes primarily to support seismic operations at the National Observatory of Athens (NOA).

A first version of the digital database of Greek active faults has been constructed. The database contains 963 faults published in peer-reviewed literature. This product may be used by geologists, seismologists and engineers working with cartographic scales 1:50000 and smaller. We exercise extreme caution to users of the database working with larger scales (e.g. 1:10000). The database is a growing database and will be subject to change as new information becomes available and new maps are published on Greek faults.

5. Acknowledgments

Some aspects of this work were funded by Action 625 of the COST project of EU (http://www.cost.esf.org/), by EU project PREVIEW, by ESA project TERRAFIRMA and by the Greek Secretariat for Research and Technology (GSRT), Ministry of Education, Greece. We thank our COST colleagues for the useful exchange of ideas. We are indebted to Spyros Pavlides, Luigi Piccardi, Anastasia Kiratzi, Gerald Roberts, Kevin White, Ricardo Caputo, Stefano Salvi, Vincenzo Spina and Ioannis Koukouvelas for discussions on active faulting and comments during field trips. We also thank Lina Alexandropoulou, Sotiris Valkaniotis and Fotini Kounavi for help with data collection and GIS processing. The paper got useful reviews from A. Chatzipetros and E. Lekkas. The database is freely accessible from the Internet (www.gein.noa.gr).

Disclaimer: This digital product is provided by the copyright holders "as is". In no event shall the copyright owner be liable for any direct, indirect, incidental, special, exemplary, or consequential damages as a result of its use.

6. References

Ambraseys N. and Jackson J. 1990. Seismicity and associated strain of central Greece between 1890 and 1988, *Geophys. J. Int*., 101, 663-708.

Ambraseys N. and Jackson J. 1998. Faulting associated with historical and recent earthquakes in the Eastern Mediterranean region, *Geophys. J. Int*., 133, 390-406.

Armijo R., Lyon-Caen H. and Papanastassiou D. 1992. East-west extension and Holocene normal fault scarps in the Hellenic arc, *Geology,* 20, 491-494.

Benetatos C., Roumelioti Z., Kiratzi A.and Melis N. 2002. Source parameters of the M 6.5 Skyros island (North Aegean Sea) earthquake of July 26, 2001, *Annals of Geophysics*, 45, 3-4.

Caputo R., Catalano S., Monaco C., Romagnoli G., Tortorici G. and Tortorici L. 2010. Active faulting on the island of Crete (Greece), *Geophysical Journal International*, 183, 111–126.

Caputo R. and Pavlides S. 1993. Late Cenozoic geodynamic evolution of Thessaly and surroundings (central-northern Greece), *Tectonophysics*, 223(3-4), 339-362.

Caputo R. 1996. The active Nea Anchialos Fault System (Central Greece): comparison of geological, morphotectonic, archaeological and seismological data, *Annali di Geofisica*, 39(3), 557-574.

Caputo R, Chatzipetros A., Pavlides S. et al. 2012. The Greek Database of Seismogenic Sources (GreDaSS): state-of-the-art for northern Greece, *Annals of Geophysics*, 55(5), 859-894.

Chatzipetros A., Kokkalas S., Pavlides S. and Koukouvelas I. 2005. Paleoseismic data and their implication for active deformation in Greece, *Journal of Geodynamics*, 40, 170-188.

Crone AJ, Machette MN and Bowman J.R. 1997. Episodic nature of earthquake activity in stable continental regions revealed by palaeoseismicity studies of Australian and North American Quaternary faults, *Australian Journal of Earth Sciences*, 44(2), 203-214.

Cundy A.B., Kortekaas S., Dewez T., Stewart I.S., Kollins P.G., Cruddace I.W., Maroukian H., Papanastasiou D., Gaki-Papanastasiou P., Pavlopoulos K. and Dawson A. 2000. Coastal wetlands as recorders of earthquake subsidence in the Aegean: a case study of the 1894 gulf of Atalanti earthquakes, central Greece, *Marine Geology*, 170, 3-26.

Delibasis N., Drakopoulos J. K., Fytrolakis N., Katsikatsos G., Makropoulos K.C. and Zamani A. 1981. Seismotectonic Investigation of the area of Crete Island, *Proc. of the Intern. Symp. on the Hellenic Arc and Trench (H.E.A.T.)*, Athens, 1, 121-138.

Doutsos T. and Poulimenos G. 1992. Geometry and Kinematics of active faults and their seismotectonic significance in the Western Corinth-Patras rift (Greece), *J. Structural Geology*, 14(6), 689-699.

EC-8 2002. Eurocode 8: Design of structures for earthquake resistance, Part 5: Foundations, retaining structures and geotechnical aspects, Draft No5, Revised Final Project Team Draft (preStage 49), May 2002, Doc CEN/TC250/SC8/N318.

ETOPO2 2004. Available online at: http://www.ngdc.noaa.gov/mgg/global/relief/ETOPO2/

Galanakis D., Pavlides S.band Mountrakis D. 1998. Recent brittle tectonic in Almyros – Pagasitikos, Maliakos, N. Euboea & Pilio, *Bulletin of the Geological Society of Greece*, XXXII/1, 263-273.

Ganas A., Chousianitis K., Batsi E., Kolligri M., Agalos A., Chouliaras G. and Makropoulos K. 2013. The January 2010 Efpalion earthquakes (Gulf of Corinth, Central Greece): earthquake interactions and blind normal faulting, *Journal of Seismology*, 17 (2), 465-484.

Ganas A., Palyvos N., Mavrikas G., Kollias S. and Tsimi C. 2010. Geomorphological and geological observations at the coast of Tripiti hill (Heraklion harbour, Crete), in relation to reported active faulting, *Proceedings of XIX CBGA Congress*, Thessaloniki, Greece, 99, 11-20.

Ganas A., Serpelloni E., Drakatos G., Kolligri M., Adamis I., Tsimi Ch. and Batsi E. 2009. The Mw 6.4 SW Achaia (Western Greece) Earthquake of 8 June 2008: Seismological, Field,

GPS Observations, and Stress Modeling, *J. of Earthquake Engineering,* 13(8), 1101 — 1124.
Ganas A. and Parsons T. 2009. Three-dimensional model of Hellenic Arc deformation and origin of the Cretan uplift, *J. Geophysical Research*, 114, B06404, doi: 10.1029/2008JB005599.
Ganas A., Pavlides SB., Sboras S., Valkaniotis S., Papaioannou S., Alexandris GA., Plessa A.and Papadopoulos GA. 2004. Active Fault Geometry and Kinematics in Parnitha Mountain, Attica, Greece, *Journal of Structural Geology*, 26, 2103-2118.
Ganas A., Roberts G.P. and Memou Tz. 1998. Segment boundaries, the 1894 ruptures and strain patterns along the Atalanti Fault, Central Greece, *Journal of Geodynamics*, 26(2-4), 461 - 486.
Ganas A. 1997. Fault Segmentation and Seismic Hazard Assessment in the Gulf of Evia Rift, central Greece, *Unpublished PhD thesis*, University of Reading, UK, 369pp.
Geological Survey of Japan, AIST, Active fault database of Japan, web site assessed July 1, 2013, Available at http://riodb02.ibase.aist.go.jp/activefault/index_e.html
Goldsworthy M, Jackson J. and Haines J. 2002. The continuity of active fault systems in Greece, *Geophys. J. Int*. 148, 596 – 618.
Goldsworthy M. and Jackson J. 2000. Active normal fault evolution in Greece revealed by geomorphology and drainage patterns, *Journal of the Geological Society*, London, 157, 967-981.
Goldsworthy M. and Jackson J. 2001. Migration of activity within normal fault systems: examples from the Quaternary of mainland Greece, *Journal of Structural Geology,* 23, 489-506.
Hatzfeld D., Pedotti G., Hatzidimitriou P. and Makropoulos K. 1990. The strain pattern in the western Hellenic arc deduced from a microearthquake survey, *Geophys. J. Int*., 101, 181-202.
Hollenstein Ch., Muller M.D., Geiger A. and Kahle H.G. 2008. Crustal motion and deformation in Greece from a decade of GPS measurements, 1993-2003, *Tectonophysics*, 449(1-4), 17-40.
IGME 1989. Seismotectonic map of Greece with seismogeological data, 1 map on 4 sheets, 1:500000 scale.
ISI web of knowledge: Available at http://isknowledge.com Copyright © 2013 Thomson Reuters
Jackson J. 1994. Active tectonics of the Aegean region, *Annual Review of Earth and Planetary Sciences*, 22, 239-271.
Jenkins D.A. 1972. Structural development of Central Greece, *The American association of Petroleum Geologists Bulletin* , 56(1), 128-149.
King G., Sturdy D. and Whitney J. 1993. The landscape geometry and active tectonics of northwest Greece, *Geological Society of America Bulletin*, 105, 137-161.
Kokkalas S., Pavlides S., Koukouvelas I., Ganas A. and Stamatopoulos L. 2007. Paleoseismicity of the Kaparelli fault (eastern Corinth Gulf): Evidence for earthquake recurrence and fault behavior, *Bollettino della Societa Geologica Italiana*, 126 (2), 387-395.
Koukouvelas I. K.and Aydin A. 2002. Fault structure and related basins of the North Aegean Sea and its surroundings, *Tectonics,*.21(5), 1046, doi: 10.1029/2001TC901037.
Koukouvelas I.K., Stamatopoulos L., Katsonopoulou D. and Pavlides S. 2001. A palaeoseismological and geoarchaeological investigation of the Eliki fault, Gulf of Corinth Greece, *Journal of Structural Geology*, 23, 531-543.
Kreemer C. and Chamot-Rooke N. 2004. Contemporary kinematics of the southern Aegean and the Mediterranean Ridge, *Geophysical J. International*, 157, 1377-1392.
Laigle M., Hirn A., Sachpazi M. and Roussos N. 2000. North Aegean crustal deformation: An active fault imaged to 10 km depth by reflection seismic data, *Geology,* 28(1), 71-74.
Laigle M., Hirn A., Sachpazi M. and Clément C. 2002. Seismic coupling and structure of the Hellenic subduction zone in the Ionian Islands region, *Earth and Planetary Science Letters*, 200 (3-4), 243-253.
Laigle M., Sachpazi M. and Hirn A. 2004. Variation of seismic coupling with slab detachment and upper plate structure along the western Hellenic subduction zone, *Tectonophysics*, 391(1-4), 85-95.

Lekkas E. 2001. The Athens earthquake (7 September 1999): intensity distribution and controlling factors, *Engineering Geology*, 59, 297-311.

Lorito S.,Tiberti M.M, Basili R., Piatanesi A. and Valensise G. 2008. Earthquake-generated tsunamis in the Mediterranean Sea: Scenarios of potential threats to Southern Italy, *J. Geophys. Res.*, 113, B01301, doi:10.1029/2007JB004943.

Louvari E., Kiratzi A.A. and Papazachos B.C. 1999. The Cephalonia Transform fault and its extension to western Lefkada Island (Greece), *Tectonophysics*, 308, 223-236.

Machette M.N. 2000. Active, capable, and potentially active faults - a paleoseismic perspective, *Journal of Geodynamics*, 29(3-5), 387-392.

Maravelakis M.J. 1943. Geologic and macroseismic study of the devastated earthquake of Larisa of 1 March 1941. *Triakontapentaeteris of Prof. N. Criticos*, Athens, 2, 176-193 (in Greek).

Mariolakos I., Fountoulis I., Logos E. and Lozios S. 1989. Surface faulting caused by the Kalamata (Greece) earthquakes (13/9/86), *Tectonophysics*, 163, 197 - 203.

Mariolakos I., Papanikolaou D., Symeonidis N., Lekkas S., Karotsieris Z. and Sideris C. 1981. The deformation of the area around the eastern Corinthian Gulf affected by the earthquakes of February to March 1981, *Proc. Int. Symp. Hellenic Arc and Trench*, Athens, 400–420.

Maroukian H., Gaki-Papanastassiou K., Papanastassiou D. and Palyvos N. 2000. Geomorphological Observations in the coastal zone of Kyllini Peninsula, NW Peloponnesus – Greece, and their relation to the seismotectonic regime of the area, *J. Coastal Research* 16(3), 853-863.

Mascle J., Le Quellec P., Leite O. and Jongsma D. 1982. Structural sketch of the Hellenic continental margin between the western Peloponnesus and eastern Crete, *Geology*, 10,113-116.

McKenzie D. 1978. Active tectonics of the Alpine-Himalayan belt: the Aegean Sea and surrounding regions, *Geophys. J.R. Astr. Soc*., 55, 217-254.

Mercier J.L., Carey-Gailhardis E., Mouyaris N., Simeakis K., Roundoyannis T. and Anghelidhis C. 1983. Structural analysis of recent and active faults and regional state of stress in the epicentral area of the 1978 Thessaloniki earthquakes (northern Greece), *Tectonics,* 2(6), 577-600.

Mettos A., Rontogianni Th., Papadakis G., Paschos P., Georgiou Ch. 1991. New geological data of the Neogene deposits of N. Euboea, *Bulletin of the Geological Society of Greece,* XXV/3, 71-83.

Morewood N.C. and Roberts G.P. 1999. Lateral propagation of the surface trace of the south Alkyonides normal fault segment, central Greece: its impact on models of fault growth and displacement – length relationships, *Journal of Structural Geology*, 21, 635-652.

Morewood N.C. and Roberts G.P. 2001. Comparison of surface slip and focal mechanism slip data along normal faults: an example from the eastern Gulf of Corinth, Greece, *Journal of Structural Geology*, 23, 473-487.

Morewood N.C. and Roberts G.P. 2002. Surface observations of active normal fault propagation: implications for growth, *Journal of the Geological Society London*, 159, 263-272.

New Zealand Ministry for the Environment (available on June 2013, web access) http://www.mfe.govt.nz/publications/rma/planning-development-active-faults-dec04/html/page11.html

Pantosti D., De Martini P.M., Papanastassiou D., Lemeille F., Palyvos N. and Stavrakakis G. 2004, Paleoseismological trenching across the Atalanti fault (Central Greece): evidence for the ancestors of the 1894 earthquake during the Middle Ages and Roman times, *Bulletin of the Seismological Society of America*, 94(2), 531-549.

Papanikolaou D. I., Mariolakos H. D., Lekkas E. L. and Lozios S.G. 1988. Morphotectonic observations on the Asopos basin and the coastal zone of Oropos. Contribution to the neotectonics of Northern Attica, *Bulletin of the Geological Society of Greece*, XX, 251-267.

Papanikolaou D., Vassilakis E. and Parcharidis I. 1998. Satellite images of short wavelength radiation for structure detection in shallow waters case study: Aegina – Agistri islands, Saronikos gulf, *Bulletin of the Geological Society of Greece* , XXX/1, 105-111.

Papanikolaou D. 1989. Geotectonic map of Greece. Special Publ. No 1, in Papanikolaou & Sassi eds., *Geol. Soc. Greece - IGCP project 276, Newsletter No 1*, Athens.

Papazachos B.C, and Delibasis N.D. 1969. Tectonic stress field and seismic faulting in the area of Greece, *Tectonophysics*, 7(3), 231-255.

Papazachos B. C.,Mountrakis D.M., Papazachos C.B., Tranos M.D., Karakaisis G.F. and Savvaidis A.S. 2001, The faults that caused the known strong earthquakes in Greece and surrounding areas during 5th century B.C. up to present, *Proc. 2nd Conf. Earthquake Eng. and Eng. Seism.*, Thessaloniki, Greece, 1, 17–26.

Pavlides S.B. and Mountrakis D.M. 1987. Extensional tectonics of north-western Macedonia, Greece, since the late Miocene, *Journal of Structural Geology*, 9(4), 385-392.

Pavlides S.B. and Tranos M.D. 1991. Structural characteristics of two strong earthquakes in the North Aegean: Ierissos (1932) and Agios Efstratios (1968), *Journal for Structural Geology*, 13(2), 205-204.

Pavlides S.B., Zouros N.C, Chatzipetros A.A., Kostopoulos D.S. and Mountrakis D.M. 1995. The 13 May 1995 western Macedonia, Greece (Kozani Grevena) earthquake; preliminary results, *Terra Nova*, 7, 544–549.

Pavlides S., Valkaniotis S. and Chatzipetros A. 2008. Seismically capable faults of Greece and their use in seismic hazard assessment, *Proceedings of the 4th International Conference on Earthquake Geotechnical Engineering,* Thessaloniki, 25-28 June 2007, Paper 1609.

Pavlides S., Caputo R., Sboras S., Chatzipetros A., Papathanasiou G. and Valkaniotis S. 2010. The Greek Catalogue of Active Faults and Database of Seismogenic Sources, *Bulletin Geological Society of Greece*, XLIII/1, 486-494.

Photogrammetric Engineering and Remote Sensing, Grids and Datums, December 2002. Available at: http://www.asprs.org/resources/Grids/12-2002-hellenic.pdf

Piccardi L. 2000. Active fault at Delphi, Greece: Seismotectonic remarks and a hypothesis for the geologic environment of a myth, *Geology*, 28(7), 651-654.

Roberts G. P. and Ganas A. 2000. Fault-slip directions in central and southern Greece measured from striated and corrugated fault planes: Comparison with focal mechanism and geodetic data, *Journal of Geophysical Research*, 105(B10), 23443-23462.

Roberts S. and Jackson J. 1991. Active normal faulting in Central Greece: an overview. In: Roberts A. M., Yielding G. & Freeman B. eds., The geometry of normal faults, *Geological Society London Publication*, 56, 125-142.

Sboras S. 2012. The Greek Database of Seismogenic Sources: seismotectonic implications for North Greece, *PhD Thesis*, University of Ferrara, Ferrara, 252 pp.

Shaw B. and Jackson J. A. 2010. Earthquake mechanisms and active tectonics of the Hellenic subduction zone, *Geophysical Journal International*, 181(2), 966-984.

Skouphos T. 1894. Die swei grossen Erdbeben in Lokris am 8/20 und 15/27 April 1894, *Zeitschrift Ges. Erdkunde zu Berlin*, 24, 409-474.

Stefatos A., Papatheodorou G., Ferentinos G., Leeder M. and Collier R. 2002. Seismic reflection imaging of active offshore faults in the Gulf of Corinth: their Seismotectonic significance, *Basin Research*, 14, 487-502.

Taymaz T., Jackson J. and McKenzie D. 1991. Active tectonics of the north and central Aegean Sea, *Geophys. J. Int*., 106, 433-490.

Underhill J. R. 1988. Triassic evaporates and Plio-quaternary diapirism in Western Greece, *Journal of the Geological Society, London*, 145, 269-282.

Wessel P. and Smith W.H.F. 1995. New Version of the Generic Mapping Tools Released, *EOS Trans. AGU*, 76, 329.

WSSPC (Western States Seismic Policy Council), 1997. Active fault definition for the Basin and Range Province, *WSSPC Policy Recommendation 97-1 White Paper*, May 22, 1997, San Francisco, CA. p. 3.

Δελτίο της Ελληνικής Γεωλογικής Εταιρίας, τομ. XLVII , 2013
Πρακτικά 13ου Διεθνούς Συνεδρίου, Χανιά, Σεπτ. 2013

Bulletin of the Geological Society of Greece, vol. XLVII 2013
Proceedings of the 13th International Congress, Chania, Sept. 2013

CONTINUOUS MAGNETOTELLURIC OBSERVATIONS IN WESTERN CRETE AS A TOOL FOR THE STUDY OF THE HELLENIC SUBDUCTION ZONE

Kalisperi D.[1], Rigakis I.[1], Makris J.P.[1], Romano G.[2] and Vallianatos F.[1]

[1] Technological Educational Institute of Crete, Department of Natural Resources and Environment, dkalisperi@chania.teicrete.gr

[2] CNR - Istituto di Metodologie per l'Analisi Ambientale, C.da Santa Loja, Tito Scalo, 85050 Potenza, Basilicata

Abstract

In the frame of the "MagnetoTellurics in studying Geodynamics of the hEllenic ARc (MT-GEAR)" project, a new continuous monitoring Magnetotelluric (MT) station has been installed in Western Crete. The new permanent MT-station, designed and constructed incorporating contemporary technology, is solar powered, fully telemetric, and the data transfer can be performed alternatively through 3G network or a satellite link. The selected site for the installation resulted from an exploratory MT survey, among other prospective sites aggregating MT qualifications. The purpose of the operation of a permanent MT observatory is twofold. The primary objective is to act as remote reference station to the ongoing MT survey (at selected Islands of southern Aegean) of the geodynamics of the Hellenic Subduction Zone. In addition, possible apparent resistivity variations as well as electric and/or magnetic field transient anomalies are investigated, while it would be attempted to associate these variations with seismic activity.

Key words: *Magnetotellurics, Remote Reference, MT Monitoring, MT-GEAR, Seismoelectromagnetism, Hellenic Subduction Zone, Crete, Southern Aegean.*

Περίληψη

Στα πλαίσια υλοποίησης του ερευνητικού έργου "MagnetoTellurics in studying Geodynamics of the hEllenic ARc (MT-GEAR)", ένας νέος μαγνητοτελλουρικός (MT) σταθμός συνεχούς παρατήρησης εγκαταστάθηκε στη Δυτική Κρήτη. Ο νέος, μόνιμος MT-σταθμός, που σχεδιάστηκε και κατασκευάστηκε ενσωματώνοντας σύγχρονη τεχνολογία, τροφοδοτείται με ανανεώσιμη, ηλιακή ενέργεια, είναι πλήρως τηλεμετρικός και η μεταγωγή των δεδομένων πραγματοποιείται εναλλακτικά είτε μέσω δικτύου κινητής τηλεφωνίας (3G) είτε μέσω δορυφορικής ζεύξης. Η θέση εγκατάστασης, που προέκυψε από διερευνητικές MT διασκοπήσεις, επιλέχθηκε ανάμεσα σε άλλες υποψήφιες θέσεις που συγκέντρωναν τις προδιαγραφές για MT. Ο σκοπός της λειτουργίας του μόνιμου MT-σταθμού είναι διττός. Ο κύριος αντικειμενικός στόχος είναι να αποτελεί σταθμό αναφοράς για τις εξελισσόμενες MT-διασκοπήσεις (σε επιλεγμένα νησιά του Νοτίου Αιγαίου) που ερευνούν τη γεωδυναμική της Ελληνικής Ζώνης Υποβύθισης. Επιπροσθέτως, διερευνώνται πιθανές μεταβολές της φαινόμενης αντίστασης της γεωηλεκτρικής δομής, όπως επίσης και ηλεκτρικές και/ή μαγνητικές μεταβατικές ανωμαλίες με σκοπό να επιχειρηθεί η συσχέτισή τους με τη σεισμική δραστηριότητα.

Λέξεις κλειδιά: *Μαγνητοτελλουρική μέθοδος, Τεχνική Απομακρυσμένου Σταθμού, Συνεχής παρακολούθηση MT δεδομένων, MT-GEAR, Σεισμοηλεκτρομαγνητικά, Ελληνική Ζώνη Υποβύθισης, Κρήτη, Νότιο Αιγαίο.*

1. Introduction

Crete is located in a prominent position in the fore-arc of the Hellenic Subduction Zone (HSZ), i.e. on top of the shallow portion of the presently active region of convergence (Spakman et al., 1988; Papazachos et al., 1995). It lies in the southern Aegean Sea (34° N-37° N, 21° E-29° E) among the islands of Kithira, Kassos, Karpathos and Rhodes, which those five islands consist the Hellenic Arc (Angelier, 1976). This arcuate feature, extending from the Peloponnese in the northwest to the island of Crete in the south, is the seismically most active region in western Eurasia due to subduction of the oceanic African lithosphere beneath the Eurasian plate (Vallianatos & Makris, 2000; Snopek et al., 2007). Due to the fact that the African plate moves to the north, compression between the Arabian and Eurasian plate is caused (Molnar & Tapponier, 1975). The rate of convergence consists of a 3-4 cm/year SSW-ward movement of Crete relative to stable Eurasia (Jackson, 1994; Noomen et al., 1999; Bohnhoff et al., 2001) and an 1 cm/year northward movement of Africa towards Eurasia (McKenzie, 1970; Bohnhoff et al., 2001), resulting in a net convergence rate of 4 to 5 cm/year at the plate boundary. The Benioff zone seismicity reaches down to ca. 180 km (Makris & Röwer, 1986), being situated at a depth of ca. 140 km underneath the magmatic arc, with volcanic activity on the islands of Santorini, Nisyros etc in the Aegean Sea. This procedure results in the movement of the Aegean and Anatolia lithospheric plates to the west, and then the gravitational spreading of the Aegean to the east Mediterranean (McKenzie, 1978; Le Pichon & Angelier, 1979; Angelier et al; 1981). This gravitational spreading of the Aegean is proved by the large amount of normal faults (Upper Miocene) (Aubouin & Dercourt, 1965; Aubouin, 1971; McKenzie, 1978; Le Pichon & Angelier, 1979; Angelier et al., 1981; Peters, 1985; Mascle & Martin, 1990). For this reason, Crete and Aegean Islands provide excellent onshore access to the internal structure of the fore-arc at various levels (Seidel, 2003).

The aforementioned area is very interesting both for its structural geological setting and, of course, for its historical (Pirazzoli, 1996; Stiros, 2001) and recent seismicity (Nikolintaga et al., 2008). Therefore, apart from the obvious study of seismotectonics, it is considered to be an excellent area to attempt to associate variations in electric (Huang and Liu, 2006) and magnetic fields and/or changes in the geoelectrical structure of subsoil (Nagao et al., 2002) with seismic activity (Merzer and Klemplerer, 1997). Literature is replete with reports of pre-earthquake phenomena, mainly of electric, magnetic or electromagnetic nature. Comprehensive reviews can be found in Johnston (1997), Tzanis & Vallianatos (2002), while much additional information exists in the collections edited by Hayakawa & Fujinawa (1994).

The magnetotellurics is a passive geophysical exploration technique that utilizes a broad spectrum of naturally occurring geomagnetic variations as a power source for electromagnetic source induction in the earth. As such, MT is distinct from active geoelectric techniques (Kaufman & Keller, 1981; Simpson & Bahr, 2005). In the 1950s, Tikhonov (1950) and Cagniard (1953) realized that if electric, E, and magnetic, B, field variations are measured simultaneously then complex ratios (impedances) can be derived that describe the penetration of electromagnetic fields into the earth. The penetration depths of electromagnetic fields within the earth depend on the electromagnetic sounding period, and on the earth's conductivity structure. By inverting the impendance tensor, which linearly relates the two horizontal electric components to the horizontal magnetic ones, the electrical resistivity distribution of the Earth's interior can be defined.

Continuous MT observations can be used both for applying the Remote-Reference-Technique (Gamble et al, 1979) and of course in order to provide information on seismoelectromagnetic

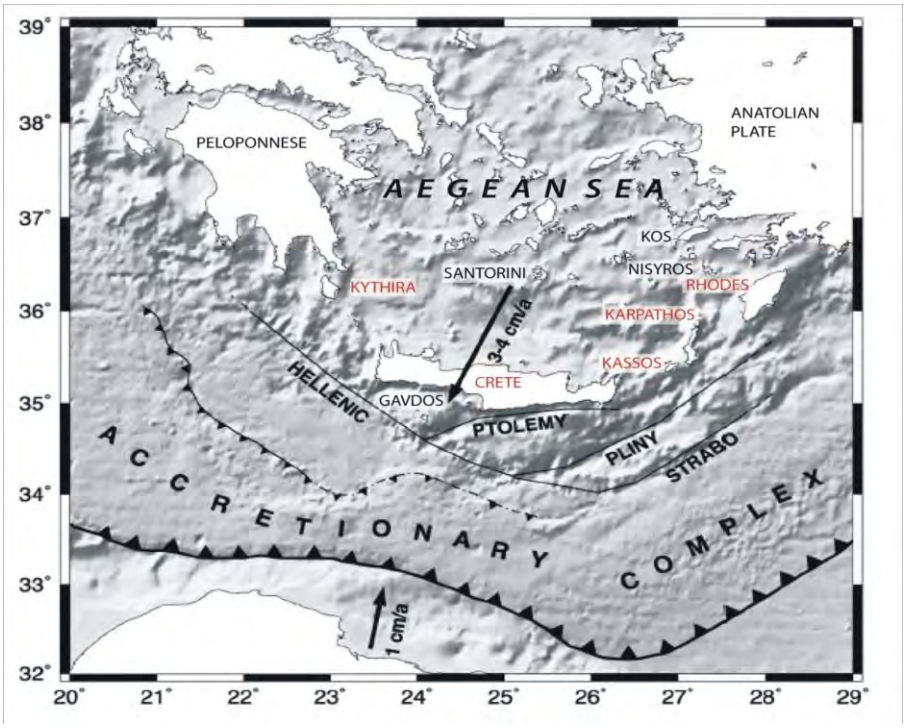

Figure 1 - Generalized map of the main tectonic elements of the South Aegean region (after Le Pichon & Angelier, 1979; Jackson, 1994) depicting the geodynamic framework of the south Hellenic Arc, which is consisted by five islands, highlighted with red color. See text for more explanation.

phenomena, such as: a change in resistivity or a generation of EM fields of internal (geodynamic) origin (Svetov et al, 1997). Globally there are many monitoring MT stations in Japan (Wakuya station and Esashi station), in Taiwan (located on Penghu Island), in Greece (Zlotnicki et al, 2006) in Italy (Balasco et al, 2008; Balasco et al, 2004), in Russia (Svetov et al, 1997), in Germany (Eydam & Munoz, 2011), etc operating either as remote reference stations or for earthquake prediction research.

Since early 2013 a new magnetotelluric (MT) monitoring station has been installed by Laboratory of Applied Geophysics and Seismology of Technological Educational Institute of Crete (LGS-TEICR) at Omalos Plateau (35.33N, 23.89E), Western Crete, Greece, in the frame of MT-GEAR project. Simultaneously during 2013, Electromagnetic Measurements (Magnetotellurics and Transient Electromagnetics - TEM) in selected sites in Southern Aegean -on Crete and on Aegean Islands across the Hellenic Arc (Kithira, Karpathos and Rhodes) but also at Santorini, Mylos, Folegandros, Gavdos, Nisyros, Kos, Tilos, Astipalaia, Southern Peloponnese, etc.- are being acquired. Several MT-TEM field campaigns have been organized at the aforementioned selected islands during this year for the study of the geoelectric structure of the Hellenic Subduction Zone and of course data from the Omalos' MT reference station will be used for the application of the remote reference technique.

The overall aim of this research is actually to produce important results concerning the geoelectrical structure of the fore-arc of the HSZ, using the permanent MT station as a remote station and to attempt to associate variations in electric and magnetic fields and changes in the geoelectrical structure with seismic activity.

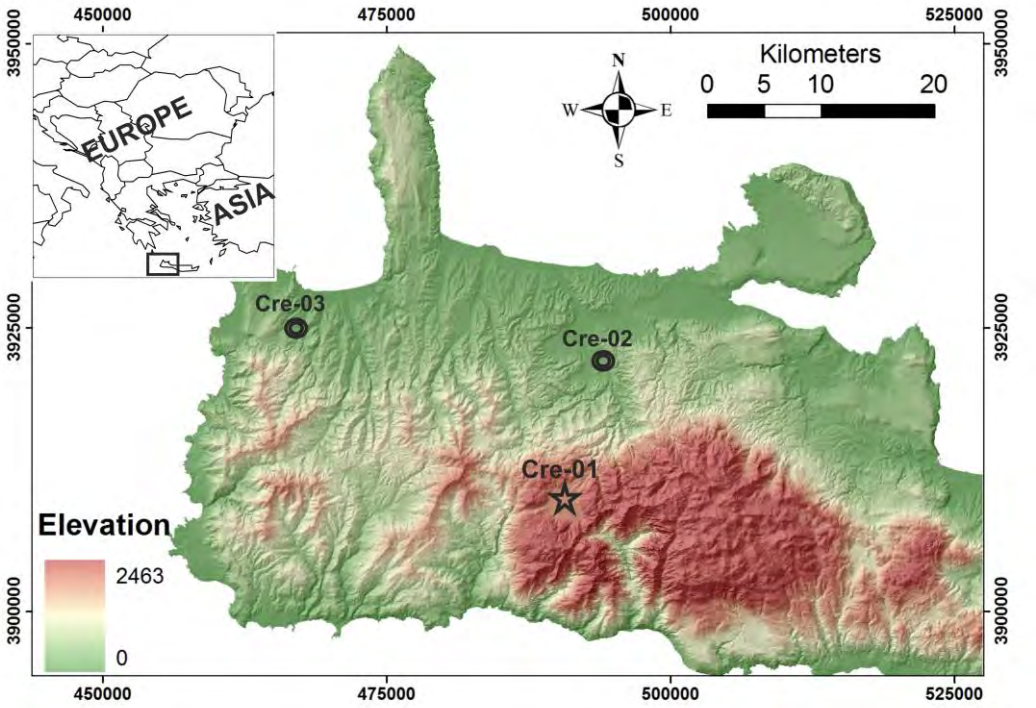

Figure 2 - Star indicates the Magnetotelluric (MT) monitoring station in Omalos (Cre-01). Circles indicate two MT surveys which took place in Fournes (Cre-02) and Kastelli (Cre-03). The Remote Reference (RR) technique was applied in order to improve MT data quality of Cre-02 and Cre-03 by using Cre-01 as RR.

2. The Permanent MT Station at Omalos

Laboratory of Geophysics and Seismology of TEI of Crete owns two complete systems to conduct magnetotelluric surveys. Each MT system comprises a MT24LF Magnetotelluric 24-bit Low Frequency receiver (developed by EMI Technology Centre owned now by Schlumberger SpA) that uses a power-efficient CPU and dual high- and low-speed 24-bit A/D acquisition, external GPS combined with a high-accuracy internal oscillator for time synchronization, three high sensitivity, very low noise Magnetic Field Induction Sensors in the range 10,000s – 1kHz and Pb-PbCl2 non-polarized electrodes with 100m cables. The MT system uses a CompactFlash memory card for data storage.

MT24LF is portable MT equipment that records orthogonal electric and magnetic fields which are processed to provide tensor impedance measurements for interpreting complex 2D and 3D subsurface geoelectric structures. Once sensor and hardware setup and installation in the field is completed, the MT acquisition phase is set up, controlled and stopped by software running on a PC that is connected to MT24LF receiver.

The location of the appropriate reference site was a complicated task, as the landscape of Western Crete has bold relief. Finally, data quality of 11 sites across western Crete was tested. Every MT system was left recording at every site for about 3 nights with sampling rate 6.25Hz in continuous mode and bursts of 500Hz every 12 hours for 30 minutes. Omalos site was selected as the best area, far away from current sources, pipelines or metallic fences. High quality data were found and the new permanent monitoring MT station was installed there. However, in the future annually snowfalls maybe disqualify the site during winter period.

Here, we present the transformation of the above portable, in-situ configured and controlled MT system, to a permanent MT-station featuring continuous unmanned operation with long-time autonomy, full remote control and telemetry.

The developed permanent MT-station comprises of the following basic units (Figure 3):

- Solar Panel 12V/95W combined with a battery of 60AH for energy storage.
- 3G Router for wireless internet access through mobile network
- Low Power Field Computer (netbook type)
- MT24LF receiver with sensors
- System Controller based on MSP430F5438A Microcontroller

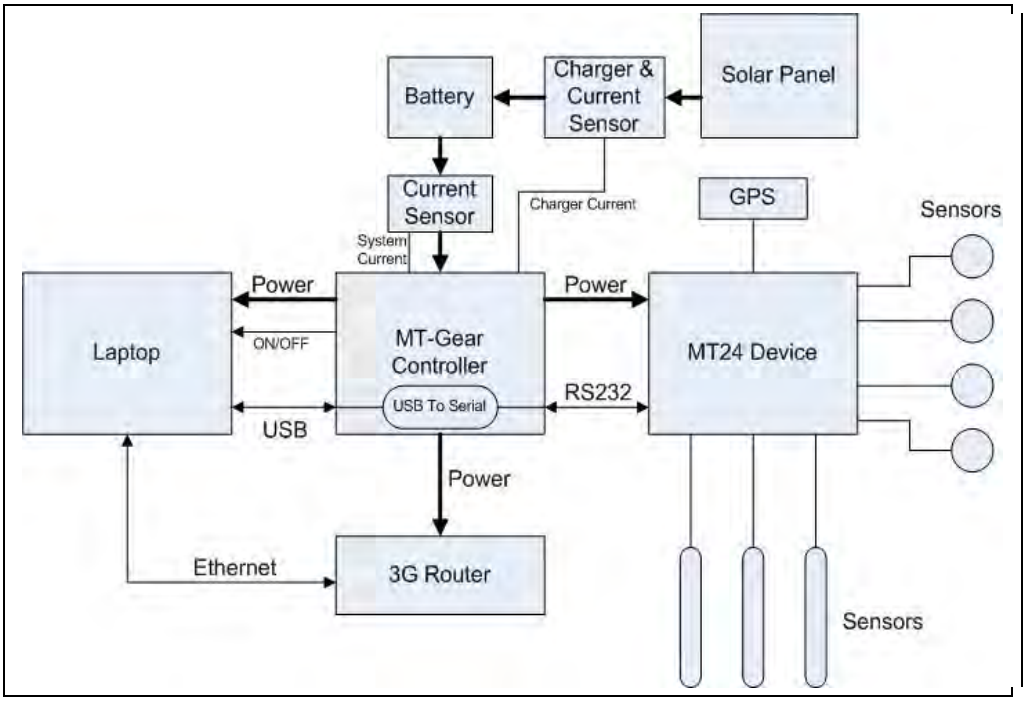

Figure 3 – Block diagram depicting the basic units and modules of the developed permanent MT-station, incorporating advanced remote control technology and telemetry.

A fundamental as well as crucial point to deal with, in the direction to develop a permanent station in the field, is uninterruptible power. As Crete is characterized by a great average of daily sunny hours (8.67) and more than 300 days of sunshine per year, renewable energy, namely solar energy, was the straightforward selection for providing station with energy autonomy. The solar panel is suitably selected in the sense that in a sunny day close to the aforementioned average is capable to fully charge the battery which in turn is able to power the whole MT-station for about 10 days without any sunshine.

The System Controller stands for the "remote master control" of the MT-station. It checks all the units of the station and provides the variety of the necessary constant and stable power voltages: +12 Volts for the 3G Router, +19 Volts for the Field Computer, ±12 Volts and +6 Volts (with low noise and galvanic isolation) for the MT24LF receiver. Furthermore, the System Controller is equipped with a GSM module in order to accept remote commands from a distant user. In addition, it incorporates a converter USB to Serial (galvanically isolated) enabling transparent serial communication and data transfer between the Field Computer and the MT24LF receiver.

Finally, the System Controller checks and records all the vital parameters and status of the permanent MT-station, i.e., charge current, system current, battery voltage, laptop status, MT24LF Status, 3G router status and all this information is available to distant user through GSM.

The Field Computer hosts the software for the setup MT24LF system, the start and stop of the acquisition and the retrieval of the collected MT-data. Of course it is remotely controlled by means of the 3G Router using either remote desktop or Teamviewer applications. The Field Computer is normally in shutdown state and it is activated, when remote access to it, is requested. The operation of the developed permanent MT-station has two distinct modes:

- The mode where only the MT24LF system is working as a regular standalone magnetotelluric measuring equipment. The MT-data are continuously recorded to its internal memory (Compact Flash). In this mode the power consumption is to the minimum and all communication is idle.
- The mode where all system units are on. In this mode, there is availability for the distinct user to access remotely the Field Computer. In this mode, with software we developed it is possible to directly and remotely give commands to MT24LF and download the collected MT-data to the base (the premises of TEI of Crete at Chania).

In order for the permanent MT-station to exchange mode of operation, it needs to be called (through the GSM module in the System Controller) by the distinct user and then the appropriate instruction (DTMF code) has to be keyed. The distinct user is able to use either fixed or mobile phone.

3. Results

3.1. MT Data Analysis and Processing

In this study three data sets of apparent resistivity were analyzed, from Cre-01, Cre-02 and Cre-03 sites. The frequency of data recording was set to 6.25Hz in continuous mode. The apparent resistivity curves ρxy and ρyx, related respectively to the off-diagonal components of impedance tensor Zxy and Zyx, were estimated using the procedure and the Robust Transfer Function Estimation Program for data reduction described in Egbert, 1997.

Two different MT processing methods were applied to the MT data: the robust Single Site processing method (*zss*) and the Remote Reference (*zrr*, Gamble *et al.*, 1979; Egbert and Booker 1986) processing method. Figure 4 shows the apparent resistivity curves estimate for the Cre-01, Cre-02 and Cre-03 sites with the two above-mentioned methods. In *zrr* estimates, we use the magnetic field recorded at Cre-01, i.e. Omalos site, as a reference field. Single Station processing seems to generally give better results than the RR one. As expected, RR method works well for long period where, especially for *xy* component, the two methodologies provide quite similar results (past 10s the three curves in fig. 6a are fairly coincident). For Cre-02, a visual inspection of the time series, highlighted a strong presence of noise affecting mainly the electric field. The noise presence can be a possible explanation for the low quality of the results both with the SS and RR processing especially in period range 1-10s, the «dead band», where signal to noise ratio is generally low.

3.2. Magnetotelluric Monitoring of Geodynamic Processes at Omalos Area

MT data from Omalos monitoring MT station (Cre-01) have not used yet for the investigation of the existence of temporal anomalous patterns in the geoelectrical structure and in that case, their correlation with the simultaneously observed seismic activity. In the frame of MT-GEAR project it will be attempted the correlation of any apparent resistivity fluctuations with local seismicity and regional strong events that may occur.

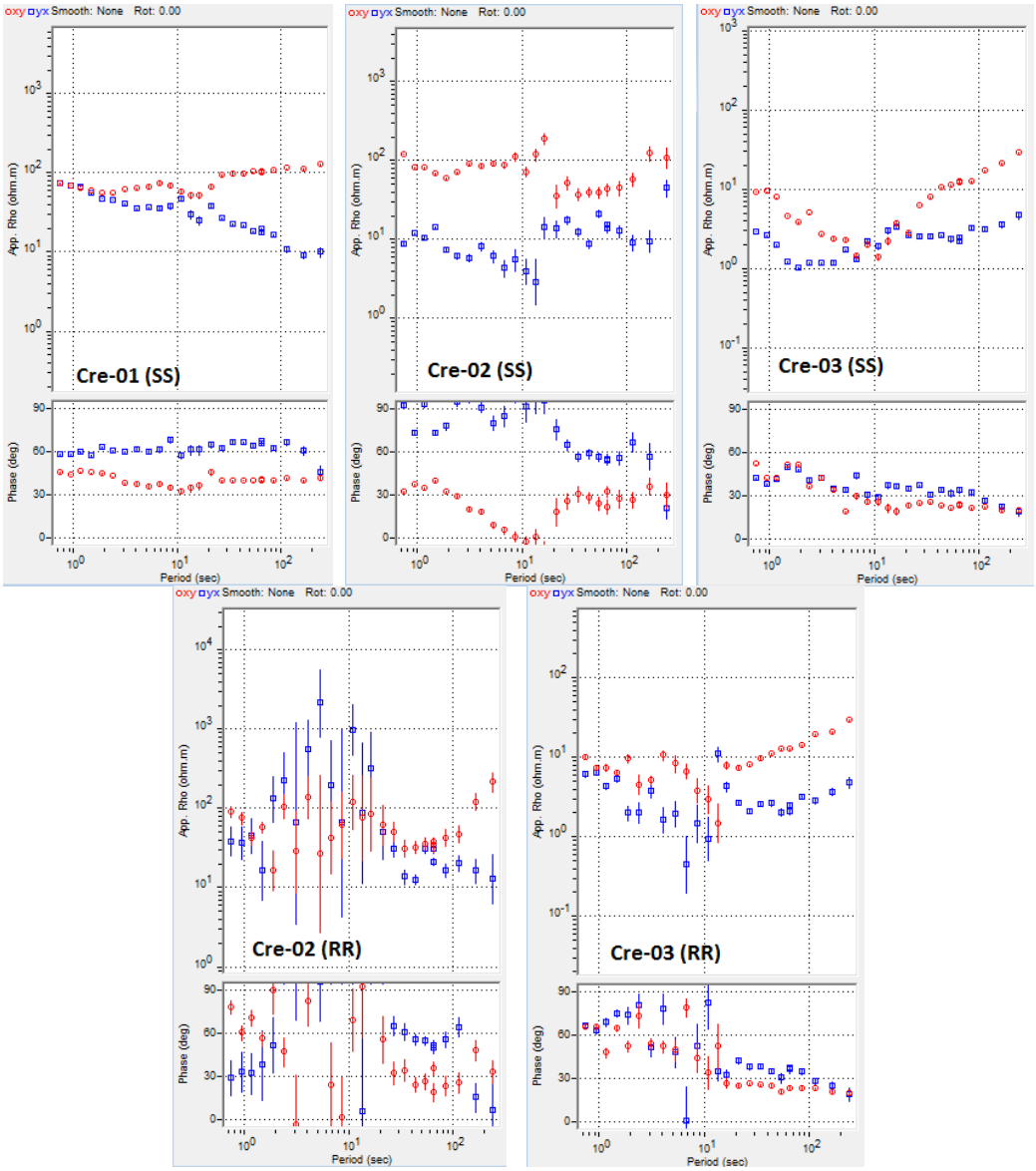

Figure 4 - Above they are shown the resistivity curves ρxy and ρyx and phases of Cre-01, Cre-02 and Cre-03 sites after using the robust Single Site processing method (*zss*). Below they are shown the results of referencing data from Cre-02 and Cre-03 to the permanent referencing site Cre-01.

4. Conclusions

Since early 2013 a new, continuous MT-monitoring station (Cre-01) has been installed by Laboratory of Applied Geophysics and Seismology of TEI of Crete at Omalos Plateau, Western Crete, Greece, in the frame of MT-GEAR project. New technology was developed for the remote control and the telemetry and the data transfer can be efficiently performed through a 3G Router using remote desktop applications. Cre-01 site was used as reference for MT measurements in western Crete (Cre-02 and Cre-03 sites). However, robust Single Site processing method (*zss*) furnished better results. RR processing seems to suffer much more than the SS when the local data are noisy (as the case of Cre-02). Future analysis will take this into account in order to increase

estimates reliability. High quality reference data are being continuously recorded since early 2013, improving MT data quality from campaigns across southern Aegean. Future task is the correlation of any apparent resistivity fluctuations with local seismicity.

5. Acknowledgments

The project is co-funded by the European Union and the Greek State in the framework of the action 'Support of Postdoctoral Researchers', which falls under the Fourth Strategic Objective of the Operational Programme (OP) 'Education and Lifelong Learning (EdLL)'.

6. References

Angelier J. 1976. Sur la neotectonique de l'arc egeen externe: les failles normales Est-Quest et l' extension submeridienne cretoise, *C.R. Acad. Sci. Paris,* (D), 282, 413-416. (in French).

Angelier J., Dumont J.F., Karamanderesi H., Poisson A., Simsek S. and Uysal S. 1981. Analyses of fault mechanisms and expansion of southwestern Anatolia since the Late Miocene, *Tectonophysics*, 75, T1-T9.

Aubouin J. and Dercourt J. 1965. Sur la geologie de l' Egee: regard sur la Crete (Greece), *Bull. Soc. Geol. France*, (7), t. VII, 787-821. (in French).

Aubouin J. 1971. Reflexion sur la tectonique de faille plio-quaternaire, *Geol. Rdsch.,* 60, 833-848. (in French).

Balasco M., Colangelo G., Lapenna V., Loddo M., Siniscalchi A. and Telesca L. 2004. Measuring apparent resistivity in a seismically active area of southern Italy, *Phys. Chem. Earth*, 29: 329-337.

Balasco M., Lapenna V., Romano G., Siniscalchi A. and Telesca L. 2008. A new magnetotelluric monitoring network operating in Agri Valley (Southern Italy): study of stability of apparent resistivity estimates, *Annals of Geophysics*, Vol.51, N.1: 265-273

Bohnhoff M., Makris J., Papanikolaou D. and Stavrakakis G. 2001. Crustal investigation of the Hellenic subduction zone using wide aperture seismic data, *Tectonophysics*, 343, 239-62.

Cagniard L.1953. Basic theory of the magnetotelluric method of geophysical prospecting, *Geophysics,* 18, 605-645

Egbert G.D. and Booker J.R. 1986. Robust estimation of geomagnetic transfer functions, *Geophys. J. R. Astron. Soc.*, 87, 173-194.

Egbert G.D. 1997. Robust multiple-station magnetotelluric data processing, *Geophys J. Int*., 130, 475-496.

Eydam D. and Munoz G. 2011. The Permanent Magnetotelluric Remote Reference Station, Schmucker-Weidelt-Kolloquium, Neustadt an der Weinstraße, 19.–23. September 2011

Gamble T.D., Goubaou W.M. and Clarke J. 1979. Magnetotellurics with a remote reference, *Geophysics*, 44, 53-68.

Hayakawa M. (Ed). 1999. Atmospheric and Ionospheric Electromagnetic Phenomena Associated with Earthquakes, *Terra Sci. Pub. Co*., Tokyo

Huang Q. and Liu T.2006. Earthquakes and tide response of geoelectric potential field at the Niijima station, *Chinese J. Geophys.,* 49: 1745-1754.

Jackson J. 1994. Active tectonics of the Aegean region, *Ann. Rev. Earth Planet. Sci*., 22, 239-271.

Johnston M.J.S.1997. Review of electric and magnetic fields accompanying seismic and volcanic activity, *Survey in Geophysics*, 18: 441-475.

Kaufman A. and Keller G.V.1981. The magnetotelluric sounding method, *Methods Geochem. Geophys.,* 15, pp. 583.

Le Pichon X. and Angelier J. 1979. The hellenic arc and trench system: a key to the neotectonic evolution of the Eastern Mediterranean area. *Tectonophysics,* 60:1-42.

Makris J., Röwer P.1986. Struktur und heutige Dynamik der Lithosphäre in der Ägäis. In: Jakobshagen, V. (Ed.), *Geologie von Griechenland*, Gebrüder Bornträger, Berlin, 241-256. (in German).

Mascle J. and Martin L. 1990. Shallow structure and recent evolution of the Aegean Sea: a synthesis based on continuous reflection profiles, *Mar. Geol.,* 94, 271-299.

McKenzie D.P. 1970. Plate tectonics of the Mediterranean region. Nature, 226, 239-243.

McKenzie D.P. 1978. Active tectonics of the Alpine-Himalayan Belt: the Aegean sea and the surrounding regions, *Geophys. J. R. Astron. Soc.* 55: 217-254.

Merzer M. and Klemplerer S.L. 1997. Modeling lowfrequency magnetic-field precursors to the Loma Prieta earthquake with a precursory increase in fault-zone conductivity, *Pure Appl. Geophys*., 150, 217-248.

Molnar P. and Tapponier P.1975. Cenozoic tectonics of Asia: effects of a continental collision, Science, 189, 419.

Nagao T., Enomoto Y., Fujinawa Y., Hata M., Hayakawa M., Huang Q., Izutsu J., Kushida Y., Maeda K., Oike K., Uyeda S. and Yoshino T. 2002. Electromagnetic anomalies associated with 1995 Kobe earthquake, *J. Geodyn*., 33, 401-411.

Nikolintaga I., Karakostas V., Papadimitriou E. and Vallianatos F. 2008. The 2006 Kythira (Greece), Mw6.7 Slab-pull event: Tectonic implication and the geometry of the Hellenic Wadati-Benioff zone, *Annals of Geophysics*, Vol.51, No.5-6, 823-837

Noomen R., Loohuis J. and Kampes B. 1999. Deformations in the Mediterranean area observed by space geodesy. *Geophys. Res. Abstracts 1.,* in: *Proceedings of the 24th General Assembly of the European Geophysical Soc.*, The Haague, Netherlands.

Papazachos C.B., Hatzidimitriou P.M., Panagiotopoulos D.G. and Tsokas G.N. 1995. Tomography of the crust and upper mantle in southeast Europe, *J. Geophys. Res*. 100 (B7), 12405-12422).

Peters J.M. 1985. Neogene and Quaternary vertical tectonics in the south Hellenic Arc and their effection on the concurrent sedimentation processes, *Gua paper of Geology, Amsterdam,* Series 1, No 23, 230.

Pirazzoli P., Laborel J., and Stiros S. 1996. Earthquake clustering in the Eastern Mediterranean during historical times, *Journal of Geophysical Research*, Vol. 101: 6083-6097

Seidel M. 2003. Tectono-sedimentary evolution of middle Miocene supra-detachment basins (Western Crete, Greece), *Ph.D. Thesis,* Universität zu Köln.

Simpson F. and Bahr K. 2005. *Practical Magnetotellurics*, Cambridge University Press.

Snopek K., Meier T., Endrun B., Bohnhoff M. and Casten U. 2007. Comparison of gravimetric and seismic constraints on the structure of the Aegean lithosphere in the forearc of the Hellenic subduction zone around Crete, *Journal of Geodynamics,* 44, 173-185

Spakman W., Wortel M.J.R. and Vlaar N.J.1988. The Hellenic subduction zone: a tomographic image and its geodynamic implications, *Geophys. Res. Lett*., 15, 60-63.

Stiros S. 2001. The AD 365 Crete Earthquake and Possible Seismic Clustering During the Fourth to Sixth Centuries AD in the Eastern Mediterranean: A Review of Historical and Archaeological Data, *Journal of Structural Geology*, 23, 545-562.

Svetov B.S., Kuksa Y.I. and Odintsov V.I.1997. Magnetotelluric monitoring of geodynamical processes, *Anali di Geofisica*, vol.XL.

Tikhonov A. N. 1950. The determination of the electrical properties of deep layers of the Earth's crust, *Kokl. Acad. Nauk. SSR.,* 73, 295-297.

Tzanis A. and Vallianatos F. 2002. A physical model of electrical earthquake precursors due to crack propagation and the motion of charged edge dislocations." (monograph) "Seismo Electromagnetics (Lithosphere-Atmosphere-Ionosphere Coupling)" by TERRAPUB

Vallianatos F. and Makris J. 2000. On the tectonoelectric zonation in the Hellenic Arc, *Physics and Chemistry of the Earth,* 25/3, 307-313.

Zlotnicki J., Le Mouel J.L., Kanwar R., Yvetot P., Vargemezis G., Menny P. and Fauquet F. 2006. Ground-based electromagnetic studies combined with remote sensing based on Demeter mission: A way to monitor active faults and volcanoes, *Planetary and Space Science*, 54/5: 541-557, April 2006.

Δελτίο της Ελληνικής Γεωλογικής Εταιρίας, τομ. XLVII , 2013
Πρακτικά 13ου Διεθνούς Συνεδρίου, Χανιά, Σεπτ. 2013

Bulletin of the Geological Society of Greece, vol. XLVII 2013
Proceedings of the 13th International Congress, Chania, Sept. 2013

THRUST TECTONICS IN THE CENTRAL PART OF THE EXTERNAL HELLENIDES, THE CASE OF THE GAVROVO THRUST

Kamberis E.[1], Sotiropoulos S.[1], Marnelis F.[1] and Rigakis N.[1]

[1]Hellenic Petroleum S.A. Exploration and Production of Hydrocarbons, 8[A], Chimaras Str., 15125, Maroussi, Athens, ekamperis@hotmail.gr, ssotiropoulos@helpe.gr, fedmarn@yahoo.gr, nrigakis @helpe.gr

Abstract

Thrust faulting plays an important role in the structural deformation of Gavrovo and Ionian zones in the central part of the 'External Hellenides' fold-and-thrust belt. The Skolis mountain in NW Peloponnese as well as the Varassova and Klokova mountains in Etoloakarnania are representative cases of ramp anticlines associated with the Gavrovo thrust.

Surface geology, stratigraphic data and interpretation of seismic profiles indicate that it is a crustal-scale thrust acted throughout the Oligocene time. It is characterized by a ramp-flat geometry and significant displacement (greater than 10 km). Out of sequence thrust segmentation is inferred in south Etoloakarnania area.

Down flexure and extensional faulting in the Ionian zone facilitated the thrust propagation to the west. The thrust emplacement triggered halokenetic movement of the Triassic evaporites in the Ionian zone as well as diapirisms that were developed in a later stage in the vicinity of the Skolis mountain.

Key words: *thrusting, thrust propagation, normal faulting.*

Περίληψη

Οι επωθήσεις διαδραματίζουν σημαντικό ρόλο στην παραμόρφωση των ζωνών Ιονίου και Γαβρόβου σε ότι αφορά το κεντρικό τμήμα της ζώνης πτυχών και επωθήσεων των Εξωτερικών Ελληνίδων. Το όρος Σκόλις της ΒΔ Πελοποννήσου καθώς και τα όρη Βαράσοβα και Κλόκοβα της Αιτωλοακαρνανίας αποτελούν αντιπροσωπευτικά δείγματα αντικλίνων τα οποία συνδέονται με την επώθηση της ζώνης Γαβρόβου.

Τα γεωλογικά και στρωματογραφικά δεδομένα καθώς και η ερμηνεία των σεισμικών προφίλ δείχνουν ότι πρόκειται για μία επώθηση σε κλίμακα λιθόσφαιρας η οποία έλαβε χώρα κατά τη διάρκεια του Ολιγόκαινου. Χαρακτηρίζεται δε από γεωμετρία επικλινούς - οριζόντιου επιπέδου (ramp - flat geometry) και από σημαντική μετατόπιση, μεγαλύτερη των 10 Km. Η εκτός ακολουθίας τμηματοποίηση της επώθησης τεκμηριώνεται στην περιοχή της νότιας Αιτωλοακαρνανίας.

Η κάμψη της λιθόσφαιρας και τα ρήγματα εφελκυσμού στην περιοχή της προχώρας (ζώνη της Ιονίου), διευκόλυναν την προελαύνουσα επώθηση προς τα δυτικά.

Η τοποθέτηση της ζώνης Γαβρόβου ενέτεινε κινήσεις εβαποριτών του Τριαδικού στην ζώνη της Ιονίου όπως επίσης και διαπειρισμούς οι οποίοι αναπτύχθηκαν σε μεταγενέστερο στάδιο στη γειτνίαση του όρους Σκόλις.

Λέξεις κλειδιά: *επωθήσεις, προελαύνουσα επώθηση, ρήγματα εφελκυσμού.*

1. Introduction

Structural and stratigraphic studies carried out in the External Hellenides in the last three decades support a model of foreland propagating thrust faults (Fleury, 1980; Brooks et al., 1988). The previous Mesozoic 'isopic' zones (Aubouin, 1959) were inverted during Tertiary, forming major thrust sheets carrying rocks from east to west onto the relatively autochton Pre-Apulian zone.

This paper focuses to Gavrovo thrust (GT) that is exposed in the central part of External Hellenides, in particular in NW Peloponnese and SW Etoloakarnania regions (Figure 1a). Surface structural and biostratigraphic data as well as subsurface data based on interpretation of seismic profiles reveal information about the geometry and the evolution of GT.

2. Tectonic Setting

In early Mesozoic times, Western Greece was part of the Apulian passive continental margin. A Triassic - early Jurassic rifting stage differentiated the Apulian margin, resulting into the formation of a series of deep basins and platforms. The collision between the Apulian and Eurasia plates in late Cretaceous and the final closure of the Neo-Tethys had as a consequence the intra-continental deformation propagating towards Apulian throughout Tertiary (Dewey et al., 1973). The end result was the 'External Hellenides' fold-and-thrust belt (FTB) representing a pile of NW-SE striking nappes separated by major foreland propagated thrust faults that become progressively younger westwards (Figure 1a). During this orogenic process, initially the Pindos zone was detached from its basement in the Late Eocene and it thrust over the flysch of the Gavrovo zone. During Oligocene, the Gavrovo zone was also involved in the ongoing deformation in the study area and it thrust over the flysch of the Ionian zone at the end of this time period.

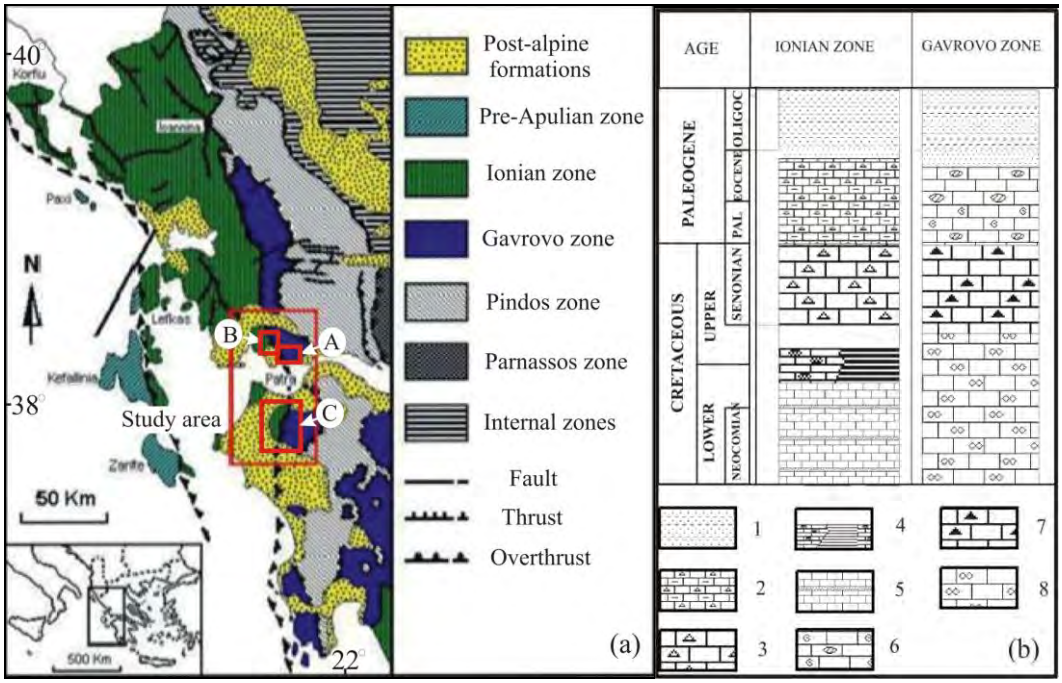

Figure 1 – (a): Location map of the study area in the central part of External Hellenides. A, B and C are locations of geological maps that will be presented in Figures 2, 4 and 5. (b): Stratigraphic columns of the Ionian and Gavrovo zones in Western Greece (1: flysch, 2: limestones-cherts with clastics, 3: pelagic limestones with clastics, 4: pelagic limestones-cherts-shales, 5: pelagic limestones-cherts, 6: platform carbonates with clastics, 7: reefal-bioclastic carbonates, 8: platform carbonates (Rigakis, 1999, partly modified).

The Ionian thrust emplacement on the pre-Apulian zone, which is considered as the slope of the Apulian platform, took place in the early Pliocene. Active compression is affecting the more external part of the FTB since Pliocene, whereas at the same time extension predominates backwards (Underhill, 1989; Doutsos & Kokkalas, 2001). Nowadays, Kefallinia transform fault delineates the structural boundary of two regions; the northern one, where collision occurs between Apulian plate and Eurasian continent, and the southern one, where an active subduction of the Ionian oceanic crust takes place beneath the Hellenic FTB (Underhill, 1989).

3. Geological Setting and Field Data

The study area is located in the south Etoloakarnania and northwest Peloponnese and it belongs to the Ionian and Gavrovo zones (Figure 1a). Thick turbiditic fan facies outcrop widely covering the carbonate sequences of above zones (IFP, 1966; BP, 1971; Fleury, 1980; Sotiropoulos et al., 2003; 2008; Kamberis et al., 2005). The upper part of the Gavrovo carbonate sequence comprises Upper Cretaceous to Eocene shallow marine carbonates (Figure 1b). They are exposed in Varassova and Klokova mountains in south Etoloakarnania as well as in Skolis mountain in northwest Peloponnese (Fleury, 1980). Eocene to earliest Oligocene transitional beds overlie conformably the carbonate series on Klokova and Skolis mountains marking the onset of the turbidites deposition in the study area (Fleury, 1980; Kamberis et al., 2000; Sotiropoulos et al., 2003).

The widespread occurrence of turbidites suggests the existence of a foreland basin that has been formed due to the westward propagation of Pindos thrust (Clews, 1989). In addition, its internal differentiation is associated with the Pindos and the GT evolution (Kamberis et al., 2000; 2005; Sotiropoulos et al., 2003). The turbidites deposition ceased in Late Oligocene revealing the age of the emplacement of GT (Kamberis et al., 2000; Sotiropoulos et al., 2003). The foreland basin was characterised by a low subsidence rate in the first stage of its evolution during late Eocene – earliest Oligocene, whereas during early Oligocene it was characterised by maximum width and high sedimentation rates. Distal fan facies were deposited in the Ionian part of the foreland basin, while more proximal facies were deposited in the same time in the Gavrovo part of the foreland basin (Sotiropoulos et al., 2003; Kamberis et al., 2005). At the end of the early Oligocene and the beginning of Late Oligocene the facies become more proximal throughout the foreland basin and this fact is associated with the westward propagation of Pindos thrust as well as with the intensive thrust fault activity in the Gavrovo zone (Kamberis et al., 2000; Sotiropoulos et al., 2003; 2008). This fault activity resulted to the successive repetitions and the overall structural thickening of the flysch sequence.

3.1 SW Etoloakarnania Area

The boundary between Ionian and Gavrovo zones is structural and it is located on the western flanks of Varassova mountain. Some authors consider that GT represents an inverse fault (Aubouin, 1959; IFP, 1966; BP, 1971), while others support that is a major thrust, accompanied with great displacement (Fleury, 1980, Kamberis et al. 2000, Sotiropoulos et al., 2003). In this position, Cretaceous limestones thrust over flysch sediments of Ionian zone (Figure 2). A west-verging narrow asymmetric anticline plunging to the north lies on the hangingwall of the GT. Its short forelimb is characterized by subvertical strata while the backlimb by east to northeast dipping strata (Figure 2). The flysch on the footwall block is intensively deformed by imbricates and tight folding in particular at the northwestern slopes of Varassova mountain (Sotiropoulos et al., 2003, Figure 2).

A second NW trending and eastward dipping thrust fault occurs at the southern part of Varassova mountain. Moreover, NNW-SSE trending normal faults dipping to the east downthrown the carbonates at the eastern flank of Varassova mountain; the latter faults could initially act as thrust faults and then as gravitational faults due to tilting of the hanging wall strata (Figure 2).

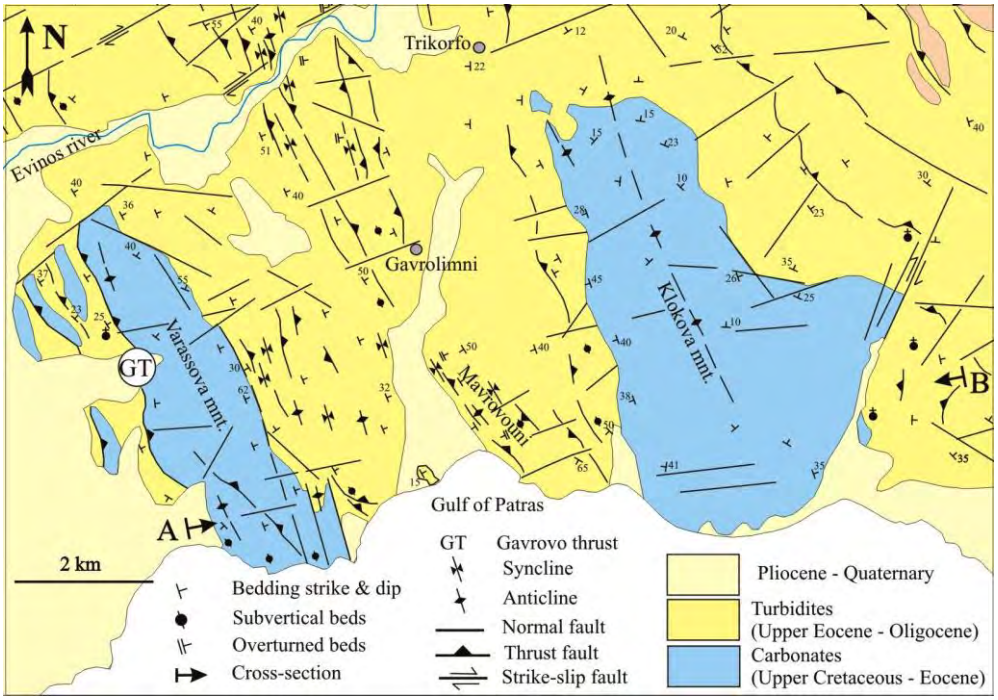

Figure 2 – Geological map of the Klokova – Varassova area. Location A in Figure 1a (Sotiropoulos, 2005).

A narrow elongated area occupied by hills (i.e. Mavrovouni hill), is located between Varassova and Klokova mountains). It represents a pop-up structure bounding to the west and to the east by thrust faults (Figures 2 & 3, Sotiropoulos et al., 2003). Heading eastwards, close to the western flank of Klokova mountain, another thrust fault was identified. It is a NNW-SSE trending and east-dipping thrust fault that runs parallel to the axis of Klokova anticline. Its northern prolongation reaches up to the Evinos river (Sotiropoulos 2005, Figure 2).

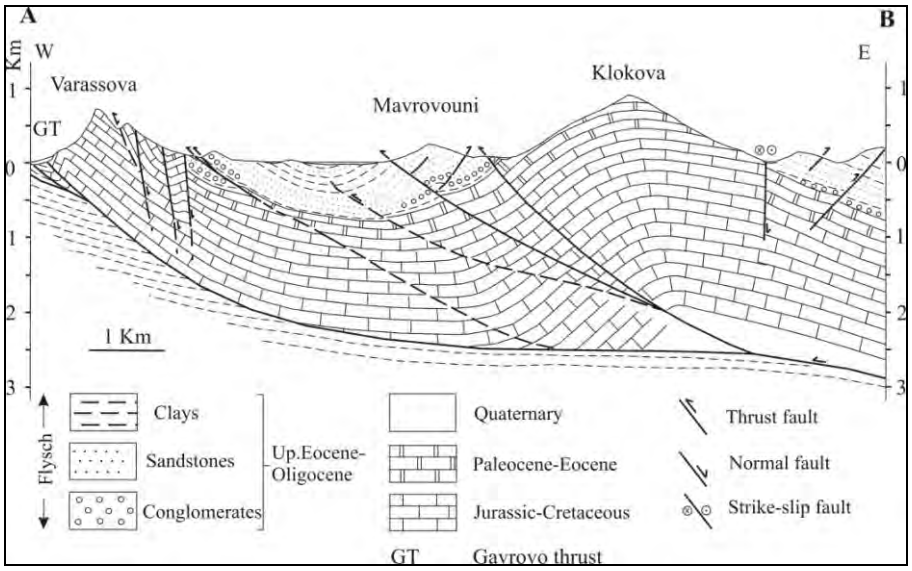

Figure 3 – Geological cross-section. Its position is shown in Figure 2 (Sotiropoulos et al., 2003).

A broad west-verging anticline plunging to the north lies at the Klokova mountain. It is asymmetric in shape with a steep forelimb and a gently dipping to the east backlimb, while its axial part is generally sub-horizontal (BP, 1971). Minor west-dipping backthrusts have been identified southeast of Klokova mountain as well as a NE-SW trending dextral strike-slip fault bring in structural contact carbonates with flysch (Figures 2 & 3). Taking into consideration the above distribution of dips on Varassova and Klokova anticlines, it is suggested that the above folds represent hangingwall anticlines closely associated with the geometry of GT (Sotiropoulos et al., 2003, Figure 3).

In an effort to track the northern prolongation of the GT, Two major elongated west verging and eastward dipping thrust fault zones have been identified northwest of Varassova mountain (Figure 4). The western fault zone runs for at least 11 km on the western flank of Arakynthos mountain reaching a width of 1.7 km at its central part (Sotiropoulos 2005, Figure 4). Most of the thrust faults strike NNW-SSE and gently dip to the east, almost parallel to the beds stratification. The younger sediments on the footwall of imbricates are of intra-Oligocene age (Sotiropoulos et al., 2003). Minor back-thrusting is observed on the eastern flank of Arakynthos mountain. The eastern thrust fault zone is an elongated one, running for at least 15 km north of the Evinos river and separating two distinct areas. The eastern one which is mountainous including a series of rises such as Makryvouni, Kokkaliara, Froxilia composed mainly of coarse facies of flysch. It represents the hangingwall block where there are several NW-SE striking thrust faults gently dipping to the east. The thrust activity induced the intense deformation of the hanging wall strata and the widespread thrust fault related folding (Sotiropoulos 2005, Figure 4). The western one, which is an area of low relief, is dominated by fine-grained turbitides representing the footwall block. An east-verging asymmetric syncline occurs, with a long forelimb gently dipping to the east and a short steep backlimb; the strata locally are overturned especially close to the thrust front (Figure 4). The overall structural pattern suggests that the above thrust fault zone reflects the prolongation of the GT to the north (Sotiropoulos et al. 2003, Sotiropoulos, 2005).

It is worth mentioning that the turbidites occupied the footwall of the GT are the youngest found flysch sediments in the entire study area, in particular dating from 27.2 to 23.2 MA (latest Oligocene age), predating the age of the GT emplacement (Sotiropoulos et al., 2003, 2008). Furthermore, the Pindos thrust emplacement has been dated to be of Late Oligocene age (Fleury, 1980, Sotiropoulos et al., 2003, 2008). Taking into consideration all of the above, it is suggested that Pindos and GT acted simultaneously during the Oligocene (Sotiropoulos et al., 2003; 2008).

3.2 NW Peloponnese

Skolis mountain is the most prominent topographic feature in northwest Peloponnese representing an elongated (9 km long) and narrow (1.5 km wide) structure (Figure 5). It reaches 1000 m. of altitude superimposed on a flysch low topographic relief. The GT is situated on the western flanks of Skolis mountain, trending N-S, parallel to the mountain axis (Fleury, 1980; Kamberis et al, 2000).

In this position, Cretaceous limestones thrust over Oligocene flysch (Fleury, 1980). The thrust fault is steeply dipping to the east. Several minor synthetic thrust faults as well as minor backthrusts are identified on the hangingwall of GT. The flysch on the footwall is steeply dipping to the east and it is intensively deformed close to the thrust fault stated by tight to kink folding (Kamberis et al., 2000). Imbrication is mapped on the north-western slopes of Skolis mountain induced the repetition of the carbonate series (Figure 5). The above faults are considered to be splays rooting on the main thrust fault (Kamberis et al, 2000). Concerning the age of the GT emplacement in the study area, a late Oligocene age is inferred by the age determinations of the younger flysch members that outcrop west of Skolis mountain (Kamberis et al., 2000; 2005).

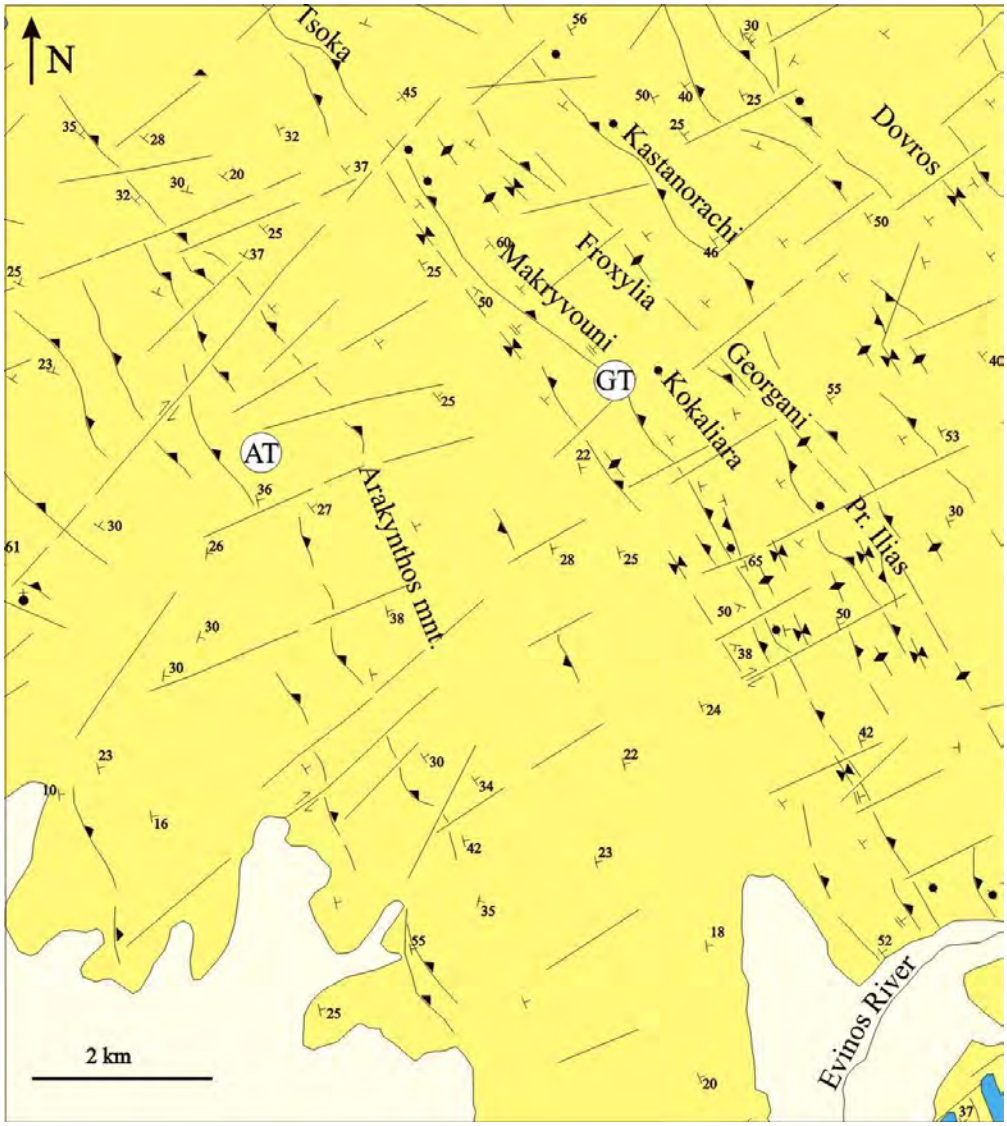

Figure 4 – Geological map of the area NW of Varassova mountain. Location B in Figure 1a. AT: Arakynthos thrust, GT: Gavrovo thrust (Sotiropoulos, 2005).

The Skolis anticline is asymmetric in shape, clearly related to the GT, (Kamberis et al., 2000). In the northern part of Skolis mountain, it represents a periclinal fold, plunging to the north, formed ahead of an advancing thrust fault. The short forelimb is dipping to the west and the long backlimb is gently dipping to the east. In the latter one, flysch overlie conformably on the Eocene carbonates. On the contrary, in the southern part of Skolis mountain, the anticline is more narrow and the carbonate strata in the backlimb are steeply dipping to the east suggesting a stronger influence of thrusting. Furthermore, on the south-eastern slopes, the carbonates are in structural contact with flysch which is gently dipping to the west (Figure 5). The contact corresponds to a major subvertical fault that in a later stage probable acted as gravitational fault, as consequence of the rotation of the hanging wall strata (Kamberis et al., 2000). It is mentioned that similar faults exist also in the eastern flank of the Varassova mountain as described before. Several E-W to WNW-ESE trending subvertical normal faults cut the earlier formed contraction structures and generally the northern ones dip to the north, while the southern ones dip to the south.

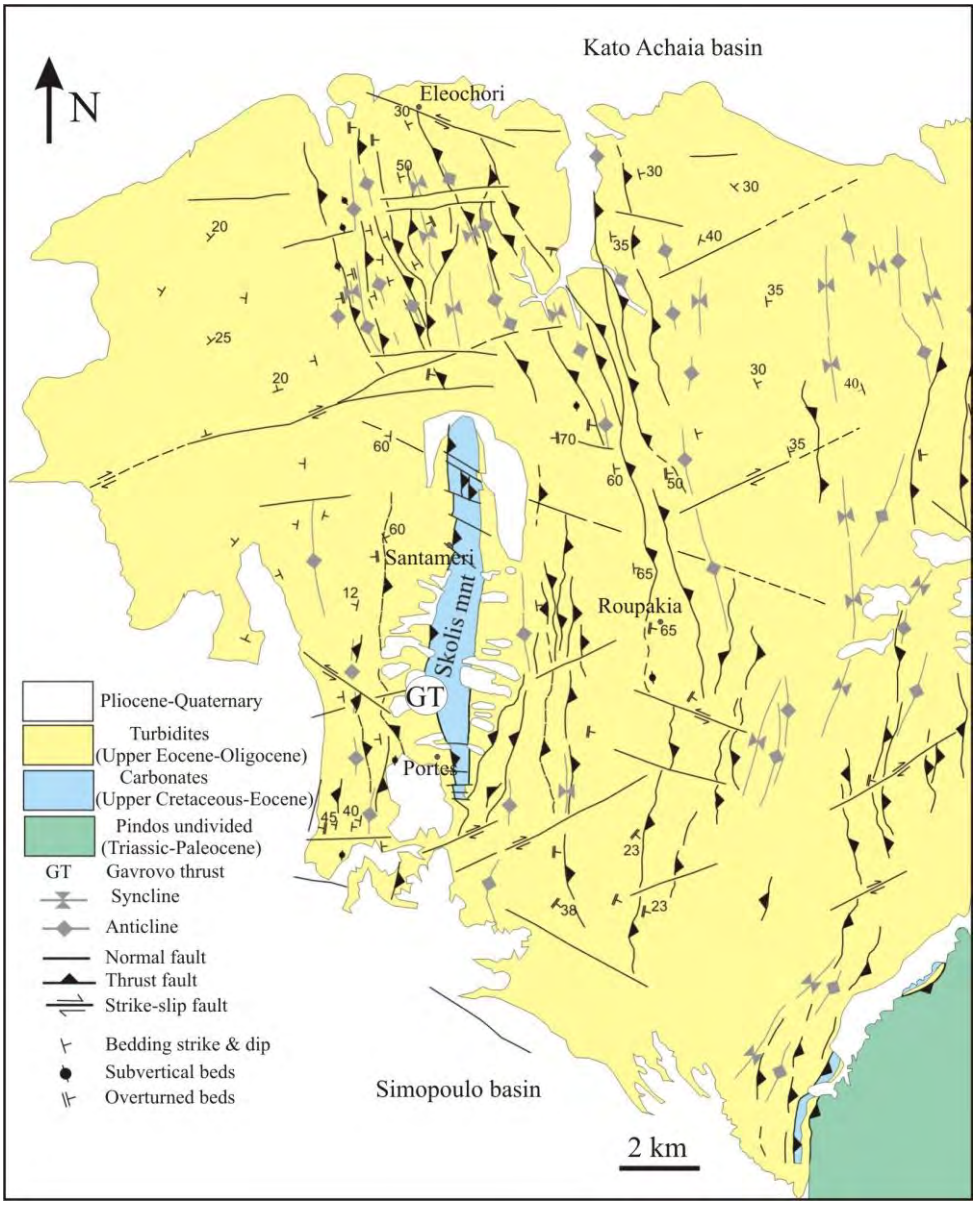

Figure 5 – Geological map of the Skolis area. Location C in Figure 1a (Kamberis et al., 2000, 2005).

An ENE-WSW trending strike-slip fault with a right-lateral sense of movement is situated north of Skolis structure, bounding the latter from a mountainous area located north of this fault (Figure 5). It consists of a series of elongated NNW-SSE to N-S trending rises with a mean altitude of 550 m. Its structural pattern is mainly controlled by a series of close-spaced west verging thrust faults (Figure 5). Thrust fault related folds do coexist, while E-W trending normal faults cut the above structures mainly close to the southern margin of Kato Achaia basin (Figure 5). Similarly a major dextral strike-slip fault seems to cut the prolongation of the GT south of Skolis mountain (Figure 5). It is worth mentioning the existence of N-S to NNW-SSE trending west-verging thrust faults and NNE-SSW trending east-verging backthrusts southwest and southeast of Skolis mountain respectively (Figure 5). East of Skolis mountain several N-S to NNW-SSE trending and eastward

dipping major thrust fault zones have been identified induced the significant structural thickening of Gavrovo flysch (Kamberis et al., 2000, 2005, Figure 5).

4. Subsurface Data

Useful subsurface information concerning the mapping of structure and the stratigraphy of the study area is derived from interpretation of seismic reflection profiles acquired for oil exploration purposes. Two seismic profiles have been selected in order to better describe of GT.

4.1 SW Etoloakarnania area

The first WSW-ENE trending seismic profile (Figure 6) is located north of Evinos river. The quality of the seismic reflectors is good since the overlying interval composed of thick flysch sequences. The Ionian zone lies on the western part of the seismic section, while in the uppermost eastern part appears the overriding Gavrovo zone. This contact is structural, corresponds to the major Gavrovo-Arakynthos system (GAT) that occupies the central part of the section. It is a major thrust gently dipping to the east, using the flysch of the Ionian zone as the detachment horizon. The propagation of GAT sheet to the west had as result the overloading and the down flexure of the Ionian zone as it is seen in the central part of seismic section (Sotiropoulos et al., 2003). At that point the flysch is very thick, reaching to a thickness of 2 sec TWT below sea level.

Sub-vertical normal faults dipping to the east affect the upper part of the carbonate sequence of the Ionian zone facilitating the bending of the Ionian zone in front of the ongoing GAT. The thrust fault splays upwards into two segments (Sotiropoulos et al., 2003). The eastern segment (GT), is short and strongly curved outcropping west of Froxylia rise. The flysch appears to be intensively deformed due to imbrication in the mountainous area around Froxilia rise and this is in agreement with the field observations in this area (Figure 4). The western segment (AT), which outcrops on the western slope of Arakynthos mountain, is longer, running almost parallel to the flysch bedding.

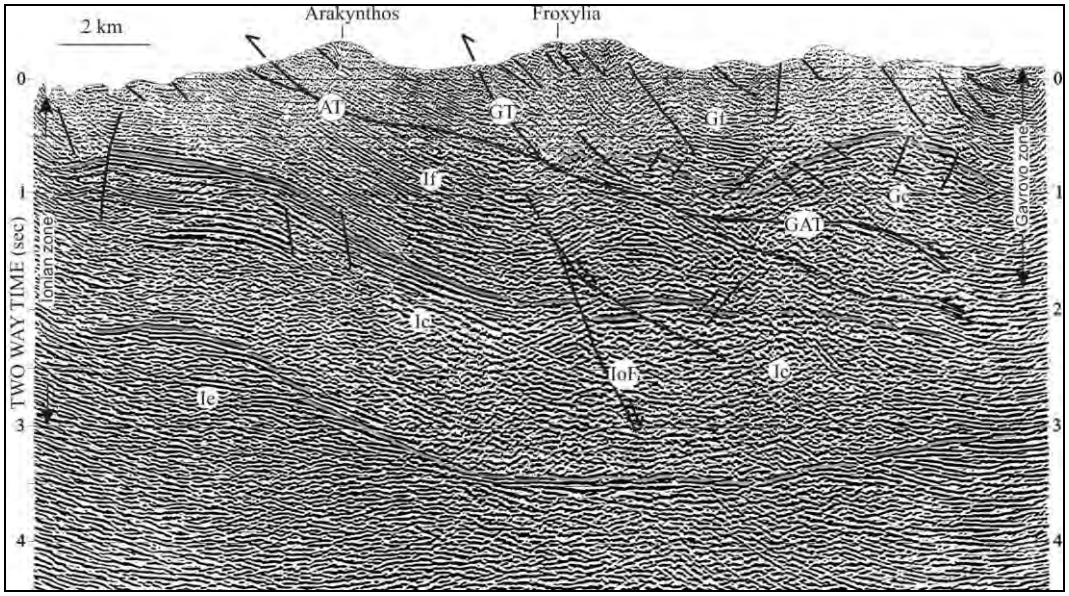

Figure 6 – Interpreted seismic reflection profile north of Evinos river (Sotiropoulos et al., 2003 partly modified). GAT: Gavrovo-Arakynthos thrust system, GT: Gavrovo splay, AT: Arakynthos splay, IoF: Ionian fault, If, Ic, Ie: flysch, carbonates and evaporites of Ionian zone, Gf, Gc: flysch and carbonates of Gavrovo zone.

The flysch age determinations on the footwall of the above thrusts indicate that the western Arakynthos segment (AT) is the older one, while the Gavrovo segment (GT) in the rear is the younger one, suggesting that they compose an out-of-sequence thrust system (Sotiropoulos et al., 2003). Two culminations that are situated on the hangingwall of the thrust fault appear on the eastern part of seismic section corresponding to the north prolongation of Varassova and Klokova anticlines. In fact, Varassova and Klokova represent two ramp anticlines clearly associated with the ramp-flat geometry of the thrust fault surface (Sotiropoulos et al., 2003). Minor back thrusts affect the backlimb of these culminations as well as minor fore thrusts affect the western limb of Klokova anticline, supporting the field observations (Figure 4).

Two features should be pointed out in the footwall of the GT. The first one refers to the probable existence of a duplex beneath the Klokova anticline, while the second one, which is located beneath the eastern segment of GT, is a thrust related structure (Figure 6). Moreover, it is worth mentioning the existence of a subvertical normal fault (IoF in Figure 6) beneath Froxylia mountain that seems to predetermine the position of the thrust fault in its hangingwall, as well as the position of the Gavrovo thrust ramp formed in a later stage. In other words, we consider that this normal fault have played an important role in the evolution of Gavrovo-Arakynthos thrust system inducing out-of-sequence thrusting in the latest stage of its evolution.

4.2 NW Peloponnese area

The GT is also well documented in the second reprocessed seismic reflection profile located south of Skolis mountain (Figure 7). The strong discontinuous reflectors in the central part of the seismic profile represent the top of the carbonates of the Gavrovo zone (Gc). These carbonates are in structural contact with flysch of the Ionian zone (If) along GT. The flysch of the Ionian zone annotates the detachment horizon (Kamberis et al., 1996) as in the case of south Etoloakarnania.

Two culminations have been identified on the hangingwall of the GT. The first narrow one reflects the southern prolongation of Skolis mountain while the second one is an open buried rollover structure (Figure 7). The latter could be related with a major listric normal fault dipping to the east, representing probably the fault on the southeastern flank of Skolis mountain, as it was described earlier in this paper in the field data.

The thrust fault is characterised by a listric geometry (Kamberis et al., 2000). The upper part of the fault represents a ramp outcropping at the western flank of Skolis mountain, while the lower part gently dips to the east, following the stratification of the Ionian flysch. The displacement is estimated to exceed the 10 km.

Based on a new interpretation of the seismic line of Figure 7, the main structural feature in the Ionian zone is a subvertical normal fault dipping to the east which is situated beneath the Skolis mountain (IoF). The extensive downthrown of the Ionian zone carbonates on the hangingwall block of this fault, suggests that it is a major normal fault. In addition, diapiric movement of the underlying Triassic evaporites may exist on the footwall block, in the vicinity to the normal fault. There are also east dipping thrust faults on the footwall of the GT west of Skolis mountain (Figure 7). They are considered to be imbricates rooting downwards on the main fault surface. Similar thrust faults are identified southwest of Skolis mountain (Figure 5). The flysch of the Gavrovo zone (Gf), in the eastern part of the seismic profile, appears to be intensively deformed by thrust faults dipping to the east. This fact is in agreement with the field data and confirms the significant structural thickening of the Gavrovo flysch (Figure 5). The decollement in the flysch sequence of the Gavrovo zone is present at the eastern part of the seismic profile. In addition, the minor folding in the Gavrovo flysch is clearly associated with the thrust activity (Figure 7).

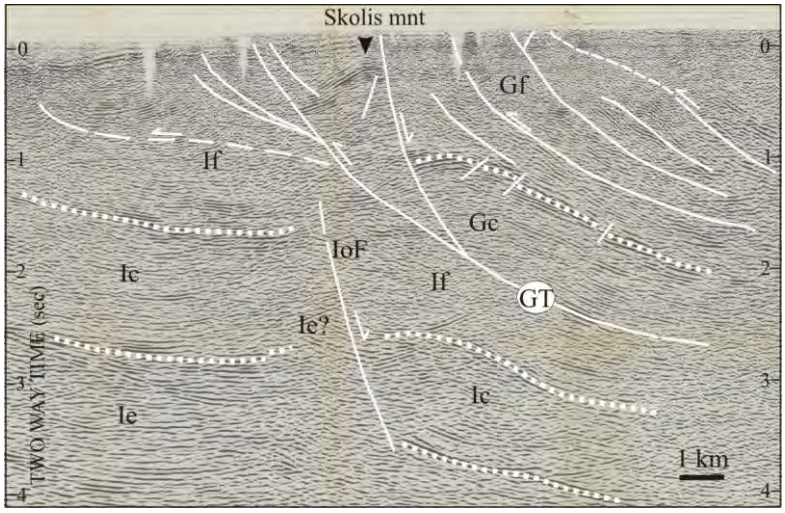

Figure 7 – Interpreted seismic reflection profile south of Skolis mountain with the same legend of Figure 6.

5. Discussion-conclusion

New field data and reinterpretation of subsurface data from northwest Peloponnese and the south Etoloakarnania support that, during Oligocene, the Gavrovo thrust acted simultaneously with the Pindos thrust. The flysch of the Ionian zone acted as the detachment horizon. The GT is well documented both on field and on seismic reflection profiles. It is characterised by a ramp-flat geometry and by significant displacement, greater than 10 km in both areas. The Klokova, Varassova and Skolis structures represent hanging wall anticlines related with the geometry of the GT. The steep relief of Skolis and Varassova mountains can be exlained by their positioning right above the frontal ramp of GT. The propagation of the GT westwards induced the flexural bending of the Ionian zone due to the thrust sheet overloading. In both regions, pre-existing sub-vertical normal faults in the Ionian zone seem to predetermine the position of the frontal ramp of the GT. In other words, there is a 'foreland influence' (term by Couples & Lewis, 1988) in the development of this major thrust (Figure 8a). The blind normal fault beneath the Skolis mountain seems to have played an important role in the structural evolution of this area. In addition, salt movement could potentially exist along this fault. The emplacement of GT could also triggered diapirism due to the overloading of the Ionian zone.

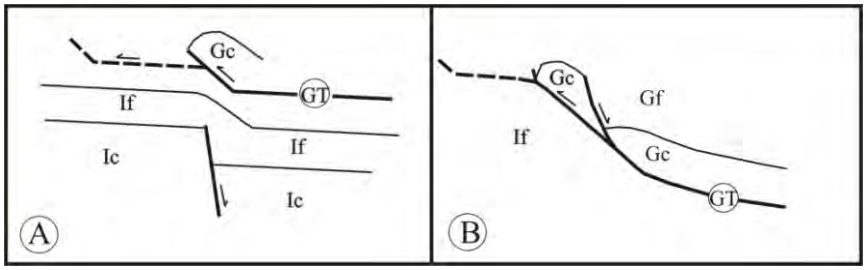

Figure 8 – Modified sketches from Couples & Lewis, 1988. (A) Influence of the foreland structure in the geometry of GT and (B) interpretation of southern part of Skolis mountain.

Such earlier formed normal faults could act in a later stage as strike-slip faults. Koukouvelas et al., 2010 consider that the strong earthquake west of Skolis mountain in summer of 2008 correlates with this major fault in front of Skolis mountain. Sub-vertical normal faults exist at the south-eastern flank of both Varassova and Skolis mountains. In the latter, the normal fault could be

important resulting to the significant downthrown of carbonates to the east, explaining a lot the seismic image (Figure 8a). In south Etoloakarnania, the GT splays upwards in two segments. The western one is longer since it is running almost parallel to the bedding of flysch, while the eastern one is shorter and it involves out-of-sequence thrusting. In both areas the northern prolongation of the GT delineates the western boundary of a mountainous area where intensive thrusting controls its internal configuration.

6. References

Aubouin J. 1959. Contribution a l'etude geologique de la Grece septentrionale:les confins de l'Epire et de la Thessalie, *Ann. Geol. Pays Hellen.* 10, 483 pp.

BP co (British Petroleum Company Limited) 1971. *The geological results of petroleum exploration in western Greece*, Institute of Geology Subsurface Researsh, Athens, 10, 73 pp.

Brooks M., Clews J., Mehs N. S. and Underhill J. R. 1988. Structural development of Neogene basins in western Greece, *Basin Research*, 3, 129-38.

Clews J. E. 1989. Structural controls on basin evolution: Neogene to Quaternary of the Ionian zone, Western Greece, *Journal of the Geological Society*, London, 146, 447-57.

Couples G. and Lewis H. 1988. 'Thrust belt' structures with 'foreland' influence; The interaction of tectonic styles, *Geol. Soc. Amer*., Memoir 171.

Dewey J. P., Pitman W. C., Ryan,W. B. F. and Bonnin J. 1973. Plate tectonics and the evolution of the alpine system, *Geological Society of American Bulletin,* 84, 3137-80.

Doutsos T. and Kokkalas S. 2001. Stress and deformation in the Aegean region, *Journal of Structural Geology*, 23, 455-472.

Fleury J. J. 1980. Evolution d'une platforme et d'un basin dans leur cadre alpin : les zones de Gavrovo-Tripolitze et du Pinde-Olonos, *Soc. Géol. du Nord*, *Special Publication 4*, 651.

IFP (Institut Francais du Petrole) 1966. Etude geologique de l' Epire (Grece nord – occidentale), *Editions Technip*, Paris, France, 306 pp.

Kamberis E., Marnelis F., Loukoyannakis M., Maltezou F., Hirn A. and Streamers Group 1996. Structure and deformation of the external Hellenides based on seismic data from offshore western Greece. In: Wessely G. & Liebl W. (Eds.): Oil and gas in Alpidic thrust belts and basins of Central and Eastern Europe, *Eur. Ass. Geo. Eng., Spec. Publ.,* 5, *Geological Society of London*, 207-214.

Kamberis E., Sotiropoulos S., Aximniotou O., Tsaila-Monopoli S. and Ioakim C. 2000. Late Cenozoic deformation of Gavrovo and Ionian zone in NW Peloponnesus (western Greece), *Annali di Geofisica,* 43, 905-19.

Kamberis E., Pavlopoulos A., Tsaila-Monopoli S., Sotiropoulos S. and Ioakim C. 2005. Deep-water sedimentation and paleogeography of foreland basins in the NW Peloponnese (Greece), *Geologica Carpathica,* 56, 503-515.

Koukouvelas I., Kokkalas S. and Xypolias P. 2010. Surface deformation during the Mw 6.4 (8 June 2008) Movri earthquake in the Peloponnese and its implications for the seismotectonics of western Greece, *International Geology Review*, 52, 249-268.

Rigakis N. 1999. Contribution to stratigraphic research on wells and outcrops of the Alpine formations in Western Greece, in relation to the petroleum generation efficiency of their organic matter, *Ph.D. Thesis,* Athens University, 255 pp.

Sotiropoulos S. 2005. Stratigraphic and structural study in South Etoloakarnania, *PhD. Thesis,* University of Patras (in Greek).

Sotiropoulos S., Kamberis E., Triantaphyllou M. and Doutsos T. 2003. Thrust sequences in the central part of the External Hellenides, *Geol. Mag.,* 140 (6), 661-668.

Sotiropoulos S., Triantaphyllou M., Kamberis E. and Tsaila-Monopolis S. 2008. Paleogene terrigenous (flysch) sequences in Etoloakarnania region (W. Greece), Plankton Stratigraphy and paleoenvironmental implications, *Geobios,* 41, 415-433.

Underhill J. 1989. Late Cenozoic deformation of the Hellenide foreland, Western Greece, *Geological Society of American Bulletin,* 101, 613-34.

Δελτίο της Ελληνικής Γεωλογικής Εταιρίας, τομ. XLVII , 2013
Πρακτικά 13ου Διεθνούς Συνεδρίου, Χανιά, Σεπτ. 2013

Bulletin of the Geological Society of Greece, vol. XLVII 2013
Proceedings of the 13th International Congress, Chania, Sept. 2013

THE MESOHELLENIC TROUGH AND THE THRACE BASIN. TWO TERTIARY MOLASSIC BASINS IN HELLENIDES: DO THEY REALLY CORRELATE?

Kilias Ad.[1], Vamvaka A.[1], Falalakis G.[1], Sfeikos A.[1], Papadimitriou E.[2], Gkarlaouni Ch.[2] and Karakostas B.[2]

[1] *Aristotle University of Thessaloniki, Department of Geology, kilias@geo.auth.gr*
[2] *Aristotle University of Thessaloniki, Department of Geophysics*

Abstract

Based on lithostratigraphic and structural data, as well as geological mapping, the mollasic Thrace Basin (ThB) in NE Greece (including the Paleogene deposits of the Axios Basin) was compared with the Mesohellenic Trough (MHT) in NW Greece. Both basins are characterized by a thick sedimentary sequence of molassic-type strata (3-5km thickness) of Tertiary age, overlain unconformably by Miocene-Pliocene and Quaternary deposits. Molassic sedimentation started almost simultaneously in both areas during the Mid-Upper Eocene but it finished in different time, in the Mid-Upper Miocene for the MHT and the Upper Oligocene for the ThB, respectively. Sedimentation in ThB was also linked with an important calc-alkaline and locally shoshonitic magmatism of Eocene-Oligocene age. We interpreted the MHT as a polyhistory strike-slip and piggy-back basin, above westward-emplacing ophiolites and Pelagonian units on the cold Hellenic accretionary prism. In contrast to MHT, the ThB evolved as a Paleogene supra-detachment basin above the strongly extended during the Eocene-Oligocene Hellenic Hinterland. The syn-depositional magmatic products, linked possibly with subduction processes in Pindos or Axios ocean(s). In any case, MHT and ThB are related to inferred oblique convergence of the Apulia plate and the internal Hellenic units.
Keywords: *Basin analysis, molasse, Hellenides, extension, compression*.

Περίληψη

Με βάση τη λιθοστρωματογραφία, την τεκτονική ανάλυση και τη γεωλογική χαρτογράφηση συγκρίθηκαν μεταξύ τους, οι μολασσικές λεκάνες της Θράκης (ThB) στη ΒΑ Ελλάδα (συμπεριλαμβάνονται οι Παλαιογενείς αποθέσεις της λεκάνης Αξιού) και της Μεσοελληνικής Αύλακας. Αμφότερες οι λεκάνες χαρακτηρίζονται από μια παχειά, μολασσικού-τύπου ιζηματογενή ακολουθία (3-5 km πάχος) Τριτογενούς ηλικίας, που καλύπτεται ασύμφωνα από Νεογενή και Τεταρτογενή ιζήματα. Η μολασσκή ιζηματογένεση αρχίζει σχεδόν ταυτόχρονα και στις δύο περιοχές κατά τη διάρκεια του Μέσου-Άνω Ηωκαίνου όμως σταματάει σε διαφορετικούς χρόνους, στο Μέσο-Άνω Μειόκαινο για τη ΜΗΤ και στο Άνω Ολιγόκαινο για τη ThB. Η ιζηματογένεση στη ThB συνοδεύτηκε επί πλέον από έναν ασβεσταλκαλικής και τοπικά σωσωνιτικής σύστασης μαγματισμό, Ηωκαινικής-Ολιγοκαινικής ηλικίας. Ερμηνεύσαμε τη ΜΗΤ ως μια πολυιστορική οριζόντιας μετατόπισης, piggy-back λεκάνη, που αποτέθηκε επάνω σε οφιόλιθους και στο Πελαγονικό κάλυμμα κατά την προς τα δυτικά τοποθέτησή τους πάνω

στο κρύο πρίσμα επαύξησης των Ελληνίδων. Αντίθετα, η ThB αναπτύχθηκε ως μια Παλαιογενή λεκάνη, πάνω σε ρήγμα διαφυγής και στις γεωλογικές ενότητες των εσωτερικών Ελληνίδων, κατά τη διάρκεια της Ηωκαινικής-Ολιγοκαινικής έκτασης των Εσωτερικών Ελληνίδων. Ο σύγχρονος με την ιζηματογένεση μαγματισμός, πιθανόν, συνδέεται με τις ορογενετικές διαδικασίες υποβύθισης του ωκεανού της Πίνδου ή του Αξιού. Σε κάθε περίπτωση MHT και ThB αναπτύχθηκαν κατά τη διάρκεια πλάγιας σύγκλισης της Απουλίας πλάκας και των Εσωτερικών Ελληνίδων.
Λέξεις κλειδιά: *Ανάλυση λεκανών, μολάσσα, Ελληνίδες, έκταση, συμπίεση.*

1. Introduction

The Mesohellenic Trough (MHT) in NW Greece (Brunn, 1956; Doutsos *et al.*, 1994; Zelilidis *et al.*, 2002; Ferrière *et al.*, 2004; Vamvaka *et al.*, 2006, 2010) and the Thrace Basin (ThB) in NE Greece (Christodoulou, 1958; Lescuyer *et al.*, 2003; Kilias *et al.*, 2006, 2012; Maravelis *et al.*, 2007; Meihold & BonDagher-Fadel, 2010) including its possible continuation into the Axios Basin (AxB; Dumurtzanov *et al.*, 2005), constitute two large late to synorogenic Tertiary molassic-type basins in the Hellenides (Figure 1). Younger, Neogene-Quaternary, unconformably overlying clastic sediments are not considered. Although these basins dominate with their size in the Hellenic orogen and the surrounding region (Figure 1; Albania, Bulgaria, Turkey; References herein-see above), and while a lot of works with different approaches were published for each basin, there still doesn't exist any comparison between the two basins until today, concerning their structural and stratigraphic evolution during the Alpine orogeny in the Hellenides. Furthermore, it is known the great industrial potential of both basins due to gold-mineralizations and their possible hydrocarbon supplies (Lescuyer *et al.*, 2003; Kontopoulos *et al.*, 1999; Zelilides *et al.*, 2002).

This work is the first attempt to compare the evolutionary history of the two basins, as well as their paleogeographic and geotectonic setting in the Hellenic orogen, at least during their molassic-type sedimentation period, taking into account our previous studies on both basins and any different published work for each basin's development. Although, both basins have a similar lithostratigraphic age, evolved mainly during the Paleogene, they differ in their structural evolution and geotectonic position in the frame of the Hellenic orogen and its evolutionary stages.

2. Geological Setting and Structural Features

The Mesohellenic Trough (MHT): The Mesohellenic Trough (MHT) is located in north-western Greece and Albania, and has a length of more than 200 km and a width of 30-40km (Figure 1). The basin developed from Middle Eocene to Upper Miocene time, related to the Alpine orogenic processes, and is sited parallel to the structural fabric of the Hellenides (i.e. NNW-SSE), between the Apulian microplate (External Hellenides, non-metamorphic) and the Pelagonian block (Internal Hellenides, metamorphic).

The basin comprises five molassic-type formations (Figure 2, 3a; Brunn 1956), overlying the Neo-Tethyan ophiolitic rocks and the transgressive Upper Cretaceous limestones or the western Pelagonian margin. Upper Miocene to Quaternary deposits overlie unconformably the molassic-type formations, which, from bottom to top, are (Figure 3a): 1) *Krania Formation* of Middle-Upper Eocene age and a thickness of 1500 m (Brunn, 1956; Wilson, 1993; Zelilidis *et al.,* 2002; Ferrière *et al.,* 2004). 2) *Eptachori Formation* of Uppermost Eocene-Lower Oligocene age and a thickness of about 1000-1200m (Brunn, 1956; Zelilidis *et al.,* 2002). 3) *Pentalophos Formation* of Upper Oligocene-Lower Miocene age, which attains a cumulative thickness of around 2500 m (Brunn, 1956; Doutsos *et al.,* 1994; Ferrière *et al.,* 2004; Zelilidis *et al.,* 2002), while in the central part of the formation it is estimated to reach a maximum thickness of 4000m (Zelilidis *et al.,* 2002). 4) *Tsotyli Formation* of Lower-Middle Miocene age and a thickness of about 1500 m (Brunn 1956; Zelilidis *et al.* 2002), and 5) *Ondria Formation* of Middle Miocene age (Burdigalian-Langian),

which remains only in a few places of the MHT with a thickness of about 350 m. With the exception of the Krania Formation in the westernmost and the southeastern parts of the MHT, the other four formations were deposited parallel to one another from west to east, respectively (Figure 2), with an overall eastward migration of the depocenters and subsidence (Brunn, 1956; Zygogiannis & Müller, 1982). Accordingly, Tsotyli formation directly rests on top of the Pelagonian microcontinent along the eastern margin of the trough. At the western edge of the basin, the strata dip towards the ENE at steep angles; dips decrease progressively away from this basin margin, whereas along the eastern margin of the basin the strata dip with a low angle towards the WSW. As a result an asymmetrical syncline is formed, controlled by structural and depositional processes (Figure 2). The MHT splits into two narrower synclines in the south separated by an uplifted structure (Theotokos-Vassiliki villages' areas; Doutsos *et al.,* 1994). Furthermore, all formations, except the Eocene Krania Formation, become coarser towards the southern part characterized by extensive fan delta deposits (Zelilidis *et al.,* 2002).

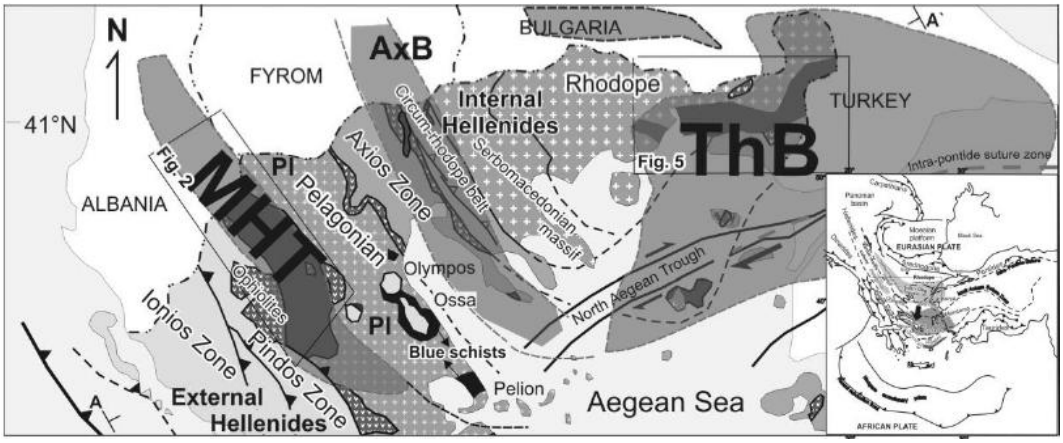

Figure 1 - Location of the Mesohellenic Trough (MHT) and the Thrace Basin (ThB) in the Hellenides and their possible paleogeographic extension in Greece and surrounding areas is shown (AxB Axios Basin; dark gray, the outcrops of the molassic strata in Northern Greece). Insert: the Hellenides as part of the Alpine orogen in the Eastern Mediterranean region; square shows the study area. The SSW migration of the Tertiary magmatic activity ih Hellenides is also indicated (from Eocene until today). A-A' cross section of Figure 6.

Numerous structural data, accrued from observations on geometry of kinematics, overprinted criteria, stratigraphic relationships and correlation between various structures, show that the basin experienced a complicated history with different tectonic episodes (T1 to T5; Figure 2, 4a; Vamvaka *et al.* 2006). These events took place in semi-ductile to brittle conditions from Middle Eocene to Quaternary time.

The first stage (T1) of the basin's development, during Middle-Upper Eocene, was contemporaneous with the final emplacement of Pindos ophiollites and culminated in deformation and uplift of Eocene strata. The Eocene sub-basins developed by crustal flexure and subsidence due to loading of the overthickened Hellenides accretionary prism. Basin evolution was associated with transpressional regime and strike-slip faults with reverse, towards NE component. During the ensuing followed basin closure, intense deformation and uplift at the end of Eocene, the sediments of the first sub-basins were deformed, and placed with a high angle at the western basin margin, locally concordant with the adjacent ophiolitic rocks. The second phase (T2) was dominated by strike-slip faults. Dextral strike-slip faults of NW-SE to NNW-SSE orientation controlled the subsidence and evolution of the basin from Lower to Upper Oligocene. Strike-slip faults, positive flower structures and rare compressional structures have been developed under a transpressional regime which is characterized only by a decrease in intensity in comparison to the first Eocene regime, and a small shift of the maximum principal stress axis (σ1) from NE-SW towards NNE-

SSW (Figure 2,4a). The third stage (T3) was characterized by low-angle normal faulting along the eastern boundary of MHT during Lower-Middle Miocene, which increased the subsidence at that part of the trough (Figure 2,4a). T3 was associated with the syn- to late orogenic collapse and detachment of the Pelagonian nappes (Kilias *et al.*, 1991a, b; Sfeikos *et al.*, 1991). The evolution of the sedimentary basin ended around Middle-Upper Miocene, followed later by rapid uplift and marine regression. A compressional event occurred during the Upper Miocene times, related to reverse and strike-slip faulting, which cut the MHT formations (T4; Figure 2,4a). Finally, extensional tectonics affected the area from Upper Miocene to present-day related to high angle normal faults, some of which are great active faults (T5).

Figure 2 - Geological-structural map of the MHT (modified after Brunn 1956, Zelilidis *et al.*, 2002, Doutsos *et al.*, 1994, Vamvaka *et al.*, 2006). Schmidt diagrams (equal area, lower hemisphere) show the fault planes and slip directions, as well as the calculated paleostress axes (inversion method Angellier 1979; σ1>σ2>σ3) for each tectonic event (T1-T5). Numbers in circles correspond to the tectonic events. AFT and ZFT ages from Pelagonian basement are shown in boxes.

Fission track (FT) analyses were also performed on the MHT sediments and their bordering Pelagonian basement rocks, towards the comprehension of the MHT development. FT data from detrital apatite from the MHT (Figure 3a; Vamvaka *et al.,* 2010) are characterized by two main age populations (i.e. Eocene and Upper Cretaceous to Paleocene ages) and confirm the adjacent to MHT Pelagonian microcontinent as the main source of the detrital material. Eocene AFT age populations (between 50 and 30 Ma) in the Eocene (up to Miocene) sedimentary strata indicate a proximal position of the Pelagonian microcontinent, which shows the same or even younger AFT ages. Upper Cretaceous to Paleocene age populations (between ~60 and ~100 Ma) point to a more distant or structurally higher (now eroded) source area. This is also concluded from the FT age pattern in the relevant units in the southern F.Y.R.O.M. (Former Yugoslavia, Republic of Macedonia), where a clear AFT age gradient from higher age in the east to lower ages in the west is documented (Most *et al.,* 2001). From AFT age components of samples deriving from the western part of the trough, the Pelagonian microcontinent is denoted as the probable, at least partly, source area of those deposits since the beginning of Upper Oligocene. No correlation with AFT ages of the western bordering basement rocks was available due to inappropriate lithology.

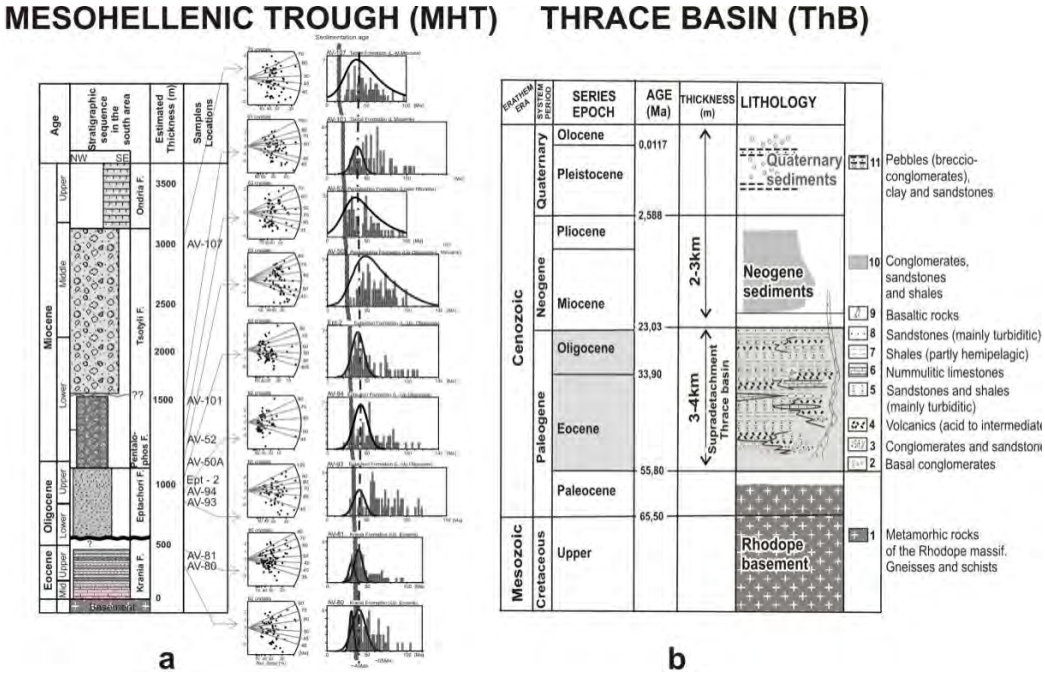

Figure 3 - Schematic lithostratigraphic columns of the MHT (a) and the Thb (b). Apatite FT data from the MHT-formations are also shown (Vamvaka *et al.*, 2010; Kilias *et al.*, 2012). The continuous line (a) refers to the stratigraphic age of the basin deposits.

According to the FT results, the Eocene orogenic event caused only weak thermal overprinting in the rocks of the Pelagonian microcontinent. In its eastern part, the AFT ages show only partial resetting, if any, whereas in its western part the ages were clearly reset during the Eocene event. AFT age-elevation relations, correlation of zircon and apatite FT ages from the same samples, and thermal modelling, based on AFT ages and track length distributions, were all used to reconstruct the low-temperature cooling history of the Pelagonian basement adjacent to the MHT. The results document fast cooling and exhumation in the Eocene that was possibly related to the erosion subsequent of the Eocene thrusting (Kilias *et al.* 1991a,b; Schermer *et al.* 1993), followed by slow cooling and exhumation during Oligocene and Miocene time. This scenario is confirmed by the AFT data from the detrital material in the MHT sedimentary strata, and the increasing lag times resulted for increasing stratigraphic age. The slow cooling period (between ~30 to 10 Ma)

coincides with a stagnation period or crustal extension and possible reheating; this could have been responsible for the partial rejuvenation of the ages of the detrital apatites showed for the oldest (Eocene) formation of the sediment sequence of the MHT (Figure 3a).

The conclusions deduced from the FT results meet the conclusions from the structural analysis, both for the Eocene event and the subsequent change in the tectonic regime. Heating of the western Pelagonian microcontinent adjacent to the MHT, during Lower-Middle Eocene, was associated to thrusting, and directly followed by fast cooling and exhumation in Middle-Upper Eocene. The slower cooling and exhumation in the continuing during Oligocene is associated to the strike-slip faults (T2) which cause localized uplift and subsidence (in the area of MHT), while less vertical movements are produced in other places (e.g., the Pelagonian micro continent). The Miocene extensional period (T3) is also shown from thermal modelling of track length distribution, which indicates a prolonged stay in the same temperature range (or reheating) around ~25 to 10 Ma. This can be caused by crustal thinning and rise of the geothermal gradient, started already since Oligocene-Miocene time, accompanying an extensional period. In the latter thermal model, an enhanced uplift is also predicted during the last 10 Ma, which is in consistence with the filling of the basin with sediments and the uplift of the area.

Geodynamically, the MHT evolved as a piggyback basin in a foreland setting above westward-emplacing ophiolites and higher Pelagonian units (Figure 4a; Wilson, 1993, Doutsos *et al.,* 1994, Ferrière *et al.,* 2004; Vamvaka *et al., 2006*), while great importance is given to the role of strike-slip faults in the structural evolution of the MHT (Vamvaka *et al.,* 2006, 2010). Successive stages and changing tectonic regimes recognised in MHT formation are met in strike-slip basins, while experiencing alternating periods of extension and compression. The changing structural settings and repeated episodes of rapid subsidence and uplift, variable depths along the axis of the basin, asymmetry and big length-to-width ratios (4:1), axial infill subparallel to the principal displacement zones, abrupt lateral and vertical facies variations, and of course the presence of strike-slip

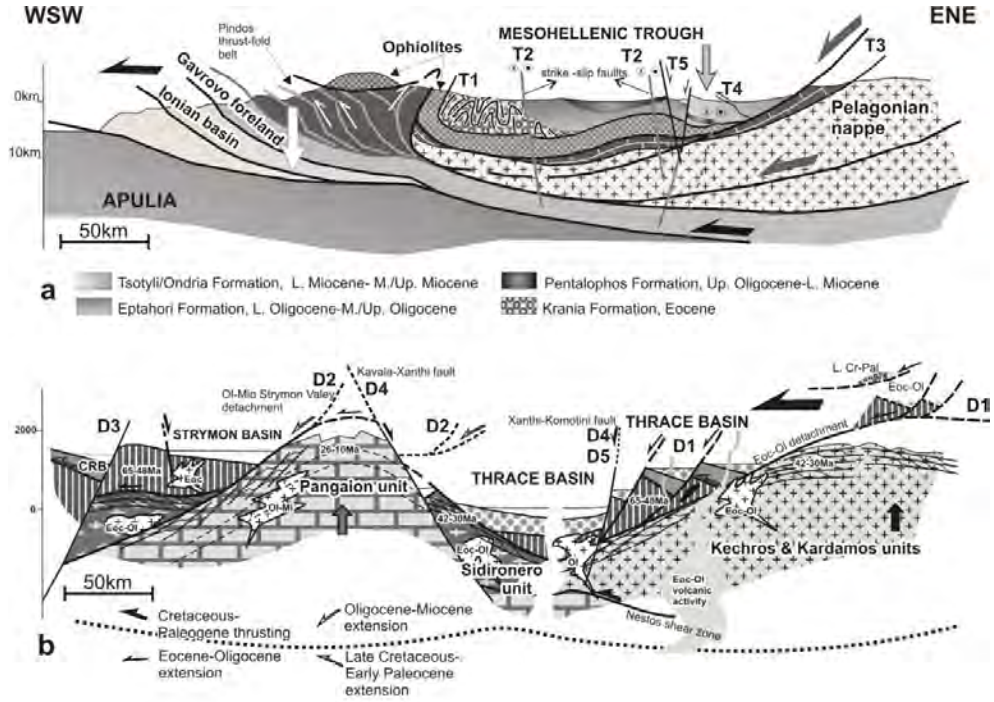

Figure 4 - Schematic cross sections through the MHT (a) and the Thb (b) showing the successive deformational stages related to the basins building (a. Vamvaka *et al.*, 2006; b. Kilias *et al.*, 2012). Legend as in Figures 2 and 5.

faults as certainly observed to bound the western side of the MHT, are some indicative characteristics of the MHT, typical criteria for the recognition of long-lived strike-slip zones and related basins. As the trough developed due to different tectonic events reported earlier, it corresponds to the pattern of polyhistory strike-slip basins (classification after Busby & Ingersoll, 1995).

In conclusion, our interpretation for the evolution of MHT suggests successive tectonic events, in response to which MHT developed, involving isostatic crustal flexure, strike-slip faults, associated with reverse dip slip component, and normal faulting (Figure 4a). This differs from previous interpretations that envisaged foreland flexure related to west-dipping backthrusting (Doutsos *et al.,* 1994), or subsidence associated with asymmetrical flexure and normal faulting (Ferrière *et al.,* 2004).

The Thrace Basin (ThB): The deposits of the Trace Basin in Greece (ThB) consist molassic-type sedimentary rocks of Paleogene age overlain unconformably by a thick (1-2 km) Neogene-Quaternary sedimentary sequence (Figure 3b, 4b, 5; Christodoulou, 1958; Kopp, 1965; Mainhold and Bon Dagher, 2010). More than 90% of the total surface of the ThB is covered by younger Neogene to Quaternary sediments and the Aegean Sea. About 10% of the Paleogene exposed outcrops of the basin is extended in the NE Greek mainland, from the Pangaion mountainous range until the Greek -Turkey borders, and the North Aegean islands of Limnos and Samotraki (Figure 1, 5).

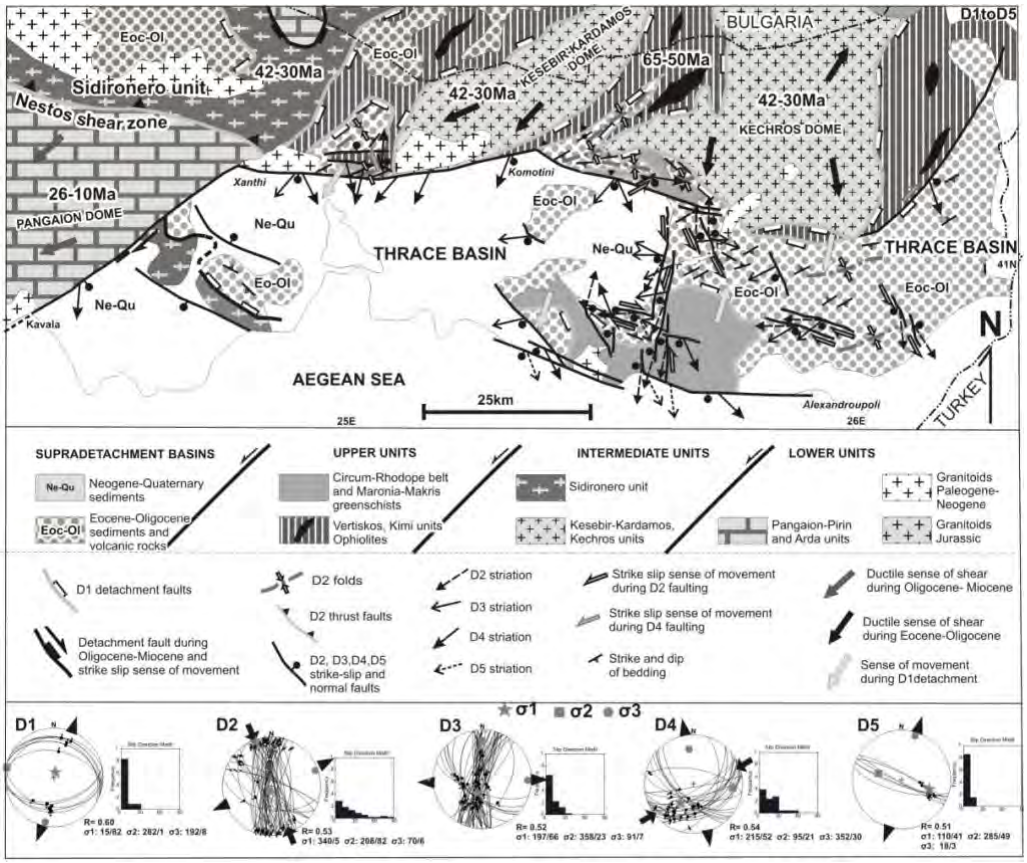

Figure 5 - Geological-structural map of the Thb and the Greek part of the Rhodope massif (modified after Kilias *et al.*, 2012; Burg, 2012). The main structures and kinematics for each tectonic event (D1-D5) are illustrated. Fault –striae data and the deduced paleostress field (σ1>σ2>σ3) direction for each tectonic event are also shown (inverse method, Angelier, 1979; equal area, lower hemisphere).

Some small outcrops of Paleogene sediments along the Axios Basin beneath Neogene-Quaternary sediments (Figure 1) were regarded as equivalent infilling products to the Paleogene ThB sedimentary rocks. The Paleogene molassic sediments of the ThB, as well as their equivalent of the Axios Basin show an age from Middle-Upper Eocene to Oligocene (Christodoulou, 1958; Dragomanov *et al.*, 1986; Roussos, 1994; Mainhold and Bon Dagher, 2010). They constitute a complicated stratigraphic sequence composed by intercalation of bedded conglomerates, breccias, conglomerates, sandstones, nummulitic limestones, turbiditic layers and shales (Figure 3b).

Sedimentation started during Lutetian- Bartonian time with initial deposition of continental sediments (mainly breccias, conglomerates and sandstones), followed during Upper Eocene-Oligocene by marine turbiditic type deposits and limestones. The sediments of the ThB lie in places on the basement rocks of the Rhodope massif and in other places on the low-grade metamorphic Permo-Triassic, volcanosedimentary Nea Makri unit (Figure 5; Bonev *et al.*, 2006; Kilias *et al.*, 2012; Burg, 2012). The total thickness of the Paleogene sedimentary sequence is estimated to 2-3 km (Christodoulou, 1958; Kopp, 1965; Burchfiel *et al.*, 2003), although in the Turkish part of the broader Thrace Basin, where its depocenters are developed, a thickness of about 9 km is reported (Goeruer and Okay, 1996). Moreover, Roussos (1994) refers that also in some parts of the Greek ThB, which are covered by the Neogene-Quaternary sediments or the Aegean Sea, the sedimentary deposition can reach a thickness of ca. 9 km.

The molassic-type sediments of both Thrace and Axios Basins, are intercalated by a lot of calc-alcaline and partly shoshonitic-type, acid to intermediate volcanic products of the same age, Mid-Upper Eocene to Oligocene (Christofides *et al.*, 2004; Dumurtzanov *et al.*, 2005; Figure 3b, 4b). Magmatic activity was further related to gold-mineralization of great economical importance.

Detail structural analysis and geological mapping, as well as study of the kinematics of deformation of the sedimentary-volcanic sequence of the Thrace Basin and its boundaries with the basement rocks of the Rhodope massif and Nea Makri unit, show a complicated structural evolution of the basin. It can be recorded in five progressive tectonic events (D1 to D5) from Eocene to Quaternary time (Figure 4b, 5). Subhorizontal entension dominates during the overall deformational history (Kilias *et al.*, 2012).

D1 is characterized by low angle normal detachment faults recognized at the tectonic boundaries of the Paleogene basin formation with the basement rocks, where no reworking took place due to younger tectonic events. D1 detachment faults strike mainly E-W to NW-SE with S-SW-ward dip direction. Some deviations of these rates are observed at different parts of the basin (Figure 4b, 5). Top to SW to SSW sense of shear dominates along the D1 fault planes but in some places an opposite top to the NE-NNW sense of movement is also recognized. D2 evolved during Oligocene-Miocene time and is related to the further opening and reconstruction of the Trace Basin. D2 is characterized by transpressional tectonics and formation of large conjugate strike-slip faults and extensional fractures, as well as thrust faults and folds with N-NW or S-SE sense of movement (Figure 5). D2-extension remains again NE-SW oriented, ca. parallel to the D1-extension, while compressional component of deformation is developed parallel to the Y-axis of the strain ellipsoid. D3 is responsible for high-angle normal faults dismembering the Eocene-Oligocene molassic basin into Neogene grabens. Some D2 strike-slip faults are reactivated during D3 event, as it is clearly concluded by the existence on their fault planes of oblique, to the strike-slip movements, D3-striations with normal sense of movement. D3 event takes place during Miocene-Pliocene time while D3 extension continues about at the same orientation, NE-SW to ENE-WSW, with the earlier D1 and D2 events. The D4-event is related to large WNW-ESE to NE-SW normal oblique fault zones some of which are older, reactivated during D4, as it is indicated by the existence of at least two striations` generations on their fault planes, with the younger one to be compatible with the D4 kinematics. D4 structures are also characterized by minor oblique reverse faults. Extension orientation changes slightly during D4 to NNW-SSE, associated with a subhorizontal ENE-WSW contraction (Figure 5). Some of the D4 fault zones

remain active until present time (D5). They form large active faults reactivated during the present stress field in the area defined by the earthquake focal mechanisms and characterized by a NNE-SSW oriented subhorizontal extension (Figure 5).

We interpret the Paleogene ThB in NE Greece mainland as a supradetachment basin above the stretched, during the Tertiary, Rhodope massif of the Hellenic hinterland (Kilias *et al.*, 2012). The Paleogene volcanosedimentary infilling of the Axios Basin is regarded as equivalent to the Greek Thrace Basin sedimentary sequence (Figure 4b).

3. Discussion-Conclusions

Molassic-type sedimentation starts in both basins, MHT and ThB including the paleogene sequence of the Axios Basin, simultaneously during Mid-Upper Eocene time (Lutetian-Bartonian) but it finishes at different time, at the Mid-Upper Miocene for the MHT and the Upper Oligocene for the Thb and its equivalent part of the Axios Basin. This Tertiary, westwards progressive delay of the sedimentary stoppage in both areas, is compatible with the W-SW-wards orogen migration of the Hellenides during the Tertiary (Kilias *et al.*, 1999). Neogene-Quaternary sediments lie discordantly on the molassic deposits of the basins, forming the last intramontane basins of Hellenides. Furthermore, the ThB and its equivalent sequence of the Axios Basin is characterized by abundant volcanic products associated with granitoid intrusions of similar age into the Rhodope basement rocks under syn- to late orogenic extension (Kilias & Mountrakis, 1998, Marchev *et al.*, 2006). Nevertheless, important strike-slip movements of Oligocene-Miocene age associated with transpressional or transtensional structures are common during both basins` evolution, showing the great significance of such strike-slip movements along the Hellenides during the Tertiary. Both basins show further analogous deformational setting during the Neogene-Quaternary time with the development of local compressional structures followed again by a general extension regime. Active faults with about the same kinematics, NNE-SSW for the Thb and NNW-SSE for the MHT, dominate also in both areas.

The MHT was evolved as an intramontane piggy-back basin above the ophiolitic nappe and the higher Pelagonian units, during their westward traveling upon the cold Hellenic accretioniary prism (Figure 4a, 6). This geotectonic position, on the cold accretionary prism (Lower plate), interprets well the total lack of any magmatic activity during the basin evolution. Initial isostatic crustal flexure associated possibly with back-thrusting toward east (Mid-Upper Eocene), strike-slip faulting (Oligocene-Miocene) and finally normal detachment faulting towards west (Lower-Middle Miocene) were the main motor mechanisms related to basin evolution (Vamvaka *et al.*, 2006, 2010). Some different interpretations for the basin evolution were proposed by Ferriere *et al.* (2004) or Doutsos *et al.* (1994), who envisaged asymmetrical flexure controlled by normal faulting or foreland depression related to backthrusting towards east, respectively. In contrast to the MHT, at least the studied part of the Greek ThB, including the Paleogene deposits of the Axios Basin, evolved as a Paleogene supradetachment basin above the strongly stretched, during the Eocene-Oligocene, Hellenic Hinterland (Figure 4b, 6; Kilias *et al.*, 1999, Bonev *et al.*, 2006). Exhumation of deep crustal levels took place about simultaneously with basin subsidence and migration of deformation towards W-SW, as well as with the progressive change of the tectonic conditions from ductile to brittle during the Paleogene – Neogene (Kilias *et al.*, 1999, 2012). The origin of the Upper Eocene-Oligocene syndepositional magmatic activity could be attributed to the subduction processes evolved during the Paleogene more further to the W-SW in Pindos or Axios ocean(s). So that it is concluded that extension and basin formation in the Rhodope province took place simultaneously with contraction, nappe stacking and crustal thickening as well as HP/LT metamorphism at the more external parts of the Hellenides towards the foreland (Figure 6).

However, Marchev *et al.* (2005) explain the origin of the Paleogene magmatism and the simultaneous extension and crustal thinning of the Rhodope continental curst due to convective removal of the lithosphere and mantle diapirism, while Tranos (2009) and Maravelis *et al.* (2007)

regard the Thrace Basin as a fore-arc basin but without clear evidence about the existence or position of a Tertiary accretionary prism associated to the basin formation.

In conclusion, according to our descriptions about the structural evolution and stratigraphic features of the MHT and ThB (including the Axios Basin), we assume that both basins constitute independent basin structures, evolved in different geotectonic positions and do not represent lateral continuation. The ThB evolved on the stretched and thinned upper plate of the Hellenic hinterland, above of a subducted slab of the lower plate during the Tertiary (Figure 6). Basin subsidence was associated with tectonic denudation and exhumation of deep crustal metamorphic rocks of the Rhodope province, as well as with abundant magmatic products. The MHT was evolved on the cold, thick crustal part of the External Hellenides, in the foreland area behind the Tertiary accretionary prism of the Hellenides and the Tertiary subduction zone (lower plate during the Tertiary orogenic processes) so that no important magmatic activity accompanied the sediments deposition during the basin evolution (Figure 6).

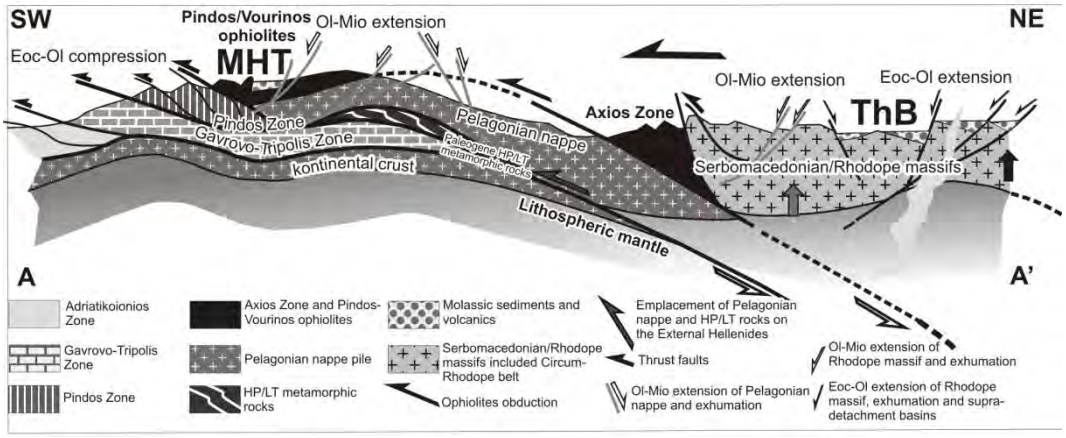

Figure 6 - Cross section through the Hellenides showing the geotectonic position of the MHT and ThB during the Tertiary orogenic processes in Hellenides. Extension acts simultaneously with compression during orogenic evolution.

In any case, MHT and ThB tectonic history seems to be related to an overall oblique plate convergence of the Apulia plate (External Hellenides) and the Internal Hellenides units during the Tertiary, as it could be inferred by the important Tertiary strike-slip motions dominated in both areas (Vamvaka *et al.*, 2006, 2010; Tranos *et al.*, 1999).

4. Acknowledgments

The research was supported by the projects, "PENED 2003" and "Pythagoras II" by GSRT, and the "Excellence Post-doc Scholarship" by RC AUTh. The authors would like to thank two anonymous referees and the editor M. Manoutsoglou for careful reviews and their insightful comments and suggestions on the manuscript.

5. References

Angelier J. 1979. Determination of the mean principal direction of stresses for a given fault population, *Tectonophysics,* 56, T17-T26.

Bonev N., Burg J.-P. and Ivanov Z. 2006. Mesozoic-Tertiary structural evolution of an extensional gneiss dome - The Kesebir-Kardamos dome, eastern Rhodope (Bulgaria-Greece), *Intern. J. Earth Sci.*, 952, 318-340.

Brunn J.H. 1956. Contribution a l' étude geologique du Pinde serpentrional et d' une partie de la Macedoine occidentale, *Ann. Géol. Pays Hellénique*, 7, 1-346.

Burg J.-P. 2012. Rhodope: From Mesozoic convergence to Cenozoic extension. Review of petro-structural data in the geochronological frame, in: Skourtsos, M. and Lister G., eds., The Geology of Greece: *Journal of virtual Explorer, 42*.

Burchfiel B.C., Nakov R. and Tzankov T. 2003. Evidence from the Mesta half-graben, SW Bulgaria, for the Late Eocene beginning of Aegean extension in the Central Balkan Peninsula, *Tectonophysics*, 375(1-4), 61-76.

Busby C.J. and Ingersoll R.V. 1995. *Tectonics of sedimentary basins*, Cambridge, Mass., U.S.A., Blackwell Science, Oxford, 579 pp.

Christodoulou G. 1958. Über das Alter einiger Formationen von Samothraki (in Greek with German summary), *Bull. Geol. Soc. Greece,* III/1, 40-45.

Christofides G., Pécskay Z., Eleftheriadis G., Soldatos T. and Koroneos A. 2004. The Tertiary Evros volcanic rocks (Thrace, Northeastern Greece): Petrology and K/Ar geochronology, *Geologica Carpathica*, 55(5), 397-409.

Doutsos T., Koukouvelas I., Zelilidis A. and Kontopoulos N. 1994. Intracontinental wedging and post-orogenic collapse in the Mesohellenic trough, *Geolog. Rundschau*, 83, 257-275.

Dragomanov L.K., Grigorov V., Ioncher A., Jelev A. and Darakchieva St. 1986. Lithological indications of the presence of Middle Eocene in the Eastern Rhodopes, *Ann. Higher Inst. Mining Geol.*, 32, 37-41 (In Bulgarian with an English abstract).

Dumurdzanov N., Serafimovski T. and Burchfiel B.C. 2005. Cenozoic tectonics of Macedonia and its relation to the South Balkan extensional regime, *Geosphere*, 1(1), 1-22.

Goeruer N. and Okay A.J. 1996. A fore-arc origin for the Thrace basin, NW Turkey, *Geol. Rundsch.*, 85, 662-668.

Ferrière J., Reynaud J.-Y., Pavlopoulos A., Bonneau M., Migiros G., Chanier F., Proust, J.-N. and Gardin S. 2004. Geologic evolution and geodynamic controls of the Tertiary intramontane piggyback Meso-Hellenic Basin, Greece, *Bul.Soc.Géol. France,* 175, 361-381.

Kilias A., Fasoulas C., Priniotakis M., Sfeikos A. and Frisch W. 1991a. Deformation and HP–LT metamorphic conditions at the tectonic window of Kranea (W Thessaly, Northern Greece), *Z. dt geol. Ges.*, 142, 87-96.

Kilias A., Frisch W., Ratschbacher L. and Sfeikos A. 1991b. Structural evolution and metamorphism of blueschists, Ampelakia nappe, eastern Thessaly, Greece, *Bull. Geol. Soc. Greece*, 25, 81-89.

Kilias A. and Mountrakis D. 1998. Tertiary extension of the Rhodope massif associated with granite emplacement (Northern Greece), *Acta Vulcanologica,* 10(2), 331-337.

Kilias A., Falalakis G. and Mountrakis D. 1999. Cretaceous-Tertiary structures and kinematics of the Serbomacedonian metamorphic rocks and their relation to the exhumation of the Hellenic hinterland (Macedonia, Greece), *Intern. J. Earth Sci.,* 88(3), 513-531.

Kilias A., Falalakis G., Gemitzi A. and Christaras V. 2006. Faulting and paleostress evolution in the Maronia-Petrota basin. Evidence of active faults, *Bull. Tethys Geol. Soc.*, 1, 7-16.

Kilias A., Falalakis G., Sfeikos A., Papadimitriou E., Vamvaka A. and Gkarlaouni Ch. 2012. The Thrace basin in the Rhodope province of NE Greece – A tertiary supradetachment basin and its geodynamic implications, *Tectonophysics,* doi:10.1016/j.tecto.2012.05.008.

Kopp K.O. 1965. Geologie Thrakiens III : Das Tertiaer zwischen Rhodope und Evros, *Ann. Géol. Pays Hellénique*, 16, 315-362.

Lescuyer J.L., Bailly L., Cassard D., Lips A.L.W., Piantone P. and McAlister M. 2003. Sedimenthosted gold in south-eastern Europe: the epithermal deposit of Perama, Thrace, Greece, in: Eliopoulos D.G. et al., eds., *Mineral exploration and sustainable development*, 499-502, Millpress, Rotterdam.

Meinhold G. and BonDagher-Fadel M. 2010. Geochemistry and biostratigraphy of Eocene sediments from Samothraki island, NE Greece, *N. Jb. Geol. Palaeont. Abh.,* 256(1), 17-38.

Marchev P., Kaiser-Rohrmeier M., Heinrich C., Ovtcharova M., von Quadt A. and Raicheva R. 2005. Hydrothermal ore deposits related to post-orogenic extensional magmatism and core complex formation: The Rhodope Massif of Bulgaria-Greece, *Ore Geol. Rev.*, 27, 53-89.

Most Th., Frisch W., Dunkl I., Balogh K., Boev B., Avgerinas A. and Kilias A. 2001. Geochronological and structural investigations of the northern Pelagonian crystalline zone - Constraints from K/Ar and zircon and apatite fission track dating, *Bull. Geol. Soc. Greece*, 34, 91-95.

Kontopoulos N., Fokianou T., Zelilidis A., Alexiadis C. and Rigakis N. 1999. Hydrocarbon potential of the middle Eocene–middle Miocene Mesohellenic piggyback basin (central Greece): a case study, *Marine and Petroleum Geology*, 16, 811-824.

Maravelis A., Konstantopoulos P., Pantopoulos G. and Zelilidis A. 2007. North Aegean sedimentary basin evolution during the Late Eocene to Early Oligocene based on sedimentological studies on Lemnos island (NE Greece), *Geol. Carpathica*, 58, 455-464.

Papanikolaou D., Lekkas E., Mariolakos E., and Mirkou R., 1988. Contribution on the geodynamic evolution of the Mesohellenic trough, *Bull. Geol. Soc. Greece*, 20, 17-36.

Roussos N. 1994. Stratigraphic and paleogeographic evolution of the Paleogene Molassic basins of the Northern Aegean, *Bull. Geol. Soc. Greece*, 32, 275-294.

Schermer E.R. 1993. Geometry and kinematics of continental basement deformation during the Alpine orogeny, Mt. Olympos region, Greece, *J. Struct. Geol.*, 15, 571-591.

Sfeikos A., Boehringer C., Frisch W., Kilias A., and Ratschbacher L. 1991. Kinematics of Pelagonian nappes in Kranea area, North Thessaly, *Bull. Geol. Soc. Greece*, 25, 101-105.

Tranos M., 2009. Faulting of Lemnos island: a mirror of the North Aegean Trough (Northern Greece), *Tectonophysics*, 467, 72-88.

Tranos M.D., Kilias A. and Mountrakis D., 1999. Geometry and kinematics of the Tertiary post-metamorphic Circum Rhodope Belt Thrust System (CRBTS), Northern Greece, *Bull. Soc. Geol. Greece*, 33, 5-16.

Vamvaka A., Kilias A., Mountrakis D. and Papaoikonomou J. 2006. Geometry and structural evolution of the Mesohellenic Trough (Greece), a new approach. In: Robertson A.H.F. and Mountrakis D. eds., Tectonic Development of the Eastern Mediterranean Region, *Geological Society of London, Special Publications,* 260, 521-538.

Vamvaka A., Spiegel C., Frisch W., Danišík M. and Kilias A. 2010. Fission track data from the Mesohellenic Trough and the Pelagonian zone in NW Greece: Cenozoic tectonics and exhumation of source areas, *Intern. Geol. Review*, 52(2-3), 223-248.

Wilson J. 1993. The anatomy of Krania basin, northwest Greece, *Bull. Soc. Geol. Greece*, 28(1), 361-368.

Zelilidis A., Piper D.J.W. and Kontopoulos N. 2002. Sedimentation and basin evolution of the Oligocene-Miocene Mesohellenic basin, Greece, *AAPB*, 86, 161-182.

Zygogiannis N. and Müller C. 1982. Nannoplankton-Biostratigraphie der tertiären Mesohellenischen Molasse (Nordwest-Griechenland), *Z. dt geol. Gesel.*, 133, 445-455.

Δελτίο της Ελληνικής Γεωλογικής Εταιρίας, τομ. XLVII , 2013
Πρακτικά 13ου Διεθνούς Συνεδρίου, Χανιά, Σεπτ. 2013

Bulletin of the Geological Society of Greece, vol. XLVII 2013
Proceedings of the 13th International Congress, Chania, Sept. 2013

RE-EXAMINING THE STRESS FIELD OF THE BROADER SOUTHERN AEGEAN SUBDUCTION AREA USING AN UPDATED FOCAL MECHANISM DATABASE

Kkallas Ch.[1], Papazachos C.B.[1], Scordilis E.M.[1] and Margaris B.N.[2]

[1] Geophysical Laboratory, Aristotle Univ. of Thessaloniki

[2] Institute of Engineering Seismology & Earthquake Engineering, Thessaloniki

Abstract

We have employed the data of EGELADOS temporary network (October 2005-April 2007) to determine 88 focal mechanism solutions from Southern Aegean Sea using the RAPIDINV algorithm (Cesca et al., 2010). The new focal mechanism solutions determined, complemented with the previously available ones for Southern Aegean Sea provide the basis for a detailed examination of the stress field, using the distribution of P and T axes. To obtain the stress field we applied the method of Gephart and Forsyth (1984), namely the grid search inversion approach of Gephart (1990a,b), which incorporates the P and T axes of selected focal mechanisms. For the inversion, the initial stress solutions were computed by the "average" kinematic P and T-axis approach of Papazachos and Kiratzi (1992). The stress-inversion allows choosing the "ideal" fault plane corresponding to the minimum misfit rotation about an axis of general orientation which is needed to match an observed fault plane/slip direction with one consistent with the final stress model.
Key words: *Southern Aegean subduction zone, Stress field, Fault plane solutions.*

Περίληψη

Χρησιμοποιήσαμε δεδομένα από το δίκτυο EGELADOS (Οκτώβριος 2005-Απρίλιος 2007) και υπολογίσαμε 88 νέους μηχανισμούς γένεσης στην περιοχή του Ν. Αιγαίου με τη χρήση του αλγορίθμου RAPIDINV algorithm (Cesca et al., 2010). Οι μηχανισμοί αυτοί, σε συνδυασμό με παλαιότερα στοιχεία χρησιμοποιήθηκαν για τον προσδιορισμό του ενεργού πεδίου τάσεων, όπως προτείνεται από την κατανομή των αξόνων P και T. Για τον προσδιορισμό αυτό χρησιμοποιήθηκε η μεθοδολογία των Gephart and Forsyth (1984) και ειδικότερα η μέθοδος αναζήτησης του Gephart (1990a,b), η οποία χρησιμοποιεί τους άξονες P και T των μηχανισμών γένεσης. Για την αντιστροφή, οι αρχικές λύσεις βασίστηκαν στη λύση των μέσων κινηματικών αξόνων P και T των Papazachos and Kiratzi (1992). Η διαδικασία αντιστροφής επιτρέπει τον καθορισμό των "ιδανικών" ρηγμάτων των μηχανισμών γένεσης, με βάση την προσαρμογή των παρατηρημένων και αναμενόμενων από το πεδίο τάσεων διανυσμάτων ολίσθησης τα οποία προκύπτουν με τη βοήθεια της μεθόδου αντιστροφής.
Λέξεις κλειδιά: *Ζώνη κατάδυσης Ν. Αιγαίου, Πεδίο τάσεων, Μηχανισμοί γένεσης.*

1. Introduction

The broader Southern Aegean area (Figure 1) is one of the most active tectonically region of the western Eurasia (Figure 1). In this region, the Nubia lithospheric plate subducts under the Aegean microplate, which in turn overrides the Nubia plate (Papazachos and Comninakis, 1971; McKenzie, 1972). The dominant tectonic feature of the area is Hellenic trench, which runs almost parallel to Hellenic outer sedimentary arc and the inner volcanic arc. The South Aegean deformation is driven primarily by the fast moving (~33 mmyr^{-1}) Aegean upper plate overriding a nearly stalled (~5 mm mmyr^{-1}) Nubian lower plate (Ganas and Parson, 2009). A well-developed Benioff zone has been identified (e.g. Papazachos et al., 2000), with medium-to-large transpressional intermediate-depth events, mainly occurring in the depth range of 60-90km, with maximum depths of the order of 180km. The subduction is associated with the generation of volcanic activity along the Hellenic volcanic arc in southern Aegean (Fytikas et al, 1985), with the volcanic centre of Santorini in Central Cyclades, being the most active volcano of the area. Much work has been already done on active tectonics of the southern Aegean (Papazachos and Comninakis, 1971; McKenzie, 1970, 1978; Hatzfeld et al., 1989; Benetatos et al., 2004; LePichon et al., 1995; Reilinger et al., 1997; Papazachos, 1999; McClusky et al., 2000; among others). Due to the tectonic complexity of the Aegean Sea we employed recent seismological data from the EGELADOS temporary network (October 2005-April 2007) to study the active tectonics in southern Aegean. Using the data of the EGELADOS temporary network we determined 88 new focal mechanisms, which, in combination with previously published mechanisms, comprise a significant data set, which can be used for the re-evaluation of the stress field of the broader Southern Aegean Sea.

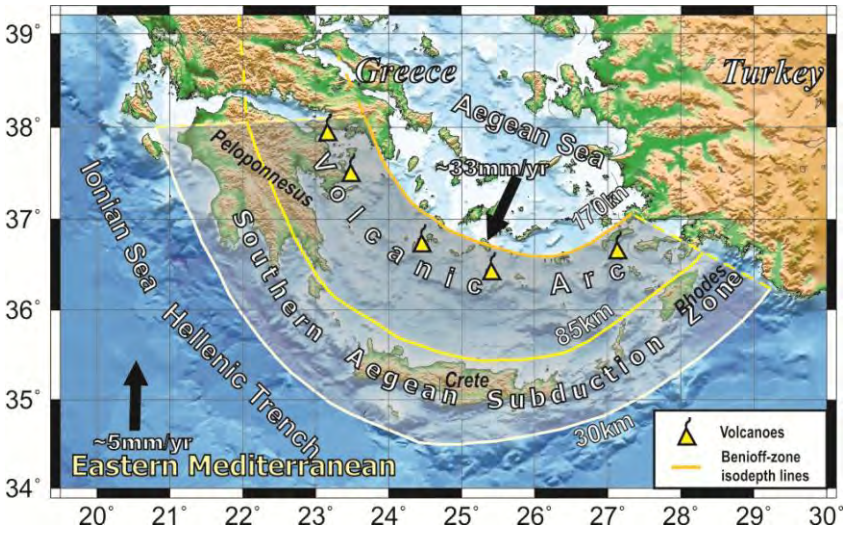

Figure 1 - Schematic geotectonic map of the broader southern Aegean area. Plate motions are depicted by solid vectors. The volcanic arc and the Benioff-zone isodepths are also shown (modified from Papazachos et al. 1998, Karagianni et al., 2005).

2. Data Used

The main data source of this work is the EGELADOS temporary network (http://www.gmg.ruhr-uni-bochum.de/geophysik/seismology/research/egelados.html), (October 2005 – April 2007). EGELADOS (Exploring of the Geodynamics of Subducted Lithosphere Using an Amphibian Deployment of Seismographs) is the largest amphibian seismological network ever deployed in southern Aegean, including 65 land and 24 OBS stations (http://geofon.gfz-potsdam.de/waveform/archive/network.php?net=11), covering almost the entire Hellenic subduction area (Figure 2). We also used data from the Euro Mediterranean Seismological Center

(EMSC) and Harvard (CMT solutions) databases from 2003 to 2011, as well as solutions published in a large number of previous studies (e.g. Papazachos et al., 1983; Benetatos et al., 2004; Kiratzi and Louvari, 2003; Taymaz et al.,1991; Louvari et al., 1999; Kiratzi et al.,1991; Yilmazturk and Burton, 1999; Arvidsson & Ekstrom, 1998; Bernard et al., 1997; Louvari et al., 2001; Kiratzi and Louvari, 2003; Vamvakaris et al., 2006).

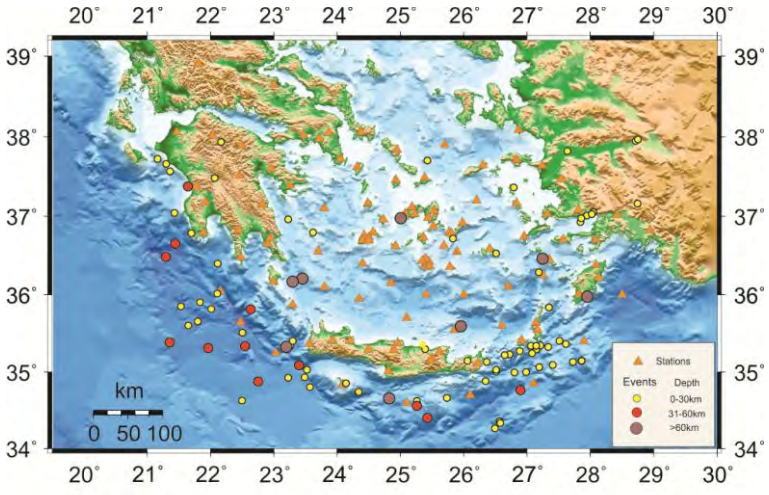

Figure 2 – Station distribution and seismic events for EGELADOS network.

3. Applied method

3.1. Estimation of Fault Plane Solutions

For the fault plane solution determination from the EGELADOS data, we employed the RAPIDINV processing software (Cesca et al., 2010). RAPIDINV is based on a *python* module which has been developed in order to simplify the process of kinematic inversion using the Kiwi tools (kinherd.org). The FPS estimation uses both waveform and spectral fitting kinematic inversion (Heimann et al., 2008; Cesca S., et al., 2010), exhibiting model flexibility, a small number of inverted parameters and the possibility for full automation. The main methodological difference is that the method employs a spectral fitting process in the first step, constraining only some of the FPS parameters. The spectral fitting is performed by a grid-walk, a Levenberg-Marquadt approach or a combination of both procedures. The Green functions are precomputed and organized in an efficient HDF5 database, allowing the acceleration of the process. Its lower time consumption renders the Kiwi tools suitable for near real-time moment tensor inversion.

After the first step (Figure 3), where the 4 candidate fault planes, depth and moment are determined, a waveform fitting is performed (for any or both type of body waves, surface waves or even full-waveform) to select the final 2 fault planes (Figure 4). Finally, in a third step, a kinematic inversion is performed for an extended source, allowing the selection of the candidate fault-plane and its rupture directivity. The inversion resulted in the determination of focal parameters for 88 earthquakes with a depth range from 2 to 98 km and moment magnitudes M ranging from 3.5 to 6.6. The final data set of the determined fault plane solutions, as well as existing fault plane solutions from previous works, earlier described, is presented in Figure 5.

3.2. Stress Tensor Inversion

In order to provide an initial estimate of the stress field variability in the study area, we employed the representative “average focal mechanism tensor” using the approach of Papazachos and Kiratzi (1992). According to this method, an average “focal mechanism” tensor, F, is calculated, which is

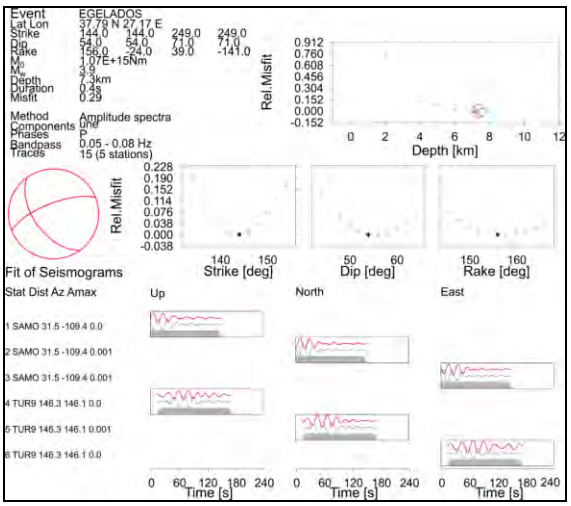

Figure 3 - Sample output of step 1 of the inversion (spectral inversion), where 4 candidate fault planes of the focal mechanism is determined. The retrieved parameters in this step are the fault plane strike, dip, rake, as well as the event M_0 and event depth.

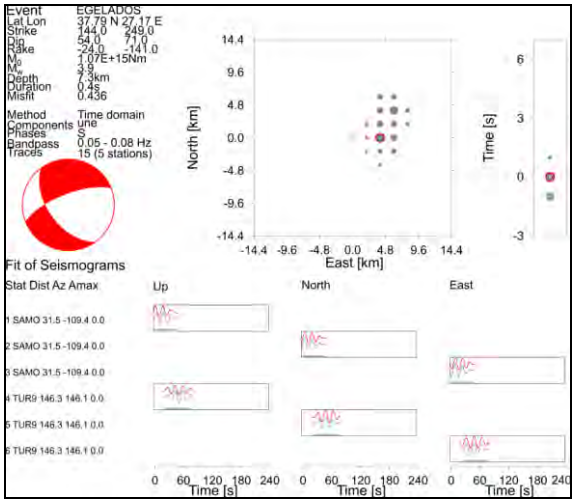

Figure 4 - Sample output step 2 of the inversion (waveform fitting). The waveforms are fit in the time domain, allowing the centroid location (space and time domain) and the retrieval of the compressive/dilatational quadrants.

a function of the strike, ζ, dip, δ, and rake, λ of the corresponding fault plane (Aki and Richards, 1980), and the eigenvalues of this average "focal mechanism" tensor F correspond to the average P, T and N (null) axes. Therefore, the method defines "average" kinematic (P, T and N) axes, which are assumed to be identical with the principal stress axes. In our case data weighting was used depending on the moment magnitude of each event. In order to perform this initial assessment of the stress field in the Southern Aegean Sea by the use of seismological data (Figure 5), we separated the area in smaller sub-regions with common seismotectonic characteristics and a relative fault plane solution homogeneity, so that they can be considered as locally representative.

Figures 6 and 7 present the spatial distribution of the average P and T axes for the depth ranges of 0–30 km and >30km, using the Papazachos and Kiratzi (1992) method, while Figure 8 shows the corresponding average focal mechanisms, separated in 5 typical groups. The first two groups (red

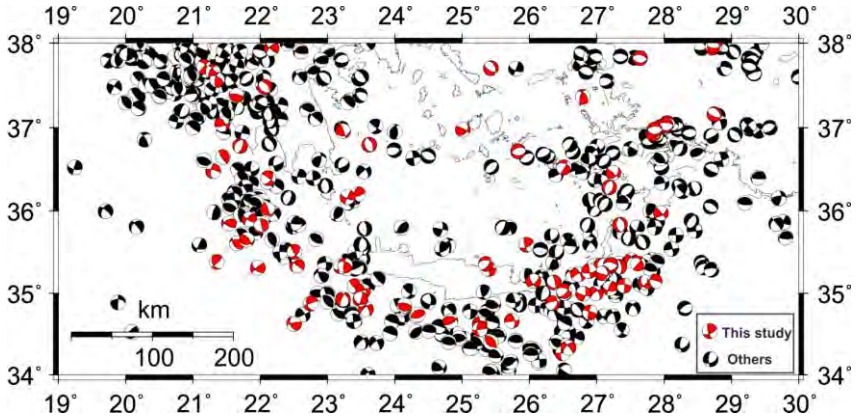

Figure 5 - Distributions of the new (RAPIDINV algorithm - red color) and the previously published (black color) focal mechanism solutions for the Southern Aegean area.

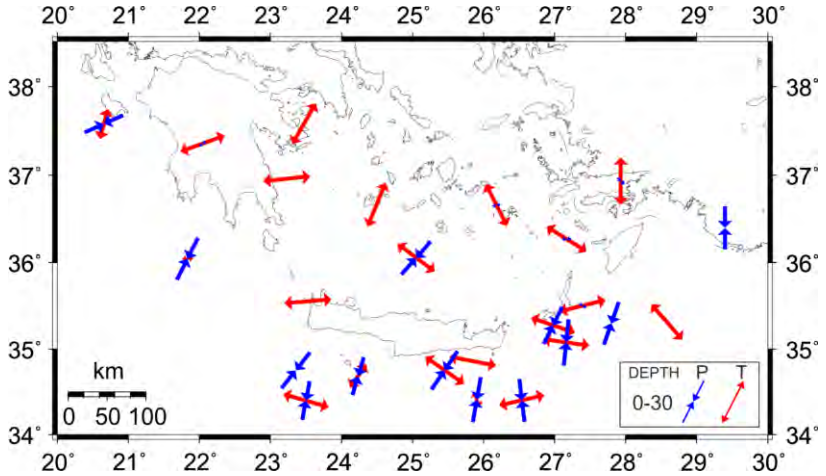

Figure 6 - Horizontal projection of P-axes (converging arrows) and T-axes (diverging arrows) from the method of the Papazachos and Kiratzi (1992) for the depths of 0-30km.

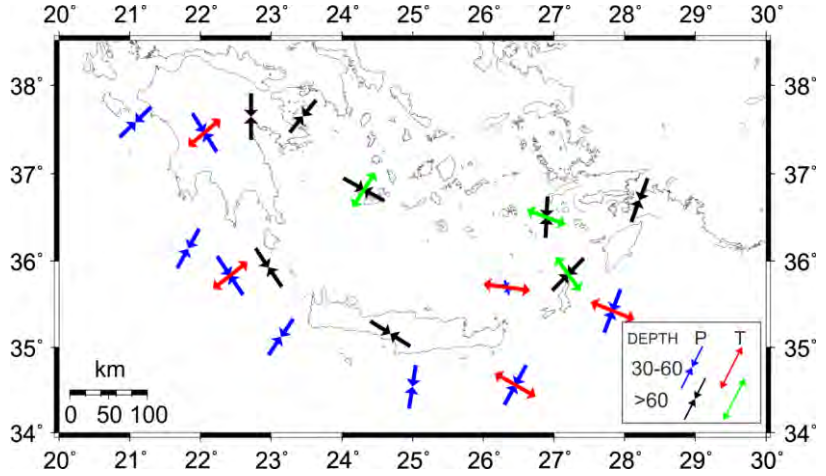

Figure 7 - Horizontal projection of P-axes (converging arrows) and T-axes (diverging arrows) from the method of the Papazachos and Kiratzi (1992) for depths >30km.

and green FPS) corresponds to ~E-W normal faults of the volcanic arc and ~N-S normal faults of the outer (sedimentary) arc, showing a ~N-S and E-W extension field, respectively. The outer arc is characterized by typical thrust faults (blue FPS) that maintain a roughly constant NW-SE orientation, while the brown FPS depict strike-slip events, that mostly cluster along the Strabo and Pliny trenches in the outer SE Aegean arc. Finally, the black FPS correspond to typical transpressional intermediate-depth events, with a clear down-dip extension and arc-parallel compression.

New results can be also inferred for intermediate depth events. Shallower events (close to the outer arc) exhibit a typical down-dip extension and in-slab compression, that shows as early as 30-60km for the Peloponnesus and SW Kythira area (see Figure 7), hence at much shallower depths than earlier considered. Extension (σ_3) axes become more horizontal at larger depths (Milos and Karpathos groups) and towards Rhodes. The results are somewhat similar to Rondogianni et al. (2011), however the stress changes proposed in the previous work near Rhodes (σ_1-σ_2 interchange with depth) are not detected in this work, where the stress field in Rhodes and Kos (different depth ranges) seems to be quite similar (figures 7 and 8), probably due to the use of extremely large regions by Rondogianni et al. (2011).

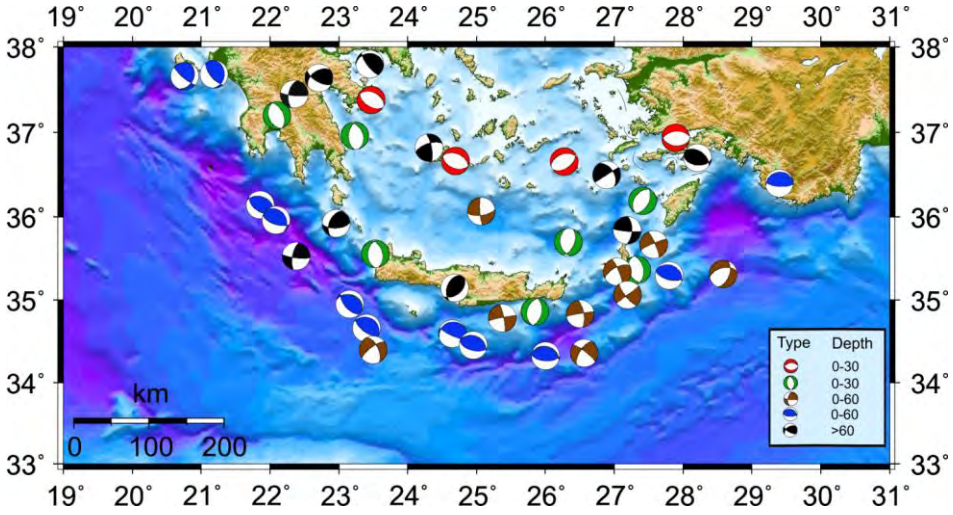

Figure 8 - Average focal mechanisms using the approach of Papazachos and Kiratzi (1992).

In order to confirm the results of Figures 6 and 7, we used the FMSI computer program developed by Gephard and Forsyth (1984) and Gephard (1990a, b) to obtain the stress field from fault plane solutions. In this method the orientation of fault planes and slip directions provided by a large population of earthquake focal mechanisms can be used to determine best fit regional principal stress directions. Four stress parameters are calculated: three of them define the orientation of the main three stress-axes σ_1, σ_2 and σ_3 and the parameter $R=(\sigma_2-\sigma_1)/(\sigma_3-\sigma_1)$, which specifies the magnitude of the intermediate σ_2 compressive stress direction, relative to maximum σ_1 and minimum σ_3 compressive stress directions, under the assumption of uniform stress in the source region. The analysis allows for the possibility that the failure occurs on pre-existing zones of weakness of any orientation. Using this approach we determined the three principal stress directions and the parameter R, as well the associated uncertainty. As initial principal stress solution we used the "average" kinematic (P, T and N) axis previously estimated using the approach of Papazachos and Kiratzi (1992). Figures 9 and 10 presents the P and T axes for the 0–30 km and >30km depth range for the results of the Gephart and Forsyth (1984) method. The obtained results shows very small azimuthal difference for the P and T axes between the two methods.

The obtained results from both methods are in excellent agreement with the previous knowledge for the region. The distribution of the focal mechanisms 0-60 km (blue colour) as shown in Figure 8, shows thrust faulting that dominates in the outer part of Hellenic trench which starts south of the

island of Zakynthos, runs along the western part of the Hellenic Arc and extends up to the coasts of Turkey. The P-axes appear to be almost normal to the strike of the arc and sub-parallel to the arc in its eastern part. The distribution of the normal shallow (0-30km) focal mechanisms (green colour) running parallel to the thrust zone shows a normal faulting zone with E–W trending T-axes connected with the sedimentary arc (Papazachos et al., 1984; Liotier, 1989; Armijo et al., 1992). An important new feature is that the trend of the normal focal mechanisms along the volcanic arc runs parallel to the local strike of the volcanic arc. At the eastern edge of the arc, near Rhodes island, a dominant zone of strike–slip faulting is identified (brown colour), associated with complex processes of subduction. Strike-slip faulting (black colour) with a significant thrust component is found along subducted Benioff zone, in accordance with earlier studies (e.g. Papazachos et al., 2000, Benetatos et al., 2004), with the P-axes running almost parallel to the strike of the arc. A new feature is that the T axεs of deeper events (>100km) become almost horizontal under the volcanic arc, not showing down-dip extension as in earlier studies for shallower events (60-100km).

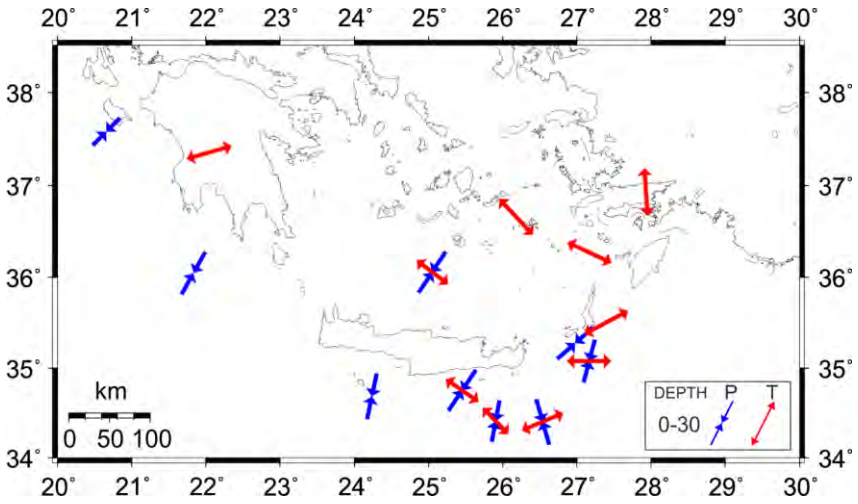

Figure 9 - Horizontal projection of P-axes (converging arrows) and T-axes (diverging arrows) from the method of the Gephart and Forsyth (1984) for depths 0-30km.

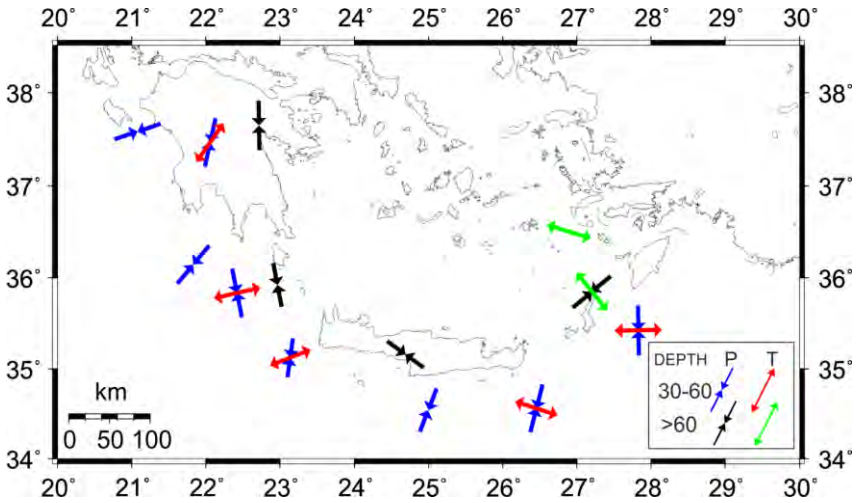

Figure 10 - Horizontal projection of P-axes (converging arrows) and T-axes (diverging arrows) from the method of the Gephart and Forsyth (1984) method for depths >30km.

3.3. Fault Determination

The application of the stress–tensor inversion allowed the determination of the plane corresponding to the minimum misfit rotation around any arbitrary axis which brings one of the nodal planes, its slip direction and the sense of slip into an orientation that is consistent with the stress model. For each FPS the misfit is determined for each modal plane. The nodal plane with the smaller misfit is usually assumed as the "ideal" fault planes on which the corresponding earthquake occurred. However, it is clear that this selection is arbitrary if both nodal planes exhibit similar misfit values which are either small (both planes are acceptable) or very large (both could be considered as "incompatible" with the determined stress field). Taking into account the average FPS solution uncertainty of 10° for fault planes and P/T axes, we considered the difference of the misfit values of the two planes as a quality measure for the selection procedure. In order to obtain more robust results we have assumed that if the misfit calculated for both fault planes (main and auxiliary) is relatively small (typically <2–3 times the average uncertainty, i.e. 25°) and their difference is less than the average uncertainty (10°), then both planes should be considered and included in the results of this study, as they are practically indistinguishable with respect to their misfit.

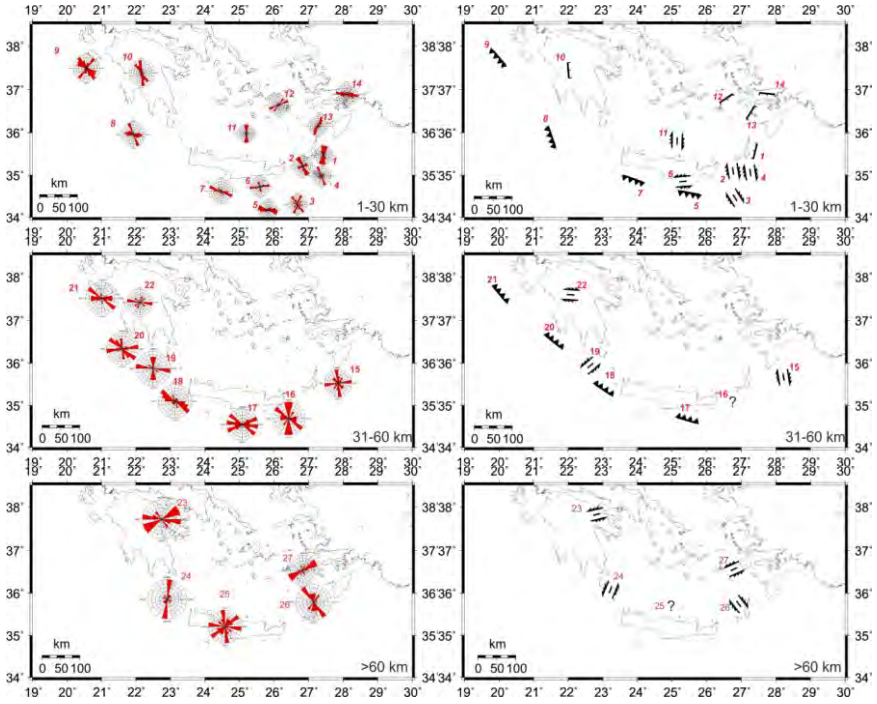

Figure 11 - Fault planes identified by the stress tensor inversion method as candidates for the "actual" seismic faults. The rose diagrams present the corresponding fault distributions.

In Figure 11 the average fault planes from each group identified by the stress inversion are presented as linear elements. The distribution of the identified faults is also presented with a rose diagram. Lund & Slunga (1999) tested the advantages and disadvantages of the method thoroughly and they concluded that the algorithm of Gephard & Forsyth (1984) does not always pick the correct nodal plane as fault but in some case the auxiliary plane is picked as fault plane. This clearly occurs for the shallow thrust faults (0-30 km), as is appears that the Aegean subducts under Nubia plate, contrary to what is observed. This is reversed for deeper thrust events, which show a normal thrusting pattern. An excellent similarity is observed for fault number 11 with results of (Kiratzi, 2012) who to found a prominent N–S strike-slip character of motion for the sequence of January 2012.

4. Conclusions

The combined application of both approaches confirm earlier findings and provide a locally novel and more detailed view of the active stress field in the broader Southern Aegean subduction area. In general, 5 main types of faulting and stress patterns are recognized: (a) Thrust faulting at depths up to 60 km with a dominant NW-SE direction, following the general local trend of the Hellenic arc, with the P axis having a constant strike, almost perpendicular to the arc-strike in its western and central parts, and sub-parallel to the arc in its eastern part, (b) Normal faulting with T-axes showing ~N-S extension, almost perpendicular to the strike of the volcanic arc at depths up to 30 km, (c) Normal faulting with T-axes showing along—arc extension, running almost parallel to the strike of the arc at depths up to 30 km, (d) Strike-slip faulting with a significant thrust component, corresponding to intermediate-depth events along the subducted Benioff zone, at depths gradually increasing from 50km (in the Crete-Kythira area) to ~100-120km in the southern Aegean volcanic arc region and, (e) Strike–slip faulting near the south-eastern edge of the Hellenic arc up to 60 km. The transition from thrust faulting (group a) to the transpressional intermediate-depth events (group d) occurs at shallower depths under Peloponessus and Kythira than previously considered, while the previously suggested stress-complexity near Rhodes by Rondogianni et al. (2011) is not supported by the present study results.

5. Acknowledgments

The GMT system (Wessel and Smith, 1998) was used to plot some figures. This work has been partly supported by the 3D-SEGMENTS project of the ARISTEIA-I call funded by EC European Social Fund and the Greek Secretariat of Research and Technology.

6. References

Aki K. and Richards P. 1980. *Quantative Seismology: Theory and Methods,* Freeman, San Francisco, California, 557 pp.

Baker C., Hatzfeld D., Lyon-Caen H., Papadimitriou E.and Rigo A. 1997. Earthquake mechanisms of the Adriatic Sea and western Greece, *Geophys. J. Int.* 131, 559–594.

Benetatos C., Kiratzi A., Papazachos C., and Karakaisis G. 2004. Focal mechanisms of shallow and intermediate depth earthquakes along the Hellenic arc, *Journal of Geodynamics,* 37, 253–296, doi:10.1016/j.jog.2004.02.002

Bird P. 2003. An updated digital model of plate boundaries, *Geochemistry Geophysics Geosystems*, 4(3), 1027, doi:10.1029/2001GC000252

Cesca S., Buforn E., and Dahm T. 2006. Moment tensor inversion of shallow earthquakes in Spain*, Geophys*. J. Int., doi: 10.1111/j.1365-246X.2006.03073.x.

Cesca S., Heimann S., Stammler K. and Dahm T. 2010. Automated point and kinematic source inversion at regional distances, *J. Geophys*. Res., doi:10.1029/2009JB006450.

Ganas A. and Parsons T. 2009. Three-dimensional model of Hellenic Arc deformation and origin of the Cretan uplift, *Journal of Geophysical Research,* 114: doi: 10.1029/2008JB005599.

Gephart J.W. 1990a. Stress and the direction of slip on fault planes, *Tectonics*, 9, 845-858.

Gephart J.W. 1990b. FMSI: a FORTRAN program for inverting fault/slickenside and earthquake focal mechanism data to obtain the regional stress tensor, *Comput. Geosci*. 16 (7), 953–989.

Gephart J. and Forsyth W. 1984. An improved method for determining the regional stress tensor using earthquake focal mechanism data: applications to the San Fernando earthquake sequence, *J. Geophys*. Res., 89, 9305-9320.

Hatzfeld D., Pedotti G. and Hatzidimitriou R. 1989. The Hellenic subduction beneath the Peloponnesus: First results of a microearthquake study, *Earth Planet*. Sci. Lett., 93, 283-291.

Heimann S., Cesca S., Krüger F. and Dahm T. 2008. Stable estimation of extended fault properties for medium-sized earthquakes using teleseismic waveform data, *Geophysical Research Abstracts*, pp. EGU2008– A–07,568.

Karagianni E.E., Papazachos C.B., Panagiotopoulos D.G., Suhadolc P., Vuan A. and Panza G.F. Shear velocity structure in the Aegean area obtained by inversion of Rayleigh waves, *Geophys. J. Int*., 160, 127-143, 2005.

Kiratzi A., and Louvari E. 2003. Focal mechanisms of shallow earthquakes in the Aegean Sea and the surrounding lands determined by waveform modelling: A new database, *Journal of Geodynamics,* 36, 251–274; doi:10.1016/S0264-3707(03)00050-4.

Kiratzi A. A. 2013. The January 2012 earthquake sequence in the Cretan Basin, south of the Hellenic Volcanic Arc: focal mechanisms, rupture directivity and slip models, *Tectonophysics*, 586, 160-172, http://dx.doi.org/10.1016/j.tecto.2012.11.019.

Lund B. and Slunga R. 1999. Stress tensor inversion using detailed microearthquake information and stability constraints: Application to Ölfus in southwest Iceland, *J. Geophys. Res*., 104:14947-14964.

Le Pichon X., Chamot-Rooke N., Lallemant S., Noomen R. and G. Veis. 1995. Geodetic determination of the kinematics of central Greece with respect to Europe: Implications for eastern Mediterranean tectonics. *Journal of Geophysical Research,* 100, 12,675–12,690.

Louvari E., Kiratzi A.A. and Papazachos B.C. 1999. The Cephalonia Transform Fault and its extension to western Lefkada Island (Greece), *Tectonophysics 308*, 223–236.

McKenzie D. 1972. Active tectonics of the Mediterranean region, *Geophys. J. R. Astr. Soc*. 30, 109–185.

McKenzie D. 1978. Active tectonics of the Alpine-Himalayan belt: the Aegean Sea and surrounding regions, *Geophys. J. R. Astr. Soc*. 55, 217–254.

McClusky S.S., Balassanian A., Barka C., Demir S., Ergintav I., Georgiev O., Gurkan M., Hamburger K., Hurst H., Kahle K., Kastens G., Kekelidze R., King V., Kotzev O., Lenk S., Mahmoud A., Mishin M., Nadariya A., Ouzounis D., Paradissis Y., Peter M., Prilepin R., Reilinger I., Sanli H. and Seeger A. 2000. Global Positioning System constraints on plate kinematics and dynamics in the eastern Mediterranean and Caucasus, *J. Geophys. Res*., 105, 5695–5719.

Fytikas M., Innocenti F., Manetti P., Peccerillo A., Mazzuoli R. and Villari L. Tertiary to Quaternary evolution of volcanism in the Aegean region, doi: 10.1144/GSL.SP.1984.017.01.55, *Geological Society*, London, Special Publications, 17, 687-699, 1984.

Oral M.B., Reilinger R.E., Toksoz M.N., King R.W., Barka A.A., Kiniki J. and Lenk D. 1995. GPS offers evidence of plate motions in eastern Mediterranean, *EOS*, 76, 9-11.

Papazachos B.C. 1990. Seismicity of the Aegean and the surrounding area, *Tectonophysics, 178*, 287–308.

Papazachos B.C. and Comninakis P. E. 1971. Geophysical and tectonic features of the Aegean arc, *J. Geophys. Res.* 76, 8517–8533.

Papazachos B.C., Kiratzi A.A., Hatzidimitriou P.and Rocca A. 1984. Seismic faults in the Aegean area, *Tectonophysics,* 106, 71–85.

Papazachos B.C. and Papazachou C.B. 1997. *The earthquakes of Greece*. Ziti Publ. Thessaloniki, Greece, 304pp.

Papazachos B.C., Papadimitriou E.E., Kiratzi A.A., Papazachos C.B. and Louvari E.K. 1998. Fault plane solutions in the Aegean sea and the surrounding area and their tectonic implications, *Bolletino di Geofisica Teorica ed Applicata* , 39, 199-218.

Papazachos B.C., Karakostas V.G., Papazachos C.B.and Scordilis E.M. 2000. The geometry of the Wadati-Benioff zone and the lithospheric kinematics in the Hellenic arc, *Tectonophysics,* 319, 275–300.

Papazachos C.B. and Kiratzi A.A. 1992. A formulation for reliable estimation of active crustal deformation and its application to central Greece, *Geophys. J. Int.,* 111, 424–432.

Papazachos C.B. and Kiratzi A.A., A formulation for reliable estimation of active crustal deformation and its application to central Greece, *Geophys. J. Int*., 111, 424-432., 1992.

Papazachos C.B. 1999. Seismological and GPS evidence for the Aegean-Anatolia interaction, *Geophys. Res. Lett.*, 17, 2653-2656.

Reilinger R.E., McClusky S.C., Oral M.B., King R.W., Toksoz M.N., Barka A.A., Kinik I., Lenk O. and Sanli I. 1997. Global positioning system measurements of present-day crustal movements in the Arabia-Africa-Eurasia plate collision zone, *J. Geophys*. Res., 102, 9983-9999.

Rontogianni S., Konstantinou N.S., Melis C.P. Evangelidis Slab stress field in the Hellenic subduction zone as inferred from intermediate-depth earthquakes (2011), *Earth, Planets and Space*, 63 (2), 139-144.

Taymaz T., Jackson J.and McKenzie D. 1991. Active tectonics of the north and central Aegean Sea, *Geophys*. J. Int., 106, 433–490.

Yilmazturk A. and Burton P.W. 1999. Earthquake source parameters as inferred from body waveform modeling, southern Turkey, J. *Geodynamics*, 27, 469-499.

Δελτίο της Ελληνικής Γεωλογικής Εταιρίας, τομ. XLVII , 2013
Πρακτικά 13ου Διεθνούς Συνεδρίου, Χανιά, Σεπτ. 2013

Bulletin of the Geological Society of Greece, vol. XLVII 2013
Proceedings of the 13th International Congress, Chania, Sept. 2013

THE GEOTECTONIC EVOLUTION OF OLYMPUS MT. AND ITS MYTHOLOGICAL ANALOGUE

Mariolakos D.I.[1] and Manoutsoglou E.[2]

[1] National and Kapodistrian University of Athens, Faculty of Geology and Geoenvironment, Department of Dynamic, Tectonic & Applied Geology, Panepistimioupoli, Zografou, GR 157 84, Athens, Greece, mariolakos@geol.uoa.gr

[2] Technical University of Crete, Department of Mineral Resources Engineering, Research Unit of Geology, Chania, 73100, Greece, emanout@mred.tuc.gr

Abstract

Mt Olympus is the highest mountain of Greece (2918 m.) and one of the most important and well known locations of the modern world. This is related to its great cultural significance, since the ancient Greeks considered this mountain as the habitat of their Gods, ever since Zeus became the dominant figure of the ancient Greek religion and consequently the protagonist of the cultural regime. Before the generation of Zeus, Olympus was inhabited by the generation of Cronus.

In this paper we shall refer to a lesser known mythological reference which, in our opinion, presents similarities to the geotectonic evolution of the wider area of Olympus.

According to Apollodorus and other great authors, the God Poseidon and Iphimedia had twin sons, the Aloades, namely Otus and Ephialtes, who showed a tendency to gigantism. When they reached the age of nine, they were about 16 m. tall and 4.5 m. wide. Having then realized their powers, because of their gigantic proportions, they decided to climb Olympus and fight the Gods, exile Zeus and the others, and wed two Goddesses. Otus was to marry Hera and Ephialtes Artemis.

But they did not know how to climb such a high mountain, so they decided to construct a "ladder", by putting mount Ossa on top of mount Olympus and mount Pelion on top of Ossa. This description coincides with the geological and tectonic evolution of the wider Olympus area. But, these complex tectonic processes were completed about 8 – 10 m.a., i.e. millions of years before the appearance of humans, therefore it is impossible that these morphotectonic processes were witnessed by man, so the similarities between the myth of Aloades and the tectonic evolution of the area must be purely coincidental. But are they, or is there more here?

Key words: *Aloades, Otus, Ephialtes, Pilion, Ossa.*

Περίληψη

Ο Όλυμπος, το υψηλότερο όρος της Ελληνικής Χερσονήσου (2918 μ.) είναι ένας από τους πιο γνωστούς τόπους στο σύγχρονο κόσμο, επειδή εδώ οι αρχαίοι Έλληνες είχαν τοποθετήσει την κατοικία των θεών τους, από τότε που ο Δίας έγινε η κυρίαρχη προσωπικότητα της αρχαιοελληνικής θρησκείας. Στην εργασία αυτή θα αναφερθούμε σε μια αναφορά της Ελληνικής μυθολογίας που παρουσιάζει μεγάλες ομοιότητες με την γεωτεκτονική εξέλιξη του Ολύμπου.

Δελτίο της Ελληνικής Γεωλογικής Εταιρίας, τομ. XLVII , 2013
Πρακτικά 13ου Διεθνούς Συνεδρίου, Χανιά, Σεπτ. 2013

Bulletin of the Geological Society of Greece, vol. XLVII 2013
Proceedings of the 13th International Congress, Chania, Sept. 2013

THE GEOTECTONIC EVOLUTION OF OLYMPUS MT. AND ITS MYTHOLOGICAL ANALOGUE

Mariolakos I.D.[1] and Manoutsoglou E.[2]

[1] National and Kapodistrian University of Athens, Faculty of Geology and Geoenvironment, Department of Dynamic, Tectonic & Applied Geology, Panepistimioupoli, Zografou, GR 157 84, Athens, Greece, mariolakos@geol.uoa.gr

[2] Technical University of Crete, Department of Mineral Resources Engineering, Research Unit of Geology, Chania, 73100, Greece, emanout@mred.tuc.gr

Abstract

Mt Olympus is the highest mountain of Greece (2918 m.) and one of the most important and well known locations of the modern world. This is related to its great cultural significance, since the ancient Greeks considered this mountain as the habitat of their Gods, ever since Zeus became the dominant figure of the ancient Greek religion and consequently the protagonist of the cultural regime. Before the generation of Zeus, Olympus was inhabited by the generation of Cronus.

In this paper we shall refer to a lesser known mythological reference which, in our opinion, presents similarities to the geotectonic evolution of the wider area of Olympus.

According to Apollodorus and other great authors, the God Poseidon and Iphimedia had twin sons, the Aloades, namely Otus and Ephialtes, who showed a tendency to gigantism. When they reached the age of nine, they were about 16 m. tall and 4.5 m. wide. Having then realized their powers, because of their gigantic proportions, they decided to climb Olympus and fight the Gods, exile Zeus and the others, and wed two Goddesses. Otus was to marry Hera and Ephialtes Artemis.

But they did not know how to climb such a high mountain, so they decided to construct a "ladder", by putting mount Ossa on top of mount Olympus and mount Pelion on top of Ossa. This description coincides with the geological and tectonic evolution of the wider Olympus area. But, these complex tectonic processes were completed about 8 – 10 m.a., i.e. millions of years before the appearance of humans, therefore it is impossible that these morphotectonic processes were witnessed by man, so the similarities between the myth of Aloades and the tectonic evolution of the area must be purely coincidental. But are they, or is there more here?

Key words: *Aloades, Otus, Ephialtes, Pilion, Ossa.*

Περίληψη

Ο Όλυμπος, το υψηλότερο όρος της Ελληνικής Χερσονήσου (2918 μ.) είναι ένας από τους πιο γνωστούς τόπους στο σύγχρονο κόσμο, επειδή εδώ οι αρχαίοι Έλληνες είχαν τοποθετήσει την κατοικία των θεών τους, από τότε που ο Δίας έγινε η κυρίαρχη προσωπικότητα της αρχαιοελληνικής θρησκείας. Στην εργασία αυτή θα αναφερθούμε σε μια αναφορά της Ελληνικής μυθολογίας που παρουσιάζει μεγάλες ομοιότητες με την γεωτεκτονική εξέλιξη του Ολύμπου.

Σύμφωνα με τον Απολλόδωρο, η Ιφιμέδεια, που ήταν παντρεμένη με τον Αλωέα, απέκτησε με τον Ποσειδώνα δύο γιους, τον Ώτο και τον Εφιάλτη, που τους ανέθρεψε ο Αλωεύς, γι' αυτό και πήραν το όνομα «Αλωάδες». Οι δύο αυτοί γιοι του Ποσειδώνα είχαν τάσεις γιγαντισμού, με αποτέλεσμα όταν έγιναν εννέα ετών να έχουν αποκτήσει εννέα πήχες πλάτος και εννέα οργιές ύψος (≈ 16 μ.). Συνειδητοποιώντας τις διαστάσεις και τις δυνάμεις τους, αποφάσισαν να ανέβουν στον Όλυμπο, να διώξουν τον Δία και τους άλλους θεούς, και να γίνουν κυρίαρχοι του κόσμου. Για να ανέβουν στον Όλυμπο αποφάσισαν να κατασκευάσουν μια κλίμακα, τοποθετώντας το Πήλιο πάνω στην Όσσα και αυτήν πάνω στον Όλυμπο, ενώ παράλληλα άρχισαν να μετατρέπουν τμήματα της ξηράς σε θάλασσα κ.λπ.
Η περιγραφή αυτή του Απολλόδωρου συμπίπτει με την γεωλογική και τεκτονική δομή και εξέλιξη του Ολύμπου που, ως γνωστό, αποτελεί ένα τεκτονικό παράθυρο, αφού λόγω αναθόλωσης, έχουν διαβρωθεί οι ενότητες της Όσσας και του Πηλίου που είχαν επωθηθεί. Όλες αυτές οι διεργασίες όμως είναι πολύ παλαιότερες από την εμφάνιση του ανθρώπινου γένους και συνεπώς ο άνθρωπος δεν μπορεί να υπήρξε μάρτυρας αυτών. Άρα πρόκειται για απλή σύμπτωση. Είναι όμως;
Λέξεις κλειδιά: *Αλωάδες, Ώτος, Εφιάλτης, Πήλιο, Όσσα.*

1. Introduction

Mountains as physiogeographical units are among the most significant factors that shaped the Greek civilization. Many features of Greek civilization and its historical development are related to these Mountains and their geographical distribution.

In Greek Mythology and according to Theogony of Hesiod (8th-7th century BC) the Gaia (Earth) gives initially birth to Uranus, who protects Gaia by covering her from all sites, and afterwards shapes her form by giving birth to the Mountains (Ούρεα). That is why Sophocles (496-406 BC) describes Gaia as "..Mountainous who feeds everything", (Ορεστέρα παμβώτι Γα, Φιλ. 394).

Although the Greek Mountains are not very high, their predominance in the landscape couldn't be ignored by the Greeks and their Mythology. The Greek Mountains, not only were not hostile against humans, but they also hosted the Gods of Ancient Greeks. The Mountains do not cause natural disasters like the rivers with their flooding, or the Sea when she is "enraged" and particularly with her climate-related eustatic level rises that deprived large and fertile lands from the pre-historic humans. The Mountains are hostile only to those that climb them under adverse conditions. According to Theogony of Hesiod (8th-7th century BC) but also other ancient sources, the Mountains are not personified, as it happens with rivers. Although there are some exceptions, like Mt Olympos and Mt Kissavos who according to later folk poetry "were fighting". Why these Mountains are "fighting" is something that needs further investigation.

One of the interpretations relates to the flow of Peneios river through the Tempe Valley in conjunction to, or as a result of, an earthquake event. In this case the rockfalls from both Mountains would have had been a tremendous physiogeological process, and together with the produced noise, it should definitely have left traces in the historical memory of the pre-historic settlers of the area; as it is well established the area has been occupied continuously from the Pre-historic times from tools that were discovered in the Peneios terraces (Schneider, 1968, 1979). However and beyond the initiation of Peneios flow, the whole area is tectonically active and hence every earthquake, even of small magnitude, would have been accompanied by rockfalls.

According to the Authors' opinion, the most important reason that the Mountains were not personified is attributed to the fact that the Mountains do not "intervene" and do not disturb human lives. Any impact seems to be a result of a passive interaction.

Mt Taygetus for example is a morphotectonic structure, an outcrop, which due to its volume and height, prevents the contact among inhabitants of the Eurotas Valley of Lakonia and of Messinian plain. This situation though is passive and does not alter. The Mountains are indeed dynamic systems since their formation is controlled by large boundary faults, which in most cases are seismogenic. Such re-activations though, do not occur daily or periodically every year. A marginal neotectonic active fault can be actually inactive for many thousand years.

On the contrary, the rivers, beyond the fact they are essential for the daily human survival, they represent rather dynamic physiogeographic systems, which display annual periodicity. River dynamics are so intense both in terms of lateral distribution and flow that have an immanence and direct impact on human lives. How many times we do not hear for humans being drowned after a thunderstorm due to river floods? The river Kephissos for example, displays totally dry periods, during which humans and farming are endangered by drought, alternating with wet periods after heavy rains, when it is not unusual for the water to escape the embankments and cause casualties among people and animals. Hence, it is absolutely reasonable to refer often to Kephissos, and its tributaries or to Ilissos and Asopos rivers. Why is it necessary to refer to Mt Aegaleo, the small mountain that crops close and north of Kephissos river? The mountains of Aegaleo or Hymettus do not disturb the pre-historic humans. Therefore, only rivers where personified and not the mountains.

The great Goddess Gaia (Γαία) – our Mother Earth – created the mountains and left them quietly, so that they can deliver only prosperous goods to the humankind; it is in the mountains that humans hunt, it is there that water springs, there are the caves to protect us, and there we can find timber and metals to develop our societies.

The Mountains however, played an additional important role in the cultural development of the pre-historic civilizations. Due to the Mountains height and thus being closer to the skies, they were, and still are, the places where humans try to get in touch with the Gods; particularly when the apexes are within the clouds.

Therefore, the twelve Gods had their residence in Mt Olympus, the highest Greek Mountain.

After all, Zeus was born in a mountain, which according to the tradition is Mt Dicte, and was raised on a different mountain, that of Mt Ida (Ιδαίο Άντρο, Cave of Zeus) both in Crete island. In a different version, Zeus was born in Arcadia in Peloponnese and not in Crete, but still on a mountain, that of Mt Lycaeus, with its apex called Cretaea; there according to the Myth Rhea gave born to Zeus.

2. Mt Olympus

Mt Olympus (+ 2918 m) is the highest mountain of Greek Peninsula and one of the most important and well known places of the modern world.

This results from its enormous cultural value, since here the ancient Greeks placed the residence of the twelve Gods, from the time that Zeus set aside the firstborn Poseidon, and became the Ruler of the ancient Greek Religion, and subsequently the Leader of the mainstream cultural development, not only of the Historic but also for a large timespan into the Pre-historic Period.

Everything was virtually starting off and ending in Mt Olympus; there were the most important decisions taken, and there was the ethos and ethics of the ancient Greek world developed. Mt Olympus was actually the decision-making center during the course of the Pre-Historic humans.

Nevertheless, Mt Olympus was not the God's Residence from the beginning, due to the fact that it couldn't sustain life during the ice ages, since it was covered with snow or ice during the period before the climatic Optimum of the Holocene.

As a result Mt Olympus must have been declared as “Heaven Residence” once the ice retreated and melted. Zeus, as a God of the Eastern Mediterranean cannot reside in a place covered by ice. Zeus is not a God of Northern Europeans; He is a God of the Aegean.

And this is the main reason that Mt Olympus is not the birth place of any significant God. Poseidon for example was born in the hillsides of Mt Alisio opposite the village of Nestani, in Mutinia (Arcadia).

Olympus should have become the God’s Residence when the climate ameliorated significantly and the conditions were similar to nowadays. This took place approximately 6,000 y BP. The period between 6-4 ky BP, known as Holocene Climatic Optimum, coincides also to the end of the Neolithic Era and the beginning of the Copper Age.

Mt Olympus of Macedonia (N. Greece), is the residence of Zeus, as well as the residential place of all Gods, hence it is termed “Heaven Residence” («Ουράνια Κατοικία»). Mt Olympus has a central role in Greek Mythology, as it is the location where Zeus throws away Hephaestus, when the later wants to intervene in favour of Hera. From Olympus Zeus throws his lightning against the Titans, and it is there that he decides upon the fates of Achilles and Hector. Moreover, Mt Olympus was the residence of Cronus that was the leader of the Titans generation.

Other mountains of the same name occur in Elis, Arcadia, Attica, etc.

Mountains with this name exist in many other parts of the world, such as in the State of Washington in the USA. The name of that Mountain was envisioned by the first Greek who arrived in the area, after Columbus, Juan de Fuca (Ioannis Fokas) from Cephalonia.

Mountains named Olympus exist elsewhere also, as for example in Cilicia of Asia Minor, in nowadays Turkey. In an effort to prove that the cradle of Western Civilization lies in Turkey various parties claim that the “Heaven Residence” is not located in Mt Olympus in Macedonia of Greece but in Mt Olympus of Cilicia. However, these claims are at least groundless, since they fail to explain how the Twelve Gods could fight against the Titans during the War of Titans (Titanomachy), who were located in Mt Othrys, from an Olympus too far away like the one in Cilicia.

2.1. Designation of Mt Olympus Name

Markos Mousouros (1470-1517), a great scholar and professor during the Renaissance, in his dictionary “Etymologicum Magnum Lexikon" mentions that the name Olympus means the Sky (Ουρανό) and the very high Mountains, and it derives from the word "ολολαμπής" that reflects to the Sky or from the phrase "ολλύειν τους ώπας δια του κρύους" (meaning “infects the ears from the cold”) that suits to the mountains.

The German philologist and linguist Georg Curtius (1820-1885), in his book "Grundzüge der Griechishen Etymologie", mentions that the word Olympus (Όλυμπος) derives from the root –λαμπ (lamp) – which is interpreted as “bright” or “white” (he considers the letter «υ» being Aeolic).

The linguist and writer Menos Filintas (1870-1934) in his book "Glossognosia and Glossographia Hellenic" rejects the derivation of the word “Olympus” from the root –λαμπ-ω (lamp –ing) and argues that many names of mountains, rivers and general location of ancient Greece is of Semitic origin, such as Helicon, Elatia, Alpheus, Aliakmon etc. and have as first syllable the Semitic article EL or AL. According to M. Filinta the words Olympus or Oulympos, are of Semitic origin quoting the words ULUWEN - ULUEN or ULU, meaning “tall”, and the words BAS or BOS that mean “power” and actually the “divine”. Hence, ULUENBAS or ULUBOS - Oulympos - Olympus (Όλυμπος) means “at high altitude” or “power”, meaning “soaring” or “heavenly power”, “divine power” the “supreme power”. In many places additionally to the name Olympos the ancient Elympos name has been preserved in the collective memory.

Archaeologist Eutychia Poulaki during a presentation in 1985 in the series "Archaeologists discuss about Pieria" argued that the form of the word reveals a pre-Hellenic origin that means mountain or sky. And this is the reason that the name still exists in other places –apart the Divine Olympus in Macedonia – in Greece but also in Cyprus, Ionia, Bithynia, Lycia.

It is however, absolutely certain that the residence of Zeus and the other Gods during the ancient times was Mt Olympus in Pieria (Macedonia, Greece) as it is clearly identified within the first and most well-known written document of the Greek Language, the Iliad of Homer.

The Academician Agapitos Tsompanakis, in his presentation in 1995, during the "2nd Conference on Olympus" suggested that "Olympus" meant high mountain, and that wherever the Aeolians went, e.g. in Bithynia, the high mountains were called "Olympus".

In the wider Aegean there are many mountains with that name. The most famous and glorious though is the one that stands on the border between Macedonia and Thessaly.

The largest and highest mountain on planet Mars has also been named "Olympus",. It is the largest in our Solar System, with a height of 24,000 feet above the surface that surrounds it, and with a diameter of more than 500 km.

3. The Mythology

As expected, Mt Olympus is repeatedly referred in the Greek Mythology. Perhaps today is the most famous mountain in the world, along with the Himalayas because of Mt Everest, and Mount Sinai, because of its direct connection to the Jewish initially and the Christian religion afterwards, as is the place where God gave the Ten Commands to Moses.

But certainly Olympus was the most famous in antiquity, especially during the Pre-Historic Period, and of course long before the Exodus of the Jews from Egypt. And this is supported by the fact that the Gods of the ancient Greeks must have inhabit Mt Olympus since the Holocene Climatic Optimum (i.e. approx. 4,000 BC), meaning a few thousand years prior to the birth of Moses.

Indeed, taking into consideration that Mt Olympus, prior to the Twelve Gods, was the home of the Titans, then Mt Olympus is probably the oldest mountain Gods lived.

In this paper however, we will refer to a largely unknown mythological reference, which in our opinion, represents similarities to the geotectonic evolution of the wider area of Mt Olympus.

3.1. The Aloades (Οι Αλωάδες)

According to Apollodorus (Book. 1.7.4) and other great writers, the great God Poseidon acquired from Iphimedeia two sons, Otus and Ephialtes. Iphimedeia, was married to Aloeus, who was also a son of Poseidon. Iphimedeia however, who had fallen in love with Poseidon, walked many times to the seaside and taking water with her palms from the waves, she was throwing it once in her chest and sometimes in her vagina. In the end, Poseidon responded to her love and gave her the above mentioned two sons, whom Aloeus raised; hence they were named after him as Aloades.

Otus and Ephialtes, however, were prone to gigantism, that is why every year they grew a cubit wide and a fathom in height. At the age of nine they became nine cubits wide and nine fathoms high, i.e around 16m tall. Having realized their forces, due to their gigantic dimensions, and knowing that the center of decisions was Mt Olympus, home of the Twelve Gods, they decided to climb Mt Olympus and, after fighting with the Gods, to persecute Zeus and the others and take over the kingdom of heaven as well as the God's wives, for Otus he wanted Hera, and for Ephialtes he wanted Artemis. How would they climb Mt Olympus though, such a high mountain?

To climb they decided to set Mt Ossa on Olympus and Mt Pelion on Mt Ossa. In this way, they constructed a ladder. Simultaneously, they were thrown into the sea other mountains so that to

transform the sea to land, whereas other land parts they transformed them to sea. Thus, began a war that rocked the Gods (Table 1, in greek).

Nowadays the above described story is regarded as figments of the imagination, and certainly, according to the modern science of Geology, as geologists, we cannot imagine that the activities of Otus' and Ephialtes', may symbolize any geodynamic processes.

But, quite coincidentally (?), the description of the myth coincides with the geological and the tectonic structure of the regional Mt Olympus area, particularly the area between the mountains Olympus, Ossa and Pelion. Let's see how this occurs in more detail.

Table 1 **- Apollodorus (Book. 1.7.4).**

… Κανάκη δὲ ἐγέννησεν ἐκ Ποσειδῶνος Ὁπλέα καὶ Νιρέα καὶ Ἐπωπέα καὶ Ἀλωέα καὶ Τρίοπα. Ἀλωεὺς μὲν οὖν ἔγημεν Ἰφιμέδειαν τὴν Τρίοπος, ἥτις Ποσειδῶνος ἠράσθη, καὶ συνεχῶς φοιτῶσα ἐπὶ τὴν θάλασσαν, χερσὶν ἀρυομένη τὰ κύματα τοῖς κόλποις ἐνεφόρει. συνελθὼν δὲ αὐτῇ Ποσειδῶν δύο ἐγέννησε παῖδας, Ὦτον καὶ Ἐφιάλτην, τοὺς Ἀλωάδας λεγομένους. οὗτοι κατ᾽ ἐνιαυτὸν ηὔξανον πλάτος μὲν πηχυαῖον μῆκος δὲ ὀργυιαῖον· ἐννέα δὲ ἐτῶν γενόμενοι, καὶ τὸ μὲν πλάτος πηχῶν ἔχοντες ἐννέα τὸ δὲ μέγεθος ὀργυιῶν ἐννέα, πρὸς θεοὺς μάχεσθαι διενοοῦντο, καὶ τὴν μὲν Ὄσσαν ἐπὶ τὸν Ὄλυμπον ἔθεσαν, ἐπὶ δὲ τὴν Ὄσσαν θέντες τὸ Πήλιον διὰ τῶν ὀρῶν τούτων ἠπείλουν εἰς οὐρανὸν ἀναβήσεσθαι, καὶ τὴν μὲν θάλασσαν χώσαντες τοῖς ὄρεσι ποιήσειν ἔλεγον ἤπειρον, τὴν δὲ γῆν θάλασσαν, ἐμνῶντο δὲ Ἐφιάλτης μὲν Ἥραν Ὦτος δὲ Ἄρτεμιν.	… Canace had by Poseidon Hopleus and Nireus and Epopeus and Aloeus and Triops. Aloeus wedded Iphimedia, daughter of Triops; but she fell in love with Poseidon, and often going to the sea she would draw up the waves with her hands and pour them into her lap. Poseidon met her and begat two sons, Otus and Ephialtes, who are called the Aloads. These grew every year a cubit in breadth and a fathom in height; and when they were nine years old, being nine cubits broad and nine fathoms high, they resolved to fight against the gods, and they set Ossa on Olympus, and having set Pelion on Ossa they threatened by means of these mountains to ascend up to heaven, and they said that by filling up the sea with the mountains they would make it dry land, and the land they would make sea. And Ephialtes wooed Hera, and Otus wooed Artemis;

4. Geological Structure of Mt Olympus

From a geological point of view, Mt Olympus, represents a complex Alpine geological and tectonic structure. The term Alpine Structure characterises both the type of the rocks and the palaeogeographical depositional setting but also the metamorphic events, and the tectonic deformation and evolution.

Mt Olympus, the greatest tectonic window of Greece, was first described in detail by Godfriaux (1968). The Olympus geotectonic unit and comprises a continuous series of non metamorphosed to slightly metamorphosed neritic carbonate rocks, with ages ranging from Triassic to Eocene terminating in a late Eocene flysch (Kilias, 1996). Over these formations, a series of geotectonic units are emplaced, namely the HP/LT metamorphics of the Ossa Unit, and the Pelagonian Unit, which also builds Mt Pelion (Pelion Formation).

From a tectonic point of view (Figure 2), the last two geotectonic units are overthrusting each other, and more specifically Pelion Unit thrusts over Ossa Unit, and these two Units together over the first, which is the Olympus Unit of Olympus, which in Geology is termed "autochthonous", while the other two Units that have been overthrusted, we call them "allochthonous".

Today, the physiogeological processes that followed the tectonism of thrusting, particularly the gradual dome-shaped uplift of Mt Olympus, associated with faults and the subsequent erosion of

the overlying thrusting Units, led to the uncover of the “nucleus” of Olympus. This “nucleous”, which consists of rocks of the lower Units, is called "tectonic window" because it allows us to see what is inside of a geological structure.

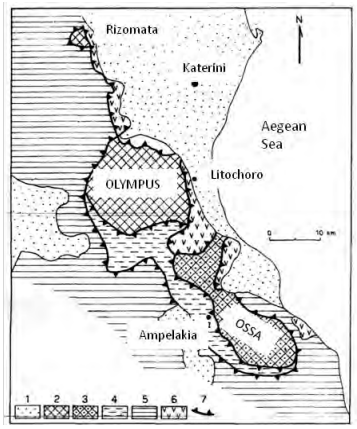

Figure 1 – Geological sketch of the wider area of the Olympus tectonic window. 1: Neogene and Quaternary deposits, 2: Autochthonous series of Olympus, 3-4: Ossa tectonic unit (3: underlain carbonate horizon, possibly analogous to the Olympus series, 4: “Ampelakia” series), 5: Pelagonian zone formations, 6: ophiolites and phyllites of the Axios zone, 7: thrusts (after Mountrakis, 1985).

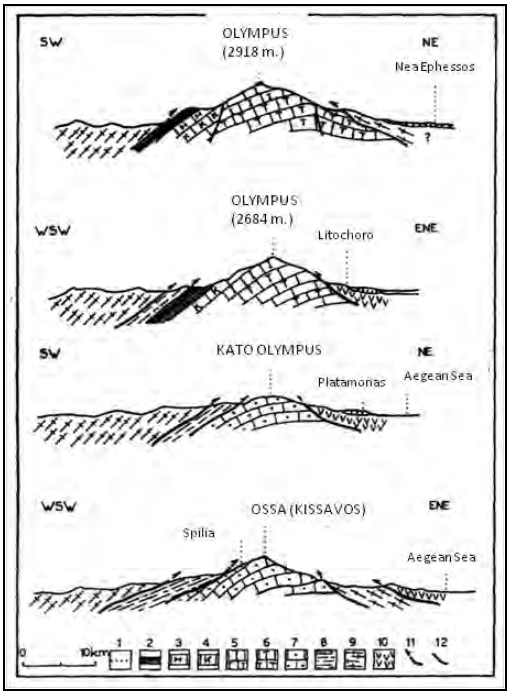

Figure 2 – Successive schematic geological sections of the Olympus – Ossa area, showing the complex nappe structure. 1: Neogene and Quaternary deposits, 2-6: 2: Autochthonous series of Olympus, 3: Eocene flysch, Eocene limestones, 4: Cretaceous limestones, 5: Jurassic limestones, 6: Triassic limestones, 7: Ossa carbonate formations, 8: “Ampelakia series”, 9: Pelagonian zone formations, 10: ophiolites, phyllites, 11: thrusts, 12: normal faults (after Mountrakis, 1985).

5. Discussion - Conclusions

These geodynamic processes, which in reality are much more complex than those described in a simplified way here and from what is shown schematically in Figures 1 and 2, belong to the oldest cycle of tectonic deformation, known as Alpine. These Alpine deformations though were completed some 8-10 My ago, meaning many millions of years before humans appeared on earth.

Therefore, the humankind could not have witnessed such morphotectonic processes. Hence, the current analogy between the activities of Aloades and the tectonic evolution of the area of Olympus should be just symptomatic.

But is it? Or is there something else?

6. Acknowledgments

The authors wish to thank the friend and colleague Dr. Stavros Kalaitzidis for his great help with the translation of the text.

7. References

Apollodorus (2nd cent. B.C.). Apanta 1, Bibliotheca, Book A, VII, 4, *KAKTOS*, Athens, 1999. (English translation by Sir James George Frazer, Loeb Classical Library Volumes 121 & 122. Cambridge, MA, Harvard University Press; London, William Heinemann Ltd. 1921,) Available online at: http://www.theoi.com/Text/Apollodorus1.html#7

Curtius G.1879. Grundzüge der Griechischen Etymologie (1858-1862, 5th ed. 1879).

Godfriaux I.1968. Étude géologique de la région de l'Olympe, *Annales Géologiques des Pays Helléniques*, 19, pp. 284.

Filintas Menos .1924. Glossognosia and Glossographia Hellenic, vol. A΄, issue 1-4, Athens, *Rallis*, 1924).

Graves R.1955. *The Greek Myths*, 2 vol. Penguin books, London.

Kilias A.1995. Tectonic Evolution of the Olympus-Ossa Mountains: Emplacement of the Blueschists Unit in Eastern Thessaly and Exhumation of Olympus-Ossa Carbonate Dome as a Result of Tertiary Extension (Central Greece), *Mineral Wealth*, 96, 7-22.

Markos Mousouros.1499. Etymologicum Magnum Lexikon

Mariolakos I. 2002. The Geoenvironmental Dimension of the Greek Mythology, *Bulletin of the Geological Society of Greece*, vol. XXXIV/6, 2065-2086, Proceedings of the 9th International Congress, Athens, September 2001

Mariolakos I. 2004.Geomythology. In Birx, J., H. (Ed.), *Encyclopedia of Anthropology*, vol. 3, 1066-1071, New York, SAGE Publ.

Migiros G.1983. Geological Study of Kato Olympos area in Thessaloniki, *Diss. Univ. Patra*, 214 p.p., Patra.

Mountrakis D.1985. The Geology of Greece, *University Studio Press*, 207 p.p. (*in greek*).

Schneider H.E. 1968. Zur quartärgeologischen Entwicklungsgeschichte Thessaliens (Griechenland), *Beiträge z. ur-u. frühgeschichtl. Archäol. d. Mittelmeer-Kulturraumes*, 6, 127 p., Bonn.

Schneider H.E. 1979. Histoire géologique du bassin néogène et quaternaire de la Thessalie, *Collection de la Maison de l'Orient méditerranéen. Série archéologique, Année 1979*, vol. 6 - No 1, pp 43-50. Available online at: http://www.persee.fr/web/ouvrages/home/prescript/article/mom_0244-5689_1979_act_6_1_1423

Δελτίο της Ελληνικής Γεωλογικής Εταιρίας, τομ. XLVII , 2013
Πρακτικά 13ου Διεθνούς Συνεδρίου, Χανιά, Σεπτ. 2013

Bulletin of the Geological Society of Greece, vol. XLVII 2013
Proceedings of the 13th International Congress, Chania, Sept. 2013

NEOTECTONIC ANALYSIS, ACTIVE STRESS FIELD AND ACTIVE FAULTS SEISMIC HAZARD ASSESSMENT IN WESTERN CRETE

Mountrakis D.[1], Kilias A.[1], Pavlaki A.[1], Fassoulas C.[2], Thomaidou E.[1], Papazachos C.[3], Papaioannou C.[4], Roumelioti Z.[3], Benetatos C.[3] and Vamvakaris D.[3]

[1] *Aristotle University of Thessaloniki, Department of Geology*

[2] *University of Crete, Natural History Museum*

[3] *Aristotle University of Thessaloniki, Department of Geophysics*

[4] *Institute of Engineering Seismology and Earthquake Engineering*

Abstract

Within the framework of this study the complicated fault system of Western Crete was napped in detail and its kinematic and dynamic setting was analysed in order to distinguish 13 major active and possible active fault zones, the seismic potential of which was assessed. Moreover, kinematic data and striations were used to estimate the corresponding stress field geometry. Two stress phases were recognized: 1st the N-S extension phase (D_1) in Mid-Upper Miocene to Lower Pliocene times forming E-W normal faults that bound the Neogene basins; 2nd the E-W extension phase (D_2) in Late Pliocene-recent times forming N-S trending active normal faults. Smaller, mainly NE-SW trending faults, with significant strike-slip component, indicate a kinematic compatibility to the D_2 phase, acting as transfer faults between larger N-S fault zones. The faults were incorporated in a detailed seismic hazard analysis together with the available seismological data, involving both probabilistic and deterministic approaches, for seismic hazard assessment of several selected sites (municipalities).

Key words: *Active deformation, seismotectonics, probabilistic approach.*

Περίληψη

Στα πλαίσια αυτής της μελέτης χαρτογραφήθηκε λεπτομερώς το πολύπλοκο σύστημα ρηγμάτων της Δυτικής Κρήτης και αναλύθηκε η κινηματική και δυναμική αυτών, με αποτέλεσμα να διακριθούν 13 μεγάλες ενεργές και πιθανά ενεργές ζώνες ρηγμάτων και να υπολογισθεί η σεισμική δυναμικότητα αυτών. Επίσης χρησιμοποιήθηκαν κινηματικοί δείκτες και γραμμώσεις ολίσθησης των ρηγμάτων για να προσδιορισθεί το πεδίο των τάσεων. Έτσι αναγνωρίσθηκαν δύο τεκτονικές φάσεις: η 1η φάση εφελκυσμού (D_1) κατά διεύθυνση Β-Ν στο Μέσο-Άνω Μειόκαινο έως Κάτω Πλειόκαινο, που προκάλεσε μεγάλα κανονικά ρήγματα παράταξης Α-Δ τα οποία οριοθετούν τις Νεογενείς λεκάνες· η 2η φάση εφελκυσμού κατά διεύθυνση Α-Δ (D_2) στο Ανώτερο Πλειόκαινο μέχρι σήμερα, προκαλώντας ενεργά κανονικά ρήγματα παράταξης Β-Ν. Παρατηρούνται επίσης μικρότερα ρήγματα παράταξης ΒΑ-ΝΔ, με σημαντική συνιστώσα οριζόντιας μετατόπισης, που δείχνουν κινηματική συμβατότητα με την D_2 φάση και λειτουρ-

γούν ως ενεργά ρήγματα μεταφοράς μεταξύ των μεγαλύτερων ενεργών ρηξιγενών ζωνών παράταξης Β-Ν. Τα ρήγματα συμπεριλήφθησαν στη λεπτομερή ανάλυση σεισμικής επικινδυνότητας, μαζί με τα διαθέσιμα σεισμολογικά δεδομένα, χρησιμοποιώντας τόσο αιτιοκρατική όσο και πιθανολογική εκτίμηση. Έτσι έγινε δυνατή η αξιόπιστη εκτίμηση της σεισμικής επικινδυνότητας για επιλεγμένες οικιστικές περιοχές (Δήμους).
Λέξεις κλειδιά: *Ενεργός παραμόρφωση, σεισμοτεκτονική, σεισμική επικινδυνότητα.*

1. Introduction

The island of Crete is situated in a fore-arc position above the active northward-directed subduction zone of the African plate beneath the Aegean lithosphere, but the seismotectonic features of the broader Aegean area are controlled by the complicated geodynamic interaction of the Aegean, Anatolian and Eastern Mediterranean lithospheres (Papazachos et al 2000). Additionaly, Crete is a structurally complicated area been strongly affected by the Alpine orogenic processes from Jurassic to present day, due to plate convergence of Eurasian and African plates and the subduction of the Tethyan oceanic crust (Bonneau 1994, Mountrakis 2006, Kilias et al 2010). Nappes stacking and compression alternate with extension, nappes collapse and exhumation of deep crustal rocks (Seidel et al 1982, Bonneau 1984, Kilias et al 1994, Fassoulas et al 1994, Jolivet et al 1996). The active deformation in Crete is revealed by the creation of new as well as the reactivation of older major faults and the occurrence of strong shallow earthquakes.

Within the framework of this study the complicated fault system of Western Crete was mapped in detail and its kinematic and dynamic setting was analysed, in order to distinguish the major active, possible and geological (inactive) fault zones. The field study was completed by the analysis of fault-slip data recognized along the main fault zones. For the calculations we employed the slickenlines orientations and fault plane data, as well as kinematic indicators to determine the slip vector and the sense of movement. Furthermore, other geological criteria were used to distinguish fault generations and different tectonic events. These results were elaborated together with the available seismological data in order to develop a seismic hazard evaluation for selected areas. For the seismic hazard analysis, both probabilistic and deterministic approaches have been used.

2. Neotectonic Analysis. Active Stress Field

The geological structure of the Crete island consists of a complicated nappes pile been stacked successively during the Alpine orogenic processes from Jurassic to Miocene times. The major compressional regime which has determined the evolution of the nappes stacking, with a SSW sense of movement, took place in Oligocene-Lower Miocene times. Compression and nappes stacking were followed during Lower-Middle Miocene by a N-S collapse, tectonic thinning and extensional exhumation of the tectonic lower nappes in a series of tectonic windows (Fassoulas et al 1994, Kilias et al 1994). During this period the first Neogene basins of the island were formed, often bordered by syn-sedimentary normal boundary faults. The extensional tectonic regime after Middle Miocene is characterized by an initial N-S sub-horizontal extension and younger neotectonic faults (Mercier et al 1989).

A detailed study of the brittle neotectonic deformation in western Crete has been realized in the framework of a large-scale seismotectonic survey for the creation of a revised neotectonic map (fig. 1) in a scale of 1:50.000 (Mountrakis et al 2012). Two distinctive stress phases were recognized, corresponding to two main brittle tectonic events in Neogene-Quaternary. The first D_1 tectonic event took place from Middle/Upper Miocene to Upper Pliocene as it affects the basins sediments of Miocene and Pliocene age, but not the younger Quaternary deposits. The major normal faults in Western Crete of E-W strike, which in some cases locally deviate to ENE-WSW and ESE-WNW, have been formed during this D_1 event. They dip mainly to the North at high angle and correspond to the initial boundary fault zones of the Neogene basins of Crete and particularly

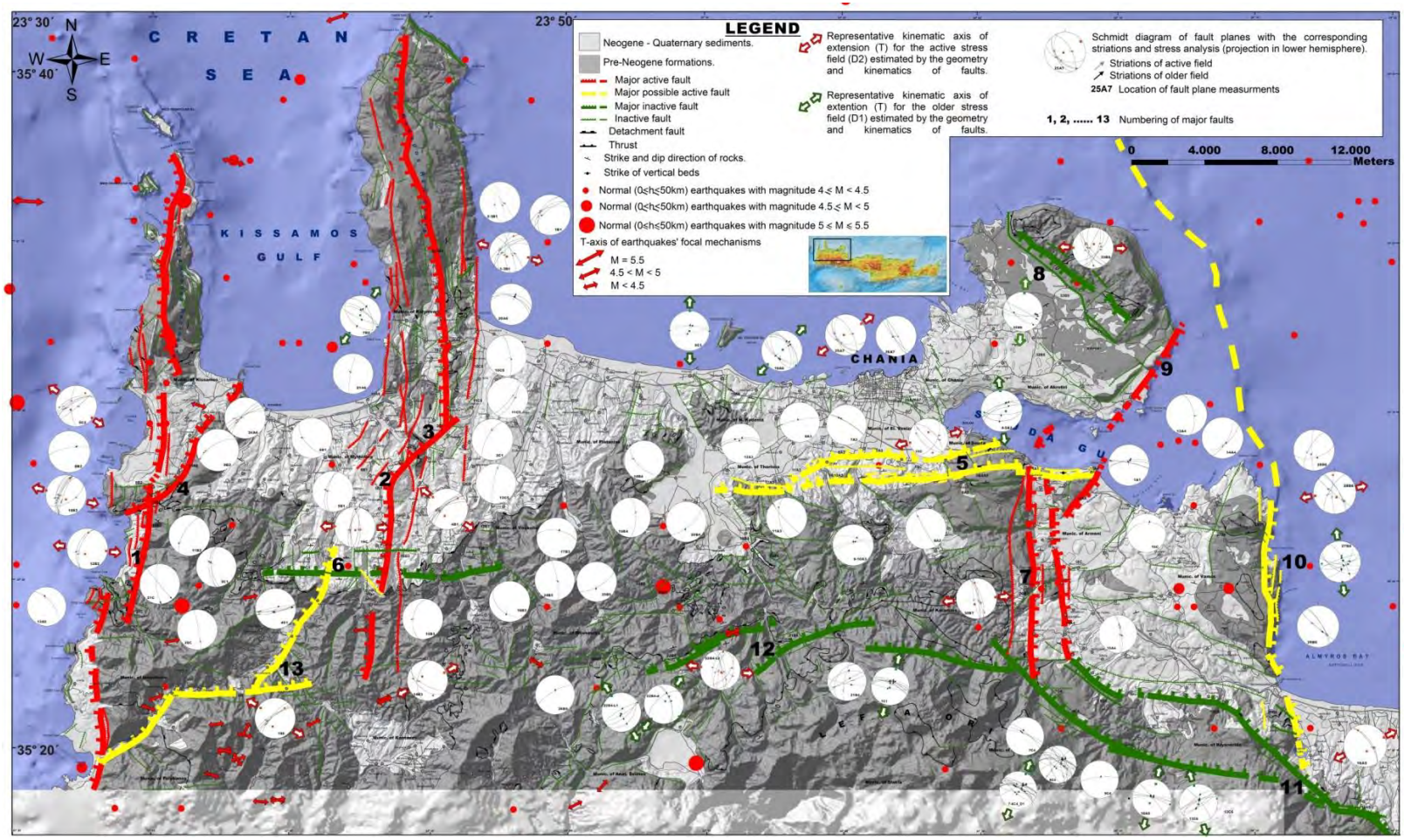

Figure 1 - Seismotectonic map of faults and surface earthquakes' epicenters of Western Crete.

in W. Crete the basins of Souda-Mournies-Agia and Georgioupoli-Vryses-Pemonia. Essentially, they represent the stage immediately following the initial Miocene expansion collapse of the nappes pile along low angle normal detachment faults, with both events showing the same dynamics and kinematics. Our results are compatible with those of the Veen & Postma (1999) for Central Crete.

The kinematic analysis of the D_1 faults shows that their fault planes present high angle dip-slip striations, dipping mostly towards the NNE to NNW. The NNW slip motion corresponds to the relatively younger one of the D_1 phase. Moreover, minor oblique normal faults trending NW-SE and NE-SW are also related to the D_1 kinematics, showing significant sinistral or dextral horizontal component of motion, respectively. Paleostress analysis for the D_1 event, using the inverse method of Angelier et al. (1982) and P-T method (Turner 1953), shows a low dipping angle minimum σ3-stress axis with a strike varying between NNE-SSW to NNW-SSE (fig. 2 & 3) for both methodes. The program Stereonett (Duyster 2000) has been used for the graphical presentation of structural data.

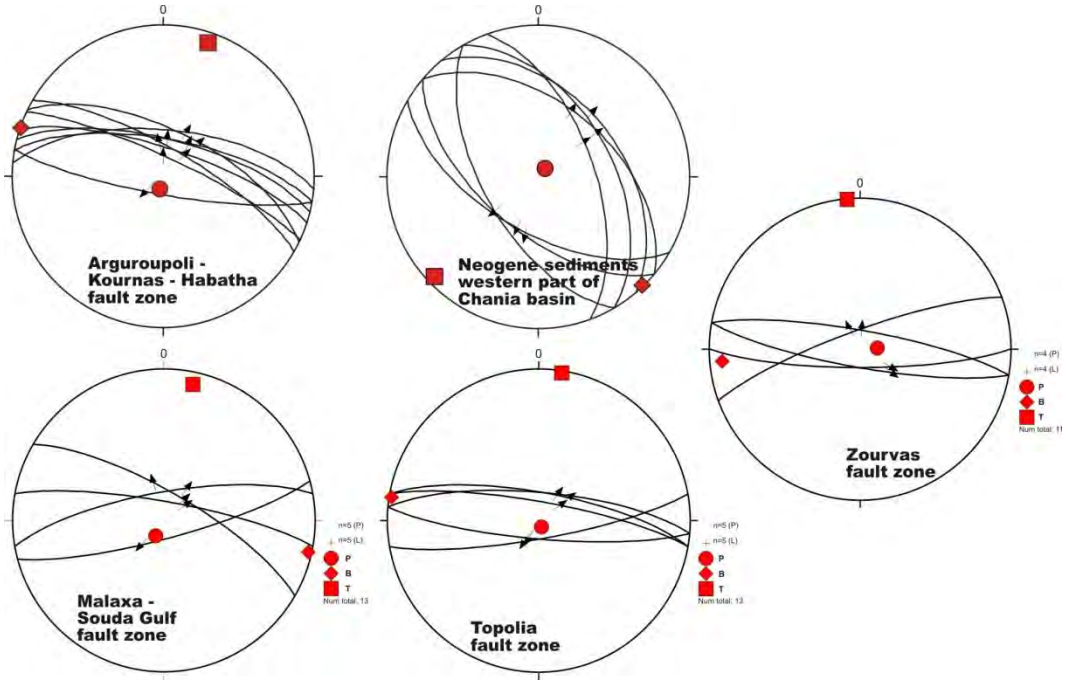

Figure 2 - Representative paleostress diagrams of $\sigma_1>\sigma_2>\sigma_3$ for the older D_1 event (lower hemisphere projection) by P-T method (Turner 1953) (see text for explanation).

The second D_2 tectonic event took place from Upper Pliocene up to present. Faults of this event overprint the previous D_1 faults, affecting usually the cataclastic fabric along the D_1 fault zones. The D_2 faults clearly affect the Pliocene sediments and have also been detected in recent Quaternary deposits, so can be characterized as active faults. They have N-S strike, varying from NNW-SSE to NNE-SSW, mostly dipping towards West. Additionaly, faults of NE-SW strike (occasionally also of NW-SE strike) are also closely related to the D_2 kinematics. These are oblique-normal faults with significant sinistral or dextral horizontal component of motion. Some of these faults seem to form major transitional rupture zones between segments of the dominant N-S faults. However, older D_1 striations are recognized on the fault surfaces of these D_2 phase oblique-normal faults, revealing a possible reactivation during D_2 tectonics, though they were initially created during the D1 event. The D_2 kinematics are also often imprinted on the older E-W D_1-faults by their reactivation as sinistral strike-slip faults, as can be derived from the horizontal

striations on their fault surface. Paleostress analysis for the D_2 tectonic event using the same methods shows a sub-horizontal minimum σ_3-stress axis, with strike ranging from WSW-ENE to WNW-ESE, with the second stress direction being the younger one. This pattern is in agreement with the active stress field along a narrow zone lying between the external NW-SW compression (due to the Eastern Mediterranean subduction under the Aegean) and the inner, back-arc ~N-S extension (e.g. Papazachos et al 1992). This narrow zone extends all the way from the Albania-Greece border and the main body of the Hellenides mountain chain up to Peloponnesus, Crete and Rhodes, following the shape of the Hellenic arc. However, its exact spatial extent is not clearly defined, since it locally exhibits partial overlapping, especially with the N-S extension area, e.g. in W. Macedonia and Epirus (Mountrakis et al., 2006).

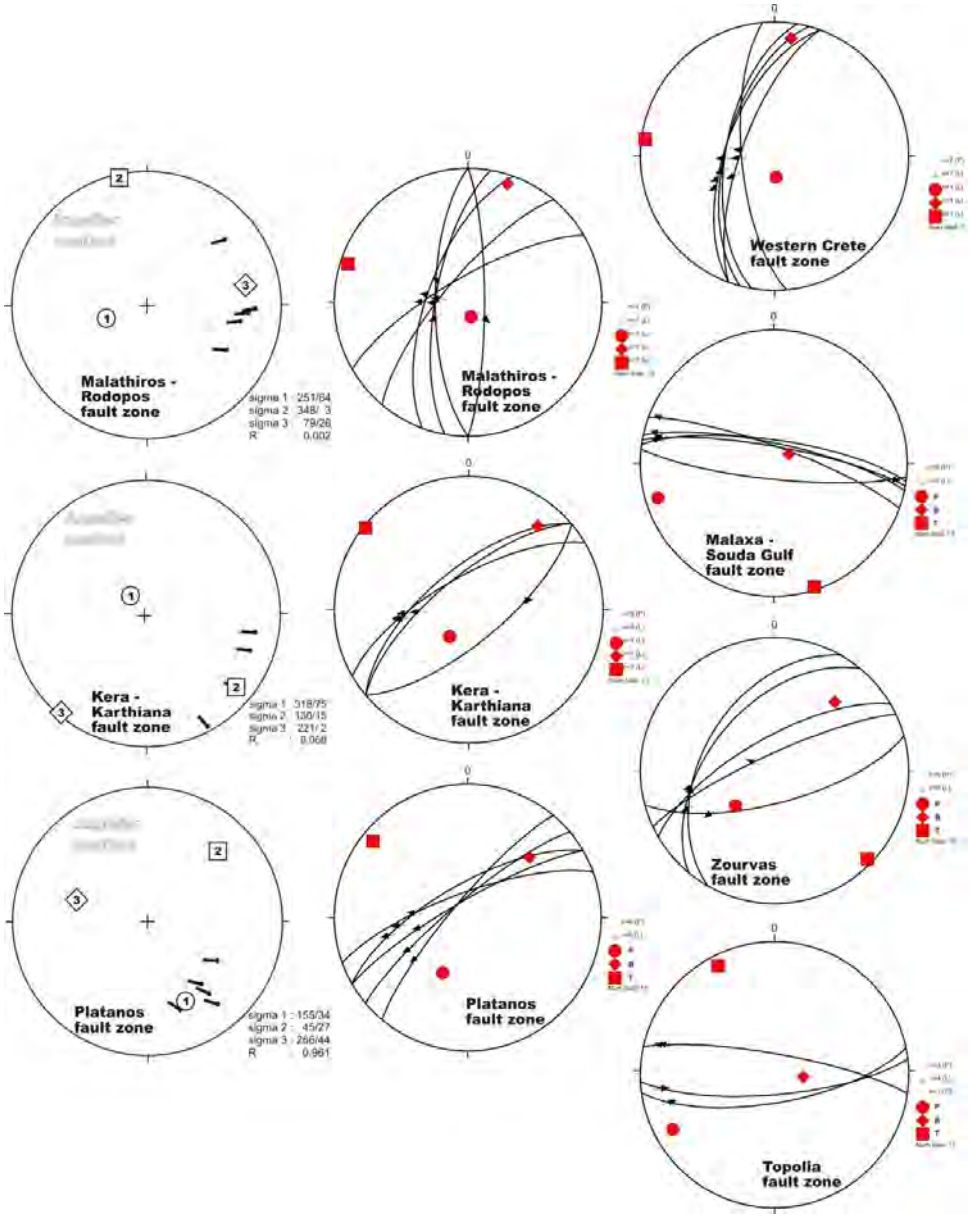

Figure 3 - Representative paleostress diagrams $\sigma_1>\sigma_2>\sigma_3$ for the D_2 event by Angelier et al. (1982) inverse method and P-T method (Turner 1953).

Correlating the active faults of the D_2 event with the available fault plane solutions of the historical-recent earthquakes ($M \geq 4.5$) in the broader study area, a very good agreement is identified, both suggesting a E-W extension regime in NW Crete mainland. The determined fault plane solutions, published by Harvad, INGV, ETH and a large number of publications, suggest a distribution of the sub-horizontal ($dip < 30^o$) principal stress axes in a consistent setting presented in figure (4). This distribution shows a clear separation of the outer arc NE-SW compression from the E-W extension regime in the NW Crete and the Kythira Island area.

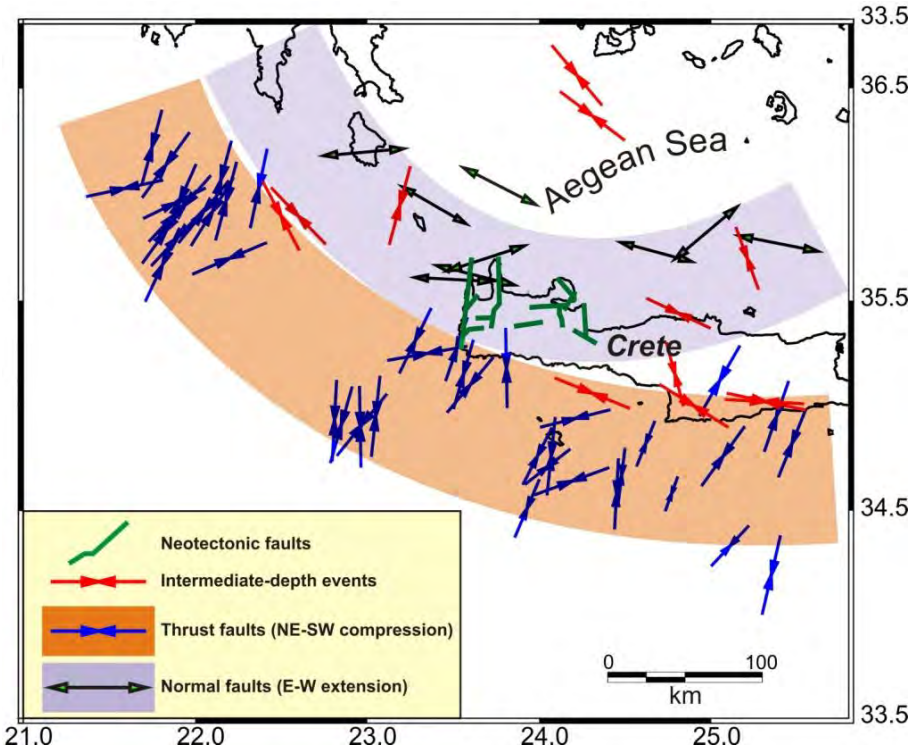

Figure 4 - Spatial distribution of the corresponding principal axes along the SW Hellenic arc, showing the clear separation of the compression area in the outer arc, with the E-W extension area along the NW Crete-Kythira area. Regional focal mechanisms, compiled from several published sources, corresponding to thrust faults along the outer Hellenic arc, intermediate-depth, strike-slip fault, with significant thrust component and normal faults have been taken into account. Intermediate-depth events exhibit a typical slab-parallel compression. The main faults mapped in this study are schematically depicted with green lines.

In order to further examine this issue, we have also collected additional fault plane solutions determined from local temporary networks installed in W. Crete or the broader area (Besnard, 1991; Chabalier et al., 1992; Hatzfeld et al., 1993; Jost et al., 2002). The corresponding distribution is presented in fig. (5a), including mainly small events with M in the range -0.2 to 3.8. The corresponding principal sub-horizontal extension axes distribution is quite consistent (fig. 5b), showing a dominant E-W extension. Using the resulting distribution, an average σ_3 extension axis was determined using the stress-tensor inversion method of Gephart and Forsyth (1984) and the average moment-tensor method of Papazachos and Kiratzi (1992). These results, also presented in fig. (5b), verify: a) The presence of an active E-W to WNW-ESE extension in W. Crete (compatible with the D_2 phase recognized from active faulting) and, b) the spatial extent of the extension regime, which covers the whole W. Crete mainland, showing that the E-W extension controls the upper crustal deformation pattern throughout the whole study area.

3. Active Faults Seismic Hazard Assessment

The D_2 major normal faults of N-S strike are compatible with the active stress-field of E-W strike and certainly display clear indications of recent activity on the basis commonly accepted geological criteria, hence they were considered as active or possible active faults. Even more some of the D_1 major normal faults of E-W or ENE-WSW strike, which are not optimally oriented with respect to the active stress-field, display indications of recent activity, operating as strike-slip faults, with the earthquake information being compatible with the strike E-W of some D_1-faults mapped in the field. These results verify that some of the major normal E-W trending faults of the D_1-phase reactivated as strike-slip faults under the E-W extensional regime of D_2 phase even in recent times. Thus finally, in W. Crete 13 major faults were identified, which exhibit clear activation or reactivation in Quaternary-recent times (Mountrakis et al., 2012). These faults numbered 1 to 13 in the seismotectonic map (fig. 1) and were distinguished as active or possible active faults. Their seismic potential was assessed on the basis of the relation logL=0.51*M-1.85 (Papazachos 1989) relating the moment magnitude, M, of the maximum expected earthquake with the total length, L, of the fault. These most important faults in W. Crete are the following:

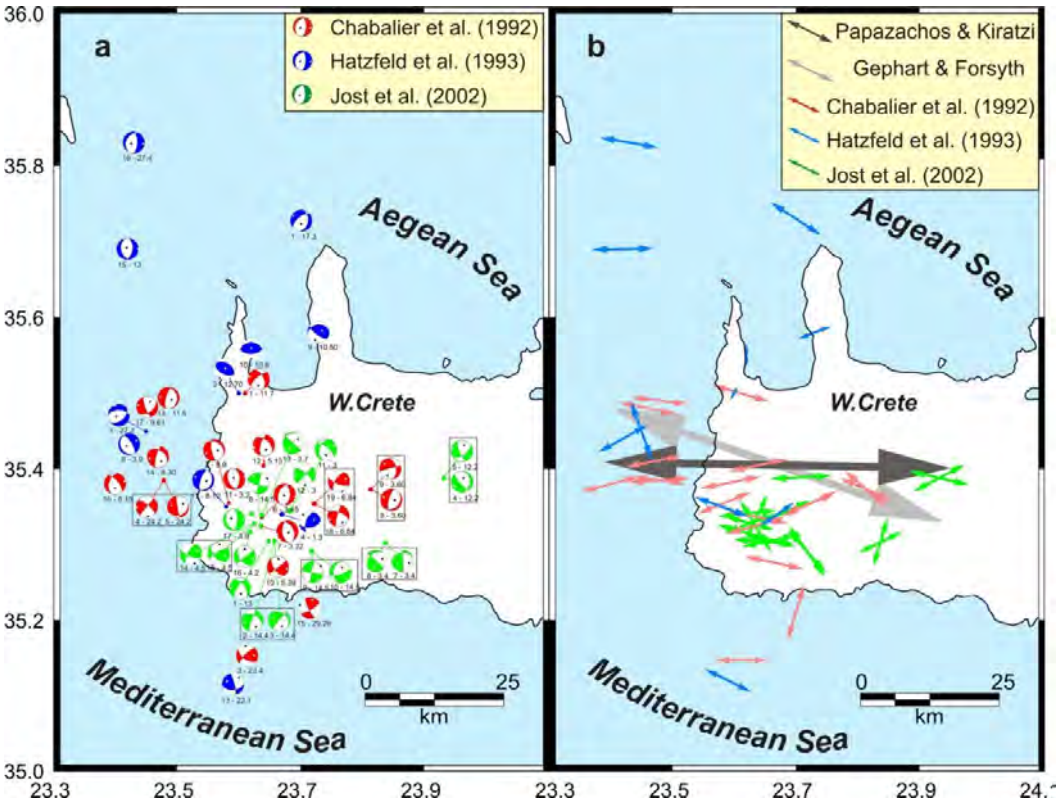

Figure 5 - a) Fault plane solutions for small-magnitude events in Western Crete. b) Spatial distribution of the corresponding principal extension axes. The average stress, computed with the methods of Gephart and Forsyth (1984) and Papazachos and Kiratzi (1992) are also presented with large grey and black arrows respectively.

1. The fault of Western Crete is an active rupture zone with a total length of 65 km and a N-S strike, dipping to the west. Its maximum expected earthquake magnitute is M=7.2. However the fault is displaying a spatial segmentation, probably suggesting its segmented activation with events of M=5.6 to 5.7 according to the partly length of the segments Gramvousa (11 km), Falasarna-Sfinari (11 km) and Kampos-Stomion (10 km). **2. The fault of Malathiros-Rodopos** is also a

large (30 km) active fault zone (trend N-S, dip W), composed by three main segments: the Rodopos (18 km), Malathyros (9 km) and Kera (4 km). The last represents a rather dextral transfer fault between the other two segments. The maximum expected earthquake magnitude is 6.5, while the segmented activation corresponds to magnitudes M-6,1 and 5.5 respectively. **3. The Kera-Karthiana** transfer active fault between the Malathiros-Rodopos segments, trends NE-SW and dips to NW. Its maximum expected earthquake magnitute is M=5.0. **4. The fault of Platanos (**trend NE-SW, dip NW) overprints the Western Crete fault. It's characterized as a lateral-normal active fault with a significant sinistral horizontal component of motion. Its total length ~10 km corresponds to a maximum magnitude of M=5.6 with its sub-segments resulting of M=5.2 and 4.8. **5. The Malaxa-Souda's Gulf possibly active fault** is a rupture zone, (E-W strike, dip N) which forms the tectonic graben of Souda's Gulf-Mournies-Myloniana. Two main slip patterns were observed on the fault surfaces: The older one corresponds to a dip-slip motion, linked to the D_1 extension and the younger to a mainly sinistral horizontal strike-slip motion related to the D_2 extensional event. The length of the fault (22 km) corresponds to a maximum magnitude of M=6.2. **6. The Topolia fault zone** of 10 km length (trend E-W, dip N) is related to the D_1 event. However, younger striations on its fault surfaces show an important strtike-slip motion compatible to D_2 kinematics of U. Pliocene-Quaternary times. **7. The Zacharias-Pemonia active fault,** (trend N-S, dip E) is composed by a system of parallel fault brances, successive tectonic terraces, and surface openings. Its total length is 11 km, resulting in a maximum magnitude of M=5.7. **8. The Akrotiri fault zone** (trend NW-SE, dip SW) is composed by pallel faults in a characteristic "doublex" structure. The kinematics of the fault (oblique downwards sense of slip) indicate that it was activated during D_2 event. **9. The Marathi active fault** (trend NE-SW, dip SE) continues beyond Souda's Gulf and is also recognized in the Ancient Aptera archaeological site. Its length (~12 km) corresponds to a maximum magnitude M=5.7. **10. The Drepanokefala – Georgioupoli possibly active fault zone,** (trend N-S, dip E) is composed by parallel fault segments, has a total length of ~12 km corresponding to a maximum magnitude M=5.8. **11. The Argiroupoli-Kournas-Habathas fault zone,** (trend NW-SE, dip NE) has a total length of 20 km. Two slip patterns were observed on its fault planes: the first corresponds to the D_1 event and the second to a strike-slip motion of the fault's reactivation during the D_2 event in U. Pliocene-Quaternary times. **12. The Zourva fault** (trend E-W, dip N) crosses the whole Western Crete. It is related to the Miocene extensional detachment of the nappes, but has been also activated during the D_1 event with dip-slip motion towards the North as well as during the D_2 event with a strike-slip component and a lateral sinistral sence of shear. Though it is not optimally oriented with respect to the active stress-field, the earthquake information be compatible with the strike of the Zourba fault. **13. The Xiropotamos-Elos-Myloi fault zone** (trend NE-SW, dip NW) is composed of three continuous segments and it is compatible with active stress field. More over, small magnitude seismicity along all segments of the zone is recorded. Expected earthquake magnitude M=5.5 for its largest segment.

For further correlation of the mapped faults with the seismicity, we have grouped all fault plane solution data in a elliptical region around each of the 13 main faults and computed average fault plane solutions using the method of Papazachos and Kiratzi (1992), and the same approach has been adopted for the neotectonic information. The results are shown in figure (6), where we present both earthquake and neotectonic information as equivalent fault plane solutions for three faults or group of faults (No 1, 2-3, 12.). The results verify the excellent agreement of neotectonic and earthquake information. The neotectonic and seismological information was used in order to perform a quatitative assessment of seismic hazard for the study area. For this reason we used all the available historical and instrumental seismicity information in order to assign appropriate quantitative seismicity measures to the previously described faults, as well as to the major thrust fault of Elafonissos that generated the 365 BC M=8.3 earthquake (Papazachos 1990), which belong to the NE-SW compression area SW of Crete.

For the historical seismicity information we mostly relied on the catalogue of Papazachos and Papazachou (2003), whereas instrumental seismicity information was based on the catalogue of the Geophysical Lab. of the Aristotle University of Thessaloniki which reports original or converted (equivalent) moment magnitudes for all events, up to 2009. The seismological information was used to determine the catalogue completeness from the Gutenberg-Richter curve and plots of the cumulative number of earthquakes versus time for several minimum magnitudes. The finally determined completeness for the W. Crete area was defined as: 1981-2002 M≥3.5; 1964-2002 M≥4.0; 1950-2002 M≥4.5. Using this completeness and the neotectonic and seismological information, we estimated appropriate seismicity parameters using elliptical areas around each of the 13 faults. Furthermore we considered the major thrust fault of Elafonissos, which strongly influences the seismic hazard assessment in the broader W. Crete area, and we also estimated the corresponding seismicity parameters for this fault. For all other areas outside the W. Crete we adopted the seismicity parameters of the zonation model proposed by Papaioannou and Papazachos (2000).

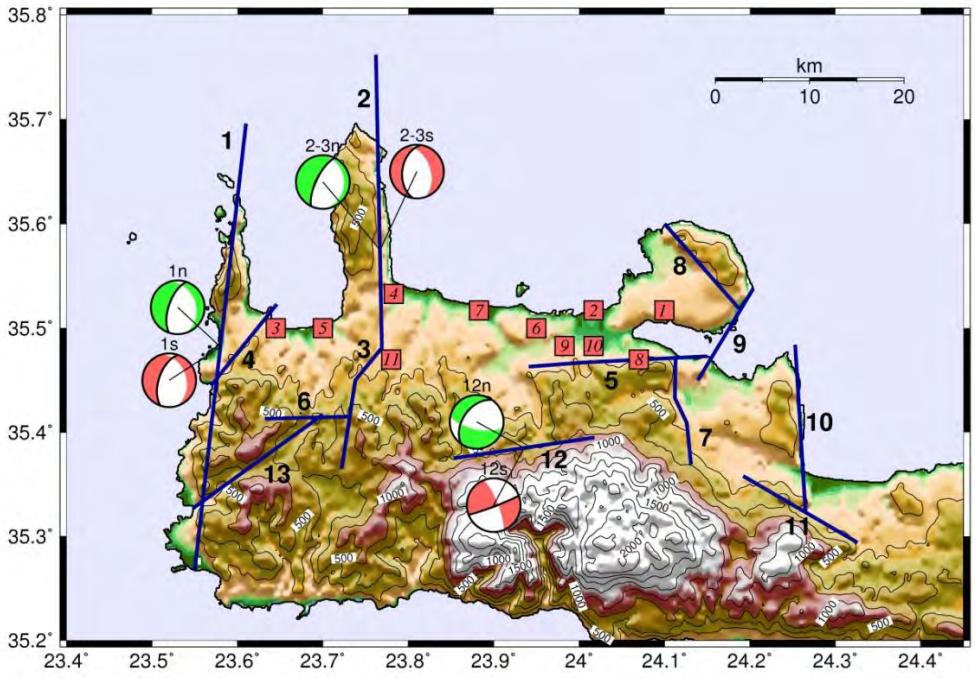

Figure 6 - Average fault plane solutions computed using the method of Papazachos and Kiratzi (1992) for faults 1 (W. Crete), 2-3 (Malathiros-Rodopos and Kera-Karthiana) and 12 (Zourva), from the available earthquake fault plane solution data (pink colored average solutions), as well as the corresponding neotectonic information from field observations (green colored average solutions). The main fault-plane is depicted with a thick line (see text for explanations). Red squares correspond to selected municipality centers for which seismic hazard analysis was performed (1:Akrotiri, 2: Chania, 3: Kissamos, 4: Kolymvari, 5: Mythimna, 6: N.Kydonia, 7: Platanias, 8: Souda, 9: Therissos, 10: Venizelos, 11: Voukolies).

In order to perform the final seismic hazard estimations we employed the PGA attenuation relation of Margaris et al. (2001) for shallow earthquakes and the relations of Theodulidis and Papazachos (1990) for intermediate-depth events. Seismic hazard estimations were performed using the Frisk88M (1995) code, appropriately modified in order to account for the different attenuation relations between shallow and intermediate-depth events, as well as anisotropic radiation of

seismic energy at the source. Moreover, pseudo-velocity response spectra PSV(T) (in cm/sec) were also computed using the relations of Theodulidis and Papazachos (1994). Estimations were performed for 11 selected major sites, corresponding to the main municipalities (fig. 6). Seismic hazard results were computed for a 10% probability exceedence in 50 yr (return period of 476 yr). In fig. 7 the results for 4 sites are presented. The sites have been selected in order to observe the gradual variation of the obtained seismic hazard results, as we move from the eastern (lower seismicity) to the westernmost (higher seismicity) part of the examined area. The results show higher seismic hazard levels for the Kissamos site, as it is affected by seismicity of the major neighboring Western Crete fault. On the other hand, the Kolymvari site exhibits quite low seismic hazard levels, despite being close to the neighboring active faults (Malathyro-Rodopos and Kera-Karthiana faults). The results verify the spatial variability of seismic hazard, suggesting that the identified active faults have an important effect on the seismic hazard assessment.

In order to quantify the effect of the seismotectonic model on the seismic hazard assessment, appropriate deaggregation of the seismic hazard results was performed for each examined site and all seismic sources affecting this site. The earthquake scenario were considered as design earthquakes and used in a stochastic simulation procedure, in order to estimate the contribution of each fault on the seismic hazard of each site, employing the methodology of Beresnev and Atkinson (1997). Using the stochastic simulation, average elastic response spectra (for 5% damping and amplification factor of β_0=2.5) were computed using a large number of simulations (typically 30) for each site. Sample results are presented in fig. (8) for the same sites as in fig. (7).

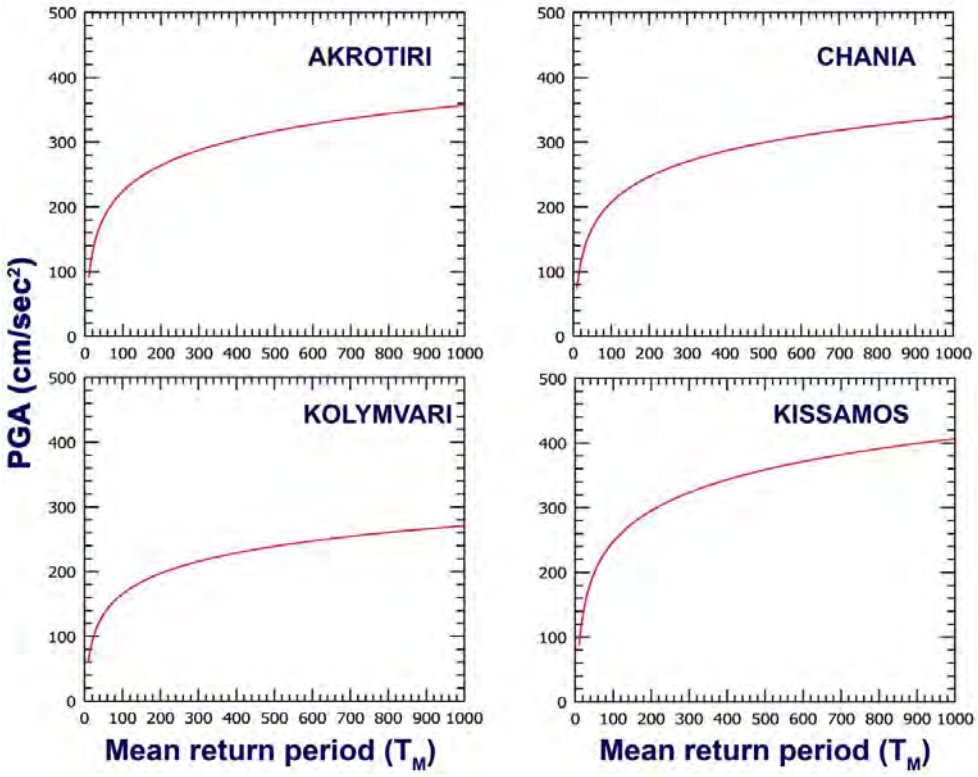

Figure 7 - Seismic hazard curves for the municipalities of Akrotiri, Chania, Kolymvari and Kissamos.

Moreover, the probabilistic elastic response spectra as determined from the initial seismic hazard analysis for two site conditions (rock and stiff soil), as well as the Greek Seismic Code (NEAK) elastic design spectra are also presented for all sites. The results additionaly confirm the strong

spatial variability of the seismic hazard in the western Crete. For sites located in the eastern (lower seismicity) part of the study area (Akrotiri, Chania) the NEAK elastic response spectra cover the probabilistic estimates from the hazard analysis. Moreover, the main contribution in seismic hazard is due to the Elafonisos thrust fault, which is almost identical to the probabilistic estimate, suggesting that the contribution of the active but low-seismicity neighboring neotectonic faults (faults 5, 7, 8, etc.) is minimal and that the main source of seismic hazard for these sites is the large thrust events that originate from the outer Hellenic arc convergence zone. A quite different situation holds for sites located in the western part of the study area. Compared to the Seismic Code design spectra, the probabilistic elastic spectra are slightly larger (up to 0.9g) at higher frequencies (2-10Hz) for Kolymvari and much larger (up to 1.45g) for frequency range (1.2 -20Hz) for the Kissamos site, suggesting that the Seismic Code spectra probably need adapting, especially for the Kissamos site. Even more important is the pattern change regarding the seismic hazard source contributions: For the Kolymvari site the contribution of the Elafonisos thrust fault is comparable to the contribution of the neighboring active Malathyros-Rodopos fault (fault 2), especially for higher frequencies (lower periods). This pattern is even more enhanced for the Kissamos site, where the neighboring faults of Western Crete (1) and Platanos (4) control the seismic hazard, while the Hellenic arc thrust fault contribution is significantly reliable smaller. This result further verifies the importance for the detailed neotectonic mapping for seismic hazard assessment.

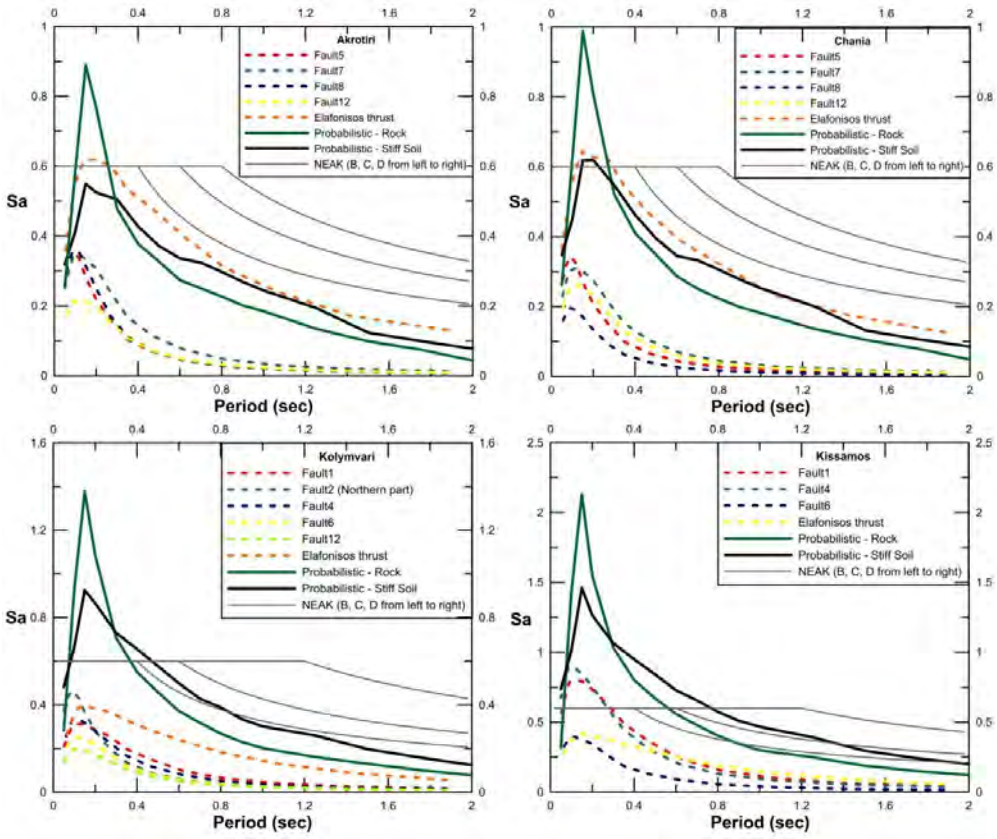

Figure 8 - Comparison of stochastic simulation elastic response spectra from the deaggregation analysis with the corresponding probabilistic elastic spectra from seismic hazard assesment and the Greek Seismic Code (NEAK) elastic response spectra for the municipalities of Akrotiri, Chania, Kolymvari and Kissamos.

4. Conclusions

After the detailed neotectonic and seismotectonic analysis we conclude that two distinctive stress phases took place. The first one (D_1, Mid-Upper Miocene to Lower Pliocene) exhibits a N-S extension and was responsible for the formation of the dominant E-W trending normal faults that control the shape of the large Neogene basins of Western Crete. The second one (D_2, Lower Pliocene to present) exhibits a E-W extension, forming mainly N-S faults, but also NE-SW trending smaller faults with significant strike-slip component, often acting as transfer zones between the larger N-S fault zones. Additionaly, some E-W faults from the previous D_1 phase are often reactivated, during the later D_2 phase, as almost pure strike-slip faults. This pattern is in excellent agreement with the seismological information, that show mostly N-S normal fault mechanisms, as well as NW-SE and NE-SW strike-slip mechanisms with significant normal component. The determined active stress field from fault plane solution data also shows a dominant E-W extension, suggesting that the D_2 phase identified by field data is an on-going active process.

Using a combination of field data and seismicity information, 13 large major fault zones were defined and characterized as active or possible active faults. They were incorporated in a detailed seismic hazard analysis, which also took into account the large thrust fault zones of the outer Hellenic arc, as well as the Benioff-zone intermediate-depth events. The probabilistic and a deterministic approach for seismic hazard evaluation, allowed not only the reliable estimation of the seismic hazard for several selected sites but also the effective deaggregation of the seismic hazard results. The seismic hazard of the westernmost part of study area is mainly controlled by the neighboring higher seismicity neotectonic faults, while the corresponding hazard of the central and easternmost part is mostly affected by the large outer arc thrust. Thus, the combined interpretation of field (neotectonic) data with seismological information is essential, not only for the better understanding of the ongoing seismotectonic processes but also for the efficient and reliable estimation of seismic hazard and the corresponding probabilistic or deterministic analysis.

5. References

Angelier J., Tarantola A., Valette B. and Manoussis S. 1982. Inversion of field data in fault tectonics to obtain the regional stress. Part I. Simple phase fault populations: a new method of computing the stress tensor, *Geophys. J. R. Astr. Soc.,* 6, 607-621.

Beresnev I. and Atkinson G. 1997. Modeling finite-fault radiation from the ωn spectrum, *Bull. Seism. Soc. Am.,* 87, 67-84.

Besnard M. 1991. Sismotectonique de l'arc egeen, resultants d'une campange de microsismicite, *PhD. Thesis,* Grenoble, France.

Bonneau M. 1984. Correlation of the Hellenic nappes in the southern Aegean and their tectonic reconstruction, In: The Geological Evolution of Eastern Mediterranean, ed. J. Dixon, & A. Robertson*, Geol. Soc. London, Sp. Publ.,* 17, 517-527.

Chabalier B., Lyon-Caen H., Zollo A., Deschamps A., Bernard P and Hatzfeld D. 1992. A detailed analysis of microearthquakes in western Crete from digital three-component seismograms. *Geophys. J. Int.,* 110, 347-360.

Duyster J. 2000. *Stereo Nett*, Microsoft Corp., Universtität Bochum.

Fassoulas C., Kilias A. and Mountrakis D. 1994. Postnappe stacking extension and exhumation of HP/LT rocks in the island of Crete, Greece, *Tectonics,* 13, 127-138.

FRisk88M 1995. *User's Manual*, ver. 1.70, *Risk* Engineering Inc., Boulder Co., 69 pp.

Gephart J. and Forsyth D. 1984. An improved method for determining the regional stress tensor using earthquake focal mechanism data: Application to the San Fernando earthquake sequence, *J. Geophys. Res.,* 89, 9305-9320.

Hatzfeld D., Besnard M., Makropoulos K. and Hatzidimitriou P. 1993. Microearthquake seismicity and fault plane solutions in the southern Aegean and its geodynamic implications, *Geophys. J. Int.,* 115, 799-818.

Jolivet L., Goffé B., Monie P., Truffert-Luxey C., Patriat M. and Bonneau M. 1996. Miocene detachment in Crete and exhumation P-T-t paths of high-pressure metamorphic rocks, *Tectonics,* 15, 1129-1153.

Jost L., Knabenbauer O., Cheng J. and Harjes H. 2002. Fault plane solutions of microearthquakes and small events in the Hellenic arc, *Tectonophysics,* 356, 87-114.

Kilias A., Fassoulas C. and Mountrakis D. 1994. Tertiary extension of continental crust and uplift of Psiloritis metamorphic core complex in the central part of the Hellenic Arc (Crete, Greece), *Geol. Rundsch.,* 83, 417-430.

Kilias A, Frisch W., Avgerinas A., Dunkl I., Falalakis G. and Ganlick H. 2010. Alpine architecture and kinematics of deformation of the Northern Pelagonian nappe pile in the Hellenides, *Austrian J. of Earth Sciences,* 103, 4-28.

Margaris B., Papazachos C., Papaioannou C., Theodulidis N., Kalogeras I. and Skarlatoudis A. 2001. Empirical attenuation relations for strong horizontal seismic motion of shallow earthquakes in Greece, *2nd Hell. Con. of Earthq. Eng. and Eng. Seism.,* Vol.1, 27-36.

Mercier J., Sorel D., Vergely, P. and Simeakis K. 1989. Extensional tectonic regimes in the Aegean basins during the Cenozoic, *Basin Res.,* 2, 49-71.

Mountrakis D. 2006. Tertiary and Quaternary tectonics of Greece, *Geol. Soc. Amer. Bull., sp. Paper*, 409, 125-136.

Mountrakis D., Tranos M., Papazachos C., Thomaidou E., Karagianni E. and Vamvakaris D. 2006. Neotectonic and seismological data concerning major active faults, and the stress regimes of Northern Greece. In: Robertson, A. & Mountrakis, D. (eds). Tect. Devel. of East. Mediterranean, *Geol. Soc. London, Sp. Publ.,* 260, 649-670.

Mountrakis, D., Kilias, A., Pavlaki, A., Fassoulas, C., Thomaidou, E., Papazachos, C., Papaioannou, C., Roumelioti, Z., Benetatos, C. and Vamvakaris D. 2012. Neotectonic study of the Western Crete. Seismic risk evaluation of the active faults, In: (Ed.) E. Skourtsos, and G. Lister, The Geology of Greece, *Journal of the Virtual Explorer*, Electronic Edition, ISSN 1441-8142, vol. 42, paper 4.

Papaioannou Ch. and Papazachos B. 2000. Time-independent and time-dependent seismic hazard in Greece based on seismogenic sources, *Bull. Seism. Soc. Am.,* 90, 22-33.

Papazachos B. 1989. A time predictable model for earthquake generation in Greece, *Bull. Seism. Soc. Am.,* 79, 77-84.

Papazachos B. 1990. Seismicity of the Aegean and surrounding area, *Tectonophysics,* 178,287-308.

Papazachos B., Karakostas V., Papazachos C. and Scordilis E. 2000. The geometry of the Wadati-Benioff zone and lithospheric kinematics in the Hellenic arc, *Tectonophysics,* 319, 275-300.

Papazachos B. and Papazachou C. 2003. *The earthquakes of Greece*, 3rd Edition, Ziti Publ., Thessaloniki, 273 pp.

Papazachos C. and Kiratzi A. 1992. A formulation for reliable estimation of active crustal deformation and its application to central Greece, *Geophys. J. Int.,* 111, 424-432.

Papazachos C., Kiratzi A. and Papazachos B. 1992. Rates of active crustal deformation in the Aegean and surrounding area, *Journal of Geodynamics,* 16, 147 -179.

Seidel E., Kreuzer H. and Harre W. 1982. A Late Oligocene/Early Miocene high pressure belt in the external Hellenides, *Geol. Jahrb.,* E 23, 165-206.

TenVeen, J. and Postma G. 1999. Roll-back controlled vertical movements of outer-arc basins of the Hellenic subduction zone (Crete, Greece), *Basin Res.,* 11, 243-266.

Theodulidis N. and Papazachos B. 1990. Strong motion from intermediate depth subduction earthquakes and its comparison with that of shallow earthquakes in Greece, *Proc. XXII Gen. Assembly ESC,* Barcelona, II, 857-864.

Theodulidis N. and Papazachos B. 1994. Dependence of strong ground motion on magnitude-distance, site geology and macroseismic intensity for shallow earthquakes in Greece: II, Peak horizontal pseudovelocity, *Soil Dyn.Earth. Eng.,* 13, 317-343.

Turner F. 1953. Nature and dynamic interpretation of deformation lamellae in calcite of three marbles, *Am. J. Sci., 4,* 276-298.

Δελτίο της Ελληνικής Γεωλογικής Εταιρίας, τομ. XLVII , 2013
Πρακτικά 13ου Διεθνούς Συνεδρίου, Χανιά, Σεπτ. 2013

Bulletin of the Geological Society of Greece, vol. XLVII 2013
Proceedings of the 13th International Congress, Chania, Sept. 2013

PALEOEARTHQUAKE HISTORY OF THE SPILI FAULT, CRETE, GREECE

Mouslopoulou V.[1], Moraetis D.[1], Benedetti L.[2], Guillou V.[2] and Hristopulos D.[1]

[1] Technical University of Crete, Department of Mineral Resources Engineering, vasiliki@mred.tuc.gr , moraetis@mred.tuc.gr, dionisi@mred.tuc.gr

[2] Centre Européen de Recherche et d'Enseignement des Géosciences de l'Environnement (CEREGE), CNRS, France, benedetti@cerege.fr, guillou@cerege.fr

Abstract

The paleoearthquake activity on the Spili Fault is examined using a novel methodology that combines measurements of Rare Earth Elements (REE) and of in situ cosmogenic ^{36}Cl on the exhumed fault scarp. Data show that the Spili Fault is active and has generated a minimum of five large-magnitude earthquakes over the last ~16500 years. The timing and, to a lesser degree, the slip-size of the identified paleoearthquakes was highly variable. Specifically, the two most recent events occurred between 100 and 900 years BP producing a cumulative displacement of 3.5 meters. The timing of the three older paleoearthquakes is constraint at 7300, 16300 and 16500 years BP with slip sizes of 2.5, 1.2 and 1.8 meters, respectively. The magnitude of the earthquakes that produced the measured co-seismic displacements, ranges from M 6.3-7.3 while the average earthquake recurrence interval on the Spili Fault is about 4200 years. The above data suggest that the Spili is among the most active faults on Crete and its earthquake parameters may be incorporated into the National Seismic Hazard Model.

Key words: *Fault, earthquake, seismic-risk.*

Περίληψη

Η παλαιοσεισμική δραστηριότητα στο ρήγμα του Σπηλίου μελετήθηκε χρησιμοποιώντας μία πρωτοποριακή μέθοδο που συνδιάζει μετρήσεις Σπανίων Γαιών (REE) και κοσμογενών ισοτόπων ^{36}Cl πάνω στην σεισμικά αποκαλυμμένη επιφάνεια του ρήγματος. Η ανάλυση των δεδομένων δείχνει ότι το ρήγμα είναι ενεργό και έχει φιλοξενήσει τουλάχιστον 5 μεγάλου-μεγέθους σεισμούς τα τελευταία 16500 χρόνια. Οι δύο πιο πρόσφατοι σεισμοί έλαβαν χώρα κατά την περίοδο 100-900 ετών πρίν από σήμερα και άθροισαν συνολικά 3.5 μέτρα σεισμικής μετατόπισης. Η χρονολογία των παλαιότερων 3 σεισμών προσδιορίσθηκε στα 7300, 16300 και 16500 χρόνια πριν από σήμερα με σεισμικές ολισθήσεις 2.5, 1.2 και 1.8 μέτρα, αντίστοιχα. Από το μέγεθος των σεισμικών ολισθήσεων συμπεραίνουμε ότι το μέγεθος των σεισμών που προκλήθηκαν από το ρήγμα του Σπηλίου κυμάνθηκε από M 6.3-7.3 ενώ ο μέσος ρυθμός επανάληψης τους ήταν ~4200 χρόνια. Τα παραπάνω δεδομένα αποκαλύπτουν ότι το ρήγμα του Σπηλίου είναι ένα από τα πιο ενεργά ρήγματα στην Κρήτη και οι

σεισμικές παράμετροί που σχετίζονται με την δραστηριότητά του πρέπει να συμπεριληφθούν στο μοντέλο σεισμικής επικινδυνότητας της Ελλάδας.
Λέξεις κλειδιά: *Ρήγμα, σεισμός, σεισμική επικινδυνότητα.*

1. Introduction and Geological Setting

Earthquakes are one of the deadliest natural disasters. About 20% of the Earth's population lives in areas of seismic hazard. Every year, there are approximately 150 large (>6M) earthquakes worldwide, causing an average of 20,000 casualties since the beginning of the 20th century and significantly impacting the economies and the sustainable development of the affected societies. Therefore, better understanding and forecasting of earthquake occurrence is one of the most pressing humanitarian goals within the sciences. Tectonic faults are breaks in the Earth's crust that grow primarily due to large magnitude earthquakes (Stein et al., 1988). Over millions of years, large cumulative displacements (e.g. >5km) accrue on faults as a result of 100's to 1000's of earthquakes; however, the systematics of this process is poorly understood. This is mainly due to the brevity of the available instrumental and/or historic earthquake record in comparison to the repeat times of large earthquakes on most faults globally. Paleoseismological investigations (i.e. fault trenching, etc.) are capable of extending the instrumental and/or historic earthquake record by including the majority of surface rupturing prehistoric earthquakes of M>6 on any particular fault (McCalpin, 1996). The identification of the timing between, and slip during, successive earthquakes on individual faults is vital in earthquake research as it highlights, and to some extent constrains, the variability associated with the complex phenomenon of earthquake occurrence (Nicol et al., 2009). Thus, paleoseismology increases the time-window over which earthquake information is available to thousands of years, providing a more realistic estimate of the seismic hazard of a particular fault.

But how exhumed carbonate fault scarps are capable of recording past earthquakes? During a large earthquake, a portion of a normal fault plane that was previously buried is suddenly exposed to the atmosphere. As further large earthquakes occur, the exposed fault plane becomes progressively larger and the succession forms a topographic escarpment, the height of which can be attributed to a number of past earthquakes (Benedetti et al., 2002). If we could identify the sections of the scarp that became successively exposed through time, we would know the number and size of the earthquakes generated by this fault. Accordingly, if we could date those sections, then we would know the timing of each earthquake.

In the case of limestone fault scarps the number, size and timing of earthquakes may indeed be constrained. As a section of a normal fault plane is suddenly exhumed, it becomes exposed to supergene weathering (rain, wind, vegetation and bacterial activity) and cosmic radiation (secondary neutrons and muons interact with Ca of the limestone scarp). The longer the surface is exposed, the more intense the weathering and the absorption of cosmic radiation. It is known that differential weathering of limestone scarps may be recorded in the chemical content of Rare Earth Elements (REE) (Manighetti et al., 2010; Mouslopoulou et al., 2011). Specifically, the concentration of REE generally decreases up-scarp, and peaks at sections of the scarp where the limestone was in direct contact with the paleosol (the limestone becomes enriched in REE while buried below the upper soil). Thus, a fault scarp is expected to include a series of rupture zones which have been weathered and exposed to radiation over significantly different time spans. The degree of weathering will reveal the number and size of the earthquakes, whereas the cosmic radiation will constrain their timing.

The primary research objective of this study is to constrain the paleoearthquake history on the Spili Fault, a fault located on the island of Crete in Greece (Figure 1a).

The Spili Fault is a normal fault that traverses the central part of Crete with a NW-SE orientation (300-320°) (Figure 1a). It extends for ca. 20 km onshore, defining along most of its length the

boundary between the Mesozoic bedrock units of Tripoli- or Pindos-limestone (upthrown block) and Pindos-flysch or ophiolites (downthrown block) (Angelier, 1979). The dip of the Spili Fault ranges from 55° SW to 75°SW. At the localities where the paleoearthquakes were identified (sites 1 and 2), the bedrock flysch is downthrown across the fault by ca. 600 m, and an elongated north-west-trending limestone ridge is formed. At the base of the ridge, a series of alluvial fans are formed by feeder streams. The fault has vertically displaced a number of alluvial fans, exposing a 10-20 m high and steep section of its carbonate fault plane. The fault plane is brecciated and, at places, polished by repeated slip movement (Figure 1b). Several slickenside striations on the main slip surface reveal a dominantly normal sense of motion, with a minor strike-slip component (i.e. 3 10/70, 308/78, 311/80 SW) (Mouslopoulou et al., 2011).

2. Research Methodology

In order to identify the number, size and timing of the large-magnitude prehistoric earthquakes that ruptured the Spili Fault, we employed a globally novel technique that involves a) identification and measurement of the Rare Earth Elements (REE) hosted in the exhumed limestone fault scarp; b) measurement of the in situ cosmogenic ^{36}Cl on each rupture zone. The former technique will provide the number and size of the earthquakes whereas the latter, the timing of the earthquakes. Specifically, paleoearthquake investigations involved 4 individual steps:

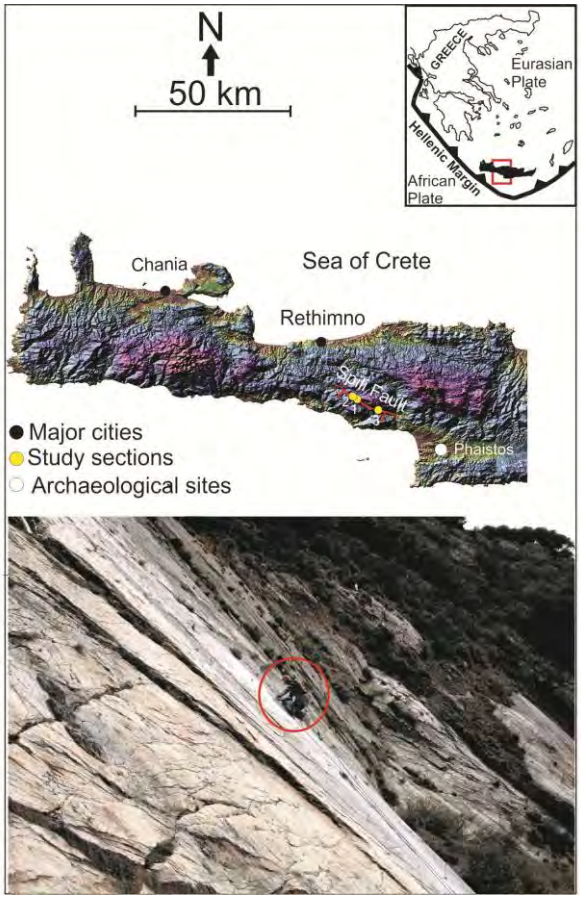

Figure 1 – Upper panel: Digital elevation model of western Crete illustrating the surface trace of the Spili Fault. The study sites are indicated by yellow circles: 1=Spili, 2=Health Center, 3=Platanes sites. Lower panel: detail of the fault plane at Site 1. Note climber for scale.

2.1. Step 1: Sampling of Exhumed Limestone Scarps for REE Analysis

Once the appropriate section was selected (Site-1), a total of 54 limestone core-samples were extracted from the exhumed fault plane in an upscarp direction, every 30 cm. Each core-sample was 4 cm long and 2cm wide. Four samples were also extracted below the soil surface, down to depth of -0.7 m.

2.2. Step 2: Identification and Measurement of REE

This stage involved the following individual steps per limestone core-sample: removal of 2mm core coating, 2cm core slicing, manual core crashing down to less than sugar grain-size, digestion of limestone grains aided by a series of acids (chemical preparation stage), centrifugation of the solutions and finally measurement of the content of REE on each sample by Inductively Coupled Plasma Mass Spectrometry (ICP-MS) equipment.

The digestion of the limestone grains (chemical preparation stage) was achieved through the following individual steps:

a) Initial dissolution with HCl until dryness for carbonates removal;

b) Dilution with HNO_3;

c) Dissolution with a mixture of HF, HNO_3 HCl and digestion in microwave;

d) Addition of EDTA and second digestion in microwave;

e) Dryness and dilution with HNO_3.

Figure 2 - Sampling the lower 15 m of the Spili Fault at Site-1 for REE analysis (a) and the lower 9 m at Site-2 for cosmogenic dating (b) using a portable drill and rock-saw, respectively.

This analysis provided the number and size of the past earthquakes on each fault and took place at the Department of Environmental Engineering at the Technical University of Crete (laboratory: Hydrogeochemical engineering and remediation of soils).

2.3. Step 3: Cosmogenic Isotope Sampling

During this stage we extracted limestone-samples for ^{36}Cl cosmogenic dating of the earthquakes. S pecifically, we used an electric rock grinder to remove a 15cm wide and 3cm thick section of the e ntire exhumed limestone fault plane. This technique is used routinely for cosmogenic isotope datin g. During this stage we extracted a total of 208 samples for ^{36}Cl cosmogenic dating. Specifically, we extracted 106 samples from the Site 1, 82 samples from Site 2 and 20 samples from Site 3.

2.4. Step 4: Cosmogenic Dating of Prehistoric Earthquakes

The last step concerns the dating of each identified earthquake by determining the concentration of ^{36}Cl as a function of scarp height. ^{36}Cl is produced primarily through interaction of cosmic rays with Ca within the calcite ($CaCO_3$) of the limestone scarp. Because the production rate of ^{36}Cl and its distribution below the surface are known, the concentration of cosmogenic ^{36}Cl can be used to calculate how long a surface has been exposed to cosmic radiation. This analysis took place at the laboratory facilities of CNRS in France (Université Aix-Marseille III).

This analysis included the following individual steps: a) sample preparation for chemical Cl extraction, b) Accelerator Mass Spectrometry (AMS) measurements and ^{36}Cl concentration determination, c) analysis of host rock chemical composition, d) analysis of colluvial wedge chemical composition and e) determination of the density of the fault scarp rocks and colluvium (Schlagenhauf et al., 2010). The final measurements of ^{36}Cl concentrations provided the timing of each earthquake.

Some information about the rock sampling and crushing:

Sampling in all cases involved extraction of carbonate rock from near-vertical (~75-80°) fault-scarps. The equipment used included an electrical generator, portable drill or rock-saw, chisel, hammer and climbing equipment (Figures 2 & 3a). Following the extraction, we manually crushed (inside an agate mortar) the REE samples, after having removed the upper 2mm of the outer core coating (Figure 3b). Each core required about 40 minutes of manual crushing. We also crushed down to sugar-grain size using an electrical mill a total of 91 limestone slabs for ^{36}Cl analysis. Each slab required about 30 minutes. Subsequently we used a sheave to separate fractions of the crushed material (the ^{36}Cl content is measured on carbonate grain-sizes ranging from 250 to 500μm).

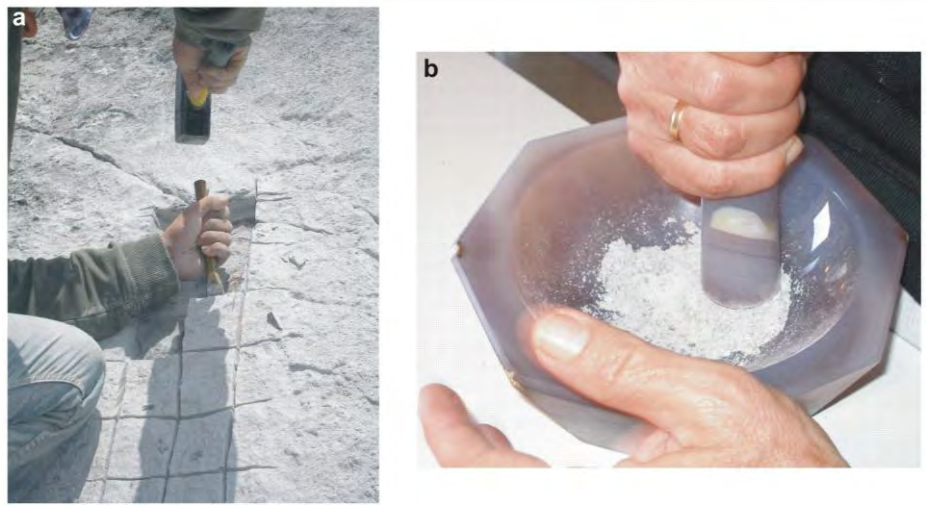

Figure 3 - (a) Sampling of the Spili Fault plane for cosmogenic dating; (b) Prior to the chemical treatment stage, carbonate cores extracted for REE analysis were manually crushed down to sugar grain size within an agate mortar.

3. Results

We successfully mapped the entire surface trace of the Spili Fault (~20 km) and identified three sections for sampling and subsequent analysis: the 'Spili' or Site-1, the 'Health Centre' or Site-2 and 'Platanes' or Site-3 (see yellow circles in Figure 1). Specifically, by combining REE measurements from the lower 15 m at Site-1 with ^{36}Cl measurements from the lower 9 m at Site-2 we recovered a minimum of seven paleoearthquakes that were accommodated by the Spili Fault and constrained the timing on the five most recent of these events.

The ^{36}Cl measurements from Site-1 are sparse and of low-concentration and thus difficult to interpret. The ^{36}Cl measurements from Site-3 are, up to date, inconclusive due to the high values of inherited Cl in the carbonates. For these reasons the above data are not included in the subsequent analysis and the timing of the identified earthquakes is based on measurements from Site 2.

3.1. Number, Size and Timing of Past Earthquake Activity on the Spili Fault

Seven paleoearthquakes have been identified to have ruptured the Spili Fault, the five most recent of which having occurred during the last ~16500 years. In the following sections, we discuss how individual earthquakes may be constrained on a fault scarp by combing the REE method with cosmogenic (^{36}Cl) dating.

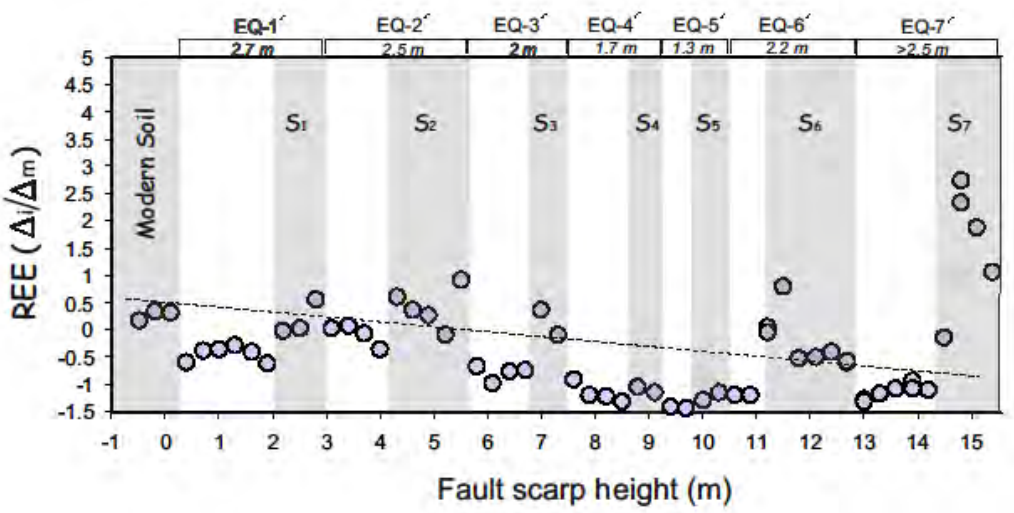

Figure 4 - (a) Plot showing the variability in the concentration of the REE as a function of sample position along the fault scarp. The Y-axis measures the difference Δi between a given concentration in core i (Ci) and the mean concentration (Cm) over the entire fault scarp collection (Δ*i*=C*i*-Cm), normalized to the mean absolute value of those differences (*Δm).* Circles correspond to the average value of 14 different REE at each locality. Domains *Si*, which are shaded grey, indicate scarp sections enriched in REE. Dashed line indicates the decreasing trend (depletion) of the average *Δi/Δm* with increasing scarp height.

REE analysis: In order to constrain the number and size of the past earthquakes that ruptured the Spili Fault we measured the REE content at 54 upscarp localities at Site-1 (Figure 4). In Figure 4, where a concentration measure (*Δi/Δm*) is plotted as a function of fault scarp height, we explore the upscarp concentration evolution of the REE average. Specifically, the Y-axis in Figure 4 measures the difference (*Δi)* between a given concentration of an element (*i*) in core (*Ci*) and the mean concentration (*Cm*) of the same element over the entire fault scarp collection (Δ*i*=C*i*-*Cm*), normalized to the mean absolute value of those differences (*Δm)*. Data reveal a nearly linear decrease of the average REE concentration with increasing scarp height (dashed line in Figure 4).

The most striking feature illustrated in Figure 4 is that, superimposed on the overall depleting trend upscarp, there is a continuous and clear signal of fluctuations in the REE concentrations as a function of fault scarp height. In detail, there are domains in which the REE concentrations are locally increased. These domains, which are highlighted by grey shading in Figure 4, are always preceded or followed by scarp sections which are characterised by lower concentrations in REE. For example, the section of the fault scarp that is currently buried up to 0.5 m below the ground surface has, on average, 60% higher REE-Y concentration compared to the section of the scarp immediately above the ground surface (Figure 4). The 60% 'drop' in the concentration persists up to the height of about 2m, where another increase of ca. 75% in the REE concentration occurs (Figure 4). Overall, our data record a minimum of seven, such *'fluctuations'* in the concentration of REE on the lowest 15m of the Spili Fault plane (Figure 4).

According to the model presented in earlier studies (Manighetti et al., 2010; Mouslopoulou et al., 2011), each concentration fluctuation is associated with an earthquake event that instantly exhumed subaerially sections of the fault scarp with depleted and elevated REE concentrations. Thus, we have identified a minimum of seven such paleoearthquakes the size of which ranges from 1.3 to 2.7 m. For more information on the REE method, its uncertainties but also the actual REE measurements that derive from the 10 lower meters of the Site-1 on Spili Fault see Mouslopoulou et al. (2011).

Cosmogenic (^{36}cl) dating: We measured and modelled the content of *in situ cosmogenic ^{36}Cl* on 41 limestone samples extracted from the lower 9 m of the fault scarp at Site-2 (Figure 5). The total scarp height at this locality is ~12 m.

The modelling of the ^{36}Cl results has taken into account the dip of the fault at Site-2, the density and the dip of the alluvial fan, the dip of the older scarp section (above the sampling site) and the shading that may be induced locally by the surrounding topography (Schlagenhauf et al., 2010).

Results indicate that the lower section (~3.5 meters) of the fault scarp is much younger than the remaining scarp. Examination of the graph in Figure 5 reveals two sharp discontinuities at 1 and 3.5 meters along the height of the scarp. These discontinuities are interpreted to result from at least two large magnitude earthquake events. The timing of these earthquakes is modelled to be at 500 (-400, +200) and 600 (±300) years BP, respectively. Following, at about 6m upscarp, there is another discontinuity, dated at 7300 (-300, +400) years BP. The large time-lag between the second and third identified earthquakes on the Spili Fault is reflected in the increased content in ^{36}Cl at six meters compared to the content measured lower on the scarp (the upper section of the scarp has been exposed to cosmic ray radiation for longer time-periods than the lower section of the scarp). This is also evident in the field, when one compares the roughness of the fault plane at different localities upscarp. Following, the 4th and 5th recorded discontinuities (earthquakes) are identified at 7.2 m and 9 m upscarp and their timing is modelled at 16300 (-100, +500) and 16500 (-500, +700) years BP, respectively (Figure 5).

The slip-sizes of the five most recent earthquakes identified at Site-2 (starting from the most recent: 1m, 2.5m, 2.5m, 1.2m and 1.8) are overall comparable to those derived from Site-1 by the REE method (starting from the most recent: 2.7m, 2.5m, 2m, 1.7m and 1.3m). Lateral slip variability is commonly observed along faults, even over short lateral distances (Schlagenhauf et al., 2011). In our case the two sites are located ~2 km apart and the slip variability observed is not surprising (perhaps with the exception of the most recent event).

Despite the fact that there have been at least 60 historically recorded large magnitude (>M6) earthquakes during the period 900-100 years BP (Papadopoulos, 2011), with some of them affecting mainly the area around Rethymnon, it is not possible to safely correlate any of the individual historic earthquakes to the identified paleoearthquakes on the Spili Fault (the uncertainties are large and include several large magnitude earthquakes).

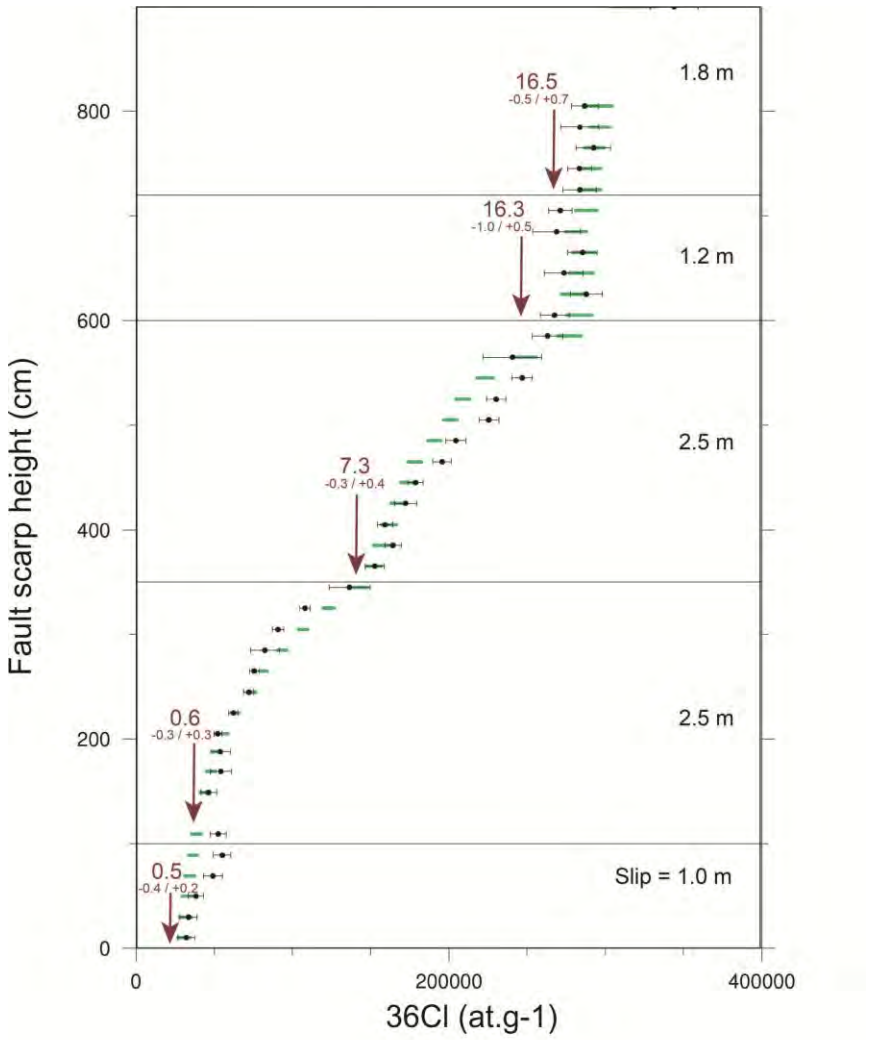

Figure 5 - Modelling (green bars) of the ^{36}Cl concentrations (black circles) that derive from the lower 9m of the Spili Fault at Site-2. Each horizontal line represents a discontinuity that is interpreted to result from at least one paleoearthquake. The timing and slip-size of each earthquake is indicated on the graph.

3.2. Earthquakes Parameters and Implications for Seismic Hazard

The Spili Fault is one of the most active faults on Crete. It has accrued 9 m of displacement over a period of 16000 years (Figure 6). Based on these measurements, the slip rate (SR) on the fault is ~ 0.6 mm/yr. Each identified earthquake on the Spili Fault produced co-seismic slip that ranged from 1 to ~2.7 m (Figure 6). Using the Wells and Coppersmiths equation M=6.69+0.74*log(MD), where MD is the Maximum Displacement per earthquake event, we derive earthquake magnitudes ranging from M 6.3-7.3.

Earthquakes of that magnitude may be highly damaging. Therefore it is important to discuss the frequency with which large magnitude earthquakes are accommodated by the Spili Fault. To achieve this, we introduce a term called 'earthquake recurrence interval'. The earthquake recurrence interval (RI) is the period of time between large magnitude events on an individual fault (McCalpin, 1996). The RI can be estimated using two different methods: 1) directly from the

earthquakes observed on the fault-scarp (observed RI) or 2) calculated from the mean single event displacement (SED) and the slip rate on the fault (estimated average RI). The methods are independent from one another and collectively provide a powerful means of estimating recurrence intervals and their variability.

Observed RI on the Spili Fault: Based on the timing of the five most recent earthquake events on the Spili Fault, that is 500, 600, 7300, 16300 and 16500 years BP and taking into account their respective uncertainties, we derive the following four RI's: 0-800, 6100-7400, 8500-9800 and 0-1000.

Therefore, based on these observed time intervals, the average observed RI on the Spili Fault over the last 16500 years is ~4200 years.

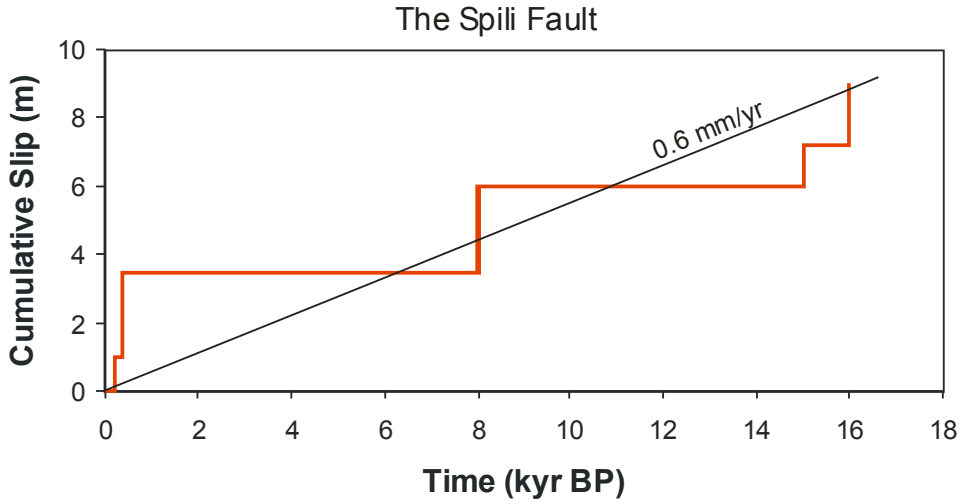

Figure 6 – Displacement versus time plot illustrating the accumulation of slip on the Spili Fault during the last 16.5 kyr. Each step corresponds to an earthquake event. The displacement rate on the fault averaged over the last 16.5 kyr is ca. 0.6 mm/yr.

Calculated RI on the Spili Fault: The value of "calculated average recurrence interval" is based on the cumulative displacement of a dated feature (fault-scarp in our case) that has been offset by multiple earthquakes. The slip per event (D) is typically estimated from the maximum or average slip documented during single earthquakes. The average D for the Spili Fault is 1.8m. Knowing that the slip rate (SR) on the fault is 0.6 mm/yr, we derive the calculated average recurrence interval based on the equation: $RI_{(calc)} = D/SR = 1800$ mm / 0.6 mm/yr = ca. 3000 years.

The above data suggest that the calculated (~3000 year) average recurrence interval on the Spili Fault is, within uncertainties, comparable to that observed (~4200 years) on the fault by dating individual earthquakes. This is encouraging because it may suggest that our sampling window (e.g. 16500) is large enough to overcome the short-term variability that often arises when we sample fault activity that is not representative of the long-term fault's behaviour (e.g. temporally clustered earthquake events). For example, the observed RI on the Spili Fault would have been much shorter had we only sampled the two most recent earthquakes on the fault. Nevertheless, as earthquakes on faults rarely occur periodically, the numbers associated with the earthquake recurrence intervals on a fault should be treated only as averages (Mouslopoulou et al., 2009).

4. Acknowledgments

We acknowledge the Latsis Foundation for partially supporting this work and C. Fassoula for useful discussions and help during fieldwork.

5. References

Angelier J. 1979. Neotectonique de l'arc egeen, *Soc. Geol. Nord. Spec. Publ.,* 3, pp. 418.

Benedetti L., Finkel R., Papanastassiou D., King G., Armijo R., Ryerson F.J., Farber D. and Flerit, F. 2002. Post-glacial slip history of the Sparta fault (Greece) determined by ^{36}Cl cosmogenic dating: evidence for non-periodic earthquakes, *Geophys. Res. Lett.,* 29, 8701-8704.

Manighetti I., Boucher E., Chauvel A., Schlagenhauf A. and Benedetti L.2010. Rare earth elements record past earthquakes on exhumed limestone fault planes, *Terra Nova*, 22, 477-482.

McCalpin J.P. 1996. Paleoseismology: San Diego, California, Academic Press, 588.

Monaco C. and Tortorici L.2004. Faulting and effects of earthquakes on Minoan archaeological sites in Crete (Greece), *Tectonophysics*, 382, 103-116.

Mouslopoulou V., Walsh J.J. and Nicol, A. 2009. Fault displacement rates on a range of time-scales, *Earth Planet. Sci. Lett*., 278, 186-197.

Mouslopoulou V., Moraetis D. and Fassoulas C. 2011. Identifying past earthquakes on carbonate faults: advances and limitations of the Rare Earth Element method based on analysis of the Spili Fault, Crete, Greece, *Earth Planet. Sci. Lett*., 309, 45-55.

Nicol A., Walsh J.J., Mouslopoulou V and Villamor P.2009. Earthquake histories and Holocene acceleration of fault displacement rates, *Geology*, 37, 911–914.

Papadopoulos G. 2011. *A seismic history of Crete*, 0-416, Edition Oselotos, ISBN: 9789609499682

Schlagenhauf A., Gaudemer Y., Benedetti L., Manighetti I., Palumbo L., Schimmelpfennig I., Finkel R. and Pou K. 2010. Using in-situ Chlorine-36 cosmo-nuclide to recover past earthquake histories on limestone normal fault scarps: A reappraisal of methodology and interpretations, *Geophys. J. Intern.,* 182, 36–72.

Schlagenhauf A., Manighetti I., Benedetti L., Gaudemer Y., Finkel R., Malavieille J. and Pou K. 2011.Earthquake supercycles in central Italy, inferred from ^{36}Cl exposure dating, *Earth Planet. Sci. Lett.,* 307, 487–500.

Stein R.S., King G.C. and Rundle J.B. 1988. The growth of geological structures by repeated earth quakes: 2 Field examples of continental dip-slip faults, *J. Geophys. Res,* 93, 13319–13331.

Wells D.L. and Coppersmith K.J. 1994. New empirical relationships among magnitude, rupture length, rupture width, rupture area and surface displacement, *Bull. Seismol. Soc. Am.,* 8, 974-100.

Δελτίο της Ελληνικής Γεωλογικής Εταιρίας, τομ. XLVII , 2013
Πρακτικά 13ου Διεθνούς Συνεδρίου, Χανιά, Σεπτ. 2013

Bulletin of the Geological Society of Greece, vol. XLVII 2013
Proceedings of the 13th International Congress, Chania, Sept. 2013

DEFINITION OF INFERRED FAULTS USING 3D GEOLOGICAL MODELING TECHNIQUES: A CASE STUDY IN TYMPAKI BASIN IN CRETE, GREECE

Panagopoulos G.[1], Giannakakos E.[1], Manoutsoglou E.[1], Steiakakis E.[2], Soupios P.[3] and Vafidis A.[4]

[1]Technical University of Crete, Dept. of Mineral Resources Engineering, Research Unit of Geology, Chania, Greece, gpanagopoulos@isc.tuc.gr, emanout@mred.tuc.gr.

[2]Technical University of Crete, Dept. of Mineral Resources Engineering, Laboratory of Applied Geology, Chania, Greece, stiakaki@mred.tuc.gr.

[3]Department of Natural Resources & Environment, Technological Educational Institute of Crete, soupios@chania.teicrete.gr

[4]Technical University of Crete, Dept. of Mineral Resources Engineering, Laboratory of Applied Geophysics, Chania, Greece, vafidis@mred.tuc.gr.

Abstract

The purpose of this paper is to recognize inferred *faults in Tympaki basin (Crete island) which cannot be observed on the surface, as the area is covered by recent deposits. The identification of the faults is crucial for the study of the sea-water intrusion in Tympaki basin that has been observed during the last years.*

3D geological modelling techniques were used for reaching the aforementioned goal. The data used include the digital elevation model (DEM) of the area, the boundary surface between *geologic* formations *and the litho - stratigraphic logs of thirty nine (39) wells. Initially a 3D stratigraphic model was set-up depicting the spatial extension of Plio-Quaternary and Neogene deposits. Next, with* emphasis on *the litho - stratigraphic logs of the wells, the boundary between the geological* formations *was defined in* a *3D* space.

The regional unconformity between the Plio-Quaternary and Neogene formations is possibly the result of tectonic activity of inferred faults. The traces of the inferred faults were drawn and they were compared with the faults suggested by previous studies.

Key words: *geological structure, 3D geological modelling technique*, *inferred faults.*

Περίληψη

Σκοπός της παρούσας εργασίας είναι ο καθορισμός πιθανών ρηγμάτων στη λεκάνη του Τυμπακίου τα οποία δεν είναι δυνατόν να παρατηρηθούν στην επιφάνεια εξαιτίας της κάλυψης της περιοχής από πρόσφατες αποθέσεις. Ο καθορισμός ρηγμάτων αποτελεί σημαντική στοιχείο στη μελέτη του προβλήματος υφαλμύρινσης που έχει παρατηρηθεί εκτεταμένα στη λεκάνη του Τυμπακίου τα τελευταία χρόνια. Η χρήση μεθόδων τρισδιάστατης γεωλογικής μοντελοποίησης αποτελεί τον τρόπο προσέγγισης αυτού του στόχου και απαιτεί τη συλλογή του συνόλου των διαθέσιμων χωρικών στοιχείων σε μια ενιαία βάση δεδομένων. Τα δεδομένα που εισήχθησαν αφορούσαν το

ψηφιακό υψομετρικό μοντέλο (DEM), τα επιφανειακά όρια των γεωλογικών σχηματισμών και τις λιθοστρωματικές στήλες από τριάντα εννέα (39) γεωτρήσεις. Αρχικά, κατασκευάστηκε το τρισδιάστατο λιθοστρωματογραφικό μοντέλο που παρουσιάζει τη χωρική κατανομή των Πλειο-Τεταρτογενών και Νεογενών αποθέσεων. Ακολούθως, με βάση τις λιθοστρωματογραφικές κολώνες των γεωτρήσεων ορίστηκαν τα γεωλογικά όρια μεταξύ των σχηματισμών στον τρισδιάστατο χώρο. Η ζώνη μετάβασης από τη μια ενότητα στην άλλη τοπικά εμφανίζεται σε διαφορετικό υψόμετρο. Τέτοιες απότομες αλλαγές θα μπορούσαν να αποδοθούν στη δράση πιθανών ρηγμάτων. Τελικά, μετά τη χωροθέτηση των πιθανών ρηγμάτων όπως προέκυψαν από τη συγκεκριμένη μεθοδολογία, γίνεται σύγκριση με τα αποτελέσματα προηγούμενων ερευνών.
Λέξεις κλειδιά: *γεωλογική δομή, πιθανά ρήγματα, τριδιάστατη γεωλογική μοντελοποίηση.*

1. Introduction

Crete is a structurally complex area that has been strongly affected by the Alpine orogenic processes in Eastern Mediterranean, due to plate convergence of Eurasian and African plates and the subduction of the Tethyan oceanic crust (Bonneau 1984; Lister et al., 1984; Mountrakis et al., 2006; Ring et al., 2010). Nappe stacking and compression alternate with extension, nappe collapse and exhumation of deep crustal rocks (Bonneau, 1984; Seidel et al., 1982; Kilias et al., 1994, 2002; Jolivet et al., 1996).

The island of Crete is situated in a fore-arc position above the active northward-directed subduction zone of the African plate beneath the Aegean plate (Petereck and Schwarze 2004). Present-day convergence rates between Libya and Crete reach 30 mm/yr in a SSW (Oral et al., 1995, Reilinger et al., 1997, McClusky et al., 2000). Given that the movement of Africa towards northward direction is approximately 10 mm/a, the overall plate convergence rate is approximately 40–45 mm/a. This convergence results to the NE-SW strong convergence compression (perpendicular to the African–Aegean plate boundaries) and to moderate extension to an arc-parallel E-W extension field (Petereck and Schwarze, 2004 and references therein).

The highly mountainous landscape in Crete and the deposits of Middle Miocene to early Late Pliocene age, which uplifted up to several hundreds of meters above the present sea-level, suggest a quite recent and rapid uplift. Along the Hellenic arc and south of Crete, the oblique convergence of the two plates explains the existence of fore-arc troughs controlled by strike-slip faults (Peterek and Schwarze, 2004 and references therein).

A large number of surface faults, such as Klima fault, Kardiotissa fault and others, indicate an intense tectonic activity in the region. The present-day surface deformation of south-central Crete is still a matter of debate. Mostly, a multi-directional extension (Duermeijer et al., 1998) has been proposed, based on fault slip data which are however hardly interpreted. Nevertheless, a dominating arc-parallel extension during Late Pliocene to Holocene time is also postulated due to young surface faulting. The existence of sinistral wrenching is evaluated as the main cause of evolution of the isolated Pliocene and younger basins in south-central Crete (Peterek and Schwarze, 2004 and references therein).

Moreover, recent studies (Chatzaras et al 2006; Tortorici et al., 2010; Kokinou et al., 2012; Klein et al., 2013) cast doubts on the duration of extension as a constantly major tectonic regime, suggesting that compression has played a crucial role beyond Middle Miocene. All these different views support the aspect that **highly** active **tectonic** setting of Crete affects the integrity and continuity of the stratigraphical units. This led to several fault-bounded blocks which bring in contact different stratigraphic units.

Several projects (FAO, 1969, 1972 & MEDIS, 2005) have been conducted in Tympaki area during the previous years. The first study performed by FAO (1969). The hydrogeological setting of the whole Messara plain (including Tympaki area) was defined, based on numerous drilling and geophysical data. More recently, in 2005 the MEDIS research project focuses for the first time on the seawater-intrusion phenomenon that had been observed in the Tympaki costal area.

The scope of the present paper is to contribute to the clarification of the tectono-stratigraphical structure of Tympaki basin, especially in the area which is covered by recent deposits, where no surface data exist. Such information will contribute to defining the hydrogeological setting of the basin.

2. Geological Setting

Crete consists of a pile of nappes that contain rock units from various geotectonic zones. These rocks belong both to External Hellenides, namely Phyllite (P-Q), Tripolis, Pindos Nappes and to Internal Hellenides, namely Arvi, Miamou, Vatos, Asterrousia Units and ophiolites, all stacked southward on the parautochthonous Permian-Tertiary Plattenkalk Group (Bonneau, 1984). The uplift and exhumation of the basement was accompanied by structural disintegration of the hanging wall, leading to formation of sedimentary basins on top of the nappe pile from Lower to Middle Miocene. Neogene sediments of Crete were subdivided by Meulenkamp (1979) into six stratigraphical groups, namely Prina, Tefelion, Vrysses, Hellenikon, Foinikia and Agia Galini Groups and the undifferentiated Pleistocene. The sedimentary characteristics of Neogene deposits reflect the tectonic regime of the Hellenic fore-arc at the time of their deposition.

The broader area of Tympaki is the westernmost part of Messara basin that is surrounded by Idi Mountains in northwest, Dikti Mountains in the northeastern side and the Asteroussia mountains in the south. Sedimentation in Messara basin started during the Middle Miocene and it resulted in deposition of sequences of conglomerates, cobbles, sands, marls and clays with abrupted lateral and vertical lithological changes.

Tympaki basin is separated from Messara basin by a tectonic horst that is named “Faistos horst” and it is oriented NNE-SSW (Figure 1). Faistos horst is filled with Neogene deposits, which are regarded as aquitard and separates hydrogeologically the Tympaki basin from the eastern part of Messara basin. There is only an approximately 2km - wide passage through the horst, on which Geropotamos river flows towards the west.

Tympaki basin exhibits a pronouncedly differentiated relief, with an almost flat south-western domain proximal to the coast, and a north eastern hilly domain proximal to Idi Mountains. The hilly landscape is because of the action of Klima fault to the north and Kardiotissa fault to the east.

The majority of Tympaki basin, especially the south western part, is covered by recent fluvio-lacustrine and alluvial deposits, while the north western domain is covered by fluvial deposits and alluvial fans (Figure 1). According to previous projects (FAO, 1972; Paritsis, 2005), the borders of the basin are defined by the tectonic contact of the aforementioned deposits with normal faults with the Neogene formations, as it is shown in the geological map of the area (Bonneau et al., 1984 and Bonneau, 1985). Apart from the fault boundaries of Tympaki basin, the same studies suggest the existence of additional normal faults that configure crucially the geometry of Tympaki basin. More specifically, according to the results of MEDIS program (Paritsis, 2005), there are also three additional inferred faults in the area (F1, F2, F3 depicted in Figure 2) which are not shown in the geological map of IGME (Bonneau et al., 1984 and Bonneau, 1985). The claim regarding the existence of these normal faults is based on the litho - stratigraphic logs of deep wells and on hydrogeological data retrieved from FAO project (FAO, 1972). These faults comprise a strike in a mean direction from NNW to SSE (Figure 2). In addition, according to a morphotectonic study in the same basin, conducted by Peterek & Schwarze (2004), similar faults exist.

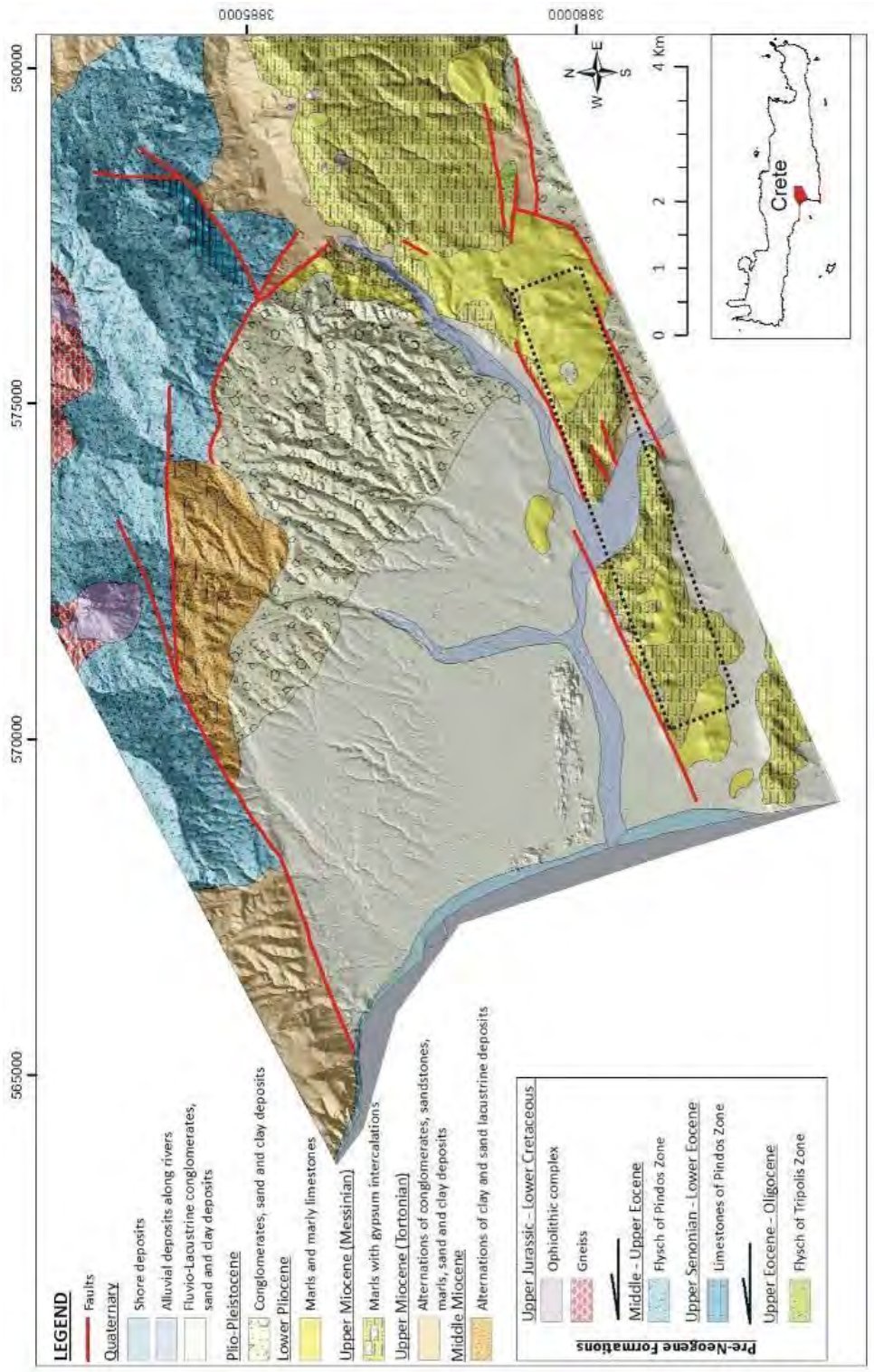

Figure 1 - Geological map of Tympaki area (after Bonneau et al., 1984 and Bonneau, 1985, modified). Dashed line shows the limits of Faistos horst.

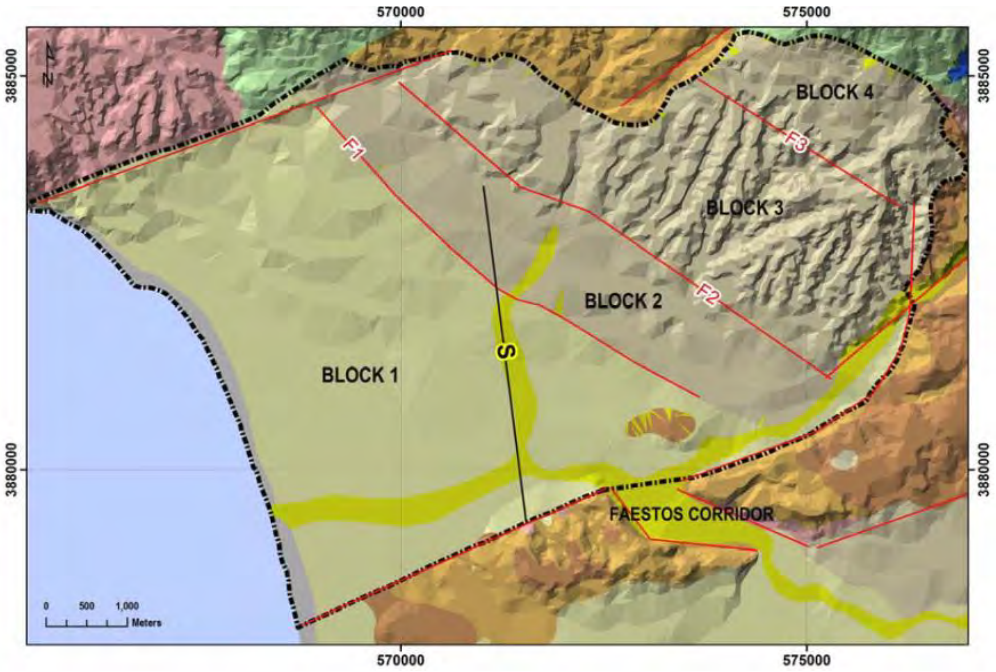

Figure 2 - Geological map of the Tymbaki basin (Paritsis, 2005). Different colours refer to different lithologies based on geological map of IGME (Bonneau et al., 1984 and Bonneau, 1985). The black dash-dot line delimits the basin boundary. F1, F2, F3 are the postulated normal faults dissecting the aquifer.

3. Methodology

3.1. General

In order to construct the 3D geological model of Tympaki basin, a GIS geological database (ArcGIS) with all the available data was created. Although data integration and cross-correlation of geology can be achieved *in* two dimensions by the GIS package, it cannot build complex surface or volumes such as geological folding and faulted structures (Kaufmann & Martin, 2008) in three dimensions. The limited capabilities in handling real 3D data with GIS packages, can be overcome using a specialized 3D geomodeling software.

Based on the above, the GIS database of Tympaki area was imported in the geomodeling software (RockWorks15, RockWare, Inc) and it was integrated by the 3D modelling process. The combined use of both types of software is desirable because it generates more complete and reliable models (Fallara et al., 2006).

The imported data comprises the digital elevation model (DEM) of the area, the surface-geological boundaries and thirty nine (39) well logs. DEM was produced from elevation data (National Cadastre & Mapping Agency S.A.) acquired from a regular grid with cell dimensions of 5m x 5m. In addition, the surface geological data comprise the digitized formation boundaries and the faults lines. Moreover, based on detailed lithological descriptions of the well logs (FAO, 1969; Municipality of Faistos), the geological formations were grouped into 23 lithological units. They were further summarized into two startigraphic units, namely Plio-Quaternary Unit and Neogene Unit (Figure 3). The former consists of clay to pebble deposits and the latter consists mainly of marls and marly limestones. It was assumed that marl formation with thickness over 10m could be regarded as a part of the Neogene.

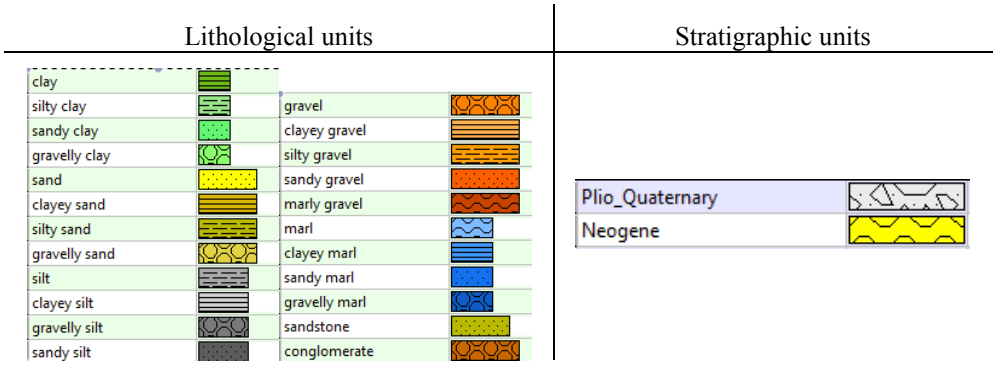

Figure 3 - The litho stratigraphic units loaded in the geomodeling software to define the structural model.

3.2. Application of 3D Modelling for the Definition of Covered Structural Model.

In sites covered by recent deposits the recognition of tectonic events is served only by morphotectonic methods, especially by the DEMs. However, there are several cases that none morphotectonic feature can be observed, like an area with flat topography. Tympaki basin is such a case, with small changes in surface elevation mainly in the southwestern part of the basin. The only way to approach the covered geological structure is to gather all the available data and to identify sound changes in the lateral continuity of the strata with reference to the borehole logs.

In the present study thirty nine (39) borehole logs were used to construct the 3D lithostratigraphic model of the area. The maximum depth of the wells reaches at about 350-400m mainly for the wells that have been drilled in the hilly part of the area. The spatial data manipulation was made easier by using the 3D modelling software. Based on the lithological descriptions of the borehole logs, the strata were subdivided into two main lithostratigraphic units, namely Plio-Quaternary and Neogene Units (Fig. 3). Twenty five (25) of the boreholes have drilled the Neogene formation near the basin borders, while none of the boreholes have reached the underlying pre-Neogene basement.

The digital 3D model was built by using all the existing data sets and the spatial distribution of the geological bodies was defined so as to be able to locate the upper and lower surface of each geological unit in any part of the basin. Especially, the definition of the surface that bounds the Plio-Quaternary and Neogene Units is crucial because any abrupt alteration in elevation could be able to supply very useful information for the definition of a fault that cannot be observed in the surface (Figure 4). The design of a contour-map for this surface is a quick and easy task, when using 3D geological modelling techniques, and it is really useful for the detection of these abrupt changes in a basin-wide scale, constituting a support tool in the design of a fault.

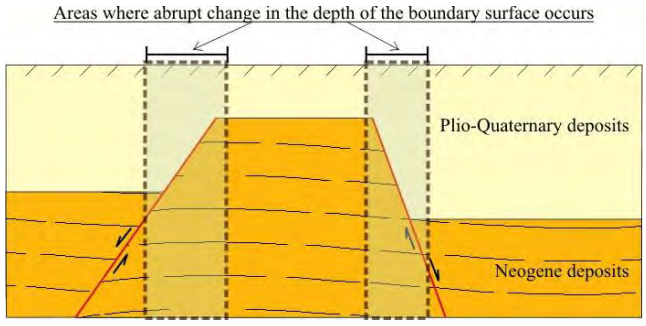

Figure 4 - The concept for identifying areas in the surface where the existence of a fault it is probable. The abrupt change of the boundary surface in depth serves as a guideline.

The surface was defined by interpolating the elevation of the lithostratigraphic contact observed in each borehole, with the remaining area between the boreholes. In this case the boreholes are regarded as reference points.

In the present study the used interpolation algorithm is triangulation. The accuracy of the resulting surfaces can be evaluated by cross-validating the model. During this process each of the observed values is regarded as unknown and the algorithm runs every time to calculate a value for it. Then, predicted and observed values are correlated, in order to calculate the correlation coefficient and to conclude regarding the reliability of the results.

Data from 25 out of 39 boreholes were used for cross-validation process, because these wells have reached up to the stratigraphical contact between Plio-Quaternary and the Neogene Units in the area (inside the basin borders).

4. Results

The boreholes data have been checked through geological sections and fence diagrams and finally led up a geological 3D model of the studied area (Figure 5). The surface that bounds the Neogene (lower) and Plio-Quaternary (upper) formation was defined reasonably well. The cross-validation showed that only 3 of the 25 predicted values were slightly to strongly different in relation to the real values, while the correlation coefficient estimated equal to 0.9959 (Figure 5).

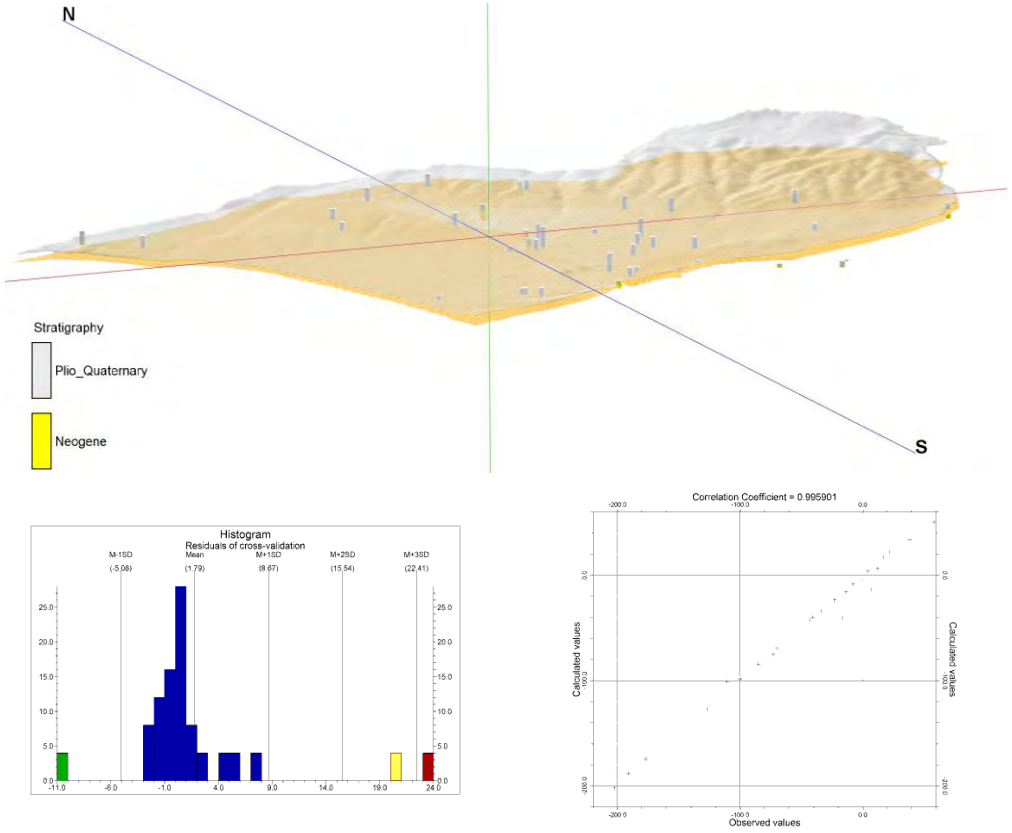

Figure 5 - 3D presentation of the upper Plio-Quaternary surface (transparent surface) and the boundary surface between Plio-Quaternary and Neogene deposits (lower surface). The spatial position of all boreholes is also shown. In the right side are shown the diagrams that resulted from the cross-validation procedure.

This surface was used as the leading surface to locate areas of any abrupt alteration in the elevation of the stratigraphic contact between Plio-Quaternary and the Neogene Units. Such abrupt alterations are interpreted in the present paper as the result of tectonic activity and for the further identification of possible faults. In order to locate easily the abrupt changes, an isodepth map showing the surface that separates the Plio-Quaternary and Neogene deposits was produced (Figure 6). The construction of the isodepth map can give a general perspective of the changes in the absolute elevation of the upper surface of Neogene formation that occur in the basin (Figure 6). Where abrupt changes occur, the existence of possible faults can be assumed. Based on this concept (Figure 3) several faults were defined. Those faults contributed in the depression or the lift of different parts of the basin (Minus and plus symbols in respect of figure 6).

It should be mentioned that the interpretation of the isodepth map was restricted in the area where enough borehole data are available, so as for the results to be as accurate as possible. Moreover, this interpretation was based on the assumption that the existence of a fault is most probable in sites where the number of the wells increases and the depth-differentiation becomes steeper.

Finally, a rose diagram of the resulting faults was constructed (Figure 7). According to this analysis, two main fault directions predominate in the region, namely NNW-SSE and ENE-WSW.

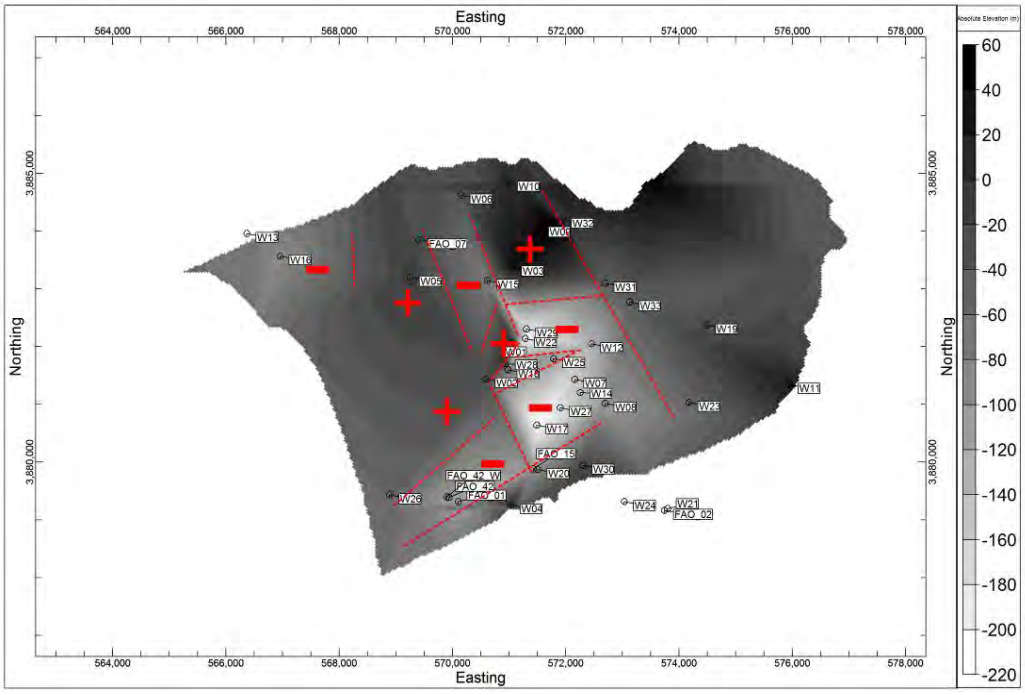

Figure 6 - Isodepth map of the upper surface of Neogene deposits in Tympaki basin. Legend shows absolute elevation in meters. The location of thirty nine (39) boreholes is also shown. Dashed lines depict inferred faults. Plus and minus symbols refer to horsts and grabens respectively.

5. Conclusions

In the present work, the litho-stratigraphic study of the area is combined with morphotectonic conclusions of previous study (Peterek & Schwarze, 2004); and as a result an enhanced concept regarding the tectono-stratigraphical structure of Tympaki basin arises.

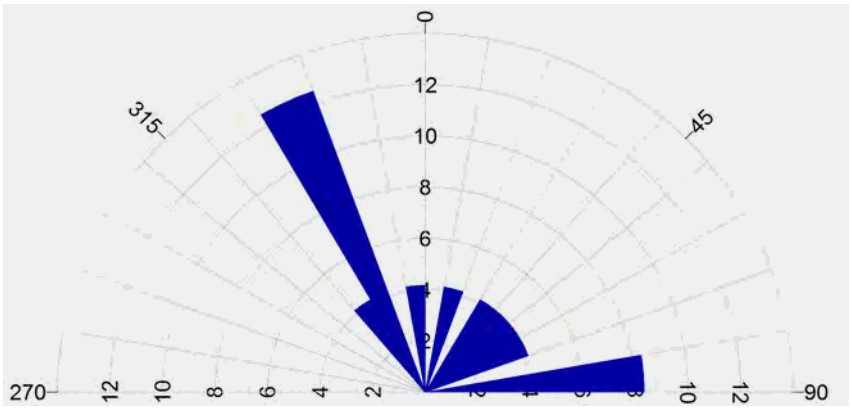

Figure 7 - Rose diagram (percent of total population) of the inferred faults resulted from the interpretation of the isodepth map (Figure 5). Bin size 10°.

The study of the lithostratigraphy, as well as the upper surface of Neogene formation provide strong evidence of faults that are not observed in the surface because the area is covered by recent fluvio-lacustrine deposits.

The analysis of the available data was conducted using an isodepth map of the top surface of the Neogene that resulted from the 3D stratigraphical model, which was constructed using a 3D geological modelling software (RockWorks15, RockWare, Inc.).

Two main fault directions were identified through the analysis. The first one has a general direction NNW-SSE, similar to the strike direction that previous studies have proposed (FAO, 1972; Peterek & Schwarze, 2004; Paritsis, 2005). The second one has a general direction from ENE to WSW direction, and it follows the strike direction of the faults that bound Tympaki basin in the Northern and Southern limit.

In other words, the drilling data lead to conclusions that are consistent with previous studies regarding the NNW-SSE strike direction; additionally, they underline the existence of a second one pronounced fault with strike direction ENE-WSW that has not been taken into account in previous underground water modelling studies. The latter direction could favour seawater intrusions because exhibit a more or less perpendicular to the coastline position.

The possibility of parallel activation of the two fault sets should make us to consider a more complicated fault-block structure of Tympaki basin that is characterized by a horst-graben structure and the simultaneous activity of crossing normal faults.

In the area where the number of the boreholes is adequate, the isodepth map defines accurately the horst and graben structure (Figure 6). However, where data were sparse the results are questionable and they should be checked by further drilling or geophysical investigation. According to the results, the top surface of the Neogene deposits has been raised in the central area of the basin, representing a horst structure. Such a conclusion should be checked with geophysical investigation up to depth of about 60 to 80m. Nevertheless, based on the available data it seems quite reasonable to reconsider the tectonostratigraphic structure of Tympaki basin and to investigate the seawater intrusion using advanced research techniques.

6. Acknowledgments

This study is part of the work that Technical University of Crete undertakes within the Work Package 1 of the BLACK SEA ERA.NET project, focusing in pollution from sea water intrusion at coastal areas (Tympaki basin).

7. References

Bonneau M. 1984. Correlation of the Hellenide nappes in the south-east Aegean and their tectonic reconstruction. In: DIXON, J. E. & ROBERTSON, A. H. F. (eds) The Geological Evolution of the Eastern Mediterranean, *Geological Society of London, Special Publications*, 17, 517-527.

Bonneau M., Jonkers H.A. and Meulenkamp J.E. 1984. Geological map of Greece (1:50.000). Timbakion sheet, *I.G.M.E.,* Athens.

Bonneau M. 1985. Geological map of Greece, 1:50.000*,* Melambes sheet, *I.G.M.E*., Athens.

Chatzaras V., Xypolias P. and Doutsos T. 2006. Exhumation of high-pressure rocks under continuous compression: a working hypothesis for the southern Hellenides (central Crete, Greece), *Geological Magazine,* 143, 859-877.

Fallara F., Legault M. and Rabeau O. 2006. 3-D integrated geological modeling in the Abitidi Subprovince (Quebec, Canada): Techniques and Applications, *Exploration and Mining Geology,* 15, 1-2, 27-41.

FAO 1972 Study of the water resources and their exploitation for irrigation in eastern Crete – Greece. Drillings and pumping tests in Messara AGL:SF/GRE 17/31, *Tech. Rep*., 26, UNDP, Iraklio.

FAO 1969. Greece: geophysical survey performed in Messara plain (Eastern Crete), *Final report*, Fondazione Ing. C. M. Lerici Del Politecnico, Milan, Italy.

Jolivet L., Goffe B., Monie P., Truffert-Luxey C., Patriat M. and Bonneau M. 1996. Miocene detachment in Crete and exhumation P–T–t paths of high-pressure metamorphic rocks, *Tectonics*, 15, 1129–1153.

Kaufmann O. and Martin T. 2008. 3D geological modeling from boreholes, cross-sections and geological maps, application over former natural gas storages in coal mines, *Computer & Geosciences*, 34, 278-290.

Kilias A.A., Tranos M. N., Oroxco M., Alonsochaves F.M. and Soto J.I. 2002. Extensional collapse of the Hellenides: a review, *Revista de la Sociedad Geological de Espania*, 15, 129-139.

Kilias A., Fassoulas C. and Mountrakis D. 1994. Tertiary extension of continental crust and uplift of Psiloritis metamorphic core complex in the central part of the Hellenic Arc (Crete Greece), *Geol. Rundschau*, 83, 417–430.

Klein T., Craddock J. P. and Zulauf G. 2012. Constraints on the geodynamical evolution of Crete: insights from illite crystallinity, Raman spectroscopy and calcite twinning above and below the 'Cretan detachment', *International Journal of Earth Sciences*, 102, 139-182.

Kokinou E., Alves T. and Kamberis E. 2012. Structural decoupling in a convergent forearc setting (southern Crete, Eastern Mediterranean), *Geological Society of America Bulletin*, 124, 1352-1364.

Lister G.S., Banga G. and Feenstra A. 1984. Metamorphic core complexes of cordilleran type in the Cyclades, Aegean Sea, Greece, *Geology*, 12, 221–225.

Meulenkamp J. E. 1979. Field Guide to the Neogene of Crete. In: Symeonidis, N., Papanikolaou, D., Dermitzakis M. (Eds.), Field Guide to the Neogene of Crete, *Publ. Dept. Geol. Paleont. Univ. Athens,* Series A, 32, 1–32.

Mountrakis D., Tranos M., Papazachos C., Thomaidou E., Karagianni E. and Vamvakaris D. 2006. Neotectonic and seismological data concerning major active faults, and the stress regimes of Northern Greece. In: Robertson M.N.F. and Mountrakis D. (eds) Tectonic Development of the Eastern Mediterranean Region, *Geological Society, London, Special Publications*, 260, 649-670.

McClusky S., Balassania S., Barka A., Demir C., Ergintav S., Georgiev I., Gurkan O., Hamburger M., Hurst K., Kahle H., Kastens L., Kekelidze G., King R.W., Kotzev V., Lenk O., Mahmoud S., Mishin A., Nadariya M., Ouzounis A., Paradissis D., Peter Y., Prilepin M., Reilinger R., Sanli I., Seeger H., Taeleb A., Toksoz M. N. and Veis G. 2000. GPS con-

straints on plate motions and deformation in the Eastern Mediterranean: Implications for plate dynamics, *J. Geophys. Res.*, 105, 5695–5719.
National Casastre & Mapping Agency S.A., DEM with grid size 5m x 5m.
Oral M. B., Reilinger R. E., Toksoz M. N., Kong R. W., Barka A.A., Kinik I. and Kenk O. 1995. Global positioning system offers evidence of plate motions in eastern Mediterranean, *EOS, Transactions, American Geophysical Union*, 76 (9), 9-11.
Papazachos C.B. 1993. Seismological and GPS evidence for the Aegean-Anatolia interaction, *Geophysical Research Letters*, 26, 17, 2653-2656.
Paritsis S.N. 2005. Simulation of seawater intrusion into the Tymbaki aquifer, South Central Crete, Greece, *Report within MEDIS project*, Study implemented on behalf of the Department of Management of Water Resources of the Region of Crete, Heraklion, Crete, Greece.
Peterek A. and Schwarze J. 2004. Architecture and Late Pliocene to recent evolution of outer-arc basins of the Hellenic subduction zone (south-central Crete, Greece), *Journal of Geodynamics*, 38, 19-55.
Reilinger R.E., McClusky S.C., Oral M.B., King R.W. and Toksoz M.N. 1997. Global Positioning System measurements of present-day crustal movements in the Arabia–Africa–Eurasia plate collision zone, *J. Geophys. Res.*, 102, 9983–9999.
Ring U., Glodny J., Will T. and Thomson S. 2010. The Hellenic Subduction System: High-Pressure Metamorphism, Exhumation, Normal Faulting, and Large-Scale Extension, *Annual Review of Earth and Planetary Sciences*, 38, 45 – 76.
Seidel E., Kreuzer H. and Harre W. 1982. A Late Oligocene/Early Miocene High Pressure Belt in the External Hellenides, *Geol. Jb.,* E 23, 165–206.
Tortorici L., Caputo R., Monaco C. 2010. Late Neogene to Quaternary contractional structures in Crete (Greece), *Tectonophysics*, 483, 203-213.

Δελτίο της Ελληνικής Γεωλογικής Εταιρίας, τομ. XLVII , 2013
Πρακτικά 13ου Διεθνούς Συνεδρίου, Χανιά, Σεπτ. 2013

Bulletin of the Geological Society of Greece, vol. XLVII 2013
Proceedings of the 13th International Congress, Chania, Sept. 2013

CLAY MINERALS FROM THE ARKITSA FAULT GOUGE ZONE, IN CENTRAL GREECE, AND IMPLICATIONS FOR FLUID FLOW

Papoulis D. [1], Romiou D. [1], Kokkalas S.[1] and Lampropoulou P[1].

[1] *University of Patras, Department of Geology, Papoulis@upatras.gr, skokalas@upatras.gr*

Abstract

Clay minerals in shallow fault rocks are increasingly recognized as key to the mechanical and seismogenic behavior of faults and fluid flow circulation within the fault core and the surrounding damage zone. We therefore studied fault-gouge mineralogy from samples derived from the ENE-trending Arkitsa fault zone, in east-central Greece, in order to testify if the fault is acting as a channel for fluid flow and whether the conditions that characterize the flow can be identified.

Clay-gouge samples were collected within the fault core zone, as well as in the broader fault damage area. Consequently, the samples were analyzed by X-Ray Diffraction, SEM and Electron microprobe analyses. The minerals that were identified within the centre of the fault zone are: Montmorillonite, corrensite, illite, micro-calcite, dolomite, quartz, plagioclase and K-feldspars. The absence of corrensite, a clay mineral usually formed in hydrothermal conditions, in the samples from the broader fault damage area indicates that the circulation of hydrothermal fluids is mostly confined within and around the fault core zone. The assemblages within the fault gouge zone and especially the presence of corrensite, combined with the absence of laumontite, indicate hydrothermal alteration at neutral to alkaline conditions and a temperature range at about 100-150 ^{o}C.

Key words: *fault zone, chlorite/smectite, hydrothermal fluids, fault damage*

Περίληψη

Η παρουσία αργιλικών ορυκτών σε πετρώματα ρηξιγενών ζωνών παίζει σημαντικό ρόλο στη μηχανική και σεισμική συμπεριφορά των ρηγμάτων καθώς και στην κυκλοφορία των ρευστών τόσο μέσα στον πυρήνα των ρηγμάτων όσο και στην ευρύτερη ζώνη διάρρηξης. Στην εργασία αυτή έγινε ορυκτολογική ανάλυση στην ΑΒΑ-διεύθυνσης ρηξιγενή ζώνη της Αρκίτσας με σκοπό να εξεταστεί εάν η ρηξιγενής ζώνη αποτελεί δίαυλο ρευστής φάσης και να αναγνωριστούν τα χαρακτηριστικά της κυκλοφορίας των ρευστών. Τα πλούσια σε αργιλικό υλικό δείγματα συλλέχθηκαν τόσο στον πυρήνα όσο και στην ευρύτερη ρηξιγενή ζώνη και αναλύθηκαν με τη χρήση Περιθλασιμετρίας ακτίνων Χ και ηλεκτρονικής μικροσκοπίας σάρωσης και μικροανάλυση. Στον πυρήνα της ρηξιγενούς ζώνης αναγνωρίστηκαν αργιλικά ορυκτά όπως, μοντμοριλλονίτης, κορενσίτης και ιλλίτης καθώς και μικροκρυσταλλικός ασβεστίτης, δολομίτης, χαλαζίας, πλαγιόκλαστο και

αλκαλικός άστριος. Η απουσία του κορενσίτη, ενός αργιλικού ορυκτού που συνήθως σχηματίζεται σε υδροθερμικές συνθήκες, από την ευρύτερη ζώνη διάρρηξης υποδηλώνει ότι η κυκλοφορία των ρευστών περιορίστηκε κυρίως εντός και περιμετρικά του πυρήνα του ρήγματος. Οι ορυκτολογικές παραγενέσεις στη ρηξιγενή ζώνη και κυρίως η παρουσία του κορενσίτη, σε συνδυασμό με την απουσία του λωμοντίτη, υποδεικνύουν συνθήκες υδροθερμικής εξαλλοίωσης σε ουδέτερο προς αλκαλικό περιβάλλον και σε θερμοκρασίες 100-150 ^{o}C.
Λέξεις κλειδιά: *ρηξιγενής ζώνη, χλωρίτης/σμεκτίτης, υδροθερμικά ρευστά, ζώνη διάρρηξης.*

1. Introduction

Clays have a number of rather unique properties as a consequence of clay mineral sheet silicate structure, size (nanocrystals) and in many of them, especially some of the most common, significantly charged particle surfaces. The presence of clay minerals within faults has been shown to influence significantly the flow of fluids in sedimentary basin (Knipe, 1993). Clay minerals as well as clay mineral growth affect anisotropy, permeability, porosity and fault strength (Morrow et al., 1984; Wintsch et al., 1995; Wibberley, 1999; Warr & Cox, 2001; Solum et al., 2003).

The shear strength of drained clays and pure clay minerals show strong variations depending on particle anisotropy and layer-charge as it has been shown by many laboratory testing (e.g. Rosenquist, 1962; Rosenquist, 1984; Müller-Vonmoos & Loken, 1989).
Clay minerals, because of their hydrous nature, can induce fluid pressure variations by storing or releasing water by hydration-dehydration reactions (Bruce, 1984; Vrolijk, 1990). This process is particularly important in the presence of smectite which can generate significant fluid pressures at low confining pressures by particle swelling (Koukouvelas & Papoulis, 2009). Variations in the

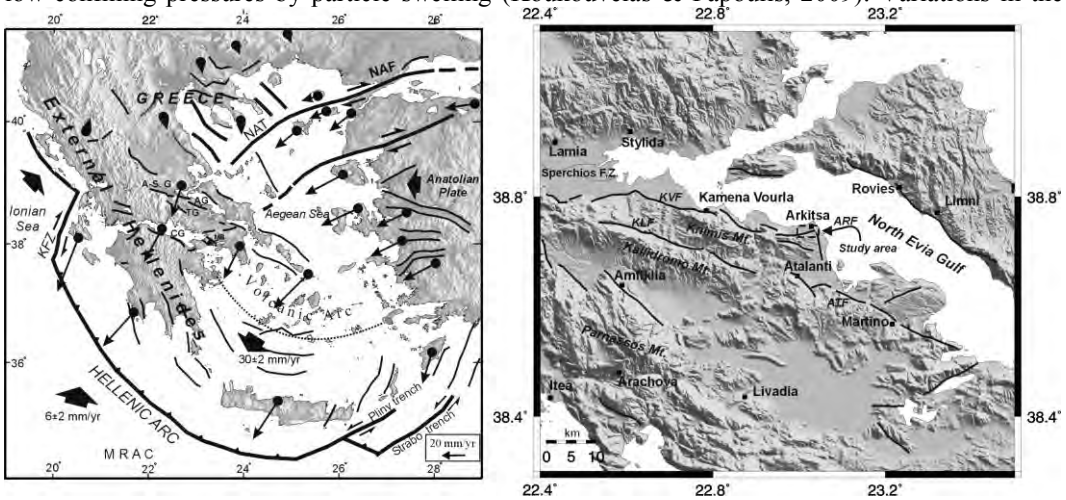

Figure 1 - (left): Simplified map showing the main structural features along the Hellenic Peninsula, as well as the main active structures. The mean GPS horizontal velocities in the Aegean plate are shown with respect to a Eurasia fixed reference frame. CG: Corinth graben, TG: Tithorea graben, AG: Atalanti graben, A-S.G: Almyros-Sperchios graben, MB: Megara basin. NAT: North Aegean Trough, NAF: North Anatolia Fault, KFZ: Kephalonia transform fault, MRAC: Mediterranean Ridge Accretionary Complex. Map modified from Kokkalas et al. (2006); (right): Map of central Greece close to the North Evia Gulf showing the main fault traces and the study area (arrow pointing to dashed rectangle). ATF: Atalanti fault, ARF: Arkitsa Fault; KLF: Kallidromo fault, KVF: Kamena Vourla fault.

type as well as the hydration state of smectite, and therefore fluid pressure fluctuations, are strongly influenced by deformation and changes in effective pressure (Morrow et al., 1992; Fitts & Brown, 1999; Moore & Rymer, 2012).

The aim of this study is to testify whether the fault is acting as a channel for flow and if the conditions which characterizing the flow can be identified. Additionally we intend to estimate the rate and conditions (e.g. temperature) of fluid transportation and to investigate the influence of the presence of clay minerals during this procedure.

2. Geological Setting of the study area

Since the Upper Miocene to present, the area of Central Greece is currently undergoing active N-S to NE-SW regional extension, with rates on the order of 1-2 mm/yr (Clarke et al., 1998), in response to the complex tectonic interplay between subduction beneath the Hellenic Arc, back-arc extension in the Aegean, and the westward movement of the Anatolian plate (e.g. Doutsos & Kokkalas, 2001; Kokkalas et al., 2006). In central Greece, much of the extensional strain is localised into a number of WNW-ESE trending grabens, which are mostly characterised by complex geometries in map view (Fig.1: right), and a high degree of segmentation along strike (Doutsos & Poulimenos, 1992; Ganas et al., 1998; Kokkalas et al., 2007). Most of the major range bounding normal faults are thought to have been active in the Pleistocene, but the relative time of their activity is not well constrained. Some historical earthquakes in the region are known, but none can be directly associated with Arkitsa fault zone or any other fault with certainty, except the 1894 rupture events of Atalanti fault (Ambraseys & Jackson, 1990).

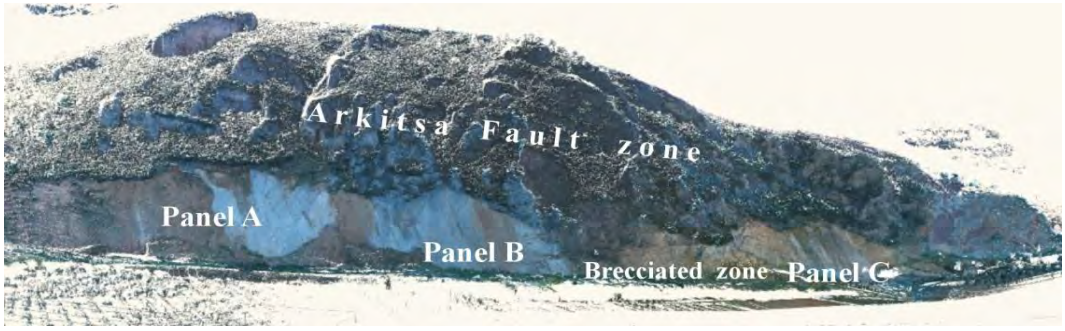

Figure 2 - Plan view image of the Arkitsa fault zone showing the three fault panels (A, B, C). The sampling area is on the left part of the picture-left part of panel A (LiDAR image; Jones et al., 2009-view towards south).

The study site for this work is the area of spectacularly exposed fault surfaces of the Arkitsa fault zone (Fig. 2), firstly reported by Jackson & McKenzie (1999), located on the southern side of the northern Gulf of Evia in central Greece. The Arkitsa fault zone, together with Ag. Konstantinos fault and Kamena Vourla fault (KVF) towards the west, form a WNW-ESE left stepping, north-dipping fault margin that link with the southern margin of the Almyros-Sperchios graben (Fig.1: right). The Arkitsa fault zone, which has a length of ~10 km, separates Late Triassic – Jurassic platform carbonates in the footwall from Lower Pliocene to Quaternary sediments in the hangingwall (Kokkalas et al., 2007). Below the carbonate units a characteristic Middle/Late Triassic volcano-sedimentary sequence is formed (Pe-Piper & Panagos, 1989). The amount of fault throw apparently varies along strike, typical of highly segmented fault zones. A minimum throw for the Arkitsa fault zone, based on Neogene-Holocene sediment thickness on the hangingwall block plus the scarp height and topographic relief of the footwall block, is estimated to be around 500-600m (Jones et al., 2009). Thus, a slip rate of 0.2-0.3 mm/yr can be calculated for Arkitsa fault zone, taking into account that faults of Evia rift zone started their activity in the last 2-3 My (Ganas et al., 1998).

The Arkitsa fault is best exposed in an outcrop 500 m south of the main Athens – Lamia national road, where recent quarrying activity during the last 20 years has removed most of the hangingwall colluviums, revealing fresh exposures of the upper ~65 m of three large fault panels (Kokkalas et al., 2007). The geomorphological expression of Arkitsa area, the back-tilted terraces on the Arkitsa fault hangingwall block, as well as the fresh ~1m band of unweathered limestone at the contact between the scree and fault plane before the quarrying, suggest Holocene seismic activity along this fault.

3. Sampling and Analytical Methods

Three clay-gouge samples were collected within the fault core zone both from the centre and the periphery (Ar11, Ar12, Ar13; Fig.3a, b). In order to compare the mineralogy of the clay gouge zone with the colluvial sediments outside the fault, two representative samples were collected from the broader fault damage area (Ar4, Ar6; Fig. 3a).

The mineralogical analyses of the samples were conducted by X-ray diffraction (using a Bruker D8 advance diffractometer, with Ni-filtered and CuKα radiation). XRD patterns were obtained from oriented or random powder samples in a 2θ range of 2° to 60° at a scanning rate of 2 °/min. Random powder mounts of selected samples were prepared by gently pressing the powder into the cavity holder. Oriented clay powder samples were prepared by the dropper method.

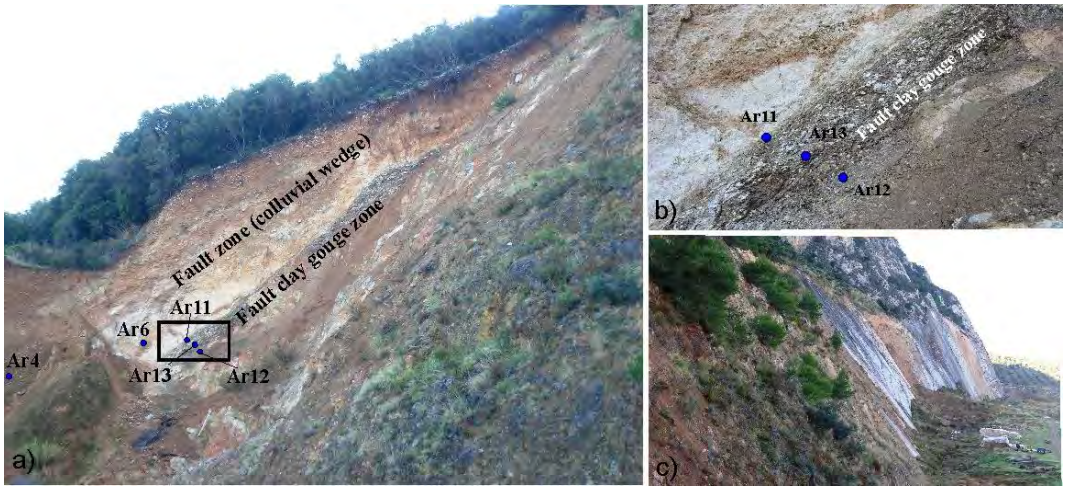

Figure 3 - (a) View of the Arkitsa Fault gouge zone and the colluvial wedge deposits adjacent to the eastern part of the scarp with sample locations. Rectangle shows the detailed area of Fig.3b (b) Detailed view of the fault clay gouge zone with location of the samples. (c) Side view of Arkitsa fault scarp showing the two of the three curved fault panels and the fault gouge zone between them.

Minerals morphology and chemical composition were examined using a Scanning Electron Microscope (SEM) JEOL 6300 equipped with an Energy Dispersive Spectrometer (EDS). The chemical composition of the minerals was determined using natural and synthetic standards and 20kV accelerating voltage with 10nA beam current. Microanalyses were performed on epoxy resin-impregnated polished and carbon or gold coated thin sections and sample powders mounted directly on the sample holder. In order to verify our results, minerals morphology and their chemical composition were also examined by using a SEM LEO SUPRA 35VP.

4. Results and Discussion

The mineralogical analyses of the collected samples were conducted by a combination of X-Ray Diffraction, SEM and Electron microprobe analyses (Figs 4, 5 and 6). The samples from the periphery of the fault clay gouge (samples Ar11, Ar12) are characterized by the presence of smectite (montmorillonite-determined using SEM-EDS) and calcite (Fig. 4e). The minerals that were identified within the centre of the fault clay gouge zone are: Smectite, corrensite, illite, micro-calcite, dolomite, quartz, plagioclase and K-feldspars (Table 1). These minerals do not coexist but are discriminated in two different assemblages. The Ar-13 lighter color assemblage is characterized by the presence of the clay mineral corrensite, as well as smectite (saponite) and illite that coexist with dolomite and plagioclase while K-feldspars are absent (Figs 4c, d, 5a, b and 6a, b). The presence of the above assemblage is confined in a thin zone (about 1cm thickness). The Ar-13, dark color assemblage is characterized by the presence of the clay mineral smectite, K-feldspars and in small amounts of illite while plagioclase is absent (Figs 4a, b, 5c, d and 6c). It should be noted that the type of smectite, as well as the mixed-layer (corrensite in the lighter color assemblage) and K-feldspars were identified using SEM-EDS (Fig. 6). The mineralogical analyses of the samples from the broader area showed the presence of calcite and in some cases montmorillonite, while corrensite and saponite are absent (Table 1, Fig. 4f).

The presence of corrensite is considered to be very important because is a regular mixed-layer chlorite-smectite clay mineral and more specifically chlorite-saponite. The presence of a different type of smectite (montmorillonite and not saponite) in the other assemblage, within the centre of the fault clay gouge, indicates that these two different assemblages represent probably different events or procedures. This is supported by the fact that the samples from the periphery of the fault clay gouge are characterized by the presence of montmorillonite and calcite and the absence of corrensite, as well as dolomite. In any case the assemblages found within the centre of the fault clay gouge did not form at the same time or place.

Taking into consideration that corrensite is usually formed in hydrothermal environments (Meunier, 2005), its absence in the samples from the broader fault damage area indicates the circulation of hydrothermal fluids only within the fault core zone. Saponite and corrensite may have been also originated when cooling, low P_H Mg-rich fluids invaded the Mesozoic platform carbonate series, that form the Arkitsa footwall, while calcite dissolution caused P_H to increase. The diagenetic formation of corrensite from saponite at depth and its uplift is not the case because saponite in diagenetic conditions would rather be transformed to palygorskite, which is not observed on any sample from Arkitsa. Additionally, the diagenetic transformation of smectite to chlorite is taking place not only through corrensite but via a continuous series of mixed-layers chlorite-smectite from pure saponite (near the surface) to pure chlorite at depth. The uplift would allow us not only to trace corrensite but a series of chlorite-smectite mixed-layers, which is clearly not the case here. In hydrothermal environments, the successive disappearance of saponite and corrensite at certain depths enable the following reaction to be written: saponite → corrensite → chlorite, (Beaufort et al., 1997). It is therefore, reasonable to suggest that the formation of corrensite is hydrothermal rather than diagenetic.

The assemblages within the fault gouge zone can provide important information about the conditions of their formation. The presence of corrensite, combined with the absence of chlorite and laumontite, indicate hydrothermal formation at neutral to alkaline conditions and a temperature range at about 100-150 ^{o}C (Meunier, 2005). The presence of the above assemblage confined in a thin zone (about 1cm thickness) indicates that the hydrothermal fluids were circulating only within this part of the fault zone and for a short period of time. It is therefore reasonable to assume that the hydrothermal fluids were elevated during a seismic event and from a zone at depth that reached temperatures on the order of 100-150 ^{o}C. In this way the alteration was confined in a thin zone in the centre of the fault gouge where the circulation of the hydrothermal fluids was taking place.

Table 1 - Mineralogical compositions of the studied samples within the fault clay gouge zone and two representative samples from the surrounding fault colluvial wedge.

Sample N° - Location	Clay Minerals	Quartz	Calcite - Dolomite	Feldspars
1 – (Ar 13) centre of the fault clay gouge zone (dark color).	+ Montmorillonite + illite	+	± Calcite	± K-Feldspars
2 – (Ar 13) centre of the fault clay gouge zone (light color)	+Corrensite + Saponite +illite	+	+ Dolomite	+ Plagioclase
3 –4 (Ar 11-Ar12) lower boundary of the fault clay gouge zone.	+ Montmorillonite	+	+ Calcite	-
4 (Ar 4)- Fault damage zone (colluvial deposits).	-	+	+ Calcite	-
5 (Ar 6) – Fault damage zone (colluvial deposits)	± Monmorillonite	+	+ Calcite	-

+: Presence, -: Absence, ±: traces

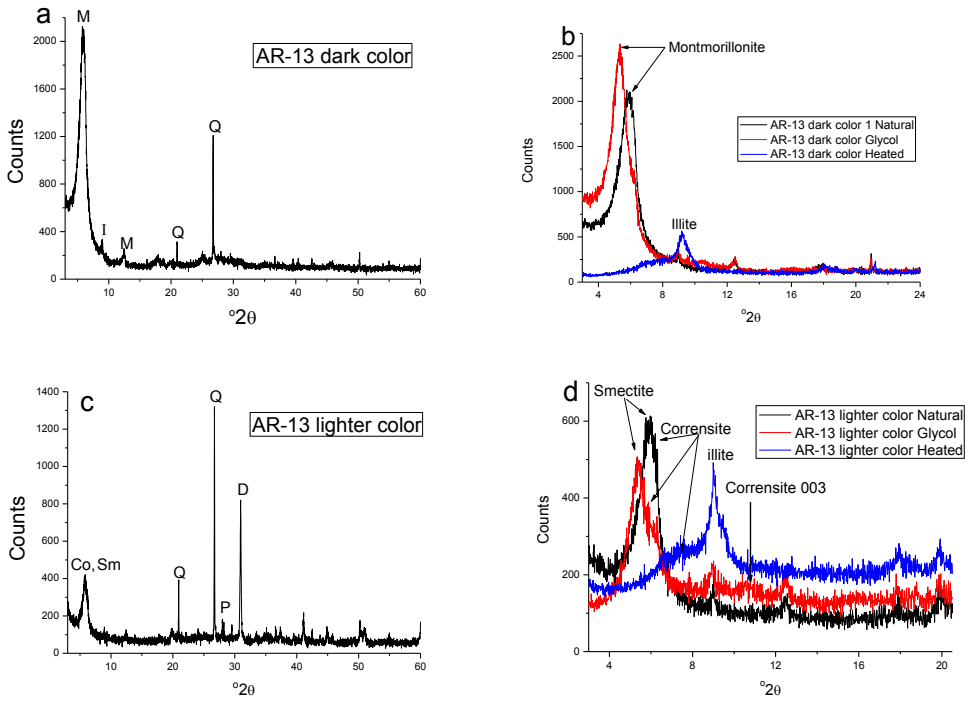

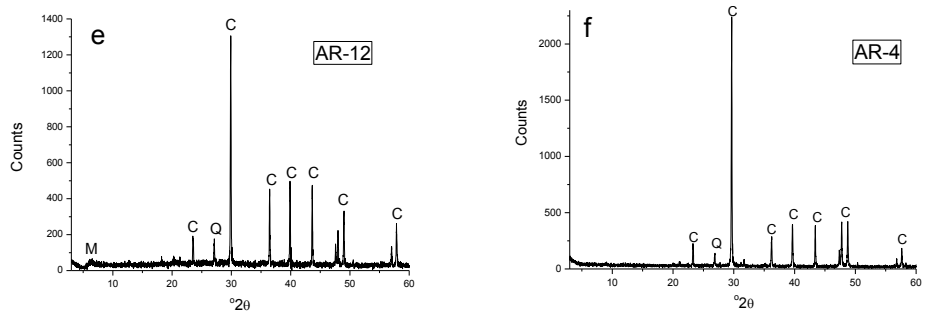

Figure 4 - XRD patterns of the assemblage Ar-13 dark color within the fault zone of bulk sample (a) and clay fraction (air dried-natural, glycolated and heated) showing the presence of smectite (b) XRD patterns of the assemblage Ar-13 lighter color within the fault zone of bulk sample (c) and clay fraction (air dried-natural, glycolated and heated) showing the presence of smectite and corrensite (d) XRD patterns of a sample (Ar-12) from the periphery of the fault gouge showing the presence of smectite (M) and calcite (e) and of a representative sample Ar-4 from the broader fault zone area (f) (M: montmorillonite, I: illite, Co: corrensite, Sm: Smectite (saponite) Q: quartz, P: plagioclase, D: dolomite and C: calcite).

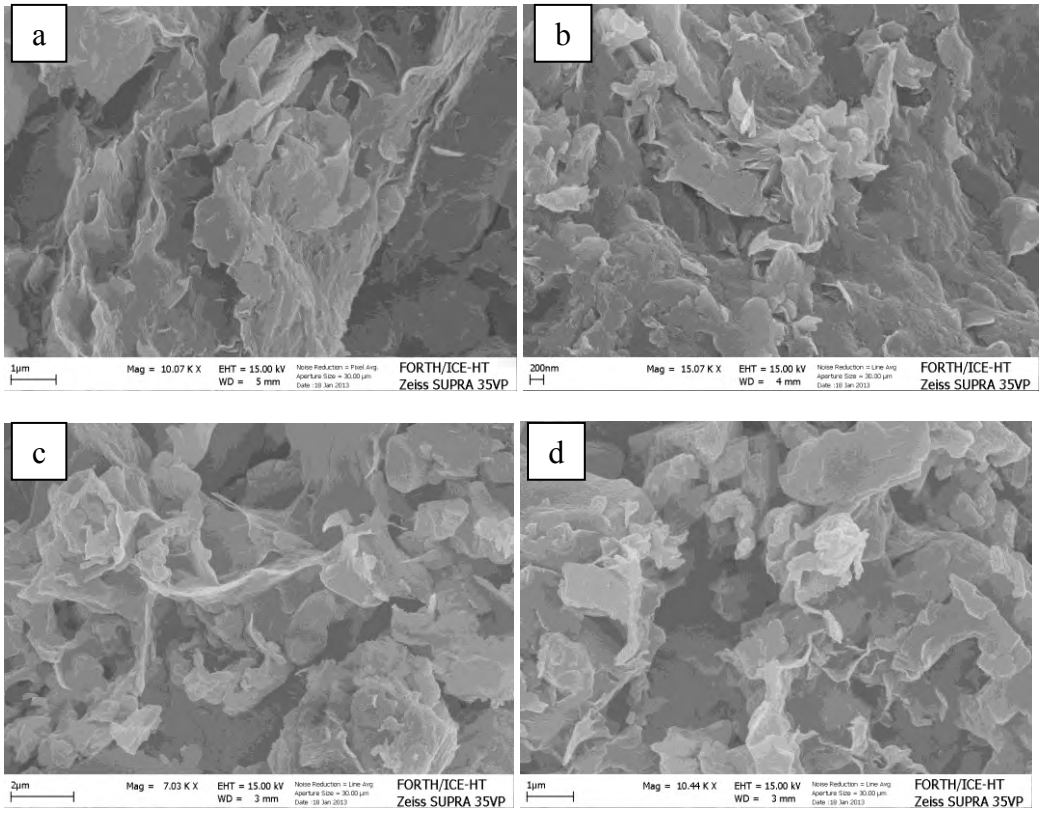

Figure 5 - SEM micrographs of (a) saponite and (b) corrensite of the assemblage Ar-13 lighter color within the fault zone (c, d) montmorillonite of the assemblage Ar-13 dark color within the fault gouge.

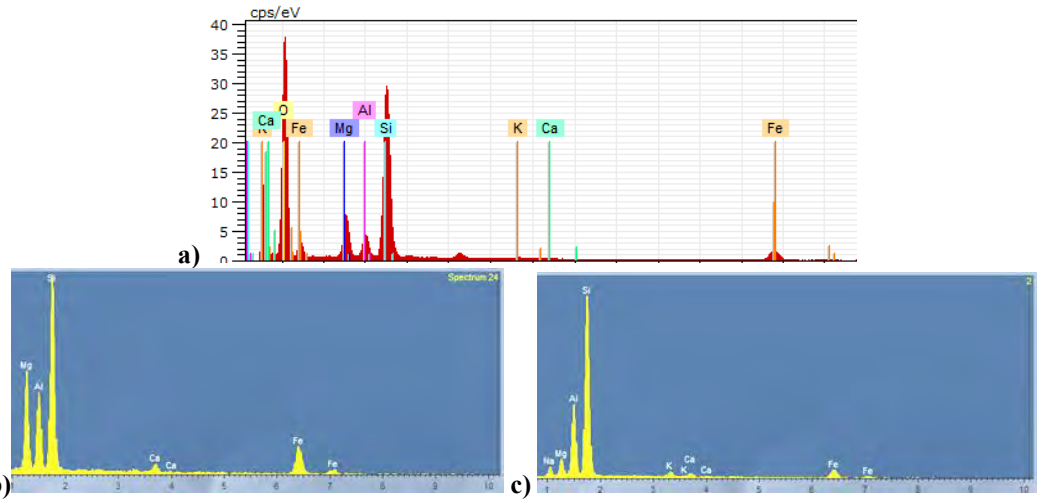

Figure 6 - SEM-EDS spectra of a) saponite and b) corrensite of the assemblage Ar-13 lighter color and c) montmorillonite of the assemblage Ar-13 darker color.

5. Conclusions

Clay samples were collected within the Arkitsa fault gouge zone, as well as in the broader fault damage area. The mineralogical analyses of the samples within the core of the fault zone revealed the presence of the minerals: Montmorillonite, corrensite, illite, micro-calcite, dolomite, quartz, plagioclase and K-feldspars. The absence of corrensite, a clay mineral usually formed in hydrothermal conditions, in the samples from the broader fault damage area indicates that the circulation of hydrothermal fluids was confined only within and around the fault core zone. The assemblages within the fault clay gouge zone and especially the presence of corrensite, combined with the absence of laumontite, indicate hydrothermal alteration at neutral to alkaline conditions and a temperature range at about 100-150 ^{o}C. The hydrothermal alteration appears to be caused by fluids ascending from deeper zones (~3-5 km), that circulated upwards through voids formed during a co-seismic slip event between the fault blocks.

6. Acknowledgments

The authors would like to thank Dr. Drakopoulos of the Foundation for Research and Technology-Hellas (FORTH) Institute of Chemical Engineering and High Temperature Chemical Processes (ICE/HT) Rio-Patras, Greece, for his help with SEM micrographs.

7. References

Ambraseys N. and Jackson J. 1990. Seismicity and associated strain of central Greece between 1890 and 1988, *Geophys. J. Int.,* 101, 663-708.

Beaufort D., Baronnet A., Lanson B. and Meunier A. 1997. Corrensite: a single phase or a mixed layered phyllosilicate of the saponite-chlorite conversion series? The case study of the Sancerre-Couy deep drill-hole (France), *American Mineralogist*, 82, 109-124.

Bruce C.H. 1984. Smectite dehydration-its relation to structural development and hydrocarbon accumulation in Northern Gulf of Mexico basin, *AAPG Bulletin*, 68, 673-683.

Clarke P.J., Davies R.R., England P.C., Parsons B., Billiris H., Paradissis D., Veis G., Cross P.A., Denys P.H., Ashkenazi V., Bingley R., Kahle H.-G., Muller M.-V. and Briole R. 1998. Crustal strain in central Greece from repeated GPS measurements in the interval 1989-1997, *Geophysical Journal International,* 135, 195-214.

Doutsos T. and Poulimenos G. 1992. Geometry and kinematics of active faults and their seismotectonic significance in the western Corinth-Patras rift (Greece), *Journal of Structural Geology,* 14, 689-699.

Doutsos T. and Kokkalas S. 2001. Stress and deformation in the Aegean region, *Journal of Structural Geology,* 23, 455-472.

Fitts T.G. and Brown K.M, 1999. Stress-induced smectite dehydration: ramification for patterns of freshening and fluid expulsion in the N. Barbados accretionary wedge, *Earth and Planetary Science Letters*, 172, 179-197.

Ganas A., Roberts G. and Memou P. 1998. Segment boundaries, the 1894 ruptures and strain patterns along the Atalanti fault, central Greece, *Journal of Geodynamics*, 26, 461-486.

Jackson J. and McKenzie D. 1999. A hectare of fresh striations on the Arkitsa fault, central Greece, *Journal of Structural Geology*, 21, 1-6.

Jones R.R., Kokkalas S. and McCaffrey K.J.W. 2009. Quantitative Analysis and Visualisation of non-planar fault surfaces using Terrestrial Laser Scanning ("LiDAR") - the Arkitsa Fault, central Greece as a case study, *Geosphere*, v.5, no.6, 465-482.

Knipe R.J. 1993. The influence of fault zone processes and diagenesis on fluid flow. In: Horbury A.D., Robinson A.G. (eds) Diagenesis and basin development. *AAPG, Studies in Geology*, 36, 135-148.

Kokkalas S., Xypolias P., Koukouvelas I. and Doutsos T. 2006. Postcollisional contractional and extensional deformation in the Aegean region, *in* Dilek, Y., and Pavlides, S., eds., Post-collisional tectonics and magmatism in the Mediterranean region and Asia: *Geological Society of America Special Paper, 409*, 97–123.

Kokkalas S., Jones R.R., McCaffrey K.J.W. and Clegg P. 2007. Quantitative fault analysis at Arkitsa, Central Greece, using terrestrial laser-scanning (LiDAR), *Bull. Geol. Soc. Greece*, vol. XXXX, 1959-1972.

Koukouvelas I.K. and Papoulis D. 2009. Fluid involvement in the active Helike normal Fult, Gulf of Corinth, Greece, *Journal of Structural Geology*, 31, 237-250.

Meunier A. 2005. *Clays*, Springer-Verlag, pp. 473, ISBN 3-540-21667-7

Moore D. and Rymer M. 2012. Correlation of clayey gouge in a surface exposure of serpentine in the San Andreas Fault with gouge from the San Andreas Fault Observatory at Depth (SAFOD), *Journal of Structural Geology*, 38, 51-60.

Morrow C.A. Radney B. and Byerlee J. 1984. Permeability of sault gouge under confining pressure and shear stress, *Journal of Geophysical Research Bulletin*, 89, 3193-3200.

Morrow C.A. Radney B. and Byerlee J. 1992. Frictional strength and the effective pressure law of montmorillonite and illite clays. In: Evans, B and Wong, T.F. (eds) *Fault Mechanics and Transport Properties of Rocks*, Academic Press, New York, 69-88.

Müller-Vonmoos M. and Loken T. 1989. The shearing behaviour of clays, *Applied Clay Science*, 4, 125-141.

Pe-Piper G. and Panagos A.G. 1989. Geochemical characteristics of the triassic volcanic rocks of Evia: petrogenetic and tectonic implications, *Ofioliti,* 33-50.

Rosenquist I. 1962. The influence of physicochemical factors upon the mechanical properties of clays, *Clays and Clay Minerals*, 9, 12-23.

Rosenquist I. 1984. The importance of pore water chemistry on mechanical and engineering properties of clay soils, *Philosophical Transactions of the Royal Society, Series A*, 311, 369-383.

Solum J.G., van der Pluijm B.A., Peacor D.R. and Warr L.N. 2003. Influence of phillosilicate mineral assemblages, fabrics, and fluids on the behavior of the Punchbowl Fault, southern California, *Journal of Geophysical Research*, 108(B5): 5-1-5-12.

Vrolijk P. 1990. On the mechanical role of smectite on subduction zones, *Geology*, 18, 703-707.

War L.N. and Cox S. 2001. Clay mineral transformations and weakening mechanisms along the Alpine Fault. New Zeland, *Geological Society of London, Special Publication,* 186, 85-101.

Wibberley C. 1999. Are feldspar-to-mica reactions necessarily reaction-softening processes in fault zones? *Journal of Structural Geology,* 21, 1219-1227.

Wintsch R.P., Christoffersen R. and Kronenberg A.K. 1995. Fluid-rock reaction weakening of fault zones, *Journal of Geophysical Research*, 100(B7): 13021-13032.

Δελτίο της Ελληνικής Γεωλογικής Εταιρίας, τομ. XLVII , 2013
Πρακτικά 13ου Διεθνούς Συνεδρίου, Χανιά, Σεπτ. 2013

Bulletin of the Geological Society of Greece, vol. XLVII 2013
Proceedings of the 13th International Congress, Chania, Sept. 2013

ALONG-STRIKE VARIATIONS IN THE HELLENIDE-ANATOLIDE OROGEN: A TALE OF DIFFERENT LITHOSPHERES AND CONSEQUENCES

Ring U.[1], Gessner K.[2], Thomson S.[3] and Markwitz V.[2]

[1]*Department of Geological Sciences, Stockholm University, Stockholm, Sweden, uwe.ring@geo.su.se*

[2]*Centre for Exploration Targeting, The University of Western Australia, M006, 35 Stirling Highway, Crawley 6009, Australia*

[3]*Department of Geosciences, University of Arizona, Gould-Simpson Building, 1040 E. 4th St., Tucson, AZ 85721-0077, USA;*

Abstract

Structure and exhumation history of the Hellenide-Anatolide Orogen in the Aegean Sea region and the adjacent Anatolian peninsula is controlled by along-strike variations of pre-Alpine palaeogeography. In the Hellenides, Mesozoic extension created ribbon-like continental fragments of thinned and dense lithosphere that pinch out eastwards. In the east, the relatively large Anatolide microcontinent mostly escaped Mesozoic extension and lithospheric thinning, presumably because it had a distinctly different, thicker and more depleted lithosphere. In the Aegean transect these along-strike differences in lithosphere structure ultimately resulted in sustained high-pressure metamorphism followed by progressive slab retreat since about 60 Ma. Further east, collision of the Anatolide microcontinent at about 42 Ma formed a south verging greenschist-facies thrust-and-fold belt. Pronounced slab retreat in the Aegean forced differential extension resulting in a broad sinistral wrench corridor that started to from at 24-23 Ma. Since then, extension in both regions mainly controlled denudation. This review highlights how differences in pre-orogenic architecture control lithospheric thickening and the subsequent exhumation of high-pressure rocks, and how large-scale continental extension evolves.
Key words: *Hellenides, Anatolides, lithospheric tear.*

1. Introduction

Much of the conceptual understanding of the development of orogens is still largely based on the assumption of cylindricity, i.e. the premise of structural continuity along strike. However, lithospheric architecture and strain in orogens usually vary substantially, both across and along strike. The causes for along-strike variations are likely to differ in individual orogenic belts, but pre-orogenic paleogeography, continental architecture, the nature of the accreting lithospheric fragments and kinematic/geometric variations at the lithospheric scale potentially play an important role. Along-strike changes in orogens have a profound impact on how major orogenic processes proceed in time and especially in space along strike.

Conceptual and numerical models of generic and regionally specific orogens suggest that deformation is mainly driven by external forcing by the sinking slab (Royden, 1993), but also internally,

by gravitational instabilities within the thermally weakened overriding plate (Houseman et al., 1981). Here we present an example of along-strike variations in the Hellenide-Anatolide Orogen in the eastern Mediterranean showing that regions controlled by slab sinking can occur in close proximity to region whose development is controlled by delamination.

Presently the transition from the Hellenide Orogen of Greece and the Anatolide Belt of west Turkey (aka Menderes Massif) is marked by a drastic change in topography, i.e. the changeover from the Aegean Sea basin into the Turkish mainland (Figure 1) (Gessner et al., 2013). Recent field-based studies show that differences in pre-orogenic paleogeography caused the Hellenide Orogen of eastern Greece and the Anatolide Belt of western Turkey to evolve in different ways (Gessner et al., 2011). We believe that better identification and understanding of those differences will potentially clarify how eastern Mediterranean subduction zones evolved, how pre-orogenic architecture and lithospheric structure controls crustal thickening, the exhumation of high-pressure rocks, and especially how large-scale continental extension evolves.

Figure 1 - Highly simplified tectonic map of the Mediterranean plate boundary zone showing retreating, advancing, and major transcurrent plate boundaries (barbs on overriding plate). Shown are the three major plates (Eurasia, Africa, Arabia) and, schematically, microplates between the three major plates; these microplates are currently forming (e.g., Anatolia) or have been amalgamated to Eurasia in the past (e.g., Adria). Vertical lines indicate highly extended regions above retreating plate boundaries (after Ring et al., 2010).

2. Setting

2.1. Paleogeography

In the eastern Mediterranean, the Adriatic plate (Adria for short) pinches out towards the east. Figure 2 shows a paleogeographic reconstruction of the area (Gessner et al., 2001a). The eastern edge of Adria is characterized by ribbons of normal thickness continental crust and intervening parts of highly stretched and thinned crust which were, at least in part, oceanic (Robertson et al., 1991). The stretching and oceanization resulted from Mesozoic rifting processes in and before the early Cretaceous when Adria was the northern part of the African plate. These rifting processes ultimately separated Adria from Africa. Further east, Neotethys broadened (Robertson et al., 1991) and a number of continental blocks that rifted off Gondwana in the Jurassic and Cretaceous occur. In the eastern Mediterranean the continental block east of Adria was Anatolia (Figure 2). Below we outline major difference in lithospheric architecture between Adria (Aegean Sea region) and Anatolia (west Turkey).

2.2. Regional Structure

The Hellenide orogen of Greece and the Anatolide belt of western Turkey form an arcuate orogen

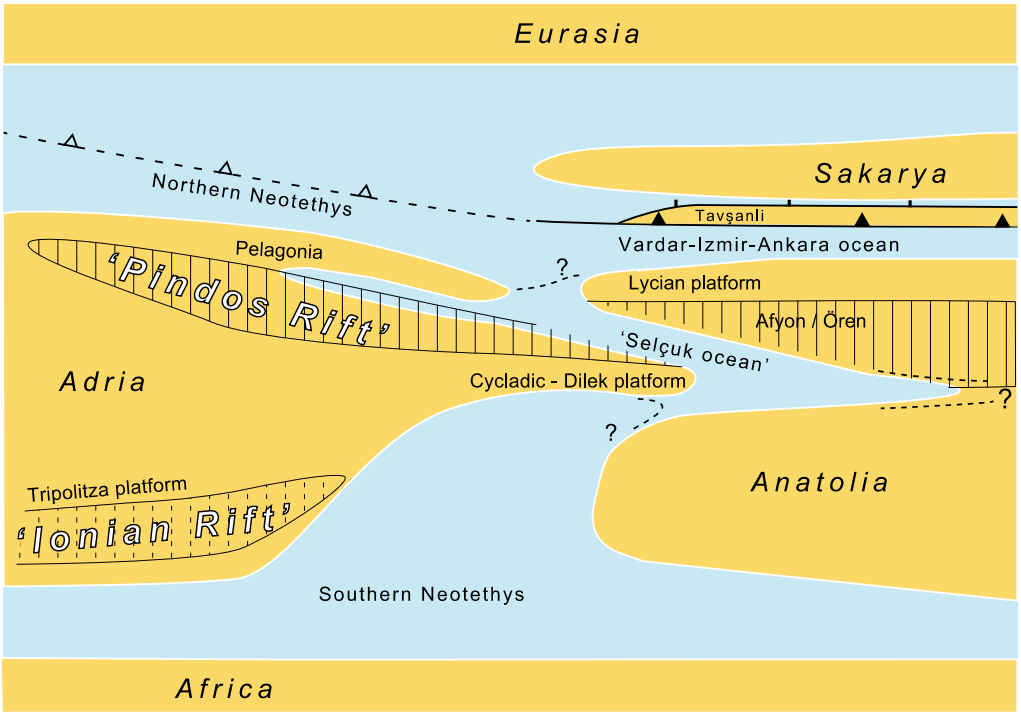

Figure 2 - Paleotectonic reconstruction of the eastern Mediterranean (after Gessner et al., 2013).

to the north of the present-day active Hellenic margin which marks the site of northnortheastwards underthrusting of the African plate underneath Europe. Both regions consist of a nappe stack, which is fringed to the north by the Late Cretaceous to Paleogene Vardar-İzmir-Ankara suture (Figure 3) zone, referred to as suture zone in the remainder of the paper. This Neotethyan suture separated units of Eurasian affinity in the north (Rhodope and Sarkaya zones) from Adria-derived continental units in Greece and a Gondwana-derived continental fragment in west Turkey (Anatolia) to the south. We will use this suture zone as our marker and describe the tectonic units below it from the Hellenide Orogen in the Aegean Sea region and the Anatolide belt in west Turkey. We will show that the nappe piles in both regions are characterized by nappes with different lithologies, PTt history and have different crustal architectures (Gessner et al., 2013).

2.2.1. Hellenide Orogen

In the Aegean Sea transect, the general architecture of the nappe pile is commonly north dipping. The uppermost nappe, referred to as Upper Unit, consists of the composite Cycladic ophiolite nappe made up of non-metamorphosed to greenschist-facies ophiolitic rocks and tectonically intercalated low-pressure metamorphic rocks of Late Cretaceous age (Jolivet et al., 1996). We regard this Upper Unit as part of the suture zone. The basement-cover sequence of the Pelagonian Zone occurs below the suture zone. Only parts of the Pelagonian Zone show evidence for Late Cretaceous high-pressure metamorphism, whereas other parts of the Pelagonian Zone escaped metamorphism (Jolivet and Brun, 2010). The Pelagonian Zone is made of a Paleozoic basement with a Paleozoic and Mesozoic carbonate cover overlain by Jurassic ophiolite obducted toward the end of the Jurassic (Jacobshagen, 1986).

Below the Pelagonian Zone is the Cycladic Blueschist Unit, which is generally considered part of the Pindos Zone (Jolivet and Brun, 2010; Ring et al., 2010). The Cycladic Blueschist Unit is a continental unit with an Eocene-Oligocene flysch (Özer et al., 2001). The major tectonic members of the Cycladic Blueschist Unit are in decending order: (i) A melange-like assemblage of ophiolitic rocks and garnet-mica schist embedded in a serpentinitic and shaly matrix (Ring et al., 1999). (ii)

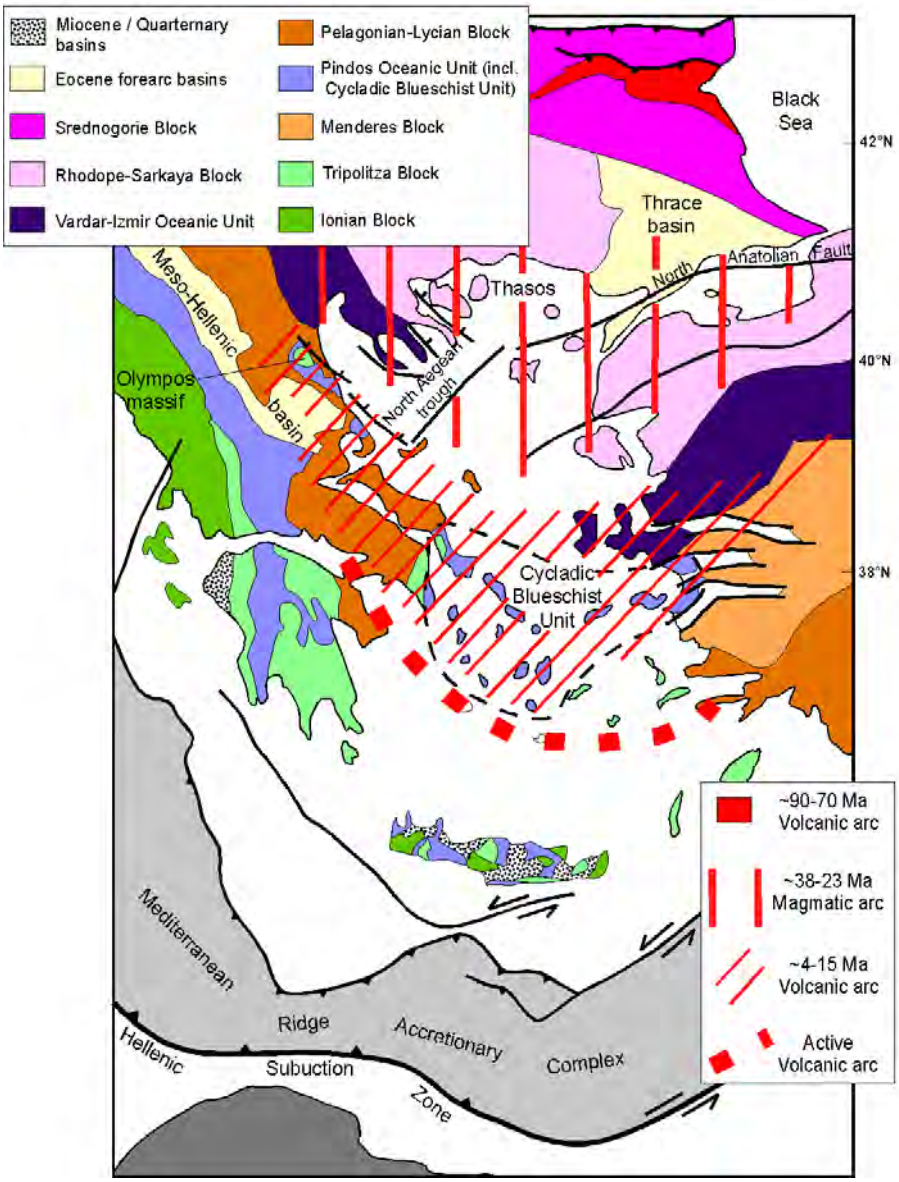

Figure 3 - Map of Hellenide-Anatolide orogen in the Aegean Sea – west Turkey transect. Simplified tectonic map of the Aegean region showing the main tectonic zones above the Hellenic subduction zone. The Mediterranean Ridge represents the modern accretionary wedge that is bounded to the north by a major backthrust system. Red line patterns indicate the positions of subduction-related magmatic-arc rocks from ~38 Ma to the Recent. The migration of this magmatic arc in the overriding plate mimics the retreat of the Hellenic slab. Also shown (in red) in the north is a volcanic arc related to the subduction of the Vardar-Izmir Oceanic Unit at ~90 Ma (after Jolivet and Brun, 2010 and Ring et al., 2010).

A shelf sequence composed of marble, metapelite, quartzite and metabasite that has been intruded by Triassic granitoids (Ring et al., 1999). (iii) A Carboniferous basement nappe made up by augengneiss, garnet-mica schist and dolomitic marble (Ring et al., 1999). The various nappes of the

Cycladic Blueschist Unit have all undergone high-pressure metamorphism at PT conditions of 12-20 kbar and 450-550°C between 53 to 30 Ma (see reviews in Jolivet and Brun, 2010 and Ring et al., 2010). Below the Cycladic Blueschist Unit occurs the Tripolitsa Zone. The latter underwent high-pressure metamorphism at 8-14 kbar and 350-450°C in windows in the Cyclades and Amorgos and very-low-grade metamorphism in Crete (Jolivet et al., 1996; Shaked et al., 2000). The underlying Ionian Zone is made up by the Plattenkalk and Phyllite-Quartzite units in Crete. At least the Phyllite-Quartzite Unit also shows an increase in high-pressure conditions from Crete (10-12 kbar and 350°C in central Crete) to the W (18 kbar and 400°C) and N (>13 kbar and 500–600°C in Amorgos) (Rosenbaum et al., 2007). The entire nappe pile has been thrust over the East Mediterranean Accretionary Complex, which started to from at 19 Ma and is being underthrust beneath Crete as the leading edge of the overriding plate.

In summary, the various units below the suture zone in the Aegean transect shows evidence for sustained high-pressure metamorphism. Jolivet and Brun (2010) and Ring et al. (2010) showed that the age for this metamorphism becomes younger from north to south towards lower structural units and reflects stages of the southward retreat of the subducting Hellenic slab.

2.2.2. Anatolide Belt

The overall structure of the Anatolide Belt of west Turkey is that of a dome-shaped nappe pile (Sengör et al., 1984). The non- to weakly metamorphosed Lycian Nappes represent a Mesozoic carbonate platform that makes up the highest tectonic unit below the suture zone. Below the Lycian Nappes follows the high-pressure metamorphosed continental Tavşanlı-Afyon-Ören Unit, with a Late Cretaceous (70-60 Ma) age for the high-pressure overprint (Sherlock et al., 1999). The Tavşanlı-Afyon-Ören Unit is underlain by the Cycladic Blueschist Unit, the latter of which has a similar tectonometamorphic history as in the Aegean Sea region (Gessner et al., 2011) and has been metamorphosed at high-pressure conditions around 42-40 Ma (Candan et al., 1997). The Cycladic Blueschist Unit in west Turkey has a lower sedimentary unit, the Dilek Nappe, composed of a shelf sequence comprising metapelite, quarzite, metabasite lenses and metabauxite-bearing marble. The Dilek Nape is overlain by the Selcuk melange, an assemblage of ophiolitic rocks embedded in a serpentinitic and shaly matrix. The Cycladic Blueschist Unit in west Turkey rests along the out-of-sequence Cyclades-Menderes Thrust above the Menderes Nappes (Gessner et al., 2013). The Menderes Nappes consists of four individual nappes, which, and this is an important point of our review, do not show any signs for a high-pressure overprint (Ring et al., 2001). It is important to note that detailed studies by various groups has demonstrated that the entire sequence below the two magneisocarpholite-kyanite-chloritoid bearing rocks does not show any relics for a high pressure overprint (Regnier et al., 2003), indicating that most probably the entire Menderes Nappes did not undergo high-pressure metamorphism.

In descending order the Menderes Nappes consist of: (1) The Selimiye Nappe containing Paleozoic sequence of schist, marble and quartzite. (2) The Çine Nappe made up by a Pan-African basement unit consisting of metagranite, augengneiss, metabasite and metapelite. Intrusion of most of the magmatic rocks took place at the Precambrian/Cambrian boundary and in part cut the penetrative amphibolite-facies tectonometamorphic fabric in the Çine Nappe (Gessner et al., 2001a). (3) The Bozdağ Nappe consisting of metapelite and quartzofeldspathic rock, which have been intruded by Pan-African and Triassic granitoids. Especially the Triassic granitoids cut the penetrative amphibolite-grade tectonometamorphic fabric in the Bozdağ Nappe. (4) The greenschist-facies Bayındır Nappe at the base containing schist and marble, the latter of which has Late Cretaceous rudists (Özer et al., 2001). The above described nappe pile has been thrust in a southerly direction onto the non-metamorphosed Mesozoic Bey Dağları carbonate platform in Miocene times (van Hinsbergen, 2010).

We stress, that the architecture of the Hellenide Orogen and the Anatolide Belt is strikingly different. As discussed in Ring et al. (1999), the Dilek nappe and the Selcuk melange can be correlated with nappes of the shelf sequence and the overlying ophiolitic melange of the Cycladic Blueschist

Unit in the Aegean and therefore might serve as a vertical marker. The intrusion of Triassic granitoids, which are interpreted to be related to the final closure of Paleotethys to the north (Sengör et al. 1984), into this shelf sequence indicates that it was the northern passive margin of Tethys. The Carboniferous basement of the Cycladic Blueschist Unit underlies this marker and has no counterpart in western Turkey. In contrast, some of the Menderes Nappes have a Pan-African basement and underlie this marker. This demonstrates that both regions belong to different crustal provinces. Therefore, both regions had different lithospheres before the onset of orogeny, and it is conceivable, and actually very likely, that the mantle components of the different lithospheres were different as well. Because only Adria had an anomalously heavy lithospheric mantle, pronounced roll-back and sustained high-pressure metamorphism characterizes the Aegean Sea region. In west Turkey, the lighter lithosphere of Anatolia halted subduction and the Menderes Nappes escaped sustained high-pressure metamorphism.

2.3. Topography

The differences in orogenic structure are reflected in a different morphologic development of both regions (Gessner et al., 2013). The Hellenide Orogen in the Aegean is largely under water and the islands either represent updomed footwalls of metamorphic core complexes or are horst structures due to post-core-complex high-angle normal faulting. The highest mountain peaks are on either side of the Aegean Sea basin (Mt. Ochi, 1394m, in southeast Evia and Kerkis, 1414m, in west Samos). Within the central Aegean peaks rarely reach 1000m (e.g. Mt. Zas in Naxos, 999m). The islands are separated from each other by Miocene to Recent graben structures with water depths of the order of 1000-2000m.

In contrast, the entire Anatolide Belt of west Turkey is emergent. The topographic evolution shows a two-stage history. After a first phase of lithospheric scale extension at the Oligocene/Miocene boundary (for details see below), an areally extensive erosion surface formed by mid-Miocene times (Yilmaz et al., 2000). This erosion surface shows that an orogenic plateau of unknown elevation had formed in west Turkey. The mid-Miocene erosion surface has then been significantly deformed from the Pliocene to the Recent by fragmentation of the plateau by the Kuzey and Güney detachment systems of the Central Menderes metamorphic core complex (Gessner et al., 2001b). In the footwalls of the two detachment systems a mountainous topography with peak elevations >2000m developed. It is likely that the topography and high elevation are the incised remains of the former plateau.

2.4. Magmatic Evolution

Most plutonic and volcanic rocks in the Aegean have enriched isotope signatures, which together with pronounced enrichment of incompatible elements, indicate mantle refertilization by a subduction component similar to continent-derived sediments subducted at the present Hellenic Trench (Siebel and Altherr, 2002) and reflect a history of melting processes above the long-lived southward retreating Hellenic subduction zone. The transfer of heat and juvenile melts from the mantle varied probably in response to episodic roll-back of the subducting lithospheric slab, as suggested by punctuated crystallisation age spectra within and among individual granitoid plutons. Detailed studies on the silicic plutonic rocks in the central Aegean document an episodic crystallisation history from 11 to 17 Ma, with peraluminous (S-type) granitoids systematically older than closely associated metaluminous (I-type) granitoids (Bolhar et al., 2010).

Post-collisional magmatism in western Anatolia began in the Eocene, and propagated from north to south (Dilek and Altunkaynak, 2007). The youngest plutonic rocks in the Menderes Massif are the Salihli and Turgutlu granodiorites with ages of 16-15 Ma (Glodny and Hetzel, 2007). The two granodiorites have a subduction zone geochemical signature, which may have been inherited from earlier subduction events in the region. During the evolution of the Eocene and Oligo-Miocene volcano-plutonic rocks, this subduction influence decreased and crustal contamination increased through time. In the early Miocene, alkaline bimodal magmatic rocks became more prominent (Dilek and Altunkaynak, 2007). The final phase of magmatism produced late Miocene to Quater-

nary alkaline to super-alkaline volcanic rocks with progressively more potassic compositions. Asthenospheric upwelling caused by partial delamination of the lithospheric root beneath the western Anatolian orogenic belt was likely responsible for the melt evolution of these alkaline volcanics (Dilek and Altunkaynak, 2007).

The alkaline basaltic activity since the Miocene was temporally distinct from the older subduction-related magmatism. Most of these alkaline volcanics occurs along the Aegean Sea / Turkish coastline (Agostini et al., 2007). The intraplate character of this alkaline association indicates that the mantle wedge, previously metasomatized by slab-derived material, was replaced by the upwelling of asthenospheric mantle as a result of rupturing of the downgoing slab.

2.5. Lithospheric Structure

Crustal thickness in the Aegean Sea region is variable. In the Cyclades it is around 30 km and towards the south the crust thins to about 15 km in the Cretan Sea south of the present volcanic arc. Underneath Crete the crust thickens again to some 40-50 km in the west and 30 km in eastern Crete (Knapmeier and Harjes, 2000). The thick crust underneath western Crete is due to underthrusting of sediments; this underplating process diminishes to the east and eventually stops in the southeast Aegean.

The results show a general trend of westward crustal thinning from 36 km in central Anatolia to 28–30 km in the central Menderes Massif to 25 km beneath the Aegean Sea. The results also indicate that crustal thinning in the Aegean is not uniform in the N-S extensional direction. The crust is thinner in the central Menderes Massif (28–30 km of crustal thicknesses) and the Cycladic Massif (25–26 km) than in surrounding regions where crustal thicknesses are 32–34 km.

The Aegean is 'underthrust' by Eocene and younger nappes (van Hinsbergen et al., 2005), all of which record high-pressure metamorphism at depth of 40-70 km (Ring and Layer, 2003). The entire former lower crust and the lithospheric mantle section of the incoming Adriatic plate has been subducted.

The lithosphere of Adria pinches out the east (Figure 2) and this appears to be marked by a lack of subduction-related seismicity to the east of Crete (Knapmeier and Harjes, 2000), the reduced crustal thickness in eastern Crete and the shallowing and disappearance of the Pliny and Strabo furrows in the Rhodos basin (Figures. 1, 3).

The crustal thickness of the Anatolide Belt in west Turkey is of the order of 40 km and thus significantly thicker than in the Aegean Sea region (Makris and Stobbe, 1984). Van Hinsbergen et al. (2010) argue that the Anatolide Belt of west Turkey is still underlain by its own continental lower crust. In contrast to the Aegean Sea region, there is no evidence that the Anatolide Belt is 'underplated' by Eocene and younger nappes (Ring et al., 1999; van Hinsbergen, 2010). Based on tomographic images and a new gravity model of the Moho from west Turkey van Hinsbergen et al. (2010) and Gessner et al. (2013) further argue that the Anatolide Belt does not have a mantle lithosphere, but is instead overlying asthenosphere directly. Such a view is supported by geophysical data of Meier et al. (2007) showing an ‘asthenospheric window’ beneath west Turkey. Van Hinsbergen (2010) suggests that the delamination of the lithospheric mantle started at about 45 or so to the north of the Anatolide belt and continued until about 35 Ma, for the slab to be able to accommodate ongoing Africa-Europe convergence. However, Prelevic et al. (2010) showed that magma compositions in west Anatolia is alkaline bimodal since the early Miocene, and that magmatic activity progressed from north to south, and volcanic rocks became higher in potassium towards the west. There is also isotopic evidence for a drastic shallowing of the source region of mafic magma since the early Miocene (Prelevic et al., 2010). These data strongly support the hypotheses that the removal of the lithospheric mantle below west Anatolia started in the early Miocene. The development of the mid Miocene erosion surface on the plateau may have either been caused by shallowing of subduction or is due to dynamic topography caused by the delamination of the lithospheric mantle.

Mantle tomography images suggest a tear in the downgoing slab in the west of Turkey (de Brooder et al., 1999). Such a tear would explain the drastic differences in lithospheric structure and tectonic evolution between the Aegean Sea and west Turkey. However, it is not known when this tear formed. Ring et al. (2010) proposed that it formed in the early Miocene. Berk Biryol et al. (2011) interpreted a new gravity anomaly and crustal thickness models to support a mantle-scale discontinuity across the Aegean coastline of Anatolia. Gessner et al. (2013) suggest an early Miocene age for this discontinuity.

3. Discussion

3.1. Differential extension

Fission track data (Figure 4, 5) reflect marked differences in the mid/late Miocene cooling history between the Aegean Sea region and western Anatolia (Ring et al., 2010). In the central Aegean, ongoing extension above the southward retreating Hellenic subduction zone was aided in the mid Miocene by the southward migration of the magmatic arc into the Cyclades region and the central Aegean underwent a major phase of lithospheric extension between about 15-8 Ma (Ring et al., 2010). At the same time in the mid Miocene a peneplain associated with plateau formation occurred in west Anatolia (Yilmaz et al., 2000). The regional cooling ages as discussed in Ring et al. (2003) suggest that extensional deformation largely ceased during that time in west Anatolia.

There is a ridge of old fission track ages along the west Anatolian coastline, which is interpreted to reflect a lack of Miocene detachment faults along the west Anatolian coastline. The Menderes detachments taper out to the west while the Aegean detachments have not laterally propagated into west Anatolia (Figure 3). In map view this geometry defines two spatially separated extension provinces divided by the ridge of old fission track cooling ages. A simple 3D elastic model of two simultaneously moving laterally tapering detachment fault systems should cause extension perpendicular to the slip directions of the two detachment systems (Bernhard Grasemann, written communication, 2011). Such E-W extension has in fact been reported from Samos Island in the easternmost Aegean right at the Turkish coastline by Ring et al. (1999). ZFT cooling ages indicate that E-W extension commenced ≥20 Ma (Ring et al., 2010).

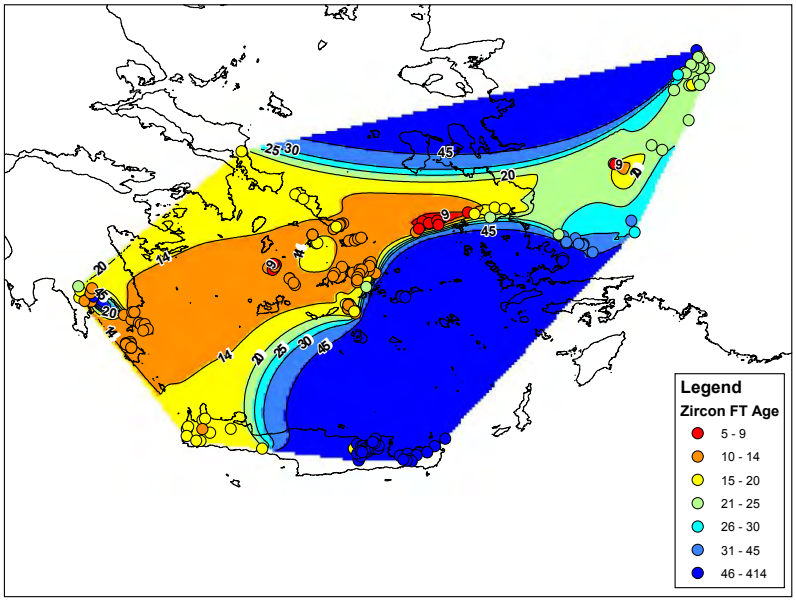

Figure 4 - Contoured map showing zircon fission track ages in the Aegean Sea region and adjacent west Turkey.

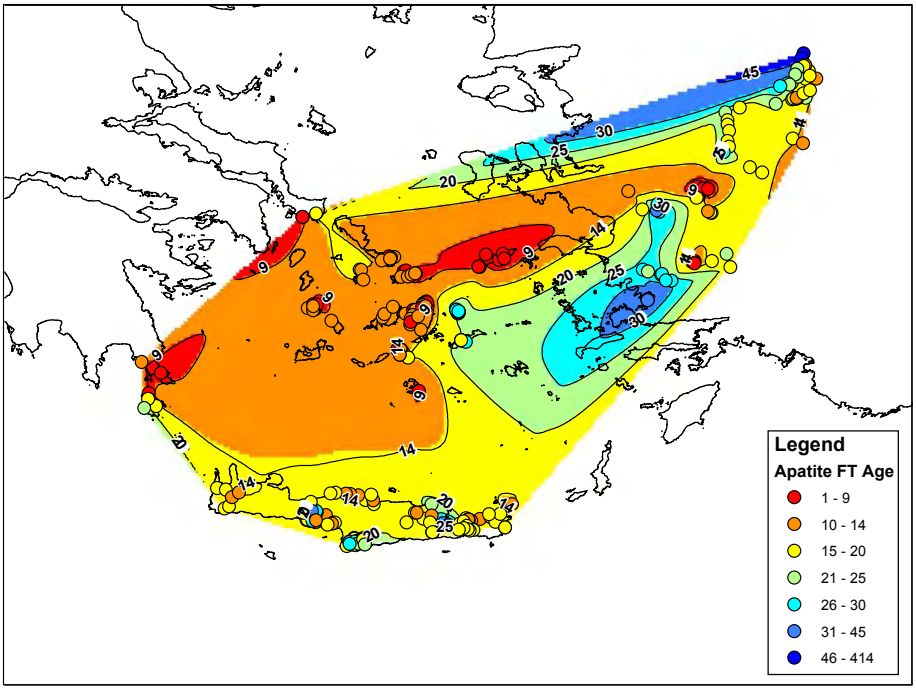

Figure 5 - Contoured map showing apatite fission track ages in the Aegean Sea region and adjacent west Turkey. Note 'ridge' of fairly old fission track ages in west Turkey.

Because extension in the Aegean Sea is greater by a factor of >3 than in west Anatolia, the detachment faults caused differential extension since the onset of extension at the Oligocene/Miocene boundary. The onset of E-W extension in Samos Island coincides well with the onset of differential extension across the Aegean and west Anatolia. The region that accommodated this differential extension coincides with the ridge of old FT ages.

3.2. Sinistral Wrench Corridor - West Anatolia Transfer Zone

The most prominent extensional structures in western Turkey are Miocene to recent E-W trending graben. Two of these grabens – the Gediz graben in the north and the Büyük Menderes graben in the south – delimit the Central Menderes Metamorphic Core Complex. The area north of the Central Menderes Metamorphic Core Complex – the northern Menderes Massif – displays a pattern of NE-striking basins bounded by basement domains. South of the Central Menderes Metamorphic Core Complex similar basins strike NNW rather than NE. Both the NE- and the NNW-striking basins appear to have formed contemporary with early manifestations of the E–W graben, but are much shallower.

We propose that shearing during sinistral strike slip has caused transtensional folding with a wavelength of tens of kilometers in the Menderes Massif. This large-scale near-simple-shear deformation accommodates a gradient in crustal extension forced by pronounced retreat of the Hellenic subduction zone since the earliest Miocene, which appears to be spatially restricted to the Aegean Sea region causing the curvature of the Hellenic slab. Folding caused uplift of basement in the anticlines, while providing accommodation space for the Miocene basins in the synclines. Transtensional folding is followed (accompanied?) by the tectonic denudation of the Central Menderes Metamorphic Core Complex, which also appears to have accommodated higher extensional strain towards its western limit. Our model provides an explanation for the geometry and timing of Neogene basins in the Menderes Massif.

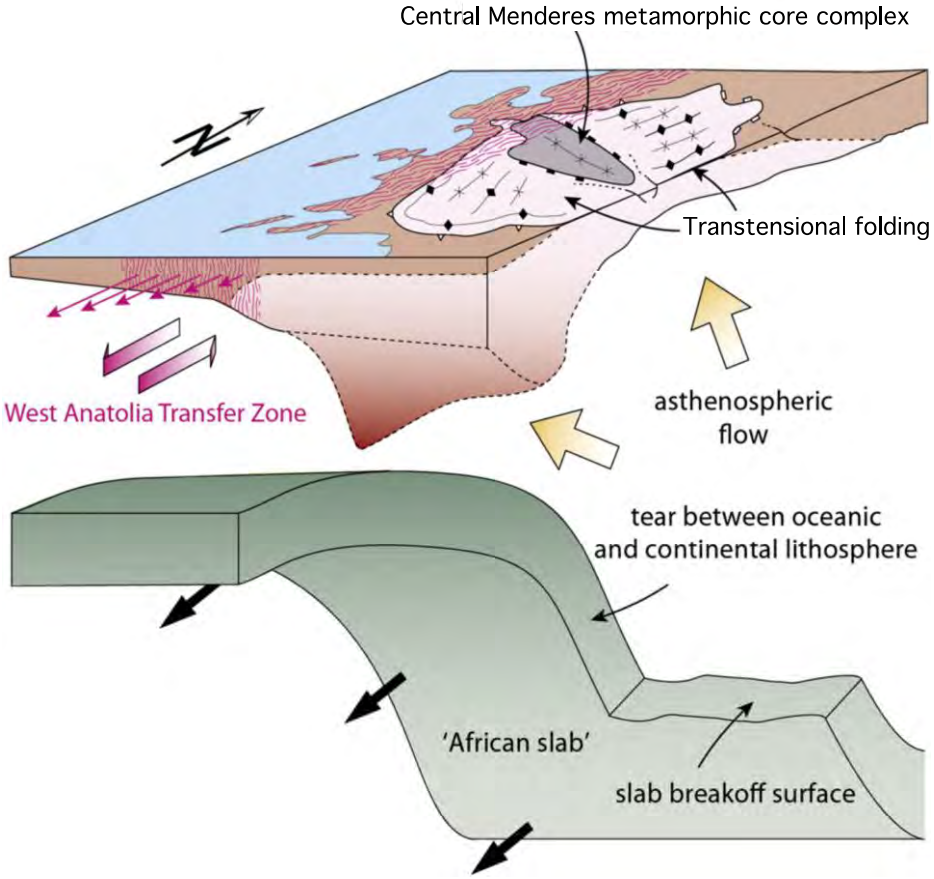

Figure 6 - Conceptual model of the present slab dynamics at the Aegean/Turkish border. The retreat of the Aegean slab with its vertical edge maintains a transtensional situation that controls diffuse brittle deformation along the coast and inboard of the Aegean.

3.3. Tectonic interpretation

Gessner et al. (2013) showed that there are marked differences in Bouguer gravity data between the Aegean Sea region and western Anatolia. The gravity data define a N-S oriented boundary between a gravity high in the Aegean and lower gravity values below west Anatolia. Seismic velocity anomalies show a sharp vertical boundary between the fast, cold and dense African slab below the Aegean and a slow, hot and buoyant asthenospheric region below the Menderes Massif, the West Anatolia Transfer Zone.

Recent reviews of Aegean tectonics by Jolivet and Brun (2010) and Ring et al. (2010) highlight the common opinion that the slab of the downgoing Adria/Africa slab reached the 660km discontinuity at about the Oligocene/Miocene boundary, then was draped over this discontinuity causing a dramatic phase of rollback. This pronounced rollback caused widespread extension in the Aegean Sea region and may have also triggered extension in adjacent west Anatolia. The very different lithosphere of the Adriatic and Anatolian slab behaved very differently. The more buoyant Anatolian slab did not roll back. This differential lithospheric behaviour caused a tear in the downgoing slab along the boundary of the different lithosphere along the west Anatolian coastline.

The slab tear allowed the asthenosphere of the incoming African slab to flow lateral around the retreating slab and aided rollback resulting in faster extension in the Aegean Sea region. We think that enhanced rollback/extension is basically reflected by the widespread fission track cooling ages of 15 to 8 Ma in the central Aegean.

The subduction of continental material in west Anatolia resulted in the major along-strike differences. Subduction of continental material commonly results in delamination and/or rupture of the oceanic slab (Sacks, 1990), which detaches and sinks into the mantle leaving behind positively buoyant continental material that rebounds isostatically (Milsom, 1986) resulting in rapid surface uplift above the rebounding slab. The rebound was probably enhanced by the lateral flow of the asthenosphere around the retreating Adriatic slab. This flow may indeed have heated the lithosphere of west Anatolia making it thermally and mechanically unstable more unstable. The rebound ultimately caused the Miocene Plateau in west Anatolia. The asthenospheric flow under west Anatolia is also capable of explaining the lamporite geochemistry associated with plateau formation.

The tectonic model argued for here calls for very different evolutions of the Aegean Sea region and west Anatolia. The rollback of the slab in the Aegean Sea ultimately created the free space for the westward extrusion of Anatolia commencing in the late Miocene and propagating into west Anatolia.

4. References

Agostini S., Doglioni C., Innocenti F., Manetti P., Tonarini S. and Savaşçin M.Y. 2007. The transition from subduction-related to intraplate Neogene magmatism in the Western Anatolia and Aegean area, *Special Paper of the Geological Society of America*, 418, 1-15.

Berk Biryol C., Beck S.L., Zandt G. and Özacar A.A. 2011. Segmented African lithosphere beneath the Anatolian region inferred from teleseismic P-wave tomography, *Geophy. J. Inter.,* 184, 1037-1057.

Bolhar R., Ring U. and Allen C.M. 2010. An integrated zircon geochronological and geochemical investigation into the Miocene plutonic evolution of the Cyclades, Aegean Sea, Greece: Part 1 – Geochronology, *Contributions Mineralogy Petrology,* 160, 719-742, DOI: 10.1007/s00410-010-0504-4.

Candan O., Dora O.Ö., Oberhänsli R., Oelsner F. and Dürr S. 1997. Blueschist relics in the Mesozoic cover series of the Menderes Massif and correlations with Samos Island, Cyclades, *Schweiz.Mineralog. Petrograph. Mitt.,* 77, 95-99.

de Boorder H., Spakman W., White S.H. and Wortel M.J.R.1998. Late Cenozoic mineralization, orogenic collapse and slab detachment in the European Alpine Belt, *Earth Planet. Sci. Lett.,* 164, 569–575.

Dilek Y. and Altunkaynak S.2007. Cenozoic crustal evolution and mantle dynamics of postcollisional magmatism in western Anatolia, *Intern. Geol. Rev.,* 49, 431–453.

Gessner K., Ring U., Passchier C.W. and Gungor T.2001a. How to resist subduction: evidence for large-scale out-of-sequence thrusting during Eocene collision in western Turkey, *J. Geol. Soc.,* 158, 769-784.

Gessner K., Ring U., Johnson C., Hetzel R., Passchier C.W. and Gungor T. 2001b. An active bivergent rolling-hinge detachment system: Central Menderes metamorphic core complex in western Turkey, *Geology,* 29, 611-614.

Gessner K., Ring U. and Güngör T. 2011. Field guide to Samos and the Menderes Massif; along-strike variations in the Mediterranean Tethyan Orogen, *GSA field trip guide 22*.

Gessner K., Gallarado L., Markwitz V., Ring U. and Thomson S.N. 2013. What caused the denudation of the Menderes Massif: Review of crustal evolution, lithospheric structure, and dynamic topography in southwest Turkey, *Gondwana Research*, 24, 243-273.

Glodny J.and Hetzel R. 2007. Precise U–Pb ages of syn-extensional Miocene intrusions in the central Menderes Massif, western Turkey, *Geol. Mag.,* 144, 235-246.

Houseman G.A., McKenzie D.P. and Molnar P. 1981. Convective instability of a thickened boundary layer and its relevance for the thermal evolution of continental convergent belts, *J. Geophys. Res.,* 86, 6115-6132.

Jacobshagen V.1986. *Geologie von Griechenland*, Borntraeger, Berlin.

Jolivet L., Goffé B., Monié P., Truffert-Luxey C. and Bonneau M. 1996. Miocene detachment in Crete and exhumation P-T-t paths of high-pressure metamorphic rocks, *Tectonics,* 15, 1129-1153.

Jolivet L. and Brun J.P. 2010. Cenozoic geodynamic evolution of the Aegean, *Intern. J. Earth Sci.,* 99, 109-138.

Knapmeyer M. and Harjes H.P. 2000. Imaging crustal discontinuities and the downgoing slab beneath western Crete, *Geophys. J. Internat.,* 143, 1–22.

Makris J. and Stobbe C. 1984. Physical properties and state of the crust and upper mantle of the Eastern Mediterranean Sea deduced from geophysical data, *Marine Geol.,* 55, 347-363.

Özer S., Sözbilir H., Özkar I., Toker V. and Sari B. 2001. Stratigraphy of Upper Cretaceous-Palaeogene sequences in the southern and eastern Menderes Massif (western Turkey), *Intern. J. Earth Sci.,* 89, 852-866.

Prelevic D., Akal C., Foley S.F., Romer R.L., Stracke A. and van den Bogaard P.2010a. Postcollisionsl mantle dynamics of an orogenic lithosphere: lamproitic mafic rocks from SW Anatolia, Turkey, Tectonic Crossroads: Evolving Orogens of Eurasia-Africa-Arabia, Ankara, pp. 18-12.

Regnier J.L., Ring U., Passchier C.W., Gessner K. and Gungor T. 2003. Contrasting metamorphic evolution of metasedimentary rocks from the Cine and Selimiye nappes in the Anatolide belt, western Turkey, *J. Metam. Geol.*, 21, 699-721.

Ring U., Gessner K., Gungor T. and Passchier C.W. 1999. The Menderes Massif of western Turkey and the Cycladic Massif in the Aegean - do they really correlate?, *J. Geol. Soc.,* 156, 3-6.

Ring U. and Layer P.W. 2003. High-pressure metamorphism in the Aegean, eastern Mediterranean: Underplating and exhumation from the Late Cretaceous until the Miocene to Recent above the retreating Hellenic subduction zone, *Tectonics,* 22 TC001350.

Ring U., Glodny J., Will T. and Thomson S.N.2010. The Hellenic subduction system: High-pressure metamorphism, exhumation, normal faulting and large-scale extension, *Annual Rev. Earth Planet. Sci.* 38, 45-76.

Robertson A.H.F., Clift P.D., Degnan P.J. and Jones G.1991. Palaeogeographic and palaeotectonic evolution of the Eastern Mediterranean Neotethys, *Palaeogeo., Palaeoclimat., Palaeoecol.* 87, 289-343.

Rosenbaum G., Ring U. and Kühn A. 2007. Tectono-metamorphic evolution of high-pressure rocks from the island of Amorgos (Central Aegean, Greece*), Journal of Geological Society London,* 164, 425-438.

Royden L.H. 1993. Evolution of retreating subduction boundaries formed during continental collision, *Tectonics,* 12, 629-638.

Sengör A.M.C., Satir M. and Akkök R.1984. Timing of the tectonic events in the Menderes massif, western Turkey: implications for tectonic evolution and evidence for Pan-African basement in Turkey, *Tectonics* 3, 693-707.

Sherlock S., Kelley S., Inger S., Harris N., Okay A. 1999. 40Ar-39Ar and Rb-Sr geochronology of high-pressure metamorphism and exhumation history of the Tavsanli Zone, NW Turkey, *Contrib. Mineral. Petrol.,* 137, 46-58.

van Hinsbergen D.J.J., Hafkenscheid E., Spakman W., Meulenkamp J.E. and Wortel R. 2005. Nappe stacking resulting from continental lithosphere below subduction of oceanic and Greece, *Geology,* 33, 325-328.

van Hinsbergen D.J.J., Kaymakci N., Spakman W. and Torsvik T.H. 2010. Reconciling the geological history of western Turkey with plate circuits and mantle tomography, *Earth Planet. Sci. Lett.,* 297, 674-686.

Yilmaz Y., Genç S.C., Gürer F., Bozcu M., Karacik Z., Altunkayak S.and Elmas A. 2000. When did the western Anatolian grabens begin to develop? In: Bozkurt, E., Winchester, J.A., Piper, J.D.A. (Eds.), Tectonics and Magmatism in Turkey and the surrounding area, pp. 353-384.

Δελτίο της Ελληνικής Γεωλογικής Εταιρίας, τομ. XLVII , 2013
Πρακτικά 13ου Διεθνούς Συνεδρίου, Χανιά, Σεπτ. 2013

Bulletin of the Geological Society of Greece, vol. XLVII 2013
Proceedings of the 13th International Congress, Chania, Sept. 2013

COSEISMIC SURFACE DISPLACEMENT VARIABILITY IN RELATION TO LITHOLOGY

Rondoyanni Th.[1], Lykoudi E.[1] and Kalogeras E[1].

[1]National Technical University of Athens, School of Mining and Metallurgical Engineering, Department of Earth Sciences, rondo@central.ntua.gr, elykoudi@metal.ntua.gr

Abstract

The variability of coseismic surface displacement along reactivated normal faults in the Aegean region is investigated. Seismotectonic data of past earthquakes associated with ground deformation and surface rupturing have been collected and analysed. Geological maps presenting the displacement at different sites along the fault traces have been compiled, as well as plots illustrating the corresponding relation between displacement and lithology. The main conclusion of this work is the strong correlation between regional lithology and coseismic surface displacement. Along a reactivated fault, the displacement observed in the recent geological formations is at least twice the displacement observed in the geological bedrock. It must be noted that the ratio of maximum to minimum displacement values along a certain active fault could be high as 5:1. Moreover, the potential displacements determined on the basis of existing empirical relationships, correspond to those observed in the bedrock. These findings could be taken into consideration in seismic hazard analysis during urban and engineering design.
Key words: *Seismotectonics; Earthquake rupturing; Fault reactivation.*

Περίληψη

Αντικείμενο της παρούσας εργασίας είναι η διερεύνηση της διαφοροποίησης του μεγέθους της συν-σεισμικής επιφανειακής μετατόπισης κατά μήκος ενός ενεργού ρήγματος, σε σχέση με τη λιθολογία των γεωλογικών σχηματισμών. Για το σκοπό αυτό αξιολογήθηκαν δεδομένα από σεισμούς της Ελλάδας που συνδέονται με την ανάδραση κανονικών ρηγμάτων και για τους οποίους υπήρχαν επαρκή και αξιόπιστα στοιχεία. Συντάχθηκαν οι αντίστοιχοι γεωλογικοί χάρτες, όπου σημειώθηκαν οι σεισμικές μετατοπίσεις στις διάφορες θέσεις παρατήρησης. Έγιναν επίσης διαγράμματα με το μέγεθος της μετατόπισης κατά μήκος κάθε ρήγματος καθώς και κάθε σεισμού που μελετήθηκε. Το κύριο συμπέρασμα αυτής της έρευνας είναι ότι υπάρχει άμεση σχέση του μεγέθους της επιφανειακής σεισμικής μετατόπισης κατά μήκος του ίδιου ρήγματος με τη λιθολογία των γεωλογικών σχηματισμών που αυτό επηρεάζει. Οι μετατοπίσεις αυτές εμφανίζουν το μεγαλύτερο μέγεθος στις μη συνεκτικές τεταρτογενείς αποθέσεις, όπου αυτό είναι τουλάχιστον διπλάσιο από το αντίστοιχο μέγεθος στα πετρώματα του γεωλογικού υποβάθρου. Σημειώνεται ότι η αναλογία της μέγιστης με την ελάχιστη τιμή της μετατόπισης κατά μήκος του ίδιου ρήγματος μπορεί να φθάσει έως και 5:1. Διαπιστώθηκε επίσης ότι οι σεισμικές μετατοπίσεις που προβλέπονται από τις εμπειρικές σχέσεις έχουν μέγεθος που συμφωνεί με το μέγεθος των μετατοπίσεων που

έχουν καταγραφεί στο γεωλογικό υπόβαθρο, οπότε πρέπει οι εκτιμήσεις να αναφέρονται αντίστοιχα σε αυτές.
Λέξεις κλειδιά: *Σεισμοτεκτονική, Σεισμικές διαρρήξεις, Ανάδραση ρηγμάτων.*

1. Introduction

The occurrence of surface rupturing and displacement along reactivated faults during strong earthquakes often results in severe structural damage due to additional ground deformation. Consequently, potential surface displacement is taken into consideration in seismic hazard analysis during urban and engineering design. To estimate future seismic surface displacement, many researchers have established empirical relations between fault length, earthquake magnitude and seismic displacement; the models proposed by Wells and Coppersmith (1994) based on worldwide data are the most commonly used. In Greece, the relations suggested by Pavlides and Caputo (2004) based on earthquake data of the Aegean region are also applied.

These relations give a range of values for average and maximum displacement observed during past earthquakes; however, no particular consideration is given to the variability of displacement depending on the differentiation of the lithologies crossed by the fault. Therefore, in the probabilistic hazard assessment of fault displacement dealing with shallow earthquakes, surface displacement is considered to depend mainly on fault length.

Displacement variability along fault trace has been noted by Sigbjörnsson and Olafsson (2004) for shallow strike-slip earthquakes with almost vertical fault plane, in the South Iceland Seismic Zone. Rockwell and Klinger (2011), by presenting new measurements for the 1940 and 1979 surface ruptures along the Imperial fault of Southern California, have reported that lateral slip varies substantially along fault-strike by more than 30%, over distances of tens to hundreds of meters. Similar results concerning slip variability have been determined after the 1999 Izmit and Duzce earthquakes in Turkey (Barka and Akyuz, 2002). The above mentioned works are focusing on the uncertainty of the collected seismic fault displacement data and on the need for closely spaced measurements; however, they are not presenting any correlation between this variability and the lithology along the fault trace.

The purpose of the present work is to investigate the influence of the lithology, of different geological formations crossed by a reactivated fault, on the magnitude of coseismic surface displacement along this fault. Information concerning shallow strong earthquakes associated with surface faulting in the Aegean region was collected and differentiations along the faults were studied. The studied earthquakes were related to the reactivation of normal faults under an extensional stress field.

2. Evaluation of Displacement Data

Certain historical and recent earthquakes in the Aegean region have exhibited surface deformation and coseismic rupturing of tectonic origin. Detailed information about coseismic surface displacement is limited, due to the fact that systematic seismotectonic studies were undertaken in Greece during the last 35 years. Moreover, there are some ambiguities as to the recorded values of coseismic displacement attributed to the following factors: incompleteness of data reflecting only part of the total fault length, sparse field measurements, recording of non-tectonic deformation, inclusion of gravitational phenomena or compaction of loose sediments and even false measurements. Besides, seismic fault traces along normal faults can be mapped and measured less confidently than fault traces along strike-slip faults.

The most ancient information, in Greece, for coseismic displacement concerns the 464 B.C. Sparta earthquake with an estimated magnitude Ms=7.2 and referred displacement about 3m, the largest recorded in the Greek territory **(**Armijo et al., 1991**)**. Field data, but non systematic measurements, concerning coseismic displacements exist for a number of about 30 earthquakes (Papazachos and

Papazachou, 2003; Pavlides and Caputo, 2004). Information for the last 120 years is referred to the earthquakes of Atalanti (1894), Ierissos (1932), Larissa (1941), Corinth (1953), Sophades (1954), Aghios Efstratios (1968), Thessaloniki (1978), Almyros (1980), Acarnania (1983), Corintian Gulf (1981), Kalamata (1986), Aigio (1995), Kozani (1995), Konitsa (1996), Andravida (2008), Oichalia (2011) (Figure 1). However, accurate data enabling comparison of coseismic displacement with lithology are available for the earthquakes of Atalanti (1894), Thessaloniki (1978) and Corinth (1981). Some others, even strong and disastrous earthquakes, were associated with minor surface rupturing and vertical displacements of the order of few centimetres. As example, the cases of 1986 Kalamata and 1995 Aigio earthquakes could be mentioned (Figures 2a and 2b). This work is a first attempt towards identifying a relation between surface coseismic displacements and affected

Figure 1- Map of Greece showing the year and the location of the earthquake faults.

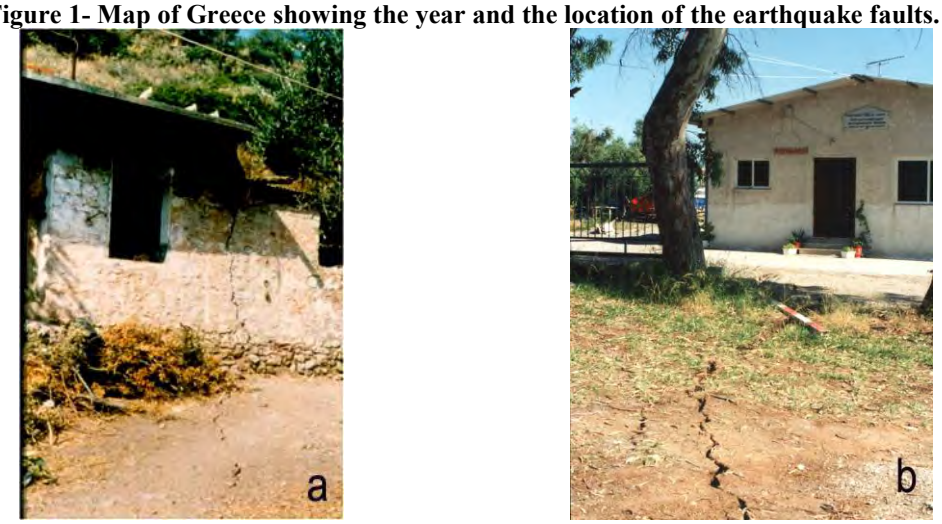

Figure 2- Open seismic cracks, without vertical displacement, formed during the 1986 Kalamata (a) and 1995 Aigio (b) earthquakes.

lithologies in an extensional seismotectonic regime, like the one dominating in Greek territory. For the evaluation of the relation between seismic displacement and affected lithologies at different sites along seismic faults, seismogeological maps were compiled, as presented hereafter. In these maps, the sites where data of coseismic surface displacement are available along reactivated faults were also noted. Then, a statistical evaluation of all available data was performed on the basis of plots illustrating seismic displacements along each fault as well as seismic displacements corresponding to each lithology.

2.1. The 1981 Corinth Earthquakes

The 1981 Corinth earthquakes constitute a good example for the study of coseismic displacement, because, in addition to the completeness of data, surface ruptures have affected a variety of geological formations allowing valuable comparisons and evaluations. The Corinthian Gulf is an active graben structure presenting intense seismicity and a rate of extensional deformation of the order of 30mm/yr NS (Billiris et al., 1991). Many past earthquakes have been accompanied by surface rupturing (Figure 3), coastal subsidence, landslides and liquefaction. Such phenomena observed during the 1981 earthquakes, were located at the eastern part of Corinthian gulf (Koukis and Rozos, 1982). Three main events were recorded, the first on February 24 (Ms=6.7), the second on February 25 (Ms=6.4) and the third on March 4 (Ms=6.3). The geological formations affected by seismic ruptures are coastal and alluvial deposits, scree and talus cones, limestone breccias, Plio-Pleistocene formations (marls, clays, sandstones and conglomerates), flysch, limestones and dolomites, schists-phyllites and ophiolites.

During the February 24 earthquake, large normal faults were reactivated in the southern part of the Gulf (in the Perachora peninsula) and the resulting seismic ruptures followed their traces (Figure 4). The total length of surface ruptures was about 15 km and displacements reached a maximum of 150 cm, usually ranging from 30cm to 70cm**.** During the March 4 earthquake, seismic cracks were observed in the northern part of the Gulf (Kaparelli area), over a total length of 12km (Figure 5).

The cracks were arranged in two branches, where displacements ranged from 50 to 70cm (personal observations; Jackson et al., 1982). The plots of Figures 6 and 7, show clearly the difference in the magnitude of seismic displacement between the geological formations of the bedrock and those of the recent formations. Only in certain seismic cracks in Pleistocene and alluvial deposits, observed in Kaparelli area, that had a variable azimuth, the displacement was of the order of few centimeters, because these cracks represented a polydeformed transfer zone between two main fault segments.

Figure 3 – View of the surface rupture in Kaparelli region.

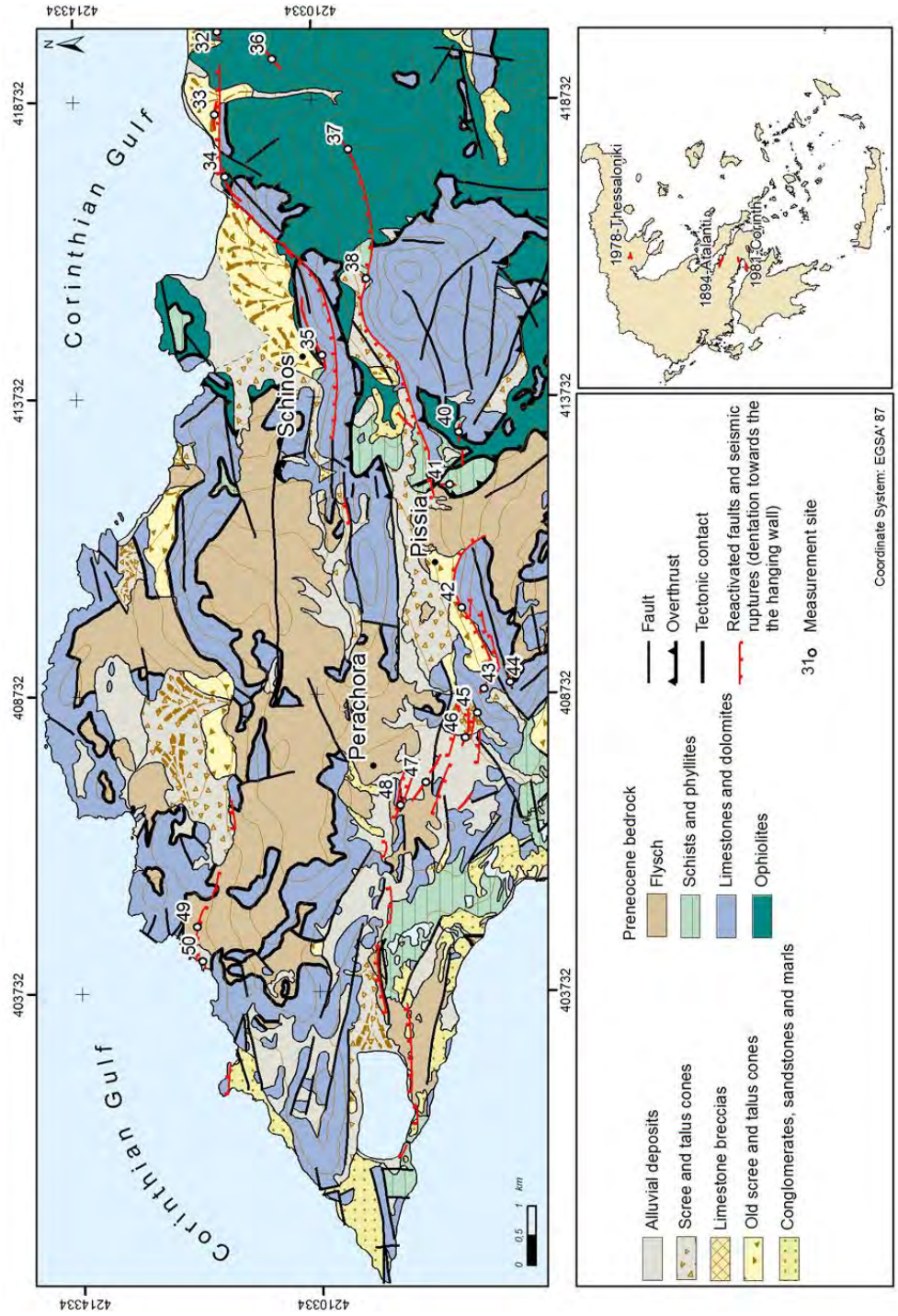

Figure 4 - Geological map of Perachora peninsula (southern part of the eastern Corinthian gulf) illustrating the 1981 seismic ruptures (based on the geological map of Greece in scale 1:50.000; Jackson et al., 1982; Rondoyanni & Koukis, 1989). The numbers correspond to the sites where displacement data were available. In the inset map, the studied seismic faults are located.

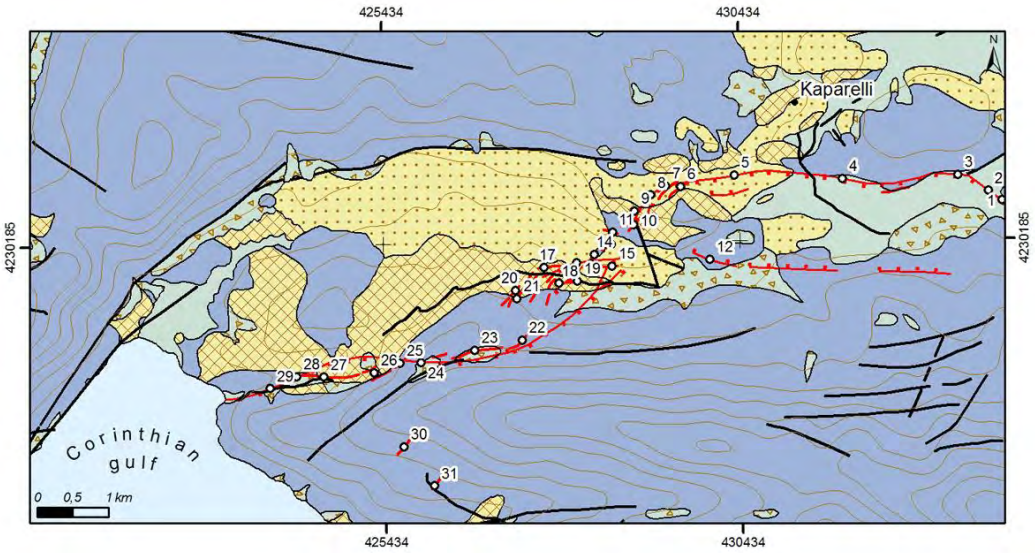

Figure 5 - Geological map of Kaparelli region (northern part of the eastern Corinthian gulf) illustrating the 1981 seismic ruptures (based on the geological map of Greece in scale 1:50.000; Jackson et al., 1982; Rondoyanni & Koukis, 1989). The numbers correspond to the sites where displacement data were available. The geological formations as noted in Figure 4.

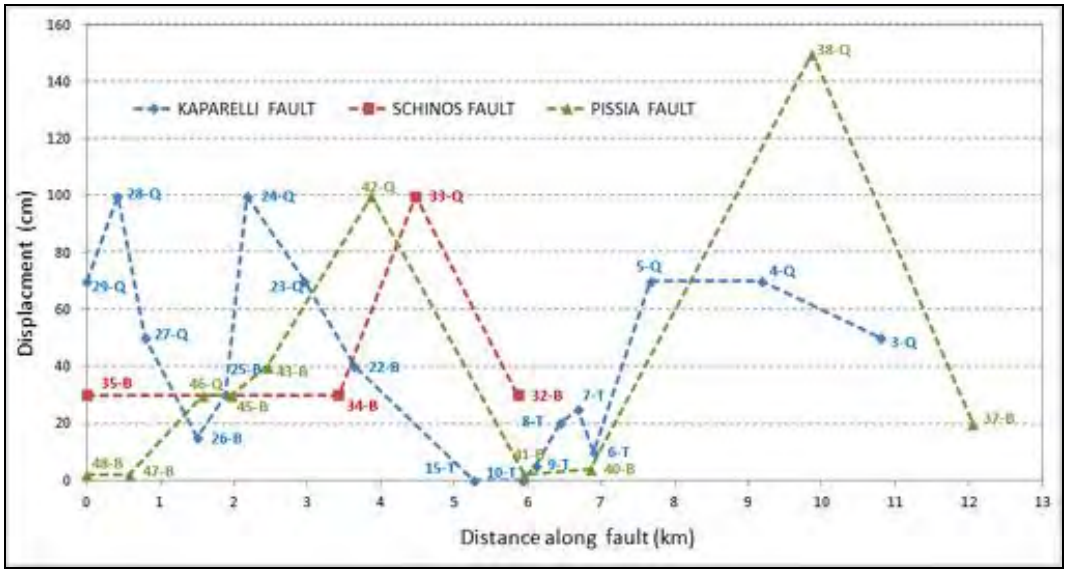

Figure 6 - Coseismic surface displacement along the 1981 reactivated faults (Schinos and Pissia faults are shown in Figure 4; Kaparelli fault in Figure 5). The numbers correspond to the sites noted also in Figures 4 and 5. Sites not presented in Figure 4 correspond to open seismic cracks with no vertical displacement. Lithology notation: B: Bedrock, Q:Quaternary unconsolidated geological formations, T:Transfer zone of Kaparelli fault.

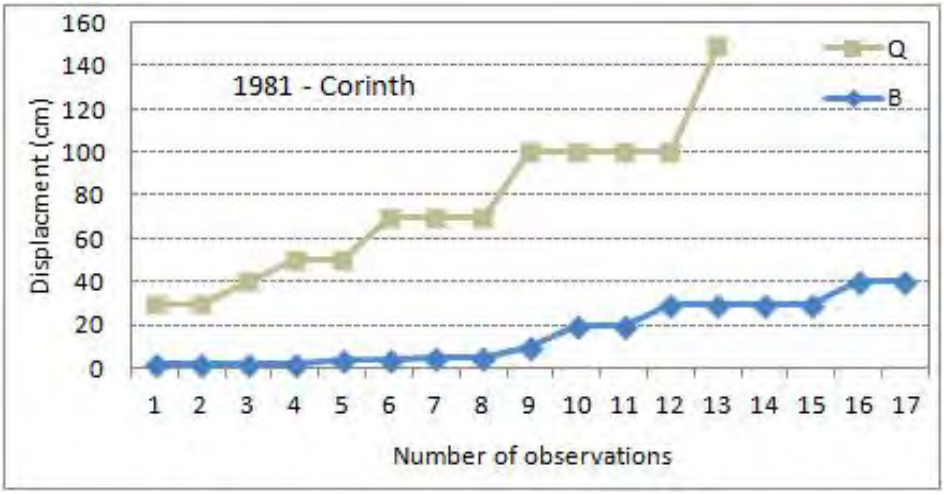

Figure 7 - Displacement of 1981 Corinth seismic ruptures in relation to lithology (B:Bedrock, Q:Quaternary unconsolidated geological formations).

As it concerns the magnitude of coseismic displacement according to existed relationships for the reactivated fault length of about 13km, an average displacement of 40cm and a maximum displacement of 65cm could be estimated, according to Wells and Coppersmith (1994) while according to Pavlides and Caputo (2004) the maximum displacement would be of the order of 45cm. The displacement measurements, in the Corinth epicentral area, showed displacements ranging from 30-60cm in the bedrock and 120cm in the quaternary deposits. Or, the correlation with the field data shows a good agreement of the estimated magnitudes with the measurements in the bedrock.

2.2. The 1978 Thessaloniki earthquake

During the 1978 Thessaloniki earthquake (Ms=6.5), seismic cracks were observed in the epicentral area, which is mainly covered by unconsolidated to medium consolidated formations such as alluvial deposits, scree and talus cones, lacustrine sediments and Plio-Pleistocene deposits (marls, clays, sandstones, conglomerates), while the geological bedrock consists of gneisses and schists (Figure 8). According to Mercier et al. (1983) and Mountrakis et al. (1983), along surface ruptures a maximum displacement of 20 cm was measured in the recent formations and a displacement of some centimeters in the gneisses (Figure 9). The length of each crack extended locally over a few hundred meters, but the total length of the deformed zone was about 12 km in length. It should be noted that the size of surface displacement appears to be smaller than this estimated according to existing relationships, considering both the magnitude of the earthquake and the length of the fault. This is maybe due to the fact that the seismic fault has caused diffuse surface deformation.

2.3. The 1894 Atalanti earthquakes

The seismic sequence of April 1894 consisted of two strong earthquakes of estimated size Ms=6.4-6.6 and Ms=6.9-7.0. The reactivated fault was a normal fault striking ESE-WNW and dipping to the North. According to the descriptions concerning the surface displacement along the fault trace, measured in scattered locations, the highest value was observed to the boundary of the bedrock with the Atalanti alluvial plain (Skufos, 1894; Papavassiliou, 1894**)**. The geological formations affected by the surface faulting are alluvial deposits, talus cones, neogene deposits (mainly marly limestones), mesozoic limestones and dolomites, palaeozoic clastic formations and ophiolites. According to existing data, the displacement ranges from 30cm in the bedrock to 120cm in the talus cones and alluvial deposits (Figure 9). The term “bedrock” includes the preneogene formations as well as well compacted Neogene deposits.

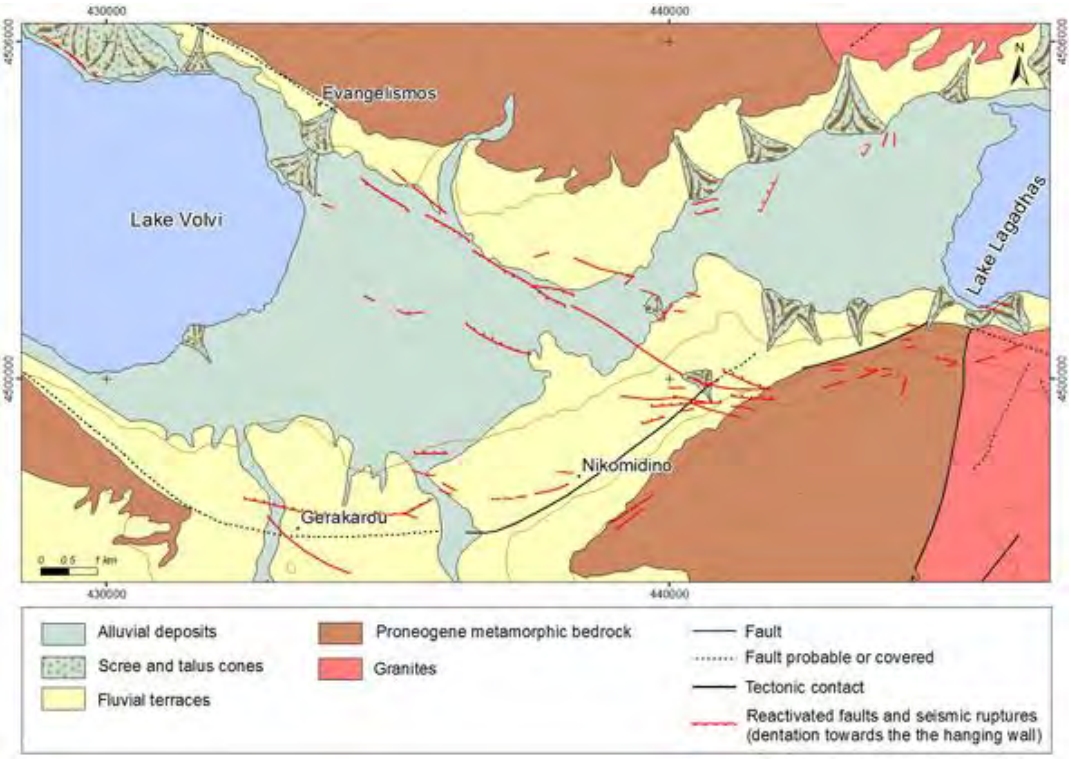

Figure 8 - Geological map of the epicentral Thessaloniki illustrating the 1978 seismic ruptures (based on the geological map of Greece in scale 1:50.000 - sheets Thermi and Zagliverio; Mercier et al., 1983; Mountrakis et al., 1983).

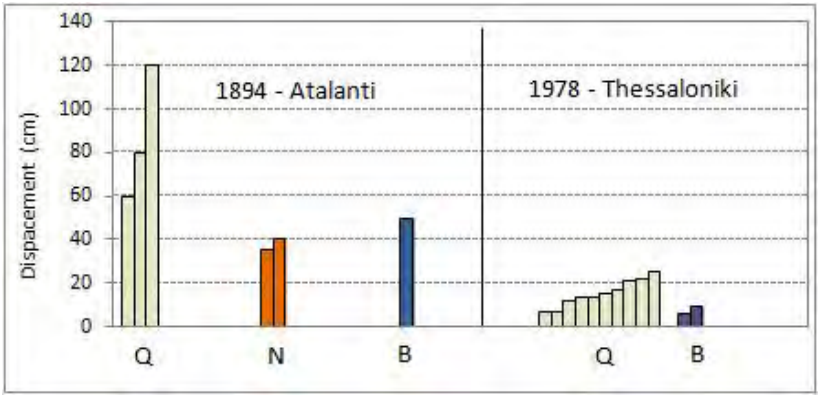

Figure 9 - Displacement of 1894 Atalanti and 1978 Thessaloniki seismic ruptures in relation to lithology (B:Bedrock, N:Neogene formations-mainly marly limestones, Q:Quaternary un-consolidated geological formations).

3. Conclusions

The estimation of the size of coseismic surface displacement along an active fault is an important factor for the assessment of fault activity and the resulting hazard. The existing empirical relationships between earthquake magnitude, fault length and seismic displacement are generally

used for this estimation. However, the size of the displacement along a reactivated fault varies significantly, depending largely on the lithology of the geological formations affected by the seismic ruptures.
By correlating displacement size with lithology along a number of reactivated normal faults in the Aegean region, the following conclusions can be drawn:

- There is a strong correlation between coseismic surface displacement and regional lithology.
- The displacement observed in the recent geological formations (alluvial deposits, talus cones and unconsolidated basin infillings) is at least twice than that occurred in the geological bedrock (limestones, schists, gneisses, ophiolites). It must be noted that the ratio of maximum to minimun displacement values along a certain active fault could be high as 5:1. The term "bedrock" includes both the pre-neogene geological formations and the neogene compacted rocks as well; along the same fault, similar values of displacement have been observed in the mesozoic limestones and the neogene marly limestones.
- In certain cases, where seismic ruptures cross a strong morphology, the size of the displacement is enhanced by gravitational effects, while in the boundary between bedrock and alluvial deposits it may be amplified by the compaction of loose soil.
- The potential future displacements along the active faults determined on the basis of the existing empirical relationships are in accordance with those observed in the bedrock. This observation must be also taken into consideration in seismic hazard analysis during urban and engineering design in the vicinity of active faults.

4. References

Armijo R., Lyon-Caen H., and Papanastassiou D. 1991. A possible normal-fault rupture for the 464 BC Sparta earthquake, *Nature, 351 (6322), 137–139.*

Barka A., Akyuz H. S. 2002. The surface rupture and slip distribution of the 17 August 1999 Izmit earthquake (M7.4), *North Anatolian fault*, BSSA (Special Issue on the 1999 Izmit and Duzce, Turkey, Earthquakes, N. Toksoz (ed.)), 92(1), 43–60.

Billiris H., Paradissi D., Veis G., England P., Featherstone W., Parsons B., Cross P., Rands P., Rayson M., Sellers P., Ashkenazi V., Davison M., Jackson J. and Ambraseys N. 1991. Geodetic determination of tectonic deformation in central Greece from 1900 to 1988, *Nature,* 350, 124–129.

Jackson J.A., Gagnepain J., Houseman G., King P., Papadimitriou P., Soufleris C., Virieux, J. 1982. Seismicity, normal faulting and the geomorphological development of the Gulf of Corinth (Greece): the Corinth earthquakes, *Earth Planet. Sci. Lett., 57, 377– 397.*

IGME (Institute of Geology and Mineral Exploration) 1978. Geological map of Greece in scale 1:50.000, *Sheets "Perachora" and "Kaparelli".*

IGME (Institute of Geology and Mineral Exploration), 1984. Geological map of Greece in scale 1:50.000, *Sheets "Thermi" and "Zagliveri".*

Koukis G and Rozos D. 1982. Geological and geotechnical characteristics of the earthquakes of February-March 1981 in the Corinthian gulf, *Proceedings of Athens Academy, 57, 406-425.*

Mercier J.L., Carey–Gailhardis E., Mouyaris N., Simeakis K., Rondouyannis Th. and Anghelidhis Ch. 1983. Structural analysis of recent and active faults and regional state of stress in the epicentral area of the 1978 Thessaloniki earthguakes (Northern Greece), *Tectonics, 2, 6, 577-600.*

Mountrakis D., A. Psilovikos and Papazachos B. 1983. The *geotectonic* regime of the 1978 Thessaloniki earthquakes, in: Papazachos, B. C. and P. G. Carydis (eds.), The Thessaloniki, Northern Greece, earthquake of June 20, 1978 and its seismic sequence, *Technical Chamber of Greece, 11 - 27.*

Papavassiliou M.S. 1894. On the earthquakes of Lokris (Greece) April 1894, *C. R. Ac. Scienc. Paris, T, CXIX:1.*

Papazachos B and Papazachou C., 2003. *The Earthquakes of Greece*, Ziti ed., Thessaloniki, 273 pp.

Pavlides S. and Caputo, R. 2004. Magnitude versus faults' surface parameters: uantitative relationships from the Aegean, Te*ctonophysics*, 380(3–4), 159–188.

Rockwell T.K. and Klinger Y. 2011. The variability of along-strike co-seismic slip: A new example from Imperial fault of southern California. *2nd INQUA-IGCP-567 International Workshop on Active Tectonics, Earthquake Geology, Archaeology and Engineering, Corinth, Greece, 200-203.*

Rondoyanni Th. and Koukis G. 1989. Neotectonics and recent seismic activity in the eastern Corinthian gulf, Greece. Geotechnical implications, *Bull. AFEQ,* 2me serie, n° 39, 171-180.

Sigbjörnsson R. and Olafsson S. 2004. On the South Iceland earthquakes in June 2000: Strong-motion effects and damage, *Bollettino di Geofisica Teorica e Applicata. 45, 131-152.*

Skufos Th. 1894. Die zwei grossen Erdbeben in Lokris am 8/20 und 15/27 April 1984, *Zeitschrift Ges. Erdkunde zu Berlin, vol. 29. 409 pp.*

Wells D. and Coppersmith K. 1994. New empirical relationships among magnitude, rupture length, rupture width, rupture area, and surface displacement, *B.S.S.A., 84, 974-1002.*

Δελτίο της Ελληνικής Γεωλογικής Εταιρίας, τομ. XLVII , 2013
Πρακτικά 13ου Διεθνούς Συνεδρίου, Χανιά, Σεπτ. 2013

Bulletin of the Geological Society of Greece, vol. XLVII 2013
Proceedings of the 13th International Congress, Chania, Sept. 2013

STRIKE SLIP TECTONICS AND TRANSTENSIONAL DEFORMATION IN THE AEGEAN REGION AND THE HELLENIC ARC: PRELIMINARY RESULTS

Sakellariou D.[1], Mascle, J.[2] and Lykousis V.[1]

[1] *Institute of Oceanography, Hellenic Centre for Marine Research, Greece, sakell@hcmr.gr, vlikou@hcmr.gr*

[2] *Observatoire Océanologique de Villefranche, France, mascle@obs-vlfr.fr*

Abstract

Recently acquired offshore seismic and swath bathymetry data from the Hellenic Arc, the Ionian Sea and the South and North Aegean Sea, including the Hellenic Volcanic Arc and the Cyclades plateau, along with geological and tectonic data from Plio-Quaternary basins exposed on the Hellenic Arc indicate that strike slip tectonics has played a major role in the southwestward extension of the Aegean crustal block, the development of the offshore neotectonic basins and the spatial distribution of the volcanic activity along the Volcanic Arc. Transtensional deformation, accommodated by (sinistral or dextral) strike slip zones and related extensional structures, prevail throughout Plio-Quaternary, since the North Anatolian Fault broke westwards into the North Aegean. Incipient collision of the Hellenic Forearc south of Crete with the Libyan promontory and consequent lateral escape tectonics led to the segmentation of the Hellenic Arc in distinct blocks, which move southwestwards independently from each other and are bounded by strike slip faults.
Key words: *Plio-Quaternary, fault-zones, neotectonic basins, volcanic activity.*

Περίληψη

Ερμηνεία και ανάλυση πρόσφατων σεισμικών τομών και δεδομένων πολυδιαυλικής βυθομετρίας από το Ελληνικό Τόξο, το Ιόνιο και Αιγαίο Πέλαγος, μαζί με ερμηνεία παλαιότερων σεισμικών τομών από τις ίδιες περιοχές και συνεκτίμηση χερσαίων γεωλογικών και τεκτονικών δεδομένων οδηγούν στο συμπέρασμα ότι ρήγματα οριζόντιας ολίσθησης και πλαγιο-εφελκυστική παραμόρφωση αποτελούν σημαντικό παράγοντα για την παραμόρφωση της περιοχής του Αιγαίου στη διάρκεια του Πλειο-Τεταρτογενούς, την δημιουργία νεοτεκτονικών λεκανών και τον γεωγραφικό προσδιορισμό της ηφαιστειακής δραστηριότητας κατά μήκος του Ηφαιστειακού Τόξου. Πλαγιο-εφελκυστική παραμόρφωση εκφραζόμενη με δεξιόστροφα και αριστερόστροφα ρήγματα οριζόντιας ολίσθησης επικρατεί μετά την προέλαση του Ρήγματος Βόρειας Ανατολίας στο Βόρειο Αιγαίο. Η έναρξη της σύγκρουσης μεταξύ της μικρο-πλάκας του Αιγαίου με την Αφρικανική Πλάκα νότια της Κρήτης προκάλεσε φαινόμενα "τεκτονικής πλευρικής διαφυγής" κατά μήκος του Ελληνικού Τόξου και τον διαχωρισμό του σε επιμέρους τεκτονικά τεμάχη, τα οποία κινούνται προς ΝΔ και οριοθετούνται μεταξύ τους με ρήγματα οριζόντιας ολίσθησης.
Λέξεις κλειδιά: *Πλειο-τεταρτογενές, ρηξιγενείς ζώνες, νεοτεκτονικές λεκάνες, ηφαίστεια.*

1. Introduction

Active tectonics, deformation and high seismicity of the Aegean region have been the subject of many studies during the last 40 years with the aim to understand the implications of plate tectonics for continental deformation. Early studies have used seismologic data, active fault distributions, and seafloor bathymetry to define the major tectonic boundaries of the Aegean and infer the magnitude and sense of relative motions across them (McKenzie, 1972, 1978; Le Pichon and Angelier, 1979, 1981; McKenzie and Jackson, 1983; Taymaz *et al*., 1991). These and other pioneering studies have shown that earthquake faulting parameters, distribution and sense of motion on mapped active faults display close relationship between them (McKenzie, 1972, 1978; Le Pichon and Angelier, 1981; McKenzie and Jackson, 1983; Taymaz *et al*., 1991; Goldsworthy *et al*., 2002) but have not led to the formulation of a widely accepted kinematic model for the Aegean deformation. In the last 20 years GPS surveys have contributed to the quantification of the contemporary deformation of the Aegean region and provided important clues to the understanding of the large-scale kinematics (Billiris *et al*., 1991; Le Pichon *et al*., 1995; Davies *et al*., 1997: Clarke *et al*., 1998; Briole *et al*., 2000; McClusky *et al*., 2000; Nyst & Thatcher, 2004). The westward extrusion of Anatolia continental block along the North Anatolian Fault, the NNE-ward subduction of the Eastern Mediterranean lithosphere beneath the Hellenic Arc, the subsequent SSW-NNE extension of the Aegean back-arc region, the collision of NW Greece with the Apulian block in the northern Ionian Sea north of the Kephallonia Fault and the incipient collision with the Libyan promontory south of Crete (Mascle et al, 1999) are the main, active processes. The boundaries of the actively deforming part of the Aegean are defined by the following geotectonic features (Figure 1):

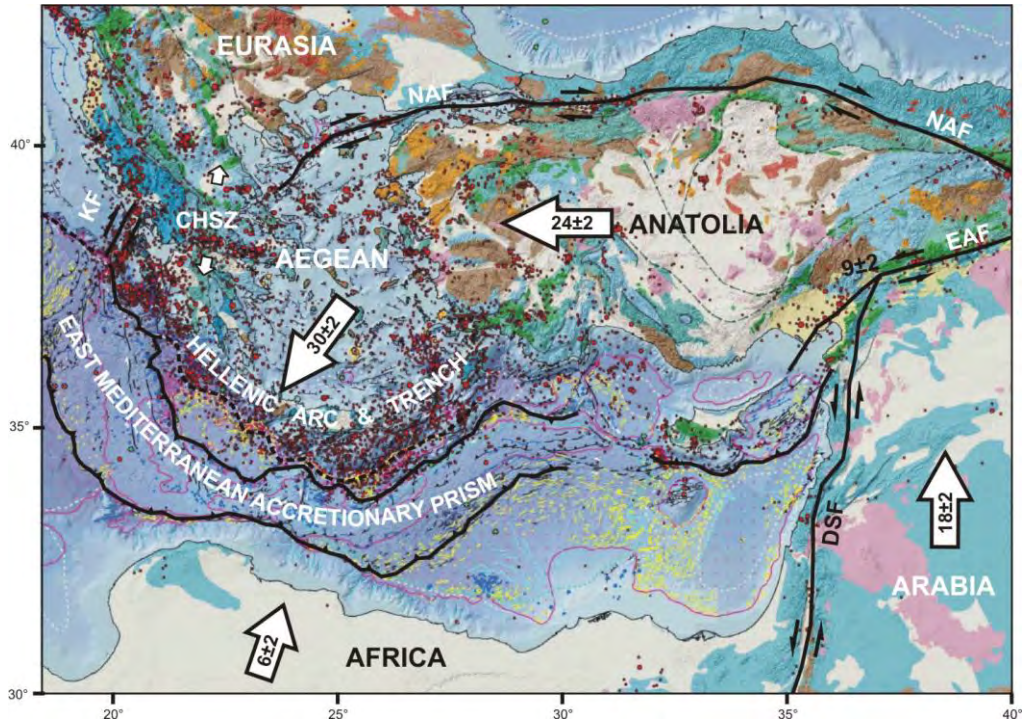

Figure 1 - Morpho-tectonic map of the East Mediterranean (extracted and modified from Mascle & Mascle, 2012) with main structural features and major tectonic boundaries of the actively deforming Aegean Region. Mean GPS horizontal velocities after McClusky *et al* (2000). DSF: Dead Sea Fault, EAF: East Anatolian Fault, NAF: North Anatolian Fault, KF: Kephallonia Fault, CHSZ: Central Hellenic Shear Zone.

1. The westward prolongation of the dextral, strike-slip North Anatolian Fault (NAF) into the Aegean Sea along the North Aegean Trough (NAT) marks the boundary between the relatively non-deforming Eurasian Continent to the north and the deforming Aegean to the south.
2. The Hellenic Trench, a series of deep, elongate basins aligned along the Hellenic Arc defines the southeast, south and west boundary of the Aegean continental block to the East Mediterranean Ridge, the accretionary prism developed above the NE-ward subduction of the East Mediterranean oceanic crust.
3. The Kephallonia Fault (KF), a SSW-NNE trending, dextral, strike slip fault which separates the active part of the Hellenic Arc to the southeast from the inactive one to the north.
4. The Central Hellenic Shear Zone (Papanikolaou & Royden, 2007), a diffuse boundary, an area of active extensional deformation, which accommodates transferring of stress between the northern tip of the Kephallonia Fault and the southwestern tip of the North Anatolian Fault.

Most of the previous studies (McKenzie, 1972, 1978; McKenzie and Jackson, 1983, 1986; Taymaz *et al*., 1991; Le Pichon *et al*., 1995; Armijo *et al.,* 1996; McClusky *et al*., 2000; Goldsworthy *et al*., 2002; Nyst & Thatcher, 2004; Kokkalas *et al*, 2006) propose that active deformation is mostly concentrated along the boundaries of relatively rigid, smaller, tectonic blocks while they do not exclude isolated zones of deformation in their interior. In this paper we present preliminary results from the interpretation of recently acquired seismic profiles and swath bathymetry data and re-evaluation of older seismic data and suggest that NE-SW trending, dextral and sinistral strike slip fault-zones and transtensional deformation has played a major role in the southwestward extension of the Aegean Region during Plio-Quaternary.

2. Materials and Methods

In this paper we present preliminary results derived from the:

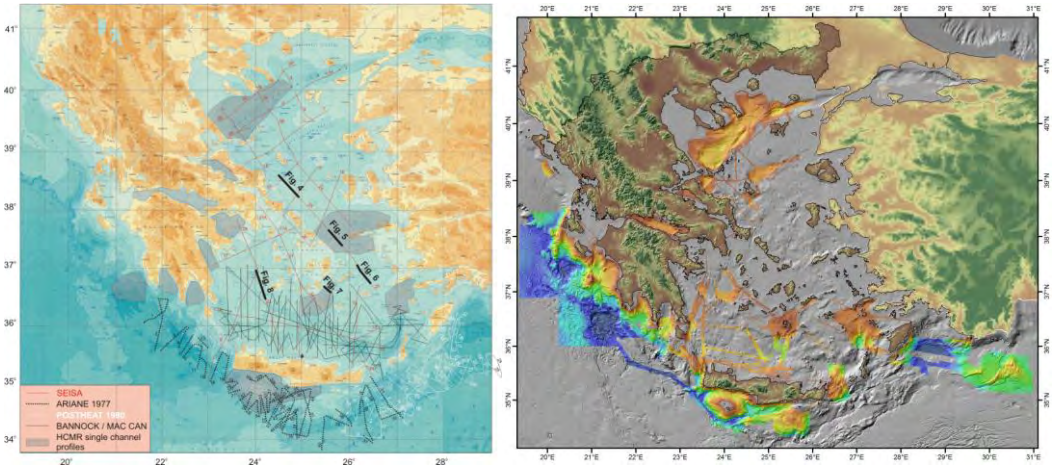

Figure 2(left) - Location map of continuous seismic profiles (multi channel, sparker) and single channel seismic profiles acquired during various cruises in the last 40 years in the Aegean Region and used for this study.

Figure 3(right) - Color-scaled swath bathymetry acquired by R/V AEGAEO (HCMR) since 2000 superimposed on gray-scaled shaded bathymetry (GEBCO) in the Aegean region.

5. Re-interpretation of continuous seismic and sparker profiles obtained during the missions ARIANE 1977, POSTHEAT 1980, SEISA 1974 (Martin, 1987; Mascle & Martin 1990), Bannock 1981 (Bartole *et al*, 1983), MAC CAN 1986 (Rossi *et al*, 1988) (Figure 2).
6. Interpretation of single channel seismic profiles obtained by HCMR during the last decades (Figure 2) in the frame of several projects and cruises: HERMES - south and southwest Crete, KM3Net - Southwest Peloponnese, THERA - Santorini area (Sigurdsson *et al*, 2006; Sakellariou *et al*, 2010), Gulf of Corinth (Moretti et al, 2004; Lykousis *et al*, 2007; Sakellariou *et al*, 2007a), AMPHITRITE - North Evia Gulf (Sakellariou *et al*, 2007b), North and South Ikarian Basins (Lykousis *et al*, 1995) and other (Figure 2).
7. Swath bathymetry data obtained in the Aegean Region by HCMR aboard R/V AEGAEO (Figure 3) and the swath bathymetry map of the Mediterranean Sea (Brossolo *et al*, 2012).
8. Review of published information and data on the active fault pattern in the offshore Aegean Region (Figure 8).

3. Results

3.1. North Aegean Sea

It is widely accepted that the North Aegean Trough is a transtensional basin developed along the right-lateral North Anatolian Fault (Angelier, 1979; Sengor, 1979; Hancock and Barka, 1980) since early Pliocene Pliocene (Armijo *et al*, 1999). Multi-channel and single channel profiles along with swath bathymetry data (Mascle & Martin, 1990; Koukouvelas & Aydin, 2002: Papanikolaou *et al*, 2002, 2006) indicate oblique opening of the basin marked by NE-SW strike-slip faults along the margins and within the basin, E-W strike slip faults in the basins and NW-SE normal faults along the Pelion and Athos margins.

The area between the North Aegean Trough and the Cyclades Plateau is regarded as a typical right-lateral strike-slip faulting regime (e.g. Mascle & Martin, 1990; Taymaz *et al.,* 1991; Kiratzi and Louvari, 2003). By using swath bathymetry and seismic profiling data we have mapped the most prominent Plio-Quaternary depocenters of this area with sediment thickness in excess of 0.5 seconds two-way travel-time and the major faults which bound them (Figure 8). The North Skyros Basin and the South Skyros Basin have developed along the southern branch of the North Anatolian Fault (Figure 4), while NW-SE trending apparently normal faults accommodate extension and subsidence of the basins. Cavo d' Oro and Lesvos Basins are two depocenters developed on the southern side of NE-SW running Cavo d' Oro - Lesvos Fault Zone (Figure 4). Like before, E-W to NW-SE trending normal faults contribute to the transtensional deformation and the creation of these two basins. Further south, a third major NE-SW trending fault zone separates the North Ikarian Basin and the Mykonos Basin to the north from the structural high of Ikaria, Samos and Mykonos Islands and the shallow ridge connecting them. Strike-slip sense of movement along this fault zone has been already proposed by Mascle & Martin (1990) and by Lykousis *et al* (1995).

Focal mechanisms of shallow earthquakes occurred in this region (Kiratzi & Louvari, 2003) strongly indicate that all three strike-slip fault zones mentioned above (south branch of North Anatolian Fault, Cavo d' Oro - Lesvos fault zone, North Ikarian fault zone) display right lateral sense of movement, like the North Anatolian Fault does.

3.2. South Aegean Sea

NE-trending strike-slip faults in the eastern part of the South Aegean Sea have been recognized by Mascle and Martin (1990) south of Santorini and Anafi. Piper & Perissoratis (2003) have mapped pronounced 040°-trending set of faults in the area from Kos and Nisyros through Amorgos and Astypalea to Santorini with narrow basement ridges and abrupt basin inversion, which strongly suggests a strike-slip regime. Figure 6 shows the structure of the Amorgos Basin depocenter on the

hangingwall of the apparent normal, NE-SW trending, S-facing Amorgos fault and one more, subvertical, apparently (left- or right-) lateral fault crosscutting the uplifted ridge. This fault pattern is in line with the interpretation proposed by Mascle & Martin (1990) and Piper & Perissoratis (2003).

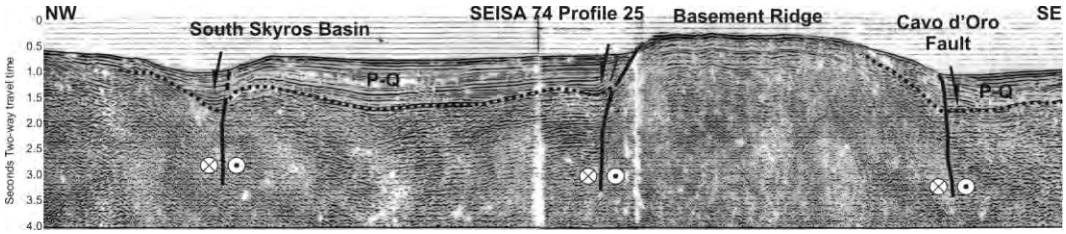

Figure 4 - Continuous seismic profile (SEISA 74) through the Southern Skyros Basin and Cavo D' Oro North Basin. Base of Plio-Quaternary deposits is shown as dotted line. Major basin bounding faults are subvertical and have been interpreted as dextral strike slip faults.

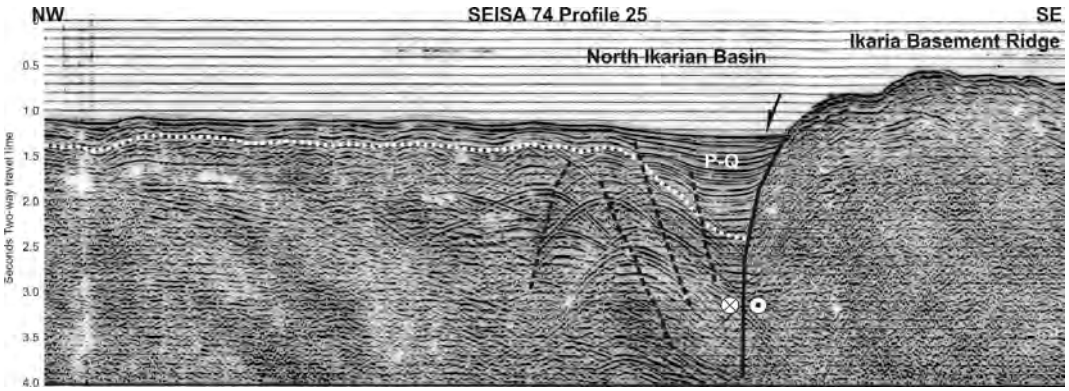

Figure 5 - Continuous seismic profile (SEISA 74) through the western part of the North Ikarian Basin and the Basement Ridge between Mykonos and Ikaria. The North Ikarian fault is subvertical or dips steeply northward. The North Ikarian Basin has developed under the transtensional regime in the hangingwall of the fault.

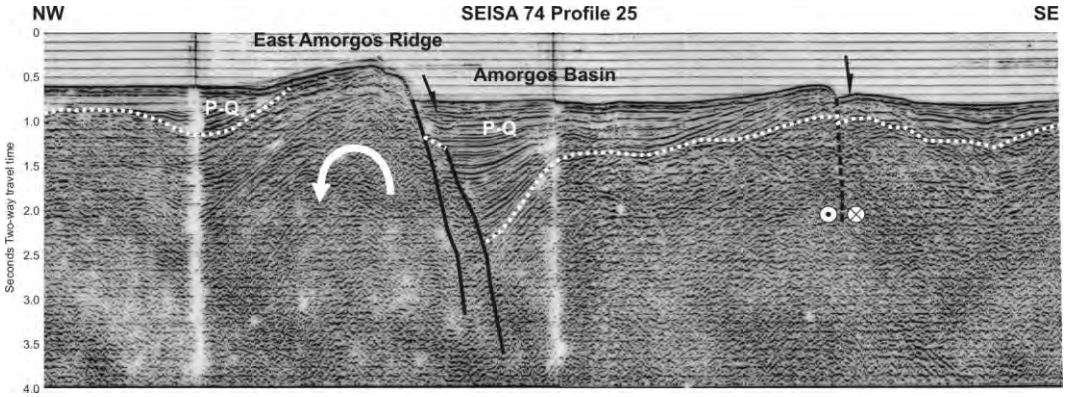

Figure 6 - Continuous seismic profile (SEISA 74) east of Amorgos. The E-W trending, South-facing, east termination of Amorgos fault is apparently a normal fault which has accommodated extension of the transtensional Amorgos Basin. Note the vertical fault (pressumably sinistral strike-slip), which crosscuts the ridge located between Amorgos (North) and Astypalea (South).

In early nineties Papazachos and Panagiotopoulos (1993) have observed five clusters of strong, shallow and intermediate, earthquake epicentres corresponding to 060° trending faults, which coincide with the volcanic fields at Sousaki, Methana, Milos, Santorini and Nisyros. Tibaldi *et al* (2008) suggest that Nisyros volcanic field has developed within a major NE-trending graben with strong evidence of left-lateral strike-slip component. In accordance to that, Sakellariou *et al* (2010) have proposed that the Santorini-Koloumbo volcanic field has developed within and along the transtensional NE-SW trending Anydros basin and that the volcanic centers of Christiana, Kameni and Koloumbo are aligned along a major strike-slip fault-zone. Piper & Perissoratis (2003) have shown that the offshore area north and south of Milos is strongly offset by prominent N-S faults and at least one major NE-trending active fault and argue that this fault pattern is a consequence of NE-trending sinistral shear.

Figure 7 shows a re-interpreted seismic profile (modified after Mascle & Martin, 1990) through the southern tectonic boundary of Mirtoon Basin and the NE-SW trending ridge southwest of Milos. Note that, with the exception of Antimilos, all volcanic centers of Milos field are aligned in NE-SW direction, parallel to the trend of the shear proposed by Piper & Perissoratis (2003). In that sense, Mirtoon Basin may have formed within a transtensional regime and is bounded by NE-SW strike slip and NW-SE normal faults. Re-evaluation of the multi-channel seismic profiles from the western part of the South Aegean Sea indicates that the Argolikos and Antikythera Basins display similar structural configuration.

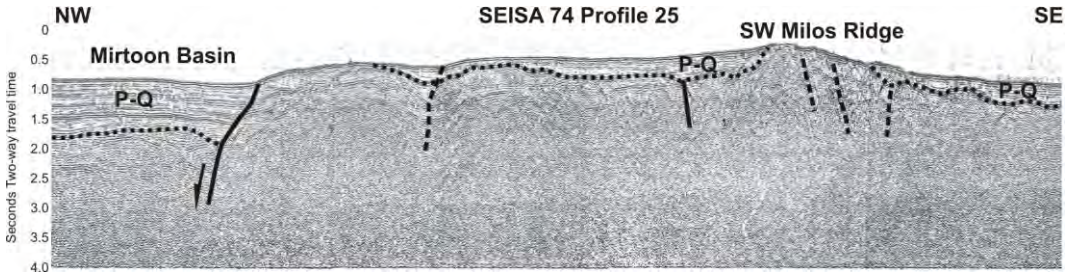

Figure 7 - Continuous seismic profile (SEISA 74) west of Milos. Note the sharp tectonic boundary of the Plio-Quaternary depocenter below the Myrtoon Basin towards S-SE and the structural high southwest of Milos, which is crosscut by subvertical faults.

In the eastern part of the South Aegean Sea Rossi et al (1986) recognized significant sinistral strike slip tectonics which led to the formation of major depocenters like Karpathos and Kamilonisi Basins (Fig. 8). Swath bathymetry data have revealed major, NE-SW trending, tectonomorphological structures, parallel or sub-parallel to the Plinian and Strabon trenches, as well as NNE-SSW oriented faulting. Kamilonosis and Syrna Basins are bounded by NE-SW trending major faults while Karpathos Basin, and the straits between Crete and Kassos and between Karpathos and Rhodes have developed due to the activity along NNE-SSW trending, apparently normal faults which to the north and south connect to NE-SW trending faults.

3.3. Hellenic Arc and Trench

Ten Veen & Kleinspehn (2003) describe a very similar fault pattern on Crete: based on observation in Messara Basin they propose that Plio-Pleistocene basins both offshore and onshore Crete are controlled by sinistral 070° strike-slip faults and secondary 020° extensional oversteps. This is the case among others for the Iraklion Basin as well as for Eastern Crete where the NNE-SSW trending Ierapetra fault connects two major NE-SW oriented, offshore strike slip faults (Figure 8).

Swath bathymetry data along the Hellenic Arc south of Crete show that the outer edge of the Aegean microplate is sinistrally offset by two NE-SW trending strike-slip fault zones, the SE Cretan Trough and the Pliny Trough fault zones, while Strabo Trench marks the southeastern boundary of the microplate towards the East Mediterranean Ridge accretionary prism. Similar offset of the Hel-

lenic Trench is observed SW of Crete, in line with the prolongation of the SW Cretan Trough fault zone. South and Southwest Peloponnese is characterized by NNW-SSE trending, predominantly normal faults which change progressively to the west to N-S direction.

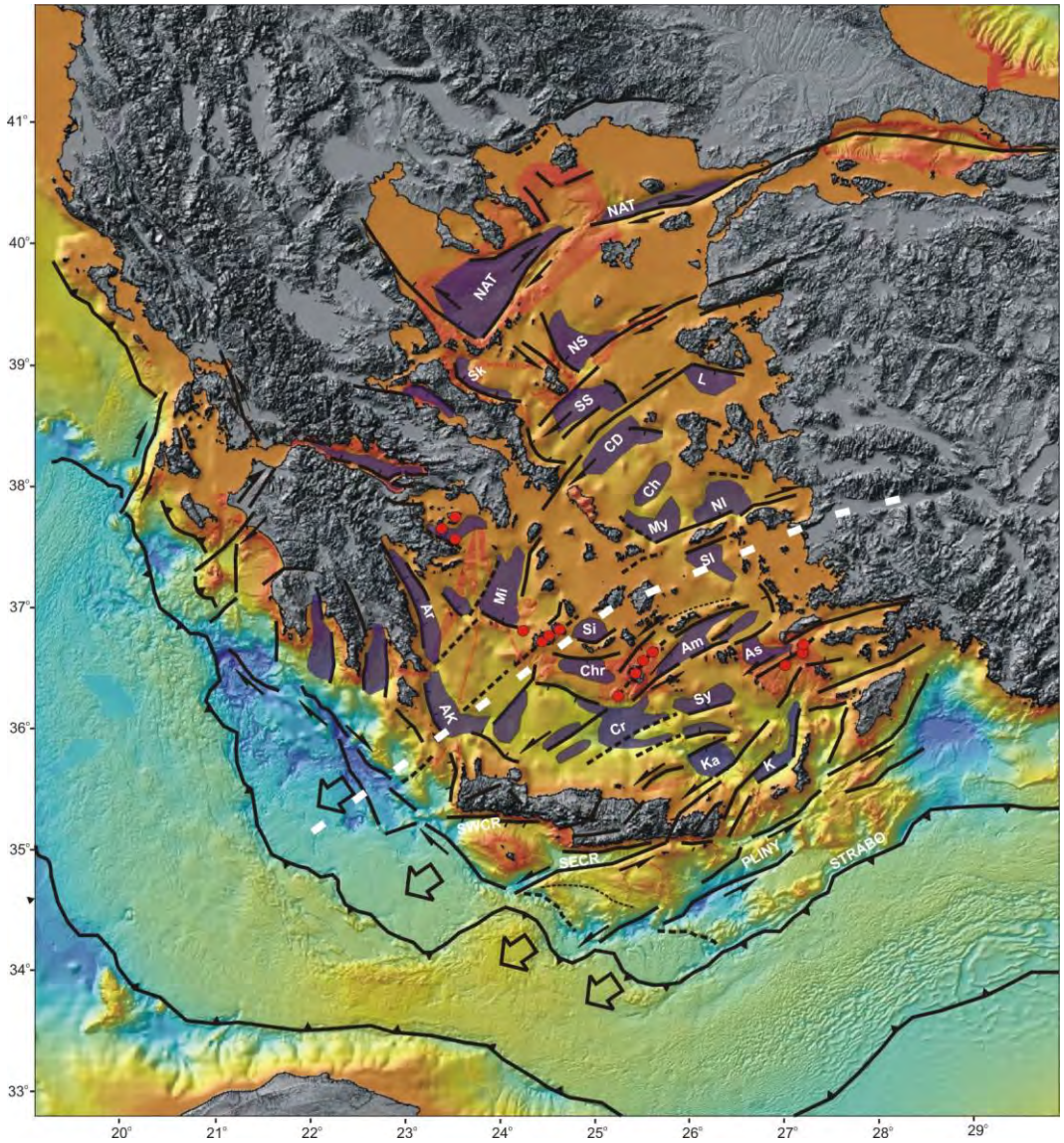

Figure 8 - Simplified tectonic map of the Aegean Region with major faults and fault zones, sense of movement and main Plio-Quaternary depocenters shown in transparent blue color. Swath bathymetry and relief extracted from Brossolo *et al* (2012). Faults after Mascle & Martin (1990), Piper & Perissoratis (2003) and new data. NE-SW, curved, dashed, white line marks the Mid-Aegean Lineament. Abbreviations of basins: NAT: North Aegean Trough, NS: North Skyros, SS: South Skyros, Sk: Skopelos, L: Lesvos, CD: Cavo d' Oro, My: Mykonos, NI: North Ikaria, SI: South Ikaria, Mi: Mirtoon, Ar: Argolikos, Si: Sikinos, Chr: Christiana, Am: Amorgos, Sy: Syrna, Cr: Cretan, Ak: Antikythera, Ka; Kamilonissi, K: Karpathos, SWCR: Southwest Cretan Trough, SECR: Southeast Cretan Trough.

Further north, west of Peloponnese and off the Ionian Islands, right lateral, NE-SW trending, strike slip faulting prevails, parallel to the Kephallonia Fault, as deduced from earthquake focal mechanisms (Kitatzi & Louvari, 2003) and from seismic profiling and swath bathymetry data.

4. Discussion - Conclusions

Mascle & Martin (1990) concluded that Late Miocene N-S extension in the South Aegean Sea shifted towards a NE-SW direction since Early Pliocene, perpendicular to the Ionian branch of the Hellenic trench, where pure convergent plate motion occurs. The former E-W structures have been slightly rotated to ENE-WSW direction progressively activated as transcurrent features (Martin, 1987). They suggested that the Aegean Sea can be viewed as a stretching continental domain cut into several ENE-WSW trending and elongated crustal terranes, all more or less independent of each other and moving progressively towards the southwest. Piper & Perissoratis (2003) proposed that much of the deformation resulting from the interaction of the Eurasian, African and Anatolian-Aegean plates is taken up at the southern margin of the Aegean microplate, in the South Aegean arc. This deformation may have played an important role in the creation and distribution of volcanism along the Hellenic Volcanic Arc. The change in tectonic style observed since Early Pliocene corresponds to the time when the North Anatolian Fault broke into the North Aegean sea (Armijo et al., 1999). Ten Veen & Kleinspehn (2003) believe that post-Miocene transtension has driven Hellenic forearc kinematics. Since Early Pliocene, incipient collision with Libyan promontory blocked further expansion of the Aegean plate south of western Crete and induced forearc slivers to be displaced northeastward and sheared sinistrally, as the Cretan–Rhodes forearc was simultaneously stretched.

Although this work is still in progress, our preliminary results suggest that deformation since Early Pliocene, when the North Anatolian Fault reached North Aegean, is strongly controlled by right and left lateral strike slip faulting distributed within the entire Aegean Region between the North Aegean Trough to the north and the southeastern branch of the Hellenic Arc to the south (Figure 8).

Transtensional deformation and development of major extensional structures in the Central and North Aegean Sea, Mainland Greece, Peloponnese and the Ionian branch of the Hellenic Arc is driven by right-lateral strike slip faulting following the kinematics of Kephallonia and North Anatolian Faults which form the northern tectonic boundary of the expanding Aegean microplate. The Central and Southern Aegean Sea along with the southern and southeastern branches of the Hellenic Arc are subject to left-lateral strike slip faulting, in accordance with the kinematics of the southeastern tectonic boundary of the Aegean microplate. The Mid-Aegean Lineament (Fig. 8), an imaginary line passing south of Samos and Ikaria Islands, over Central Cyclades plateau and through the West Cretan strait, marks the boundary between right-lateral (to the north) and left lateral (to the south) strike slip tectonics.

The southwestward expansion and stretching of the Aegean microplate during Plio-Quaternary takes place between two, more or less fixed, parallel to each other tectonic boundaries: (i) a right-lateral tectonic boundary to the north, marked by the Kephallonia and North Anatolian Faults and (ii) a left -lateral tectonic boundary to the south, marked by the southeastern branch of the Hellenic Trench (Pliny & Strabo). Deformation of the Aegean microplate is mostly dominated by transtension, driven by NE-SW trending right-lateral (north) and left-lateral (south) strike slip fault zones and associated E-W and N-S normal faults.

5. References

Angelier J. 1979. Neotectonique de l'arc Egeen, *These Doct*., Univ. Paris VI.

Armijo R., Meyer B., King G., Rigo A. and Papanastassiou D. 1996. Quaternary evolution of the Corinth rift and its implications for Late Cenozoic evolution of the Aegean, *Geophys. J. Int*, 126, 11 – 53.

Armijo R., Meyer B., Hubert A. and Barka A.1999.Westward propagation of the North Anatolian f ault into the northern Aegean: timing and kinematics, *Geology*, 27, 267–270.
Bartole R., Catani G., Lenardon G. and Vinci A.1983. Tectonics and sedimentation of the southern Aegean Sea, *Boll. Oceanol. Teor. App.,* 1, 319-340.
Billiris H. et al.1991. Geodetic determination of tectonic deformation in central Greece from 1900 to 1988, *Nature*, 350, 124– 129.
Briole P. et al. 2000. Active deformation of the Corinth rift, Greece: Results from repeated Global Positioning System surveys between 1990 and 1995, *J. Geophys. Res*., 105, 25,605– 625.
Brosolo L., Mascle J. and Loubtrieu B. 2012. MorphoBathymetry of the Mediterranean Sea, Map 1/4.000.000. 1st Edition, Published by the Commission for the Geological Map of the Worl d (CGMW) and UNESCO), 2012
Clarke P. J. et al.1998. Crustal strain in central Greece from repeated GPS measurements in the int erval 1989–1997, *Geophys. J. Int*., 135, 195– 214.
Davies R., England P., Parsons B., Billiris H., Paradissis D. and Veis G. 1997. Geodetic strain of Greece in the interval 1892– 1992, *J. Geophys. Res*., 102, 24,571– 24,588.
Goldsworthy M., Jackson J. and Haines J. 2002. The continuity of active faults in Greece, *Geophy s. J. Int.*, 148, 596– 618.
Hancock P.L and Barka A.A. 1980. Plio-Pleistocene reversal of displacement on the North Anatoli an Fault Zone, *Nature*, 286(5773)5: 91-594.
Kiratzi A. and Louvari E. 2003. Focal mechanisms of shallow earthquakes in the Aegean Sea and t he surrounding lands determined by waveform modelling: a new database*, J. Geodyn*., 36 (1–2), 251–274.
Kokkalas S., Xypolias P., Koukouvelas I. and Doutsos T. 2006. Postcollisional contractional and extensional deformation in the Aegean region. In Dilek, Y., and Pavlides, S., eds., Post-collisional tectonics and magmatism in the Mediterranean region and Asia: *Geological Society of America,* Special Paper 409, 97–123, doi: 10.1130/2006.2409(06).
Koukouvelas I. and Aydin A. 2002. Fault structure and related basins of the North Aegean Sea and its surroundings, *Tectonics*, 21, No. 5, 1046, doi:10.1029/2001TC901037, 2002
Le Pichon X. and Angelier J. 1979. The Hellenic Arc and trench system: A key to the neotectonic evolution of the eastern Mediterranean area, *Tectonophysics*, 60, 1 –42.
Le Pichon X. and Angelier J.1981. The Aegean Sea, *Philos. Trans. R. Soc. London, Ser. A,* 300, 35 7– 372.
Le Pichon X., Chamot-Rooke N., Lallemant S., Noomen R. and Veis G.1995. Geodetic determinat ion of the kinematics of central Greece with respect to Europe, J. Geophys. Res., 100, 12,67 5– 12,690.
Lykousis V., Anagnostou C., Pavlakis P., Rousakis G. and Alexandri M.1995. Quaternary sedimentary history and neotectonic evolution of the eastern part of the Central Aegean Sea, Greec e, *Mar. Geol.,* 128, 59-71.
Martin L.1987. Structure et évolution récente de la meer égée: apports d'une étude par sismique ref lection, *Thése Doct.*, Univ. Paris VI.
McClusky S. et al. 2000. Global Positioning System constraints on plate kinematics and dyna-mics in the eastern Mediterranean and Caucasus, J. Geophys. Res., 105, 5695–5719.
McKenzie D. P. 1972. Active tectonics of the Mediterranean region, *Geophys. J. R. Astron. Soc*, 3 0, 109– 185.
McKenzie D. P. 1978. Active tectonics of the Alpine Himalayan Belt, the Aegean Sea and surroun ding regions, Geophys, *J. R. Astron. Soc.*, 55, 217–252.
McKenzie D. P. and J. A. Jackson. 1983. The relationship between strain rates, crustal thicken-ing, paleomagnetism, finite strain and fault movements within a deforming zone, *Earth & Plan et. Sci. Lett.*, 65, 182–202.
McKenzie D. and Jackson J. 1986. A block model of distributed deformation by faulting, *J. Geolo g. Soc. London*, 143, 349–353.
Mascle J. and Martin L.1990. Shallow structure and recent evolution of the Aegean Sea: A synthesis based on continuous reflection profiles, *Marine Geology*, 94, 271-299.

Mascle J., C. Huguen J., Benkhelil N., Chamot-Rooke E., Chaumillon J.-P., Foucher R., Griboulard A., Kopf G., Lamarche A., Volkonskaia J., Woodside T. and Zitter 1999. Images may show start of European-African Plate collision, *EOS Trans.*, AGU 80 (1999) 421-428.

Mascle J. and Mascle G. 2012. Geological and Morpho-Tectonic Map of the Mediterranean Domain. Published by the Commission For The Geological Map Of The World (CGMW) and UNESCO.

Nyst M. and Thatcher W. 2004. New constraints on the active tectonic deformation of the Aegean, *J. Geoph. Res.*, 109, B11406, doi:10.1029/2003JB002830, 2004

Papanikolaou D., Alexandri M., Nomikou P. and Ballas D. 2002. Morphotectonic structure of the western part of the North Aegean Basin based on swath bathymetry, *Marine Geology*, 190, 465-492

Papanikolaou D., Alexandri M. and Nomikou P. 2006. Active faulting in the north Aegean basin, *Geol. Soc. America*, Sp. Paper 409, 189-209, doi:10.1130/2006.2409(11).

Papanikolaou D.J. and Royden L.H. 2007. Disruption of the Hellenic arc: Late Miocene extension al detachment faults and steep Pliocene-Quaternary normal faults—Or what happened at Co rinth?, *Tectonics*, 26, TC5003, doi:10.1029/2006tc002007.

Papazachos B.C. and Panagiotopoulos D.G. 1993.Normal faults associated with volcanic activity a nd deep rupture zones in the southern Aegean volcanic arc, *Tectonophysics*, 220, 301-308.

Piper D.J.W. and Perissoratis C. 2003. Quaternary neotectonics of the South Aegean arc, *Mar. Geo l.*, 198, 259-288.

Rossi S., Got H., Taviani M. and Martin L.1986. Elements structuraux de la mer de Crete orientale et du Golfe d'Antalya (Mediterranee orientale), *Mem. Soc. Geol. It.*, 36, 153-164.

Sakellariou D., Lykousis V., Alexandri S., Kaberi H., Rousakis G., Nomikou P., Georgiou P. and Ballas D.2007a. Faulting, seismic-stratigraphic architecture and Late Quaternary evolution of the Gulf of Alkyonides basin – East Gulf of Corinth, Central Greece, *Basin Research*, 19/2, 273-295.

Sakellariou D., Rousakis G., Kaberi H., Kapsimalis V., Georgiou P., Kanellopoulos Th. and Lykousis V. 2007b. Tectono-sedimentary structure and late quaternary evolution of the north Evia gulf basin, Central Greece: preliminary results, *Bulletin of the Geological Society of Greece*, vol. XXXVII/1, p. 451-462.

Sakellariou D., Sigurdsson H., Alexandri M., Carey S., Rousakis G., Nomikou P., Georgiou P. and Ballas D. 2010. Active tectonics in the Hellenic Volcanic Arc: the Kolumbo submarine volcanic zone, *Bulletin of the Geological Society of Greece*, XLIII, No 2, 1056-1063

Sengor A.M.C. 1979. The North Anatolian transform fault: its age, offset and tectonic significance , *J.Geol. Soc. London*, 136, 269-282.

Sigurdsson H., Carey S., Alexandri M., Vougioukalakis G., Croff, K., Roman C., Sakellariou D., Anagnostou C., Rousakis G., Ioakim C., Gogou A., Ballas D., Misaridis T. and Nomikou P. 2006, Marine Investigations of Greece's Santorini Volcanic Field, *EOS*, Vol 87, 34.

Taymaz T., Jackson J. A. and McKenzie D. 1991. Active tectonics of the north and central Aegean Sea, *Geophys. J. Int.*, 106, 433–490.

ten Veen, J.H. and Kleinspehn K.L. 2003. Incipient continental collision and plate-boundary curvature: Late Pliocene–Holocene transtensional Hellenic forearc, Crete, Greece, *Journal of the Geological Society, London*, Vol. 160, 2003, 161–181.

Tibaldi A., Pasquare F.A., Papanikolaou D. and Nomikou P. 2008. Tectonics of Nisyros Island, Greece, by field and offshore data, and analogue modeling, *Journal of Structural Geology,* 30, 1489–1506.

Δελτίο της Ελληνικής Γεωλογικής Εταιρίας, τομ. XLVII , 2013
Πρακτικά 13ου Διεθνούς Συνεδρίου, Χανιά, Σεπτ. 2013

Bulletin of the Geological Society of Greece, vol. XLVII 2013
Proceedings of the 13th International Congress, Chania, Sept. 2013

MORPHOTECTONIC ANALYSIS OF KOZANI BASIN (WESTERN MACEDONIA, GREECE)

Simou E.[1], Karagkouni V.[1], Papantoniou G.[1], Papanikolaou D.[1] and Nomikou P.[1]

[1] National and Kapodistrian University of Athens, Faculty of Geology and Geoenvironment, Department of Dynamic, Tectonic and Applied Geology, erinisim@gmail.com, vasilikikaragouni@gmail.com, gapap@live.com, dpapan@geol.uoa.gr, evinom@geol.uoa.gr,

Abstract

Kozani Basin is located in northern-central Greece and constitutes the southernmost of the Plio-Pleistocene basins of western Macedonia. Quantitative and qualitative analysis of morphological slope values, as well as the analysis of the drainage pattern in Kozani Basin confirms that the current topographic relief reflects intense neotectonic activity. Synthetic Morphotectonic Map of the under study area was carried out by means of the combined use of: (a) Digital Elevation Model (DEM), (b) Slope Distribution Map, (c) Morphological Slope Map and (d) Drainage Pattern Map. The composition of the digital modelling in conjunction with the regional geological setting, allows the identification of the main morphological discontinuities and lineaments that result from morphotectonic interpretation. The high morphological slope values indicate well-defined morphotectonic features, which mainly trend NE - SW and, secondarily, NW - SE. Distinct tectonic structures are mostly recognized in the SE margin of Kozani Basin, which is characterized by intense topographic relief. The main large-scale tectonic structure trends NE - SW and corresponds to the major Aliakmonas marginal fault zone that bounds the Kozani basin to the south. On the other hand, the NW margin's features are indiscernible; thus, the criteria for their recognition are based on the existence of the river terraces, which reflect the tectonic control. The results of our studies are presented on the Morphotectonic Map, which is followed by our 3D model of Kozani Basin.

Key words: *tectonic geomorphology, Aliakmonas fault zone, morphotectonic structures.*

Περίληψη

Η λεκάνη της Κοζάνης αποτελεί τη νοτιότερη Πλειο-Πλειστοκαινική λεκάνη της δυτικής Μακεδονίας. Η ποιοτική και ποσοτική ανάλυση των μορφολογικών κλίσεων, καθώς και η ανάλυση του υδρογραφικού δικτύου στην περιοχή μελέτης επιβεβαιώνουν πως η σημερινή μορφή της αντανακλά έντονη νεοτεκτονική δραστηριότητα. Ο Μορφοτεκτονικός Χάρτης προέκυψε από τη σύνθεση του ψηφιακού μοντέλου αναγλύφου, την κατανομή μορφολογικών κλίσεων και την ερμηνεία του υδρογραφικού δικτύου. Τα παραπάνω, σε συνδυασμό με τη γεωλογία της περιοχής, οδήγησαν στον προσδιορισμό των κύριων μορφολογικών ασυνεχειών. Οι κυριότερες τεκτονικές δομές, διεύθυνσης ΝΔ-ΒΑ, εντοπίζονται στο ΝΔ περιθώριο της λεκάνης, το οποίο χαρακτηρίζεται από έντονο τοπογραφικό ανάγλυφο. Κύρια μορφοτεκτονική δομή αποτελεί η ρηξιγενής ζώνη του Αλιάκμονα, που οριοθετεί τη λεκάνη της Κοζάνης προς

νότο. Το ΒΔ περιθώριο της λεκάνης χαρακτηρίζεται από ήπιο ανάγλυφο, το οποίο καθιστά δυσχερή τον εντοπισμό των τεκτονικών στοιχείων. Οι μορφοτεκτονικές παρατηρήσεις συνοψίζονται στους χάρτες και το 3D μοντέλο που παρατίθενται.
Λέξεις κλειδιά: *ενεργός τεκτονική, μορφογραμμώσεις, ρηξιγενής ζώνη Αλιάκμονα.*

1. Introduction

Kozani basin is geographically situated in northern-central Greece and constitutes the southernmost of the Plio-Pleistocene basins of western Macedonia (Parcharidis et al, 2001). The above inland basin, which trends NE – SW, is bounded by Askion Mt. and Vourinos Mt. to NW and SE respectively, Kamvounia Mts. to the south and Pieria Mts. to E-SE (Figure 1).

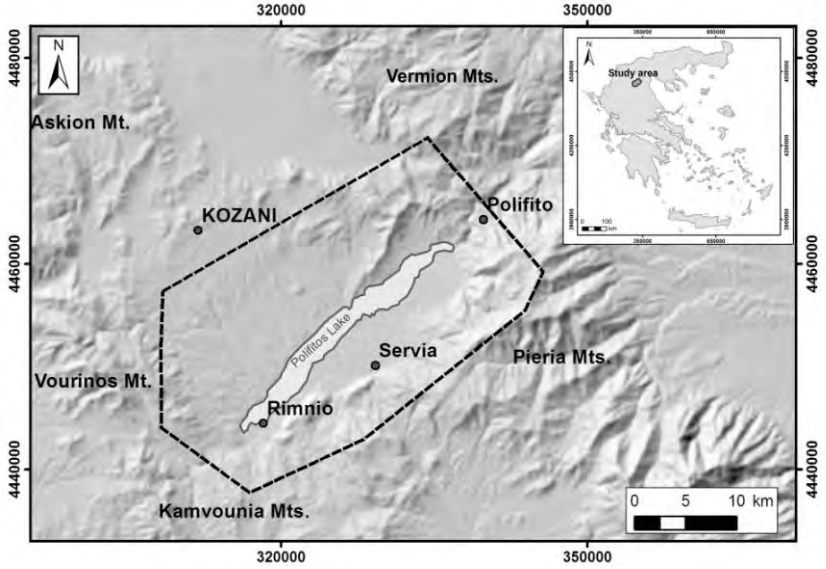

Figure 1 – Geographical location of the Kozani basin (GGRS87). The dashed line outlines the study area.

Mountrakis et al. (1998), have studied the several successive tectonic events related to the development of the Kozani basin. Knowing the resulting tectonic data, which correspond to our project area, we attempted to discriminate the significant tectonic structures of Kozani basin by mainly assessing the regional geomorphological and geological conditions. More specifically, the aim of the project has been the fault recognition by applying morphostructural analysis, which was based on the qualitative and quantitative interpretation of the topography, the slope distribution and the drainage pattern development in the study area.

2. Methodology

Since there was a large number of data in different formats (raster and vector) the GIS methodology has been the most suitable for our analysis. ArcGIS 10 package has been used for the data processing and the map composition and Surfer V. 10 / Rockware for the final 3D modelling. The construction of the Slope Distribution Map, the Morphological Map and the Drainage Pattern Map was based on: (i) the determination and classification of the morphological slope values, (ii) the evaluation of the morphological discontinuities and (iii) the drainage pattern interpretation, which were carried out in order to identify the neotectonic structures and their possible morphological expression. The aim of the above procedure was the construction of the Morphotectonic Sketch Map, which presents the major tectonic structures of the project area.

3. Geological Setting

3.1. Geotectonic Structure

The alpine basement of the Kozani neotectonic basin (Figure 1) is geotectonically located in the medial tectonometamorphic zone (Papanikolaou, 1984; Papanikolaou, 1986; Papanikolaou et al., 2004), also known as Pelagonian geotectonic unit (Mountrakis, 1985). The geological formations that can be observed in the wider Kozani area are the following (Neotectonic Map of Greece, Kozani Sheet, Scale: 1:100 000, Mountrakis et al. 1999):

- **Alpine Formations (Figure 2): (a) Eastern Greece Unit formations.** They outcrop at the SE and WNW part of the study area. They are Mesozoic carbonate formations, which mainly consist of Triassic-Jurassic crystalline limestones and dolomites, **(b) Flambouro Unit formations**, which mainly consist of upper Palaeozoic gneisses and amphibolites. They outcrop at the SW part of the study area and constitute the basement of the Pelagonian zone (Papanikolaou, 1986), and **(c) Vourinos Ophiolite Complex.** The ophiolite formations consist of basaltic lavas, dacites, diorites, gabbro and, mainly, peridotites (Mavridis & Kelepertzis, 1993).
- **Post-alpine Formations (Figure 2).** They are **Holocene deposits** (alluvial deposits and scree material) and thick sequences of **Plio-Pleistocene sediments**, composed by fluvial and lacustrine coarse-grained, unconsolidated clastic material (loose conglomerates, clays, sands and sandstones).

3.2. Tectonics

Previous studies and structural analyses that were carried out in western Macedonia (Pavlides S., 1985; Pavlides et al., 1987; Mountrakis et al., 1993; Mountrakis et al., 1998; Burchfiel et al., 2008) determined the successive tectonic events, which have taken place during the Tertiary evolution. In Early Oligocene, the regional extensional stress field formed NNW-SSE trending normal faults. Middle-Late Miocene was characterised by two compressional deformation stages; (i) an ENE-WSW compressional event responsible for NNW-SSE trending reverse faults, as well as dextral strike-slip transfer faults of E-W to NE-NW direction and (ii) a NNE-SSW compressional stress field, which activated E-W trending reverse faults. A Late Miocene–Pliocene subsequent extensional deformation event, expressed by NNW-SSE trending normal faults, started forming the Kozani - Ptolemais basin. The extensional stress field remained active during Early-Middle Pleistocene and formed the existing half-graben structure controlled by NE-SW to ENE-WSW basin's marginal faults, which are related to steep scarps, drainage asymmetries and other morphotectonic features which were also interpreted on the following morphotectonic analysis.

3.3. Geomorphology

3.3.1. Drainage Pattern Analysis

The drainage pattern in Kozani basin is characterized by intense asymmetry, especially between the NW and SE margin. The drainage disorders reveal the tectonic structures that have significant influence on the current topographic relief, as presented on the Synthetic Drainage Pattern Map (Figure 2). The project area is mainly characterized by parallel drainage pattern (Figure 2 - area 1). The streams are straight, trending NW-SE to NNW-SSE in both margins, with very few tributaries. Flow is accumulated towards SE and NW at the NW and SE margin of the basin respectively. Parallel drainage pattern indicates the smooth to moderate steep slopes (Howard, 1967), which are identified at the northwest part of the study area (Figure 2) and consist of unconsolidated post-alpine formations; lacustrine deposits and mostly sands, clays, marls, sandstones and conglomerates, which comprise easily erodible material. The elongated streams (~10-15km in length) can be explained by the tilting of the NW part of the basin towards N (Goldsworthy & Jackson, 2000), as a result of the major active NE-SW trending tectonic structure, which is known

as the Aliakmonas fault zone. Tilting of fault blocks can also be interpreted by local asymmetries of the drainage pattern which develops on the alpine basement (Mesozoic carbonate formations of Eastern Greece unit) in area 3 (Figure 2). Flow in the few existing tributaries might be related to the differential erosion rates, which depend on the geological background.

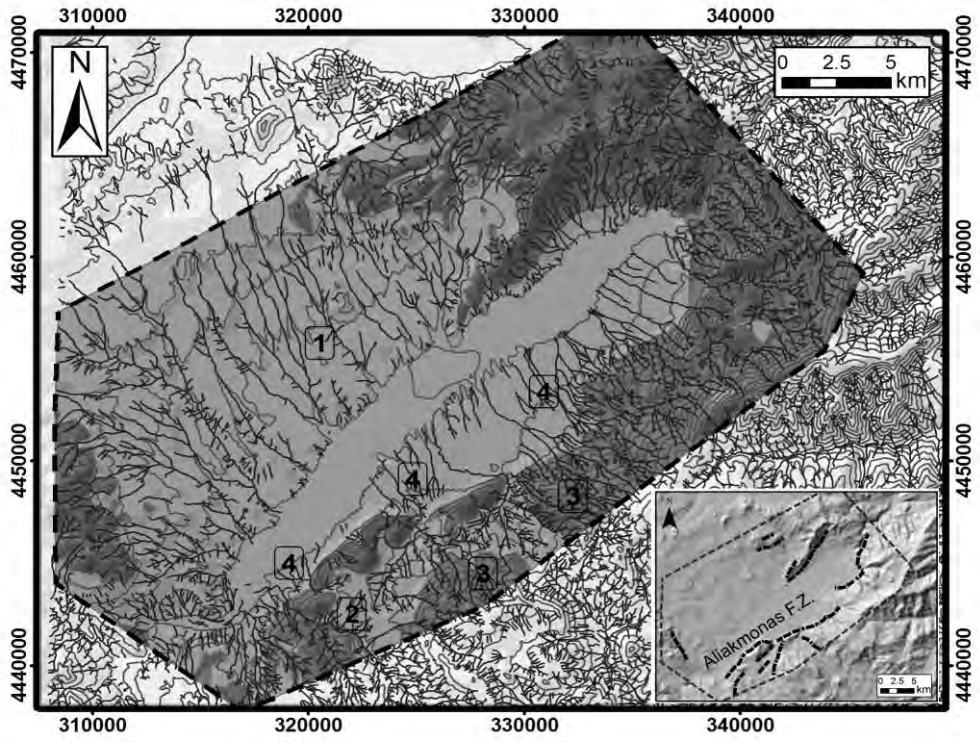

Figure 2 – Synthetic Drainage Pattern Map (GGRS87). Dark and light grey colours indicate the alpine basement and the post-alpine sediments respectively (after Mavridis & Kelepertzis, 1993; Mountrakis et al., 1999). The picture on the right bottom corner presents the morphotectonic features that can be interpreted by the local drainage asymmetries (numbers are explained in the text).

Rectangular drainage pattern develops locally in the SE margin of the basin (area 2 of Figure 2). The tectonic activity is controlled by the predominant joint systems, which characterize the alpine basements formations.

Drainage asymmetries in the SE margin of the Kozani basin may also indicate the fault segmentation of the main large scale Aliakmonas fault zone (Goldsworthy & Jackson, 2000). The drainage flows from the footwall (SE margin – Alpine basement) to the hanging wall (NW margin – Post-alpine sediments) at the lower topographic areas, which seem to be related to the ends of the fault segments (Figure 2 - areas 4). The small catchments are more related to the lithology rather than the tectonic setting, as they indicate the karstification of the Mesozoic carbonate bedrock at the southeast part of the study area.

Drainage pattern analysis in combination with the following morphological slope values has contributed in the morphotectonic interpretation of the Kozani basin.

3.3.2. Slope Distribution and Morphological Slope Analysis

The geomorphological signatures that have affected topography allow the configuration of the active faulting in the study area. Topographic map and slope distribution map processing contributed to the distinction of two main areas in the Kozani basin: the NW margin, characterized by smooth topographic relief and the SE margin, which is characterized by steeper slopes. More specifically, the project area was analysed with regard to the slope distribution. The results of the slope values analysis are presented on the Slope distribution map (Figure 3) and the Morphological slope map (Figure 4).

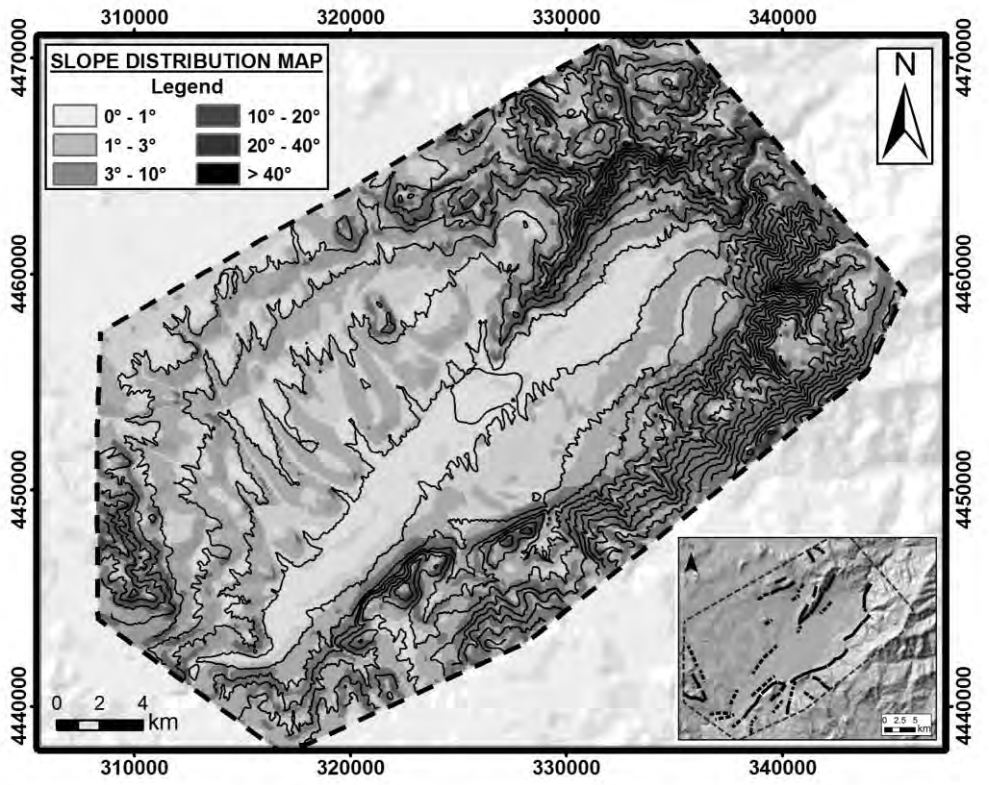

Figure 3 –Slope Distribution Map of Kozani basin (GGRS87). The slope values are in degrees. The picture on the right bottom corner presents the tectonic features that can be interpreted after the classification of the slope values.

On the slope distribution map, the slope values are distinguished in 6 classes: (i) flat areas of 0°-1° (basinal area), (ii) areas of mean morphological slope values of 1°-3°, (iii) areas of 3°-10°, (iv) areas of 10°-20°, (v) areas of 20°-40° and (vi) steeper areas of > 40°. This classification aims to indicate areas characterized by abrupt change of slope values, which reflect the position of active tectonic structures (S and SE part of the project area – Figure 3). On the contrary, the areas of negligible change of the slope values, suggest plain areas on post-alpine formations related to river terraces or basinal areas (NW part of the project area – Figure 3).

The morphological slope map (Figure 4) reaffirms the above results. It constitutes a quantitative map, which aims to present not only the slope values but the direction of the slopes as well, indicating thereby the overall shape of the basin. The slope discontinuities (Figure 4) that can be distinguished are related to the active tectonic structures of Kozani basin.

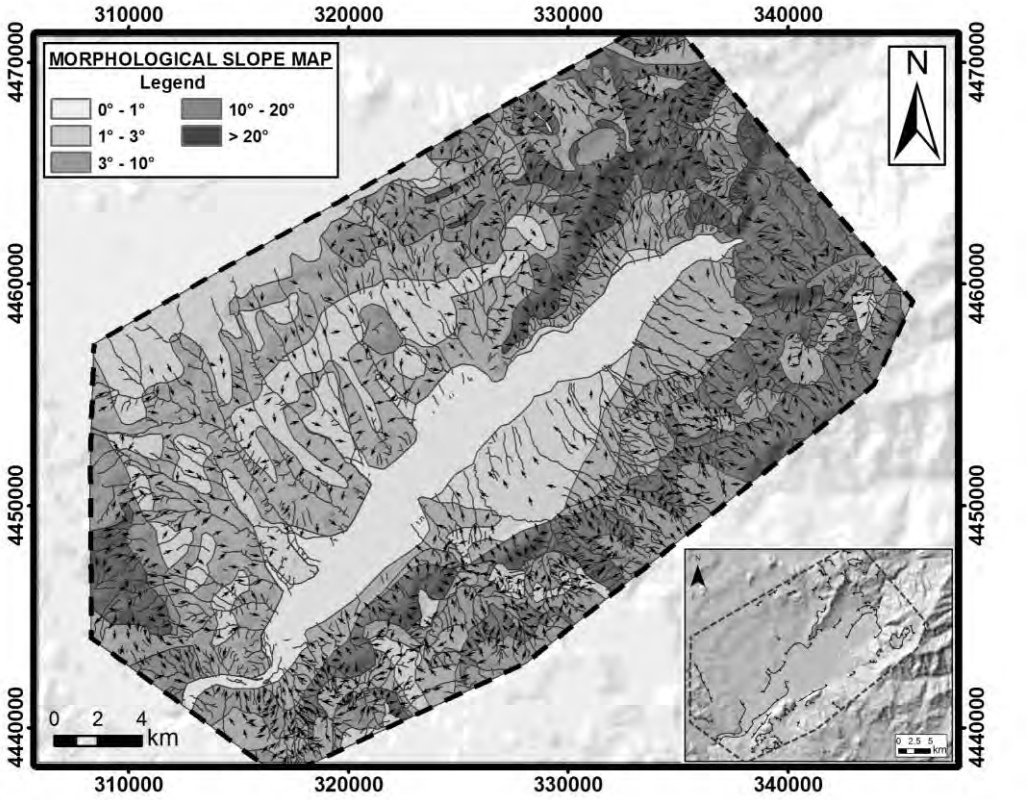

Figure 4 – Morphological Slope Map of Kozani basin (GGRS87), presenting the slope values classification (in degrees). The arrows indicate the dip direction of the slopes. The picture on the bottom right corner illustrates the slope discontinuities.

4. Morphotectonic Interpretation - Results

The morphotectonic interpretation, accomplished by the compilation of the previously presented maps, has led to the construction of the Morphotectonic sketch map (Figure 5), which illustrates the major morphotectonic features of the project area.

The overall morphology of Kozani basin seems to be controlled by the large-scale faults, which can be defined by the abrupt alternations of the morphological slope values (Figure 4) and the local drainage asymmetries (Figure 2). The defined tectonic structures of the basin, as it can be concluded by the statistical analysis (Figure 5 – rose plots), are developed primarily in a NE – SW direction and, secondarily, in a NW – SE one, following the slope direction distribution. It is remarkable that the most significant NE – SW trending faults can be related to the borders of the basin, where the alpine basement outcrops. In the study area, more than 30 morphotectonic structures could be determined by using exclusively the morphological indices and are presented on the morphotectonic map of Figure 5.

Knowing the tectonic data according to the regional tectonic setting of Kozani area, further analysis of the most significant determined structures was attempted in combination with the available bibliographic references. The major active tectonic structure of the Kozani basin is the NE-SW trending Aliakmonas fault zone (Figure 5 – segments 1 & 2). It can be observed at the SE part of the project area and comprises a major extensional tectonic feature (Papanastasiou et al.,

1998; Mountrakis et al., 1998; Mountrakis et al., 1999), discernible especially because of its significant effect on the topographic relief. The Aliakmonas fault zone length exceeds 80km and constitutes of 3 segments, which can be verified mainly by the drainage pattern. More specifically, the drainage occurs from the footwall of the Aliakmonas fault zone (SE margin of the basin) to the hanging wall (NW margin of the basin) at the lower topographic areas (Goldsworthy & Jackson, 2000), which seem to be associated to the ends of the fault segments (Figure 2 - areas 4). Two of the three fault segments belong to the project area and correspond to the Rymnio fault and the Servia fault (Figure 5).

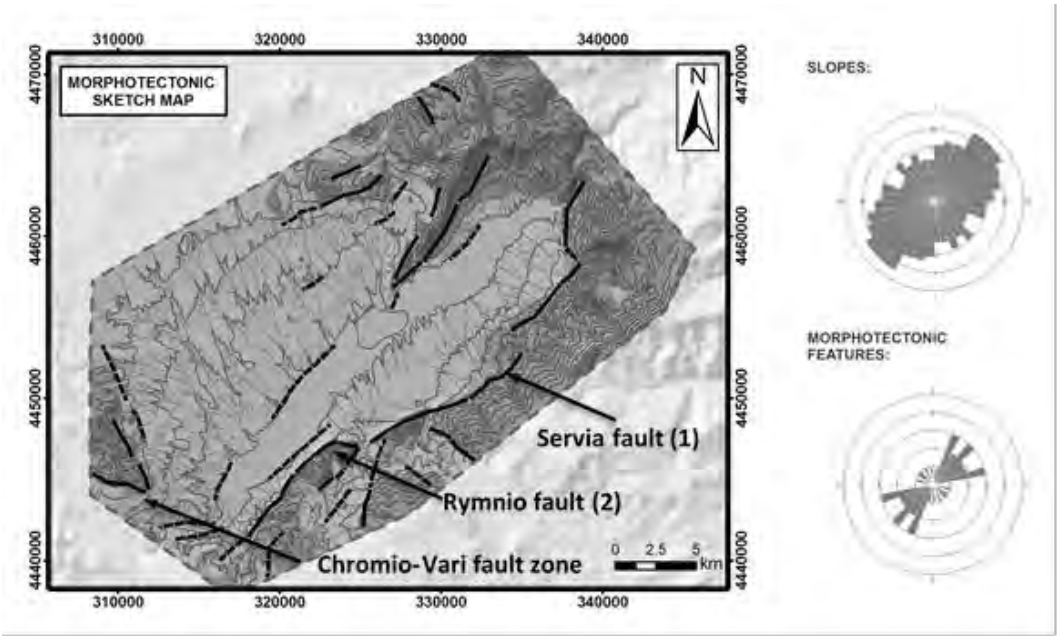

Figure 5 –Morphotectonic Sketch Map (GGRS87), presenting the most significant morphotectonic features in Kozani basin (black continuous lines for the distinct - dashed for the probable structures). Dark and light grey colours indicate the alpine basement and the post-alpine sediments respectively. Rose plots (statistical analysis) on the right illustrate the main directions of the slope and the morphotectonic features.

Servia fault (Figure 5; Figure 6) lies in the northern part of the Aliakmonas fault zone and bounds the Kozani basin to the south. It corresponds to one of the most prominent morphotectonic features of the project area, trending NE – SW and dipping ~60° towards NW (Papanastasiou et al. 1998). The fault surface is distinct due to the steep slopes that develop in the alpine basement.

Rymnio fault (Figure 5) constitutes the middle part of the Aliakmonas fault zone and consists the Servia fault extension towards SW. It is not as distinct structure as the Servia fault in the field, though it can easily be recognised in the morphotectonic map (Figure 5). The Rymnio fault, dipping 80°-85° near surface and about 30° deeper (Mountrakis et al, 1998) comprises the main seismogenic structure, which, according to certain researchers, is related to the 13th May 1995 Kozani earthquake (Lekkas et al., 1996; Drakatos et al., 1998). Servia fault was not activated during the earthquake event, possibly because it is geomorphologically separated from the Rymnio fault segment.

Another significant tectonic feature, which is partly observed in the project area, is the Chromio-Vari fault zone (Figure 5). This feature contributes a WNW-ESE trending, secondary antithetic normal fault, which develops in the hanging wall of the Aliakmonas fault zone. It comprises a

seismogenic structure that exceeds 15 km in length, bounds partially the Vourinos ophiolithic complex formations and is covered by the Plio-Pleistocene formations (Mountrakis et al., 1998).

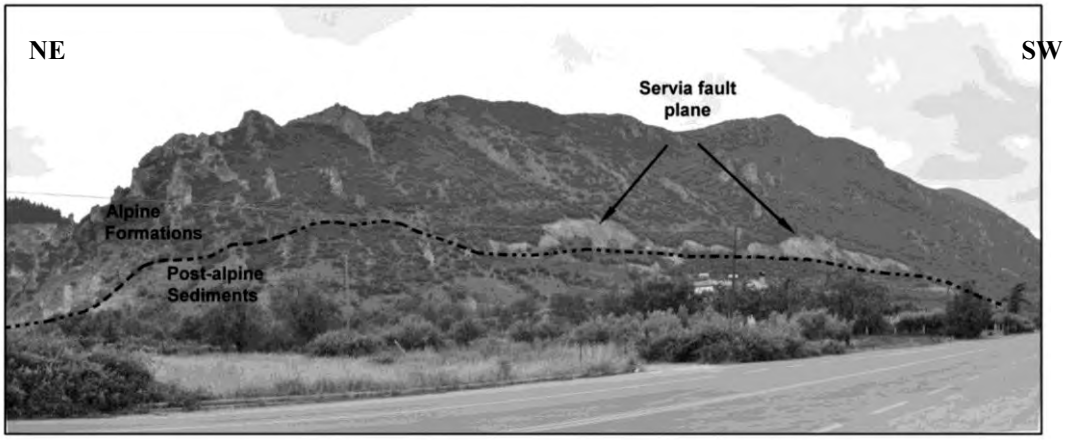

Figure 6 – Panoramic view of Servia fault segment.

On the other hand, the NW part of the project area where the north marginal fault of the basin is considered to be buried under the Plio-Pleistocene sequences, is characterized by smooth topographic relief. The mean morphological slope values, ranging between 1°-10° (Figure 3; Figure 4) and the undisturbed parallel drainage pattern (Figure 2 – area 1) indicate the insignificant effect of the active tectonics on that part of the basin, which is characterized by the development of river terraces on the hanging wall of the Aliakmonas fault zone. The study of the Kozani basin by using optical and radar satellite data (Parcharidis et al., 2001) is in accordance with our results, concerning the distribution of the NE-SW trending morphotectonic lineaments.

The morphotectonic features presented on our Morphotectonic Map can be related to the tectonic features that have been already mapped in the wider area of Kozani (Mountrakis et al., 1999).

5. Discussion

The paper deals with the compilation of a morphotectonic map for the Kozani basin, based on digital modelling in combination with the regional geological, tectonic and geomorphological setting. Both on local and regional scales, the quantitative characterization of landforms (Morphological slope map – Figure 4) based on DEM analysis (Slope distribution map – Figure 3), contributes to the identification of tectonic lineaments and the characterization of the structural properties of faults on a morphological basis.

The relief, the slope parameters, the drainage pattern asymmetries and the hypsometric high surface roughness support the neotectonic uplift which is accommodated by tectonic features developed primarily in a NE – SW direction, representing the transverse disruptive structures of the E – W oblique opening of Late Pliocene – Quaternary. Moreover, the identified secondary NW – SE trending faults reflect the Oligocene – Miocene extensional stage which corresponds to the last time at which extension was accommodated on arc-parallel structures (Papanikolaou & Royden, 2007).

The morpho-structural analysis which was operated for the project area gives an accurate scheme of the geometry of the Kozani basin and distinction of the most significant morphotectonic structures, which are presented on our Morphotectonic sketch map (Figure 5) and the following 3D model (Figure 7).

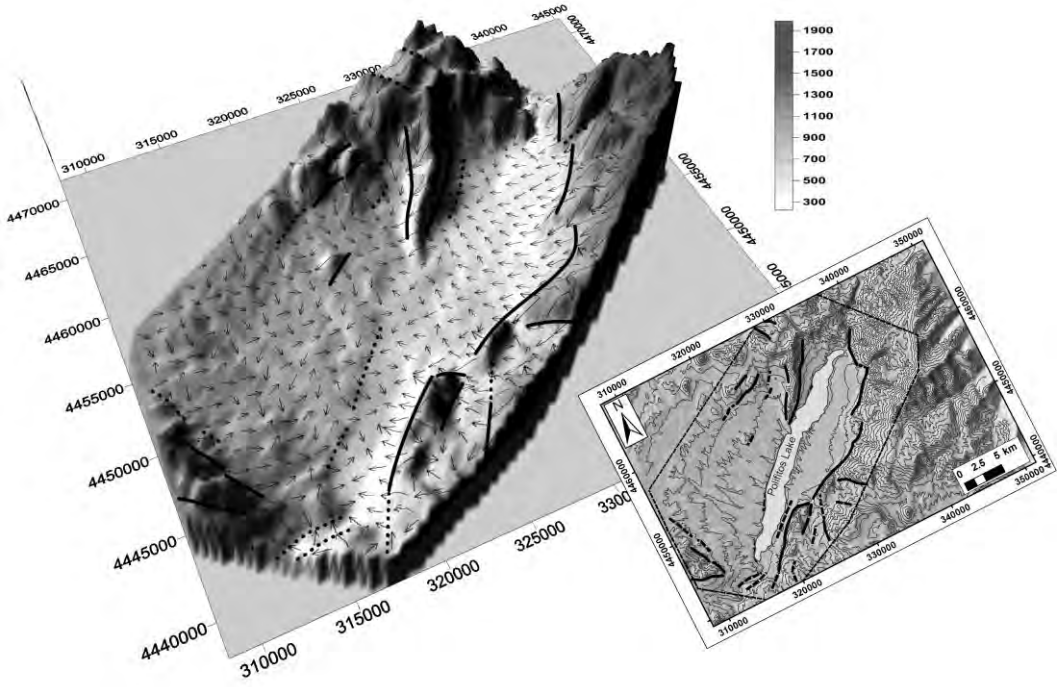

Figure 7 – 3D model of Kozani basin and the relevant Morphotectonic Sketch Map (GGRS87), which illustrate the significant morphotectonic structures of the project area (black continuous lines for the distinct - dashed for the probable structures). View from SSW - (Surfer V. 10 / Rockware).

6. References

Burchfiel B.C., Nakov R., Dumurdzanov N., Papanikolaou D., Tzankov T., Serafimovski T., King R.W., Kotzev V., Todosov A. and Nurce B. 2008. Evolution and dynamics of the Cenozoic tectonics of the south Balkan extensional system, *Geosphere*, *4* (6), 919-938.

Drakatos G., Papanastasiou D., Papadopoulos G., Skafida H. and Stavrakakis G. 1998. Relationship between the 13 May 1995 Kozani–Grevena (NW Greece) earthquake and the Polyphyto artificial lake, *Engineering Geology, 51*, 65-74.

Goldsworthy M. and Jackson J. 2000. Active normal fault evolution in Greece revealed by geomorphology and drainage patterns, *Journal of the Geological Society of London*, 157, 967-981.

Howard A.D. 1967. Drainage analysis in geological interpretation: A summation, *The American Association of Petroleum Geologists Bulletin, 51*, 11, 2246-2259.

Lekkas E., Fountoulis I., Lozios S., Kranis Ch. and Adamopoulou E. 1996. Neotectonic Implications of Grevena - Kozani Earthquake (May 13, 1995, W. Macedonia, Greece). *International meeting* on results of the May 13 1995 *earthquake of West Macedonia: One year after,* Kozani, 1996, 76-80.

Mavridis A. and Kelepertzis A. 1993. Geological map of Greece, *Knidhi Sheet*, Scale 1:50,000, I.G.M.E.

Mountrakis D. 1985. *Geology of Greece*, University Studio press – Thessaloniki (in Greek).

Mountrakis D., Kilias A. and Zouros N. 1993. Kinematic analysis and tertiary evolution of the Pindos-Vourinos Ophiolites (Epirus-Western Macedonia, Greece), *Bull. Geol. Soc. Greece, Vol. XXVIII/I*, 111-124.

Mountrakis D., Pavlides S., Zouros N., Astaras Th. and Chatzipetros A. 1998. Seismic fault geometry and kinematics of the 13 May 1995 Western Macedonia (Greece) earthquake, *J. Geodynamics, 26*, 2-4, 175-196.

Mountrakis D., Kilias A., Pavlides S., Vavliakis E., Tranos M., Zouros N., Spyropoulos N., Chatzipetros A., Karakostas V., Skordilis M., Gkountromichou Ch. and Thomaidou E. 1999. *Neotectonic Map of Greece*, Kozani Sheet, Scale 1:100,000. Faculty of Sciences, School of Geology, Aristotle University of Thessaloniki.

Papanastasiou D., Drakatos G., Voulgaris N. and Stavrakakis G. 1998. The May 13, 1995, Kozani-Grevena Earthquake, *J. Geodynamics, 26*, 2-4, 233-244.

Papanikolaou D. 1984. The three metamorphic belts of the Hellenides: a review and a kinematic interpretation, *Geological Society of London*, *Special Publications*, 17, 551-561.

Papanikolaou D. 1986. *Geology of Greece*, National and Kapodistrian University of Athens (in Greek).

Papanikolaou D., Bargathi H., Dabovski C., Dimitriu R., El-Hawat A., Ioane D., Kranis H., Obeidi A., Oaie G., Seghedi A. and Zagorchev I. 2004. The TRANSMED Atlas – Geological and geophysical framework of the Mediterranean and the surrounding areas. A publication of the Mediterranean Consortium for the 32nd International Geological Congress, Springer.

Papanikolaou D. and Royden L. 2007. Disruption of the Hellenic arc: Late Miocene extensional detachment faults and steep Pliocene – Quaternary normal faults – Or what happened at Corinth?, *Tectonics, 26,* TS5003.

Parcharidis I., Nikolakopoulos K., Serelis K. and Baskoutas I. 2001. Integrated Use of Optical and Radar Satellite Data for Active Faults and Corresponding Displaced Landforms in Kozani Basin. Greece, *Geocarto International, 16*, 17-23.

Pavlides S. 1985. Neotectonic evolution of Florina – Vegoritis – Ptolemais basin, *Phd Thesis*, Aristotle University of Thessaloniki.

Pavlides S. and Mountrakis D. 1987. Extensional tectonics of northwestern Macedonia, Greece, since the late Miocene, *Journal of Structural Geology, 9*, 385-392.

Δελτίο της Ελληνικής Γεωλογικής Εταιρίας, τομ. XLVII , 2013
Πρακτικά 13ου Διεθνούς Συνεδρίου, Χανιά, Σεπτ. 2013

Bulletin of the Geological Society of Greece, vol. XLVII 2013
Proceedings of the 13th International Congress, Chania, Sept. 2013

MICROSTRUCTURAL FINITE STRAIN ANALYSIS OF THE HAFAFIT GRANITOIDS DOMES SOUTH CENTRAL EASTERN DESERT OF EGYPT

Thabet I.[1& 2], Kilias A.[2] and Kamh S.[1]

[1] Geology Department, Faculty of Science Tanta University, Tanta, Egypt, eslam642004@yahoo.com.,kilias@geo.auth.gr, kamh2002@yahoo.com.

[2]Geology and Palaeontology Department, School of Geology, Aristotle University of Thessaloniki, Greece.

Abstract

The Wadi Hafafit Culmination (WHC) can be subdivided into two main units which are separated by Nugrus thrust shear zone. The WHC domes are occupies the southern part of the Central Eastern Desert of Egypt and is cored by five separated gneissic granitoids ranging in composition from tonalite to granodiorite having compositions consistent with hydrous partial melting of a mafic source suggesting subduction-related magmatism. The leucogranites along thrust zones is related to the late phase of metamorphism of Hafafit rocks. The five main domes of the WHC have been labeled A dome occupies the northern part of WHC, B and C domes occupies the central eastern part of WHC, D dome occupies the central western part of WHC and E dome occupies the southern part of WHC. The fourth domes A, B, C and E are affected by more than one deformation event but D dome is affected by one deformation event. The domes not uniform throughout the WHC according radial pattern of stretching lineation but these domes of WHC were subjected and affected by late-orogenic extension that was controlled by the Najd transform faults and that resulted in exhumation of the WHC domes are oriented NW-SE parallel to the trend of the left-lateral shear zones of Najd fault system.

Key words: *Wadi Hafafit Culmination, Strain analysis, Deformations, Najd fault.*

1. Introduction

Some of the most conspicuous Precambrian structures in the Eastern Desert of Egypt are met with in the Migif-Hafafit area. This area is characterized by huge open regional folds trending NW-SE. The WHC has been studied by El Ramly etal. (1984) as part of a collaborative project between the Geological Survey of Egypt and University of Mainz, West Germany. This study was based essentially on the detailed lithological field mapping of this area by El Ramly in the late fifties together with photo-interpretation. The most spectacular antiform is a structural culmination composed of several granitoid-cored gneiss domes. These domes is raced for about 55km from Wadi Shait in the north to Wadi El Gemal in the south. The WHC is bordered in the east by the Hangaliya-Zabara range and in west by the vast plain of gneissic granitoids which are pierced by conspicuous trachyte plugs (e.g. Gabal Hamrt Salma and Gabal El Nuhud). The maximum width of this antiform is 17Km. Hashad (1990) interpreted the granitic gneisses at the core of domes as

gneissic granitic intrusions. They named the rock assemblage above the core granite and below the psammitic gneiss as a metamorphosed and deformed ophiolitic mélange assemblage, whereas the psammitic gneiss as a metamorphosed sedimentary unit of a quartozo-feldspathic composition. Several models have been postulated to explain the WHC four tectonic models were proposed to decipher their origin: (1) development of fault-bend fold "antiformal stacks" (e.g.Hafafit domal structure; Greiling et al.,1988a), (2) orogen-parallel crustal extension (e.g. HaFafit, Sibai and Meatiq domal structures; Wallbrecher et al., 1993; Fritz et al., 1996, 2002; Bregar et al., 2002; Loizenbauer et al., 2001; Abdel Wahed, 2008; Khudeir et al., 2008), (3) emplacement within regional domal structures (Ibrahim and Cosgrove, 2001) followed by extension parallel to their fold axes (e.g. Sibai dome, Fowler et al., 2007), and (4) interpreted the WHC as a result of fold interference patterns involving multiply deformed sheath folds (Fowler and El Kalioubi, 2002). The domal structure (WHC) represents the largest antiformal structures in the Nubian Shield. It is considered as one of spectacular structures in the Eastern Desert, but its structural history has not been entirely clarified. The WHC has been subdivided into five separated gneissic domes (labeled A-E core gneisses; of various aerial extends (El Ramly and Greiling, 1988). El Bahariya and Abd El Wahed (2003) considered the granitoid cores together with the genetically related foliated metagabbro to represent the oldest rocks in the Hafafit area. The tectonic evolution of the WHC has been interpreted as a result of fold interference paterns involving multiply deformed sheath folds (Fowler and El Kalioubi, 2002) or as aconsequence of tectono-magmatic and tectono-metamorphic processes in an active continental margin tectonic setting (El Bahariya and Abd El Wahed, 2003). The P-T conditions for the different mineral assemblages in order to place some constraints on the petrogenesis of the migmatitic rock association as well as the tectonic processes which accompanied metamorphism and orogenesis (El Bahariya, 2008). The structural characteristics of the northern dome (dome A) of WHC, field descriptions of the dome and surrounding are discussed with emphases to their relations with the overlying Pan-African cover nappes and the bounding ductile shear zones and suggested that the emplacement of gneissic core occurred during accretion of the Pan–African nappes, later strike-slip shear zones of Najd Fault System and the associated Subsidiary shear arrays postdate emplacement of the dome (Shalaby, 2010). Our main aim of this study is to examine the finite strain, variation pattern in gneissic granitoids in five domes of WHC to known tectonic evaluation of this culmination.

2. Geological Setting

The present paper deals with the all granitoids that cored domes of the WHC which is bordered by latitudes 24° 35′ 00′′ N and 24° 51′ 00′′ N and longitudes 34° 30′ 00′′ E and 34° 45′ 00′′ E. The WHC has been subdivided into five separated gneissic domes (labeled A-E core gneisses; of various aerial extends (El Ramly and Greiling, 1988) (Fig.1a, b). These domes are composed of medium grade gneisses and are separated from the overlying low grade metamorphic rocks by low angle thrust zones. The rock assemblages in Hafafit area could be grouped into two main units which are separated by Nugrus Thrust. The eastern unit (Nugrus unit) is composed mainly of low grade mica-schists and metavolcanics. This unit is associated with remnants of ophiolitic altered ultramafic and metagabbros.The western unit (Hafafit unit) forms Hafafit domes and includes from core to rim. Granite and gneiss of tonalitic and granodiorite composition, banded amphibolites which is is overthrusted by ultramafic rocks, alternating bands of biotite- and hornblende-gneiss and the psammitic gneiss at the rim of the domal structure. In some parts, the amphibolites are associated with metagabbro (Abd El-Naby and Frisch, 2006). Both units have been intruded by undeformed leucogranites, especially along thrust zones. The present contribution describes the microstructural characteristics of the all from north to south of WHC field descriptions of domes and surrounding with relations of Pan-African and the bounding ductile shear zones. The WHC constitutes an elongated folded belt in Southern Eastern Desert that is about 150 square kilometers, trending NW–SE parallel to the orientation of the Najd fault system. It has evolved and was exhumed in close connection with the activity of this shear zone

system. These granitoids domes are white or greyish white since they consist essentially of oligoclase and quartz with some biotite, hornblende and minor orthoclase. Tonalite prevails in the core of the northernmost dome (dome A), where the peripheral zone is strongly foliated and encloses conformable bands of the foliated metagabbro which several hundreds of meters in length. In places, the tonalite is invaded by numerous, thin pegmatite veinlets giving the erroneous impression of migmatites. The outer rim of this core tonalite is highly injected with white pegmatite veins; it acquires a conspicuous white colour which is accentuated by the weathering and kaolinization of oligoclase. At the northern closure of the dome, highly altered, irregulary-shaped, small masses of rusty brown serpentinite are enclosed in this outer rim, where they are transformed along the peripheries of the intruding pegmatite veins into fibrous anthophyllite (Rasmy, 1974). Stern and Hedge (1985) gave an age of 680 Ma to these tonalites. Whereas the domes B, C and D formed tonalite to granodiorites, the dome E with the conspicuous feature of Naslet Maghar is tonalitic.

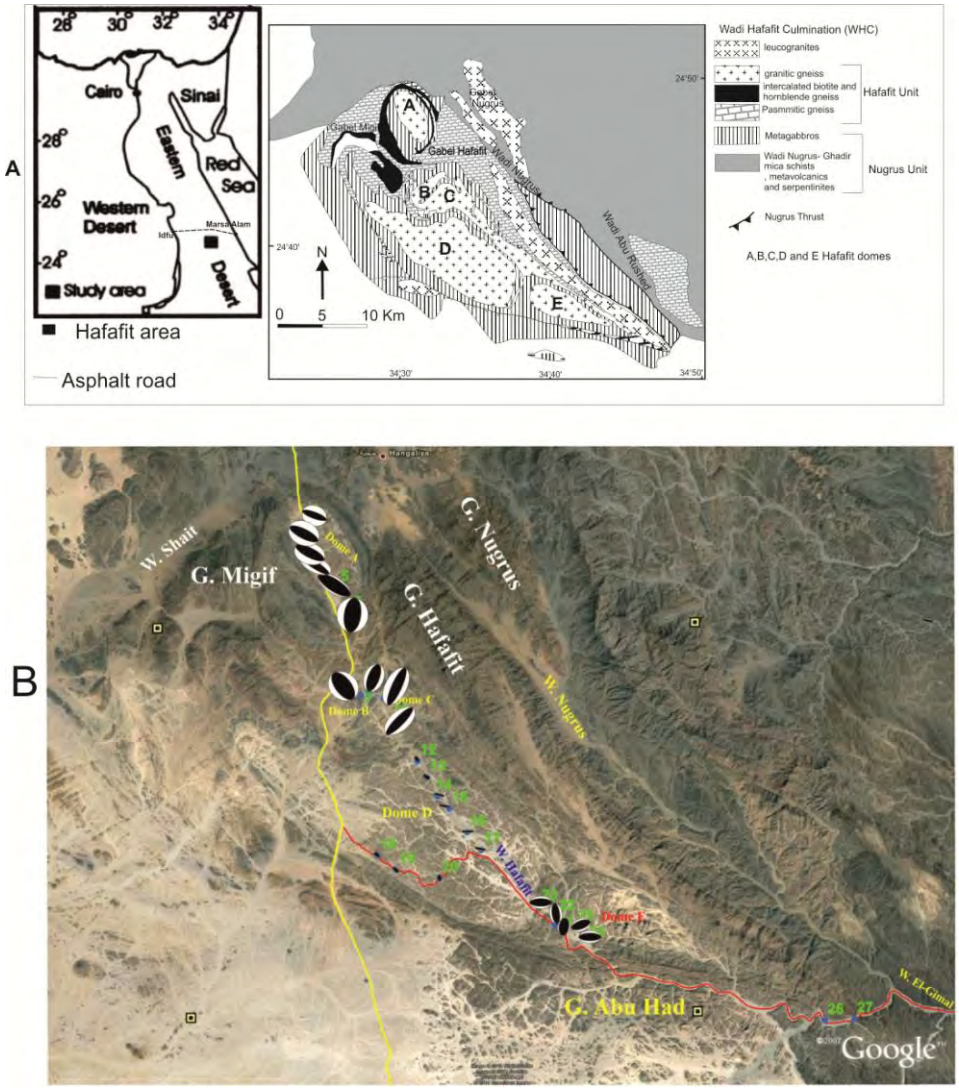

Figure 1 - A- Simplified geological map of Wadi Hafafit area showing major rock types and tectonic structure (modified after El Ramly etal., (1993), B- Photo showing strain ellipsoids in cored granitoids domes of Hafafit.

3. Finite-Strain Analysis

3.1. Field Investigations and Sampling:

24 samples were collected from the Hafafit granitoids domes (for samples localities refer to (Fig. 1b). The Fry and Projection methods used on quartz or feldspar crystal from 6 gneissic tonolite (Dome A), 4 gneissic tonalite and granodiorite (Dome B and C), 9 gneissic tonalite and gneissic granodiorite (Dome D) and 5 gneissic tonalite (Dome E).

Applying the Fry method and projection analysis included: (i) preparation of thin sections along two mutually perpendicular axis (X, Y and Z) subparallel to the XZ and YZ principal planes; (ii) take photographs by polarized microscope; and (iii) employ ‘’fabric 8’’ program for determining the shape and directions of ellipsoid in each deformation.

3.2 Techniques Used in Strain Analysis:

To quantify the finite strain in the Hafafit granitoids domes, feldspars and quartz have been analysed by Fry and Projection techniques (Fry 1979; Ramsay 1967; Ramsay & Huber 1983; Panozzo, 1984). Two-dimensional strain measurements were made on XY, XZ andYZ sections ($X \geq Y \geq Z$, finite strain axes) in order to estimate the three dimensional strain geometry. The Fry strains are thought to represent the matrix strain, for Fry analysis, the central points of more than 70 feldspar or quartz grains per section were used to calculate strain. The strain estimates were used to calculate the finite-strain ellipsoid according to the modified least-square technique of Owens (1984).

At first the three principal strain directions X, Y and Z have to be determined ($X \geq Y \geq Z$; Principal strain axes). For this purpose, the rock sample is cut parallel to lineation, which represents the plane of flattening (XZ) at the maximum extension direction X, which are normal to the foliation and parallel to lineation (XZ). The intermediate strain direction, Y, is defined by its orthogonality with X and Z, which are normal to foliation and lineation (YZ). After having cut the samples in the Rxz and Ryz directions, Rxy direction has been calculated in accord with the following equation:

$Rxy=Rxz/Ryz$

In addition, the stretches Sx, Sy and Sz, which are parallel to principle axes X, Y and Z respectively, enable the following calculation (S) according to (Kassem and Abd El Rahim, 2010).

$Sy= \sqrt[3]{(R_{xz}/R^2_{xy})}$

$Sx=R_{xy} \times Sy$

$Sz=1/(Sx \times Sy)$

3.3 Results of Finite-strain Analysis:

The sample localities for finite strain analysis are shown in Fig. 1 b, the strain data are summarized in tables 1and 2.

3.3.1 Deformation structures:

In microstructural investigations were made on thin section cut parallel to the foliation (XY), normal to the foliation and parallel to the lineation (XZ) and normal to the foliation and lineation (YZ).

The granitoids domes of the Hafafit is very heterogeneously deformed in the field, where feldspar grains and quartz show different microstructural features in same dome of granite in thin section are extremely smeared out with aspect ratios in XZ and YZ section. The development of normal

Table 1 – Direction of finite strain axes and stretches for samples from granitoids domes of Gabel Hafafit.

Domes	Rock types	sample no	long.	lat.	X			Y			Z		
					Trend	Plunge	Stretch	Trend	Plunge	Stretch	Trend	Plunge	Stretch
Dome A	Gneissic Tonalite	1BA	34° 30' 09'' E	24° 49' 13'' N	330	19	1,25	48	43	1,14	310	70	0,70
		2AA	34° 29' 59'' E	24° 48' 33'' N	330	36	1,35	229	15	1,00	120	50	0,74
		3BA	34° 30' 07'' E	24° 48' 18'' N	330	31	1,29	7	70	1,07	300	55	0,72
		3CA	34° 30' 07'' E	24° 48' 18'' N	330	32	1,11	3	69	1,05	302	55	0,86
		4BA	34° 30' 20'' E	24° 47' 50' N	330	46	1,25	281	59	1,02	300	40	0,79
		6AA	34° 37' 05'' E	24° 49' 13'' N	157	35	1,30	160	73	1,21	125	50	0,63
Dome B&C	Gneissic Tonalite &Gneissic granodiorite	7AB	34° 32' 06'' E	24° 44' 12'' N	150	22	1,20	243	7	1,09	350	67	0,77
		8BB	34° 32' 09'' E	24° 44' 06'' N	185	25	1,17	92	6	1,12	350	64	0,76
		9AB	34° 32' 06'' E	24° 43' 54'' N	205	9	1,42	102	51	0,97	290	30	0,72
		10AB	34° 32' 36'' E	24° 43' 45'' N	225	3	1,20	133	35	1,10	320	55	0,76
Dome D	Gneissic Tonalite &Gneissic granodiorite	12BD	34° 33' 42'' E	24° 41' 48'' N	150	47	1,15	246	5	1,10	340	43	0,79
		13BD	34° 34' 01'' E	24° 41' 18'' N	310	41	1,30	340	23	1,08	340	45	0,71
		14BD	34° 34' 22'' E	24° 40' 43'' N	310	51	1,41	320	15	0,95	340	35	0,75
		15BD	34° 34' 45'' E	24° 40' 20'' N	280	21	1,41	16	16	1,01	140	63	0,70
		16BD	34° 35' 21'' E	24° 39' 36'' N	250	0	1,45	160	50	1,12	340	40	0,61
		17BD	34° 35' 49'' E	24° 39' 03'' N	300	42	1,35	50	21	1,16	160	40	0,64
		18BD	34° 36' 30'' E	24° 41' 10' N	310	34	1,12	339	61	1,05	295	55	0,85
		19BD	34° 32' 57'' E	24° 38' 28'' N	310	70	1,22	49	3	1,03	140	20	0,80
		20BD	34° 34' 24'' E	24° 38' 12'' N	10	16	1,14	268	36	1,13	120	50	0,78
Dome E	Gneissic Tonalite	21BE	34° 38' 16'' E	24° 36' 43'' N	325	28	1,44	220	26	1,02	95	50	0,68
		22BE	34° 38' 18'' E	24° 36' 58'' N	350	10	1,35	250	43	1,08	90	45	0,68
		23BE	34° 37' 43'' E	24° 37' 18'' N	10	8	1,17	276	29	0,98	115	60	0,87
		24CE	34° 39' 02'' E	24° 36' 11'' N	250	36	1,23	11	35	1,06	130	35	0,76
		25BE	34° 39' 02'' E	24° 36' 24'' N	310	38	1,43	212	10	1,07	110	50	0,65

Table 2 – Finite strain data for samples from granitoids domes of Gabel Hafafit.

Hafafit domes	Sample no	Method	Rxz	Ryz	Rxy	Stretch			Principal strain ratio
						Sx (X)	Sy (Y)	Sz (Z)	K
Dome A	1BA	Fry	1,79	1,63	1,098	1,253	1,141	0,700	0,156
	1BA	Projection	1,12	1,07	1,047	1,054	1,007	0,942	0,669
	2AA	Fry	1,83	1,35	1,356	1,354	0,999	0,740	1,016
	2AA	Projection	1,22	1,07	1,140	1,116	0,979	0,915	2,007
	3BA	Fry	1,78	1,48	1,203	1,289	1,072	0,724	0,422
	3BA	Projection	1,18	1,15	1,026	1,066	1,039	0,903	0,174
	3CA	Fry	1,29	1,23	1,049	1,106	1,055	0,857	0,212
	3CA	Projection	1,27	1,05	1,210	1,154	0,954	0,909	4,204
	4BA	Fry	1,59	1,29	1,233	1,251	1,015	0,787	0,802
	4BA	Projection	1,21	1,18	1,025	1,075	1,048	0,888	0,141
	6AA	Fry	2,06	1,91	1,079	1,305	1,210	0,633	0,086
	6AA	Projection	1,22	1,08	1,130	1,113	0,985	0,912	1,623
Dome B&C	7AB	Fry	1,57	1,42	1,106	1,202	1,087	0,765	0,251
	7AB	Projection	1,08	1,08	1,000	1,026	1,026	0,950	0,000
	8BB	Fry	1,54	1,48	1,041	1,170	1,125	0,760	0,084
	8BB	Projection	1,37	1,11	1,234	1,191	0,965	0,870	2,133
	9AB	Fry	1,96	1,34	1,463	1,421	0,971	0,725	1,361
	9AB	Projection	1,32	1,08	1,222	1,173	0,960	0,889	2,778
	10AB	Fry	1,58	1,45	1,090	1,199	1,100	0,759	0,199
	10AB	Projection	1,17	1,15	1,017	1,060	1,042	0,906	0,116
Dome D	12BD	Fry	1,45	1,39	1,043	1,148	1,100	0,792	0,111
	12BD	Projection	1,29	1,14	1,132	1,135	1,003	0,879	0,934
	13BD	Fry	1,82	1,51	1,205	1,299	1,078	0,714	0,403
	13BD	Projection	1,22	1,14	1,070	1,093	1,021	0,896	0,502
	14BD	Fry	1,89	1,27	1,488	1,412	0,949	0,747	1,809
	14BD	Projection	1,15	1,13	1,018	1,054	1,036	0,916	0,136
	15BD	Fry	2	1,43	1,399	1,409	1,007	0,704	0,927
	15BD	Projection	1,31	1,29	1,016	1,100	1,083	0,840	0,053
	16BD	Fry	2,37	1,83	1,295	1,453	1,122	0,614	0,356
	16BD	Projection	1,09	1,04	1,048	1,045	0,997	0,959	1,204
	17BD	Fry	2.1	1,8	1,167	1,348	1,156	0,642	0,208
	17BD	Projection	1,32	1,19	1,109	1,136	1,024	0,860	0,575
	18BD	Fry	1,33	1,24	1,073	1,126	1,050	0,846	0,303
	18BD	Projection	1,14	1,13	1,009	1,048	1,039	0,919	0,068
	19BD	Fry	1,53	1,29	1,186	1,220	1,029	0,796	0,637
	19BD	Projection	1,61	1,4	1,150	1,228	1,068	0,763	0,375
	20BD	Fry	1,46	1,45	1,007	1,137	1,129	0,779	0,015
	20BD	Projection	1,28	1,13	1,133	1,132	0,999	0,884	1,021
Dome E	21BE	Fry	2.12	1.5	1,413	1,442	1,020	0,680	0,827
	21BE	Projection	1,14	1,09	1,046	1,060	1,014	0,930	0,511
	22BE	Fry	1,98	1,59	1,245	1,351	1,085	0,682	0,416
	22BE	Projection	1,12	1,07	1,047	1,054	1,007	0,942	0,669
	23BE	Fry	1,34	1,12	1,196	1,170	0,978	0,873	1,639
	23BE	Projection	1,2	1,08	1,111	1,101	0,991	0,917	1,388
	24CE	Fry	1,61	1,39	1,158	1,231	1,063	0,765	0,406
	24CE	Projection	1,27	1,08	1,176	1,143	0,972	0,900	2,202
	25BE	Fry	2,2	1,64	1,341	1,434	1,069	0,652	0,534
	25BE	Projection	1,24	1,07	1,159	1,128	0,974	0,910	2,275

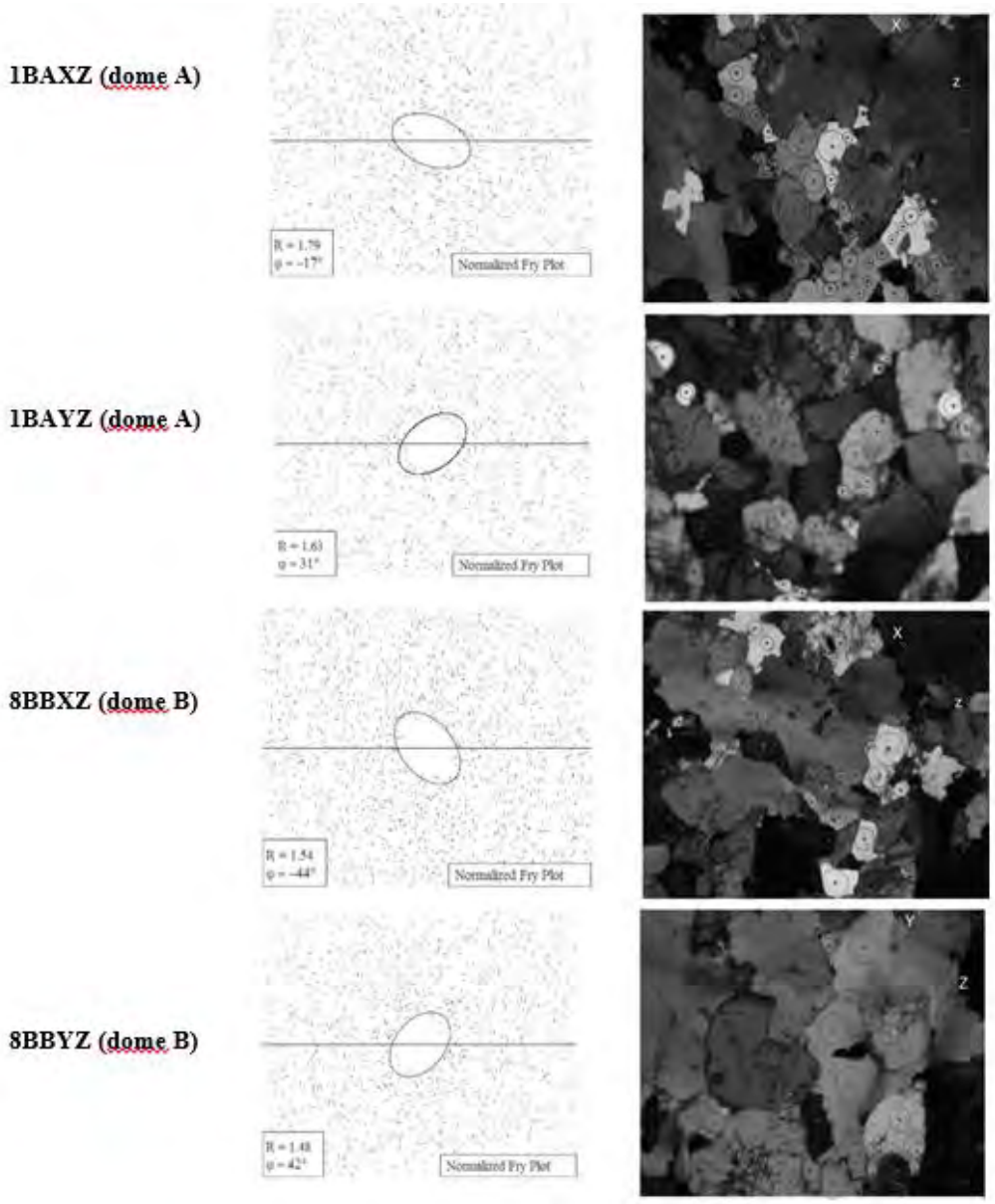

Figure 2 - Fry analysis along XZ and YZ principle finite strain planes and original samples surfaces to which fry applied.

tonalite and granodiorite showing hypidomorphic texture to gneissic tonalite and gneissic granodiorite. In the gneissic granite, the main-phase foliation is a gneissic foliated defined by elongated, dynamically recrystallized feldspar and quartz crystals and alignment of biotite and hornblende (Figs.2, 3).

3.3.2 Magnitudes of Finite Stretches:

The sample localities for finite strain analysis are shown in (Fig. 1 b). The strain data are summarized in tables 1& 2 shown in a Flinn diagram in (Fig.4), the flinn diagram shows the

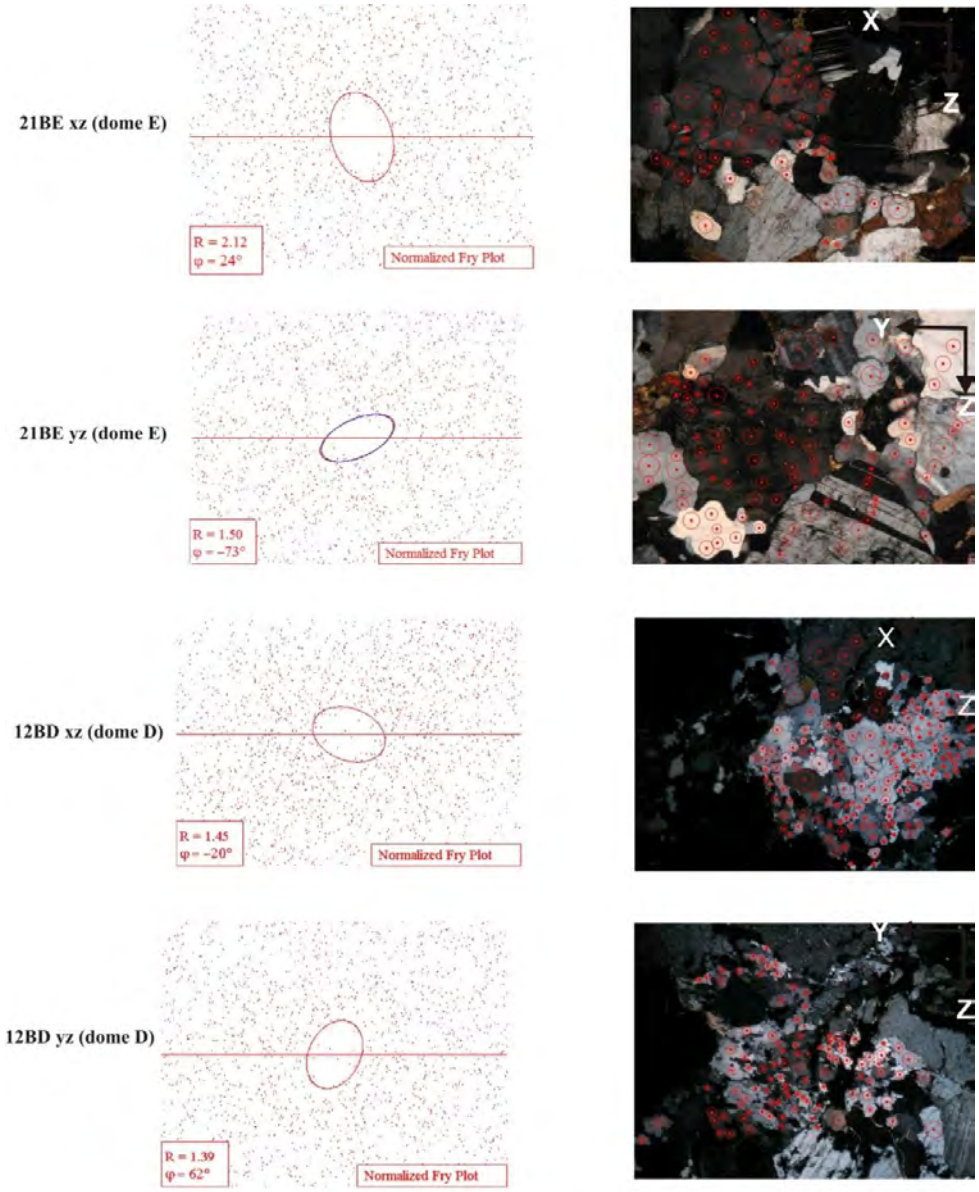

Figure 3 – Fry analysis along XZ and YZ principle finite strain planes and original samples surfaces to which fry applied.

relative shapes of the strain ellipsoids, i.e. prolate vs oblate. To infer strain type, i.e constrictional vs flattening, information on volume strain is needed.

As shown in Table 2, Projection strains are not fundamentally different from Fry strains; in some cases, the Fry strains are slightly greater than the projection strains. Therefore, our studied samples show that there was no significant difference in deformation behavior between the biotite and Hornblende matrix and the feldspar-quartz porphyroclasts during the accumulation of finite strain during deformation conditions. Furthermore, finite strain in the gneissic tonalite in dome A is of the same order of magnitude as those from the gneissic tonalite to granodiorite of domes B&C and the gneissic tonalite dome E which suggests similar deformation behavior in both lithologies but dome D have another deformation behavior about this domes. In general, the strain ellipsoids in

domes A, B,C and E have oblate and prolate strain symmetry but the strain ellipsoids in dome D have oblate symmetry only. In the dome (A) The axial ratios in XZ sections range from 1.12 to 2.06 with Sx ranging from 1.05 to 1.35. The stretches in the Z direction, Sz range from 0.63 to 0.94 indicating vertical shortening. Sy ranges from 0.95 to 1.20 showing both contraction and extension in this direction.

The strain data verify pronounced heterogeneous deformation of the gneissic tonalite as shown in the field. In dome B&C the axial ratios in XZ sections range from 1.08 to 1.96 with Sx ranging from 1.025 to 1.42. The stretches in the Z direction, Sz range from 0.72 to 0.95 indicating vertical shortening. Sy ranges from 0.95 to 1.12 showing both contraction and extension in this direction. The strain data verify pronounced heterogeneous deformation of the gneissic tonalite to granodiorite as shown in the field. In the dome (E) the axial ratios in XZ sections range from 1.12 to 2.20, with Sx ranging from 1.06 to 1.44. The stretches in the Z direction, Sz range from 0.65 to 0.94 indicating vertical shortening. Sy ranges from 0.97 to 1.08 showing both contraction and extension in this direction. The strain data verify pronounced heterogeneous deformation of the gneissic tonalite as shown in the field. In the dome (D)The axial ratios in XZ sections range from 1.09 to 2.37 with Sx ranging from 1.045 to 1.45. The stretches in the Z direction, Sz range from 0.61 to 0.95 indicating vertical shortening. Sy ranges from 0.99 to 1.20 showing extension in this direction. The strain data verify pronounced homogeneous deformation of the gneissic tonalite and gneissic granodiorte. All domes A, Band C and E of Hafafit granitoids showing flattening and constricitional strains but dome D showing only flattening this means found different events of deformation.

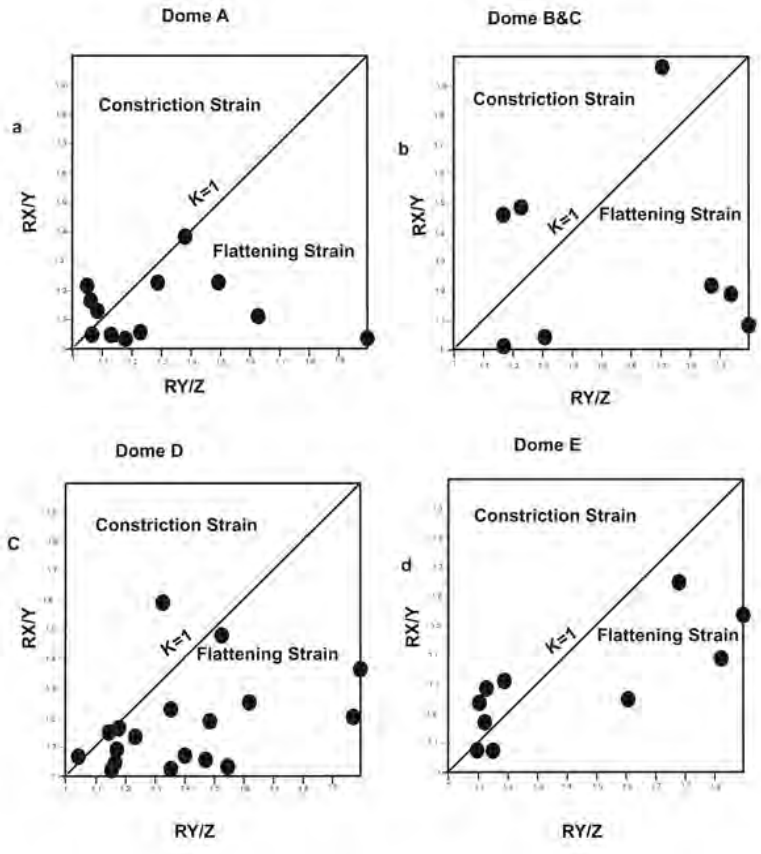

Figure 4 – Flinn diagram showing strain symmetry as obtained by fry and projection methods for Hafafit domes.

5. Discussion

The data show oblate and prolate symmetry (flattening and constriction strains) in gnessic granitoids of domes A, B, C, E but show oblate syemmetry (flattening strain) only in granitoids of dome D this indicates that the time of deformation represents the accumulation of ductile to britle not same time and not same deformation events. This means the granitoids domes of Hafafit are subjected to two different stage of deformation. The early stage of deformation the domes A, B, C, E are affected by more than one deformation event so we observed that the direction of long axis (x) of strain ellipsoid in these gneissic granitoids domes have set W/WSW to N/ENE But granitoids of dome D not affected by this deformation stage. The late stage of deformation all granitoids domes are subjected to general one deformation event so the direction of long axis (x) of strain ellipsoid are common in these domes SE to NW this inductors in cored domes of Hafafit according tectonic evoluation.

Structural observations in WHC show that the culmination is bounded from east and west by two non-parallel left-lateral strike-slip shear zones; namely, Nugrus and El Gemal shear zones, where they intersect south of dome "E" by a pivot and spread away northward, giving rise to the V-geometry for the whole culmination (Fig. 5). Published structural data in WHC (e.g. Greiling et al., 1988b; Fritz et al., 1996; Fowler and El Kalioubi, 2002; El Naby et al., 2008; Fowler and Osman, 2009; Shalaby, 2010) elucidate:

1. Northwestward tectonic transportation on thrust zones with gradual decrease of shortening across the culmination from south to north, which is indicated by stronger buckling in dome "E" at the pivot and weak buckling in dome "A" northward. Fabrics in cross-sections parallel to stretching lineation show evidences of northwestward ductile stretching involved within gneissic bands especially in domes located further north.
2. Opposite to pivot and especially north of zone between domes "A" and "B", ductile normal shears are frequent, dipping mostly shallowly to NW. These extensional fabrics are reactivated into brittle normal faults of regional extend. (e.g. Shait normal fault)
3. The northern area is intensively crossed by roughly E–W trending dykes that rather disappear southward.
4. The dome "B" and "C" is crossed by N–S trending left-lateral strike-slip fault. Displacement on this fault is fading towards zero at dome "D".
5. Late –orogenic extension and crustal thining that controlled by the Najd transform faults that resulted in exhumation of the Hafafit domes through acombination of transpression and lateral extrusion.

6. Conclusions

The strain analysis of the deformation in WHC domes south central Eastern Desert of Egypt indicates that ductile deformation show oblate and prolate symmetry (flattening and constriction strains) in gnessic granitoids of WHC domes A, B, C, E and show oblate syemmetry (flattening strain) only in granitoids of dome D. The oblate symmetry (flattening) on all domes due to late orogenic extension and crustal thining associated the Najd transform fault that resulted exhumation of the WHC domes, The domes A, B, C and E show prolate symmetry (constriction strains for this reasons:

1. Dome A sheared with Shait-Nugrus Shear zone (SNSZ) after post arc collision structure (Fowler and Osman, 2009).
2. Dome B &C shows constriction strain becouse more complex patterns of superimposed interference folds and sheared with Shait-Nugrus Shear zone (SNSZ) (Fowler and El Kalioubi, 2002).
3. Dome E is indicated by stronger buckling in dome "E" at the pivot of two shear zones (Nugrus and El Gemal shear zones).

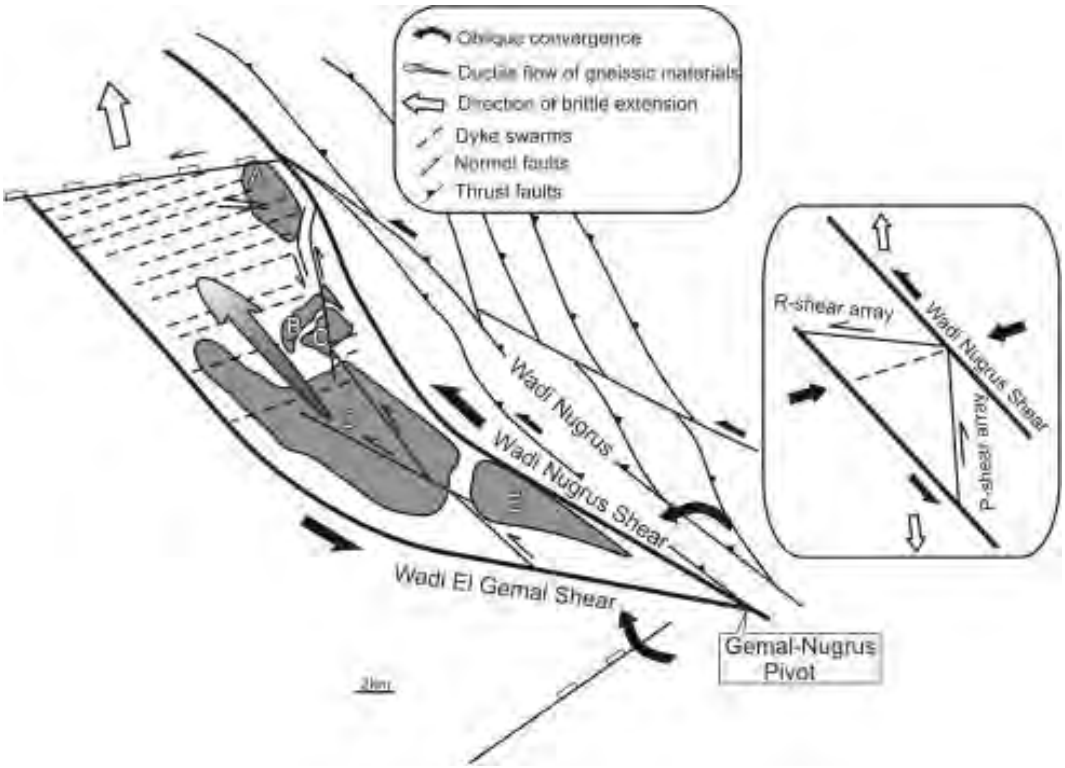

Figure 5 - Simplified structural map for the WHC, collected from landsat images and different literatures (e.g. Greiling et al., 1988b and Fritz et al., 1996; Fowler and El Kalioubi, 2002, Fowler and Osman, 2009 and Shalaby, 2010) The V-geometry for the whole culmination is formed with intersection of two non-parallel left-lateral strike-slip shear zones (Nugrus and El Gemal shear zones) at a pivot, located south of dome "E", while they spread away northward. Stronger domal buckling close to the pivot and weak buckling further north, northwestward ductile stretching in gneissic domes located further north with development of early ductile, later brittle, Sha'it normal faults, the frequent distribution of E–W trending dykes to north and their rather disappear southward, are structural elements that satisfy the synthetic component of the scissor-like deformation model described by Fowler and Osman (2001). In this model, exhumation of Hafafit gneisses is expected to be accomplished by Late –orogenic extension and crustal thining that controlled by the Najd transform faults that resulted in exhumation of the Hafafit domes through a combination of transpression and lateral extrusion.

7. Acknowledgments

Our thanks are due to Greece Scholarships Foundation (IKY) for supporting the doctoral studies in Aristotle University Thessaloniki (Greece) our thanks are also Professor Mohamed Abdel Wahed (Tanta University) for helping me in field work.

8. References

Abd El-Naby H. and Frisch W. 2006. Geochemical constraints from the Hafafit Metamorphic Complex (HMC): evidence of Neoproterozoic back-arc basin development in the central Eastern Desert of Egypt, *Journal of African Earth Science*, 45, 173-186.

Abdel Wahed M. 2008. Thrusting and transpressional shearing in the Pan-African nappe southwest El-Sibai core complex, Central Eastern Desert, Egypt, *Journal of African Earth Science*, 50, 16-36.

Bregar M., Bauernhofer A., Pelz K., Kloetzli U., Fritz H. and Neumayr P. 2002. A late neoproterozoic magmatic core complex in the Eastern Desert of Egypt; emplacement of granitoids in a wrenchtectonic setting, *Precambrian Research*, 118, 59–82.

El Bahariya G. A. and Abd El-Wahed M. A. 2003. Petrology, mineral chemistry and tectonic evolution of the northern part of Wadi Hafafit Area, Eastern Desert, Egypt, *The 3rd international Conference on the Geology of Africa,* Assiut, Egypt, 2, 201-231.

El Bahariya G.A. 2008. Geology and petrology of neoproterozoic syntectonic anatectic migmatites around Wadi abu Higlig, Hafafit region, Eastern Desert, Egypt, *Egyptian Journal of Geology*, 52, 25-54.

El Ramly M.F. and Greiling R. 1988. Wadi Hafafit Area- *1:100.000 Geology map*, Technische Fachhoochschule, Berlin.

El-Ramly M.F., Greiling R., Kröner A. and Rashwan A.A.A. 1984. On the tectonic evolution of the Wadi Hafafit area and environs, Eastern Desert of Egypt, *Bulletin of the Faculty of Science, King Abdulaziz University*, 6,113–126.

El Ramly M.F., Greiling R.O., Rashwan A.A. and Rasmy A.H. 1993. Explanatory note to accompany the geological and structural maps of Wadi Hafafit area, Eastern Desert of Egypt, *Geological Survey of Egypt,* Paper No. 68.

Fowler A. and El Kalioubi B. 2002. The Migif-Hafafit gneissic complex of the Egyptian Eastern Desert: fold interference patterns involving multiply deformed sheathfolds, *Tectonophysics*, 346, 247-275.

Fowler A.R., Khamees H. and Dowidar H. 2007. El Sibai gneissic complex, Central Eastern Desert, Egypt: Folded nappes and syn-kinematic gneissic granitoid sheets—not a core complex, *Journal of African Earth Sciences,* 49(4), 119–135

Fowler T.J. and Osman A.F. 2001. Gneiss-cored interference dome associated with two phases of late Pan-African thrusting in the Central Eastern Desert, Egypt, *Precambnan Research*, 108, 17–43.

Fritz H., Dalmeyer D.R., Wallbrecher E., Loizenbauer J., Hoinkes G., Neumayr P. and Khudeir A.A. 2002. Neoproterozoic tectonothermal evolution of the Central Eastern Desert, Egypt: a slow velocity tectonic process of core complex exhumation, *Journal of African Earth Sciences,* 34, 543–576.

Fritz H., Wallbrecher E., Khudier A.A., Abu El Ela F. and Dallmeyer R.D. 1996. Formation of Neoproterozoic metamorphic core complexes during oblique convegence, Eastern Desert, Egypt, *Journal of African Earth Sciences,* 23, 311–329.

Fry N. 1979. Random point distributions and strain measurement in rocks, *Tectonophysics*, 60, 806–807.

Greiling R.O., Abdeen M.M., Dardir A.A., El Akhal H., El Ramly M.F., Kamal El Din G.M., Osman A.F., Rashwan A.A., Rice A.H. and Sadek M.F. 1994. A structural synthesis of the Proteorozoic Arabian–Nubian Shield in Egypt, *Geologische Runschau,* 83, 484–501.

Greiling R.O., Kröner A., El-Ramly M.F. and Rashwan A.A. 1988. Structural relationships between the southern and central parts of the Eastern Desert of Egypt: details of a fold and thrust belt. In: El-Gaby S, Greiling RO (eds) *The Pan-African belt of NE Africa and Adjacent Areas. Earth Evolution. Sciences,* Vieweg, 121–145.

Habib M. E., Ahmed A.A. and El-Nady O. 1985. Two Orogenies in the Meatiq Area of the central; Eastern Desert, Egypt, *Precambrian Research*, 30, 83-111.

Hassan M.A.and Hashad A.H. 1990. Precambrian of Egypt. In: Said R (ed) *The Geology of Egypt*, Balkema, Rotterdam, 201–248.

Ibrahim S. and Cosgrove J. 2001. Structural and tectonic evolution of the Umm Gheig/El-Shush region, central Eastern Desert of Egypt, *Journal of African Earth Sciences*, 33, 199–209.

Kassem M. K. and Abd El Rahim H. 2010. Finite-strain analysis of metavolcano-sedementry rocks at Gabel El Mayet area, Eastern Desert, Egypt, *Journal of African Earth Sciences*, 58, 321-330.

Khudeir A., Abu El-Rus M., El-Gaby S., El-Nady O. and Bishara W. 2008. Sr–Nd isotopes and geochemistry of the infrastructural rocks in the Meatiq and Hafafit core complexes, Eastern Desert, Egypt: evidence for involvement of pre-Neoproterozoic crust in the growth of Arabia*n, Nubian Shield Island Arc*, 17, 90–108

Owens W. H. 1984. The calculation of a best-fit ellipsoid from elliptical sections on arbitrarily oriented planes, *Journal of Structural Geology*, 6, 571-578.

Panozzo R., 1984. Two dimensional strains from orentation of lines in aplane, *Journal of Structural Geology*, 6, 215-221.

Ramsay J.G. 1967. *Folding and fracturing of rocks,* McGraw-Hill, New York.

Ramsay J.G. and Huber M.I. 1983. *The techniques of modern structural geology*, v. 1, Strain Analysis, Academic, New York, 307.

Rasmy A.H. 1974. Petrological, mineralogical and genetic studies of the Hafafit pegmatites and related mineralization, *Ph.D thesis*, Faculty of Science Ain Shams Univ., Cairo.

Shalaby A. 2010. The northern dome of Wadi Hafafit culmination, Eastern Desert, Egypt. Structural setting in tectonic framework of a scissor-like wrench corridor, *Journal of African Earth Science.*

Stern R.J. and Hedge C.E. 1985. Geochronologic and isotopic constraints on Late Precambrian crustal evolution in the Eastern Desert of Egypt, *American Journal of Sciences*, 28, 97–127.

Wallbrecher E., Fritz H., Khudeir A.A. and Farahat F. 1993. Kinematics of Pan-African thrusting and extension in Egypt. In: Thorweihe U, Schandehneier H (eds) *Geoscientific Research in Northeast Africa*, Balkema, Rotterdam, 27–30.

Δελτίο της Ελληνικής Γεωλογικής Εταιρίας, τομ. XLVII , 2013
Πρακτικά 13ου Διεθνούς Συνεδρίου, Χανιά, Σεπτ. 2013

Bulletin of the Geological Society of Greece, vol. XLVII 2013
Proceedings of the 13th International Congress, Chania, Sept. 2013

GROUNDWATER QUALITY CHARACTERISTICS OF THE ANAVISOS BASIN

Angelakopoulou E.[1], Koumantakis I.[2], Vasileiou E.[2] and Stathopoulos N.[2]

[1]*Msc Agriculturist, Amedaiou Han 1, 11525, Athens, Greece, eva_angelak@yahoo.gr*

[2] *National Technical University of Athens, School of Mining & Metallurgical Engineering, Laboratory of Engineering Geology & Hydrogeology, Heroon Polytechniou 9, 15780, Athens, Greece., koumantakisioannis@gmail.comelvas@metal.ntua.gr, nstath@metal.ntua.gr*

Abstract

The Anavisos basin is located in the southern part of Attica and it is a part of the coastline in the Saronikos Bay. The basin covers an area about 110,91 km^2. The water needs for potable uses of the area are covered by EYDAP and irrigational needs by private drillings and wells. The salinization of the groundwater and the degradation of the water quality had also been observed in the past in the study area. In this research, the most recent chemical analysis showed that the salinity appears extended in the coastal zone as it was in previous decade. The salinization has proceeded into the inland, so the groundwater is characterized as saline and improper for any use in some cases. The main cause for the sea intrusion is the over-pumping exploitation of the coastline aquifers. The rational developments of the area, the lack of a sewerage system, are the main reasons for the degradation of the groundwater in the basin. Additionally there is not a wastewater treatment system in the area, for reusing these waters.
Key words: *Anavisos basin, groundwater, Saronikos, salinization.*

Περίληψη

Η λεκάνη της Αναβύσσου βρίσκεται Νότια του νομού Αττικής και βρέχεται από τον κόλπο Σαρωνικού. Η συνολική έκταση της υπό μελέτης περιοχής είναι 110,91 km^2. Οι υδρευτικές ανάγκες της περιοχής καλύπτονται σήμερα από το δίκτυο της ΕΥΔΑΠ, ενώ οι αρδευτικές από ιδιωτικές γεωτρήσεις και πηγάδια. Στη λεκάνη της Αναβύσσου είχε εντοπισθεί και στο παρελθόν πρόβλημα υφαλμύρωσης του υπόγειου υδροφόρου και ποιοτική υποβάθμιση των υπόγειων νερών. Σε αυτή την εργασία, οι πρόσφατες αναλύσεις έδειξαν ότι το φαινόμενο της υφαλμύρωσης είναι εξίσου έντονο, με την προηγούμενη δεκαετία. Η υφαλμύρωση έχει προχωρήσει σε ένα μέτωπο μεγαλύτερο από την ακτή, προς την ενδοχώρα, έχοντας υποβαθμίσει σε μεγάλο βαθμό την ποιότητα των υπόγειων νερών, περιορίζοντας τις χρήσεις τους ή καθιστώντας τα ακατάλληλα. Προφανής αιτία του προβλήματος, είναι η υπεράντληση των υπόγειων νερών. Για την ποιοτική υποβάθμιση των υπόγειων νερών, ευθύνεται η οικιστική ανάπτυξη, η ανυπαρξία αποχετευτικού δικτύου, η ύπαρξη πολυάριθμων απορροφητικών βόθρων και η έλλειψη μονάδας βιολογικού καθαρισμού των λυμάτων.
Λέξεις κλειδιά: *Λεκάνη Αναβύσσου, Σαρωνικός, υφαλμύρωση υπόγειων υδροφόρων.*

1. Introduction

The Anavisos basin is located in the southern part of Attica, the south and west part of it, is wetted by the Saronikos Bay (Figure 1). The research area includes mostly the part of Saronikos municipality; the main villages in the basin are Anavisos and Palea Fokea. The total area is 110, 91 km^2. The average altitude of the area is about 100 m (Pavlopoulos, 1997). Potable water needs of the area are currently covered by EYDAP and the irrigational ones by private drillings and wells.

The aim of this paper was to investigate the water quality in Anavisos basin, to compare this during the time 2001-2011 and to suggest a rational water management.

In the Anavisos basin, salinization and degradation of the groundwater quality had also been observed in the past. The saline front has moved further into the inland and has degraded significantly the ground's water quality, restricting or prohibiting the use of it.

The increase water demands have been caused by the constant residential development of the area, in combination with the population growth and the intense agricultural activities in the area. The touristic development in the area also influences the rational water management. The main reason for the deterioration of water quality is the intense farming due to the overuse of fertilizers, the unrefined residential wastewater, the dumps, the intrusion of the sea water and the two cemeteries, those of Anavisos and Palea Fokea.

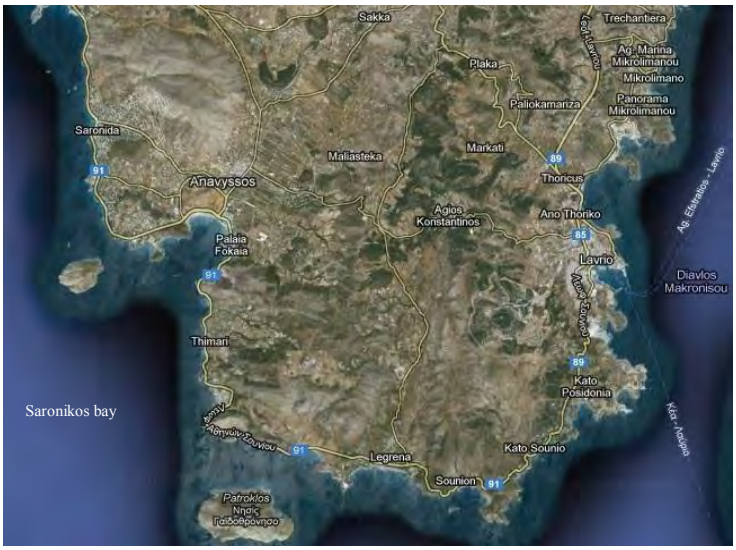

Figure 1 - Geographic position of the studying area (www.googlemap.com).

2. Geology

The southern part of Attica presents a complex of geotectonic structure. The southeastern Attica belongs to the Pelagonian zone. Especially the preneogene formations that are developed in the area are metamorphic and semi-metamorphic formations which are marbles, dolomitic marbles, micas schist and phyllites (Pavlopoulos, 1997)

The main part of the study area is covered by Quaternary deposits. These deposits are mainly recent deposits, older and recent fluvial deposits. Karst marbles are often found in the area, especially in the hills and the mountainous zones. Neogene sediments mainly dominate in the western part of the area. These geological formations are consisted of conglomerates, marls, sandstones, sands and clays. Karstified marbles are located in several parts of the area, especially in the southern part.

3. Hydrogeology

In the study area, are developed high permeable (marbles) permeable (conglomerates), impermeable (schists, ophiolite-very low permeability and clays, marls, lacustrine low permeability) and semi-permeable formations (fine grained and fluvial deposits) (Figure 2).

In the Neogene sediments a significant aquifer system is developed southern of Palea Fokea. This aquifer has hydraulic connection with the karstic formations of Gerakina and Asfakeris and lateral recharge from the marbles of Olympos. The alluvial deposits in the mountain ridge, have small thickness and poor recharge, because of the limited run off. In Quaternary deposits there is also an aquifer system of high capacity, which is consisted of shallow unconfined aquifers and deeper confined ones, mainly in the lowland area. In the carbonate formations of Anavisos is developed a karstic aquifer in the north part of the study area.

The main recharge of the aquifers comes from the infiltration of the precipitation, via the percolation from riverbeds and the surface run off in the impermeable formations. The alluvial deposits are in hydraulic contact by the sea because of this, sea intrusion takes place during the period of overexploitation of the coastal aquifers. The marbles don't have any connection with these sediments. These marbles are isolated from impermeable and semi-permeable rocks, which protect the aquifer from sea intrusion. On the contrary the hill of Asfakeris ends to the sea (Mposinakou, 2002).

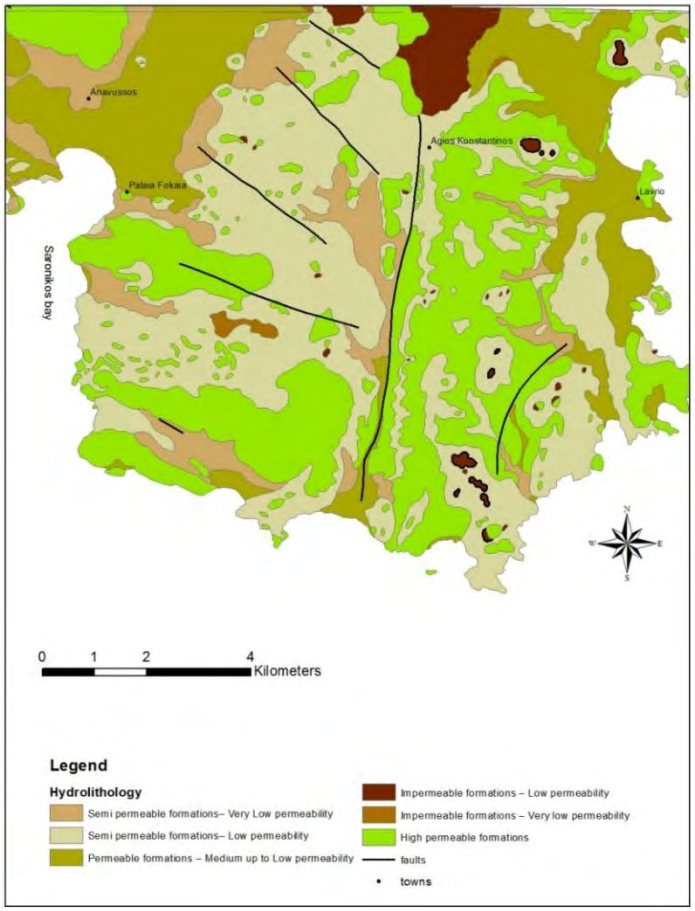

Figure 2 - Hydrogeological map of Anavisos basin.

4. Meteorological Data

The climate of Anavisos basin is Mediterranean, mostly the rainfalls are observed during the cold season, as in the summer there are many drought periods. Meteorological data from the Helenic National Meteorological Service, were evaluated from the three nearest stations in the study area: Elliniko (in the period 1955-2004), Markopoulo (time period 1971-2009) and Spata (time period 1974-2004).

The average annual rainfall was estimated at about 403,9 mm, which is considered as law value. During the period from May to September the average monthly rainfall is lower than 20 mm and as a result there isn't recharge to the aquifers. The average annual temperature is 17,4 ˚ C. The average annual real evapotranspiration was calculated at 305,88 mm (76%) by Thornthwhaite method. Lack of water is observed from April to October, whereas replenishment of soil humidity is taking place in November. Recharge is observed during the period from December until March (figure 3). The diagram of climatic water balance by Thornthwhaite method is described.

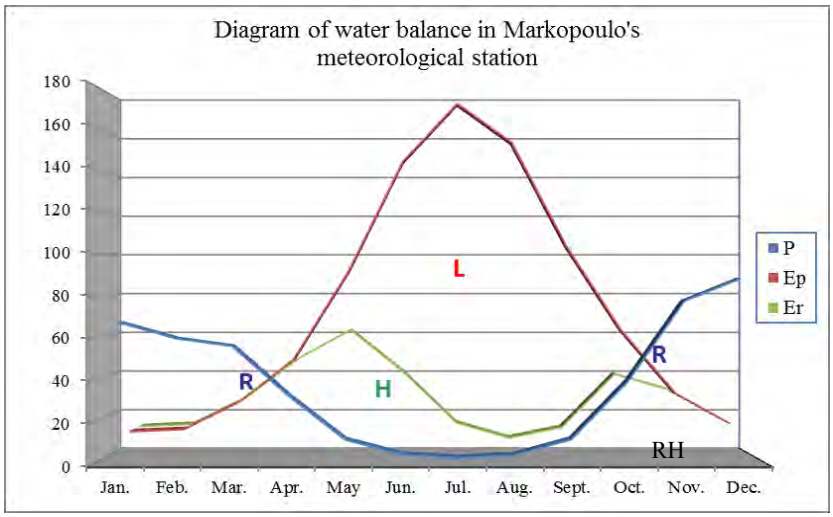

Figure 3 - Water balance in Markopoulo's station according to Thornthwaite, R: Surplus of Water, H: Use of soil humidity, L: Lack of water, RH: Replenishment of soil humidity.

5. Hydrochemistry

Several samplings were taken in two different periods (February-March and August 2011) from seventeen drills and wells of the study area. Physical parameters were measured in situ (pH, EC, Tem, D.O) and the chemical analyses of major anions and cations were done in the Laboratory of Engineering Geology & Hydrogeology, in the School of Mining and Metallurgy Engineering. The results of those measurements from the sampling period of August were compared with the previous sampling from Mposinakou (2001), for the same period. The statistical analysis of them is presented to the Table 1.

High average values of EC, (over 2000 μS/cm), were estimated for both years 2001 and 2011. The high values of EC were measured in a distance of almost 5,4 km from the coastline (Figure 4).The spatial distribution of chloride concentration is similar to the one of the EC. The correlation between these parameters is proved by the following diagram for the measurements of the year 2011 (Figure 5).

High average concentration of Cl (over 300 mg/l) are appeared to a distance about 2,1 km from coastline, for the year 2001 (Bosinakou, 2001). The high concentration of chloride in groundwater must be correlated to the high value of E.C, as a result of the sea intrusion.

Table 1 - Statistical analysis of sampling in the year of 2001 and 2011.

Chemical Elements	2001 (30 samples)			2011(17 samples)		
	Min	Max	Average	Min	Max	Average
EC (μS/cm)	412,00	8410,00	2571,21	334,00	7860,00	2242,48
Cl (mg/l)	19,00	2368,00	497,36	9,00	2221,00	372,47
NO_3 (mg/l)	4,50	208,00	84,47	5,00	118,00	49,64
Na^+ (mg/l)	12,00	860,00	234,89	34,33	650,21	220,37
Ca^{+2} (mg/l)	44,05	403,68	161,65	52,46	220,26	133,64
Mg^{+2} (mg/l)	17,50	332,42	86,09	5,19	228,18	72,83
HCO_3^- (mg/l)	168,36	445,30	345,23	143,68	672,22	417,66
SO_4^{-2} (mg/l)	32,00	440,00	219,60	33,00	450,00	209,65

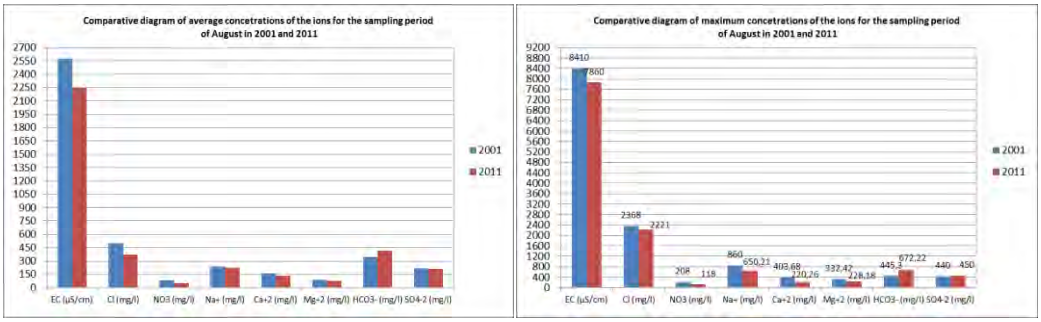

Figure 4 - Statistical diagrams of chemical elements for the years 2001 and 2011.

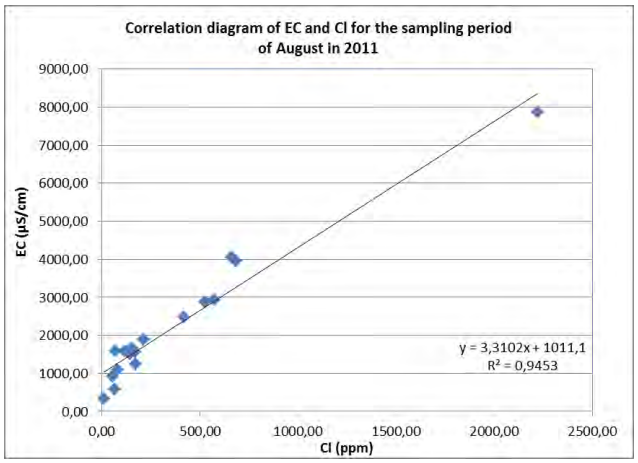

Figure 5 - Correlation diagram of EC and Cl for the time period of August in 2011.

The high concentration of nitrates in the area, is combined with the intense agricultural activity that is occurred in the area, the use of fertilizers and the numerous of non absorbent sinks that exist in the area. Other sources of pollution for nitrate could be considered the two cemeteries, which are located the near the villages of Anavisos and Palea Fokea. Angelakopoulou (2011)

The classification of the water samples, according to the hydrochemical diagrams of Durov, Piper,Wilcox, Schoeller, are mentioned for the year 2011, (Table 2). The hydrochemical diagrams of Piper, Wilcox, Schoeller are presented below (Figure 6).

As it is obvious, from the table 1 and figure 4, the water quality in 2011 is improved compared to the time period of 2001. All the average concentrations of ions and E.C, in 2011 are lower than the ones of 2001. The common time period for both sampling is on August, the low season for the water table, due to the dry summer. During this decade from 2001 up to 2011, the rainfall was increased significantly. In the time period of 1999 until 2001, the rainfall in this basin was very low (247 -346 mm, respectively for each year), on the contrary after the year of 2002, there were ``rich`` recharge from the precipitation to the groundwater, as it was almost doubled (525 mm the average rainfall from 2002 until 2010). This can justify the little change in water quality. In 2001, there was not significant recharge, the extended dry season caused overexploitation of the coastal aquifers and the sea intrusion. In the next years, there was recharge to the aquifers with ``fresh``

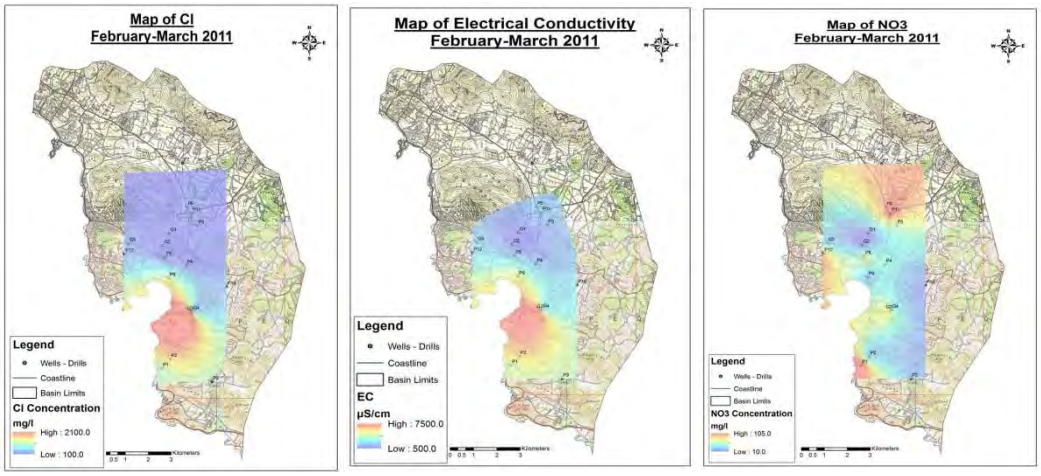

Figure 6 - Distribution Maps of a) E.C. b) Cl^- c) NO_3^- for the period of February-March 2011.

Table 2 - Classification of groundwater according to Durov, Piper, Wilcox, Schoeller diagrams, for the year 2011.

	February-Mars 2011	August 2011
Durov	• 5th field (simple water mixing) for the majority of water samples.	
Piper	• Calcium-magnesium water for the majority of water samples. Calcium-magnesium chloride-sulfate waters dominate and calcium-magnesium carbonate waters follow. • Regarding the cations' concentration: Mixed type water for the majority of water samples. • Regarding the anions' concentration: Mixed type water for the majority of water samples, carbonate waters and chloride waters follow respectively.	
Wilcox	• C3-S1 category for the majority of water samples (moderate water quality, appropriate for the use of irrigation under restrictions). Exceptions: • G1 and G2 water samples, C2-S1 category (good to moderate water quality). • P10 water sample, C4-S1 category (moderate to bad water quality). • P1, P3, P9 water samples, C4-S2&S3 (bad water quality).	• C3-S1 category for the majority of water samples (moderate water quality, appropriate for the use of irrigation under restrictions). Exceptions: • G1 and G2 are moving to C3-S1 category (moderate water quality). • P5 and G4 water samples, C2-S1 category (good to moderate water quality). • P10 water sample, C4-S1 category (moderate to bad water quality). • P3, P8, P9, P10 water samples, C4-S2 (bad water quality).
Schoeller	• Saline water is dominated in the south and in the central part of the basin. • The coastal aquifers of Anavisos and Palea Fokea are also saline • Fresh water in the South and East part of the basin, at the Olympos' mountain. Fresh water in G4 (Palea Fokea), whereas the water from G3 characterized as saline.	

water from the rainfall and it helped a little to decrease the extreme high concentrations, but not at an acceptable level. The sea intrusion is extended in the coastal zone. It is similar the results from the measurements for the wet season (February and March, figure 6). The values of E.C and chloride are very high in the coastal zone, without significant changes to the respective measurements of August.

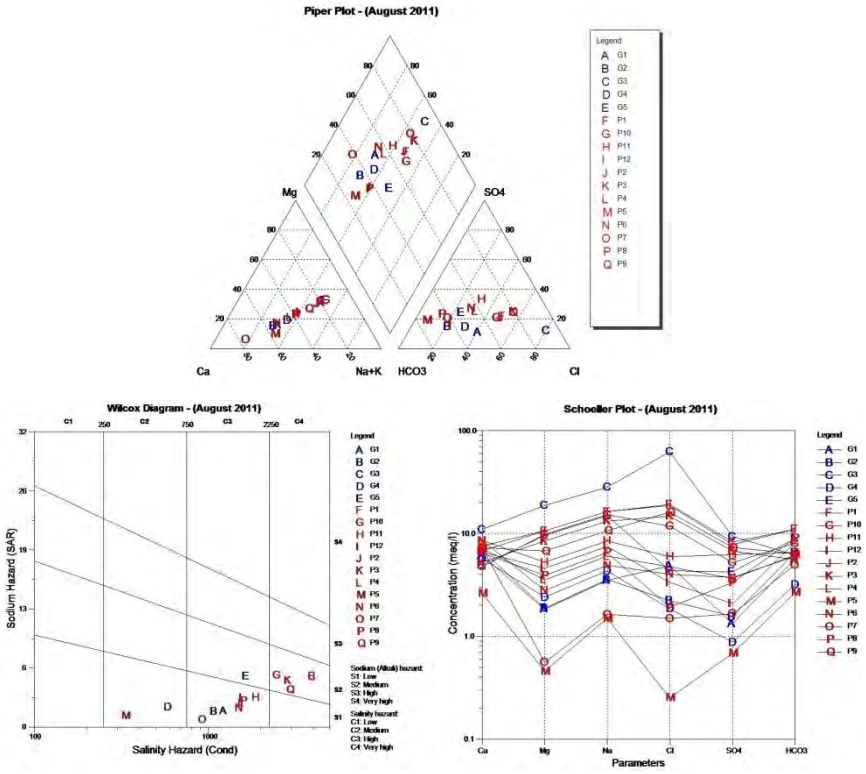

Figure 7 - Hydrochemical diagrams of Piper, Wilcox, Schoeller.

6. Water Economy

Regarding the water quality, none of the samples was proper for potable use, apart from those of G1 and G2 drills in the Olympo's marbles, which are of good quality and the one from G5 as well.

The water samples were also classified according to their use for irrigation. The classification was based on the following factors that indicate irrigation water quality: Salinity, which was estimated by measuring the electrical conductivity, infiltration, which was estimated by measuring Sodium Adsorption Ratio (S.A.R.), and the ions of Cl, Na and HCO_3. According to this classification, two out of seventeen water samples, P5 and P7 (in the central and north part of the basin respectively) are suitable for irrigating the most cultivation. Ten out of seventeen samples are suitable for irrigating resistant cultivations (such as barley, wheat, zucchini, olive, pomegranate, palm, fig, peanut, clover, cucumber, tomato, melon, asparagus). The samples P1, P2, P3 (in the south part of the basin) and P9 (in the Anavisos village) are suitable only for irrigational use in some very resistant to salinity cultivations (such as barley, wheat, zucchini). Finally, one sample, G3 (in the Palea Fokea, village) is completely improper for irrigation. (Misopolinos, 1991; Tsakiris, 2004)

After examining the cultivations of Anavisos and Palea Fokea for 2010, the dominating cultivations are wheat and vineyards, which are mainly not irrigated, diverse vegetables, citrus and nuts, almonds, peanuts which are irrigated and olive trees. A large area is also covered by urban green. Totally, in the Palea Fokea village 2.316.000 m^2 are disposed to agricultural use (including 10.000

m2 of urban green), 431.000 m2 of which are irrigated. In the Anavisos village, 3.625.000 m^2 are disposed to agricultural use (including 35.000 m^2 of urban green), 2.613.000 m2 of which are irrigated. The total irrigation water needs of the area was estimated to be about 1.705.675 m^3, 274.442 m3 for Palea Fokea and 1.431.233 m^3 for Anavisos (Saronikos Municipality, Agricultural Department).

The re-use of the wastewater, after treatment, is being proposed as a solution to the problem of the water resources of the area. The wastewater is proposed to be used for the irrigation needs during the summer and for the artificial recharge of the aquifers, under control. According to a study on a new wastewater treatment in Saronikos municipality, the total annual production of wastewater is expected to be about 2.599.200 m^3. A part of it, 1.705.675 m^3, could be disposed to cover the irrigation needs and the rest 893.525 m^3 to the artificial recharge of the aquifers. Taking into consideration the minimum water necessities per cultivation for Attica water status according to C.Y.A. F 16/6631/89, the total water necessities were estimated for Palea Fokea and Anavisos and are presented in the following Table 3. The minimum water necessities per cultivation were calculated after summing the minimum water needs per cultivation category according to its factor plant, for the months from April to September when irrigation is necessary.

7. Conclusions-Discussion

The area is characterized from the increasing water demands and the overexploitation of the aquifers by over pumping. Due to the fact that the phenomenon of degradation of groundwater quality is extended all over the area, the water is improper for different uses in most of the cases. Additionally, the lack of natural recharge compounded the hydrological conditions, because of the small rainfall in the area. The overexploitation of the coastal aquifers, especially during the drought period, has caused the sea intrusion and thus the salinization of the aquifers even to the inland. During 2011, the phenomenon of salinization seems to be more expanded from the coastline than it is appeared to be during 2001. Moreover, the intense farming and overuse of fertilizers have caused an intense nitrate pollution of groundwater.

Some proposals regarding the rational water management are presented below:

- Restricting over-pumping in order to cover irrigation needs that will help to reduce the salinization in the coastline from Palea Fokea to Anavisos.
- The mountainous aquifers of Olympos, Keratovouni and Merenta should be investigated in order to exploit them, which have available water deposit of good quality.
- A number of constructions could take place in specific areas, such as flood control and anti-corrosion constructions that will also contribute to the artificial recharge of the aquifers and thus will increase the groundwater volume and improve its quality.
- Rehabilitation of dumps and quarries is proposed in order to avoid water pollution.
- Improvement of the sewer system in order to stop leaking ,which pollute groundwater.
- Establishment of a wastewater treatment specified to permit the reuse of wastewater in order to cover irrigation or other needs (except for that of drinkable water).
- The existing of numerous absorbable wells and the lack of wastewater treatment.
- Local governance should focus on sustainable management of local water resources.

The re-use of the wastewater, after treatment, is being proposed as a solution to the problem of the water resources of the area. The wastewater is proposed to be used for the irrigation needs during the summer and for the artificial recharge of the aquifers, under control. According to a study on a new wastewater treatment in Saronikos municipality, the total annual production of wastewater is expected to be about 2.599.200 m^3. A part of it, 1.705.675 m^3, could be disposed to cover the irrigation needs and the rest of it about 893.525 m3, could be used to the artificial recharge of the aquifers.

Table 3 - Cultivations and irrigation water needs of Palea Fokea and Anavisos.

Irrigated cultivations of Palea Fokea Municipality (2010)			
Cultivation	**Minimum Water necessities (m^3/m^2/year)**	**Area (m^2)**	**Water Consumption per year (m^3)**
Tomatoes, beans, zucchini, okra, eggplant, Other Horticulture	0,67	201.000	134067
Peanut trees	0,62	150.000	93150
Almond,	0,62	35.000	21735
Citrus	0,52	35.000	18340
Urban green (mainly grass)	0,72	10.000	7150
SUMMARY			**274.442**
Irrigated cultivations of Anavisos Municipality (2010)			
Vegetables	0,67	8.000	5336
Cauliflower	0,67	2.000	1334
Spinach	0,67	6.000	4002
Leeks	0,67	2.000	1334
Onion	0,67	20.000	13340
Celery	0,67	1.000	667
Radish	0,67	2.000	1334
Peas	0,67	60.000	40020
Beans	0,67	30.000	20010
Lettuce	0,67	10.000	6670
Chicory	0,67	2.000	1334
Tomatoes	0,67	30.000	20010
Green beans	0,67	8.000	5336
Okra	0,67	1.000	667
Zucchini	0,67	5.000	3335
Cucumbers	0,67	2.000	1334
Eggplants	0,67	2.000	1334
Peppers	0,67	3.000	2001
Artichokes	0,67	1.000	667
Olives trees	0,52	1200.000	628800
Peanut trees	0,62	250.000	155250
Citrus trees	0,52	900.000	471600
Pear trees	0,62	33.000	20493
Urban green (mainly grass)	0,72	35.000	25025
SUMMARY			**1.431.233**
TOTAL SUMMARY			**1.705.675**

As a general remark, the re-use of the wastewater would be the solution not only to create new water deposits in the area, but also to improve the quality of water resources. Wastewater can be used for the sustainable management of the area's water resources. Groundwater's over-pumping from drills and wells could be restricted if wastewaters cover the increased irrigation needs during the summer. Also the treated wastewaters could be used for artificial recharge of the aquifers, considering that, they will be of good quality and to continues monitoring.

9. References

Angelakopoulou P. 2011. Water Resources status of the Anavisos basin with emphasis to groundwater, *postgraduate study* DPMS 'Water Resources Science and Technology', National Technical University of Athens, Athens 2011

C.Y.A. F 16/6631/89. Determination of minimum and maximum irrigation water necessities for the sustainable use of irrigation water.

Helenic National Meteorological Service, Meterological data from the stations Elliniko (time period 1955-2004), Markopoulo (time period 1971-2009) and Spata (time period 1974-2004).

Kallergis G. 1986. Applied Hydrogeology, Volume A, T.E.E. Athens 1986

Koumantakis I. etc. 1986. Plain of Anavisos and Palaia Fokaia, *Research Project* in National Technical University of Athens, Athens 1986

Koumantakis I. Groundwater quality, Course Notes 'Advanced Hydrogeology', DPMS 'Water Resources Science and Technology', National Technical University of Athens

Koumantakis I. Saronikos Municipality Water Resources, Course Notes Course Notes 'Advanced Hydrogeology', DPMS 'Water Resources Science and Technology', National Technical University of Athens

Kounis G. 1998. Hydrogeological study of Attica. Athens, IGME

Misopolinos N. 1991. Problematic Soils Study, Prevention, Improvement, Editions Giahoudi – Giapouli, Thesaloniki

Mposinakou P. 2002. Hydrogeological study of the area of the Anavisos basin, *postgraduate study* DPMS 'Water Resources Science and Technology', National Technical University of Athens, Athens 2002

Pavlopoulos K. 1997. GAIA No 2: Geomorphological Evolution of South Attica', E.K.P.A.: Geology Department

Saronikos Municipality, Agricultural Department, Cultivations in Anavisos and Palaia Fokea for the year 2010

Tsakiris G. 2004. Water Resources-Irrigation water quality, postgraduate study DPMS 'Water Resources Science and Technology', National Technical University of Athens, Athens 2011

Δελτίο της Ελληνικής Γεωλογικής Εταιρίας, τομ. XLVII , 2013
Πρακτικά 13ου Διεθνούς Συνεδρίου, Χανιά, Σεπτ. 2013

Bulletin of the Geological Society of Greece, vol. XLVII 2013
Proceedings of the 13th International Congress, Chania, Sept. 2013

DELINEATION OF RECHARGE AREAS OF THE AQUIFER SYSTEMS OF CORINTHIA PREFECTURE BY THE USE OF ISOTOPIC EVIDENCE

Antonakos A.[1] and Nikas K.[2]

[1] *General Secretariat for Civil Protection, Evagelistrias 2, 105 63, Athens, aantonako@yahoo.gr*

[2] *IGME. 1st Spirou Louis St., Olympic Village, 13677 Acharnae. nikas1kostas@gmail.com*

Abstract

The results of a ground water isotopic research program conducted during the period 2004-2008 by an IGME/Hydrogeology Department team in the area of North Korinthian prefecture are presented here. 69 ground water samples were collected during the period 6/2007 and analyzed in the laboratory of Isotope Hydrology of NCSR "Demokritos" for Oxygen isotopes $\delta^{18}O$ and Tritium. From the spatial distribution of $\delta^{18}O$, the conglomerate aquifer systems seem to be recharging from their outcrop areas and possibly laterally from the karstic systems that outcrops in higher altitudes. The rest aquifer systems of the area seem to be recharging exclusively from their outcrop areas with the exception of the Vocha coastal alluvial aquifer which seem to be recharging almost totally from waters coming from higher altitudes. According to the spatial distribution of Tritium in both Sikion–Velo and Vrachati–Lechaio areas, low Tritium values are observed which are indicative of the fact that the aquifer system of those areas are recharged from vertical seepage from the riverbeds of Asopos and Rachiani rivers respectively. Contrariwise in the area of Krines–Zevgolatio the high values of Tritium reveal the lateral recharge from the adjacent marine terraces and marl aquifers.

Key words: *$\delta^{18}O$, Tritium, aquifer, lateral recharge.*

Περίληψη

Στα πλαίσια των εργασιών του έργου "Καταγραφή και αποτίμηση των υδρογεωλογικών χαρακτήρων των υπόγειων νερών και των υδροφόρων συστημάτων της χώρας" που πραγματοποίησε το ΙΓΜΕ/Διεύθυνση Υδρογεωλογίας και με σκοπό την αποσαφήνιση των συνθηκών τροφοδοσίας και εκφόρτισης των υδροφόρων συστημάτων πραγματοποιήθηκε δειγματοληψία και ισοτοπικές αναλύσεις $\delta^{18}O$ και Τριτίου σε 69 υδροσημεία από την ευρύτερη περιοχή του νομού Κορινθίας. Οι αναλύσεις πραγματοποιήθηκαν στο εργαστήριο Ισοτοπικής Υδρολογίας του Ε.Κ.Ε.Φ.Ε «Δημόκριτος». Από την κατανομή του $\delta^{18}O$, προκύπτει ότι τα υδροφόρα συστήματα των κροκαλοπαγών τροφοδοτούνται απευθείας από την περιοχή στην οποία αναπτύσσονται επιφανειακά ή ενδεχομένως και πλευρικά με υπόγειο νερό των καρστικών υδροφόρων που προέρχεται από περιοχές με υψηλότερο υψόμετρο. Τα υπόλοιπα υδροφόρα συστήματα της περιοχής έρευνας φαίνεται να τροφοδοτούνται αποκλειστικά από τις περιοχές στις οποίες οι σχηματισμοί που φιλοξενούν την υδροφορία αναπτύσσονται επιφανειακά, με εξαίρεση τον παράκτιο προσχωματικό υδροφόρο της Βόχας ο οποίος σχεδόν στο σύνολό του φαίνεται να τροφοδοτείτε από νερό που προέρχεται από υψηλότερα υψόμετρα.

Από την κατανομή Τριτίου στο τμήμα Σικυώνος - Βέλου και στο τμήμα Βραχατίου-Λεχαίου σχετικά χαμηλές τιμές Τριτίου παρατηρούνται, γεγονός που φανερώνει ότι ο υδροφόρος στις περιοχές αυτές τροφοδοτείται επαγωγικά από τους ποταμούς Ασωπό και Ράχιανη αντίστοιχα. Αντίθετα στο τμήμα Κρήνες-Ζευγολατιό οι υψηλές τιμές Τριτίου φανερώνουν πλευρική τροφοδοσία από τους παρακείμενους υδροφόρους των θαλάσσιων αναβαθμίδων και των μαργών.
Λέξεις κλειδιά: *$\delta^{18}O$, Τρίτιο, υδροφόρος, πλευρική τροφοδοσία.*

1. Introduction

As part of the project Nº 12 "Study of Water Resources of North Peloponnese Water District, with Emphasis on Quality Characteristics and Seawater Intrusion Phenomena" (Nikas and Antonakos, 2010) which respectively was part of the broader project "Inventory and valuation of the hydrogeologic character of groundwater and aquifer systems in the Hellenic country", funded by the 3rd EU Framework budget and in order to fully assess the hydrochemical conditions and clarify the conditions of the aquifer recharge and discharge, groundwater isotopic analyses were conducted for a series of samples collected from the area of Korinthia prefecture.

2. Geological and Hydrogeological Setting

The study area is located in the northeastern part of Peloponnesus Greece, in the central part of Korinthia prefecture area and it is approximately 902 Km^2 in area (Figure 1). The geological bedrock consists of the carbonate sediments of the Trapezona sequence (a transition zone between Pindos and Pelagonian geotectonic zones) in the southeastern part of the study area and the carbonate sediments and flysch of the Pindos and Tripolis zones in the southwestern part of the study area (Katsikatsos, 1992).

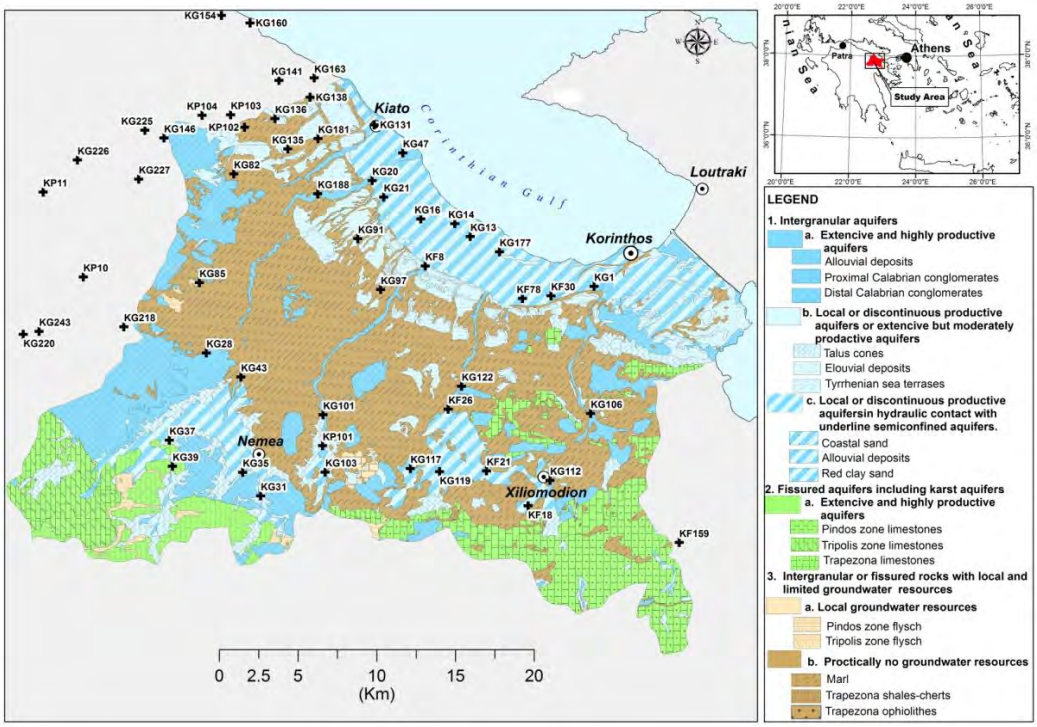

Figure 1 – Hydrogeological map of the study area with the location of the sampling points.

The Trapezona carbonate sequence consists of plated limestones of Triassic to Upper Jurassic age with nodules and thin bands of chert. In Middle Jurassic, this sequence was intermingled and interbedded with the shale-chert formation made up of bedded sandstone, clay and marl with ophiolithic bodies.

The Tripolis zone consists mostly of the dolomitic limestone of the limestone series of Upper Jurassic to Eocene age which is unconformably overlaid by the Tripolis zone flysch formation.

The Pindos zone formation in the study area consists of Upper Cretaceous platy limestones which are unconformably overlaid by the flysch formation. Pindos zone is geotectonically overthrusted on the Tripolis zone with a general NE-SW thrust direction.

The main part of the study area is covered by post orogenic sediments of Pliocene to Holocene age which uncomformably overlay the bedrock formations. They consist of Pliocene lacustrine marls interbedded by thin layers of conglomerates and sandstones, fluvial (proximal and distal) cemented conglomerates of Calabrian age, sea terraces of Tyrinian age, eluvial deposits consisting of alterations of red sand, clay, sandy loam and loose conglomerates of Pleistocene age and finally recent alluvial deposits and talus cones.

From the hydrogeological point of view six major hydrogeological units (aquifers and aquitards) can be distinguished (Antonakos and Lambrakis, 2007) according to the classification proposed by IAH and implemented thereafter in the International Hydrogelogical Map of Europe (Nikas et al., 2010):

- The carbonate aquifers of the bedrock system which are fully karstic for the Trapezona sequence and Tripolis zone and partly karstic for the Pindos zone. They are highly productive aquifers with an average thickness of 100 to 400 m and hydraulic conductivity values ranging from 0.34 to 775.6 m/day (Nikas et al., 2008).
- The flysch formations of Tripolis and Pindos zones and the shale-chert formations of the Trapezona sequence which can be distinguished here as the confining (impermeable) units in the whole aquifer system.
- The Pliocene marl aquifer that develops almost exclusively in the thin beds of sandstones and conglomerates which are found here interbedded within the whole marl formation. It is a confined type of aquifer with an average thickness of 2-10 m and generally low hydraulic conductivity values (0.086 m/day).
- The Calabrian conglomerates aquifer with an average thickness of 50-100 m and high values of hydraulic conductivity (129.6 m/day).
- The aquifer that develops within the eluvial and sea terraces formations, with an average thickness of 30-50 m and medium to high hydraulic conductivity values (1.72 m/day) (Voudouris et al., 2000).
- The aquifer that develops within the recent alluvial and talus cone deposits with an average thickness of 40-60 m and hydraulic conductivity values ranging from 8.64 to 69.12 m/day. This aquifer is, in the most of the cases, in hydraulic contact with the adjacent or underlying aquifer of eluvial and sea terraces formations and is laterally recharged from them.

The impermeable stratum that underlies all the aquifers of the post orogenic sediments is in general the lacustrine marls of the Pliocene marl formation.

The mean annual precipitation in the study area is 594 mm which in quantitative terms corresponds to mean annual rainfall water volume of $536.5*10^6 m^3$. The water balance parameters have been computed based on the procedures described by Thornthwaite and Mather (1955). An amount 67.5% of the annual precipitation, namely $360.9*10^6 m^3$, is lost via the process of evapotranspiration while 19.1%, namely $102.6*10^6 m^3$, infiltrates and recharges the groundwater

system. The rest 13.4%, namely 71.8*10^6 m^3, discharges to the sea as surface runoff (Voudouris et al., 2007).

A major part of the study area, namely 49.9%, is covered with intensive cultivations (vineyards, fruit trees, olive groves) which are widely spread in the whole extent of the study area. The use of inorganic fertilizers in these cultivations has a great polluting effect on groundwater. The composition of these fertilizers is mainly ammonium sulfate and ammonium nitrate so the major expected pollutant in the study area is nitrogen mainly in the form of nitrates. A big part of the coastal zone of the study area is covered by urban and suburban areas which add an extra environmental pressure to the groundwater of the costal alluvial aquifer system.

3. Materials and Methods

3.1. Research Framework

Analyses were performed in the laboratory of Isotope Hydrology of NCSR "Demokritos". More specifically, sampling of groundwater was conducted from 69 sample points during the period 6/2007 and isotopic analyzes were carried out afterwards for the determination of $\delta^{18}O$ and Tritium concentration. The method used for the analysis of stable isotopes was the Isotope Ratio Mass Spectrometry (IRMS). The measurement accuracy was ± 0.22 ‰ for the value of $\delta^{18}O$ and ± 0.51 ‰ for the value of $\delta^{2}H$.

3.2. Isotopic Hydrology Basic Principles

The Isotopic hydrology is a field of hydrology that uses isotopic dating to estimate the age and ori gins of water and of movement within the hydrologic cycle. It evolves the behavioral examination of stable (^{18}O, ^{2}H, ^{13}C) and radioactive (^{14}C, ^{3}H) isotopes, during the water cycle.

More specifically, with Isotope Hydrology the altitude of the recharge area of an aquifer can be det ermined, as well as, the mixing between different types of groundwater, the degree of mixing of su rface and groundwater, the rate of evaporation, the inflow and outflow of surface water systems, th e groundwater salination and the groundwater residence time in aquifers (Matiatos et al., 2010).

As isotopic ratio, R, of an isotope in a water sample, the ratio of the number of atoms of the isotop e in the sample to the total number of atoms of the same element in the sample, is defined:

Equation 1 – Isotopic Ratio

$$R = \frac{\textbf{number of atoms of the isotope}}{\textbf{number of atoms of the element}}$$

As "isotopic fractionation" the modification of an isotopic ratio (e.g., $^{18}O/^{16}O$) during the transition of the molecules of a compound from one phase to another or during the transition of a chemical reaction, **is defined**. When a process does not attain isotopic fractionation, it is said that the isotopes involved in this process are in isotopic equilibrium.

Because the three isotopic species of water have different molecular mass, they exhibit also differences in their physicochemical properties (e.g. lighter molecules of $H_2{}^{16}O$ which can evaporate more easily than the heavier $H_2{}^{18}O$). Thus, during the various stages of the water cycle (evaporation, condensation), a part of the environment is enriched in one isotopic species, while another becomes poorer. There is, therefore, a change in the isotopic ratio and that is called "isotopic fractionation» (Kendall and Caldwell, 1998).

Due to the importance of the behavior of the $^{18}O/^{16}O$ ratio, another example of Oxygen isotopic fractionation within the water cycle is mentioned hereafter. During the evaporation of ocean water, the steam that arises is poorer in heavy isotopes (^{18}O, ^{2}H). When the uplifting steam encounters the cold layers of air it forms a condensate (cloud) which is richer than the original uplifting steam in heavy isotopes. The steam that remains is thus poorer in isotopes than the original. The water

falling as rain is more concentrated, while the remaining steam is further moved towards the interior of continents, where it meets new coldest areas resulting in new compression and further reduction in its content in heavy isotopes.

The decreasing of the content of a steam in heavy isotopes is more intense, as the condensation temperature is less. So rain falling in coastal areas has almost the same isotopic composition as seawater where, in contrast, rainwater falling on the mainland is generally poorer in both heavy isotopes, the rate of difference being increasing as the distance from the sea gets greater. In general, the rainwater that falls on the highlands occurs more depleted in heavy isotopes than the rainwater that falls on coastal plains (Kalergis and Leontiadis, 1983).

In this context, the high precision of the measurements of mass spectrometry allows us to differentiate between rainwater that comes from areas with difference in altitude, within a range of 200 meters.

Isotopic fractionation occurs, as already mentioned also during chemical reactions (e.g. when groundwater reacts with minerals found within the aquifer system).

To quantify the effects of isotopic fractionation, in a reversible chemical reaction or phase change, under equilibrium conditions, in the form A ↔ B, the Isotopic Fractionation Ratio or Fractionation Coefficient α, is introduced:

Equation 2 – Isotopic Ratio

$$a = \frac{R_i}{R_v}$$

Where i: the fluid phase and v: the steam phase

Isotopic Fractionation Ratio α, depends on the temperature and more specifically it increases when the temperature decreases.

The isotopic ratio cannot be measured accurately because changes can happen even during the measuring process. But with the mass spectrometer measurement the difference of the isotopic ratio of a sample from an acknowledged standard measurement can be measured with great accuracy. The most commonly used standard is the SMOW (Standard Mean Ocean Water) for the isotopes ^{18}O and ^{2}H which approximates the average isotopic composition of the ocean water (International Atomic Energy Agency, 1981).

This difference is denoted by the Greek letter δ, is measured in parts per million and is given by the following equation:

$$\delta(‰) = \frac{(R_x - R_{st})}{R_{st}} \cdot 1000$$

Where R_x is the isotopic ratio of the sample and R_{st} is the isotopic ratio of the standard.

If the value of δ is positive (R_x - R_{st}> 1), then the sample is richer than the standard in heavy isotopes. If the value of δ is negative (R_x - R_{st} <1), then the sample is poorer than the standard in heavy isotopes (Kendall et al., 1995).

For example, if we have a water sample with $\delta^{18}O$ = - 5 ‰, we get the information that the sample has 5 ‰ ^{18}O less than the standard.

The main changes in the isotopic composition of natural waters take place in the atmosphere and in surface waters. Water found in soil and subsoil retains the characteristics of meteoric and surface water infiltrating the ground (unless mixed with other waters of different isotopic origin).

The International Atomic Energy Agency (IAEA) has done a lot of research on the field of oxygen and hydrogen isotopes in precipitation, since 1961, and has created 144 research centers, many of which are still operative. These centers include islands, coastal and inland areas. The main conclusions of IAEA studies can be summarized as follows (Leontiadis et al., 1996):

- Meteoric waters are poorer in heavy isotopes than seawater.
- The oceans have stable isotopic composition.
- Concentrations of ^{2}H and ^{18}O in seawater vary proportionally.
- The concentration of heavy isotopes in precipitation decreases as the condensing temperature decreases (temperature effect). This general conclusion leads to a series of different effects on isotopic composition of natural waters:
- Reduction of the isotopic composition in precipitation with increasing latitude and altitude (latitude effect, altitude effect),
- Seasonal variation of the isotopic composition in precipitation (seasonal variation),
- Reduction of the isotopic composition with increasing amount of precipitation (amount effect),
- Reduction of the isotopic composition in precipitation with increasing distance from the ocean (continental effect).
- Intense evaporation affects the proportional relationship between values of $\delta^{2}H$ and $\delta^{18}O$ (kinetic effect).

Tritium (^{3}H) is a radioactive isotope of hydrogen with a half-life of 12.26 years. It is produced in the nature in the upper atmosphere, as a result of the influence of cosmic radiation on nitrogen molecules. The tritium produced in this way reacts with oxygen in the air and forms water, which falls to the earth within the whole rainwater volume. The concentration of rainwater in natural tritium is between 6 and 15 units of tritium (one unit is equivalent to a tritium atom every 1018 hydrogen atoms). The balance between the constant rate of production of natural tritium, constant rate of decay and the various changes in the water cycle in nature was disrupted by thermonuclear tests in the atmosphere. Large quantities of tritium were then passed in the troposphere, from where they still return to the atmosphere (Christodoulou et al., 1993).

Systematic measurements of the tritium content of rainwater started since 1961 in a number of stations established around the world. The tritium concentration in rain water reached about 6000 tritium units (TU) in 1963 and then decreased, but is still at a higher level than it used to be in the period before 1952.

In areas of similar latitude, a satisfactory correspondence in the value of mean concentration of tritium in rainwater is observed. Nevertheless, regardless of the latitude, the various regions may be classified into groups, which are affected only by air masses of the same origin and in which therefore, the tritium isolines are presented parallel. Thus, it is possible and with reasonable accuracy, the reference to the history of tritium for a particular area, being afterwards presented, by correlating that area with another typical area.

When an amount of water is exposed to the ground surface, equilibrium appeared between the rate of atmosphere uptake and the rate of tritium loss: the latter being occurred as a result either to tritium reactions or from other unidentified causes. On the other hand it is obvious that when water isolates itself from the atmosphere, the concentration of tritium found in these waters also decreases, according to the known laws of radioactive isotopes decay. By measuring therefore the amount of reduction, it is possible to calculate the elapsed time since the water was isolated from the atmosphere. Because, and as a consequence of thermonuclear tests, the tritium concentration in rainwater has not been stable in the past 50 years, any age assessment of groundwater requires the

prior knowledge of the values of tritium in rainwater when the actual recharge took place. For the relevant mathematical manipulation, these values constitute the "input function"(Mook, 2005).

Tritium is used for dating groundwater, for relatively recent ages up to a past few decades. For the study of dynamics of groundwater systems, in which water has a mean age of over 500 years, a **^{14}C** isotope which has a half-life of 5730 years is used instead.

In this study we have not proceeded to the exact determination of the average residence time of water in aquifers because of the lack of adequate number of tritium measurements of both groundwater and seasonal rainwater samples. We limited therefore the usage of tritium values found in groundwater samples, for comparisons reasons only, for the purpose that they could reveal the relative residence time of water in different aquifers spatially differentiated among themselves by the different examined points (areas) within the whole study area.

4. Results

The altitude effect of the precipitation on isotopic composition has been determined for the study area, by using data coming from three specific rain gauge stations namely, Thission, Patras, Pendeli of the Global Network of Isotopes in Precipitation (G.N.I.P.). This Network was constructed by the International Atomic Energy Agency (I.A.E.A.) in cooperation with the World Meteorological Organization (W.M.O.). The selection here of these three specific stations (Patras, Thission, Pendeli), out of the whole GNIP network, was based on the fact that they have showed the longest and most complete time series from all the available stations, while at the same time they are located closer to the study area.

Regression analysis between $\delta^{18}O$ values and altitude values for the three stations gave a linear relationship as shown in figure 2. The $\delta^{18}O$ values and altitude values of the groundwater sampling points show the same, descending with altitude relationship, with all groundwater sampling points located beneath the GNIP network regression line, which is interpreted that their mean altitude of recharge is most likely to be higher than the actual altitude at the sampling site.

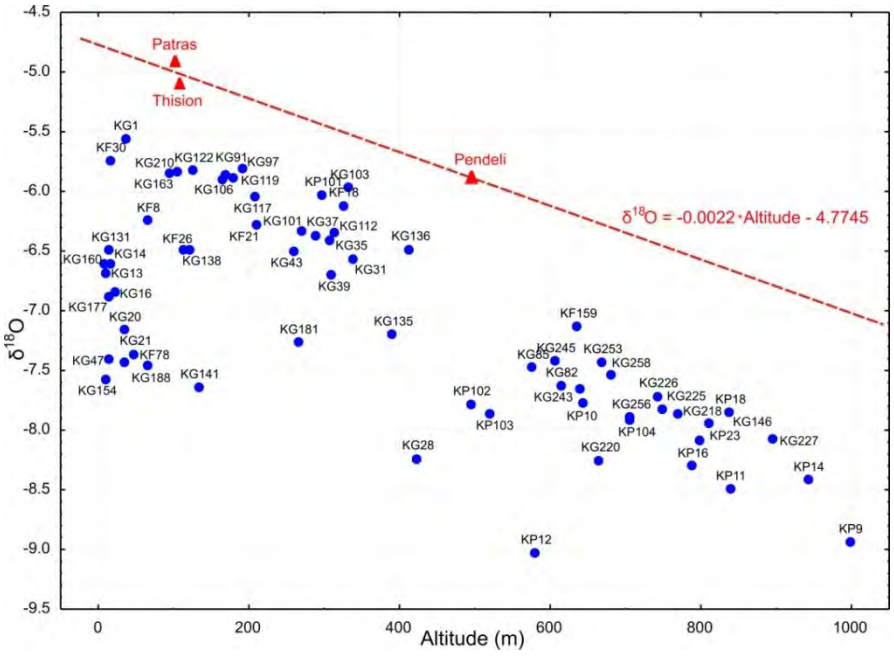

Figure 2 – Diagram of the observed mean $\delta^{18}O$ values in groundwater versus altitude values of the corresponding sampling points.

The points that are very close to the line show that the mean altitude of the recharge area is almost the same with the elevation of sampling. On the contrary, sample points plotted very far from the line illustrate that they are mainly recharged from much higher altitudes than the one of the sampling site.

If we calculate residuals values for the groundwater sampling points, i.e. the difference between measured values of $\delta^{18}O$ and estimated values of $\delta^{18}O$, the latter's being derived from the regression equation shown in figure 2, we can eventually estimate the spatial distribution of residual values by using the spatial interpolation methods. The result of this procedure is shown in the map of Figure 3.

As it can be seen from this map, Vocha coastal alluvial aquifer has high residual values and seems to be recharging entirely by groundwater coming from higher elevations. This water may be transferred into the aquifer in two ways. Either laterally from adjacent aquifers or by induced recharge coming mostly from the rivers and streams that flow through the alluvial aquifer system and their flow constituted mostly by their base flow. In the first case, ground water in the alluvial aquifer should have longer residence times in the aquifer, and hence relatively high tritium values, whereas in the second case ground water should have a short residence time and hence low values of tritium.

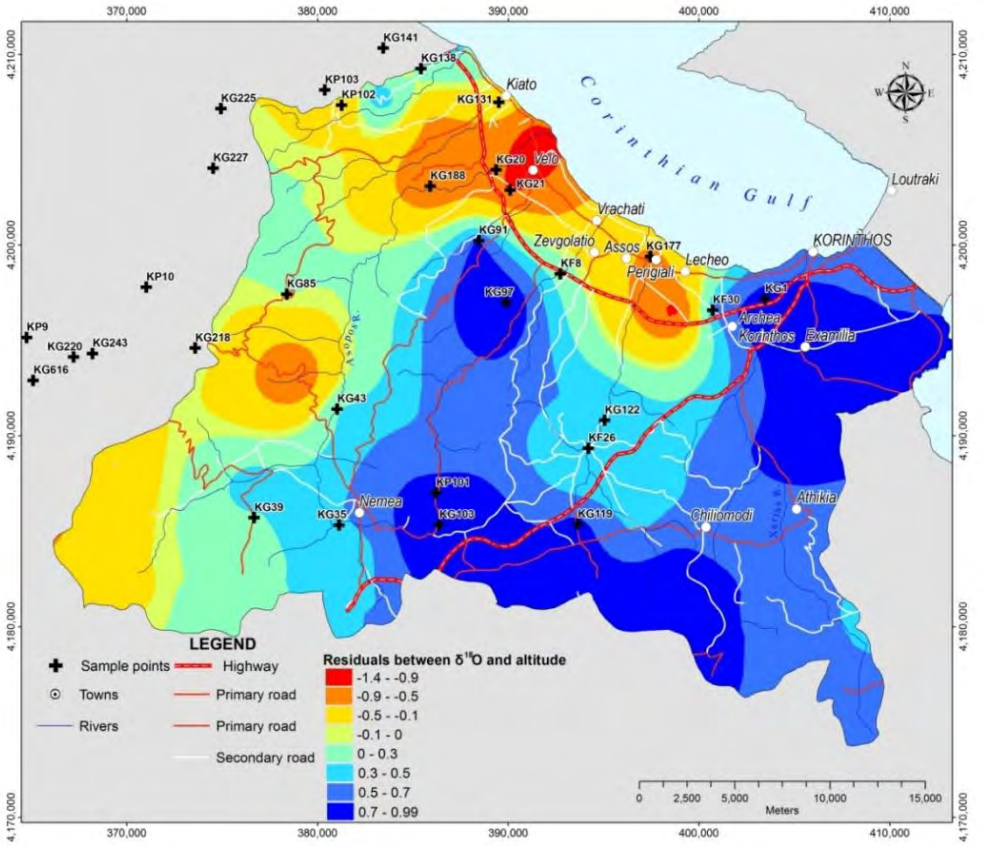

Figure 3 – Residuals between measured and estimated values.

As it can also be seen from the map of Figure 3, the aquifer systems of conglomerates W-NW of Nemea appear to be recharging directly from rainwater falling in the areas where they outcrop or possibly laterally via underground water coming from karst aquifers that outcrop at higher altitudes. The rest of the aquifer systems of the study area appear to be recharging exclusively

from areas where the geological formations within those areas form aquifers that outcrop with the exception of the carbonate karst aquifers in the SW edge of the study area which appear to be recharging from slightly higher altitudes and from the marl aquifers lying SW of Nemea. (Antonakos, 2012).

As shown in the spatial distribution of tritium map in Figure 4, Sikyon - Velo and Vrahati-Lecheo areas have relatively low rates of tritium, indicating that the groundwater in these areas is recharged inductively by Asopos and Rachiani riverbeds respectively. On the contrary the high tritium values in Krines- Zevgolatio area indicate lateral recharge from the adjacent aquifers of the marine terraces and marls formation.

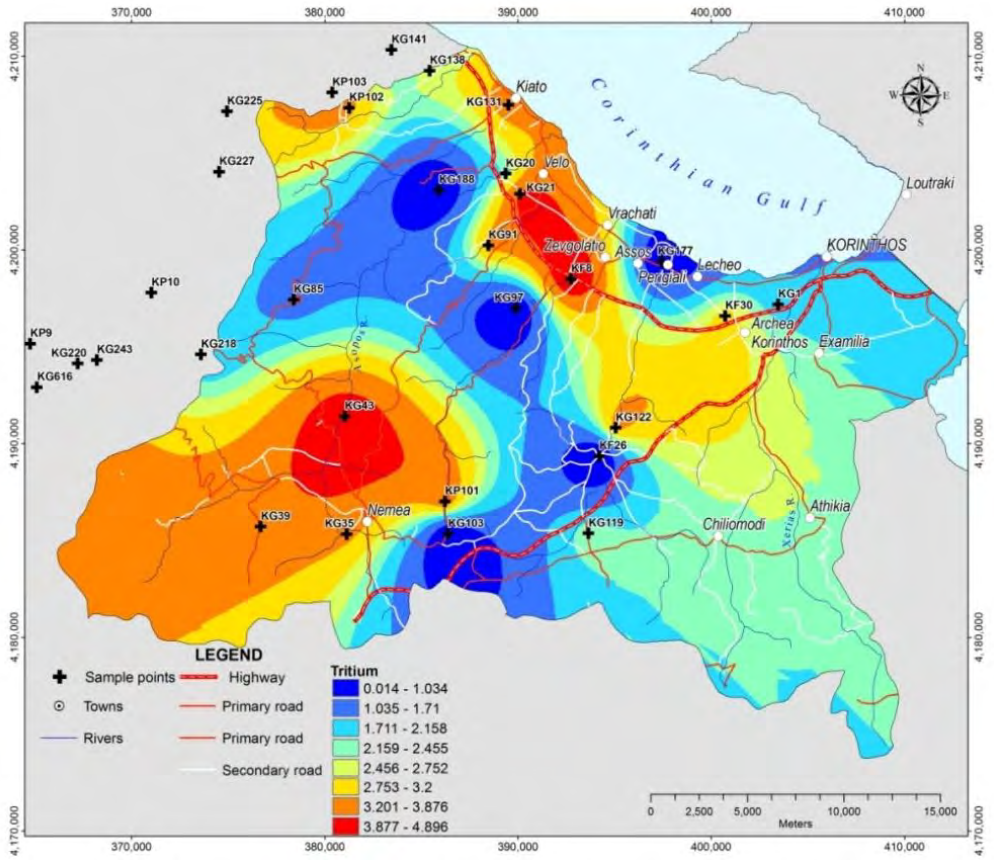

Figure 4 – ^{3}H spatial distribution map of the study area.

High values of tritium are also observed in the granular aquifer system of Nemea and mostly in the Koutsi area, without being noticing the expected otherwise high residual values between measured and estimated values of $\delta^{18}O$. In this case, the low observed residual values indicate that the recharge of groundwater comes exclusively from direct infiltration of meteoric water into the groundwater system; hence the high prices of tritium observed, reflect the problematic recharge and discharge of water, totally resulting in the long residence time of waters within the groundwater system of the local aquifer.

5. Conclusion and Discussion

Isotopic Hydrology can be a valuable tool for the determination of recharge mechanism of aquifers, particularly in areas of complex geological and hydrogeological structure. In the case of the study area by using $\delta^{18}O$ and ^{3}H values in groundwater samples and by studying their spatial distribution

either independently or in comparison, we were able to clarify the recharge mechanism of aquifers and also to determine possible explanations for their groundwater hydrochemical composition.

6. Acknowledgments

The authors wish to express their thanks to Dr. Nikolaos Zouridakis, senior research scientist in the Isotope Hydrology Laboratory of Physical Chemistry of NCSR "Demokritos", for the implementation of the isotopic analyses and for his valuable knowledge on isotopic hydrology issues which was kindly transferred to us.

7. References

Antonakos A. 2012. Use of Geographic Information Systems (G.I.S.) for Environmental Hydrogeology problems in Corinthian Prefecture, *Doctoral Thesis*, Patras University Academic Colection, pp. 307. Available online at: http://hdl.handle.net/10889/5773

Antonakos, A., Lambrakis, N., 2007. Development and testing of three hybrid methods for the assessment of aquifer vulnerability, *Journal of Hydrology*, 333: 288-304.

Christodoulou Th., Leontiadis I.L., Morfis A., Payne B.R. and Tzimourtas S., 1993. Isotope hydrology study of Axios River plain in northern Greece. *J. Hydrol*., 146: 391-404.

International Atomic Energy Agency (IAEA), 1981. Statistical treatment of environmental isotope data in Precipitation. *Tech. Rep*., Ser. No. 206, IAEA, Vienna.

Kallergis G. and Leontiadis I.L., 1983. Isotope hydrology study of Kalamos Attikis and Assopos river plain areas in Greece, *J. Hydrol*., 60: 209-225.

Katsikatsos G. 1992. Geology of Greece. Patras University, O.P.E.B., Pages 451

Kendall C. and Caldwell E. A. 1998. Fundamentals of Isotope Geochemistry, In: C. Kendall and J.J. McDonnell (Eds.), Isotope Tracers in Catchment Hydrology, Elsevier Science, Amsterdam, pp. 51-86.

Leontiadis I.L., Vergis S. and Christodoulou T., 1996. Isotope hydrology study of areas in Eastern Macedonia and Thrace, Northern Greece, *Journal of Hydrology* 182: 1-17

Matiatos I., Alexopoulos A., and Zouridakis N., 2010. Use of stable isotopes in the determination of the mean altitude of recharge and the investigation of function mechanism of spring waters in Argolis peninsula (Greece). Bulletin of the Geological Society of Greece, 2010 Proceedings of the 12th International Congress.

Mouk W.G. 2005. *Introduction to Isotope Hydrology,* London, Taylor and Francis Publications, 223 pp.

Nikas K. and Antonakos A. 2010. Water Resources of North Peloponnese Water District, with Emphasis on Quality Characteristics and Seawater Intrusion Phenomena, IGME study in compliance with the EU 3rd Framework Program. 80 pp, 47 thematic map sheets. 7 separate annexed volumes. IGME Library.

Nikas K., Antonakos A., Kallergis G., and Kounis G. 2010. International Hydrogeological Map of Europe: Sheet D6 "Athina". *Bulletin of the Geological Society of Greece*, 2010, Proceedings of the 12th International Congress Patras. XLIII, No 4: p. 1821-1830

Nikas K., Antonakos A., Maravegias D. 2008. Study of hydraulic parameters of carbonate aquifers of Gavrovo-Tripolis and Olonos-Pindos isopic zones in Peloponnese, *Mineral Wealth*, 147: 7-30

Thornthwaite C.W. and Mather J.R. 1955. The water balance. Thornthwaite Ass. Lab., New Jersey. In: Climatology 8 (1), 1-37.

Voudouris K.S., Mavrommatis Th.P. and Antonakos A., 2007. Hydrologic balance estimation using GIS in Korinthia prefecture, Greece Adv. Sci. Res., 1, 1–8, 2007, Available online at: www.adv-sci-res.net/1/1/2007/

Voudouris K., Panagopoulos, A. and Koumantakis J., 2000. Multivariate statistical analysis in the assessment of hydrochemistry of the northern Korinthia Prefecture alluvial aquifer system, Peloponnese, Greece, *Natural Resources Research*, 9(2), 135–143.

Δελτίο της Ελληνικής Γεωλογικής Εταιρίας, τομ. XLVII , 2013
Πρακτικά 13ου Διεθνούς Συνεδρίου, Χανιά, Σεπτ. 2013

Bulletin of the Geological Society of Greece, vol. XLVII 2013
Proceedings of the 13th International Congress, Chania, Sept. 2013

ENVIRONMENTAL PRESSURES TO THE WATER RESOURCES IN THE WIDER AREA OF RODITSA, IN SPERCHIOS RIVER DELTA OF EASTERN CENTRAL GREECE

Katsifa M.[1], Koumantakis I.[2], Stathopoulos N.[2] and Vasileiou E.[2]

[1] Msc in Water Resources Science and Technology (WRST) NTUA, Civil Engineer N.Chochlia 13 Roditsa, 35100, Lamia, mkatsifa@hotmal.com

[2] National Technical University of Athens, School of Mining Engineering & Metallurgy, Section of Geological Sciences, Laboratory of Engineering Geology & Hydrogeology, Iroon Polytechneiou 9, Athens 15780 koumantakisioannis@gmail.com, nstath@metal.ntua.gr, elvas@metal.ntua.gr

Abstract

The aim of this paper is to describe the ``pressures`` in the water environment, focusing in the water quality regime. The study area is located in the east – southeast of Lamia, southwest of the mountain Orthris, up to Maliakos gulf. The groundwater quality, regarding its irrigative use, ranges between good and moderate. The main sources of water deterioration are agricultural activities and sea intrusion near the coastline. Similar conditions are observed in the surface water of the area. Concerning the qualitative suitability of the water for irrigation, in the majority of the area's surface water samples that were tested, there is a fluctuation between good and moderate. The hydrological data from the karstic springs were evaluated and several estimations were made, for describing their hydrodynamic regime. Certain proposals are suggested for the sustainable management of the water resources, concerning the proper use of the karstic springs and surface water, the reuse of sewage water, the exploitation of groundwater and a number of further actions that should be taken under consideration based on the European legislation
Key words: *karstic springs, salinization, Maliakos gulf, irrigation.*

Περίληψη

Σκοπός της εργασίας αυτής είναι να περιγράψει τις ``πιέσεις`` που ασκούνται στο υδατικό περιβάλλον , με έμφαση στο ποιοτικό καθεστώς. Η περιοχή έρευνας βρίσκεται ανατολικά-νοτιοανατολικά της Λαμίας και εκτείνεται νοτιοδυτικά του όρους Όθρυς, μέχρι το Μαλιακό κόλπο. Η ποιότητα των υπογείων νερών για αρδευτική χρήση, κυμαίνεται από καλή έως μέτρια. Οι κύριες πηγές υποβάθμισης της ποιότητας των νερών, είναι οι αγροτικές δραστηριότητες και η διείσδυση της θάλασσας στην παραλιακή ζώνη. Παρόμοιες συνθήκες παρατηρούνται στα επιφανειακά νερά της περιοχής. Τα ποιοτικά χαρακτηριστικά των επιφανειακών νερών εμφανίζονται από καλά έως μέτρια. Τα υδρολογικά δεδομένα των καρστικών πηγών εκτιμήθηκαν και υπολογίστηκαν προκειμένου να περιγραφεί το υδροδυναμικό καθεστώς των πηγών. Προτείνονται κάποιες λύσεις για αειφόρο διαχείριση των υδατικών πόρων, με σκοπό τη σωστή διαχείριση των καρστικών πηγών, των επιφανειακών νερών, την επαναχρησιμοποίηση των υγρών λυμάτων, την εκμετάλλευση των υπογείων νερών και

μια σειρά πρόσθετων ενεργειών που πρέπει να ληφθούν σύμφωνα με την Ευρωπαϊκή νομοθεσία.

Λέξεις κλειδιά: *καρστικές πηγές, υφαλμύρινση, Μαλιακός κόλπος, άρδευση.*

1. Introduction

The area of interest belongs to the water compartment of Eastern Central Greece and is located on the east – southeast side of Lamia city and southwest of Orthris Mountain. The area is part of Sperchios river delta, whose estuaries end up in Maliakos Gulf. Part of Maliakos Gulf shoreline is the eastern natural limit of the research area. The altitude of the area fluctuates between 0 and 4,5m, with small slopes that do not exceed 3% (Papadimitriou N. 2010).

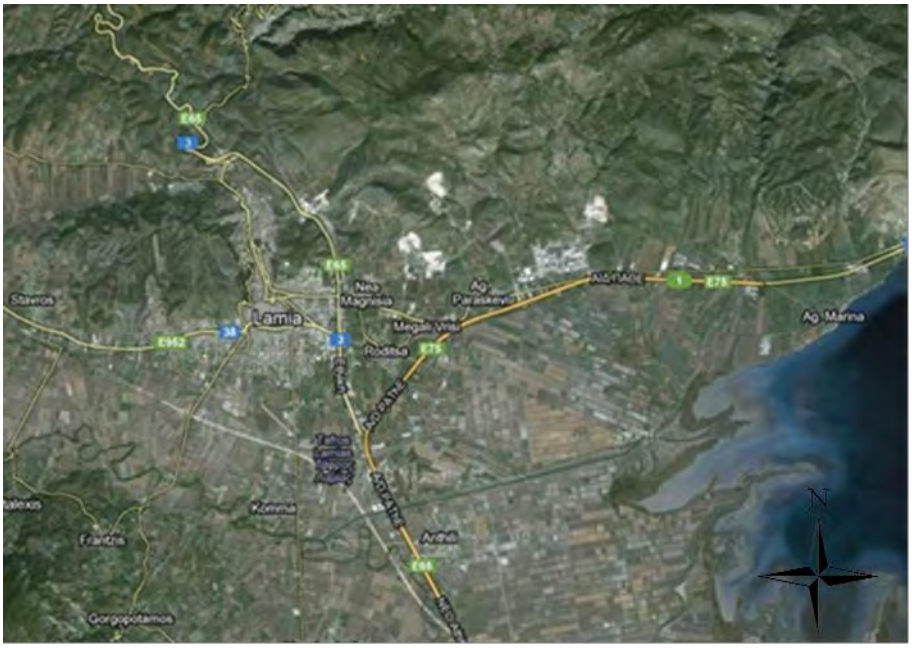

Figure 1 - Location of the study area.

2. Materials and Methods

2.1 Geology-Hydrogeology

Throughout the wider extent of the research area we find alluvial deposits. These geological formations are, either recent deposits coming from the sediment yield of Sperchios River and other local streams, or material coming from the mountainsides of Orthris of the same limestone and schist formations on which it is deposited.

The soil types that are found in the area, are intercalations of clay and clay-silts, with interjecting thin layers of sand, sand-silt and argillaceous sand with gravels. The succession and thickness of the intercalations differs per place.

The area is part of Sperchios river hydrological system and the aquifer system of Lamia. Hydro-lithologically consists of deltaic alluvial deposits of Sperchios River, which consist of alternations of coarse and fine-grained materials. In the northern part of the area, in mountain Orthris frindge, Lamia's Karstic system is deployed.

The composition of the alluvial deposits varies; they have high permeability and consist of unbound materials, pebble and breccia of various size, gravels- and sand that alternate with low permeability materials, such as clay and silts. The deployed aquifer system, due to these alternations, is separated in two individual confined aquifers and one unconfined (M.W.S.C.L., LRI – NAGREF, 2009).

The aquifer system of Lamia consists of karstified Upper-Cretaceous limestone that in its base is in contact with impermeable formations of the schist-crest conformation. This limestone aquifer discharges through Megali Vrusi, Sfageio and Mauromantila springs.

In the lowland part of the research area, due to variations in the granulometric gradation of recent deposits, confined and unconfined aquifers are deployed. The recharge of these aquifers is accomplished through water infiltration by the rivers and streams, through the direct infiltration in the detrital cone and in the coarse deposits of the lowland areas and to some extent by sideway transfusions of the karstic fringe towards the recent deposits of the lowland part.. In the low-level region there is a large number of boreholes and wells that are used mainly for irrigation purposes (Tsoumas V., Zorapas V. 2010).

The hydraulic conductivity and capacity of Lamia's karstic system varies. Specifically, in the area of Ag Paraskeui (where the springs of Megali Vrusi are found), the system is characterized of high capacity; while in the area of Mauromantila is of moderate to insignificant capacity (Dimitressas D. 1999).

In the eastern part, in Sperchios delta and near the shores of Maliakos Gulf, there are clay-silt formations with some layers of sand, which are found in small extent and limited thickness. These aquifers are of low capacity and are not suitable for productive drillings.

In the eastern fringes of Sperchios basin that surround the lowland deltaic area of the river, fanglomerates and detrital cones are deployed, formations with important aquifer dynamics, as well as karstic aquifers of high capacity (Tsoumas V., Zorapas V. 2010).

2.2 Hydrodynamic Conditions

In the area of interest there are many springs and the most important of them is Megali Vrusi spring. The following diagram (Figure 2) presents the monthly fluctuation (average, maximum, minimum) of the recharges of Megali Vrusi springs, for the time period 1961 – 2010.

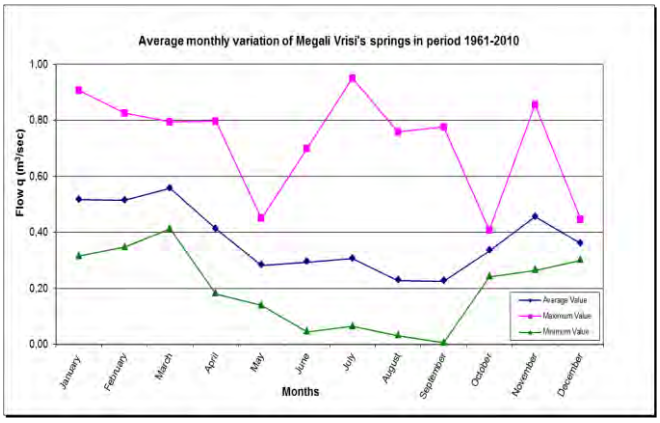

Figure 2 - Average monthly discharge in Megali Vrusi springs.

The irrigative needs of the area are mainly covered by the surficial water of Sperchios River. Due to the increased needs during the summer months, the irrigation of the crops, at the land-redistribution zone of Roditsa, is carried out also with the exploitation of groundwater, through the six public drillings, but mainly through private drillings (at least 35 private drillings).

3. Water Quality of Research area

For the research of the water quality status in the area, adequate sampling took place in selected points, simultaneously with the beginning of the irrigation period (4 – 5/7/2011), both from the surficial recipients (Sperchios diversion, German moat, Ksirias, Megali Vrusi springs) and groundwater through the drillings.

Table 1 - Chemical analysis of Groundwater.

ID	Station ID	Physical features - parameters				Main Cations (mg/l)				Main Anions (mg/l)			
		T (°C)	PH	E.C. (μS/cm)	TDS (mg/l)	Ca^{++}	Mg^{++}	Na^{++}	K^{++}	HCO_3^-	Cl^-	SO_4^-	NO_3^-
G2	Mavromadila	19,7	7,2	624	406	98	3	19	2	289	30	7	25,1
G3	Agia Paraskevi	18,4	7,4	582	378	90	24	14	1	307	25	23	62,7
G4	Stergiopoulou	18,4	7,8	1492	970	128	32	159	32	199	351	54	31,6
G5	Xatzikosta	18,3	8	294	191	34	2	15	1	167	21	15	13,9
G6	Tsaina	18,4	8,1	442	287	17	1	38	2	231	54	24	38,8
G7	Ftelies	18,1	8	358	233	65	1	8	1	268	10	7	1
G8	Zardas a	18,1	8	711	462	28	6	6	1	423	7	1	3,2
G9	Stathopoulos	18,9	8,1	491	319	26	1	6	1	356	8	2	9,2
G10	Kontos a	18,7	7,9	429	279	44	11	5	1	277	5	3	15
G11	Kontos b	18,5	7,7	511	332	84	12	18	2	212	29	25	63,1
G12	Agios Panteleimon	18	7,6	604	393	113	15	17	1	312	23	23	48,6
G13	Zardas b	18,2	7,4	882	573	145	39	21	2	451	34	42	74,3

Table 2 - Chemical analysis of Surface water.

ID	Station ID	Physical features - parameters				Main Cations (mg/l)				Main Anions (mg/l)			
		T (°C)	PH	E.C. (μS/cm)	TDS (mg/l)	Ca^{++}	Mg^{++}	Na^{++}	K^{++}	HCO_3^-	Cl^-	SO_4^-	NO_3^-
Th1	Before dam	20,4	7,7	487	317	83	17	21	4	275	13	39	8,4
Th2	Cross Spercheos - canal T1	21,1	8	485	315	83	15	20	4	265	11	38	13,2
Th3	German Trench before Ksirias riverbed	21,2	7,7	981	638	96	65	26	5	540	25	69	26,1
Th4	Ksirias riverbed before German Trench	23,2	8,1	372	242	47	19	21	4	218	14	23	13,7
Th5	Soil trench before the canal leading to Roditsa	20	8	470	306	83	15	23	4	271	17	42	16,8
Th6	German Trench before Biological Treatment	21,4	8	596	387	64	39	24	5	345	19	33	6,6
Th7	Springs of Megali Vrisi	18,4	7,3	567	369	91	14	24	5	287	21	11	38,5
Th8	Pumping - station	23,7	7,6	4700	3055	103	106	517	168	331	1224	200	6,9
Th9	New riverbed - exit to Maliakos Gulf	23,4	7,9	1864	1212	86	48	177	55	276	393	95	7,8
Th10	German trench after Biological treatment	25,1	7,8	882	573	74	24	34	8	433	44	37	6,2
Th11	New riverbed - before German trench	21,1	7,8	527	343	80	16	21	4	264	12	39	6,5

Table 3: Water type of each sample.

ID (Groundwater)	Station ID	HYDROCHEMICAL TYPE
G2	Mavromadila	Ca-HCO_3
G3	Agia Paraskevi	Ca-Mg-HCO_3
G4	Stergiopoulou	Na-Ca-Cl-HCO_3
G5	Xatzikosta	Ca-Na-HCO_3
G6	Tsaina	Na-HCO_3-Cl
G7	Ftelies	Ca-HCO_3
G8	Zardas a	Ca-HCO_3
G9	Stathopoulos	Ca-HCO_3
G10	Kontos a	Ca-Mg-HCO_3
G11	Kontos b	Ca-HCO_3
G12	Agios Panteleimon	Ca-HCO_3
G13	Zardas b	Ca-Mg-HCO_3

3.1 Groundwater Quality

In Table 1 concerning groundwater, the water type HCO_3 that appears in all the samples is clearly noticed and it could be attributed to the mineralogical composition of the various geological formations, through which the groundwater flows. These can be karstic formations (e.g. limestone), marl formations, or in general formations with many carbonic compounds, like for example the alluvial deposits.

In addition, the following lab results that came of the chemical analysis of the samples are worth mentioning:

- In the drilling G4, high concentrations of Cl (35 mg/l) and Na (159 mg/l) were measured, fact that implies salinization (Figure 3).The high concentrations of Cl^- is due to the sea intrusion. There are not samples near the coastline; the blue dashed line is the actual limit of the measurements. The eastern part of this limit is a ``false`` picture of the Kriging method used by the Surfer software.
- In the drilling G3, high values of anions, HCO_3, Cl, SO_4 and NO_3 (62,7 mg/l) were measured. The increased values of Cl, SO_4, HCO_3, are probably due to wring leakage from the sanitary landfill waste area or/and from the cemetery, that neighbours with the drilling (the cemetery 50 m west and Lamia's waste disposal area 2,5 km northwest of the drilling). The geological background of the area favours this possible hydraulic communication. The increased values of NO_3 have as possible sources the wrings of the neighbouring cemetery, the fertilizers or/and the livestock wastes of the area.

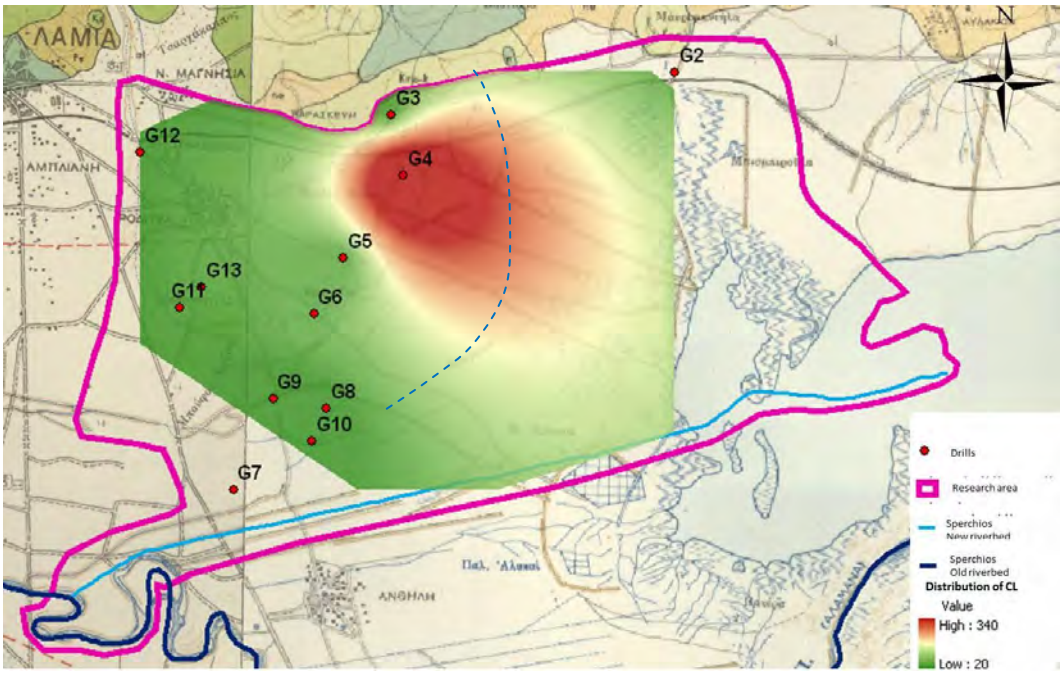

Figure 3 - Distribution map of Cl^- in groundwater.

- The increased values of NO_3 that were measured in G2, as well as in the private drillings G11 and G13, which cover the irrigation needs in cultivations south of the settlement, are due to the use of fertilizers (Figure 4). Noteworthy is the combinatorial irrigation – fertilization system, in which the fertilizer is put in "tanks", which are connected to the drilling and through the water flow is led to the cultivations.

The water quality for ten of the drillings is placed, according to SAR index, in the category C2-S1 therefore characterized as of good up to moderate quality (Table 4 - according to Wilcox diagram).The drillings G4 and G13 belong to the category C3-S1, moderate up to very moderate quality (the water can be used under specific conditions).

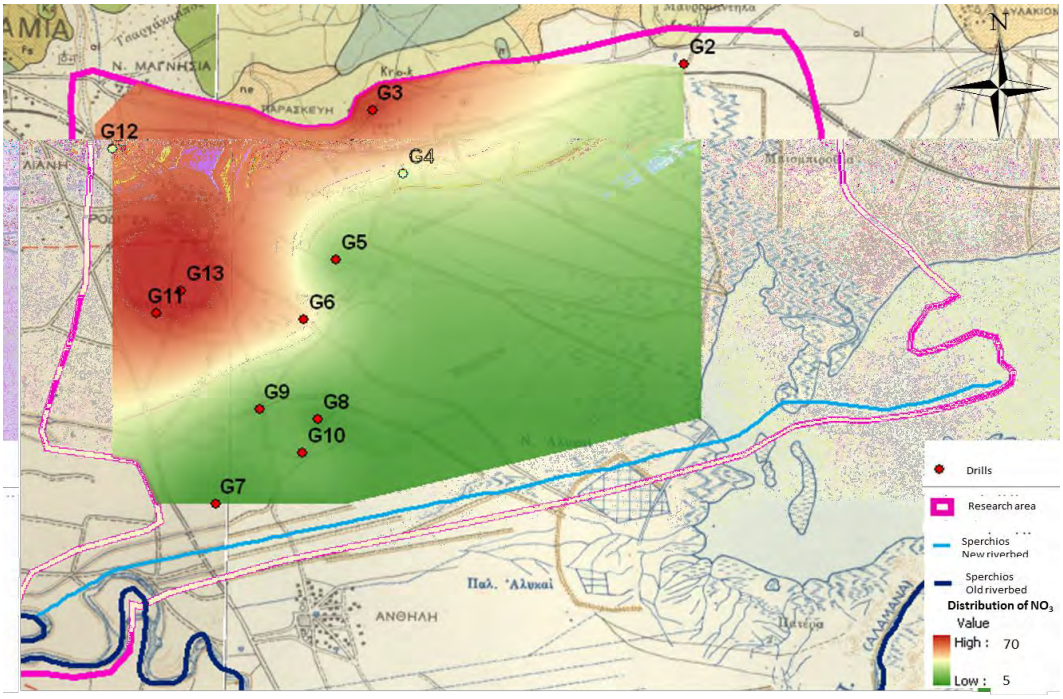

Figure 4 - Distribution map of NO_3^- in groundwater.

3.2 Surface Water Quality

The results from the chemical analyses of surface water are shown in Table 2. In Sperchios old riverbed, the sampling points were Th1, Th2 and Th5.

The samples Th3, Th6, Th10 refer to specific points along the Lamia – German moat. The sampling point Th3 is placed before the moat's junction with Ksirias stream, Th6 east of the national road, before the junction with the Unit of Biological Treatment and finally Th10 in the end of the moat just before its estuary to Sperchios new riverbed – diversion. Sample Th3 has higher concentrations of TDS, Ca, Mg, HCO_3, SO_4 and NO_3 ions, in comparison with the other two samples.

It would be useful to mention that the German moat is a recipient of smaller streams, before Ksirias stream, of the drainage networks of the arable areas such as Komma and Amouri, as well as of these settlement's sewage due to lack of a proper sewage network. The wastes of a local industry also end up in the moat.

The increased value of Cl ions, in sampling point Th10 in the end of the German moat, just before the junction with Sperchios new riverbed, must also be noted. The sample Th4 was taken from Ksirias stream, before the junction with Lamia – German moat.

The water of Ksirias stream does not burden the moat's water, as its chemical characteristics are of better quality compared with the ones it meets. This fact is confirmed and by the in situ observations of the natural characteristics of the samples Th3 and Th4 during the sampling. The

sample Th3 showed increased turbidity, high viscosity, intense stench and green colour. On the contrary the main characteristic of sample Th4 was the increased turbidity.

The increased values of TDS (>1000 mg/l – saline or brackish water), as well as of the ions Na (Figure 5) and Cl, are data showing salinization (Figure 6), fact that is attributed to intrusion of the sea front inwards the estuaries of Sperchios new riverbed. Comparing the two sampling points Th10 and Th11, it is noticed that the German moat's water that ends up to the new riverbed – diversion (Th10) has increased values of TDS as well as of ions HCO3 and Cl, relatively with the sample of Sperchios new riverbed (Th11).

Sample Th8 was taken by the moat that gathers the pumping station's water and directs it to the sea. All waters of the drainage network of the area's cultivations end up in there. The chemical analysis shows particularly increased values of TDS (the highest measured value among all the surficial samples taken), as well as in all ions except NO_3. Noteworthy are also the high values of Cl and SO_4. It is relatively safe to attribute these high concentrations in the effect of seawater, as the sampling point has a distance of about 1 km from the sea. Sample Th7 was taken from the karstic springs of Megali Vrusi.

The water from the springs presented the highest measured value of NO_3 among all the surficial samples. The increased concentration of NO_3, is probably due to the neighbouring cemetery, as well as to the sanitary landfill waste site located north of Megali Vrusi springs, in the area of Agia Paraskevi.

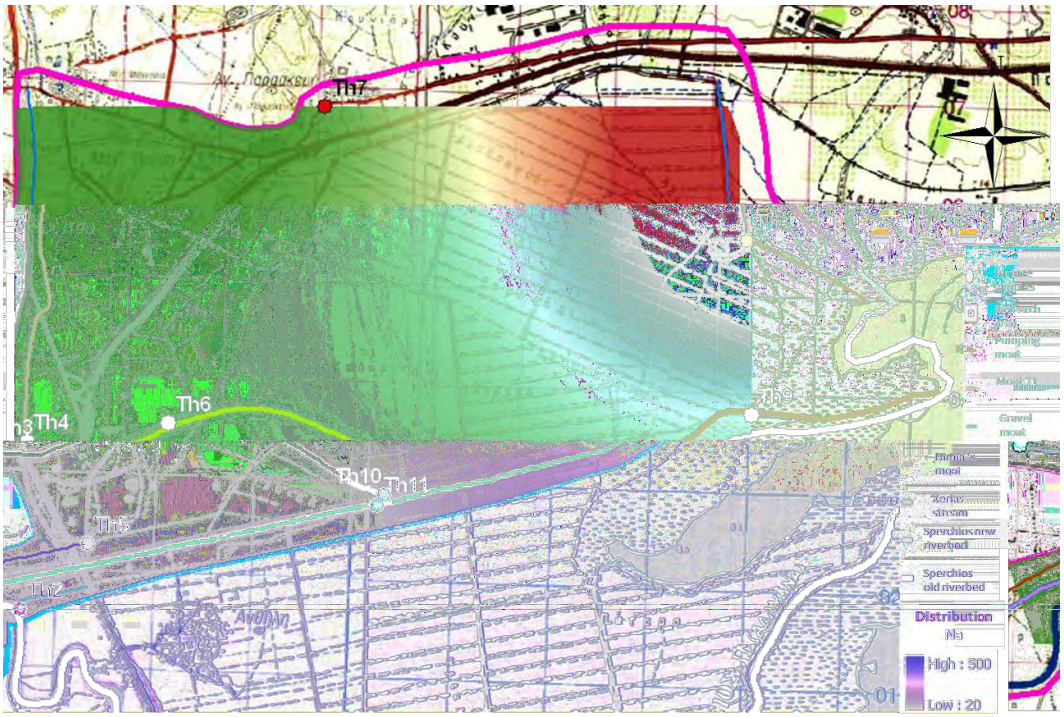

Figure 5 - Distribution of Na in surface waters.

According to Table 4 and the categories of irrigative water, it is observed that the surficial water of seven samples belongs to the category C2-S1, meaning that their quality is from good up to moderate. Samples Th3, Th9, Th10, belong to the category C3-S1, meaning that their quality is from moderate to very moderate. Finally sample Th8 is of very bad quality (category C4-S3) and should not be used in any case.

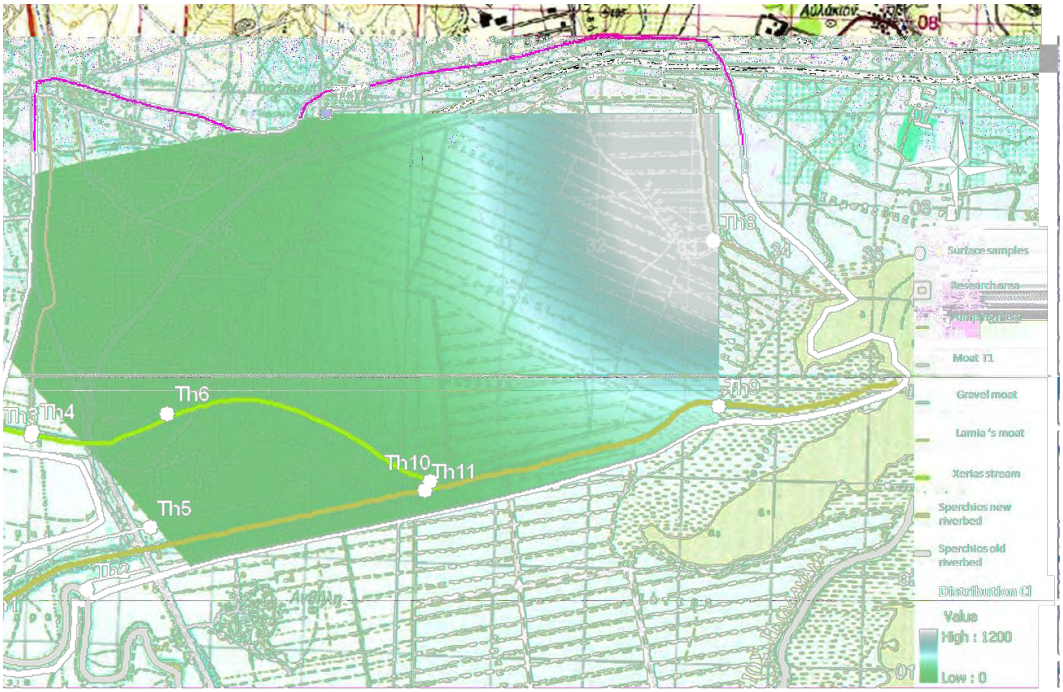

Figure 6 - Distribution of Cl in surface waters.

Table 4 - Classification of Wilcox diagram.

Sample ID (underground)	Station ID	WILCOX CLASSIFICATION	QUALITY
G2	Mavramadila	C2-S1	GOOD TO MODERATE
G3	Agia Paraskevi	C2-S1	GOOD TO MODERATE
G4	Stergiopoulou	C3-S1	MODERATE TO VERY MODERATE
G5	Katzikosta	C2-S1	GOOD TO MODERATE
G6	Tsairia	C2-S1	GOOD TO MODERATE
G7	Fteries	C2-S1	GOOD TO MODERATE
G8	Zardas a	C2-S1	GOOD TO MODERATE
G9	Stathopoulos	C2-S1	GOOD TO MODERATE
G10	Kontos a	C2-S1	GOOD TO MODERATE
G11	Kontos b	C2-S1	GOOD TO MODERATE
G12	Agios Panteleimon	C2-S1	GOOD TO MODERATE
G13	Zardas b	C3-S1	MODERATE TO VERY MODERATE

Sample ID (surface water)	Station ID	WILCOX CLASSIFICATION	QUALITY
Th1	before dam	C2-S1	GOOD TO MODERATE

4. Results and Discussion

Based on the existent water conditions in the area, the exploitation of the surficial water is considered to be imperative. The karstic springs of Megali Brysh can contribute up to a very important level. In the non-irrigative periods, the water from the spring through canals ends up in the pumping station and from there to the sea in Maliakos Gulf. Storing these water quantities will have a double benefit. This supply will be available during the summer period covering the water shortage and in addition it could be used for artificial enrichment of the area's aquifers. Therefore the over-pumping will be reduced, thus protecting the groundwater reserves, increasing also at once their quantity with the help off the artificial enrichment.

The construction of small containment dams along Ksirias stream watercourse is also suggested, so that new water reserves will be gathered, able to be used for covering the irrigative needs of Roditsa and Megali Brysi settlements, as well as for artificial enrichment of groundwater. These small dams can also withhold the sediment yield of the stream.

The adoption of more efficient irrigative methods would help in a more rational management of the area's water resources. The "drop" irrigative method has the highest degree of efficiency

(90%) and a variety of other advantages, such as the decrease of water loss due to minimum surficial runoff. Furthermore, this method works with low energy cost, due to low pressure requirements and because is unaffected by the wind.

The application of a new pricing policy for the consumers would help in the reduction of pressures in the area's water resources. The cost of irrigative water should be calculated based on water consumption and not based on the cultivated acres.

The constant briefing of producers and farmers, as well as the promotion of specific actions, that will contribute in the acquisition of the proper culture over the subject of rational exploitation of irrigative water, will induce important results. The "cultivation" of a saving philosophy concerning the water resources, followed by the encouragement for adopting new methods (such as the construction of common private drillings, proper pumping and irrigation in specific daily hours, thus minimizing the water losses), targeting towards the reduce of over-pumping of groundwater and in general the inappropriate water use.

The reuse of urban waste for irrigation purposes, with the requirement of completion of trustworthy studies and of all the procedures and their implementation according to the environmental terms, it would probably be an effective solution for the decrease of pumping for irrigation purposes.

5. References

Dasenakis E., Kastritis A., Mpourou P., Paraskevopoulou B. and Triantafullaki S. 2005. Transport of pollutant in Sperchios basin and the effects in the coastal zone. 5th National Conference: Integrated Management of Water Resource in a basin.Xanthi

Dimitressas D. 1999. Hydrogeological Study-Water balance in the region of water subtraction in Roditsa -M.Vrusi – Avlaki. Lamia, Geological department, DEB Fthiotidas

Katsifa D. Maria. 2011. Water resources within the area of Roditsa Delta of Spercheos river of Fthiotida county, with emphasis on hydrochemistry and quality, *Master thesis*, NTUA.

Municipal Water and Sewerage Company of Lamia (M.W.S.C.L), Land Reclamation Institute (LRI)-National Agricultural Research Foundation – (NAGREF) 2009, Study of the environmental effects for the use of treated waste waters from the treatment unit of Lamia for irrigation reasons, Lamia.

Papadimitriou N. 2010. Study for the work Irrigational net of Sperchios estuary Company of Fthiotida's development.

Tsoumas B. 1991. The provision of brackish areas in the peripheral zone of Maliakos - causes of contamination of surface and groundwater to the Maliakos bay, Paper presented at the 2nd Conference Fthiotida prefecture.

Tsoumas B. and Zorapas B. 2010.Recording on the groundwater data of Eastern Sterea Hellas, Infrastructure and Measurement in the catchments of Evritania, Fokida and Fthiotida Hydrogeological study IGME, Athens.

Tsoumas B. and Zorapas B. 2010. Recording on the groundwater data of Eastern Sterea Hellas. Infrastructure and Measurement in the catchments of Evritania, Fokida and Fthiotida Hydrogeological study-Field measurements, IGME, Athens.

Δελτίο της Ελληνικής Γεωλογικής Εταιρίας, τομ. XLVII , 2013
Πρακτικά 13ου Διεθνούς Συνεδρίου, Χανιά, Σεπτ. 2013

Bulletin of the Geological Society of Greece, vol. XLVII 2013
Proceedings of the 13th International Congress, Chania, Sept. 2013

HYDROGEOLOGICAL REGIME AND GROUNDWATER OCCURENCE IN THE ANTHEMOUNTAS RIVER BASIN, NORTHERN GREECE

Kazakis N.[1], Voudouris K.[1], Vargemezis G.[2] and Pavlou A.[1]

[1]*Laboratory of Engineering Geology & Hydrogeology, Department of Geology, Aristolte University of Thessaloniki, Greece.*

[2]*Laboratory of Applied Geophysics Department of Geology Aristotle University of Thessaloniki, Greece.*

Abstract

The Anthemountas river basin is located in northern Greece and covers an area of 374 km^2. The mountainous part of the basin consists of ophiolitic, crystalline and carbonate rocks, whereas the lowlands comprise Neogene and Quaternary sediments. Porous aquifers are developed in neogene *and quaternary deposits of confined and/or unconfined conditions. Karstic aquifers are developed in the carbonate rocks and there are aquifers in the Mesozoic and Palaeozoic fissured rocks. The water demands of the basin are mainly met by the exploitation of the porous aquifers through a large number of boreholes (more than 1000). The aquifers of fissured rocks discharge through cold springs without significant flow rate. Thermal hot springs are recorded across the Anthemountas fault discharging a mixture of geothermal fluids and cold water from the karst aquifer. According to their hydrogeological and lithological characteristics, porous aquifers can be divided into the subsystems of Galatista and Galarinos in the eastern part of the Anthemountas basin, Vasilika-Risio-Thermi and Tagardes-Trilofos in the western part and Peraia-Agia Triada and AUTh farm-Makedonia airport in the coastal area. For the determination of the aquifers (geometry and anatomy), their recharge mechanisms and hydraulic connection, data from geological maps, lithological profiles, geoelectrical soundings and tomographies, pumping tests and groundwater level measurements are used.*

Key words: *Aquifer systems, Fissured rocks, Springs, Geoelectrical soundings.*

Περίληψη

Η λεκάνη του Ανθεμούντα βρίσκεται στη βόρεια Ελλάδα και έχει έκταση 374 km^2. Στα ορεινά τμήματα της περιοχής συναντώνται οφιολιθικά, ανθρακικά και κρυσταλλοσχιστώδη πετρώματα, ενώ το πεδινό τμήμα αποτελείται από Τεταρτογενή και Νεογενή ιζήματα. Στα τεταρτογενή και νεογενή ιζήματα αναπτύσσονται ελεύθεροι και υπό πίεση υδροφορείς, στα ανθρακικά πετρώματα καρστικοί, ενώ και υδροφορείς στα διερρηγμένα κρυσταλλικά πετρώματα. Οι υδατικές ανάγκες της περιοχής καλύπτονται κυρίως από την εκμετάλλευση των πορώδων υδροφορέων με μεγάλο αριθμό γεωτρήσεων (>1000). Οι υδροφορείς των διερρηγμένων πετρωμάτων εκφορτίζονται από ψυχρές πηγές χωρίς σημαντικές παροχές. Κατά μήκος του ρήγματος του Ανθεμούντα εντοπίζονται γεωθερμικές πηγές όπου σε ορισμένες περιπτώσεις εκφορτίζουν νερό από

ανάμειξη γεωθερμικών ρευστών και ψυχρού από τον καρστικό υδροφορέα. Σύμφωνα με τα υδρογεωλογικά και λιθολογικά χαρακτηριστικά τους οι πορώδεις υδροφορείς χωρίστηκαν στα υποσυστήματα της Γαλάτιστας και του Γαλαρινού στα δυτικά, των Βασιλικών-Ρυσίου-Θέρμης και Ταγαράδων-Τριλόφου στο κέντρο της λεκάνης και της Περαίας-Αγίας Τριάδας και Αγροκτήματος ΑΠΘ-Αεροδρόμιο Μακεδονία στο παράκτιο τμήμα. Για τον καθορισμό της γεωμετρίας και δομής των υδροφορέων, την υδραυλική επικοινωνία και τα υδραυλικά τους χαρακτηριστικά χρησιμοποιήθηκαν δεδομένα από λιθολογικές τομές, δοκιμαστικές αντλήσεις, βυθοσκοπήσεις και ηλεκτρικές τομογραφίες, καθώς και μετρήσεις στάθμης.
Λέξεις κλειδιά: *Διαρρηγμένα πετρώματα, Πηγές, Υπόγειοι υδροφορείς, Γεωηλεκτρικές διασκοπήσεις.*

1. Introduction

Groundwater is of major importance in the Anthemountas basin because it is the main supply of water for domestic, irrigation, industrial and livestock uses. Population of the basin is 56,000 people, agricultural land covering 52%, livestock units (about 100) and a large number of industrial and commercial units can describe the main needs of water supply in the area. The water demands are covered by the exploitation of the porous aquifers through a large number of boreholes (greater than 1000). On the other hand a small number of boreholes are drilled in fissured rocks, located mainly in fault zones. Cold springs with no significant discharge are recorded in the wider area.

The aim of this work is the determination of the aquifers type, geometry and anatomy, hydraulic characteristics, recharge mechanisms and their hydraulic connection. These data are necessary to determine groundwater reserves and are useful for rational exploitation in order to avoid future quantitative and qualitative degradation.

2. Geomorphological and Geological Settings

The Anthemountas basin is located in northern Greece at the eastern part of the Thermaikos gulf and covers an area of 374 km^2 with high hills of semi-mountainous relief, according to Dikau's (1989) classification. The mean altitude and slope of the study area are 259 m and 20%, respectively, with a good developed dendritic drainage network.

From a geological point of view, the Anthemountas basin is a part of the Servo-Macedonian, Circum-Rhodope and Paeonian geotectonic zone (Mountrakis, 1985). The mountainous part of the basin consists of Mesozoic ophiolitic, crystalline and carbonate rocks whereas in the lowlands Neogene and Quaternary sediments represent 65% of the formations. The Neogene sediments are mainly located at the southern part of the area and consist of sandstone-marl (sandstones, marls, sands and gravels), red-clay (clay with lenses of sands) and conglomerate series (conglomerates, gravels, sands). The Quaternary sediments are alluvial deposits (sands, gravels and clays) in the western part of the basin and terrace systems (sands, pebbles) in the east (Figure 1). Carbonate rocks outcrop in the south-central part of the basin near Agia Paraskevi and Tagarades and consist of Triassic limestones. Leucocratic gneiss represents the largest percentage of the metamorphic rocks in the basin. The fault pattern of the study area is quite complex with WNW-ESE to E-W and NE-SW normal faults (Tranos et al., 2004). The Anthemountas fault is the longest in the area (32 km) and is characterised as active (Tranos et al., 2003; Zervopoulou et al., 2007).

3. Materials and Methods

For the determination of the aquifers, their recharge mechanisms and hydraulic connection, data from geological maps, lithological profiles, geoelectrical soundings and tomographies, pumping

tests and groundwater level measurements have been used (Figure 2). The aquifer type and geometry has been determined from the geological maps and lithological profiles (150) of boreholes. From the geoelectrical vertical soundings (47), the material of the vadose zone was defined, while geoelectrical tomographies were used to identify the anatomy of the aquifer layers after calibration with lithological data based on Vargemezis and Fikos'assignment (2010).

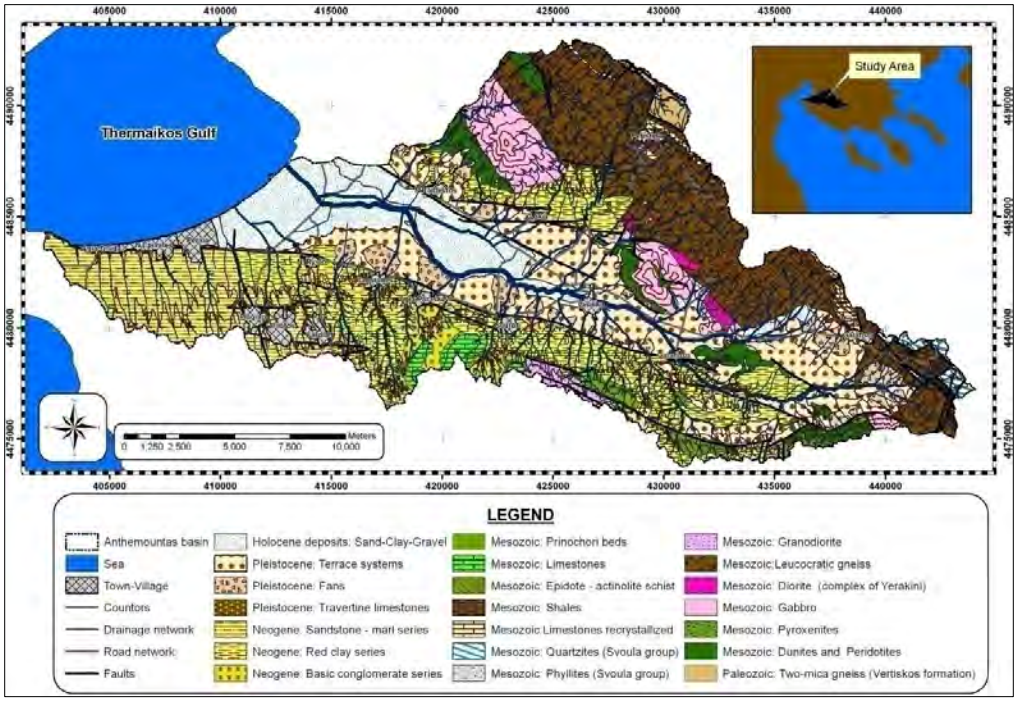

Figure 1 - Geological and topographic map of Anthemountas basin (Modified from IGME, Sheets Thessaloniki, Epanomi, Vasilika, Thermi, Polygiros and Zagliveri).

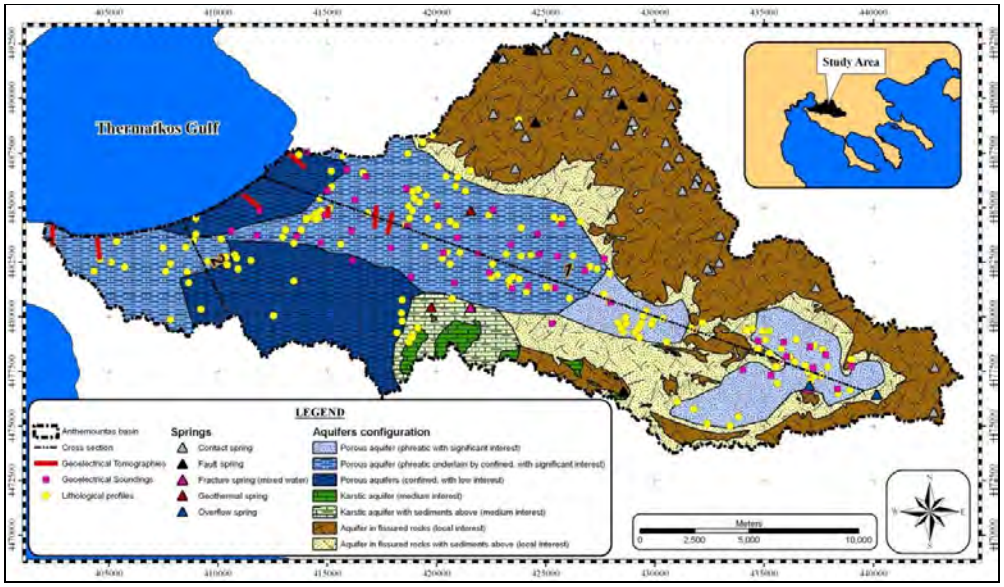

Figure 2 - Aquifers configuration, springs and locations of used data in the Anthemountas basin.

Water level measurements were performed in 136 boreholes for four periods: wet, May 2010-11 and dry, September 2009-2010. Pumping tests were performed in 6 boreholes and pumping data from 135 lithological profiles were used to evaluate the hydraulic characteristics of the porous aquifers. Constant rate pumping tests were used to determine the storativity and specific capacity, which is defined as the ratio of discharge to drawdown at the pumping borehole. Springs were mapped from the geological maps and field investigation. All collected data were stored, analysed, managed and displayed using geographic information systems (G.I.S.).

The Schlumberger array has been applied in order to measure the 47 geoelectrical soundings in the area. The exact location of each VES (Vertical Electric Sounding) can be seen on Figure 2. The distance in between the current electrodes (AB) varied between 30 and 50 meters aiming to get information about the vadose zone. Measurements were taken with Syscal (V11.4) IRIS instrument and the inversion has been done by the use of IPI2WIN software (Alexei et al. 1990-2001). The RMS values varied between 0.5% and 7%.

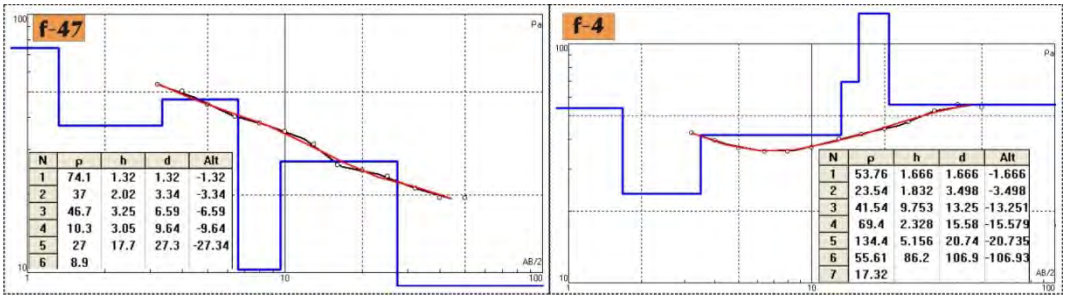

Figure 3 - Example of interpretation for 2 representative VES measured in Nea Raidestos (F-47) and Galatista (F-4).

Some typical examples of the results are presented in Figure 3 where the original measurements (black line with white circles) along with the resulting (by the forward modelling) curve (red colour) and the corresponding table of resistivity (ρ), depth (d) and thickness (h) of each identified layer.

The resistivity values have been calibrated according to geological information revealed from boreholes in the area and geoelectrical layers have been transformed to geological units according to the following table.

Table 1 - Calibration of resistivity values.

Resistivity (Ohm-m)	Geological Unit
0-10	Clay
10-20	Clayey sand
20-30	Sandy clay with thin layers of gravel
30-50	Gravel
50-80	Marl
>80	Conglomerate

According to the calibration table, the distribution of the thickness of the clay layers is shown in the map of Figure 4. The areas with green color are characterized by the absence of clay layers representing unconfined aquifers, while the areas with significant thickness of clay layers (orange and red color) correspond to areas with confined aquifers.

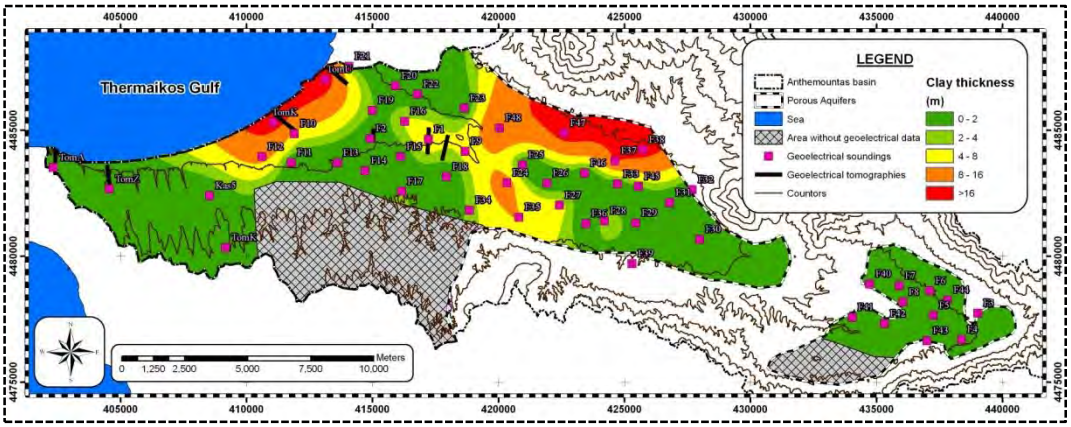

Figure 4 - Distribution of clay layers in vadose zone according to the geoelectrical survey.

4. Results

According to the geological formations, three categories of aquifers have been determined in the Anthemountas river basin, which are: aquifers in fissured rocks, karstic and porous aquifers.

The aquifers of fissured rocks have local interest in fault zones with discharges ranging from 30–80m^3/h and covering an area of 177 km^2 although 52 km^2 are under sediments. A large number of contact and fault springs (greater than 50) are located in fissured rocks without significant flow rates (1–5 m^3/h), which discharge periodically during the winter and spring (Figure 5a).

Karstic aquifers are located in the south-central part of the basin, near to Agia Paraskevi and Tagarades villages, covering an area of 5 km^2 and 11 km^2, respectively. Fault springs discharge mixed geothermal and cold water across the Anthemountas fault (Kazakis, 2013); the most well-known is Voskina spring (Figure 5b) near the village of Souroti. According to Nimfopoulos et al. (2002), a karstic aquifer underlies the sediments of the basin and controls the composition of the hosted hydrothermal waters, which are mixed with meteoric water and discharged through.

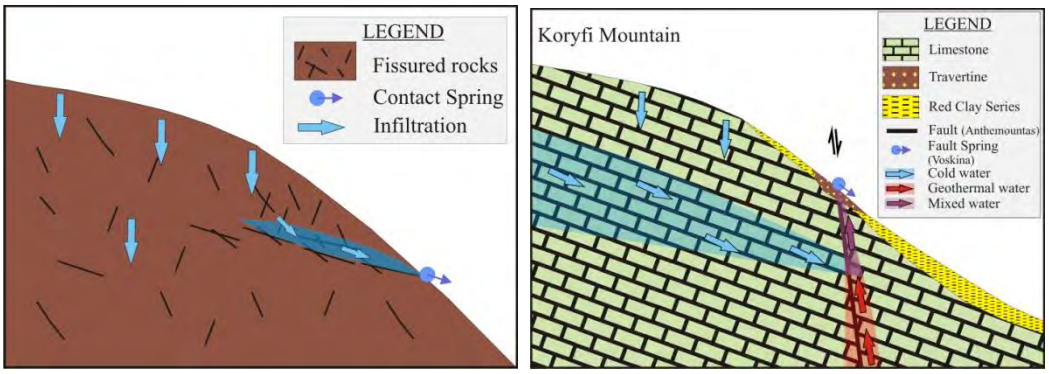

Figure 5 - (a) Contact spring in fissured rocks, (b) Fault spring with mixed water in Karst.

Porous aquifers cover an area of 181 km^2 and are developed mainly in the lowlands. According to their hydrogeological and lithological characteristics, porous aquifers can be divided into the sub-systems of Galatista and Galarinos in the eastern part of the Anthemountas basin, Vasilika-Risio-Thermi and Tagardes-Trilofos in the western part and Peraia-Agia Triada and AUTh farm-Makedonia airport in the coastal area (Figure 2). The sub-systems are described below and their hydraulic characteristics represented in Table 2.

- **Galatista:** Located in the western part of the Anthemountas basin, the Galatistas sub-basin covers an area of 24 km^2. An unconfined aquifer underlain by a confined aquifer is developed in the centre of the basin (Theodosiou and Latinopoulos, 2006). Its thickness ranges from 15 to 100 m, consisting of pebbles, gravel and sand. Groundwater level varies from 8 m below ground surface (b.g.s.) in the centre to 100 m (b.g.s.) in the southern part. The sub-system is hydraulically isolated from the other systems, because it is surrounded by crystalline rocks. The unconfined aquifer is recharged from directly infiltrating precipitation, percolation water from streams and the Anthemountas River and from fissured aquifers, whereas the confined aquifer is recharged from both unconfined and fissured aquifers.
- **Galarinos**: This is placed between the villages of Galarinos and Vasilika and has an area of 9 km^2. The thickness of the sediments varies from 140 to 180 m. The main aquifer is unconfined with a small confined aquifer below. Its thickness ranges from 40 to 80 m. The materials of the aquifer system consist of gravel, sand and sandy clay. Groundwater level varies from 60 m in the eastern part to 25 m in the western part. Groundwater recharge in this aquifer occurs via the following mechanisms: direct infiltration from rainfall, percolation from the Anthemountas River and lateral subsurface inflows from the aquifers of the fissured rocks. Aquifers of the fissured rocks are detected below the porous aquifers of the sub-system, as a result of the small thickness of the sediments. This is the main difference to the Vasilika-Risio-Thermi sub-system, with which it is in direct hydraulic contact.

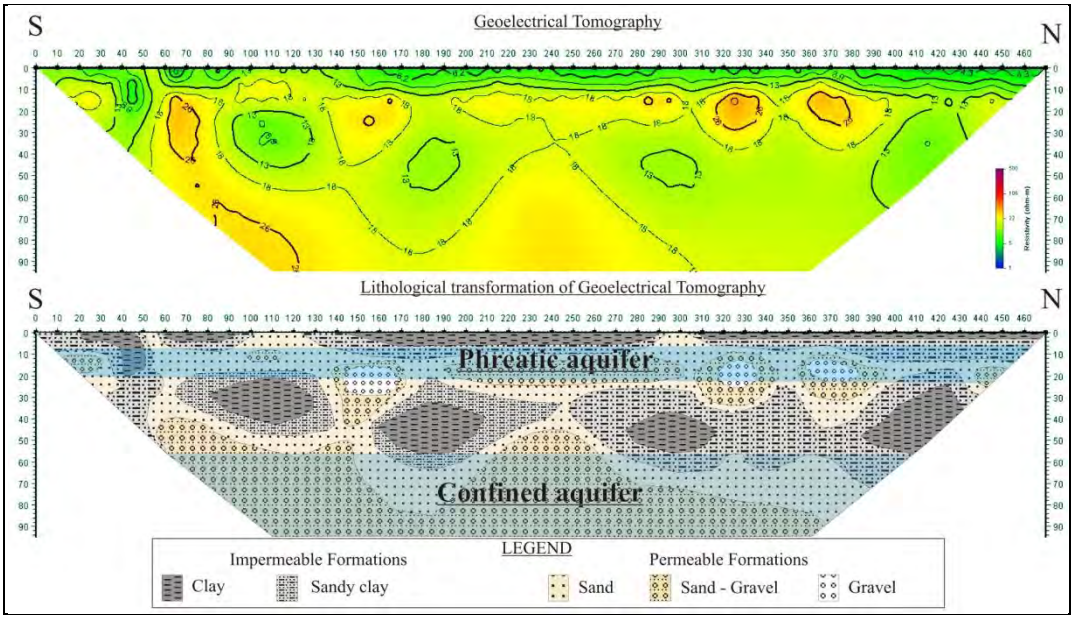

Figure 6 - (Up) Geoelectrical tomography of Vasilika-Risio-Thermi sub-system, (Below) lithological cross section based on geoelectrical tomography and lithological profiles.

- **Vasilika-Risio-Thermi:** This is located in the centre of the basin between Vasilika, Neo Risio and Thermi with a total area of 70 km^2. The thickness of the sediments is greater than 800 m in Vasilika (Vargemezis and Fikos, 2010) and greater than 1000 m near to Neo Risio (Thanassoulas, 1983). Quaternary deposits are up to 300 m thick and the aquifers developed within them contain fresh water; geothermal fluids are found beneath these deposits (Kolios et al., 2007). A phreatic aquifer was detected at a depth of up to 30–40 m (Nagoulis, 1998) with hydraulic connection with the confined aquifer through the

discontinuities of the clay lens (Figure 6). Furthermore, the construction of boreholes, exploiting both two aquifers favours the connection. The phreatic aquifer is converted to confined conditions in places, due to surface clay layers, mainly in the centre of the sub-system. The material of the aquifers consists of sand, sand-silt and gravel. Recharge of the sub-system occurs via infiltration of rainfall water, percolation from the Anthemountas River and torrents (Tagarades, Trilofos) and lateral inflows from the karstic aquifer in the southern part and the fissured rocks aquifer in the north. Groundwater level of the phreatic and confined aquifers ranges from 8−20 m in the western part to 25−40 m in the eastern part. Both aquifers are united in the area of Vasilica village, which constitutes the boundary with the Galarinos sub-system.

- **AUTh farm-Makedonia airport:** The phreatic aquifer of the Vasilika-Risio-Thermi sub-system is confined in the coastal area with the exception of some parts of AUTh farm (Fikos, 2000). For this reason, it is separated from the Vasilika-Risio-Thermi sub-system, although the two aquifer systems are in hydraulic connection. This sub-system covers an area of 7 km^2 in the northern coastal part and is recharged by infiltration of rainfall and from the Vasilika-Risio-Thermi. Groundwater level varies from 5 to 20 m below ground surface or from 10 to 20 m below sea level and shows negative piezometry due to overexploitation of the aquifer. The aquifer materials consist of sands and gravels.

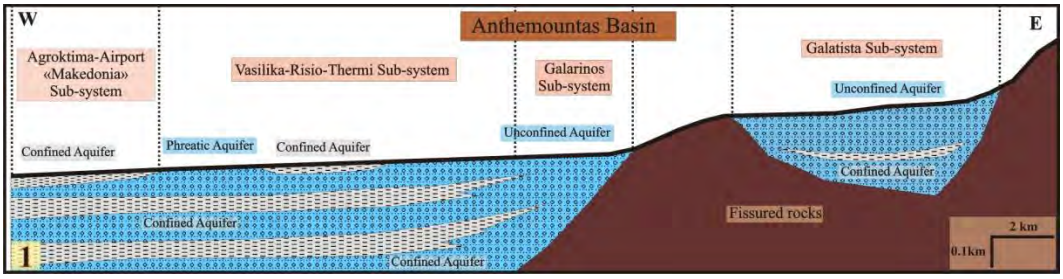

Figure 7 - Hydrogeological cross section from Galatista to Costal area (1).

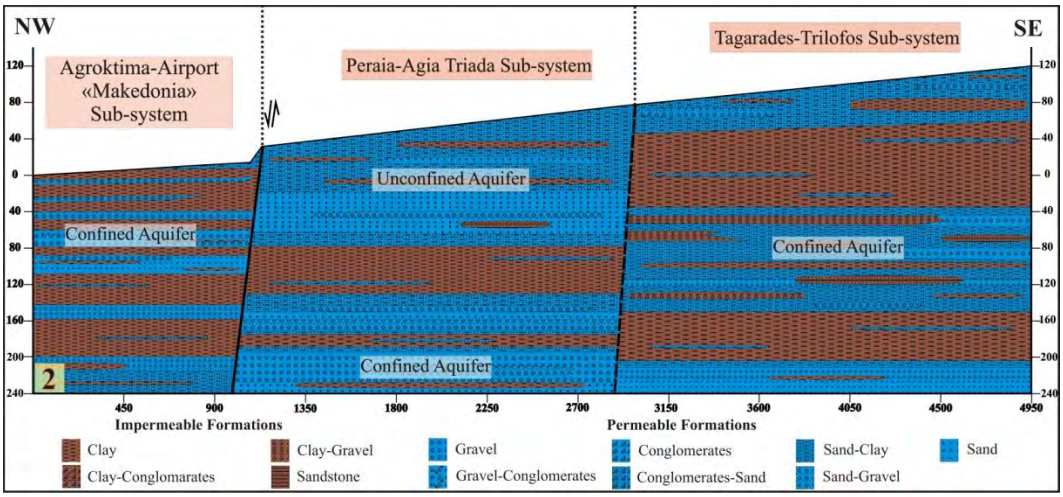

Figure 8 - Hydrogeological cross section (2) of the south-west part of Anthemountas basin.

- **Tagarades-Trilofos:** This is located in the north-western part of the basin and covers an area of 42 km^2. The Anthemountas fault form the boundary with the Vasilika-Risio-Thermi

sub-system. The aquifer consists of a small thickness (15-20 m) of parallel layers of sand with clay and gravel under confined conditions. The yield of the boreholes ranges between 4 and 10 m^3/h, while groundwater level varies from between 60 to 120 m b.g.s. without significant variation between the dry and wet periods. The sub-system is recharged mainly by infiltration of rainwater and by the percolation from streams and from the karst aquifer in the east.

- **Peraia-Agia Triada:** It covers an area of 22 km^2 located in the south-western part from the coast to the Tagardes-Trilofos sub-system. The aquifer system is divided to the upper unconfined aquifer with a mean thickness of 80 m and the deeper confined aquifer below 200 m. The two aquifers have the same piezometric head (Koumantakis, 2006) with negative values due to overexploitation (Voudouris and Kazakis, 2011). The unconfined aquifer consists of sand and some layers of gravel with groundwater level varying from 10 m near to the coast to 100 m in the hills of the southern part. The sub-system is recharged via infiltration, percolation from streams and inflows from the Tagarades-Trilofos sub-system.

In Figure 9, the spatial distribution of groundwater heads (metres above sea level) for the period of May 2010 is given. The groundwater flow direction in the Galatistas sub-system is mainly from west to east and southwest to northeast in the southern part revealing a hydraulic connection and recharge from the aquifer of the fissured rocks. In the western part of the study area the direction of groundwater is northwest to southeast in the north and from northwest to southeast in the south, whereas in the coastal area it is from the sea towards the mainland, which is due to seawater intrusion from overexploitation and the low natural recharge of the aquifer.

In Table 2, the hydraulic characteristics of the Anthemountas river basin sub-systems are shown. Hydraulic conductivity values range between 1.5×10^{-6} m/s and 5×10^{-6} m/s. The value of storativity (S) varies from 10^{-4} to 3×10^{-1}. The values of specific capacity range between 2–270 m^2/h. The effective porosity varies from 15% to 26%.

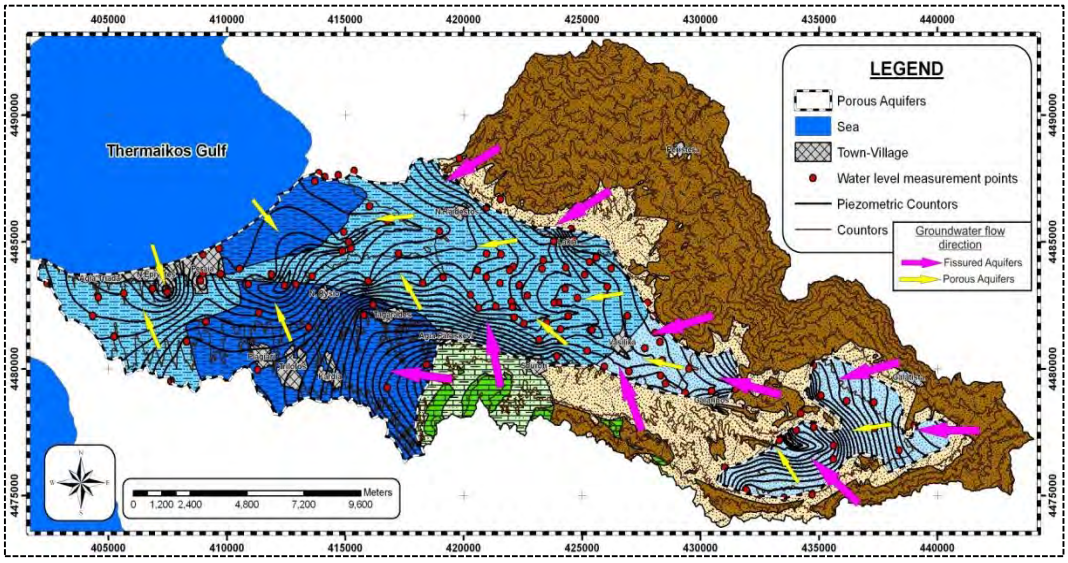

Figure 9 - Piezometric map and groundwater flow of porous aquifers of Anthemountas basin (May 2010).

Table 2 – Hydraulic characteristics of Anthemountas basin sub-systems.

Sub-system	Aquifers Thickness (m)	Yield of boreholes (m^3/h)	Specific Capacity (m^2/d)	Hydraulic Conductivity (m/d)	Storativity (%)	Effective porosity (%)
Galatista	15-100	25-80	28-60	1.3-3.5	0.1-10	15-23
Galarinos	15-80	30-160	15-270	0.3-8.6	1-30	17-24
Vasilika-Risio-Thermi	15-170*	20-160	28-270	1.3-43.2	0.01-5	16-26
Tagardes-Trilofos	15-50*	4-10	2-20	0.1-0.5	0.01-0.1	15-19
Peraia-Agia Triada	45-120*	30-60	28-230	1.7-10.4	0.05-5	19-24
AUTh farm-Macedonia airport	50-100*	30-80	60-250	1.7-13.8	0.01	19-26

*Until the depth of 300 m

5. Conclusions

From the analysis of hydrogeological and geophysical data in the Anthemountas river basin (North Greece), the following conclusions can be drawn:

Porous aquifers are divided into the sub-systems of Galatista, Galarinos, Vasilika-Risio-Thermi, Tagardes-Trilofos, Peraia-AgiaTriada and AUTh farm-Makedonia airport. In the sub-systems of Galatista, Galarinos and Peraia-AgiaTriada the main aquifer is phreatic and the yield of the boreholes varies from 25 to 160 m^3/h.

The confined aquifer is the most important in the Vasilika-Risio-Thermi and AUTh farm-Makedonia airport sub-systems with significant values of yield from boreholes ranging between 15–170 m^3/h. The Tagarades-Trilofos sub-system consists of parallel confined aquifers without significant discharge due to the low thickness of the aquifers and the mix of clay in the aquifer media.

Fissured rock aquifers and karstic aquifer discharge groundwater through springs. Piezometric maps reveal the subsurface hydraulic connection between the aforementioned aquifers and porous aquifers. The main direction of groundwater flow in the Anthemountas river basin is E-W, while overexploitation in the coastal area has caused an inversion of the flow from the sea towards the mainland.

6. Acknowledgements

This scientific work was carried out within the framework of PhD thesis of Nerantzis Kazakis and financially supported by the STATE SCHOLARSHIPS FOUNDATION OF GREECE (IKY).

7. Reference

Bobachev A. and Modin I.and Shevnin. 2000. Geoscan M Ltd, IPI2Win software, Moscow, Russia.

Dikau R. 1989. The application of a digital relief model to landform analysis, in: Raper, J. F. (Ed.) 1989: Three dimensional applications in Geographical Information Systems, Taylor and Francis, London, pp. 51-77.

Fikos I. 2000. Diachronic study of free aquifers using the method of electric tomography: A case study in Northern Greece, *MSc Thesis*, Department of Geology, Aristotle University of Thessaloniki (in Greek).

Fikos I., Ziankas G., Rizopoulou A. and Famelos S.2005. Water balance estimation in Anthemountas river basin and correlation with underground water level, *Global NEST Journal*, Vol. 7, No 3, pp. 354-359.

I.G.M.E. Geological Maps of Greece, Scale 1:50.000, Sheets: Thessaloniki, Epanomi, Vasilika, Thermi, Polygiros, Zagliveri.

Kazakis N.2013. Groundwater pollution risk assessment in Anthemountas basin. *PhD Thesis*, Department of Geology, Aristotle University of Thessaloniki (in Greek).

Kim J.H. 2009. DC2DPro-2D interpretation system of DC resistivity tomography User's Manual and Theory KIGAM, S. Korea.

Kolios N., Koutsinos S. and Arvanitis A. 2007. Construction supervision and evaluation results of geothermal drilling, municipality of Thermi, Thessaloniki. I.G.M.E. *Unpublished Technical Report* (in Greek).

Koumantakis I. 2006. Geological investigation, Municipality of Thermaikos. *Final technical report of research project*. National Technical University of Athens (Unpublished).

Mountrakis D.1985. *Geology of Greece*, University Studio Press, Thessaloniki (in Greek).

Nagoulis A. 1998. Hydrological study of Anthemountas basin, ANATOLIKI S.A. *Unpublished Technical Report* (in Greek).

Nimfopoulos M.K., Hadjispyrou S.A., Polya D.A., Michailidis K.M.and Trontsios G. 2002. Geochemical conditions and environmental pollution from hydrothermal waters of the Anthemous basin. Thessaloniki district, N. Greece, *6th Pan-Hellenic Geographical Conference (Volume II)*, Thessaloniki 2002, pp. 428-435.

Thanassoulas C.1983. Geophysical study of Anthemountas basin (V.E.S.), IGME. Unpublished Technical Report (in Greek).

Theodossiou N.and Latinopoulos P.2006. Evaluation and optimisation of groundwater observation networks using the Kriging methodology, *Environmental Modelling & Software* 21, pp. 991-1000.

Tranos M.D., Meladiotis I.D. and Tsolakopoulos E.P.2004. Geometrical characteristics, scaling properties and seismic behavior of the faulting of the Chortiatis region and Anthemountas basin (Northern Greece). *5th Int. Symposium on Eastern Mediterranean Geology*, Thessaloniki, Vol. 2, pp. 888-89.

Tranos M., Papadimitriou E. and Kilias A.2003. Thessaloniki–Gerakarou Fault Zone (TGFZ): the western extension of the 1978 Thessaloniki earthquake fault (Northern Greece) and seismic hazard assessment, *Journal of Structural Geology* 25, pp. 2109–2123.

Vargemezis G. and Fikos I. 2010. Large Scale Vertical Electrical Soundings survey in Anthemountas river basin for evaluating hydraulic communication between sub basin aquifers. *Proc. of the 12th International Congress*, Patras, May, 2010. *Bulletin of the Geological Society of Greece, Vol. XXXVIII*, pp. 1953-1961.

Voudouris K. and Kazakis N.2011. The impacts of urbanization on groundwater of Peraia area, Thermaikos. *Proceeding* of *4th Environmental Conference of Macedonia*, 18-20 March, Thessaloniki, pp. 1-10 (in Greek).

Zervopoulou A., Chatzipetros A., Tsiokos L., Syrides G. and Pavlides S.2007. Non-seismic surface faulting: The Peraia fault case study (Thessaloniki, N. Greece). *4th International Conference on Earthquake Geotechnical Engineering*, June 25-28, Thessaloniki, Greece, Paper No 1610.

Δελτίο της Ελληνικής Γεωλογικής Εταιρίας, τομ. XLVII , 2013
Πρακτικά 13ου Διεθνούς Συνεδρίου, Χανιά, Σεπτ. 2013

Bulletin of the Geological Society of Greece, vol. XLVII 2013
Proceedings of the 13th International Congress, Chania, Sept. 2013

FLOOD AND GROUNDWATER MANAGEMENT FOR THE MOUNTAIN PLATEAU OF OMALOS BASED ON GEOINFORMATICS TECHNIQUES

Kourgialas N.N.[1] and Karatzas G.P.[1]

[1]*Department of Environmental Engineering, Technical University of Crete, Greece, nektarios.kourgialas@enveng.tuc.gr; karatzas@mred.tuc.gr*

Abstract

A viable approach for flood and groundwater management in a mountain Plateau based on geoinformatics techniques is presented in this work. The proposed water management plan has two components: (a) the determination of the flood-hazard areas, and (b) the estimation of groundwater flow. For the first component, six factors were considered in order to estimate the spatial distribution of the flood hazardous areas: elevation, slope, land use, rainfall intensity, geology, and flow accumulation, The study area was divided into five regions characterized by different degrees of flood hazard ranging from very low to very high. The produced map of flood-hazard areas identifies the areas at high risk of flooding. The second component includes a groundwater management approach for estimating groundwater flow and the potential contamination risk. The proposed methodology can be used to objectively compare different scenarios based on anthropogenic interventions that can affect the flood-prone areas or the groundwater flow dynamic. All these approaches were applied at the Omalos Plateau in the White Mountains of Crete in Greece.

Key words: *flood-hazard areas, GIS, groundwater hazard management, Omalos Plateau.*

Περίληψη

Στην παρούσα μελέτη, με βάση τη χρήση γεωπληροφορίας σε περιβάλλον GIS, παρουσιάζεται μια βιώσιμη διαχειριστική προσέγγιση πλημμυρικών φαινομένων και υπογείων υδάτων σε ορεινά οροπέδια. Το προτεινόμενο διαχειριστικό πλάνο αποτελείται από δύο συνιστώσες: (α) τον καθορισμό των πλημμυρικά επικίνδυνων περιοχών, και (β) την εκτίμηση της ροής των υπογείων υδάτων. Για την πρώτη συνιστώσα, μελετήθηκαν έξι παράγοντες που σχετίζονται άμεσα με την χωρική κατανομή των επικίνδυνων σε πλημμυρικά φαινόμενα περιοχών: υψόμετρο, κλίση, χρήσεις γης, ένταση βροχής, γεωλογία, και συσσώρευση επιφανειακής απορροής. Η περιοχή μελέτης χωρίστηκε σε πέντε επιμέρους περιοχές οι οποίες χαρακτηρίζονται από διαφορετικούς βαθμούς πλημμυρικής επικινδυνότητας από πολύ χαμηλή έως πολύ υψηλή. Ο δημιουργούμενος χάρτης πλημμυρικού κινδύνου καθορίζει τις περιοχές εκείνες με αυξημένο κίνδυνο εμφάνισης πλημμυρών. Η δεύτερη συνιστώσα περιλαμβάνει μια διαχειριστική προσέγγιση υπογείων υδάτων για την αξιολόγηση της υπόγειας ροής και τον πιθανό κίνδυνος ρύπανσης. Η προτεινόμενη μεθοδολογία μπορεί να χρησιμοποιηθεί για τη μελέτη διαφορετικών σεναρίων ανθρωπογενών

παρεμβάσεων που μπορεί να επηρεάσουν τις πλημμυρικά επιρρεπείς περιοχές ή τη δυναμική της ροής των υπογείων υδάτων. Όλες οι παραπάνω προσεγγίσεις εφαρμόστηκαν στο οροπέδιο του Ομαλού στα Λευκά Όρη της Κρήτης στην Ελλάδα.
Λέξεις κλειδιά: *Πλημμυρικά επικίνδυνες περιοχές, Γεωγραφικά Συστήματα Πληροφοριών, Διαχείριση ρύπανσης υπογείων υδάτων, Οροπέδιο Ομαλού.*

1. Introduction

The number of flash flood events has increased significantly all around the world over the last three decades. Especially, in mountainous areas flash floods are very common where rapid snowmelt or heavy rainfalls are quickly transformed into runoff. These events, due to the high capacity of transport, can be characterized as the most significant weather-related hazards in many mountain Plateaus all around the world, causing considerable economic and human losses (Ballesteros *et al.* 2010). The main causes of flash floods are climatic changes, changes in land use and other anthropogenic interventions. The most common anthropogenic interventions are urban growth, the partial or total cover of torrent banks, watercourse alignment, improperly dimensioned bridges, deforestation and the consequent erosion, the construction of roads or other structures across the watercourse, subsidence observed in flat regions due to anthropogenic interventions such as overpumping, and finally, the change or deviation of the watercourse (Kourgialas and Karatzas 2011).

In addition, in mountain Plateaus the role of groundwater management is very important. Specifically, hydrogeologic settings in Mediterranean mountain areas are typically characterized by the occurrence of fractured-rock aquifers (Wireman 2003). As the population density and agricultural activity increases in these fractured-rock settings the management of groundwater supplies becomes a very crucial issue. In addition, in these regions there has been an increase in anthropogenic contamination of groundwater resources. As a result of this increasing stress on water resources in these mountain regions, groundwater scientists have recognized the need to develop easy to handle methods and tools for characterizing groundwater contaminant transport risk.

The availability of detailed climatic and hydrogeological data in mountain regions is in general limited hindering the use a detail modelling approach. Thus, in flash floods studies, precipitation records and flow data have been widely used (Chiang and Chang 2009); however, the use of systematic data on flash floods presents several challenges in mountainous catchments as representative instrumental records are not normally available in these environments (Ballesteros *et al.* 2010). Thus, in ungauged mountainous areas where expensive and time consuming hydrological-hydraulic simulations are not possible the use of an effective Geographic Information Systems (GIS) management tool is essential to delineate the flood prone areas (Manfreda *et al.* 2008). Furthermore, the synthesis of available data and the mapping of the relationships between groundwater hazard and the elements at risk require the use of tools such as GIS. Nowadays, integrated approaches of GIS and remote sensing technology are capable of providing the base for quantitative analysis of an environmental process with an appropriate degree of accuracy.

The aim of this work is to present an integrated and easy to handle GIS tool that incorporates geoinformatics techniques for flood and groundwater management in mountain Plateau. The proposed water management tool has two components: (a) the determination of the flood-hazard areas, and (b) the estimation of groundwater flow and the potential contamination risk under current and future anthropogenic pressures and activities. All these approaches were applied at the Omalos Plateau in the White Mountains of Crete in Greece.

2. The Study Area

The Omalos Plateau is the largest active polje of Western Crete (Greece) and covers an area of approximately 6 km^2 (3x2 km). The elevations of this Plateau range from 1032 to 1360 m above sea level within the boundaries of the Natura 2000 site 'Lefka Ori' (GR 4340008) (Figure 1). The mean annual temperature is 9.3 ^{o}C and monthly means range from 2.2 ^{o}C in January to 19.3 ^{o}C in July (data from the period 1994 to 2012 from the meteorological station of Omalos plain). The mean annual rainfall for that period is 1600 mm. The Plateau consists of Post-Mesozoic sediments (recent deposits) which lie on the "Trypali" metamorphic carbonates and the Plattenkalk carbonate group. The later formations are karstified at Omalos. The term karstification refers to geological processes mainly involving dissolution. These processes create unique morphological characteristics such as dolines, whose size varies from several meters to few hundreds of meters, or a polje which often results from more than one dolines or karstic structures (Hamdan *et al.* 2012). The Omalos plain is both cultivated with cereals and fruit trees and grazed by sheep and goats. As the anthropogenic innervations and agriculture, in the study area, have become more intensive a proper management plan regarding the flood phenomena and the protection of groundwater supplies is a challenge.

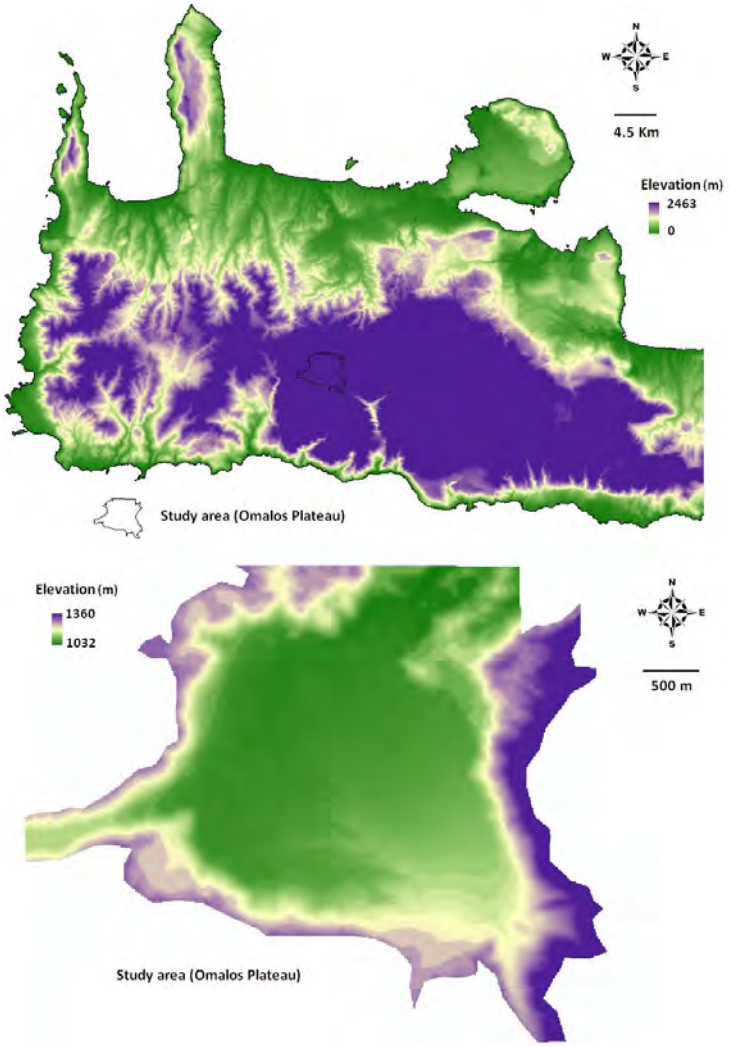

Figure 1 – Topography of the study area (Omalos Plateau).

3. Materials and Methods

3.1. Estimating the Flood Hazardous Areas in the Omalos Plateau

In order to estimate the flood hazardous areas the study area was divided into five regions characterized by different degrees of flood hazard (very high, high, moderate, low and very low). This classification is performed by considering the factors that form and influence a flood and by assigning relative weights to them. This process is performed in a Geographic Information Systems (GIS) environment and thematic maps are produced for each parameter. The linear combination of the thematic maps and the selection of the weights yield the final map of flood hazardous areas.

For the estimation of the flood hazardous areas in the Omalos Plateau, six (6) thematic maps were created using GIS Arc Map environment: elevation, slope, land use, rainfall intensity, geology, and flow accumulation. The factors used in this study were selected due to their general relevance to the flood hazards and according to literature surveys (Yahaya *et al.* 2010; Kourgialas and Karatzas 2011). All of these maps were georeferenced to the Greek Coordinate System EGSA'87. The produced raster maps were 10×10 m, i.e., a 100 m² raster unit.

The original data include the topographic maps (1:5000) and the monthly rainfall values from seven stations located in the surrounding area. The Digital Elevation Model (DEM) for the terrain was first created by using the 3D Analyst tool. Corine 2006 and remote sensing methods (aerial photographs) were used to determine the land use map, while the traditional field explorative geological mapping was used to determine the geological map of the Omalos Plateau. The DEM was used to determine the flow direction in each raster cell. This process was followed by the ident ification of the water accumulation points. The flow concentration map, which indicates the number of cells that hydrologically contribute to each raster cell was developed by using the flow direction map combined with a suitable algorithm (flow accumulation - Arc Hydro). Output cells with a high flow accumulation (pixels) are areas of concentrated flow (Kourgialas and Karatzas 2011).

In order to determine the rainfall intensity, the meteorological data of seven meteorological station s in the surrounding area of the Omalos Plateau, shown in Figure 2, were used. Specifically, the re-corded meteorological data from stations M1, M2, M3, and M6 was for the period 1999-2011, from station M7 the period was 1960-2010, while for stations M4 and M5 the time period was 2007-2012. The rainfall intensity map was created by using the Modified Fournier Index methodology (Morgan 2005):

$$MFI = \sum_{1}^{12} \frac{p^2}{P}, \quad (1)$$

where *MFI*: the Modified Fournier Index, $\sum_{1}^{12}$: the 12-month summation, *p*: the average monthly rainfall, and *P*: the average annual rainfall.

The MFI indicator expresses the sum of the average monthly rainfall intensity at a station. In the present study, at each station the territorial contribution of the MFI index values were considered using the spline interpolation method (Kourgialas and Karatzas 2011).

3.2. Estimating the Groundwater Direction and Groundwater Contamination Risk in the Omalos Plateau

For estimating the groundwater contamination risk in the extended area of the Omalos Plateau the equipotential contours map was created in a GIS environment. This map describes the groundwater flow direction in the study area. Combining this information with the recorded faults

in the extended area of the Omalos Plateau the groundwater hazard can be estimated. The original data for the creation of the above maps include: a) land uses based on Corine 2006 and aerial photographs, b) hydrogeological layers maps, c) soil maps, and d) groundwater level data from wells in the study area. Specifically, in this study the recorded groundwater level data was obtained from four wells for the time period 2004-2012 (Figure 3). These data was the only available from the Omalos Plateau.

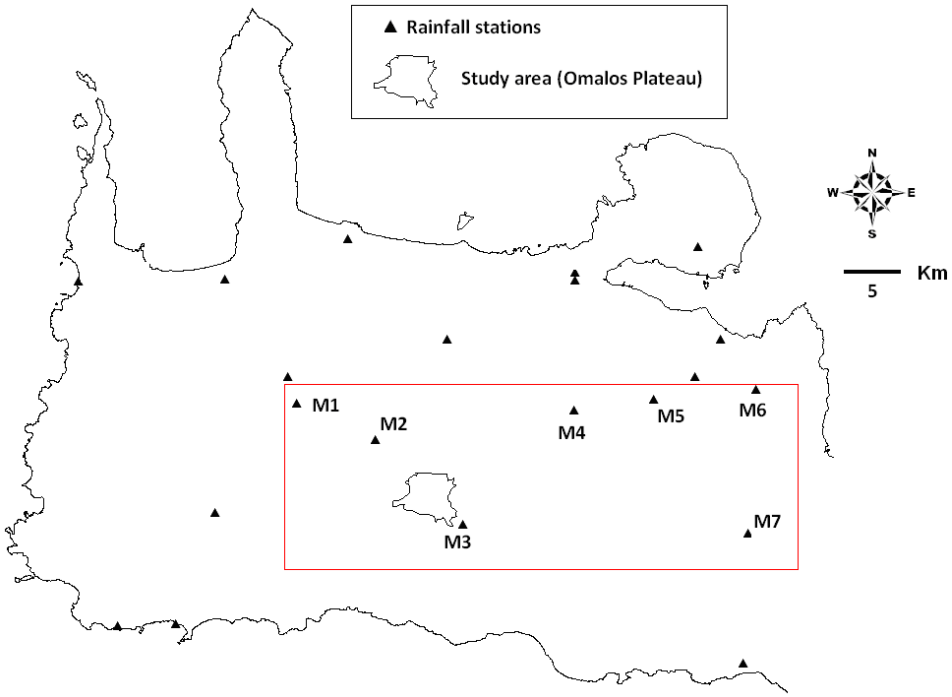

Figure 2 - Locations of the Meteorological stations.

Figure 3 – Observation well locations.

4. Results and Discussion

4.1. Flood Prone Areas

The six factors introduced in section 3.1 were used to estimate the flood hazardous areas and create the corresponding map. The effect of each factor is mapped as five different hazard levels: very high (20-year flood), high (100-year flood), moderate (200-year flood), low (500-year flood), and very low (>500-year flood). Among these factors, flow accumulation, slope, elevation and rain fall intensity have numeric values, whereas geology and land use are expressed in descriptive form . In the case of the numeric-valued factors, five different hazard classes were identified on the base s of the Jenk's Natural Breaks classification (Smith 1986). In the case of the non numeric-valued factors, classification depends mainly on the influence of the factor on the generation of flood process. For instance, for the geology factor, a karstic geology indicates a very low flood hazard. In the case of the land use factor, limited land cover (low land cover percentage) indicates a very high flood hazard.

The flood hazardous areas cannot be estimated by considering the effect of each factor separately. The integration of all factors is necessary in order to obtain the overall flood hazardous areas map. Since all factors do not have the same degree of influence on the hazardous areas, a weighting approach, where a different weight is assigned to each factor, was applied while the factor weights were determined by employing the methodology presented by Kourgialas and Karatzas (2011). Based on this methodology, the effects of each factor on all other factors are depicted in Figure 4. A solid line between two factors indicates that one factor has a main effect on the other pointed by the arrow, that is, a change of the first factor has a direct effect on the other (main avenue). A dashed line between two factors indicates that one factor has a secondary effect on the factor pointed by the arrow, that is, a change of the first factor has an indirect effect on the other (minor avenue). For example, flow accumulation has a main effect on land use and a secondary effect on slope. In order to quantify the two different types of effects, one (1) point is assigned to a main effect and half a point (½) to a secondary (Shaban *et al.* 2006). Then, the rate for a factor is computed as the summation of the points corresponding to the effects emanating from the factor.

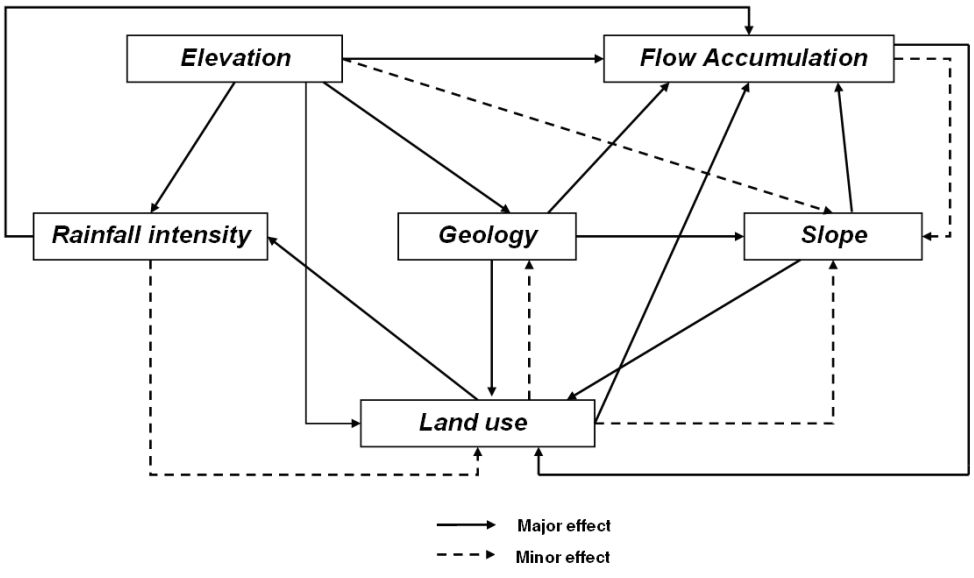

Figure 4 - A schematic depiction of the interaction between factors that influence the flood hazard (Kourgialas and Karatzas 2011).

Based on the above weighting approach and according to Kourgialas and Karatzas (2011) the contribution of each factor to the flood hazardous areas, expressed as a percentage, is for the elevation: 31.49%, slope: 14%, land use: 21%, rainfall intensity: 10.5%, geology: 12.52%, and flow accumulation: 10.5%.

The resulting map of hazardous areas includes the combination of the above six variables that are related directly to any flood event that occurs in the area of study. Specifically, the six maps that were developed after the classification method (Figure 5) were combined using a weighted linear combination approach in a GIS environment.

According to this technique each factor is multiplied by its percentage weight and the summation of all factors yields the final hazardous areas map (Shaban *et al.* 2006):

$$S = \sum w_i x_i \,, \quad (2)$$

where, S is the final hazardous areas map, w_i is the weight of factor i (percentage) and x_i is the rate of the factor i.

The factors (maps) were combined according to Equation (2) and the final flood hazardous areas map was produced (Figure 6). According to this figure, the study area of Omalos Plateau can be classified with respect to flood hazard from high to very low. Based on the results, the south-east parts of the Omalos Plateau can be characterized as high flood prone areas.

4.2. Groundwater Risk under an Intensive Agriculture

Nowadays, due to intensive agricultural activities in the study area, of particular interest is the hypothetical scenario of charging pollutants (e.g. fertilizers, pesticides) and whether it may create environmental problems in the extended area.

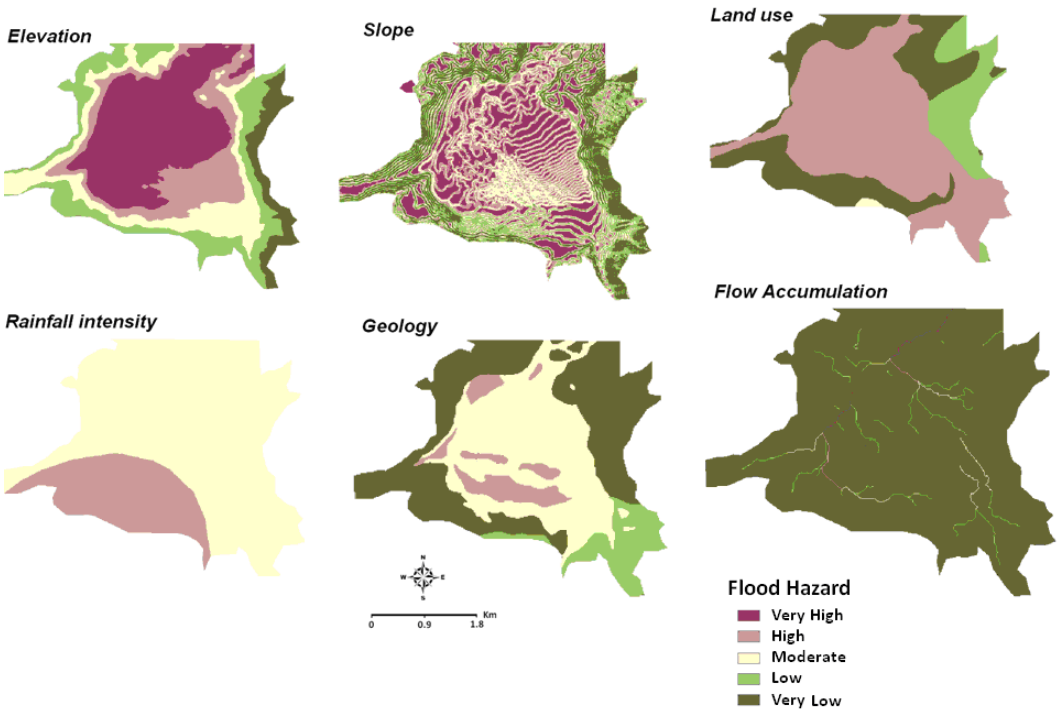

Figure 5 - Flood hazard maps for each factor.

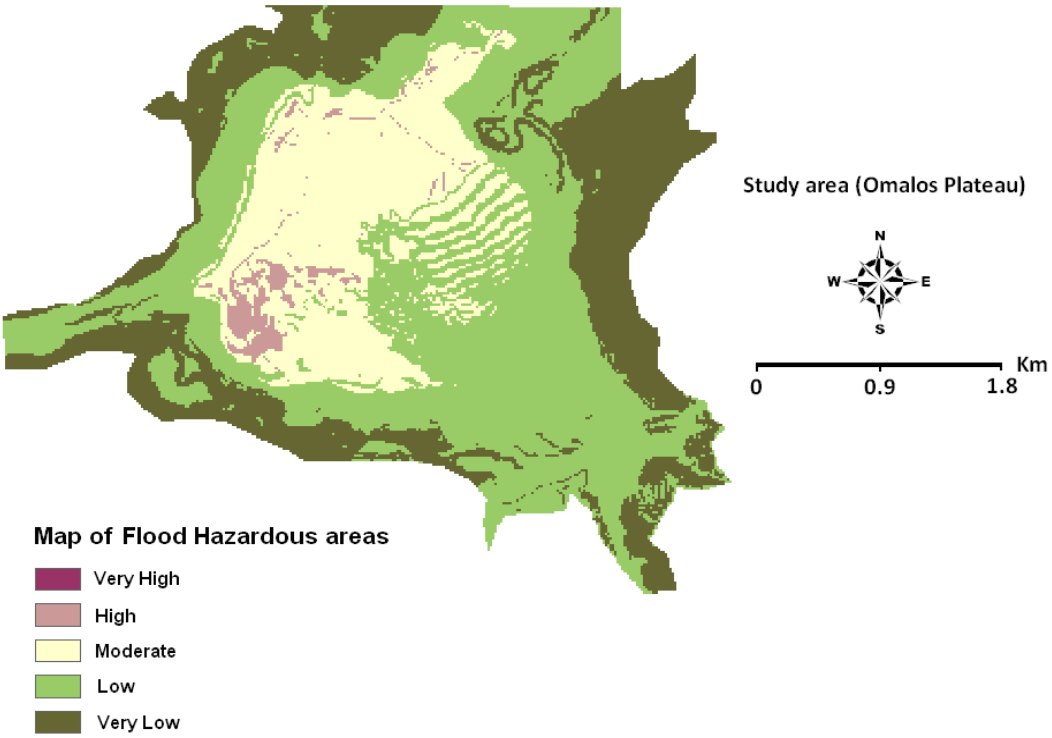

Figure 6 - Final flood hazardous map for the study area.

In answering this question the map of equipotential lines for an extended area of Omalos Plateau was created (Figure 7). This map was based on the groundwater level data from four wells in the Omalos Plateau. Figure 7 also describes the flow direction, perpendicular to the equipotential lines, and the existing faults in the region. According to this figure the direction of groundwater flow is north-west, through this flow direction groundwater encountered many large and small faults that direct groundwater in the north at Meskla and Agia springs (Figure 8). At this point it is very important to mention that: a) based on the groundwater level data, the aquifer in the extended area of the Omalos Plateau is shallow (3-7m), b) the study area receives significant amounts of rainfall, fact that lead to a rapid recharging of groundwater resources, and c) the groundwater flow in the study area discharges through the Meskla and Agia springs. These springs supplies drinking water important settlements in the Prefecture of Chania.

Based on the above, the highly significant groundwater contamination risk in the study area of Omalos Plateau from any excessive use of agrochemicals through intensification of agricultural activity is obvious. Any deposition of contaminants such as nitrates in this area may have the final recipient of the springs Meskla and Agia in the center and north of the Prefecture of Chania, respectively.

The above results are confirmed by the results of previous studies where a tracing method was performed by the Institute of Geological and Mineral Exploration (IGME) in 1989 and 1987 in the Omalos Plateau (Knithakis 1993). Specifically, dye was poured into carbonate rocks of the Omalos Plateau at an altitude of 1050 meters to monitor the groundwater flow connection of this region with the springs discharge in the northern and northeastern part of the White Mountains. As a result, the poured dye was detected in many discharge springs of the Prefecture of Chania such as the Meskla and Agia.

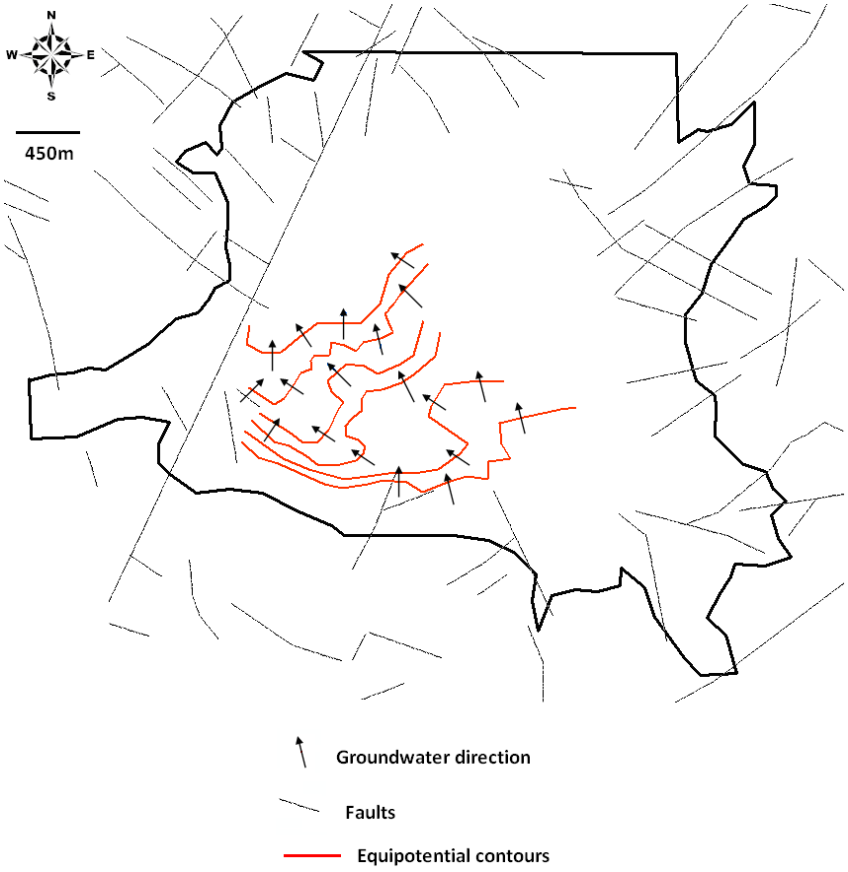

Figure 7 – Water table contour lines, faults and flow direction.

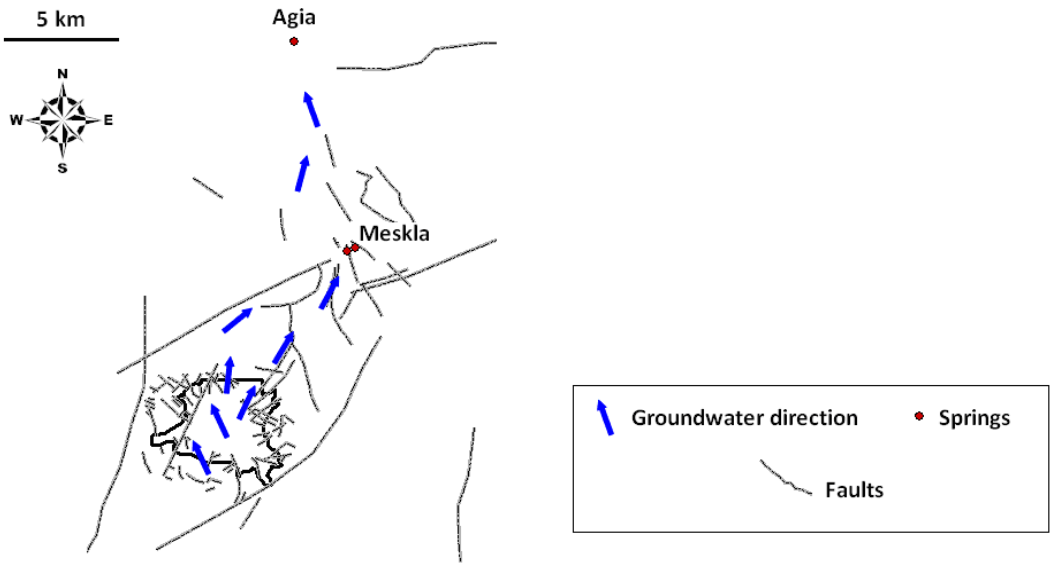

Figure 8 – Groundwater flow direction to springs.

5. Conclusions

This work presents a combined approach on flood and groundwater management. Specifically, in this work a method to evaluate the flood prone areas as well as a simple approach to estimate the groundwater contamination risk in the Omalos Plateau is presented**.** Based on the results of this study:

- The flood hazard phenomena in the study area can be characterized as high in south-western side of the Omalos Plateau, while in the rest parts as moderate to very low.
- The karstic aquifer of the Omalos Plateau can be characterized by many large faults and shallowness. All these features contribute to a high groundwater contamination risk in the Plateau from the increasing use of fertilizers and pesticides. Regarding the possible contamination in surrounding areas, especially the spring discharge of Meskla and Agia the groundwater hazard can be classified as very high.

It is very important to mention that the accuracy of groundwater flow direction in the study area should be verified using data from extra monitoring wells. The estimation of flood and the groundwater hazardous areas are fundamental components of a water management strategy. The proposed work could become a useful tool for the better organization of a management plan regarding the determination of the potential flooding areas and the areas of high groundwater contamination risk.

6. References

Ballesteros C.J.A., Eguibar M., Bodoque M.J., Diez-Herrero A., Stoffel M. and Gutierrez-Perez I. 2011. Estimating flash flood discharge in an ungauged mountain catchment with 2D hydrau lic models and dendrogeomorphic palaeostage indicators, *Hydrological Processes,* 25(6), 9 70-979.

Chiang Y.M. and Chang F.J. 2009. Integrating hydrometeorological information for rainfall-runoff modelling by artificial neural networks*, Hydrological Processes,* 23(11), 1650–1659.

Corine Land Cover 2006 for Greece, *European Environmental Agency*.

ESRI 2008. ArcView 9.2 User Manuals, Environmental System Research Institute, 380 New York Street, Redlands, CA, 92373 USA.

Hamdan A.D., Economou N., Kritikakis G., Andronikidis N., Manoutsoglou E., Vafidis A., Panagratis P. and Apostolidou G. 2012. 2D and 3D imaging of the metamorphic carbonates at Omalos plateau/polje, Crete, Greece by employing independent and joint inversion on resistivity and seismic data, *International Journal of Speleology*, 41, 199-209.

Knithakis M. 1993. Institute of Geological and Mineral Exploration (IGME), (in Greek).

Kourgialas N.N. and Karatzas G.P. 2011. Flood management and a GIS modelling method to asses s flood-hazard areas–a case study*, Hydrological Sciences Journal,* 56(2), 1-14.

Manfreda S., Sole A. and Fiorentino M. 2008. Can the basin morphology alone provide an insight into floodplain delineation? *WIT Transactions on Ecology and the Environment,* Vol. 118, 47-56, www.witpress.com

Morgan R.P.C. 2005. Soil erosion and conservation*, Blackwell Publishing Ltd,* Oxford UK.

Shaban A., Khawlie M. and Abdallah C. 2006. Use of remote sensing and GIS to determine recharge potential zones: the case of Occidental Lebanon, *Hydrogeology Journal*, 14(4), 433-443.

Smith R.M. 1986. Comparing traditional methods for selecting class Intervals on choropleth map, *The Professional Geographer*, 38(1), 62-67.

Wireman M., 2003. Characterization and Management of Ground Water Resources in Fractured – rock Hydrogeologic Settings, *Groundwater Monitoring and Remediation*, 23, no. 3/ Summer 2003.

Yahaya S., Ahmad N. and Abdalla R.F. 2010. Multicriteria Analysis for Flood Vulnerable Areas i n Hadejia-Jama'are River Basin, Nigeria, *European Journal of Scientific Research*, 42(1), 7 1-83.

Δελτίο της Ελληνικής Γεωλογικής Εταιρίας, τομ. XLVII , 2013
Πρακτικά 13ου Διεθνούς Συνεδρίου, Χανιά, Σεπτ. 2013

Bulletin of the Geological Society of Greece, vol. XLVII 2013
Proceedings of the 13th International Congress, Chania, Sept. 2013

ASSESSMENT OF GROUNDWATER POLLUTION IN RELATION TO HEAVY METALS OF THE ALLUVIAL AQUIFER OF THRIASION PLAIN (NW ATTICA)

Kyriazis D. [1], Zagana E. [2], Stamatis G. [1], Fillippidis F. [1] and Psomiadis E[1].

[1]Institute of Mineralogy-Geology, Agricultural University of Athens, Iera Odos 75, GR 11855 Athens, Greece, stamatis@aua.gr , dskiriazis@yahoo.com,, filippidis_fil@hotmail.com, mpsomiadis@aua.gr

[2]Institute of Hydrogeology, Department of Geology, University of Patras, GR 26110, Rio-Patras, Greece, e-mail: zagana@upatras.gr

Abstract

In this study the hydrogeological and hydrochemical characteristics of Thriasion Plain are presented focusing mainly on the presence of heavy metals in the alluvial aquifer. Two main aquifer systems exist in the study area: a) the karst aquifer hosted in the karstified carbonate formations, which structure the bedrock and the margins of the alluvial basin and b) the phreatic aquifer within the Quaternary deposits of the Thriasion Plain.

Coastal and submarine groundwater discharges show the direct connection of the aquifers with the sea causing intense salinization in both aquifers. The phreatic aquifer is characterized by high levels of TDS (483 – 13,067 mg/l) and correspondingly high degree of hardness (15.7 to 165.7 ^{o}dH). High concentrations of Na^{+}, Cl^{-}, SO_4^{2-}, NO_3^{-}, NH_4^{+} and PO_4^{3-} reflect the diverse anthropogenic influences on the aquifer. The strong presence of heavy metals, Cd, Cu, Fe, Mn, Ni, Pb, Sr and Zn has been determined in the most of the samples. Their origin is associated with geogenic factors, such as the occurrences of bauxites, oxides derived from the alteration of rocks, especially shischts, organic matter within the Plio-Pleistocene sediments of the region, as well as with intense pressures from anthropogenic activities. In some cases the groundwater is improper not only for human consumption but also for many other uses.

Key words: *Hydrochemistry, heavy metals, phreatic aquifer, Thriasion Plain.*

Περίληψη

Στην παρούσα εργασία παρουσιάζονται τα υδρογεωλογικά και υδροχημικά χαρακτηριστικά της περιοχής του Θριάσιου Πεδίου, εστιάζοντας κυρίως στην παρουσία των βαρέων μετάλλων στα υπόγεια νερά του προσχωματικού υδροφορέα. Στην περιοχή εντοπίζονται δυο ευδιάκριτες μεταξύ τους υδροφορίες, η καρστική υδροφορία που αναπτύσσεται εντός των καρστικοποιημένων ανθρακικών σχηματισμών, οι οποίοι δομούν τα περιθώρια και το υπόβαθρο της προσχωματικής λεκάνης και η φρεάτια υδροφορία που αναπτύσσεται εντός των Τεταρτογενών αποθέσεων. Η άμεση επικοινωνία των υδροφόρων με τη θάλασσα έχει ως αποτέλεσμα την έντονη υφαλμύρωση τους. Η υδροχημική έρευνα έδειξε, υψηλά επίπεδα αλατότητας και σκληρότητας, υψηλές συγκεντρώσεις στα κύρια στοιχεία Na^{+}, Cl^{-},

SO_4^{2-}, NO_3^-, NH_4^+ και PO_4^{3-} και στα βαρέα μέταλλα Cd, Cu, Fe, Mn, Ni, Pb, Sr και Zn, τα οποία αντικατοπτρίζουν τις ποικίλες γεωγενείς και ανθρωπογενείς επιδράσεις που υφίσταται ο εκμεταλλευόμενος υδροφορέας. Η άναρχη ανθρωπογενής δραστηριότητα που συντελείται στο Θριάσιο Πεδίο, σε συνδυασμό με την θαλάσσια διείσδυση, έχουν συμβάλλει στη συνεχή υποβάθμιση της ποιότητας των υπόγειων νερών με αποτέλεσμα το περιορισμό της δυνατότητας εκμετάλλευσης τους, όχι μόνον για την ανθρώπινη κατανάλωση αλλά και για πολλές άλλες χρήσεις.
Λέξεις Κλειδιά: *Υδροχημεία, βαρέα μέταλλα, φρεάτια υδροφορία, Θριάσιο πεδίο.*

1. Introduction

Thriasion plain is an area characterized by several and intense human activities. Along the coastal zone and in the central part of the area intense building activity takes place, while in the north part the cultivation of vegetables prevails. The uncontrolled installation of various crafts and large industrial units, the operation of the military airport, the dense network of roads with the traffic of heavy vehicles are some features of the area. In recent decades the increased industrial activity has imposed significant environmental pressures in Thriasion Plain. These continual changes in land use, from cultivated land and pastures to industrial use, were not accompanied by the necessary infrastructures and implement measures (sewage treatment, biological waste water treatment, etc.) causing air, soil and groundwater pollution.

Soil studies, which have been conducted in the area of Thriasion plain, have recorded high loads of heavy metals in soil horizons resulting in surface- and groundwater pollution by mobilizing them (Massas *et al.,* 2013). Previous hydrogeological investigations in the study area have shown intense salinization of groundwater, in both coastal and inland region, where the front of seawater intrusion is detected in about 8.5 km away from the coast. At the same distance from the coast is also detected the high pollutant load that characterizes the alluvial aquifer due to various anthropogenic pressures (Kuna *et al.,* 1991; Karavitis *et al.,* 2001, Paraschoudis 2002; Lioni *et al.,* 2008, Iliopoulos *et al.,* 2011, Christides *et al*., 2011). In this paper the results of a hydrogeochemical study conducted in Thriasion plain are presented. The purposes of the study were the investigation of the general groundwater quality, the evolution of the degradation of the groundwater quality from human activities (urban waste, agriculture, livestock, industry, etc.), emphasizing in the presence of heavy metals, as well as the determination of the suitability of water for various uses.

2. Study Area

The study area is located in the northwestern part of Attica (Figure 1). The mountains in the eastern, northern and western part form the relief of the area. The Aigaleo Mt (453m) at the southeastern delimits Thriasion plain from Attica basin. Parnitha Mt. (700m) and Patera Mt (450m) defines Thriasion Plain to the east and north and to the west respectively, while in the south the study area is surrounding by Saronic Gulf. Low altitudes, from 0 to 100 m, dominate in the lowland area of Thriasion plain, which is a paleo-karstic depression older than Quaternary of age. It presents a semicircular shape. During Quaternary it has been filled with fluvial and lacustrine deposits with thickness up to 200m. Low limestone hills outcrop locally in this region. These could be defined as “residual hills” characteristic for the advanced stage of the kartsification of the area.

Geology: The study area belongs geotectonically to Pelagonian Zone and is built up by alpine and post – alpine formations. Alpine formations consist of Triassic-Jurassic dolomitic limestones and limestones of Cretaceous age. The dolomitic limestones consist of thick bedded up to imbedded often dolomitized limestones fragmented, fractured and intensely karstified with a variable thickness of approx 300-700 m. They occur in the eastern, northern and northwestern part of the

region covering most of its surface. The low part of Cretaceous limestones are thin bedded, locally marly, with a thickness of approx. 100m and of Kenomanian age, while the middle part are thick bedded (Touronian age), with intense smell of bitumen and a thickness of approx 80m. Finally the upper part consists of thin bedded limestones that underlie the flysch formation with a thickness of 40m (Senonian age). They occur mainly at the northwestern of Thriasion Plain and at places in the northwestern part of the plain.

The post alpine deposits consist of semi-consolidated Neogene formations and unconsolidated Quaternary deposits. The Neogene formations in the eastern part of Thriasion plain consist at their low parts of alternating layers of lacustrine mainly marls, clays and sandstones, while the upper parts are continental deposits mainly conglomerates and red mud. The Quaternary deposits consist of old Pleistocene and Holocene alluvial deposits.

The Pleistocene sediments covering the northern part of Thriasion Field with a significant thickness of 100m are mostly torrential deposits, pebbles, gravel and sands of various origins. They usually occur with strong diagenesis as breccia-conglomerates including irregular intercalations of sand clays with calcareous debris. The Holocene sediments developed mainly in the coastal zone of Thriasion plain (Dounas *et al.*, 1971; Katsikatsos *et al.*, 1986) comprise clastic material, recent alluvial deposits and recent talus conus with a thickness of about 2 to 10m.

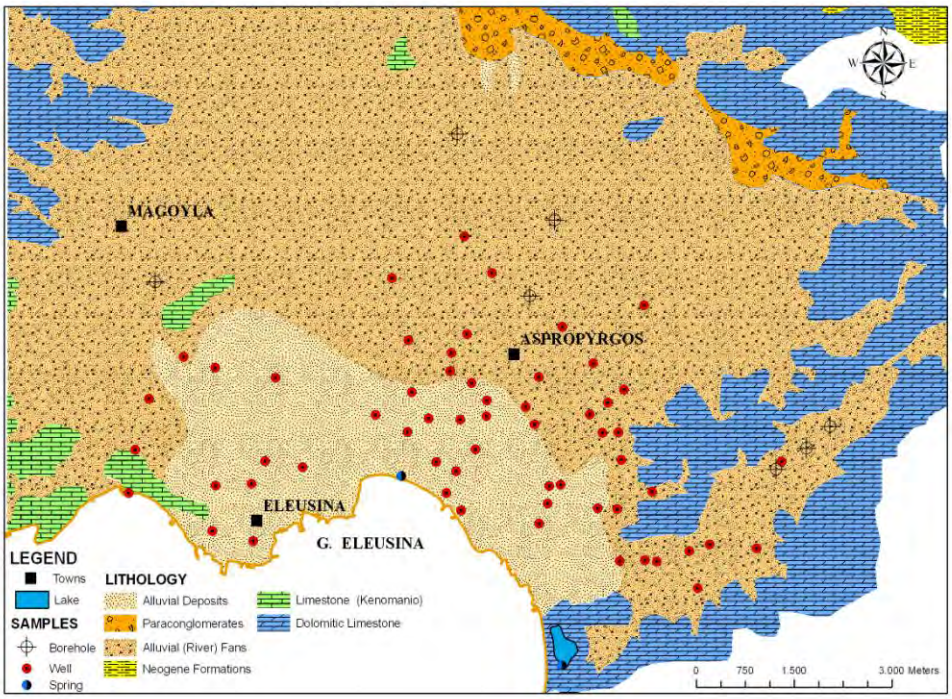

Figure 1 - Geological map of the study area (Digitized by IGME geological map 1:50 000, Sheet Athens to Eleusis (Katsikatsos et al. 1978)) and sampling points.

Hydrogeology: The climate of the study area is characterized as Mediterranean, semi-arid, with mild winters and hot summers. The average annual rainfall ranges between 300 and 400mm, with an average value of 390mm. The average annual temperature varies from 17^{o} C and 19^{o} C. The carbonate formations, which occur in great extent in Thriasion plain, are intensely fragmented and karstified, due to the tectonic activity of the area. Within these formations a highly productive karst aquifer is developed. The average hydraulic conductivity is estimated to be 10^{-3} m/s (Paraschoudis 2002). Paleozoic schist formations are the impermeable bedrock of the karst aquifer.

Coastal and submarine springs at lower topographic places drain the karst aquifer. A significant amount of karst water discharges in Koumoundourou Lake located at the SE part, while another amount of the karst water flows towards the Eleusinian Gulf in the SW part of the plain. Finally karst water flows and feeds lateral the alluvial aquifer. Within the Quaternary deposits a significant aquifer is developed. It undergoes intense exploitation through wells and boreholes for drinking and irrigation purposes. The discharge rate of the wells is over $20m^3$/sec, while the discharge rate of the boreholes ranges from 100 – 150 m^3/h (*Kounis et al., 1991, Parasxoudis 2001)*. The hydraulic conductivity ranges between 10^{-2} m/s and 10^{-4} m/s. The replenishment of the aquifer is realized by the infiltration of the rainwater, the infiltration of surface water, through the coarse sediment of its streambed as well as by the lateral feed of the karst system. In the coastal zone the aquifers adjoin the sea. Moreover the overexploitation of aquifer caused the decrease of the water level. Thus seawater intrusion phenomena occur resulting in the salinization of the groundwater.

3. Hydrochemistry

Material and Methods*:* During the wet period (December 2006) 51 samples from wells and 14 samples from boreholes were collected. The physicochemical parameters, temperature (T), electrical conductivity (EC) and pH, were measured from untreated samples in-situ using the portable devices WTW/LF-330 for electrical conductivity and WTW/330i for pH.

The samples were collected in two different types of polyethylene bottles (100 ml and 1000ml volume). The first bottle type of 100 ml volume was filtered on site through 0.45μm pore size Millipore filters. It was then acidified to a pH about 2 with 65% ultra-pure HNO_3 for heavy metals determination, Cd, Cu, Fe, Mn, Ni, Pb, Sr and Zn (Table 1). The second non-acidified aliquot (1 L volume) was retained to determine major cation analyses and non-metal ions (Ca^{2+}, Mg^{2+}, Na^+, K^+, HCO_3^-, Cl^-, SO_4^{2-} NO_3^-, NH_4^+ and PO_4^{3-}) (Table 1). Total Hardness, Calcium Hardness, Temporal Hardness as well as Cl^- were determined with titration kits. The parameters SO_4^{2-}, NO_3^-, NO_2^-, NH_4^+, PO_4^{3-} and SiO_2 were determined by spectral photometry (HACH DR/3000) using the suitable HACH kits. The parameters Ca^{2+}, Mg^{2+}, Sr, Fe, Mn, Cu, Cr, Ni, Pb, Cd and Zn were determined by atomic absorption spectroscopy (GBC/908AA), while Na^+ και K^+ using Flamephotometer (INTECH/420). All the analyses were conducted at the laboratory of Mineralogy-Geology, Agriculture University of Athens.

Groundwater quality: The groundwater of the study area is characterized by a wide range of physicochemical parameters values. The water of the wells generally presents, except in certain cases, high concentrations of salts (TDS: 535-13,567 mg / l), high hardness (TH: 14.6-165.7 ^{0}dH), high salinization due to seawater intrusion (Na^+: 4.0-4045.9 mg/l, Cl^-: 17.7-7269.7 mg/l and SO_4^{2-}: 8.2-782 mg/l) and high concentrations of compounds of anthropogenic origin (NO_3^-:5.7- 293 mg/l, NH_4^+: 0.01-16.06 mg/l and PO_4^{3-}: 0.10-16 mg/l). The presence of all these elements and compounds reflects the geogenic and anthropogenic influences in the aquifer. The highest concentration is observed in the samples of the wells in the phreatic aquifer, which are located within the residential area, close to industrial units. In the most samples the concentrations exceed the upper allowable limits given by the Directive concerning the water quality for human use (EEC98/83 1998).

As is shown in Piper diagram (Figure 2) groundwater samples are classified mainly in three groups: i) In the first group belong the geo-alkaline waters with Ca-Mg-HCO_3 and Ca-Mg-Na-HCO_3-Cl-SO_4 hydrochemical types. ii) In the second group belong the brackish waters with Na-Cl-HCO_3 and Na-Cl hydrochemical types. They are mixed waters from sea water and karst water. iii) In the third group belong the water samples from wells and boreholes in the lowland of Thriasion plain, which present a geo-alkaline with high percentage of alkaline character. The hydrochemical types Ca-Mg-Na-HCO_3, Ca-Mg-Na-Cl-HCO_3 and Mg-Na-Cl-SO_4-HCO_3 prevail in this group, which exhibit seawater impacts. A small number of samples from boreholes present the

hydrochemical types Ca-HCO_3 and Ca-Mg-HCO_3 revealing the recharge of the area with fresh karst water.
As it shown in Durov diagram (Figure 3) cation – exchange processes (Ca-HCO_3, Mg-HCO_3) and reverse cation - exchange processes (Na-Cl, Mg-Cl and Ca-Cl) take place in the area, while a significant number of the samples undergo mixing from sea water and fresh groundwater.

Table 1 - Results of hydrochemical analyses.

Samples		51 Samples of wells			14 Samples of boreholes		
		min	max	mean	min	Max	mean
Ta	^{0}C	11.5	20.2	16.2	13.5	19.4	17.4
EC	μS/cm	674	23,100	3671	629	3780	1676
pH		7.0	8.27	7.4	7.12	7.9	7.43
Tot. Hardness	^{0}dH	14.6	165.7	53.4	15.7	85.9	38.2
Temp. Hardness	^{0}dH	11.7	41.3	24	15.4	31.1	20.6
Perm. Hardness	^{0}dH	0.0	154	29.7	0.0	68.0	18.8
Ca^{2+}	mg/l	49.6	584.8	189.8	61.6	272.0	135.4
Mg^{2+}	mg/l	10.6	421	115.7	26	286.3	85.4
Na^{+}	mg/l	11.8	4045.9	412.5	29.6	540	129.4
K^{+}	mg/l	0.3	166	17.5	1.9	18	6.9
HCO_3^{-}	mg/l	256.2	899.7	523.9	335.5	677.1	440.3
Cl^{-}	mg/l	39.0	7269.5	821.4	17.7	939.7	346.8
SO_4^{2-}	mg/l	22.8	782	232.8	8.2	268.7	94.2
NO_3^{-}	mg/l	5.7	293	91.3	12.8	239.3	93
NH_4^{+}	mg/l	0.01	16.06	2.85	0.55	4.30	1.74
PO_4^{-}	mg/l	0.1	1.14	0.35	0.12	1.05	0.3
SiO_2	mg/l	0.5	26.4	15.8	9.6	20.8	16.6
Cd	ppm	0.027	0.064	0.046	0.028	0.072	0.049
Cu	ppm	0.058	1.05	0.106	0.061	0.188	0.092
Fe	ppm	0.001	0.636	0.154	0.001	0.279	0.138
Mn	ppm	0.007	0.610	0.085	0.046	0.112	0.077
Ni	ppm	0.001	0.282	0.111	0.001	0.300	0.125
Pb	ppm	0.002	0.417	0.221	0.006	0.454	0.241
Sr	ppm	0.613	4.016	2.281	0.689	2.370	1.925
Zn	ppm	0.001	0.400	0.062	0.005	0.535	0.108
TDS	mg/l	535	13567	2423	770	2714	1353

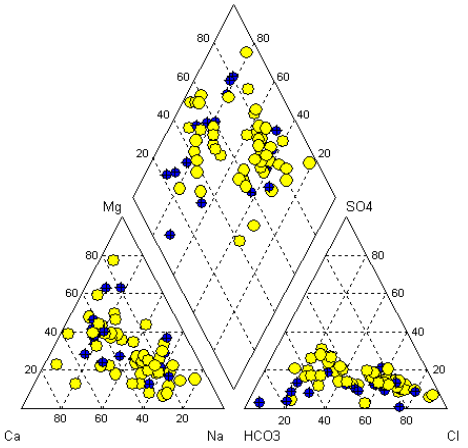

Figure 2 - Classification of groundwaters in the Piper diagram (○: wells. ●: boreholes).

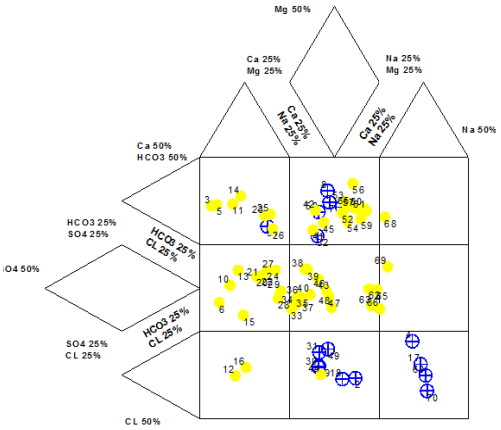

Figure 3 - Classification of groundwaters based on Durov diagram (○: wells. ●: boreholes).

Heavy metals: The groundwaters of the study area present high concentrations of the heavy metals Cd, Cu, Fe, Mn, Ni, Pb, Sr and Zn. The concentration of Fe_{tot} ranges from 0.001 to 0.636ppm, while in 51% of the samples the concentration exceeds 0.2 ppm, the upper limit given by the Directive concerning the water quality for human use (EEC98/83 1998). Mn concentration varies between 0.007 and 0.610ppm, while in 74% of the samples the concentration exceeds 0.05ppm, the upper limit given by the Directive concerning the water quality for human consumption. Ni concentration varies between 0.001 and 0.29ppm, while in 59% of the samples the concentration exceeds 0.02ppm, the upper limit given by the European Directive. All the samples present Cd concentrations between 0.027-0.072ppm exceeding the upper limit of 0.005ppm. The concentration of Pb ranges from 0.002-0.454ppm, presenting in 95% of the samples values above the upper limit of 0.010ppm. The concentrations of Cu and Zn range from 0.058-1.050ppm and 0.001-0.535ppm respectively and do not exceed the upper limits of 2.0 ppm and 5.0ppm respectively (WHO 1993, EU-98/83 1998). The concentration of Sr is high and ranges from 0.613-4.016ppm. It could be attributed to the disillusion of the minerals selestine ($SrSO_4$) and strontianite ($SrCO_3$) included in the sediments and evaporates. The highest concentration of the heavy metals is associated with geogenic factors, such as the occurrences of bauxites, oxides derived from the alteration of rocks and the organic matter within the unconsolidated sediments of the region, which is characterized for its ability to bind the heavy metals. Intense pressures from anthropogenic activities, such as air pollutants from traffic and gas industrial plants, the function of Eleusis military airport, industrial and municipal waste, waste dumps and agricultural crops could also contribute to the significant presence of heavy metals in the groundwaters of the area.

The spatial distribution of heavy metals is shown in Figure 4. The presence of Fe prevails in the west part of the area, while Mn, Ni and Zn occur in the groundwaters in the east part of the area. This could be attributed to the presence of the landfill of Ano - Liosia located at the eastern margins of Thriasion plain. Cd, Cu, Pb and Sr present higher concentrations in the central and north part of the area. Their distribution is associated with both occurrences of bauxite in the north and west of Thriasion Field and the existence of distributed manufacturing units and the lack of waste water treatment facilities.

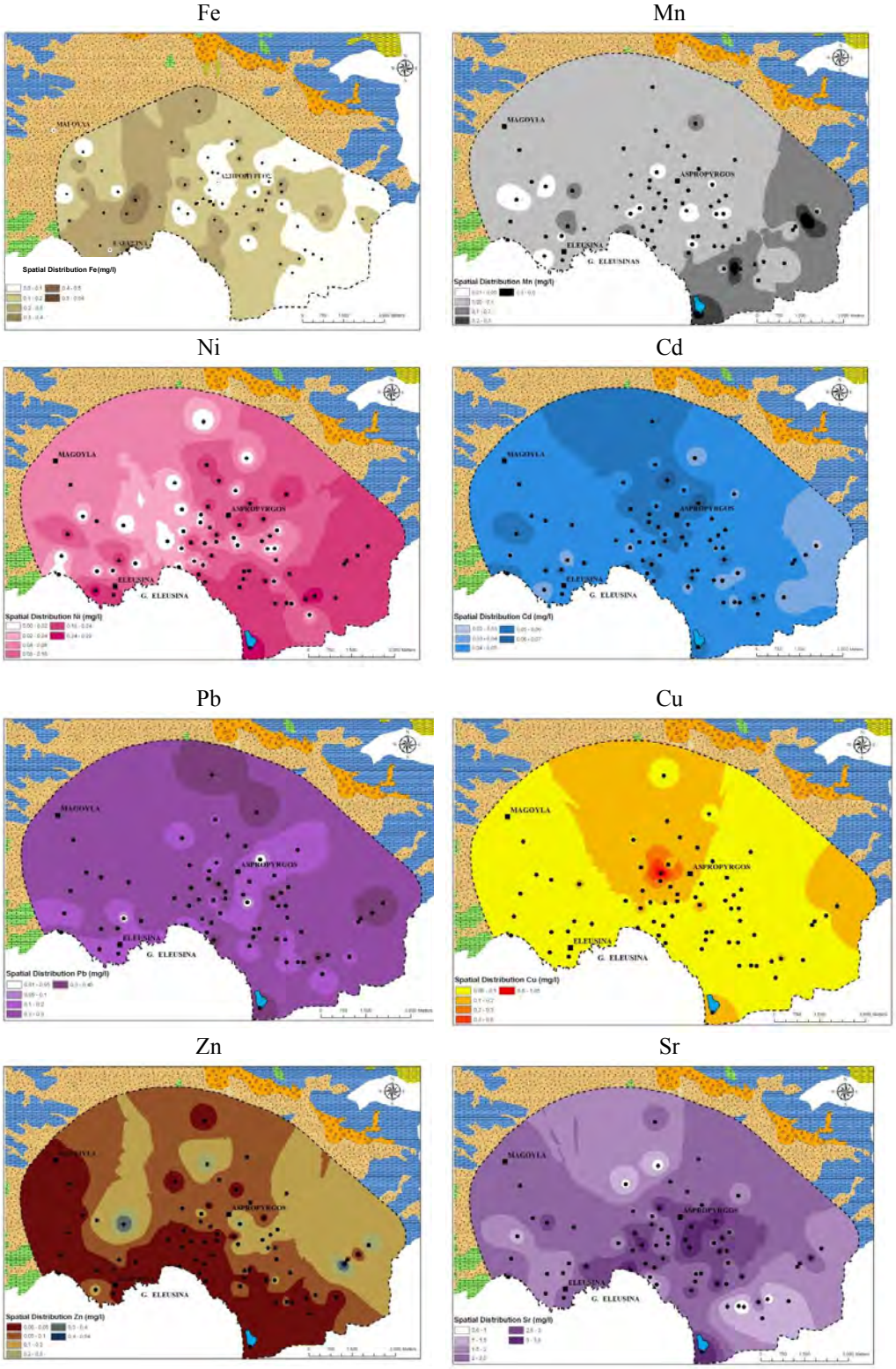

Figure 4 - Spatial distribution of heavy metals in groundwater at the Thriasio plain area. (Fe, Mn, Cd, Pb, Ni, Cu, Zn and Sr).

To detect relationships exist between the various elements and parameters, factor analysis is used with the statistical program SPSS. The method collects data into groups which are called factors. The load factors show how important is the participation of the respective variable factor (Davis 1986).

Table 2 - Results of factor analyses.

Elements	Factor 1	Factor 2	Factor 3	Factor 4
Ca	.230	**.768**	-.123	-.129
Mg	**.724**	.299	-.276	-.110
Na	**.951**	.043	.010	.100
K	**.894**	-.222	.051	.120
Cl	**.953**	.140	-.072	-.003
SO_4	**.866**	.307	-.067	.068
NO_3	-.234	**.794**	-.271	.075
Pb	-.059	.039	.057	**.760**
Zn	-.139	-.002	.100	**-.691**
Ni	-.092	-.162	**.634**	-.049
Mn	.071	-.098	**.689**	.231
Sr	.355	**.731**	.060	.139
Cd	.151	-.035	**-.697**	.340
% of Variance	**32.2**	**15.7**	**12.0**	**10.1**

In Table 2 is shown that the first group, which accounts for 32.2% of the variance in the data matrix connecting the ions Mg^{2+}, Na^{+}, K^{+}, Cl^{-} and SO_4^{2-}. It represents the brackish waters resulting from the seawater intrusion in the aquifers of the study area. The second group accounts for 15.7% of the total variance, connecting elements Ca^{2+}, Sr and NO_3^{-}. The coexistence of these shows the use of fertilizers. The relationship between nitrate and calcium could be explained as ion exchange relationship between the ion of ammonium resulting from the hydrolysis of ammonia fertilizer and calcium that is a component of carbonate minerals in the area. The coexistence of Ca^{2+} and Sr^{2+} is directly related to the chemical affinity of the two elements. The third and fourth groups accounts for 12% and 10.1% of the total variance, respectively. They connect the elements Ni, Mn, Cd, Pb and Zn that could be associated with the dissolution of bauxites and various oxides and obviously with different anthropogenic impacts.

4. Conclusions

Two systems developed in the study area, the karst system that structures the east, north and west margins of the basin and the greatly expanded in size clastic system of Quaternary age. In the coastal zone where the contact of carbonate rocks with the sea is immediate, intense salinization of karst waters takes place. The high concentrations of the main elements and heavy metals reveal the degradation of the alluvial aquifer, which could be attributed to both natural factors and anthropogenic impacts. These concentrations values exceed the upper limits for human consumption and the majority of groundwater samples are characterized as inappropriate. This is attributed to geogenic factors and other anthropogenic impacts, as Thriasion plain undergoes intense environmental pressure from various human activities.

4. References

Christides A., Mavrakis A. and Mitilineou A. 2011. A case of intense seawater intrusion to aquifer of the Thriasio Plain. Greece, *Proceedings of the 12th International Conference on Environmental Science and Technology (12th ICEST)*. Vol B:152-159.

Davis J.C. 1986. Statistics and data analysis in geology, Wiley, New York.

Dounas A. 1971. The geology between Megara and Erithres area. *PhD Thesis,* University of Athens.

EU Council directive 98/83 1998. Council Directive 98/83/EC of the European Parliament on the quality of water intended for human consumption, The European Parliament and the Council of the European Union, Off J L 330.

Iliopoulos V., Stamatis G. and Stournaras G. 2011. Marine and human activity effects on the groundwater quality of Thriasio Plain, Attica, Greece, *Advances in the Research of Aquatic Environment. Environmental Earth Sciences*. 3. 409-416. DOI: 10.1007/978-3-642-24076-8-48.

Karavitis C., Bosdogianni A. and Vlachos E. 2001. Environmental Management approaches and water resources in the stressed region of Thriassion, Greece, Global Nest: *the Int. J*. Vol 3. No 2. p. 131-144.

Katsikatsos G. et al 1986. Geological Map Athens-Eleusis 1:50.000. I.G.M.E.

Kounis G. and Siemos N. 1991. Spot hydrogeological investigation of the aquifers of Thriassio Plain for supply of Hellenic Petroleum Company, IGME.

Lioni A. Stournaras G. and Stamatis G. 2008. Degradation of Groundwater quality of Thriassio Plain through Natural Factors and human activity. *Proceedings* of the 8th Hydrogeological Congress of Greece. vol.2 p.577.

Massas I., Kalivas D., Ehaliotis C. and Gasparatos D. 2013. Total and available heavy metal concentrations in soils of the Thriassio Plain (Greece) and assessment of soil pollution indexes, *Environ Monit Assess*.

Paraschoudis B. 2002. Hydrogeological study of West Attica, *Unpublished report,* Ministry of Agriculture

WHO 1993. Guidelines for drinking water quality. vol.1. 2nd ed. World Health Organization. Geneva.

Δελτίο της Ελληνικής Γεωλογικής Εταιρίας, τομ. XLVII , 2013
Πρακτικά 13ου Διεθνούς Συνεδρίου, Χανιά, Σεπτ. 2013

Bulletin of the Geological Society of Greece, vol. XLVII 2013
Proceedings of the 13th International Congress, Chania, Sept. 2013

SPATIAL – TEMPORAL ANALYSIS, VARIATION AND DISTRIBUTION OF PRECIPITATION IN THE WATER DISTRICT OF CENTRAL – EASTERN GREECE

Lappas I.[1], Tsioumas V.[1] and Zorapas V.[1]

[1]National Centre of Sustainable Development – Institute of Geology and Mineral Exploration, Sector of Water Resources and Environment, Department of Hydrogeology, 13677 Acharnai, Athens, Greece

Abstract

In this study, the spatial and temporal distribution of precipitation in the Water District of Central – Eastern Greece is investigated for the 42-year period (1968 – 2009) by using monthly mean data from 35 rainfall gauges, with adequate spatial coverage. The basic objective is to infer the pattern of spatial variation of rainfall over the study area based on meteorological observations. The accurate estimation of rainfall's spatial distribution is needed whenever hydrological modelling is undertaken at the watershed scale for model calibration and validation. By using timeseries analysis and geostatistical methods, the regional and seasonal precipitation change and regime of this region during over 40 years is analyzed. However, this input is subject to uncertainty due to the random nature of rainfall. For all stations, uniformity checking and appropriate completion (where needed) took place and it appears that orography plays significant role as far the amount of rainfall is concerned. The results indicate that high variations in regional rainfall estimation occur in the mountainous areas, while the variance decreases in shadow areas in all seasons. The analysis of rainfall showed that there exists a wide variation in the rainfall amounts with variation from 382.4mm to 1397mm with a significantly decreasing trend.

Key words: *Regional – seasonal variation, timeseries analysis, trends, geostatistical methods, orography.*

Περίληψη

Στη μελέτη αυτή, η χωρική και χρονική κατανομή των βροχοπτώσεων στο υδατικό διαμέρισμα της Κεντρικής – Ανατολικής Ελλάδα διερευνάται για μια περίοδο 42 ετών (1968 – 2009) χρησιμοποιώντας μέσα μηνιαία δεδομένα από 35 βροχομετρικούς σταθμούς, με επαρκή γεωγραφική κάλυψη. Ο βασικός στόχος είναι να απεικονισθεί η χωρική μεταβολή των βροχοπτώσεων πάνω από την περιοχή μελέτης, με βάση μετεωρολογικές παρατηρήσεις. Η ακριβής εκτίμηση της χωρικής κατανομής της βροχής είναι απαραίτητη κάθε φορά, που υδρολογικά μοντέλα γίνονται σε κλίμακα λεκανών απορροής για την βαθμονόμηση και την επαλήθευσή τους. Με τη χρήση ανάλυσης χρονοσειρών και γεωστατιστικών μεθόδων, διερευνάται η εποχιακή μεταβολή των κατακρημνισμάτων κατά τη διάρκεια των 40 ετών. Ωστόσο, αυτή υπόκειται σε αβεβαιότητα λόγω της τυχαίας φύσης των βροχοπτώσεων. Για όλους τους σταθμούς έλαβε χώρα έλεγχος της ομοιομορφίας και κατάλληλη ολοκλήρωση (όπου απαιτήθηκε) και φάνηκε ότι η ορεογραφία παίζει σημαντικό ρόλο, σε ό,τι

αφορά το ύψος των βροχοπτώσεων. Τα αποτελέσματα δείχνουν ότι οι υψηλές διακυμάνσεις στην εκτίμηση της βροχής συμβαίνουν στις ορεινές περιοχές, ενώ η διακύμανση μειώνεται σταδιακά σε ομβροσκιερές περιοχές σε όλες τις εποχές. Η ανάλυση των βροχοπτώσεων έδειξε ότι υπάρχει μεγάλη διακύμανση στα ποσά της βροχόπτωσης κυμαινόμενα από 382.4mm έως 1397mm, με σημαντικά πτωτική τάση.
Λέξεις κλειδιά: *Εποχική μεταβολή, ανάλυση χρονοσειράς, τάσεις, γεωστατιστικές μέθοδοι, ορεογραφία.*

1. Introduction

Climate change is one of the most critical issues for scientists from many areas, owing to its potentially serious global effects on both natural environment and human life. Today, climatic change has direct effects on increasing global temperature, altered precipitation patterns, melting glaciers and rising sea level (Hultstrand et al., 2008). The spatial and temporal distribution is crucial for advancing our ability to model and predict weather and climate changes. Its distribution is also important for water management, agriculture, electrical power, flood control, drought and flood monitoring on all spatial scales (Kusre, 2012).

Precipitation data are recorded by meteorological stations and rainfall gauges and the interpolation of climate data took place using several methods, such as graphical methods, including precipitation – elevation analysis and isohyets mapping (Subyani, 2004). Numerical methods including optimal interpolation such as kriging and its variants were developed in an attempt to spatially distribute rainfall. Analyzing the trend of climatic timeseries data is a methodology allowing the understanding of a potential trend in a given period of time. Identifying ascending or descending trends in climatic variables requires specific techniques, owing to the random values of climatic data. Predictions of average, maximum and minimum rainfall changes within the study area point to different patterns based on the location of regions. The aim of this study is to estimate the spatial distribution of long-term precipitation data obtained from 48 meteorological and rainfall stations and to identify trends on an annual, seasonal and monthly scale between 1968 and 2009.

2. Data Sources, Acquisition and Preparation. Research Methodology

The study is based on monthly precipitation data from 48 meteorological / rainfall stations situated across the Water District of Eastern – Central Greece where the investigated period is 1968-2009. The variability of seasonality for this climatic parameter is investigated as well as the irregularity of monthly precipitation distribution is analyzed providing a tool to determine the degree of climate's continentally character (Hatzianastassiou, 2008). Monthly rain gauge datasets are distributed irregularly throughout the Water District, but with a fairly good uniform density (Figure 1, left). The monthly mean precipitation timeseries are provided by the Hellenic National Meteorological Service (HNMS), the Ministry of Agricultural Development and Food (MADF) and the Ministry of Environment, Energy and Climate Change (MEECC). It is pointed out that several meteorological / rainfall stations beyond the Water District's limits have been taken into account in order to obtain a more representative picture of precipitation's spatial distribution (Figure 1, left).

In case there are missing data in the timeseries the following procedure is applied: first, the corresponding monthly mean substitutes the missing values; second, the correlation matrix is computed among the timeseries in order to select the surrounding timeseries with characteristics that most closely resemble those of the station with missing data; a linear spatial regression is then derived to interpolate the missing values so as to create reference timeseries for testing inhomogeneities. The statistical behaviour of the timeseries can be described on the basis of mean, maximum and minimum value, range, median, standard deviation, coefficients of skewness and kurtosis taken as measure of variability. Statistical analysis consists of a) sample concentration using histograms and empirical distribution functions, b) theoretical model adaptation (selection of

a suitable distribution function, parameters' estimation and statistical control and adaptation), c) statistical forecast (variable estimation for a given return period or exceedance probability) and d) use of theoretical distributions for stochastic simulation procedures (Petalas, 2004).

The distribution of precipitation reveals strong gradients, with higher values corresponding to the West and North (over 1,100mm/yr) and lower values obtained towards the Southeast (below 400mm/yr). There are also inland regions with a relatively low precipitation regime.

3. Study Area's Location and Geomorphology

The Water District of Eastern – Central Greece administratively belongs to the Eastern Greece Prefecture, with longitude between $21^0 49' - 24^0 37'$ and latitude between $37^0 55' - 39^0 19'$

The Water District's total area is approximately $12.23 \times 10^3 km^2$, where the mainland is bounded by the mountains of Orthris, Timphristos, Giona – Parnassos and Parnitha from the North, Northwest, Southwest and Southeast respectively. The rest of the area is surrounded by sea (Figure 1, left). The maximum elevation of the Water District is 2,431m, with the average elevation being at 417.5m, while the elevation 50% reaches 237m. The mountainous areas occupy a total of 9.2%, the semi-mountainous zone represents 14.9%, while the hills and valleys cover 38.8% και 37.1% respectively mostly concerning the coastal areas. In conclusion, the area's topographic relief can be considered flat to hilly. Analyzing the elevations of the study area's relief it is concluded that 20.2% of the total area concerns the altitude of 0-100m, 42.0% the altitude of 100-400m, 19.0% the altitude of 400-700m, 9.6% the altitude of 700-1000m and 9.2% the altitude over 900m (Figure 1, right). Finally, the prevailing geomorphological slopes are of the order of $0\text{-}10^0$ with percentage of 57.6% followed by those with values of $10\text{-}20^0$ (27.7%), $20\text{-}30^0$ (12.1%) and $30\text{-}45^0$ (2.5%), while slopes over 45^0 participate only with percentage of 0.04%.

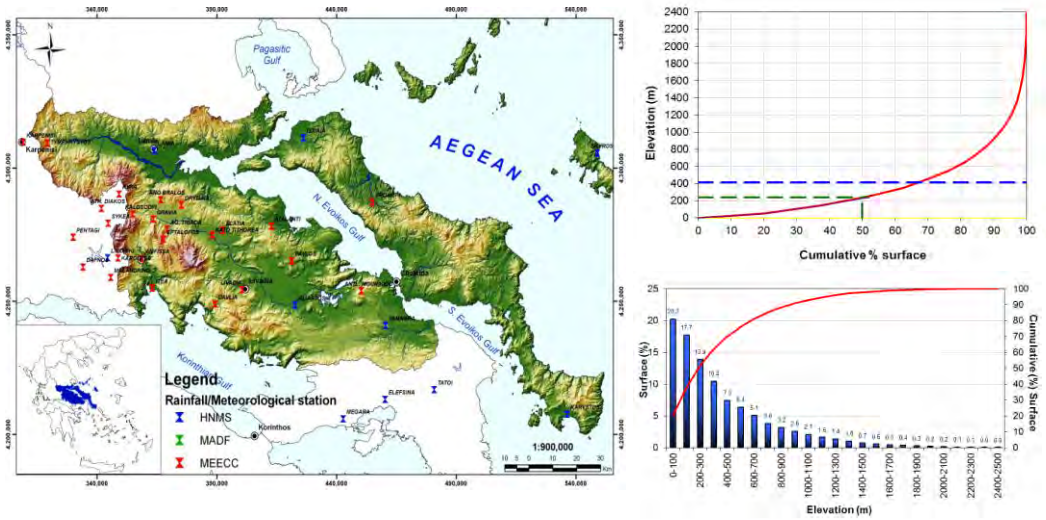

Figure 1 - (left) Geomorphological relief and rainfall / meteorological stations' geographical distribution of the Eastern – Central Greece Water District, (right) elevation vs. cumulative surface curve as well percentage of surface per 100m elevation.

4. Monthly, Seasonal and Annual Distribution of Precipitation Data

Processing of precipitation on a monthly basis was performed in order to determine those months with the greatest rainfall values contributing to the groundwater replenishment within the study area. The below histogram (Figure 2, left) shows that the most wet and humid month of the year is December followed by November and January. Instead, the months with the lowest rainfall are

July, August and June. Also, it can be shown that the major rainfall events start in October, reach their peak in December and remain at high levels until March. It has to be mentioned that some of the rainfall stations did not have continuous data for the 42-year period, so firstly the nearest stations (with almost similar geographical characteristics) with the strongest correlation were used in order to fill the missing data (double mass curve and regression functions with r>0.7).

In Pie chart (Figure 2, right) the seasonal rainfall distribution of all the stations is illustrated. As seen, winter accumulates precipitation at a rate of 40.4%, followed by 37.2% during fall, spring rate by 15.2%, while during summer season rainfall takes place only by 7.1%. Evaluating the two basic periods of a hydrological year (wet and dry) it seems that 77.6% of annual precipitation corresponds to wet period and only 22.3% to the dry one. Concerning the mean overannual rainfall (Figure 3), the highest values are recorded at Ath. Diakos, Dafnos, Pira and Pedayi gauges, while the lowest ones at Skyros, Mouriki, Itea, Megara and Elefsina stations. The arithmetic mean annual precipitation of the study area is 819.1mm, while the average rainfall values range between 1,397mm (Ath. Diakos station) and 382.4mm (Elefsina station). Based on the median value the rainfall stations with the highest and lowest values are the same as those mentioned above (Figure 4). Finally, as far as the highest and the lowest annually recorded rain values are concerned, Megara station represents the minimum annual rainfall (114.1mm in the year 1989), while Ath. Diakos rain gauge represents the maximum one (2,196.8mm in the year 1987).

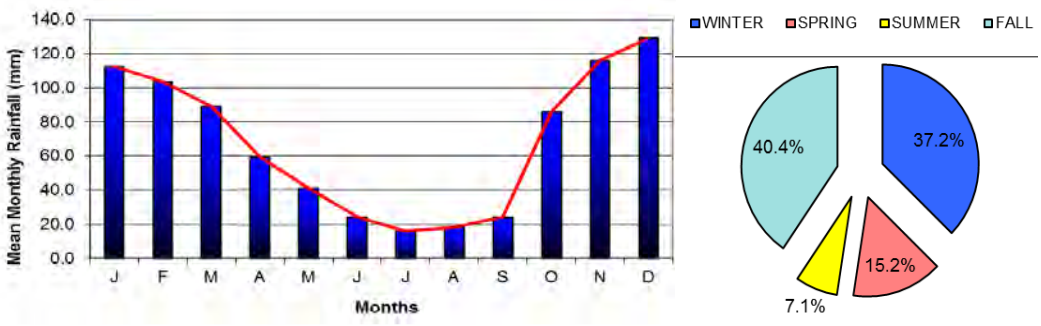

Figure 2 - (left) Histogram of monthly precipitation distribution, (right) pie of seasonal precipitation distribution within the Water District of Eastern – Central Greece.

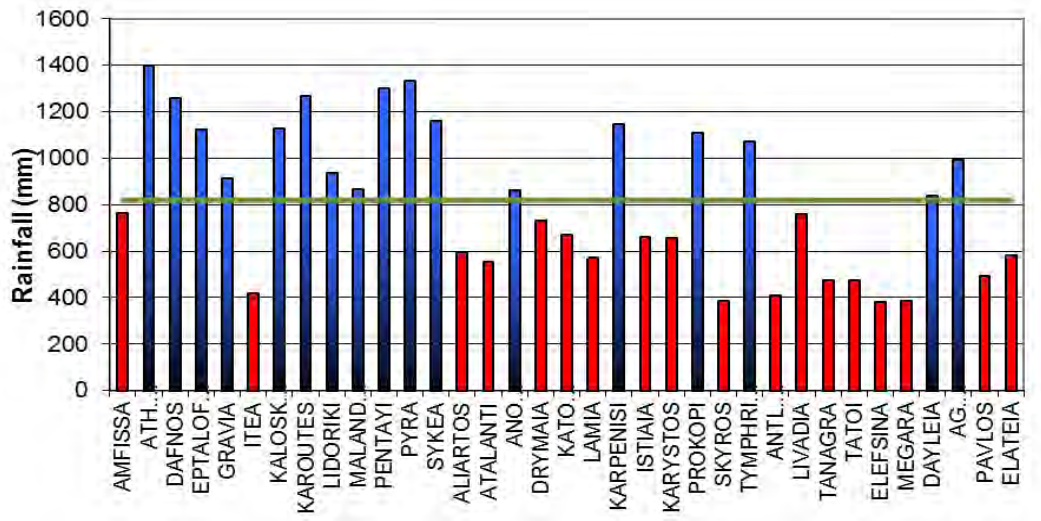

Figure 3 - Mean overannual precipitation of the stations within the study area. The thick green line corresponds to the arithmetic mean rainfall (819.1mm).

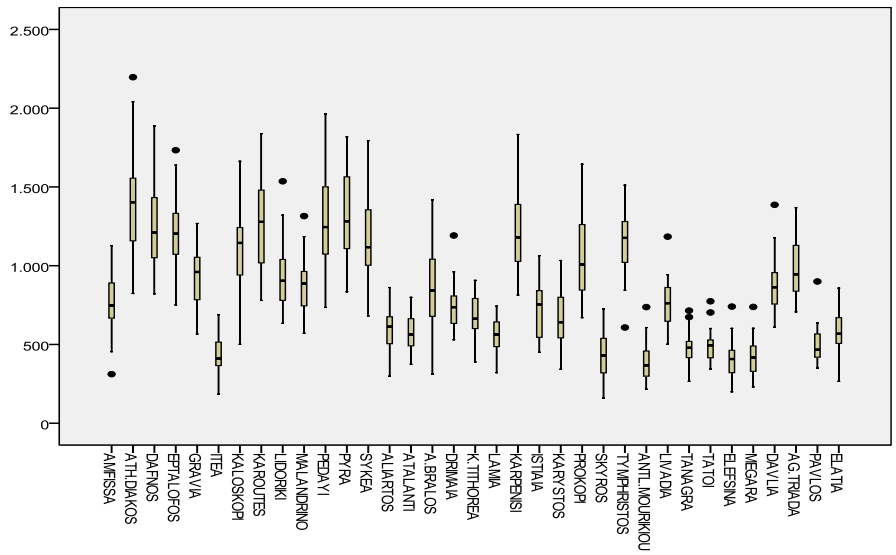

Figure 4 - Boxplot of the annual rainfall of the study area's stations. The linear extensions represent the highest and lowest observed values, the upper and lower limit of the box the percentiles of 75% and 25% respectively and the solid circles the outliers.

The key factor that affects the annual rainfall of a region is the land surface elevation. Thus, an estimation and identification effort of a mathematical relationship correlating rainfall with altitude is made within the study area. Evaluating the rainfall data from all the rain stations it seems that correlation coefficient between rainfall and stations' altitude is quite low (r^2=0.57) having applied the least squares method. Thus, it is obvious to determine two different regression functions: the one belonging to inland of Eastern – Central Greece and the other to Evia region with Sporades islands. The regression functions are expressed by the following equations:

Equation 1 - Regression functions between rainfall and elevation

P = 0.80Z + 452.6 (inland region)
P = 0.83Z + 444.4 (Evia and Sporades islands)

where P the rainfall and Z the elevation of each station. In both cases, the correlation coefficient is satisfactory ($r^2 \geq 0.70$), as it seems that besides the elevation there are other local factors (e.g. stations exposure on air masses, proximity to the sea, complex topographic relief with valleys and mountains etc.) that affect the precipitation values. From the first equation it is concluded that rainfall increases by 80mm every 100m of elevation, while the mean annual rainfall at sea level is 452.6mm (Figure 5, left). Similarly, in the second equation precipitation increases by 83mm every 100m of elevation, while the mean annual rainfall at sea level is 444.4mm (Figure 5, right).

It has to be mentioned that the second regression function (Evia and Sporades islands) is derived by very few rain stations (4) due to lack of reliable data from other rain gauges (no adequate data and very poor correlation, that is, r^2<0.5) thus, being under further discussion, analysis and research. Subsequently, the mean surface rainfall distribution is calculated with the geostatistical method Ordinary kriging (Figure 6, left). In addition, the variation between rainfall and stations' elevation is illustrated (Figure 6, right) using the above regression functions.

One of the most basic rainfall analyses is the statistical distribution in time so as to thoroughly examine the rainfall variation in an overannual scale and the various trends occurring in a given return period (Baltas, 2007). In Figure 7, the overannual precipitation variation and trend of the indicatively chosen meteorological / rainfall stations are depicted and as a result there is an obvious rainfall decline, making the groundwater replenishment even more difficult.

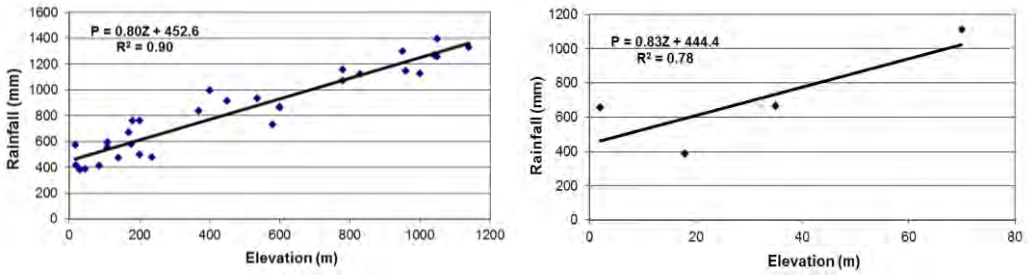

Figure 5 - Regression functions between rainfall and elevation for the inland region (left) and for Evia region and Sporades islands (right).

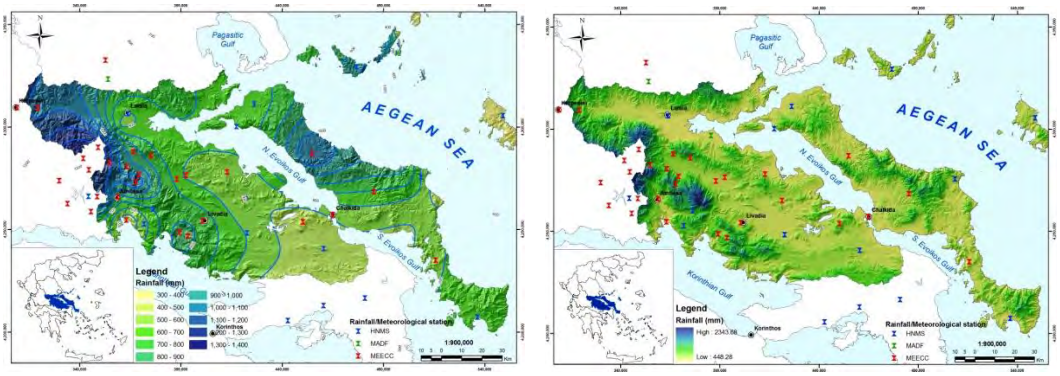

Figure 6 - (left) Surface rainfall distribution within the study area based on the geostatistical method Ordinary kriging, (right) precipitation – elevation variation using the regression functions.

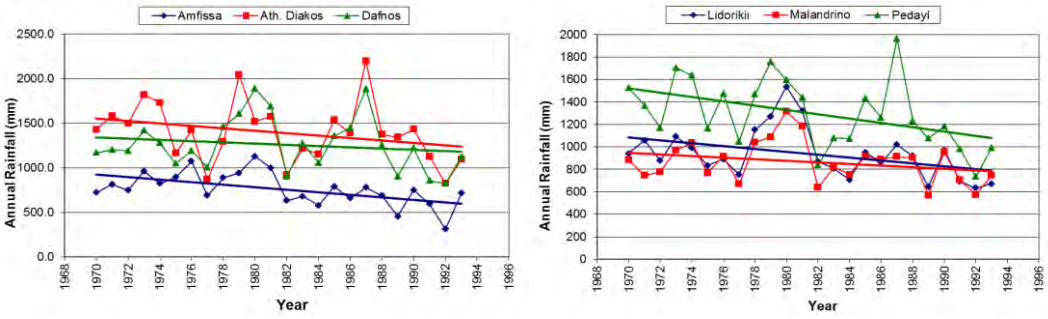

Figure 7 - Mean annual rainfall fluctuation for indicative meteorological stations in the Eastern – Central Greece Water District.

5. Probable Maximum Precipitation – PMP

Probable maximum precipitation represents the worst possible weather event and is the theoretical maximum rainfall of specific duration occurred but not exceeded in a given area, at a given location and time of year and under well – known meteorological conditions. One way of calculating PMP is the statistical method by Hershfield (Chen, 2007, Keramaris, 2008). This method is based upon the statistical characteristics (mean and standard deviation) of the annual maximum rainfall timeseries of a meteorological station. According to this method, the point PMP estimation h_m is directly derived by the mean value h and standard deviationη s_H of the annual maximum precipitation sample, namely by applying the following equation (Figure 8):

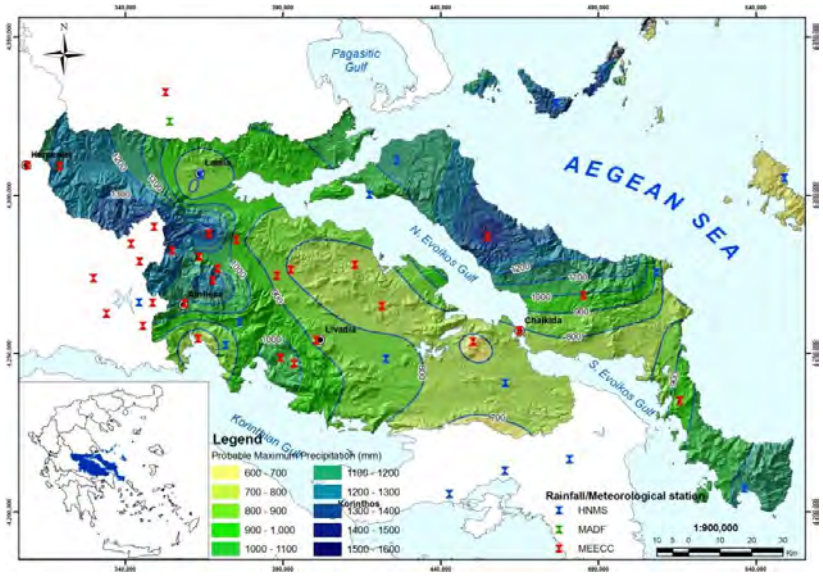

Figure 8 - Surface distribution of Probable Maximum Precipitation within the study area according to the geostatistical method Ordinary kriging.

Equation 2 - PMP calculation by Hershfield

$$h_m = \bar{h} + k_m \cdot s_H$$

where k_m is a dimensionless coefficient given by the following equation based on many rainfall samples statistical analysis:

Equation 3 - Calculation of the dimensionless coefficient k_m

$$k_m = 20 - \ln\left(\frac{\bar{h}}{130} + 1\right) \cdot \left(\frac{24}{d}\right)^{0.4} \quad (\bar{h} \text{ in mm, d in hours})$$

It has to be mentioned that PMP estimation, derived by the above equations, is refered to the point rainfall (Bostan, 2010, Fu, 2009).

6. Climatic Characteristics

Analyzing the study area's climatic characteristics, correlation between air temperature and rainfall takes place, so as the dry months to be determined according to Gaussen and De Martonne equations, while SPI (Standardized Precipitation Index) is determined based on rainfall data. Finally, the region is climatically classified according to Köppen and Thornthwaite classifications. Monthly Drought index by De Martonne is given by the following equation (Baltas, 2007, 2008):

Equation 4 - Monthly drought index by De Martonne

$$I_{DM} = 12P_m / (T_m + 10)$$

where P_m is the monthly rainfall in mm and T_m the mean monthly air temperature in ^{0}C.

The value $I_{DM} = 20$ defines, according to De Martonne, a limit under which the ground soil has irrigation needs. The annual temperature range and the mean annual rainfall of each station are taken into account in order to apply the above equation. The monthly index I_{DM} is applied for each month based on mean monthly temperature and rainfall data for each gauge (the mean value of

each month was calculated). Indicatively, only two rain stations are demonstrated in this paper due to lack of space, covering the one a mountainous area and the other a valley one to clearly show the meteorological and climatological spatial – temporal variation. From Figure 9, above (a, b), it seems that at Lamia station during the period from April to September – October the Drought index I_{DM} is lower than 20, which means that the ground soil needs to be irrigated. Accordingly, at Lidoriki station the ground soil needs irrigation from May to September. As far as the rest of the rain gauges is concerned, those covering the mountainous areas have similar characteristics with Lidoriki rain station and the ones located to semi-mountainous and valley areas behave like Lamia station, that is, irrigation period from April to September.

According to Gaussen, a month is considered dry when P<2T, where P and T are the mean monthly rainfall and temperature respectively. In order to examine the Gaussen criterion (Figure 9, below, c, d), the unit of the rainfall axis should be twice that of the air temperature one (2mm of rain correspond to 1^0C). As it seems at Lidoriki station the dry months are represented by June until September, while at Lamia one, the driest months are represented by May until September.

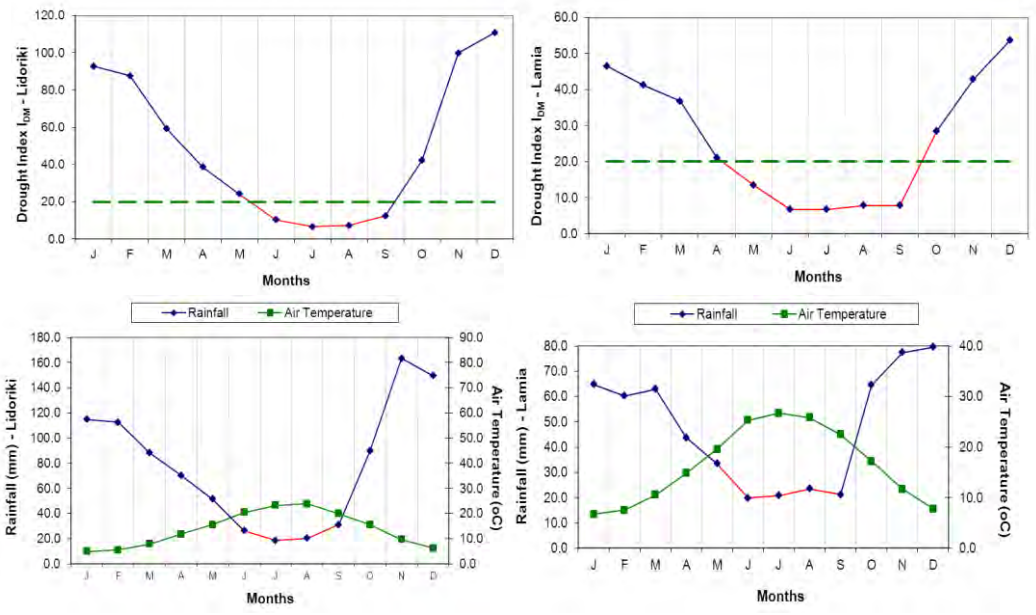

Figure 9 - (above) Monthly variation of Drought index I_{DM} according to De Martonne at Lidoriki and Lamia rain stations (a, b), (below) rainfall and air temperature correlation at Lidoriki and Lamia stations according to Gaussen criterion (c, d).

SPI is a drought indication quantifying the precipitation deficit for different time periods, thus reflecting its influence on the groundwater resources availability within a region. The mathematical relationship giving SPI is the following:

Equation 5 – Standard Precipitation index (SPI)

$$SPI = (X_i - \overline{X})/\sigma$$

where Xi is the precipitation during the year i, $\overline{X}$ the mean rainfall for a specific time period and σ the standard deviation of rainfall during the specific time period. SPI takes both negative and positive values, from which the first ones correspond to drought events, while the second ones represent wet and humid events. From Figure 10, it seems that during the period 1988 – 1992 there is an extensive moderate to severe drought, unlike other years which occurs periodically a rotation between dry and wet periods.

Köppen climatic classification is based upon the statistical analysis of the climate impact on several factors such as temperature and rainfall regime. According to Köppen classification, the majority of weather stations belong to Csa climatic type. This type represents the Mediterranean climate characterized by mild, wet winters and mild, warm and dry summers due to the impact of subtropical anticyclones.

Thornthwaite climatic classification studies the relationship between vegetation and climate of each region and determines the temperature effect as well as the rain effectiveness. The rain effectiveness upon the vegetation is a function of rain and evaporation. According to this classification, the study area's climate is considered semi-arid to arid and dry, sometimes strongly influenced by the sea (Figure 11).

As mentioned before, only two (2) indicative rain stations, due to lack of space, were used covering both mountainous and lowland areas in order to determine the spatial and temporal difference and variation between the rain gauges within the Eastern – Central Greece Water District. The rest rain gauges follow, more or less, the same meteorological pattern depending on the elevation for each station.

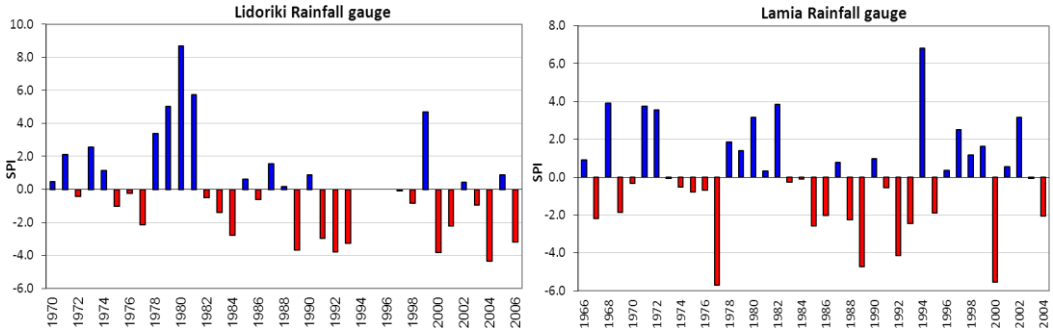

Figure 10 - Annual variation of SPI to indicative rainfall gauges at the Eastern – Central Greece Water District.

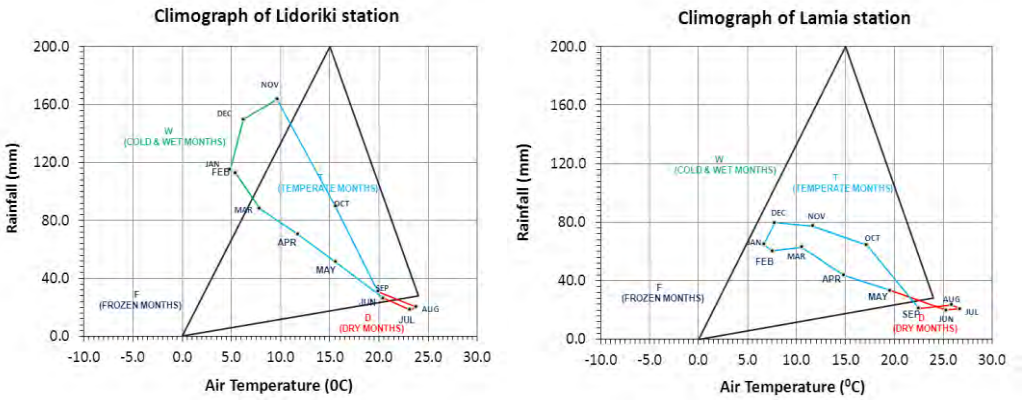

Figure 11 - Climograph of rainfall – temperature at Lidoriki (left) and Lamia stations (right).

7. Conclusions – Remarks

At the Water District of Eastern – Central Greece there is a satisfactory number of meteorological / rainfall stations which enables to deliver the most important statistical characteristics of monthly, seasonal and annual rainfall. The arithmetic mean annual precipitation is 819.1mm with a distinct

rainfall differentiation between the mountainous and lowland gauges because of the intense topographic relief and rain's orographic role. Generally, a significant decline in precipitation may be observed throughout the stations' operation. Specifically:

- The time period from November to January is the rainiest, while the driest one is between June and August. During a hydrological cycle the months with the highest rainfall (wet period) thus replenishing the groundwater resources are October until March (>90mm for each month).
- The regression functions determined by the equations $P=0.80Z+452.6$ and $P=0.83Z+444.4$ for the inland region and Evia as well Sporades islands respectively, have significant correlation coefficient (over 70% in both cases). Where no sufficient data exist there should be made further discussion, analysis and thorough exploration and research.

8. Acknowledgements

The authors would like to thank the Hellenic National Meteorological Service, the Ministry of Agriculture Development and Food and the Ministry of Environment, Energy and Climate Change for the precipitation and temperature data provided for the accomplishment of the present study.

9. References

Baltas E. 2007. Spatial Distribution of Climatic Indices in Northern Greece, *Meteorological Applications*, 14, 69-78 pp.

Baltas E. 2008. Investigation of the Spatial – Temporal Distribution of Climatic Parameters in Greece, *8th International Hydrogeological Congress of Greece – 3rd MEM Workshop on Fissured Rocks Hydrology*, Athens.

Bostan P. and Akyürek Z. 2010. Spatio-Temporal Analysis of Precipitation and Temperature Distribution over Turkey, *The International Archives of the Photogrammetry, Remote Sensing and Spatial Information Sciences*, Vol. 38, Part II. *14th International Symposium on Spatial Data Handling*.

Chen X. and Liu D. 2007. Spatial Distribution and Temporal Variation of Rainfall in Guangdong Province, China, *Methodology in Hydrology*, *Proceedings of the Second International Symposium on Methodology in Hydrology*, IAHS Publ. 311, 491–497 pp.

Fu C., Xie J., Liu Z., Wang M., and Liu Y. 2009. A Study of Spatial and Temporal Distribution Law about Temperature and Precipitation in the Northeast of China, *Remote Sensing and GIS Data Processing and Other Applications*.

Hatzianastassiou N., Katsoulis B., Pnefmatikos J., and Antakis V. 2008. Spatial and Temporal Variation of Precipitation in Greece and Surrounding Regions Based on Global Precipitation Climatology Project Data, *Journal of Climate*, Vol. 21.

Hultstrand D., Parzybok T., Tomlinson E. and Kappel B. 2008. Advanced Spatial and Temporal Rainfall Analyses for Use in Watershed Models, *The Third Interagency Conference on Research in the Watersheds*.

Keramaris E. 2008. Study of Distribution Time of Rainfalls in Greece. *8th International Hydrogeological Congress of Greece – 3rd MEM Workshop on Fissured Rocks Hydrology*, Athens.

Kusre C. and Singh S. 2012. Study of Spatial and Temporal Distribution of Rainfall in Nagaland (India), *International Journal of Geomatics and Geosciences*, Vol.2, No.3.

Petalas C., Pliakas F., Diamantis I. and Kallioras A. 2004. Study of the Distribution of Precipitation in District of Eastern Macedonia and Thrace for the Period 1964 – 1998, *Bulletin of Greek Geological Society*. *Proceedings of the 10th International Congress*, Thessaloniki.

Subyani A. 2004. Geostatistical Study of Annual and Seasonal Mean Rainfall Patterns in Southwest Saudi Arabia, *Hydrological Sciences, 49(5)*.

Δελτίο της Ελληνικής Γεωλογικής Εταιρίας, τομ. XLVII , 2013
Πρακτικά 13ου Διεθνούς Συνεδρίου, Χανιά, Σεπτ. 2013

Bulletin of the Geological Society of Greece, vol. XLVII 2013
Proceedings of the 13th International Congress, Chania, Sept. 2013

ANALYSIS OF TEMPORAL HYDROCHEMICAL AND ISOTOPIC VARIATIONS IN SPRING WATERS OF EASTERN PELOPONNESUS (GREECE)

Matiatos I. and Alexopoulos A.

Faculty of Geology and Geoenvironment – National and Kapodistrian University of Athens, 15784 Panepistimiopolis, Athens, Greece

Abstract

The temporal variation of groundwater hydrochemistry has been used to support observations on the nature of groundwater circulation inside geological terrains of various lithological formations in Eastern Peloponnesus. In the present study, variations in groundwater physical-chemical properties such as electric conductivity, CO_2 partial pressure, and calcite saturation index were used to give indications with regard to the nature of the geological formation, the groundwater residence time, and the mode of water circulation inside the hydrogeological systems. Additional isotopic values ($\delta^{18}O$) were defined in order to support the aforementioned objectives. The seasonal variations of these properties during three years of monitoring were determined for individual springs appearing in the geological setting of Argolis peninsula, which is mostly composed of carbonate (karstificated in places), ophiolitic and flysch formations. The variation of the parameters was also approached by calculating the coefficient of variation used to detect whether the groundwater flow is of diffuse or/and conduit type. Coefficient of variation values of less than 5% were considered as indicative of the diffuse flow type and therefore a long contact residence time, while higher values were associated with fast-flowing water. However, the isotopic measurements and the overall hydrochemical analysis combined with in situ observations, related to the flow characteristics of the springs, revealed that a spring can be fed by a common diffuse type system although it shows a rather high coefficient of variation.
Key words: *Coefficient of variation, hydrochemistry, stable isotopes, groundwater, flow system.*

Περίληψη

Η χρονική μεταβολή των υδροχημικών παραμέτρων των υπόγειων νερών αποτελεί ένα χρήσιμο εργαλείο για την ερμηνεία της κυκλοφορίας του νερού μέσα σε λιθολογικά διαφορετικούς γεωλογικούς σχηματισμούς στην ανατολική Πελοπόννησο. Στην παρούσα μελέτη, εξετάστηκαν οι χρονικές διακυμάνσεις διαφόρων φυσικών-χημικών παραμέτρων του υπόγειου νερού, όπως η ηλεκτρική αγωγιμότητα, η μερική πίεση του CO_2, ο δείκτης κορεσμού σε ασβεστίτη προκειμένου να δώσουν πληροφορίες σχετικά με τη φύση του γεωλογικού σχηματισμού, το χρόνο παραμονής των υπογείων υδάτων, καθώς και το είδος της κυκλοφορίας του νερού μέσα στα διάφορα υδρογεωλογικά συστήματα. Ταυτόχρονα, προσδιορίστηκαν οι χρονικές μεταβολές των σταθερών ισοτόπων ($\delta^{18}O$) με στόχο την περαιτέρω υποστήριξη των

συμπερασμάτων. Οι εποχιακές διακυμάνσεις όλων των εξεταζόμενων μεταβλητών κατά τη διάρκεια τριών ετών προσδιορίστηκαν για ανεξάρτητες πηγές που εντοπίζονται στο γεωλογικό περιβάλλον της χερσονήσου της Αργολίδας, η οποία συνίσταται ως επί το πλείστον από ανθρακικούς (καρστικοποιημένους κατά θέσεις), οφιολιθικούς και φλυσχικούς σχηματισμούς. Για τη μελέτη της χρονικής διακύμανσης των παραμέτρων προσδιορίστηκε επίσης ο συντελεστής μεταβλητότητας ο οποίος χρησιμοποιείται για να διαπιστωθεί αν η ροή του υπόγειου νερού είναι διάχυτης μορφής ή/και λαμβάνει χώρα μέσα σε αγωγούς. Τιμές του συντελεστή μεταβλητότητας μικρότερες από 5% θεωρούνται ενδεικτικές της ροής διάχυτης μορφής και, συνεπώς, ενός μεγαλύτερου χρόνου παραμονής του νερού στο υπέδαφος, ενώ οι υψηλότερες τιμές του συντελεστή μεταβλητότητας συνδέονται με υψηλότερης ταχύτητας ροή. Ωστόσο, η ανάλυση των ισοτοπικών και όλων των υδροχημικών παραμέτρων σε συνδυασμό με επιτόπου παρατηρήσεις έδειξε ότι μια πηγή μπορεί να τροφοδοτείται από ένα σύστημα ροής διάχυτης μορφής, ακόμα και αν εμφανίζει έναν υψηλό συντελεστή μεταβλητότητας.
Λέξεις κλειδιά: *Συντελεστής μεταβλητότητας, υδροχημεία, σταθερά ισότοπα, υπόγειο νερό, τύπος ροής.*

1. Introduction

Aquifers often discharge their water through large or small discharge springs. In regions where the ground water lies at shallow depths and where there is much localized recharge through sinking streams, the springs often show considerable seasonal variation in their physical-chemical characteristics. On the other hand, springs originating from higher depths showing possible fluctuations in discharge tend to maintain their physical-chemical characteristics constant in time (Liu et al., 2007; Shuster and White, 1971).

Groundwater flow is mainly determined by the regional geology. The stratigraphic position of the water hosting geological formations with respect to non-permeable capping, and large structural features controlling the position of recharge and discharge areas determine the subsurface hydrogeological conditions. Within a particular hydrogeological setting, groundwater systems may consist of primary or/ and secondary porosity in the forms of small fractures, joints, bedding planes and intergranular matrix largely unmodified by solution, or there may be a well integrated system of pipes and conduits (White, 2007; Gabrovsek and Dreybrodt, 2001; Ternan, 1974; Newson, 1972; Shuster and White, 1971). There are two end member groundwater flow systems (Singhal and Gupta, 2010; Shuster and White, 1971): l) a diffuse flow (Darcian) in granular aquifers or in fractured aquifers along small interconnected openings measured in centimeters or less and 2) a conduit (turbulent) flow through integrated conduit systems with water flowing, often turbulently, through solution passages and fractures measured in centimeters to meters. The flow characteristics in carbonate rocks can be explained by discrete fracture flow, equivalent porous medium and double porosity models. A ‘triple porosity’ model has also been conceptualized in well developed karst aquifers consisting of matrix, fracture and conduit porosities (Kresic, 2007).

The objective of the present study is to investigate the variations in the hydrochemical and isotopic parameters of small discharge spring waters occurring in Argolis peninsula and to relate these variations to the type of flow system. Emphasis has been given on the geochemistry of the species and their statistically approached variation with season. Moreover, the identification of the flow system has given insight in the residence time of the groundwater in the geological formations.

2. Geology - Hydrogeology

As illustrated in the geological map (Figure 1), the largest part of the peninsula is occupied by the thick bedded limestones of Trapezona (Triassic–Jurassic age) with cherts and coarse-grained

carbonate and ophiolitic breccias in the upper parts (Baumgartner, 1985). In the lower parts, volcanic formations were identified at many sites (Gaitanakis and Photiades, 1991; Renz, 1906). The ophiolitic mélange consisting mainly of pillow lavas and dolerites, and locally of cherts, siltstones, serpentinised mafic and ultramafic rocks, is typical in the peninsula. A flysch tectonic mélange characterised mainly by the presence of silts, sandstones and marls, occupies the largest part of Adheres mountain ridge. In this matrix, turiditic rocks of different lithologies, such as volcanic rocks, radiolarites, limestones, granodiorites (Photiades and Keay, 2000) pyroclastic rocks, andesites, dolomites (Aranitis, 1963), quartz sandstones, serpentinites and basalts (Clift and Robertson, 1989), are present. A 'post-Ypresian' flysch, which represents alterations of calcareous schists, marls, sandy marls, sandstones, conglomerates and limestones, covers mainly the Nafplio–Lygourio basin (Kantas, 1991; Baumgartner, 1985). 'Akros formation' made up of neritic limestones of Cretaceous age, which successively become pelagic in the upper parts, and followed by marls and flysch outcrop mainly in the foothills of Mountains Arachnaio and Dhidhima (Decrouez, 1975). At the bottom of the formation, there is a tectonic mélange (Heliokastro area) of 'sheared' serpentinites and clastic slices of several rocks, such as dunits, basalts, cherts and limestones (Gaitanakis and Photiades, 1993; Photiades and Economou, 1991).

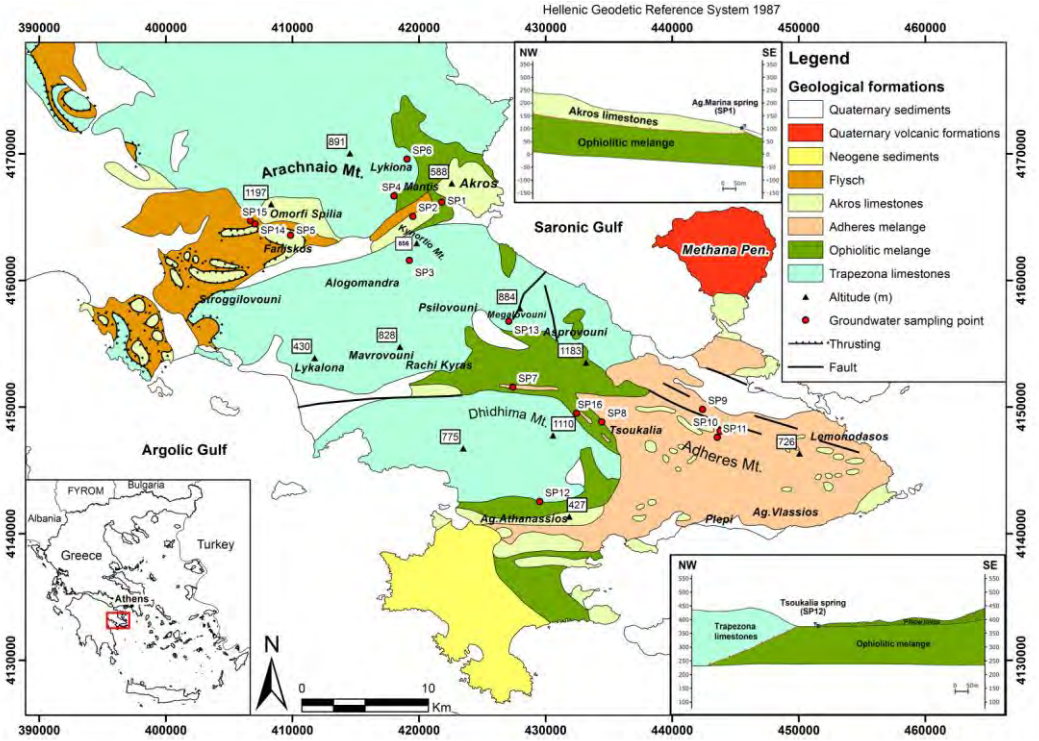

Figure 1 - Geological map of the study area, the location of the groundwater sampling sites and cross sections of two representative springs.

Neogene deposits of Miocene–Pliocene age occupy the Porto Cheli–Kranidi geological trough, in the southwestern part of the peninsula (Gaitanakis and Photiades, 2007). The sequence includes calcareous marls, marly limestones and conglomerates with sandstones intercalations. A quaternary volcanic formation consisting of loose volcanic sediments with tuff blocks and dacide and andesite domes (Fytikas et al., 1980), covers almost the entire Methana peninsula. Finally, recent deposits of Quaternary age, composed of alluvial fans, debris cones and loose sediments of silts, sands and pebbles are mainly lying inside the regional basins of the peninsula.

In the absence of recorded aquifers' hydraulic parameters, a modified qualitative hydrolithological classification (Matiatos and Alexopoulos, 2011) of the aforementioned geological formations has been used to define the hydrogeological status in the peninsula. Hence, the geological formations have been classified in the following categories and subcategories (Table 1):

Table 1 - Hydrolithological classification of the geological formations in the study area and spring water sampling sites.

Category	Subcategory	Geological formations	Spring water sampling site
Aquifers in which flow is mainly inter-granular	Local productive aquifers of small thickness or extensive but moderately productive aquifers	Recent deposits (alluvial fans, debris cones, loose sediments of silts, sands and pebbles)	SP2
Fissured aquifers with secondary porosity	a. Extensive aquifers with high productivity	Limestones of Triassic-Eocene age	SP1, SP12, SP14, SP15
	b. Local productive aquifers of small thickness or extensive but moderately productive aquifers	Limestones of limited extent inside the flysch formations and the tectonic mélange Pelagic limestones of Mesozoic age	SP9
Fissured or granular rocks forming insignificant aquifers or strata with essentially no groundwater resources	a. Local or extensive aquifers with low productivity	Neogene sediments Ophiolitic mélange Flysch sediments & tectonic mélange of Adheres Mountain	SP5 SP3, SP4, SP6, SP7, SP8, SP13, SP16 SP10, SP11
	b. Strata with essentially no groundwater resources	Quaternary volcanic formations	

The complex stratigraphy and the tectonic activity of the area have given the Argolis peninsula a substantial lithological heterogeneity in horizontal and vertical directions, which has led to the formation of independent aquifer systems and the appearance of a number of individual springs mainly of small discharge allocated in carbonate formations, as well as in less permeable lithologies, such as the ophiolitic mélange and the flysch sediments (Figure 1). The latter is evidenced by the presence of springs as well as of numerous wells and boreholes.

In situ geological and hydrogeological observations have revealed that the majority of the water bearing geological formations appearing in the peninsula show primary or/ and secondary porosity. Therefore, the groundwater systems occurring in them are expected to have diffuse flow through small fractures and the granular matrix of the rock, where the water seeps slowly through the aquifers. On the contrary, groundwater flow in conduits is expected to be dominant in the karstified carbonate formations, such as those observed in the Arachnaio and Dhidima Mountains.

3. Methodology

The present study examines the isotopic and physical-chemical characteristics of 16 spring sites, allocated in the Argolis peninsula to evaluate the sensitivity of processes to environmental change induced by geochemical factors. The campaign was carried out between March 2005 and March 2008, and the springs were continually monitored in situ for temperature, alkalinity, pH and electrical conductivity (EC). Moreover, all the springs were sampled at their mouth in order to

minimise the groundwater exposure to ambient air and evaporation. Laboratory major ion analyses (Ca, Mg, Na, K, NO_3, Cl, SO_4) as well as laboratory isotopic analyses ($\delta^{18}O$) were performed on a monthly basis during the whole sampling period.

For the $\delta^{18}O$ measurements, the samples were collected in 20 ml polyethylene containers which were first rinsed in sample water several times and then filled to the top to minimise the air entrapment. For the major cation element analyses, the samples were filtered through 0.45-μm filters and collected in acid-rinsed 100 ml polyethylene bottles. For the major anion element analyses the samples were collected in 500 ml polyethylene bottles. Once the samples were taken, they were stored in a portable fridge until they were transported to the laboratory for the analyses.

Water temperature, pH and specific electrical conductivity were measured in situ by WTW350i instruments with ±0.1% for pH and ±0.5% for EC reading limits. Alkalinity was determined by acid titration using methyl orange. Major ion analysis was performed photometrically in the Faculty of Geology and Geoenvironment (University of Athens, Greece). All the isotopic analyses were performed in the Isotope Hydrology Laboratory of National Center of Scientific Research (NCSR) 'Demokritos' (Athens, Greece). In particular, the stable isotope ratio of oxygen ($^{18}O/^{16}O$) was determined by conventional mass spectrometry (SIRA Series II) with an overall precision of 0.1 ‰. The measurements were expressed in delta (δ) notation as per mille (‰) deviation from the reference Vienna Standard Mean Ocean Water (VSMOW).

The fluctuations in the seasonal concentrations have been reduced to a single number for each spring by calculating the coefficient of variation defined by the equation below:

Equation 1 - Coefficient of variation

$$CV = \sigma / X * 100 \quad (1)$$

where σ is the standard deviation and X is the arithmetic mean.
The coefficient of variation classifies the spring as conduit flow or diffuse flow type when CV is more or less than 5%, respectively (Shuster and White, 1971). Values of CV less than 5% also indicate a long contact residence time of the groundwater. Coefficient of variation, determinable from the seasonal series, has been identified as a useful index of aquifer type, although Atkinson (1977) indicates that additional parameters (e.g. geomorphological characteristics) should be also taken into account in the interpretation. The carbon dioxide partial pressure (P_{CO2}) is an indicative parameter of the capacity of water to dissolve carbonates. Hence, higher values of P_{CO2} in water result in increasing the water capacity to dissolve carbonates. The determination of P_{CO2} has been calculated with the software package PHREEQC based on the following mass-action equation when the concentration of HCO_3 and the pH value are known (Freeze and Cherry, 1979):

Equation 2 - Mass action equation

$$K_{H2CO3} = [H^+] [HCO_3^-] / [H_2CO_3] \quad (2)$$

Equation 3 - Carbon dioxide partial pressure equation

$$P_{CO2} = [H_2CO_3] / K_{CO2} \quad (3)$$

where the brackets mean ionic activity, and:

$[H^+]$ is the ionic activity of hydrogen;

K_{H2CO3} is an equilibrium constant = $10^{-6.35}$ at 25°C;

K_{CO2} is an equilibrium constant = $10^{-1.47}$ at 25°C;

P_{CO2} is the carbon dioxide partial pressure expressed in bars or atmospheres.

4. Results and Discussion

4.1 Water Quality

The mean values for the physical-chemical variables analyzed in the groundwater samples are summarized in Table 2. These values have been used for groundwater quality assessment. Hence, as depicted in the Piper diagram (Figure 2), the largest number of spring waters is plotted in the left corner of the diamond-shaped field. On the metals triangle, many samples lie very close to and along the segment that connects the calcium and the magnesium ions. On the right triangle, the majority of the samples plotted in the left corner suggest a significant content in HCO_3. The Ca–HCO_3 water type predominates in the region as it characterises 81.3% of the groundwater samples. The Mg–HCO_3 water type is represented by 18.7% of the samples. The Ca–HCO_3 type refers to the groundwater samples that were taken from aquifers located in carbonate formations, sandstones and conglomerates. The Mg–HCO_3 type includes the spring waters that mainly discharge the ophiolitic mélange, since the presence of minerals rich in magnesium is typical for this formation (e.g. SP16).

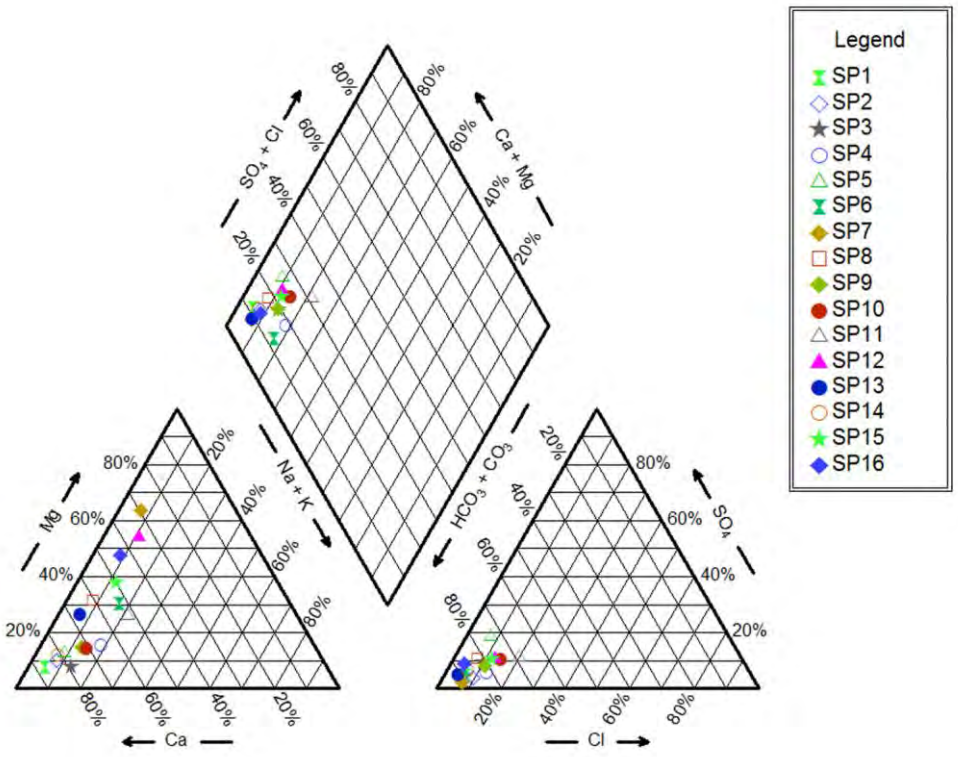

Figure 2 - Piper diagram for the definition of groundwater chemical types.

4.2 Temporal variations

Hydrochemographs of continuous water-quality data from springs have been widely used as indicators of aquifer characteristics (Liu et al., 2007; Andreo et al., 2002; Raeisi and Karami, 1997). In the present study, hydrochemographs of $LogP_{CO2}$, $\delta^{18}O$, HCO_3, pH, SI_{cal} and water temperature have been constructed in order to assess the hydrochemical indicators of groundwater flow. Additionally, the coefficient of variation for electrical conductivity (EC) (Table 2) has been calculated to classify springs according to the groundwater flow type occurring in the subsurface.

Table 2 - Hydrochemical and stable isotopic results in groundwater samples

Sample ID	pH	EC (μS/cm)	Water Temp. (°C)	Ca^{2+} (mg/l)	Mg^{2+} (mg/l)	Na^{+} (mg/l)	K^{+} (mg/l)	HCO_3^{-} (mg/l)	Cl^{-} (mg/l)	SO_4^{2-} (mg/l)	NO_3^{-} (mg/l)	$LogP_{CO2}$ (atm)	SIcal	$\delta^{18}O$ (‰ SMOW)	CV§ (EC)	N†
SP1	7.02	709.7	19.2	138.0	7.3	9.6	0.70	408.8	15.2	14.9	10.9	-1.55	0.19	-6.18	4.16	20
SP2	7.16	725.4	18.0	129.4	9.4	14.2	1.10	387.5	22.4	10.9	20.0	-1.69	0.25	-6.14	2.46	19
SP3	7.58	657.6	17.5	114.0	6.6	22.2	0.79	354.1	24.1	30.1	8.9	-2.13	0.57	-6.44	5.82	14
SP4	7.92	486.0	18.8	72.2	10.2	23.5	0.12	260.7	23.1	14.3	8.6	-2.57	0.61	-6.44	5.20	20
SP5	7.65	737.1	17.9	123.1	12.0	15.7	0.83	339.0	19.6	63.4	20.6	-2.21	0.60	-6.16	3.81	10
SP6	7.50	828.3	16.6	95.3	33.4	35.4	1.17	457.9	16.4	26.7	8.3	-1.96	0.45	-5.48	13.71	12
SP7	7.60	637.5	16.1	43.5	57.6	12.4	0.41	392.0	17.0	6.3	9.0	-2.10	0.19	-6.30	4.22	20
SP8	7.11	859.3	17.7	114.6	36.3	17.9	1.41	425.2	19.1	37.5	52.2	-1.61	0.15	-6.28	2.78	19
SP9	8.03	535.5	17.8	80.9	10.0	17.0	0.81	275.8	22.1	20.9	5.2	-2.65	0.79	-6.64	5.84	19
SP10	7.86	601.5	16.0	95.5	11.7	22.8	0.60	305.7	34.2	32.1	4.1	-2.45	0.69	-6.73	4.99	19
SP11	7.55	660.0	14.2	105.2	13.6	24.8	0.73	329.5	32.7	47.6	4.0	-2.14	0.43	-6.71	4.23	10
SP12	7.67	808.3	17.8	64.4	61.3	23.7	1.02	396.2	38.2	41.7	26.3	-2.10	0.44	-5.07	3.43	19
SP13	7.25	769.4	17.9	117.3	28.2	13.9	0.58	464.1	4.7	2.0	1.1	0.15	0.13	0.18	5.85	18
SP14	7.84	554.6	17.8	97.7	8.7	10.2	0.39	320.6	13.8	18.2	4.2	-2.40	0.74	-6.67	14.45	16
SP15	7.75	803.5	18.4	96.6	44.3	27.5	0.43	441.5	39.4	44.2	5.6	-2.18	0.74	-6.50	7.26	15
SP16	7.47	731.1	16.7	75.9	50.1	17.6	0.28	418.8	12.1	30.3	26.2	-1.95	0.33	-6.24	4.01	15

Note: The measurements represent pluriannual mean values (sampling period: October 2005–March 2008), §: Coefficient of variation, †: Number of samples

The coefficient of variation of EC values vary between 2.4% and 14.4%. The majority of the springs (SP1, SP2, SP5, SP7, SP8, SP10, SP11, SP12, SP16) show CV values below 5.0% indicating a dominant diffuse flow system in the aquifers, whereas seven springs (SP3, SP4, SP6, SP9, SP13, SP14, SP15) are characterised by CV values above 5.0%. Electrical conductivity variance in springs SP3, SP4, SP9 and SP13 is very close to 5.0% and in combination with in situ geological and hydrogeological observations it can be assumed that the groundwater flow in these aquifers is mainly taking place through small fractures and the matrix of the rock, where the water seeps slowly. In three springs (SP6, SP14 and SP15), the CV of EC has been calculated far above the 5.0%, outlining that groundwater flow is mainly occurring in conduits. Two of these springs (SP14 and SP15) are located in karstified carbonate formations, hence the assumption can be justified by the regional geology. Spring SP6 outcrops inside the ophiolitic mélange, meaning that a conduit flow system is probably not a valid assumption. In situ observations have revealed that the groundwater of the specific spring is very close to the surface, hence the water is very much affected by the atmospheric conditions. Moreover, its discharge is very small resulting in its ephemeral function and the waters been stagnant until the spring starts again its operation.

The observed variation of bicarbonate concentrations (Figure 3) follows more or less the seasonal pattern of $LogP_{CO2}$ in a yearly cycle, with the highest values occurring in summer and the lower in winter. Several springs (e.g. SP5, SP10) tend to show their highest bicarbonate concentrations in the summer, when the highest $LogP_{CO2}$ occurs; also expected when considering equations 2 and 3. This is attributed to the fact that the CO_2 partial pressure in water is strongly related to the transpiration by plant roots and microbes in the soils. In summer, root transpiration in soil is stronger and carbon dioxide is more generated (Liu et al., 2007; Liu et al., 2006; Atkin et al., 2000), hence this explains the seasonal change. However, there are springs (e.g. SP6, SP14) where the highest $LogP_{CO2}$ and bicarbonate values occur in the early wet period which can be related to the flushing of soluble components stored during the earlier dry periods which are washed out by the first recharge events (Khayat et al., 2008; Bakalowicz et al., 1974).

In most cases, the groundwater in aquifers is close to saturation with respect to calcite (Figure 3); hence the majority of the springs are calcite supersaturated. Only when the groundwater is decreased in pH or enriched in CO_2, the spring waters show lower Saturation Index with respect to calcite. Calcite supersaturation during the rainy season is controlled by variations of pH in the recharge events. Therefore, seasonal variations are not easily observed. Typically, saturation of calcite can be reached at the beginning of a rainy season (Khayat et al., 2008) and that is the case of several springs in the study area (e.g. SP8, SP12, SP13). Moreover, high SI_{cal} values indicate a solution rate decrease and a longer residence of water in the aquifer which can be attributed to low flow capacities (Jacobson and Langmuir, 1974).

The stable isotopes contribute in the investigation of the groundwater circulation as the stable isotopic content is very much affected by temperature variations resulting in fractionation phenomena. Hence, the lowest and highest $\delta^{18}O$ values are observed in lowest and highest water temperatures, respectively (Clark and Fritz, 1997). In the study area, the measured $\delta^{18}O$ values of the spring waters reflect seasonal variations typical for the northern hemisphere with minimum values in winter and maximum values in summer (Figure 3). However, the $\delta^{18}O$ values of September 2006 are more negative than expected which can be attributed to a heavy recharge event which is typically exhausted relative to the $H_2{}^{16}O$, resulting in relatively low $\delta^{18}O$ values (Clark and Fritz, 1997). Moreover, the fluctuations of $\delta^{18}O$ values can be regarded as weak indicating of good mixing of infiltrated and ground waters.

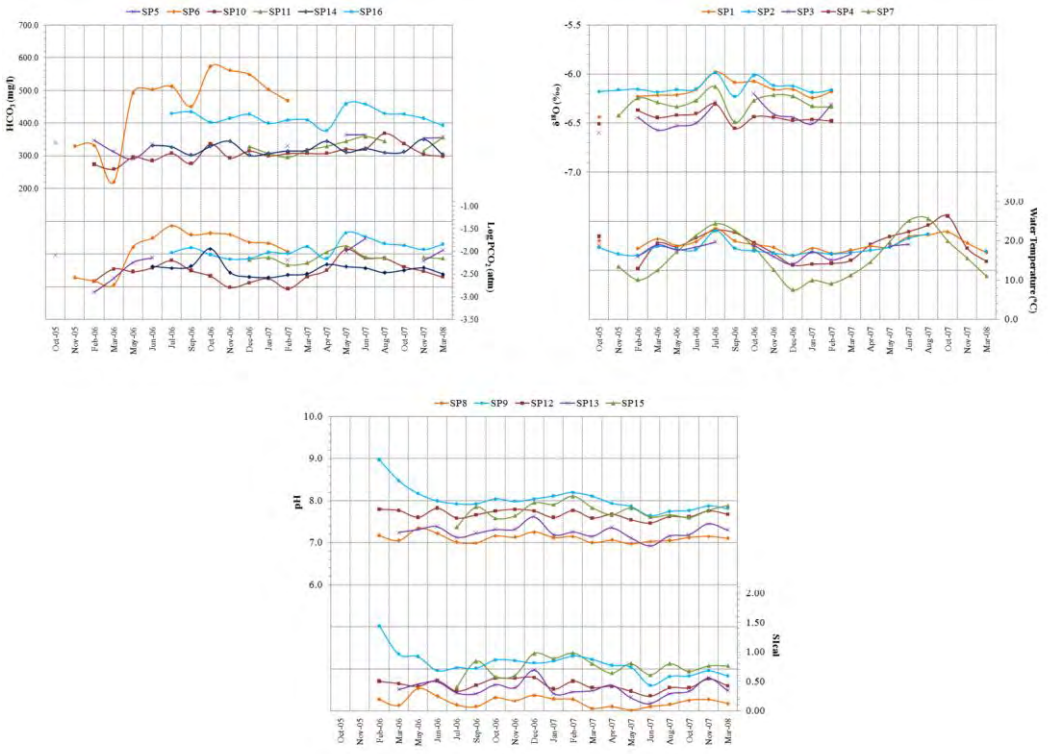

Figure 3 - Temporal variations of physical-chemical and isotopic parameters.

5. Conclusion – Remarks

Natural discharge of flow systems in Argolis peninsula occur through a number of small discharge springs because of stratigraphic or structural features. This paper presents the seasonal variations of three hydrological year continuous physical-chemical and isotopic data from these springs through the construction of representative hydrochemographs and the determination of the coefficient of variation. These variations were found for pH, electric conductivity, CO_2 partial pressure, HCO_3 and calcite saturation of the springs. The results have shown that the diffuse flow type characterises the majority of the springs while the karstic springs are mainly related to conduit flow system.

Temporal variations of data have also revealed the strong correlation between stable isotopic values and the water temperature, as the $\delta^{18}O$ values become more positive in the summer and more negative in the winter. The bicarbonate values follow more or less the variation of $LogP_{CO2}$ in a yearly cycle, indicating that the CO_2 partial pressure in water is strongly related to the transpiration by plant roots and microbes in the soils, while the opposite is related to the flushing of soluble components stored during the earlier dry periods which are washed out by the first recharge events. Moreover, the majority of the springs are supersaturated with respect to calcite and strongly correlated to pH variations. Supersaturation of calcite, which indicates a longer residence time, is mainly reached at the beginning of a rainy season.

6. Acknowledgements

The author would like to thank the director as well as the personnel of the Isotope Hydrology Laboratory of NCSR ‘Demokritos’ (Athens) for providing the stable isotope analyses.

7. References

Andreo B., Carrasco F., Bakalowicz M., Mudry J. and Vadillo I. 2002. Use of hydrodynamic and hydrochemistry to characterise carbonate aquifers. Case study of the Blanca–Mijas unit (Malaga, southern Spain), *Environmental Geology*, 43: 108–119 pp.

Aranitis S. 1963. Die Entstehung der Eruptivgesteine vom Hermioni–Gebiet und die mit ihnen verbundene Vererzung, *Ann Geol Pays Hell*, 14: 211 pp.

Atkin O.K., Edwards E.J. and Loverys B.R. 2000. Response of root respiration to changes in temperature and its relevance to global warming, *New Phytologist*, 147: 141-154 pp.

Atkinson T.C. 1977. Diffuse flow and conduit flow in limestone terrain in the Mendip Hills, Somerset (Great Britain), *Journal of Hydrology*, 35: 95-110 pp.

Bakalowicz M., Blavoux B. and Mangin A. 1974. Apports du tracage isotopique naturel a la connaissance du fonctionnement d'un systeme karstique-teneurs en oxygen-18 de trios systems des Pyrenees, France, *Journal of Hydrology*, 23: 141-158 pp.

Baumgartner P.O. 1985. Jurassic Sedimentary Evolution and Nappe Emplacement in the Argolis Peninsula (Peloponnesus, Greece), *Mém Soc Helv Sci Nat*., 99 (1): 137 pp.

Clark I.D. and Fritz P. 1997. Environmental Isotopes in Hydrogeology, Lewis Publishers, New York, 328 pp.

Clift P.D. and Robertson H.F. 1989. Evidence of a Late Mesozoic Ocean Basin and Subduction–Accretion in the Southern Greek Neo–Tethys, *Geology*, 17: 559.

Decrouez D. 1975. Étude stratigraphique et micropaléontologique du Crétacé d'Argolide (Péloponnèse, Grèce), *PhD Thesis*: University of Geneva.

Freeze R.A. and Cherry J.A. 1979. Groundwater, Prentice-Hall, Englewood Cliffs, New Jersey.

Fytikas M., Innocenti F. and Mazzuoli R. 1980. Methana Sheet – Geological Map in Scale 1:50000, *IGME*, Athens, Greece.

Gabrovsek F. and Dreybrodt W. 2001. A model of the early evolution of karst aquifers in limestone in the dimensions of length and depth, *Journal of Hydrology*, 240: 206–224 pp.

Gaitanakis P. and Photiades A.D. 2007. Spetses Sheet – Geological Map in Scale 1:50000. *IGME*, Athens, Greece.

Gaitanakis P. and Photiades A.D. 1993. New Data on the Geology of Southern Argolis (Peloponnesus, Greece), *Bull Geol Soc Greece*, 28: 247 pp.

Gaitanakis P. and Photiades A.D. 1991. Geological Structure of SW Argolis (Peloponnesus, Greece), *Bull Geol Soc Greece*, 25: 319 pp.

Jacobson R.L. and Langmuir D. 1974. Controls on the quality variations of some carbonate spring waters, *Journal of Hydrology*. 23: 247-265 pp.

Kantas K. 1991. Hydrogeological Explanation of Salt–Water Intrusion in Karstic Aquifers in the NE Argolis Limestones (Peloponnesus, Greece), *Bull Geol Soc Greece*, 25: 183 pp.

Khayat S., Möller P Geyer S., Marei A., Siebert C. and Hilo F.A. 2008. Hydrochemical variation in the springs water between Jerusalem–Ramallah Mountains and Jericho Fault, Palestine. *Environ Geol*, 57: 1739–1751 pp.

Kresic N. 2007. Hydrogeology and Groundwater Modeling, 2nd ed., CRC Press, Boca Raton, FL, 805 pp.

Liu Z., Li Q., Sun H. and Wang J. 2007. Seasonal, diurnal and storm-scale hydrochemical variations of typical epikarst springs in subtropical karst areas of SW China: Soil CO_2 and dilution effects, *Journal of Hydrology*, 337: 207-223 pp.

Liu Z., Li Q., Sun H., Liao C., Li H., Wang J. and Wu K. 2006. Diurnal variations of hydrochemistry in a travertine-depositing stream at Baishuitai, Yunnan, SW China. *Aquatic Geochemistry*, 12: 103–121 pp.

Matiatos I. and Alexopoulos A. 2011. Application of stable isotopes and hydrochemical analysis in groundwater aquifers of Argolis Peninsula (Greece), *Isotopes in Environmental and Health Studies,* 47 (4), 512–529 pp.

Newson M.D. 1972. Comments on seasonal fluctuations in the chemistry of limestone springs, by Shuster, E.T. and White, W.B. *Journal of Hydrology*, 16: 49-51 pp.

Photiades A.D. and Ecomomou G.S. 1991. Alteration hydrothermale sous–marine des basaltes et des dolerites (facies zeolitique) de l'unité moyenne 'volcanique' de l'Argolide septentrionale (Péloponnèse, Grèce), *Bull Geol Soc Greece*, 25: 301 pp.

Photiades A.D. and Keay S. 2000. Mid–Late Jurassic Granodiorite Basement in Southern Argolis Peninsula (Greece), Tectonostratigraphic Implications, in *Proceedings of the 3rd International Conference on the Geology of the Eastern Mediterranean*, edited by I. Panayides et al. *Geological Survey Department*, Lefkosia, Cyprus, 2000, 233–239 pp.

Raeisi E. and Karami G. 1997. Hydrochemographs of Berghan karst spring as indicators of aquifer characteristics, *Journal of Cave and Karst Studies*, 59(3): 112-118 pp.

Renz C., 1906. Trias und Jura in der Argolis. *Z. dtsch. geol. Ges.*, 58: 379-395 pp.

Shuster E.T. and White, W.B. 1971. Seasonal fluctuations in the chemistry of limestone springs: a possible means for characterizing carbonate aquifers, *Journal of Hydrology*, 14: 93-128 pp.

Singhal B.B.S. and Gupta R.P. 2010. *Applied Hydrogeology of Fractured Rocks*, 2nd Edition, Springer, 408 pp.

Ternan J.L. 1974. Comments on the use of calcium hardness variability index on the study of carbonate aquifers: with reference to central Pennines, England, *Journal of Hydrology*, 16: 317-334 pp.

White W.B. 2007. Groundwater Flow and Transport in Karst, in *The Handbook of Groundwater Engineering* edited by J.W. Delleur, CRC Press, Boca Raton, FL, 18–1 to 18–36 pp.

Δελτίο της Ελληνικής Γεωλογικής Εταιρίας, τομ. XLVII , 2013
Πρακτικά 13ου Διεθνούς Συνεδρίου, Χανιά, Σεπτ. 2013

Bulletin of the Geological Society of Greece, vol. XLVII 2013
Proceedings of the 13th International Congress, Chania, Sept. 2013

GROUNDWATER QUALITY OF THE COASTAL AQUIFERS IN THE EASTERN PART OF THERMAIKOS GULF (FROM AGGELOCHORI TO KALLIKRATEIA)

Pavlou A.[1], Soulios G.[1], Dimopoulos G.[1], Tsokas G.[2], Mattas C.[1], Kazakis N.[1] and Voudouris K.[1]

[1] *Laboratory of Engineering Geology and Hydrogeology, School of Geology, Aristotle University of Thessaloniki, thanasis_pavlou@yahoo.com, gsoulios@geo.auth.gr, gdimop@geo.auth.gr, cmattas@geo.auth.gr, kazakis@geo.auth.gr, kvoudour@geo.auth.gr*

[2] *Exploration Geophysics Laboratory, School of Geology, Aristotle University of Thessaloniki, gtsokas@geo.auth.gr*

Abstract

The study area is located in the coastal area of the eastern Thermaikos Gulf, covering an area of 252 km^2. The area is characterised by intense agricultural activity, and during the past few years it has undergone considerable residential development. From a geological point of view, the area consists of Quaternary alluvial coastal deposits, river terraces and Neogene deposits (marly limestones and sandstone-marl series). The bedrock formations are Jurassic limestone and Mesozoic granite. The main aquifer system is developed within the sand, gravel, and sandstone layers of the Quaternary deposits as well as within the sandstone-marl series. This paper investigates the relationship between the groundwater quality and groundwater level. Groundwater sampling and water level measurements took place in April and September 2010. The results of chemical analyses indicate degradation of the groundwater quality. The sources of the groundwater pollution are seawater intrusion due to the overexploitation of the coastal aquifers, fertilizers from the agricultural activities and the disposal of untreated wastewater in torrents.
Key words**:** *over-pumping, water level drawdown, salinization.*

Περίληψη

Η περιοχή έρευνας καταλαμβάνει το παράκτιο τμήμα του ανατολικού Θερμαϊκού κόλπου, καλύπτοντας έκταση 252 Km^2. Η περιοχή χαρακτηρίζεται από έντονη γεωργική δραστηριότητα, ενώ τα τελευταία χρόνια παρουσιάζει μεγάλη οικιστική ανάπτυξη. Γεωλογικά η περιοχή αποτελείται από Τεταρτογενείς αποθέσεις και Τριτογενείς αποθέσεις (μαργαϊκοί ασβεστόλιθοι, ψαμμιτομαργαϊκή σειρά). Το υπόβαθρο συνίσταται κυρίως από ασβεστόλιθους του Ιουρασικού και γρανίτη του Μεσοζωικού. Η κύρια υδροφορία της περιοχής αναπτύσσεται σε στρώματα άμμων, χαλικιών, καθώς και ψαμμιτών των Τεταρτογενών αποθέσεων και της «ψαμμιτομαργαϊκής σειράς» που εναλλάσσονται με αργίλους. Στην εργασία αυτή γίνεται σύγκριση της μεταβολής της ποιότητας του υπόγειου νερού σε συνάρτηση με τη μεταβολή της στάθμης του υπόγειου υδροφόρου ορίζοντα. Πραγματοποιήθηκαν δειγματοληψίες και μετρήσεις της στάθμης του υπόγειου νερού σε 2 περιόδους (Απρίλιος 2010 – Σεπτέμβριος 2010). Λόγω της αυξημένης άντλησης του νερού για

την άρδευση και ύδρευση παρατηρείται σε ορισμένα τμήματα της περιοχής έρευνας υποβάθμιση της ποιότητας του νερού (υψηλές τιμές νιτρικών ιόντων, λόγω νιτρορύπανσης γεωργικής προέλευσης και χλωριόντων, λόγω διείσδυσης της θάλασσας), λόγω της υπερεκμετάλλευσης του υπόγειου υδροφορεά.
Λέξεις κλειδιά: *υπεράντληση, πτώση στάθμης, υφαλμύριση.*

1. Introduction

The studied area is located in the south part of Thessaloniki Prefecture, in the coastal part of Eastern Thermaikos Gulf, extending from Aggelochori–Thessaloniki (Megalo Emvolo) to Nea Kallikrateia–Chalkidiki (Figure 1). Administratively, the area belongs to the regional units (former Prefectures) of Thessaloniki and Chalkidiki and to the Municipalities of Thermaikos, Thermi, and Nea Propontida–Chalkidiki. The population is 27,447 inhabitants (National Statistical Service of Greece, 2001).

Figure 1-Topographic map of the study area.

Rapid population growth occurred since 1981, with a great intra-annual variation due to the increase observed during the summer months. The main activity of the residents in the study area is intensive agriculture. Cereals, fruit and vegetables, cotton, vineyards and olives are the main products. A few residents work in small and large industries, mostly in the Industrial Area of Lakomma, and some are self-employed (e.g. fishermen). The needs for irrigation and domestic water supply are covered by 750 boreholes. The pollution is detected in loose sediments (sandy clays, clays) of moderate to very low permeability. The main pollution sources are untreated waste effluent from oil mills and cheese dairies and uncontrolled waste disposal sites (UWDS). Pollution from the oil mill waste effluent can be associated with the high acidity of the groundwater due to the low pH (3.0–4.5), high temperature, high percentage of suspended solids and high organic load (Voudouris et al., 2000). The increased values of nitrate and chloride ions, which are mainly attributed to the agricultural activities, are associated

with the use of nitrogenous fertilisers and groundwater over-pumping that favours seawater intrusion, respectively (Voudouris et al., 2004; Soulios, 2004).

1.1. Description of the Study Area

The surface of the studied area is 252.5 km^2. The perimeter is 95.6 km, the maximum length is 31.4 km and the maximum width is 16 km. The terrain is described as flat to semi-hilly, due to the significant extension of the Neogene formations of horizontal to slightly inclined layers with different hardness as well as to erosion by torrents. The elevation is generally low, except in the northeastern part of the area where the altitude of some bed formations can reach 535 m asl. The mean altitude of the area was calculated as 96.5 m using GIS, and the mean inclination was estimated to 5.1 %. The coastal areas present a very typical morphology, being alternately steep and flat. The flat coasts are formed at the stream mouths into the sea and they consist of alluvial deposits. The hydrographic network is moderately developed and has a dendritic to parallel form (Figure 1). Flow is observed during heavy rainfall, with a NNE-SSW direction, and is characterised as torrential. The bifurcation ratio has been calculated as 3.72, which indicates a naturally developing hydrographic network and drainage density equal to 1.55 km/km^2. The value of drainage frequency is estimated at 3.01/km^2.

1.2. Geological Setting

The studied area geotectonically belongs to the Interior Greek zones and specifically to Paeonia zone (Mountrakis, 2010). It consists of a Mesozoic bedrock covered by Neogene and Quaternary sediments (Lalechos & Bison, 1969; Mollat et al., 1978).

Bedrock formations:

- Early-Late Jurassic granite-granodiorite of Monopigado: biotite and two-mica granite traversed by pegmatite veins
- Jurassic limestone: fine-to medium-grained, overlaying locally thin layers of sandstone

Neogene sediments:

- Basic conglomerate series of Lower–Middle Miocene age: consists of bedrock gravels of various sizes and sandy, sandy mud to loamy cementing material
- Red clay series of Upper Miocene age: composed of red to tile-coloured silty clay with lenses of shingle-sand-sandstone with cross bedding, mud clay sand, fine marl and clay appearing at sites
- Sandstone marl series of Pontian age (Upper Miocene): consists of alternating sand layers (fine-grained to coarse-grained), clayey marl and clay, with interbedded, (not very cohesive) sandstones, breccias, fine layers of sandstone-breccias, calcareous sandstone and limestone
- Fresh-water limestone of the Pliocene period: the deposition took place in a shallow lake microenvironment (Syrides, 1990). It is a mainly marly limestone, often containing gravels and other materials of local origin.

Quaternary sediments:

- Upper terrace system of Pliocene age: mainly made up of quartzite pebbles and metamorphic rocks containing a small proportion of limestone
- Lower terrace system of the Holocene period: found in streams and mostly consists of pebbles, sand, limestone and schist pebbles
- Eluvial mantle: covers the Neogene deposits and consists of their weathering products
- Sediments of coastal lakes and lagoons: mainly sands and sandy clays
- Coastal deposits: consist of beach ridges and sand dunes
- Alluvial deposits: consist of sedimentary material (clays, sands, grits) from the weathering of Neogene formations

The area has been affected by the extensional phase of Quaternary, resulting in NNW-SSE and NE-SW main fault systems. These small and medium-scale faults have small surface traces.

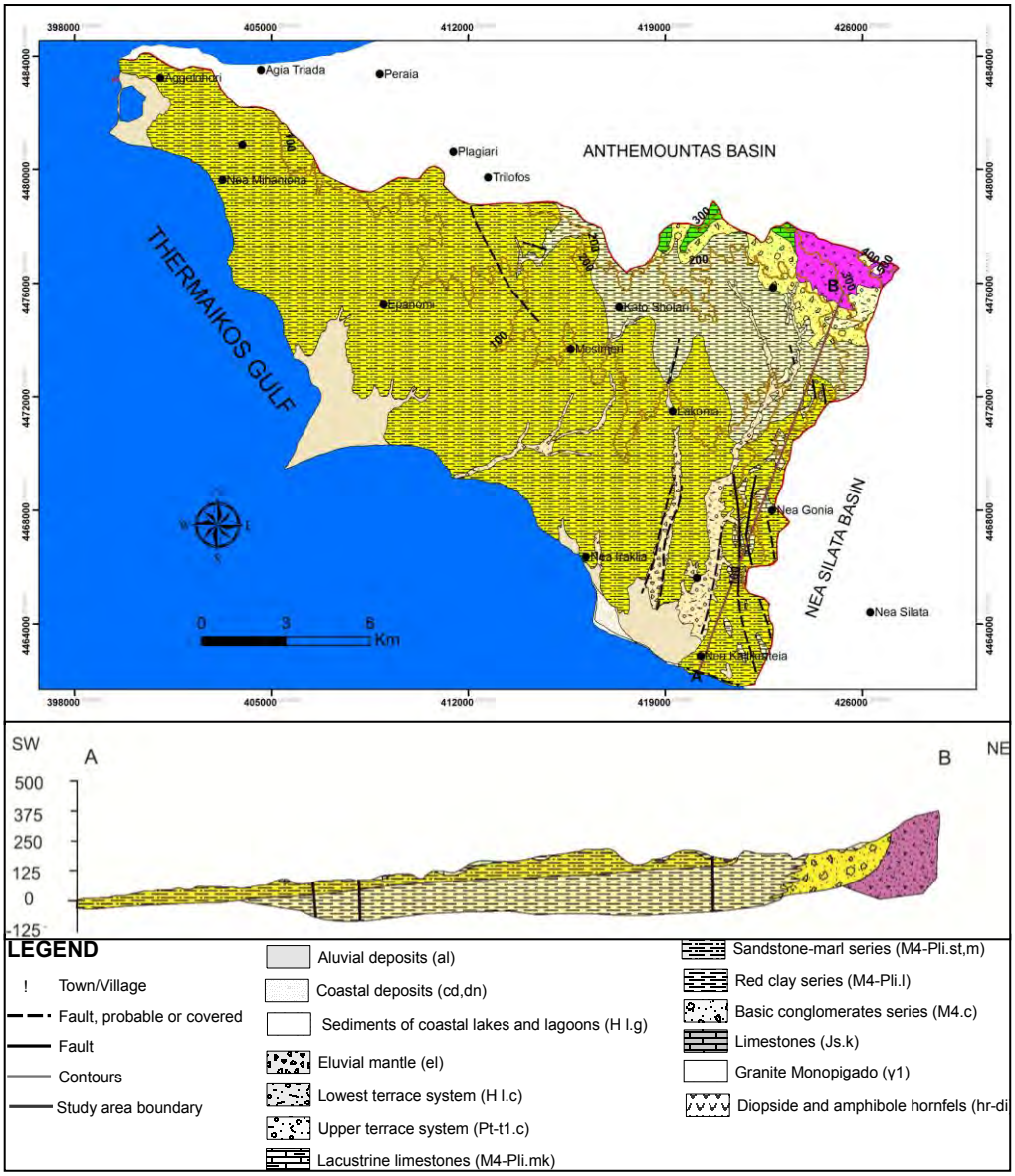

Figure 2 - Geological map of the study area and sketched geological section along settlements N. Kallikrateia-N. Gonia-Monopigado of SW-NE direction.

2. Hydrogeological Setting of the Study Area

2.1. Water Level Measurements and Results

The main aquifers have developed within the Quaternary geological formations and the fine layers of sands, sandstones and pebbles of the sandstone marl series, which covers the largest part of the area. Data from available lithological sections show that the yield of the boreholes ranges from 8 to 140 m^3/h with a mean value of 60 m^3/h. The drilling depth ranges from 40 m

in the coastal part to 360 m in the central and northern part of the area, with the average depth at 210 m. The lowest yields (5–20 m^3/h) are recorded in the northern part of the area, which consists of Neogene sediments (red clays, conglomerates) and defines the recharge area of the aquifer, while the highest yields (50–140 m^3/h) are recorded in the coastal areas of Aggelohori, Mihaniona, Epanomi, and Kallikrateia. The region between the settlements of Mesimeri, Kato Sholari, Lakoma, Nea Gonia and the northern boundary of the studied area presents the most adverse hydrogeological conditions.

The upper aquifers are unconfined ($T=1–5.10^{-3}$ m^2/s; $k=1.10^{-3}$ m/s) and are formed along the torrents. The deep underlying aquifers are in confined to semi-confined conditions. According to Koumantakis (2006), the piezometric level of both aquifer systems is identical, while their hydraulic features are heterogeneous. The confined aquifers are mostly characterised by good to moderate groundwater capacity ($T=1.10^{-3}–1.10^{-5}$ m^2/s; $k=5.3.10^{-5}$ m/s). The transmissivity in some parts of the hilly area (Trilofos – Kardia – Kallikratia – Nea Gonia) is relatively low ($T\leq10^{-5}$ m^2/s), resulting in low borehole yields (15–20 m^3/h) from the depth of 350 m (Institute of Geology & Mineral Exploration/IGME, 2008; Papageorgakakis & Koumantakis, 1978).

The groundwater level in the area was measured in 80 boreholes used for various purposes (irrigation, water supply, etc). According to the international specifications, each measurement was preceded by pumping interruption for an adequate time period, there was no pumping during the measurements in the neighbouring area and the same measurement was always performed from the same point using the same instrument. Measurements of the water level were carried out during both the wet and dry periods, in April 2010 and September 2010, respectively.

It was shown that the maximum depth of the groundwater level in April 2010 was 148.7 m (below ground surface) and the minimum was 0.44 m (b.g.s.), while in September 2010 the corresponding depths ranged from 0.45 m to 149.32 m. A water table map is shown in Figure 3 (the groundwater level values are measured above the sea level). The groundwater flow lines follow the NE-SW direction and groundwater flows from the internal part of the basin to the coastal part. The negative values of the water level contours, occurring mostly near the coastal zone, indicate that the intrusion of seawater is possible. The groundwater level drawdown (Figure 4) observed between the two periods ranges from 5.84 m to 0.01 m, while the average value is about 1 m. The highest drawdown is observed in the southern part of the area, where the largest increase in resident population and visitors is recorded during the summer months, resulting in increased water needs.

2.2. Groundwater Sampling and Results

Groundwater sampling was carried out at the end of the wet and dry periods (April and September) of 2010. These periods represent the highest and lowest groundwater levels and are considered to be the most suitable for studying any changes in hydrochemical parameters. Fifty nine (59) samples were collected at the end of the wet period and sixty three (63) samples at the end of the dry period. In situ measurements of pH and electrical conductivity (E.C.) were conducted, while the value of major ions concentration (Ca^{2+}, Mg^{2+}, Na^{+}, K^{+}, HCO_3^{-}, Cl^{-} , SO_4^{2-} and NO_3^{-}) was determined in the Engineering Geology & Hydrogeology Laboratory, Dept. of Geology, Aristotle University.

Based on the results of chemical analyses, it is concluded that the cation composition of the groundwater is Ca>Mg>Na>K, except for samples from the coastal zone, where Na is the predominant cation. The anion composition of the groundwater is HCO_3>Cl>NO_3 (fresh water) or Cl>HCO_3>NO_3 (water affected by seawater intrusion). The Ca-Mg-HCO_3 chemical water type is the dominant type in inland areas (fresh water) and Na-Cl water type is the type of water affected by seawater intrusion in coastal areas.

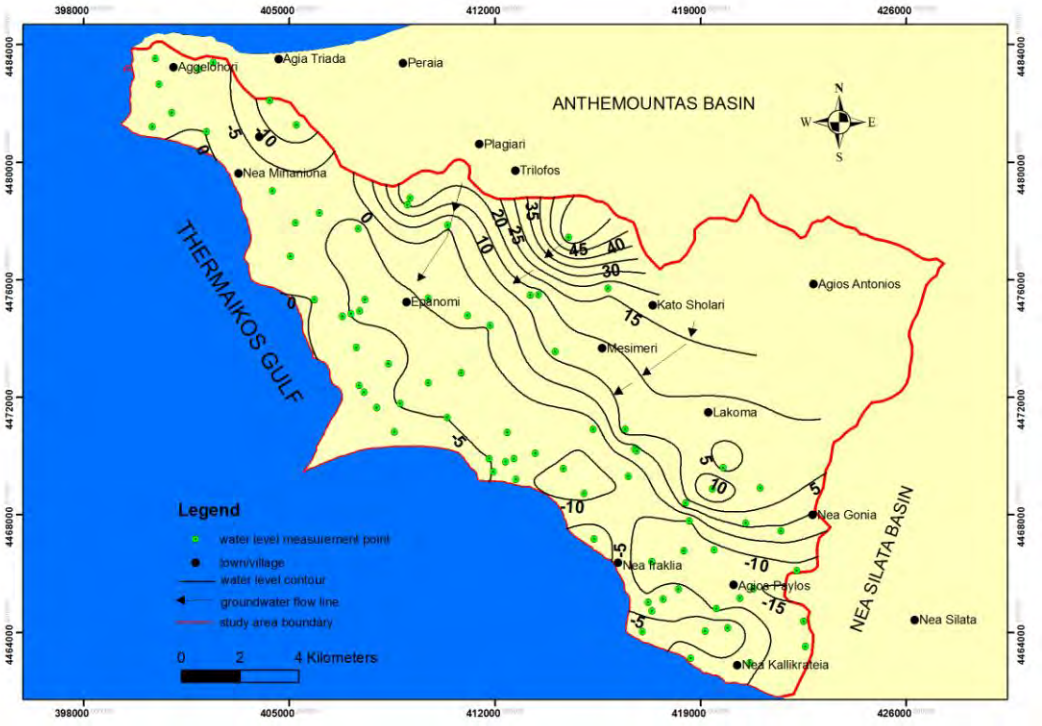

Figure 3 -Water table map, April 2010.

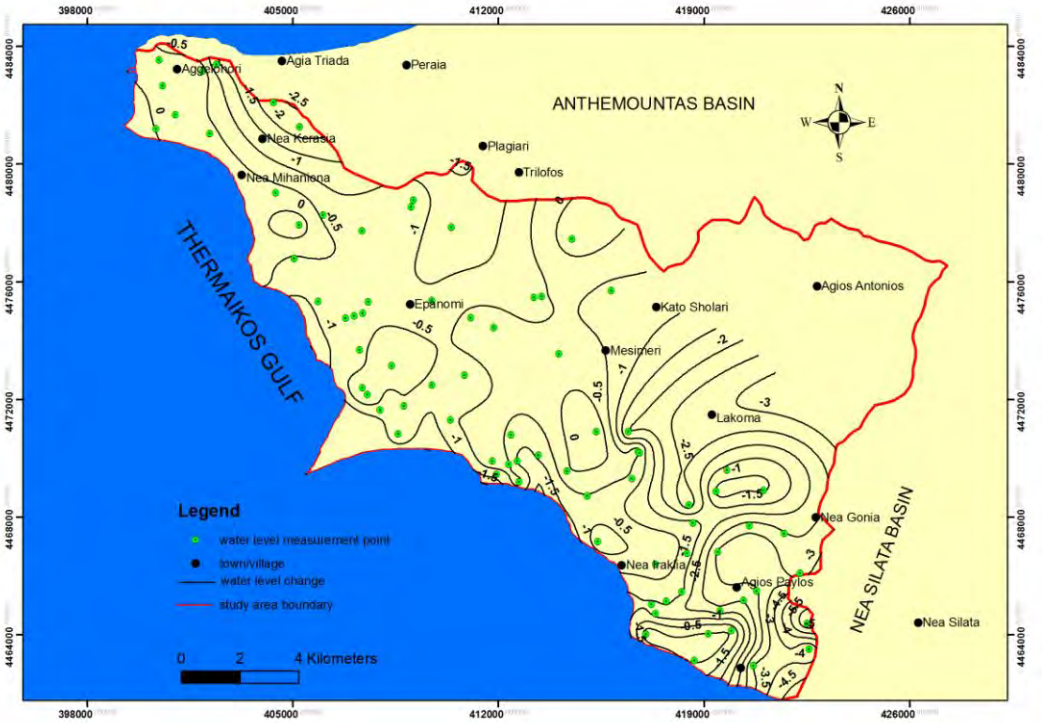

Figure 4 -Water level change during the period of April 2010-September 2010.

High concentrations of Cl^-, Na^+ and NO_3^- ions are locally recorded, rendering most of the samples not suitable for drinking. Regarding the nitrates, the NO_3 concentration exceeds the maximum admissible limit of 50 mg/l (set by EU Council for drinking water) in 30 % of the boreholes, rendering groundwater unsuitable for human consumption. Increased concentrations in chloride ions and nitrates are recorded in the coastal zone and are clearly attributable to the seawater intrusion due to groundwater over-pumping to meet irrigation demands.

The problem of salinisation of the coastal aquifers has been examined by many researchers in Greece (Diamantis & Petalas, 1989; Petalas & Diamantis, 1999) and worldwide (Henry, 1970; Todd, 1953; Pulido-Leboeuf, 2004), as it is among the main causes of groundwater degradation in coastal areas. Figures 5 and 8 illustrate the spatial distribution of chloride and nitrate ion concentration, respectively, in the study area. The change in chloride ion concentration between dry and wet periods is depicted in Figure 6. It emerges that during the dry period the value of chloride ion concentration is higher than during the wet period in the majority of groundwater samples. This increase in the coastal areas is obviously attributed to the seawater intrusion due to water level drawdown. The groundwater level change in relation to the chloride ion concentration change between the two periods is illustrated in Figure 7. As can be seen from the diagram, the chloride ions tend to rise as the groundwater level decreases. On average, an increase in chloride ions by 25 mg/l is observed with a 1 m groundwater level drawdown. In addition, there is a decline in nitrates from the wet to the dry period. This can be explained by the fact that fertilisation takes place during the summer months, while infiltration and transportation from the upper soil layers to the aquifers is much higher during winter due to rainfall. The effect of fertilisation on the groundwater quality is evident after the infiltration processes are completed.

Figure 5 - Spatial distribution of chloride ions concentration (April 2010).

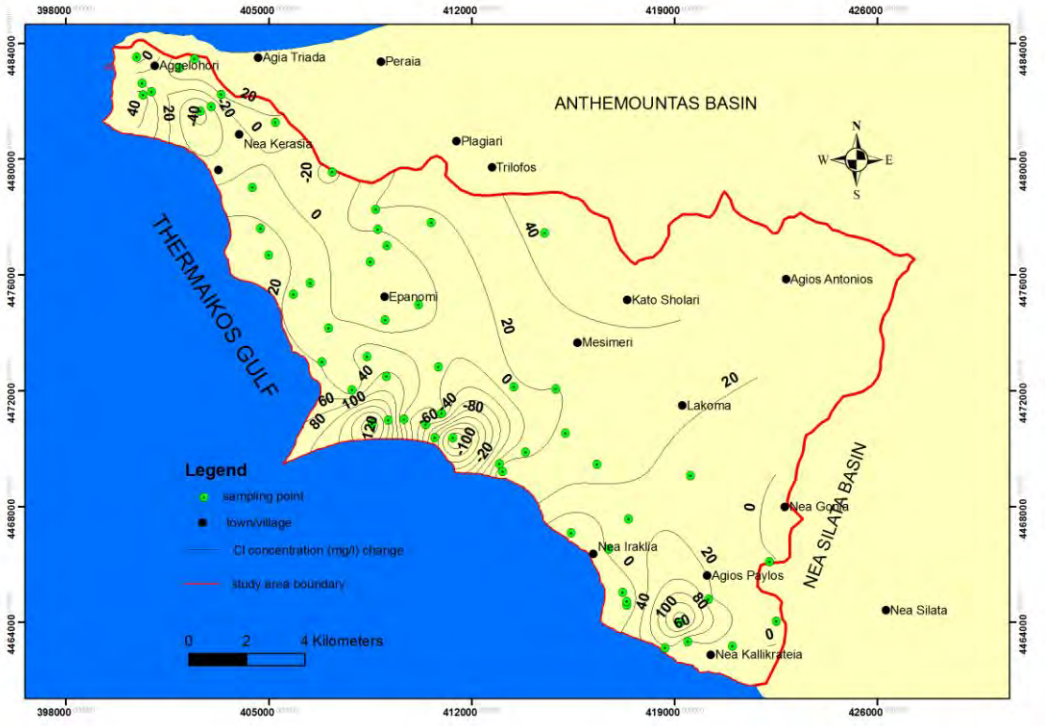

Figure 6 - Chloride ions concentration change, during the period April 2010- September2010.

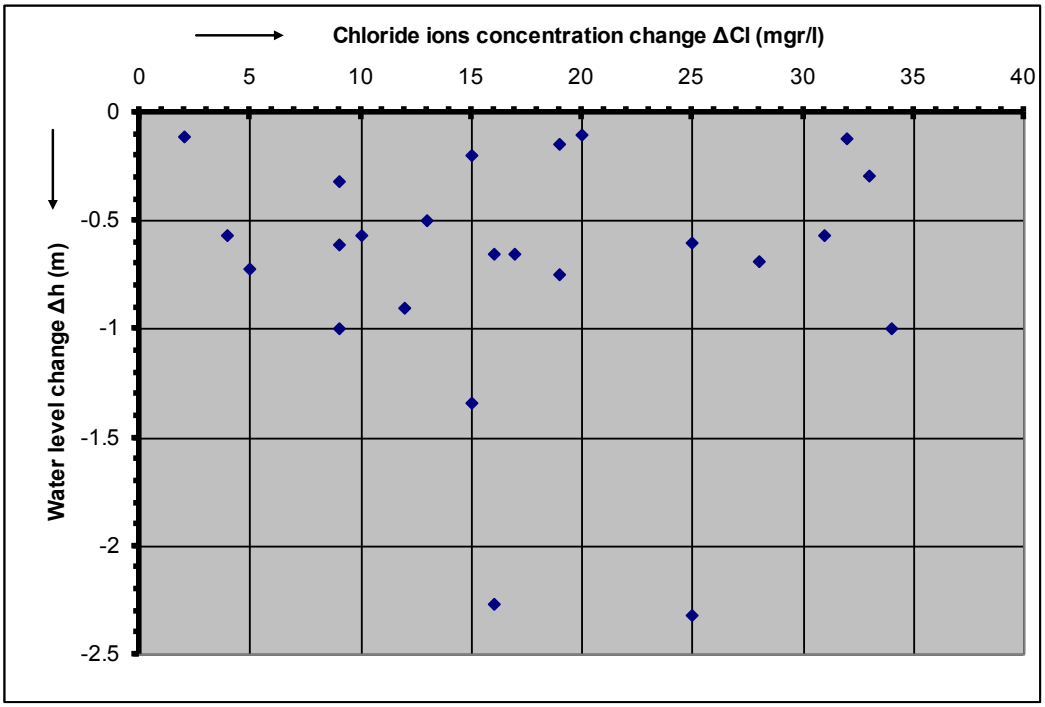

Figure 7 - Relation between water level change and Cl^- concentration change during April 2010- September 2010.

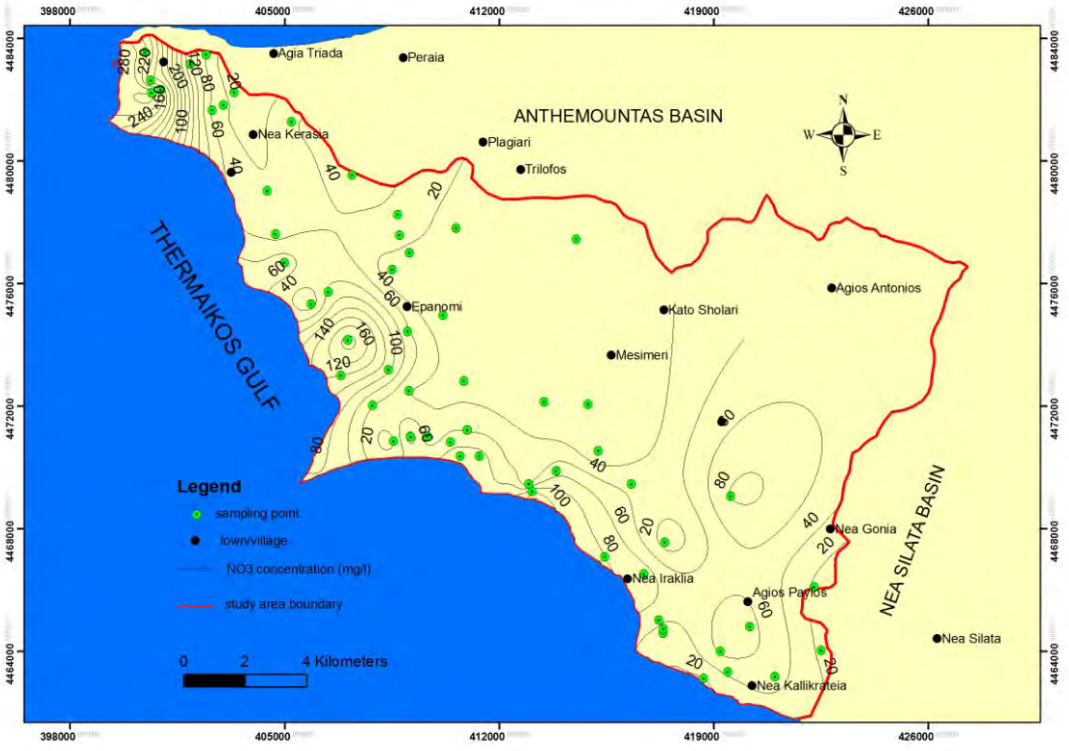

Figure 8 - Spatial distribution of nitrate ions concentration (April 2010).

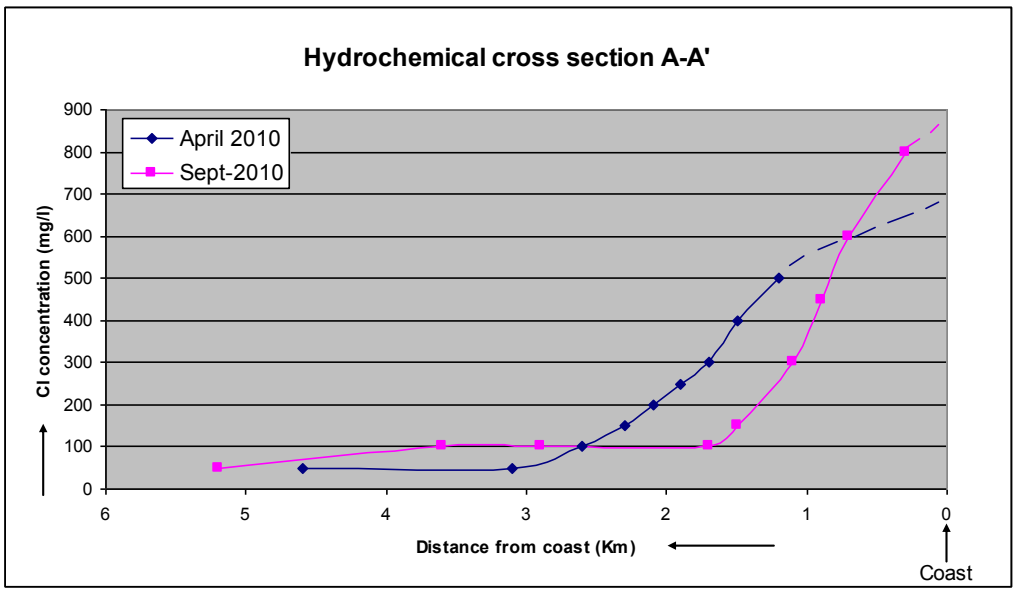

Figure 9 – Hydrochemical cross section (Cl^- concentration).

At a distance of 2.5 km from the coast an increase of the Cl^- concentration was observed according to the hydrochemical cross sections in Figure 9. Seawater intrusion is insignificant in inland areas. An intra-annual fluctuation is also observed, with high Cl values at the end of the dry period (September).

3. Conclusions

An increased concentration of chloride ions has been detected in the coastal zone of the studied area, attributed to seawater intrusion as a result of over-pumping and groundwater level change. There is also an increased concentration of nitrates due to the use of nitrogenous fertilisers for agricultural purposes. The nitrate concentration decreases during the dry period owing to over-pumping and increases at the end of the wet period due to infiltration. A systematic monitoring programme for both quality and quantity should be established in selected boreholes to mitigate seawater intrusion phenomena and nitrate pollution on a large scale.

4. References

Diamantis J. and Petalas C. 1989. Sea water intrusion into coastal aquifers of Thrace and its impact on the environment, *Toxic. and Env. Chemistry,* v. 20-21, p. 291-305.

Henry H.R. 1960. Salt intrusion into coastal aquifer, *Intern. Assoc. Scientific Hydrology, publ. n^o 52,* p. 478-487.

I.G.M.E. 2008. Further characterization of the aquifers, Directive 2000/60/EC-Implementation of Article 5, Report volume.

Koumantakis I., 2006. Geological problems and their treatment at Thermaikos Municipality, Research programe *Final Report*, N.T.U.A.

Lalechos N. and Bison G. 1969. Geological Map of Greece 1:50000 Sheet Epanomi, *Editions I.G.M.E.*

Mollat H., Antoniadis P., Christodoulou G., Parginos D. and Kourmoulis N. 1978. Geological Map of Greece 1:50000 Sheet Vasilika, *Editions I.G.M.E*.

Mountrakis D. 2010. *Geology and geotectonical evolution of Greece*, University Studio Press, 374 pp.

Papageorgakakis I. and Koumantakis I. 1978. Hydrogeological study of Chalkidiki and Anthemounta and Epanomi basins, Technical Report*, Agriculture Ministry.*

Petalas C. and Diamantis I., 1999. Origin and distribution of saline groundwaters in the upper Miocene aquifer system, coastal Rhodope area, northeastern Greece, *Hydrogeology Journal*, v.7, issue 3, 305-316.

Pulido-Leboeuf P. 2004. Seawater intrusion and associated processes in a small coastal complex aquifer (Castell de Ferro, Spain), *Applied Geochemistry*, v. 19, issue 10, 1517-1527.

Soulios, G., 2004. *General Hydrogeology*, *volume III*, Kyriakidis bros publishing house*,* Thessaloniki, 250 pp.

Syrides G. 1990. Lithostratigraphic, biostratigraphic palaeogeographic study of the Neogene - Quetarnary sentimentary deposits of Chalkidiki Peninsula, Macedonia, Greece. *PhD Thesis*, School of Geology, A.U.TH., 230 pp.

Todd D.K. 1953. Sea water intrusion in coastal aquifers, *Amer. Geophys. Union trans,* v. 34, n^o 5, p. 749-754

Voudouris K., Panagopoulos A., Daniil D. 2000. Implications to surface water quality of Korinth's Prefecture from anthropogenic activities, *Proc. of Intern. Conference "Protection and Restoration of the Environment* V", Vol. I, 235-242.

Voudouris K., Panagopoulos A. and Koumantakis I. 2004. Nitrate pollution in the coastal aquifer system of the Korinthos Prefecture (Greece), *Global Nest: The International Journal*, vol. 6, n.1, 31-38.

Δελτίο της Ελληνικής Γεωλογικής Εταιρίας, τομ. XLVII, 2013
Πρακτικά 13ου Διεθνούς Συνεδρίου, Χανιά, Σεπτ. 2013

Bulletin of the Geological Society of Greece, vol. XLVII 2013
Proceedings of the 13th International Congress, Chania, Sept. 2013

IS THE CONSTRUCTION OF A SANITARY LANDFILL ACCEPTABLE IN A KARSTIC AREA? THE CASE OF THE SANITARY LANDFILL SITE IN FOKIDA, CENTRAL GREECE

Soulios G.[1], Mattas C.[1], Kaklis T.[1], Sotiriadis M.[1], Voudouris K.[1] and Dimopoulos G.[1]

[1] *Aristotle University of Thessaloniki, School of Geology, Department of Geology, Laboratory of Engineering Geology and Hydrogeology*

gsoulios@geo.auth.gr, cmattas@geo.auth.gr, kaklis@geo.auth.gr, msotiria@geo.auth.gr, kvoudour@geo.auth.gr, gdimop@geo.auth.gr

Abstract

This paper investigates the suitability of a specific site for the construction of a sanitary landfill. The following works were performed: detailed geological mapping at a scale of 1:5,000, a geological-hydrogeological cross-section of the sanitary landfill, drilling exploration including the construction of a deep borehole for the detection of any perched aquifer, core logging and in situ permeability tests, implementation of the DRASTIC and EPIC methods to estimate the aquifer's vulnerability. Finally estimation of the total annual amount of solid waste that will be deposited into the sanitary landfill and determination of the pollution load.
Key words: *karstic aquifer, vulnerability, solid waste.*

Περίληψη

Για τη μελέτη της καταλληλότητας μιας συγκεκριμένης θέσης ως Χ.Υ.Τ.Υ. πραγματοποιήθηκαν οι εξής ερευνητικές εργασίες. Εκπόνηση λεπτομερούς γεωλογικής χαρτογράφησης σε αρχική κλίμακα 1:5.000 και στη συνέχεια κατασκευή γεωλογικής-υδρογεωλογικής τομής που περνάει από τη θέση του Χ.Υ.Τ.Υ. Στη συνέχεια εκτελέσθηκε γεωτρητικό πρόγραμμα τόσο με βαθιά γεώτρηση για τη διαπίστωση ύπαρξης στάθμης υπόγειου υδροφόρου ορίζοντα όσο και δειγματοληπτικές γεωτρήσεις με δοκιμές εισπίεσης. Επιπλέον, εφαρμόσθηκαν μέθοδοι εκτίμησης της τρωτότητας υποκείμενου υδροφόρου στρώματος (DRASTIC και EPIC). Τέλος υπολογίσθηκε ο ετήσιος όγκος απορριμμάτων που θα τοποθετούνται στο Χ.Υ.Τ.Υ., ο οποίος δίνει και το μέγεθος του ρυπαντικού φορτίου.
Λέξεις κλειδιά: *καρστικός υδροφορέας, τρωτότητα, στερεά απόβλητα.*

1. Introduction

The Association for Waste Products Management of the Prefecture of Fokida assigned to us the task of researching the suitability of the "Vartos" area as a place for the construction of a sanitary landfill. The proposed area, as shown in Figure 1, is located between Parnassos and Gkiona Mountains, at a distance approximately 3 km northwest of Eleonas village, which is the closest

populated place to the study area. The site satisfies the general requirements arising from the legal framework. The whole area is mainly constituted by karst limestone formations and there is a general view among the geologists that "a priori" the karst areas are improper for the construction of sanitary landfill. We assume that this generalised conception needs to be evaluated in cases like the present one.

The siting of a landfill is a difficult, complex and protracted process requiring evaluation of many different criteria (Chang et al., 2008; Vatalis & Manoliadis, 2002). Research on the suitability of a site for the construction of a sanitary landfill mainly comprises investigation of the transmission of pollutants underground and especially in groundwater bodies. This case is different from the case of selection of the most suitable site amongst others proposed sites which meet the basic suitability criteria (Soulios, 2006).

2. Geological Structure

2.1. Geotectonic Setting

The area belongs to the Parnassos- Giona geotectonic Unit (Renz, 1940) that has been studied in detail by Celet (1962). The northeast part of the study area forms a nappe structure upon Cenomanian limestones of the Sub-Pelagonian zone (Aubouin, 1959).

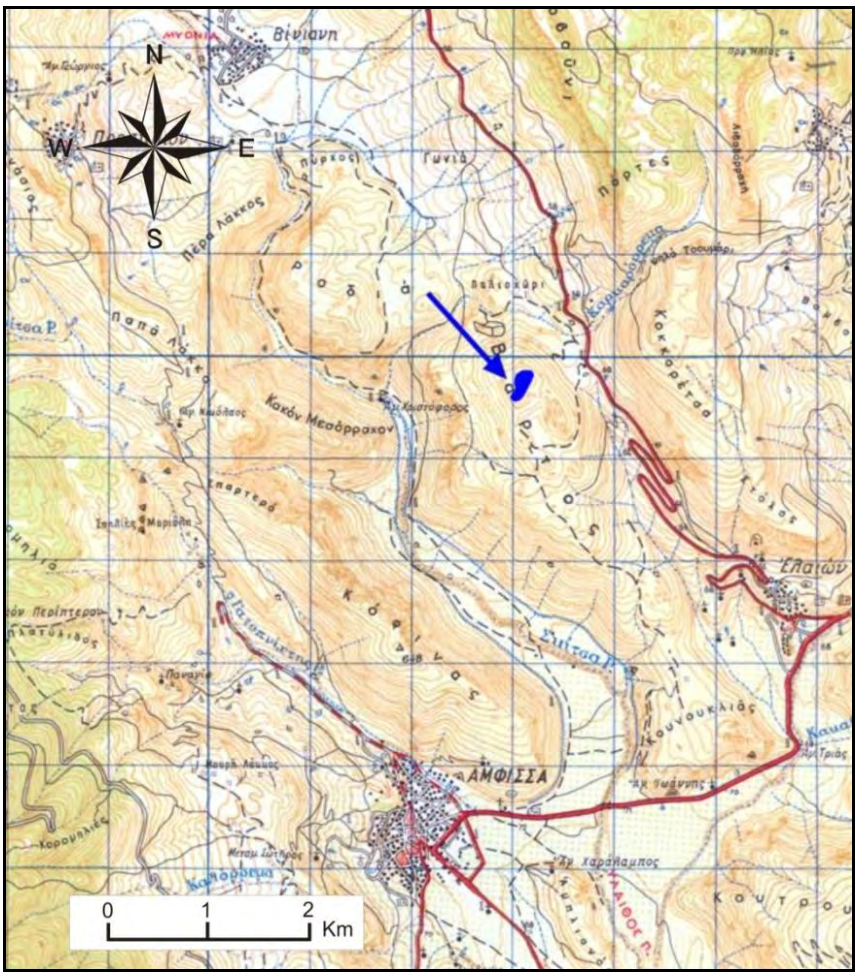

Figure 1 - Site of the studied sanitary landfill.

2.2. Geological Formation

According to the IGME (Institute of Geology and Mineral Exploration) geological map, scale 1:50,000 (Papastamatiou, 1960), the geological formations that appear around and close to the study area (Figure 2), are the following (from the most recent to the oldest):

Post-alpine formations:

- Man made soil deposits , sediments, fragmented materials
- Quaternary deposits (clays, sands, gravels)

Parnassos–Giona unit formations:

- Flysch (P.K.11): thin, laminated, in places clayed, reddish, or calcareous greenish brown or dark mudstone. The age of this formation is Palaeocene–Eocene and its thickness is around 150–250 m.

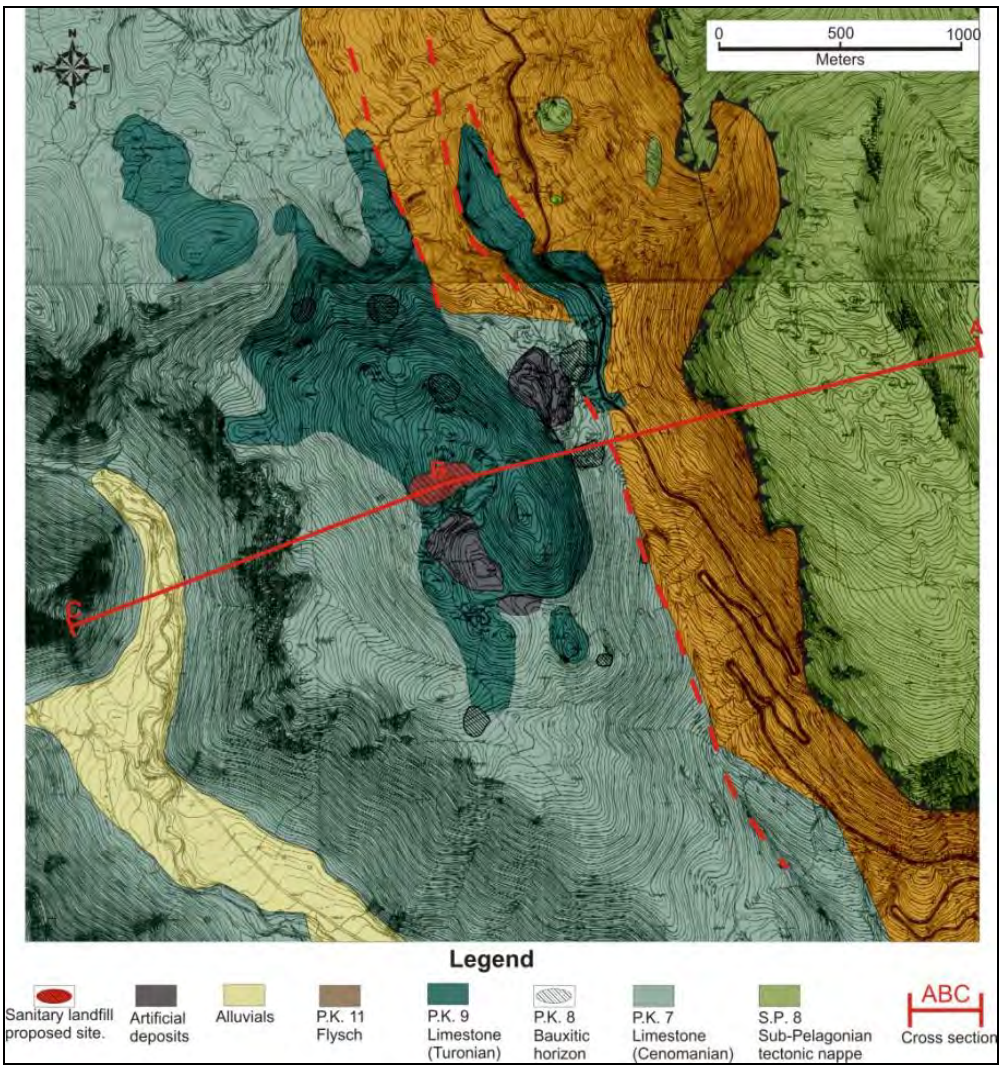

Figure 2 - Geologic map of the studied area.

- Limestone (P.K. 9): variegated (grey, dark grey, sub-white), medium-bedded to thick-bedded, and intensely karstified. A rich fauna of Rudistae fragments is located in this

formation. The age of this formation is Upper Cretaceous (Turonian-Senonian) and its thickness varies between 100 and 150 m.

- Bauxitic horizon (P.K.8): the upper (third) bauxitic horizon. There is no monocline or continuous presence and appearance. Its age is Cenomanian–Turonian.

Limestones (P.K.7): black, yellow-black, yellow-white, yellow-grey, and marly by positions. Their lithology varies vertically and laterally. They are medium-bedded and massive in some places. Little to moderate karst is present in this formation. Its age is Middle–Upper Cretaceous (Cenomanian). Its thickness is more than 400–500 m. This limestone forms the base of the sanitary landfill.

Sub–Pelagonian mass formations

- Limestone tectonic nappe consisting of fragmented whitish, blackish, mainly medium-bedded limestones (S.P.8). In places and mainly at the base it carries a clay-sandstone series. Its age is Turonian–Maestrichtian. Its thickness varies across the area, but in the study area ranges from 250 m to 300 m.

2.3. Tectonic Setting

Regarding tectonics, folding (syncline folds, anticlinal folds) with a large radius of curvature is present. The folding axis has a direction of NNW to SSE, with or without a minor sinking angle. The tectonic of the area is characterized by large block structure in opposition to the multi folding structures which appear in neighbouring areas (Pindos mass etc).

The faults mainly have a vertical direction with vertical movement, with or without a small horizontal movement.

3. Drilling Exploration

3.1. Drilling Programme

For the detailed study of the geological basement on which the sanitary landfill will be constructed, the following works were performed:

- Drilling of a 140 m deep borehole for the detection of any perched or epikarstic aquifers. The water level of the main aquifer at the location where the sanitary landfill will be constructed is at a depth of 500 m below the ground surface.
- Logging and sampling from four boreholes with a depth up to 20–22 m with complete core sampling. The hydraulic conductivity was determined at every 3 meter intervals using the Lugeon or Maag method.

3.2. Deep Borehole Evaluation

The deep borehole did not encounter the aquifer. The drilling was completed in May 2009; therefore if a perched aquifer exists it would have been detected.

3.3. Core Sampling Borehole Evaluation

Interesting results were derived from the core logging, sampling and permeability tests, as illustrated in Figure 3 that refers to one of the boreholes. The results are as follows:

- The degree of fracturing can be characterized as usual to low and the karstification very low.
- The hydraulic conductivity ranges from 10^{-5} m/sec to 10^{-7} m/sec, and it corresponds to geological formations that are semi-pervious to impervious. Taking into account that this coefficient corresponds to the horizontal conductivity, that is, the one that is parallel to the layering, it is obvious that the vertical conductivity will be significantly smaller. Therefore, the entire geological formation on which the sanitary landfill will be constructed can be considered impervious or marginally semi-pervious, that implies the diffusion of pollutants.

4. Hydrogeology

4.1. Hydro-lithology

From a hydrolithological point of view, the geological formations are classified as follows:

- Flysch (PK11), which can be considered as an impervious formation.
- Limestones of Turonian–Senonian age (PK9), karstified and very permeable, as deduced from the field investigation.
- Limestones of Cenomanian age (PK7), which have locally moderate to low permeability or impermeability in places or along bedding, as deduced from the results of permeability tests. Locally they are marly and they are characterized by low karstification or no karstification.
- The sub-Pelagonian tectonic nappe consisting of limestone of Turonian-Maestrichtian age that is permeable. A productive aquifer is developed within this formation.

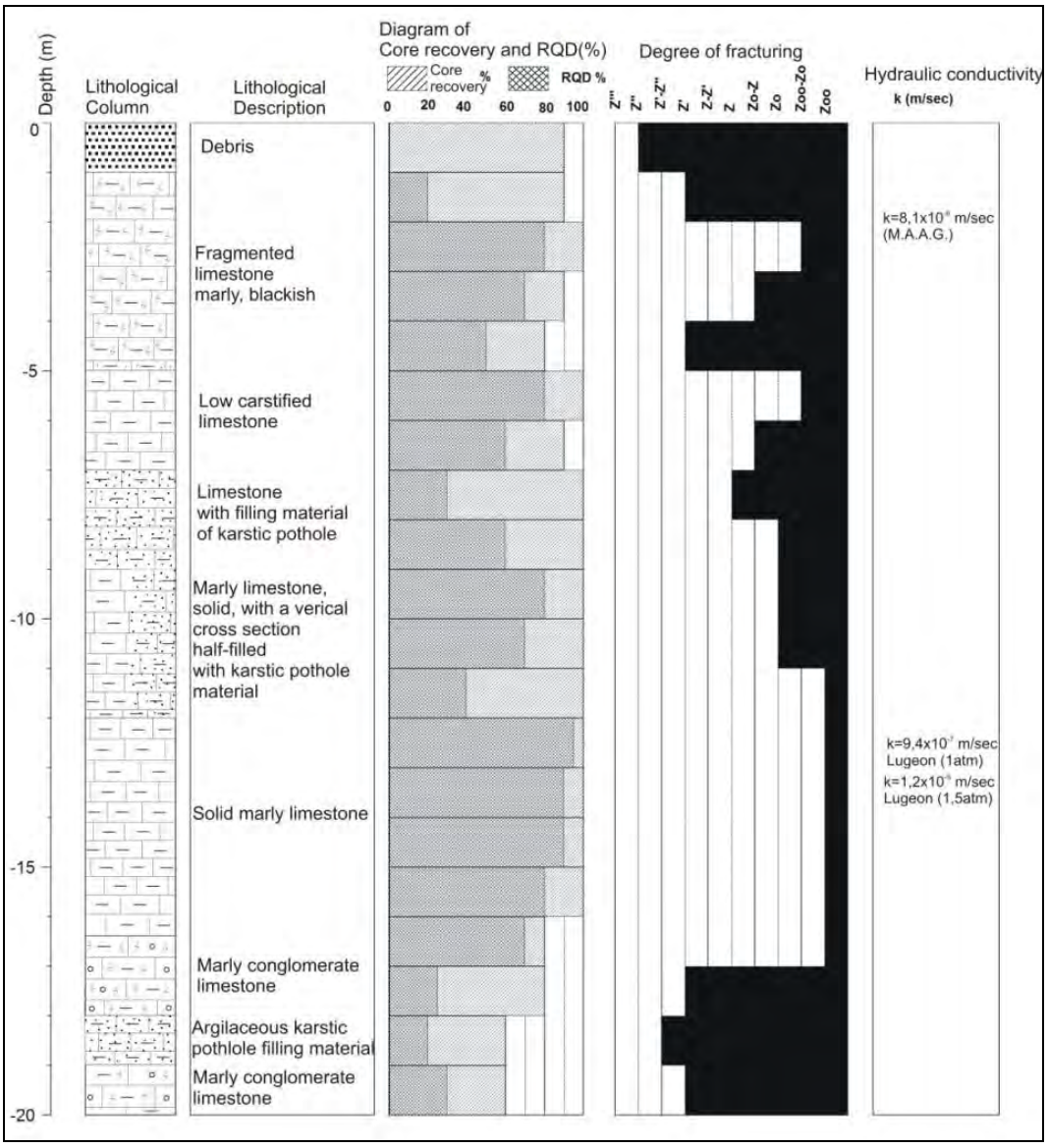

Figure 3 - Geological-geotechnical column of a constructed borehole.

4.2. Aquifer Systems

In Figure 4, a geological-hydrogeological section ABC is shown. From this section the following conclusions can be drawn.

- An aquifer system is developed within the sub-Pelagonian nappe and is discharged through Elaionas springs. The impervious basement is made up of flysch (PK11) of the Parnassos zone.
- As deduced from the existing boreholes, the depth to the water table is approximately 200 m below the ground surface or 500 m below the bottom of the proposed sanitary landfill site. It is concluded that the underlying geological formation (locally semi-impervious to impervious) may eliminate the risk of pollution from the sanitary landfill.

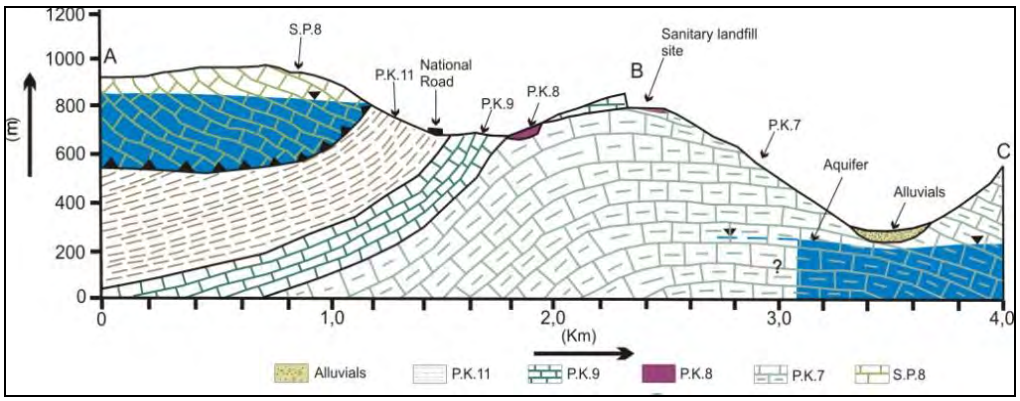

Figure 4-Indicative geological cross section (symbols as shown in Figure 2).

5. Vulnerability Assessment

5.1. Karstic Aquifer Vulnerability Assessment Methods

The degree of aquifers protection against pollution from human activities is expressed by vulnerability. In order to assess the vulnerability, many methods have been developed, each of which uses different numbers of parameters. In this work two methods (DRASTIC, EPIC) of intrinsic vulnerability were applied. The application of these methods has led to the design of vulnerability maps, which are useful tools for groundwater protection and land use planning (Panagopoulos et al., 2009; Voudouris et al., 2010; Kazakis & Voudouris, 2011).

5.2. DRASTIC Method

DRASTIC (Aller et al., 1987) is a method for "any type of aquifer" that has some limitations in application to karstic aquifers (Polemio et al., 2009). The higher the DRASTIC Index (DI), the greater the groundwater pollution potential or the aquifer's vulnerability (Doerfliger et al., 1999). The DI values range from 23 (absolutely not vulnerable) to 230 (absolutely vulnerable). Based on the results, the DI value for the proposed sanitary landfill site is 102, indicating low to moderate vulnerability.

5.3. EPIC Method

The EPIC method was designed to be applied to karstic aquifers and takes into consideration four karst attributes (Gogu & Dessargues, 2000): epikarst, protective cover, infiltration conditions, and karst network. Based on the results of the application of the EPIC method, the protection factor in the proposed sanitary landfill site was estimated to be 29, indicating low vulnerability, similar to the result of the DRASTIC method.

It is concluded that the aquifer system below the proposed sanitary landfill site has low to moderate vulnerability and for this reason there will be no pollution risk from the construction of the particular sanitary landfill to either groundwater or surface water due to the absence of torrents in the wider region.

6. Solid Waste Production in Fokida Prefecture – Sanitary Landfill Technical Standards

6.1. Population of Fokida Prefecture

According to the 2001 census, the population of Fokida Prefecture, (except of the Municipality of Efpalinio, which is not under the jurisdiction of the Association for Waste Products Management), is 42,000 inhabitants. 25% of them do not reside permanently in Fokida. However, during the summer, the population increases due to tourism. The equivalent population is estimated to be 40,000–42,000 inhabitants.

6.2. Waste Production

According to a study of this specific area (Sanozidou, 2008), the annual solid waste amount (except for Efpalinio) is estimated to be 17,658 tons. Based on data provided by the Association for Waste Products Management, this amounts to 16,994 tons. The waste production in Fokida is assumed to be, 1.1 kg/person per day (according to the statistical mean of Greece) and the annual amount is estimated to approximately 17,000 tons. Taking into account a population increase in the following 10–20 years, the total annual amount will reach 20,000 tons, assuming that the recorded economic recession in our country during the last five years does not affect the production of solid waste.

6.3. Waste Composition

There are many published papers regarding the composition of the solid waste (e.g. Tchobanoglous et al., 1993; Soulios, 2006; Voudouris, 2009). In this paper we accept that the most representative composition is the one mentioned in the Joint Ministerial Decree 50910724/2003, according to which 70% of the waste is recyclable after sorting, while this percentage decreases to 50% if the sorting takes place at household level.

6.4. Technical Standards

The technical standards for sanitary landfills were established by the Joint Ministerial Decree (J.M.C.) 114218 (Official Government Gazette 10116B'/17-11-1997) and Ministerial Decree 29407/3508 (Official Government Gazette 1572B'/16-12-2002). Nevertheless, the placement of a natural clay layer is suggested for additional environmental protection.

Based on the above, the annual amount of waste that will arrive at the sanitary landfill will be 10,000 tons at most and probably less. This amount determines the pollution load and the environmental risk of the sanitary landfill under study, which is proportionally very small, compared, for example, to Mavrorachi landfill (Thessaloniki Prefecture), which receives 400,000 tons annually (Soulios 2006).

7. Conclusions

The geological basement at the sanitary landfill site consists of marly limestones, characterized by low karstification, and hydraulic conductivity value ranging between 10^{-5} and 10^{-7} m/s. The subjacent aquifer lies at a depth of 500 m below the bottom of the proposed sanitary landfill. Implementation of the DRASTIC and EPIC methods indicated that the aquifer has low to moderate vulnerability to pollution. The annual solid waste weight is approximately 10,000 tons, which does not indicate a high pollution load. Finally, special construction standards (see §6.4)

should be applied in order to eliminate any risks of pollution. Using geological-hydrogeological criteria, the specific site is considered suitable for the construction of a sanitary landfill.

8. References

Aller L., Bennet T., Lehr J.H., Petty RJ. and Hackett G. 1987. DRASTIC: a standardized system for evaluating groundwater pollution potential using hydrogeological setting, *EPA/600/2-87/035. US Environmental Protection Agency,* 163 pp.

Aubouin J. 1959. Contribution a l'étude géologique de la Grèce septentrionale: les confins de l' Epire et de la Thessalie, *A.G.P.H.,* 10, 484pp.

Celet P., 1962. Contribution à l'étude géologique du Parnasse-Kiona et d'une partie des régions méridionales de la Grèce continentale, *Ann. Geol. Pays Hell.,* 13, 446 pp.

Chang N, Parvathinathanb G. and Breden J.B. 2008. Combining GIS with fuzzy multicriteria decision making for landfill siting in a fast-growing urban region, *Journal of Environmental Management* 87, 139-153.

Doerfliger N., Jeannin P.Y. and Zwahlen F. 1999. Water vulnerability assessment in karst environments: a new method of defining protection areas using a multi-attribute approach and GIS tools (EPIK method), *Environmental Geology 39 (2),* 165-176.

Gogu R.C. and Dessargues A. 2000. Sensitivity analysis for the EPIK method of vulnerability assessment in a small karstic aquifer, S. Belgium. *Hydrogeology Journal*, 8, 337-345.

Kazakis N. and Voudouris K., 2011. Comparison of three applied methods of groundwater vulnerability mapping: A case study from the Florina basin, Northern Greece, Advances in the research of aquatic environment, (Eds: Lambrakis N., Stournaras G., Katsanou K.), Springer. *Proc. of 9th International Conference on Hydrogeology,* Kalavrita, October 5-8, 2011, 2, 359-367.

Panagopoulos G., Antonakos A. and Lambrakis N., 2005. Optimization of the DRASTIC method for groundwater vulnerability assessment via the use of simple statistical methods and GIS. *Hydrogeology Journal*, 14, 894-911.

Papastamatiou I., 1960. Geological mapping of Greece 1:50.000, Sheet Amfissa, *I.G.M.E. Publications*.

Polemio M., Casarano D. and Limoni P.P. 2009. Karstic aquifer vulnerability assessment methods and results at a test site (Apulia, southern Italy), *Natural Hazards and Earth System Sciences*, 9, 1461-1470.

Renz, C. 1940. Die Tectonic der Griechisen Gebirge, *Mem. Acad. Athens,* 8, 171 pp.

Sanozidou M. 2008. Environmental study consideration of the Fokida Prefecture Sanitary Landfill, *Unpublished Technical Report* submitted to the Association for waste products management of Prefecture of Fokida (in Greek)

Soulios G., 2006. *General Hydrogeology*, IV, University Studio Press Publications.

Tchobanoglous G., Theisen H. and Vigil S.A. 1993. *Integrated solid waste management,* McGraw-Hill, 978 pp.

Vatali, K. and Manoliadis O. 2002. A two-level multicriteria DSS for landfill site selection using GIS: Case study in western Macedonia Greece. *Journal of Geographic Information and Decision Analysis*, Vol. 6, No 1, 49-56.

Voudouris K. 2009. *Environmental Hydrogeology,* Thessaloniki, Tziola Publications, 460 pp (in Greek).

Voudouris K., Kazakis N., Polemio M. and Kareklas, K. 2010. Assessment of intrinsic vulnerability using DRASTIC model and GIS in the Kiti aquifer, Cyprus, *European Water,* 30, 13-24.

Δελτίο της Ελληνικής Γεωλογικής Εταιρίας, τομ. XLVII , 2013
Πρακτικά 13ου Διεθνούς Συνεδρίου, Χανιά, Σεπτ. 2013

Bulletin of the Geological Society of Greece, vol. XLVII 2013
Proceedings of the 13th International Congress, Chania, Sept. 2013

WATER RESOURCES MANAGEMENT IN SPERCHIOS RIVER BASIN, USING SWOT ANALYSIS

Stathopoulos N.[1], Rozos D.[1] and Vasileiou E.[1]

[1] National Technical University of Athens, School of Mining Engineering & Metallurgy, Section of Geological Sciences, Laboratory of Engineering Geology & Hydrogeology, Iroon Polytechneiou 9, Zografou Campus,Athens 15780

nstath@metal.ntua.gr, rozos@metal.ntua.gr, elvas@metal.ntua.gr

Abstract

SWOT (Strengths, Weaknesses, Opportunities and Threats) analysis is a useful tool for sustainable development and decision making about environmental planning and water resources management. This analysis was applied in order to evaluate the water resources of the wider area of Sperchios River.

Sperchios River basin, with an average altitude of approximately 810m, covers an area of 2116 km^2. The river is recharged by many streams of permanent and periodic flow and discharges in Maliakos Gulf. The steep slopes, which are present within approximately 2/3 of the total length of the river course, form a rather mountainous topography (streamy, with crucial flooding peaks and very intense sediment yield). Only in the last downstream part of Sperchios course, the topography gradually changes into a lowland relief, with an extent at the river mouth of 1830 km^2. At this part of Sperchios severe cases of flooding have been occasionally observed and reported.

Regarding the SWOT applications on the wider area of Sperchios River, various data were processed (geological, meteorological, hydrological, hydrogeological, land use, socio-economic and environmental parameters) in order to suggest a water management planning in the area.

Key words: *Maliakos Gulf, environmental pressures, sustainable management.*

Περίληψη

Η μέθοδος SWOT (δυνάμεις, αδυναμίες, ευκαιρίες, κίνδυνοι) είναι ένα χρήσιμο εργαλείο για την βιώσιμη ανάπτυξη και την λήψη αποφάσεων ως προς τον περιβαλλοντικό σχεδιασμό και την διαχείριση των υδατικών πόρων. Η ανάλυση αυτή εφαρμόστηκε με σκοπό την αξιολόγηση των υδατικών πόρων της ευρύτερης περιοχής του Σπερχειού ποταμού.

Η υδρολογική λεκάνη του Σπερχειού ποταμού, με μέσο υψόμετρο περίπου 810m, καλύπτει μια έκταση 2116 km^2. Ο ποταμός τροφοδοτείται από ρέματα της περιοχής, μόνιμης και περιοδικής ροής, και εκφορτίζεται στον Μαλιακό κόλπο. Οι έντονες κλίσεις που επικρατούν σχεδόν στα 2/3 της συνολικής έκτασης της πορείας του ποταμού, σχηματίζουν μια ιδιαιτέρως ορεινή τοπογραφία (χειμαρρική, με οξείες αιχμές πλημμυρών και πολύ έντονη στερεοπαροχή). Μόνο στο τελευταίο τμήμα της διαδρομής ο Σπερχειός μετατρέπεται σε πεδινό ποταμό και διασχίζει χαμηλές

περιοχές, με την εκβολή του να καλύπτει έκταση 1830 km^2. Σε αυτό το τμήμα του ποταμού σοβαρές περιπτώσεις πλημμυρών έχουν παρατηρηθεί και καταγραφεί.
Για τις εφαρμογές της μεθόδου SWOT, στην ευρύτερη περιοχή του Σπερχειού ποταμού, συγκεντρώθηκαν διάφορα δεδομένα (γεωλογικά, υδρογεωλογικά, μετεωρολογικά, υδρολογικά, χρήσεων και κάλυψης γης, οικονομικο-κοινωνικές και περιβαλλοντικές παράμετροι) και έγινε επεξεργασία αυτών, προκειμένου να προταθεί ένα μοντέλο διαχείρισης των υδατικών πόρων της λεκάνης.
Λέξεις κλειδιά: *Μαλιακός κόλπος, περιβαλλοντικές πιέσεις, βιώσιμη διαχείριση.*

1. Introduction

Sperchios River basin extends from the east of Maliakos Gulf up to Tymfristos mountain in the west. From south the basin is delimited by the mountains Oiti and Kalidromo and from north by the mountain Orthris. The extent of the basin is almost 2116km^2, with an average altitude of 810m (Kakavas, 1984).

Sperchios riverbed is recharged by streams of permanent and periodic flow. The river's valley, in the 2/3 of its length, has steep slopes, which give to the river a rather mountainous – streamy character, with crucial flooding peaks and very intense sediment yield. On the contrary, at the last third of its course, Sperchios gradually transforms in a lowland river crossing low altitude areas, often causing severe flooding (Koutsogiannis, 2007).

The dominating land use of the basin is agriculture, therefore the water needs and mainly the irrigation needs are particularly increased. The proper water resources management of Sperchios basin is considered to be of high importance.

This paper constitutes a first approach in the area's water resources management via SWOT method analysis. The aim of this work is to locate all SWOT parameters in order a management model for water resources to be applied in the area of interest.

The conclusions and results of this paper are based on primary research that took place in the area, including conversations on targeted questions with citizens and local authorities, concerning the SWOT parameters that were evaluated as of great importance for this work.

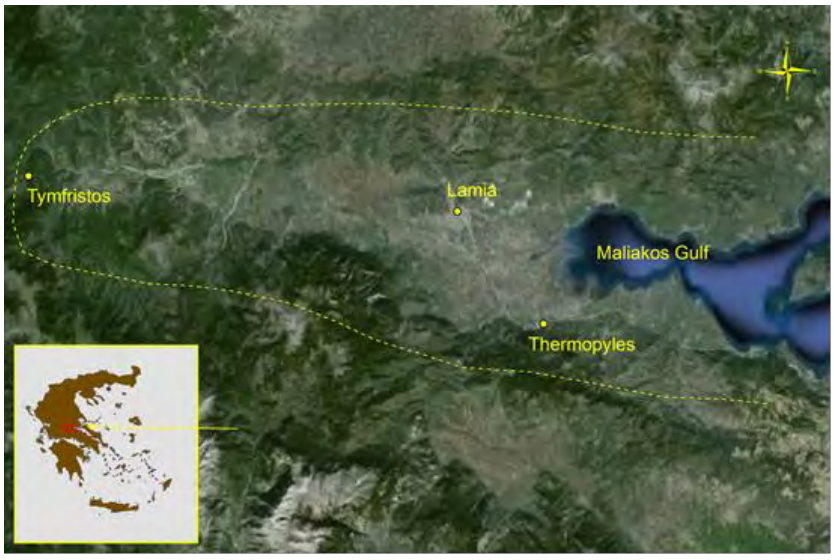

Figure 1 - Location of the study area.

Swot analysis is found to be a useful managerial tool, incorporating interdisciplinary issues-engineering, scientific, legislative, economic and social, which are difficult to quantify, in order to identify the main environmental problem of the study area, which is overexploitation of the groundwater resources (Kallioras et.al. 2010).

As groundwater becomes more critical, many countries increasingly face the challenges of multiple and competing stakeholders, competing uses of groundwater and variegated policy approaches for groundwater management (Kallioras et.al. 2010).

Groundwater is one of the most valuable natural resources in Greece, playing a vital role in the economy of the country. However, one could argue that this sensitive natural resource has been mismanaged during the last 60 years, which has led to a general qualitative as well as quantitative deterioration of the country's groundwater resources (Kallioras et. al., 2010).

Swot analysis is a form of market analysis introduced by Albert Humphrey at Stanford University in the 1960's and 1970s and is an acronym of its main components: strengths, weaknesses, opportunities and threats. It was subsequently applied as a general managerial tool in several scientific fields, including economics, law, environmental sciences and engineering, has been used in many case studies in water resources management and Engineering (Diamantopoulou and Voudouris, 2008).

2. Methodology

2.1. Geological Data

The creation of Sperchios basin is a result of tectonic movements, subsequent to the Alpine orogenesis cycle, mainly of faults of north – south and east – west direction. In the following time period the basin was filled with clastic sediments that came from the erosion of the basement's formations (IGME, 2010).

In the wider area, four unities of the Alpine orogenesis cycle are observed. North and south-southeast the Subpelagonian zone, in the center and south the Parnassos – Giona zone and in the west Pindos zone and upper Pindos zone (IGME, 2010).

Lithologically, Sperchios basin is separated in three unities: a) in the west, where flysch and clastic formations of Pindos unity are found, b) in the north-northeast, where limestone, ophiolite and schist-crest formations of Parnassos – Giona zone are found, c) in the south southeast, where lime-stone of Parnassos – Giona zone is the dominating formation (Psomiadis E.,2010).

The central part of Sperchios basin is covered by Quaternary formations, which consist of river and land deposits, such as clays, sands, conglomerates, detrital cones, stream deposits and breccia, whose composition and spreading depend on the adjacent or subjacent older formations. In the areas where hot manifestations are observed, deposition of hot spring limestone is noticed (traver-tine) (IGME, 2010).

The Neogene sediments, continental, lacustrine or marine, which can be found in north-east and south-east part of Sperchios basin and mostly in the borders, consist of cohesive marl, siltstones, clays, conglomerates and marly limestone with small lignite insertions (IGME, 2010).

The basement consists mainly of schist, limestone, dolomite, ophiolite, schist-crest and flysch formations (IGME, 2010).

2.2. Hydrogeology Data

The formations of Sperchios basin present different hydrogeological characteristics, due to their lithological composition, porosity and water permeability. Based on these data the formations are separated in the following categories (Kakavas N., 1984):

i. *Permeable formations*. This category includes carbonic rocks, conglomerates of lacustrine Pleistocene sediments, coarse materials of detrital cones, old and modern fanglomerates, as well as modern deposits of the riverbed.

ii. *Semi-permeable up to permeable formations.* This category includes the deep Sperchios delta deposits and the areas with alternations of sands, clays and grits, resulting in the creation of sub-confined and confined (artesian) aquifers. In addition, this category includes the ophiolite formations, as in this specific area they present increased permeability, due to secondary porosity caused by intense tectonism.

iii. *Semi- permeable formations.* This category includes the Quaternary deposits, consisting of mixed coarse and fine-grained materials. This heterogeneity develops limited and discontinuous aquifers. These formations are considered to be the flood deposits of Sperchios River, consisting of silt with layers of sand per places.

iv. *Impermeable formations.* In this category belong the formations that are considered to have permeability values from10^{-6} up to 10^{-9} m/sec. Referring to the study area, these are the schist-crest and flysch formations beside the conglomerates and limestone layers, the older Sperchios deposits of silt-clays and the limestone tuffs of the thermal springs' deposits.

Two large categories of aquifers are distinguished in Sperchios basin (Kakavas N., 1984):

i. Aquifers deploying in the alluvial deposits, which are both unconfined and confined (artesian). The unconfined aquifer that is formed almost in the whole surface of the alluvial deposits is heterogeneous. Its capacity is characterized as moderate up to satisfactory. The confined aquifer is found in deeper layers and especially where frequent alternations of coarse and fine-grained materials exist.

ii. Aquifers of carbonic formations. The limestone formations of Orthris, Kalidromo and Oiti, are intensely tectonized, fragmented and karstified, with increased porosity and water permeability. Three karstic systems are being formed, of Lamia – Stylida, of Oiti and of Kalidromo – Oiti. The first system is discharged through Agia Paraskeui, Sfagia and Mauromantila springs, the second one through the spring complexion of Kompotades – Meksiates and finally the last one through Mauroneria springs.

2.3. Meteorological Data

The climate ranges from dry to semi-humid. The average temperature is 16,8 ^{o}C in Lamia. The rainfall distribution at all stations is normal (figure 2), there is a linear regression between rainfall and the altitude in the area. The analysis of meteorological data showed decrease of rainfall (about 4 mm/yr) and runoff (3 mm/yr). The annual rainfall in the area is about 893 mm/yr. In Lamia meteorological station, in the east coastal part of the area, the average precipitation is about 561 mm. The total amount of evaporation is high, approximately 72%, the infiltration and the surface runoff is 28%. There is strong correlation between water table and discharge, as it is shown in figure 3 (Stathopoulos et. al, 2012).

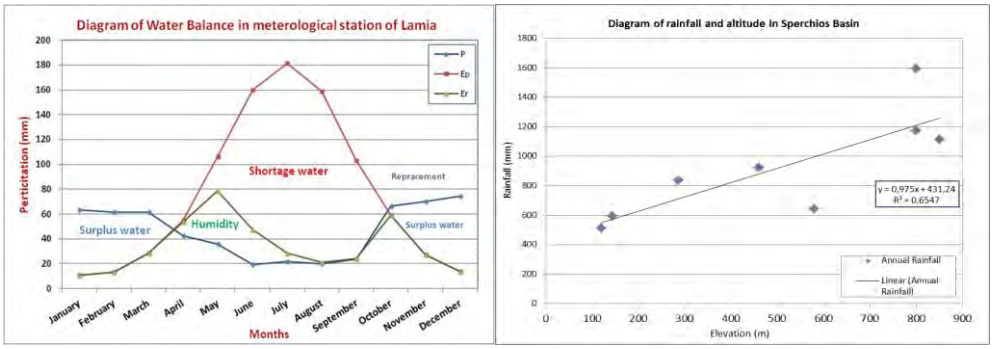

Figure 2 - Climatic diagram of water balance in Lamia and the correlation of rainfall and altitude (Stathopoulos et. al, 2012).

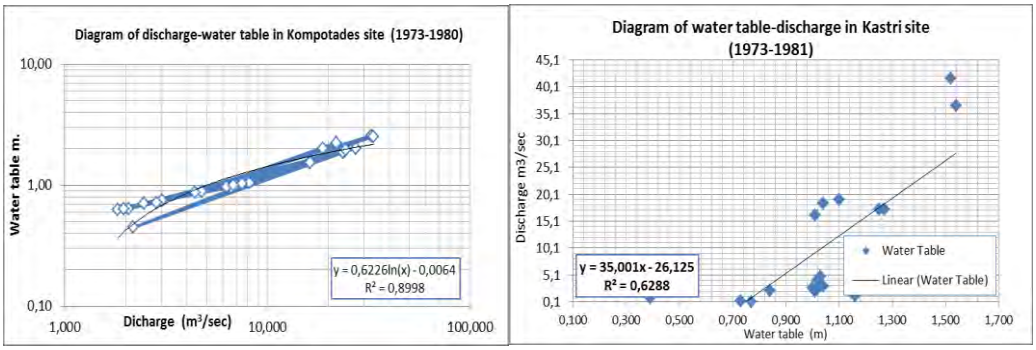

Figure 3 - Correlation diagram of water table and discharge in Kompotades and Kastri site (Stathopoulos et. al, 2012).

2.4. Land Use and Land Cover

Figure 4 presents the Land Cover map (Corine 2006) of the study area. As it can be noticed in table 1, the highest land cover percentage refers to hard leaf vegetation (about 20%). The main Land uses are the agricultural areas with significant natural vegetation as well as and the complex cultivation systems.

2.5. Water Quality Data

Sperchios River is the natural runoff recipient of the wider part of agricultural areas in Fthiotida prefecture. The waste from the city of Lamia, after partial processing and carbon and nitrogen removal, as well as the processed waste of Lamia's industrial area, also end up in Sperchios River. Sperchios River in the upstream part of its course is of better quality, while in the downstream part it deteriorates gradually, with the highest deterioration occurring in the deltaic part.

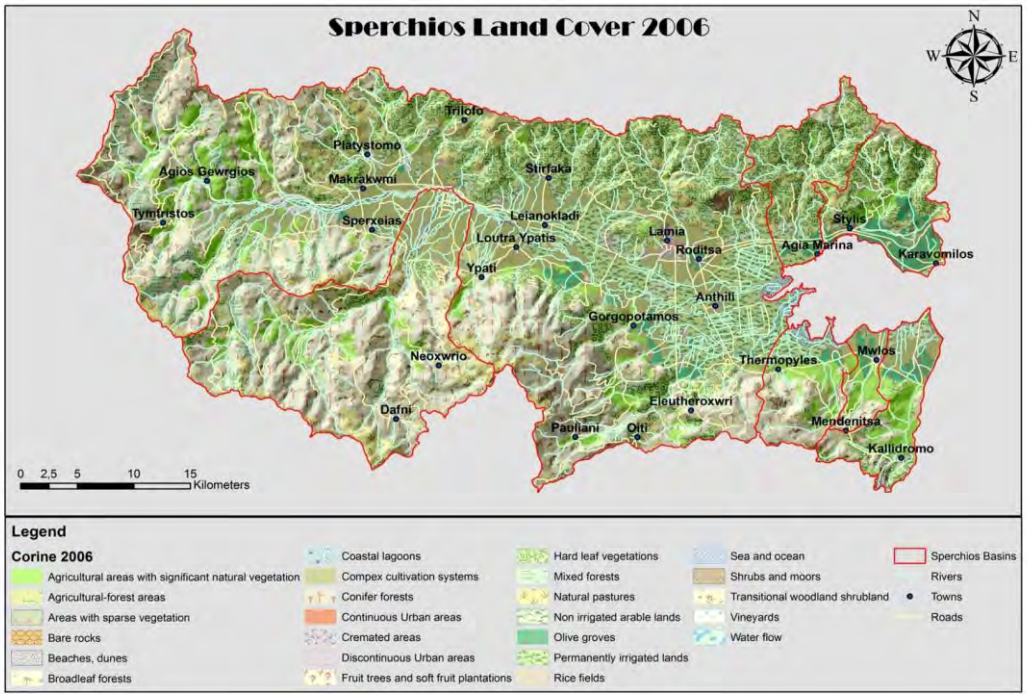

Figure 4: Land Cover/Use map – Corine 2006 (Stathopoulos et. al, 2012).

Table - Land Cover/Use percentages (Corine 2006).

Sperchios Basin Land cover - Land use	Percentages (%)
Transitional woodland shrubland	10,04
Broadleaf forests	8,20
Natural pastures	7,44
Conifer forests	13,80
Olive groves	2,84
Agricultural areas with significant natural vegetation	8,13
Compex cultivation systems	12,07
Mixed forests	3,68
Hard leaf vegetations	19,67
Non irrigated arable lands	3,61
Permanently irrigated lands	6,58
Other various land cover/use	3,94

Figure 5 - Pollution from fertilizers in Sperchios River (lowland area).

Based on the analysis of the hydro-chemical data from 99 samples of groundwater during the period from September 2005 up to August 2006, is noted that (Koutsogiannis, 2007):

- The electrical conductivity (EC) ranges between 323- 1370 μS/cm with an average value of 680μS/cm. Augmentation of the EC is recorded towards the coastal area, due to the loading of groundwater with salts as it flows and also due to sea intrusion.
- The nitric ions range between 0 – 155 mg/l with an average value of 28 mg/l (the limit of European Union for potable water is 50 mg/l). High values come of human activities and mainly because of intense agricultural activity with the application of fertilizers, as well as from the lack of sewage system and use of septic sinks in many areas. Thus per places groundwater becomes improper for potable use.
- Phenomena caused by sea intrusion are detected in the eastern part of Sperchios deltaic area.
- The concentration of Cl ions ranges between 7-174 mg/l with an average value of 29 mg/l.

Figure 6 - Obvious soil salinization in Sperchios delta area.

3. SWOT Analysis

SWOT analysis (figure 7) is a useful tool for planning development and decision making and has widely been applied to environmental planning and water resource management (AHRD 2001, Baser 2001).

Strengths and weaknesses are factors of the system (internal issues), while opportunities and threats are factors of the external environment (external issues). In other words, a SWOT analysis helps to find the best match between environmental trends (opportunities and threats) and internal capabilities and facilitate a strategic approach to administration (Richards 2001). Concerning the application of SWOT analysis, it is necessary to minimize or avoid both weaknesses and threats. Weaknesses should be converted into strengths (Danca 2000). Likewise, threats should be converted into opportunities.

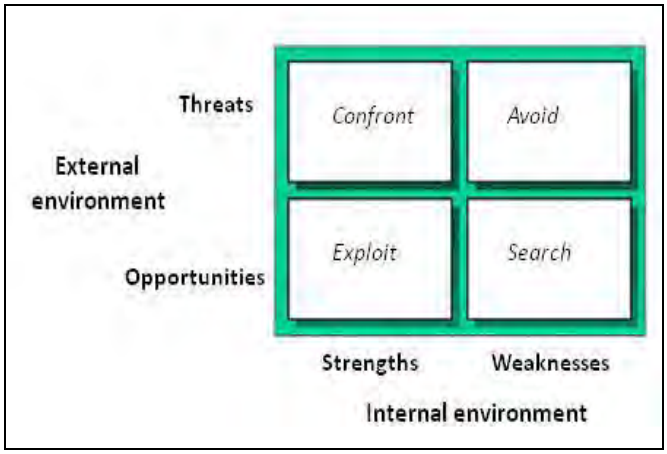

Figure 7 - SWOT analysis diagram.

The Strengths of the basin are:

- The capacity of river Sperchios, whose runoff crosses the whole basin, is significant (annual runoff 693,1hm^3). (Koutsogiannis, 2007)
- The availability of the surface water deposits during the wet and dry period.
- The existence of recent hydrogeological studies is an advantage for the rational water resource management, as it can provide new data and contribute to the planning of better strategies in order to achieve water sustainability.
- The existence of important thermal-springs in many sites of the basin that can be exploited for social-economic development of the area.
- The existence of karstic aquifers with annual water deposits of about 136hm^3/yr (Koutsogiannis, 2007).
- The existence of many environmentally protected areas (Natura).
- Water quality in the upper part of Sperchios River, is generally good. The water recharge is rich in quantity and of very good quality, thus improving and renewing, in a sufficient rate, the deteriorated water caused by human activities. Stathopoulos (2008), noticed the degradation of water quality by nitrate pollution and chloride because of the sea intrusion.
- There are biological treatment units in the wider area

The weaknesses of the basin are:

- Increased water demands, mainly during summer period
- The overexploitation of the area's water recourses for irrigative purposes.
- The lack of adequate monitoring data (groundwater levels, quality data, torrents, etc.). Especially, in Sperchios River (one of the most important rivers in Greece) there is no kind of monitoring for quality or discharge.
- The extended use of fertilizers, causing nitrate pollution.
- The salinization of coastal aquifers, mainly due to over-pumping of groundwater for irrigation purposes and also due to natural sea intrusion.
- Quality deterioration of the area's water resources, due to urbanization (urban wastes).
- In the lower part of Sperchios, the water quality is deteriorated
- The total basin is characterized as in high risk for erosion
- In most of the villages there are septic sinks, which cause problems to water quality. The lack of a proper sewage system in the area must be mentioned.
- Water deterioration caused by industrial wastes.
- The periodic flooding of the lowland areas via Sperchios River due to extreme rainfall events.
- Urbanization, construction of public transportation network infrastructure.

The opportunities of the basin are:

- There are many biological treatment units in the area, which doesn't work at this time. The operation of them will help to the proper management of the waste waters.
- The existence of thermal springs. This is a significant factor for the touristic development of the area and the financial regeneration.
- The EU Framework Directive (2000/60/EC). This Directive provides new legislation and opportunities for the sustainable management of water resources.
- The directive requires the establishment of monitoring programs covering groundwater quantitative and qualitative status.

- Directive 2006/21/EC of the European Parliament and of the Council of 15 March 2006 on the management of waste from extractive industries and amending Directive 2004/35/EC - Statement by the European Parliament, the Council and the Commission.
- There are many protected areas in the basin (Natura), fact that is very important, because the legislation can restrict the environmental pressures in these regions.
- Hydropower plants were proposed for covering the needs of energy in the basin

The threats of the basin are:

- The improper waste treatment, which is a complex problem
- The extensive pumping could cause possible subsidence
- The area's erosion is extended and the sediment yield of the river is increased with various effects to the environment.
- The area is in risk for natural hazards (landslides)
- Cremated areas (forest fire)
- Pollution of Maliakos gulf
- Shrinkage of natural biodiversity in the area
- The climate changes in correlation with the overexploitation of the surface and groundwater resources.

4. Conclusions

The main environmental pressures of groundwater resources of Sperchios basin are:

- Urbanization
- Agricultural activities
- Over-exploitation of water resources
- Salinization
- Lack of rational environmental management
- Industrial pollution

According to SWOT analysis it is necessary to minimize the weaknesses and convert the threats to opportunities. In addition, strengths and opportunities should be matched to optimize the water resources of the basin. Based on the SWOT analysis results the following actions are suggested:

- ✓ The reduction of over-pumping in order to preserve the water deposits, which shrink also due to climate changes, will protect the area from landslides and subsidence. This action will aid also in the suspension of sea intrusion and salinization.
- ✓ Proper use of the water treatment plants of the area (optimization of the active ones and operation start for the inactive ones). These actions will increase the water supply of the area and thus the groundwater pumping will be minimized.
- ✓ Adoption of new cultivation methods, in order to reduce fertilizing and preserve the area from desertification.
- ✓ Construction of small interception works along Sperchios river flow, as wells as in the basin's stream network in order to contain water quantities and use them for the area's water needs.
- ✓ Installation of - suitable equipment for monitoring a) the river's discharge, quality, sediment yield, flooding peaks and b) the water table of coastal drills so that sea intrusion and salinization will be controlled and ameliorate.
- ✓ Implementation of projects concerning the area's sustainable water resources management is considered to be of high importance.
- ✓ Credible implementation of the EU Directive 2000/60/EC.

5. References

Academy of Human Resources Development 2001. Performing a SWOT analysis, http://www.academyofhrd.org/clsot.htm

Baser O. 2001. SWOT analysis: a practical guide for young managers, http://www.baserler.com.tr/onur/isletme/management%20skills-swot.htm.

Danca A. 2000. An explanation of the SWOT analysis process, http://www.stfrancis.edu/ba/ghkickul/stuwebs/btopics/works/swot.htm.

Daskalaki P. and Voudouris K. The impacts of the irrational water resources management on the groundwater quality of Greece, http://www.srcosmos.gr/srcosmos/showpub.aspx?aa=8804

Diamantopoulou P. and Voudouris K. 2008. Optimization of water resources management using SWOT analysis: the case of Zakynthos Island,Ionian Sea, Greece, Environ Geol., 54, 197-211.

IGME 2010. Recording and evaluating of groundwater's hydrogeological characteristics and the aquifer system of Greece, 3rd Community Support Framework, Athens

Kakavas N. 1984. Hydrological water balance of basin of Sperchios river, *Phd Thesis*, Athens.

Kallioras A., Pliakas F., Diamantis I., Kallergis G., 2010. SWOT analysis in groundwater resources management of coastal aquifers: a case study from Greece, *Water International*, Vol. 35, No 4, 425-441.

Koutsogiannis D. 2007. Project plan of water resources management of the country, Ministry of Development – Directory of Water Dynamic and Natural Resources, Athens.

Psomiadis E. 2010. Research of the geomorphological and environmental changes in the hydrological basin of Sperchios River by using new techniques, *Phd thesis*, Agricultural University of Athens.

Richards H. 2001. *Modeling and decision support tools. Department of Engineering*, University of Cambridg,. http://www-mmd.eng.cam.ac.uk/people/ahr/dstools/paradigms/swot.htm

Stathopoulos N., Vasileiou E., Charou E., Perrakis A., Kallioras A., Rozos D. and Stefouli M. 2012.Coupling of remote sensing, climate and hydrologic data for assessing coastline changes in R. Sperchios estuary (Maliakos Gulf, Greece), *Geophysical Research Abstracts*, Vol. 14, EGU2012-9712, 2012 EGU General Assembly 2012, Vienna 22-27 April, Austria.

Δελτίο της Ελληνικής Γεωλογικής Εταιρίας, τομ. XLVII , 2013
Πρακτικά 13ου Διεθνούς Συνεδρίου, Χανιά, Σεπτ. 2013

Bulletin of the Geological Society of Greece, vol. XLVII 2013
Proceedings of the 13th International Congress, Chania, Sept. 2013

DEVELOPMENT OF MULTI-CRITERIA DECISION SUPPORT SYSTEM (DSS) COUPLED WITH GIS FOR IDENTIFYING OPTIMAL LOCATIONS FOR SOIL AQUIFER TREATMENT (SAT) FACILITIES

Tsangaratos P.[1], Pizpikis T.[1], Vasileiou E.[1], Pliakas F.[2], Schuth C.[3] and Kallioras A.[1,4]

[1] *National Technical University of Athens, School of Mining and Metallurgical Engineering, Athens, 15780, Greece (ptsag@metal.ntua.gr)*

[2] *Democritus University of Thrace, Department of Civil Engineering, Xanthi, 67100, Greece.*

[3] *Technical University of Darmstadt, Institute of Applied Geosciences, Darmstadt, 64287, Germany.*

[4] *Helmholtz Centre for Environmental Research – UFZ, Leipzig, 04318, Germany.*

Abstract

Managed Aquifer Recharge is a wide-spread well-established groundwater engineering method which is largely seen as an alternative potential major source for water and this conclusion becomes even more pronounced in semi-arid and/or arid areas, such as the Mediterranean Basin. The process of site selection for the installation of a MAR facility is of paramount importance for the feasibility and effectiveness of the project itself, especially when the facility will include the use of waters of impaired quality as a recharge source.

The main objective of this study is to present the developed framework of a multi-criteria Decision Support System (DSS) that integrates within a dynamic platform: the main groundwater engineering parameters associated with MAR applications together with the general geographical features which determine the effectiveness of such a project. The proposed system will provide an advanced coupled DSS-GIS tool capable of handling local MAR-related issues -such as hydrogeology, topography, soil, climate etc., and spatially distributed variables -such as societal, economic, administrative, legislative etc., with special reference to Soil-Aquifer-Treatment technologies. The new SAT-selection tool in question is integrated in ArcGIS software -within a user friendly environment- where data can be processed and displayed using Arc tools for spatial analysis.

Key words: *Managed Aquifer Recharge-MAR, Soil-Aquifer-Treatment-SAT, Decision Support System-DSS, Geographical Information Systems-GIS, groundwater management.*

Περίληψη

Η διαχείριση του εμπλουτισμού των υδροφορέων αποτελεί μια ευρέως διαδομένη τεχνική, ιδιαίτερα σε υδρολογικά ευαίσθητες περιοχές, όπως αυτές της Μεσογειακής Λεκάνης, όπου οι υδατικοί πόροι είναι περιορισμένοι. Η επιλογή της χωροθέτησης έργων τεχνητού εμπλουτισμού (Τ.Ε.) αποτελεί μια πολύπλοκη διαδικασία το

αποτέλεσμα της οποίας καθορίζει εν πολλοίς και την ίδια την αποτελεσματικότητα του έργου. Η εν λόγω διαδικασία περιπλέκεται εντονότερα όταν πρόκειται για τη χρηση νερών εμπλουτιμού υποβαθμισμένης ποιότητας.
Βασικός στόχος της παρούσας εργασίας είναι η παρουσίαση ενός πρόδρομου εργαλείου πολυ-κριτιριακού Συστήματος Λήψης Αποφάσεων, το οποίο ενσωματώνει σε μια δυναμική πλατφόρμα: τόσο τις τεχνικές του Τ.Ε. όσο και τα γεωγραφικά χαρακτηριστικά που καθορίζουν την αποτελεσματικότητα του έργου. Το προτεινόμενο σύστημα αποτελεί προχωρημένο εργαλείο σύζευξης Συστημάτων Λήψης Αποφάσεων και Γεωγραφικών Πληροφοριών ικανό να αξιολογεί κρίσιμα ζητήματα που αφορούν σε έργα Τ.Ε. –γεωλογικά, υδρογεωλογικά, κλιματολογικά, νομικά, κοινωνικά, οικονομμικά κ.α. – με ιδιαίτερη έμφαση σε συστήματα Επεξεργασίας-Εδάφους-Υδροφόρου. Το συγκεκριμένο εργαλείο πρόκειται να ενσωματωθεί στο λογισμικό ArcGIS, σε περιβάλλον φιλικό προς το χρήστη, όπου η προβολή και επεξεργασία χωρικών δεδομένων μπορεί να πραγματοποιηθεί με τη χρήση Arc tools.
Λέξεις κλειδιά: *Διαχείριση Εμπλουτισμού Υδροφορέων, Τεχνητός Εμπλουτσιμός, Συστήμα Επεξεργασίας Εδάφους-Υδροφόρου, Πολυ-κριτιριακό σύστημα Λήψης Αποφάσεων, Διαχείριση Υπόγειων Νερών.*

1. Introduction

Artificial recharge (AR) systems are engineered systems where surface water is put on or in the ground for infiltration and subsequent movement to aquifers to augment groundwater resources (Bower, 2002); while some of their most typical objectives include: (i) the minimization of seawater intrusion by forming a hydraulic barrier along the coast, (ii) the demonstration of aquifers as effective underground water reservoirs, and, (iii) to improve the quality of the water through Soil-Aquifer-Treatment (SAT) or geo-purification. The type of system to be selected for artificial recharge of groundwater and how it should be designed and managed for optimum performance depends entirely on local conditions of soil, hydrogeology, topography, water availability (quality, continuous, or interrupted supply), and climate (Bower, 2004). Dillon (2005,) summarizes all available groundwater engineering techniques for Managed Aquifer Recharge (MAR): Aquifer Storage and Recovery (ASR); Aquifer storage transfer and recovery (ASTR) (Dillon et al., 2008); bank filtration; injection wells; dune filtration; infiltration ponds; percolation tanks; rainwater harvesting; Soil Aquifer Treatment (SAT); sand dams; underground dams; recharge releases.

SAT facilities are engineered synthesis of MAR and wastewater re-use and/or reclamation technology, renovating waters of impaired quality into indirect potable levels. Groundwater recharge with reclaimed municipal wastewater presents a wide spectrum of technical and health challenges that must be carefully evaluated prior to undertaking a project (Asano and Cotruvo, 2004). SAT systems typically remove essentially all suspended solids, biochemical oxygen demand (BOD), and pathogens (viruses, bacteria, protozoa, and helminthic eggs). Concentrations of synthetic organic carbon, phosphorous, and heavy metals are greatly reduced, while nitrogen can either be left in the water if needed as fertilizer for irrigation use or can be removed in the pretreatment process.

Within a site suitability problem, site selection is the outcome of a process, which evaluates a variety of needs for the prospective location and the suggestion of an area on the basis of a proper assessment of the land. The process described above is the main objective and the prime prerequisite in an AR system scheme while the performance of AR scheme clearly depends on the ability of the decision makers to collect and analyze the proper geographic data. However, large number of parameters and the extent of their interrelationships among these parameters cause difficulties in decision making, as complex regional hydrological and hydrogeological characteristics make site selection for AR systems a very demanding task.

The complexity in which the spatial problem results, may require processing at a level that exceeds a decision maker's cognitive ability. The role of Geographical Information System (GIS) and Multi Criteria Decision Analysis (MCDA) techniques is to support the decision maker in achieving greater effectiveness and efficiency of decision making while solving spatial decision problems. In addition the combination of GIS and MCDM provides the decision maker with support in all stages of decision making, that is, in the preparation stage (collecting and storing data), design, and choice phases of the decision making process. A number of criterion weighting procedures based on the judgment of decision makers have been proposed in the multi – criteria decision bibliography. Some of the most popular procedures include: ranking, rating, pair-wise comparison and trade-off analysis (Malczewski, 1999). Each method differs in terms of their accuracy, degree of easiness to use, understanding and theoretical foundation and to choice the best for our problem requires discussion, field verification and iterative modifications. In this study the pair-wise comparison method was used in the context of the Analytic Hierarchy Process (AHP) in order to identify suitable sites for SAT applications in Attica Prefecture within a GIS tool. The product can be seen as an effective tool which can be used by water authorities and/or water utility companies for the integrated management of municipal wastewater.

2. Materials and Methods

2.1. Framework

Decision-making can be regarded as a process, which helps in the selection of a course of actions among several alternative scenarios. Every decision-making process produces a final choice (Reason, 1990), while the proposed framework usually involves three main phases: (a) Problem Definition Process (PDP), (b) Constraint Mapping Process, (CMP), (c) Suitability Mapping Process (SMP).

2.1.1. Problem Definition Process

The problem definition process is the first and most essential process that involves recognition and definition of the decision problem. In water resources planning and management, SAT has proved to be an effective countermeasure to water scarcity problems. In order to identify the suitable sites and produce a preliminary suitability map, one has to integrate Multi Criteria Decision Analysis (MCDA) techniques into a Geographical Information System (GIS). MCDA combines appropriate technical, economical, social and environmental criteria and weights them with respect to their importance to SAT; while GIS provides spatial analysis of the aforementioned criteria. Several MCDA techniques were used in many fields for site selection and land allocation; ELECTRE, PROMETHEE, AHP, TOPSIS, AIM, etc. (Gilliams et al., 2005; Gomez and Barredo, 2005; Zhong-Wu et al., 2007). However, only few of them are integrated into GIS (Gomez and Barredo, 2005; Marinoni, 2004), among which the Analytic Hierarchy Process (AHP) is the most widely applied. AHP was established by Thomas Lorie Saaty in the 1970s (Saaty, 1980) and used to determine the priority of different decision alternatives via pairwise comparisons with respect to common criteria.

2.1.2. Constraint Mapping Process

A constraint map represents the limitations of the value that attributes and decision variables may assume. In this phase the main objective is to avoid conflicts in decision-making. Areas of interest to other planning projects or which are non-feasible for SAT implementation are excluded from further analysis. The developed constraint map serves as a "mask" for the next process of SMP.

2.1.3. Suitability Mapping Process

The next step is to set the evaluation criteria; a step that involves specifying:

- A comprehensive set of objectives that reflect all concerns relevant to the decision problem.

- Measures for achieving those objectives; so-called attributes.

The degree to which the objectives are met, as measured by the attributes, is the basis for comparing alternatives. The evaluation criteria are associated with geospatial entities and relationships among geospatial entities and therefore can be represented in the form of thematic or data layer maps. The information about the relative importance of the criteria is usually obtained by assigning a weight to each criterion. The value of the weight represents its importance relative to other criteria under consideration, in which the larger the value, the more important the criterion in the overall utility (Malczewski, 1999). The next section (2.2) provides in more detail a description about the methodology followed during the Suitability Mapping Process.

2.2. Step by Step SMP

The methodology involves the following steps: (a) select essential criteria of suitability to SAT, (b) use GIS to manage the related data layers, (c) develop a decision hierarchy structure, (d) standardise each criterion, (e) identify priorities for each of the decision criteria, (f) estimate the Suitability Index (S_i) and (g) extract best-suitable sites based on their S_i value.

The first critical step during the phase of SMP is the selection of the appropriate and relevant surface, subsurface, spatial and non-spatial data such as geological maps, geomorphological, lineaments, slope inclination and slope orientation maps, land use cover, road infrastructure, power lines, proximity to water source and groundwater pollution. The next step is to convert all the data layers into a common scale, a process called standardization. It is of paramount importance that the classes of each factor have to be standardized into a common scale. The rating of the classes within each factor is based on the relative importance of each class obtained from expert knowledge or statistical assumptions. To standardize the classes to a uniform rating scale, Equation 1 is be applied.

Equation 1 – standardized rank values

$$newValue = \frac{(oldValue - \min(oldValue))}{\max(oldValue) - \min(oldValue)} * (\max(newRange) - \min(new(Range)) + \min(newRange)$$

Where, min (newRange) = 1, and max (newRange) = 3.

As already discussed the AHP method was used in this study to systematically assign preferences based on Saaty's proposal (Saaty, 2000). The method assists in determining the importance of each of the selected factor in the SMP. The method involves six essential steps: (i) define the unstructured problem, (ii) develop the AHP hierarchy, (iii) pair wise comparison, (iv) estimate the relative weights, (v) check the consistency and (vi) obtain the overall rating. The AHP reduces the complexity of a decision problem to a sequence of pair-wise comparisons, which are synthesized in an interaction matrix. The AHP method constructs a hierarchy of decision criteria and through the pair-wise comparison of each possible criterion pair a relative weight for each decision criterion is produced. Each comparison is a two-part question determining which criterion is more important, and how much more important, using a numerical relational scale (Table 1).

The next phase is to combine all the weighted factors by using the Weighted Linear Combination (WLC) method in order to obtain the Suitability Index. WLC is one of the widest known and most commonly used MCDA methods (Malczewski 1999, Ayalew et al. 2005). The method involves multiplying the weight value assigned for each factor by the standardized rank values given to each class and numerically added according to Equation 2 in order to produce the Suitability Index Map (S_i). Each pixel of the final S_i map, obtains a value that ranges between 0.1 and 1, whereas 0.1 corresponds to the most unsuitable setting and 1 corresponds to the most suitable.

Table 1 - Scale of importance between two parameters in AHP (Saaty, 2000).

Scale	Intensity of importance	Definition
1	Equally	Two activities contribute equally to the Objective
3	Moderately	Experience and judgment slightly to moderately favour one activity over another
5	Strongly	Experience and judgment strongly or essentially favour one activity over another
7	Very strongly	An activity is strongly favoured over another and its dominance is showed in practice.
9	Extremely	The evidence of favouring one activity over another is of the highest degree possible of an affirmation.
2,4,6,8	Intermediate values	Used to represent compromises between the references in weights 1, 3, 5, 7 and 9

Equation 2 – Suitability Index (S_i) for each pixel

$$S_{pi} = \sum_{j=1}^{n} Fw_j * cf_j$$

where pi the i^{th} pixel, Fw_j the weight of the j^{th} factor and cf_j the standardized ratings of class k^{th} of the j^{th} factor.

3. Case Study Application

3.1. Problem Definition – General Characteristic of the Study Area

The Region of Attica covers an area of 3,207 km^2, containing more than half the population of Greece, surrounded by (1,413 m), Kitheronas (1,400 m), Penteli (1,108 m), Hymettus (1,025 m) and Aegaleo (469m). The basin of Attica, Thriasio plain, Mesogea, Megara and the coastal zone of Marathonas and Nea Makri, are the main parts of the lowlands with a mean elevation of 115 m. Attica Water District involves the entire Region of Attica, the islands of Aegina, Salamina and Makronisos and small parts of Sterea Ellada and Peloponnese (IGME, 2010).

The climate of the study area is Mediterranean continental, with relatively mild wet winters and hot-dry summers. The average temperature is 16–18°C (Koutsogiannis, 2007). The average annual precipitation is 400 mm, ranging from less than 400 mm -within the south coastal areas- to 600 mm at the mainland and 1,000 mm on the mountainous zones, the highest values observed in the mountain Kitheronas and Parnitha (IGME, 2010). The two main rivers are Illissos and Kifissos, which in the urbanized areas have been channelized, discharging into Saronikos Gulf.

Attica consists of two geological units, the basement with rock formations -Paleozoic to Upper Cretaceous (marbles, dolomites, limestones, phyllites, schists and conglomerates of flysch)- and the clastic cover of Neogene and Quaternary deposits of the Plio-Pleistocene (sands, gravels, conglomerates, marls, clays, sandstones, lacustrine). The lithological formations have been the effect of successive tectonic movements and deep erosion in both the vertical and the horizontal.

Permeable geological formations cover a significant amount of the total area; with karstified limestones being the major ones, covering mainly the eastern and western part of the region. The

total water availability is app. 449 hm^3 and this amount consists of 259 hm^3 surface water and 190 hm^3 groundwater (Koutsogiannis, 2007). Three major aquifer systems are developed in Attica region: a) the karst aquifer systems -at the eastern and western parts-, b) the aquifer systems which are composed of unconsolidated materials -mainly present in coastal plain areas-, and c) the aquifer systems present in fractured formations.

Figure 1, shows the geographical location of the study area, including the morphological relief as well as the locations of the Wastewater Treatment Plants (WWTP) of Athens Water Supply & Sewage Co SA (EYDAP). The number and location of WWTP facilities were considered as one of the most important parameters taken into account for the DSS, as they involve the major source of recharge water for the SAT systems.

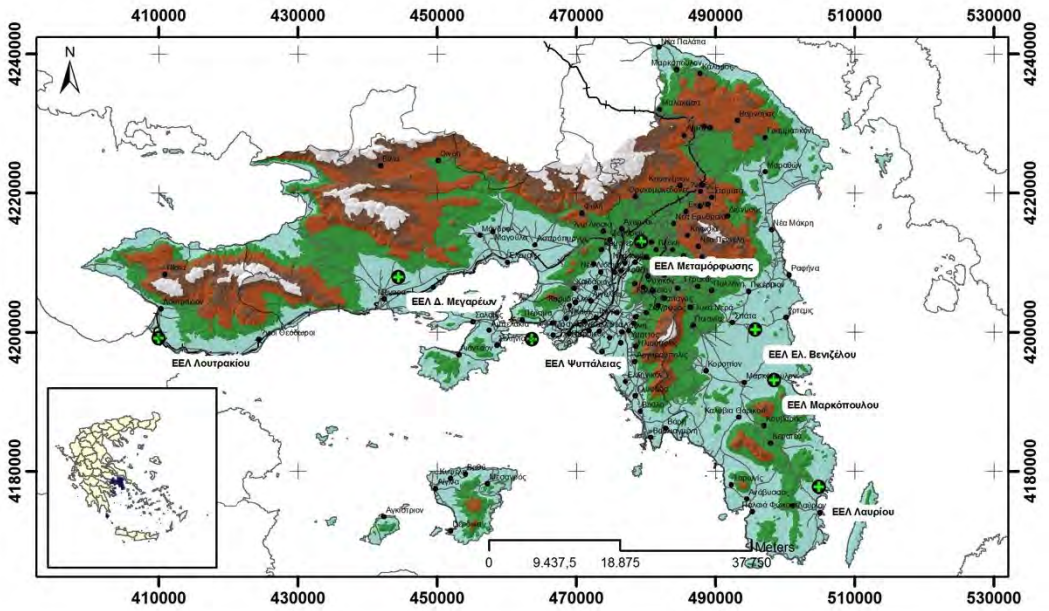

Figure 1 – Study area.

3.2. Selecting the Appropriate Criteria

Geology plays a very important factor for SAT, since it depicts the content of a large part of the vadose zone. In general, suitable sites should present a very low clay fraction in order to fulfil high hydraulic conductivity conditions and perform good complementary wastewater purification (Anane et al., 2008).

Depth to water table is a technical criterion of ample importance as it represents the thickness of the vadose zone in which the treated wastewater will undergo appropriate purification processes before it percolates in the saturated zone. The unsaturated layer should be thicker than 5m (Asano et al., 2007) to enhance SAT, and to avoid any chance of contaminating the underlying aquifer.

Considering the topographic characteristics and more specifically the slope values, the steeper the surface profile appears the less suitable for aquifer recharge it is. Suitable areas for SAT are those with slope ranging from flat to 15^o. Higher slopes increase runoff and soil erosion and lower slope indicate areas of high priority (EPA, 2004). The slope thematic layer was derived from Shuttle Radar Topography Mission Digital Elevation Model (SRTM DEM) 90m – resolution after projecting from UTM to EGSA ’87. In general the existing land use of an area provides information about the land availability for implementing SAT. In urban areas or of industrial use

the implementation is not – feasible. As stated by EPA (2004) the main criteria concerning the economic criteria should be the transport distance from the WWTP to the potential application site, which should not exceed 8 km, and also the difference in elevation with WWTP level.

3.3. Constraint Mapping Process

Alternatives that do not meet the constraints are referred to as non- feasible or unaccepted. Under conjunctive screening an alternative is accepted if it meets specified standards or thresholds for all evaluation criteria. The study takes into consideration four constraint criteria: (a) protective areas, (b) distance to groundwater pollution source, and (c) land use cover. For each constraint criterion a threshold value is assigned in order to produce the constraint map (Table 2).

Table 2 – Land use types for MAR Constraint Mapping Process

Constraint Criteria		Threshold value
Land use types	Permanent crops, natural vegetation, rivers	Feasible
	Agricultural areas, irrigated areas, quarries, urban areas	Non- feasible
Proctective areas	Natura 2000, etc.	Non- feasible
Distance to groundwater pollution source	> 500m	Feasible
	< 500m	Non- feasible

The process involves the preparation of the final constraint map that is the product of the sum of each individual constraint map. Figure 2 shows the constraint thematic layers and the final constraint map.

3.4. Suitability Mapping Process

In order to rank the suitability of a given study area, a weight for each criterion is assigned. Weighting expresses the criterion degree of relevance or preference relatively to the other criteria. The methodology followed for SMP proceeds in weighting through the pair-wise comparison between the elements for each hierarchical level (Saaty, 1980). Table 3 shows the produced pair-wise matrix for the main decision criteria, while Figures 3 to 5 show the three main thematic layer criteria, namely: (a) hydrolithological characteristics, (b) aquifer depth and (c) slope inclination.

Figure 3, shows the spatial distribution of the suitability criteria based on the hydrolithological characteristics of the study area. Three main categories were used, based on the geological formations present, with unconsolidated formations assigned as posing the most suitable conditions.

Figure 4 presents the depth to groundwater table, i.e. the thickness of the unsaturated zone within the major unconsolidated aquifer bodies of Attica, where SAT can be potentially applied. It is considered as being one of the most important suitability criteria for SAT site selection because the necessary treatment is obtained by filtration as the wastewater percolates through the vadose zone (with a critical thickness of at least 5m), and then some distance laterally through the aquifer.

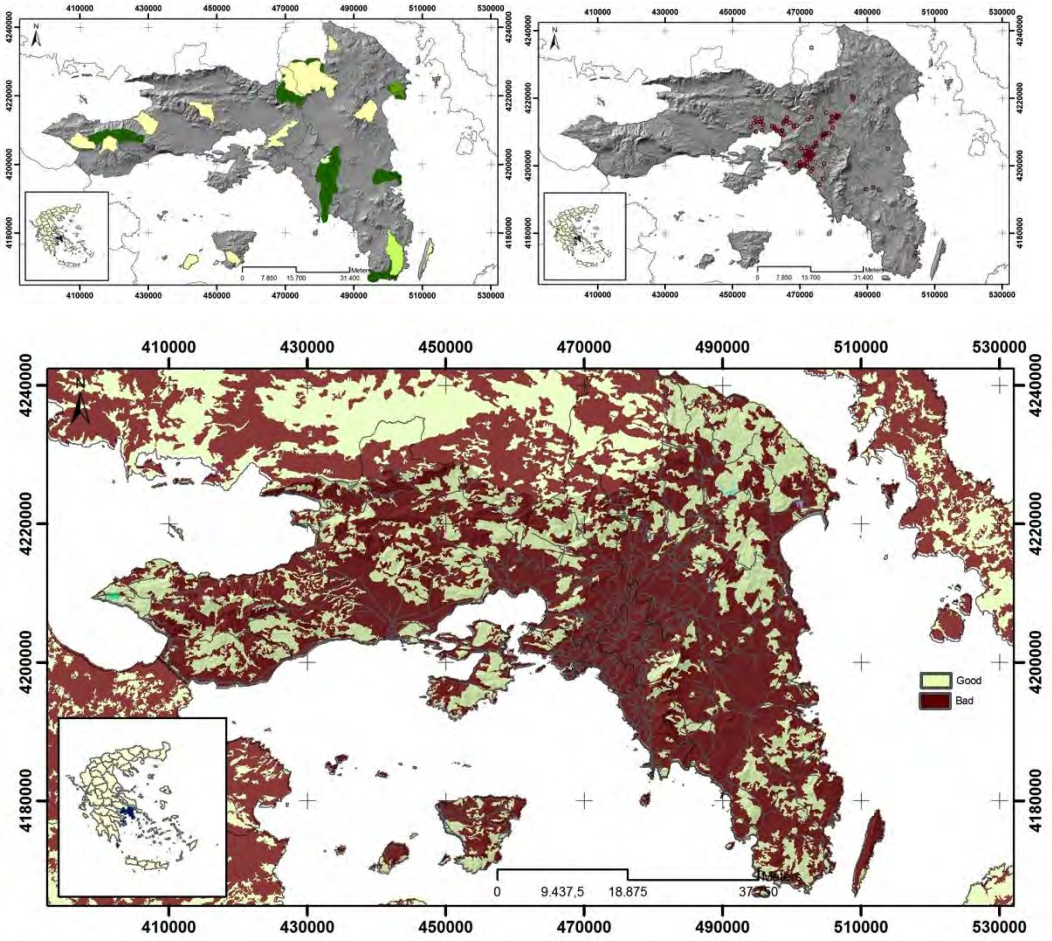

Figure 2 – Constraint criteria a. protected areas, b. industries, c. land use.

Table 3 – Pair-wise comparison matrix for evaluating the relative importance of the selected criteria for SAT.

	F1	**F2**	**F3**	**F4**	**F5**	**w**
F1	1	1	5	7	9	0.398
F2	1	1	5	7	9	0.398
F3	1/5	1/5	1	3	4	0.112
F4	1/7	1/7	1/3	1	3	0.059
F5	1/9	1/9	1/4	1/3	1	0.033
λmax	5.1845					
CI	0.0461					
CR	0.0412					

F1: Hydrolithological characteristics, F2: Aquifer Depth, F3: Slope Inclination, F4: Distance from Residential Centres, F5: Distance from WWTP.

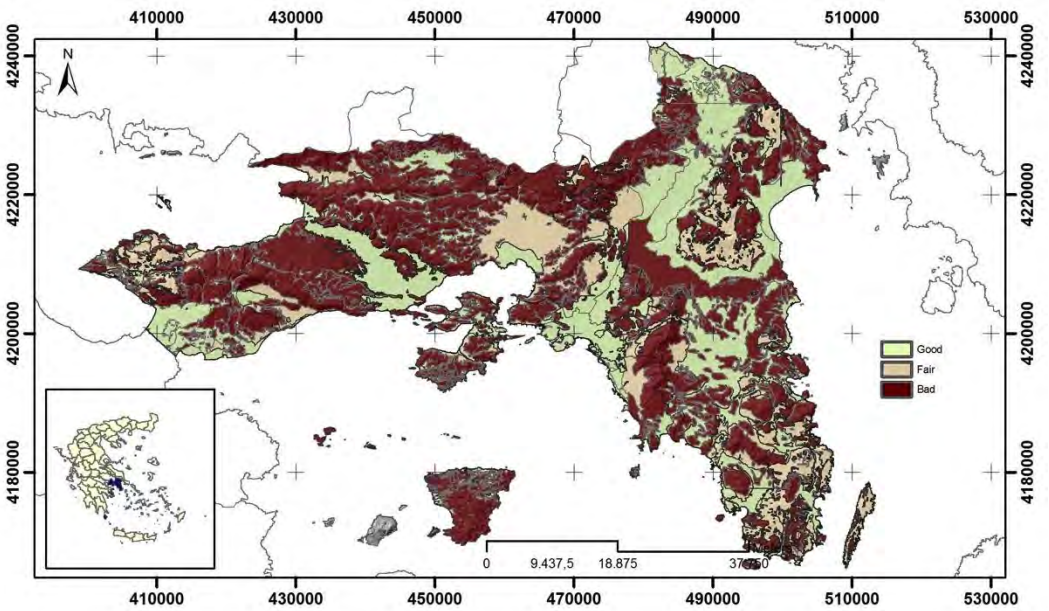

Figure 3 – Hydrolithological characteristics.

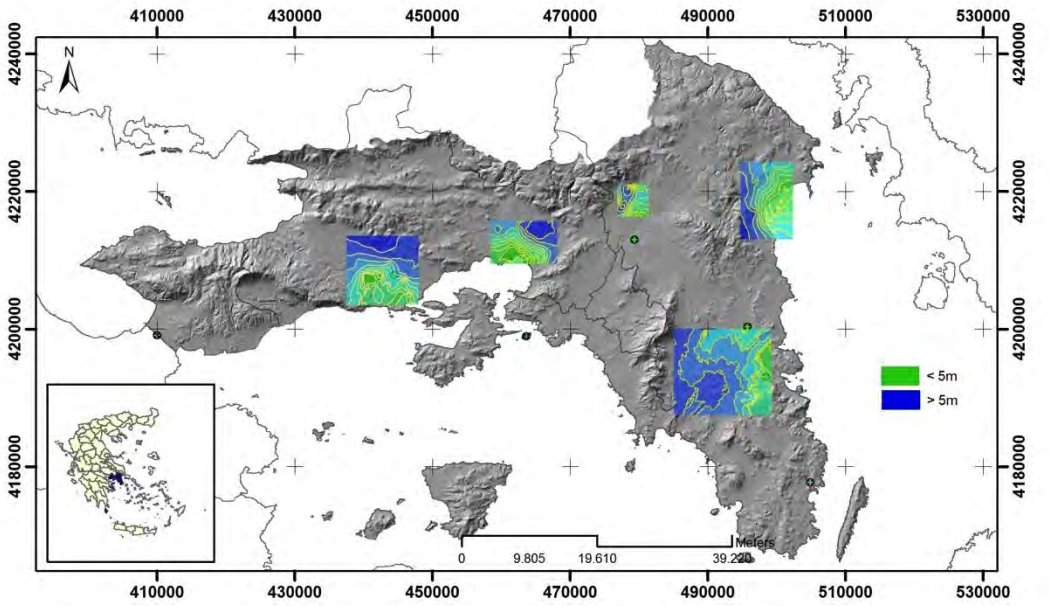

Figure 4 – Unsaturated zone thickness.

Figure 5 shows the distribution of slope inclination for the study area of Attica. Suitable areas for SAT are those with slope ranging from flat to 15^{o}, while higher slopes increase runoff and soil erosion and lower slope indicate areas of high priority (EPA, 2004). Additionally, the lower the slopes, the most feasible the construction works during the basins preparation phase.

Figure 6 shows the final suitability map, and is produced after the synthesis of all the aforementioned suitability maps. Since SAT systems, require a source of reclaimed wastewater, final suitability map also contains the locations of the WWTP of EYDAP, highlighting the radius of optimal distance (8km from the SAT facilities).

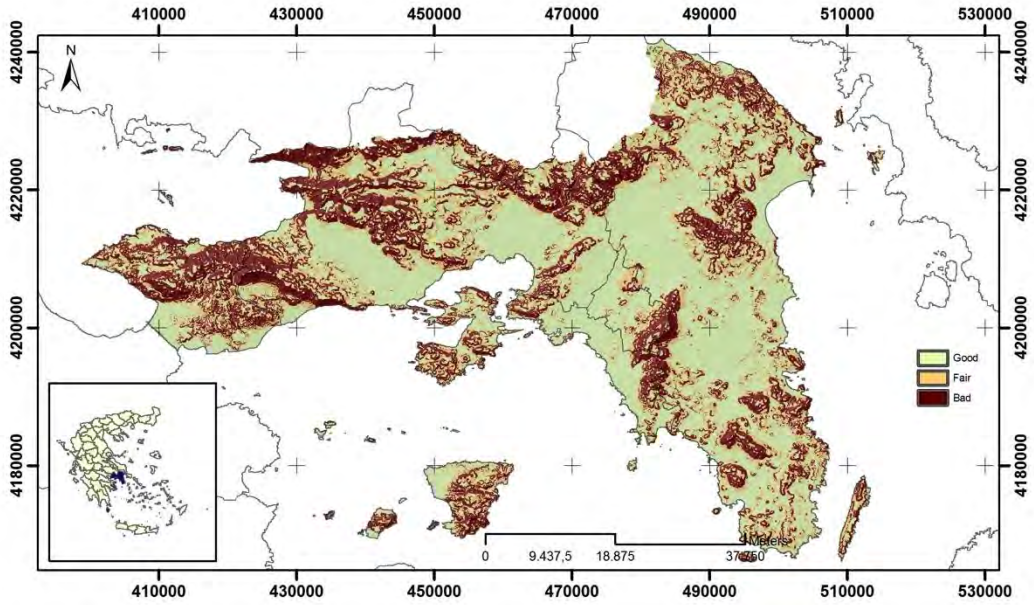

Figure 5 – Slope Inclination.

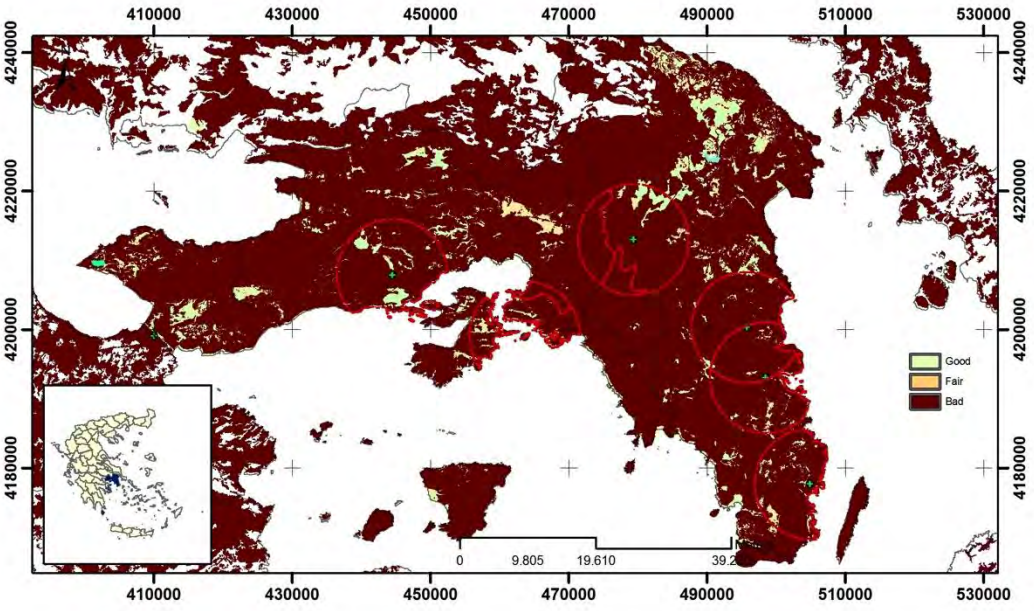

Figure 6 – Final suitability map.

4. Conclusions

SAT is a cost-effective natural wastewater treatment and reuse technology, while Abel et al., (2012) quote that it is an environmentally friendly technology that does not require chemical usage and is applicable to both developing and developed countries. Through the use of innovative analytical tools, the removal/transformation of wastewater effluent organic matter (EfOM) have been tracked through SAT systems (Amy and Drewes, 2007).

In the present study, a single-objective AHP integrated with a GIS was carried out to identify potential sites for SAT installations in Attica Region. Major criteria were selected, taking into account hydrolithological settings, unsaturated zone thickness, slope inclination, and economic aspects related to the proximity of the WWTP with the potential SAT locations and the difference of elevation between the suitable area and the WWTP. Hydrolithological characteristics and aquifer depth have been found to be the most significant factors, as they are directly related to the geopurification processes during downward effluent filtration.

Site selection analysis involves a great number of objectives, criteria, alternatives and decision parameters, resulting in a complex decision environment. The developed framework promotes clear thinking and better understanding of the spatial problem of Aquifer Recharge together with reducing errors in importance judgement. One of the advantages of the methodology it that it also allows checking the consistency to the user's input weight for each criterion.

A final composite Suitability map of the study area is obtained calculating the S_i for each pixel (i), according to equation 2 (Figure 6). The map is reclassified into 3 classes, good fair and bad. Since most of the study area involves mountainous zones and highly urbanized areas, the spatial distribution of locations preferable for SAT facilities are quite limited for the study area.

This work can be considered as a valuable managerial tool that technically supports the decision makers for integrated water resources management. Further developments could be achieved by multi objectives analysis, including other types of artificial recharge systems such as shallow or deep injection wells, induced recharge, artificial wetlands, infiltration trenches etc.

5. References

Abel C.D.T., Sharma S.K., Malolo Y.N., Maeng S.K., Kennedy M.D., Amy G.L. 2012. Attenuation of Bulk Organic Matter, Nutrients (N and P), and Pathogen Indicators During Soil Passage: Effect of Temperature and Redox Conditions in Simulated Soil Aquifer Treatment (SAT), *Water Air Soil Pollution*, 223, pp. 5205–5220.

Amy G., and Drewes J. 2007. Soil Aquifer Treatment (SAT) as a Natural and Sustainable Wastewater Reclamation/Reuse Technology: Fate of Wastewater Effluent Organic Matter (EfOM) and Trace Organic Compounds, *Environ Monit Assess*, 129, pp. 19–26.

Anane M., Kallali H., Jellali S. and Ouessar M. 2008. Ranking suitable sites for Soil Aquifer Treatment in Jerba Island (Tunisia) using remote sensing, GIS and AHP-multicriteria decision analysis, *Int. J. Water*, Vol. 4, Nos. 1/2, pp.121–135.

Asano T. and Cotruvo J.A. 2004. Groundwater recharge with reclaimed municipal wastewater: health and regulatory considerations, *Water Research*, 38, pp. 1941–1951.

Asano T., Burton F.L., Leverenz H. L. Tsuchihashi R. and Tchobanoglous G. 2007. *Water Reuse, Issues, Technologies, and Applications*, Metcalf & Eddy | AECOM.

Ayalew L. and Yamagishi H., 2005. The application of GIS-based logistic regression for landslide susceptibility mapping in the Kakuda-Yahiko Mountains, Central Japan, *Geomorphology* 65(1–2), 15–31.

Bower H. 2002. Artificial recharge of groundwater: hydrogeology and engineering, *Hydrogeology Journal*, 10, pp. 121–142.

Bower H. 2004. Artificial recharge of groundwater: systems, design and management, Hydraulic Design Handbook, McGraw-Hill, Chapter 24, pp. 24.1-24.44.

Dillon P. 2005. Future management of aquifer recharge, *Hydrogeology Journal*, 13, pp. 313-316.
Dillon P., Page D., Vanderzalm J., Pavelic P., Toze S., Bekele E., Sidhu J., Prommer H., Higginson S., Regel R., Rinck-Pfeiffer S., Purdie M., Pitman C. and Wintgens T. 2008. A critical evaluation of combined engineered and aquifer treatment systems in water recycling, *Water Science and Technology*, 57(5), pp. 753-762.
Environmental Protection Agency, E.P.A. – Guidelines for Water Reuse. EPA/625/R-04/108, U.S. Agency for Inter. Development, Washington, DC, USA, 2004
Gilliams S., Raymaekers D., Muys B. and van Orshoven J. 2005. Comparing multiple criteria decision methods to extend a geographical information system on afforestation, *Computers and Electronics in Agriculture*, Vol. 49, pp.142–158.
Gomez M. and Barredo J.L. 2005. Sistemas de Informacion Geograficay Evaluacion Multicriterio en la Ordenacion del Territorio, 2nd ed., RA-MA edition.
Institute of Geology & Mineral Exploration, IGME, 2010. Recording and evaluating of groundwater hydrogeological characteristics and the aquifer systems of Greece, Athens, *Internal Report.*
Koutsogiannis D. 2007. Project plan of water resources management of the country, Ministry of Development – Directory of Water Dynamic and Natural Resources , Athens.
Malczewski J. 1999. GIS and Multicriteria Decision Analysis (John Wiley and Sons, New York, 1999).
Marinoni O. 2004. Implementation of the analytical hierarchy process with VBA in ArcGIS. – Computers and Geosciences 30: 637-646, Amsterdam.
Saaty T.L. 1980. The Analytic Hierarchy Process, McGraw-Hill, New York.
Saaty T.L. 2000. Fundamentals of Decision Making and Priority Theory with the Analytic Hierarchy Process. 2nd Edn., RWS Publications, Pittsburg, USA.
Zhong-Wu L. Guang-Ming Z., Hua Z., Bin Y. and Sheng J. 2007. The integrated eco-environment assessment of the red soil hilly region based on GIS – a case study in Changsha City, China, *Ecological Modelling*, Vol. 202, pp.540–546.

Δελτίο της Ελληνικής Γεωλογικής Εταιρίας, τομ. XLVII , 2013
Πρακτικά 13ου Διεθνούς Συνεδρίου, Χανιά, Σεπτ. 2013

Bulletin of the Geological Society of Greece, vol. XLVII 2013
Proceedings of the 13th International Congress, Chania, Sept. 2013

THE ROLE OF KEFALOVRUSO AND AMOURIO SPRINGS IN THE HYDRODYNAMIC CONDITIONS OF POTAMIA ELASSONA BASIN

Vasileiou E.[1] and Koumantakis I.[1]

[1] National Technical University of Athens, School of Mining Engineering & Metallurgy, Section of Geological Sciences, Laboratory of Engineering Geology & Hydrogeology, Iroon Polytechneiou 9, Zografou Campus,Athens 15780
elvas@metal.ntua.gr, koumantakisioannis@gmail.com,

Abstract

Two lignite deposits have been found in the Neogene basin of Potamia, located in Elassona area in central Greece. The water resources of the region affect critically the exploitation of the mineral deposits. The detailed hydrogeological research of the area is imperative before starting the mining activities. Two groups of springs discharge near the study area. The karstic springs of Kefalovruso are in the north-west boundaries of the Neogene basin and the springs of Amourio are located in the Quaternary alluvial deposits, in the central part of the area. This paper includes the analysis of the hydrogeological conditions of the springs, the processing of the water-measurements (water supply, water level) and their correlation with the area's meteorological data. The time series of hydrological data, from 1972 to 2008, were evaluated for both springs and several parameters were estimated in order to investigate the function and the capacity of the springs. The relation between the recharge system of the springs and the area's groundwater dynamics is also analysed.
Key words: *karstic, hydrogeology, Thessaly, discharge, recharge.*

Περίληψη

Δυο λιγνιτικά κοιτάσματα έχουν εντοπιστεί στη λεκάνη των νεογενών της Ποταμιάς, που τοποθετείται στην Ελασσόνα στην κεντρική Ελλάδα. Οι υδατικοί πόροι της λεκάνης επηρεάζουν την εξόρυξη αυτών των κοιτασμάτων. Η λεπτομερής υδρογεωλογική έρευνα της περιοχής κρίνεται απαραίτητη πριν την έναρξη της μεταλλευτικής δραστηριότητας. Δυο είδη πηγών εκφορτίζονται στην περιοχή έρευνας, Οι καρστικές πηγές Κεφαλοβρύσου, στα βόρειο-δυτικά όρια της λεκάνης και οι πηγές Αμουρίου που αναβλύζουν στα Τεταρτογενή, στις αλλουβιακές αποθέσεις στο κεντρικό τμήμα της λεκάνης. Στην εργασία αναλύονται, οι υδρογεωλογικές συνθήκες των πηγών, αξιολογούνται οι υδρομετρήσεις (στάθμη, παροχές) και η συσχέτιση τους με τα μετεωρολογικά δεδομένα της περιοχής. Πραγματοποιήθηκε επεξεργασία της χρονοσειράς των υδρολογικών δεδομένων από το 1972 μέχρι το 2008 και για τις δυο πηγές, ενώ διάφοροι παράμετροι υπολογίστηκαν, για να διερευνηθεί η λειτουργία και η δυναμικότητα των πηγών. Διερευνήθηκε η τροφοδοσία του συστήματος των πηγών και η αλληλεπίδραση τους με το υπόγειο υδατικό δυναμικό της Ποταμιάς.
Λέξεις κλειδιά: *καρστικές πηγές ,υδρογεωλογία ,Θεσσαλία, παροχές, τροφοδοσία.*

1. Introduction

Potamia basin is located in the municipality of Elassona, in Thessaly, Central Greece. In this basin, two lignite deposits of 187,5x10^6 tn (Domeniko -167x10^6 tn and Amourion- 20,5x10^6 tn) have been identified (Dimitriou 1997). Two significant springs of Amourio and Kefalovruso influence the hydrogeological conditions of Potamia basin. Amourio springs discharge alluvium aquifer, in an elongated forehead at elevation of 170 m asl. They adrain out , in two different sites, the first 1 km south-east of Magoula village and the second about 2,5 km north of Amourio village. According to Panila (1999), the discharge of Amourio springs caused by the development of lignite layers at a depth of 60 meter, the lignite deposit constitutes the barrier for the groundwater flow.

The high capacity karstic aquifer of Krania, is drained out by the significant karstic spring, which is located 800 m north of the Kefalovruso village. It is a front of springs about 30 m long, at an altitude of 255 m.

The water of these two springs (Amourio and Kefalovruso) recharges the Quaternary sediments of the basin and covers irrigation and water supply needs for the wider area. Amourio springs are located at the western boundaries of the lignite deposits, thus the interaction of these springs with the mining activity is very interesting. Kefalovruso springs do not have direct hydraulic connection with the future lignite mine, but they affect the lignite exploitation via the recharge of the alluvial aquifer in the basin.

2. Geology-Hydrogeology

2.1.Amourio Springs

The alluvial aquifer is primarily replenished by recharge from the infiltration of Elassonitikos River and the percolation of the precipitation in the upstream alluvial area.

The rainfall through infiltration enriches the shallow unconfined aquifer and the deeper alluvial aquifers of Potamia (some of these deeper aquifers are confined or semi-confined).Groundwater flows under the bed of old streams, while the morphological slopes or the less impermeable formations force it to discharge on surface, via Amourio springs.

There is probably an additional supply to the springs from the karstic aquifers, which are developed in the marbles of Evagelistria and Paleokastro area (Figure 2). These marbles are hydrologically isolated from the main marble mass, which is developed at the north-west area of Kamvounia. There are no spring discharges in the surface of marbles and alluvial in the area of Evagelistria, which means that there is hydraulic underground connection between these formations and thus it recharges the alluvial deposits of Potamia and Amourio springs. Groundwater, from these marbles, flows downstream Elassonitikos River and ends up to the springs. Additional quantities from the river's infiltration must be considered.

Figure 1 - Image of Amourio (on the left) and Kefalovruso (on the right) springs.

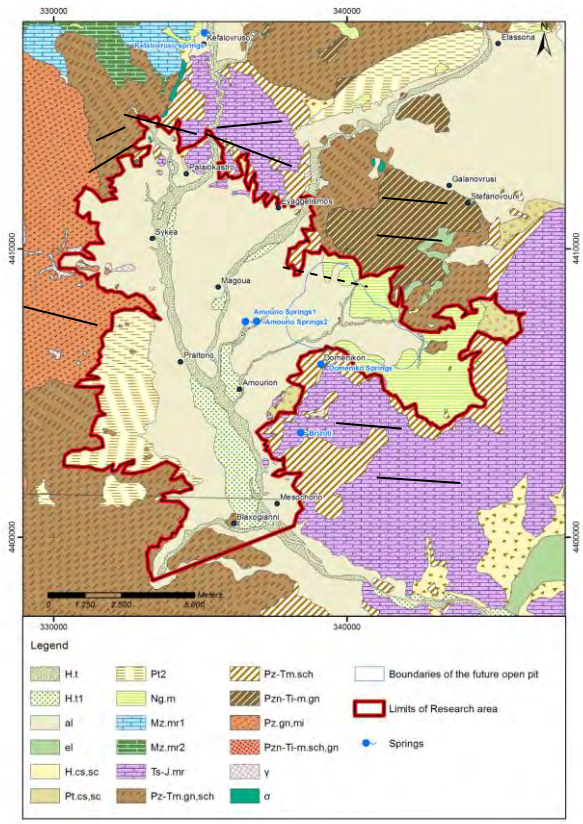

Figure 2 - Geological map of the south part of Elassona basin (Vasileiou, 2011).

2.2.Kefalovruso Springs

The karstic aquifer is developed in the carbonate formations of Krania. The average water table elevation is about 256 m asl, for the period 1988-1992 (Manakos, 1999). The infiltration from the precipitation is the main recharge for this aquifer. Deskati and Paliomantano streams run off the karstic mass and the percolation through them recharges additionally the karstic aquifer.

In 1962, a low dam was constructed at a distance of 20 meters from the main discharge points and an artificial lake was created that covers approximately an area of 3000 m^2. The basement of the dam and the lake consist of impermeable Neogene clay formations.

The water discharge through the dam's extractor ends up in a canal, leading to the river Boulgaris. The villages of Kefalovruso, Valanida, Paleokastro and Sukea are supplied with water from the discharge of Kefalovruso springs. The karstic aquifer is exploited by pumping drills, at the upper area of the discharge point. The water flows naturally, through channels, to Paleokastro and Sukea.

The tectonic settings of the marbles formations in the area are the main reason for the existence of these springs, as the groundwater flow blocked by almost impermeable formations such as the crystalline schist, gneiss of Pelagonian zone and sediments with clay and marl composition, of Neogene and Quartenary.

The contact between marbles and schists in the discharge points is a result of the area's tectonism - during Miocene (at the end of tectonic movements, the Pelagonian had overthrusted to Krania marbles).

The springs occur, due to the fault which is located, in a distance of 2,5 Km south of their location (Manakos &Tasios, 1998). The fault cannot be seen in the discharge points, as it is filled with Neogene and Olocene deposits.

3. Materials and Methods

3.1. Hydrological Data of Amourio

The available time series of monthly water measurements cover the period of 1972-2008 (Region of Thessaly-Department, Ministry of Agriculture). According to these data the average discharge of the springs was estimated at about 0,417 m^3/s. The minimum value, for the period of 35 years was measured in August 1990 (0.003 m^3/s) and the maximum in April 1987 (2,767 m^3/s). The average scaling value for July is about 0,40 m^3/s and for August about 0,362 m^3/s. During summer, while the irrigational needs are increased, the discharge of the springs is almost concurred with the average scaling. This fact is significant and rare for Greece (Vasileiou, 2011).

Another interesting data for the springs is the low ratio between the maximum and minimum discharge value for the whole time period. The small fluctuation among the average monthly discharges proves the good regulation of the aquifer. In 1990, this ratio was higher than the others, probably due to the extended dry period (1988-1990) that was recorded by the nearest meteorological station of Magoula. In this period, the annual precipitation was estimated in half of the value of the average annual rainfall (445,5mm), in the same station (Vasileiou, 2011).

The maximum average monthly discharges are recorded in April (0,50 m^3/sec) and the minimum in November (0,31 m^3/sec) (Table 1). Figure 3, presents the annual changes of springs discharge, where the downward trend is obvious through the last 35 years. Only in the years of 1982, 1987, 1996, 1997, high values were observed. The average annual discharge was estimated at about 13 $x10^6$ m^3. The flow is continuous, but the discharge is often low, during this time. The flood runoff (2,77 m^3/sec) in April of 1987, was in instant correlation with the precipitation in that period (approximately 671 mm of rainfall in 1987, 90 mm in March of the same year and 57,40 mm in April at Magoula station), which was very high and extreme in comparison to the values of the other years (Vasileiou,2011).
Specifically, on August of 1996, the high discharge value must be correlated with the increased rainfall of that month (71mm) and the previous one (47,70mm). These values are high for the summer period in this area.
The average water table measurement in the artificial lake was evaluated at about 0,539 m (reference level the bottom of the lake). The highest value of water table measurement is about 0,85 m and the lowest about 0,33m. There is a wide range between these measurements that is confirmed by the standard deviation of statistical sample which is 0,113.

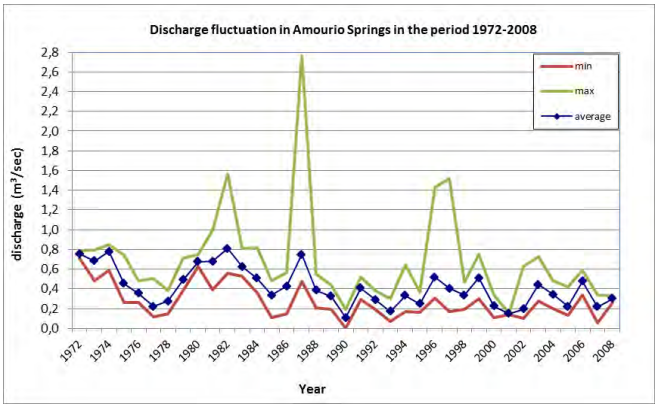

Figure 3 - Diagram of discharge fluctuation for the period 1972-2008, in Amourio springs.

Table 1 - Statistical data for the period 1972-2008, in Amourio springs.

Months	Average Discharge m^3/sec	Minimum Discharge m^3/sec	Maximum Discharge m^3/sec
January	0,39	0,14	0,72
February	0,42	0,15	0,79
March	0,42	0,12	0,81
April	0,50	0,12	**2,77**
May	0,44	0,15	0,83
June	0,44	0,12	0,85
July	0,40	0,04	0,82
August	0,36	**0,003**	1,43
September	0,36	0,04	0,99
October	0,35	0,04	1,56
November	0,31	0,06	0,77
December	0,38	0,11	1,52
Average	**0,41**		

There is a strong relation between the spring's discharge and the level of water. Figure 4 presents the correlation between the rainfall in Magoula meteorological station and the discharge of Amourio springs. In specific years (1993, 2002 and 2005), when the precipitation was significant, the measured discharges were low. Additionally in the year of 1997 and 2003, even though the rainfall was low, the spring's discharge was high. These deviations increase the possibility that the groundwater recharges by the karstic system of Evaggelismos-Paleokastro as well. This karstic system is developed in higher elevation; therefore the precipitation is higher than Magoula's station.

During the dry periods, when there is no water inflow into the aquifer, the dynamic water reserve from which the spring outflows decreases as a function of time, and the groundwater level declines. Maillet (1905) suggested that the discharge of a spring is a function of the water volume held in storage and described it by the simple exponential equation (Milanovic 1981; Ford & Williams 2007):

$Qt = Q_o * e^{-at}$

Maillet's (1905) equation recession analysis of the discharges of Amourio springs were performed, and recession coefficients (a) and dynamic volume (storage capacity, Vs) of the aquifer were calculated. The recession (discharge) coefficients of Amourio springs were estimated at a constant value of $a=7,99x10^{-3}$ day^{-1} and dynamic volume (storage capacity) values are $Vs=3,51\times10^6$ m^3. This equation was tested and presented, in this paper, for a period of three years and as the differences among the results was very small, was regarded as graphical errors. These three years had measurements for all the time period and were representative for the precipitation in the area. The system was evaluated as simple and well operated. The discharge of the springs is not directly affected by the monthly variations of the precipitation.

The value of the recession coefficient derives from the hydrogeological characteristics of the aquifer, especially by the effective porosity and transmissivity. Small values of the coefficient indicate very slow drainage of the aquifer with large storage capacity. The springs of this type of aquifer

are mostly permanent. Large values of the coefficient (the recession curve is steep) indicate rapid drainage through the conduits and little underground storage (Milanovic 1981; Ford & Williams 2007).

Figure 4 presents the hydrograph of discharge fluctuation in the year of 2005. The red part of the line corresponds to the dry season of the year.

Table 2 - Maillet equation recession analysis in Amourio springs.

	1999	2003	2005
a d^{-1}	$7{,}99x10^{-03}$	$3{,}37x10^{-03}$	$7{,}99x10^{-03}$
W m^3	$3{,}51x10^{6}$	$1{,}56x10^{7}$	$3{,}51x10^{6}$
q_o m^3/sec	0,730	0,610	0,325

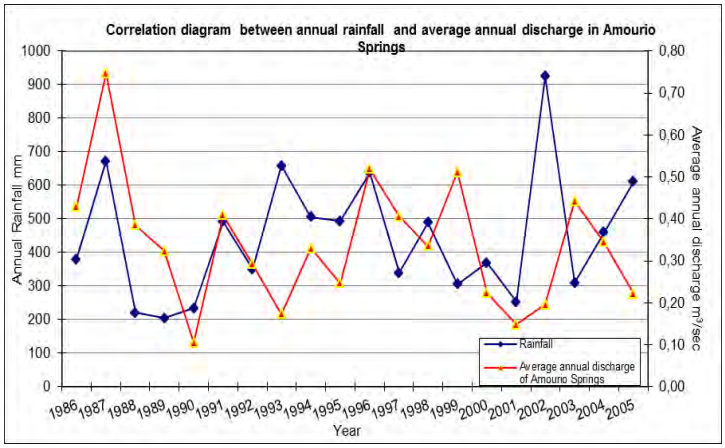

Figure 4 - Correlation diagram of rainfall and discharge of Amourio springs

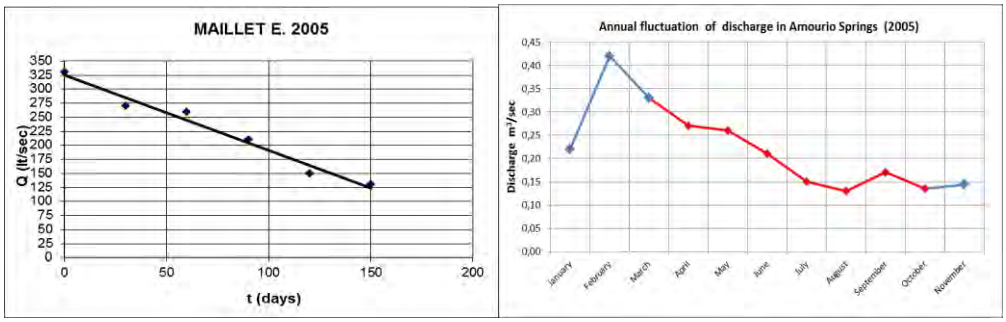

Figure 5 - Hydro-diagram of Maillet for Amourio springs

3.3. Hydrological Data of Kefalovruso

The average discharge of Kefalovruso spring for the period 1972-2008, was estimated at 1,277m^3/s. The average maximum spring's discharge was measured in April (1,8 m^3/s) , the minimum in August of 2001 (0,12 m^3/s) and the maximum in December of 1982 (5,120 m^3/s). The average discharge for July was measured at 1,19 m^3/s (although it is a dry season with increased water demands in the area). In the next months, the average monthly discharges are lower, the average minimum value is observed in October (0,683 m^3/s). It increases in November and December, but remaining in low values until June (Vasileiou, 2011).

The ratio of maximum and minimum values is low (average ratio 4,08) for each year, ranging between 1,35 (1972) and 5,33 (1984), that indicates a well regulated aquifer, which is distinguished

by a well interconnected karstic system. The spring's function isn't affected significantly from the pumping and this is proved by the observed small drawdown of the water table (Vasileiou, 2011).

Figure 6 presents, the discharge fluctuation of the springs per time. It is obvious that there is a decrease of flow rate during last 35 years. The spring's discharge is continuous and the annual value is estimated at about 40,27 x10^6 m^3. Figure 7 presents the water table fluctuations at the artificial lake. The highest water table level was at 0,62 m in 1983 and the change was 0,45 m for the last 35 years (bottom of the lake). The average water table in the lake was estimated at 0,35m. The combinational diagram shows a strong correlation between rainfall (meteorological station of Giannota) and spring's discharge after 1997.

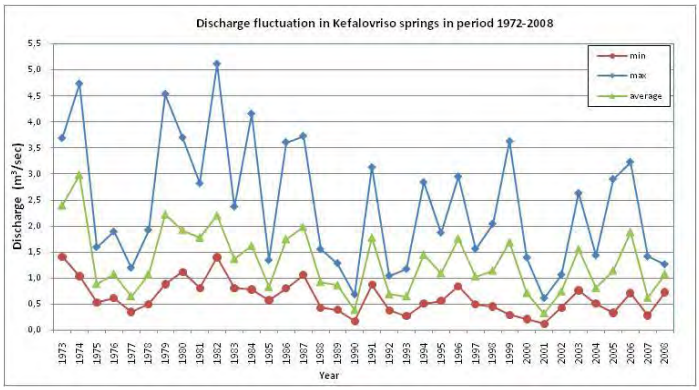

Figure 6 - Diagram of discharge fluctuation for the period 1972-2008, in Kefalovruso springs.

Table 3: Statistical data for the period 1972-2008, in springs of Kefalovruso.

Μήνες	Average discharge (m^3/sec)	Min (m^3/sec)	Max (m^3/sec)
January	1,464	0,500	4,540
February	1,549	0,420	2,900
March	1,769	0,480	3,700
April	1,806	0,470	3,790
May	1,637	0,210	3,620
June	1,657	0,140	4,740
July	1,187	0,130	4,520
August	0,822	0,120	4,430
September	0,816	0,170	2,880
October	0,683	0,200	1,400
November	0,894	0,280	2,430
December	1,040	0,400	5,120
Average	**1,277**		

Maillet's equation was applied for the karstic spring of Kefalovruso for the dry period of the years 1986, 1994 and 2005, the results are presented in Table 4.The values of the recession coefficients calculated for Kefalovruso springs and small changes in the discharge through the years indicate that the karstic aquifer of Krania has a large storage capacity and the drainage occurs very slowly. The discharges of the springs are not directly affected by the monthly variations of the precipitation.

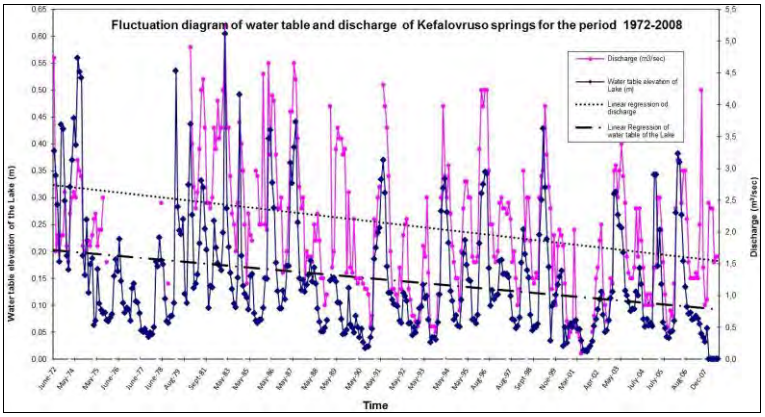

Figure 7: Diagram of water table in the lake and discharge of Kefalovruso springs.

The high values of coefficient (10^{-2}) indicate a poor operated karstic system and that the drainage occurs very quickly. These values of the recession coefficients are different from the calculated ones ($a=10^{-3}$) by Manakos (1999), for the years 1989, 1990 and 1992. Manakos (1999) mentioned that the karstic spring of Kefalovruso is the main discharge point of the karstic system of Krania

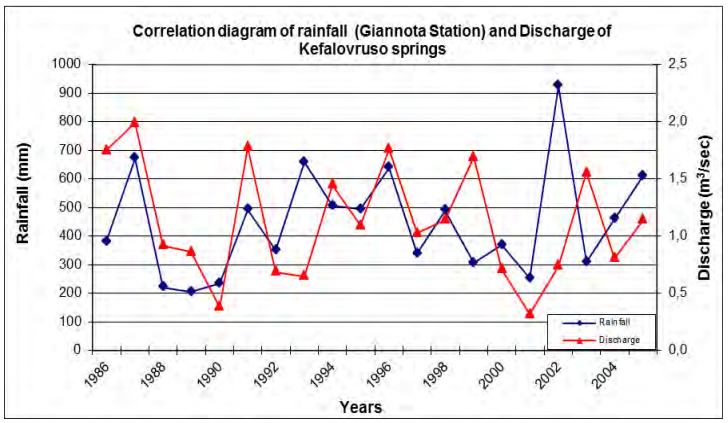

Figure 8 - Diagram of rainfall and discharge in Kefalovruso springs.

According to table 4, the different values of q_o and W_o, that were calculated in these three years, are justified by the rainfall recharge fluctuations.

Figure 9 presents the operation of the springs during dry and wet season, where the significant changes of discharge are observed in the year of 2005. The red part of the line represents the dry season for the spring, which is the time period for Maillet equation analysis.

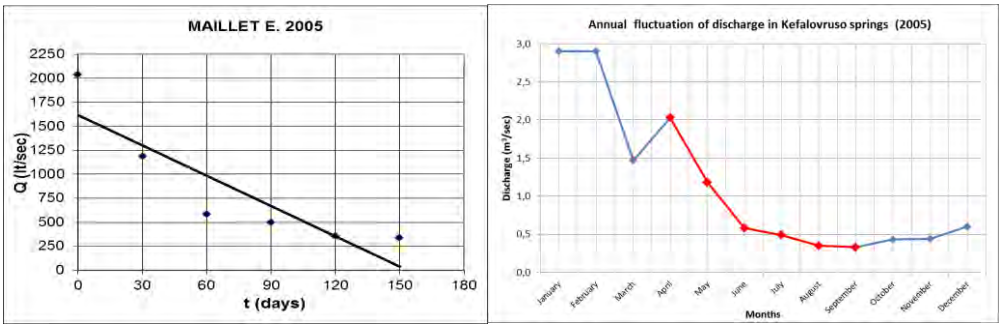

Figure 9 - Hydro-diagram of Maillet.

Table 4: Maillet equation recession analysis in Amourio springs.

	1986	1994	2005
a d^{-1}	$1{,}21x10^{-2}$	$1{,}20x10^{-2}$	$1{,}35x10^{-2}$
W m^3	$2{,}46x10^7$	$1{,}98\ x10^7$	$1{,}04\ x10^7$
q_o m^3/sec	3,450	2,750	1,625

4. Conclusions-Discussion

The flow rate and the capacity of Amourio and Kefalovruso springs were examined in this paper. The hydrogeological conditions of Potamia basin are affected significantly from these two springs.

The springs at Kefalovruso are the main discharge point of Krania karstic aquifer. These springs as well as the percolation of Titarisios River are the main recharge a source for the aquifers of the basin's filling (at the northern boundaries of Potamia basin). It was estimated that an average quantity of $28x10^6$ m^3/year percolate in the karstic mass of Krania (Vasileiou, 2011). Significant quantities from the springs flow through channels towards the villages in the north covering their water needs (Sukea, Paleokastro). Additionally, the basin is crossed by Titarisios River ($109\ x10^6$ m^3/year), which is formed by the conflux of Boulgaris and Elassonitikos rivers. Boulgaris River has an additional supply by Kefalovruso springs and some small torrents in the west boundaries of the area. The recharge of the basin is additionally supported by the infiltration of the rivers. The recharge from Boulgaris and Elassonitikos rivers is rich, as it comes from other hydrological basins in higher elevations, in which the rainfalls are higher (Vasileiou et. al., 2011).

The overlaying marbles of the Pelagonian series are of limited extent and thickness, especially in Evagelismos area and in the basin's basement. The total recharge volume of the marbles was estimated at about $3x10^6$ m^3/year. Therefore they are of minor importance concerning their water storage capacity. The marbles of Paleokastro recharge - Amourio spring and increased their discharge rate. The area has two main characteristics, the extended agricultural activities and the over-exploitation of the water resources (for covering irrigation and potable needs). A volume over $9{,}5x10^6$ m^3/year is being pumped from wells, mainly along Titarisios river and Amourio springs (Vasileiou, 2011).

Based on the piezometric map (Figure 10) of the basin (Vasileiou, 2011), there is rich recharge from Krania marbles at the north, via Kefalovruso springs. The karstic aquifer of Paleokastro contributes a moderate quantity of water to the alluvial aquifer in the north-east part of the basin and to Amourio springs. In the basin two aquifers are developed, the one of them is unconfined the underlying of the lignites. These springs have the most important role to the hydrodynamic conditions of the basin.

In Amourio area the lignite deposit cannot be exploited, because of the hydrogeological and hydrological conditions in this area. The problems concerning the recharge and high hydraulic over heads of the confined aquifer will cause significant difficulties, fact that makes the exploitation of this lignite field financially forbidden (Vasileiou et al., 2011). On the contrary the recharge that comes from the karstic springs of Kefalovruso, doesn't influence directly the mining activity.

Both springs contribute to the recharge of the basin and are the discharge points of two significant aquifer systems. The role of the springs is very important to the rational water management of the basin, as well as for the planning of every mining or other human activity in the area, which can change the water balance. The water capacity and importance for the area must always be under serious consideration. Protection and optimum exploitation of water resources in the area are necessary.

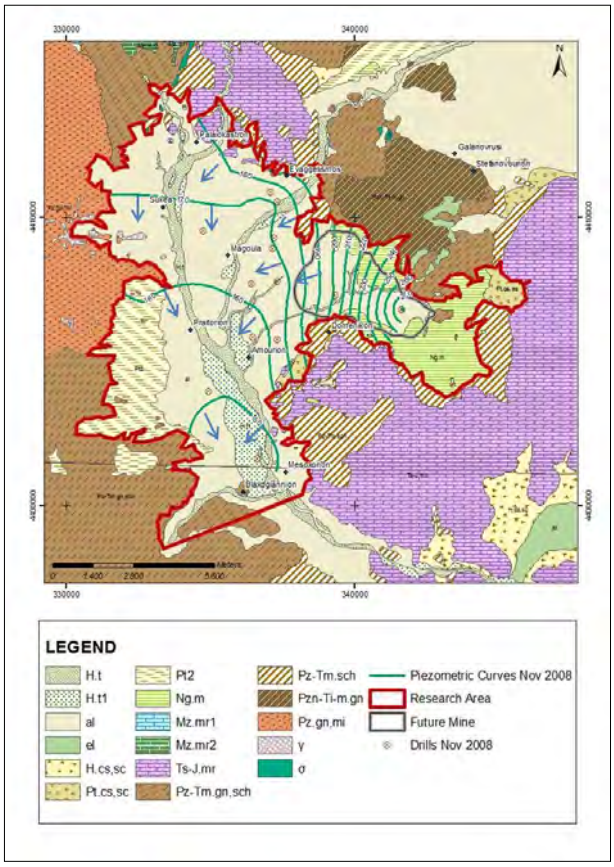

Figure 10: Piezometric map of Potamia basin in November 2008.

5. References

Dimitriou D. 1997. The lignite deposit of Domeniko and its importance in energetic economy of our country. IGME Athens.

Ford D. and Williams P. 2007. Karst Hydrogeology and Geomorphology.- John Wiley & Sons, pp. 562, Chichester.

Maillet E. 1905. Essais d'Hydraulique souterraine et fluviale- Hermann, pp. 218, Paris.

Manakos G.1999. Hydrogeological behaviour and stochastic modeling of the karstic aquifer of Krania in Elassona. *Phd thesis* in Aristoteleio University of Thessaloniki.

Manakos G. and Tassios G. 1998. Hydrogeological research of the great carbonate masses of Thessaly. The karstic aquifer of Krania, *Technical Report*, IGME, Thessaloniki.

Milanovic P.T. 1981. Karst Hydrogeology, *Water Resources Publications*, pp. 434, Littleton.

Region of Thessaly-Department, Ministry of Agriculture

Vasileiou E. 2011. Hydrogeological conditions of Potamia area, in Elassona. The effects of the future exploitation of the two lignite deposits in the water resources. *Phd Thesis* in NTUA,.

Vasileiou E. and Koumantakis I. 2011. The exploitation of lignite deposits in relation with the surface and groundwater in the mining area. The case study of Potamia basin, in Thessaly, Greece, *11th IMWA Congress-Aachen*, Germany 4-11 September.

Δελτίο της Ελληνικής Γεωλογικής Εταιρίας, τομ. XLVII , 2013
Πρακτικά 13ου Διεθνούς Συνεδρίου, Χανιά, Σεπτ. 2013

Bulletin of the Geological Society of Greece, vol. XLVII 2013
Proceedings of the 13th International Congress, Chania, Sept. 2013

TRACE ELEMENT CONTENT AND MORPHOLOGICAL CHARACTERISTICS IN MICROSCALE OF COMMERCIALLY AVAILABLE CLAYS USED AS COSMETIC PRODUCTS

Giouri K.[1], Papadopoulos A.[1], Bourliva A.[1], Tzamos E.[1], Papadopoulou L.[1] and Filippidis A.[1]

[1] Aristotle University of Thessaloniki, School of Geology, Department of Mineralogy-Petrology-Economic Geology, agiouri@geo.auth.gr, argpapad@geo.auth.gr, annab@geo.auth.gr, tzamos@geo.auth.gr, lambrini@geo.auth.gr, anestis@geo.auth.gr

Abstract

Two kinds of clays (one white and one green) available in pharmacies and herbalist's shops in the Greek market have been studied for their concentrations in trace elements, namely As, Be, Cd, Cr, Hg, Ni, P, Pb, Sb, Se, Te, Tl and Zr. According to EC Regulation 1223/2009, the presence of the analyzed trace elements and their compounds, are prohibited in cosmetics. The most abundant trace elements of the white clay are P (330 ppm), Pb (220 ppm) and Zr (11 ppm), while for the green clay are P (1250 ppm), As (43 ppm), Cr (31 ppm), Pb (30 ppm) and Ni (23 ppm). Compared to the global shale average concentration of elements, Pb is enriched 11-times in the white clay and As is enriched 3-times in the green clay. The depleted trace elements of the white clay are As, Cd, Cr, Hg, Ni, P, Sb, Se, Te, Tl and Zr, while of the green one are Cr, Hg, Ni, Sb, Te, Tl and Zr. Concerning the morphological characteristics, differences were observed in the particle size and shape between the white and green clay aggregates.

Key words: *Industrial minerals, Microporous natural raw materials, Inorganic contaminants.*

Περίληψη

Δύο είδη αργίλων (λευκή και πράσινη) που διατίθενται σε φαρμακεία και ειδικά καταστήματα στην Ελληνική αγορά, μελετήθηκαν για τις συγκεντρώσεις τους σε ιχνοστοιχεία, ειδικότερα σε As, Be, Cd, Cr, Hg, Ni, P, Pb, Sb, Se, Te, Tl και Zr. Σύμφωνα με τον Κανονισμό 1223/2009 της Ευρωπαϊκής Επιτροπής, η παρουσία των αναλυθέντων ιχνοστοιχείων και των ενώσεών τους, απαγορεύεται στα καλλυντικά. Τα ιχνοστοιχεία με τις υψηλότερες συγκεντρώσεις στη λευκή άργιλο είναι P (330 ppm), Pb (220 ppm) και Zr (11 ppm), ενώ στην πράσινη άργιλο είναι P (1250 ppm), As (43 ppm), Cr (31 ppm), Pb (30 ppm) και Ni (23 ppm). Σε σύγκριση με τη μέση περιεκτικότητα των χημικών στοιχείων στους αργιλικούς σχιστόλιθους (παγκόσμιος μέσος όρος), ο Pb είναι εμπλουτισμένος κατά 11-φορές στη λευκή άργιλο και το As είναι εμπλουτισμένο κατά 3-φορές στην πράσινη άργιλο. Τα ιχνοστοιχεία με μειωμένη περιεκτικότητα στη λευκή άργιλο είναι As, Cd, Cr, Hg, Ni, P, Sb, Se, Te, Tl και Zr, ενώ στην πράσινη άργιλο είναι Cr, Hg, Ni, Sb, Te, Tl και Zr. Όσον αφορά τα

μορφολογικά χαρακτηριστικά, εντοπίστηκαν διαφορές τόσο στο μέγεθος όσο και στο σχήμα των συσσωματωμάτων μεταξύ της λευκής και πράσινης αργίλου.
Λέξεις κλειδιά: *Βιομηχανικά ορυκτά, Μικροπορώδεις φυσικές πρώτες ύλες, Ανόργανοι ρυπαντές.*

.

1. Introduction

Cosmetic products are designed to be placed in contact with external parts of the human body. In these cases they require a consistency suitable for application. Because of their high specific surface area, optimum rheological characteristics and/or excellent sorptive capacity which are being studied by many researchers, clay minerals have been used in several health care formulations (Patel et al., 1986; Christidis et al., 2006; López-Galindo et al., 2007; Viseras et al., 2007; Rathossi et al., 2011; Christidis, 2012). This is because when dispersed in polar solvents, they possess enough viscosity to remain in contact with the application area (Murray, 2000; Carretero, 2002; Silva et al., 2011).

In order to be suitable for topical application, clays must comply with a number of compositional requirements (Galán et al., 1985; López-Galindo and Viseras, 2004). Specifically, they must have low or zero toxicity. Their high adsorption capacity can cause the accumulation of trace elements and some of them are considered as potentially toxic (López-Galindo et al., 2007; Silva et al., 2011). Cosmetics content in European Community is regulated, with EEA relevance, by the EU Regulation 1223/2009-a simplification of the Council Directive 76/768/EEC (EC 2009).

Cosmetic clays are available in various colours (white, green, red, pink, yellow etc.), which reflect differences in mineralogical and organic content. In the present study, white and green clays being commercially available in the Greek market were analysed for their content of As, Be, Cd, Cr, Hg, Ni, P, Pb, Sb, Se, Te, Tl and Zr. Moreover, morphological characteristics were also determined.

2. Materials and Methods

Two commercial cosmetic clays available in pharmacies and herbalist's shops in the Greek market were studied. The samples were studied in their bulk form, as they were already available in powder.

2.1. Sample Identification

According to their colour which is probably affected by the mineralogical composition and organic matter, the clays analysed were classified according to their commercial names in two kinds: white (WC1) and green (GC1).

2.2. Chemical Analyses

The chemical analyses were performed at the Acme Analytical Laboratories (Vancouver, Canada). Trace elements in the clays were extracted using the aqua regia digestion, while their concentrations were determined in all samples by ICP-MS. The elements analysed were selected because their occurrence, as well as their compounds, are excluded in cosmetic ingredients, including clays, by the EU Regulation 1223/2009.

2.3. Morphology

The morphology of the clays in microscale was evaluated with a JEOL J.S.M. 840A scanning electron microscope at the Scanning Microscope Laboratory, Aristotle University of Thessaloniki. The samples were coated with carbon – average thickness of 200 Å– using a vacuum evaporator JEOL-4X.

3. Results and Discussion

The health impact of the presence of several trace elements in the natural environment is potentially heavy. Cosmetic clays are commercial products based on natural raw materials, thus they must comply with several regulations concerning their chemical composition. According to EU Regulation 1223/2009, the presence of As, Be, Cd, Cr, Hg, Ni, P, Pb, Sb, Se, Te, Tl, Zr and their compounds in cosmetic ingredients, including clays must be excluded (Table 1).

Table 1 – Some of the trace elements that occur in the list of substances prohibited in cosmetic products, according to EC Regulation 1223/2009, ANNEX II (EC 2009).

Reference Number	Chemical Name / INN
40	Sb and its compounds
43	As and its compounds
54	Be and its compounds
68	Cd and its compounds
97	Cr, chromic acid and its salts
221	Hg and its compounds, except those special cases included in Annex V
279	P and metal phosphides
289	Pb and its compounds
297	Se and its compounds with the exception of selenium disulphide under the conditions set out under reference No 49 in Annex III
312	Te and its compounds
317	Tl and its compounds
391	Zr and its compounds, with the exception of the substances listed under reference number 50 in Annex III, and the zirconium lakes, pigments or salts of the colouring agents when listed in Annex IV
1093	Nickel

Significant concentrations of the trace elements mentioned above have been measured in the white and green clay samples (Table 2 and Figure 1). The investigated clays contain 1.2 and 43.2 ppm As (corresponding for white and green respectively), 1.9 and 3.0 ppm Be, <0.01 and 0.27 ppm Cd, 0.7 and 31.1 ppm Cr, <5 and 17 ppb Hg, 0.5 and 23.1 ppm Ni, 330 and 250 ppm P, 220.10 and 30.10 ppm Pb, 0.33 and 0.20 ppm Sb, <0.1 and 0.4 ppm Se, <0.02 and 0.03 ppm Te, 0.23 and 0.47 ppm Tl, 10.6 and 0.6 ppm Zr.

In general, green clay contains higher concentrations than the white clay in all trace elements, apart from Pb, Sb and Zr. The most abundant trace elements of the white clay are P (330 ppm), Pb (220 ppm) and Zr (11 ppm), while for the green clay are P (1250 ppm), As (43 ppm), Cr (31 ppm), Pb (30 ppm) and Ni (23 ppm).

Compared to the average concentration of elements in shales (Shale average) (Turekian & Wedepohl, 1961 and Mason & Moore, 1982) Pb is enriched 11-times in the white clay and As is enriched 3-times in the green clay. When the ratio of an element concentration to that of Shale average is >2 the element is considered to be enriched and when it is <0.5, is considered to be depleted. The depleted trace elements of the white clay are As, Cd, Cr, Hg, Ni, P, Sb, Se, Te, Tl and Zr, while for the green one are Cr, Hg, Ni, Sb, Te, Tl and Zr.

Concerning morphological characteristics in microscale, the white clay (WC1) consists of small aggregates of flaky microparticles (Figure 2a). Single aggregates have a size of about 25μm. The green clay (GC1) shows a different morphology (Figure 2b). It consists of globular aggregates with sizes that exceed 50μm in diameter. However, it appears to be formed by platy particles, similar to the ones observed in the white clay. Yet, Transmission Electron Microscopy (TEM) is able to provide more information concerning the real and detailed morphology of clays.

4. Conclusions

The chemical analysis of the samples revealed that they contain trace elements, whose presence is prohibited in cosmetic products.

Compared to the Shale average, the white clay is enriched in Pb, while the green one is enriched in As. Both kinds of clays are depleted in Cr, Hg, Ni, Sb, Te, Tl and Zr. Moreover, the white one is also depleted in As, Cd, P, and Se.

Concerning morphological characteristics in microscale, white clay consist of small aggregates of flaky microparticles, while green clay consist of globular aggregates.

In any case, further investigation concerning the bioavailability of the trace elements determined in clays used in cosmetics, is essential.

Table 2 – Trace element content of the studied clay samples (Shale average after Turekian & Wedepohl, 1961 and Mason & Moore, 1982).

		Detection Limit	WC1	GC1	Shale Average (SA)	WC1:SA	GC1:SA
As	*ppm*	0.1	1.2	**43.2**	13	0.09	**3.32**
Be	*ppm*	0.1	1.9	3.0	3	0.63	1.00
Cd	*ppm*	0.01	<0.01	0.27	0.3	<0.03	0.90
Cr	*ppm*	0.5	0.7	**31.1**	90	0.01	0.35
Hg	***(ppb)***	5	<5	17	400	<0.01	0.04
Ni	*ppm*	0.1	0.5	**23.1**	68	0.01	0.34
P	*ppm*	10	**330**	**1250**	700	0.47	1.79
Pb	*ppm*	0.01	**220.10**	**30.10**	20	**11.01**	1.51
Sb	*ppm*	0.02	0.33	0.20	1.5	0.22	0.13
Se	*ppm*	0.1	<0.1	0.4	0.6	<0.17	0.67
Te	*ppm*	0.02	<0.02	0.03	2.2	<0.01	0.01
Tl	*ppm*	0.02	0.23	0.47	1	0.23	0.47
Zr	*ppm*	0.1	**10.6**	0.6	160	0.07	<0.01

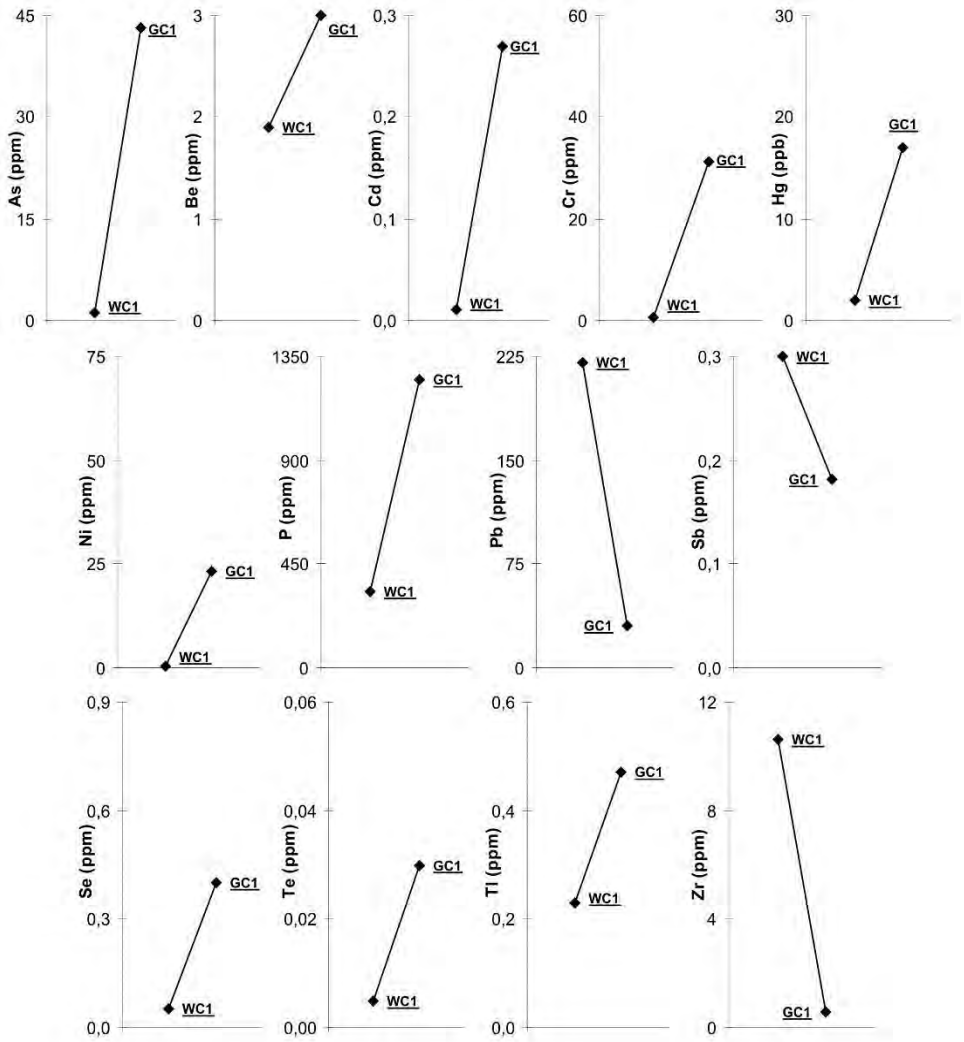

Figure 1 – Variation of trace elements concentrations among the studied samples.

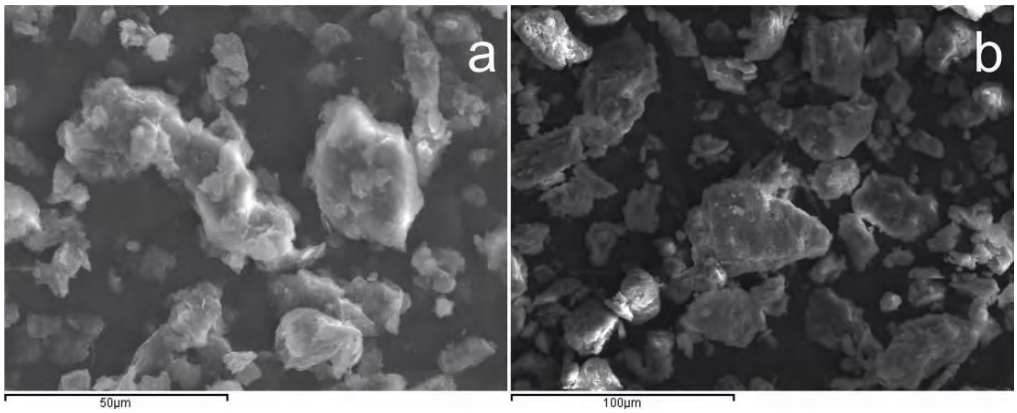

Figure 2 – SEM microphotographs of the studied samples. (a) White clay (WC1) and (b) Green clay (GC1).

5. References

Carretero M.I. 2002. Clay minerals and their beneficial effects upon human health. A review, *Appl. Clay Sci.*, 21, 155–163.

Christidis G.E. 2012. Assessment of Industrial Clays. In Bergaya F. et al. (eds): *Handbook of Clay Science, 2nd edition*, Elsevier, Amsterdam (in press).

Christidis G.E., Blum A.E. and Eberl D.D. 2006. Influence of layer charge and charge distribution of smectites on the flow behaviour and swelling of bentonites, *Appl. Clay Sci.*, 34, 125-138.

EC 2009. Regulation (EC) No 1223/2009 of the European parliament and of the Council of 30 November 2009 on Cosmetic products, *Official Journal of the European Union*, L342 (22.12.2009), 59-209.

Galán E., Liso M.J.and Forteza M. 1985. Minerales utilizados en la industria farmacéutica, *Bol. Soc. Esp. Mineral.*, 8, 369–378.

López-Galindo A. and Viseras C. 2004. Pharmaceutical and cosmetic application of clays. In Wypych, F., Satyanarayana, K.G. (eds.), *Clay Surfaces: Fundamentals and Applications,* Elsevier Ltd, 267–289.

López-Galindo A., Viseras C. and Cerezo P. 2007. Compositional, technical and safety specifications of clays to be used as pharmaceutical and cosmetic products, *Appl. Clay Sci.*, 36, 51–63.

Mason B. and Moore C.B. 1982. *Principles of Geochemistry*, Wiley, New York, 344p.

Murray H.H. 2000. Traditional and new applications for kaolin, smectite, and palygorskite: a general overview, *Appl. Clay Sci.*, 17, 207–221.

Patel N.K., Kennon L. and Levinson R.S. 1986. Pharmaceutical suspensions, In Lachman, L., Lieberman, H.A., Kanig, J.L. (eds.), *The Theory and Practice of Industrial Pharmacy, 3rd ed*., Lea and Febiger, Philadelphia, 479–501.

Rathossi C., Lambropoulou P., Skourlis K. and Katagas C. 2011. Mineralogical and microstructure of clay-bearing sediments of NE Peloponnese (Greece): Indices for physical and mechanical behaviour in civil engineering works, *Clay Miner.*, 47 (2), 259-274.

Silva P.S.C., Oliveira S.M.B., Farias L., Fávaro D.I.T. and Mazzili B.P. 2011. Chemical and radiological characterization of clay minerals used in pharmaceutics and cosmetics, *Appl. Clay Sci*., 52, 145-149.

Turekian K.K. and Wedepohl K.H. 1961. Distribution of elements in some major of the earth's crust, *Geol. Soc. Am. Bull*., 72, 175–192.

Viseras C., Aguzzi C., Cerezo P. and Lopez-Galindo A. 2007. Uses of clay minerals in semisolid health care and therapeutic products, *Appl. Clay Sci.*, 36, 37–50.

Δελτίο της Ελληνικής Γεωλογικής Εταιρίας, τομ. XLVII , 2013
Πρακτικά 13ου Διεθνούς Συνεδρίου, Χανιά, Σεπτ. 2013

Bulletin of the Geological Society of Greece, vol. XLVII 2013
Proceedings of the 13th International Congress, Chania, Sept. 2013

ANALYTICAL GEOCHEMISTRY IN THE SERVICE OF MEDICINE: AN EXPERIMENTAL STUDY OF URINARY STONES FROM NORTHERN GREECE

Iordanidis A.[1] and Garcia-Guinea J.[2]

[1]Department of Geotechnology and Environmental Engineering, Technological Educational Institute (TEI) of Western Macedonia, Kila, 50100 Kozani, Greece, aiordanidis@yahoo.co.uk and andior@teikoz.gr

[2]Museo Nacional Ciencias Naturales, CSIC, Abascal 2, 28006 Madrid, Spain

Abstract

Knowledge of the precise human biomineral composition may allow physicians to recommend an appropriate prophylactic therapy for the patient and thus prevent or delay the stone recurrence. The present study focuses on the application of complementary analytical techniques to the characterization of human urinary stones. Several gallbladder and renal stone samples were obtained from patients dwelling in areas of northern Greece. A comprehensive analytical study took place, employing the following, common in analytical geochemistry, techniques: Environmental Scanning Electron Microscopy (ESEM) coupled to Energy Dispersive System (EDS), X-Ray Diffraction (XRD), thermogravimetry (TG), μRaman spectroscopy and Cathodoluminescence (CL). A detailed determination of morphological, micro-structural, molecular, chemical and mineralogical characteristics of the urinary stone samples was achieved. It was evident by our study the application of powerful analytical techniques could substantially help the medical advisors to ascribe a medical treatment of diseases related to stone formation.

Keywords: *Human Calculi**,** ESEM-EDS, Raman, XRD, Cathodoluminescence.*

Περίληψη

Στην παρούσα μελέτη εφαρμόζονται μέθοδοι της αναλυτικής γεωχημείας στον αναλυτικό χαρακτηρισμό δειγμάτων βιο-ορυκτών, που λήφθηκαν από ασθενείς που διαβιούν στη βόρειο Ελλάδα και πάσχουν από νεφρολιθίαση και χολολιθίαση. Χρησιμοποιήθηκαν οι κάτωθι συνδυασμένες τεχνικές για τον ενδελεχή χαρακτηρισμό των προαναφερθέντων δειγμάτων: Ηλεκτρονική μικροσκοπία σάρωσης συζευγμένη με σύστημα διασποράς ενέργειας (ESEM-EDS), καθοδοφωταύγεια (CL), περιθλασιμετρία Ακτίνων Χ (XRD), Raman φασματοσκοπία και θερμική ανάλυση(TG). Πραγματοποιήθηκε αναλυτικός χαρακτηρισμός των δειγμάτων πέτρας νεφρών και χολής και προσδιορίστηκαν λεπτομερώς τα μορφολογικά, μικρο-δομικά, μοριακά, χημικά και ορυκτολογικά χαρακτηριστικά τους. Έγινε αντιληπτό ότι η χρήση των αναλυτικών αυτών βιο-γεωχημικών μεθόδων μπορεί να συνεισφέρει στην ιατρική επιστήμη, βοηθώντας τους θεράποντες ιατρούς στην αντιμετώπιση των ασθενειών που σχετίζονται με σχηματισμό πέτρας στο ουροποιητικό σύστημα.

Λέξεις κλειδιά: *Ηλεκτρονική μικροσκοπία, καθοδοφωταύγεια, περιθλασιμετρία Ακτίνων Χ, Raman φασματοσκοπία, θερμική ανάλυση.*

1. Introduction

Urinary stones are generally comprised of organic and inorganic compounds (mainly of calcium, phosphate, magnesium salts, oxalate, and uric acid). They occur in varieties of shape, size and crystalline to amorphous structure and range in color from creamy white, yellow, black and brown. There is also variation in the size of stones ranging from few millimeters to 5 cm. The pathogenesis of human stones is complex and is not completely understood.

An elevated number of nephrolithiasis and cholelithiasis (i.e. formation of renal and gallbladder stones respectively) incidents has been observed among patients dwelling in northern Greece, especially within Western Macedonia province (Iordanidis et al., 2010, 2011). This increasing frequency, related to different epidemiological factors and diseases, prompted us to carry out an analytical investigation on this kind of human stones. Such analytical studies, incorporating both non-destructive and destructive analytical methodologies, have been conducted worldwide, providing significant information on the formation and composition of human calculi and helping the physicians to take prophylactic measures for the patients (Grunhage and Lammert, 2006; Abboud 2008a, 2008b).

In the present study, the application of complementary analytical techniques, such as Environmental Scanning Electron Microscope coupled to Energy Dispersive System (ESEM-EDS), μRaman spectroscopy, X-Ray Diffraction (XRD), Thermogravimetry (TG) and Cathodoluminescence (CL) is attempted in order to provide a more comprehensive determination of the renal and gallbladder stones.

2. Materials and Methods

Several urinary (renal and gallbladder) samples were supplied by the surgeons of the General Public (Mamatsio) Hospital of Kozani and the Central (Genimatas) Hospital of Thessaloniki, northern Greece. The stones were washed and dried before analysis. Samples were cut and two types of block sections were prepared: polished ones, which were used for the Scanning Electron Microscopy and μRaman spectroscopy and unpolished ones for the X-Ray Diffraction (XRD) and Cathodoluminescence (CL) analyses. Moreover, a tiny amount of each sample was ground for the thermal analyses.

A Philips QUANTA 200 Environmental Scanning Electron Microscope (ESEM), coupled with an Oxford INCA Energy 200 Energy Dispersive System (EDS) was used for the chemical analyses and the recording of pictures, under back-scattered electron (BSE) mode.

Cathodoluminescence (CL) spectra were collected on polished slabs, at low vacuum mode without coating to keep open way out to the CL emission, using a Gatan MonoCL3 detector with a PA-3 photomultiplier attached to the ESEM.

The Raman spectra of samples were recorded with a Thermo Scientific DXR Raman Microscope with a 780 nm laser beam, which has a point-and-shoot Raman capability of 1-μm spatial resolution, setting the power value of the sample irradiation at 12 mW. The average spectral resolution in the Raman shift range of 100-3000 cm^{-1} was 5 cm^{-1}.

For the X-ray diffraction (XRD), a Phillips PW1710/00 diffractometer was used with a CuKa radiation source, equipped with a graphite monochromator. The XRD patterns were obtained by step scanning from 2º to 64º (2θ in steps of 0.020º; 4 s per step) and compared with the XRD card files of the Joint Committee on Powder Diffraction Standards.

Thermogravimetry (TG) analyses were recorded with a thermal analyzer Model 851e Mettler Toledo in N_2 atmosphere. Thermal treatments were performed at a heating rate of 10ºC min^{-1} from room temperature up to 1000ºC.

3. Results and Discussion

The macroscopic views of four characteristic gallbladder and one renal calculi, which were analyzed in our study, are shown in Figure 1.

The first gallstone is a 'black pigment' urinary stone with a spherulitic, fragile and porous structure. The ESEM images (Figure2) reveal a massive appearance with micro nodules. The chemical composition of this gallstone, as revealed by EDS analysis, consists of CaO (44.17 %) and CO_2 (52.15 %), indicating the presence of calcium carbonate minerals. The Raman spectra of two different regions of observation revealed two types of minerals, a calcium carbonate (most favourably ascribed to aragonite) and a bilirubin phase. Finally, the XRD pattern (Figure 4-1) shows a characteristic hump between 10^o and 30^o of 2θ angle, ascribed to amorphous organic phases and aragonite mineral, with its characteristic peaks of d-spacing (3.35, 3.27, 1.97 and 1.87 Å).

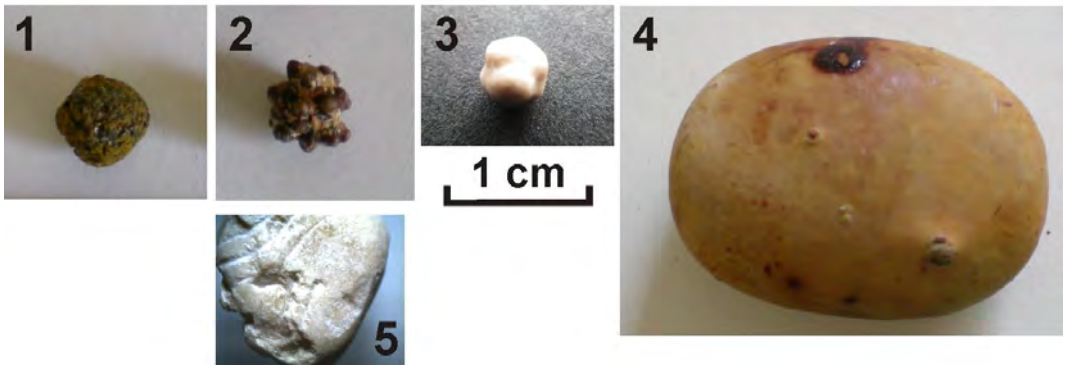

Figure 1 - Macroscopic images of the four gallbladder (No 1 - 4) and one renal (No 5) stones analyzed in this study.

The second sample in an asteroidal assemblage of pale-coloured nodules. The concentric structure is more evident under ESEM observation (Figure 2). Based on the chemical composition (EDS) of distinct layers within the gallbladder, we can conclude that the inter-bedded layers have a variable composition of calcium carbonate, calcium hydroxyl-apatites and Ca-oxalates. The phosphorous-rich areas are in fact grains intercalated in the concentric matrix. A typical Ca-oxalate mineral (either whewellite [$CaC_2O_4.H_2O$)] or weddellite [$CaC_2O_4.2H_2O$]) was determined with Raman spectroscopy. The XRD analysis of this sample revealed amorphous organics along with carbonate (characteristic peaks of d-spacing at 5.87, 3.64 and 2.97 Å) and oxalate (peak at 5.19 Å) minerals.

The third sample is a white spherical calculus, with a size of approximately 5 mm and rather dense and hard comparing to the previous ones. The ESEM/EDS analysis inferred a purely organic (CO_2 100 %) material (Figure 2). The Raman spectroscopy revealed a very distinct molecule of cholesterol with sharp and clear peaks (Figure 3). The XRD pattern of the same sample provided information of a mixture of cholesterol crystalline structures (characteristic peaks of d-spacing at 5.21, 4.11 and 4.89 Å) and organic-rich phases, most probably assigned to oxalic acids (peak at 5.56 Å). Precipitation of cholesterol from supersaturated bile leads to the gallstone formation and is related to several different pathways, which in turn include nucleation, crystallization, growth and agglomeration of cholesterol crystals (Jayalakshmi et al., 2009; Athanasiadou et al., 2013).

The fourth gallstone is approximately 3cm long with a pale colour and a pebble-like appearance. An ideal concentric structure is shown in the ESEM image (Figure 2). Numerous layers are inter-bedded. The growth of the gallbladder calculus occurs around an initially formed nucleus. The EDS analysis determined a gallstone rich in carbon (CO_2 68.34%) and nitrogen (N_2O_5 31.44%). The Raman spectra revealed a well-crystallized molecule of uric acid. Uric acid is a heterocyclic compound of carbon, nitrogen, oxygen, and hydrogen with the chemical formula $C_5H_4N_4O_3$. This

is also confirmed by the XRD analysis (Figure 4), in which very distinctive peaks of uric acid crystals are revealed (peaks at 6.55, 5.61. 3.85, 3.27, 3.10 and 2.24 Å). Whereas it is usual to have variation in composition from the core to the outer surface of such mixed calculi (Wilson et al., 2010), in our study, several zones throughout the calculus were analyzed by EDS and Raman spectroscopy, indicating a composition of a rather pure uric acid.

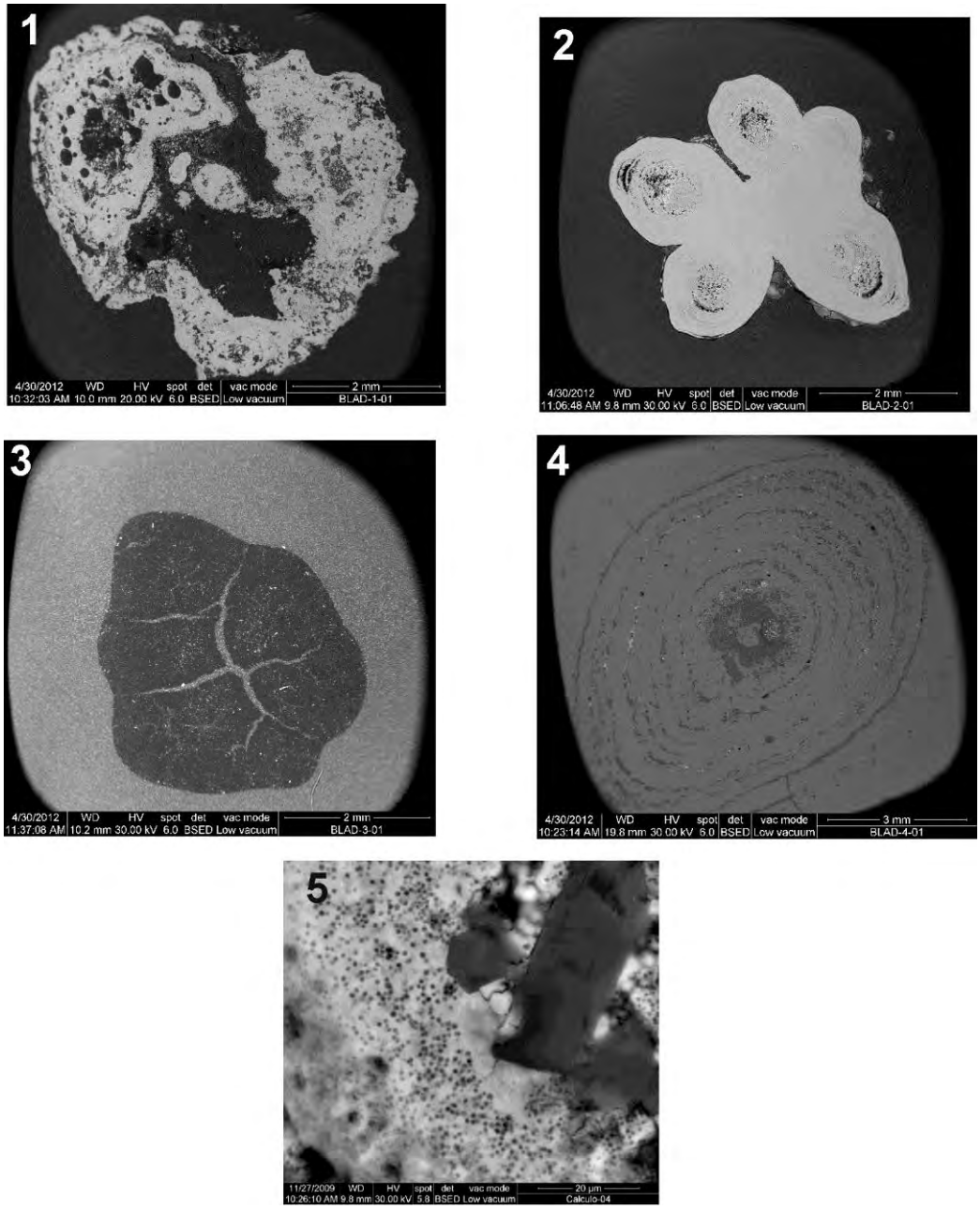

Figure 2 - ESEM images of five urinary stones: (1) calcium-rich gallbladder No1; (2) gallbladder No2, rich in apatites, calcium carbonates and oxalates; (3) the organic-rich gallstone No 3; (4) the amino-acidic gallstone No 4; (5) hexagonal cystine crystals (dark) and microbial remnants (white pores) of the renal stone No5 .

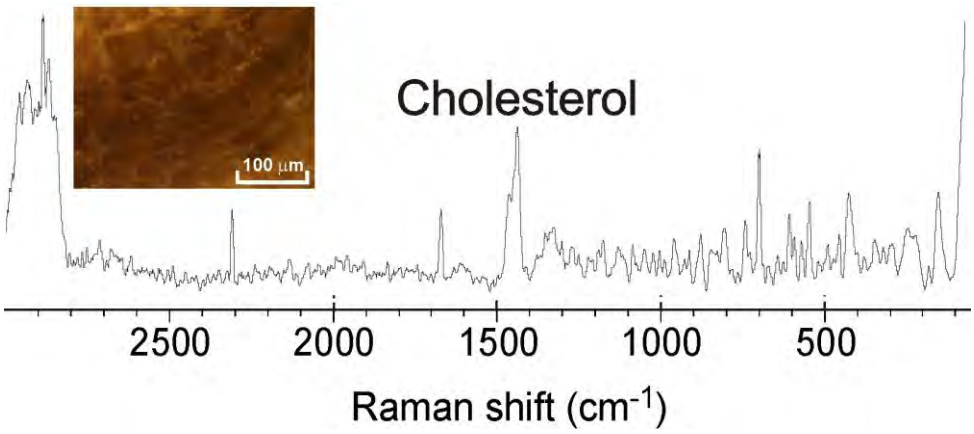

Figure 3 - Raman spectrum and microscopic views using the con-focal Raman microscope of the cholesterol sample No 3.

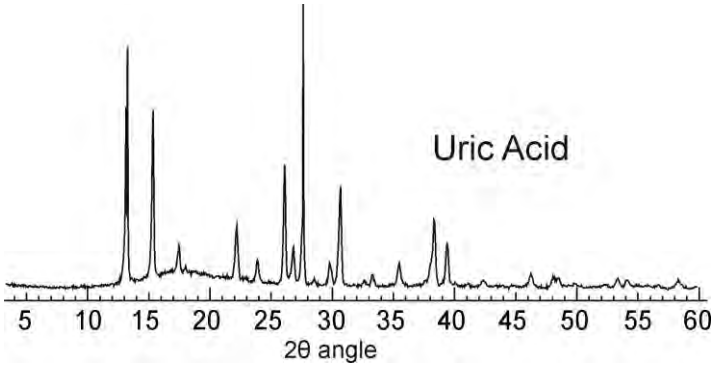

Figure 4 - Characteristic XRD peaks of the Uric Acid crystals of sample No 4.

A characteristic concentric texture is clearly shown for the No5 renal calculus. Using ESEM, thick cystine layers inter-bedded with thin calcium hydroxyl-apatite layers are observed. The elevated concentrations of sulphur are clearly shown under EDS, while calcium and phosphorous prevail within the apatite regions. Characteristic hexagonal cystine crystals are observed under higher magnification (Figure 2). The mineralogical (XRD) analysis revealed a clear L-cystine structure (the less soluble amino-acid found in the urine) (Figure 4). The thermal analysis revealed the characteristic endothermic peak at 246 ^{o}C found in L-cystine and a high amount of mass loss (90%), as expected for such an organic compound (Figure 5).

The cathodoluminescence (CL) technique was employed as a complementary method to all the aforementioned techniques (ESEM-EDS, Raman, XRD, TG) to investigate the calculi samples. To our knowledge, there has not been published any CL analytical results on human stones in the global. Thus, it could be regarded as a first attempt to utilize the cathodoluminescence spectroscopy for the analysis of gallbladder calculi. Figure 6 contains characteristic CL spectra of the mineral constituents of the cystine calculus No5. Cathodoluminescence spectra were obtained from several areas of the stone. The chemically pure collagen displays similar and more intense CL plots than hydroxyapatite, thus producing a significant mask of the CL emission, whereas the CL emission peaks at 325 (L-cystine-apatite) and 310 nm (Ca-oxalate) could be associated to oxygen hole centre emission defects coupled with C—OH precursor bonds. For the gallbladder stones (No 1-4), in general, two intensive peaks are determined in all the CL spectra, one between 300 and 310 nm, with an intensity varying between 3800 and 8000 a.u., and another rather broad between 600 and 620 nm, with a considerably lower intensity. These analytical data of

cathodoluminescence could be regarded as reference for any related future studies, notwithstanding that our CL experiments are launching cathodoluminescence technique as a significant analytical technique for biomaterials characterization.

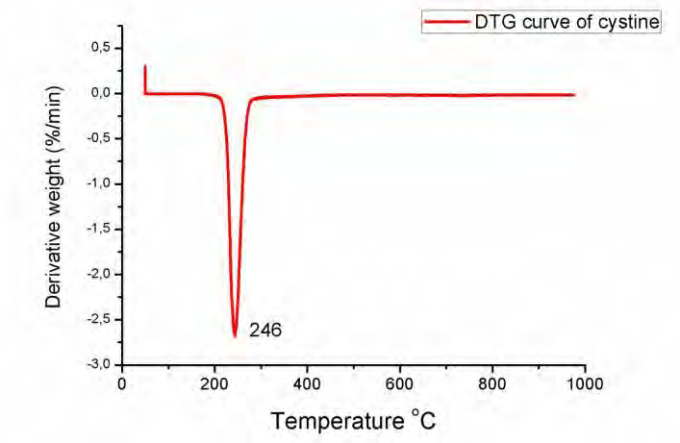

Figure 5 - Derivative Thermogravimetric (DTG) curve of cystine calculus No5.

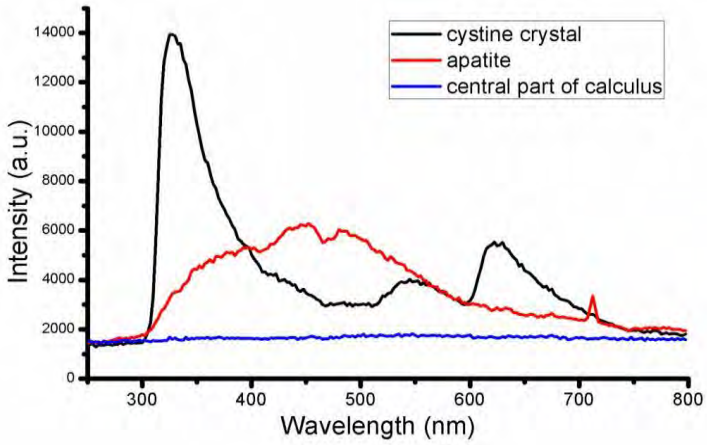

Figure 6 - CL emission spectra of three characteristic areas of cystine calculus No5: central calculi part, apatite mineral and cystine crystal.

In synopsis, the employment of complementary methodologies provided a comprehensive characterization of the human calculi. It is noticeable that certain constituents could not be detected by one single methodology, a fact that clearly demonstrates the significance of using combined techniques such as the electron microscopy imaging and EDS chemical analysis, micro-Raman molecular spectroscopy, X-ray Diffraction for the detection of crystalline phases and the Cathodoluminescence probe for the relationships between defects and emission. Our study proves that the application of powerful analytical techniques could substantially help the medical advisors. In particular, having a thorough micro-chemical and structural analysis of an urinary stone, the medical treatment of diseases related to stone formation could be better scheduled. Knowledge of the precise bio-mineral composition may allow physicians to recommend an appropriate prophylactic therapy for the patient and thus prevent or delay the cystine stone recurrence.

4. Acknowledgements

The technical staff from the Museo Nacional Ciencias Naturales, CSIC, Madrid (Rafael Gonzalez Martin, Manuel Castillejo, Laura Tormo Cifuentes, Marta Furió Vega, Alberto Jorge García, Cristina Paradela) for their help in conducting the analyses are gratefully acknowledged. We are also indebted to the physicians form the National Hospital of Kozani (Giousef Chisam, Angelopoulos Angelis and Doulgeralis Michael) and Dr. Papadopoulou Lambrini from the School of Geology, Aristotle University of Thessaloniki, for their collaboration.

5. References

Abboud I.A. 2008a. Concentration effect of trace metals in Jordanian patients of urinary calculi, *Environmental Geochemistry and Health*, 30, 11–20.

Abboud I.A. 2008b. Mineralogy and chemistry of urinary stones: patients from North Jordan, *Environmental Geochemistry and Health*, 30, 445–463.

Athanasiadou D., Godelitsas A., Sokaras D., Karydas A.G., Dotsika E., Potamitis C., Zervou M., Xanthos S., Chatzitheodoridis El., Chye Goo, H. and Becker U., 2013. New insights into the chemical and isotopic composition of human-body biominerals. In: Cholesterol gallstones from England and Greece, *Journal of Trace Elements in Medicine and Biology,* 27 (2), 79-84.

Grunhage F. and Lammert F. 2006. Pathogenesis of gallstones: a genetic perspective, *Best Practice & Research Clinical Gastroenterology*, 20 (6), 997-1015.

Iordanidis A., Garcia-Guinea J., Correcher V. and Goundas I., 2011. Optical and spectral observations on cystine, oxalate and apatite renal calculi, *Spectroscopy Letters*, 44 (7-8), 490-494.

Iordanidis A., Garcia-Guinea J. and Goundas, I., 2010. Microchemical and microstructural characteristics of cystine (a renal stone), *XIX Congress of the Carpathian Balkan Geological Association*, Thessaloniki, Greece, 23-26 September 2010, pp. 166

Jayalakshmi K., Sonkar K., Behari A., Kapoor V.K. and Sinha N, 2009. Solid state 13C NMR analysis of human gallstones from cancer and benign gall bladder diseases, *Solid State Nuclear Magnetic Resonance*, 36, 60–65.

Wilson E.V., Junaid Bushiri M. and Vaidyan V.K. 2010. Characterization and FTIR spectral studies of human urinary stones from Southern India, *Spectrochimica Acta Part A*, 77, 442–445.

Δελτίο της Ελληνικής Γεωλογικής Εταιρίας, τομ. XLVII , 2013
Πρακτικά 13ου Διεθνούς Συνεδρίου, Χανιά, Σεπτ. 2013

Bulletin of the Geological Society of Greece, vol. XLVII 2013
Proceedings of the 13th International Congress, Chania, Sept. 2013

CHEMOSTRATIGRAPHY OF THE TOARCIAN OCEANIC ANOXIC EVENT FROM THE IONIAN ZONE, GREECE

Kafousia N.[1], Karakitsios V.[1], Mattioli E.[2] and Jenkyns H. C.[3]

[1] National and Kapodistrian University of Athens, Faculty of Geology and Geoenvironment, Department of Hist. Geology - Paleontology, nkafousia@geol.uoa.gr, vkarak@geol.uoa.gr,

[2] Laboratoire de Géologie de Lyon UMR 5276 CNRS, Université Lyon 1, ENS Lyon, Campus de la Doua, Bâtiment Géode, F-69622 Villeurbanne Cedex, France, emanuela.mattioli@univ-lyon1.fr

[3] Department of Earth Sciences, University of Oxford, South Parks Road OXFORD OX1 3AN, United Kingdom, Hugh.Jenkyns@earth.ox.ac.uk

Abstract

A global perturbation in the carbon cycle has been recorded in the Early Toarcian (~ 183 Ma) and is marked by enhanced organic-carbon burial and mass extinction. It is also associated with high palaeotemperatures, both positive and negative excursions in carbon-isotope ratios, and the development of anoxic to euxinic conditions in marine environments: together these phenomena have been designated as constituting an Oceanic Anoxic Event. Here we provide a high-resolution, multiproxy biostratigraphic and chemostratigraphic study from a section that belongs to the central Ionian Zone in Greece. Calcareous nannofossil distribution, as well as the TOC, $\delta^{13}C_{carb}$ and $\delta^{13}C_{org}$, have all been determined. The nannofossil zones NJT 5b, NJT 6 and NJT 7 have been recognized in the section. In the NJT 5b zone a small positive excursion in TOC and negative excursion in $\delta^{13}C_{carb}$ is recorded, tentatively assigned to the Pliensbachian/Toarcian boundary. In the NJT 6 zone, the main negative carbon-isotope excursion characteristic of this interval is developed, associated with a relative increase in TOC. The difference in this section, compared with sections from the Pindos Zone but in common with sections elsewhere, is the record of a positive excursion in the NJT 7 zone in both organic and carbonate carbon isotopes. This study offers new biostratigraphic and geochemical data for the Ionian Zone, and further illustrates the impact of Toarcian Oceanic Anoxic Event in the Tethyan region.

Key words: *Jurassic, total organic carbon, carbon isotopes, biostratigraphy, geochemistry.*

Περίληψη

Κατά τη διάρκεια του Κατώτερου Τοάρσιου (~ 183 Μα), έχει καταγραφεί μια παγκόσμια αναταραχή στον κύκλο του άνθρακα, η οποία έχει σημαδευτεί από αύξηση στον ρυθμό ενταφιασμό του οργανικού άνθρακα και μαζικές εξαφανίσεις ειδών. Επίσης, έχει συσχετιστεί από υψηλές παλαιοθερμοκρασίες, θετικές και αρνητικές μεταβολές στα ισότοπα του άνθρακα και με τη δημιουργία ανοξικών έως ευξινικών συνθηκών στα θαλάσσια περιβάλλοντα. Ο συνδυασμός όλων αυτών των φαινομένων θεωρείται ότι αποτελεί ένα Ανοξικό Γεγονός. Σε αυτή την εργασία, παρουσιάζεται μια υψηλής

ανάλυσης μελέτη όπου συνδυάζονται βιοστρωματογραφικά και χημειοστρωματογραφικά δεδομένα, σε μια τομή της κεντρικής Ιόνιας Ζώνης. Στα πλαίσια της εργασίας, αναγνωρίστηκαν οι συναθροίσεις των ασβεστολιθικών ναννοαπολιωμάτων καθώς και οι συγκεντρώσεις των TOC, $\delta^{13}C_{carb}$ και $\delta^{13}C_{org}$. Αναγνωρίστηκαν οι Ζώνες NJT 5b, NJT 6 και NJT 7. Στη Ζώνη NJT 5b παρατηρείται μια μικρή θετική μεταβολή στις συγκεντρώσεις του TOC και μια αρνητική μεταβολή στο $\delta^{13}C_{carb}$, που οδηγούν στην αναγνώριση του ορίου Πλιενσβάχιο/Τοάρσιο. Στην Ζώνη NJT 6, αναπτύσσεται η κύρια αρνητική μεταβολή στα ισότοπα του άνθρακα, η οποία είναι χαρακτηριστική για το συγκεκριμένο επίπεδο, σε συνδυασμό με αύξηση των συγκεντρώσεων του TOC. Η διαφορά αυτής της τομής, σε σύγκριση με τομές από τη Ζώνη της Πίνδου, είναι η εμφάνιση θετικής μεταβολής και στα δύο ισότοπα του άνθρακα στην Ζώνη NJT 7. Αυτή η μελέτη δίνει νέα βιοστρωματογραφικά και γεωχημικά δεδομένα για την Ιόνια Ζώνη και διαφωτίζει περαιτέρω τον αντίκτυπο του Τοάρσιου Ωκεάνιου Ανοξικού Γεγονότος στην περιοχή της Τηθύος.
Λέξεις κλειδιά: *Ιουρασικό, ολικός οργανικός άνθρακας, ισότοπα του άνθρακα, βιοστρωματογραφία, γεωχημεία.*

1. Introduction

The Toarcian Oceanic Anoxic Event (T-OAE) constitutes one of the most profound environmental changes of the Mesozoic Era (Jenkyns, 1988). Marine depositional settings across the globe, show evidence for global warming (Bailey et al., 2003; Jenkyns, 2003; Suan et al., 2008), mass extinction (Little and Benton, 1995; Wignall, 2001) and probable ocean acidification (Hermoso et al., 2012; Hönisch et al., 2012; Trecalli et al., 2012). A major perturbation in the global carbon (Cohen et al., 2007) and sulphur cycle (Gill et al., 2011; Newton et al., 2011) during the Toarcian has been recorded. The carbon perturbation is marked by a negative excursion in carbon isotopes interrupting an overarching positive trend, that has been recorded in terrestrial wood (Hesselbo et al., 2000; Hesselbo et al., 2007; Al-Suwaidi et al., 2010), marine organic matter and carbonate (Jenkyns and Clayton, 1986; Suan et al., 2008; van Breugel et al., 2006; Woodfine et al., 2008).

In this paper, we present biostratigraphical (calcareous nannofossils) and geochemical (wt% TOC, δ^{13}Ccarb, and δ^{13}Corg) data from the Toarcian sediments of the central Ionian Zone (Petousi section), a marine basin that constituted part of the southern Tethyan margin (Bernoulli and Renz, 1970). Age equivalent deposits in Greece have recently chemostratigraphically studied in Pindos Zone (Karakitsios et al., 2010; Kafousia et al., 2011), corresponding to a deep-sea ocean-margin basin that formed in mid-Triassic times along the northeastern part of Apulia.

2. Geological Setting

The Ionian Zone of NW mainland Greece is one of most external Hellenides (Paxos Zone, Ionian Zone, Gavrovo Zone; Aubouin, 1959). This domain corresponds to the southern passive continental margin of the Neotethys Ocean. This Ocean's opening started in Early Mesozoic while its closure took place during the Late Mesozoic–Early Cenozoic (Karakitsios, 1992, 1995; Laubscher and Bernoulli, 1977). The Ionian Zone constitutes of rocks that range from Triassic evaporites through a varied series of Jurassic to Upper Eocene mixed carbonate–siliciclastic–siliceous sediments, overlain by Oligocene flysch. During the Early Jurassic, northwestern Greece was covered by a vast carbonate platform (IGRS-IFP, 1966; Bernoulli and Renz, 1970; Karakitsios, 1992, 1995). In the Pliensbachian, extensional stresses that are related to the opening of the Neotethys Ocean, began to act in the area and caused the differentiation of the Ionian Zone from the adjacent Zones (Karakitsios, 1992, 1995). These Zones (Paxos and Gavrovo) remained carbonate platforms, while the Ionian Zone became an area of strong subsidence and faulting with the development of pelagic conditions (Karakitsios, 1995). This palaeogeographic evolution is recorded in the pelagic

Siniais Limestone and the laterally equivalent Louros Limestones of Pliensbachian age (Karakitsios and Tsaila-Monopolis, 1988; Dommergues et al., 2002; Karakitsios, 1992).

The initial formation of the Ionian Basin was followed by an internal differentiation into smaller sub-basins with half-graben geometry; in most cases these sub-basins did not exceed 5 km across (Karakitsios, 1995). This had as a result abrupt changes in thickness of the syn-rift formations, which take the shape of syn-sedimentary wedges. In the deeper parts of the half-grabens, these wedges include complete Toarcian-Tithonian successions, while in the elevated parts of the half-grabens; the succession is interrupted by unconformities (Karakitsios, 1992, 1995). The directions of syn-sedimentary structures (e.g. slumps and syn-sedimentary faults) indicate that deposition was controlled both by structures formed during extension related to the opening of the Neotethys Ocean and the halokinesis of evaporites at the base of the Ionian Zone succession (Karakitsios, 1992, 1995). In the Early Berriasian the post-rift sequence began with the pelagic Vigla Limestone, whose deposition was effectively synchronous throughout the Ionian Basin (Karakitsios et al. 1988; Karakitsios, 1992; Karakitsios and Koletti, 1992). The Vigla Limestone blankets the syn-rift structures and, in some cases, directly overlies pre-rift units (e.g. Pantokrator Limestone). As a consequence, the base of the Vigla Limestone represents the break-up unconformity of the post-rift sequence in the Ionian Basin (Karakitsios, 1992). Long-standing differential subsidence during the deposition of the Vigla Limestone, as shown by the marked variation in the thickness of this formation, was probably due to the continued halokinesis of the basal-Ionian Zone evaporites. This palaeogeographic configuration persisted with minor off- and onlap movements along the basin margin until the Late Eocene, when orogenic movements and flysch sedimentation began. The particular geometry of the restricted sub-basins that were formed during the syn-rift period of the Ionian Zone may have favored increased organic-matter burial during the Toarcian–Tithonian interval (Baudin et al. 1990; Karakitsios, 1995; Rigakis and Karakitsios, 1998; Karakitsios and Rigakis, 2007). Toarcian black shales in the Ionian Zone were described first by Renz (1910), who compared them with the Posidonienschiefer of Germany, and sedimentological details were given by Walzebuck (1982). In this paper we demonstrate that the Lower Toarcian organic-rich laminated black shales, deposited in the different palaeogeographic environments of the Ionian sub-basins, record a global rather than a local event.

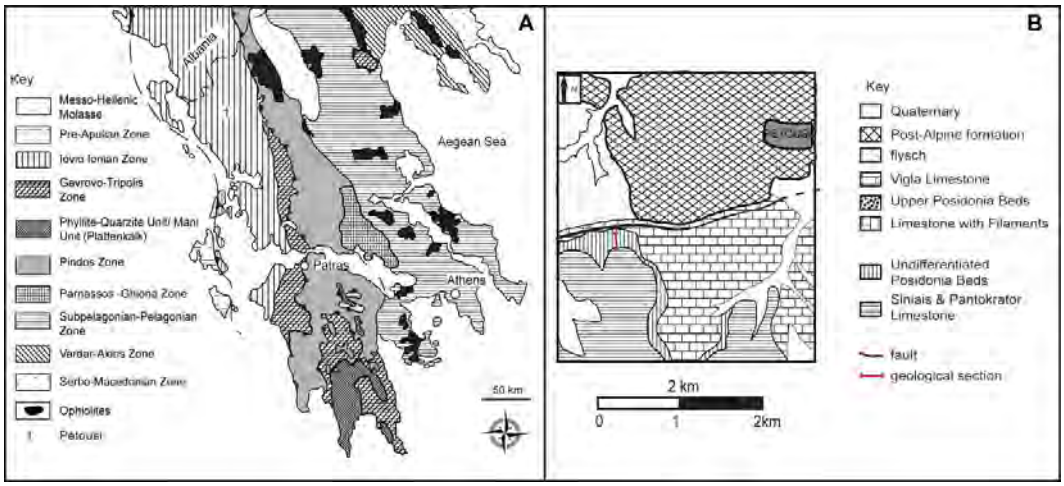

Figure 1 – A: structural map of Greece, B: geological map of the Petousi section.

2.1. Petousi Section

The Petousi section (39º30´N, 20º35´E), was first described by Karakitsios (1992). It is located around 2 km WSW from Petousi village, south of the Petousi–Paramithia road, in Thesprotia prefecture. The studied outcrop is of excellent quality even though it is locally covered by vegetation.

The section begins with the uppermost metres of the Siniais Limestone: white to grey limestones, with thin layers of black shales intercalations. It continues with the Undifferentiated Posidonia Beds, which begins with 10 m of black shales followed by a yellow-green chert rich in *Posidonia* (*Bositra buchi*).

Figure 2 – Petousi section.

3. Materials and Methods

A total of 139 samples from Petousi, were analysed for their wt% TOC using a direct combustion and automatic titration method through a Strohlein Coulomat 702 analyser. Duplicate samples were used; one of them was roasted at 420ºC overnight to remove organic carbon. Both samples were then combusted at 1220ºC to decompose the calcium carbonate. The gaseous products of combustion are released (a Urea Peroxide tablet is removing SO_2) and fed to barium perchlorite solution at stable temperature 10ºC and pH 10 with resultant change in pH. An electrolytically titration is bringing the pH back to the original value. The quantity of electricity needed for this purpose gave an absolute determination of the amount of carbon present. The difference between the samples that had (C_a) and had not (C_b) been roasted at 420ºC gave a measure of the value of TOC. Reproducibility of the samples was usually better than 0.1%. The result was given in counts and the following formula was used for the final result.

Equation 1

$$\%C = \frac{counts \times 0.2}{weight(mg)} \qquad \%TOC = \%Ca - \%Cb$$

For carbonate carbon-isotope composition, 211 bulk sediment samples were analysed. The powdered samples were cleaned using 10% H_2O_2 followed by acetone ($(CH_3)_2CO$) and then dried at 60ºC for at least 30 minutes. Samples were then reacted with purified orthophosphoric acid at 90ºC and analysed on-line using a VG Isogas and Prism II mass spectrometer. Corrections were applied and the results are reported through the δ notation, in ‰ deviation from the Pee Dee Belemnite (PDB) standard. The calibration of the PDB was performed via the laboratory standard that was calibrated against NBS19 and Cambridge Carrara marble. Reproducibility of replicate analyses of the standards was usually better than 0.1‰.

Equation 2

$$\delta X = \frac{Rx(sample) - Rx(standard)}{Rx(standard)} \times 1000$$

For 97 samples organic carbon-isotope composition was calculated. The samples were decarbonated using 3 M HCL for the removal of $CaCO_3$ and put in a warm surface for the removal of the rest CO_3^{2-} for 8 hours. Samples were then rinsed with distilled water, centrifuged and rinsed again until pH was neutral and then dried in an oven at 60ºC. A quantity of 4 to 50 mg (depending on the amount of organic carbon) was weighed out into a 8x6 mm tinfoil cup and placed in an Europa Scientific Limited CN biological sample converter connected to a 20–20 stable isotope gas ratio mass spectrometer. Carbon isotope ratios were measured against a laboratory nylon standard ($\delta^{13}C$ = -26.1 ± 0.2% and) and expressed relative to Peedee belemnite (PDB) and reported through the δ notation. Reproducibility is better that ± 0.2‰. All the above analyses were undertaken at the University of Oxford.

A set of 24 samples was investigated for the content of calcareous nannofossils. Smear-slides were prepared from the powdered rock according to the technique described in Bown & Young (1998), then analyzed in an optical polarizing Leitz microscope at x1250. Nannofossils were counted for each sample in a surface area of the slide varying between 2 and 3 cm^2 at the Laboratoire de Géologie de Lyon, Université Claude Bernard.

4. Results

4.1. Biostratigraphy

The samples that were studied from Petousi section show a diverse and relatively rich nannofossil assemblage, although preservation is moderate to poor. *Schizosphaerella*, *M. jansae* and some small *Lotharingius* (*L. hauffi* and *L. frodoi*) are the dominant forms in the assemblage. In the base of the section, corresponding to the Siniais Limestone, NJT 5b Subzone was identified based on the presence of *Calyculus* spp. and *L. sigillatus*. This zone spans the Pliensbachian/Toarcian boundary (Mattioli & Erba, 1999). Higher in the section, the NJT 6 Zone is identified; starting at 5.4 m with the FO of *C. superbus* and ending at 9.8 m with the FO of *D. striatus* that marks the onset of the NJT 7 Zone.

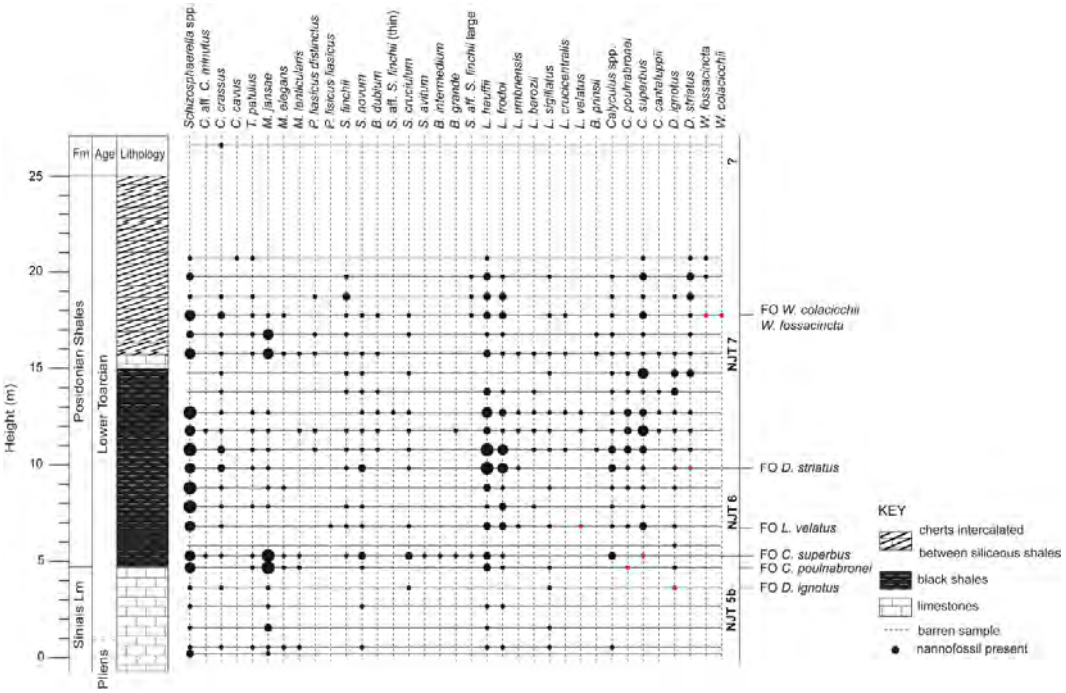

Figure 3 – Calcareous nannofossil biostratigraphy of Petousi section. Relative abundance per square surface unit was estimated. Four abundance classes were defined: rare, frequent, common and abundant. These classes are represented by a different size of black dots.

4.2. Chemostratigraphy

4.2.1. Wt% Total Organic Carbon (TOC)

TOC values in the Siniais Limestone begin at very low values, ~ 0-1 wt%. In the basal Undifferentiated Posidonia Beds, where there are black shales, TOC values begin to rise marking a positive excursion that reaches values up to 4.86 wt% over a 2-metre interval. Higher in the section, values are lower and fluctuate between ~ 0 and 3 wt%.

4.2.2. Carbon-Isotope Ratio

In Figure 3 it can be seen that both carbonate and organic-carbon $\delta^{13}C$ profiles show a small disturbance at the 2- metre level of the section. This, together with the small excursion in the TOC data and the biostratigraphy, designate that this is the Pliensbachian/Toarcian boundary. Up-section, isotopic values of bulk carbonate remain stable around 1.3‰. The values show a marked ~ 1‰ decrease, that spans less than 1 m, half a metre above the NJT 5b/NJT 6 boundary. Above this level and for 11 metres, values increase recording a positive excursion of only ~ 1‰. Higher in the section, values decrease again.

Above the Pliensbachian/Toarcian boundary $\delta^{13}C_{org}$ fluctuates around a background value of -29‰. At the NJT5b/NJT6 boundary, values fall and define the negative excursion that spans 2 metres of the section where values drop to -33‰. Following this excursion, values begin to rise reaching values up to -30‰. Up-section, values goes up and down until the 9.5-metre level of the section. At this point a positive excursion that lasts for 2 metres and reaches values up to ~ -26‰ is recorded. Above this level, $\delta^{13}C_{org}$ attains background values (~-29‰) to the top of the section.

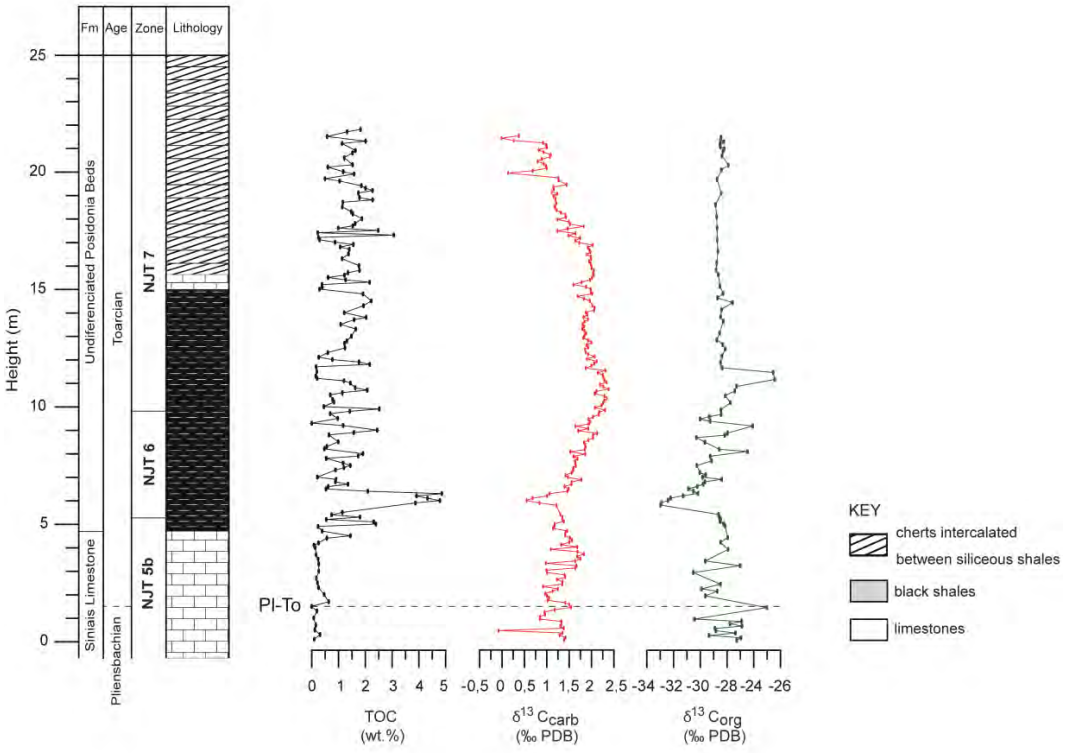

Figure 4 – Lithostratigraphic log, bulk TOC, $\delta^{13}C_{carb}$, and $\delta^{13}C_{org}$ profiles through Petousi section.

5. Discussion

Calcareous nannofossil analysis from the Petousi section reveals the age of the studied formations. The Upper part of the Siniais Limestone belongs to Subzone NJT 5b *Lotharingius sigillatus*, spanning the Late Pliensbachian–basal Toarcian interval (Mattioli and Erba, 1999; Mattioli et al., 2009). The small negative followed by a small positive excursion in carbonate carbon-isotopic data in the same formation, confirms that there is the Pliensbachian–Toarcian boundary. The small negative

carbon-isotope excursion probable represent a global event, since it has been recorded in many areas (Bodin et al., 2010; Hesselbo et al., 2007; Kafousia et al., 2011; Littler et al., 2010; Sabatino et al., 2009).

The lower part of the overlying stratigraphic formation (Undifferentiated Posidonia Beds) belongs to the Nannofossil Zone NJT 6 *Carinolithus superbus*. This Zone is encapsulated in the ammonite zones polymorphum/tenuicostatum and levisoni/serpentinus in Tethyan sections where ammonite biostratigraphy is available (Mattioli and Erba, 1999; Mattioli et al., 2009).

Total organic carbon values in the Petousi section from the Ionian Zone are comparable with coeval Tethyan sections. TOC values over the interval of the negative carbon-isotope excursion reach values up to ~ 5%. These values are similar to those in certain pelagic sections from the Southern Alps of Italy (Jenkyns, 2010; Jenkyns et al., 2001; Pancost et al., 2004).

In the Petousi section the negative carbon-isotope excursion and the increase in TOC, that are the main characteristics of the Toarcian Oceanic Anoxic Event, take place in the NJT 6 zone. The difference in this section, compared to sections from the Pindos Zone (Kafousia et al., 2011), is that in the NJT 7 zone is recorded a positive excursion, in both organic and carbonate carbon isotopes.

All the above data indicate that the Toarcian Oceanic Anoxic Event took place in the Ionian Zone but sedimentation and the geochemistry of seawater has been affected by local palaeoenviromental conditions.

6. Acknowledgments

The authors would like to thank Dr Norman Charnley and Mr Steve Wyatt (Earth Sciences Department) and Dr Peter Ditchfield (Archaeological Research Laboratory) for analyses performed during a visit of NK to Oxford University. NK would acknowledge the European Association of Organic Geochemists (EAOG) for the travel scholarship, which she received; and the University of Athens SARG for co-funding the field work.

7. References

Al-Suwaidi A.H., Angelozzi G.N., Baudin F., Damborenea S.E., Hesselbo S.P., Jenkyns H.C., Manceñido M.O. and Riccardi A.C. 2010. First record of the Early Toarcian Oceanic Anoxic Event from the Southern Hemisphere, Neuquén Basin, Argentina, *Journal of the Geological Society*, 167, 633-636.

Aubouin J. 1959. Contribution a l 'étude géologique de la Grece septentrionale; les confins de l'Epire et de la Thessalie, *Annales Géologiques des Pays Helléniques*, 10.

Bailey T.R., Rosenthal Y., McArthur J.M. and van der Schootbrugge B. 2003. Paleoceanographic changes of the Late Pliensbachian-Early Toarcian interval: a possible link to the genesis of an Oceanic Anoxic Event, *Earth and Planetary Science Letters*, 212, 307-320.

Baudin F., Herbin J.P., Bassoulet J.P., Dercourt J., Lachkar G., Manivit H. and Renard M. 1990. Distribution of organic matter during the Toarcian in the Mediterranean Tethys and Middle East, In Huc, A.Y. (Ed.), Deposition of organic facies.73-92, *American Association of Petroleum Geologists, Studies in Geology*, 30, 73-92.

Bernoulli D. and Renz O. 1970. Jurassic carbonate facies and new ammonite faunas from Western Greece, *Eclogae Geologicae Helvetiae*, 63/2, 573-607.

Bodin S., Mattioli E., Fröhlich S., Marshall J.D., Boutib L., Lahsini S. and Redfern J. 2010. Toarcian carbon isotope shifts and nutrient changes from the Northern margin of Gondwana (High Atlas, Morocco, Jurassic): Palaeoenvironmental implications, *Palaeogeography, Palaeoclimatology, Palaeoecology*, 297, 377-390.

Bown P.R. and Young J. 1998. Chapter 2: techniques. In Bown, P.R. (Ed.), *Calcareous Nannofossil Biostratigraphy,* 17, Dordrecht, Kluwer Academic Publishing, 314 pp.

Cohen A.S., Coe A.L. and Kemp D.B. 2007. The Late Palaeocene–Early Eocene and Toarcian (Early Jurassic) carbon isotope excursions: a comparison of their time scales, associated environmental changes, causes and consequences, *Journal of the Geological Society*, 164, 1093-1108.

Dommergues J.-L., Karakitsios V., Meister C. and Bonneau M. 2002. New ammonite data about the earliest syn-rift deposits (Lower Jurassic) in the Ionian Zone of N-W Greece (Epirus), *Neues Jahrbuch fuer Geologie und Palaeontology, Abhandlungen*, 223, 299-316.

IGRS-IFP 1966. *Etude géologique de l'Epire* (Grèce nord-occidentale), 306.

Gill B.C., Lyons T.W. and Jenkyns H.C. 2011. A global perturbation to the sulfur cycle during the Toarcian Oceanic Anoxic Event, *Earth and Planetary Science Letters*, 312, 484-496.

Hermoso M., Minoletti F., Rickaby R.E.M., Hesselbo S.P., Baudin F. and Jenkyns H.C. 2012. Dynamics of a stepped carbon-isotope excursion: Ultra high-resolution study of Early Toarcian environmental change, *Earth and Planetary Science Letters*, 319–320, 45-54.

Hesselbo S.P., Grocke D.R., Jenkyns H.C., Bjerrum C.J., Farrimond P., Morgans Bell H.S. and Green O.R. 2000. Massive dissociation of gas hydrate during a Jurassic oceanic anoxic event, *Nature*, 406, 392-395.

Hesselbo S.P., Jenkyns H.C., Duarte L.V. and Oliveira L.C.V. 2007. Carbon-isotope record of the Early Jurassic (Toarcian) Oceanic Anoxic Event from fossil wood and marine carbonate (Lusitanian Basin, Portugal), *Earth and Planetary Science Letters*, 253, 455-470.

Hönisch B., Ridgwell A., Schmidt D.N., Thomas E., Gibbs S.J., Sluijs A., Zeebe R., Kump L., Martindale R.C., Greene S.E., Kiessling W., Ries J., Zachos J.C., Royer D.L., Barker S., Marchitto T.M., Moyer R., Pelejero C., Ziveri P., Foster G.L. and Williams B. 2012. The Geological Record of Ocean Acidification, *Science*, 335, 1058-1063.

Jenkyns H.C. 1988. The early Toarcian (Jurassic) anoxic event; stratigraphic, sedimentary, and geochemical evidence, *American Journal of Science*, 288, 101-151.

Jenkyns H.C. 2003. Evidence for rapid climate change in the Mesozoic-Palaeogene greenhouse world, *Phil. Trans. R. Soc. Lond. A*, 361, 1885-1916.

Jenkyns H.C. 2010. Geochemistry of oceanic anoxic events, *Geochemistry Geophysics Geosystems*, 11, doi:10.1029/2009GC002788.

Jenkyns H.C. and Clayton C.J. 1986. Black shales and carbon isotopes in pelagic sediments from the Tethyan Lower Jurassic, *Sedimentology*, 33, 87-106.

Jenkyns H.C., Gröcke D.R. and Hesselbo S.P. 2001. Nitrogen isotope evidence for water mass denitrification during the Early Toarcian (Jurassic) Oceanic Anoxic Event, *Paleoceanography*, 16, 593-603.

Kafousia N., Karakitsios V., Jenkyns H.C. and Mattioli E. 2011. A global event with a regional character: the Early Toarcian Oceanic Anoxic Event in the Pindos Ocean (northern Peloponnese, Greece), *Geological Magazine*, 148, 619-631.

Karakitsios V. 1992. Ouverture et inversion tectonique du bassin Ionien (Epire, Grèce), *Annales Géologiques des Pays Helléniques*, 35, 185-318.

Karakitsios V. 1995. The influence of preexisting structure and halokinesis on organic matter preservations and thrust system evolution in the Ionian basin, Northwest Greece, *American Association of Petroleum Geologists Bulletin*, 79, 960-980.

Karakitsios V., Danelian T. and De Weve, P. 1988. Datations par les Radiolaires `a Filaments, Schistes `a Posidonies superierieurs et Calcaires de Vigla (zone Ionienne, Epire, Gr`ece) du Callovien au Tithonique terminal, *C. R. Acad. Sci. Paris*, 306, 367-372.

Karakitsios V., Kafousia N. and Tsikos H. 2010. A Review of Oceanic Anoxic Events as recorded in the Mesozoic sedimentary record of mainland Greece, *Hell. J. of Geosc.*, 45, 123-132.

Karakitsios V. and Koletti L. 1992. Critical revision of the age of the basal Vigla Limestones (Ionian Zone, Western Greece), based on nannoplankton and calpionellids, with paleogeographical consequences, in: Hamersmid B., Young J. (Eds.), *Proceedings of the fourth international nannoplankton association conference, Knihovnika Zemniho Plynu a Nafty*, Prague, pp. 165-177.

Karakitsios V. and Rigakis N. 2007. Evolution and Petroleum potential of Western Greece, *Journal of Petroleum Geology*, 30, 197-218.

Karakitsios V. and Tsaila-Monopolis S. 1988. Données nouvelles sur les niveaux supériers (Lias inférieur-moyen) des Calcaires de Pantokrator (zone Ionienne moyenne, Epire, Grèce continenetale). Description des Calcaires de Louros, *Revue de Micropaléntologie*, 31, 49-55.

Laubscher H. and Bernoulli D. 1977. Mediterranean and Tethys, In: A.E.M. Nairn (ed.): *The ocean margins, vol.: Structural history of the Mediterranean basins*, 129-132.

Littler K., Hesselbo P.S. and Jenkyns H.C. 2010. A carbon-isotope perturbation at the Pliensbachian-Toarcian boundary: evidence fromthe Lias Group, NE England, *Geological Magazine*, 147, 181-192.

Little C.T.S. and Benton M.J. 1995. Early Jurassic mass extinction: A global long-term event, *Geology*, 23, 495-498.

Mattioli E. and Erba E. 1999. Synthesis of calcareous nannofossil events in Tethyean Lower and Middle Jurassic successions, *Rivista Italiana di Paleontologia e Stratigrafia*, 105, 343-376.

Mattioli E., Pittet B., Petitpierre L. and Mailliot S. 2009. Dramatic decrease of pelagic carbonate production by nannoplankton across the Early Toarcian anoxic event (T-OAE), *Global and Planetary Change*, 65, 134-145.

Newton R.J., Reeves E.P., Kafousia N., Wignall P.B., Bottrell S.H. and Sha J.G. 2011. Low marine sulfate concentrations and the isolation of the European epicontinental sea during the Early Jurassic, *Geology*, 39, 7-10.

Pancost R.D., Crawford N., Magness S., Turner A., Jenkyns H.C. and Maxwell J.R. 2004. Further evidence for the development of photic-zone euxinic conditions during Mesozoic oceanic anoxic events, *Journal of the Geological Society of London*, 161, 353-364.

Renz C. 1910. Stratigraphische Untersuchingen im griechischen Mesozoikum und Palaeozoikum, *Jahrbuch d. k. k. geol. Reichsanstalt*, 60, 421-636.

Rigakis N. and Karakitsios V. 1998. The source rock horizons of the Ionian Basin (NW Greece), *Marine and Petroleum Geology*, 15, 593-617.

Sabatino N., Neri R., Bellanca A., Jenkyns H.C., Baudin F., Parisi G. and Masetti D. 2009. Carbon-isotope records of the Early Jurassic (Toarcian) oceanic anoxic event from the Valdorbia (Umbria-Marche Apennines) and Monte Mangart (Julian Alps) sections: palaeoceanographic and stratigraphic implications, *Sedimentology*, 56, 1307-1328.

Suan G., Mattioli E., Pittet B., Mailliot S. and Lecuyer C. 2008. Evidence for major environmental perturbation prior to and during the Toarcian (Early Jurassic) oveanic anoxic event from the Lusitanian Basin, Portugal, *Paleoceanography*, 23, PA1202.

Trecalli A., Spangenberg J., Adatte T., Föllmi K.B. and Parente M. 2012. Carbonate platform evidence of ocean acidification at the onset of the early Toarcian oceanic anoxic event, *Earth and Planetary Science Letters*, 357–358, 214-225.

van Breugel Y., Baas M., Schouten S., Mattioli E. and Sinninghe Damsté J.S. 2006. Isorenieratane record in black shales from the Paris Basin, France: Constraints on recycling of respired CO2 as a mechanism for negative carbon isotope shifts during the Toarcian oceanic anoxic event, *Paleoceanography*, 21, PA4220.

Walzebuck J.P. 1982. Bedding types of the Toarcian black shales in NW-Greece, In: Einsele G., Seilacher A. (Eds.), *Cyclic and event stratification*, Springer, 512-525 pp.

Wignall P.B. 2001. Large igneous provinces and mass extinctions, *Earth-science reviews*, 53, 1-33.

Woodfine R.G., Jenkyns H.C., Sarti M., Baroncini F. and Violante C. 2008. The response of two Tethyan carbonate platforms to the early Toarcian (Jurassic) oceanic anoxic event: environmental change and differential subsidence, *Sedimentology*, 55, 1011-1028.

Δελτίο της Ελληνικής Γεωλογικής Εταιρίας, τομ. XLVII , 2013
Πρακτικά 13ου Διεθνούς Συνεδρίου, Χανιά, Σεπτ. 2013

Bulletin of the Geological Society of Greece, vol. XLVII 2013
Proceedings of the 13th International Congress, Chania, Sept. 2013

MOLECULAR, CHEMICAL AND MORPHOLOGICAL EVIDENCE FOR HEMATITE BIOGENICITY AT THE QUATERNARY CAPE VANI MN-(BA-FE) DEPOSIT, MILOS, GREECE

Kilias S.P.[1], Chatzitheodoridis E.[2] and Lyon I.[3]

[1] National and Kapodistrian University of Athens, Faculty of Geology and Geoenvironment, Department of Economic Geology -Geochemistry, kilias@geol.uoa.gr

[2] National Technical University of Athens, School of Metallurgical and Mining Engineering, Department of Geological Sciences, eliasch@metal.ntua.gr.

[3] The University of Manchester, School of Earth, Atmospheric and Environmental Sciences M139PL, Manchester, UK.

Abstract

Many aspects of the biotic or abiotic origin of iron-rich sedimentary rocks consisting mainly of hematite, an important indicator for exobiology, remain unresolved. Here, we use combined optical microscopy, scanning electron microscopy and energy dispersive X-ray spectrometry (SEM-EDS), Raman spectroscopy and time-of-flight secondary ion mass spectrometry (TOF-SIMS), to image the spatial distribution, and determine the composition, of potential biogenic markers (microbial microfossils, trace elements, organic ion species) in hematite-microstromatolites and oncolite-like microstructures. These structures are identified in iron-rich material cementing a Quaternary fossil-beach conglomerate deposit in the Cape Vani area, NW Milos Island, Greece. The combined detection of morphological, chemical, and molecular organic-ion, biomarkers closely associated with possible hematite microfossils within microstromatolite laminae, strongly supports microbial mediation for their formation, and indicates that hematitic microlamination may be used as a biosignature for Fe-rich biomats on Earth and for their detection in extra-terrestrial materials. The Cape Vani hematite-microstromatolites may contribute to growing our understanding of the function of microorganisms in the genesis of modern and ancient Fe deposits.
Key words: *TOF-SIMS, microfossils, organic biomarkers, microstromatolites.*

Περίληψη

Η γένεση ιζηματογενών πετρωμάτων πλούσιων σε σίδηρο, κυρίως αιματίτη, μέσω βιολογικών ή αβιοτικών διεργασιών, η κάποιου συνδυασμού αυτών, παραμένει άλυτο επιστημονικό πρόβλημα. Στην εργασία αυτή χρησιμοποιήσαμε έναν συνδυασμό αναλυτικών μεθόδων που συμπεριλαμβάνουν οπτική μικροσκοπία, ηλεκτρονική μικροσκοπία σάρωσης και μικροανάλυση (SEM-EDS), φασματοσκοπία Raman και φασματομετρία μάζας χρόνου πτήσης δευτερογενών ηλεκτρονίων (time-of-flight secondary ion mass spectrometry, TOF-SIMS), για να προσδιορίσουμε την χωρική κατανομή και την σύσταση εν δυνάμει γεωβιολογικών δεικτών (π.χ. μικροβιακά

μικροαπολιθώματα, ιχνοστοιχεία, οργανικές ιοντικές ενώσεις) σε αιματιτικούς μικροστρωματόλιθους και μικροδομές από αιματίτη που μοιάζουν με oncolites (ονκόλιθους). Οι μικροδομές αυτές προσδιορίστηκαν σε υλικό πλούσιο σε σίδηρο που αποτελεί συνδετικό υλικό παράλιου κροκαλοπαγούς Τεταρτογενούς ηλικίας από την ευρύτερη περιοχή του ακρωτηρίου Βάνι, στη ΒΔ Μήλο. Ο προσδιορισμός μορφολογικών, χημικών και οργανικών μοριακών ιοντικών βιοδομών σε συνδυασμό με πιθανά μικροαπολιθώματα από αιματίτη, υποδηλώνουν μικροβιακή μεσολάβηση στον σχηματισμό των τελευταίων, και υποδεικνύουν ότι μικροστρωματόλιθοι από αιματίτη μπορεί να χρησιμοποιηθούν ως βιοδείκτες για τη ύπαρξη σιδηρούχων βιο-υλικών στη Γη, και για την ανίχνευση τους σε εξωγήινα υλικά. Η μελέτη των αιματιτικών μικροστρωματόλιθων του ακρωτηρίου Βάνι μπορεί να συμβάλει στην κατανόηση των λειτουργιών των μικροοργανισμών στην γένεση τόσο σύγχρονων όσο και παλαιών κοιτασμάτων σιδήρου.
Λέξεις κλειδιά: *TOF-SIMS, μικροαπολιθώματα, οργανικοί βιοδείκτες, μικροστρωμα-τόλιθοι*.

1. Introduction

Many aspects of the sedimentary origin of iron-rich rocks and soils, consisting mainly of hematite, an important indicator for exobiology, remain unresolved (Bekker et al., 2010; Bishop, 1998). Most prismatic or platy hematite in an iron-ore formation is the result of post depositional or diagenetically late upgrade processes; however, the Fe oxidation mechanisms, i.e. biological versus non-biological, currently are not determined with certainty (Ohmoto et al., 2006; Beukes and Gutzmer, 2008). Primary micron-sized hematite spheroids are scarce in the geological record, and they have only been reported from modern iron oxide deposits of the Red Sea (Taitel-Goldman and Singer, 2002), and Archean banded iron formations (BIF) of the Hamersley Province, Australia (Ayres et al., 1972); these hematite spheroids have been interpreted as aqueous deposited low-temperature early diagenetic products (Bekker et al., 2010). Moreover, nanophase (nm-sized) grey spherulitic hematite, known to be formed by both biotic and abiotic aqueous-fluid processes on Earth, has been spectroscopically identified on the Martian surface, and raised the possibility of liquid water and biological activity on Mars (Bishop, 1998).

Here, we are undertaking a laboratory study of laminated iron oxide-bearing cement samples from a fossil-beach conglomeratic deposit, NW Milos Island, Greece. The conglomerate forms an interbed in Early Quaternary volcaniclastic sandstones/sandy tuffs which host the Cape Vani Mn-Ba-Fe oxide deposit that is known as a distinct littoral to tidal-flat metallogenic environment related to the activity of ancient microbial mats and white smoker-type seafloor hydrothermal venting (Kilias, 2012). The scope of the paper is to document micron-sized spheroid hematite occurrences, and morphologic (i.e. fossil microbes, filaments, or biofilm) and chemical (i.e. organic) biomarkers, in an attempt to decipher the origin of hematite.

2. Materials and Methods

Polished sections of the Vani fossil-beach conglomeratic ferruginous cement is prepared for study. These were sputtered with either carbon or gold for avoiding charging in insulating areas, for EPA and ToF-SIMS analysis. Especially for the ToF-SIMS analysis, a smaller sample was cut to allow its easy insertion into the sample holder and the ultra-high vacuum chamber. This was also required to allow quick vacuum generation, since the sample contains a high number of pores. Optical, scanning electron microscopy and analysis (SEM/EDS) (National and Kaposdistrian University of Athens and National Technical University of Athens), micro-Raman (National Technical University of Athens) and Time-of-Flight mass spectrometry (University of Manchester) techniques were used to investigate the ferruginous cement. Reflected optical

microscopy and imaging was performed with a Carl Zeiss Axioskop 40 microscope at various magnifications. Scanning electron microscopy and electron probe analysis were performed on a Jeol 6380LV electron microscope. On this instrument, a liquid nitrogen cooled Energy Dispersive Spectrometer (EDS) from Oxford Systems is installed. Acquisition is controlled through the INCA software. To achieve high-resolution secondary electron images and backscattered electron images, the acceleration voltage was set to 30kV and the smallest slit size (1) available was used. Chemical analysis was performed at 20kV and with a beam current on the sample of about 1nA. Raman spectra were acquired with a confocal Renishaw Ramascope RM1000 Raman micro-spectrometer, attached to a Leica DMLM optical microscope. A 632.8nm He-Ne laser is probed on the sample, on a spot size of less than 1.5μm when using the ×100 objective lens and with energy, at the spot, of less than 5mW. Rayleigh scattering is reduced by an edge filter whose cut-off is at about 180cm^{-1}. The entrance slit to the spectrometer was set to 50μm. The spectra acquisition system is composed of a grating of 1800lines/mm and a 576×384pixel Peltier-cooled CCD camera. Spectra acquisition was made in continuous scanning mode. Final spectra are accumulated scans of a few individual spectra, each of 10 seconds integration time. The TOF-SIMS instrument used in this study is the "IDLE" instrument, and it is described in detail in Henkel et al. (2006). Mass-resolved spectra were acquired by sputtering with a pulsed gold ($^{197}Au^{+}$) primary ion beam set at 25kV acceleration voltage. The beam size was about 1μm, defining the spatial resolution of the acquired ion maps. The ion map manipulation and handling software is the "spaceTOF" (Chatzitheodoridis et al., 2005). The surface of the sample was always thoroughly cleaned prior to analysis by sputtering with a direct current ion beam in scanning mode. Positive and negative secondary ion spectra were acquired using both low mass and high mass resolution (about 500 and 2500, respectively).

3. Results

3.1. Morphologic and Mineralogical Biosignatures

The main volume of the sample is a ferruginous deposit, which glues together various detrital crystals, and partly fossilising biological material (cyanobacterial cells and their EPS). The detrital crystals are various common minerals, such as feldspar, Ti-magnetite, zircon and manganese minerals. Optical and scanning electron microscope (SEM) investigation of the ferruginous cement has revealed that it occurs as finely (micrometre scale) laminated colloform or botryoidal structures that bear morphological similarities to microstromatolites (e.g. Allwood et al., 2006; Lazăr et al., 2012) (Figure 1). The microstromatolites consist mainly of a remarkable cyclic repetition of growth laminae consisting of chainlike concentrations of spheroidal/coccoidal structures of variable size, aligned parallel to the microlamination, enclosed in a gel-like mucoid film (Figures 1, 3). Oncoidal microstromatolites also occur, forming the cortices of rounded and bulbous oncoid-like structures, and are developed as closely packed build-ups surrounded by colloform or botryoidal microstromatolites; they range in size from 50 to 200 μm and have a globular to elongated/flattened shape. In general, microlamination is a result of a combination of differential porosity, and weathering of the film material, as well as size variability of the spheroids/coccoids. The laminae are composed mainly of hematite and organics (see below). Detrital silicates (adularia, chlorite) represent a minor component of some laminae and when present, are mainly found in specific detrital layers. This indicates that stromatolite growth was mainly controlled by in situ precipitation.

Hematite in the microstromatolites was identified by Raman spectroscopy (Figure 2). This hematite compares very well to a metamorphic hematite used as reference and to hematite measured by Shim and Duffy (2001), with only minor offsets of the peak positions. One exception is a wide peak centred at 660.6cm^{-1}, which is normally a forbidden band for Raman but IR-active. This peak has been interpreted to represent either surface resonance of incomplete symmetry of hematite, due to stress-induced defects or the first overtone of the 1318.3cm^{-1} peak (Shim and Duffy, 2001), or, due to impurities (Zoppi et al., 2005). Partial transformation to magnetite due to

the effect of the laser beam has been also suggested (Ulubey et al., 2008; Bouchard and Smith, 2003), however, it seems not applicable here due to the very low energy of the beam used, and its presence to all performed analyses irrespectively of conditions, except for our standard hematite spectrum. A peak at 658cm^{-1} is reported by Bikiaris et al. (1999) and is attributed to the Al-O-Si bond of clays, e.g. kaolinite. Vani hematite samples do contain traces of clay, however, this peak in our spectra, is interpreted as a result of disorder (Shim and Duffy, 2001) due to its high intensity.

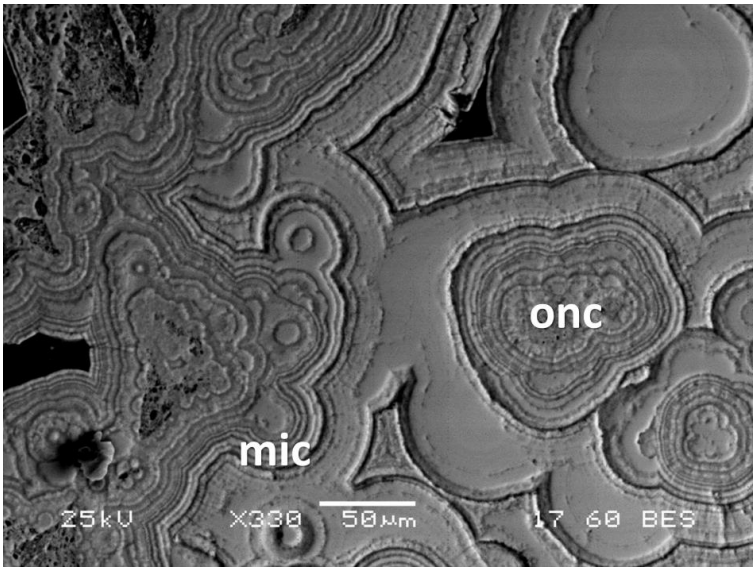

Figure 1 - ackscattered electron (BSE) image of micrometre-scale ferruginous microstromatolites (mic) and oncoidal microstromatolites (onc) cementing a fossil-beach conglomerate, NW Milos Island, Greece.

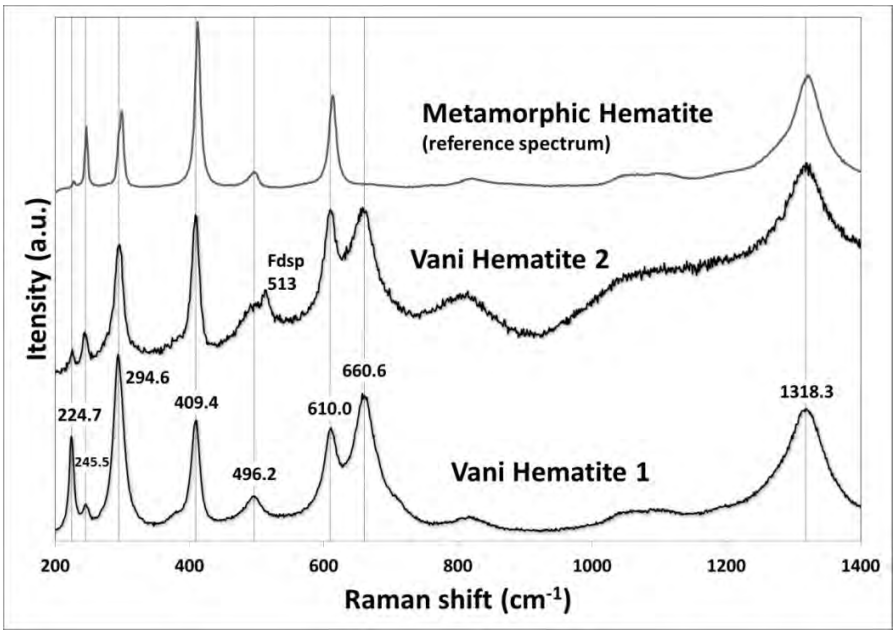

Figure 2 - Raman spectra of Vani hematite (spectra 1 and 2) compared to a reference highly ordered hematite of metamorphic origin. The Vani hematite 2 spectrum shows additionally a feldspar peak (Fdsp; 513cm^{-1}).

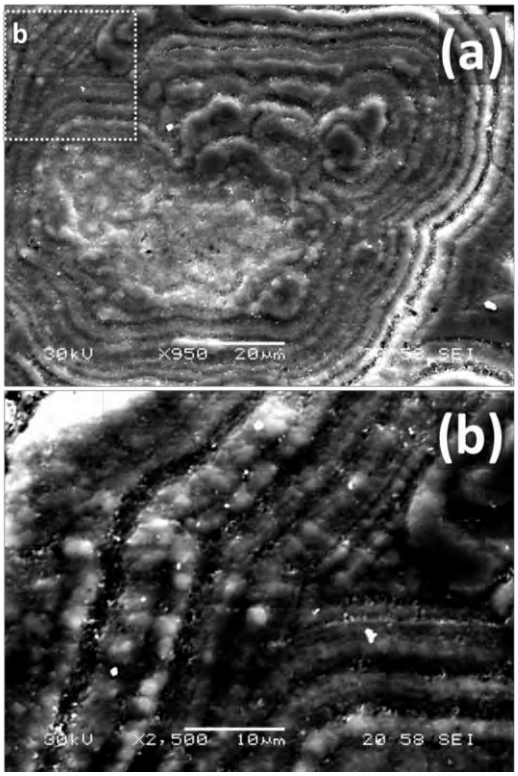

Figure 3 - Sequence of progressively higher magnification of backscattered electron images o f chain like concentrations of spherical/coccoidal hematite structures with variable size (b) di stributed along microstromatolitic laminae (a) composed of bands ranging from 2 to 5 µm thi ckness of mainly hematite and organics, plus Mn, Na, Ca, and lesser K (see below).

3.2. Molecular Biomarkers

In order to set the inorganic frame on which organics sit, firstly a set of ToF-SIMS ion maps of the major elements is given (Figure 4), together with the total ion image which is the sum for all counts measured in each pixel. Iron ion map coincides with the stromatolitic texture. Dark areas on Figure 4 indicate voids or silicate mineral composition, i.e. such as feldspars, or chlorite. The results obtained by TOF-SIMS demonstrate the presence of Mn, Mg, Si, Na, Ca, Al and lesser K, within the microstromatolitic lamination (Figure 4). This elemental distribution may indicate detrital silicate minerals along the specific lamina, most probably fine distributions of clays, micas and feldspars. Especially on the bright spots that concentrate on the bottom-right of the images, mainly feldspars are located, as evidenced also from electron probe investigations. This zone is also composed of more diffused Mn, Mg, Na and Ca. Probably these elements are present in the matrix of hematite as well. The very limited occurrence of K in this layer compared to the rest of the area, together with the enrichment in Na is intriguing. This might be resolved if the molecular ion maps of hydrocarbons are considered, as shown on Figure 5.

Figure 5 demonstrates that the hematitic lamina already described is preferentially enriched in carbonaceous material in the form of hydrocarbon fragments. Hydrocarbon fragments with odd (C_{2n+1} H_x) and even (C_{2n} H_x) number of carbon atoms, as well as organic molecules containing oxygen, seem to be especially rich in this layer. Mono-carbonic chains (C_n) show an even distribution coinciding with the iron-rich area. These chains probably have a different origin e.g. contamination. To investigate the distribution of hydrocarbons as well, a detailed analysis of the mass spectrum was performed and the intensities of the peaks were measured. The result is shown in Figure 6, which demonstrates a systematic abundance of hydrocarbon fragments.

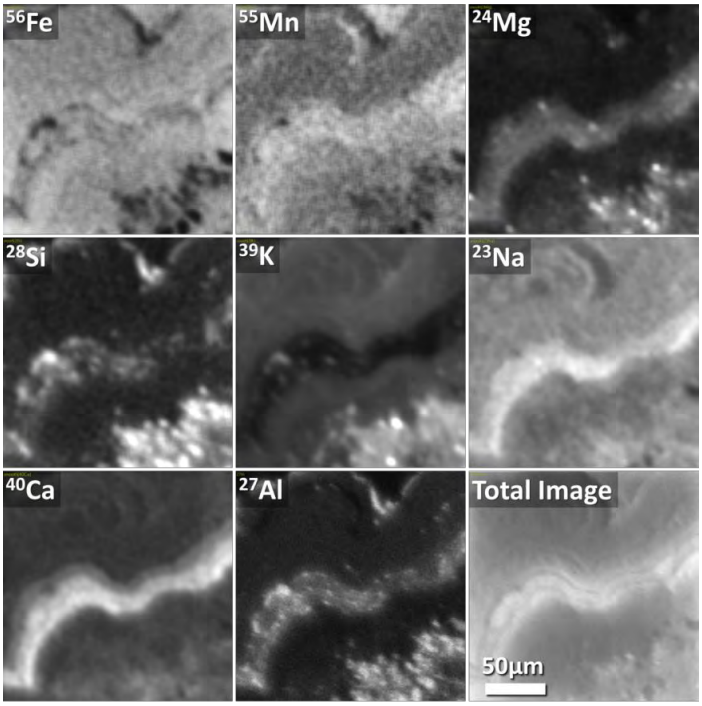

Figure 4 - ToF-SIMS ion maps of major elements. "Total Image" is the total ion image, which is composed of all ions of the spectrum acquired from each pixel.

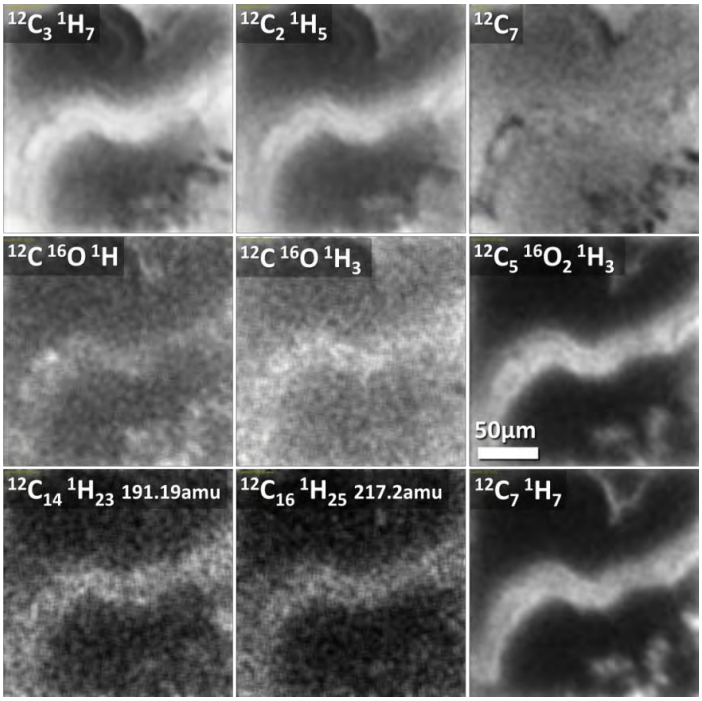

Figure 5 - ToF-SIMS molecular ion maps of the carbonaceous matter in hematite lamina of the Vani microstromatolites. Note the good correspondence between hematitic coccoidal microfossils and the distribution of globular carbonaceous matter, i.e. $C_5O_2H_3$, C_7H_7, and C_3H_7.

4. Discussion-Conclusions

The biogenicity and syngenicity of the morphological and chemical signatures were evaluated according to a series of published criteria (Westall et al., 2011; Schopf et al., 2010). The Vani hematite-rich conglomeratic cement shows typical features of microstromatolitic microbialites, i.e. laminated organosedimentary deposits resulting from benthic microbial community trapping and binding clastic sediment particles and/or inducing mineral precipitation (Burne and Moore, 1987; Burkhalter, 1995). The microbialites exhibit two main morphological fabrics: (i) hematitic microstromatolites (Burkhalter, 1995), and (ii) hematitic oncoidal microstromatolites (Cavalazzi et al., 2007) (Figure 1). The Vani Fe-microstromatolites show features extremely similar to typical biogenic stromatolites, such as non-isopachous micrometer-scale alternations of smooth to wrinkly growth laminae, linked domical pseudocolumns with continuous bridging laminae between them, hemispherical to bulbous 3-D laminae shape, and thickening of laminae over the crests of the domes (Allwood et al., 2006; Rossi et al., 2006)(Figures 1, 3). Hematitic oncoidal microstromatolites form the cortices of rounded and bulbous, oncoid-like structures and occur as closely packed build-ups surrounded by colloform banded microstromatolites; they range in size from 50 to 200 μm and have a globular to elongated/flattened shape. The strongest evidence that these structures are stromatolitic microbialites, however, is the outstanding profusion of fossil microbes in the form of hematitic spheroids, in the stromatolitic laminae. The hematitic spheroids have morphological characteristics consistent with colonies of coccoidal fossil microbial cells (Schopf et al., 2010), and the polymer film maintains morphological details identical to fossil extracellular polymeric substances (EPS) produced by the cells (Westall et al., 2000). This, combined with the alignment of the coccoidal fossil microbes parallel to the convex outward microlamination, offer strong evidence that microbes were active and not fortuitous in the development of such microstructures (Rossi et al., 2006).

Carbonaceous material, i.e. odd and even chained C_x-H_y ionic molecules, C_x-O_y-H_z molecules and mono-carbonic chains C_x, was identified in the hematite laminae using TOF-SIMS in a highly systematic abundance (Figure 6). Carbonaceous material occurs as micrometer-sized heterogeneously distributed chain-like globular clusters, as well as diffuse film-like material that coats both the hematite microfossils and their substrate, and it is exclusively associated with the hematite laminae. Moreover, according to Siljeström et al. (2010) hopanes and steranes constitute organic lipid biomarkers, indicative of cyanobacteria. Their diagnostic molecular ions are at 191.19amu for hopanes and 217.2amu for steranes. Both peaks exist in the spectra of the studied section of hematite and they follow the same pattern with the rest of the organic fragments (Figure 6). Therefore, it can be inferred that the carbonaceous material is indicative of the existence of biological material trapped in and/or with hematite.

According to its organic nature and in conjunction with the biomorphological evidence presented, the organic-rich hematite spheroidal and filmy material is thus interpreted as Fe- bio-mineralised fossil bacterial cells and associated fossil EPS, likely produced by iron-oxidising micro-organisms (Westall et al., 2000; Heim at al., 2012). Along with the presence of Fe, local selective enrichments of microstromatolitic laminae with inorganic bio-essential elements such as Mn, Na, Ca, ±K detected by ToF-SIMS, further support microbial mediated reactions. The combined detection of morphological, chemical and molecular ion biomarkers in the Cape Vani hematitic microstromatolites and oncolite-like structures clearly supports microbial mediation for their formation, and indicates that this microlamination may be used as a biosignature for Fe-rich biomats on Earth and for their detection in extraterrestrial materials. Moreover, the Cape Vani microstromatolites may contribute to growing our understanding of the function of microorganisms in the genesis of modern and ancient Fe and associated Mn deposits.

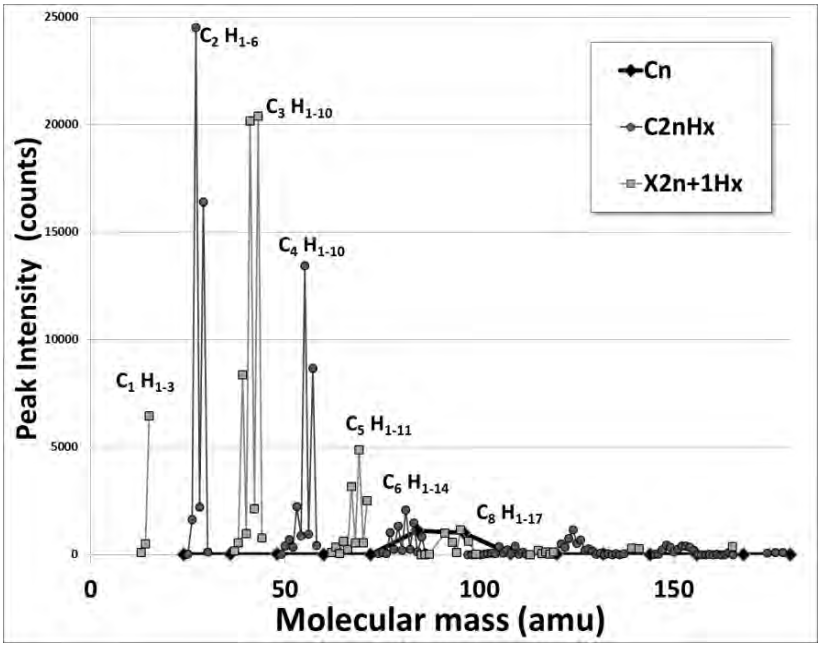

Figure 6 - Distribution patterns of mono-carbonic chains (C_n), and hydrocarbon fragments with even ($C_{2n}H_x$) and odd ($C_{2n+1}H_x$) number of carbon atoms.

5. Acknowledgments

Funding by the Special Account for Research Grants of the National and Kapodistrian University of Athens to SPK is thankfully acknowledged.

6. References

Allwood A.C., Walter M.R., Kamber B.S., Marshall C.P. and Burch I.W. 2006. Stromatolite reef from the Early Archaean era of Australia, *Nature,* 441 (7094), 714-718.

Ayres D.E. 1972. Genesis of iron-bearing minerals in banded iron formation mesobands in the Dales Gorge Member, Hamersley Group, Western Australia, *Economic Geology*, 67, 1214−1233.

Bekker A., Slack J.F., Planavsky N., Krapež B., Hofmann A., Konhauser K.O. and Rouxel O.J. 2010. Iron formation: the sedimentary product of a complex interplay among mantle, tectonic, oceanic, and biospheric processes, *Economic Geology*, 105, 467-508.

Beukes N.J., and Gutzmer J. 2008. Origin and paleoenvironmental significance of major iron formations at the Archean-Paleoproterozoic boundary, *Reviews in Econ. Geol.*, 15, 5−47.

Bikiaris D., Sister Daniilia, Sotiropoulou S., Katsimbiri O., Pavlidou E., Moutsatsou A.P. and Chryssoulakis Y. 1999. Ochre-differentiation through micro-Raman and micro-FTIR spectroscopies: application on wall paintings at Meteora and Mount Athos, Greece, *Spectrochimica Acta*, 56, 3-18.

Bishop J.L. 1998. Biogenic catalysis of soil formation on Mars? *Orig. Life Evol. Biosph.*, 28(4-6), 449-459.

Bouchard M. and Smith D.C. 2003. Catalogue of 45 reference Raman spectra of minerals concerning research in art history or archaeology, especially on corroded metals and coloured glass, *Spectrochimica Acta*, 59, 2247-2266.

Burkhalter R.M. 1995. Ooidal ironstones and ferruginous microbialites: origin and relation to sequence stratigraphy (Aalenian and Bajocian, Swiss Jura Mountains), *Sedimentology,* 42, 57–74.

Burne R.V. and Moore, L.S. 1987. Microbialites: organosedimentary deposits of benthic microbial communities, *Palaios,* 2, 241–254.

Cavalazzi B., Barbieri R. and Ori G.G. 2007. Chemosynthetic microbialites in the Devonian carbonate mounds of Hamar Laghdad (Anti-Atlas, Morocco), *Sedimentary Geology,* 200, 73-88.

Chatzitheodoridis, E., Lyon I.C. and Vgenopoulos A. 2005. Interactive geochemistry in the micro- and submicron scale: a visual software tool for ion map extraction, manipulation and analysis from TOF-SIMS spectra. In IMA05: The *4th International Conference on Instrumental Methods of Analysis, Modern Trends and Applications*, Iraklion, Crete, Greece, 2-6 October 2005.

Heim C., Lausmaa J., Sjövall P., Toporski J., Dieing T., Simon K., Hansen B.T., Kronz A., Arp G., Reitner J. and Thiel V. 2012. *Geobiology*, 10, 280-297.

Henkel T., Tizard J., Blagburn D., Lyon I. 2006. Interstellar dust laser explorer (IDLE): A new instrument for submicron analyses of stardust-quantification of laser SNMS. *Applied Surface Science*, 252, 7117-7119.

Kilias S.P. 2012. Microbial-mat related structures in the Quaternary Cape Vani manganese oxide(-barite) deposit, NW Milos island-Greece, in Noffke N., and Chafetz H., (Eds.), *Microbial Mats in Siliciclastic Depositional Systems Through Time*, SEPM (Society for Sedimentary Geology) Special Publication, 101, 97-100.

Lazăr I., Grădinaru M. and Petrescu L. 2013. Ferruginous microstromatolites related to Middle Jurassic condensed sequences and hardgrounds (Bucegi Mountains, Southern Carpathians, Romania). *Facies*, 59, 359-390.

Ohmoto H., Watanabe Y., Yamaguchi K.E., Naraoka H., Haruna M., Kakegawa T., Hayashi K. and Kato Y. 2006. Chemical and biological evolution of early Earth: Constraints from banded iron formations, *Geological Society of America Memoir,* 198, 291−331.

Rossi C., Lozano R.P., Isanta N. and Hellstrom J. 2006. Manganese stromatolites in caves: El Soplao (Cantabria, Spain), *Geology,* 38, 1119-1122.

Schopf W.J., Kudryavtsev A.B., Sugitani K. and Walter M.R. 2010. Precambrian microbe-like pseudofossils: A promising solution to the problem. *Precambrian Research,* 179, 191-205.

Shim S.-H. and Duffy T. S. 2001. Raman spectroscopy of Fe_2O_3 to 62GPa, *American Mineralogist*, 87, 318-326.

Siljeström S., Lausmaa J., Sjövall P., Broman, C., Thiel V. and Hode T. 2010. Analyses of hopanes and steranes in single oil-bearing fluid inclusions using time-of-flight secondary ion mass spectrometry (ToF-SIMS), *Geobiology*, 8, 37-44.

Taitel-Goldman N. and Singer A. 2002. Metastable Si-Fe phases in hydrothermal sediments of Atlantis II Deep, Red Sea, *Clay Minerals*, 37, 235−248.

Ulubey A., Fazlioglu I., Erdogu B. 2008. Pigment identification in Hellenistic ceramics from the Tuz Gölü region of central Anatolia by confocal Raman spectroscopy, *Ceramics*, 52, 201-204.

Westall F., Foucher F., Cavalazzi B., De Vries S.T., Nijman W., Pearson V., Watson J., Verchovsky A., Wright I., Rouzaud J-N., Marchesini D., and Anne S. 2011. Volcaniclastic habitats for early life on Earth and Mars: A case study from ~3.5 Ga-old rocks from the Pilbara, Australia, *Planetary and Space Science*, 59, 1093-1106.

Westall F., Steele A., Toporski J., Walsh M., Allen C., Guidry S., McKay D., Gibson E. and Chafetz H. 2000. Polymeric substances and biofilms as biomarkers in terrestrial materials: Implications for extraterrestrial samples, *J. Geophys. Res.*, 105(E10), 24511–24527, doi:10.1029/2000JE001250.

Zoppi A., Lofrumento C., Castellucci E.M., Migliorini M.G. 2005. The Raman spectrum of Hematite: possible indicator for a compositional or firing distinction among Terra Sigillata wares, *Annali di Chimica*, 95, 239-246.

,Δελτίο της Ελληνικής Γεωλογικής Εταιρίας, τομ. XLVII , 2013 Πρακτικά 13ου Διεθνούς Συνεδρίου, Χανιά, Σεπτ. 2013

Bulletin of the Geological Society of Greece, vol. XLVII 2013 Proceedings of the 13th International Congress, Chania, Sept. 2013

PRELIMINARY RESULTS OF REE-Y SORPTION ON CARBONATE ROCKS

Moraetis D.[1, 2] and Mouslopoulou V.[2,3]

[1] *Technical University of Crete, Department of Environmental Engineering moraetis@mred.tuc.gr*

[2] *Technical University of Crete, Department of Mineral Resources Engineering*

[3] *German Research Centre of Geosciences, GFZ, Potsdam, Germany, vasso@gfz-potsdam.de*

Abstract

The Rare Earth Elements and Yttrium (REE-Y) have recently been proposed as good proxies for identifying rupture zones on carbonate fault scarps. Indeed, fluctuations in the REE-Y concentrations along a fault plane may be linked to the number and size of earthquakes that ruptured the fault. The enrichment is attributed to the contact of the soil with the carbonate fault scarp. Our study presents preliminary results from a series of experiments that aim to shed light on the mechanism associated with the REE-Y sorption on the limestone-soil interface. Rain simulation pot experiments, kinetic and isotherm batch experiments were employed to describe the mechanism of REE-Y sorption in calcite. Results reveal fast REE-Y sorption on the limestone surface after the simulation of five years of rainfall. The fast REE-Y sorption is also supported by the kinetic experiments. Isotherm tests show the higher affinity of calcite in the Light Rare Earth (LREE) compared to the Heavy Rare Earth Elements (HREE). The sorption of the REE in the form of carbonate complexes is proposed as a plausible mechanism of REE-Y incorporation into the limestone.

Περίληψη

Οι σπάνιες γαίες και το ύτριο (REE-Y) θεωρούνται καλοί δείκτες για τον προσδιορισμό σεισμικών ζωνών κατά μήκος της επιφάνειας ενός ασβεστολιθικού ρήγματος (καθρέφτης ρήγματος). Η συγκεκριμένη τεχνική θεωρείται αποτελεσματική στην αναγνώριση του αριθμού και του μεγέθους των σεισμών. Πρόσφατες εργασίες έχουν επαληθεύσει την ύπαρξη ενός μηχανισμού εμπλουτισμού των ασβεστόλιθων σε σπάνιες γαίες όταν είναι σε επαφή με το έδαφος. Τα πρώτα αποτελέσματα από την διερεύνηση του μηχανισμού εμπλουτισμού του ασβεστόλιθου σε REE-Y παρουσιάζονται στην υποβαλλόμενη εργασία. Τα πειράματα προσομοίωσης βροχής πέντε ετών (σε γλάστρες) έδειξαν ταχύ εμπλουτισμό της επιφάνειας ασβεστόλιθου σε REE-Y. Τα πειράματα κινητικής έδειξαν επίσης ταχεία ρόφηση REE-Y, ενώ οι δοκιμές ισόθερμης ρόφησης έδειξαν μεγαλύτερη επιλεκτικότητα σε ελαφριές (LREE) σπάνιες γαίες σε σχέση με τις βαριές (HREE). Ο μηχανισμός ρόφησης των σπανίων γαιών με τη μορφή ανθρακικών συμπλόκων θεωρείται πιθανός μηχανισμός ρόφησης των REE-Y στην επιφάνεια των ασβεστολίθων.

1. Introduction

The Rare Earth Elements (REE) have been widely used as provenance indices either to describe the water hydrology or sediments origin (Dia et al., 2000; Roy et al., 2012). Furthermore soil processes, like argilluviation, carbonation etc., have been described through the REE fate and transport in soil horizons (Laveuf and Cornu, 2009). Other geological processes like biogeochemical conditions in paleo-seawater (Shields and Stille, 2001) and weathering processes have also used the REE as primary indices (Patino et al., 2003). The REE-Y concentration measured along the carbonate scarp of the Magnola Fault (Italy) revealed remarkable fluctuations that match with the rupture zones identified independently by Cl^{36} (Palumbo et al. 2004; Carcalliet et al., 2008). Manighetti at el. (2010) verified on the very same fault scarp that the REE-Y enrichment occurs due to the contact of the limestone with paleo-soils. Mouslopoulou et al. (2011) identified at least four zones of REE-Y enrichment on a fault of unknown earthquake history in Crete (the Spili Fault). The new proxies for the identification of paleo-earthquakes on carbonate faults are promising and the sound validation of the mechanism of REE enrichment on the limestone would enhance confidence that REE may be used prior to the costly method of Cl^{36} to constrain the slip history on carbonate faults.

Limestones have been proposed in various studies as adsorbents for heavy metals in the environment (Sdiri, 2012; Komnitsas et al., 2004; Godelitsas et al., 2003). The presence of carbonate minerals like calcite may have a direct or indirect effect in metal adsorption in limestones (Papadopoulos and Rowell, 1988). The direct effect is through their surface reactivity and the indirect is through their effect in the pH of reactive solutions. The metal incorporation in calcite can be a) with adsorption in the calcite surface through ion exchange with Ca or with complexation with carbonate groups bound in a disordered, hydrated surfaces (Zachara et al., 1988) and b) with precipitation (metal precipitates $MeCO_3$) in solutions with high ionic strength metal solutions. The adsorption of metals in calcite showed to vary among different sorbates. For example, Zn appears to be adsorbed and rapidly desorbed (reverse reaction) whereas, Mn and Cd appear to be rapidly absorbed with very slow desorption rate (almost irreversible) (Papadopoulos and Rowell, 1988). pH changes in the presence of limestone is accompanied by carbonate (CO_3^{2-}) release. REE shows high affinity of solution complexation with carbonates. The solubility of REE in most limestone aquifers is influenced partly by the solution complexation with carbonates and partly from the REE adsorption on charged surfaces like clays and oxides. It has been reported that Heavy Rare Earth Elements (HREE) are being more sorbed in clay surfaces compared to Light Rare Earth Elements (LREE). Moreover, the same has been observed in the Carrizo sand aquifer of Texas (Tang and Johannesson, 2005a). Thus, the calcite behaviour with respect to the metal adsorption is complex and the majority of the studies focus on the adsorption of the heavy metals and no data exist with respect to the REE-Y sorption in calcite.

In the case of REE-Y, little has been done to characterize the sorption processes on the interface between limestone and soil (Figure 1). To elucidate the mechanism responsible for the REE-Y enrichment we conducted a series of pot, kinetic and batch experiments.

2. Materials and Methods

The present study includes two experimental parts: a) the pot experiments with the placement of limestone bricks within pots which are filled with soil and b) the kinetic and isotherm sorption experiments. In the second part of experiments, the limestone was grinded in less than 250 μm. The grinded limestone for the kinetic and isotherm sorption experiment was aged by storing 0.5 limestone in 14 L of 0.02 mol/L $NaHCO_3$. The aging process enhances the dissolution of small crystallites and crystallite with defects and the re-precipitation of uniform crystalline calcite, with less free energy in the surface. All kinetic and isotherm tests were performed with this aged limestone. Ce, Eu and Yb were selected to represent Light, Medium and Heavy Rare Earth

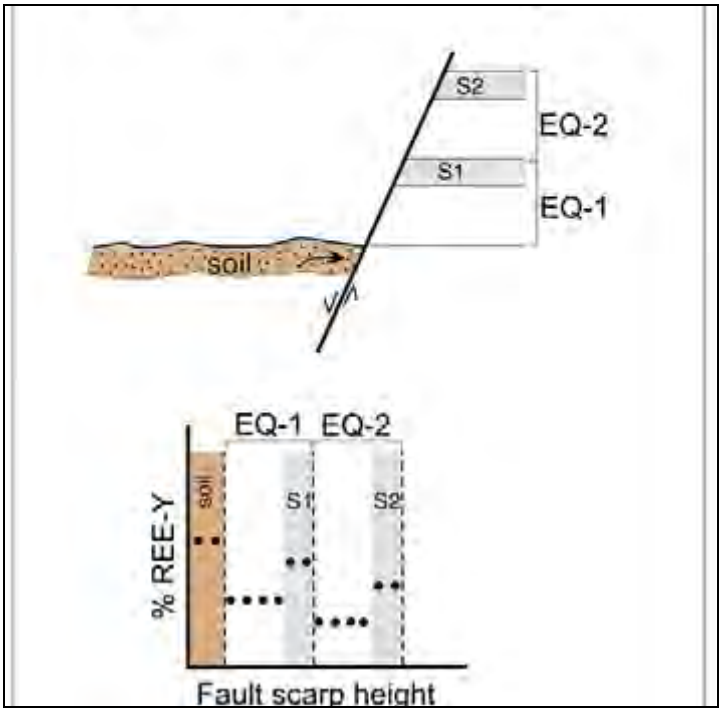

Figure 1 - Diagram illustrating the mechanism of REE-Y enrichment along a carbonate fault scarp. S1 and S2 represent paleo-ground levels which have been exhumed due to the successive earthquakes EQ1, EQ2. Modified from Mouslopoulou et al. (2011).

presented by Mouslopoulou et al. (2011). The oxidation states of each element was not considered in the present study and we calculate the bulk removal of Ce, Yb, La from each test (kinetic, isotherm etc.) The tests were performed in atmospheric CO_2 (p CO_2=3.2). The Ce, Eu and Yb standards which were used for the solutions preparation (1000 ppm) were certi-pure in 2-3% HNO_3 from Merck Company.

2.1. Pot Experiments

Pot experiments were operated to simulate the limestone fault plane while buried under the ground surface (paleosoil-rock interaction). Thus, we removed orthogonal limestone segments from the fault plane (see Figure 2a & b) and covered the entire surface of the brick with waterproof silicon resin apart from the 2/3 of the front surface (see Figure 2c). The bricks were placed into pots (Figure 2d) and covered with soil which was sampled from the very colluvium wedge at the foot of the Spili Fault on Crete. The rain filtered through each pot was 4.2 litters per year of simulation according to the average rainfall in the area (600 mm) and normalised to the pot diameter (6 cm). A total of five years were simulated whereas in between simulations the pots were dried with natural aeration (average 30^o Celsius). Synthetic rain of specific ionic strength ($5.6*10^{-4}$ mol/L) and pH (5.39) was used in pot experiments following the chemical analysis of rain from Samara et al. (1992). The salts that were used for synthetic rain comprised of $CaSO_4.2H_2O$, KCl, $MgCl_2.6H_2O$, $NaNO_3$, whereas HCl, H_2SO_4 and HNO_3 were used for pH adjustment. Tests were conducted at 25^{o}C and 15^{o}C. All pot experiments were obtained in triplicates.

2.2. Kinetic and Isotherm Tests

Kinetic and isotherm tests were conducted in solid/solution ratio of 1/40. The pH for both tests was 7.59. With the use of Mineql we calculate the composition of the solutions in equilibrium with calcite at this pH. We applied the aqueous speciation reactions and equilibrium constants given by

Zachara et al. (1988). The time intervals were 3h, 6h, 12h, 1d, 5d, 7d for the kinetic tests, hence the REE concentrations was 10^{-4} mol/L. The isotherm tests were conducted with the REE concentration of 10^{-3}, 10^{-4}, 10^{-5}, 10^{-6}, 10^{-7} mol/L at pH 7.59. After the addition of the REE standard the pH dropped in 5.6 in both kinetic and isotherm tests. We adjusted the pH at the isotherm test with the use of NaOH, whereas the kinetic test was left to equilibrate without pH adjustment. The calcite equilibrium solution in both kinetic and isotherm experiments were prepared by mixing $HClO_4$, $CaCl_2O_8$, $NaHCO_3$, NaOH.

Figure 2 - (a) and (b) The bricks were detached from the carbonate fault plane by using electric saw; (c) waterproof silicon coverage of the brick; (d) brick placement into pots filled with soil; (e) brick removal after 5 years of rain simulation.

3. Results

3.1. Pot Experiments

The results of the pot experiments after simulating 5 years of rainfall at two different temperatures (15º and 25º Celsius) are illustrated in Figure 3. The difference (% change) in REE-Y concentration between the outer surfaces A1, B1 (which were in contact with the soil) on each brick and the deeper parts A2, B2 was calculated as $100*(Conc_{A1,B1,D1} - Conc_{A2,B2,D2})/ Conc_{A2,B2,D2}$. The $Conc_{A1,B1,D1}$ refers to the concentration in each of the A1, B1 or D1 segments whereas the $Conc_{A2,B2,D2}$ refers to the concentration of the immediately deeper A2, B2 and D2 segments (as shown in Figure 3). At temperatures of 25º Celsius, the average increase recorded in the A1 and B1 segments was 40% and 23%, respectively. At temperatures of 15º Celsius, the average increase recorded in the A1 and B1 segments was 36 and 5%, respectively. In contrast, D1 segment shows lower REE-Y concentration compared to D2 segment (approximately -45% for both tests temperatures; minus refers to decrease in concentration). The limestone at 15º Celsius experiment showed generally lower enrichment in REE-Y compared to that recorded at 25º Celsius (Figure 3).

3.2. Kinetic and IsothermRresults

The results from the isotherm sorption tests and the kinetic sorption tests are shown in Figure 4. The limestone selectivity was higher for Ce compared to Eu and Yb and that remained stable for both tested temperatures. There was a slight increase in the limestone affinity for the REE in the temperature of 15ºC, especially for Ce and Yb as it is evident from the slope of the line. The linearity of the sorption isotherm, as depicted in the log-log diagram of Figure 4a & b, resembles the isotherm of Freundlich.

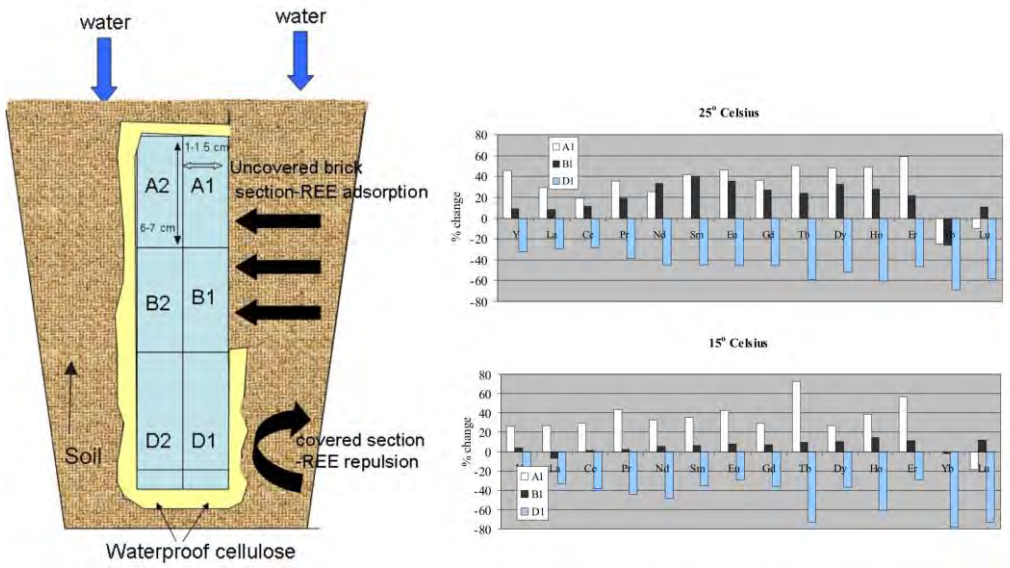

Figure 3 - Schematic diagram illustrating a pot experiment that involves a limestone brick buried within a soil. The results (in the two plots) derive by comparing the REE-Y concentration in A1 and A2, B1 and B2 and D1 and D2 segments on each brick at two different temperatures (15° and 25° Celsius).

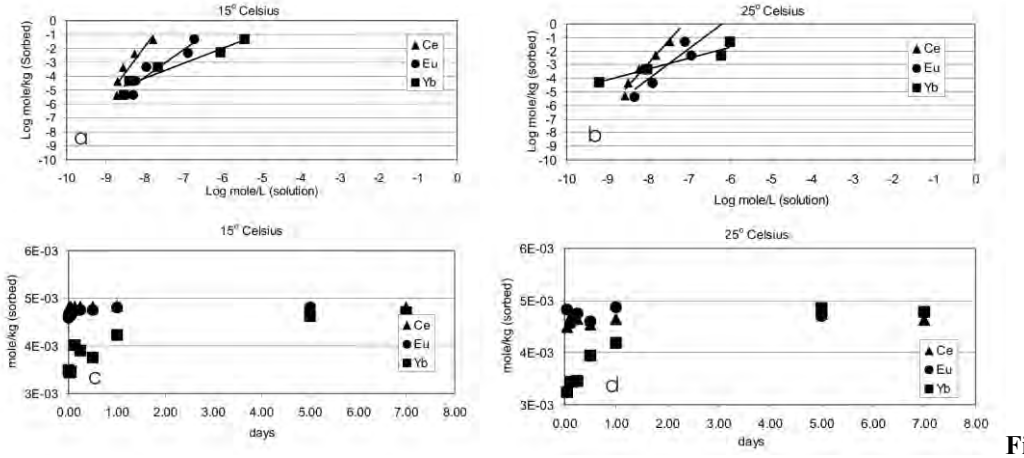

Figure 4 - (a) and (b) Sorption isotherm tests for Ce, Eu and Yb at two different temperatures; (c) and (d) kinetic sorption tests for Ce, Eu and Yb at two different temperatures.

The kinetic test shows immediate sorption for Ce and Eu and slower sorption for Yb (up to the 1st day of the experiment). The three REE reached identical the same sorption level after the 1st day. The kinetic test at the 7th day shows a slight decrease in the sorption of all three REE. Thus, REE with high atomic number (e.g. Yb) show slower sorption in the 1st day of the kinetic test compared to REE with lower atomic number (Ce, Eu).

4. Discussion

4.1. Pot Experiments

Preliminary results show that there is indeed a mechanism which is responsible for the recorded increase in the concentration of REE on the limestone, at localities where the latter is in direct

contact with the soil. The REE enrichment on the buried surfaces A1 and B1 was clear, as was the non-enrichment of the D1 surface. The enrichment was achieved in pot-experiments after simulating five years of rainfall. Thus, two conceptual models may arise: a) the REE-Y escape from the soil through a soil solution and subsequently they are sorbed by the limestone surface b) the limestone surface is weathered due to its contact with acidic soil solution and the REE-Y, which were already in the limestone, dissolute and become subsequently re-sorbed (precipitate) in the limestone surface. The latter is thought to be impossible considered the level of % percentage change in the REE-Y concentration and the short duration of the experiment. It would require extreme dissolution of the limestone surface to change the REE-Y content at a depth of 1.5 cm (Figure 3). Thus, the plausible scenario is the one that supports the origin of the REE-Y from the soil.

The measurements of the chemical parameters in the infiltrates from the pot experiments revealed lower pH values and higher calcium content for the pot experiment at 15º Celsius (Figure 5).

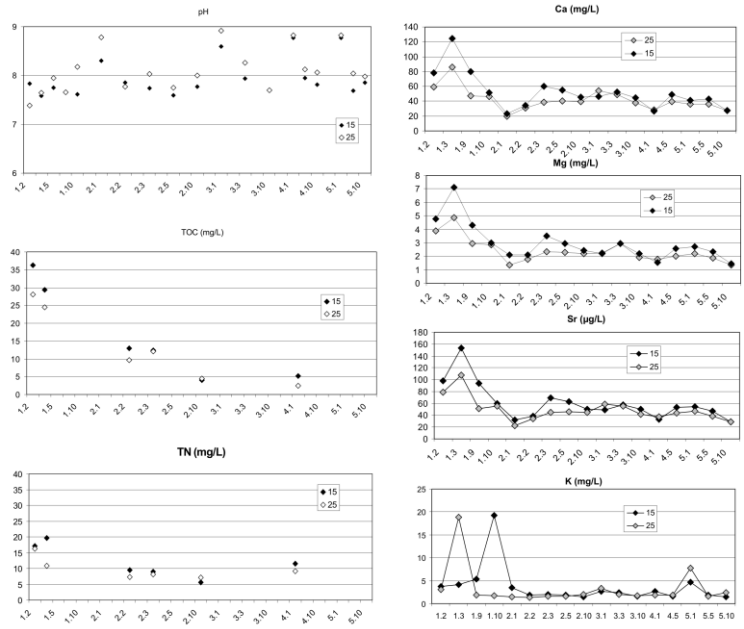

Figure 5 - Chemical and physical parameters measured in the infiltrates from the pot experiments. X axis represents five years of the simulated rainfall; hence the number in the decimal digit is the number of rain event for each year.

Considering that chemical species such as Ca and Sr in the infiltrates were originated from dissolution of calcite and dolomite, higher dissolution was observed in the pot experiments at temperatures of 15º Celsius. Higher concentrations were observed also for Mg at temperatures of 15º Celsius compared to 25 º Celsius. Potassium was approximately identical to both temperatures, mainly because potassium originated from ion exchange reactions rather than dissolution reactions. The higher degree of calcium leaching in the pot experiments at 15º Celsius (compared to that at 25º Celsius) is due to higher organic content in the infiltrates which lower the soil solution pH (Figure 5). The high activity of H^+ was balanced by calcite dissolution either from the soil or the uncovered limestone surface. The chemical conditions and reactions at 15º Celsius increase the calcite dissolution which, in turn, increased the carbonates. Thus the lower REE-Y sorption at limestone surface at 15º Celsius was probably related to the mineralization of organic matter from soil microorganisms. The latter has a two-fold effect: a) lowering of the pH in the soil solution which may facilitate the desorption of REE-Y from clays, oxides and organic host sites and b) the

dissolution of calcite in the limestone with rapid increases in the pH and sorption of the REE-Y on the limestone surface.

4.2. Kinetic and Isotherm Experiments

The % of the REE removal in the sorption isotherms was 98-99%, 96-99% 97-99% for Ce, Eu and Yb, respectively. No plateau was reached in the sorption test and the calcite capacity for REE sorption is considered high. Moreover, the preferable sorption of LREE has been observed mainly in sorption onto metal oxides (Koeppankastrop et al., 1991) and it has been attributed to stronger complexation of HREE, with carbonate anions which hold HREE in solution. There is a controversy whether the REE are strongly bound with carbonates and dicarbonates, or whether there is a strong effect of the ionic radii among the competitive cations in the case of sorption reactions (Coppin et al., 2002). In our case, the competitive cation was Ca^{2+}. Comparing the calcium content in solution between the kinetic test and the isotherm test we record higher calcium concentration (by up to 1 order of magnitude) in the kinetic experiment compared to the isotherm experiment. This occurred because the kinetic test reached equilibrium without correcting the solution pH, whereas in the isotherm test the pH was corrected (Figure 6). The lack of pH adjustment in the kinetic test increased the calcite dissolution after the addition of the REE standard solution (very acidic solution), whereas in the isotherm tests Ca precipitated due to the addition of NaOH. The higher ionic strength in the kinetic test had no effect on the fast sorption of Ce and Eu. The final sorption was 17% higher in the kinetic test, with higher ionic strength (ca. I=1.2) than that recorded in the isotherm test of low ionic strength (ca. I=0.2) Thus, ionic size effect in high ionic strength solution has no significant effects in the REE sorption. Moreover, the calcite dissolution in the kinetic test appears to have inevitably increased the CO_3^{2-} as it probably created complexes with REE.

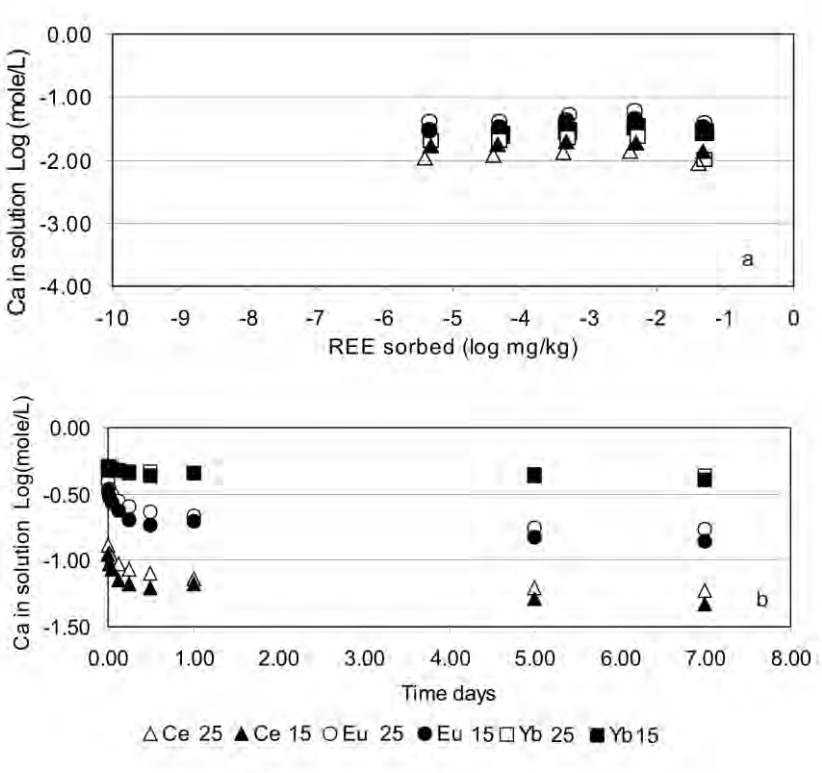

Figure 6 - The calcite content in the (a) isotherm and (b) kinetic experiments.

The kinetic test shows that the maximum REE sorption for all ionic radii species is attained after 24 hours; this is considered to be a fast reaction. The inferred high concentration of CO_3^{2-} in the kinetic has not impeded the fast REE sorption in calcite. Fast REE sorption was also observed in sand by Tang and Johannesson (2005a). The same authors observed a slight decrease in the REE sorption after 12 h; that was attributed to limited dissolution of the sorbent solid phases. In our experimental set up the slight decrease in the REE sorption is observed after the 5th day. The fast sorption rate is mainly attained by a physisorption (adsorption) reaction compared to chemisortpion (absorption). The remark effect in pH experiment was the lower sorption rate for Yb compared to the remaining REE during the first day. The slower sorption rate for Yb may be attributed to the high affinity of Yb to create carbonate complexes which hold it in solution at least for the first 24 hours. Hence, we infer that due to the high dissolution of calcite in our batch experiments, the REE forms complexes with carbonates. Thus, the sorption of the REE on the calcite surface should occur in the form of $REECO_3^+$, $REEHCO_3^{2+}$.

5. Conclusions

The fast sorption of the REE-Y was evident both in pot experiments and kinetic tests. Due to the high calcite dissolution in our tests, we inferred that the REE were bound in carbonates and bi-carbonates, which were sorbed onto the calcite surface. The mechanism of REE-Y enrichment in the limestone involved the three successive steps of: a) REE-Y release from the soil as a result of the pH reduction due to bioturbation; b) sorption on the limestone surface due to calcite dissolution which increased the pH and c) enhancement in the REE-Y sorption. Further studies will focus on the nature of the sorption and the associated oxidation states of REE; however here we propose a physisorption, which progressively changes to inner sphere complexes, as a plausible mechanism for the inclusion of the REE-Y within the limestone surface.

6. Acknowledgments

This work was accomplished with the financial support of John S. Latsis Public Benefit Foundation. We sincerely thank the chemist Saru Maria-Liliana for the REE-Y measurements with ICP-MS and the Laboratory of Hydrogeochemical Engineering and Remediation of Soils for hosting us.

7. References

Carcaillet J., Manighetti I., Chauvel C., Schlagenhauf A. and Nicole J.M. 2008. Identifying past earthquakes on an active normal fault (Magnola, Italy) from the chemical analysis of its exhumed carbonate fault plane, *Earth Planet. Sc. Lett.,* 271, 145–158.

Coppin F., Berger G., Bauer A., Castet S. and Loubet M. 2002. Sorption of lanthanides on smectite and kaolinite, *Chem. Geol.*, 182, 57–68.

Dia A., Gruau G., Olivié-Lauquet G., Riou C., Molénat J. and Curmi P. 2000. The distribution of rare earth elements in groundwater: Assesing the role of source-rock composition, redox changes and colloidal particles, *Geochim. Cosmochim. Ac.,* 64, 4131-4151.

Godelitsas A., Astilleros J.M., Hallam K., Harissopoulos S. and Putnis A. 2003. Interaction of calcium carbonates with lead in aqueous solutions, *Environ. Sci.Technol.,* 37, 3351-3360.

Komnitsas K., Bartzas G. and Paspaliaris I. 2004. Efficiency of limestone and red mud barriers: laboratory column studies, *Miner. Eng.,* 17, 183-194.

Koeppankastrop D., DeCarlo E.H. and Roth M. 1991. Amethod of investigate the interaction of rare earth elements in aqueous solution with metal oxides, *J. Radioanal. Nucl. Ch.,* 152, 337-346.

Laveuf C. and Cornu S. 2009. A review on the potentiality of Rare Earth Elements to trace pedogenetic processes, *Geoderma,* 154, 1-12.

Manighetti I., Boucher E., Chauvel A., Schlagenhauf A. and Benedetti L. 2010. Rare earth elements record past earthquakes on exhumed limestone fault planes, *Terra Nova,* 22, 477–482.

Mouslopoulou V., Moraetis D. and Fassoulas C. 2011. Identifying past earthquakes on carbonate faults: advances and limitations of the Rare Earth Element method based on analysis of the Σpili Fault, Crete, Greece, *Earth Planet Sc. Lett.,* 309, 45-55.

Palumbo L., Benedetti L., Bourles D., Cinque A. and Finkel R. 2004. Slip history of the Magnola fault (Apennines, Central Italy) from 36 Cl surface exposure dating: evidence for strong earthquakes over the Holocene, *Earth Planet. Sc. Lett.,* 225,163–176.

Patino L.C., Velbel M.A., Price J.R. and Wade J.A. 2003. Trace element mobility during spheroidal weathering of basalts and andesites in Hawaii and Guatemala, *Chem. Geol.,* 202 (3–4), 343–364.

Papadopoulos P. and Rowell D.L. 1988. The reactions of cadmium carbonate surfaces, *J. Soil Sci.,* 39, 23-36.

Roy P.D., Caballero M., Lozano S., Morton O., Lozano R., Jonathan M.P., Sánchez J.L. and Macías M.C. 2012. Provance of sediments deposited at paleolake San Felipe, western Sonora Desert: Implications to regimes of summer and winter precipitation during last 50 cal kyr BP, *J. Arid Environ.,* 81, 47-58.

Samara C., Tsitouridou R. and Balafoutis Ch. 1992. Chemical composition of rain in Thessaloniki, Greece in relation to meteorological conditions, *Atm. En.,* 26B, 359-367.

Sdiri A., Higashi T., Jamoussi F. and Bouaziz S. 2012. Effects of impurities on the removal of heavy metals by natural limestones in aqueous systems, *J. Environ. Manage.,* 93, 245-253.

Shields G. and Stille P. 2001. Diagenetic constrains on the use of cerium anomalies as paleoseawater redox proxies: an isotopic and REE study of Cambrian phosphorites, *Chem. Geol.,* 175, 29-48.

Tang, J., Johannesson, K.H., 2005a. Adsorption of rare earth elements onto Carrizo sand:experimental investigations and modeling with surface complexation. *Geochim. Cosmochim. Ac.,* 5269, 5247–5261.

Zachara J.M., Kittrick J.A., Harsh J.B., 1988, The mechanism of Zn^{2+} adsorption on calcite. *Geochim. Cosmochim. Ac.,* 52, 2281-2291.

Δελτίο της Ελληνικής Γεωλογικής Εταιρίας, τομ. XLVII , 2013
Πρακτικά 13ου Διεθνούς Συνεδρίου, Χανιά, Σεπτ. 2013

Bulletin of the Geological Society of Greece, vol. XLVII 2013
Proceedings of the 13th International Congress, Chania, Sept. 2013

TOC AND $CaCO_3$ CONTENT IN OLIGOCENE SHELF DEPOSITS ON LEMNOS ISLAND AND THEIR RELATION WITH DEPOSITIONAL CONDITIONS

Nioti D.[1], Maravelis A.[2], Tserolas P.[1] and Zelilidis A.[1]

[1]University of Patras, Department of Geology, Laboratory of Sedimentology, 26504 Patras, Greece, A.Zelilidis@upatras.gr

[2] School of Environmental and Life Sciences, University of Newcastle, Callaghan 2308 NSW, Australia, Angelos.Maravelis@newcastle.edu.au

Abstract

A series of seventy seven samples from outcrops of mudstones were analyzed in order to evaluate their total organic carbon (TOC) and calcium carbonate (CaCO3) concentrations. Results showed that TOC ranges between 0% to 1.15% (with a mean value of 0.34%) introducing that Oligocene shelf deposits on Lemnos island have fair to good conditions to be potential source rocks. Analysis of $CaCO_3$ presented a range between 1.37% to 42.52% (with a mean value of 16.95%). The comparison of TOC and $CaCO_3$ suggests that the two parameters are either inversely or positively related. The inversely related contents, high TOC and low $CaCO_3$, may indicate anoxic conditions, whereas low TOC and high $CaCO_3$ occur in oxic conditions due to the decomposition of TOC. The CO_2 produced by decomposition of organic carbon and production of organic acids reduces the pH in pore water enough to dissolve any $CaCO_3$ that reaches the sediment water interface. On the other hand, a positive relation, with both high TOC-$CaCO_3$ contents, could be related with oxic conditions and high sedimentation rate or incidents of abrupt death and bury of great amounts of benthic organisms (TOC) increasing the maintenance of organic material in the sediment.

Key words: *Lemnos island, source rock, $CaCO_3$, TOC.*

Περίληψη

Αναλύθηκαν εβδομήντα εφτά δείγματα από επιφανειακές εμφανίσεις ιλυολίθων με σκοπό να προσδιοριστούν η ποσότητα του συνολικού οργανικού άνθρακα (TOC) και του ανθρακικού ασβεστίου ($CaCo_3$). Το συνολικό οργανικό υλικό κυμαίνεται από 0% έως 1.15% (με μέση τιμή 0.34%) δείχνοντας ότι οι αποθέσεις υφαλοκρηπίδας ηλικίας Ολιγοκαίνου, στο νησί της Λήμνου έχουν μέτριες έως καλές δυνατότητες να είναι μητρικά πετρώματα. Το ποσοστό του ανθρακικού ασβεστίου κυμαίνεται από 1.37% έως 42,52%, με μέση τιμή 16,95%. Η σύγκριση των αποτελεσμάτων μεταξύ TOC και $CaCO_3$ προτείνει ότι οι δύο παράμετροι έχουν είτε αρνητική ή θετική συσχέτιση. Η αρνητική συσχέτιση των ποσοστών, TOC υψηλό και $CaCO_3$ χαμηλό μπορεί να συσχετιστεί με ανοξικές συνθήκες, ενώ TOC χαμηλό και $CaCO_3$ υψηλό, εξ' αιτίας της αποικοδόμησης του TOC σε οξικές συνθήκες. Το CO2 που παράγεται από την αποσύνθεση του οργανικού υλικού και η παραγωγή οργανικών οξέων μειώ-

νουν το pH του νερού των πόρων τόσο ώστε να επιτρέπεται η διάλυση όσου $CaCO_3$ φτάνει στην διεπιφάνεια ιζήματος- νερού. Από την άλλη μεριά, η θετική συσχέτιση, με υψηλά και τα δύο TOC και $CaCO_3$, μπορεί να συσχετιστεί με οξικές συνθήκες και μεγάλο ρυθμό ιζηματογένεσης και απότομο θάνατο και ταφή μεγάλων ποσοτήτων βενθικών οργανισμών αυξάνοντας έτσι τη διατήρηση του οργανικού υλικού στο ίζημα.

Λέξεις κλειδιά: *Λήμνος, μητρικό πέτρωμα, ανθρακικό ασβέστιο, οργανικός άνθρκας.*

1. Introduction

Continental shelves constitute one of the preferential zones for the productivity of biomass, which is converted into hydrocarbons (Biju- Duval, 2002). A typical source rock consists of fine sediments that release enough hydrocarbons so as to form a remarkable concentration of oil or natural gas (Brooks et. al., 1987). Source rock prediction requires an understanding of the structural and stratigraphic evolution of the sedimentary layers inside a basin. Characterizing the organic matter from sedimentary rocks is now widely recognized as a critical step in the evaluation of the hydrocarbon potential (Lafargue et. al., 1998).

The amount of organic matter in rocks is usually measured as the total organic carbon content (TOC) and expressed as a percentage of the dry rock. At this study sequence stratigraphy has been combined with total organic carbon (TOC) analysis to develop a model of TOC accumulation in marine source rocks. Various factors play a role in the preservation of organic matter, notably the oxygen content of the water column and sediment (oxic versus anoxic), primary productivity of new organic matter by plants, water circulation, and sedimentation rate (Demaison and Moore, 1980; Emerson, 1985). Anoxic conditions are critical to the preservation of organic matter in sediments. Source rock prediction is therefore concerned primarily with the predicting where and when in the geological past anoxic conditions are likely to have existed. Anoxic conditions develop where oxygen demand exceeds oxygen supply. Oxygen demand is high in areas of high organic productivity (Allen and Allen, 2005).

Studies of numerous global samples of different ages have led to the conclusion that the minimum TOC value required for the designation as an immature source rock is 0.5 wt% (Hunt, 1979; Hedberg and Moody, 1979, Tissot and Welte, 1984).

In present study a series of seventy seven samples were chosen from outcrops of shelf deposits in order to measure the TOC and $CaCO_3$ content and after correlation to introduce the factors that influence the above relation and their influence on depositional environments.

2. Geological Setting

The Thrace Basin has been considered as a fore arc basin of the 'contracted' type (Görür and Okay, 1996; Maravelis and Zelilidis, 2010a) and is the largest and thickest Tertiary sedimentary basin of the eastern Balkan region (Turgut et al., 1991; Turgut and Eseller, 2000). It is exposed on Hellenic, Turkish and Bulgarian territory and comprises an important hydrocarbon province (e.g. Turgut and Eseller, 2000; Siyako and Huvaz, 2007; Maravelis and Zelilidis, 2010b; Maravelis and Zelilidis, 2012). A large accretionary prism in the Central Aegean region bounds the basin on the seaward side, and the landward flank was bound by an active volcanic arc, the Rhodope Zone. Most of the basin strata are Lower Eocene to Upper Oligocene and form thick sedimentary successions (up to 9000 m) made of deep-sea fan deposits (Turgut et al., 1991; Turgut and Eseller, 2000). Sedimentation along the basin margin was dominated by deposition of carbonates during the Eocene and by deltaic bodies, prograding towards the basin center, in the Oligocene (Sümengen and Terlemez, 1991; Turgut et al., 1991).

The Greek part of the Thrace Basin in Lemnos Island and Rhodope was mainly influenced by two major sediment inputs (Maravelis and Zelilidis, 2010b, 2013). The southern part (Lemnos) was significantly affected by the accretionary prism and associated ophiolitic units (Maravelis and Zelilidis,

2010a, 2012) while the northern part (Greek Rhodope) reflects a Circum-Rhodope Belt influence (Maravelis and Zelilidis, 2010b). On Lemnos, the source area contributed significant a volume of ultramafic, gabbro, basalt, chert, and possibly some volcaniclastic detritus of variable grain size into the forearc basin and was probably located south-southwest of Lemnos (Maravelis and Zelilidis, 2010a). The source area was probably rugged and rapidly eroded, causing the ophiolitic bedrock to be deeply incised, enabling a significant amount of coarse-grained material from the uplifting source area to be transported to the Lemnos area (Maravelis and Zelilidis, 2010b, 2013).

This material was deposited in submarine fans in the Lemnos area, which, as a result of tectonic activity, are overlain by shelf deposits (Maravelis et al., 2007). The submarine fan is a sand-rich system, which comprises a basin-floor fan overlain by a slope fan, suggesting submarine fan progradation. Both basin-floor and slope fans are characterized by monotonous alternations of sandstone and mudstone beds (Maravelis et al., 2007).

The shelf environment at Lemnos consists of sandstones interbedded with very thin mudstone beds. Many types of sandstone appear featureless, although others show grooves and tool marks. Internal structures are dominated by a prominent parallel lamination. The sandstone beds show, generally a single set of ripple cross-laminae at the top. Mudstones commonly contain a high proportion of coal debris. Upwards, this unit grades from a sand dominant to an almost completely mud-dominant sequence that consists of massive, homogeneous green or green-grey mudstones (Maravelis et al. 2007).

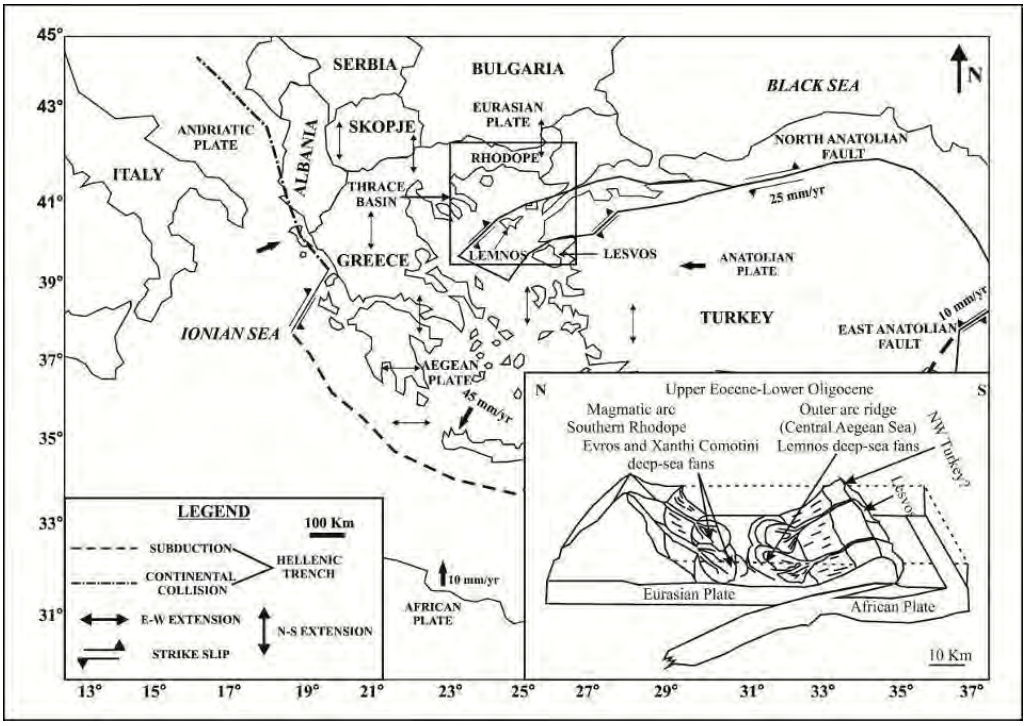

Figure 1 - Simplified sketch map and plate tectonic configuration of the Eastern Mediterranean and adjacent region and schematic diagram illustrating the north-east Aegean Sea tectonic setting (Modified from Maravelis & Zelilidis, 2010a).

During the Miocene, Lemnos was the site of volcanic activity resulting in accumulation ofmagmatic rocks (Pe-Piper and Piper, 2001). Both plutonic and volcanic rocks accumulated, principally trachyandesites and dacites, and cover a large part of the studied area. These rocks have been interpreted as belonging to the high-K province along the Aegean–Anatolian boundary (Pe-Piper et al., 2009). In particular, they belong to the northern, 'shoshonitic province' that includes the islands of Samothrace,

Lemnos and Lesvos (Pe-Piper et al., 2009). These high-K rocks, mostly of intermediate composition, indicate ensuing calc-alkaline orogenic volcanism, emitted from large volcanic centers. Upwelling of asthenospheric mantle has been invoked to account for their genesis (Pe-Piper et al., 2009). The end of the Miocene is characterized by the deposition of conglomerates, marls and calcareous sandstones. Local Pleistocene porous calcareous and locally oolitic limestones and Holocene alluvial, coastal deposits and dunes are sparse.

3. Stratigraphy

Studied shelf deposits, up to 84m thick, consist of four sedimentary cycles of repetition character, start with mud and terminate upwards with an increasing grain size either of sand with mud or only of sand (Figure 2).

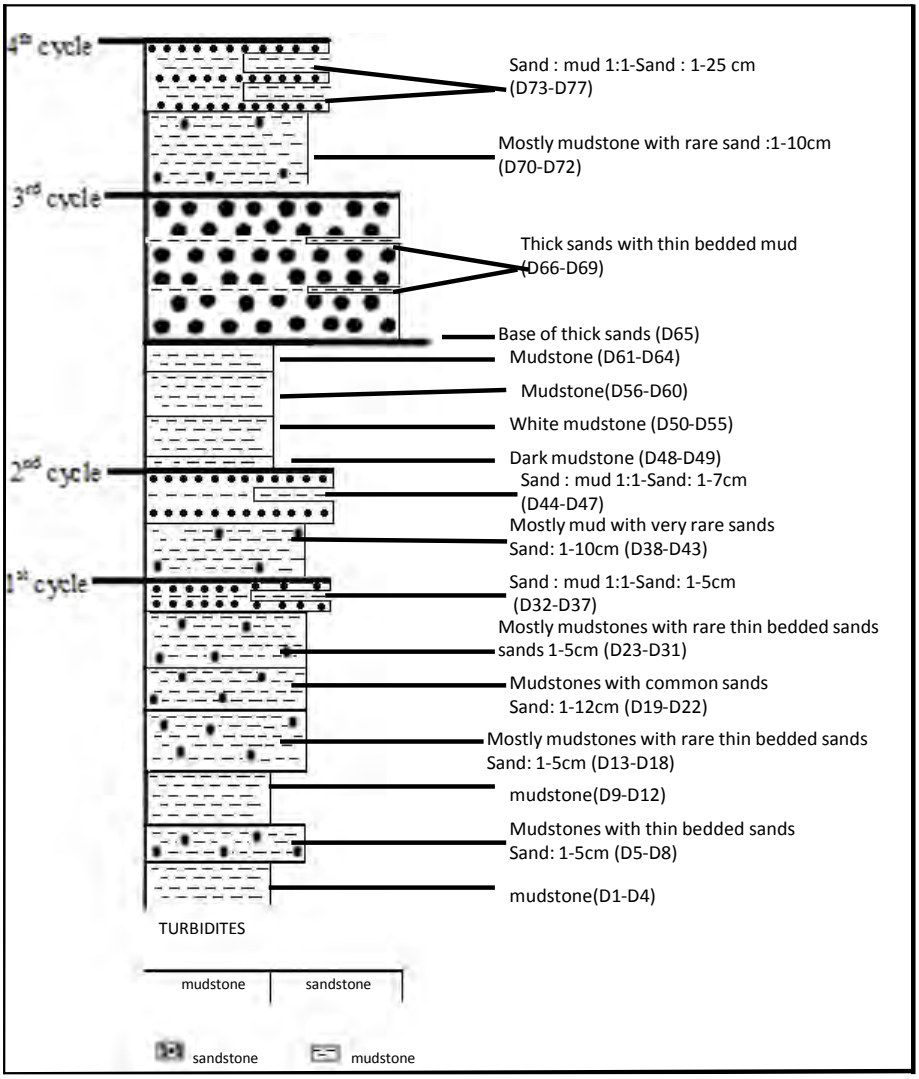

Figure 2 - Stratigraphic column of sediments samples of the study area.

The fact that the cycles are completed with sand indicates that the processes of sand transport and deposit were of a higher energy than those of mud transport and deposit. More specifically, the first sedimentary cycle is 36.5m thick, and consists of 6 mudstone layers (33m thick) and a layer

of sandstone which overlies the mudstones about 3.5 meters thick. The second sedimentary cycle is composed of a mudstone layer (7m thick) and a sandstone layer (6m thick) and has an overall thickness of 13 meters. The third sedimentary cycle includes 4 layers of mudstones (15m thick) and a thick sandstone layer with a total thickness of about 17.5 meters. The last sedimentary cycle, up to 17m thick, is formed by a mudstone layer (10m thick) and a layer of sandstone (7m thick).

4. Methodology and Results

4.1. Materials and Methods

The TOC % concentrations were evaluated with the use of the titration method by Gaudette et al. 1974. 10 ml of potassium dichromate (K2Cr2O7) were added and mixed thoroughly. Then 20 ml of concentrated sulfuric acid (H2SO4, 96%) were added and the mixture was stirred with a gentle shake for one minute. This is done carefully to achieve full contact (reaction) of the precipitate with the reagent while avoiding residue on the walls of the bottle and not in contact with the reagents. After 30 minutes, the solution was diluted with 200 ml distilled water and afterwards 10 ml of phosphoric acid (H3PO4, 85%) ,0,2 gr of sodium fluoride (NaF) and 15 drops of indicator difenylaminis were added. The solution was back-titrated with a solution of ferrous ammonium sulfate regularity 0,5 N (FeSO4 (NH4) 2 (SO4) 6H2O). The color develops from dull green-brown to green by adding approximately 10 ml of the ferric solution. The color continues to change with the addition of 10 to 20 drops of the ferric solution until very bright green. The same procedure is followed in a blank sample (a sample containing no precipitate) per ten samples.

For the determination of calcium carbonate (CaCO3) % concentration of the samples, the method for cleaving the CaCO3 with CH3COOH (acetic acid) is used as described by Varnavas, 1979. This method relies on the full decomposition of calcium carbonate (CaCO3) with acetic acid (CH3COOH), to form a soluble salt of calcium acetate ((CH3COO) 2Ca) and escape the produced carbon dioxide (CO2).

4.2. TOC Results

Organic carbon content (Figure 3) of the Lemnos studied sediments exhibits variable contents ranging from 0 to 1.15% with an average value of 0.34% and these values prove that the studied rocks have from poor to good source rock potential. Generally, TOC value is characterized by an intense fluctuation throughout the stratigraphic column. At the first sedimentary cycle (samples D1-D37), a sudden negative shift in the TOC rations occurs over the samples D1 and D35 with 0% TOC. At the second sedimentary cycle (samples D38-D47), TOC values reach a peak at D40-1.03%. At the third sedimentary cycle (samples D48-D69) TOC values reach a peak at D67-1.15% and D68-0.98% while D51, D53, D54, D55, D57, D58, D59, D66, D69 contain 0% TOC. At the fourth sedimentary cycle (samples D70-D77) and at the top layer of the stratigraphic column D70, D71, D73, D75, D76 contain 0% TOC. The average TOC content presents a general decreasing trend through each sedimentary cycle (Figure 3).

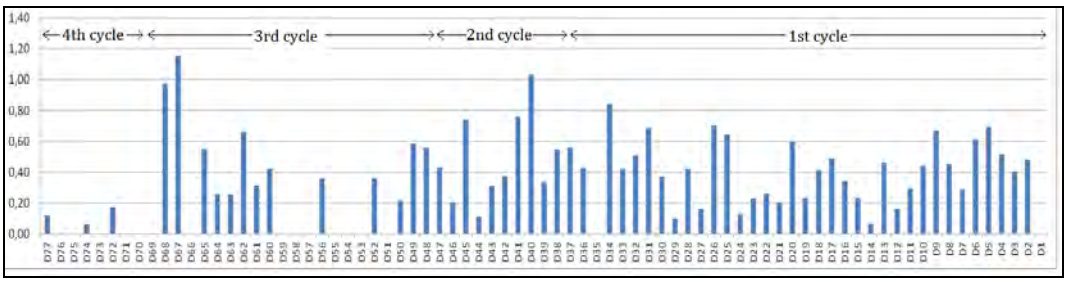

Figure 3 - TOC percentages in sediments of study area.

4.3. CaCO3 Results

Variation of $CaCO_3$ throughout the stratigraphic column is presented in Figure 4 with Ca-CO_3variable content ranging from 1.37 to 42.52% with an average value of 16.95%.

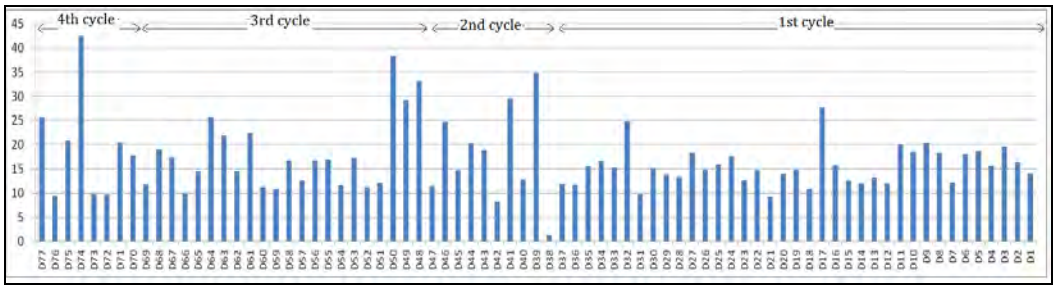

Figure 4 - Calcium carbonate percentages in sediments of study area.

At the first sedimentary cycle, (samples D1-D37) max values of $CaCO_3$ occur at D17-27.67% and at D32-24.74% while minimum values occur at samples D21-9.24% and D31-9.82%. At the second sedimentary cycle (samples D38-D47), the elevated values are punctuated by major peaks at D39-34.85% and D41-29.58% while its minimum values correspond to samples D38-1.37% and D42-8.23%. At the third sedimentary cycle (samples D48-D69), occur major peaks at D48-33.13%, D50-38.3% while minimum values occur at D66-9.98% and D59-10.9%. At the fourth sedimentary cycle (samples D70-D77) $CaCO_3$ reaches a peak of 42.52% at D74 and D77-25.71% as well as minimum values at D76-9,42% and at D72-9.74%. The average $CaCO_3$ content presents a general increasing trend through each sedimentary cycle (Figure 4).

In the study area the results of the study of calcareous nannofossils (biostratigraphy) showed that during the lower Oligocene the cold paleoclimatic conditions led to changes in palaeoenvironment and biotic conditions at the open seas (Maravelis and Zelilidis, 2012). For example, calcareous nanofossils *Braarudosphaera bigelowii* and *Micrantholithus spp.* which were recognized at the study area indicate changes in climate at Eocene / Oligocene. These species are typical of eutrophic waters with low oxygen and salinity (Peleo-Alampay et al., 1999) and indicate the input of terrestrial material (Švábenická, 1999).

4.4. Correlation Between TOC and $CaCO_3$

TOC and CaCO3 values can be compared to one another for each sample separately observing Figure 5. The mean values for each sedimentary cycle are presented in Table 1.

At the first sedimentary cycle, TOC and CaCO3 values are increased at Sample D17 with values of 0.49% and 27.67%, respectively. At sample D26 organic matter increases while CaCO3 decreases with values of 0.70% and 14.84%, respectively. At sample D32 TOC with a value of 0.51% decreases and CaCO3 - 24.74% increases. At sample D34 both percentages increase with TOC-0.84% and CaCO3-16.61%.

Specifically, the mudstones of the first sedimentary cycle have an average of 0.38% of TOC and 15.5% of CaCO3 while the upper layer of sandstone/mudstone has an average of 0.46% TOC and 15.97% CaCO3. At the second sedimentary cycle, at sample D39 a decrease of organic material (0.33%) and an increase of CaCO3 (34.85%) are observed. An increase in organic matter (1.03%) and a decrease of CaCO3 (12.76%) is observed at sample D40. Specifically, the mudstone layer of the second sedimentary cycle has an average of 0.56% TOC and 17.6% CaCO3 while the upper layer of sandstone is described by 0.37% TOC and 17.77% CaCO3. At the third sedimentary cycle at sample D50 organic matter decreases (0.21%) and CaCO3 increases (38.3%) while at sample D67 both TOC and CaCO3 are increased with values of 1.15%, 17.42%, respectively. At the third sedimentary cycle the four layers of mudstone have a TOC average of

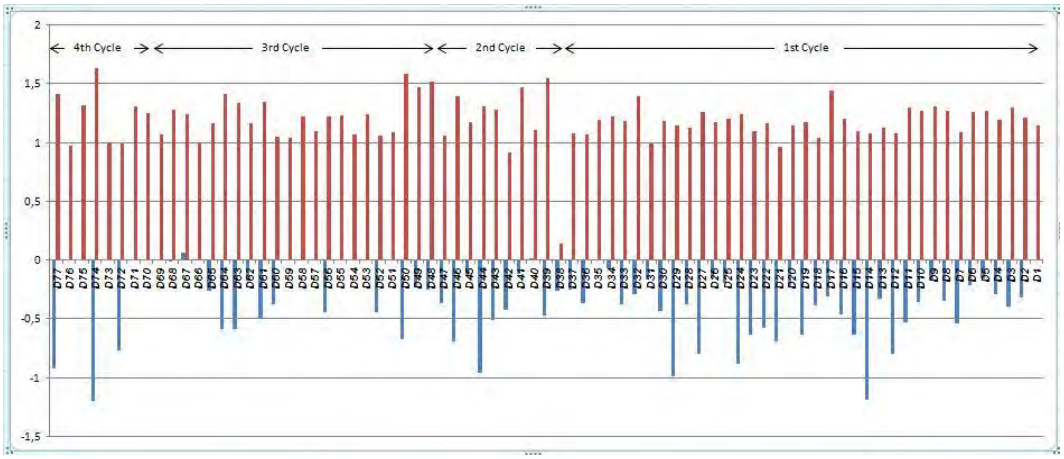

Figure 5 - TOC and $CaCO_3$ logarithmic concentrations in sediments of study area.

0.23% and a CaCO3 average of 18.99% while the sandstone layer of this cycle has percentages of 0.54% and 14.55%, respectively. At the fourth sedimentary cycle, the sample D74 has values that increase at 0.06%, for TOC and at 42.52% for CaCO3. Also, the mudstone layer of the fourth sedimentary cycle is characterized by TOC of 0.06% and CaCO3 of 16% while the layer of sandstone/mudstone has an average of 0.04% TOC and 21.71% CaCO3.

Table 1 - TOC and $CaCO_3$ percentages in sediments for each sedimentary cycle.

CYCLE	no. S	$CaCO_3$ avg	TOC avg
1st	37	15,57	0,39
2nd	8	17,67	0,48
3rd	22	17,97	0,30
4th	8	19,57	0,04

Nearly 3m with dark mudstone where samples D48-49 were taken from, contain an average of 31.21 % $CaCO_3$ and 0.57 TOC % while the overlying white mudstone of 4m (D50- D55) contain an average 17.96% of $CaCO_3$ and 0.1 TOC. The anoxic conditions predominated during deposition of the sediments of the dark mudstone while these conditions changed in an environment with higher oxygen (white mudstone).

Samples with a synchronous increase of TOC-$CaCO_3$ content occur at samples (D17, D34, D67, D74) and can be interpreted by the abrupt death and bury of a great quantity of both the shells $CaCO_3$) and the body parts (organic matter) of benthic organisms by successive layers of sediment.

On the contrary, the inverse relation between $CaCO_3$-TOC at samples D26, D32, D39, D40, D50, where increase of TOC is accompanied with decrease of $CaCO_3$ indicates that the CO_2 produced by decomposition of that organic carbon and production of organic acids reduces the pH of anoxic pore waters enough to dissolve any $CaCO_3$ that reaches the sediment-water interface (Figure 5).

While no general correlation is present throughout the sedimentary cycles (r~0) a general trend of $CaCO_3$ increase and TOC respective decrease can be observed. Furthermore, the correlation between the average % measurements for each sedimentary cycles (Table 1) is strong negative (r=-0,7). The lack of general correlation may indicate different origin for inorganic and organic carbon throughout the sedimentation process.

However, throughout the sedimentation cycles exceptions to this rule occur, where increase of $CaCO_3$ content is synchronous with increase of the TOC content. Specifically, at the closing of each cycle positive correlations occur, while the highest measurements for both parameters co-occur at the closing of the 3rd cycle. The scatter plot of the closing of the 3rd cycle is presented in Figure 7, where the positive correlation is evident (r~1). The same pattern applies for the closing of both the 1st and the 4th cycle. For each cycle, the grain size increases as we move upwards which indicates higher energy sedimentation or progradation of the deposition environment, or both. High energy sedimentation can justify the positive correlation, as the organic carbon is buried in a rate that preserves oxidization; both higher energy sedimentation rates and progradation of the depositional environment can be observed through the stratigraphic column, as there is an upward thickening trend and grain size is increasing at the end of each cycle.

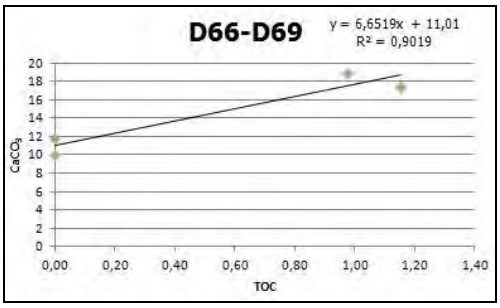

Figure 7 - TOC and $CaCO_3$ correlation for the upper part of third sedimentary cycles.

5. Discussion – Conclusions

The study of both TOC and $CaCO_3$ content for Lemnos shelf deposits and the identification of correlations between the two parameters can provide several clues about the depositional environment and conditions and the evaluation of possible source rocks. In general, the results present:

- **A poor to good TOC % content (0-1,15%). TOC average % for each cycle decreases upwards.** Taking into consideration that a source rock needs to be a fine-grained and rich in organic matter, the mudstone of the second sedimentary cycle with the most elevated percentage of TOC-0.54% may be considered as most suitable source rock in compare to all other sediments of the stratigraphic column. Also, according to the percentages of Peters and Cassa (1994), showing petroleum potential (quantity) of an immature source rock, the mudstone of second sedimentary cycle presents a fair potential to hydrocarbon production.
- **A poor $CaCO_3$ content (0,71-45%), not enough to consider the study rocks as calcareous mudstone source rocks.** The poor content indicates limited inorganic carbon supply from the terrestrial ultramaffic, gabbro, basalt and volcanoclastic detritus.
- **$CaCO_3$ and TOC % content does not present a general correlation either positive or inverse, which indicates different source supply of organic and inorganic carbon.** However a general inverse trend is observed for each sedimentary cycle and for the most significant measurements, while synchronous changes occur throughout the sequence.
- **Detailed analysis has presented positive correlation between the two parameters at the higher energy parts of the sedimentary cycles.** The coarse grained sands are of higher energy, and thus higher sedimentation rates; organic content is preserved under successive sediment accumulation in a higher rate than its oxidization. Simultaneous rapid increase in both contents, as is the case in the 3rd sedimentary cycle, can be attributed to abrupt death and bury of benthic organisms, which provide both the organic material (body parts) and the increase of calcium carbonate (shells). Biotic and enviromental changes during Oligocene, which are also indicated by the biostratigraphy of the shelf deposits (Maravelis &

Zelilidis, 2012) could justify such an event, while the rapid sedimentation preserved the geological record. Another fair assumption is that the thickening of the sandstones of the closing of the cycle could indicate elevation of the depositional environment and thus, increased terrigenous supply in both parameters.

6. References

Allen P. and Allen J. 2005. Basin Analysis: Principles and Applications, Second Edition: Blackwell Science Limited, *a Blackwell Publishing Company*, p. 423.

Aubry M.P. 1992. Late Paleogene calcareous nannoplankton evolution: a tale of climatic deterioration. In: Prothero D.R., Berggren W.A. (Eds.), Eocene/Oligocene Climatic and Biotic Evolution. Princeton University Press, pp. 272–309.

Biju-Duval B. 2002 Sedimentary geology, sedimentary basins depositional environmnents, petroleum formation. Institute Français du petrole publications, *Editions Technip*, France, p.642.

Brooks J.M., Kennicutt M.C., Fisher C.R., Mako S.K., Cole K., Childress J.J., Bidigare R.R. and Vetter R. 1987. Deep-Sea hydrocarbon seep communities; Evidence of energy and nutritional carbon sources, *Science*, 238: 1138-1142.

Burke W.F and Ugurtas G. 1974. Seismic interpretation of Thrace Basin. *Proc 2nd Petrol Congr*, Turkey, pp 227–248

Demaison G.J. and Moore G.T. 1980. Anoxic environments and oil source bed genesis, *AAPG Bulletin,* v. 64, p.1179-1209.

Doust H. and Arıkan Y. 1974. The geology of the Thrace Basin, 2, *Petroleum Congress of Turkey,* Ankara, pp. 119–136, 227–248

Emerson S. 1985. Organic carbon preservation in marine sediments, in E.T. Sundquist and W.S. Broecker, eds., The carbon cycle and atmospheric CO2: natural variations from Archean to Present: American Geophysical Union, *Geophysical Monograph 32*, p. 78-86.

Gorur N. and Okay A. 1996. A fore-arc origin for the Thrace Basin, NW Turkey. *International Journal of Earth Sciences* 85, 662-668.

Haq B.U., Hardenbol J. and Vail P.R. 1987. Chronology of fluctuating sea levels since the Triassic Science 235, 1156–1167.

Hauck J., Gerdes D., Hillenbrand Cl-D., Hoppema M., Kuhn G., Nehrke G., Völker Chr. and Wolf-Gladrow D. 2012. Distribution and mineralogy of carbonate sediments on Antarctic shelves. *Journal of Marine Systems*, 90(1), 77-87.

Hedberg H.D. and Moody J.O. 1979. Petroleum prospects of deep offshore, *Am. Assoc. Pet. Geol. Bull Bul*. 63, 286–300.

Hunt J.M. 1979. Petroleum Geochemistry and Geology. Freeman and Company, San Francisco, 617 pp.

Jackson J. and McKenzie D.P. 1988. The relationship between plate motions and seismic moment tensors, and the rates of active deformation in the Mediterranean and Middle East, *Geophysical Journal,* v. 93, p. 45–73.

Khim B.K., Kim H.J., Cho Y.S., Chi S.B. and Yoo C.M. 2012. Orbital Variations of Biogenic CaCO3 and Opal Abundance in the Western and Central Equatorial Pacific Ocean During the Late Quaternary, *Terr. Atmos. Ocean*. Sci. 23 -1, 107-117.

Lafargue E., Marquis F. and Pillot D. 1998. Rock-Eval 6 applications in hydrocarbon exploration, production, and soil contamination studies. *Revue de l'Institut Français du Pétrole* 53-4, 421-437

Maravelis A. 2009. Provenance, tectonic setting and source rock potential of the Paleogene deep-water sediments on Lemnos Island Northeast Greece. Implications of the Northeast Aegean Sea hydrocarbon potential and configuration. *PhD Thesis*, Patras Univ. press.

Maravelis A., Konstantopoulos P., Pantopoulos G. and Zelilidis A. 2007. North Aegean sedimentary basin evolution during the late Eocene to early Oligocene based on sedimentological studies on Lemnos Island (NE Greece), *Geologica Carpathica* 58, 455-464.

Maravelis A. and Zelilidis A. 2010. Organic geochemical characteristics of the late Eocene/early Oligocene submarine fans and shelf deposits on Lemnos Island, NE Greece, *Journal of Petroleum Sciences and Engineering* 71, 160–168.

Maravelis A. and Zelilidis A. 2010. Petrography and geochemistry of the late Eocene-early Oligocene submarine fans and shelf deposits on Lemnos Island, NE Greece: implications for provenance and tectonic setting*, Geological Journal* 45, 412-433.

Maravelis A. and Zelilidis A. 2012. Paleoclimatology and Paleoecology across the Eocene/Oligocene boundary, Thrace Basin, Northeast Aegean Sea, Greece, *Palaeogeography, Palaeoclimatology, Palaeoecology*, 365–366, 81-98.

Maravelis A. and Zelilidis A. 2013. Discussion to 'Unraveling the provenance of Eocene- Oligocene sandstones of the Thrace Basin, North-east Greece' by Caracciolo et al. (2011), *Sedimentology*, 58, 1988-2011. Sedimentology. 60, 860-864

Peleo-Alampay A.M., Mead G.A. and Wei W. 1999. Unusual Oligocene Braarudosphaerarich layers of the South Atlantic and their paleooceanographic implications*, J. Nannoplankton Res*. 21, 17–26.

Perincek D. 1991. Possible strand of the North Anatolian Fault in the Thrace basin, Turkey- an interpretation. TAPG Bull.75 (2), 241–257.

Peters K. and Cassa M. 1994. Applied source rock geochemistry, in Magoon, L.B., and Dow, W.G., eds., The petroleum system – from source to trap, *American Association of Petroleum Geologists Memoir* 60, p. 93-120.

Shanmugam G, Moiola R.J. 1988. Submarine fans: characteristics, models, classification and reservoir potential, *Earth Science Reviews* 24: 383-428.

Siyako M. and Huvaz O. 2007. Eocene stratigraphic evolution of the Thrace Basin, Turkey, *Sedimentary Geology*, v. 198, p. 75–91.

Švabenicka L. 1999. Braarudosphaera-rich sediments in the Turonian of the Bohemian Cretaceous Basin, Czech Republic. Cretac. Res. 20, 773–782.

Tissot B. and Welte D. 1978. Petroleum formation and occurrence. A new approach to Oil and Gas exploration. *Springer-Verlag*, Berlin.

Turgut S., Türkaslan M. and Perinçek D. 1991. Evolution of the Thrace sedimentary basin and its hydrocarbon prospectivity. In: Spencer AM (ed) Generation, accumulation, and production of Europe's hydrocarbons. *Spec Publ Eur Assoc Petrol Geosci* 1: 415–437

Turgut S. and Eseller G. 2000. Sequence stratigraphy, tectonics and depositional history in eastern Thrace Basin, NW Turkey. *Marine and Petroleum Geology* 17, 61-100.

Turgut S., Türkaslan M. and Perinçek D. 1991. Evolution of the Thrace sedimentary basin and its hydrocarbon prospectivity. In: Spencer, A.M. (Ed.), Generation, Accumulation, and Production of Europe's Hydrocarbons, *Special Publication of European Association of Petroleum Geoscientists,* pp. 415-437.

Δελτίο της Ελληνικής Γεωλογικής Εταιρίας, τομ. XLVII , 2013
Πρακτικά 13ου Διεθνούς Συνεδρίου, Χανιά, Σεπτ. 2013

Bulletin of the Geological Society of Greece, vol. XLVII 2013
Proceedings of the 13th International Congress, Chania, Sept. 2013

COMPARATIVE EVALUATION OF ROCK-EVAL AND ELEMENTAL ANALYSIS TO DETERMINE ORGANIC CARBON CONTENT IN SEDIMENT SAMPLES

Pyliotis I.[1], Hamilaki E.[2], Pasadakis N.[2] and Manoutsoglou E.[1]

[1] *Technical University of Crete, Department of Mineral Resources Engineering, Research Unit of Geology, Chania, 73100, Greece, ipyliotis@isc.tuc.gr, emanout@mred.tuc.gr*

[2] *Technical University of Crete, Department of Mineral Resources Engineering, Research Unit of Hydrocarbon Chemistry and Technology, Chania, 73100, Greece, ehamilak@mred.tuc.gr,*

pasadaki@mred.tuc.gr

Abstract

Rock-Eval and Elemental Analysis techniques are widely used in Organic Geochemistry for the determination of the organic content in sediment samples. Both techniques determine the carbon content using thermal treatment and pyrolysis and/or oxidation reactions. Due to the complex nature of the geochemical samples (different mineralogical composition, low organic carbon content, e.t.c) and the differences of their operational principles, disagreements are commonly observed between the analytical results of these techniques. In this work we studied in a systematic manner the performance of both techniques on a common sample set, consisting of immature, poor in organic carbon, sediments. It was demonstrated that both techniques applied on original and acid-treated samples, provide consistent analytical results for carbon content; that has also been showed by its mass-balance calculations showed.

Key words: *Carbonates, acid-treatment, mass-balance.*

Περίληψη

Η πυρόλυση Rock-Eval και η στοιχειακή ανάλυση είναι ευρέως διαδεδομένες τεχνικές στην Οργανική Γεωχημεία για τον προσδιορισμό του οργανικού περιεχόμενου σε δείγματα ιζημάτων. Και οι δυο τεχνικές προσδιορίζουν τον περιεχόμενο άνθρακα στα δείγματα χρησιμοποιώντας θερμική επεξεργασία και πυρόλυση ή/και καύση. Εξαιτίας της σύνθετης φύσης των γεωχημικών δειγμάτων (διαφοροποιήσεις στην ορυκτολογική σύσταση, χαμηλή περιεκτικότητα σε οργανικό άνθρακα, κ.λπ.) και των διαφορών στην αρχή λειτουργίας τους, συχνά παρατηρούνται ασυμφωνίες μεταξύ των αναλυτικών αποτελεσμάτων αυτών των τεχνικών. Στην παρούσα δημοσίευση μελετήθηκε με συστηματικό τρόπο η απόδοσή και των δύο τεχνικών σε μια κοινή ομάδα δειγμάτων, που αποτελείται από ανώριμα ιζήματα, φτωχά σε οργανικό υλικό. Αποδείχθηκε ότι και οι δύο τεχνικές, που εφαρμόστηκαν στα αρχικά δείγματα και σε δείγματα που επεξεργάστηκαν με οξύ, παρέχουν συγκρίσιμα αναλυτικά αποτελέσματα για τον περιεχόμενο άνθρακα, όπως έδειξε και ο υπολογισμός του ισοζυγίου μάζας του.

Λέξεις κλειδιά: *Ανθρακικά, επεξεργασία με οξύ, ισοζύγιο μάζας.*

1. Introduction

Rock-Eval (RE) pyrolysis (Espitalie et al 1977) is probably the most widespread analytical technique used for the estimation of the organic matter content in sediments and provides the basic quantitative data for further geochemical analyses. RE enables the rapid screening of sediment samples, without the tedious preliminary kerogen isolation, and the reliable estimation of the organic content in terms of already existing hydrocarbons (S1), pyrolyzable organics (S2), oxygen content (S3), remaining char after pyrolysis (S4) as well as of the Total Organic Carbon (TOC) present. The values of S1, S2, S3 and S4 peaks reflect the organic matter type and content as well as the time and temperature the rock sample has undergone in the subsurface. Although the development of Rock-Eval 6 systems, with their more sophisticated detection system and higher pyrolysis/oxidation temperatures, provides more accurate estimation of the quality and quantity of organic matter (Behar et al, 2001, Lafargue et al, 1998), the well-known Rock-Eval II systems with TOC module serve, till now, in numerous petroleum laboratories worldwide.

Carbon determination in sediments based on its oxidation in an oxygen atmosphere at elevated temperatures has been also widely used in organic geochemical laboratories. Today this analysis is easy to carry out using Elemental Analysers (EA), that enables the simultaneous determination of multiple elements such as hydrogen, nitrogen, sulphur, oxygen e.t.c. Due to the high oxidation temperatures used in EA the carbon determined from sediment samples comes from both organic matter as well as from carbonates that thermally dissociate during the analysis.

It has been recognized from the early days of RE use that the obtained analytical data, especially when used to assess the type of the organic matter, may be influenced by the inorganic matrix of the sample, thus leading to questionable conclusions (Katz 1983). For instance, the presence of carbonate minerals in the samples would release CO_2 during RE analysis, resulting in an increase of S3 values. Therefore, acidification of solid samples to remove inorganic from organic carbon is a widely encountered procedure in organic geochemistry, usually applied to sediments in order to improve the accuracy, especially of the S3 peak determination.

The aim of the present work was firstly to evaluate whether or not RE and EA techniques display comparable results and secondly to examine the effect of the presence of carbonate minerals in the determination of organic carbon content. In order to achieve these objectives, both techniques were applied on a sample set of immature, poor in organic carbon, sediments as well as on the acid-treated decarbonated counterparts.

2. Samples and Methods

A set consisting of twenty sediment samples, obtained from cuttings of a well penetrating neogene formations were used. The positions of the samples in the penetrated lithostratigraphic column are shown in Figure 1. The samples, after washing, to remove possible organic contaminants from drilling mud, were dried at 105^{o}C overnight, crashed and sieved through a 60 mesh sieve. Their analysis was carried out according to the following protocol:

1. Aliquots of sediments (~100mg) were analyzed in an RE II-TOC (Delsi Inc.) system connected to an A/D acquisition system, SRI-302. After a 2min purging with He, the samples were heated at 300^{o}C for 3min and afterwards were pyrolyzed up to 600^{o}C, following a temperature ramp equal to 50^{o}C/min. The CO_2 trap was functioning till 390^{o}C. The pyrolyzed sample was further burned in an air atmosphere in the oxidation oven at 600^{o}C. The S1, S2, S3, S4 values were calculated using the peak areas obtained using the PeakSimple 3.29 software, based on a previously performed calibration using standard sediment samples. The comparison of the results obtained using the above data acquisition and processing system with the ones from the RE system integrator found to be more repeatable especially when low peak areas were considered. The experimental data of RE II-TOC analysis on the original samples are shown in Table 1.

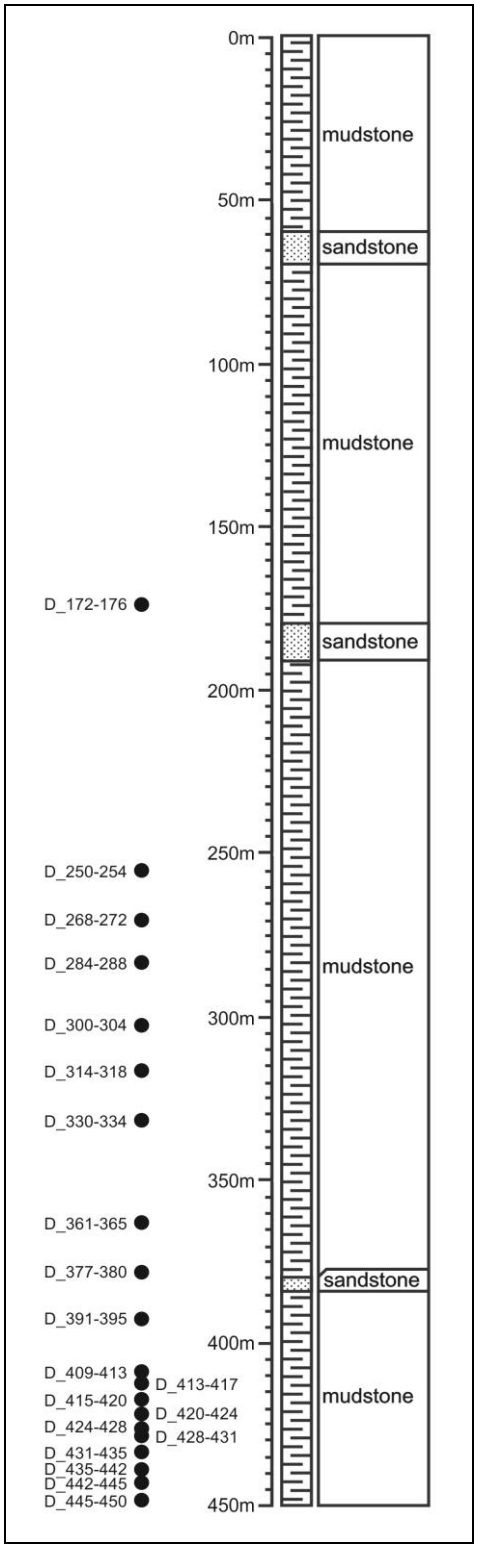

Figure 1 - Lithostratigraphic description of the well. The depths where the samples were recovered are also marked.

Table 1. Rock-Eval parameters measured and calculated from original and acid-treated samples.

			Original samples					Acid-treated					Calculated***			
Sample	**Carb.***	**Res.****	**Tmax**	**S1**	**S2**	**S3**	**TOC**	**Tmax**	**S1**	**S2**	**S3**	**TOC**	**S1**	**S2**	**S3**	**TOC**
	% w.	%	°C	mg/g sediment			% w.		mg/g sediment			% w.	mg/g sediment			% w.
D_172-176	26.26	54.80	417	0.02	0.19	0.79	0.38	413	0.08	0.60	0.47	0.64	0.15	1.09	0.49	0.35
D_250-254	29.37	57.25	408	0.02	0.30	0.67	0.48	405	0.14	0.91	0.30	0.56	0.24	1.59	0.26	0.32
D_268-272	24.91	54.84	416	0.02	0.28	0.76	0.46	409	0.12	0.98	0.26	0.64	0.22	1.79	0.35	0.35
D_284-288	24.59	58.73	409	0.03	0.34	0.74	0.52	406	0.10	0.73	0.30	0.51	0.17	1.24	0.29	0.30
D_300-304	23.85	57.24	403	0.03	0.30	0.84	0.36	406	0.17	1.05	0.46	0.60	0.30	1.83	0.30	0.34
D_314-318	25.36	56.55	416	0.02	0.30	0.64	0.24	409	0.04	0.59	0.35	0.92	0.07	1.04	0.74	0.52
D_330-334	22.10	57.28	412	0.02	0.28	0.68	0.32	405	0.09	0.50	0.31	0.58	0.16	0.87	0.54	0.33
D_361-365	23.84	53.29	409	0.02	0.37	0.69	0.41	408	0.08	0.54	0.49	0.70	0.15	1.01	0.68	0.37
D_377-380	25.40	58.07	407	0.02	0.33	0.67	0.39	401	0.13	0.60	0.34	0.62	0.22	1.03	0.48	0.36
D_391-395	22.58	55.57	408	0.01	0.36	0.67	0.47	403	0.07	0.62	0.39	0.86	0.13	1.12	0.61	0.48
D_409-413	23.59	56.03	411	0.02	0.35	0.71	0.45	405	0.07	0.51	0.36	0.65	0.12	0.91	0.48	0.36
D_413-417	27.14	57.63	406	0.03	0.40	0.67	0.50	407	0.05	0.50	0.31	0.64	0.09	0.87	0.61	0.37
D_415-420	21.92	60.45	410	0.05	0.57	0.68	0.63	406	0.08	0.48	0.31	0.66	0.13	0.79	0.48	0.40
D_420-424	29.86	57.60	409	0.02	0.64	0.74	0.50	407	0.09	0.49	0.35	0.70	0.16	0.85	0.40	0.40
D_424-428	26.52	58.55	406	0.03	0.41	0.68	0.42	407	0.07	0.44	0.38	0.57	0.12	0.75	0.48	0.33
D_428-431	25.76	57.71	408	0.04	0.59	0.62	0.52	402	0.08	0.51	0.43	0.66	0.14	0.88	0.68	0.38
D_431-435	23.55	57.37	405	0.04	0.31	0.76	0.50	406	0.09	0.51	0.38	0.71	0.16	0.89	0.66	0.41
D_435-442	24.03	59.51	406	0.02	0.58	0.58	0.48	403	0.07	0.47	0.37	0.76	0.12	0.79	0.54	0.45
D_442-445	24.39	57.92	406	0.04	0.52	0.56	0.50	401	0.10	0.45	0.33	0.65	0.17	0.78	0.52	0.38
D_445-450	26.02	57.18	403	0.02	0.54	0.74	0.40	409	0.04	0.33	0.31	0.63	0.07	0.58	0.51	0.36

* - Carbonates content (% w.) from XRD analysis, ** - % w. of sediment after acid treatment, *** - Corrected with respect to mass-loss during acid-treatment

2. Subsequently the sediment samples were acid-treated to remove carbonates by applying, in a strongly repeatable way, the following methodology: Sample aliquots (~0.5 gr) were weighted and placed in centrifuge tubes. 70 ml of HCl (2N) was added to each tube and they were left to react at 70^{o}C in an oil bath for 12h. Then, after centrifuging for 5 min at 2000 rpm, the broth was decanted, followed by at-least five washing cycles with 50 ml of distilled water until neutral pH was obtained. Specific care was taken to avoid mass-loss due to suspended particles. The remaining material was dried and weighted again to determine the sample loss due to the acid treatment. The amount of this material, expressed as fraction of the original sediment weight is shown in Table 1.

3. The two sample sets (original and acid-treated) were analyzed in a Flash 2000 Elemental Analyzer (Thermo Scientific) in CHNS mode calibrated using home-prepared standards containing carbon in low concentration (1-5%).

4. Finally the bulk mineralogy of the samples was investigated using X-ray diffraction (XRD). XRD patterns were recorded with a Bruker D8 Advance diffractometer, with Cu-Kα1 radiation, with a voltage of 40 kV and a current of 40 mA. The random powder mounts of samples were scanned with a step size of 0.02° 2θ and counting time per step 0.3s. Raw data were evaluated using EVA software. The mineralogical composition of the samples under study is shown in Table 2.

3. Results and Discussion

3.1. RE Data Evaluation

The examination of the RE analytical data (Table 1) shows that all studied sediment samples are immature, as their low Tmax values denote. Both original and acid-treated samples exhibited, as expected, identical Tmax values, indicating that organic content of the sediments remains unaltered during the acid-treatment, under the employed in this study experimental conditions. On the contrary, a comparison of the experimentally measured S1, S2, S3 and TOC values of both sample sets reveals significant differences, which are due to the fact that they are expressed on a different weight basis. In the acid-treated samples higher values of the organic content are obtained, because although they contain the same amount of organic matter as the original ones, their RE parameters have been calculated with respect to the remaining, after acid-treatment material, which is significantly less, as data in Table 1 show.

The removal of carbonates prior to the RE analysis is a common procedure in geochemical laboratories, mainly aiming to improve the accuracy of the deternination of the produced during pyrolysis of the organic matter CO_2. The procedure, being not a "standard" one, is carried out under different experimental conditions in different Labs, resulting to a removal of inorganics in a different manner. Therefore the RE analytical data reported for acid-treated samples may differ significantly as they are calculated on a different weight basis. In our case, the carbonates content, determined as the sum of the calcite and dolomite from XRD analysis (Table 2), differs significantly (more than 20% w.) from the percentage of inorganics removal measured in the Lab. Therefore it can be concluded that during carbonates removal, other minerals are also removed probably dissolved in the acid solution. It is obvious that this fraction of the inorganic matter should depend heavily on the mineralogical composition of the samples under studied. Therefore it can be recommended that, RE data obtained from acid-treated samples should be corrected based on the mass-balance from the acid-treatment itself rather than using carbonates content from XRD or other suitable analytical technique. The corrected thereby data describe correctly the original samples.

3.2. Total Carbon Mass Balance

As reported above the original sediment samples as well as the acid-treated ones were analysed in an Elemental Analyzer and their carbon content was determined. Total carbon content (% w.)

determined by EA for original and acid-treated samples, is shown in Table 3. It is obvious that the significant difference of carbon content observed between the original and the acid-treated samples is due to the presence of carbonate minerals in the inorganic matrix of the sediments. In order to check the "correctness"' of these results a mass-balance check of the measured carbon was applied. The total carbon content in the original samples may be calculated as the sum of:

1. The carbon content measured from EA on acid-treated samples (Table 3), weighted by the percentage of mass loss during treatment (Table 1).

2. The carbon content in calcite and dolomite minerals, calculated from their molecular formula and their concentration in the original samples available from XRD analysis (Table 1).

The calculated in this way total carbon content values are shown in Table 3. These values are in good agreement with the experimentally measured from EA, with their differences exhibiting a mean relative error less than 10% w. This accuracy may be considered as satisfactory, keeping in mind the nature of the samples (sediments) and their possible non-homogeneity.

Table 2. Mineralogical composition of samples from XRD analysis (% w.).

Sample	Calcite	Chlorite	Dolomite	Gypsum	Illite1Mc	Kaolinite	Plagioclase Albite	Quartz
D_172-176	19.21	12.67	7.05	0.73	25.11	2.99	10.33	21.92
D_250-254	17.30	10.71	12.07	1.80	26.52	2.09	8.58	20.94
D_268-272	15.86	6.89	9.05	0.48	24.64	3.10	11.11	28.86
D_284-288	17.93	12.58	6.66	0.67	26.18	2.64	9.28	24.04
D_300-304	16.95	10.14	6.90	1.14	30.37	3.05	11.35	20.08
D_314-318	16.97	11.05	8.39	1.34	27.97	2.37	9.00	22.90
D_330-334	15.18	11.50	6.92	1.10	28.64	2.85	10.56	23.24
D_361-365	16.70	12.65	7.14	0.81	27.68	3.08	9.97	21.98
D_377-380	15.85	11.65	9.55	0.92	25.78	2.38	9.99	23.88
D_391-395	15.95	11.70	6.63	1.15	27.96	2.69	11.24	22.68
D_409-413	15.62	11.80	7.97	1.03	29.48	2.48	8.83	22.81
D_413-417	16.89	9.95	10.25	1.07	29.36	2.48	8.61	21.40
D_415-420	15.56	13.40	6.36	1.29	27.29	2.34	9.94	23.33
D_420-424	16.80	10.71	13.06	1.07	29.35	1.52	3.56	23.92
D_424-428	17.17	12.15	9.35	1.13	25.79	2.71	8.52	23.19
D_428-431	17.47	10.66	8.29	1.04	28.20	2.74	9.13	22.47
D_431-435	16.34	11.34	7.21	0.90	28.18	2.87	9.19	23.96
D_435-442	17.25	12.77	6.78	1.09	26.90	2.58	9.55	23.07
D_442-445	17.67	10.63	6.72	1.30	26.07	2.82	10.30	24.49
D_445-450	18.01	8.34	8.01	1.58	27.54	2.34	9.34	24.83

Table 3. Total carbon content (% w.) for the original and acid-treated samples by elemental analysis.

Sample	Original samples	Acid-treated samples	Calculated*
	Carbon content % w.		
D_172-176	3.89	0.73	3.72
D_250-254	3.70	0.78	4.27
D_268-272	4.26	0.71	3.60
D_284-288	3.92	0.78	3.57
D_300-304	3.82	0.82	3.50
D_314-318	4.10	0.95	3.79
D_330-334	3.90	0.82	3.29
D_361-365	4.21	0.76	3.44
D_377-380	3.70	0.80	3.75
D_391-395	4.10	0.92	3.38
D_409-413	3.75	0.81	3.48
D_413-417	3.97	0.82	3.98
D_415-420	3.55	0.78	3.26
D_420-424	3.90	0.80	4.36
D_424-428	3.88	0.77	3.86
D_428-431	3.82	0.80	3.76
D_431-435	3.90	0.90	3.52
D_435-442	3.79	0.78	3.52
D_442-445	4.46	0.76	3.53
D_445-450	3.90	0.77	3.76

* Corrected with respect to mass-loss during acid-treatment

3.3. Organic Carbon Mass Balance

Subsequently an attempt was undertaken to examine the consistence of the determined organic content values from the two employed analytical procedures (RE and EA). Initially the organic carbon content of the original sediment samples was calculated based on the measured, using EA, carbon of acid-treated samples corrected with respect to the percent of mass-loss during acid-treatment (Table 1). These values are shown in Table 4 (col. 1). Subsequently the organic carbon

content of the samples was calculated as the sum of the measured TOC from the RE analysis of acid-treated samples, corrected for the mass-loss during acid-treatment and of the carbon content contained in the CO_2 produced during pyrolysis (S3 peak) of the same samples. These values are shown in Table 4 (col. 2). The pronounced agreement between the organic content values calculated from the two independent methodologies verifies their accuracy.

Table 4. Organic carbon content (% w.) calculated from RE and EA methodologies.

Sample	Elemental analysis	RE analysis
	% w.	
D_172-176	0.40	0.42
D_250-254	0.44	0.37
D_268-272	0.39	0.39
D_284-288	0.46	0.35
D_300-304	0.47	0.41
D_314-318	0.54	0.57
D_330-334	0.47	0.38
D_361-365	0.41	0.44
D_377-380	0.46	0.41
D_391-395	0.51	0.54
D_409-413	0.46	0.42
D_413-417	0.47	0.42
D_415-420	0.47	0.45
D_420-424	0.46	0.46
D_424-428	0.45	0.39
D_428-431	0.46	0.45
D_431-435	0.52	0.47
D_435-442	0.47	0.51
D_442-445	0.44	0.43
D_445-450	0.44	0.41

4. Conclusions

A methodology for carbonates removal from sediment samples by acid-treatment was tested and evaluated for its performance on immature sediment samples. It was verified that except of the carbonates, a significant additional fraction of the inorganic matrix was also removed during this treatment, while organic matter content of the samples was not affected.

The total carbon content of the original sediment samples, measured by EA, found to be in agreement with the one measured as the sum of the carbon content in acid-treated samples plus the carbon contained in the carbonates minerals determined quantitatively by XRD analysis.

The organic carbon content, measured using EA on acid-treated samples, is equivalent to the one determined with Rock-Eval analysis of the same samples with the addition of the carbon content in the produced CO_2 (S3 peak).

5. Acknowledgments

This research has been co-financed by the European Union (European Social Fund – ESF) and Greek national funds through the Operational Program "Education and Lifelong Learning" of the National Strategic Reference Framework (NSRF) - Research Funding Program: THALIS –UOA- "Messinian Salinity Crisis: the greatest Mediterranean environmental perturbation and its repercussions to the biota" (70/3/11605, MIS: 375405).

6. References

Barry J.K. 1983. Limitations of 'Rock-Eval' pyrolysis for typing organic matter, *Org. Geochem*. Vol. 4. No 3-4, pp. 195-199.

Behar F., Beaumont V., Penteado H.L. and De B. 2001. Rock-Eval 6 technology: performances and developments, *Oil and Gas Science and Technology 56*, 111–134.

Espitalie J.M., Madec B., Tissot J.J., Mennig and Leplat P. 1977. Source rock characterization method for petroleum exploration, *Proceedings of the 9th Annual Offshore Technology Conference*, v.3, p. 39-448.

Lafargue E., Marquis F. and Pillot D. (1998). Rock-Eval 6 Applications in Hydrocarbon Exploration, Production and Soils Contamination Studies, *Oil & Gas Science and Technology*, 53, 4, 421-437.

Δελτίο της Ελληνικής Γεωλογικής Εταιρίας, τομ. XLVII , 2013
Πρακτικά 13ου Διεθνούς Συνεδρίου, Χανιά, Σεπτ. 2013

Bulletin of the Geological Society of Greece, vol. XLVII 2013
Proceedings of the 13th International Congress, Chania, Sept. 2013

SOURCE ROCK POTENTIAL OF THE LATE MIOCENE METOCHIA FORMATION OF GAVDOS ISLAND, GREECE

Pyliotis I.[1], Zelilidis A.[2], Pasadakis N.[3], Panagopoulos G.[1] and Manoutsoglou E.[1]

[1] Technical University of Crete, Department of Mineral Resources Engineering, Research Unit of Geology, Chania, 73100, Greece

[2] University of Patras, Department of Geology, Laboratory of Sedimentology, Patra, 26110, Greece

[3] Technical University of Crete, Department of Mineral Resources Engineering, Research Unit of Hydrocarbon Chemistry and Technology, Chania, 73100, Greece

Abstract

Rock-Eval method was used to analyze 53 samples from late Miocene Metochia Formation of Gavdos Island (south of Crete Island) in order to characterize the contained organic matter and to evaluate its potential as source rock. The samples were collected from Metochia Section which consists of about 100 m thick marls-sapropels alternations. Organic matter analysis showed that the studied succession could be subdivided into two parts. The lower one, which is generally rich in organic matter and the upper one, which is poor. In the lower part the rich horizons in organic matter are characterized by Kerogen type II, III and IV, with low oxygen content, and with fair to very good potential for gas and/or oil hydrocarbon generation. Additionally, the studied samples are thermally immature. Taking into account that the studied area has never been buried in such a depth to reach conditions of maturation, as well as, that the studied section in Gavdos is connected with Messara basin located in the northeastern and, finally, that the main part of Gavdos basin, which is situated between Gavdos and Crete islands, has continuously encountered subsidence, we could conclude that sediments of Metochia Formation could act as source rocks but in the more deep central part of the Gavdos basin.
Key words: *Neogene, Rock-eval pyrolysis, Organic matter.*

Περίληψη

Η μέθοδος πυρόλυσης Rock-Eval χρησιμοποιήθηκε για την ανάλυση 53 δειγμάτων από τον Άνω Μειοκαινικό σχηματισμό των Μετοχίων της Γαύδου (νότια της Κρήτης) ώστε να εκτιμηθεί το δυναμικό του ως μητρικό πέτρωμα υδρογονανθράκων. Τα δείγματα ελήφθησαν από την τομή Μετόχια η οποία αποτελείται από μία παχιά ακολουθία, περίπου 100 m, εναλλαγών μαργών-σαπροπηλών. Η ανάλυση του οργανικού υλικού έδειξε ότι η μελετώμενη ακολουθία θα μπορούσε να χωριστεί σε δυο μέρη. Το κατώτερο το οποίο είναι γενικά πλούσιο σε οργανικό υλικό και το ανώτερο το οποίο είναι φτωχό. Στο κατώτερο τμήμα οι πλούσιοι σε οργανικό υλικό ορίζοντες χαρακτηρίζονται από κηρογόνο τύπου II, III και IV, με χαμηλό περιεχόμενο οξυγόνο, με μέτριο έως πολύ καλό δυναμικό για την παραγωγή αέριων και υγρών υδρογονανθράκων. Ε-

πιπρόσθετα, τα μελετώμενα δείγματα είναι θερμικά ανώριμα. Λαμβάνοντας υπόψη ότι η περιοχής μελέτης δεν βρέθηκε σε τέτοιο βάθος ώστε να φτάσει σε συνθήκες ωρίμανσης, ότι η μελετώμενη τομή στην Γαύδο συνδέεται με την ΒΑ ευρισκόμενη λεκάνη της Μεσσαράς και τέλος ότι το κύριο τμήμα της λεκάνης της Γαύδου, το οποίο βρίσκεται μεταξύ Γαύδου και Κρήτης, υπέστη συνεχώς καταβύθιση, μπορούμε να υποθέσουμε ότι τα ιζήματα του σχηματισμού των Μετοχίων θα μπορούσαν να λειτουργήσουν ως μητρικά πετρώματα αλλά στο βαθύτερο κεντρικό τμήμα της λεκάνης της Γαύδου.
Λέξεις κλειδιά: *Νεογενές, Πυρόλυση Rock-Eval, Οργανικό υλικό.*

1. Introduction

This paper deals with the late Miocene sediments of Metochia Formation on Gavdos Island and their source rock potential. Metochia Formation consists of a thick sequence of marls-sapropels alternations. In general, sapropels are characterized by high (>2%) TOC (Total Organic Carbon) values. These high values of TOC make sapropels to be considered as possible source rocks for the generation of hydrocarbons. In case of Metochia Formation, TOC analysis of several sapropelic samples was carried out in order to examine the hydrocarbon generating potential. The fact that numerous biogenic gas seepages have been observed in the neighbouring Messara basin (Maravelis et al., *In Press*, Panagopoulos et al., 2011), which is located at North-Eastern of Gavdos, makes TOC-analysis campaign reasonable. More specifically, the observed seepages in Messara are connected with neogene deposits that belong to Tefelion Group (according to the classification of Meulenkamp et al. (1979)) and are time-equivalent with the neighbouring neogene deposits of Gavdos (van Hinsbergen and Meulenkamp, 2006, Zachariasse et al 2011). Additionally, the studied sediments are palaeogeographically located in the southernmost edge of Aegean landmass (Fortuin, 1978) and are dominated by Aegean terrigenous supply through a drainage system that covered the whole southern area of Aegean landmass, including Messara and Gavdos basins (Fortuin, 1978; van Hinsbergen and Meulenkamp, 2006; Köhler et al., 2010). Therefore it can be assumed that both basins constituted a single one for a specific period of time.

2. Geological Settings

Gavdos Island is located about 30km southerly of Crete Island. Both Gavdos and Crete islands are between a volcanic arc in the North and a northward subduction zone in the South, which have been created from the subsidence of the African plate below the Aegean plate.

The preneogene alpine basement of Gavdos island consists of a Maastrichtian–Danian calcareous sequence topped by Eocene flysch (Vicente, 1970), belonging to the Pindos–Ethia geotectonic zone. Towards the northeastern part of the island, a Mesozoic volcano-sedimentary series is exposed (Vicente, 1970; Seidel and Okrusch, 1978), which according to Bonneu (1984) is thrusted above the Pindos–Ethia sequence.

The neogene sediments of Gavdos Island cover about one half of its surface. Anastasakis et al (1995) subdivided these neogene deposits into two distinct Formations based on lithostratigraphic and biostratigraphic criteria.

The older one is Potamos with a lower Tortonian age (Antonarakou et al, 2007). According to van Hinsbergen and Meulenkamp (2006). Potamos Formation recorded late Serravallian subsidence, containing coral limestone unconformably overlying the pre-Neogene basement, overlain by upper Serravallian mudrocks and sapropels (Anastasakis et al., 1995), deposited at around 500-600m water depth. The mudrocks and sapropels are overlain by shallow-marine sands, reflecting latest Serravallian to earliest Tortonian uplift. Zachariasse et al. (2011) suggested that Potamos Formation is time-equivalent with the fluvio-lacustrine sediments of the Viannos Formation and/or the marine Skinias Formation in central Crete. This suggestion was based on the correlation of age

estimations that Zachariasse et al. (2011) conducted for neogene sediments of Crete with age estimations that Postma et al. (1993a) and Hilgen et al. (1995) conducted for Gavdos sediments.

According to van Hinsbergen et al (2006) (and reference therein) during late Serravallian (late Middle Miocene) an east-to west running longitudinal sedimentary system connects the river sediments of Males Formation in Ierapetra area with lacustrine sediments of Viannos Formation in central Crete and deep-marine sediments of Potamos Formation on Gavdos.

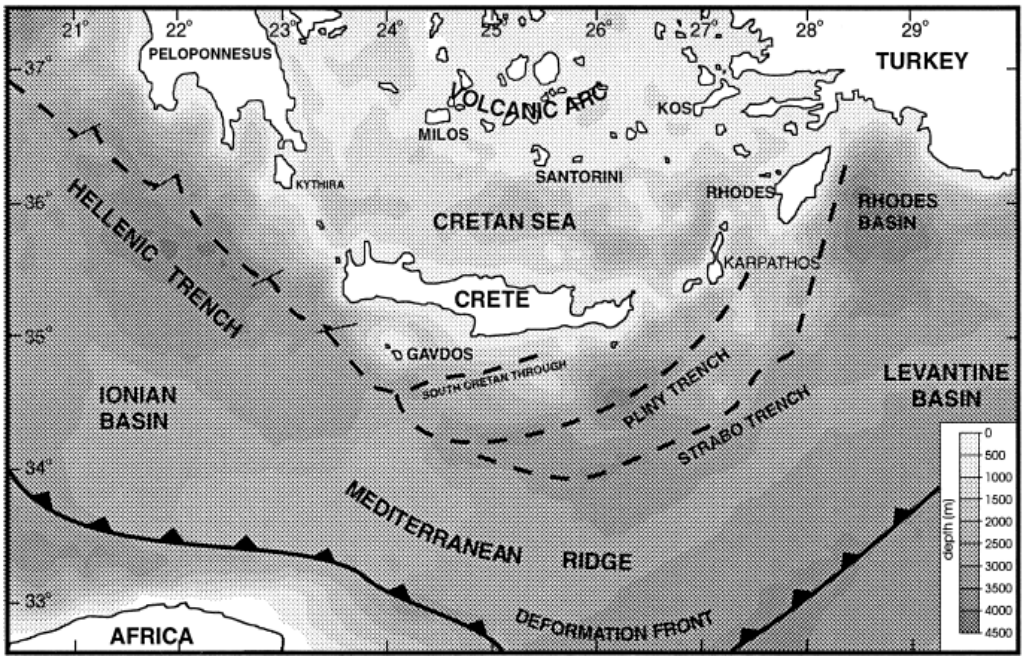

Figure 1 - Major structural features and bathymetry of the Aegean region (Duermeijer et al. 1998).

The second one is the Metochia Formation with a Tortonian-Messinian age (Postma et al., 1993a, Hilgen et al., 1995). Metochia Formation starts with a strong erosional surface over an intense angular unconformity forming on top of the alpine basement flysch beds or Potamos Formation (Anastasakis et al 1995, Drinia et al 2007). The most pronounced section of this Formation is the Metochia section, which is located in the North part of Gavdos Island. This section has a thickness more than 100m and is one of the most well studied sections in the area of Eastern Mediterranean, covering a time-span from 9.8 to 6.6 million years ago. Metochia section is composed of two subsections (Metochia B and C), which are separated by a normal fault (Krijgsman et al. 1995, Stigter 1989). These subsections are correlated on the basis of characteristic lithology patterns (Krijgsman et al. 1995).

The basal part of the Metochia section starts with a paleosol horizon, followed by estuarine sediments and shallow marine sands rich in Heterostegina, echinoderma and molluscs. These sediments are overlaid by a marls-sapropels alternations sequence which are numbered L1 to L96 (Postma et al. 1993) (or M1 to M96 according to Hilgen et al., 1995, Krijgsman et al. 1995). In the lower part of the Formation the L1-L7 marls-sapropels alternations are gradually replaced of a turbidite sequence (L8-L11). A second interval of marls-sapropels alternations overlay the turbiditic sequence. According to van Hinsbergen and Meulenkamp (2006), Metochia Formation was deposited during an episode of pronounced subsidence, with deposition of the sediment at a water depth of more than 1000 - 1200 m. Köhler et al. (2008, 2010) related a sharp decrease of the Aegean terrigenous supply being drained by fluvial systems into the Gavdos about 8,2 million years ago, with the change from paralic to marine sedimentation in central Crete at the same time.

This section is conformably overlaid by a diatomitic sequence (about 15m thick), which is covering the-time span between 6.6 and 6 million years ago (Drinia et al 2004, Gaudant et al 2005, Hilgen and Krijgsman 1999).

3. Materials and Methods

In the context of this study, sampling on Metochia B section was carried out. In Figure 2 there is the sedimentary log of Metochia B section and in Figure 3 there is a panaromic view of the sampling outcrop. Totally 53 samples were collected, among which 11 samples belong to the lower marls-sapropels alternations, 11 samples to the turbiditic sequence and 31 samples to the upper marls-sapropels alternations.

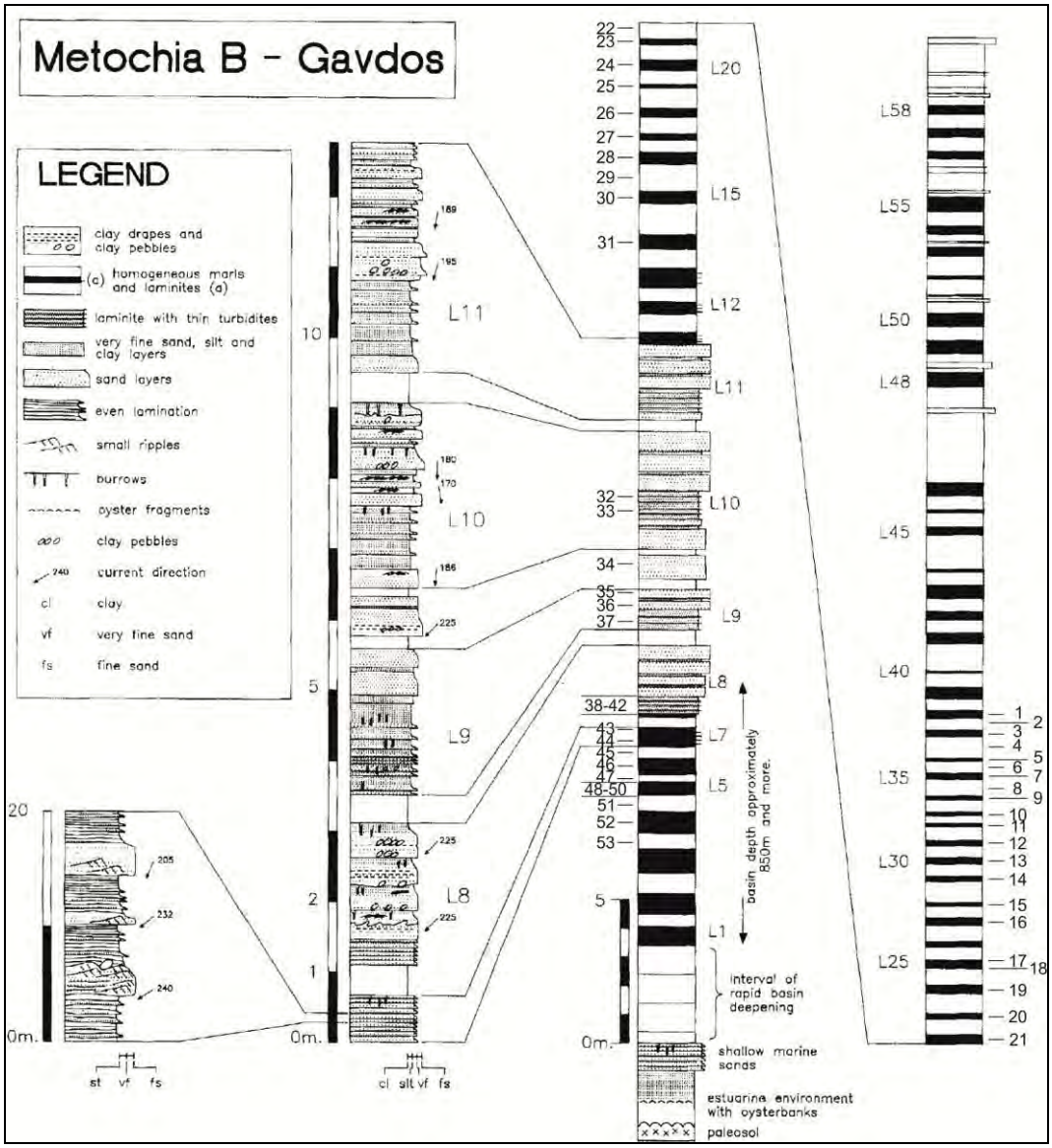

Figure 2. Sedimentary log of Metochia B section (Postma et al., 1993). Sampling horizons have been marked with numbers (1-53).

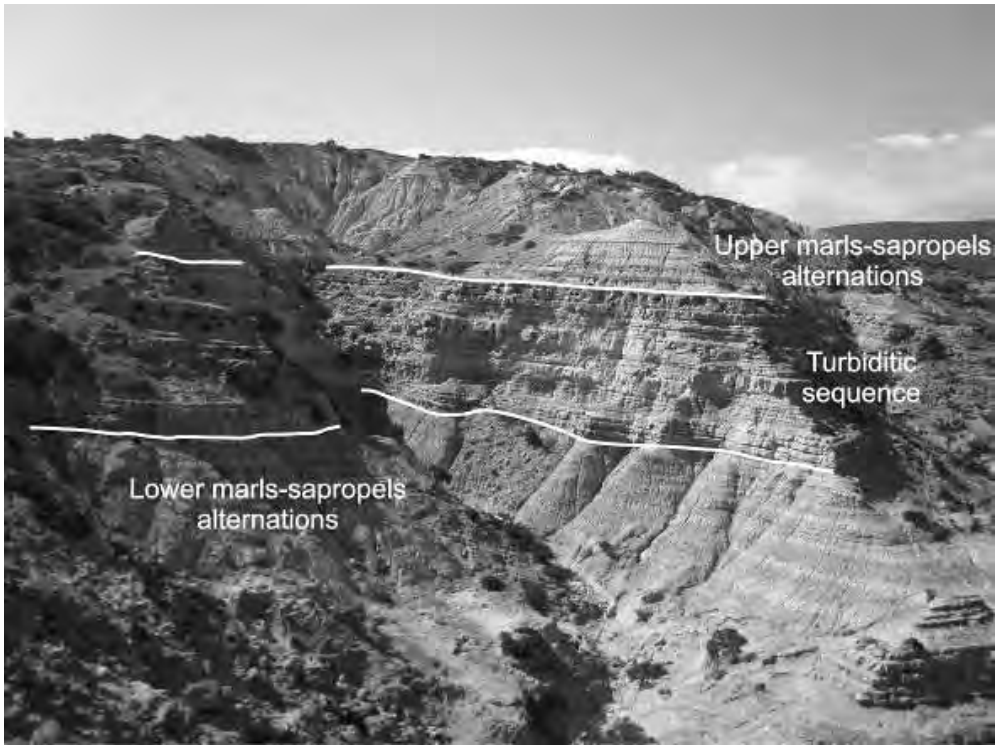

Figure 3. Panoramic view of the sampling outcrop (Metochia B section).

The samples, after being pulverized and dried at 100 oC, were analyzed in a Rock-Eval II (Delsi Inc.) analyzer following the typical experimental procedure of Espitalié et al. (1977). Each sample was heated in an inert He atmosphere for 2min at 300 oC and then pyrolyzed stepwise with increasing temperature at 600 oC with a heating rate of 25oC/min.

The measured parameters of each pyrolysis run consist of three peaks (S1, S2, and S3) and a maximum temperature value (Tmax).

- S1: the area of the S1 peak characterizes the quantity of free hydrocarbons contained in the rock sample in mg hydrocarbons/g rock.
- S2: the area of the S2 peak characterizes the quantity of hydrocarbons produced by thermal conversion of kerogen contained in the rock sample in mg hydrocarbons/g rock.
- S3: the area of the S3 peak characterizes the quantity of organic CO_2 produced during pyrolysis from the organic matter in the rock sample in mg CO_2/g rock. S3 index is an indication of the oxygen content in kerogen.
- Tmax: is the temperature which corresponds to the maximum generation of hydrocarbons from kerogen.

Additionally to these parameters during Rock-Eval pyrolysis, the total organic carbon (TOC) content of the sample is calculated from the S1, S2 and S4 peaks. The S4 peak corresponds to the CO_2 generated from the oxidation in air at 600°C of the residual carbon (after pyrolysis).

Hydrogen (HI) and Oxygen (OI) indices were calculated, using the previous parameters.

- HI: is defined as (100 x S2)/TOC. The HI is proportional to the amount of hydrogen contained within the kerogen.
- OI: is defined as (100 x S3)/100. The OI is related to the amount of oxygen contained in the kerogen.

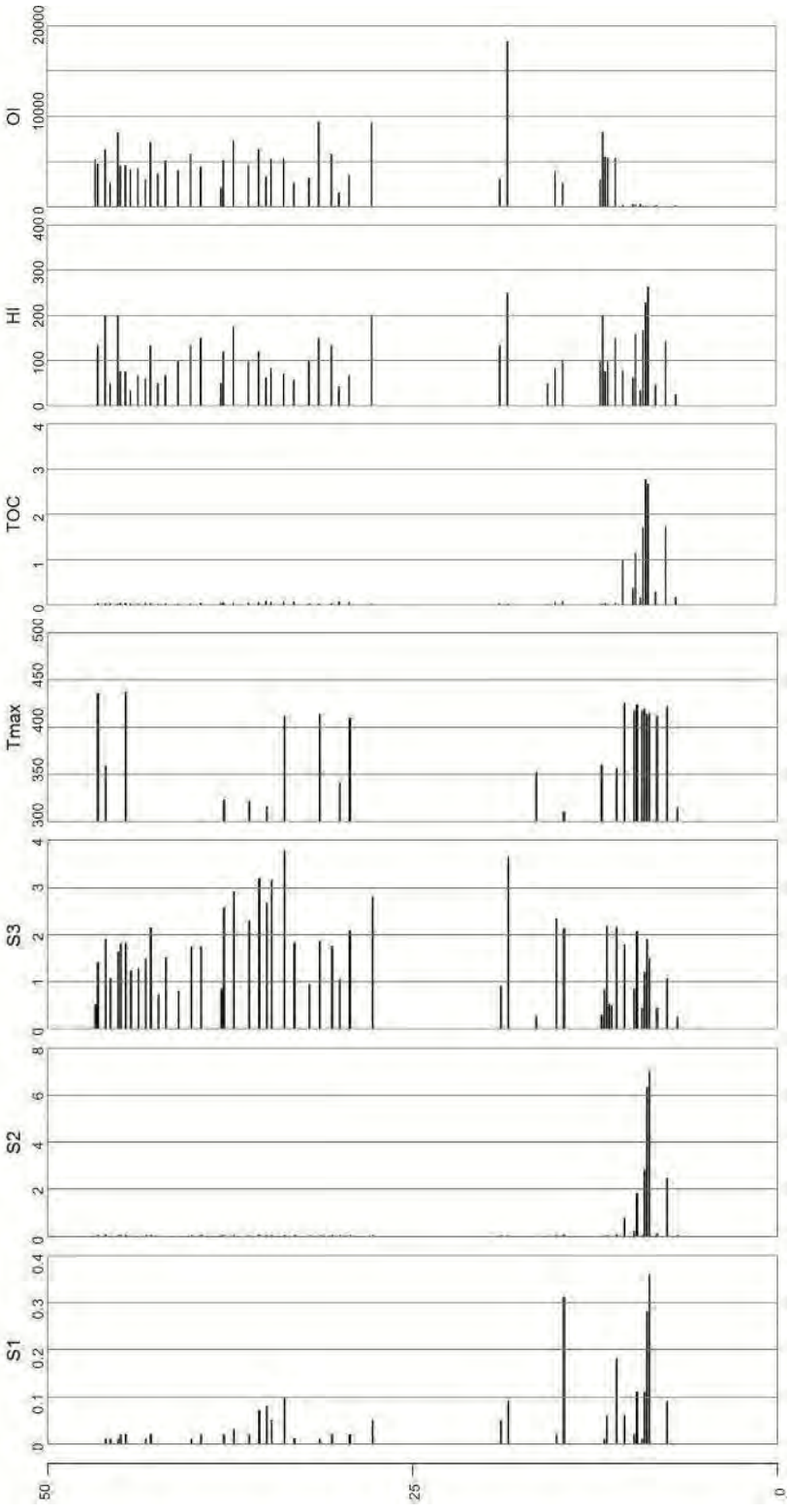

Figure 4 - Column of samples' position on the section and their corresponding S1, S2, S3, Tmax, TOC, HI and OI values.

4. Results

The experimental results of Rock-Eval pyrolysis are graphically presented at Figures 4 with respect to the sample position in the section. The interpretation of the results, regarding source rock potential is based on the study of Espitalié et al. (1977).

The S1, S2 and TOC values are higher for the lower marls-sapropels alternations compared to the ones of the turbiditic sequence and the upper marls-sapropels alternations, where they practically equal zero. The values of S1 are lower than 0.5 mg HC/g, for all samples, showing poor source rock potential. S2 values show poor source rock potential for the samples belonging the turbiditic sequence and the upper marls-sapropels alternations. The values of this index for the lower marls-sapropels alternations shows poor-to-good source rock potential. Similarly the interpretation of TOC values shows poor source rock potential for the majority of the samples, except of the samples from the lower marls-sapropels alternations, which show poor-to-very good source rock potential. S3 values are ranging between 0 and 3.78 mg CO2/g, for all the samples, indicating a kerogen with low oxygen content. In addition, Tmax values demonstrate immature organic matter.

The cross-plots of hydrogen (HI) and oxygen (OI) indices on the van Krevelen diagram as well as and HI vs Tmax diagram (Figures 5 and 6) demonstrate kerogen types III and IV. The HI vs TOC diagram (Figure 7), indicate poor oil potential but several samples show gas and oil generating potential. In these diagrams only samples from the lower marls-sapropels alternations, have been included, due to the extremely low values measured for the rest of the samples.

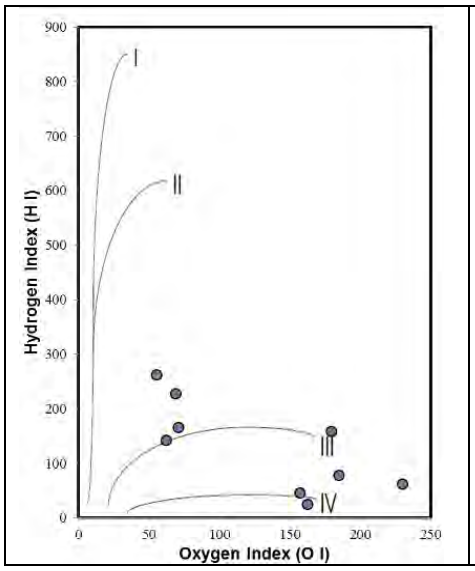

Figure 5 - Van Krevelen plot of the samples.

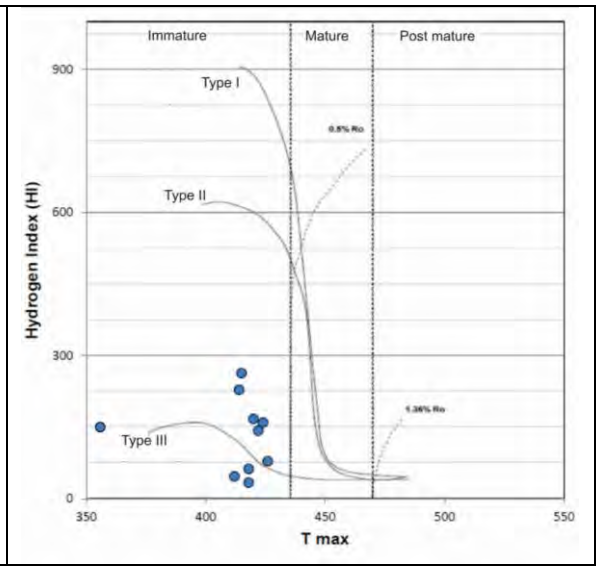

Figure 6 - Classification of the kerogen types by using Hydrogen Index vs. Tmax (°C) diagram.

5. Conclusions

The Rock-Eval pyrolysis shows that the studied succession can be subdivided into two parts. The first one corresponds to the lower marls-sapropels alternations, showing poor to very good source rock potential for gas and/or oil generation, with thermally immature organic matter. The second part corresponds both to the turbiditic sequence and the upper marls-sapropels alternations, showing poor source rock potential. Despite the low thermal maturity of the samples from the first part of the section, it could be contented that their lateral equivalents can act as potential source rocks, considering that are buried in the northern and deeper parts of Gavdos basin where maturation conditions should be more favourable.

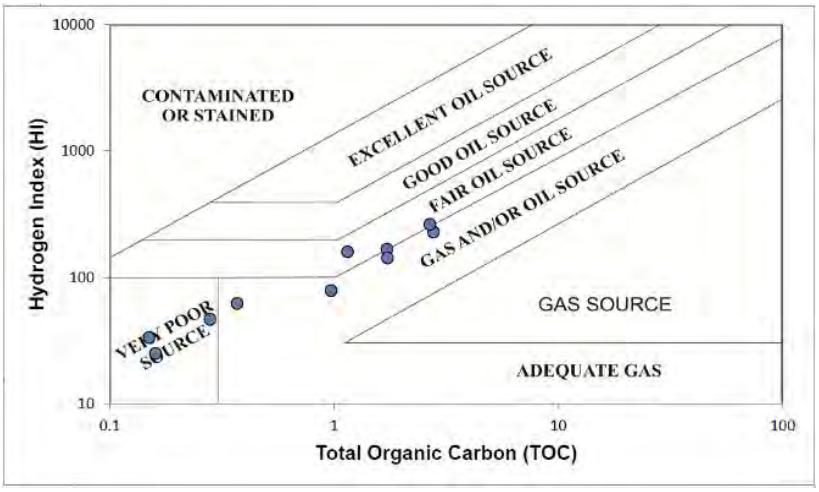

Figure 7. Hydrogen Index vs. Total Organic Carbon diagram of the samples (modified from Jackson et al., 1985).

6. Acknowledgments

This research has been co-financed by the European Union (European Social Fund – ESF) and Greek national funds through the Operational Program "Education and Lifelong Learning" of the National Strategic Reference Framework (NSRF) - Research Funding Program: THALIS –UOA- "Messinian Salinity Crisis: the greatest Mediterranean environmental perturbation and its repercussions to the biota" (70/3/11605, MIS: 375405).

7. References

Anastasakis G.C., Dermitzakis M.D. and Triantaphyllou M.V. 1995. Stratigraphic framework of the Gavdos Island Neogene sediments: *Newsl. Stratigr.* v. 32, p. 1-15.

Antonarakou A., Drinia H., Tsaparas N. and Dermitzakis M. D. 2007. Micropaleontological parameters as proxies of late Miocene surface water properties and paleoclimate in Gavdos Island, eastern Mediterranean, *Geodiversitas* 29 (3): 379-399.

Bonneau M. 1984. Correllation of the Hellenic Nappes in the south-east Aegean and their tectonic reconstruction, in Dixon, J.E., and Robertson, A.H.F., eds., The geological evolution of the eastern Mediterranean, Volume 17: *London, Geological Society of London*, p. 517-527.

Drinia H., Antonarakou A., Tsaparas N., Dermitzakis M.D. and Kontakiotis G. 2004. Foraminiferal record of environmental changes: Preevaporitic diatomaceous sediments from Gavdos island, Southern Greece, *Bulletin of the Geological Society of Greece* vol. XXXVI. p. 782-791.

Drinia H., Antonarakou A., Tsaparas N. and Kontakiotis G. 2007. Palaeoenvironmental conditions preceding the Messinian Salinity Crisis: A case study from Gavdos Island. *Geobios 40*, p. 251–265.

Duermeijer C.E., Krijgsman W., Langereis C.G. and ten Veen J.H. 1998, Post early Messinian counter-clockwise rotations on Crete: implications for the late Miocene to Recent kinematics of the southern Hellenic Arc: *Tectonophysics*, v. 298, p. 77-89.

Espitalie, J. Laport J. L., Madec M., Marquis F., Leplat P., Paulet J. and Boutefeu A., 1977. Methode rapide de characterization des roches meres de leur potential petrolier et de leur degree d' evolution, *Revue de l' Institut Francais du Petrole*, v. 1, XXXII, p. 23-42.

Gaudant J., Tsaparas N., Antonarakou A., Drinia H. and Dermitzakis M. D., 2005. The Tortonian fish fauna of Gavdos Island (Greece), *Systematic Palaeontology*, 4: 687–695.

Hilgen F.J., Krijgsman W., Langereis C.G., Lurens L.J., Santarelli A. and Zachariasse J.W. 1995. Extending the astronomical (polarity) time scale into the Miocene, *Earth Planet, Sci Lett.*, 136, 495-510.

Hilgen F.J. and Krijgsman W. 1999. Cyclostratigraphy and astrochronology of the Tripoli diatomite Formation (pre-evaporite Messinian, Sicily, Italy), Terra Nova 11, 16-22.

Jackson K.S., Hawkins P.J., Bennett A.J.R. 1985. Regional facies and geochemical evaluation of Southern Denison Trough, *APEA J*. 20, pp. 143-158.

Krijgsman W., Hilgen F.J., Langereis C.G., Lourens L.J., Santarelli A. and Zachariasse J.W., 1995. Late Miocene magnetostratigraphy, biostratigraphy and cyclostratigraphy from the Mediterranean. *Earth and Planetary Science Letters*, 136, 475-494.

Köhler C., Heslop D., Dekkers M.J., Krijgsman W., van Hinsbergen D.J.J. and von Dobeneck T., 2008. Fuzzy C-means cluster analysis on a late Miocene multiproxy data set of the eastern Mediterranean: constrains the disappearance of Crete as a sediment source, *Geochem. Geophys. Geosyst.*, p. 9.

Köhler C., Krijgsman W., van Hinsbergen D.J.J., Heslop D. and Dupont-Nivet G. (2010) Concurrent tectonic and climatic changes recorded in upper Tortonian sediments from the Eastern Mediterranean, *TerraNova*, 22, 52-63.

Maravelis A., Panagopoulos G., Pyliotis I., Pasadakis N., Manutsoglou E. and Zelilidis A. (*In press*). Source-rock potential of the Late Miocene (Tortonian-Early Messinian) sediments of the Central Crete. *Oil and Gas Science and Technology-France*.

Meulenkamp J.E. 1979. Field guide to the Neogene of Crete, Publ. *Dep. Geol. Pal. Univ. Athens*, 32, 32

Seidel E., and Okrusch M. 1978. Regional distribution of critical metamorphic minerals in Crete, in Closs H., Roeder D., and Schmidt K.E., eds., *Alps, Apennines, Hellenides*: 448-452, Schweizerbart, Stuttgart.

Stigter H. 1989. *Neogene-Recent compressional tectonics in the southern Hellenic Arc*, 34 pp., Intern. Rep. Utrecht Uni.

Postma G., Fortuin A.R. and Van Wamel W.A. 1993a. Basin-fill patterns controlled by tectonics and climate: the Neogene 'fore-arc' basins of Eastern Crete as a case history, In: *Tectonic Controls and Signatures in Sedimentary Successions* (Ed. by L.E. Frotick & R.J. Steel), pp. 335-362, International Association of Sedimentologists, Special Publications.

Postma G., Hilgen F.J. and Zachariasse W.J. 1993b. Precession-punctuated growth of a late Miocene submarine-fan lobe on Gavdos (Greece), *Terra Nova*, 5, 438-444.

Panagopoulos G., Pyliotis I., Zelilidis A., Spyridonos E., Hamdan H., Vafidis A., Manoutsoglou E., 2011. 3D modeling of biogenic gas-bearing Neogene deposits at Arkalochori region, Messara, Crete, Greece, *Proceedings of IAMG*, Saltzburg 431-440.

Van Hinsbergen D. and Meulenkamp J., 2006. Neogene supradetachment basin development on Crete (Greece) during exhumation of the South Aegean core complex, *Basin Research*, 18, 103-124.

Vicente J.C. 1970. Etude géologique de île de Gavdos (Grèce), la plus méridionale de l'Europe. *Bull. Soc. Géol. de France*, 7(12) : 481-495.

Zachariasse W.J., van Hinsbergen D.J.J. and Fortuin A.R., 2011. Formation and fragmentation of a late Miocene supradetachment basin in central Crete: implications for exhumation mechanisms of high-pressure rocks in the Aegean forearc, *Basin Research*, 23, 6, 678-701.

Δελτίο της Ελληνικής Γεωλογικής Εταιρίας, τομ. XLVII , 2013
Πρακτικά 13ου Διεθνούς Συνεδρίου, Χανιά, Σεπτ. 2013

Bulletin of the Geological Society of Greece, vol. XLVII 2013
Proceedings of the 13th International Congress, Chania, Sept. 2013

MATURITY OF DISPERSED ORGANIC MATTER IN BITUMINOUS FORMATIONS OF THE IONIAN ZONE (EPIRUS REGION, NW GREECE)

Rallakis D., Siavalas G., Oskay R.G., Tsimiklis D. and Christanis K.

University of Patras, Dept. of Geology, 265.04 Rio-Patras, Greece, rallakis@upatras.gr, christan@upatras.gr

Abstract

The main objective of this paper is to study by means of Organic Petrology techniques, the maturity of the dispersed organic matter from certain sedimentary formations of the Ionian Zone, such as the Bituminous Shale, the Upper Siliceous Vigla Formation and the Bituminous Sandstone. The samples were collected from outcropping sites located in the region of Epirus. Initially they were treated with acids (HCl-HF) to remove most of the carbonate and silicate minerals. Then a $ZnCl_2$ solution was used to concentrate the organic-rich fraction. Total Organic Carbon (TOC) content was determined applying dichromate oxidation. Polished blocks were prepared from the concentrated organic matter mounted in epoxy resin and examined under the coal-petrography microscope. Emphasis was given to maceral identification and vitrinite reflectance (R) measurements, which provide information regarding the quality and the maturity of the organic matter respectively, with implications for the petroleum generation potential regardless the level of alteration. The TOC and Rr values (4.74% and 0.68%, respectively) confirm to the oil potential of the Lower Jurassic Posidonia Shale. Nevertheless, it is suggested that detailed and higher resolution sampling focusing on the Lower Posidonia Shale, as well as organic petrography analyses coupled with Rock-Eval pyrolysis should be carried out in order to accurately determine its quality as petroleum source rocks.

Key words: *Posidonia Shale, Organic Petrology, vitrinite reflectance.*

Περίληψη

Σκοπός της εργασίας είναι η μελέτη της ωριμότητας της οργανικής ύλης ορισμένων σχηματισμών της Ιόνιας Ζώνης, όπως οι αργιλικοί σχίστες του ανώτερου και κατώτερου Ιουρασικού, ο Ανώτερος Πυριτικός Ορίζοντας της Βίγλας του Κρητιδικού και οι βιτουμενιούχοι Ψαμμίτες του Τριτογενούς, χρησιμοποιώντας τεχνικές Οργανικής Πετρολογίας. Τα δείγματα συλλέχθηκαν από επιφανειακές εμφανίσεις στην Ήπειρο. Αρχικά χρησιμοποιήθηκαν οξέα (HCl-HF) για να απομακρυνθεί το μεγαλύτερο μέρος των ανθρακικών και πυριτικών ορυκτών. Το συμπύκνωμα που προέκυψε, αναμίχθηκε με $ZnCl_2$ συγκεκριμένης πυκνότητας, ώστε να επέλθει βαρυτικός διαχωρισμός του πετρώματος σε ελαφρύ και βαρύ κλάσμα. Το οργανικό μέρος οξειδώθηκε χημικά για να υπολογιστεί η περιεκτικότητα σε Ολικό Οργανικό Άνθρακα. Στιλπνές τομές παρασκευάστηκαν με ανάμιξη του οργανικού υλικού με διάλυμα εποξικής ρητίνης και μελετήθηκαν στο ανθρακοπετρογραφικό μικροσκόπιο.

Έμφαση δόθηκε στην ανακλαστικότητα βιτρινίτη και τον προσδιορισμό των maceral. Εφαρμόστηκε επίσης περιθλασιμετρία ακτίνων Χ. Διαπιστώθηκε ότι οι αργιλικοί σχίστες του κατώτερου Ιουρασικού περιέχουν οργανική ύλη (TOC: 4,74%), ο βαθμός ωριμότητας (Rr 0,68%) της οποίας βρίσκεται εντός του παραθύρου πετρελαίου. Ωστόσο περαιτέρω έρευνα εστιασμένη στους Κατω-Ιουρασικούς αργιλικούς σχίστες με Posidonia, με τη βοήθεια της Οργανικής Πετρολογίας και της πυρόλυσης Rock-Eval είναι αναγκαία, προκειμένου να διαπιστωθεί η ποιότητά τους ως μητρικά πετρώματα υδρογονανθράκων.
Λέξεις κλειδιά: *ανακλαστικότητα βιτρινίτη, σχίστες με Posidonia, Οργανική Πετρολογία.*

1. Introduction

The Ionian geotectonic zone (Figure 1) occupies the western part of Greece; the NW part of the zone has been studied over the last forty years in search for hydrocarbons (e.g. IGRS-IFP, 1966; BP, 1971; Jenkins, 1972; Karakitsios and Rigakis, 1996; 2007; Rigakis and Karakitsios, 1998; Avramidis and Zelilidis, 2001; Avramidis et al., 2002; Karakitsios, 2003; Zelilidis et al., 2003; Kokkinou et al., 2005).

According to Karakitsios and Rigakis (1996) the organic-rich facies of the Ionian Zone are: the shale of the Triassic breccias that have entered the gas window with a TOC value up to 11.15% and a petroleum potential of 74.02 mg HC/g of rock; the Lower and Upper *Posidonia* Beds (or shale) with TOC content from 1.05-9.82% and type I and II organic matter that is highly oil-prone; and the Vigla shale with TOC values from 1.44% to 2.44% and type I, II organic matter being at an early stage of maturation.

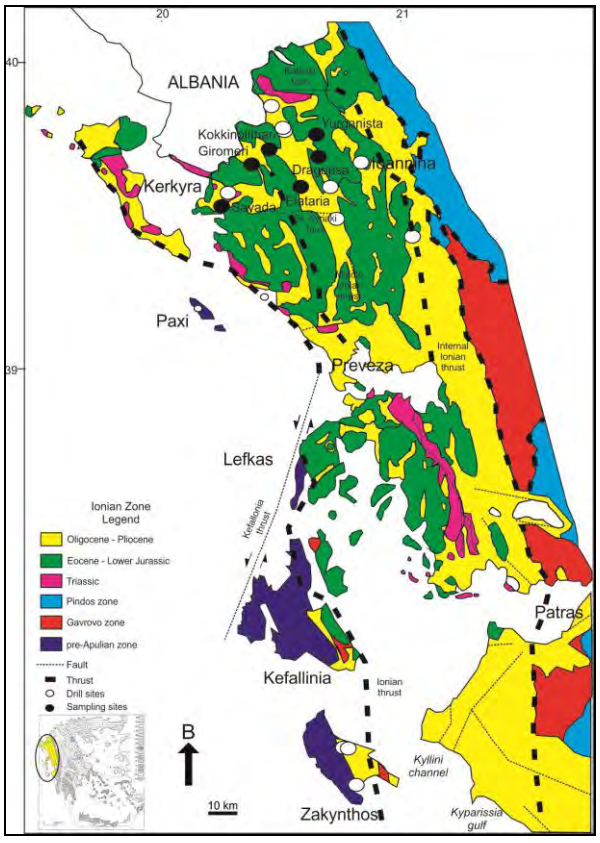

Figure 1 - Geological map of the Ionian Zone. Sampling sites are marked as black circles (after Zelilidis et al., 2003; Karakitsios and Rigakis, 2007; modified).

This study aims to provide with scientific data regarding the hydrocarbon potential of certain sedimentary formations of the Ionian Zone, by means of Organic Petrology techniques.

2. Geological Setting

Ionian Zone is part of the external Hellenides. During the early stages of formation, in Mesozoic times, the Ionian Zone was a submarine basin which separated the pre-Apulian platform in the west, from the Gavrovo Zone in the east (Figure 2). It is also divided in three sub zones, the External (pre-rift), the Axial (syn-rift) and the Internal one (post rift) that experienced significant differences into their sedimentation (Karakitsios, 2007).

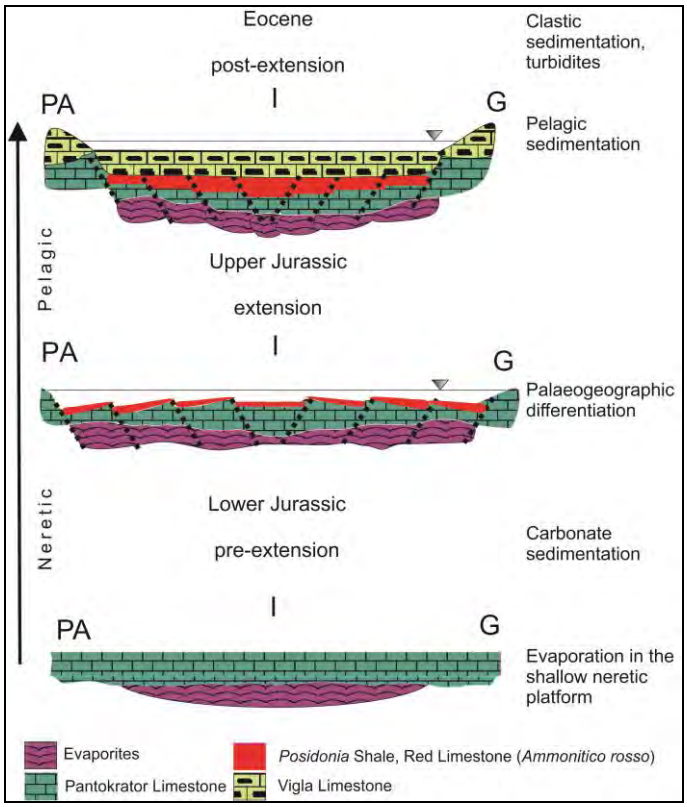

Figure 2 - Evolution of the Ionian Zone (modified after Jones and Robertson, 1991); (PA: Pre-Apulian platform, I: Ionian Zone, G: Gavrovo Zone).

From Lower Jurassic to Eocene, the sedimentation gradually changed from neretic to pelagic. In Early Triassic the excessive evaporation led to the deposition of evaporites that consistute the bedrock of the Ionian Basin (Figure 3). Later, in Lower Jurassic the sedimentation changed to carbonate-dominated (neretic) resulting in the deposition of the Pantokrator limestone. In Middle Jurassic the palaeogeographic evolution of the basin started with the deposition of the red limestone containing *Ammonitico rosso* in the shallow parts of the basin and the *Posidonia* shale in the deepest parts; the shale is distinguished into the Lower and the Upper *Posidonia* Beds corresponding to Toarcian and Callovian-Tithonian age, respectively.

In the transition from Jurassic to Cretaceous, the whole region was included in the foreland basin of Pindos Thrust and this affected the sedimentation, which gradually passed to pelagic with the deposition of the Vigla limestone. Turbidite deposits of Tertiary age overlie the Mesozoic carbonate rocks (Zelilidis et al., 2003; Karakitsios, 2007). All over the Ionian Zone, the formations containing considerable concentrations of organic matter are the following, from bottom to top:

- The shale included in the Triassic evaporites
- The marls in the basis of *Ammonitico-rosso* limestone
- The Lower and Upper *Posidonia* Beds
- The Upper Siliceous formation of Vigla
- The turbidite sandstone (flysch)

The Lower (LPB) and Upper (UPB) Jurassic *Posidonia* Beds, the Cretaceous shale and the Miocene sandstone, are the formations on which this study focuses.

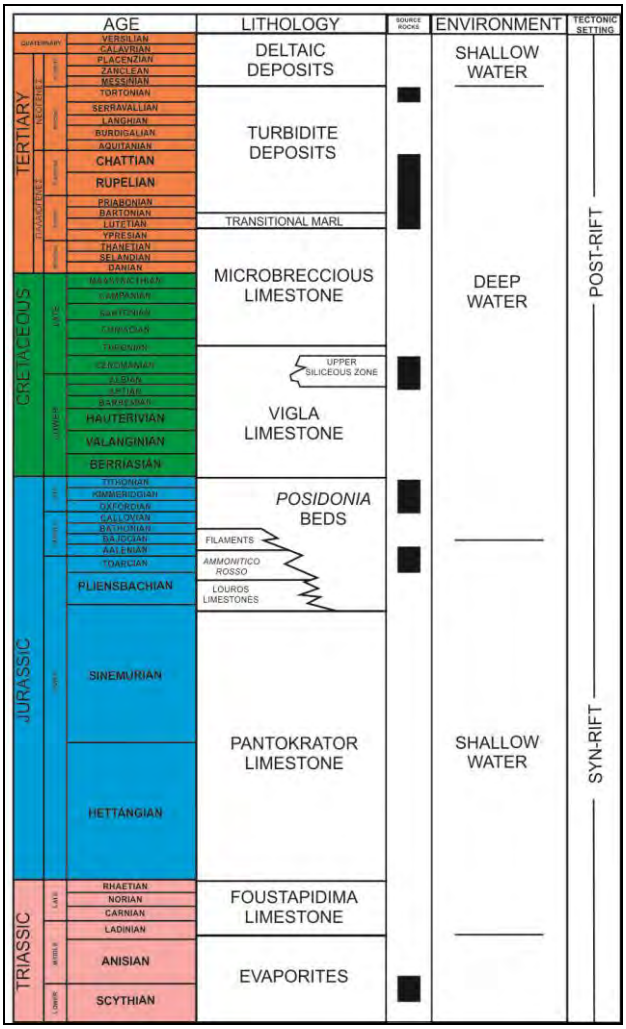

Figure 3 - Lithostratigraphical column of the Ionian Zone (Zelilidis et al., 2003, and references herein).

3. Sampling

Sampling took place in the areas of Elataria, Giromeri, Dragopsa, Kokkinolithari, Yurganista and Sayada in the region of Epirus (Figure 1). Eighteen samples in total, namely eleven from the Lower Jurassic Bituminous Shale strata, two from the Upper Jurassic Bituminous Shale strata, one from the Upper Cretaceous Upper Siliceous Vigla Formation and four from the Miocene Bituminous Sandstone, part of the Turbidite Formation, were picked up from outcrops (Table 1).

Table 1 - Coordinates of the sampling sites based on World Geodetic System (WGS 84).

Sample	Formation/Age	North (φ)	East (λ)	Altitude (m a.s.l.)
Elataria (#1)	Medium to low thickness limestone with chert nodules/Lower Jurassic	39º32'23.50"	20º32'20.5"	680.1±6.9
Elataria (#2)	Limestone with chert and bituminous shale alternations/Lower Jurassic	39º32'18.70"	20º30'14.4"	644±43.5
Giromeri (#1)	Shale poor in bitumens with chert nodules/Lower Jurassic	39º39'8.30"	20º19'11.7"	360±30
Giromeri (#2)	Shale poor in bitumens with chert alternations/Lower Jurassic	39º39'1.20"	20º19'35.3"	360±30
Dragopsa	Turbidite sandstone with organic matter/Miocene	39º35'52.2"	20º40'52.2"	674.5±11
Kokkinolithari	Shale with chert alternations in contact with limestone/Upper Jurassic	39º39'32.1"	20º23'45.3"	390±15
Yurganista	Siliceous shale/Upper Cretaceous	39º38'8.12"	20º38'6.23"	160±10
Sayada	Shale in contact with mudstone/Upper Jurassic	39º32'13.7"	20º32'10.3"	122.6±20.4

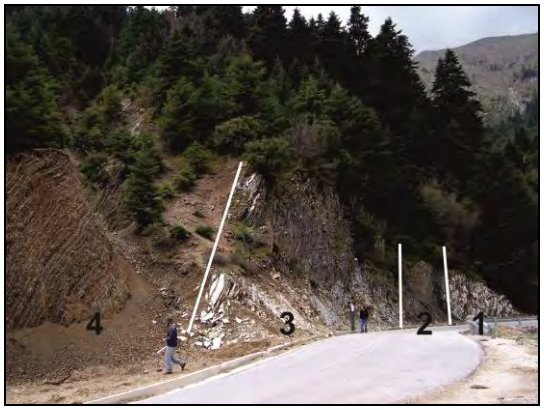

Figure 4 - The Triassic to Upper Jurassic sequence of the Ionian Zone at Elataria site: 1) Pantokrator limestone, 2) Lower *Posidonia* beds (LPB), 3) Intermediate limestone, 4) Upper *Posidonia* beds (UPB).

4. Methodology

The samples were treated firstly with an HCl (3M), then with an HF (6M) solution to remove the carbonates and the silicates, respectively. The concentrated residue was then mixed with a $ZnCl_2$ solution (1.6 g/ml) to apply density (or gravity) separation. The floating (organic-rich) substance was rinsed with deionized water and then freeze dried to remove moisture. The samples (Ø < 3 mm) were then mounted in epoxy resin. Polished blocks were prepared according to ISO 7404-2 (2009). Organic Petrography techniques including random vitrinite reflectance (Rr) measurement and maceral identification, under white incident light and blue-light excitation, were applied on the polished blocks. A Leica DMRX coal-petrography microscope with oil immersion lens, in a total magnification of 500x, was used. The vitrinite reflectance measurement was conducted following ISO 7404-5 (2009). Theoretically, a hundred measurements should be taken on huminite/vitrinite in each polished block (Ø 3 cm), but a satisfactory mean average can also be achieved with less

measurements depending on the organic matter content of the studied sample. The maceral classification was based on the ICCP (1971, 2001) & Sýkorová et al. (2007) nomenclature.

Total Organic Carbon (TOC) content was determined by oxidizing the organic part (Jackson, 1958). This method is based on the oxidation of organic matter with a potassium dichromate/sulphuric acid solution and the calculation of organic carbon through the determination of dichromate excess in the solution. Thus, a wide range of organic forms except for the highly refractory fraction can be oxidized. The TOC values are calculated according to a formula based on the Walkey-Black method (Nelson and Sommers, 1996). Although the actual organic carbon of these samples may have been slightly underestimated, the results could be considered reliable. For verification purposes automatic elemental analysis (AEA) has been applied on several samples, using a CHNS (EAGER 200) Carlo Erba Elemental Analyser calibrated against CP1 material (ASTM D5373, 2004). Loss on Ignition (LOI at 550ºC for 4 h) was applied to estimate the organic matter content under ASTM (D 3174-2004) standards.

The mineralogical composition of the shale samples was determined applying X-ray diffraction on whole rock samples. A Bruker D8 X-ray diffractometer equipped with a LynxEye® detector was used for the mineralogical analyses. The mineral phases in the diffractograms were identified using EVA software.

5. Results and Discussion

It must be stated that the results should only be considered preliminary and adequate to qualify areas for further research, since they were obtained from outcrop samples, which have been affected by weathering; however, vitrinite reflectance can be considered a reliable measure of organic matter maturity even in the case of outcrop samples provided that the external highly weathered part is removed prior sampling. The outcrops are of a limited extent and contain chert intercalations, complicating laboratory tests. In more detail some of the outcrops sampled are as follows:

Elataria: Medium-bedded limestone with chert nodules. Thickness of the bituminous shale formation is approximately 1 m, with alternations of non-bituminous shale. The limestone strata display medium to small thickness with chert intercalations thicker than 5 m (Figure 4, 5a).

Girομeri: Lower bituminous shale intercalated with limestone and chert nodules (Figure 5b).

Sayada: Upper shale mixed with silt material. The total thickness of the target formation is approximately 30 cm (Figure 5c).

Yurganista: Poor in bitumens shale alternating with limestone (Figure 5d).

Figure 5 - The outcrops at the sampling sites: (a, b) Lower *Posidonia* Shale at Elataria and Girομeri, respectively, (c) Upper *Posidonia* Shale at Sayada, (d) Upper Siliceous Vigla Formation at Yurganista.

The Elataria and (to a lesser extent) the Giromeri samples contain significant quantities of TOC reaching up to 4.75%. All other samples display very low contents.

The Rr of the Lower Shale in the studied area of Elataria ranges between 0.5 and 0.7%, corresponding to a maturation stage within the oil window (Taylor et al., 1998). The liquid hydrocarbon generation commences at a Rr 0.5-0.6%. Nevertheless the important build up begins between 0.6 and 0.85% and cannot exceed 1.8% for kerogen type III source rocks (Petersen, 2002). The organic matter in the rest of the samples appears rather immature displaying Rr < 0.5%, i.e. out of the oil window, and in some cases (e.g. at Kokkinolithari; 0.15% Rr) equivalent to recent organic matter.

Amorphous organic matter (particulate organic components that appear structureless at the scale of light microscopy; Mendonça Filho et al., 2011) was dominant in all the studied samples. Macerals of the vitrinite, liptinite and inertinite groups are also present. The liptinite group includes typical macerals of kerogen types I and II. Kerogen type I derives from green and blue algae that sustain in reductive environments whereas type II originates from natural wax, lipids and plant resins. In general, the samples are poor in vitrinite. The dispersed organic matter in type I and II rocks is capable of yielding liquid and gas hydrocarbons (Tissot and Welte, 1984). Figure 6 displays some abundant types of organic matter contained in the studied samples.

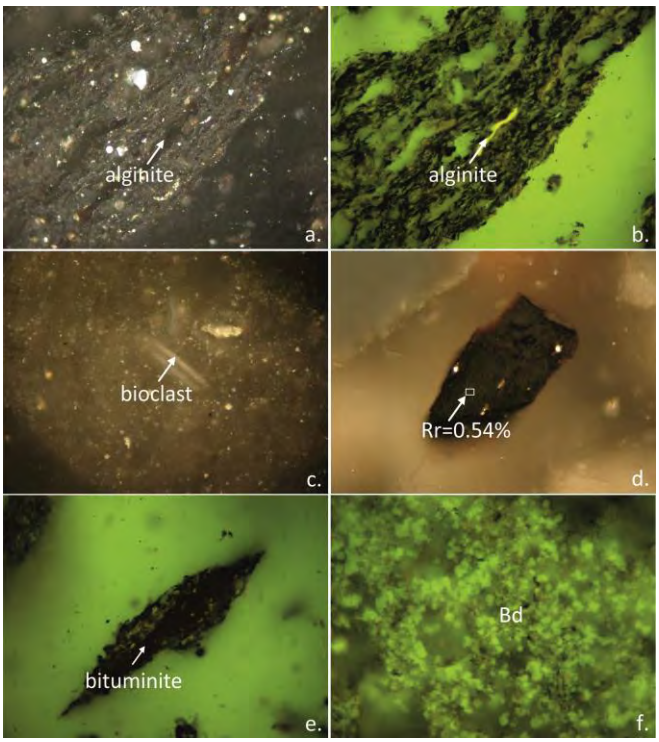

Figure 6 - Photomicrographs taken under oil-immersion, magnification 500X, photograph width is 265 µm: a, b. Alginite under white light (a) and blue light excitation (b), c. Bioclast, d. Vitrinite under white incident light, e. Bituminite under blue light excitation, f. Bitumen drops under blue light excitation.

Table 2 displays the results of the detailed characterization of the samples. The Elataria samples display the highest TOC and LOI values, whereas the reflectance falls close (0.49%) or within (0.68%) the oil window. The Dragopsa sandstone samples contain two different varieties of macerals appropriate for reflectance measurements, one displaying Rr ~0.29% (huminite) and another one ~0.90% (vitrinite). According to Avramidis et al. (2002) the submarine fans have the potential to yield hydrocarbons. This is in agreement with the high vitrinite content of the Dragopsa sample, typical for kerogen type III being gas-prone.

Table 2 - Total organic carbon and elemental carbon contents, loss on ignition and mean random vitrinite reflectance (*: sandstone sample, **: no vitrinite, L: Liptinite, V: Vitrinite, I: Inertinite; Characterization after Tyson, 1989, 1995).

Sample	TOC (%)	C (%)	LOI (%)	Mean Rr%	Maceral groups	Characterization
Elataria (#1)	2.87	3.69	8.79	0.49	L>V>I	Excellent source potential
Elataria (#2)	4.75		11.38	0.68		Modal range for marine 'black shale' source rocks
Giromeri (#1)	0.92	0.39	2.44	0.40		'Fair' source potential
Giromeri (#2)	0.25		3.02	0.31		'Poor' source potential Deep-sea facies
Sayada	0.46	0.59	3.65	**	I>V>L	'Poor' source potential
Kokkinolithari	0.30	0.16	0.79	0.15		'Poor' source potential
Yurganista	0.28	0.31	4.47	0.26		'Poor' source potential Deep-sea facies
Dragopsa*	0.34	1.43	7.31	0.29/0.90	V>I>L	Industry limit for carbonate source rocks

The qualitative mineralogical composition of the studied samples is presented in Table 3. Elataria #1 & 2 and Giromeri #1 & 2 samples are merged due to similar mineralogical composition. Quartz is the major component. Chlorite, albite, calcite, chrysotile and montmorillonite were also identified. The mineralogical composition is used here as a supplementary tool, in order to better interpret the results from TOC determination and LOI. Calcite is present at low concentration in four samples and lacks from the rest. Thus total carbon values, especially for both Elataria samples, can be considered to be equal to TOC. Additionally, the presence of hydroxyl-bearing minerals (chrysotile, chlorite, montmorillonite) indicates that LOI overestimates the actual organic matter content. For this reason the ratio between TOC and LOI is higher than 2 being typical for sedimentary organic matter (Schumacher, 2002).

Table 3 - Mineralogical composition of the samples (M: Major, m: Minor, t: Trace)

Sample	Quartz	Chlorite	Albite	Calcite	K-Feldspar	Chrysotile	Clay
Elataria	M			t			m
Giromeri	M			m			m
Dragopsa	M	m	m	M	t	m	
Kokkinolithari	M						
Yurganista	M						m
Sayada	M	m	m	m			m

In order to evaluate the source-rock potential, the TOC and Rr values (Table 2) were plotted on the diagram of Figure 7. Only the Elataria samples are promising to have acted as petroleum source-rocks. All other samples display a relatively immature stage of diagenesis and despite the adequate organic matter type and content (e.g. the Giromeri samples) cannot be characterized as good source rocks.

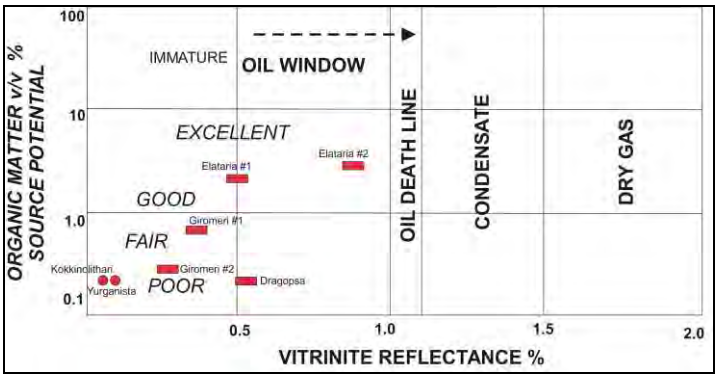

Figure 7 - Source potential to maturation scheme (after Cook, 2011).

6. Conclusion

The Lower Jurassic *Posidonia* shale (e.g. at Elataria sampling site) seems to have the potential to generate hydrocarbons. In general, the abundance of liptinite group macerals (alginite, sporinite) is typical for kerogen types I and II being highly oil prone. The vitrinite reflectance values in addition to the high TOC content set the samples within the oil window. Of course, detailed and higher resolution sampling focusing on the Lower *Posidonia* Shale, as well as organic petrography analyses coupled with Rock-Eval pyrolysis should be carried out in order to accurately determine its quality as petroleum source rocks.

7. Acknowledgements

The authors would like to thank Dr. Konstantina Katsanou for her field work assistance, as well as Dr. Paraskevi Lamprpoulou for the X-Ray Diffraction analyses, Mr. Panagiotis Mpalasis (all from Dept. of Geology, Univ. of Patras) for polishing the blocks. Mr. Dimitrios Vachliotis (Lab of Instrumental Analyses, Faculty of Sciences, Univ. of Patras) is thanked for the elementary analyses.

8. References

American Society for Testing and Materials (ASTM) D3174, 2004. Standard method for ash in the analysis sample of coal and coke from coal. In: *2004 Annual Book of ASTM Standards, Gaseous Fuels, Coal and Coke*, American Society for Testing and Materials, PA, Philadelphia, Vol. 05.06, pp. 322-326.

American Society for Testing and Materials (ASTM) D5373, 2004. Standard test methods for instrumental determination of carbon, hydrogen and nitrogen in laboratory samples of coal and coke. In: *2004 Annual Book of ASTM Standards, Gaseous Fuels; Coal and Coke*, vol. 05.06., ASTM, Philadelphia, PA, pp. 504-507.

Avramidis P. and Zelilidis A. 2001. The nature of deep-marine sedimentation and palaeocurrent trends as an evidence of Pindos foreland basin fill conditions, *Episodes*, 24(4), 252-256.

Avramidis P., Zelilidis A., Vakalas I. and Kontopoulos N. 2002. Interactions between tectonic activity and eustatic sea-level changes in the Pindos and Mesohellenic basins, NW Greece: Basin evolution and hydrocarbon potential, *J. Petrol. Geol.*, 25(1), 53-82.

British Petroleum Company Limited (BP) 1971. The geological results of petroleum exploration in western Greece, *Inst. Geol. Subs. Res*., Athens, 10, 1-73.

Cook A. 2011. The Role of Organic Petrology in Oil and Gas Exploration, *ICCP Training Course on Dispersed Organic Matter*, pp. 119-126.

Institut de Géologie et Recherches du Sous-Sol, Institut Français du Pétrole (IGRS-IFP), 1966. Étude Géologique de l'Épire, *Ministére de l'Industrie*, Athénes, 306 pp.

International Committee for Coal Petrology (ICCP) 1971, *International Handbook of Coal Petrography*, 1st suppl. to 2nd edn. Centre National de la Recherche Scientifique, Paris.
International Committee for Coal and Organic Petrology (ICCP) 2001. The new inertinite classification (ICCP System 1994), *Fuel*, 80, 459-471.
International Organization for Standardization (ISO) 7404-2 2009. Methods for the Petrographic Analysis of Coals - Part 2*: Methods of Preparing Coal Samples,* International Organization for Standardization, Geneva, Switzerland, 12 pp.
International Organization for Standardization (ISO) 7404-5, 2009. Methods for the Petrographic Analysis of Coal - Part 5: *Methods of Determining Microscopically the Reflectance of Vitrinite*, International Organization for Standardization, Geneva, Switzerland, 14 pp.
Jackson M.L. 1958. *Soil Chemical Analysis*, Prentice-Hall Inc., Englewood Cliffs, NJ.
Jenkins D.A.L. 1972. Structural development of western Greece, *AAPG Bulletin*, 56, 128-149.
Jones G. and Robertson A.H.F. 1991. Tectonostratigraphy and evolution of the Mesozoic Pindos ophiolite and related units, northwestern Greece, *J. Geol. Soc.of London*, 148, 267-288.
Karakitsios V. 2003. Evolution and Petroleum Potential of the Ionian Basin (Northwest Greece), *AAPG International Conference*, (September 21-24, Barcelona, Spain), 7 pp.
Karakitsios V. 2007. Studying the carbonates from Triassic to Eocene in the Ionian Zone, *25th IAS Meeting of Sedimentology*, 2007, Patras-Greece, Field Trips Guide Book, p.123-142.
Karakitsios V. and Rigakis N. 1996. New oil source rocks in Greek Ionian basin, *Oil and Gas J.*, 12, 56-59.
Karakitsios V. and Rigakis N. 2007. Evolution and petroleum potential of western Greece, *J. Petrol. Geol.*, 30(3), 197-218.
Kokkinou E., Kamberis E., Vafidis A., Monopolis D., Ananiadis, G. and Zelilidis A. 2005. Deep seismic reflection data from offshore western Greece: a new crystal model for the Ionian Sea, *J. Petrol. Geol*., 28, 81-98.
Mendonça Filho J.G., Menezes T.R. and Mendonça J.O. 2011. Organic Composition (Palynofacies Analysis), *ICCP Training Course on Dispersed Organic Matter*, pp. 33-81.
Nelson D.W. and Sommers L.E. 1996. Total carbon, organic carbon and organic matter. In: *Methods of soil analysis part3: Chemical methods*, Sparks D.L., Page A.L., Helmke P.A., Loeppert R.H., Soluanpour P.N., Tabatabai M.A., Johnston C.T., Sumner M.E. (Eds), Soil Science Society of America, Inc. and American Society of Agronomy, Inc., Madison, Wisconsin, USA. pp. 961-1010.
Petersen H.I. 2002. A re-consideration of the 'Oil Window' for humic coals and kerogen type III source rocks, *J. Petrol. Geol.*, 25(4), 407-432.
Rigakis N. and Karakitsios V. 1998. The source rock horizons of the Ionian Basin (NW Greece), *Marine Petrol. Geol.,* 15, 593-617.
Schumacher B.A. 2002. Methods for the Determination of Total Organic Carbon (TOC) in Soils and Sediments, United States Environmental Protection Agency, *NCEA-C-1282*, 23 pp.
Sýkorová I., Pickel W., Christanis K., Wolf M., Taylor G.H. and Flores D. 2005. Classification of huminite – ICCP System 1994, *Int. J. Coal Geol*., 62, 85-106.
Taylor G.H., Teichmüller M., Davis A., Diessel C.F.K., Littke R. and Robert P. 1998. *Organic Petrology,* Gebrüder Borntraeger, Berlin, Stuttgart, 704 pp.
Tissot B.P. and Welte D.H. 1984. *Petroleum Formation and Occurrence*, 699 pp.
Tyson R.V. 1989. Late Jurassic palynofacies trends, Piper and Kimmmeridge Clay Formations, UK onshore and northern North Sea. In: *Northwest European Micropalaeontology and Palynology*, Batter, D.J., Keen, M.C. (Eds), The British Micropalaeontological Society Series, Ellis Horwood, Chichester, pp. 135-172.
Tyson R.V. 1995. *Sedimentary Organic Matter. Organic facies and palynofacies,* Chapman and Hall, London, 615 pp.
Zelilidis A., Piper D.J.W., Vakalas I., Avramidis P. and Getsos K. 2003. Oil and gas plays in Albania: Do equivalent plays exist in Greece?, *J. Petrol. Geol*., 26(1), 29-48.

Δελτίο της Ελληνικής Γεωλογικής Εταιρίας, τομ. XLVII , 2013
Πρακτικά 13ου Διεθνούς Συνεδρίου, Χανιά, Σεπτ. 2013

Bulletin of the Geological Society of Greece, vol. XLVII 2013
Proceedings of the 13th International Congress, Chania, Sept. 2013

ENVIRONMENTAL MAGNETISM: APPLICATION TO CAVE SEDIMENTS

Aidona E.[1], Pechlivanidou S.[2] and Pennos Ch.[2]

[1] *Department of Geophysics, School of Geology, Aristotle University of Thessaloniki, 54124 Thessaloniki - Greece, aidona@geo.auth.gr*

[2]*Department of Physical Geology, School of Geology, Aristotle University of Thessaloniki, 54124 Thessaloniki – Greece sophiap@geo.auth.gr, pennos@geo.auth.gr*

Abstract

Environmental magnetism techniques allow a rapid, low cost and sensitive characterization of sediments and can be applied in a wide range of environments. More specific, magnetic properties can be successfully used to reconstruct paleoenvironmental and paleoclimatic conditions in rockshelter and cave sites. Cave sediments, imprint the environmental conditions at the Earth's surface at the time of deposition since are well protected both at the interior and at the entrance of the cave systems. In addition, many cultural sequences and archaeological artifacts are well preserved in rockshelter and cave sediment records and can be effectively used for paleoenvironmental interpretations. In this study we present data from two different cave sites from Northern Greece. In the first cave (Maronia Cave) magnetic measurements were performed in two cores 80 and 90 cm, respectively, located inside the cave area. High values of magnetic susceptibility are directly linked with the human activity inside the cave, while lower values show deposition under infiltration and fluvial processes. In the second cave (Mikro Eptamilon Cave), magnetic susceptibility and frequency dependent magnetic susceptibility depicted from a sedimentary sequence with a thickness of 200 cm, located in the entrance of the cave. Results lead to conclusions concerning the velocity of the paleo-flow likely related to the paleoclimatic conditions that dominated the broader area.

Key words: *Magnetic susceptibility, human activity, paleoenvironmental conditions, N. Greece.*

Περίληψη

Οι τεχνικές του περιβαλλοντικού μαγνητισμού επιτρέπουν έναν γρήγορο, χαμηλού κόστους και ευαίσθητο χαρακτηρισμό των ιζημάτων και μπορούν να χρησιμοποιηθούν σε διαφορετικά περιβάλλοντα. Πιο συγκεκριμένα, οι μαγνητικές ιδιότητες μπορούν με επιτυχία να χρησιμοποιηθούν για την ανακατασκευή των παλαιοπεριβαλλοντικών και παλαιοκλιματικών συνθηκών σε βραχοσκεπές και σπήλαια. Τα ιζήματα των σπηλαίων αποτυπώνουν τις περιβαλλοντικές συνθήκες που επικρατούσαν στην επιφάνεια της Γης κατά την απόθεσή τους λόγω του προστατευμένου χώρου που βρίσκονται είτε στο εσωτερικό είτε στην είσοδο των σπηλαίων. Επιπρόσθετα, αρκετά αρχαιολογικά ευρήματα είναι καλά προστατευμένα στις βραχοσκεπές και στα ιζήματα των σπηλαίων βοηθώντας μας έτσι αποτελεσματικά στις παλαιοπεριβαλλοντικές ερμηνείες. Στην παρούσα μελέτη παρουσιάζονται δεδομένα από δύο διαφορετικά σπήλαια της Β. Ελλά-

δας. Στο πρώτο (Σπήλαιο Μαρώνειας) πραγματοποιήθηκαν μετρήσεις μαγνητικές επιδεκτικότητας σε δύο πυρήνες 80 και 90 εκ. αντίστοιχα μέσα από το σπήλαιο. Υψηλές τιμές της επιδεκτικότητας συνδέονται με την ανθρώπινη δραστηριότητα μέσα στο σπήλαιο, ενώ οι χαμηλές υποδεικνύουν την απόθεση των ιζημάτων από ποτάμιες διεργασίες. Στο δεύτερο (Μικρό Σπήλαιο Επταμύλων) μετρήθηκε η μαγνητική επιδεκτικότητα και το ποσοστό της εξαρτώμενης από τη συχνότητα επιδεκτικότητα σε μία ιζηματογενή σειρά με πάχος ~ 200 εκ., που βρίσκεται στην είσοδο του σπηλαίου. Τα αποτελέσματα οδηγούν σε συμπεράσματα σχετικά με την ταχύτητα της παλαιοροής που πιθανώς συνδέεται με τις παλαιοκλιματικές συνθήκες που επικρατούσαν στην ευρύτερη περιοχή.
Λέξεις κλειδιά: *Μαγνητική επιδεκτικότητα, ανθρώπινη δραστηριότητα, παλαιοπεριβάλλον, Β. Ελλάδα.*

1. Introduction

During the last decades, environmental magnetism methods have been utilized into a wide range of environments to provide a fast, low cost and sensitive characterization of sediments (Thompson and Oldfield, 1986; Evans and Heller, 2003). Iron-containing minerals are extremely sensitive to environmental processes occurring on Earth's surface and therefore mineral magnetic measurements have been widely applied to assess past environmental changes. Paleoclimatic/environmental alterations have been well documented from lake sediments (e.g. Paasche et al, 2004), loess (e.g. Verosub et al., 1993), marine deposits (e.g. Yang et al., 2008; Aidona and Liritzis, 2012) and archaeological sediments (Aidona et al., 2001; Tsatskin and Nadel 2003), based on mineral magnetic properties.

Furthermore, environmental magnetism techniques have been successfully used in cave sites to detect both past environmental conditions and human imprints. Caves as well as rockshelters act as important sediment traps that record paleoenvironmental conditions, since are well protected environments (Collcutt 1979; Karkanas 2001; Woodward & Goldberg, 2001). Moreover, karstic sites were attractive locations for human activity, preserving many cultural sequences and archaeological artifacts. Magnetic studies on sedimentary sequences mainly found at the entrance of cave systems depict the environmental signal of these sediments; Ellwood et al. (1996, 2004) and Sroubek et al. (2001, 2007) performed paleoclimatic reconstructions from mineral magnetic measurements (magnetic susceptibility and remanence parameters), obtained on clastic sediments deposited into the entrance of caves in the Mediterranean region. Also, magnetic properties have been applied as anthropogenic indicators related to burning activities (e.g. Woodward 1997).

In this study, the suitability of the magnetic susceptibility to record paleoenvironmental conditions on cave deposits is tested in two cave sites from northern Greece, the Maronia Cave and the Mikro Eptamilon Cave. The two karstic sites differ in terms of past human activity; the Maronia Cave is a well known archaeological site in contrast to the Mikro Eptamilon Cave where no archaeological remains were found. Magnetic susceptibility was measured on sediment samples in order to depict both the natural and anthropogenic signal of the cave deposits.

2. Study Area

2.1. Maronia Cave

The Maronia Cave is located at the Koufoplati hill (3 km NW of the Maronia village) (Figure 1). It has an elongated shape in N - W direction, with a total length of 350 m and width ranging from 15 m to 50 m. The main entrance of the cave is located 150 m above mean sea level (Figure 2a). The Maronia Cave developed in a relatively thin layer of eroded Nummulitic limestones of Middle Eocene age (Melfos et al., 2005; Pavlides et al., 2008). The limestones are strongly fissured and fractured, slightly inclined towards the west and contain several species of fossilized foraminifera,

algae, corals, sea urchins, bivalves and bryozoan (Vaxevanopoulos and Melfos, 2010). Detailed study of the cave based on the morphological features and microthermometric analyses on calcite spars documents that the speleogenetic processes are closely related with thermal ascending fluids (Vaxevanopoulos & Melfos, 2010). Epigenetic processes resulting to sediment accumulation control the subsequent evolution of the Maronia Cave.

During the last six years, numerous findings from the Maronia Cave have been excavated from the Ephorate of Paleoanthropology and Speleology of Northern Greece. The excavation of new profiles in the entrance of the cave brought to light important data concerning the use of the cave during the prehistoric and historic years. Traces of the oldest habitation are dating this phase back to early copper age II. After a long period with no evident anthropogenic use of the cave, the second occupation phase is observed, dating to the 7th century A.D. Another big gap occurred in the following centuries ending up with the last habitation level in the end of the 12th beginning of the 13th century A.D. (Panti and Miteletsis, 2008).

2.2. Mikro Eptamilon Cave

The Mikro Eptamilon Cave is located at the foothills of the southern-eastern part of Mount Menikio (Serres Prefecture, northern Greece) (Figure 1) and belongs to a broader cave complex that is developed in Paleozoic marbles. The cave consists of lenticular in cross section corridors following the strata of the marbles that suggest the epi-phreatic origin of the cave. At the entrance of the Mikro Eptamilon Cave, which revealed during the works of marble exploitation in 1965, a naturally deposited sequence of clastic sediments alternating with chemical deposits approximately 200 cm thick, is lying uncomfortably on the bedrock marbles (Figure 2b).

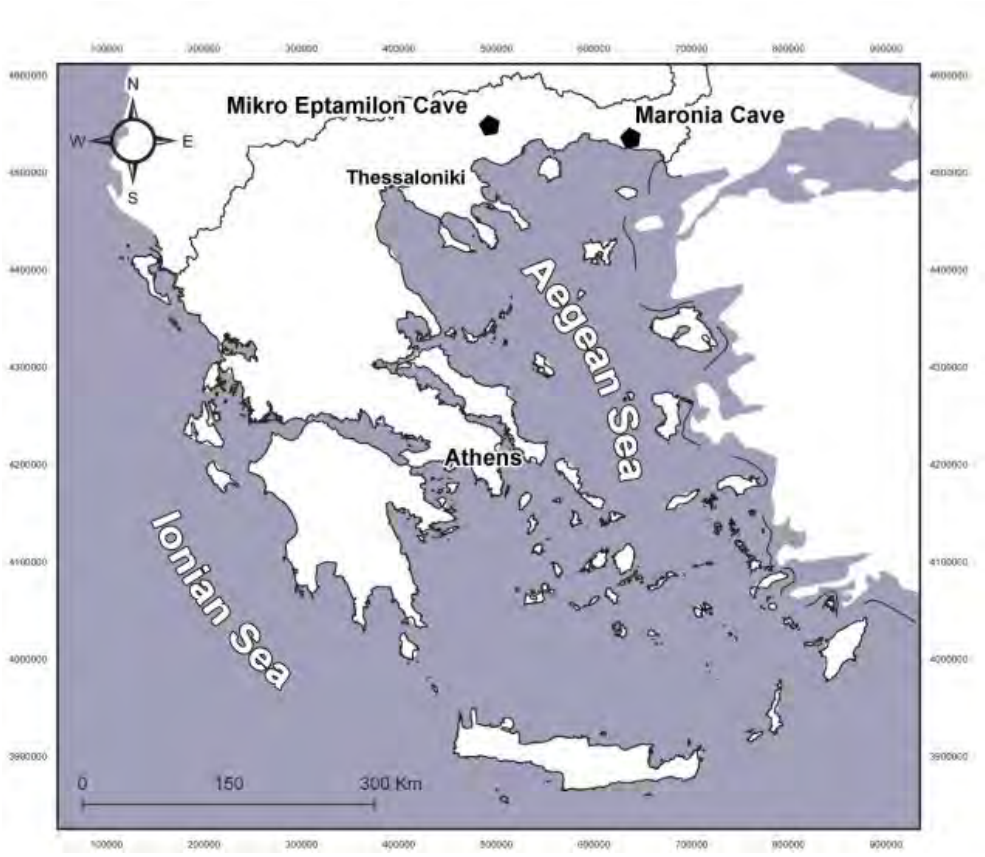

Figure 1 - Location map of the Maronia Cave and the Mikro Eptamilon Cave.

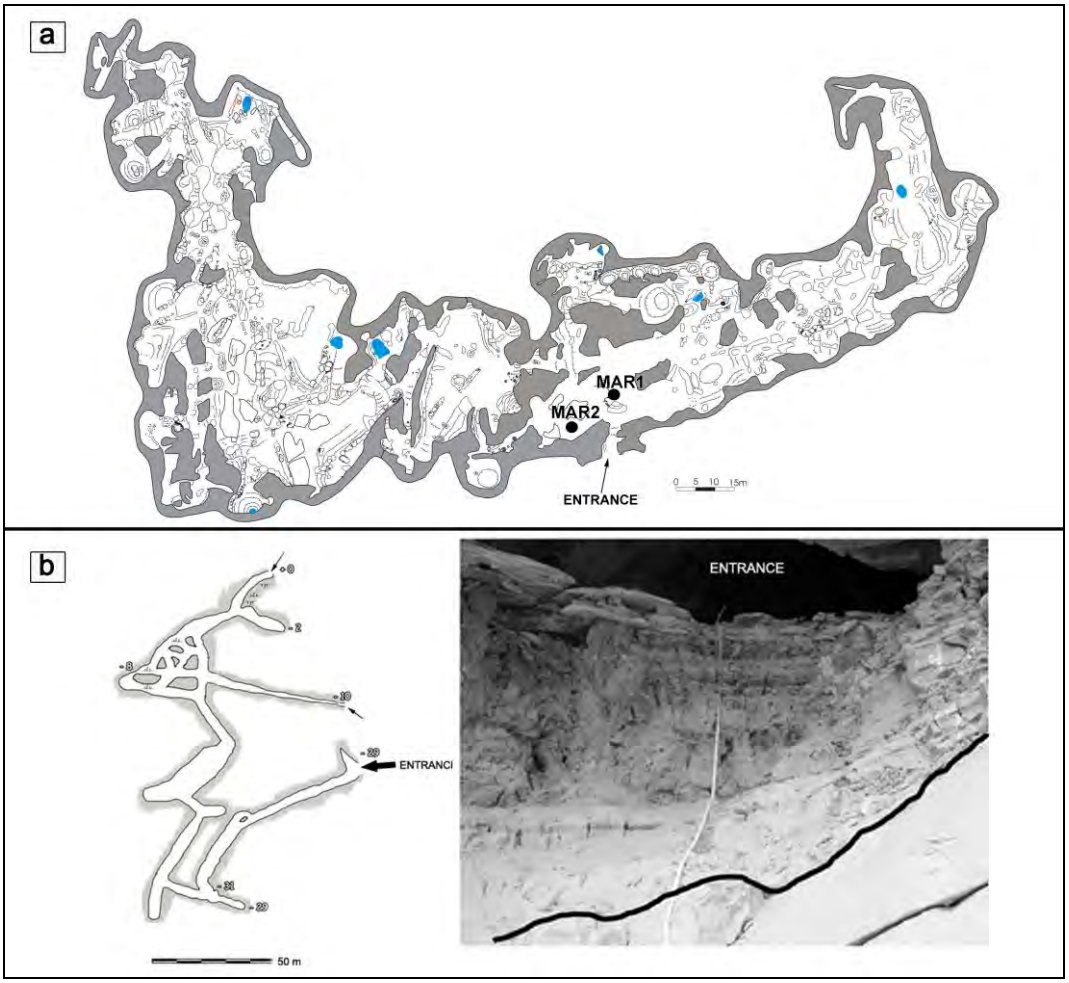

Figure 2 - Plan view of (a) the Maronia Cave with location of the studied vibracores MAR1 and MAR2 (from Pavlides et al., 2008) and (b) the Mikro Eptamilon Cave (in detail the studied sedimentary sequence at the entrance of the cave) (from Pechlivanidou et al., 2011).

3. Methodology

Magnetic susceptibility is a measure of the ease, which a material can be magnetised. The volume susceptibility is defined by the relation $\kappa=M/H$, where M is the acquired magnetisation when a uniform magnetic field (H) is applied. In SI units both M and H are expressed in A/m consequently k is dimensionless. Mass specific susceptibility χ is defined as: $\chi = \kappa/\rho$ where ρ is the density and has m^3/Kg units in SI.

Volume magnetic susceptibility (κ_{lf}) was measured on clastic and chemogenic sediments from the Maronia Cave using a Bartington MS2E meter (resolution: 2 $x10^{-6}$ SI on 0.1 range). Two vibracores, 80 cm and 90 cm respectively, retrieved from the interior of the cave (Figure 2a). The cores were split in half and surface measurements performed continuously with a step of 2.5 cm.

At the Mikro Eptamilon Cave, bulk sampling was performed continuously throughout the sedimentary sequence at the entrance of the cave (Figure 2b). Samples were packed in plastic boxes (2 x 2 x 1.6 cm^3), weighted and mass magnetic susceptibility was measured both at low (0.465 kHz ± 1%) and high (4.65 kHz ± 1%) frequency with a Bartington MS2B dual frequency

sensor. The dual frequency enabled the estimation of the frequency dependent magnetic susceptibility (χ_{fd}) which indicates the presence of ferrimagnetic grains close to the superparamagnetic stable single domain (SP) transition (Evans and Heller, 2003). Moreover, the variation of the magnetic susceptibility with temperature was estimated for selected samples, using the Bartington furnace in free air.

4. Results

4.1. Maronia Cave

Magnetic susceptibility shows a great variability across the studied cores from the Maronia Cave. Figure 3 shows the downcore variations of κ_{lf} for MAR1 and MAR2. κ_{lf} values are significantly low for the upper 20 cm of MAR1, ranging from $21*10^{-6}$SI to $45*10^{-6}$SI. Between 20 - 65 cm, magnetic susceptibility values increase to $211.3*10^{-6}$SI, while are decreasing until the depth of 80 cm to $7.5*10^{-6}$SI. From 80 cm to the end of MAR1, magnetic susceptibility increases again reaching the value of $348.8*10^{-6}$SI (Figure 3).

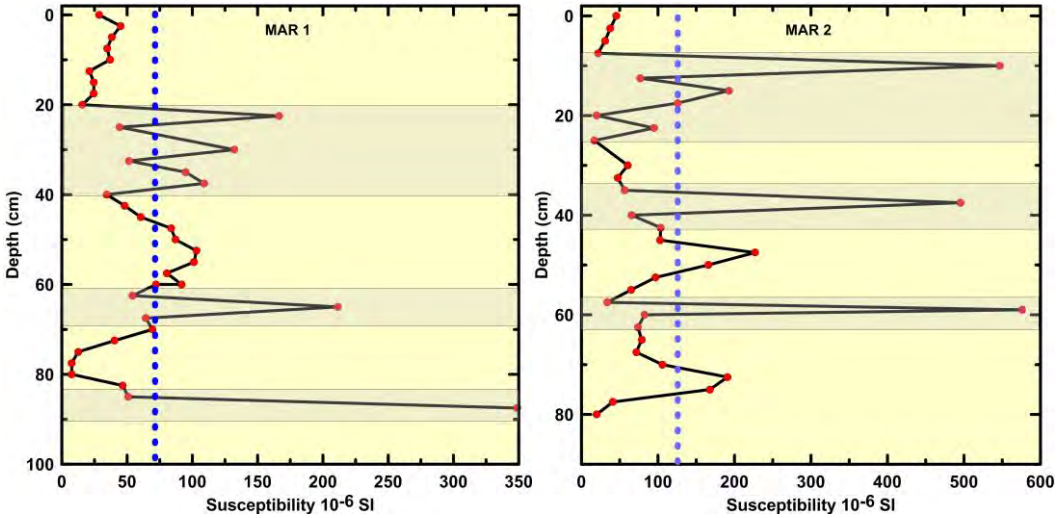

Figure 3 - Downcore variations of magnetic susceptibility (κ_{lf}) for MAR1 and MAR2, from the Maronia Cave. Grey zones indicate the enhanced layers, while blue line corresponds to the mean values for each core.

A similar trend in the magnetic susceptibility depicted for MAR2 (Figure 3). κ_{lf} values ranging from 21.7*10-6SI to 45.6*10-6SI at the upper part of the core until the depth of 7.5 cm. From 7.5 cm to 20 cm, magnetic susceptibility values are significantly higher with a maximum value of 547.7*10-6SI, while from 20 cm to 35 cm, are decreasing, reaching a minimum value of 17*10-6SI. From 35 cm to 75 cm, there is a distinct downcore increase in κlf and maximum values are detected at 37.7 cm, 50 cm, 59 cm and 72.5 cm. An exception occurs between 52.5 - 57.5 cm depth, where κlf values are gradually decreasing to 33.8*10-6SI. From 75 cm to the end of MAR2, κlf decreases reaching a value of 19.9*10-6SI.

4.2. Mikro Eptamilon Cave

Magnetic analysis of sediment samples derived from the sedimentary sequence at the Mikro Eptamlon Cave is shown on Figure 4. Both the magnetic susceptibility (χ_{lf}) and the frequency dependent susceptibility (χ_{fd}) show distinct variations with depth. Increased magnetic susceptibility values observed between 85 cm and 165 cm depth, showing a maximum value of $80.5*10^{-8}$ m^3/Kg at 100 cm depth. The upper and the lower part of the sequence depicts rather small magnetic susceptibility values, ranging between 7.8 - 22.8 $*10^{-8}$ m^3/Kg. Frequency magnetic susceptibility

(χ_{fd}) shows a more complicated trend across the studied sequence. χ_{lf} values are generally increasing until the depth of 138 cm, from 138 cm to 100 cm are decreasing and from 100 cm to the upper part of the sequence are increasing again. Maximum χ_{fd} values (> 14%) depicted at 26 cm, 48 cm, 50 cm, 135 cm, 145 cm and 190 cm, depth. The two pick values (~ 30%) observed at 15 cm and 138 cm depth, are considered as erroneous measurements since they do not seem realistic (Dearing, et al., 1996), hence are excluded for further interpretation.

Additionally, the variation of magnetic susceptibility with temperature was studied in selected samples. In Figure 5 the heating curve of the sample located at 100cm depth (showing the maximum susceptibility value Fig.4a) is displayed. A clear susceptibility drop near 585^{0}C is observed, suggesting the existence of nearly stoichiometric magnetite. The drop of susceptibility in the range of 300^{0}C is interpreted as the conversion of metastable cubic maghemite to weakly magnetic rhombohedral hematite (Deng et al., 2005). Moreover, Liu et al. (2005) further showed that this susceptibility decrease results from the inversion of fine-grained maghemite to hematite. Such a susceptibility drop is more prominent for paleosol samples and is consistent with the idea that paleosol contains more fine-grained pedogenic maghemite grains.

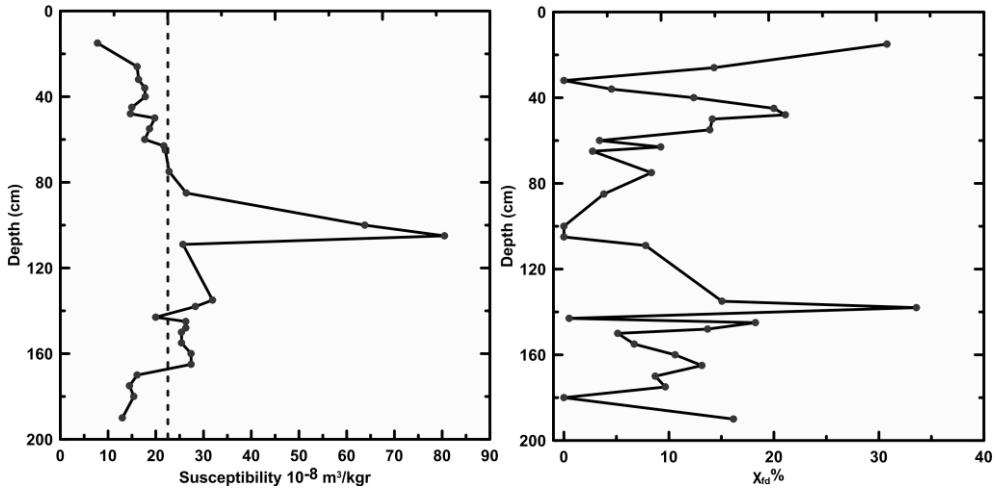

Figure 4 - Magnetic susceptibility (χ_{lf}) and frequency dependent susceptibility (χ_{fd}) variations with depth, recorded from the sedimentary sequence at the Mikro Eptamilon Cave (location is shown in Fig. 2b).

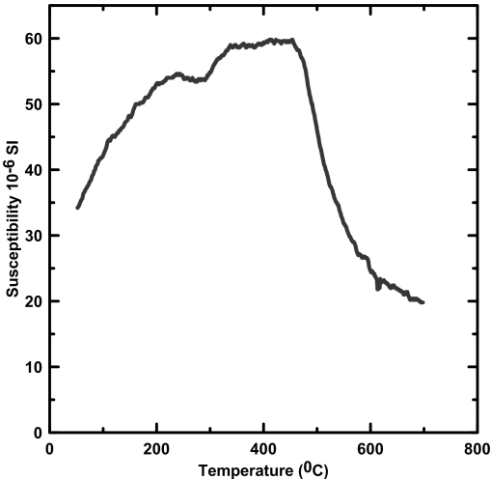

Figure 5 - Variation of the magnetic susceptibility with temperature.

5. Discussion

As it is well known, magnetic susceptibility shows enhanced values in the buried archaeological human occupation layers. As it is reported by several authors (e.g. Dalan 2006, 2008) this enhancement is due to an increase in fine grained magnetite or maghemite.

Similar behaviour it is observed in the case of Maronia Cave. The variation of the magnetic susceptibility across the two cores from this cave records the anthropogenic influence on these sediments. Three evident picks are observed in both cores and they exhibit a clear correlation (Figure 3, grey zones). These enhanced layers are related with the human occupation that took place inside the cave. Archaeological findings confirm the existence of different occupation levels dating from Neolithic period until 13th century A.D. Several authors have been led to similar conclusions in archaeological trenches. Aidona et al., (2001) reported that enhanced values of magnetic susceptibility could correlate with the habitation layer of the studied settlement, indicating that magnetic susceptibility measurements are capable of distinguishing the archaeological layers of the site from those where the complex was abandoned and provide additional evidence for the occupation periods of the complex. Additionally, Dalan (2008) identified a buried archaic soil layer by its correlation with high values of susceptibility. Sediments depicting lower magnetic susceptibility values were not influenced by human activities in the Maronia Cave and have likely been deposited under infiltration and fluvial processes.

The variation of the magnetic susceptibility in the sedimentary sequence from the Mikro Eptamilon Cave exhibits a different behavior. All χ values are much lower than the ones from the Maronia Cave as it is shown from the comparison of their mean values (Figures 3, 4). So, it is evident that the sediments deposited in the Mikro Eptamilon Cave are natural and they are not affected by any anthropogenic influence. This is also confirmed by the lack of any archaeological remains in the cave. The observed variability in the magnetic susceptibility (Figure 4) is likely due to changes of the paleoflow inside the Mikro Eptamilon Cave, primarily controlled by climate alterations. During periods of increased flow a larger amount of magnetic minerals is transferred and deposited inside the cave, resulting in higher magnetic susceptibility values. In contrast, during periods of low flow conditions the depositional energy was not capable enough to carry a significant amount of ferrimagnetic minerals (e.g. magnetite). In addition, the presence of rather small magnetic grains (SP grains) at the upper and the lower part of the studied section obtained from χ_{fd} values (Figure 4), indicates low energy conditions. The detected variability in both the magnetic susceptibility and the frequency dependent magnetic susceptibility is also consistent with detailed grain size analysis (Pechlivanidou, et al., 2011) that further support possible changes of the paleoflow.

Moreover, the increased magnetic susceptibility values are considered to indicate warmer paleoclimatic conditions between 85 cm - 105 cm depth, while magnetic susceptibility lows indicate cooler climatic conditions at the upper and the lower parts of the studied sequence. Ellwood et al., (1996) and Šroubek et al., (2001) have also proposed paleoclimatic reconstructions on cave sites from the Mediterranean region based on magnetic susceptibility variations. These variations were attributed to the growth of extremely fine- grained magnetite and/or maghemite formed by pedogenic processes during warm and humid climatic periods and redeposition into the cave sites. As it is known, the magnetic behavior of many minerals varies with temperature. All magnetic minerals have a temperature point (Curie temperature) above which they become paramagnetic. So, when the magnetic susceptibility is recorded continuously with the increase of the temperature (the so-called thermomagnetic experiment) it is possible to detect from the shape of the temperature–susceptibility curves the presence of magnetic minerals which are present.

In figure 5 such a variation of the magnetic susceptibility with temperature is shown. The shape of the curve and especially the decrease observed around 300°C indicates the presence of maghemite. The above indication further reinforces the suggestion of warmer climatic conditions since the

formation of maghemite is possibly due to effects of pedogenetic processes on sediments washed into the Mikro Eptamilon Cave area.

6. Conclusions

Environmental magnetism techniques used in the present study proved to be a useful tool for detecting the paleoenvironmental conditions under which sediment deposition took place inside the two studied caves. Both the natural and anthropogenic signal of the cave deposits was detected based on magnetic susceptibility measurements. In the case of the Maronia Cave three different occupation levels were well distinguished from the magnetic susceptibility data, while in the Mikro Eptamilon Cave, the variation of the magnetic parameters were correlated with changes of the paleoflow controlled by paleoclimatic alterations.

In order to complete and reinforce our preliminary results further magnetic analyses are required, such as the estimation of remanence parameters. The most important issue for the continuation of this kind of research is the dating of the sediments with independent dating techniques (e.g. U/Th, 14C dating techniques). Being able to correlate magnetic variations with marine oxygen isotope stages as well as with archaeological data, will lead us to safer conclusions regarding the past environmental changes imprinted on cave sediments.

7. Acknowledgments

The authors would like to express their gratitude to the archaeologists Panti, A., Miteletsis, M. and Syros, A. of the Ephorate of Paleoanthropology and Speleology of the Northern Greece for their help during the sampling and the evaluation of the archaeological data.

8. References

Aidona E., Sarris A., Kondopoulou D. and Sanakis Y. 2001. Application of Magnetic and Spectrometry Methods in the Detection of Human Activity in Soils: A Case Study in the Archaeological Site of Kitros (N. Greece), *Archaeological Prospection,* 8, 187-198.

Aidona E. and Liritzis I. 2012. Magnetic Susceptibility and Radioactivity Changes of Aegean and Ionian Sea Sediments during Last Glacial/Interglacial: Climatic and Chronological Markers, *Journal of Coastal Research*, 28, 2, 342 – 353.

Collcutt S.N. 1979. Analysis of Quaternary cave sediments, *World Archaeology* 10, 290-301.

Dalan R. 2006. A geophysical approach to buried site detection using down-hole susceptibility and soil magnetic techniques, *Archaeological Prospection,* 13, 182-206.

Dalan R.2008. A review of the role of magnetic susceptibility in archaeogeophysical studies in the USA: Recent Developments and Prospects. *Archaeological Prospection,* 15, 1–31.

Dearing J.A., Dann R.J.L., Hay K., Lees J.A., Loveland P.J., Maher B.A. and O'Grady K. 1996. Frequency-dependent susceptibility measurements of environmental materials, *Geophysical Journal International,* 124, 228-240.

Deng C., Vidic N.J., Verosub K.L., Singer M.J., Liu Q., Shaw J. and Zhu R. 2005. Mineral magnetic variation of the Jiaodao Chinese loess//paleosol sequence and its bearing on long-term climatic variability, *Journal of Geophysical Research*, 110, B03103.

Ellwood B.B., Harrold F.B., Benoist S.L., Thacker P., Otte M., Bonjean D., Long G.J., Shahin A.M., Hermann R.P. and Grandjean F. 2004. Magnetic susceptibility applied as an age-depth-climate relative dating technique using sediments from Scladina Cave, a Late Pleistocene cave site in Belgium, *Journal of Archaeological Science*, 31, 283-293.

Ellwood B.K., Petruso K.M., Harrold F.B. and Korkuti M. 1996. Paleoclimate characterization and intra-site correlation using magnetic susceptibility measurements and example from Konispol Cave, Albania, *Journal of Field Archaeology*, 23, 263-271.

Evans M. and Heller F. 2003. Environmental Magnetism - Principles and Applications of Enviromagnetics, Academic Press, pp. 293.

Karkanas P. 2001. Site formation processes in Theopetra Cave: A record of climate change during the late Pleistocene and early Holocene in site formation processes in Theopetra Cave, *Geoarchaeology: An International Journal*, 16, 373-399.

Liu Q.S., Jackson M.J., Banerjee S.K., Maher B.A., Deng C.L., Pan Y.X., Zhu and R.X. 2005. Mechanism of the magnetic susceptibility enhancements of the Chinese loess, *Journal of Geophysical Research,* 110, B12107.

Melfos V., Chatzipetros A., Chatzopoulou A., Vasileiadou M.K., Lazarides G., Vaxevanopoulos M., Syrides G., Tsoukala E. and Pavlides S. 2005. Geological, petrographical and paleonotological study of the Maronia cave in the Eocenic limestones of Thrace, *Bulletin of the Geological Society of Greece*, XXXVII, 37, 153-167.

Paasche Ø., Løvlie R., Dahl S.O., Bakke J. and Nesje A. 2004. Bacterial magnetite in lake sediments: late glacial to Holocene climate and sedimentary changes in northern Norway, *Earth and Planetary Science Letters*, 223, 319–333.

Panti A. and Miteletsis M. 2008. The excavation of Polifimo Maronia Cave, Prefecture of Rhodope: Preliminary study, 2008, *Proceedings of the 20th AEMTh*, University of Thessaloniki, Thessaloniki, Greece (in Greek).

Pavlides S., Tsoukala E., Chatzipetros A., Chatzopoulou A., Melfos V., Vasileiadou M.K., Lazarides G. and Vaxevanopoulos M. 2008. The Maronia cave in the nummulitic limestone (Thrace, Greece), Geology & Palaeontology, in Ch. Petreas (ed*), Procceedings of the 14th International Congress of Speleology (ICS),* Athens, 88-90.

Pechlivanidou S., Aidona E., Vouvalidis K., Pennos Ch. and Albanakis K.2011. Geomorphological, sedimentological and magnetic susceptibility analysis of sediments in the 'Mikro' Eptamilon Cave, Serres, Greece, *Bulletin of the Geological Society of Greece*, XLIV, 37-46.

Šroubek P., Diehl J.F. and Kadlec J. 2007. Historical climatic record from flood sediments deposited in the interior of Spirálka Cave, Czech Republic, *Palaeogeography, Palaeoclimatology, Palaeoecology*, 251, 547-562.

Šroubek P., Diehl J.F., Kadlec J. and Valoch K. 2001. A Late Pleistocene paleoclimate record based on mineral magnetic properties of the entrance facies sediments of Kulna Cave, Czech Republic, *Geophysical Journal International*, 147, 247-262.

Thompson, R. and Oldfield F. 1986. Environmental Magnetism. Allen and Unwin, pp. 227, London.

Tsatskin A. and Nadel D. 2003. Formation processes at the Ohalo II submerged prehistoric campsite, Israel, inferred from soil micromorphology and magnetic susceptibility studies. *Geoarchaeology: An International Journal*, 18, 409-432.

Vaxevanopoulos M. and Melfos V. 2010. Hypogenic features in Maronia cave, Thrace, Greece. Evidence from morphologies and fluid inclusions, *Bulletin of the Geological Society of Greece*,, XLIII/2, 948-957.

Verosub K.L., Fine P., Singer M.J. and Tenpas J. 1993. Pedogenesis and paleoclimate - interpretation of the magnetic-susceptibility record of chinese loess-paleosol sequences, *Geology*, 21, 1011-1014.

Woodward J.C. 1997. Late Pleistocene rockshelter sedimentation at Klithi, in: Bailey, G. N. (Ed.), Klithi: *Palaeolithic Settlement and Quaternary Landscape in Northwest Greece. Volume 2: Klithi in its Local and Regional Setting,* Cambridge: McDonald Institute, pp. 361-376.

Woodward J.C. and Goldberg P. 2001. The Sedimentary Records in Mediterranean Rockshelters and Caves: Archives of Environmental Change, *Geoarchaeology: An International Journal*, 16, 327-354.

Yang X., Grapes R., Zhou H. and Yang J. 2008. Magnetic properties of sediments from the Pearl River Delta, South China: Paleoenvironmental implications, *Science in China Series D: earth Sciences* 51: 56-66.

Δελτίο της Ελληνικής Γεωλογικής Εταιρίας, τομ. XLVII , 2013
Πρακτικά 13ου Διεθνούς Συνεδρίου, Χανιά, Σεπτ. 2013

Bulletin of the Geological Society of Greece, vol. XLVII 2013
Proceedings of the 13th International Congress, Chania, Sept. 2013

GEOCHEMICAL MAPPING OF URBAN SOILS IN ATHENS, GREECE- PRELIMINARY RESULTS

Argyraki A.[1], Kelepertzis E.[1], Fligos G.[1], Athanasiou E.[1], Gardiakos K.[1] and Kourgia V.[2]

[1] National and Kapodistrian University of Athens, Faculty of Geology and Geoenvironment, Department of Economic Geology and Geochemistry, argyraki@geol.uoa.gr, kelepert@geol.uoa.gr

[2] National and Kapodistrian University of Athens, Faculty of Chemistry

Abstract

Urban geochemistry is a fast growing scientific discipline mainly because of the profound impact of large cities on the environment as well as the increase in the world's urban population. The present study aims to produce the urban geochemical map of Athens, based on multi-element analysis of surface soils (0-10 cm) with emphasis in the spatial distribution of potentially harmful elements (PHEs). Soil sampling was based on a regular 1km x 1km grid, laid over the survey area covering more than 200 km^2. Sampling locations within the grid cells were selected giving priority to playgrounds, schools and urban parks. The < 100 μm fraction of a total of 320 soil samples were analysed by Flame Atomic Absorption Spectroscopy for Pb, Zn, Cu, Cd, Cr, Ni, Co and Mn after aqua regia dissolution. Average content of Pb (62 mg/kg), Cu (36 mg/kg), Zn (91 mg/kg) and Mn (465 mg/kg) in soil was lower than reported concentrations from other European cities while Cr (74 mg/kg), Ni (89 mg/kg) and Co (16 mg/kg) were relatively enriched. Geochemical maps were plotted within GIS enabling recognition of spatial trends in elemental concentrations and potential sources of the elements. The research outcome will contribute to the evaluation of quality characteristics of urban soils in Athens and drive attention to areas of any environmental or health risks.

Key words: *Heavy metals, environmental contamination, GIS.*

Περίληψη

Η αστική γεωχημεία είναι ένας αναπτυσσόμενος επιστημονικός τομέας κυρίως λόγω των περιβαλλοντικών επιπτώσεων από την εξάπλωση των πόλεων και την αύξηση του αστικού πληθυσμού. Η παρούσα εργασία έχει ως στόχο τη γεωχημική χαρτογράφηση των επιφανειακών (0-10 cm) εδαφών της Αθήνας με έμφαση στη χωρική κατανομή δυνητικά βλαβερών χημικών στοιχείων. Η δειγματοληψία υπαίθρου πραγματοποιήθηκε βάσει τετραγωνικού κανάβου ισοδιάστασης 1 km και κάλυψε συνολική έκταση περίπου 200 km^2, με προτεραιότητα σε παιδικές χαρές, σχολεία και πάρκα. Αναλύθηκαν320 εδαφικά δείγματα κοκκομετρίας < 100 μm με την τεχνική της φασματοσκοπίας ατομικής απορρόφησης μετά από διαλυτοποίηση με βασιλικό ύδωρ και προσδιορίστηκαν τα στοιχεία Pb, Zn, Cu, Cd, Cr, Ni, Co και Mn. Οι μέσες συγκεντρώσεις των στοιχείων Pb (62 mg/kg), Cu (36 mg/kg), Zn (91 mg/kg) και Mn (465 mg/kg) είναι χαμηλότερες των αντίστοιχων συγκεντρώσεων άλλων Ευρωπαϊκών πόλεων ενώ οι

συγκεντρώσεις των Cr (74 mg/kg), Ni (89 mg/kg) και Co (16 mg/kg) υψηλότερες. Το γεωχημικό ανάγλυφο αποτυπώθηκε σε περιβάλλον ΓΣΠ δίνοντας τη δυνατότητα προσδιορισμού διαφορετικών πηγών των στοιχείων. Τα αποτελέσματα της έρευνας συμβάλουν στην εκτίμηση της ποιότητας των εδαφών της Αθήνας και αποτελούν πολύτιμο εργαλείο στην αναγνώριση περιοχών περιβαλλοντικής επικινδυνότητας.
Λέξεις κλειδιά: *Βαρέα μέταλλα, περιβαλλοντική ρύπανση, ΓΣΠ.*

1. Introduction

Urban geochemical mapping studies are useful for establishing a baseline for the urban environment, satisfying the legislative-driven demand for geochemical information on the urban chemical environment, locating polluted areas, assessing the contribution of parent materials and anthropogenic activity to the geochemical baseline, assessing risks to other compartments of the urban environment (e.g. groundwater) and identifying sources of potentially harmful elements (PHEs) (Johnson and Ander, 2008). Within this frame many cities around the world have been mapped with respect to PHEs content in soil (Kelly et al., 1996; Li et al., 2004; Madrid et al., 2002; Cicchella et al., 2008; Andersson et al., 2010). In Greece, a few publications exist on the soil geochemistry of urban areas (Demetriades, 2010; Massas et al. 2010; Massas et al. 2013) however systematic geochemical maps of urban soils do not exist for any of the major cities.

The present study aims to produce the urban geochemical map of Athens, the capital city of Greece with population exceeding 3 million (2011). The study was implemented by multi-element analysis of surface soils (0-10 cm) and this paper is focused on the spatial distribution of PHEs. Geochemical maps were plotted within GIS enabling recognition of spatial trends in elemental concentrations and potential sources of the elements. The preliminary results presented here, enable the identification of spatial patterns in elemental concentration corresponding to lithology and anthopogenic activity. The research outcome will contribute to the evaluation of quality characteristics of urban soils in Athens and drive attention to areas of any environmental or health risks.

2. Materials and Methods

2.1. Soil Sampling and Chemical Analysis

Soil sampling was based on a regular 1km x 1km grid, laid over the survey area covering more than 200 km^2. The 281 sampling locations within the grid cells were selected giving priority to playgrounds, schools and urban parks. Sampling depth was 0-10 cm. At each sampling site, samples were collected in sealable plastic bags after removing debris and surface vegetation. Five-fold composite samples were collected by mixing sample increments from the four corners and the centre of a 10 m square. Sampling duplicates were collected from 20 random sites by collecting a second soil sample about 200 m away from the original point at random direction but within the same $1km^2$ sampling cell. A balanced Analysis of Variance (ANOVA) experimental design was subsequently applied by performing duplicate analysis for each of the field duplicate samples. This allowed the estimation of *geochemical* (between sampling sites), *sampling* (between sampling duplicates) and *analytical* (between analytical duplicates) variances as proportions of the total variability in the data set (Ramsey and Elisson, 2007; Argyraki, 2010).

The < 100 μm fraction of a total of 341 soil samples was analysed by Flame Atomic Absorption Spectroscopy for Pb, Zn, Cu, Cd, Cr, Ni, Co and Mn after *aqua regia* dissolution. All analytical procedures were performed in the Laboratory of Economic Geology and Geochemistry, University of Athens. Sampling and analytical quality was assessed by applying the duplicate method (Ramsey and Elisson, 2007) and inclusion of blanks and 3 certified reference materials (NIST SRM2709, NIST SRM2711 and ISE921) in random positions within the analytical batches.

2.2. Data Processing and GIS Application

Analytical results were inspected for systematic differences between batches and for outlying values. Subsequent statistical analysis was performed by calculating the basic descriptive statistics for the measured parameters including minimum, maximum, mean, median and standard deviation values. Factor analysis, a multivariate statistical method, was applied on the normal scores of concentration values in order to group the studied elements according to their inter-correlations and define geochemical processes that control their distribution in soil. Presentation and interpretation of the spatial patterns in PHEs soil content was enabled by using a GIS system within the ArcMap platform. Apart from the geochemical data, layers of spatial information that were inserted in the GIS included the topography and local geology of Athens. These data were provided by the Department of Dynamic Geology of UoA.

3. Results and Discussion

3.1. Descriptive Statistics

The descriptive statistics of heavy metal concentrations are presented in Table 1. Average concentrations reported in the literature for other European cities are also provided for comparison.

All elements showed positively skewed distributions- median values were always lower than means. Athens soils showed relatively lower concentrations in Mn, Cu, Pb and Zn than most European cities but were enriched in Ni, Cr and Co. Further statistical processing of the data by applying factor analysis grouped the elements in 3 groups accounting for 85% of the total variation (Table 2). The first factor included Ni, Cr and Co with high positive loadings and was interpreted as lithogenic, the second included Cu, Pb and Zn and the third Mn. Copper, Pb, Zn and Mn are typical elements indicating the influence of anthropogenic activities on soil characteristics in urban environments since they were used extensively throughout history (Albanese and Cicchella, 2012). Especially Pb was one of the most significant contaminants in urban environments throughout the 20th century as a consequence of its use in urban smelters, in paint and its presence as tetraethyl lead in gasoline.

Table 1 - Statistical summary of heavy metal concentrations (mg/ kg) in urban soils from Athens extracted by aqua regia dissolution (n=281). Average concentrations for some European cities are also given for comparison purposes.

	Ni	Cr	Co	Mn	Cu	Pb	Zn
Mean	89	74	16	465	36	62	91
Standard Deviation	56	41	3.3	185	32	125	77
First quartile	63	51	14	377	22	32	54
Median	82	68	16	445	29	41	72
Third quartile	99	88	17	525	37	57	104
Minimum	26	19	5.8	121	8.5	9	14
Maximum	616	500	41	2200	316	1930	833
Trondheim (Norway)[1]	45	65			39	81	112
Napoli (Italy)[2]	11.6	15.3	7.3	683	94	204	223
Sevilla (Spain)[3]	21.9	39.4		471	68.2	137	145
Galway (Ireland)[4]	20.7	33.3	5.6	674	33.2	78.4	99.3

[1]Andersson et al., 2010, [2]Cicchella et al., 2008, [3]Madrid et al., 2002, [4]Zhang 2006

Table 2 – Rotated factor loadings and communalities based on normal score data of heavy metal concentrations in 281 urban soils of Athens.

Variable	Factor 1	Factor 2	Factor 3	Communality
Ni	0.935	0.058	0.157	0.902
Cr	0.912	0.146	0.077	0.859
Co	0.820	0.090	0.333	0.791
Mn	0.310	0.143	0.929	0.980
Cu	0.263	0.851	0.182	0.826
Pb	0.088	0.879	-0.030	0.781
Zn	-0.029	0.883	0.110	0.793
% Variance	0.364	0.333	0.150	0.847

3.2. Spatial Heterogeneity within the Sampling Cells

One-way analysis of variance was applied on the results from duplicate sampling and analysis. The technique was implemented using the computer program ROBAN. EXE, adapted from a published program (AMC, 1989) and available from the (UK) Royal Society of Chemistry web site. It was found that while analytical variance was within acceptable limits, accounting for small proportions (1.8 % - 12 %) of the total variance for all the elements, sampling variance contributed higher percentages than the geochemical variance in most instances. This was attributed to the high degree of soil heterogeneity within the separation distance of sampling duplicates (about 200 m). Indeed urban soils are subject to hundreds of human-driven forcings resulting in wide differences in elemental concentrations inside the urban net (Hursthouse et al. 2004; Bain et al. 2012). Densely populated areas amplify human-driven fluxes through waste generation at spots or through abrupt changes in land use within areas smaller than 1 km^2 which was the used sampling spacing in this study. Based on these facts it was decided not to interpolate the concentration values, as this would result in an erroneous smoothing effect, but rather present them as graduated size symbols on the constructed maps.

3.3. Spatial Distribution of PHEs

The spatial distribution of the studied elements is presented in two maps as integrated indexes of the lithogenic (Cr+ Ni +Co) (Figure 1) and anthropogenic (Pb + Zn +Cu) (Figure 2) elements. The grouping of elements was based on results from the factor analysis and the class intervals were defined based on natural breaks in the histograms of integrated data. Distinct patterns were observed between the two maps. Specifically, the lithogenic elements displayed maximum concentrations towards the periphery of the Athens Basin, along two axes running parallel to the foot hills of Agaleo and Hymettus Mountains. These areas are characterised not only by outcropping of Alpine rocks but also by the presence of serpentinised members of ophiolithic sequences (Papanikolaou et al. 2004) (Figure 3). The spatial correlation between maximum concentrations of Cr, Ni and Co and these lithological types provides further evidence on the geogenic origin of these elements. On the contrary maximum concentrations of Pb, Zn and Cu are plotted in the core area of the city of Athens, around the hills of Acropolis and Lycabetus as well as around Piraeus Port.

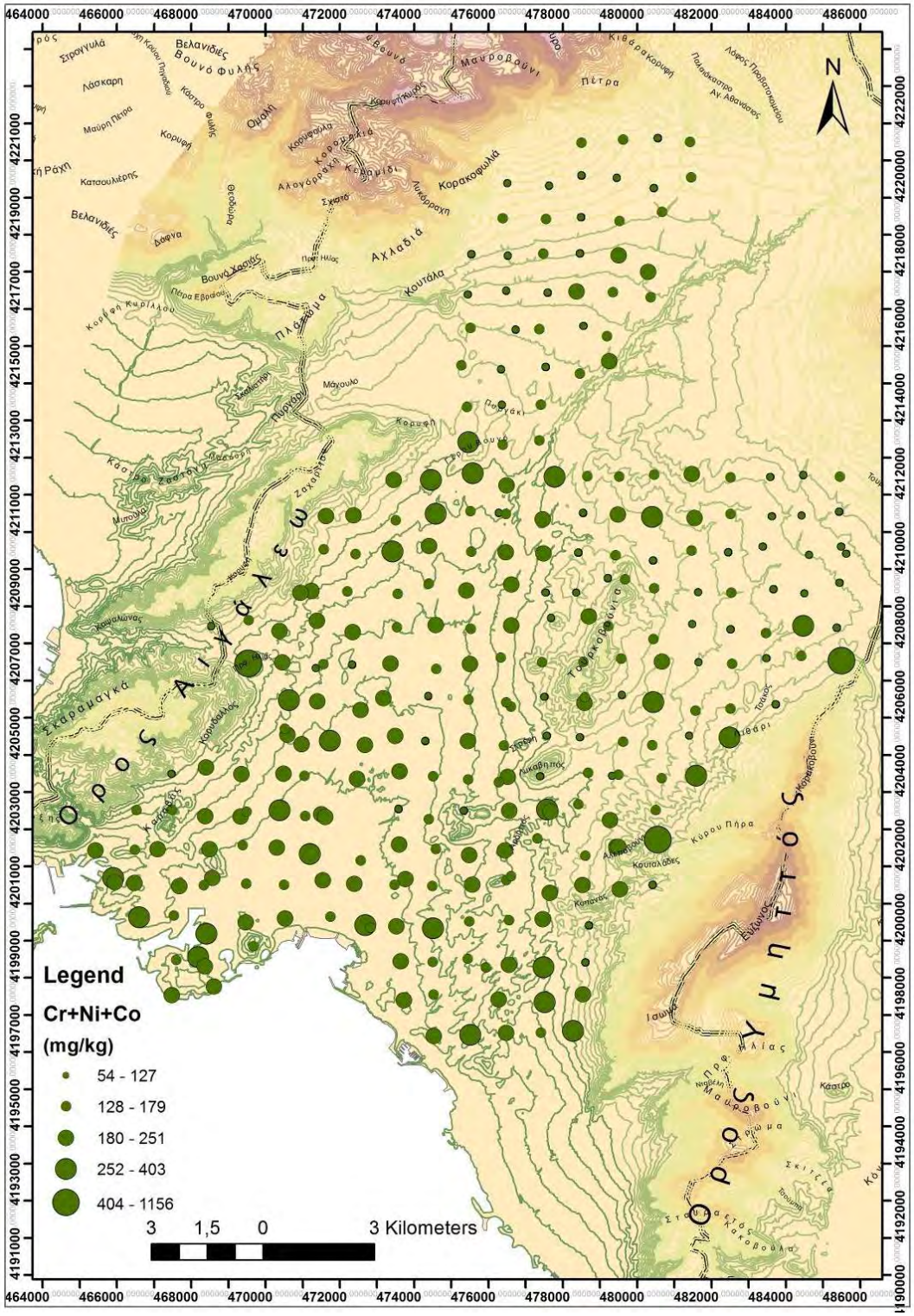

Figure 1 - Graduated symbol map showing the spatial distribution of the integrated index for the lithogenic elements Cr, Ni and Co in Athens soils.

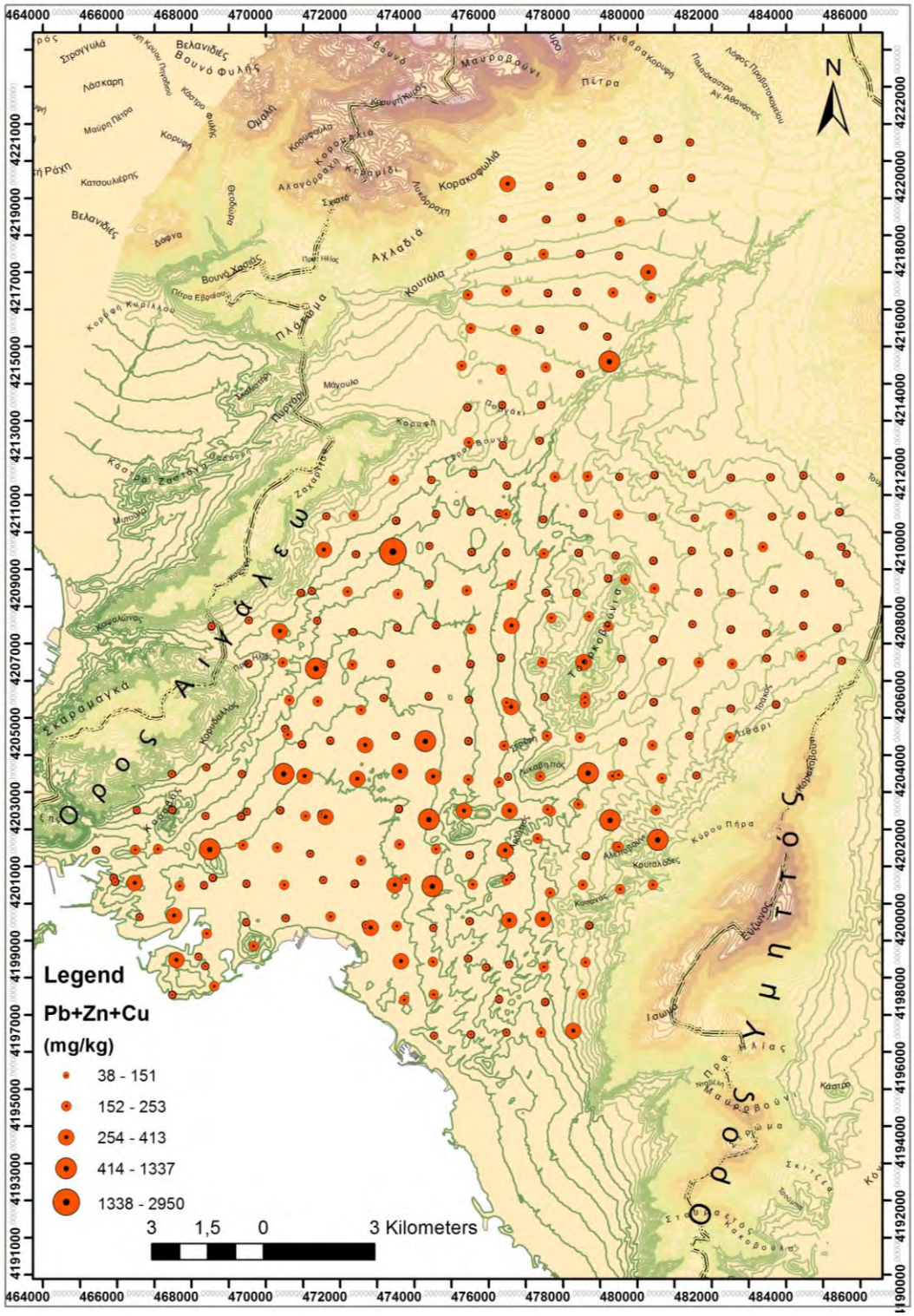

Figure 2 - Graduated symbol map showing the spatial distribution of the integrated index for the anthropogenic elements Pb, Zn and Cu in Athens soils.

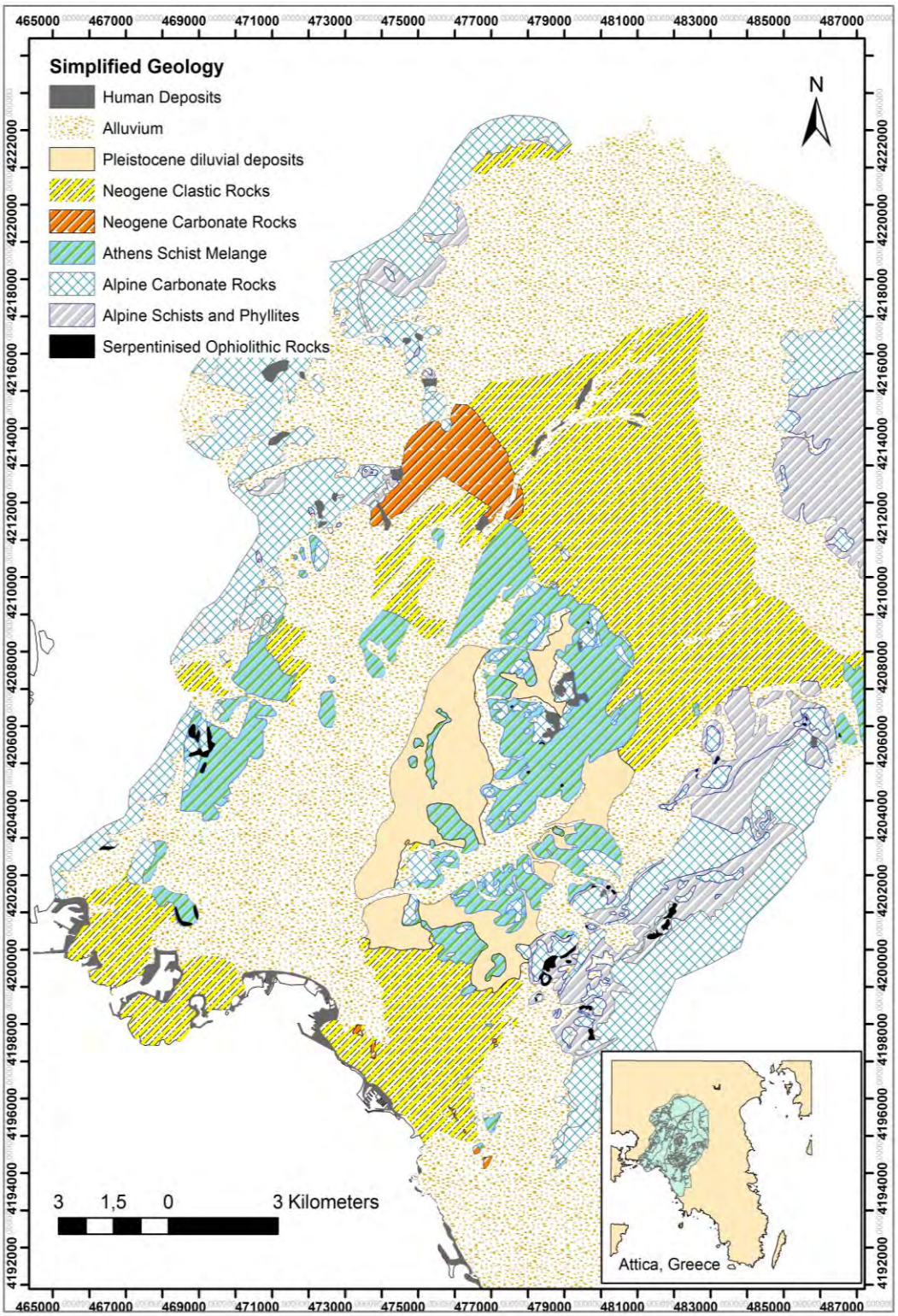

Figure 3 - Simplified geological map of the Athens Basin. Modified from Papanikolaou et al. 2004.

High concentrations of this group of elements extend towards the western part of the city in the industrial areas of Elaionas, while some isolated high values are observed in the periphery of the study area. Although the results presented here are preliminary, the spatial trend of Pb, Zn and Cu is probably linked to factors such as timing of urbanization, age of infrastructure, population density, vehicular traffic and amount of green spaces (Lyons and Harmon, 2012). In general, Pb, Zn and Cu have been repeatedly shown to be related to vehicular pollution (Li et al., 2004; Morton-Bermea et al., 2009). Further work will explore these relationships by utilizing statistical techniques and GIS in order to define the most significant of the contributing factors. Also, urban soils are considered to be sinks of PHEs deposited by atmospheric fallout, usually as adsorbed species onto particulate matter. Such secondary enrichment results in enhanced extractability and high bioavailability (Kierczak et al., 2008; Albanese and Ciccella, 2012) and calls for evaluation of the significance of geochemical anomalies in relation to lithological characteristics and human activities.

4. Conclusions

Systematic data on soil geochemistry of the city of Athens, covering the total extend of the metropolitan area are presented for the first time. In this study preliminary results on aqua regia extracted concentrations of PHEs were evaluated and compared to reported literature data from other European cities. It was found that Athens soils had lower concentrations of Pb, Cu, Zn and Mn but were relatively enriched in Cr, Ni and Co. Geochemical maps were plotted within GIS enabling recognition of spatial trends in elemental concentrations and potential sources of the elements. The group of Cr, Ni and Co was interpreted as being of geogenic origin and displayed spatial association of maximum values with ophiolithic rock outcrops in the periphery of the Athens Basin, while the group of Pb, Cu and Zn showed maximum concentrations in the centre of the city indicating anthropogenic influence. Further work within the GIS will exemplify relationships between spatial data such as population density, age of urban development and automobile traffic intensity and heavy metal concentrations in soil. The research outcome will contribute to the evaluation of quality characteristics of urban soils in Athens and drive attention to areas of any environmental or health risks.

5. Acknowledgments

This project was funded by the John S. Latsis Public Benefit Foundation. The sole responsibility for the content lies with its author/s.

6. References

Albanese S. and Cicchella D. 2012. Legacy problems in urban geochemistry, *Elements* 8, 423-428.

Analytical Methods Committee 1989. Robust Statistics – How not to reject outliers, Part 1, Basic Concepts, *Analyst*, 114, 1693-1697.

Andersson M., Ottesen R.T. and Langedal M. 2010. Geochemistry of urban surface soils – Monitoring in Trondheim, Norway, *Geoderma*, 156, 112-118.

Argyraki A. 2010. Analysis of Variance to estimate sampling uncertainty, in: B. Geelhoed (Ed.), *Approaches in Material Sampling*, IOS Press, Amsterdam, 61-88.

Bain D. J., Hale R. L. and Wollheim W. M. 2012. Hotbeds of biogeochemical diversity: Insights from urban long-term ecological research sites, *Elements*, 8, 435-438.

Cicchella D., De Vivo B., Lim, A., Albanese S., McGill R.A.R. and Parrish R.R, 2008. Heavy metal pollution and Pb isotopes in urban soils of Napoli, Italy, *Geochemistry: Exploration, Environment, Analysis*, 8, 103-112.

Demetriades A. 2010. The Lavrion urban geochemical study, in: C.C. Johnson, A., Demetriades R.T., Ottesen and J. Locutura (Editors), *Mapping the urban chemical environment,* Wiley, London.

Hursthouse A., Tognarelli D., Tucker P., Ajmone-Marsan, F., Martini C. and Madrid L. 2004. Metal content of surface soils in parks and allotments from three European cities: initial Pilot Study results, *Land Contam Reclam*, 12, 189-196.

Johnson C.C. and Ander E. L. 2008. Urban geochemical mapping studies: how and why we do them, *Environmental Geochemistry and Health, 30*, 511-530.

Kelly J., Thornton, I. and Simpson, P.R. 1996. Urban Geochemistry: A study of the influence of anthropogenic activity on the heavy metal content of soils in traditionally industrial and non-industrial areas of Britain, *Applied Geochemistry*, 11, 363-370.

Kierczak J., Neel C., Aleksander-Kwaterczak U., Helios-Rybicka E., Bril H. and Puziewicz J. 2008. Solid speciation and mobility of potentially toxic elements from natural and contaminated soil: A combined approach, *Chemoshpere*, *73*, 776-784.

Li X.D., Lee S.L., Wong S.C., Shi W.Z. and Thornton I. 2004. The study of metal contamination in urban soils of Hong Kong using a GIS-based approach, *Environmental Pollution,* 129, 113-124.

Lyons W. B. and Harmon R.S. 2012. Why urban geochemistry? *Elements*, 8, 417-422.

Madrid L., Díaz-Barrientos E. and Madrid F. 2002. Distribution of heavy metals contents of urban soils in parks of Sevilla, *Chemosphere*, 49, 1301-1308.

Massas I., Ehaliotis C., Kalivas D. and Panagopoulou G. 2010. Concentrations and availability indicators of soil heavy metals; the case of children's playgrounds in the city of Athens (Greece), *Water, Air, and Soil Pollution, 212*(1–4), 51–63.

Massas I., Kalivas D., Ehaliotis C. and Gasparatos D. 2013. Total and available heavy metal concentrations in soils of the Thriassio plain (Greece) and assessment of soil pollution indexes, *Environmental Monitoring and Assessment*, DOI 10.1007/s10661-013-3062-1.

Morton-Bermea O., Hernández-Álvarez E., González-Hernández G., Romero F., Lozano R. and Beramendi-Orosco, L.E. 2009. Assessment of heavy metal pollution in urban topsoils from the metropolitan area of Mexico city, *Journal of Geochemical Exploration*, 101, 218-224.

Papanikolaou D.I, Lozios S.G., Soukis K. and Skourtsos E. 2004. The geological structure of the allochthonous 'Athens Schists', *Bulletin of the Geological Society of Greece vol. XXXVI, Proceedings of the 10th International Congress,* Thessaloniki, April 2004, 1550-1559 (in Greek with English abstract).

Ramsey M.H. and Ellison S.L.R., (eds) Eurachem/EUROLAB/CITAC/Nordtest/AMC Guide. 2007, *Measurement uncertainty arising from sampling; a guide to methods and approaches*, Eurachem.

Zhang C. 2006. Using multivariate analyses and GIS to identify pollutants and their spatial patterns in urban soils of Galway, Ireland, *Environmental Pollution*, 142, 501-111.

Δελτίο της Ελληνικής Γεωλογικής Εταιρίας, τομ. XLVII , 2013
Πρακτικά 13ου Διεθνούς Συνεδρίου, Χανιά, Σεπτ. 2013

Bulletin of the Geological Society of Greece, vol. XLVII 2013
Proceedings of the 13th International Congress, Chania, Sept. 2013

COMPARATIVE GEOCHEMISTRY OF THREE URBAN STREAMS IN ATHENS: KIFISSOS- PODONIFTIS- PIKRODAFNI

Argyraki A.[1], Paraskos F.[1], Marmara M.[1], Papadopoulou K.[1] and Maglaropoulou A.[1]

[1] National and Kapodistrian University of Athens, Faculty of Geology and Geoenvironment, Department of Economic Geology and Geochemistry, Panepistimiolpolis Zographou, Athens, argyraki@geol.uoa.gr

Abstract

The geochemistry of three urban streams in Athens was analysed and compared on the basis of major elements and heavy metals content in water and active sediment. The studied streams of Kifissos, Podoniftis and Pikrodafni run through the Athens basin of a total area of 540 km^2 but differ with respect to the origin of their headwaters i.e., Parnitha, Penteli and Hymettus mountains. The main aim of the study was to determine the geochemical signature of water and sediment within the Athens hydrological basin and evaluate the effect of natural and anthropogenic environment on these water courses. A total of 56 stream water samples were obtained and analysed for major anions, cations and heavy metals (Mn, Cr, Cu, Zn, Pb) as well as nitrate and phosphate concentrations. Active stream sediments were collected at 22 locations along the streams and were analysed for heavy metals (Pb, Zn, Cu, Mn, Cr, Ni, Cd). Results indicated that rock weathering, rather than atmospheric or pollution influx is the dominant process affecting the major ion geochemistry of stream flow in the urban setting. However, Kifissos and Podoniftis waters had higher nitrate and phosphate concentrations indicating greater influence by anthropogenic activities. In general the quality characteristics of water and sediment in the study area were found to be in a good state regarding the studied parameters.
Key words: *hydrogeochemistry, surface water, heavy metals, urban pollution.*

Περίληψη

Παρουσιάζονται τα υδρογεωχημικά χαρακτηριστικά τριών αστικών ρεμάτων της Αθήνας και γίνεται σύγκριση ως προς το περιεχόμενο κυρίων στοιχείων και ιχνοστοιχείων στο νερό και το ενεργό ίζημα. Τα ρέματα που μελετήθηκαν, Κηφισός, Ποδονίφτης και Πικροδάφνη, διατρέχουν το Λεκανοπέδιο Αθηνών αλλά πηγάζουν από γεωλογικά διαφοροποιημένες περιοχές δηλαδή την Πάρνηθα, την Πεντέλη και τον Υμηττό. Ο κύριος στόχος της έρευνας ήταν να προσδιοριστεί ο γεωχημικός χαρακτήρας του νερού και του ιζήματος των ρεμάτων ως προς τους φυσικούς και ανθρωπογενείς παράγοντες που των διαμορφώνουν. Αναλύθηκαν συνολικά 56 δείγματα ύδατος και προσδιορίστηκαν οι συγκεντρώσεις των κύριων στοιχείων και των βαρέων μετάλλων Mn, Cr, Cu, Zn, Pb. Επίσης ενεργό ίζημα από 22 θέσεις κατά μήκος των ρεμάτων αναλύθηκε για τα μέταλλα Pb, Zn, Cu, Mn, Cr, Ni, Cd. Διαπιστώθηκε ότι ο κύριος παράγοντας ελέγχου του χημισμού του νερού είναι η αποσάθρωση των πετρωμάτων. Ωστόσο το

νερό του Κηφισού και της Πικροδάφνης έδειξε μεγαλύτερη επιβάρυνση σε νιτρικά και φωσφορικά ιόντα. Γενικά η ποιοτική κατάσταση του νερού και του ιζήματος των τριών ρεμάτων κρίνεται ικανοποιητική ως προς τις παραμέτρους που μελετήθηκαν.
Λέξεις κλειδιά: *Υδρογεωχημεία, επιφανειακό νερό, βαρέα μέταλλα, αστική ρύπανση.*

1. Introduction

The city of Athens is the most populated area of Greece with a population of 3,074,160 million (in 2011) and is also the 4th most populous European Union capital (2004). The ever increasing urbanization has lead to uncontrollable development around Athens 3 main streams of Kifissos, Pikrodafni and Podoniftis. All three streams have been the recipients of local runoff as well as uncontrollable industrial and residential discharge. The river banks have been altered in many different ways, including, development of houses within the rivers' protection zones. This has resulted in extensive anthropogenic pollution which has disrupted the natural ecosystem.

Microbial contamination due to wastewater is a very common threat in urban environments while contamination by metals and industrial compounds is a long-term concern in industrialized cities (Wong et al. 2012). In this study the geochemistry of water samples and stream sediment samples, from all three streams, has been analysed and compared over a period of one year. The main objective was to determine whether the streams are capable of retaining their natural geochemical characteristics despite the effect of other influxes. In addition, the level of anthropogenic effect on the water course was determined, in order to evaluate the current geochemical state of the streams.

2. Description of Study Area

The examined streams of Kifissos, Pikrodafni and Podoniftis are all situated in, and run through, the Athens Basin. The basin covers a total of 540 km^2 and is bounded by the mountains of Egaleo, Parnitha, Penteli and Hymettus. The streams derive from geologically different areas (Figure 1), influencing their water and sediment geochemical characteristics. Kifissos springs mainly from Mount Parnitha, Pikrodafni from Mount Hymettus whereas Podoniftis from Mount Penteli.

The geology of Attica is quite complex and is consisted of four main alpine geotectonic units (Papanikolaou et al 2004a): a) The lowest-basement unit (relatively autochthon) comprises the metamorphosed formations of Athens and can be found in Mount Penteli and Mount Hymettus. Formations include marble, dolomite, and mica-schist amongst others. b) The Alepovouni unit found in the western side of Mount Hymettus, also characterized by metamorphic formations. c) The Sub-Pelagonian unit, which can be found in Mount Egaleo and Mount Parnitha and consists of carbonate formations such as limestone and dolomitic limestone. d) The Upper Unit of Athens which is basically found in all the internal part of the basin and is divided into two napes. The lower nape is considered to be a "mélange" and was often referred to, as the 'Athens Schist', whereas the upper nape is comprised of limestone.

Kifissos is the longest river of the basin at approximately 33.7 km long and is also considered to be the main pluvial water recipient. As it was previously mentioned it derives from Mount Parnitha and discharges into the Saronic Gulf. Since it springs from Mount Parnitha, it goes through carbonate formations and is therefore expected to have high Ca^{2+} and HCO_3^- concentrations. For the most part it is inaccessible and specifically, for its last 15 km, starting at the area of Nea Halkidona, it is channeled under a highway (Kifissos Avenue) until it discharges into the Saronic Gulf. In terms of its geomorphology, the river is presently in a state of constant erosion.

Until the Upper Miocene the river's basic level was around 100-140 m higher than what it is today (Papanikolaou et al., 2004b). Kifissos is considered to be the most polluted river of the basin. Up

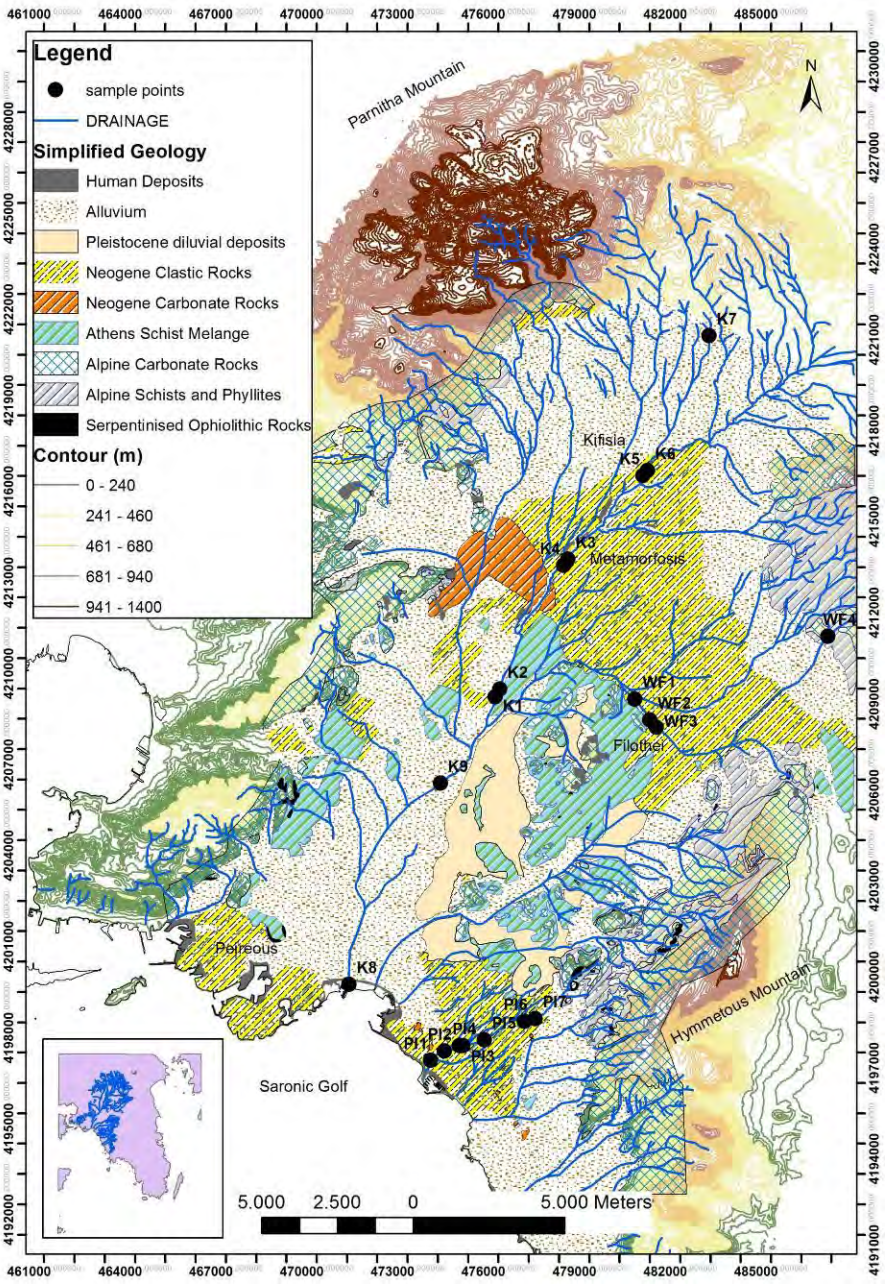

Figure 1 – Location of sampling sites plotted on the simplified geological map of Athens Basin, modified from Papanikolaou et al. 2004a.

until today it has been the recipient of industrial and residential waste, despite numerous legislative protection acts. Many houses and local industries are situated within the 1st class protection zone (A) which is a 50 meter wide zone, along both sides of the river bank.

The Pikrodafni stream is approximately 9.3 km long and is located in the south-western part of the city of Athens. Its drainage basin is around 22.4km^2 and it springs from the western side of Mount Hymettus discharging in the Saronic Gulf (Alimos area). It is considered to be in a better state than the Kifissos River and is one of the few streams of Athens which have been characterized as being

of special environmental interest. Around 6.6 km of its length is in its natural state whereas the remaining part is channeled. Pikrodafni has not reached a balanced geomorphological state and is in a continuous state of erosion, as is Kifissos (Papanikolaou et al, 2004b). It also has a continuous, yearlong flow. Despite the fact that there have been attempts for its rehabilitation it is considered to be a degraded natural environment. It is the recipient of local runoff and residential discharge. One of the biggest problems though is the fact that along the river banks there has been uncontrolled and illegal building. Even though the natural habitat has been disrupted various local species of fauna and flora have been reported. The Greek Ornithological association has reported 32 species of birds near the river mouth (2011), which are more than have been reported at the Kifissos River. Out of the reported species, 2 belong in the Greek Red Data Book of threatened species.

The stream of Podoniftis is considered to be a tributary of Kifissos. It is the smallest of the 3 studied streams, since a large part of it runs underground. It springs from the Mountain of Penteli and is then channeled underground until it reaches the area of Filothei in which it runs above ground naturally. Its drainage basin is around 14.3 km^2 and is mainly comprised of carbonate formations which therefore affect the waters chemistry. Podoniftis is considered to be in the best state in comparison to the other 2 streams. The stream has a wide variety of flora and fauna, but there have not been extensive analyses of the species. Characteristic examples of fauna are the frog Rana Ridibunda as well as the nightingale Luscina Magarhynchos. The most characteristic flora species are the Platanus orientalalis, Nerium Oleander and Hedera Helix .

3. Materials and Methods

3.1. Sampling and Analysis of Water

A total of 56 stream water samples were collected from 20 sampling stations covering the 3 streams (Figure 1), 27 of which from Kifissos, 21 from Pikrodafni and 8 from Podoniftis. The samples of Kifissos and Pikrodafni were obtained 3 times during a year long period whereas the samples of Podoniftis twice. All sampling occurred between the period of June 2011 and November 2012. The samples were collected under a wide range of flow conditions, including base and peak flow periods. Water samples were collected in 1L polyethylene sampling bottles which were rinsed 3 times with stream water before collecting the final sample. In situ measurements included parameters such as Total dissolved solids (TDS), Electrical Conductivity, temperature (T), pH and Eh. Samples which were collected for heavy metal analyses were filtered on the site through a plastic syringe fitted with a 0.45μm filter and were acidified using 1ml of nitric acid (HNO_3). They were then refrigerated until analyses were conducted.

Heavy metal (Pb, Mn, Co, Cd, Cr, Cu, Ni, Zn) concentrations were measured by Atomic Absorption Spectrometry (both FAAS and GAAS). Major anion (SO_4^{2-}, PO_4^{3-}, NO_3^-, Cl^-) concentrations were determined with the use of a HACH DR/4000 spectrophotometer. Total and Ca hardness, from which concentrations of Ca^{2+} and Mg^{2+} were derived, and the bicarbonate anion (HCO_3^-) were measured using the HACH digital titrator, whereas concentrations of K^+ and Na^+ were measured on a flame photometer. All samples which were obtained for the determination of major anion and cation concentrations were unacidified. They were filtered through a 0.45μm filter membrane in the lab and analysed within 24 hours of their collection. All analyses were performed in the Laboratory of Economic Geology and Geochemistry, University of Athens.

3.2. Sampling and Analysis of Active Stream Sediment

Stream sediment samples were collected once from each stream, 8 of which were from Kifissos, 10 from Podoniftis and 4 from Pikrodafni, accounting to a total of 22 samples. The sediment sampling also occurred during the year 2011-2012. Field samples were collected with a shovel and treated appropriately by drying in an air oven at 60 ^oC followed by sieving in order to prepare the laboratory samples of 150 μm. Heavy metals were extracted using a mixture of hot nitric (HNO_3)

and hydrochloric (HCl) acids. The concentrations of Pb, Mn, Co, Cd, Cr, Cu, Ni, Zn and Fe were determined by Flame Atomic Absorption Spectrometry (FAAS). Scanning Electron Microscopy (SEM) analysis was performed on most of the water filters, whereas X-Ray Diffraction (XRD) was used for mineralogical analyses of selected sediment samples.

4. Results and Discussion

4.1. Major Parameters of Water Chemistry

Ranges of values for the major measured parameters in water samples from the three streams are presented in Table 1. Also in Table 1 are given the respective median values from Greece Mainland Rivers (Skoulikidis et al. 2006) for comparison. The latter values are representative of water quality in more 'pristine' environments, away from urban centres, however they belong in the same geological and climatic zone with respect to national spatial scale.

Table 1 - Summary of concentration ranges for major water parameters in the studied streams. Median values of river water from mainland Greece (Skoulikidis et al. 2006) are also given for comparison.

Water Parameter	Pikrodafni	Kifissos	Podoniftis	Median values of Greek mainland rivers
T (°C)	17-27	8-28	12- 23	12.6
pH	7.7-8.4	7.2-9.0	7.3-8.0	8.2
EC (μS/cm)	790-1260	1.1-1476	770- 1228	294
Ca^{2+} (mg/ L)	90-96	97- 182	68-148	30.4
Mg^{2+} (mg/ L)	23-29	0-16	6-35	6.9
Na^{+} (mg/ L)	39-110	27-210	43-111	8.5
K^{+} (mg/ L)	5.5-8.2	1.4-23	1.7-7	1.9
HCO_3^{-} (mg/ L)	248-500	290-453	274-386	128
SO_4^{2-} (mg/ L)	76-121	32-700	60-100	15.8
Cl^{-} (mg/ L)	46-174	7.4-118	11-191	6.4
NO_3^{-} (mg/ L)	2-24	1-26	2-48	2.3
PO_4^{3-} (mg/ L)	0.45-8.9	0.31-14.4	0.04-4.50	0.5

These zones have been developed as a part of an integrated national ecological quality assessment and classification system. As expected most of the major parameters in the urban streams water, even when comparing their minimum values, exceed the median values of mainland stream water. Profound differences exist for EC, Na^{+}, SO_4^{2-} and Cl^{-}, indicative of urban impact on water quality (Wong et al. 2012). Atmospheric deposition and storm-water runoff in urban environments contains a variety of leached constituents including H_2SO_4, HNO_3, organic matter, trace metals and industrial compounds. Furthermore, the leakage, direct discharge or irrigation of wastewater (even when treated) can degrade water quality by increased concentrations of dissolved ions (e.g. Ca^{2+}, Cl^{-}, Na^{+}, SO_4^{2-}), nutrients (e.g. N, P) and pathogenic organisms. With respect to measured nutrient concentrations of NO_3^{-} and PO_4^{3-}, collected data show a high degree of variability related to seasonal fluctuations as well as presence of point sources along the flow path of the studied streams (Figure 2). When compared to the Nutrient Classification System developed by Skoulikidis et al. (2006), most samples fall within the 'moderate' to 'bad' quality categories.

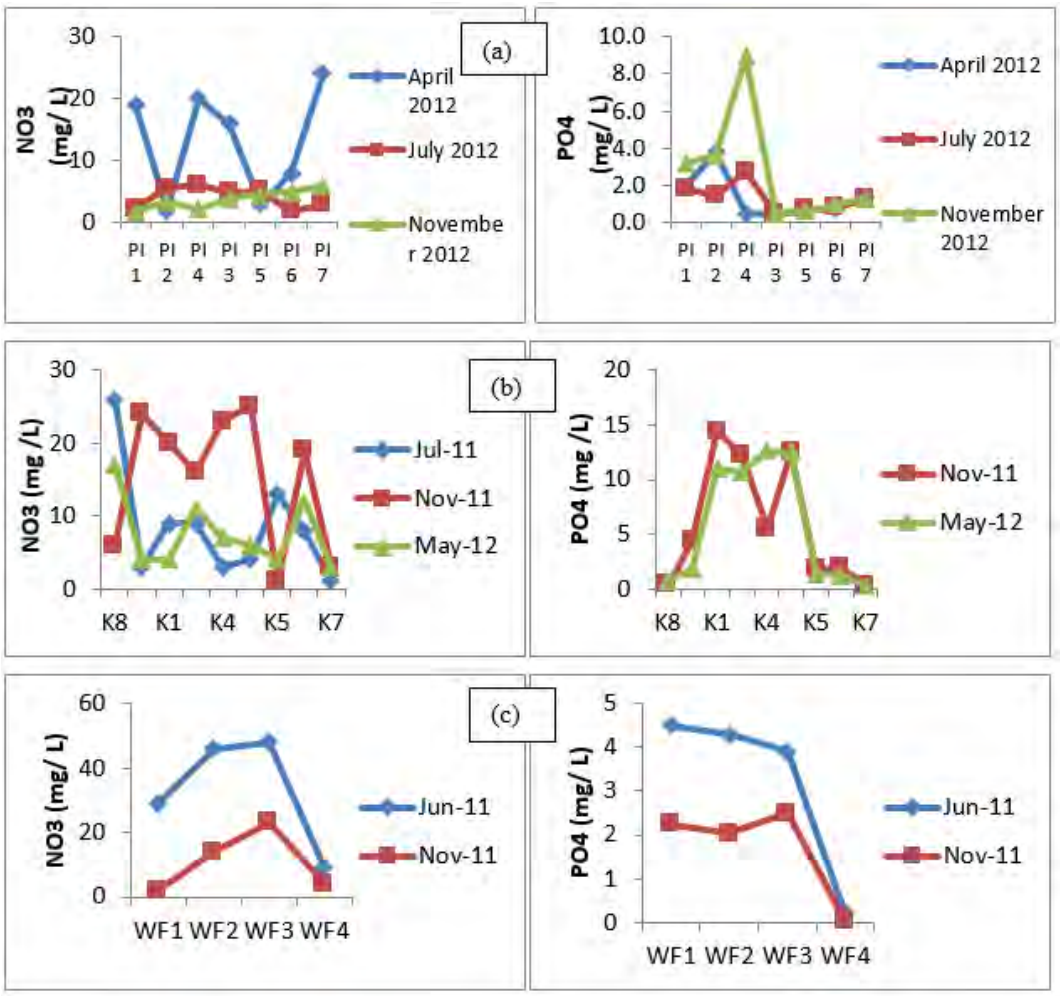

Figure 2 – Variation in NO_3^- and PO_4^{3-} concentrations in water along the studied streams. (a) Pikrodafni, (b) Kifissos, (c) Podoniftis. Data are presented downstream (left) to upstream (right).

Overall concentrations of the measured nutrients in the studied streams showed differences within the same sampling period (March- May 2012) (Figure 3). The highest values of NO_3 were measured in samples from Podoniftis and the lowest in Kifissos, while PO_4 was higher in Kifissos and had minimum values in Pikrodafni. It is noted that this comparison is only indicative considering differences in the spatial extend of sampling along the three streams. Kifisos had the highest concentrations of NO_3^- during the second sampling period (November 2011) in the areas of Kifisia (sampling point K6), Metamorphosis (Sampling points K3,K4) and Nea Halkidona (Sampling point K9). Point sources such as a livestock stable near the sampling area in Kifisia and greenhouse farming near the sampling area in Metamorphosis are the most likely causes of elevated levels of NO_3^-. In the area of Nea Halkidona concentrations were related to the high population density of this region, which had a consequent effect on the urban runoff which feeds into the river. High PO_4^{3-} concentrations were observed in the areas of Metamorphosis and Nea Philadelphia (sampling points K1-K4).This is probably related to the existence of greenhouse farms adjacent to the sampling points which use fertilizers and pesticides, that possibly leak into the river. The abrupt increase in the concentrations of NO_3^- and PO_4^{3-} in sample point WF3 of Podoniftis coincides with the river emerging from its underground channeled bed. The 2 to 4 fold

increase in concentrations compared to those observed in the headwaters at Penteli may be explained by unregulated discharges into the river along its underground course. Also worth noting is the significant decrease in concentration of both parameters with distance along the open course of the river through Filothei, probably explained not only by dilution but also by biologically mediated redox reactions taking place in the open air. Anomalous high values in the above mentioned parameters concentrations in Pikrodafni are attributed to point sources along the river course as they are mainly observed at tributaries of minor side inflows.

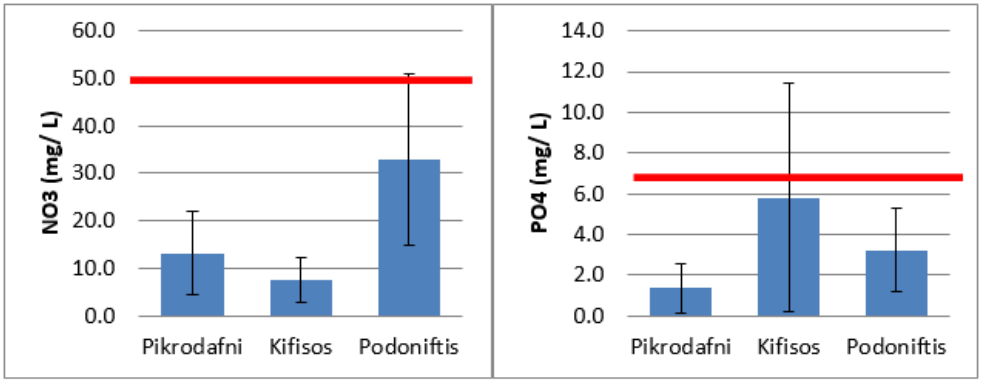

Figure 3 – Comparison of NO_3^- and PO_4^{3-} concentrations in water from the three studied streams during spring 2012. Bars denote one standard deviation. Thick horizontal lines indicate the upper concentration limit in drinking water.

Differences between the studied streams' water quality in terms of major ions were identified by plotting the data on a Piper diagram (Figure 4). Water type derived from this diagram reflects catchment and geological characteristics influencing ion concentrations. Although anthropogenic influence has affected water quality, clustering of water samples in the Piper diagram demonstrates

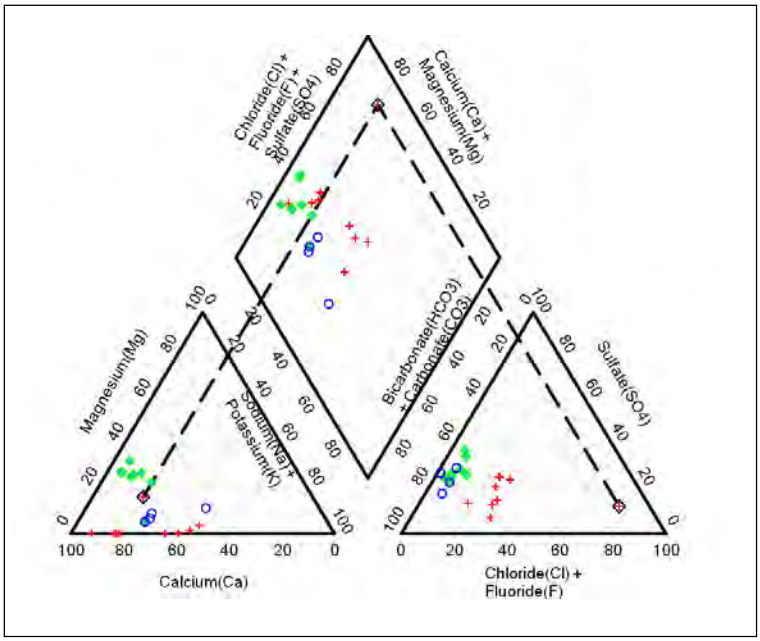

Figure 4 – Piper diagram showing differences in water type between the three studied streams. Crosses denote Kifissos samples, diamonds Pikrodafni samples and open circles Podoniftis samples.

the geological control over some of the major elements, especially Mg which is higher in samples from Pikrodafni mirroring the contribution of Hymettus dolomite marble dissolution in water quality characteristics.

The health of urban waterways is also reflected in their ability to support and maintain a balanced community of organisms of substantial species diversity. Although the study of biological diversity was beyond the scope of this research, some evidence of the streams' ability to support natural habitats was provided by the abundant numbers of diatoms observed by SEM on used water filters (Figure 5). Diatoms have been used as indicators of environmental change in rivers and lakes as several genera respond to eutrophication (Harding and Kelly, 1999; Stevenson and Pan, 1999). Detailed studies of diatom assemblages in rivers and streams can be statistically analysed to establish their relationship to the environmental factors, thus providing valuable data for bioassessment of river health.

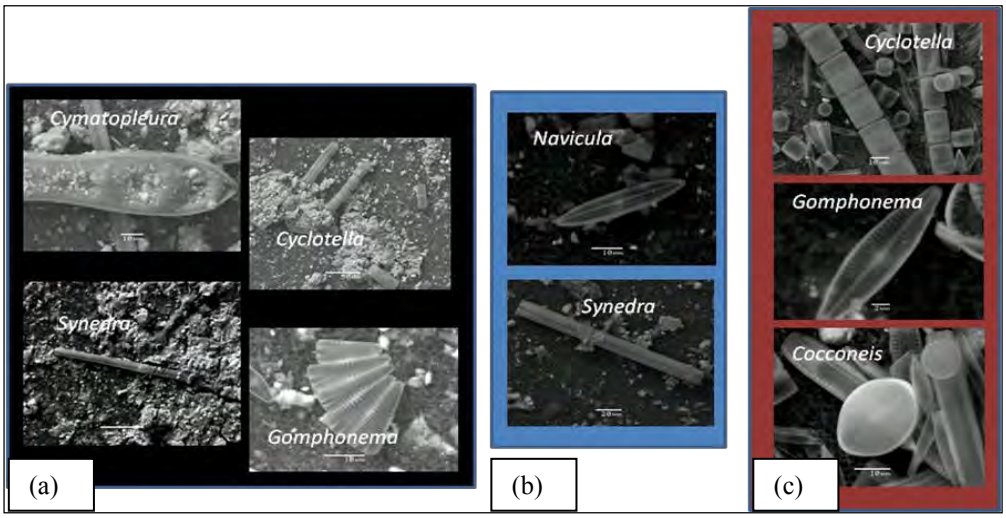

Figure 5 – SEM microphotographs of water filters in backscattered electron mode, showing abundant numbers of diatoms of various genera in the studied streams. (a) Kifissos, (b) Podoniftis, (c) Pikrodafni.

4.2. Heavy Metals in Water and Stream Sediment

Urban runoff can have elevated turbidity and high concentrations of metals such as Cu, Fe, Pb and Zn as a result of erosion from roads, parking lots and buildings. However the most significant source of heavy metals in urban environments is industry (Paul and Meyer, 2001). Measured concentrations of heavy metals in water samples from this study were not significant. Most of the determined parameters were below detection limits for all samples and all sampling periods. The three metals that showed measurable concentrations were Mn, Ni and Cu (Figure 6). From this only Mn in Kifissos samples reached the concentration of 50 μg /L but was near 10 μg /L in the samples from the other two streams. Ranges in concentrations of heavy metals in the stream sediment samples are presented in side by side boxplots in Figure 7.

Concentrations of all metals were within the expected background values and comparable to concentrations measured in urban soils of Athens (Massas et al. 2010). The highest concentrations of all metals were measured in samples from Pikrodafni and maximum concentrations were determined for Mn among all heavy metals. High concentrations of this particular element are probably linked to biogeochemical processes within the streamwater-sediment interface. Data of heavy metal concentrations are also comparable to values reported by Panagiotopoulos et al. (2010) for surficial and sub-surficial sediments obtained from the lower course of the Kifissos

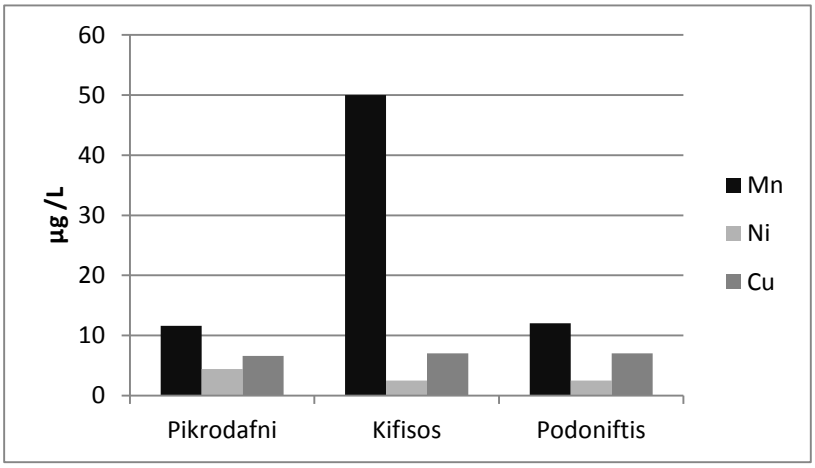

Figure 6 – Comparison of heavy metal concentrations in water samples from the three streams during the spring 2012 sampling campaign.

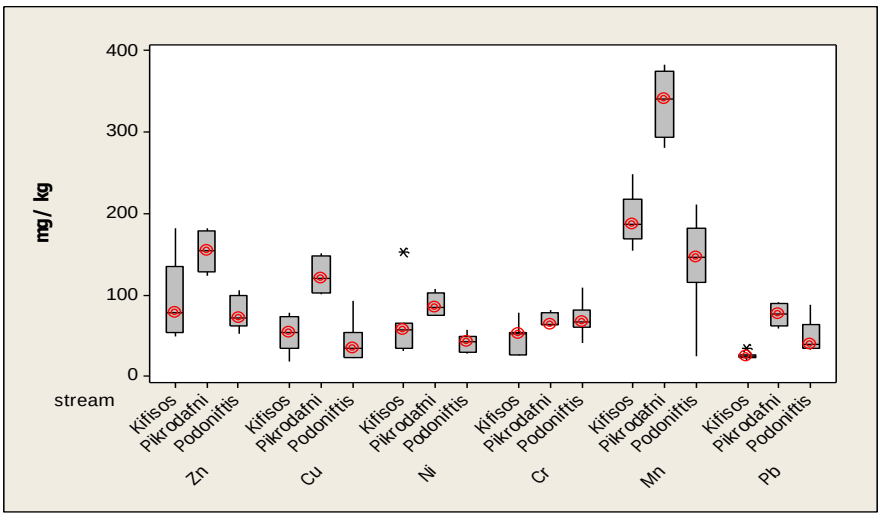

Figure 7– Box plots of heavy metal concentrations in stream sediments showing values within the normal background expected in urban environments.

River. In their study, the calculated enrichment factors for the identified heavy metals, with the baseline taken from a pristine area in the adjacent Saronikos Gulf, were very low. In contrast, the enrichment factors for the measured hydrocarbons were particularly high. This data underscore that the study of pollution in such environments is multicomponent, thus we must reserve judgement about the general quality of the urban stream systems.

5. Conclusions

The geochemistry of three urban streams in Athens was analysed and compared on the basis of major elements and heavy metals content in water and active sediment. Results indicated that rock weathering, rather than atmospheric or pollution influx is the dominant process affecting the major ion geochemistry of stream flow in the urban setting. Water samples from different streams are of a different Ca-Na-HCO_3 type indicating the effect of different lithological types on water chemistry. However, Kifissos and Podoniftis samples had higher nitrate and phosphate concentrations indicating greater influence by anthropogenic activities. Heavy metals in water did not have signif-

icant concentrations. Also, heavy metal concentrations in sediment samples were generally low; samples from Pikrodafni showed relatively higher concentrations than the other two streams.

In general the quality characteristics of water and sediment in the study area were found to be in a relatively good state regarding the studied parameters, capable of supporting abundant diatom populations. With appropriate management, the abiotic substrate of the studied streams could provide an opportunity for the evolution of a healthy ecosystem and development of so needed 'green belts' within the urban environment of Athens.

6. References

Harding J.P.C. and Kelly M.G. 1999. Recent developments in algal based monitoring in the UK, in: Prygiel et al. (eds) Use of algae for monitoring rivers III, *Agence de l'eau Artois Picardie*, France. Pp 26-34.

Massas I., Ehaliotis, C., Kalivas D. and Panagopoulou, G. 2010. Concentrations and availability indicators of soil heavy metals; the case of children's playgrounds in the city of Athens (Greece), *Water, Air, and Soil Pollution*, 212(1–4), 51–63.

Panagiotopoulos I., Kapsimalis V., Hatzianestis I., Kanellopoulos T.D. and Kyriakidou C. 2010. Environmental status of the metropolitan river (Kifissos) of Athens, Greece, *Environmental Earth Science*, 61, 983-993.

Papanikolaou D.I., Lozio S.G., Soukis K. and Skourtsos E., 2004a. The geological structure of the allochthonous 'Athens Schists', *Bulletin of the Geological Society of Greece vol. XXXVI, Proceedings of the 10th International Congress,* Thessaloniki, April 2004, 1550-1559 (in Greek with English abstract).

Papanikolaou D., Bassi E. K., Kranis H. and Danamos G., 2004b. Paleogeographic evolution of the Athens Basin from Upper Miocene to present, *Bulletin of the Geological Society of Greece vol. XXXVI, Proceedings of the 10th International Congress*, Thessaloniki, April 2004, 816-825 (in Greek with English abstract).

Paul M.J. and Meyer J.L. 2001. Streams in the urban landscape. *Annu. Rev. Ecol. Syst.,* 32, 333-365.

Skoulikidis N. Th., Amaxidis Y., Bertahas I., Laschou S. and Gritzalis K.. 2006. Analysis of factors driving stream water composition and synthesis of management tools—A case study on small/medium Greek catchments. *Science of the Total Environment*, 362, 205-241.

Stevenson R.J. and Pan Y. 1999. Assessing environmental conditions in rivers and streams with diatoms, in: Stoermer E.F. and Smol J.P (eds) The Diatoms: Applications for the Environmental and Earth Sciences. *Cambridge University Press*, UK. Pp.334-351.

Wong C. I., Sharp J.M., Hauwert N., Landrum,J. and White K. M. 2012. Impact of urban development on physical and chemical hydrogeology, *Elements*, 8, 429-434.

Δελτίο της Ελληνικής Γεωλογικής Εταιρίας, τομ. XLVII , 2013
Πρακτικά 13ου Διεθνούς Συνεδρίου, Χανιά, Σεπτ. 2013

Bulletin of the Geological Society of Greece, vol. XLVII 2013
Proceedings of the 13th International Congress, Chania, Sept. 2013

NEUTRALIZATION OF SLUDGE AND PURIFICATION OF WASTEWATER FROM SINDOS INDUSTRIAL AREA OF THESSALONIKI (GREECE) USING NATURAL ZEOLITE

Filippidis A.[1], Godelitsas A.[2], Kantiranis N.[1], Gamaletsos P.[2], Tzamos E.[1] and Filippidis S.[1]

[1] Division of Mineralogy-Petrology-Economic Geology, Department of Geology, Faculty of Sciences, Aristotle University of Thessaloniki, Panepistimioupoli, 54124 Thessaloniki, Greece.

2 Department of Geology and Geoenvironment, School of Sciences, University of Athens, Panepistimioupoli Zografou, 15784 Athens, Greece.

Abstract

The commixture of sludge from Sindos industrial area of Thessaloniki with high quality HEU-type natural zeolite (tuff with 86 wt.% clinoptilolite-heulandite) in equal proportions, resulted in odourless and cohesive zeosludge. Also, the treatment of wastewater of pH 7.8 from the same area with high quality HEU-type natural zeolite (88 wt.% clinoptilolite-heulandite) resulted in production of clear water of pH 7.3, free of odours and improved quality parameters by 60% for the NO_3^- content, 76% for the chemical oxygen demand (COD), 100% for P_2O_5 and Cr contents. Simultaneously, a precipitate of odourless and cohesive zeosludge was produced. The odourless and cohesive zeosludge produced either by the commixture of sludge with the natural zeolite or as precipitate from the treatment of industrial wastewater with the natural zeolite and coagulants, is suitable for safe deposition, since the fixation of the hazardous components in the micro/nano-pores of the HEU-type zeolite, as well as the meso- and macro-porous of natural zeolite, prevents their leaching by the rain water, protecting thus the quality of soils, surface and ground waters.
Key words: *Economic Geology, Waste treatment, environmental mineralogy, waste management.*

Περίληψη

Η ανάμειξη λάσπης από τη βιομηχανική ζώνη Σίνδου Θεσσαλονίκης με υψηλής ποιότητας φυσικό ζεόλιθο τύπου-HEU (τόφφος με 86 %κ.β. κλινοπτιλόλιθο-ευλανδίτη) σε ίσες ποσότητες, έδωσαν άοσμη και συνεκτική ζεολάσπη. Επίσης, η κατεργασία υγρών αποβλήτων pH 7,8 από την ίδια βιομηχανική ζώνη με υψηλής ποιότητας φυσικό ζεόλιθο τύπου-HEU (88 %κ.β. κλινοπτιλόλιθο-ευλανδίτη), έδωσε διαυγές νερό pH 7,3, ελεύθερο από οσμές και βελτιωμένες τις ποιοτικές παραμέτρους κατά 60% για τα NO_3^-, 76% για το χημικά απαιτούμενο οξυγόνο (COD), 100% για τα P_2O_5 και το Cr. Ταυτόχρονα, προέκυψε άοσμη και συνεκτική ζεολάσπη ως ίζημα. Η άοσμη και συνεκτική ζεολάσπη που προέκυψε είτε από την ανάμειξη της λάσπης με τον φυσικό ζεόλιθο, είτε ως ίζημα από την κατεργασία των βιομηχανικών υγρών αποβλήτων με φυσικό ζεόλιθο και κροκιδωτικά, είναι κατάλληλη για ασφαλή απόθεση, επειδή η καθήλωση των επιβλαβών συστατικών στους μίκρο/νάνο-πόρους του ζεόλιθου τύπου-HEU καθώς και στους μέσο- και μάκρο-πόρους του φυσικού ζεόλιθου, αποτρέπει την έκπλυσή

τους από το νερό της βροχής, προστατεύοντας έτσι την ποιότητα των εδαφών, επιφανειακών και υπόγειων υδάτων.
Λέξεις κλειδιά: *Κοιτασματολογία, Κατεργασία αποβλήτων, περιβαλλοντική ορυκτολογία, διαχείριση αποβλήτων.*

1. Introduction

Natural zeolite deposit corresponds to a rock which contains high amounts of one or more from the 80 natural phases of zeolites. The zeolite with the numerous applications is the HEU-type zeolite (clinoptilolite-heulandite) that shows tabular crystals and contains micro/nano-pores in a framework of channels with 10- and 8-member rings, in dimensions of 7.5x3.1 Å, 4.6x3.6 Å and 4.7x2.8 Å (Baerlocher et al. 2007; Mitchell et al. 2012). For nutritional, pharmaceutical, medical, environmental, cattle-raising, agricultural, aqua-cultural and industrial uses, the required HEU-type zeolite (clinoptilolite-heulandite) content should be greater than 75 wt.%. The presence of fibrous zeolites (e.g., erionite, mordenite, scolecite, mesolite, natrolite, roggianite, mazzite, ferrierite) is inhibitory for the use of natural zeolite (Tsirambides and Filippidis 2012).

Almost every industrial area is served by sludge and wastewater treatment facilities that aim to treat sludge and wastewater and dispose them in a safe manner using a variety of techniques (e.g., anaerobic, aerobic, coagulation/precipitation, composting). High quality HEU-type natural zeolites, display unique physical and chemical features and have a great variety of environmental, industrial, aquacultural and agricultural applications (e.g. Tserveni-Gousi et al. 1997; Colella and Mumpton 2000; Bish and Ming 2001; Kallo 2001; Ming and Allen 2001; Tchernev 2001; Filippidis and Kantiranis 2007; Filippidis et al. 2008; Filippidis 2010; Tzamos et al. 2011; Vogiatzis et al. 2012). The production of odourless-cohesive zeosludge using sludge from Sindos industrial area in proportions 20:80 and 40:60 (sludge:natural zeolite), as well as the purification of 300 mL Sindos industrial area wastewater using 0.1 and 0.2 g of natural zeolite, have been previously investigated (e.g. Filippidis et al. 2011a,b, 2012).

The present study investigates the neutralization of sludge from Sindos industrial area of Thessaloniki using high quality natural zeolite in proportion 50:50 (sludge:natural zeolite), as well as the purification of 300 mL Sindos industrial area wastewater using 0.4 g of high quality natural zeolite.

2. Materials and Methods

The natural zeolite samples used (Fig. 1) were supplied by GEO-VET N. Alexandridis & Co O.E. The mineralogical composition of natural zeolite samples were determined by X-Ray Powder Diffraction (XRPD). The XRPD analysis was performed using a Philips PW1710 diffractometer with Ni-filtered CuK_{α} radiation. The counting statistics were: start angle 3º, end angle 65º 2θ and scanning speed 1.2º/min. Semi-quantitative estimates of the abundance of the mineral phases were derived from the XRPD data, using the intensity (counts) of certain reflections, the density and the mass absorption coefficient for CuK_{α} radiation of the minerals present. The combined methods of SEM-EDS, thermal treatment and XRPD, revealed that the HEU-type zeolite contained in the zeolitic tuffs, presents characteristics of group I zeolite (clinoptilolite) and of group II (intermediate heulandite) (Kantiranis et al. 2006, Filippidis and Kantiranis 2007).

The natural zeolite was powdered in agate mortar and passed all through sieve < 0,5 mm. The sludge was mixed with natural zeolite in equal proportions, in a high-speed shaker for 5 seconds. The produced zeosludge was left to dry at room temperature for 24 hours. The wastewater was treated at room temperature with < 0.5 mm grain-size of natural zeolite in batch-type experiment. In 300 mL wastewater 0.4 g of natural zeolite was added under continuous stirring for 3 minutes followed by the addition of 0.1 mL of polyaluminium chloride and 2 mL of cationic

polyelectrolyte. The overflow and the precipitated zeosludge were separated by filtering. The zeosludge was dried overnight at room temperature. The starting wastewater and the overflowed clear water, were analyzed for (method): pH (Electrometric), Chemical Oxygen Demand (method of K_2CrO_6), P_2O_5 (Molecular Absorption Spectrophotometry), NO_3^-, Cu, Zn and Cr (Atomic Absorption Spectroscopy).

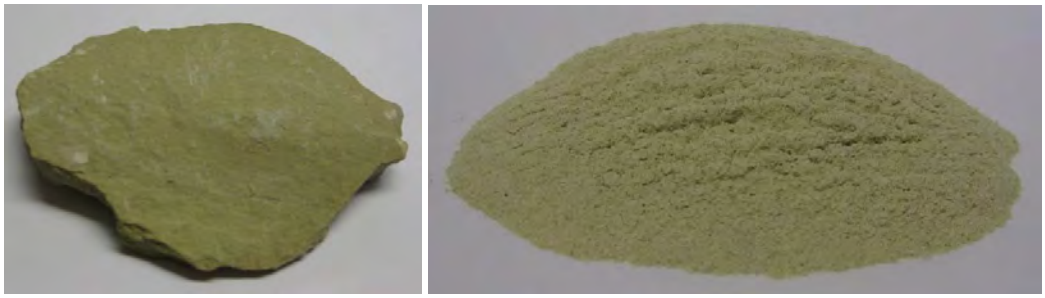

Figure 1 - Natural zeolite rock (left) and its powdered sample with grain-size <0.5 mm (right).

3. Results

The semi-quantitative mineralogical composition of natural zeolite samples used are presented in Table 1. The natural zeolite used for the sludge treatment contains 86 wt.% HEU-type zeolite (clinoptilolite-heulandite), 4 wt.% mica + clay minerals, 5 wt.% feldspars (plagioclase + alkali-feldspar) and 5 wt.% SiO_2-phases (quartz + cristobalite). The natural zeolite used for the wastewater treatment contains 88 wt.% HEU-type zeolite, 4 wt.% mica + clay minerals, 5 wt.% feldspars and 3 wt.% SiO_2-phases. The small differences observed between the natural zeolite samples concerning their semi-quantitative mineralogical composition are within the standard deviation of the XRPD method.

Table 1 - Semi-quantitative mineralogical composition (wt.%) of the natural zeolite samples.

Minerals	**Natural zeolite used for sludge treatment**	**Natural zeolite used for wastewater treatment**
HEU-type zeolite (clinoptilolite-heulandite)	86	88
Mica + Clay minerals	4	4
Feldspars (plagioclase + alkali-feldspar)	5	5
SiO_2-phases (quartz + cristobalite)	5	3
Total	100	100

The commixture of sludge from Sindos industrial area of Thessaloniki with the high quality HEU-type natural zeolite (86 wt.% clinoptilolite-heulandite) in equal proportions, resulted to odourless and cohesive zeosludge (Fig. 2).

The treatment of wastewater of pH 7.8 from Sindos industrial area of Thessaloniki with the high quality HEU-type natural zeolite (88 wt.% clinoptilolite-heulandite) resulted in production of clear water of pH 7.3, free of odours and improved quality parameters by 60% for the NO_3^- content, 76% for the chemical oxygen demand (COD), 100% for P_2O_5 and Cr contents (Table 2 and Fig. 3). Simultaneously, a precipitate of odourless and cohesive zeosludge was produced, after drying for 24 hours at room temperature (Fig. 4).

Figure 2 - Left: Raw sludge from Sindos industrial area of Thessaloniki, Right: Odourless and cohesive zeosludge (sludge:natural zeolite 50:50).

Table 2 - Quality characteristics of Sindos Industrial Area Wastewater (SIAW), overflowing Clear Waters treated with 0.1g (CW-0.1), 0.2g (CW-0.2) and 0.4g (CW-0.4) of natural zeolite and relevant improvement (±%).

Parameter (detection limit)	SIAW	CW-0.1[1]	±%	CW-0.2[2]	±%	CW-0.4[3]	±%
pH (0.1)	7.8	7.3	6	7.4	5	7.3	6
Chemical Oxygen Demand (COD), mg/L (15)	239	73	69	63	74	58	76
P_2O_5, mg/L (0.3)	9.1	bdl	100	bdl	100	bdl	100
NO_3^-, mg/L (2)	35	16	54	15	57	14	60
Cu, mg/L (0.1)	bdl	bdl	-	bdl	-	bdl	-
Zn, mg/L (0.1)	bdl	bdl	-	bdl	-	bdl	-
Cr, μg/L (5)	35	8	77	6	83	bdl	100

[1]Filippidis et al. (2011a), [2]Filippidis et al. 2011b, [3]Present study, bdl: below detection limit.

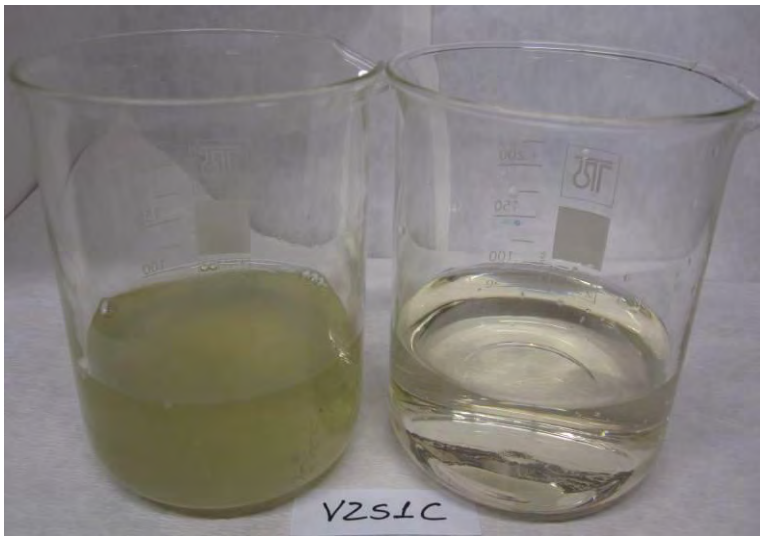

Figure 3 - Raw wastewater from Sindos industrial area of Thessaloniki (left) and clear water after the natural zeolite treatment (right).

Figure 4 - Odourless and cohesive zeosludge, dried at room temperature for 24 hours.

4. Discussion and Conclusions

The natural zeolite is of high quality, on average contains 87 wt.% HEU-type zeolite (clinoptilolite-heulandite), 4 wt.% mica + clay minerals, 5 wt.% feldspars (plagioclase + alkali-feldspar) and 4 wt.% SiO2-phases (quartz + cristobalite).

The commixture of industrial sludge with high quality natural zeolite produced odourless and cohesive zeosludge, suitable for safe disposal. The treatment of industrial wastewater of pH 7.8 with high quality HEU-type natural zeolite resulted in the production of clear water of pH 7.3, free of odours and improved quality parameters by 60% for the NO_3^- content, 76% for the chemical oxygen demand (COD), 100% for P_2O_5 and Cr contents. Simultaneously, a precipitate of odourless and cohesive zeosludge was produced. The increase of the added amount of natural zeolite from 0.1g to 0.4g, resulted in purification improvement by 6% for NO_3^-, 7% for COD and 23% for Cr, while for pH and P_2O_5 improvement was almost the same (Table 2).

The odourless and cohesive zeosludge produced either by the commixture of sludge with the natural zeolite or as precipitate from the treatment of industrial wastewater with the natural zeolite, is suitable for safe disposal, since the fixation of the hazardous components in the micro/nano-pores of the HEU-type zeolite, as well as the meso- and macro-porous of natural zeolite, prevents their leaching by the rain water, protecting thus the quality of soils, surface and ground waters (Filippidis 2010).

High quality HEU-type natural zeolite, sorb bacteria, fungi, gases, inorganic, organic and organometallic compounds, controls to neutral the pH of soils and waters, enriching in oxygen the waters (oxygenous currents), acting as acceptor and donor of protons, exhibiting thus an amphoteric character. The pH increase of the acidic waters is attributed to the binding of H^+ to the Lewis basic active sites of the HEU-type zeolite, while the pH decrease of the basic waters is attributed to the removal of OH^- from Brønsted acidic active sites and/or from the exchangeable hydrated cations of the HEU-type zeolite. The sorption of gases results in the oxygen enrichment of air and in remarkable malodour decrease (e.g. Filippidis et al. 1996, Charistos et al. 1997, Godelitsas et al. 1999, 2001, 2003, Filippidis and Kantiranis 2007).

The sorption and fixation of the different components by the micro/nano-pores of the HEU-type zeolite, as well as the meso- and macro-pores of the natural zeolite, are attributed to absorption (ion exchange), adsorption and surface precipitation processes. Important role in these processes play the surface Brønsted acidic and Lewis basic sites of the HEU-type zeolite structure. Due to the existence of these active sites, HEU-type zeolite reacts with the positively or/and negatively charged chemical species, even with molecules in gas condition. These chemical processes are

related to sorption and fixation physicochemical phenomena of ions and molecules, and concerns both the structural void spaces (micro/nano-pores) and the surface of the HEU-type zeolite crystals, consequently the meso- and macro-pores of the natural zeolite (e.g. Misaelides et al. 1995, Godelitsas et al. 1999, 2001, 2003, Kallo 2001, Kantiranis et al. 2011).

5. Acknowledgements

We express our gratitude to the company GEO-VET N. Alexandridis & Co O.E., for the supply of the natural zeolite samples.

6. References

Baerlocher Ch., McCuster L.B. and Olson D.H. 2007. *Atlas of Zeolite Framework Types*. 6th revised edition, Elsevier, Amsterdam.

Bish D.L. and Ming D.W. 2001. *Natural Zeolites: Occurrence, Properties, Applications*. Mineralogical Society of America, Washington DC.

Charistos D., Godelitsas A., Tsipis C., Sofoniou M., Dwyer J., Manos G., Filippidis A. and Triantafyllidis C. 1997. Interaction of natrolite and thomsonite intergrowths with aqueous solutions of different initial pH values at 25^{o} C in the presence of KCl: Reaction mechanisms, *Applied Geochemistry*, 12, 693-703.

Colella C. and Mumpton F.A. 2000. *Natural Zeolites for the Third Millenium*. De Frede Editore, Napoli.

Filippidis A. 2010. Environmental, industrial and agricultural applications of Hellenic Natural Zeolite, *Hellenic Journal of Geosciences*, 45, 91-100.

Filippidis A. and Kantiranis N. 2007. Experimental neutralization of lake and stream waters from N. Greece using domestic HEU-type rich natural zeolitic material, *Desalination*, 213, 47-55.

Filippidis A., Godelitsas A., Charistos D., Misaelides P. and Kassoli-Fournaraki A. 1996. The chemical behavior of natural zeolites in aqueous environments: Interactions between low-silica zeolites and 1M NaCl solutions of different initial pH-values, *Applied Clay Science*, 11, 199-209.

Filippidis A., Apostolidis N., Paragios I. and Filippidis S. 2008. Zeolites clean up, *Industrial Minerals*, 487 (April), 68-71.

Filippidis A., Tsirambides A., Kantiranis N., Tzamos E., Vogiatzis D., Papastergios G., Papadopoulos A. and Filippidis S. 2011a. Purification of wastewater from Sindos industrial area of Thessaloniki (N. Greece) using Hellenic Natural Zeolite, 9th International Hydrogeological Congress, Kalavrita, Greece. Environmental Earth Sciences, Springer-Verlag Berlin, *Advances in the Research of Aquatic Environment*, vol. 2, 435-442.

Filippidis A., Tsirambides A., Tzamos E., Vogiatzis D., Papastergios G., Georgiadis I., Papadopoulos A. and Filippidis S. 2011b. Purification of wastewater from Thessaloniki industrial area using Hellenic natural zeolite, *21st Panhellenic Chemistry Congress, Thessaloniki, Greece, 9-12/12/2011, Proceedings*, 8p (in Greek with English abstract).

Filippidis A., Godelitsas A., Tzamos E., Gamaletsos P. and Filippidis S. 2012. Production of odourless-cohesive zeo-sewagesludge and zeo-sludge with natural zeolite, *4th International Congress of Hellenic Solid Waste Management Association, Athens, Greece, Proceedings*, 6p. (in Greek).

Godelitsas A., Charistos D., Dwyer J., Tsipis C., Filippidis A., Hatzidimitriou A. and Pavlidou E. 1999. Copper (II)-loaded HEU-type zeolite crystals: characterization and evidence of surface complexation with N,N-diethyldithiocarbamate anions, *Microporous and Mesoporous Materials*, 33, 77-87.

Godelitsas A., Charistos D., Tsipis A., Tsipis C., Filippidis A., Triantafyllidis C., Manos G., and Siapkas D. 2001. Characterisation of zeolitic materials with a HEU-type structure modified by transition metal elements: Definition of acid sites in Nickel-loaded crystals in the light

of experimental and quantum-chemical results, *Chemistry European Journal*, 7(17), 3705-3721.

Godelitsas A., Charistos D., Tsipis C., Misaelides P., Filippidis A. and Schindler M., 2003. Heterostructures patterned on aluminosilicate microporous substrates: Crystallisation of cobalt (III) tris(N,N-diethyldithiocarbamato) on the surface of HEU-type zeolite, *Microporous and Mesoporous Materials*, 61, 69-77.

Kallo D. 2001. Applications of natural zeolites in water and wastewater treatment. In: *Natural Zeolites: Occurrence, Properties, Applications*, eds. D.L. Bish and D.W. Ming, Mineralogical Society of America: Washington DC, Reviews in Mineralogy and Geochemistry, 45, 519-550.

Kantiranis N., Chrissafis C., Filippidis A. and Paraskevopoulos K. 2006. Thermal distinction of HEU-type mineral phases contained in Greek zeolite-rich volcaniclastic tuffs, *European Journal of Mineralogy*, 18(4), 509-516.

Kantiranis N., Sikalidis K., Godelitsas A., Squires C., Papastergios G. and Filippidis A. 2011. Extra-framework cation release from heulandite-type rich tuffs on exchange with NH4+, *Journal of Environmental Management*, 92, 1569-1576.

Ming D.W. and Allen E.R. 2001. Use of natural zeolites in agronomy, horticulture and environmental soil remediation, in: *Natural Zeolites: Occurrence, Properties, Applications*, eds. D.L. Bish and D.W. Ming, Mineralogical Society of America: Washington DC, Reviews in Mineralogy and Geochemistry, 45, 619-654.

Misaelides P., Godelitsas A., Filippidis A., Charistos D. and Anousis I. 1995. Thorium and uranium uptake by natural zeolitic materials, *The Science of the Total Environment*, 173/174, 237-246.

Mitchell S., Michels N.L., Kunze K. and Perez-Ramirez J. 2012. Visualization of hierarchically structured zeolite bodies from macro to nano length scales, *Nature Chemistry*, 4, 825-831.

Tchernev D.I. 2001. Natural zeolites in solar energy heating, cooling and energy storage. In: *Natural Zeolites: Occurrence, Properties, Applications*, eds. D.L. Bish and D.W. Ming, Mineralogical Society of America: Washington DC, Reviews in Mineralogy and Geochemistry, 45, 589-617.

Tserveni-Gousi A.S., Yannakopoulos A.L., Katsaounis N.K., Filippidis A. and Kassoli-Fournaraki A. 1997. Some interior egg characteristics as influenced by addition of Greek clinoptilolitic rock material in the hen diet, *Archiv fur Geflugelkunde*, 61(6), 291-296.

Tsirambides A. and Filippidis A. 2012. Exploration key to growing Greek industry, *Industrial Minerals*, 533 (February), 44-47.

Tzamos E., Kantiranis N., Papastergios G., Vogiatzis D., Filippidis A. and Sikalidis C. 2011. Ammonium exchange capacity of the Xerovouni zeolitic tuffs, Avdella area, Evros Prefecture, Greece, *Clay Minerals*, 46, 179-187.

Vogiatzis D., Kantiranis N., Filippidis A., Tzamos E. and Sikalidis C. 2012. Hellenic Natural Zeolite as a replacement of sand in mortar: Mineralogy monitoring and evaluation of its influence on mechanical properties, *Geosciences*, 2, 298-307.

Δελτίο της Ελληνικής Γεωλογικής Εταιρίας, τομ. XLVII , 2013
Πρακτικά 13ου Διεθνούς Συνεδρίου, Χανιά, Σεπτ. 2013

Bulletin of the Geological Society of Greece, vol. XLVII 2013
Proceedings of the 13th International Congress, Chania, Sept. 2013

REMOVAL OF MALACHITE GREEN DYE FROM AQUEOUS SOLUTIONS BY DIASPORIC GREEK RAW BAUXITE

Georgiadis I.K.[1], Papadopoulos A.[1], Filippidis A.[1], Godelitsas A.[2], Tsirambides A.[1] and Vogiatzis D.[1]

[1]Aristotle University of Thessaloniki, School of Geology, Department of Mineralogy-Petrology-Economic Geology, igeorgia@chem.auth.gr, argpapad@geo.auth.gr, anestis@geo.auth.gr, ananias@geo.auth.gr, dvogias@geo.auth.gr

[2]National and Kapodistrian University of Athens, Faculty of Geology and Geoenvironment, Department of Mineralogy and Petrology, agodel@geol.uoa.gr

Abstract

Raw bauxite from Klisoura mine (Prefecture of Fokida, Greece) containing 72 wt.% diaspore, 16 wt.% hematite, 6 wt.% quartz, 4 wt.% anatase and 2 wt.% calcite, has been used for the removal of malachite green dye from aqueous solutions. The batch type experiments were conducted with 10 ml of solution, at pH = pH_{ZPC} = 6.7 and contact time 1 h. The initial concentration of malachite green dye was 10 mg/l, the bauxite quantity was 0.02 g, 0.04 g, 0.06 g, 0.1 g and 0.2 g. The highest adsorption capacity achieved was 4.5 mg/g (90% removal) using 0.02 g bauxite. The removal capacity of raw bauxite is comparable to other non-conventional adsorbents, such as neem sawdust, sugar cane dust and cane root carbon.
Key words: *Wastewater treatment, textile wastewater, adsorption, industrial minerals and rocks.*

Περίληψη

Ακατέργαστος ελληνικός βωξίτης από το μεταλλείο της Κλεισούρας (Νομός Φωκίδας) που περιέχει 72% κ.β. διάσπορο, 16% κ.β. αιματίτη, 6% κ.β. χαλαζία, 4% κ.β. ανατάση και 2% κ.β. ασβεστίτη, χρησιμοποιήθηκε για την απομάκρυνση της χρωστικής «πράσινο του μαλαχίτη» από υδατικά διαλύματα. Τα πειράματα τύπου batch εκτελέστηκαν σε διάλυμα 10 ml, σε pH = pH_{ZPC} = 6,7 και χρόνο επαφής 1 h. Η αρχική συγκέντρωση της χρωστικής «πράσινο του μαλαχίτη» ήταν 10 mg/l, ενώ οι ποσότητες του βωξίτη ήταν 0,02 g, 0,04 g, 0,06 g, 0,1 g και 0,2 g. Η μεγαλύτερη προσροφητική ικανότητα που παρατηρήθηκε ήταν 4,50 mg/g (90% απομάκρυνση) με τη χρήση 0,02 g βωξίτη. Η ικανότητα του ακατέργαστου βωξίτη στην απομάκρυνση της χρωστικής, είναι συγκρίσιμη με άλλα μη συμβατικά προσροφητικά, όπως πριονίδι από δέντρο neem, σκόνη ζαχαροκάλαμου και στάχτη ριζών καλαμιών.
Λέξεις κλειδιά: *Κατεργασία υγρών αποβλήτων, υγρά απόβλητα υφαντουργίας, προσρόφηση, βιομηχανικά ορυκτά και πετρώματα.*

1. Introduction

Removal of pollutants from wastewater is of crucial importance in environmental protection. The removal of non-biodegradable pollutants is of great interest due to their heavy potential environ-

mental impact. Several types of industrial dyes are commonly considered as non-biodegradable pollutants. Malachite green (a N-methylated diaminotriphenyl methane) dye is a commonly used non-biodegradable industrial dye.

Malachite green dye may have serious impact on human health and the environment in general. It has been reported to cause carcinogenesis, mutagenesis, chromosomal fractures, teratogenecity and respiratory toxicity. Histopathological effects of malachite green dye include multi-organ tissue injury (Srivastava et al., 2004). Despite all these facts, malachite green dye is still in use in aquaculture and other industries, and no effective alternative to it has yet been found.

Adsorption on activated carbon has been proven to be effective in removing dyes from aqueous solutions. However, activated carbon is still considered expensive and currently the research is focused on the development of low-cost adsorbents for this purpose. Low-cost adsorbents include natural, agricultural and industrial by-product wastes. They are attractive because of their abundant availability at low or no cost and their good performance in removing dyes from aqueous solutions.

Numerous adsorbents for malachite green dye have been used. Activated carbon from pine sawdust (Akmil-Basar et al., 2005), commercially available powdered activated carbon (Kumar and Sivanesan, 2006), activated carbon from lignite (Onal et al., 2007), carbon based adsorbent from the pyrolysis of waste materials from paper industry and pine bark (Mendez et al., 2007) and bentonite (Bulut et al., 2008). A number of non-conventional sorbents (Crini, 2006) such as sugarcane dust, algae, sawdust, bottom ash, fly ash, de-oiled soya, maize cob, peat, iron humate, mixed sorbents, microbial biomass, activated slag, waste product from agriculture, magnetic nanoparticle and coal have been tested for malachite green dye adsorption: Sugar cane dust (Khattri and Singh, 1999), neem sawdust (Khattri and Singh, 2000), chemically modified rice straw (Gong et al., 2006), hen feathers (Mittal, 2006), cyclodextrin based adsorbent, (Crini et al., 2007) rubber wood (Kumar and Sivanesan, 2007), lemon peel (Kumar, 2007) and Arundo donax root carbon (Zhang et al., 2008) were also used. An extensive review on nonconventional low-cost adsorbents for dye removal was reported by Das et al. (2009). For the same purpose, surfactant modified alumina has also been used (Das et al., 2009). High quality natural zeolite have been used for the purification of dye-work wastewaters (Filippidis, 2008, 2010, 2013; Filippidis et al., 2008).

Bauxite ore may exhibit a variety of colors and is mainly composed of amorphous and/or crystalline alumina oxides and hydroxides, namely gibbsite, boemite and diaspore. It is mainly used for the production of aluminum metal. Additionally, bauxite is used for numerous non-metallurgical end uses. Through the Bayer process, bauxite is converted to alumina (Al_2O_3); especially activated alumina is used as adsorbent, desiccant and catalyst, while calcined alumina is used in abrasives, ceramics and refractories. Hard-burned (sintered) calcined alumina is used for the production of tabular alumina and principally for high performance refractory materials. Finally, fused alumina is mainly used for abrasives and refractories (e.g., Harben and Dickson, 1983; Benbow, 1988; Bolger, 1997; Crossley, 2001; Harben, 2002; Taylor, 2003).

The present study investigates, for the first time, the ability of diasporic raw bauxite (a low-cost adsorbent) to remove the malachite green dye from aqueous solutions.

2. Materials and Methods

The bauxite sample used in this study was obtained from b3 bauxitic horizon of the Klisoura open pit mine, Prefecture of Fokida, Central Greece. In the Parnassus–Ghiona geotectonic zone or Parnassus zone, three bauxitic horizons were formed, b1) Middle/Upper Jurassic, b2) Kimmeridgian/Tithonian and b3) Upper Aptian, Lower Albian, Lower Senonian (e.g., Kiskyras, 1982; Tataris, 1986).

Polished and polished thin sections of the bauxite have been studied. The mineralogical composition of the samples was determined by X-Ray Powder Diffraction (XRPD) analysis, using a

Philips diffractometer with Ni-filtered CuKα radiation on randomly oriented samples. The sample was scanned from 3° to 43° 2θ at a scanning speed of 1.2°/min. Semi-quantitative estimates of the abundance of the mineral phases were derived from the PXRD data, using the intensity (cps) of specific reflections, the density and the mass absorption coefficients for CuK_α radiation of the minerals present.

The chemical composition of the sample was measured by a Perkin Elmer 3300 Atomic Absorption Spectrometer with a graphite furnace following standard wet chemical methods. The loss of ignition (LOI) of the bauxite sample was determined gravimetrically by firing 0.8 g of the powder at 925°C for 45 min.

The raw bauxite sample was crushed by the use of agate mortar to a particle size < 63μm. Prior to the adsorption experiments the pulverized raw bauxite was dried by heating (75°C for 24 h). The pH at the potential of zero charge of the adsorbent (pH_{ZPC}) was determined using the pH drift method (Jia et al., 2002; Govindasamy et al., 2009): A solution of 0.01 M NaCl was prepared and eleven aliquots of 50 ml each were taken; their pH was fixed between 2 and 12 using 1 M HCl and 1 M NaOH solutions. In every aliquot 0.1 g of adsorbent was added and the final pH of the suspension was measured (Hanna pH 301 pH/ion meter) after 24 h.

Malachite green dye (malachitgrün-oxalat pro analysi, C.I. 42,000, FW=927.10 g/mol, Merck) was used as adsorbate, without further purification. Stock solution was prepared by diluting exactly 400 mg of malachite green dye in one litre of deionized water. The working solutions were prepared by the appropriate dilution of this solution. The adsorption of malachite green dye on natural bauxite was investigated in batch mode experiments using the standard immersion method (Rouquerol et al., 1999). For this reason, working solutions of initial concentration 10 mg/l in malachite green dye were prepared. Their pH was fixed to the desired value by using 1 M HCl and 1 M NaOH solutions. Sealing test tubes were used containing aliquots of 10 ml of solution with 0.02 g, 0.04 g, 0.06 g, 0.1 g and 0.2 g of powdered raw bauxite. They were shaken for 1 h in 20 rpm and then centrifuged in 3000 rpm for 15 min. The concentration of the remaining malachite green dye in the supernatant solution was then measured using SHIMADZU UV-1700 PharmaSpec spectrophotometer at λ=619 nm (measured value). All the adsorption studies were carried out at ambient temperature.

3. Results and Discussion

The texture of the studied bauxite sample is oolitic (Figure 1). The oolits are usually smaller than 2 mm, their shape is round or elliptic and are usually consisted of Al-minerals (diaspore) and Fe-minerals (hematite). More specifically, the oolite consists of either a mineral or mainly of concentric shells of alternating mineral composition, which indicate varying deposition conditions. Usually, either the diasporic oolits are surrounded by an outer hematite shell or hematite can be found as distinguished spots into the main mass. Finally, hematite can be found as a filling material at the rock cracks.

The XRPD analysis revealed that the bauxite sample contains 72 wt.% diaspore (theoretical chemical forlula AlOOH), 16 wt.% hematite (Fe_2O_3), 6 wt.% quartz (SiO_2), 4 wt.% anatase (TiO_2) and 2 wt.% calcite ($CaCO_3$). The mineralogical composition of the raw bauxite is in good agreement (Table 1).

The determination of pH_{ZPC} (i.e. the pH at which the mineral's surface charge becomes zero) is of great importance for bauxite, as its major mineral constituent (diaspore) encompass hydroxyl ions into their strucrure; the latter are very reactive, contributing to the total mineral electric charge. At $pH < pH_{ZPC}$ raw bauxite exhibits a net positive charge, whereas at $pH > pH_{ZPC}$ a net negative charge (Krauskopf and Bird, 1995). The studied sample demonstrates $pH_{ZPC} = 6.7$. In comparison, hematite has pH_{ZPC} between 5 and 9, goethite has pH_{ZPC} ranging around 7.5 and gibbsite has pH_{ZPC}

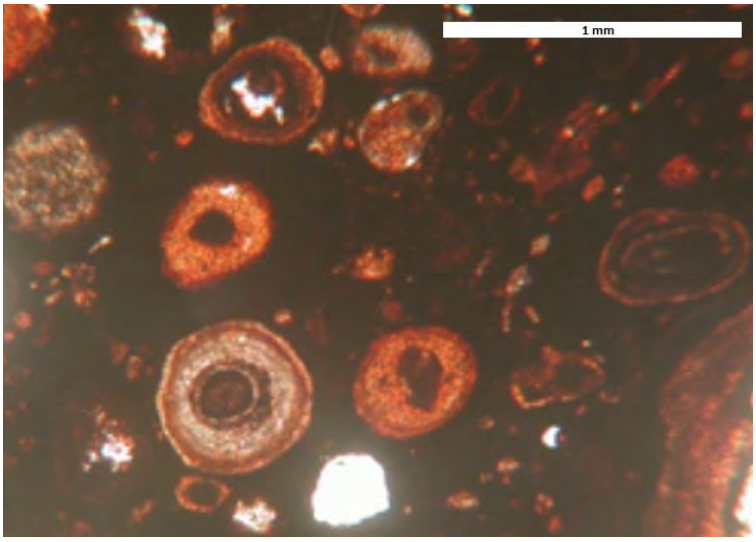

Figure 1 - Oolitic texture of the bauxite used (photomicrograph, polarizing microscope, +N).

Table 1 – Semi-quantitative mineralogical and chemical composition of the bauxite used.

Mineralogical composition (wt.%)		Chemical composition (wt.%)			
Diaspore	72	SiO_2	6.42	Na_2O	0.12
Hematite	16	Al_2O_3	59.54	TiO_2	3.84
Quartz	6	Fe_2O_3	15.16	MnO	0.01
Anatase	4	CaO	0.64	P_2O_5	0.15
Calcite	2	MgO	0.08	LOI (loss on ignition)	13.51
Total	100	K_2O	0.02	Total	99.49

= 9 (Krauskopf and Bird, 1995). For alumina a value of $pH_{ZPC} = 9.15$ and poor adsorption capacity for malachite green dye at pH < pH_{ZPC} has been reported (Das et al., 2009). In general, the suspension of oxides in an aqueous solution must form distinct surface charge sites due to the following mechanism (Prado et al., 2008; Preocanin and Kallay, 2006):

$$MOH_2^+ \leftrightarrow MOH + H^+$$

$$MOH \leftrightarrow MO^- + H^+$$

and especially when hydroxyl ions are attached to aluminium cations, the following mechanism is proposed (Krauskopf and Bird, 1995):

$$Al-OH + H^+ \rightarrow Al-OH_2^+$$

$$Al-OH + OH^- \rightarrow Al-O^- + H_2O$$

The former reaction is favoured in acid solutions and the latter in basic solutions.

The effect of adsorbent dosage for malachite green dye removal at initial concentration 10 mg/l and solution pH = $pH_{ZPC} = 6.7$ is presented in Table 2 and demonstrated in Figure 3. The optimum solid to solution ratio was 0.1 g of bauxite powder to 10 ml of solution.

Table 2 – Adsorption of malachite green (MG) dye by bauxite (In all experiments: Solution volume = 10 ml, pH = 6.7 and contact time = 1 h).

Initial concentration of MG (mg/l)	Amount of bauxite added (g)	Concentration of MG after 1 h (mg/l)	Adsorption of MG (%)
10	0.2	0.36	96.4
10	0.1	0.13	98.7
10	0.06	0.15	98.5
10	0.04	0.29	97.1
10	0.02	1.00	90.0

The maximum adsorption capacity is approximately 99 % with 0.1 g and 0.06 g of bauxite per 10 ml of malachite green dye solution. This value is comparable to other non-conventional adsorbents, such as neem sawdust, sugar cane dust, hen feathers and arundo donax root carbon (Khattri and Singh, 1999, 2000; Mittal, 2006; Zhang et al., 2008).

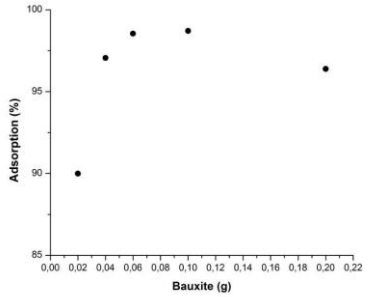

Figure 3 - Adsorption (%) of malachite green dye onto raw bauxite.

This non linear solid to solution dependence is already well documented (Limousin et al., 2007). The reasons for this effect may include, the aggregation of the suspended particles (Voice et al., 1983; Di Toro et al., 1986), the occupied volume of the suspended particles (Celorie et al., 1989), the solute transfer rate onto the surface of the adsorbent (Nandi et al., 2008) and the potential splitting of the amount of dye compounds adsorbed onto the unit weight of the adsorbent (Govindasamy et al., 2009). The optimum experimental value for solid to solution ratio for geomedia, would be a value representative of the natural conditions. The latter though demonstrate such value in general too high to be used in batch experiments (e.g. in solids the ratio tends to unity) (Limousin et al., 2007). For malachite green dye concentrations of 20 mg/l $\leq C_o \leq$ 100 mg/l, solid to solution ratio equal to 1:100 g/ml, solution pH = 5.3 ± 0.2, surfactant-modified alumina as adsorbent and at ambient temperature, the optimum time for malachite green removal was 30 min (Das et al., 2009).

In general, the decreasing order of adsorption capacities for various types of cationic dyes onto activated alumina (as amount of dye adsorbed per one gram of sorbent) is: Crystal violet > malachite green > rhodamine B > methylene blue (Singh et al., 1975). Malachite green values of $4.615 \cdot 10^{-5}$ g/g (with k = 0.1248 min^{-1}) and $7.590 \cdot 10^{-5}$ g/g (with k = 0.1139 min^{-1}) were also reported and the first order rate law for the adsorption process was found to be followed (Singh et al., 1975). The adsorption of malachite green onto surfactant-modified alumina fits into the Langmuir model isotherm, with q_{max} = 185 mg/g (Das et al., 2009). In this study, the maximum adsorption capacity recorded (q_{max}) was 4.5 mg/g for initial adsorbent quantity of 0.02 g.

4. Conclusions

The Greek raw bauxite as adsorbent is composed mainly of diaspore, with lesser hematite, quartz, anatase and calcite.

The adsorption capacity of diasporic raw bauxite increases up to approximately 99% for contact time 1 h, initial malachite green dye concentration 10 mg/l, solution pH = pH_{ZPC} = 6.7 and solution volume 10 ml. More specifically, for adsorbent dosage up to 0.06 g per 10 ml of solution, the adsorption capacity increases rapidly to 99%, then stabilizes to that value as the adsorbent amount increases up to 0.1 g and then slightly diminishes as more adsorbent is added.

The data presented, in conjunction were other literature, suggest that the phenomenon is more suitably described as a physical sorption process.

5. References

Akmil-Basar C., Onal Y., Kilicer T. and Eren D. 2005. Adsorption of high concentration malachite green by two activated carbons having different porous structures, *J. Hazard. Mater. B,* 127, 73–80.

Benbow J. 1988. Bauxite: Aluminating non-metallurgical sectors, *Industrial Minerals,* 252, 67-83.

Bolger R. 1997. Non – refractory bauxite, Variety but not much spice, *Industrial Minerals,* March 1997, 21-29.

Bulut E. Ozacaar M. and Ayhan Sengil I. 2008. Adsorption of malachite green onto bentonite: equilibrium and kinetic studies and process design, *Micropor. Mesopor. Mat.,* 115/3, 234-246.

Celorie J.A., Woods S.L., Vinston T.S. and Istok J.D. 1989. A comparison of sorption equilibrium distribution coefficients using batch and centrifugation methods, *J. Environ. Qual.,* 18, 307–313.

Crini G. 2006. Non-conventional low-cost adsorbents for dye removal: A review. *Bioresour. Technol.,* 97, 1061–1085.

Crini G., Peindy H.N., Gimbert F. and Robert C. 2007. Removal of C. I. basic green 4 (malachite green) from aqueous solutions by adsorption using cyclodextrin-based adsorbent: kinetic and equilibrium studies, *Separ. Purif. Technol.,* 53, 97–110 and references cited therein.

Crossley P. 2001. Bauxite in 2001-getting a grip on supply, *Industrial Minerals,* 401, 27-41.

Das A.K., Saha S., Pal A. and Maji S.K. 2009. Surfactant-modified alumina: An efficient adsorbent for malachite green removal from water environment, *J. Env. Sci. Health, Part A: Toxic/Hazardous Substances and Environmental Engineering,* 44/9, 896-905.

Di Toro D.M., Mahony,J.D., Kirchgraber P.R., O'Byrne A.L., Pasqual, L.R. and Piccirilli D.C. 1986. Effects of nonreversibility, particle concentration, and ionic strength on heavy metal sorption, *Environ. Sci. Technol.,* 20, 55–61.

Filippidis A., 2008. Treatment and recycling of municipal and industrial waste waters using Hellenic Natural Zeolite: A Review, *AQUA, 3rd Intern. Conf. Water Science and Technology with emphasis on water and climate*, Athens, Greece, Proc., 5p.

Filippidis A. 2010. Environmental, industrial and agricultural applications of Hellenic Natural Zeolite, *Hellenic Journal of Geosciences*, 45, 91-100.

Filippidis A. 2013. Industrial and municipal wastewater treatment by zeolitic tuff, *Water Today*, January, Volume-V (issue-X), 34-38.

Filippidis A., Apostolidis N., Paragios I. and Filippidis S. 2008. Purification of dye-work and urban wastewaters, production of odorless and cohesive zeo-sewage sludge, using Hellenic Natural Zeolite, *1st Intern. Conf. Hazardous Waste Management*, Chania, Greece, Proc., 8p.

Gong R., Jin Y., Chen F., Chen J. and Liu Z. 2006. Enhanced malachite green removal from aqueous solution by citric acid modified rice straw, *J. Hazard. Mater. B,* 137, 865–870.

Govindasamy V., Sahadevan R., Subramanian S. and Mahendradas D.K. 2009. Removal of malachite green from aqueous solutions by perlite, *Int. J. Chem. Reactor Engin.,* 7, 1-20.

Harben P.W. 2002. *The Industrial Minerals HandyBook*, Pensord, Blackwood, UK, 409 p.
Harben P.W. and Dickson E.M. 1983. Non-metallurgical grades-bauxite's crème de la crème, *Industrial Minerals,* 192, 25-43.
Jia Y.F., Xiao B. and Thomas K.M. 2002. Adsorption of metal ions on nitration surface functional groups in activated carbon, *Langmuir,* 18, 470-478.
Khattri S.D. and Singh M.K. 1999. Color removal from dye wastewater using sugar cane dust as an adsorbent, *Ads. Sci. Tech.,* 17, 269–282.
Khattri S.D. and Singh M.K. 2000. Color removal from synthetic dye wastewater using a bioadsorbent, *Water, Air, Soil Poll.,* 120, 283–294.
Kiskyras D. 1982. Characteristic features of the Greek bauxites in view of their origin, *Proc. Academy Athens,* 57, 82-95.
Krauskopf K.B.and Bird D.K. 1995. *Introduction to geochemistry (3rd ed.),* New York, McGraw-Hill, 647 pp.
Kumar K.V., Sivanesan, S. 2006. Pseudo second order kinetics and pseudo isotherms for malachite green onto activated carbon: Comparison of linear and non-linear regression methods, *J. Hazard. Mater. B,* 136, 721–726.
Kumar K. V. 2007. Optimum sorption isotherm by linear and non-linear methods for malachite green onto lemon peel, *Dyes Pigments,* 74, 595–597.
Kumar K.V. and Sivanesan S. 2007. Isotherms for malachite green onto rubber wood (Hevea brasiliensis) saw dust: Comparison of linear and non-linear methods, *Dyes Pigments,* 72, 124–129.
Limousin G., Gaudet J.-P., Charlet L., Szenknect S., Barthe`s V.and Krimissa M. 2007. Sorption isotherms: A review on physical bases, modelling and measurement, *Appl. Geochem., 22,* 249–275.
Mendez A., Fernandez F. and Gasco G. 2007. Removal of malachite green using carbon-based adsorbents, *Desalination,* 206, 147–153.
Mittal A. 2006. Adsorption kinetics of removal of a toxic dye, malachite green, from wastewater by using hen feathers, *J. Hazard. Mater. B,* 133, 196–202.
Nandi B. K., Goswami A., Das A. K., Mondal B. and Purkait M. K. 2008. Kinetic and Equilibrium Studies on the Adsorption of Crystal Violet Dye using Kaolin as an Adsorbent, *Sep. Sci. Technol.,* 43, 1382–1403.
Onal Y., Akmil-Basar C. and Sarici-Ozdemir C. 2007. Investigation kinetics mechanisms of adsorption malachite green onto activated carbon, *J. Hazard. Mater.,* 146, 194–203.
Prado A.G.S., Bolzon L.B., Pedroso C.P., Moura A.O.and Costa L.L. 2008. Nb_2O_5 as efficient and recyclable photocatalyst for indigo carmine degradation, *Appl. Catal. B,* 82, 219–224.
Preocanin T.and Kallay N. 2006. Point of zero charge and surface charge density of TiO_2 in aqueous electrolyte solution as obtained by potentiometric mass titration, *Croat. Chem. Acta,* 79, 95–106.
Rouquerol F., Rouquerol J.and Sing K. 1999. *Adsorption by powders and porous solids: Principles, methodology and applications.* San Diego, Academic Press, 485 pp.
Singh R., Gupta J.R.P. and Prasad B.B. 1975. Adsorption of cationic dyes by activated alumina, *Proc. Indian Natn. Sci. Acad.,* 41A, 163–169.
Srivastava S., Sinha R. and Roy D. 2004. Toxicological effects of malachite green, *Aquatic Toxicology,* 66, 319–329.
Tataris A. 1986. Bauxites-bauxitic clays (b2_3) of the "Intermediate" Limestone of the Parnassus-Ghiona zone. Origin of the bauxitic horizons material, *IGME, Geol. Geophys. Res., Spec. Iss.,* 449-465.
Taylor L. 2003. Bauxite's strength in diversity, *Industrial Minerals,* 432, 62-67.
Voice T.C., Rice C.P.and Weber W.J. 1983. Effects of solids concentration on the sorptive partitioning of hydrophobic pollutants in aquatic systems, *Environ. Sci. Technol.,* 17, 513–518.
Zhang J., Li Y., Zhang C. and Jing Y. 2008. Adsorption of malachite green from aqueous solution onto carbon prepared from Arundo donax root, *J. Hazard. Mater.,* 150/3, 774-782.

Δελτίο της Ελληνικής Γεωλογικής Εταιρίας, τομ. XLVII , 2013
Πρακτικά 13ου Διεθνούς Συνεδρίου, Χανιά, Σεπτ. 2013

Bulletin of the Geological Society of Greece, vol. XLVII 2013
Proceedings of the 13th International Congress, Chania, Sept. 2013

OCCURRENCE OF ARSENIC IN WATERS AND SEDIMENTS OF THE PALEA KAVALA RIVER, NE MACEDONIA, NORTHERN GREECE

Giouri K.[1], Vavelidis M.[1] and Melfos V.[1]

[1] Department of Mineralogy-Petrology-Economic Geology, Faculty of Geology, Aristotle University of Thessaloniki, agiouri@geo.auth.gr

Abstract

Inorganic arsenic (As) is a naturally occurring metal, present in various ecosystems. However, it can also be added to an aquatic system by anthropogenic activities. The aim of the present study is to determine the total As content in the Palea Kavala river (NE Macedonia, Northern Greece). The correlation between As content and some chemical and physico-chemical parameters of the samples was also examined. Research demonstrated significant As concentrations in the water and the sediments of the river. No correlation was found between As and pH, Fe, Mn in the water samples. Concerning the sediment samples, positive correlation was revealed for As with Fe and Mn content, while negative correlation was revealed between As and pH. This is probably indicative of a higher arsenic mobility in the Palea Kavala river water than in sediments. Since no anthropogenic activities were observed in the river's catchment area, elevated As concentrations are probably due to the lithology of the broader area and especially the presence of extended ore mineralizations including As-bearing sulphide minerals. However, the research in the study area is in progress since a more detailed evaluation of the local sources of As and mechanisms of As release is required.
Key words: *Inorganic contamination, heavy metals, Northern Greece.*

Περίληψη

Το αρσενικό (As) είναι χημικό στοιχείο που μπορεί να υπάρχει στα επιφανειακά υδάτινα οικοσυστήματα λόγω φυσικών αλλά και ανθρωπογενών δραστηριοτήτων. Ο σκοπός της παρούσας μελέτης είναι να προσδιοριστεί η περιεκτικότητα σε ολικό As τόσο των υδάτων αλλά και των ιζημάτων του ρέματος Παλαιάς Καβάλας, που βρίσκεται στην Ανατολική Μακεδονία (Β. Ελλάδα). Έγινε επίσης μία προσπάθεια να διερευνηθεί τυχόν συσχέτιση των συγκεντρώσεων του As με κάποιες χημικές και φυσικοχημικές παραμέτρους των δειγμάτων. Με βάση τα αποτελέσματα, δεν βρέθηκε κάποια συσχέτιση του As με τις περιεκτικότητες του Fe και Mn στα δείγματα ύδατος, καθώς ούτε και με το pH τους. Αντίθετα, προσδιορίστηκε ως θετική η συσχέτιση του As με τις συγκεντρώσεις Fe και Mn καθώς και με το pH των ιζημάτων. Οι υψηλές περιεκτικότητες As σε όλα τα δείγματα, πιθανόν να οφείλονται στην ύπαρξη μεταλλοφοριών στην ευρύτερη περιοχή έρευνας με μεικτά θειούχα ορυκτά που περιέχουν As, παρά σε ανθρωπογενείς δραστηριότητες. Παρόλα αυτά, είναι απαραίτητη περαιτέρω έρευνα, ώστε να προσδιοριστούν με μεγαλύτερη λεπτομέρεια οι πηγές του As στην περιοχή.
Λέξεις κλειδιά: *Ανόργανοι ρυπαντές, Βαρέα μέταλλα, Βόρεια Ελλάδα.*

1. Introduction

Trace elements, especially heavy toxic metals, in surface waters are attributed to natural or anthropogenic sources. In elevated concentrations, toxic metals may lead to irreversible health diseases. For this reason, the pollution of the surface aquatic systems, especially rivers, with inorganic pollutants has been attracting the attention of public and scientific community over the last few decades (Kabata-Pendias and Pendias, 2001; Suthar et al., 2009). A naturally occurring element in ecosystems is inorganic arsenic (As). It occurs in a variety of environmental media, including minerals, rocks, sedimentary deposits, soil, water and plants and usually is incorporated in sulfide minerals. Nevertheless, arsenic can also originate from anthropogenic activities and transmitted in the environment as a contaminant through sewage discharge or use of fertilizers in agriculture (Nordstrom, 2002; Hoang et al., 2010).

Arsenic contamination in water has caused severe health problems around the world, since it causes serious natural hazards when exceeding the established standards. The association between arsenic and human health effects is well described by numerous related surveys globally. Furthermore, the chemical analysis of river sediments is very useful when studying inorganic contamination in an area (Förster and Salomons, 1991; Abernathy et al., 2003 and references therein).

The objective of the present study is to determine the presence of the total arsenic content in water and sediments of the Palea Kavala river and examine if there is any correlation with chemical and physico-chemical parameters of the samples. Palea Kavala river is located 6 km north of the Kavala city, in northeastern Greece (Figure 1). It emanates from the Lekani mountains and passing through the Palea Kavala village it flows towards the Philippoi plain. When entering the plain, due to the extensive karst formations, the river disappears into the sediments.

2. Geological Setting

Geologically the study area belongs to the lower Pangeon unit of the Rhodope massif, consisting mainly of gneisses overlain by marbles. In the Palea Kavala area the metamorphic rocks of the Rhodope massif, were intruded by the Kavala pluton of a Lower Miocene age (21-22 Ma). The latter has the characteristics of an I-type intrusion and is mainly composed of amphibole-biotite granodiorite. Alluvial deposits which consist of clays, sands and gravels overlie the crystalline rocks (Kronberg, 1970; Kronberg and Melidonis, 1970; Christofides, 1996; Vavelidis et al., 1997; Melfos et al., 2008) (Figure 1).

The Palea Kavala region contains ~150 minor hydrothermal–magmatic base- and precious-metal occurrences within the Kavala pluton and the surrounding metamorphic rocks of the Rhodope massif. These occurrences have variable metal assemblages that include Fe-Mn-(Pb±Zn±Ag), Fe-Mn-Au, Fe-As-Au, Fe-Cu-Au and Bi-Te, but most are weathered and oxidized. Primary metallic minerals consist of pyrite, arsenopyrite, chalcopyrite, pyrrhotite, galena, sphalerite, tetrahedrite-tennantite, petzite, bismuthinite, tetradymite, cosalite, bismuthinite, lillianite, proustite, pyrargyrite, argentite, jalpaite, stephanite and native gold. Arsenic is mainly related with arsenopyrite, proustite and tennantite (Vavelidis et al., 1996a,b; Melfos et al., 2008; Fornadel et al., 2011).

3. Materials and Methods

3.1. Sample Collection

Seven sites were sampled for water (PKW1 to PKW7) and thirteen sites for their sediments (PK1 to PK13) downstream the Palea Kavala river (Figure 1). Water and sediment sampling was carried out in November 2009, after the dry season, and in May 2010, after the rainy season, leading to fourteen in total water samples.

Water sampling was performed with plastic bottles of 300 ml capacity, rinsed with distilled water. Following that, the samples were delivered on the same day to the laboratory. Sediment samples were collected at the top of the riverbeds and their banks, avoiding the input of other materials. All sediment samples were collected with a plastic shovel and were put in plastic bags.

3.2. Laboratory Treatment of Samples

The water samples were filtered through 0.45 μm Whatman filter paper, acidified with HNO_3 (1:1) to pH 2, and stored at 4° C in polyethylene plastic bottles until they were sent for analysis.

At the laboratory, after the removal of organic material, sediment samples were dried in an oven at 60˚ C. They were gently ground with rolling pin to disaggregate the samples but not break down the grains themselves, sieved to collect less than 0.063 mm grain size and stored in polyethylene bags until they were sent fir analysis. The <0.063 mm fraction was used due to the fact that the environmentally available trace elements mainly remain in this fraction, because of its larger specific area. Therefore, fine sediments have been used by many researchers in order to investigate river pollution (Kabata-Pendias and Pendias, 2001; Salomons, 1995).

3.3. Sample Analysis

The physico-chemical parameter pH of the water was measured in the field during sampling, using a portable combined instrument. The pH of sediments was measured at the laboratory using a digital pH-meter. The chemical analyses were performed at the Acme Analytical Laboratories (Vancouver, Canada). Metals in the sediments were extracted using the aqua regia digestion, while their concentrations were determined in all samples by ICP-MS.

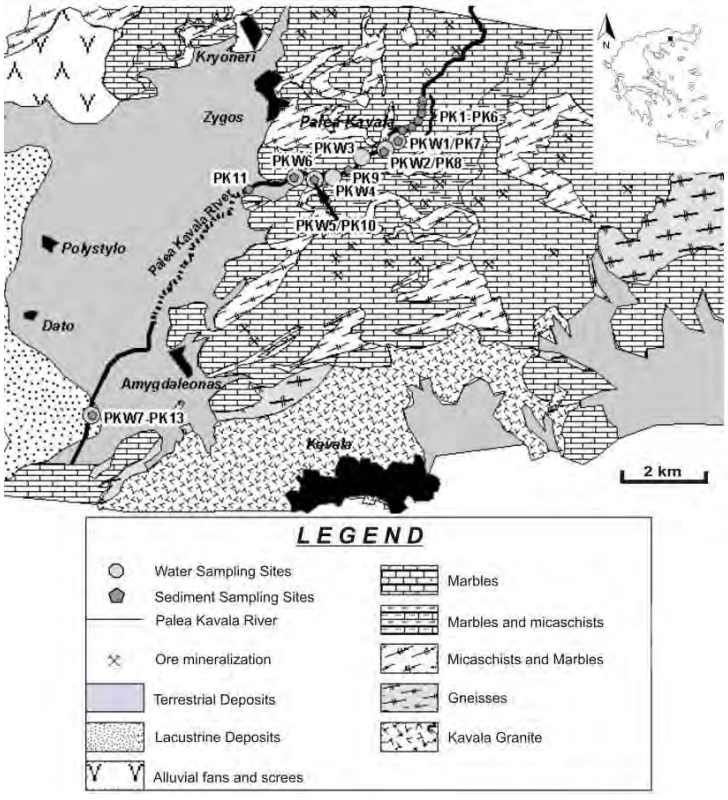

Figure 1 - Geological map of the studied area with the Palea Kavala river and sampling sites (according to Kronberg, 1970; Kronberg and Melidonis, 1970 with modifications).

4. Results and Discussion

The results of the physico-chemical analyses and of heavy metals content in water and sediment samples are shown in Table 1 and Table 2, respectively. The pH values were approximately neutral to slightly alkaline, with a range of 7.36 to 8.14. The range of concentration for As and Mn in the water samples was 15.9- 59.9 ppb and 0.5-152 ppb, respectively.

Arsenic content after the wet season ranges from 28.9 to 59.9 ppb, and after the dry season from 15.9 to 37.4 ppb. This demonstrates that arsenic levels after the dry season (November 2009) are higher than the respective ones which followed the wet season (May 2010). It is apparent, therefore, that arsenic contents were higher during the period of a low river flow (Figure 2). This has also been confirmed by previous studies (Giouri et al., 2012), according to which significant variations of As content were found in most of the sites. However, clear trends in these changes between wet and dry season were not determined, as it was also concluded by the coefficient of determination (R2). According to its value (R2=0.60) there was found a positive but moderate correlation between wet and dry season As concentrations.

Table 1 - Results of the pH and the As, Mn concentrations in surface waters of the Palea Kavala river.

Number of samples		pH	As (ppb)	Mn (ppb)
n=14 (PKW1a–PKW7a→Nov-2009) (PKW1b–PKW7b→May-2010)	min	7.36	15.9	0.5
	max	8.14	59.9	152.0
	median	7.63	35.9	2.8
	mean	7.71	38.7	22.7

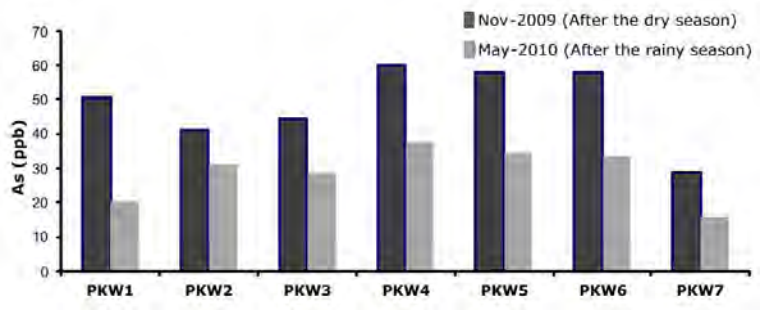

Figure 2 - Variation in the concentrations of As in the water samples collected downstream P alea Kavala river, for both sampling periods.

Table 2 - Results of the pH and the As, Mn, Fe concentrations in the sediments of the Palea Kavala river.

Number of samples		pH	As (ppm)	Mn (ppm)	Fe (wt %)
n=13 (PK1 – PK13)	min	6.33	51.3	405	1.6
	max	8.18	705.5	5268	4.0
	median	7.58	170.1	822	3.6
	mean	7.37	231.0	1097	3.1

The pH values of the sediments range from 6.33 to 8.18, without any drastic differences among sampling sites. As and Mn concentrations are high in all samples, ranging from 51.3 to 705.5 ppm and from 405 to 5268 ppm, respectively. Fe was also relatively high varying from 1.6 to 4.0 wt% (Table 2 and Figure 3). From the diagram in Figure 3, it can be concluded in general that the variation in As concentrations, follow the variations of Mn and Fe.

The distribution of As in water and sediments of surface streams or rivers, is related with the pH, the deliberate pollution and the release of other compounds which can adsorb arsenic. In the case of rivers, the As content may be strongly affected by geological characteristics of the drainage area of the rivers and by anthropogenic inputs. The adsorption of As on precipitated hydrous Fe and Mn oxides that exist in the sediments of the rivers, is significant. It is apparent, therefore, that the correlation between the content of As, Mn and Fe in the collected water and sediment samples should be further studied (McLaren and Kim, 1995; Smedley, P.L. and Kinniburgh, D.G., 2002; Gault et al., 2003; Sanchez-Rodas et al., 2005; Nordstrom, 2011; Sarmiento et al., 2012).

According to the water analyses results in Palea Kavala river, the relationship between As content and pH is weak but negative (Figure 4) with a correlation coefficient factor R^2=0.18. Similarly the correlation of As with Mn is also very poor, with R^2=0.0051 (Figure 4). Arsenic in water is also very poorly correlated with Fe. According to the present study, Fe in most of the samples was below detection limits, with the exception of 2 samples (data not shown). This means that there is not any relationship between As and Fe and therefore As in the water is not adsorbed because of the presence of Fe.

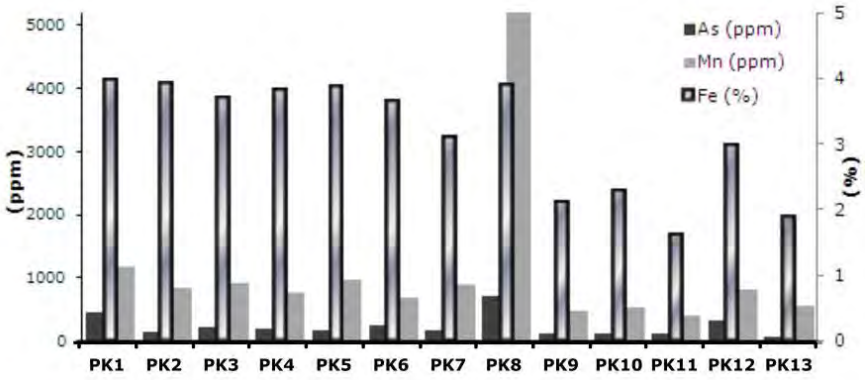

Figure 3 - Variation in the concentrations of As, Mn and Fe in the sediment samples collected downstream Palea Kavala river.

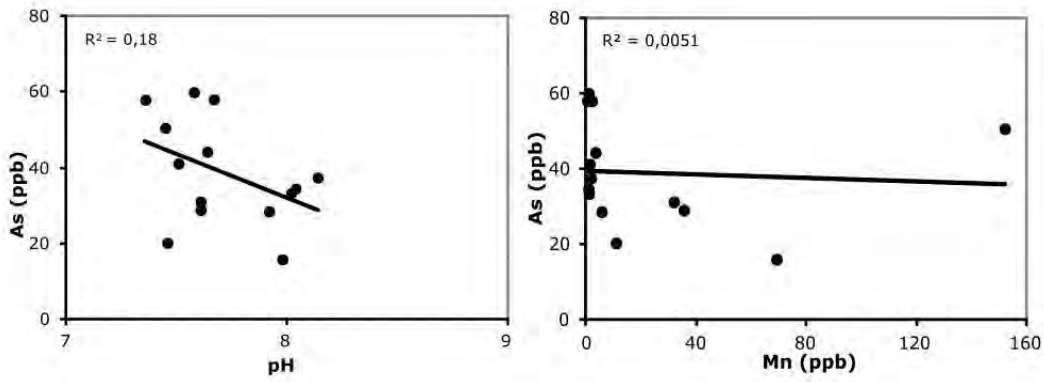

Figure 4 - Scatter plot of arsenic concentrations in the water sample in correlation with pH and Mn content.

According to the results of sediment analyses (Figure 5), a moderate negative correlation was observed between arsenic and pH (R^2=0.41). The correlation of As is stronger with Mn than with Fe. This is concluded since the value of correlation coefficient factor for As with Mn is R^2=0.77, while for As with Fe is R^2=0.30. It should be mentioned that the sample with the most elevated concentrations of As and Mn is not plotted close to the rest ones (Figure 5). However, by exempting that specific sample, the correlation between As and Mn is slightly weaker (R^2 decreases from 0.77 to 0.54), remaining still positive and relatively good. As illustrated in Figures 4 and 5, arsenic shows a closer relationship with pH, Fe and Mn in the sediments than with the corresponding parameters in water.

Since in the catchment area of Palea Kavala river any anthropogenic activities were not observed, which as a consequence can increase metal concentrations in the sediment and water, it is assumed that high arsenic content can be attributed to the geological environment. After all, some of the primary minerals that comprise the metal assemblages occurring in the Palea Kavala region, mainly arsenopyrite, proustite and tennantite (Fornadel et al., 2011), are related with the elevated As concentrations. This is also demonstrated in Figure 6, since it is revealed that higher concentrations of As are observed mainly upstream Palea Kavala river, where the majority of As-bearing ore mineralizations occur.

5. Conclusions

The purpose of the present study was to determine the total arsenic content in water and sediments of the Palea Kavala river (NE Macedonia, Northern Greece). Furthermore, it was examined if there is any correlation between As and some chemical and physico-chemical parameters in the samples.

Results of chemical analyses demonstrated considerable concentrations of As, both in water and sediments of the river. This is probably due to some geological factors such as the lithology of the broader area. Especially the presence of extended ore mineralizations which include arsenopyrite (FeAsS), proustite (Ag_3AsS_3) and tennantite ($(Cu,Ag,Fe,Zn)_{12}(As, Sb)_4S_{13}$) in metal occurrences in Palea Kavala region, and so in the river water and sediments because of weathering and transportation, can be related with As content.

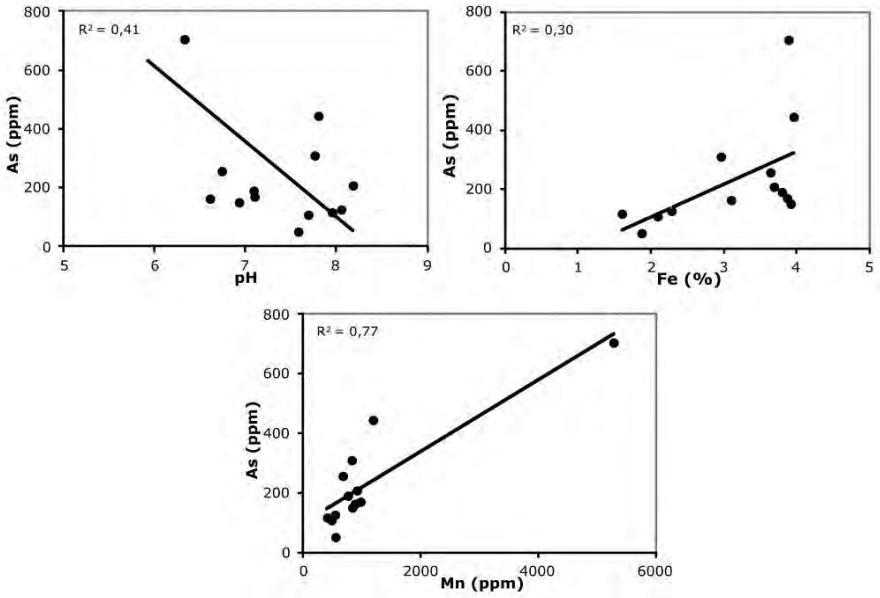

Figure 5 - Scatter plot of arsenic concentrations in every sediment sample in correlation with pH, Fe and Mn content.

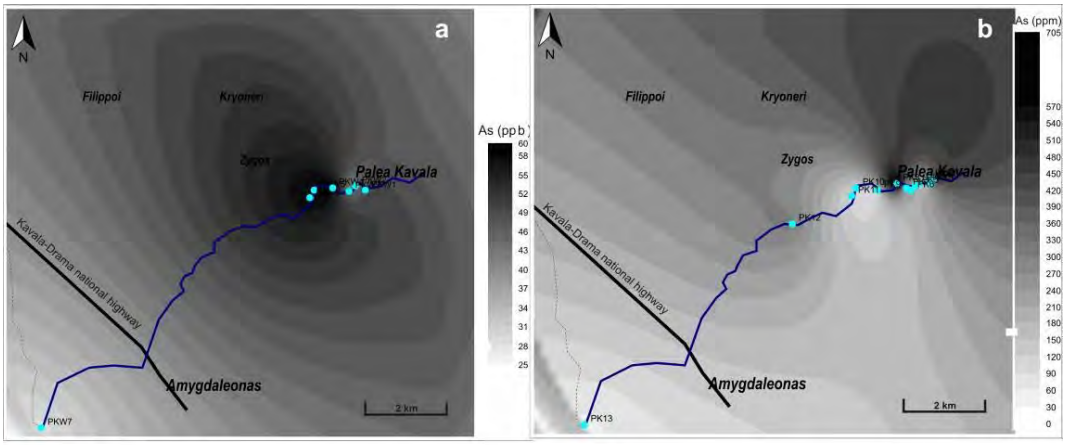

Figure 6 - Spatial distribution of $As_{(tot)}$ in the water (a) and sediments (b) of Palea Kavala river.

Physicochemical factors such as pH and the presence of Mn and Fe oxides, can contribute to the adsorption of As. However, no correlation was found between As content and pH, as well as Fe and Mn in the water samples. On the other hand, positive correlation was revealed for As with Fe and Mn and negative correlation was observed between As and pH in the sediments. It can probably be concluded that mobility of arsenic in Palea Kavala river is higher in water than in sediments. However, the research in the study area is in progress since a more detailed evaluation of the local sources of As and mechanisms of As release in surface water is required.

6. Acknowledgements

The first author (Giouri K.) would like to thank the State Scholarships Foundation of Greece for the financial support during her post-graduate studies. The authors would like to thank P. Voudouris, an anonymous reviewer and the associated editor for their constructive comments and recommendations.

7. References

Abernathy C.O., Thomasy D.J. and Calderon R.L. 2003. Toxicity and risk assessment of trace elements. Health effects and risk assessment of arsenic, *Am. Soc. Nutr. Sci.*, 1536–1538.

Christofides G. 1996. Tertiary magmatism in the Greek Rhodope Massif, northern Greece: Granitic plutons, in Knezevic V., Krstic B. (eds.), *Terranes of Serbia: The Formation of the Geologic Framework of Serbia and the Adjacent Regions*. University of Belgrade, Belgrade, 155–160.

Fornadel A.P., Spry, P.G., Melfos V., Vavelidis M. and Voudouris P.Ch. 2011. Is the Palea Kavala Bi–Te–Pb–Sb±Au district, northeastern Greece, an intrusion-related system? *Ore. Geol. Rev.*, 39, 119–133.

Förster U. and Salomons W. 1991. Mobilization of metals from sediment, in Merian, E. (eds), *Metals and their compounds in the environment*, VCH, Weinheim, 379–398.

Gault A.G., Polya D.A. and Lythgoe P.R. 2003. Seasonal variation of total dissolved arsenic and arsenic speciation in a polluted waterway, *Environ. Geochem. Health,* 25, 77–85.

Giouri A., Vavelidis M. and Melfos V. 2012. Primary approach on the evaluation of total arsenic concentration in Palea Kavala river, NE Macedonia, Northern Greece, *Proc. of the XI Protection and Restoration of the Environment International Conference*, Thessaloniki, 3-6 July, 356-364.

Hoang T.H., Bang S., Kim K.W., Nguyen M.H. and Dang D.M. 2010. Arsenic in groundwater and sediment in the Mekong River delta, Vietnam. *Environ. Pollut.*, 158, 2648-2658.

Kabata Pendias A. and Pendias H. 2001. Trace elements in soils and plants, 3rd ed. CRC Press, Boca Raton, Florida, 413p.

Kronberg P. and Melidonis N. 1970. Geological map of Greece, Krinidhes Sheet, Scale 1:50.000. IGME, Athens.

Kronberg P. 1970. Geological map of Greece, Kavala Sheet, Scale 1:50.000. IGME, Athens.

McLaren S.J. and Kim N.D., 1995. Evidence for a seasonal fluctuation of arsenic in New Zealand's longest river and the effect of treatment on concentrations in drinking water. *Environ. Pollut.,* 90 (1), 67–73.

Melfos V., Voudouris P., Vavelidis M. and Spry, P.G. 2008. Microthermometric results and formation conditions of a new intrusion-related Bi–Te–Pb–Sb±Au mineralization in the Kavala Pluton, Greece. Joint 13th All-Russian Conference on Thermobarogeochemistry/ *4th Asian and Pacific International Fluid Inclusion Society Symposium*, Moscow, Abstracts.

Nordstrom D.K. 2002. 'Public health. Worldwide occurrences of arsenic in ground water, *Science*, 296, 2143–2145.

Nordstrom D.K. 2011. Hydrogeochemical processes governing the origin, transport and fate of major and trace elements from mine wastes and mineralized rock to surface waters, *Appl. Geochem.*, 26, 1777 – 1791.

Salomons W. 1995. Environmental impact of metals derived from mining activities: processes, predictions, preventions, *J. Geochem. Explor*., 52, 5–23.

Sanchez-Rodas D., Gomez-Ariza J.L., Giraldez I., Velasco A. and Morales E. 2005. Arsenic speciation in river and estuarine waters from Southwest Spain, *Sci. Total Environ*., 345, 207–217.

Sarmiento A.M., Caraballo M.A., Sanchez-Rodas D., Nieto J.M. and Parviainen A. 2012. Dissolved and particulate metals and arsenic species mobility along a stream affected by Acid Mine Drainage in the Iberian Pyrite Belt (SW Spain), *Appl. Geochem.,* 27, 1944-1952.

Smedley P.L. and Kinniburgh D.G. 2002. A review of the source, behavior and distribution of arsenic in natural waters, *Appl. Geochem*., 17, 517–568.

Suthar S., Nema K.A., Chabukdhara M. and Gupta K.S. 2009. Assessment of metals in water and sediments of Hindon River, India: Impact of industrial and urban discharges, *J. Hazard. Mater.*, 171, 1088–1095.

Vavelidis M., Christofides G. and Melfos, V. 1996a. The Au–Ag-bearing mineralization and placer gold of Palea Kavala (Macedonia, N. Greece). In Knežević-Dorđević, V., Krstić, B. (eds.), *Terranes of Serbia: The Formation of the Geologic Framework of Serbia and the Adjacent Regions*. University of Belgrade, Belgrade, 311–316.

Vavelidis M., Gialoglou G., Melfos V. and Wagner G.A. 1996b. Goldgrube in Palaea Kavala-Griechenland: Entdeckung von Skaptehyle? *Erzmetall,* 49, 547–554.

Vavelidis M., Melfos, V. and Eleftheriadis G. 1997. Mineralogy and microthermometric investigations in the Au-bearing sulphide mineralization of Palea Kavala (Macedonia, Greece). In Papunen, H. (eds.), *Mineral Deposits: Research and Exploration — Where do They Meet?* Balkema, Rotterdam, 343–346.

Δελτίο της Ελληνικής Γεωλογικής Εταιρίας, τομ. XLVII , 2013
Πρακτικά 13ου Διεθνούς Συνεδρίου, Χανιά, Σεπτ. 2013

Bulletin of the Geological Society of Greece, vol. XLVII 2013
Proceedings of the 13th International Congress, Chania, Sept. 2013

GEOCHEMICAL EFFECT OF THE ROCK CHEMISTRY AND THE ANTHROPOGENIC ACTIVITIES ON GROUNDWATER: THE CASE STUDY OF NW EUBOEA, GREECE

Kanellopoulos C.[1] and Mitropoulos P.[2]

[1]Doctor in Geological Sciences, 15 Pindou str., Vrilissia, Athens, 15235, Greece, ckanellopoulos@gmail.com

[2]Professor in Geochemistry, University of Athens, Department of Geology and Geoenvironment Panepistimiopolis, Ilisia, 157 84, Athens, Greece, pmitrop@geol.uoa.gr

Abstract

A geochemical study of NW Euboea island ground waters was undertaken, in order to examine the possible effect of the chemical composition of the country rocks of the area as well as of the anthropogenic activities, to the concentration of environmentally important elements and chemical compounds in the groundwaters. NW Euboea consists of a great variety of rock types showing a wide range in mineralogical and chemical composition. The main groups of rocks occurring in NW Euboea are: i) various types of sedimentary rocks e.g. shale and chert formations, carbonate and clastic rocks, ii) ophiolitic rocks including peridotite, gabbro, serpentinite etc, and iii) epizonally metamorphosed basic igneous rocks, with schist and phyllite intercalations. A number of hot springs also occur in the area. The main anthropogenic activity in the area is the agricultural land use, as any significant industrial activity is absent. For that purpose, 45 water samples were collected and analyzed by Spectrophotometry for the main anions and by FP and AAS for major and a number of trace elements. On the basis of those analyses, a number of the water samples were selected and analyzed by ICP-AES and ICP-MS for a large group of mainly metallic trace elements. The interpretation of the analytical data showed clearly that the content of the groundwater for a significant group of trace elements (e.g. Cr, Ni, Zn) was considerably influenced by the chemical composition of the surrounding rocks, especially the ophiolitic and metamorphic rocks. The anthropogenic activities also affect the groundwater quality, near areas where the use of fertilizers and pesticides for agricultural purposes is extensive, resulting to the increase of various anion concentrations (NO_3^-, SO_4^{-2}, PO_4^{-3}).

Key words: *groundwater geochemistry, trace element and anion concentration, NW Euboea, Greece.*

Περίληψη

Στη παρούσα μελέτη πραγματοποιήθηκε γεωχημική έρευνα των υπόγειων ψυχρών νερών της ΒΑ Εύβοιας. Στην ΒΑ Εύβοια εμφανίζεται πληθώρα γεωλογικών σχηματισμών με πλούσια ορυκτολογική σύσταση. Οι κυριότεροι τύποι πετρωμάτων που απαντώνται είναι: i) ιζηματογενή πετρώματα, ii) πετρώματα της οφιολιθικής σειράς όπως περιδοτίτες, γάββροι, σερπεντινίτες κ.α., iii) μεταμορφωμένα βασικά

εκρηξιγενή πετρώματα με παρεμβολές σχιστόλιθων και φυλλιτών. Επίσης, στη ΒΑ Εύβοια εμφανίζονται θερμές πηγές. Οι ανθρωπογενείς δραστηριότητες στην περιοχή μελέτης είναι κυρίως αγροτικής φύσεως, ενώ απουσιάζει οποιαδήποτε σημαντική βιομηχανική δραστηριότητα. Ένας από τους σκοπούς ευρύτερης έρευνας που διεξάγεται στην περιοχή, είναι ο εντοπισμός της επιρροής των φυσικών παραγόντων και των ανθρωπογενών δραστηριοτήτων στον χημισμό των υπόγεων νερών, εδαφών κλπ. Στα πλαίσια της παρούσας μελέτης συλλέχθηκαν 45 δείγματα υπόγειων νερών, τα οποία αναλύθηκαν φασματοφωτομετρικά για τον προσδιορισμό των κύριων ανιόντων/κατιόντων και με FP και AAS προσδιορίστηκαν κύρια στοιχεία και ιχνοστοιχεία. Επιλεγμένα δείγματα αναλύθηκαν με ICP-AES και ICP-MS για τον προσδιορισμό μια μεγάλης σειράς ιχνοστοιχείων. Από την επεξεργασία των αποτελεσμάτων διαπιστώθηκε πως οι συγκεντρώσεις στα νερά, διαφόρων στοιχείων (π.χ. Cr, Ni, Zn) επηρεάζεται από την χημική σύσταση των πετρωμάτων της περιοχής και κυρίως από τα οφιολιθικά και μεταμορφωμένα πετρώματα. Οι ανθρωπογενείς δραστηριότητες διαπιστώθηκε ότι επηρεάζουν την σύσταση των υπόγειων νερών, σε περιοχές στις οποίες υπάρχει έντονη χρήση λιπασμάτων και φυτοφαρμάκων, αυξάνοντας την συγκέντρωση ανιόντων (NO^{3-}, SO_4^{-2}, PO_4^{-3}) σε αυτά.

Λέξεις κλειδιά: *γεωχημεία υπόγειων νερών, συγκεντρώσεις ιχνοστοιχείων και ανιόντων, ΒΔ Εύβοια, Ελλάδα.*

1. Introduction

Groundwater, plays a basic role in human life. The existence of sufficient groundwater resources and the maintenance of their quality is of major importance for the survival of man. It is thus indispensable, to protect these resources and ensure their sustainability. Environmental deterioration has led to a growing public concern over the potential accumulation of harmful elements and other contaminants in groundwater (Kabata-Pendias, 1995). The contamination of groundwater can pose long term environmental and health implications (Kabata-Pendias, 2007; Mueller, 1994; Needleman, 1980).

Water, whose chemical composition controls the circulation of element in ecosystems, is the main carrier of trace elements for vegetation. The prevailing opinion is that high concentrations of trace elements, which at many cases are potentially toxic, are linked with anthropogenic activities. In the present paper, a non-industrial area, where only small scale agricultural activities take place, was studied. At the study area there are occurrences of ultramafic rocks from the ophiolitic sequence. Many studies have proven that from the weathering of that type of rocks, triggers the enrichment of specific elements in nearby soils e.g. Co, Ni, Cr, As, Fe, Mn (Kanellopoulos and Argyraki, 2013; Oze et al., 2003; Gasser & Dahlgren, 1994; Alexander et al., 1989; Gough et al. 1989; Brooks, 1987; Schreier et al., 1987).

The aim of this paper is to assess the impact of both anthropogenic and natural factors on the geochemistry of groundwater.

2. Geological Setting

Euboea Island is located in central Greece. The studied area lies between latitudes 38º 58´ and 38º 50.5´ and longitudes 22º 49.5´ and 23º 10.5´. It is characterized by rocky mountainous topography and some lowland areas.

The Northeastern part of Euboea island belongs geologically to the Pelagonian and Sub-Pelagonian units, which form the western part of the internal geotectonic units of Greece (Mountrakis, 1986; Aubouin, 1959).

The study area consists of non-metamorphic rocks of the ophiolitic series, including peridotite, gabbro and serpentinite, as well as of metamorphic rocks. Large parts of NW Euboea are covered by Post Alpine formations and sediments of Quaternary to Neogene age (Fig. 1).

In the centre of the northern Evoicos gulf, the volcanogenic islands of Lichades are located (Georgalas, 1938). They are made mainly of trachyandesite lava flows, dated at 0.5 Ma (Pe-Piper and Piprer, 2002). The whole area is highly faulted due to extensional tectonics (Vavassis, 2001, Le Pichon and Angelier, 1979; McKenzie 1970; 1972). In the studied area many hot springs exist (Gioni-Stavropoulou, 1983), showing high concentrations of a large group of major and trace elements (Kanellopoulos, 2011; 2006). Finally in the areas of Loutra Edipsou and Ilia, thermogenic travertine deposits exist, created by the local hot-springs (Kanellopoulos, 2012; 2011).

3. Materials and Methods

3.1. Groundwater Sampling and Analysis

A total of 45 groundwater samples were collected (Table 1) from springs, wells and drills mainly used for agricultural activities and water supply of villages. Sensitive physicochemical parameters such as, pH, Temperature, E.C., T.D.S. were measured in the field. All the samples were vacuum filtered, acidified to a final concentration of 2% nitric acid, stored in polyethylene bottles and preserved in a refrigerator.

All the 45 water samples were analyzed in the Laboratory of Economic Geology and Geochemistry, University of Athens. The anion concentrations were measured spectrophotometrically (bicarbonate was measured by titration) while the major and trace element concentrations were measured by Flame Photometry and Atomic Absorption Spectroscopy (AAS) (Table 2).

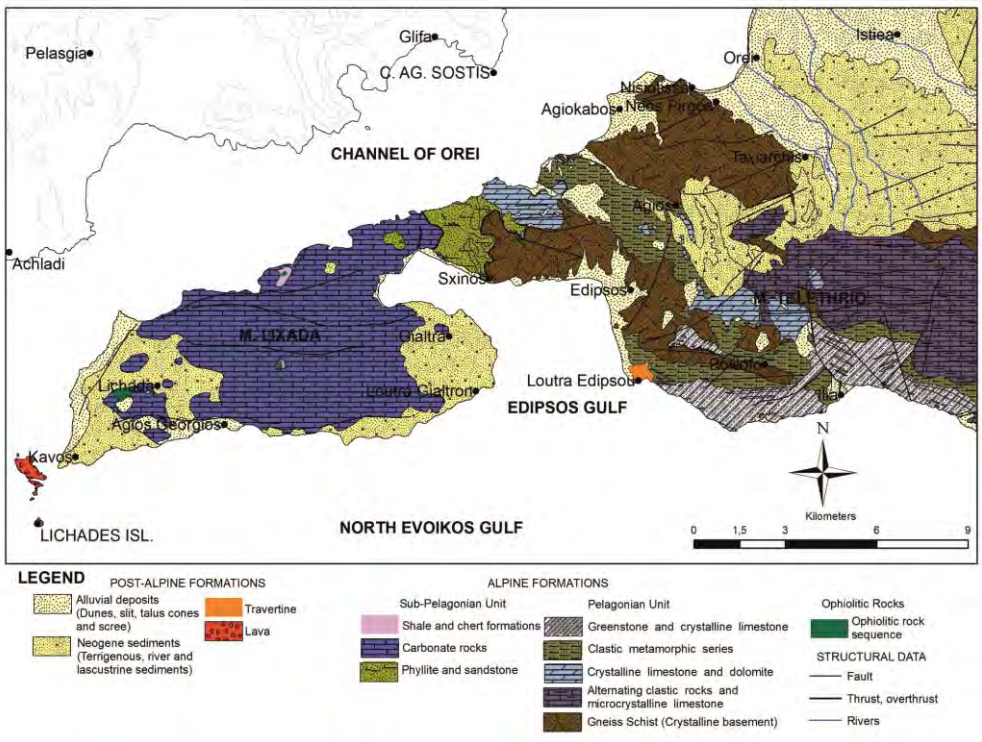

Figure 1 - Geological map of the study area (Kanellopoulos, 2011).

Table 1 - Samples locality, physicochemical parameters, hydrochemical type, SAR, EC, MH values and classification based on SAR-EC.

Code	Locality	Sampling site (depth in m)	T (ºC)	pH	TDS (g/lt)	EC* (mS/cm)	Hydroc. type	SAR-EC classif.	SAR	MH
AD-11	Edipsos-Schinos	well (4)	17.5	7.66	1.27	3.33	Ca-Cl	C3-S1	0.811	21.9
AD-22	Edipsos-Schinos	well (4)	21.9	7.85	1.77	3.55	Na-Cl	C3-S2	8.569	28.1
AD-10	Edipsos-Schinos	well (7)	23.2	7.1	3.63	7.26	Na-Cl	C2-S1	7.117	26.4
AD-16	Edipsos-Well Φ-18	well (10)	16	6.8	0.33	0.66	$Ca\text{-}HCO_3$	C1-S1	0.938	31.8
AD-17	Edipsos-Village	drill	14.45	7.45	0.41	0.84	$Ca\text{-}HCO_3$	C2-S1	0.949	43.9
AD-18	Edipsos-Old factory	drill (120)	12.2	6.99	0.475	0.96	$Ca\text{-}HCO_3$	C2-S1	1.214	35
HL-2	Ilia	spring	15	7.9	0.26	0.54	$Mg\text{-}HCO_3$	C1-S1	0.284	51.2
HL-10	Ilia	spring	18	8.27	0.25	0.51	$Ca\text{-}HCO_3$	C1-S1	0.397	46.7
AD-7	Polylofo-Vitsa	spring	15.3	7.7	0.39	0.78	$Ca\text{-}HCO_3$	C2-S1	0.759	26.1
AD-8	Polylofo- St. George M.	spring	12.7	8.1	0.27	0.53	$Mg\text{-}HCO_3$	C1-S1	0.266	50.3
GIA-1	Gialtra-3 springs	spring	21.3	6.96	0.69	1.36	$Na\text{-}SO_4$	C2-S1	2.4	43.6
GIA-2	Gialtra-Averof spring	spring	17.7	7.23	0.64	1.28	$Na\text{-}NO_3$	C2-S1	2.252	42.4
GIA-3	Gialtra	drill	19.1	7.6	0.33	0.69	$Ca\text{-}HCO_3$	C1-S1	0.997	45.1
GIA-5	Gialtra-Near Averof sp.	spring	14.1	7.7	0.37	0.74	$Ca\text{-}HCO_3$	C1-S1	0.8	49.4
GIA-6	Gialtra-3 springs	spring	20.1	8.06	0.66	1.34	$Ca\text{-}HCO_3$	C2-S1	1.838	47.3
GIA-10	Gialtra	spring	18	7.84	0.31	0.62	$Mg\text{-}HCO_3$	C1-S1	0.562	54.6
AGG-1	St. George vil.-Kamara	spring	19.9	6.96	1.18	2.37	Na-Cl	C3-S1	5.725	52.6
AGG-2	St. George village	spring	22.2	7.84	1.2	2.4	Na-Cl	C3-S1	6.224	55.2
LIX-1	Lichada	drill	17.9	7.27	0.54	1.09	$Mg\text{-}HCO_3$	C2-S1	0.506	60.2
LIX-2	Lichada	drill	23	7.85	0.52	1.05	$Mg\text{-}HCO_3$	C2-S1	0.513	60.6
AG-1	Agios	well (10)	15.35	6.91	0.61	1.23	$Ca\text{-}HCO_3$	C2-S1	1.33	25.4
AD-12	Agios-Platania	spring	12.7	7.6	0.25	0.51	$Ca\text{-}HCO_3$	C1-S1	0.273	48
AD-13	Agios-Old factory	drill (120)	14.3	7.33	0.46	0.93	$Ca\text{-}HCO_3$	C2-S1	1.026	38.6
BAR-1	Varvara	spring	15	7.39	0.51	1.03	$Ca\text{-}HCO_3$	C2-S1	0.571	41.7
AK-1	Agiokabos-Skepasti	spring	16.35	7.3	0.41	0.83	$Ca\text{-}HCO_3$	C2-S1	1.444	44.5
AK-2	Agiokabos-Xalasmata	drill	10.5	7.43	0.37	0.74	$Ca\text{-}HCO_3$	C1-S1	1.183	49.1
AK-3	Agiokabos-Restorant	drill (6)	14.3	7.25	0.39	0.8	$Ca\text{-}HCO_3$	C2-S1	0.774	33.7
AK-4	Agiokabos	drill (36)	15.8	7.3	0.32	0.64	$Ca\text{-}HCO_3$	C1-S1	0.643	40.4
AK-6	Agiokabos	drill (60)	15.2	7.19	0.33	0.66	$Ca\text{-}HCO_3$	C1-S1	0.636	38.9
AK-7	Agiokabos	drill (4)	18.3	7.96	0.46	0.93	$Ca\text{-}HCO_3$	C2-S1	1.17	28
NIS-1	Nisiotissa	well	13.1	7.24	0.42	0.85	$Ca\text{-}HCO_3$	C2-S1	1.299	31.5
NIS-2	Nisiotissa	well	14.6	7.19	0.41	0.84	$Ca\text{-}HCO_3$	C2-S1	1.696	32.8
NIS-3	Nisiotissa	drill	18.25	6.86	0.41	0.83	$Mg\text{-}HCO_3$	C2-S1	1.404	51.9
NP-1	N. Pirgos-Tsempetsis	well	17.7	7.23	0.56	1.13	$Ca\text{-}HCO_3$	C2-S1	2.19	41.2
NP-3	N. Pirgos-Lowland	drill (6)	17.5	7.45	0.53	1.07	$Ca\text{-}HCO_3$	C2-S1	0.712	45.7
NP-4	N. Pirgos-Lowland	drill (9)	15.6	7.3	0.48	0.93	$Ca\text{-}HCO_3$	C2-S1	0.837	41.6
NP-5	N. Pirgos-Arida	drill (50)	16.3	7.29	0.59	1.17	$Ca\text{-}HCO_3$	C2-S1	0.763	43.1
NP-6	N. Pirgos-New aqueduct	drill (60)	16.6	7.37	0.38	0.77	$Ca\text{-}HCO_3$	C1-S1	0.885	38.4
NP-7	N. Pirgos-Old aqueduct	drill (60)	16.6	7.36	0.9	0.44	$Ca\text{-}HCO_3$	C2-S1	0.852	44.1
NP-8	N. Pirgos-New church	well (3)	12.15	7.76	0.28	0.56	$Ca\text{-}HCO_3$	C1-S1	0.428	31.4
NP-9	N. Pirgos-Old church	drill	14.4	7.39	0.41	0.82	$Ca\text{-}HCO_3$	C2-S1	0.576	44
NP-10	N. Pirgos-Kolonaki	well (5)	14.1	7.13	0.42	0.86	$Ca\text{-}HCO_3$	C2-S1	1.278	47.4
NP-11	N. Pirgos-Kolonaki	well (5)	14.4	6.95	0.35	0.72	$Ca\text{-}HCO_3$	C1-S1	1.414	44.1
OR-1	Oreoi-School	spring	10.75	7.72	0.38	0.76	$Ca\text{-}HCO_3$	C1-S1	0.625	49.8

Table 2 - Concentrations of chemical parameters analyzed by AAS, FP, SP and titration.

	Cd	Co	Cr	Mn	Pb	Ni	Fe	Zn	Na	K	Mg	Ca	PO_4	NO_3	SO_4	Cl	HCO_3
	µg/L	µg/L	µg/L	µg/L	µg/L	µg/L	µg/L	µg/L	mg/L	mg/L	mg/L	mg/L	mg/L	mg/L	mg/L	mg/L	mg/L
AD-11	0.1	1.8	<0.2	9	<1	3	22	420	42	8	34.1	200	0.21	9.2	160	650	320
AD-22	<0.1	<0.2	0.3	1	<1	<0.6	9	150	465	5	38.1	160.5	0.23	9.7	200	848	295
AD-10	0.3	0.3	0.3	0.6	<1	<0.6	2	5	-	-	-	-	0.353	1	70	410	283
AD-16	<0.1	<0.2	0.9	0.6	<1	<0.6	7	10	34	3	19.2	68	0.25	9.7	39	36	280
AD-17	<0.1	<0.2	0.4	1	<1	0.6	2	34	39	4	34.1	72	0.14	29	70	38	313
AD-18	<0.1	<0.2	0.9	0.7	<1	<0.6	3	10	51	4	28.4	87	0.24	19.8	26	66	381
HL-2	<0.1	0.5	0.4	0.8	<1	<0.6	3	9	10	3	29.3	46	0.13	7	20	9.9	154
HL-10	-	-	-	-	-	-	-	-	-	-	-	-	0.198	0.5	38.6	2.41	213
AD-7	<0.1	1.5	<0.2	<0.5	<1	<0.6	4	17	24	5	12	56	0.12	24.2	30	20.2	292
AD-8	0.4	1.3	0.3	<0.5	<1	<0.6	8	12	9	5	26.4	43	0.04	7	19	13	224
GIA-1	<0.1	0.6	1	<0.5	<1	<0.6	15	10	107	24	39.9	85	0.25	**225.5**	620	78	272
GIA-2	<0.1	1.3	1	<0.5	<1	<0.6	12	6	97	30	36.2	81	0.15	**250.8**	95	84	240
GIA-3	<0.1	0.6	6	1	<1	0.8	12	47	40	7	33.4	67	0.17	**166.1**	41	44	198
GIA-5	<0.1	2.9	0.7	1	<1	<0.6	10	23	30	6	32	54	0.27	15	37	21.3	255
GIA-6	<0.1	<0.2	0.6	<0.5	<1	<0.6	3	<2	81	19	42.3	77.6	0.28	**217.4**	80	140.8	283
GIA-10	-	-	-	-	-	-	-	-	-	-	-	-	0.121	0.8	26.2	27.5	267
AGG-1	<0.1	<0.2	0.2	1	<1	<0.6	3	4	275	9	55.8	83	0.1	7	80	478	330
AGG-2	<0.1	<0.2	0.3	<0.5	<1	<0.6	3	<2	290	9	55.1	73.8	0.09	4.4	74	604	258
LIX-1	-	-	-	-	-	-	-	-	-	-	-	-	0.446	15.5	43	7.57	347
LIX-2	-	-	-	-	-	-	-	-	-	-	-	-	0.514	8.9	42.9	15.45	343
AG-1	<0.1	0.2	0.2	120	<1	<0.6	2	5	60	13	23.8	115	3.04	**73.5**	94	64	298
AD-12	<0.1	<0.2	<0.2	<0.5	<1	<0.6	4	8	9	5	24.1	43	0.04	7	20	8.3	234
AD-13	<0.1	0.5	<0.2	<0.5	<1	<0.6	3	13	42	6	29.8	78	0.17	18	34	60	352
BAR-1	<0.1	<0.2	0.4	0.9	<1	0.9	2	3	27	4	42.9	99	0.32	29	55	52	410
AK-1	<0.1	0.2	<0.2	12	<1	<0.6	4	51	55	4	29.7	61	0.15	5.7	37	74	292
AK-2	0.2	0.9	0.3	0.5	<1	0.6	2	46	43	4	29.8	51	0.2	5.3	29	42	300
AK-3	0.3	<0.2	<0.2	3	<1	<0.6	1	3510	32	3	26.5	86	0.15	6.2	46	28	365
AK-4	<0.1	<0.2	<0.2	17	<1	0.8	3	30	24	3	25.9	63	0.12	6.6	34	40	270
AK-6	<0.1	0.4	0.4	1.8	<1	<0.6	2	8	24	4	25.5	66	0.06	7	40	28	285
AK-7	<0.1	<0.2	<0.2	3	<1	2	2	50	44	3	18.2	77.2	0.1	5.7	54	67.2	347
NIS-1	<0.1	<0.2	0.3	2	<1	<0.6	4	6	50	3	21.5	77	1.37	18.5	80	54	230
NIS-2	<0.1	<0.2	0.9	0.5	<1	<0.6	<2	6	61	3	19.5	66	1.11	7.5	64	76	270
NIS-3	<0.1	0.5	0.3	20	<1	<0.6	3	6	53	4	34	52	0.65	9.7	22	88	230
NP-1	<0.1	0.7	0.6	80	<1	5	7	15	88	7	30.6	72	2.02	40.5	44	72	386
NP-3	<0.1	<0.2	0.3	14	<1	<0.6	9	47	34	6	47.9	94	0.24	11.9	102.5	22.4	430
NP-4	<0.1	0.6	3	1.3	<1	<0.6	6	49	36	6	35.4	82	0.39	18	39	28	366
NP-5	<0.1	0.3	3	1.5	<1	<0.6	7	47	36	6	44.1	96	0.44	33.9	80	34	426
NP-6	<0.1	<0.2	<0.2	<0.5	<1	<0.6	7	22	33	6	24.6	65	0.19	10.1	25	20	277
NP-7	<0.1	<0.2	3	1	<1	0.6	13	11	37	6	38.2	80	0.22	15.8	40	13.1	378
NP-8	<0.1	0.2	2	0.9	<1	1	3	10	15	5	17.8	64	0.3	22.9	35	13	249
NP-9	<0.1	<0.2	3	0.8	<1	<0.6	<2	9	25	4	38.1	80	0.2	13.2	37	37	242
NP-10	<0.1	0.2	0.4	1.6	<1	<0.6	3	4	50	4	33.4	61	0.43	57.6	52	54	200
NP-11	<0.1	<0.2	0.3	0.7	<1	<0.6	13	4	50	7	25.4	53	0.63	31.2	55	46	230
OR-1	<0.1	0.3	0.3	260	<1	1	3	19	27	7	42.7	71	0.18	4.8	2	20.1	380
P.V.	**5**		**50**		**10**	**20**								**50**			

(P.V. = Parametric Value set by Directive 98/83/EC; with bold red color are the values exceed P.V.)

On the basis of the above analytical data, 11 of the water samples were analyzed by Inductively Coupled Plasma–Atomic Emission Spectroscopy (ICP-AES) and by Inductively Coupled Plasma-Mass Spectrometry (ICP-MS) at the ACME Analytical Laboratories Ltd., Canada, for a series of elements (Table 3).

Detailed description of the used analytical methods as well as, the analytical quality control procedures, including analysis of blank and duplicate samples as well simultaneous analysis of Certified Reference water samples, are given in Kanellopoulos, 2011.

4. Analytical Results

4.1. Chemical Analysis

The location of the samples is presented in Table 1, while in Tables 1, 2 and 3, the physicochemical parameters analysed both in situ and in the lab, are presented.

In Figure 2A, the chemical analyses were plotted in the Piper diagram, in order to evaluate the hydrochemistry of the studied groundwater samples. In that Piper diagram, 39 of the studied groundwater samples are plotted in the same area and most of them have Ca-HCO_3 hydrochemical type (Table 1). From that group, only four samples have different hydrochemical type, as a result of the differentiation of the local bedrocks (Lichada area: LIX-1, LIX-2, Ilia area: HL-2, AD-8).

From all the studied samples only 6 are plotted separately due to their differed hydrochemical type, reflecting the impact of specific factors controlling the chemistry of the samples, like intrusion of sea water (AD-10, AD-11, AD-22, AGG-1 and AGG-2, hydr. type Na-Cl) or impact of fertilizers (GIA-1, hydr. type Na-SO_4). All the samples with Na-Cl hydrological type are from shallow aquifers located at a short distance from the shoreline (10-20m) and present high concentration of Cl (Table 2).

In order to visualize the spatial relationship between the concentrations and the geological features in the studied area, graduated symbol maps were created by plotting the results of the chemical analysis. Class intervals were selected on the basis of the statistical distribution for each element and appear with different sized symbol on the maps, representing the following concentration classes: (a) minimum- 1st quartile, (b) 1st quartile- median (baseline concentration), (c) median- 3rd quartile and (d) > 3rd quartile- maximum. These maps are presented in Figures 2E-2H.

The concentrations of Na and Cl vary in the same way (Fig. 2B), suggesting common source. The samples with higher concentrations of Cl (848 mg/L) and Na (642 mg/L) are from shallow aquifers located at short distance from the sea. For instance, samples AD-11, AD-22 and AD-10 were taken from shallow wells near the seashore at Schinos area (Fig. 2E).

The concentrations of K, NO_3, SO_4, PO_4 also co-vary satisfactorily (Fig. C), suggesting common source. The relation coefficient between K and NO_3 is 0.86. High concentrations are presented in samples located near lowlands, where agricultural activities take place (Fig. 2F).

Some samples present very high concentrations of NO_3 as compared to SO_4, PO_4 and K concentrations (e.g. GIA-1, GIA-2, GIA-3, AG-1 etc). These samples are located within or are adjacent to villages without sewerage.

Concentrations of Ni, Mg, Zn (Fig. 2G) and to a smaller extent Fe, Cr, Co show high values near the crystalline basement. These areas are mostly lowlands, usually covered by Post-Alpine formations, characteristic examples are the areas of Neos Pyrgos and Agiokampos. Also, the concentrations of Cr and Zn co-varies (Fig. 2D). Of the above elements, Zn shows some outlier values (>150 μg/L) like the AK-3 sample (3510 μg/L).

Table 3 - Concentrations of elements analyzed by ICP-MS.

		LIX-1	LIX-2	AGG-1	GIA-1	GIA-10	AD-10	HL-10	AD-18	AK-3	NIS-3	NP-7
Ag	**(µg/L)**	-	-	<0.05	<0.05	-	-	-	<0.05	<0.05	<0.05	<0.05
Al	**(µg/L)**	<100	<100	8	7	<100	<100	<100	10	5	9	6
As	**(µg/L)**	<1000	<1000	2.6	4.2	<1000	<1000	<1000	0.5	<0.5	<0.5	0 .7
Au	**(µg/L)**	-	-	<0.05	<0.05	-	-	-	<0.05	<0.05	<0.05	<0.05
B	**(µg/L)**	-	-	193	409	-	-	-	<20	91	25	48
Ba	**(µg/L)**	166	165	26	124	89	108	68	258	92	29	79
Be	**(µg/L)**	<0.11	<0.11	-	-	<0.11	<0.11	<0.11	-	-	-	-
Br	**(µg/L)**	-	-	1692	242	-	-	-	134	136	303	100
Ca	**(mg/L)**	83.1	82.4	113.6	117.1	56.6	454.2	51.5	120	109.6	67.2	103
Cd	**(µg/L)**	0.07	0.11	<0.05	<0.05	<0.05	<0.05	0.11	<0.05	0.29	<0.05	<0.05
Ce	**(µg/L)**	<0.24	<0.24	0.07	0.06	<0.24	<0.24	<0.24	0.06	0.06	0.06	0.04
Cl	**mg/L)**	-	-	522	102	-	-	-	88	46	113	35
Co	**(µg/L)**	<0.09	<0.09	0.15	0.18	<0.09	0.23	<0.09	0.21	0.14	0.16	0.15
Cr	**(µg/L)**	14	14	<0.5	0.7	<4	7	<4	1.1	<0.5	<0.5	2.4
Cs	**(µg/L)**	<0.09	<0.09	13.38	0.09	<0.09	<0.09	<0.09	0.03	<0.01	0.03	<0.01
Cu	**(µg/L)**	3	3	1.8	2.8	3	5	2	4.1	1.4	1.1	2.3
Fe	**(µg/L)**	<100	<100	600	520	<100	<100	<100	570	500	420	520
Ga	**(µg/L)**	<0.4	<0.4	-	-	<0.4	<0.4	<0.4	-	-	-	-
Ge	**(µg/L)**	<2	<2	-	-	<2	<2	<2	-	-	-	-
Hg	**(µg/L)**	-	-	0.4	<0.1	-	-	-	0.2	0.4	0.3	<0.1
K	**(µg/L)**	2630	2720	8130	21380	2250	9290	940	1140	560	950	1430
La	**(µg/L)**	<0.58	<0.58	0.06	0.05	<0.58	<0.58	<0.58	0.19	0.07	0.08	0.04
Li	**(µg/L)**	13.9	14.1	21.5	9.2	6.9	18.8	3.6	5.6	5.7	9.2	5
Lu	**(µg/L)**	<0.001	<0.001	<0.01	<0.01	<0.001	<0.001	<0.001	<0.01	<0.01	<0.01	0.01
Mg	**(mg/L)**	76.2	76.9	61.8	45	41.3	99	27.4	31.2	29	36.4	43.1
Mn	**(µg/L)**	<10	<10	1.36	0.29	<10	<10	<10	0.37	3.77	23.94	1.28
Mo	**(µg/L)**	<5	<5	1.2	0.3	<5	<5	<5	0.6	0.6	0.1	1.2
Na	**(mg/L)**	26.6	26.9	286.4	86	22.8	642.1	14.2	58.1	30.1	52.8	23.7
Nb	**(µg/L)**	<0.3	<0.3	-	-	<0.3	<0.3	<0.3	-	-	-	-
Ni	**(µg/L)**	4.9	4.4	<0.2	<0.2	1.5	6.1	1.2	0.4	<0.2	0.6	0.3
P	**(µg/L)**	<1000	<1000	44	79	<1000	<1000	<1000	41	41	41	66
Pb	**(µg/L)**	0.8	<0.4	0.1	<0.1	0.5	0.4	<0.4	<0.1	0.6	<0.1	0.1
Rb	**(µg/L)**	0.53	0.54	7.36	1.53	1.53	4.97	0.38	0.75	0.11	0.1	0.25
S	**mg/L)**	9.61	9.6	21	24	6.34	94.6	8.02	7	12	6	11
Sb	**(µg/L)**	<0.2	<0.2	<0.05	0.07	<0.2	<0.2	<0.2	0.21	0.08	<0.05	0.09
Se	**(µg/L)**	-	-	10.1	1.6	-	-	-	2.3	0.8	1.7	0.9
Si	**(µg/L)**	16100	16000	4200	13400	11800	10500	5000	12600	7600	13800	11000
Sn	**(µg/L)**	<0.8	<0.8	0.15	0.25	<0.8	<0.8	<0.8	0.31	0.21	1.15	1.71
Sr	**(µg/L)**	362	360	368	222	315	2599	240	324	264	204	289
Ta	**(µg/L)**	<0.03	<0.03	-	-	<0.03	<0.03	<0.03	-	-	-	-
Ti	**(µg/L)**	<1000	<1000	-	-	<1000	<1000	<1000	-	-	-	-
Tl	**(µg/L)**	<0.13	<0.13	<0.01	<0.01	<0.13	<0.13	<0.13	<0.01	<0.01	<0.01	<0.01
U	**(µg/L)**	1.4	1.41	2.82	0.98	1.51	9.02	1.01	2.73	1.72	0.2	3.51
V	**(µg/L)**	12.5	12.4	3	3.8	4.1	4.2	<1.3	0.6	0.3	0.5	1.2
W	**(µg/L)**	-	-	0.05	0.04	-	-	-	0.11	0.04	0.09	0.03
Y	**(µg/L)**	0.027	0.017	0.01	0.01	0.014	0.042	0.009	0.05	0.1	0.01	0.13
Zn	**(µg/L)**	30	25	11	11	<16	29	23	27	3020	12	12

(The samples LIX-1, LIX-2, GIA-10, AD-10, HL-10 analysed in Natural History museum of London labs and the rest of them in ACME labs)

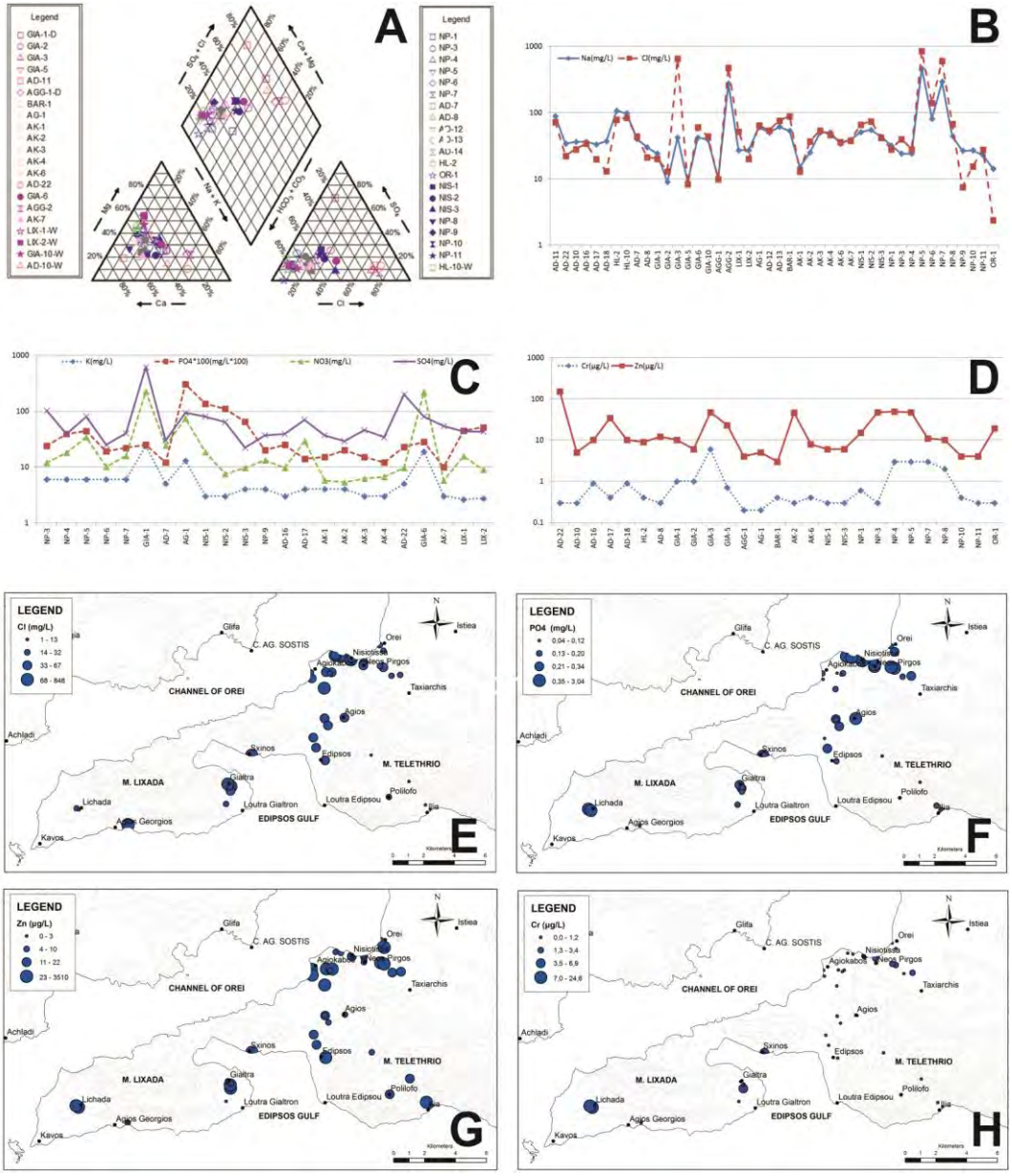

Figure 2 - (A) Chemical composition of groundwater samples plotted in Piper trilinear diagram. (B) Diagram presenting the co-varying of Na and Cl at groundwater samples. (C) Diagram presenting the variation of K, NO_3, SO_4 and PO_4 at groundwater samples from lowlands, where agricultural activities take place. (D) Diagram presenting the co-varying of Cr and Zn at groundwater samples (used only the samples in which both Fe and Zn concentrations are above detection limits). Geochemical maps showing the distribution of Cl (E), PO_4 (F), Zn (G) and Cr (H) in groundwater samples.

The water samples from the peninsula of Gialtra (Sample Codes: LIX-; AGG-; GIA- and samples AD-10, AD-11, AD-22) show the maximum concentrations for a series of elements, namely Cr (14.2 μg/L; Fig. 2H), Ni (6.1 μg/L) and Fe (35 μg/L), Zn (420 μg/L) and Co (3 μg/L).

The results of chemical analysis of groundwater samples by ICP-MS (Table 3) strongly support the relationships between elemental groundwater content and rock geochemistry.

4.2. Evaluation of Water Quality for Human Consumption

In order to assess the suitability of the studied groundwater samples, for human consumption, the analytical values with the parametric levels, imposed by the current relative legislation (Directive 98/83/EU) were compared. It is noted that the National Greek law is in agreement with that EU Directive 98/83/EU. Even though industrial activities are absent in the studied area and only agricultural activities take place, concentrations of some chemical parameters exceeded the indicator parametric value (17.7 %) and the parametric value (8.8 %) according to Directive 98/83/EC (Tables 1 and 2).

Analytically, the Mn content of the studied groundwater samples varies from 0.09 to 260 μg/L, while the parametric value given by Directive 98/83/EC is 50μg/L. This value was exceeded by three samples from the areas of Neos Pyrgos, Oreoi and Agios.

The Na content varies from 9 to 640mg/L, while the indicator parametric value is 200mg/L. Six samples, from Agios Georgios and Schinos of Edipsos exceed that value.

The Ca content ranges between 43 and 450mg/L, while the indicator parametric value is 100 mg/L. Four samples exceed it, from Agios Georgios and Schinos of Edipsos.

The NO_3 content varies from 0.5 to 250mg/L, while the parametric value is 50mg/L. Six samples from Gialtra, Agios Georgios and Neos Pyrgos exceed it.

The SO_4 content varies from 2 to 620mg/L, while the indicator parametric value is 250mg/L. Only one sample from the area of Gialtra exceeds it.

The conductivity values range between 0.4 and 7.3mS/cm, while the indicator parametric value is 2.5mS/cm. Three samples exceed it, and all these samples are from the area of Schinos of Edipsos. All the others studied chemical parameters are within the parametric values given by the Directive 98/83/EC.

4.3. Evaluation of Water Quality for Irrigation

In order to assess the suitability of groundwaters for irrigation, their quality status was assessed through Sodium Adsorption Ratio (SAR) and Magnesium Hazard (MH). The SAR in the studied groundwater samples ranges from 0.2 to 8.6 (Table 1) which, combined with the measured values of Electrical Conductivity (EC) gave information about their classification, based on the fields suggested by U.S. Salinity Laboratory (1954). So the studies samples were classified (Table 1) as follows: S1-C1 (58%), S1-C2 (33%), S1-C3 (7%) and S2-C3 (2%). The MH (Magnesium Hazard) values, in the studied samples, ranges from 21.9 to 60.6 and 18% of the samples have MH>50 (Table 1), meaning that they are not recommended for irrigation.

5. Discussion - Conclusions

The results from the study of cold groundwater, undertaken in the area of NW Euboea Greece, show that the chemical composition of the groundwater is controlled by the following three main factors: (i) the chemical composition of the local rocks (ultramafic and metamorphic), (ii) the sea, for the samples located near the seashore and (iii) the anthropogenic activities (mainly the extensive use of fertilizers and pesticides).

The results of chemical analyses through the spatial distribution of the concentrations of the various elements, show that the two main rock formations that have affected the chemical composition of the studied groundwater are the ultramafic rocks from the ophiolitic sequence as well as the metamorphic rocks occurring in the area.

In the peninsula of Gialtra, small surface occurrences of ultramafic rocks from the ophiolithic sequence are present. The water samples from that area (Lichada, Agios Georgios, Gialtra, Schinos), show the highest concentration of Cr (up to 14μg/L), Ni (6.1μg/L) as well as high concentrations of Co (up to 3μg/L), Fe (up to 35μg/L) and Zn (up to 450μg/L). Enrichment of groundwater in these elements can be attributed to the impact of ultramafic rocks. Kanellopoulos (2011) and Kanellopoulos and Argyraki (2013) proved that soils and some plant species (e.g. Alyssum chalcidicum) also present high concentrations of the same elements, especially Cr and Ni, even at long distances from the surface occurrences of the local ultramafic rocks.

High concentrations of Zn, Mg, Ni and to a smaller extent Fe, Cr, Co are observed near the metamorphic basement (e.g. Neos Pyrgos and Agiokampos). Enrichment of groundwater in those elements is attributed to the impact of metamorphic rocks dominating in this region. It must be noted that the soils in these areas also present high concentrations of the same elements and after geochemical and mineralogical analysis found that they have been enriched by the weathered material of the metamorphic rocks (Kanellopoulos, 2011). Of the above elements, Zn, shows some outlier values (>150 μg/L) like the AK-3 sample (3510 μg/L). These cases may be influenced by anthropogenic sources.

The co-variation of Cl and Na suggests that they have common source. The spatial distribution of their concentrations, points out that the samples with the highest concentrations (848 mg/L Cl; 642 mg/L Na) are from shallow aquifers near the seashore, which have been affected from the seawater and they have Na-Cl hydrochemical type, like the case of Schinos area.

Also the co-variation of K, NO_3, SO_4, PO_4, suggests their common source. The spatial distribution of their concentrations, points out that the samples with the highest concentrations located near lowlands, where agricultural activities take place. Their source is the use of fertilizers and the variability which could be observed from area to area is related to the different degree of use of each type of fertilizer. Some samples present disproportionately high concentrations of NO_3 compared to SO_4, PO_4 and K concentrations. These samples are within or adjacent to villages without sewerage, so the high concentration of NO_3 is related to residential wastewater.

It is profound that both natural and anthropogenic factors affect the groundwater quality for human consumption to such an extent that 17.7 % exceed at least one indicator parametric value and 8.8 % exceed at least one parametric value of the Directive 98/83/EC. Finally, the studied groundwater samples quality for irrigation classified based on SAR-EC as S1-C1 (58%), S1-C2 (33%), S1-C3 (7%) and S2-C3 (2%) and based on the MH (Magnesium Hazard) 18% of the samples have MH>50 and they are not recommended for irrigation.

6. References

Alexander E.B., Adamson C., Zinke P.J. and Graham R.C, 1989. Soils and conifer forest productivity on serpentinized peridotite of the Trinity Ophiolite, California, *Soil Science*, 148(6), 412-423.

Aubouin J. 1959. Contribution a l'étude géologique `de la Grèce septentrionale: Les confins de l'Epire et de la Thessalie, *Ann. Géol. Pays Hellen*, 10, 1-483.

Brooks R.R. 1987. *Serpentine and its vegetation: Portland*, OR, Dioscorides Press.

Directive 98/83/EU. *On the quality of water intended for human consumption*.

Gasser U.G. and Dahlgren R.A. 1994. Solid-phase speciation and surface association of metals in serpentinitic soils, *Soil Science*, 158, 409–420.

Georgalas G.C. 1938. Le volcans des ıˆles Likhades et de Hagios Ioannis (Kammena Vourla), *Praktika Academia Athinion*, 13, 86–98.

Gioni-Stavropoulou G. 1983. Inventory of hot and mineral springs of Greece, I, Aegean sea, *Hydrological and Hydrogeological Investigation Report*, No. 39, IGME, Athens (in Greek).

Gough L.P., Meadows G.R., Jackson L.L. and Dudka S., 1989. Biogeochemistry of a highly serpentinized, chromite-rich ultramafic area, Tehama County, California, *U.S. Geological Survey Bulletin,* 1901, 1-24.

Kabata-Pendias A. and Mukherjee A. 2007. *Trace Elements from Soil to Human*. Springer-Verlag, Berlin, New York.

Kabata-Pendias A. 1995. Agricultural problems related to excessive trace metal contents in soils, in: Salomons, W., Forstner, U., Mader, P. (Eds.), *Heavy Metals: Problems and Solutions*. Springer-Verlag, Berlin Heidelberg, pp. 3–18.

Kanellopoulos C. 2006. Geochemical research on the distribution of metallic and other elements to the groundwater in Fthiotida Prefecture and N. Euboea. *Master Thesis*, University of Athens, Greece (in Greek).

Kanellopoulos C. 2011. Geochemical research on the distribution of metallic and other elements to the cold and thermal groundwater, soils and plants in Fthiotida Prefecture and N. Euboea. Environmental impact, *Ph.D. Thesis*, University of Athens, Greece (in Greek).

Kanellopoulos C. 2012. Distribution, lithotypes and mineralogical study of newly formed thermogenic travertines in Northern Euboea and Eastern Central Greece, *Central European Geosciences*, 4(4), 545-560.

Kanellopoulos C. and Argyraki A. 2013. Soil baseline geochemistry and plant response in areas of complex geology. Application to NW Euboea, Greece, *Chemie der Erde – Geochemistry*, doi: 10.1016/j.chemer.2013.06.006

Le Pichon X. and Angelier J. 1979. The Hellenic Arc and Trench system: A key to the neotectonic evolution of the Eastern Mediterranean area, *Tectonophysics*, 60, 1-42.

McKenzie D. 1970. Plate Tectonics of the Mediterranean Region, *Nature*, 226, 239-242.

McKenzie D. 1972. Active tectonics of the Alpide – Himalayan belt: the Aegean Sea and surrounding regions (Tectonics of the Aegean Region), *Geophys. J. Roy. Astr. Soc.*, 55, 217-254.

Mountrakis D. 1986. The Pelagonian zone in Greece: A polyphase deformed fragment of the Cimmerian continent and its role in the geotectonic evolution of the Eastern Mediterranean, *Journal of Geology*, 94, 335 - 347.

Mueller M. 1994. Distribution of cadmium in the food chain (soil–plant–human) of a cadmium exposed area and the health risks of the general population, *Sci. Total Environ*., 156, 151–158.

Needleman H.L. 1980. *Low Level Lead Exposure—The Clinical Implications of Current Research*. Raven Press, New York.

Oze C., LaForce M., Wentworth C., Hanson R., Bird D. and Coleman R. 2003. Chromium geochemistry of serpentinous sediment in the Willow core, Santa Clara County, CA. U.S. Department of the interior, U.S. geological survey, *Open-File Report 03-251*.

Pe-Piper G. and Piper D. 2002. *The igneous rocks of Greece, the anatomy of an orogen*, Gebruder Borntraeger, Berlin.

Richards L.A. 1954. Diagnosis and improvement of saline and alkali soils, *Agriculture handbook*, Volume 60, US Department of Agriculture, Washington DC.

Schreier H., Omueti J.A. and Lavkulich L.M. 1987. Weathering processes of asbestos-rich serpentinitic sediments, *Soil Science Society of America Journal*, 51, 993-999.

Szabolcs I. and Darab C. 1964. The influence of irrigation water of high sodium carbonate content of soils. In: *Proceedings of 8th international congress of ISSS*, Transaction II, 803–81.

U.S. Salinity Laboratory 1954. Diagnosis and improvement of saline and alkali soils. In Richards L. A. (Ed.), *USDA agriculture handbook No. 60*. Washington, D.C.: U.S. Government Printing Office.

Vavassis I. 2001. Geology of the Pelagonian zone in Northern Evia Island (Greece): Implications for the geodynamic evolution of the Hellenides. *These de doctorat*, Univ. de Lausanne.

Δελτίο της Ελληνικής Γεωλογικής Εταιρίας, τομ. XLVII , 2013
Πρακτικά 13ου Διεθνούς Συνεδρίου, Χανιά, Σεπτ. 2013

Bulletin of the Geological Society of Greece, vol. XLVII 2013
Proceedings of the 13th International Congress, Chania, Sept. 2013

EFFECT OF WET MILLING ON THE ADSORPTION CAPACITY OF A GREEK NATURAL ZEOLITE USED FOR THE REMOVAL OF HEAVY METALS FROM SOLUTIONS

Katsimicha D.[1], Pentari D.[1], Pantelaki O.[1] and Komnitsas K.[1]

[1] Technical University of Crete, Department of Mineral Resources Engineering, dekatsi@yahoo.gr, pentari@mred.tuc.gr, olgapan@mred.tuc.gr, komni@mred.tuc.gr

Abstract

The aim of the present work is the investigation of the effect of wet milling on the adsorption capacity of a Greek natural zeolite to remove heavy metal ions from solutions. The ultimate objective is to explore the potential of producing and using fine-grained zeolite in industrial and environmental applications. For this, a rich in clinoptilolite natural zeolite, was subjected to wet milling and 3 fractions were obtained (<10 μm, 10-63 μm, and 63-200 μm). The mineralogy of each fraction was determined through powder XRD and XRF analyses, while their particle size distribution and specific surface area were determined using the Laser Beam Diffraction Technique and the BET method respectively. The adsorption of Cu^{2+}, Ni^{2+}, Mn^{2+} and Cd^{2+} ions by each zeolite fraction was investigated using different initial metal ion concentrations (10 and 100 mg/L) and contact times (up to 72 h). The concentration of the adsorbent was kept constant (5 g/L), whereas no pH adjustment took place.
The experimental results proved that wet grinding can result in the production of very fine natural zeolite (d_{50}= 4.37 μm) without any loss of crystallinity and that this fraction exhibits substantial metal ion adsorption capacity. Adsorption is best described by the Freundlich isotherm.
Key words: *zeolite, wet milling, adsorption, heavy metals, isotherms*

Περίληψη

Ο στόχος της παρούσης εργασίας είναι η διερεύνηση της επίδρασης της λειοτρίβισης στην προσροφητική ικανότητα ενός ελληνικού φυσικού ζεόλιθου ως προς την απομάκρυνση ιόντων βαρέων μετάλλων από υδατικά διαλύματα. Ο απώτερος στόχος είναι να μελετηθεί η δυνατότητα παραγωγής και χρήσης υπέρλεπτου ζεόλιθου σε βιομηχανικές και περιβαλλοντικές εφαρμογές. Για τον σκοπό αυτό, φυσικός ζεόλιθος πλούσιος σε κλινοπτιλόλιθο υποβλήθηκε σε υγρή λειοτρίβιση σε ραβδόμυλο ώστε να προκύψουν τρία κοκκομετρικά κλάσματα (<10 μm, 10-63 μm, and 63-200 μm). Η ορυκτολογία των κλασμάτων προσδιορίστηκε με την μέθοδο της Περιθλασιμετρίας Ακτίνων-Χ (XRD) και της Φασματοσκοπίας Φθορισμού Ακτίνων-Χ (XRF), ενώ η κατανομή του μεγέθους των κόκκων και η ειδική τους επιφάνεια με την τεχνική της Περίθλασης Ακτίνας Laser και την μέθοδο BET αντίστοιχα. Η προσρόφηση των ιόντων Cu^{2+}, Ni^{2+}, Mn^{2+} και Cd^{2+} από κάθε κοκκομετρικό κλάσμα ζεολίθου μελετήθηκε χρησιμοποιώντας διαφορετικές αρχικές συγκεντρώσεις ιόντων (10 και 100 mg/L) και χρόνους παραμονής (έως 72 ώρες). Η συγκέντρωση του ροφητή διατηρήθηκε σταθερή (5 g/L), ενώ δεν έλαβε χώρα ρύθμιση του pH. Τα πειραματικά αποτελέσματα απέδειξαν ότι με

υγρή λειοτρίβιση μπορεί να παραχθεί εξαιρετικά λεπτομερής ζεόλιθος (d_{50}= 4.37 μm) χωρίς απώλεια κρυσταλλικότητας και ότι αυτό το κλάσμα παρουσιάζει εξαιρετική ικανότητα προσρόφησης ιόντων βαρέων μετάλλων. Η διεργασία της προσρόφησης περιγράφεται πολύ καλά από την ισόθερμη Freundlich.
Λέξεις κλειδιά: *ζεόλιθος, υγρή λειοτρίβιση, προσρόφηση, βαρέα μέταλλα, ισόθερμες*

1. Introduction

The introduction of heavy metals to natural ecosystems has been related to many diverse human activities and is of great concern, due to the fact that these contaminants, unlike organics, are persistent in soils and non degradable, whereas if they are mobilized and released to water reservoirs may become bioavailable and threaten living organisms (Shi et al., 2009). Among several processes, such as ion-exchange, filtration, electrolytic or liquid extraction, chemical precipitation, reverse osmosis and membrane techniques (Pentari et al., 2009), adsorption can offer an easy, low-cost and effective alternative to water, wastewater and industrial effluent treatment (Wang & Peng, 2010).

Natural zeolites are hydrated alumino-silicate minerals of a porous structure with good mechanical and thermal characteristics and beneficial physicochemical properties, like high cation exchange capacity, and potential to act as molecular sieve and catalyst (Misaelides, 2011). Their usage does not introduce additional contamination in the environment, so they can find numerous environmental and industrial applications, including uptake of heavy metals from acid mine drainage, purification of waters and industrial-urban wastewaters, management of nuclear wastes, soil remediation, drying of acid-gases, production of pozzolanic cement and lightweight aggregates, zeoponic substrates for greenhouses, deodorization products and dietary supplements for animals (Mumpton, 1999; Kulasekaran and Dendi Damodar, 2011). Natural zeolitic tuffs have been found in many countries while their world mine production in 2010 has been estimated at 2.75 million tons (USGS, 2011).

The adsorption capacity of natural and modified zeolites has been studied extensively (Panayotova & Velikov, 2002; Caputo & Pepe, 2007; Castaldi et al., 2008; Ghair and Ingwersen, 2009; Motsi et al., 2011). The effect of milling on the improvement of the adsorption capacity of zeolites has been also studied by several researchers (Akçay et al., 2004; Ozkan et al., 2009; Charkhi et al., 2010). Today, researchers mainly investigate the capacity of modified or non modified nano-zeolites for the adsorption of organic contaminants (Seifi et al., 2011; Hassani Nejad-Darzi et al., 2012). Future research activities will definitely focus on the adsorption capacity of modified nano-zeolites and the decontamination of industrial solutions and soils as well as on the potential hazardous impacts of zeolite nano-particles on humans and ecosystems.

The aim of the present study is the investigation of the effect of wet milling on the crystallinity and the adsorption capacity of a Greek natural zeolite used for the removal of heavy metal ions, namely Cu^{2+}, Ni^{2+}, Mn^{2+} and Cd^{2+}, present in solutions in various concentrations. The ultimate objective is to explore the potential of using extremely fine or nano-zeolite in environmental and industrial applications.

2. Materials and Methods

2.1. Zeolite Treatment

The zeolite used in the present study originates from a natural clinoptilolite-rich deposit from the area of Petrota (Evros Prefecture, North Greece) (Filippidis et al., 2009) and its initial particle size distribution ranged between 0.3-0.8 cm. Zeolite was subjected to wet rod milling for 20 min at 47 rpm using a Sepor's 5´´ Series Batch Rod Mill Drive. Under the optimum conditions, the mill was loaded with 9 kg of hardened steel rods of 23 cm length and varying diameter (1.3-1.9 cm), 1 L water and 1 kg zeolite. The finely ground zeolite was then split in three fractions (<10 μm, 10-63

μm, 63-200 μm) using a Richard Mozley Ltd hydro-cyclone. Finally, all fractions were dried at 100 ^{o}C for 24 h and then stored in plastic bags until further analysis and use.

2.2. Characterization Studies

The chemical analysis of all three fractions was performed through X-Ray Fluorescence, using an Energy Dispersive Spectrometer S2 RANGER Bruker apparatus. Additionally, the mineralogy of the fractions was determined through Powder X-Ray Diffraction, using a XRD D8 Advance Bruker apparatus. The data were obtained at 35 kV and 35 mA, with a graphite monochromator, using CuKα radiation. The qualitative evaluation of the data was carried out with the software Diffrac Plus EVA, while the Autoquan software (based on the Rietveld method) was used for quantitative analysis.

The specific surface area of the fractions was determined using the Quantachrome Instruments Nova 2200 apparatus, according to the Brunauer, Emmett and Teller (B.E.T.) theory, while their particle size distribution through Laser Beam Diffraction, using a Mastersizer S Ver. 2.14 apparatus of MALVERN Instruments.

2.3. Experimental Methodology

Sorption experiments were carried out using solutions containing analytical grade nitrate salts of the corresponding metals: $Cu(NO_3)_2 \cdot 3H_2O$, $Ni(NO_3)_2 \cdot 6H_2O$, $Mn(NO_3)_2 \cdot 4H_2O$ and $Cd(NO_3)_2 \cdot 4H_2O$ (puriss p.a. quality, FLUKA). Batch experiments were performed at room temperature under continuous agitation. 0.5 g of air dried zeolite was added in 100 mL of metal solution in 200 mL glass beakers. Mono-component kinetic experiments were carried out for each metal ion and zeolite fraction, using two initial metal ion concentrations, namely 10 mg/L and 100 mg/L. Liquid samples were withdrawn at different periods (5 min, 15 min, 30 min, 2 h, 6 h, 18 h, 24 h, 48 h and 72 h) and filtered to determine the residual metal ion concentration with Flame Atomic Absorption Spectroscopy, using an Analyst 100 of Perkin Elmer spectrometer. pH was monitored throughout the experiments using a WTW InolabLevel1 pH meter; no pH adjustment took place.

Sorption isotherms were derived only for the finest zeolite fraction (<10 μm), which was proved to be the best adsorbent, by varying the initial concentration of each metal ion from 10 to 100 mg/L (10, 30, 50, 80 and 100 mg/L); the concentration of the adsorbent was kept constant at 5 g/L. The other conditions were kept similar to those used in kinetic studies and the retention period to reach equilibrium was maintained at 48 h. In all tests, reagent blanks and randomly selected duplicate samples were considered for quality control/assurance and precision purposes.

3. Results and Discussion

3.1. Zeolite Characteristics

The mineralogical phases, the content in oxides, the particle size distribution and the specific surface area of each zeolite fraction are presented in Table 1 and Figure 1. As shown, the main mineralogical phases in all fractions are cliniptilolite, smectite, cristobalite, quartz and other alumino-silicates (oligoclase, illite). XRD patterns also show that the crystallinity of the fine grained zeolite is not affected by wet milling. The finer fractions are enriched in clinoptilolite and smectite whereas the content of cristobalite, quartz and oligoclase decreases to a higher or lesser extent. The <10 μm fraction contains extremely fine particles (d_{50}=4.37 μm, d_{10}=1.06 μm) with a significant specific surface area (18.30 m^2/g), 65% larger than that of the 63-200 μm fraction.

Table 1 – Characterisation of each zeolite fraction.

	< 10 µm	10 – 63 µm	63 – 200 µm
Mineralogical phases (%)			
Clinoptilolite	74.91	75.38	66.61
Cristobalite	4.35	5.60	6.98
Illite	1.85	0.51	1.05
Oligoclase	2.78	2.20	7.95
Quartz	4.73	6.72	9.58
Smectite	11.37	9.59	7.83
Oxides (%)			
Na_2O	1.31	1.33	1.17
MgO	1.51	1.30	1.08
K_2O	2.97	3.22	3.20
CaO	2.43	2.39	2.14
TiO_2	0.08	0.11	0.08
MnO	0.03	0.03	0.02
Fe_2O_3	1.56	1.08	0.84
Al_2O_3	13.58	12.61	11.82
SiO_2	72.00	74.81	74.2
P_2O_5	0.00	0.00	0.00
L.O.I.	9.41	8.71	7.42
Particle Size Distribution (µm)			
d_{10}	1.06	9.05	9.98
d_{50}	4.37	32.66	92.69
d_{90}	9.81	62.61	176.91
Specific Surface Area (m^2/g)	18.30	11.86	11.08

3.2. Adsorption Capacity of Zeolite

3.2.1. Kinetics

The effect of retention time on the adsorption of each metal ion by each zeolite fraction is illustrated in Figure 2. In all cases the equilibrium was reached very quickly, in less than 24 h. The experimental results show that the finest fraction (-10 µm) exhibited the best adsorption capacity for all metal ions regardless of the initial concentration of 10 mg/L or 100 mg/L. Metal ion removal for all elements varied between 90-96% when the initial concentration was 10 mg/L; the removal percentage decreased to 67-90% when a coarser zeolite fraction (63-200 µm) was used. When the initial metal ion concentration increased to 100 mg/L, which is indeed high for most industrial effluents, the adsorption capacity of zeolite decreased substantially. In this case, the removal efficiency of the -10 µm fraction varied between 26 and 47%. As mentioned before no pH adjustment was done since this was not considered necessary; pH in all tests varied between 5.5 and 6.5. Among the metal ions tested, zeolite exhibited its highest adsorption capacity for copper and cadmium and its lowest for nickel (Fig. 2-a,c,e for initial concentration of 10 mg/L and Fig. 2-b,d,f for initial concentration of 100 mg/L).

Adsorption rates for all heavy metals were much higher in the beginning of the tests but soon reached an asymptotic plateau, where the increase of retention time did not seem to be beneficial. Table 2 shows the calculated adsorption rates for all heavy metal ions when the finest zeolite fraction was used. The retention time required to reach equilibrium was 30 min. It is observed that when the metal ion concentration was 10 mg/L adsorption rates were almost identical for Cu, Mn and Cd (3.9 mg/g/h) and slightly lower for Ni (3.5 mg/g/h). Adsorption rates differed significantly though when the high metal ion concentration was used (100 mg/L). In this case, the highest adsorption rate was recorded for Cd (16.4 mg/g/h) and the lowest for Ni (9.6 mg/g/h). Thus, the adsorption rate sequence in decreasing order was Cd>Cu>Mn>Ni and agreed with most previous studies (Erdem et al., 2004, Wang & Peng, 2010).

The adsorption rate sequence is quite well related to the ionic radius of each heavy metal ion, which is for Cd: 0.95 Å, Mn: 0.83 Å, Cu: 0.73 Å, and Ni: 0.69 Å. It is shown that the higher the ionic radius the lower, in absolute values, the hydration enthalpy for all metal ions studied (Table 3). The enthalpy of hydration, H_{hyd}, in kJ/mole, of an ion is the amount of energy released when a mole of the ion dissolves in a large volume of water forming thus an infinite dilute solution. According the Eisenman-Sherry theory of cation exchange selectivity (Eisenman, 1962, Sherry, 1969), zeolites exhibit a greater preference for larger cations, like Cd^{2+}, with greater ionic radius and lower, in absolute values, hydration enthalpy (Panayotova & Velikov, 2002, Caputo & Pepe, 2007).

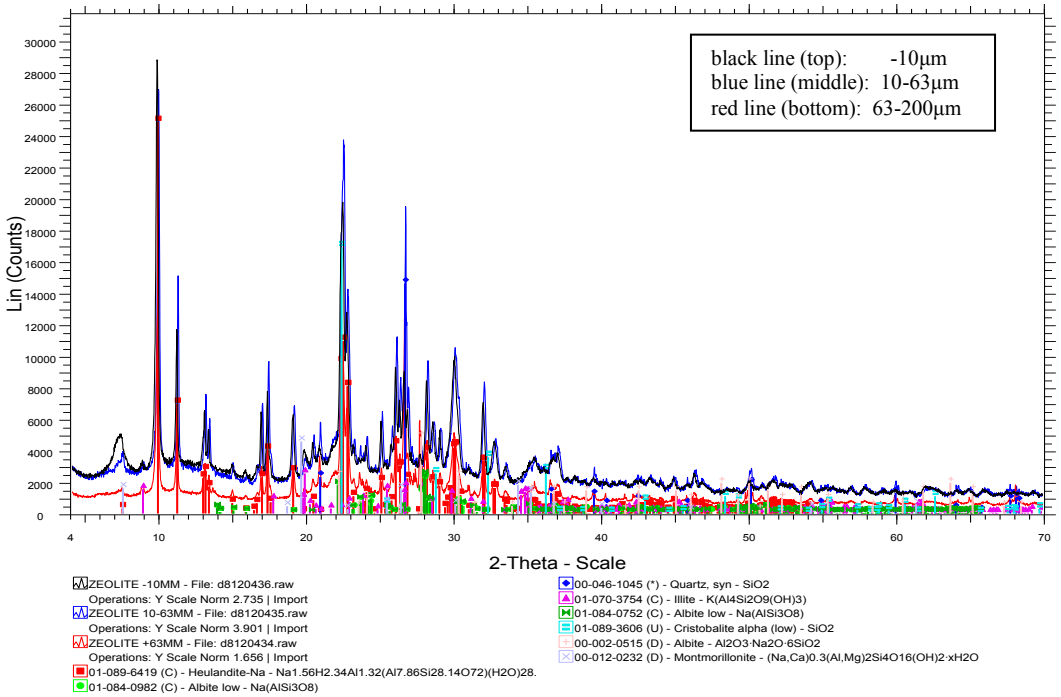

Figure 1 – XRD diffractograms of all zeolite fractions.

Table 2 - Adsorption rates (in mg metal ion/g zeolite/h) for each metal ion. Zeolite fraction -10 µm, retention time 30 min.

Initial metal ion concentration	Cu	Ni	Mn	Cd
10 mg/L	3.98	3.54	3.94	3.94
100 mg/L	13.70	9.60	10.40	16.40

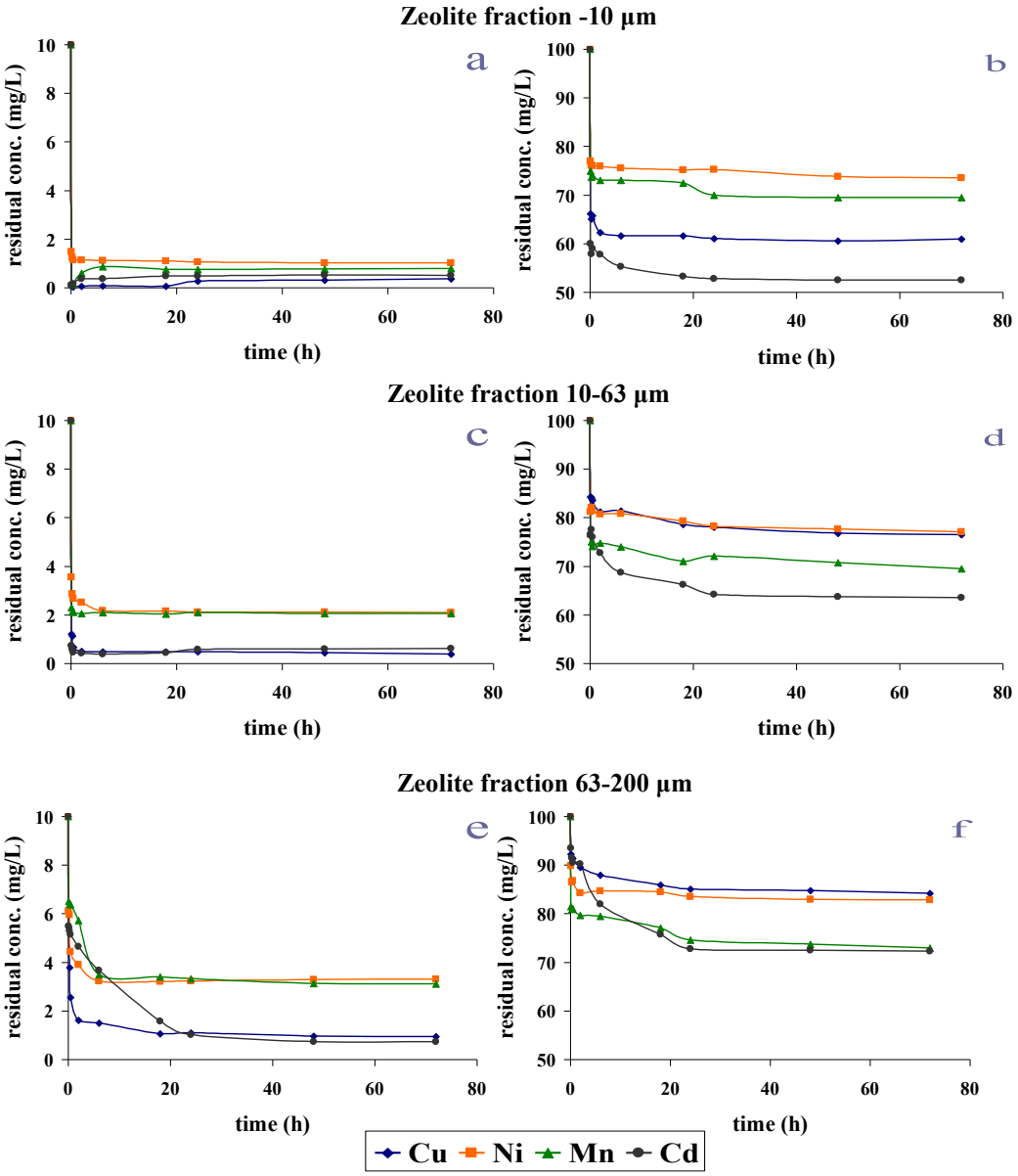

Figure 2 – Adsorption kinetics for each metal ion by each zeolite fraction. Experimental conditions: initial metal ion concentration 10 mg/L (a,c,e) and 100 mg/L (b,d,f), zeolite concentration 5 g/L.

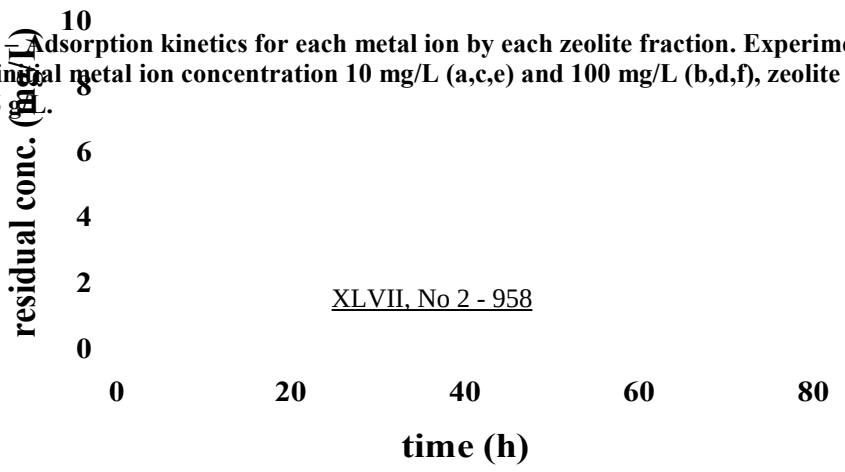

Table 3 – Ionic radii and hydration enthalpy of the metal ions studied (Marcus, 1994).

	Ionic radius (Å)	Hydration enthalpy (kJ/mole)
Cd^{2+}	0.95	-1830
Mn^{2+}	0.83	-1870
Cu^{2+}	0.73	-2120
Ni^{2+}	0.69	-2115

3.2.2. Adsorption Isotherms

The equilibrium data were analysed and tested against three different isotherm models, the Linear, the Freundlich and Langmuir respectively, in order to describe the adsorption of the four metal ions studied on the -10 μm zeolite fraction. The equations which were used for each model are:

Equation 1 - Linear model

$$q_e = K_P \cdot C_e$$

Equation 2 - Freundlich model

$$q_e = K_F \cdot C_e^{1/n}$$

Equation 3 - Langmuir model

$$\frac{q_e}{q_{\max}} = \frac{b \cdot C_e}{1 + b \cdot C_e}$$

where

q_e (mg/g), is the quantity of metal ion adsorbed per unit mass of zeolite at equilibrium,

C_e (mg/L), is the metal ion concentration at equilibrium,

K_P (L/g), coefficient related to the affinity between the adsorbent and the ion,

K_F (L/g), coefficient related to the adsorption capacity of the adsorbent

1/n (dimensionless), indicates the intensity of adsorption in relation to the heterogeneity of the adsorbent

b (L/mg), constant related to the adsorption intensity and

q_{max} (mg/g), is the maximum adsorption capacity of the adsorbent.

A non-linear regression analysis (Smyth, 2002) was carried out using the MATLAB R2012a software and the results are presented in Table 4.

Adsorption isotherms derived for each metal ion using the -10 μm fraction (Figure 3) indicated that are considered of "L" type according to the classification of Giles et al. (1974). This means that the concentration of a compound adsorbed on the solid mass decreases when the solute concentration increases, thus suggesting a progressive saturation of the solid (Limousin et al., 2007).

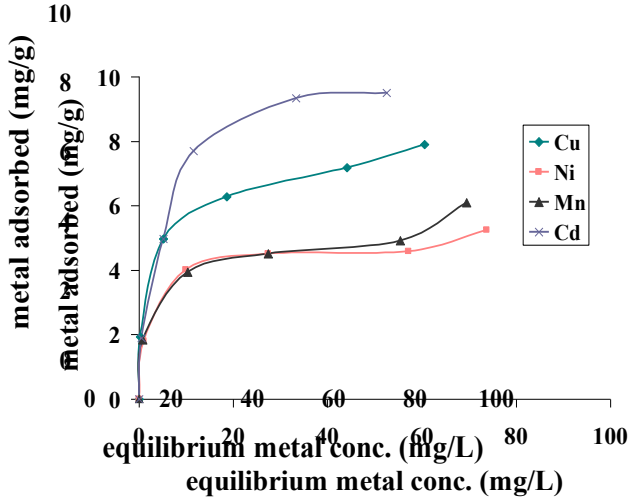

Figure 3 – Adsorption isotherms for each metal ions studied. Experimental conditions: zeolite fraction -10 µm, zeolite concentration 5 g/L, metal ion concentration 10 to 100 mg/L.

Table 4 – Model parameters for Cu, Ni, Mn and Cd adsorption by the -10 µm zeolite fraction.

Element	Linear model		Freundlich model			Langmuir model		
	K_P (L/g)	r^2	K_F (L/g)	n	r^2	q_{max} (mg/g)	b (L/mg)	r^2
Cu	0.157	0.282	3.140	4.419	0.990	7.482	0.510	0.964
Ni	0.085	0.075	2.222	5.030	0.968	4.964	0.513	0.987
Mn	0.098	0.363	2.111	4.261	0.980	5.307	0.503	0.940
Cd	0.230	0.334	3.260	3.466	0.968	10.450	0.218	0.986

As shown in Table 4 and in Figure 4, the Freundlich model fits better the experimental data; this suggests that the isotherm does not reach any plateau and consequently the studied adsorbent does not show clearly a limited adsorption capacity.

It is noted that the Langmuir isotherm describes adsorption of an ion in a single layer of an homogeneous surface of a solid particle without taking into account any interactions between the adsorbed ions or molecules. On the other hand, the Fruendlich isotherm considers an adsorbent with heterogeneous distribution of adsorption sites and takes into account potential interactions between the adsorbed ions/molecules.

It has to be mentioned that the isotherms may differ in case of simultaneous multi-component adsorption experiments. This issue is currently under investigation.

4. Conclusions

The experimental results show that by controlled wet rod milling of natural zeolite a well crystalline -10 µm fraction (d_{50}= 4.37 µm) is obtained. This fraction shows a very good adsorption capacity and can be used for the effective clean up of solutions containing up to 10 mg/L Cu^{2+}, Ni^{2+}, Mn^{2+} and Cd^{2+} ions. Adsorption is very well described by the Freundlich model.

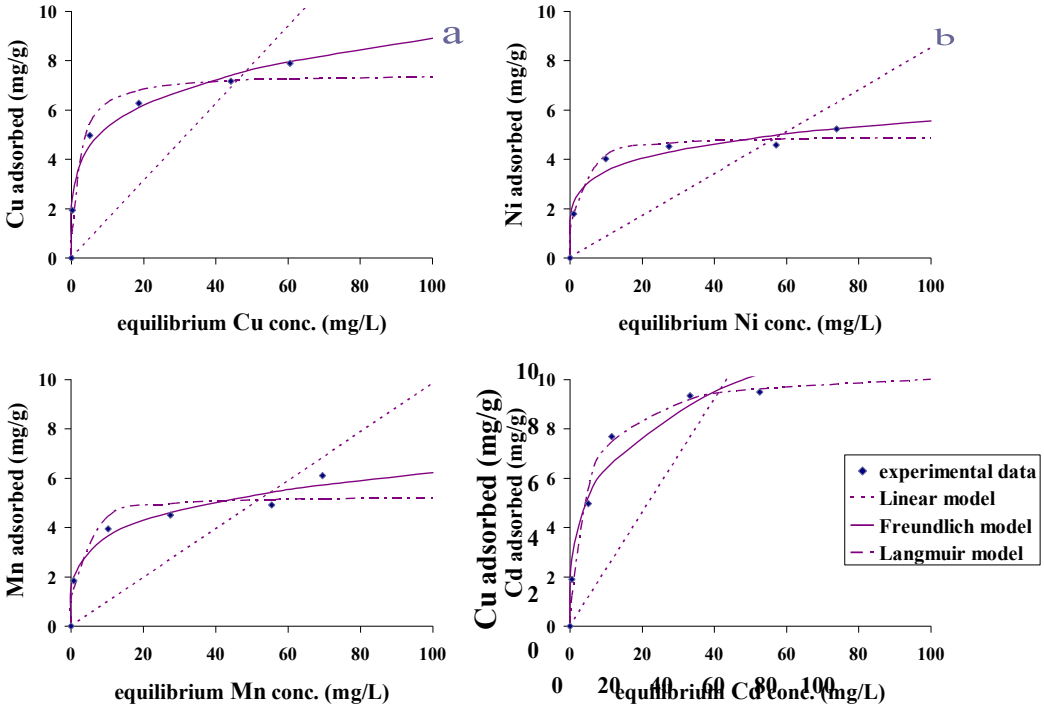

Figure 4 – Adsorption isotherms for (a) Cu, (b) Ni, (c) Mn and (d) Cd. Lines represent predicted data by Linear, Freundlich and Langmuir models while rhombus represent experimental data

5. Acknowledgements

This research has been co-financed by the European Union (European Social Fund - ESF) and Greek national funds through the Operational Program "Education and Lifelong Learning" of the National Strategic Reference Framework (NSRF) - Research Funding Program: THALES (Project title: Development of an integrated methodology for the management, treatment and valorisation of hazardous waste (WasteVal), proposal number:420). Prof. Komnitsas would also like to thank his colleague, Prof. Anestis Filippidis, School of Geology, Faculty of Sciences, Aristotle University of Thessaloniki, for the provision of the zeolite used in this work.

6. References

Akçay K., Sirkecioğlu A., Tather M., Tunç Savaşçi Ö. and Erdem-Şenatalar A. 2004. Wet ball milling of zeolite HY, *Powder Technology*, 142, 121-128.

Caputo D. and Pepe F. 2007. Experiments and data processing of ion exchange equilibria involving Italian natural zeolites: a review, *Microporous and Mesoporous Materials*, 105, 222-231.

Castaldi P., Santona L., Enzo S. and Melis P. 2008. Sorption processes and XRD analysis of a natural zeolite exchanged with Pb^{2+}, Cd^{2+} and Zn^{2+} cations, *Journal of Hazardous Materials*, 156, 428-434.

Charkhi A., Kazemian H. and Kazemeini M. 2010. Optimized experimental design for natural clinoptilolite zeolite ball milling to produce nano powders, *Powder Technology*, 203, 389-396.

Eisenman G. 1962. Cation selective glass electrodes and their mode of operation, *Biophysical Journal*, 2, 259–323.

Erdem E., Karapinar N. and Donat R. 2004. The removal of heavy metal cations by natural zeolites, *Journal of Colloid and Interface Science*, 280, 309-314.

Filippidis A., Apostolidis N., Filippidis S. and Paragios I. 2009. Purification of sewage effluents and production of odorless-cohesive sewage sludge using Hellenic natural zeolite (in Greek), *Hydrogaia*, Honorary volume for Prof. Ch. Tzimopoulos, Faculty of Engineering, Aristotle University of Thessaloniki, 425-434.

Ghair A.M. and Ingwersen J. 2009. Nanoparticulate zeolitic tuff for immobilizing heavy metals in soil: preparation and characterization, *Water, Air, and Soil Pollution*, 203, 155-168.

Giles C.H., Smith D. and Huitson A. 1974. A general treatment and classification of the solute adsorption isotherm, I. Theoertical, *Journal of Colloid and Interface Science*, 47, 755–765.

Hassani Nejad-Darzi S.K., Samadi-Maybodi A. and Ghobakhluo M. 2013. Synthesis and characterization of modified ZSM-5 nanozeolite and their applications in adsorption of Acridine Orange dye from aqueous solution, *Journal of Porous Materials*, doi: 10.1007/s10934-012-9668-9.

Kulasekaran R. and Dendi Damodar R. 2011. Chapter four: Zeolites and their potential uses in agriculture, *Advances in Agronoly*, Vol. 113, 219-241.

Limousin G., Gaudet J.P., Charlet L., Szenknect S., Bartès V. and Krimissa M. 2007. Sorption isotherms: A review on physical bases, modeling and measurement, *Applied Geochemistry*, 22, 249-275.

Marcus Y. 1994. A simple empirical model describing the thermodynamics of hydration of ions of widely varying charges, sizes and shapes, *Biophysical Chemistry*, 51 (2-3), 111-127.

Misaelides P. 2011. Application of natural zeolites in environmental remediation: A short review, *Microporous and Mesoporous Materials*, 144, 15-18.

Motsi T., Rowson N.A. and Simmons M.J.H. 2011. Kinetic studies of the removal of heavy metals from acid mine drainage by natural zeolite, *International Journal of Mineral Processing*, 101, 42-49.

Mumpton F.A. 1999. La roca magica: Uses of natural zeolites in agriculture and industry, *Proceedings of the National Academy of Sciences USA*, Vol. 96, 3463-3470.

Ozkan A., Yekeler M. and Calkaya M. 2009. Kinetics of fine wet grinding of zeolite in a steel ball mill in comparison to dry grinding, *International Journal of Mineral Processing*, 90, 67-73.

Panayotova M. and Velikov B. 2002. Kinetics of heavy metal ions removal by use of natural zeolite, *Journal of Environmental Science and Health*, A37(2), 139-147.

Pentari D., Perdikatsis V., Katsimicha D. and Kanaki A. 2009. Sorption properties of low calorific value greek lignites: removal of lead, cadmium, zinc and copper ions from aqueous solutions, *Journal of Hazardous Materials*, 168, 1017-1021.

Seifi L., Torabian A., Kazemian H., Bidhendi G.N., Azimi A.A. and Charkhi A. 2011. Adsorption of petroleum monoaromatics from aqueous solutions using granulated surface modified natural nanozeolites: Systematic study of equilibrium isotherms, *Water, Air, and Soil Pollution,* 217(1-4), 611-625.

Sherry H.S. 1969. The ion-exchange properties of the zeolites, In: Marinsky J.A. ed., *Ion Exchange: A Series of Advances*, Vol.2, Marcel Dekker, New York, 89-133.

Shi W.-Y., Shao H.B., Li H., Shao M.A. and Du S., 2009. Progress in the remediation of hazardous heavy-metal polluted soils by natural zaolite, *Journal of Hazardous Materials*, 170, 1-6.

Smyth G.K. 2002. Nonlinear regression, In: El-Shaarawi A.H. and Piegorsch W.W. eds., *Encyclopedia of Environmetrics*, Vol.3, 1405-1411, Wiley, J. & Sons, Ltd, Chichester.

USGS 2011. Zeolites (Natural), *U.S. Geological Survey, Mineral Commodity Summaries*, January 2011.

Wang S. and Peng Y. 2010. Natural zeolites as effective adsorbents in water and wastewater treatment, *Chemical Engineering Journal*, 156, 11-24.

Δελτίο της Ελληνικής Γεωλογικής Εταιρίας, τομ. XLVII , 2013
Πρακτικά 13ου Διεθνούς Συνεδρίου, Χανιά, Σεπτ. 2013

Bulletin of the Geological Society of Greece, vol. XLVII 2013
Proceedings of the 13th International Congress, Chania, Sept. 2013

ENVIRONMENTAL MONITORING OF SOIL POLLUTION IN URBAN AREAS (A CASE STUDY FROM HERAKLION CITY, CENTRAL CRETE, GREECE)

Kokinou E.[1], Belonaki C.[1], Sakadakis D.[1] and Sakadaki K. [1]

[1] *Technological Educational Institute Crete, Department of Natural Resources & Environment, Chania, Crete, Greece, ekokinou@chania.teicrete.gr*

Abstract

Main scope of the present study is to combine topographic and geological data, magnetic susceptibility and thermomagnetic analysis in order to investigate the magnetic properties of the near surface soils in possible polluted urban areas. For this purpose, a power plant with a dense traffic net around it, located in the NW section of Heraklion city in Crete was selected to be the study area. Surface soil samples have been collected from the area under investigation and they were analyzed in order to estimate the spatial distribution of the magnetic susceptibility. Loci of high values of the magnetic susceptibility within the study area gave rise to further proceed to thermomagnetic analysis of the selected samples. GIS techniques were used for mapping the magnetic measurements on the various topographic and geological features of the area. The digital elevation model was created by the digitization of the topographic map contours (1:5000 scale maps). The combination of the above techniques indicate high values of the magnetic susceptibility especially in the northeastern part of the investigated area, possibly related to pollution due to the presence of heavy metals.
Key words: *Magnetic susceptibility, thermomagnetic analysis, GIS.*

Περίληψη

Στόχος της παρούσας εργασίας είναι να συνδυάσει τοπογραφικά (1:5000), γεωλογικά δεδομένα και μαγνητικές αναλύσεις (μαγνητική επιδεκτικότητα και θερμομαγνητική ανάλυση) επιφανειακών ιζημάτων με στόχο να καθοριστούν τα χαρακτηριστικά των ιζημάτων γύρω από πιθανές πηγές ρύπανσης από βαρέα μέταλλα. Η περιοχή που επιλέχθηκε βρίσκεται κοντά στον υποσταθμό της ΔΕΗ, δυτικά της πόλης του Ηρακλείου με πυκνό οδικό δίκτυο τριγύρω. Τα αποτελέσματα δείχνουν πιθανή ρύπανση στο βορειοανατολικό κυρίως τμήμα της υπό μελέτη περιοχής.
Λέξεις κλειδιά: *Μαγνητική επιδεκτικότητα, θερμομαγνητική ανάλυση, Γ.Σ.Π.*

1. Introduction

Industrial pollution and heavy traffic constitute serious problems for fast developing countries. Magnetometry and especially magnetic susceptibility is a fast and cost-effective method for detection of environmental pollution of soils, sediments and dusts. Magnetic minerals present in soils may be either inherited from the parent rocks (lithogenic origin), formed during pedogenesis or may be stemmed by anthropogenic activities (emissions from power plants, combustion of

fossil fuel, metallurgical industries, smelters, road traffic, etc.). In the case of minor contribution of the first two sources to the magnetic properties of soils, susceptibility measurements become very important for monitoring environmental pollution, because metallurgical dusts, fly ashes and cement dust contain relatively large amount of iron phases and are therefore highly magnetic (Strzyszcz et al. 1996; Goluchowska 2001). Magnetic particles are usually deposited downwind from the industrial units on the surface of soils, streets, buildings and trees. Fly ashes with significant portion of magnetic minerals are produced by industrial processes; they are transported through atmospheric pathways and deposited on the ground. In soils, such particles penetrate downwards and accumulate in top layers and their increased concentration can be easily detected using surface magnetic measurements. Hansen et al. (1981) indicated that chromium manganese, cobalt, nickel, copper, zinc and beryllium are all significantly enriched in the 'magnetic' fraction of coal fly-ash. Beckwith et al. (1984) identified pollution sources in urban drainage systems using magnetic methods. Petrovsky & Elwood (1999) reviewed the application of magnetic susceptibility measurements in various ecosystems. Lately, more researchers investigate the usage of magnetic susceptibility as a tool for contaminated top soils and sediments (Scholger 1998; Bitykova et al. 1999; Petrovsky et al. 2001; Boyko et al. 2004, Sarris et al., 2009).

The aim of this study is to establish links between enhanced concentrations of anthropogenic magnetic particles and known sources of pollution in the catchment area. For this purpose the spatial distribution of the magnetic susceptibility and the frequency dependent susceptibility, thermomagnetic analysis, topographic and geological data are combined. This study tries to document that simple and fast in situ magnetic measurements can reflect the anthropogenic influence under certain circumstances.

2. Geology of the Study Area

The Heraklion basin (Figure 1a), where the study area is located (Figure 1b), comprises the largest Neogene basin (900 km^2). The Neogene deposits of Heraklion basin overlie basement rocks of the Upper Nappes (Gavrovo-Tripolis, Pindos and the heterogeneous Uppermost Unit). The Upper Nappes in the Psiloritis and Dikti Mts. are separated from the HP-LT metamorphic rocks of the Lower Nappes (parautochtone Plattenkalk and Phyllite-Quarzite units) by the Cretan detachment (Zachariasse et al., 2011). This fault (or faults) is in many places exposed with a sense of shear either to both S and N (Kilias et al., 1994; Fassoulas, 1999; Papanikolaou and Vassilakis, 2010), or dominantly top-to the north (Jolivet et al., 1996). This basin is mainly filled by fluvial and marine sediments of Holocene, Pleistocene, Lower-Middle Pliocene, Upper Miocene, Cretaceous – Middle Eocene and Upper Triassic-Upper Jurassic (Figure 2). The Holocene sediments (al) mainly comprise fluvial and closed basin deposits, situated in the western part of the city, on either site of the drainage network. Pleistocene – Holocene sediments (Qs) are generally located across the coastline, comprising of undivided marine terraces and coastal sands. The Heraklion formation (Pt) of Pleistocene consists of marine bioclastic limestones, sandstones with crossed bedding conglomerates and marls. The majority of the basin's interior consists of Lower-Middle Pliocene sediments (Pl.m) the so called Finikia formation, comprising of white marls or marly limestones, grayish clays with brown, often thin bedded intercalations, white beige fossiliferous marls, lamellar marls or diatomites and bioclastic limestones. The base of this formation consists in general of an unsorted "marly breccia". It overlies unconformably the Ag. Varvara formation (Mk) of Upper Miocene, consisting of bioclastic, reef limestones, marls or marly limestones (Mm) and gypsum (g). In the eastern part of Heraklion city are situated Cretaceous – Middle Eocene (Ks-Ek) limestones, grey to black, medium-thick bedded to massive bituminous locally microbreciatted and dolomitic in the upper members. Triassic –Upper Jurassic (Ts-Js.Kd) limestones, dolomitic limestones and dolomites are also present in the area. They constitute the base of the external zones tectonic nappe resulting in a local mylonitization at their base due tectonism. They are karstic, mainly in the upper members. Finally the oldest layer of this area is the Phyllites-Quartzites (ph) unit, aged Upper Palaeozoic - Upper Triassic (Krahl et al. 1983), underlain by the

Plattenkalk unit (Crete-Mani), aged Upper Palaeozoic - Lower Oligocene (Psonis 1981, Thiebault 1982, Manutsoglu 1990, Aleweld 2002).

The study area (Figure 1c-f) is located at the W section of the Heraklion city in Crete, showing a NE-SW orientated drainage network (Figure 2), named Almyros river, located near to the local power plant. The study area is mainly filled by recent alluvial (al) and Pleistocene (Pt.tm) sediments, the Finikia Formation (Pl.m), as well Triassic –Upper Jurassic (Ts-Js.Kd) limestones and the Phyllites-Quartzites (ph) unit. N-S, NW-SE and E-W trending faults prevail in the wide area.

3. Methodology

3.1. Soil Sampling

Top soil sampling was performed in the study area within a grid covering a total area of about 2.5 km^2. GPS coordinates (in EGSA_87 system) were taken from each sampling site in order to be in agreement with the available topographic data. At each site samples were taken within a depth of 0-15 cm below the surface. Soil samples were placed in plastic containers. Each of the soil samples was mixed, air-dried, disaggregated and sieved retaining the fraction smaller than 2mm in order to reduce the biasing effect of air, water and pebbles.

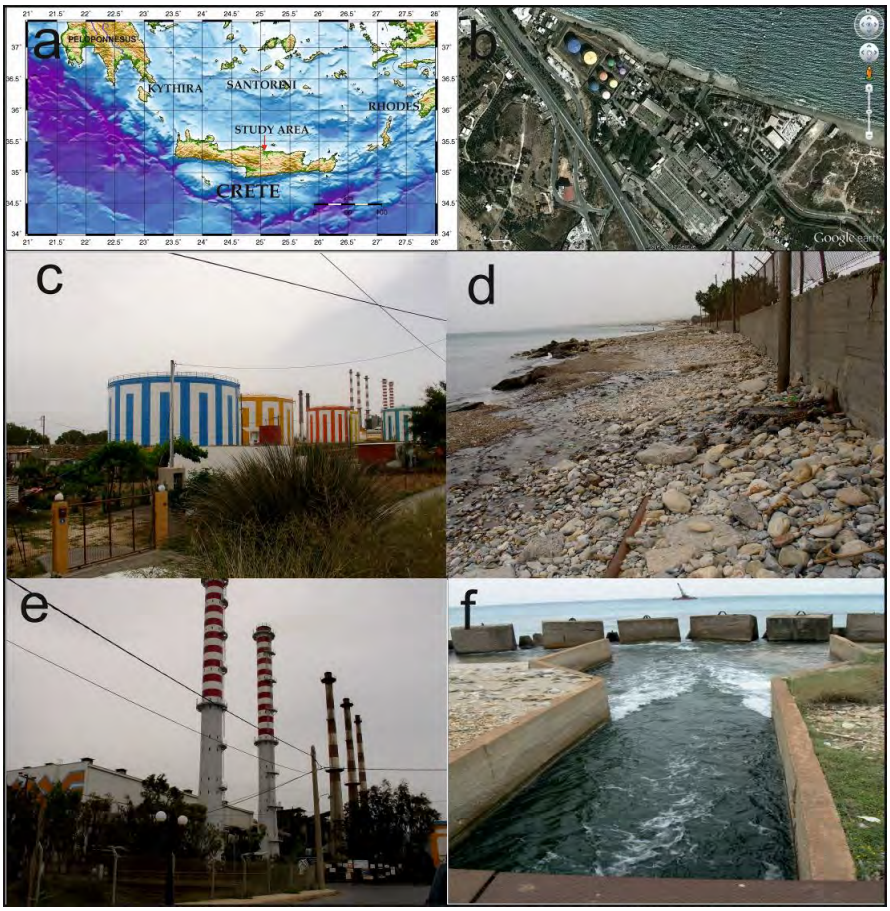

Figure 1 - a: Map of Crete showing the study area, b: the location of the power plant. Satellite imagery from Google Earth showing the wider area of interest, c-f: Detailed photos from the study area.

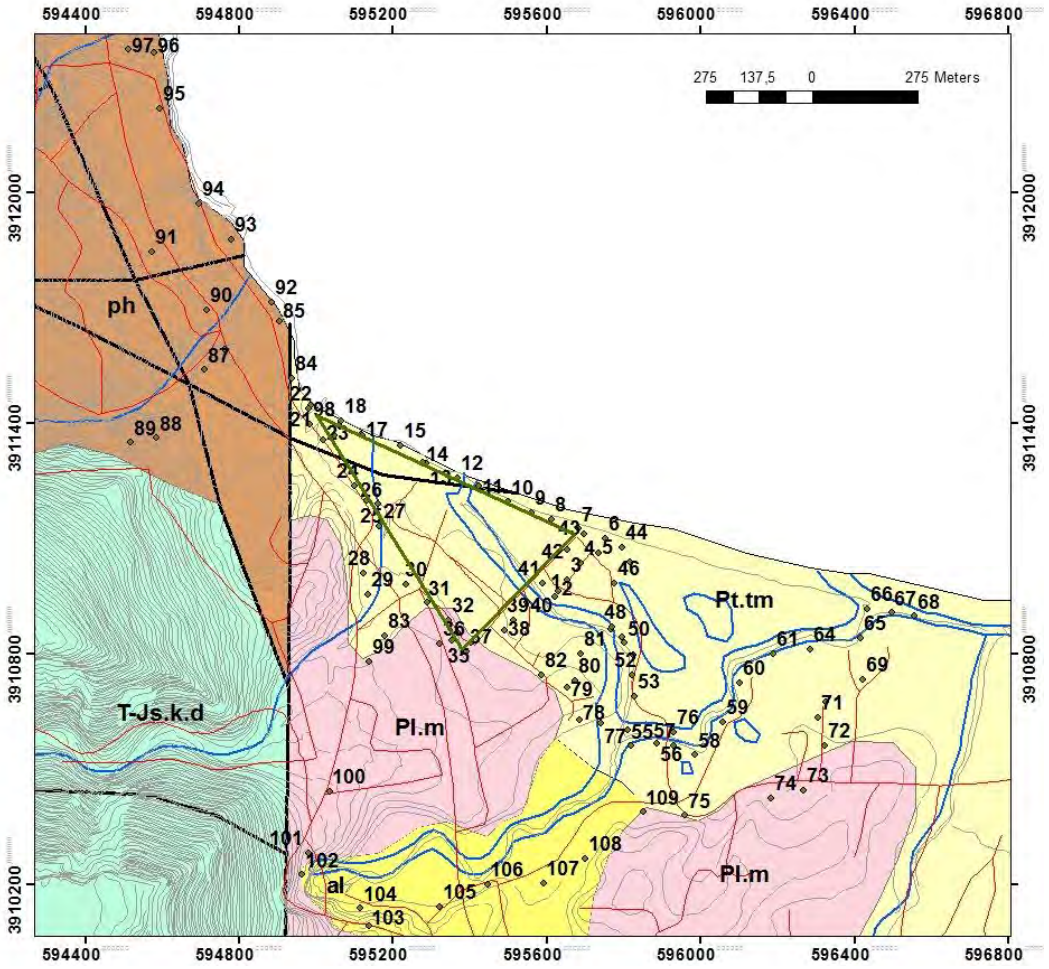

Figure 2 - Geological map of the wider area (according to geological map of IGME). Sympols: al-alluvial sed., Pt.tm-marls, sands and conglomerate, Pl.m- Finikia formation, Ts-Js.Kd - Triassic –Upper Jurassic limestones, dolomitic limestones and dolomites., ph-phyllites, Black line-fault, blue line-drainage net, Green line -power plant, Red line - traffic net, Black circle-sample location.

3.2. Magnetic Measurements

In environmental magnetism, the most often used magnetic parameter is the magnetic susceptibility (χ) which is the ratio of induced (temporary) magnetization acquired by a sample in the presence of a weak magnetic field, to the applied field itself. In the present study, the magnetic susceptibility of all samples was measured with the dual frequency version of sensor MS2B (Bartington Instruments). Accurate measurements of mass susceptibility were obtained in two frequencies (f_{low}=0.43KHz and f_{high}=4.3KHz). Further the frequency dependent susceptibility (χ_{fd} %) was calculated using the formula: χ_{fd} (%)=[(χ_{lf} - χ_{hf})/χ_{lf}]x100, where χ_{lf} the susceptibility measured in low frequency and χ_{hf} the susceptibility measured in high frequency.

Since our samples were of unknown density, mass specific measurements seemed to be more appropriate than the ones based on specific volume. A sample of 10 cm^3 tightly packed Manganese Carbonate powder (χ=99.2x10^{-6} emu/gr) was used for calibration of the instrument. The consistency of the instrument calibration was checked by measuring the susceptibility of the

calibration sample in the beginning and end of the measuring session. Samples were weighted and the subsequent susceptibility measurements in both frequencies were multiplied by a factor w_f= (10/ weight of sample) in order to normalize our measurements for a mass of 10 gr. The contribution of the plastic container was measured for 10 pieces and the average value was subtracted from all measurements.

The magnetic behavior of many minerals varies with temperature. All magnetic minerals have a temperature point (Curie temperature) above which they become paramagnetic. So, in practice, from the shape of the temperature - susceptibility curves the presence of magnetic minerals and domains can be detected. Our samples were heated with the Susceptibility Temperature Bartington Device up to 700^{o}C and cooled down to room temperature in order to identify the main magnetic

3.3. Geographic Information System (GIS)

Digitization techniques and GIS were applied for the presentation of the spatial distribution of magnetic susceptibility measurements on the topographic and geological data. In order to address the correlation between the above quantities and the geomorphologic attributes of the region, a number of maps were collected and digitized. Topographic maps of the area (scale 1:5000) were enriched through a generalization of the geological formations of the region available by 1:50000 scale geological maps of the Institute of Geological and Mineral Exploration (IGME, Vidakis et al., 1996). Faults, the Almyros river, the main and secondary roads were also digitized and fused to the Geographical Information System component of the project. The samples' location was also superimposed on the maps (Figures. 2, 3, 4).

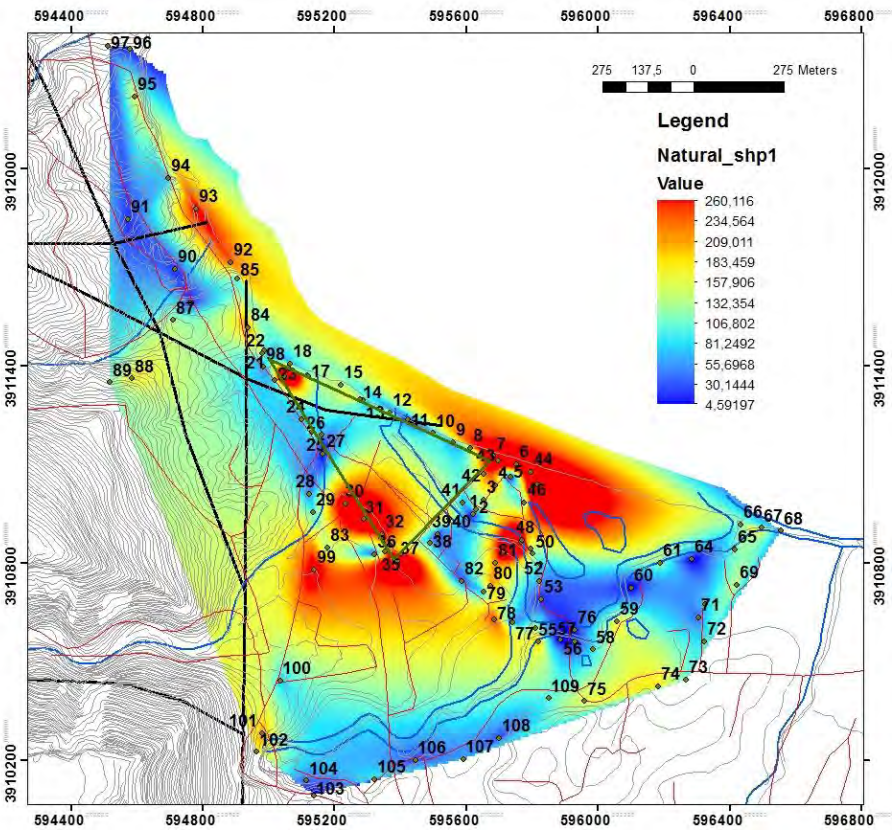

Figure 3 - Spatial distribution of the low field magnetic susceptibility (LFS) in 10-6 m3/Kg. Black line-fault, blue line-drainage net, Green line -power plant, Red line - traffic net, Black circle-sample location.

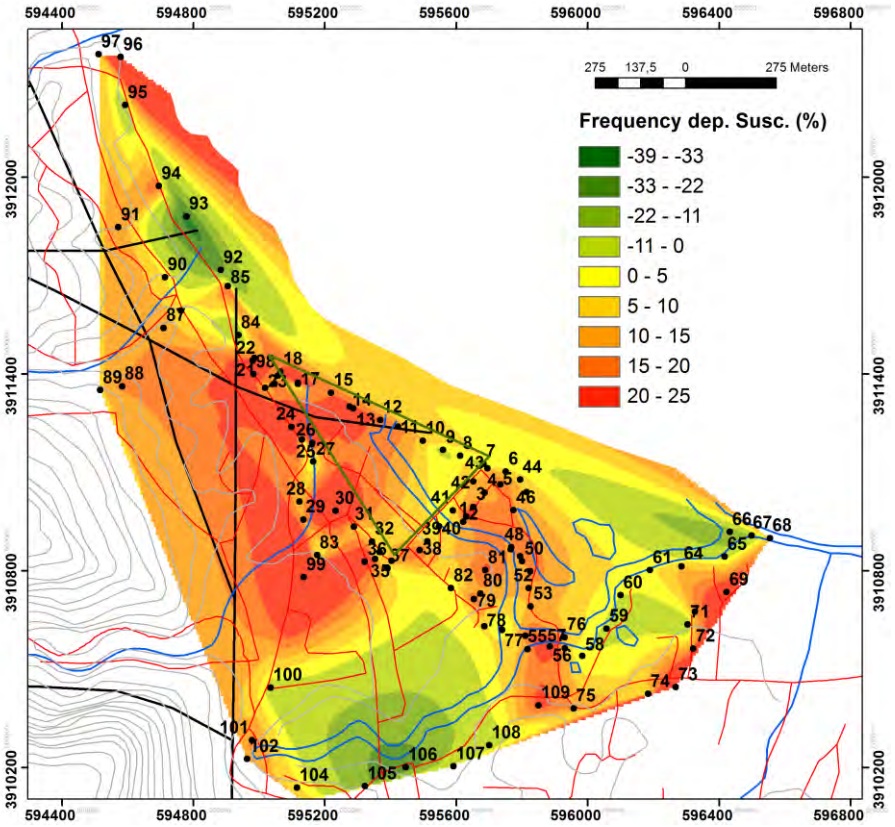

Figure 4 - Spatial distribution of the frequency dependent susceptibility χ%. Black line-fault, blue line-drainage net, Green line -power plant, Red line - traffic net, Black circle-sample location.

The digital elevation model was created by the digitization of the topographic map contours, while the cell size of the digital elevation model was 4 m. Gridding of the data was carried out using the inverse distance weighted method or the natural neighbor. Similar interpolation methods were used for creating surfaces of the spatial distribution of magnetic measurements.

4. Results and Discussion

In the present work, magnetic susceptibility and thermomagnetic measurements were conducted around a power plant with a dense traffic net, located in the W section of Heraklion city in Crete, in order to examine if the study area is an interesting place for further pollution research. The relief of the study area is steep in the western part and almost flat in the eastern part. From the geological point of view, the majority of the collected samples mainly correspond to Pliocene-Pleistocene and alluvial sediments. A few of them have been collected from the western most area covered by the Phyllites-Quartzites unit.

The distribution of the low frequency magnetic susceptibility (LFS) is presented in Figure 3. High susceptibility values, indicating possibly polluted sites, are generally detected around the power plant and across the coast. The majority of the samples selected across the drainage net show relative low χ. High frequency magnetic susceptibility (HFS) presents the same distribution as the low one. The distribution of the frequency dependent susceptibility (χ_{fd}%) shows low values (less than 5%) upstream of Almyros river and at the lower part of the high order branch. High values

(up to 25%) of the χ_{fd}% are indicated west of the power plant and at the stream of Almyros river in the vicinity of the power plant (Figure 4).

Additionally, thermomagnetic analysis indicate the presence of magnetite (Figure 5, samples 72, 102 and possibly 74) as the main magnetic mineral in the samples as well the contribution of hematite (Figure 5, sample 107). Samples, corresponding to the same geological formations and showing low magnetic susceptibility values, generally present paramagnetic behavior (Figure 6).

Presently, the morphology of the landward coastal region in the wide area of study shows alterations between small hills and small flat fields, up to the distance of 150-170 meters from the coastline. Around the study area, the relief of the coastal area is smoother including an extensive sandy beach, while southwards the relief is hilly. Concerning the geological structure of the study area, faults seem not to be related to the pollution transport. The main transmission factor in the study area seems to be the wind. The extensive nearly straight front of the coast, is unprotected from the north sector winds (mainly northern, north-eastern and partly north-western winds) (Pehlivanoglou and Papathanasoglou, 2004). High values of the magnetic susceptibility χ are orientated NW-SE that is the orientation of the study area. Northern and north-western winds usually blow in this area. The hilly relief southwards may prevent the pollution transmission to this direction. Low values of the magnetic susceptibility χ are mainly distributed in the southeastern part of the study area, even though the drainage network is also well developed in this part of the study area.

The results of our investigation generally confirm that magnetic susceptibility measurements provide the basis for an environmental study in polluted areas. Furthermore, the terrain attributes and the wind currents seem to play also an important role in the distribution of the possible pollution. In this term GIS techniques provide an excellent tool for studying the spatial distribution and relation between magnetic susceptibility, pollution mainly due to the presence of heavy metals and the natural settings of a study area.

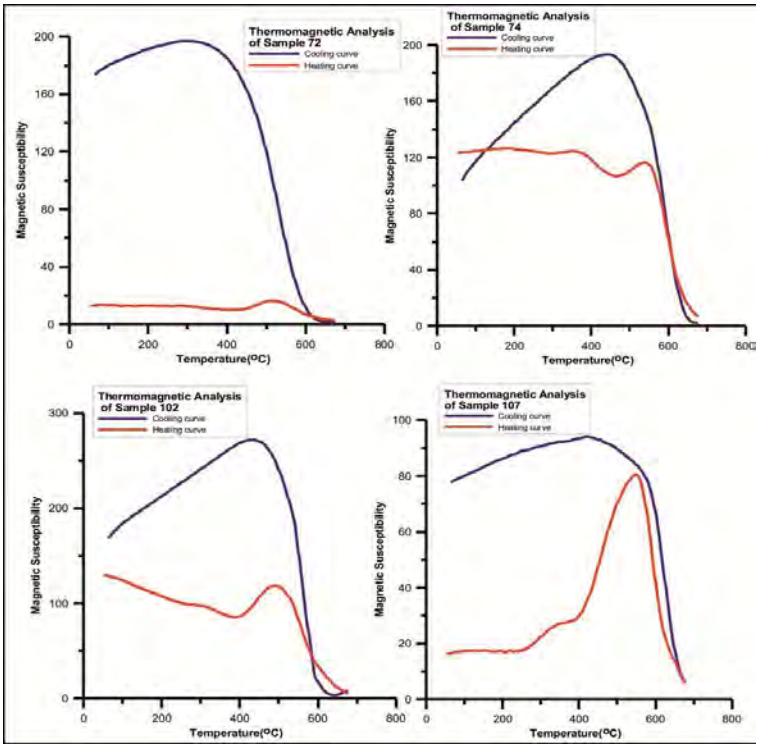

Figure 5 - Thermomagnetic curves of samples showing magnetic behavior.

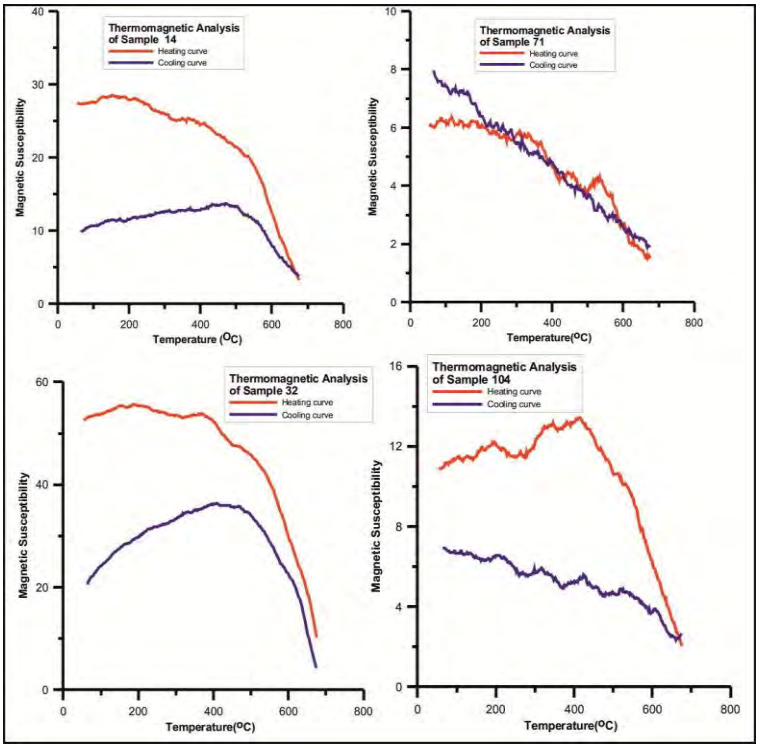

Figure 6- Thermomagnetic curves of samples showing paramagnetic behavior.

5. Conclusions

Strong contribution of the morphology and the wind currents to the pollution transport is considered for the study area. In concluding, the study area is of interest and further magnetic analyses (IRM, ARM, hysteresis loops) as well chemical analyses are proposed in order to examine the possibly polluted sites. In any case, the application of the magnetic methods should not be overestimated. Results obtained in one specific region may not be applicable to another region. Instead, detailed analysis should be carried out in order to establish basic correlations between various magnetic parameters, possible pollution (concentration of heavy metals) and natural settings. Only if such relationship is evident, magnetic measurements can be used in tracing and observing temporal and spatial variations of the pollution.

6. Acknowledgements

We would like to thank Professor Manutsoglou E. and Lecturer Aidona E. for their critical reviews, which help improved the manuscript.

7. References

Aleweld E. 2002. Seriengliederung und Deckenbau im nördlichen Taygetos-Gebirge (Südpelopon nes, Griechenland), *PhD thesis*, Universität Müchen, München, 150 pp.

Beckwith P.R. Ellis J.B. Revitt D.M. and Oldfield F. 1984. Identification of pollution sources in urban drainage systems using magnetic methods, in Balmer P., Malmqvist P.A., Sjoberg A., eds.: *Proc. of the 3rd International Conference on Urban Storm Drainage*, Chalmers University of Technology, Gotenborg, Sweden, 1313-1322.

Bityukova L. Scholger R. and Birke M. 1999. Magnetic susceptibility as indicator of environmental pollution of soils, *Tallin/ Phys. Chem. Earth*, 24, 829-835.

Boyko T. Scholger R. Stanjek H. MAGPROX Team 2004. Topsoil magnetic susceptibility mapping as a tool for pollution monitoring: repeatability of in situ measurements, *J. Applied Geophys*., 55, 249-259.

Fassoulas C. 1999. The structural evolution of Central Crete: insight into the tectonic evolution of the South Aegean (Greece), *J. Geodynam*., 27, 23-43.

Goluchowska B.J. 2001. Some factors affecting an increase in magnetic susceptibility of cement dusts, *J. Appl. Geophys*., 48, 103-112.

Hansen L.D. and Silberman D. and Fischer, G.L. 1981, Crystalline components of stack-collected, size-fractioned coal fly ash, *Environ. Sci. Technol*., 15, 1057-1062.

Jolivet L. Goffé, B. Monie P. Truffert-Luxey C. Patriat M. and Bonneau M. 1996. Miocene detachment on Crete and exhumation P-T-t paths of high-pressure metamorphic rocks, *Tectonics*, 15, 1129-1153.

Kilias A., Fassoulas C. and Mountrakis D. 1994. Tertiary extension of continental crust and uplift of Psiloritis metamorphic core complex in the central part of the Hellenic Arc (Crete,Greece), *Geol. Rundsch*., 83, 417-430.

Krahl J., Kauffmann G., Kozur H., Richter D., Forster O. and Heinritzi F. 1983. Neue Daten zur Bi ostratigraphie und zur tektonischen Lagerung der Phyllit-Gruppe und der Trypali-Gruppe a ufder Insel Kreta (Griechenland), *Geol. Rundsch*., 72, 1147-1166.

Manutsoglu E. 1990. Tektonik und metamorphose der Plattenkalk-Serie im Taygetos (Peloponnes, Griechenland), *Berliner geowiss.* Abh. (A), 129, 82 pp.

Papanikolaou D. and Vassilakis E. 2010. Thrust faults and extensional detachment faults in Cretan tectono-stratigraphy: implications for Middle Miocene extension, *Tectonophysics*, 488, 233-247.

Pehlivanoglou K.G. and Papathanasoglou, A. 2004. Geologic and Oceanographic data determining the "old foreshore zone", of the Heraklion coastal area, Crete Island, *Global Nest:the Int. J.*, 6(2), 157-166.

Petrovský E. and Ellwood B. B. 1999. Magnetic Monitoring of Air-, Land- and Water Pollution, in: B. A. Maher and R. Thompson (eds): *Quaternary Climates, Environments and Magnetism*, Cambridge University Press, Cambridge, U.K., 279–322.

Petrovsky E. Kapička A. Jordanova N. and Borůvka L. 2001. Magnetic properties of alluvial soils contaminated with lead zinc and cadmium, *J. Applied Geophys*., 48, 127-136.

Psonis K.T. 1981. About the presence of Permian (?) – Lower Triassic beds as a basement of the P lattenkalk series in the Taygetos Mt. Description of a continuous section, *Ann. Geol. Pays. Hell.*, 30, 578-587.

Sarris A., Kokinou E., Aidona E., Kallithrakas-Kontos N., Koulouridakis P., Kakoulaki G., Droulia K. and Damianovits O. 2009. Environmental study for pollution in the area of the Megalopoli power plant (Peloponnesus, Greece), *Environmental Geology*, 58, 8, 1769-1783, DOI:10.1007/s00254-008-1676-3.

Scholger R. 1998. Heavy metal pollution monitoring by magnetic susceptibility measurements applied to sediments of the river Mur (Styria, Austria), *Eur. J. Envirn. Eng. Geophys*., 3, 25-37.

Strzyszcz Z., Magiera T. and Heller F. 1996. The influence of industrial emissions on magnetic susceptibility of soils in Upper Silesia, *Studia Geophysica and Geodesia*, 40, 276 – 286.

Thiebault F. 1982. Evolution geodynamique des Hellenides externes en Peloponnese meridional (Grece), *Societe Geologique du Nord*, 6, 393 pp.

Vidakis M., Meulenkamp J.E., Koutsouveli A., Ioakim, Ch., Papazeti, E. and Skourtsi-Koronaiou, V. 1996, *Geological Map of Greece* in 1:50,000 scale – Heraklion Sheet. IGME, Athens.

Zachariasse W.J,. van Hinsbergen, D.J.J. and Fortuin A.R. 2011. Formation and fragmentation of a lateMiocene supradetachment basin in central Crete: implications for exhumationmechanisms of high-pressure rocks in the Aegean forearc, *Basin Res.*, 23, 678–701, doi: 10.1111/j.1365-2117.2011.00507.x.

Δελτίο της Ελληνικής Γεωλογικής Εταιρίας, τομ. XLVII , 2013
Πρακτικά 13ου Διεθνούς Συνεδρίου, Χανιά, Σεπτ. 2013

Bulletin of the Geological Society of Greece, vol. XLVII 2013
Proceedings of the 13th International Congress, Chania, Sept. 2013

ENVIRONMENTAL ASSESSMENT OF CONTAMINANTS IN A DOWNSTREAM AREA OF A LANDFILL

Koutsopoulou E.[1], Katsanou K.[1], Papoulis D.[1], Zagana E.[1] and Tsolis-Katagas P.[1]

[1] University of Patras, Faculty of Natural Sciences, Department of Geology, ekoutsop@upatras.gr, katsanou@upatras.gr, papoulis@upatras.gr, zagana@upatras.gr, n.tsoli-kataga@upatras.gr

Abstract

Waste disposal poses a major pollution threat to public health and the environment. Therefore, the evaluation of environmental risks associated with a landfill and the effect of landfill surface runoff was investigated. Soil samples were collected in the downstream area of the waste disposal site and their mineralogy was studied. An appraisal of the heavy metal contamination in the area was attempted. Top layers of sediments seem to interact with chemically modified surface runoff waters from the landfill. Heavy metals such as As and Pb were in significant concentrations in the sediments within a distance of 200 m from the site. Anions such as chloride, sulphate and phosphate adsorbed on clay minerals suggest the interaction of sediments with surface runoff from the waste disposal site. Inorganic parameters NH_4^+ and NO_2^- in surface water samples are above or slightly below the guidelines recommended by EE and WHO. The results indicated that environmental monitoring of the landfill is considered essential.

Key words: *waste disposal site, clay minerals, stream sediments, surface water run-off, heavy metals.*

Περίληψη

Η διάθεση των απορριμμάτων αποτελεί τη μεγαλύτερη περιβαλλοντική απειλή για τη δημόσια υγεία και το περιβάλλον. Για το σκοπό αυτό η εκτίμηση των περιβαλλοντικών προβλημάτων που σχετίζονται με έναν χώρο απόθεσης απορριμμάτων και η επίδραση των υδάτων επιφανειακής απορροής προερχομένων από το χώρο θεωρήθηκε απαραίτητη. Εδαφικά δείγματα συλλέχθηκαν στην περιοχή κατάντη του χώρου και μελετήθηκε η ορυκτολογική τους σύσταση. Παράλληλα, επιχειρήθηκε μια εκτίμηση της ρύπανσης στην περιοχή. Τα επιφανειακά ιζήματα φαίνεται να αλληλεπιδρούν με τα χημικώς τροποποιημένα ύδατα επιφανειακών απορροών που προέρχονται από το χώρο απόθεσης απορριμμάτων. Παρατηρήθηκαν υψηλές συγκεντρώσεις σε As και Pb σε απόσταση 200 m από το χώρο απόθεσης. Οι αναλύσεις αργιλικών ορυκτών έδειξαν την παρουσία χλωρίου, θείου και φωσφόρου γεγονός που ενισχύει την αλληλεπίδραση τους με ύδατα απορροών από το χώρο απόθεσης. Παράμετροι όπως NH_4^+ και NO_2^- στα ύδατα επιφανειακών απορροών βρίσκονται σε συγκεντρώσεις πάνω ή λίγο κάτω από τα όρια που προτείνονται από την ΕΕ και τον WHO γεγονός που υποδεικνύει ότι η περιβαλλοντική παρακολούθηση του χώρου απόθεσης θεωρείται απαραίτητη.

Λέξεις κλειδιά: *χώρος απόθεσης απορριμμάτων, αργιλικά ορυκτά, επιφανειακά ιζήματα, επιφανειακή απορροή, βαρέα μέταλλα.*

1. Introduction

Rational waste management is a key issue in environmental engineering in order to minimize migration of pollutants and their potential effects on human health and the environment. Although significant efforts towards reduction of waste - through physical, chemical or biological methods - have been made in recent years, the disposal of waste in landfill sites is likely to continue (Department of the Environment, 1995, Hermanns Stengele and Plötze, 2000, EPA, 2010).

A number of requirements for landfills designed to ensure environmental protection have been established by the European legislation (e.g., 1999/31/EC, 1999, 2003/33/EC, 2002, 2008/1/EC, 2008 and 2008/98/EC, 2008). Landfill sites should comply with these standards and consist of a multi-barrier system comprising a geomembrane, a clay liner and a natural geological barrier are essential requirements to conserve the quality of the environment. In the case of pollutant escape the natural geological barrier is the final barrier to the migration of pollutants. Clay minerals are widely used as geological barriers in sanitary landfills because of their effective characteristics (Arch, 1998, Dubbin, 2000, Kugler et al., 2002, Du and Hayashi, 2006). These characteristics include their long-term compatibility with chemicals and the high sorption capacity for pollutants (Hermanns Stengele and Plötze, 2000, Volzone, 2004, Li et al., 2007). These properties depend on the mineralogy of the clay material used in the waste disposal site (Sezer et al., 2003). Therefore, the selection of the location for the landfill is one of the key parameters to ensure the retention of pollutants.

In the case of pollutant escape from the landfill site, enrichment of metals in stream sediments has been reported (Mantei and Coonrod 1989, Mantei and Foster 1991, Gonçalves et al., 2004). Surface runoff waters from the landfill site seem to affect the concentrations of metals in stream sediments. The potential pollution caused by runoff waters includes the release of ammonia, nitrates and nitrites, chlorinated and non-chlorinated compounds and heavy metal ions into the environment, all of which are toxic to living organisms (Baccini et al., 1987, Kjeldsen et al., 1998, Christensen et al., 2001).

The aim of this study is to evaluate the behaviour of the clay material down gradient of an operating waste disposal facility and its effectiveness for pollution control. The environmental impact of the landfill in the downstream area was evaluated. Stream sediments were examined for possible enrichment in heavy metals since they interact with chemically modified runoff waters from the landfill. The consequences of the disposal of waste and assessment of pollution on surface water downstream of the area were also investigated.

2. Materials and Methods

2.1. Site Characteristics and Sampling

The study area covers the landfill site and the surrounding area. This operating waste disposal facility is located at approximately 37º44′37″N and 20º55′15″E, West Greece (Fig.1). Two Pleiocene fine sediment sequences comprise the geology of the landfill area, the Upper and the Lower Horizon. The Upper Horizon consists of light grey to white sandstones with clay and marly intercalations and the Lower Horizon of blue marls and marly sandstones which do not host an aquifer (Monopolis and Bruneton, 1982, Skagias, 1986, Kamberis et al., 1998). The operations of the landfill commenced in 1992. The landfill area is about 90 acres and the mean waste load that receives is 22,484 ton/year (available data from 1997 to 2009). The landfill was constructed with a composite lining system according to the multi-barrier system and EU regulations (Hermanns Stengele and Plötze, 2000) and consists of a compacted clay liner, an overlying geomembrane (HDPE) and a geotextile. Samples were collected around the landfill and from top layers of sediments from a stream system, in the vicinity of the waste disposal site. Surface runoff water samples were collected downstream of the landfill and analysed to determine chemical parameters usually considered as indicators of pollution from solid waste disposal.

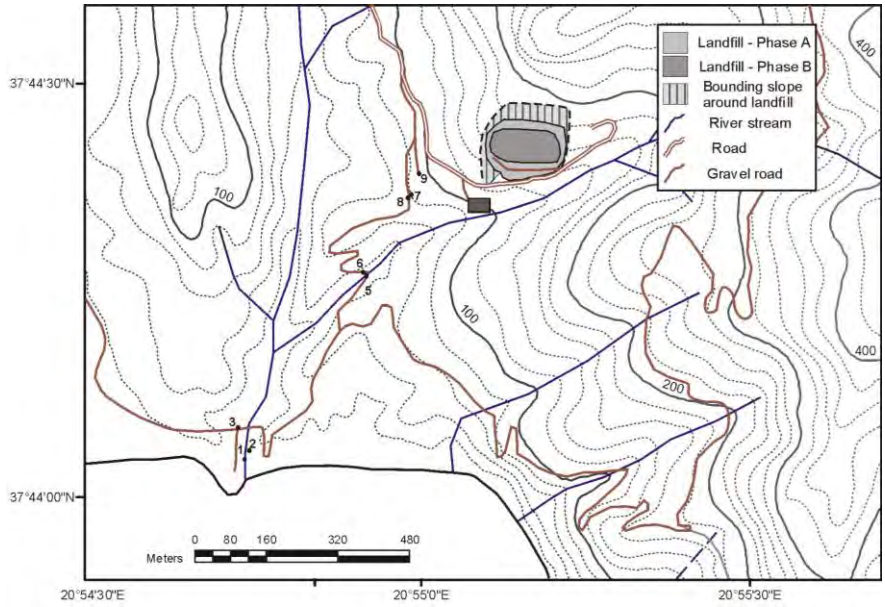

Figure 1 – Landfill site and sampling positions.

2.2. Experimental Methods

The bulk mineralogy of the samples was determined with X-Ray Diffraction, using a Bruker D8 Advance diffractometer, Ni-filtered CuKα radiation. The random powder mounts of bulk samples were scanned from 2 to 70º 2θ with a step increment of 0.015º 2θ and a count time of 0.3s per step. The <2 μm oriented specimens were prepared by sedimentation of the clay suspension onto glass slides and clay minerals were identified from three XRD patterns, after air-drying at 25 ºC, with ethylene glycol treatment, and after heating at 490 ºC for 2 hours.

The chemical composition of the minerals was determined using a Scanning Electron Microscope SEM JEOL 6300 equipped with an Energy Dispersive Spectrometer (EDS) with natural and synthetic standards and 20kV accelerating voltage, 10nA beam current. Microanalyses were performed on epoxy resin-impregnated polished and gold or carbon coated thin sections, and carbon coated sample powders mounted directly on the sample holder.

Chemical analyses were carried out in Activation Laboratories (Canada) by Instrumental Neutron Activation Analysis (INAA) and Inductively Coupled Plasma (ICP) using a 4-acid (HF, HClO4, HNO3 and HCl) digestion technique. Bulk sample chemical analyses for major and trace elements were performed in all samples, using a Thermo Jarrell-Ash ENVIRO II ICP for INAA and a Perkin Elmer Optima 3000 ICP.

Chemical parameters of surface runoff water samples were determined by Flame Atomic Absorption Spectrometry (AAS) AVANTA P, GBC, by titration and by a DR 4000 HACH Spectrophotometer.

3. Results

3.1. Mineralogy

The X-ray diffraction patterns of random powder mounts are characterised by the presence of quartz, calcite, plagioclase and clay minerals in all samples. In some of the samples K-feldspar and dolomite are also present. The clay fraction (<2μm) is dominated by chlorite, smectite, vermiculite, illite, serpentine and mixed-layer chlorite-smectite. Chlorite is characterised by the presence of

peaks at 14.2 Å, 7.1 Å, 4.74 Å and 3.55 Å which remain unaffected after ethylene glycol treatment and heating. Smectite is identified by the reflection at about 16.5 Å after ethylene glycol treatment which collapses to 10 Å after heating. Vermiculite is distinguished by the peak at 14.4 Å which is not affected by ethylene glycol treatment and collapses to10 Å after heating. Illite is identified by the peaks at10 Å, 5 Å and 3.3 which are not affected by ethylene glycol solvation and heating (Moore and Reynolds, 1989). The characteristic peaks of serpentine are observed at 7.30 Å, 3.65 Å which remain unaffected after heating treatment (Brindley and Brown, 1980). Mixed-layer chlorite-smectite is identified by the peak at 15.5 Å after treatment with ethylene glycol and at about 12 Å after heating (Thorez, 1975). Typical X-Ray Diffraction patterns of the <2 μm fraction of samples collected around the landfill and from stream sediments are shown in Figure 2.

3.2. Geochemistry

Bulk sample chemical analyses for major elements were performed in the samples and are shown in Table 1. Stream sediments (samples 1, 5 and 6, Fig.1) have the highest content in Al_2O_3, reflecting the abundance in clay minerals. Trace elements analyses (Table 2) showed that the content of As, Cu, Zn and Pb is higher in the stream sediments compared to the uncontaminated samples. Top layers of stream sediments are known to interact with runoff waters from the landfill. V and Rb are correlated with clay minerals whereas the high Ni and Cr contents reflect the presence of ultramafic components in the host rock.

Minerals present in the samples and the stream sediments were also examined by SEM-EDS for trace elements associated with pollution in waste disposal sites. SEM-EDS analyses showed traces of Cu and/or Zn in clay minerals. Anions such as chloride, sulphate and phosphate were also detected in clay minerals analyses.

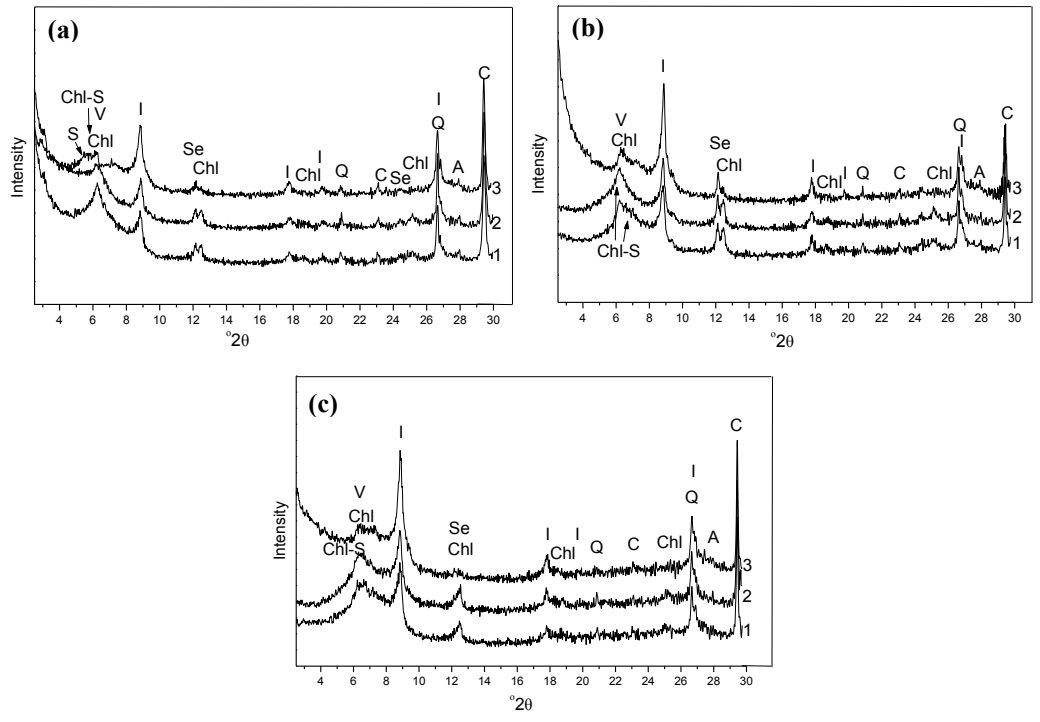

Figure 2 – X-Ray diffraction patterns of the <2 μm fraction. 1: air-dried sample, 2: glycolated, 3: heated. a) material collected downgradient of the landfill (sample 9), b) stream sediment (sample 1), c) stream sediment (sample 5). S: smectite, Chl-S: chlorite-smectite, I: illite, Chl: chlorite, V: vermiculite, Se: serpentine, Q: quartz, C: calcite, A: albite.

Table 1 - Bulk sample chemical analyses for major elements (wt %).

sample	SiO_2	Al_2O_3	Fe_2O_3	MnO	MgO	CaO	Na_2O	K_2O	TiO_2	P_2O_5	LOI
1	52.68	8.20	3.65	0.05	3.62	13.16	1.39	1.56	0.48	0.09	14.98
2	59.30	4.01	1.66	0.05	3.74	13.09	1.36	0.98	0.30	0.06	14.82
3	57.21	6.25	2.75	0.05	3.52	13.41	1.25	1.26	0.41	0.07	14.20
5	53.39	8.05	3.42	0.06	2.15	14.36	1.22	1.56	0.46	0.08	15.71
6	46.72	8.95	4.60	0.07	4.37	13.93	1.09	1.76	0.51	0.10	17.19
7	50.43	4.03	1.30	0.04	1.40	24.54	1.05	0.81	0.36	0.07	15.30
8	55.60	4.76	1.51	0.04	1.67	14.48	1.19	1.12	0.29	0.04	18.80
9	53.65	6.60	2.61	0.05	2.35	15.50	1.33	1.27	0.43	0.08	15.56

Table 2 - Bulk sample chemical analyses for trace elements (ppm).

sample	As	Cu	Zn	Pb	Ni	Cr	V	Rb
1	4.6	16	48	11	173	386	67	57
2	5.0	4	28	<5	71	2350	25	26
3	4.9	11	35	6	157	847	48	43
5	6.6	18	44	12	133	455	67	57
6	9.4	20	57	11	192	437	87	74
7	3.1	5	18	<5	56	922	24	22
8	5.2	4	18	<5	86	773	30	30
9	6.3	11	34	8	120	532	50	39

3.3. Surface Water Quality

Surface runoff water samples were collected down gradient of the disposal site and analysed to determine chemical parameters usually considered as indicators of pollution from solid waste disposal. The mean chemical composition of surface runoff water samples collected after a rainy period was compared with the mean chemical composition of rainwater from the area and is shown in Figure 3. Most cations and anions analysed were quite low and range in concentrations below the recommended values and guidelines certified by EE (1998/83/EC, 1998). Ammonium concentration was above the guidelines recommended (0.5 mg/L) and nitrite was just below the guideline value of 0.1 mg/L.

4. Discussion

The greatest environmental concern in landfill sites is the generation of leachate from infiltrating surface water leading to the contamination of surface or groundwater supplies (Hermanns Stengele and Plötze, 2000). The mineralogy of the clay material used in a waste disposal site may influence the mobility of contaminants; therefore the determination of the types of clay minerals that are present in the landfill is of great importance for the assessment of their efficiency in the retention of pollutants.

Clay minerals and especially chlorite, smectite, illite and mixed layer chlorite-smectite identified by XRD, are abundant in the area the landfill was constructed and in the stream sediments. The specific clay minerals and especially smectite are widely used as natural clay barriers in waste disposal sites (Sezer et al., 2003). This is due to the sorption capacity of clay minerals for different metals and the anion and cation adsorption behaviour under various chemical conditions (Czurda and Wagner, 1991, Venema et al., 1996, Churchman et al., 2006, Chalermyanont et al., 2009, Koutsopoulou et al., 2010).

Geochemical analyses showed that the Al_2O_3 content is higher in the stream sediments compared to the rest of the samples. MgO and Fe_2O_3 content is related to the presence of chlorite and vermiculite. SEM-EDS analyses of trioctahedral chlorites in the samples showed Mg^{2+} and Fe^{2+} as the commonest divalent cations. The high MgO content in samples 2 and 3 is due to the presence of dolomite as revealed by the mineralogical analyses. Trace elements As, Cu, Zn and Pb showed elevated concentrations in the stream sediments. Enrichment of metals in stream sediments caused by various contamination sources have been reported (Ramamoorthy and Rust, 1978, Rule, 1986). Studies have shown elevated concentrations of Cu, Pb, Zn, Cd, Ag, and Ba in stream sediments affected by landfills and water treatment facilities (Mantei and Coonrod 1989, Mantei and Foster 1991). Stream sediments interact with runoff waters from landfills and show enrichment in metal concentrations. Clay minerals adsorption of heavy metals is strongly affected by the pH and the presence of anions in the solution since metal cations are known to form complexes with inorganic ligands (McLean and Bledsoe, 1992, Undabeytia et al., 2002, Churchman et al., 2006). The interaction between the metal ions and the complexing ligands could result in the formation of a complex that is either weakly adsorbed to the soil surface or more strongly adsorbed relative to the free metal ion (Benjamin and Leckie, 1982). The presence of Cl^-, SO_4^{2-} and PO_4^{3-} adsorbed on clay minerals in the stream sediments as revealed by SEM-EDS seems to have increased the negative charge of the surface and enhanced the adsorption of metals such as Cu and Zn from surface runoff waters from the waste disposal site.

Stream sediments also showed elevated lead and arsenic concentrations. Generally, Pb is accumulated near the soil surface. Sipos et al. (2005) suggested that soil organic matter plays a decisive role in the Pb adsorption, but the fixation by clay minerals is much stronger. Arsenite As(III) and arsenate As(V), are the main species in soils and sediments with the reduced state, arsenite being more toxic, soluble and mobile than arsenate (Bhattacharya et al., 2007). However, As mobility is usually limited due to the strong sorption by clays and Fe hydroxides (Kabata-Pendias, 2011). In general, the adsorption of arsenic in the form of arsenate is stronger than in the form of arsenite while Mn oxides are effective oxidants for the transformation of As(III) into As(V) (Dechamps et al., 2003).

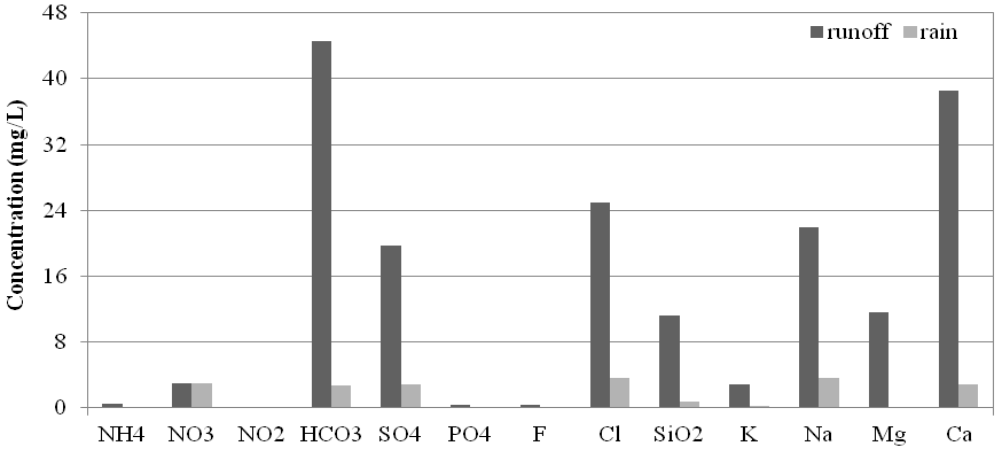

Figure 3 – Mean chemical composition of surface runoff water versus rainwater in mg/L.

The chemical composition of the surface runoff water samples showed concentrations below the maximum contaminant level (MCL) values given by European Council Directive (1998/83/EC, 1998) for the majority of the parameters. Rainwater is relatively free from impurities. However, landfill activities have the potential to deteriorate the quality of rainwater. The significance of the potential impacts will vary according to the phase of operation and the scale of the operations of the waste disposal facility. The comparison between surface runoff water and rainwater (Fig. 3) shows that the former is becoming enriched in most analysed parameters. Although the concentrations of chloride in surface runoff water are quite low, its presence in clay minerals analyses together with sulphates and phosphates could be attributed to contamination from the landfill. Chloride is usually considered as a tracer around landfill sites (Fatta et al., 1999). The ammonium concentration of the surface runoff water display elevated values that exceed the EE drinking water guidelines (1998/83/EC, 1998). Natural levels in groundwater and surface water are usually below 0.2 mg/L while anaerobic groundwaters may contain up to 3 mg/L (WHO, 2008, EPA, 2010). Ammonium in water is usually an indicator of possible bacterial, sewage or animal waste pollution and was attributed to contamination from the waste disposal site. Ammonium can also result in nitrite formation. The mean nitrite concentration (0.04 mg/L) was below the guideline value recommended (0.1 mg/L). However, its presence in the runoff water after an extended period of rainfall could only be of great concern for the operation conditions in the landfill.

5. Conclusions

The mineralogy of the naturally occurring clay material down gradient the landfill site and in the stream sediments is considered desirable in landfill sites.

Steam sediments are more abundant in clay minerals controlling the migration of pollutants. Trace elements analyses showed enrichment of As, Cu, Zn and Pb in the stream sediments compared to the uncontaminated samples. Since stream sediments are in contact with runoff waters from the landfill this could be an indication of contamination from the landfill. The presence of chloride, sulphate and phosphate adsorbed on clay minerals further contributes to the impact of clay mineralogy for pollution control.

The presence of ammonium and nitrite ions in surface runoff water is considered as human induced contamination from the landfill.

6. Acknowledgments

This research was funded by the University of Patras through the ‘K. Karatheodoris’ basic research funding scheme.

7. References

1998/83/EC, O.J.L. 1998. *Council Directive of 3 November 1998 on the quality of water intended for human consumption*, European Union legislation.

1999/31/EC, O.J.L. 1999. *Council Directive of 26 April 1999 on the landfill of waste*, European Union legislation.

2003/33/EC, O.J.L. 2002. *Council Decision of 19 December 2002 establishing criteria and procedures for the acceptance of waste at landfills pursuant to Article 16 of and Annex II to Directive 1999/31/EC on the landfill of waste*, European Union legislation.

2008/1/EC, O.J.L. 2008. *Council Directive of 15 January 2008 concerning integrated pollution prevention and control*, European Union legislation.

2008/98/EC, O.J.L. 2008. *Council Directive of 19 November 2008 on waste and repealing certain directives*, European Union legislation.

Arch J. 1998. Clay Barriers in Landfills. Environmental Interactions of Clays. *Clays and the Environment*, in: Parker, A., Rae, J.E., (Eds.), Springer-Verlag, Berlin, 207-242 pp.

Baccini P., Henseler G., Figi R., and Belevi H. 1987, Water and element balances of municipal solid-waste landfills. *Waste management and Research*, 5, 483-499.

Benjamin M.M. and J.O. and Leckie. 1982. Effects of complexation by Cl, SO4, and S2O3 on adsorption behavior of Cd on oxide surfaces. *Environ. Sci. Technol*. 16, 162-170.

Bhattacharya P., Mukherjee, A.B., Bundschuh, J., Zevenhoven, R. and Loeppert, R.H. 2007. *Arsenic in Soils and Groundwater Environment*. Elsevier, Amsterdam. 640p.

Brindley G.W. and Brown G. 1980, *Crystal structures of clay minerals and their X- ray identification*. Mineralogical soc monograph No 5.

Chalermyanon T., Arrykul S. and Charoenthaisong N. 2009. Potential use of lateritic and marine clay soils as landfill liners to retain heavy metals, *Waste Management*, 29, 117-127.

Christensen T.H., Kjeldsen P., Bjerg P.L. Jensen, D.L. Christensen J.B., Baun A., Albrechtsen H.J. and Heron C. 2001. Biogeochemistry of landfill leachate plumes, *Applied Geochemistry*, 16, 659–718.

Churchman G.J., Gates W.P., Theng B.K.G., and Yuan G. 2006. Clays and Clay Minerals for Pollution Control, in: Developments in Clay Science Vol.1., *Handbook of Clay Science*, Bergaya F., Theng B.K.G. and Lagaly G. (Eds). 625-676pp.

Czurda K.A. and Wagner J.F. 1991. Cation-transport and retardation prossesses in view of the toxic-waste deposition problem in clay rocks and clay liner encapsulation, *Eng. Geol*., 30, 103-113.

Deschamps E., Ciminelli V.S.T., Weidler P. and Ramos A.Y. 2003. Arsenic sorption onto soils enriched in Mn and Fe minerals, *Clays and Clay Minerals*, 51, 197–204.

Department of the Environment, 1995. *Making waste work: a strategy for suitable waste management in England and Wales*, HMSO, London.

Du Y.J. and Hayashi S. 2006. A study on sorption properties of Cd^{+2} on Ariake clay for evaluating its potential use as a landfill barrier material, *Applied Clay Science*, 32, 14-24.

Dubbin W.E. 2000. Intercalation of organic and inorganic contaminants by expanding layer silicates, in: J.D. Cotter-Howells L.S., Campbell E., Valsami-Jones and M. Batchelder (eds) *Environmental Mineralogy: Microbial Interactions, Anthropogenic Influences, Contaminated Land and Waste Management*, Mineralogical Society Series, 9. Mineralogical Society, London. 227-244 pp.

EPA 2010. EPA Victoria. Siting, *Design, Operation and Rehabilitation of Landfills*. Publication 788.1, availiable at: http://www.epa.vic.gov.au/

Fatta D., Papadopoulos A. and Loizidou M. 1999. A study on the landfill leachate and its impact on the groundwater quality of the greater area, *Environmental Geochemistry and Health*, 21, 175-190.

Hermanns Stengele R. and Plötze M. 2000. Suitability of minerals for controlled landfill and containment, *Environmental Mineralogy*. EMU Notes in mineralogy, Vol. 2, Chapter 8, 291-331.

Gonçalves M.A., Nogueira J.M.F, Figueiras J., Putnis C.V. and Almeida C. 2004. Base-metals and organic content in stream sediments in the vicinity of a landfill, *Applied Geochemistry*, 19, 137-151.

Kabata-Pendias A. 2011. *Trace Elements in Soils and Plants*, 4th Edition. CRC Press. Taylor and Francis Group, LLC. 505p.

Kamberis E., Ioakim, Ch., Tsaila-Monopolis St., Marnelis F. and Sotiropoulos S. 1998. Geological and palaeogeographic evolution of western Greece, during the Neogene-Quaternary period in the geodynamic setting of the Hellenic Arc, *Roman J. Stratigraph*. 78, 63-74.

Kjeldsen P., Bjerg P.L., Rugge K., Christensen T.H. and Pedersen J.K. 1998. Characterization of an old municipal landfill (Grindsted, Denmark) as a groundwater pollution source. Landfill hydrology and leachate migration, *Waste Management and Research*, 16, 14–22.

Koutsopoulou E., Papoulis D., Tsolis-Katagas P. and Kornaros M. 2010. Clay minerals used in sanitary landfills for the retention of organic and inorganic pollutants, *Applied Clay Science*, 49, 372-382.

Kugler H., Ottner F., Froeschl H., Adamcova, R., and Schwaighofer B. 2002. Retention of inorganic pollutants in clayey base sealings of municipal landfills. *Applied Clay Science*, 21, 45-58.

Li L.Y., Ohtsubo M., Higashi T., Yamaoka S., Morishita T. 2007. Leachability of municipal solid waste ashes in simulated landfill conditions, *Waste Management*, 27, 932-945.

Mantei E.J. and Coonrod D.D. 1989. Heavy metal content in the stream sediments adjacent to a sanitary landfill, *Environmental Geology and Water Science*, 13(1), 51-58.

Mantei E.J. and Foster M.V. 1991. Heavy Metals in Stream Sediments: Effects of Human Activities, *Environmental Geology and Water Science*, 18, 2, 95-104

McLean J.E. and Bledsoe, B.E. 1992. Behavior of Metals in Soils, in: Boulding, J.R. (Ed.), EPA *Environmental Assessment Sourcebook*, pp. 19-56.

Monopolis D. and Bruneton A. 1982. Ionian Sea (Western Greece): its structural outline deduced from drilling and geophysical data, *Tectonophysics*, 83, 227-242.

Moore D.M. and Reynolds R.C.Jr. 1989. *X-Ray Diffraction and the Identification and Analysis of Clay Minerals*. Oxford University Press. New York. 198-269 pp.

Ramamoorthy S. and Rust B.R. 1978. Heavy metal exchange processes in sediment water systems, *Environmental Geology*, 2(3), 165-172

Rule J. 1986. Assessment of trace element geochemistry of Hampton Roads Harbor and Lower Chesapeake Bay area sediments, *Environmental Geology,* 8(4):209-219

Sezer G.A., Türkmenoğlu A.G. and Göktürk E.H. 2003. Mineralogical and sorption characteristics of Ankara Clay as a landfill liner, *Applied Geochemistry*, 18, 711-717.

Sipos P., Nemeth T. and Mohai I. 2005. Distribution and possible immobilization of lead in a forest soil (Luvisol) profile. *Environ. Geochem. Health*, 27, 1–10.

Skagias S. 1986. *Hydrogeological Research of Zakynthos Island*. IGME, (Institute of Geology and Mineral Exploration), Athens.

Thorez J. 1975. *Phyllosilicates and clay minerals: A laboratory handbook for their X-Ray diffraction analysis*. Ed. G. Lelotte. B 4820 Dison, Belgique.

Undabeytia T., Nir S., Rytwo G., Serban C., Morillo E. and Maqueda C. 2002. Modeling Adsorption-Desorption Processes of Cu on Edge and Palnar Sites of montmorillonite, *Environ. Sci. Technol*. 36, 2677-2683.

Venema P., Hiemstra T., and van Riemsdijk W.H. 1996. Comparison of different site binding models for cation sorption: Description of pH dependency, salt dependency, and cation-proton exchange, *J. Colloid Interface Sci*., 181, 219-228.

Volzone C. 2004. Removal of Metals by Natural and Modified Clays, in: *Clay Surfaces: Fundamentals and Applications. Interface Science and Technology*. Vol. 1., F. Wypych and K.G. Satyanarayana (editors). Elsevier Academic Press. 291-320.

WHO, World Health Organization, 2008. *Guidelines for drinking-water quality*, 3rd ed. Vol. 1. incorporating 1st and 2nd addenda, Recommendations. Geneva.

Δελτίο της Ελληνικής Γεωλογικής Εταιρίας, τομ. XLVII , 2013
Πρακτικά 13ου Διεθνούς Συνεδρίου, Χανιά, Σεπτ. 2013

Bulletin of the Geological Society of Greece, vol. XLVII 2013
Proceedings of the 13th International Congress, Chania, Sept. 2013

DRASTIC METHOD TO MAP GROUNDWATER VULNERABILITY TO POLLUTION USING NITRATE MEASUREMENTS IN AGRICULTURAL AREAS

Samara T.[1] and Yoxas G.[2]

[1] *National and Kapodistrian University of Athens, Faculty of Geology and Geoenvironment, Department of Dynamic Tectonic & Applied Geology,tsamara@geol.uoa.gr*

[2]*AquaScience Consulting, Geological and Environmental Office Services, yoxas@aquascience.gr*

Abstract

DRASTIC model has been used to map groundwater vulnerability to pollution in many areas. Since this method is used in different places without any changes, it cannot consider the effects of pollution type and characteristics. Therefore, the method needs to be calibrated and corrected for that aquifer and specific land use. In this research, by correcting the rates of DRASTIC parameters, one can assess the vulnerability potential to pollution more accurately. The new rates were computed using the relationships between DRASTIC INDEX (DI) corresponding to land use and to nitrate concentration in groundwater. The proposed methodology was applied in deltaic region of alluvial aquifer of Volinaios catchment located in the northwestern part of Peloponnesus. In order to determine the quality of the ground waters, either for watering or irrigating purposes, in the study area, a sampling was made. Correlation was used to find the relationship between the index and measured pollution in each point and therefore, to modify the rates. The results showed that the modified DRASTIC is better than the original method for nonpoint source pollution in agricultural areas.

Περίληψη

Η μέθοδος DRASTIC χρησιμοποιείται για την εκτίμηση και τη χαρτογράφηση της εσωτερικής τρωτότητας των υπόγειων νερών από εξωτερικά ρυπαντικά φορτία. Δεδομένου όμως, ότι η μέθοδος εφαρμόζεται σε διαφορετικές περιοχές, χωρίς καμία τροποποίηση, την καθιστά αδύνατη να λάβει υπόψη της τις επιδράσεις του ρυπαντή, ανάλογα με το είδος και τα χαρακτηριστικά του. Συνεπώς, στη μέθοδο DRASTIC θα πρέπει να συνυπολογίζονται τόσο οι ιδιαίτεροι παράμετροι του φυσικού συστήματος του υδροφορέα, όσο και οι ιδιαίτερες συνθήκες κάθε περιοχές (χρήσεις γης). Στα πλαίσια της παρούσας εργασίας, τροποποιώντας τις παραμέτρους της τυπικής μεθόδου DRASTIC και τους αντίστοιχους συντελεστές βαρύτητας, εκτιμήθηκε ο δείκτης τρωτότητας με μεγαλύτερη ακρίβεια. Την περιοχή εφαρμογής της προτεινόμενης μεθοδολογίας αποτελεί η Δελταϊκή περιοχή του προσχωματικού υδροφόρου ορίζοντα του ποταμού Βολιναίου, στην ΒΔ/κή Πελοπόννησο.

1. Introduction

The concept of vulnerability is associated with the capacity with which a contaminant that has penetrated the soil surface reaches the aquifer, under specific land use management practices in an area of interest, while the characteristics of the contaminant and the aquifer sensitivity are set.

Vulnerability maps provide a more or less subjective view of the ability of the subsoil, to protect groundwater especially in terms of quality. The basic purpose of these maps is to divide an area into more classes, each of which will represent a different dynamic for a specific purpose and use. (Vrba&Zaporozec, 1994). The main methods of mapping and assessing intrinsic vulnerability in porous media are the following: DRASTIC (Aller et al., 1987), AVI (Van Stempvoort et al., 1993), GOD (Foster, 1987) and others. In this paper the DRASTIC method was applied, which is an index method based on hydrogeological parameters. A modification to the original method was attempted in order to include anthropogenic activity, which is extensive in the area, by adding an extra parameter that of land use. In order to assess the results, a correlation between these and nitrate ion concentration was made.

2. Methodology

The main purpose of this paper is to describe, analyze, and interpret, the geological, hydrogeological and hydrochemical conditions of the study area, in order to identify sites according to contaminant sensitivity. For this stage, the original DRASTIC method was used.

The title of this method comes from the abbreviation of the parameters taken into account: D (Depth to water), R (Recharge rate), A (Aquifer media), S (Soil cover), T (Topography), I (Impact of vadose zone) and C (Conductivity of the aquifer). The DRASTIC index (DI) is calculated by the following equation:

$$\mathrm{DI} = \sum_{i=1}^{7} r_i \cdot w_i \qquad (1)$$

where r, is the value of the parameter, and w is the value of the weighted factor. It should be noted that the grater the DI value, the greater the contaminant sensitivity of the area.

Table 1 presents the weighted factor of each parameter. It is obvious that depth to water and impact of vadose zone, are the parameters with the greater weighted factor values.

Table 1 –Assigned Weights for Typical DRASTIC parameters.

Parameter	Weight
Depth to water	5
Recharge	4
Aquifer media	3
Soil cover	2
Topography	1
Impact of vadose zone	5
Conductivity of the aquifer	3

Considering the fact that the causes of groundwater contamination are mainly anthropogenic, in addition to the fact that in the original DRASTIC method anthropogenic activity is not taken into account, the modified DRASTIC method was proposed. This method uses an additional parameter that of land uses, to include anthropogenic impact on an area.

3. Description of the Study Area

The study area includes the deltaic region of the alluvial aquifer of the river Volinaios. It is located in the northwestern area of Peloponnese, in the Achaea regional unit, approximately 15 km east of the city of Patra and consists of an approximately 11 km^2 area. The average annual temperature reaches up to 19,1^{o}C and the average annual rainfall height, up to 972 mm. According to the approximate hydraulic balance equation estimated in the study area, the actual evapotranspiration is 60.8 % of the average annual rainfall height (591 mm), the recharge area is 19.2%, and infiltration is 20% (Yoxas, 2004).

In terms of geology, the study area consists of post-Alpine sediments, which are divided into two main units:

- Pliocene-Pleistocene sediments, that consist of a conglomerate formation, a marl formation and a sand clay formation and
- Holocene sediments, that consists of alluvial deposits and scree cones.

These units are related to the folded Alpine bedrock via an angled unconformity that consists of Cretaceous pelagic and platy limestones of the Pindos Unit (Koukouvelas and Papadopoulos, 1984).

In the study area occur permeable and semi-permeable formations, which behavior depends on grain size, thickness and stratigraphic position. Therefore, alluvial and debris cone formations are characterized as permeable, while marl and sandy clay and conglomerate formations are characterized as semi-permeable. Within the alluvial formation is developed the main aquifer of the study area.

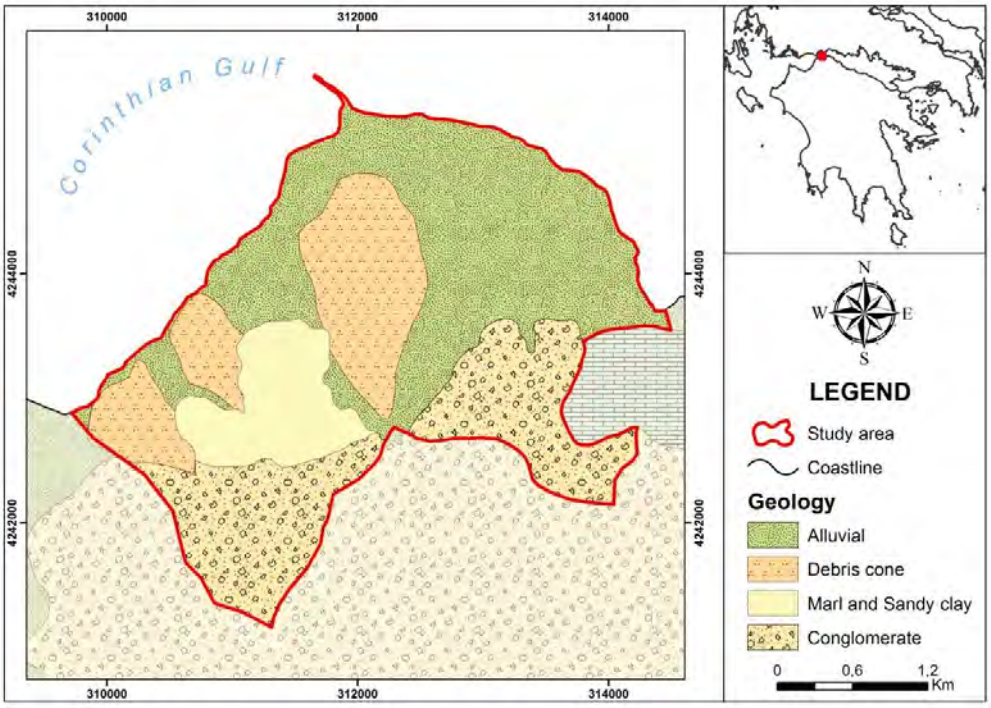

Figure 1 – Geological map of the study area (Tsoflias, 1971, modified).

According to the piezometric map (Figure 2), the hydraulic gradient ranges from 5 ‰ to 8 ‰, the general flow direction is NW and the hydraulic head ranges between +14 m to 0 m in coastal areas (Yoxas, 2004).

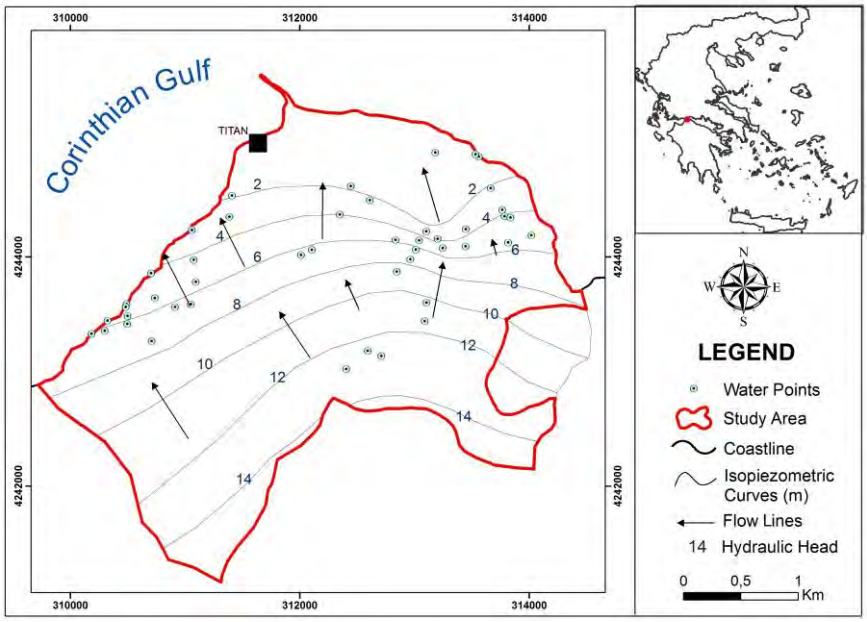

Figure 2 – Piezometric map of the study area.

4. Hydrochemical Conditions

Observation and assessment of the physical-chemical parameters of the water in the study area is imperative in order to project an image of the current quality conditions, and to verify the results of the vulnerability assessment methods (Table 2).

Table 2 – Summary statistics of physicochemical parameters of the alluvial aquifer.

Parameter	Units	Dry Period			Wet Period		
		Min	Max	Avg	Min	Max	Avg
pH	-	6.89	8.1	7.372	6.72	7.95	7.318
Eh	(mV)	22	269	179.1	-175	270	139.897
T	(oC)	10.7	19.2	15.92	10.9	23.5	16.682
E.C.	(μS/cm)	153	2040	635.1	139	1690	596.231
Na^+	mg/L	2.682	143.322	24.777	5.659	137.072	33646
K^+	mg/L	0.598	3.984	1.702	1.469	7.752	2.652
Mg^{2+}	mg/L	0	27.134	4.162	0.001	26.512	9.079
Ca^{2+}	mg/L	42.456	196.394	118.968	11.704	213.428	91.275
NH_4^+	mg/L	0	12.642	0.655	0	2.792	0.24
Cl^-	mg/L	2.7	361	51.09	3.98	344	33.018
Br^-	mg/L	0	3.866	0.533	0.07	2.95	0.358
SO_4^{2-}	mg/L	0	102	44.8	0	155.2	37.931
NO_3^-	mg/L	9.68	38.72	19.226	1.32	79.2	13.009
HCO_3^-	mg/L	112.24	434.32	258.884	107.36	484.34	266.179
O_2	mg/L	2.8	10.1	7.46	0.9	14.4	0.072

The chemical analysis (Yoxas, 2004) included defining each of the following physical parameters: Temperature (T_{wa}), electrical conductivity (E.C.), pH, redox potential (Eh),dissolved oxygen (DO_2), and the following chemical parameters: Na^+, K^+, Mg^{2+}, Ca^{2+}, NH_4^+, Cl^-, Br^-, SO_4^{2-}, NO_3^-, NO_2^-, HCO_3^-, O_2.

In order to verify the results of the application of both methods, data from hydrochemical analysis and in particular those of nitrate ions were used, because of their anthropogenic origins.

By observing the spatial distribution map of nitrate ions (Figure 3), an increase in the concentration of nitrate ions is noted in both the western and eastern section of the study area. In the northern, central and southwestern section, the lowest values are observed.

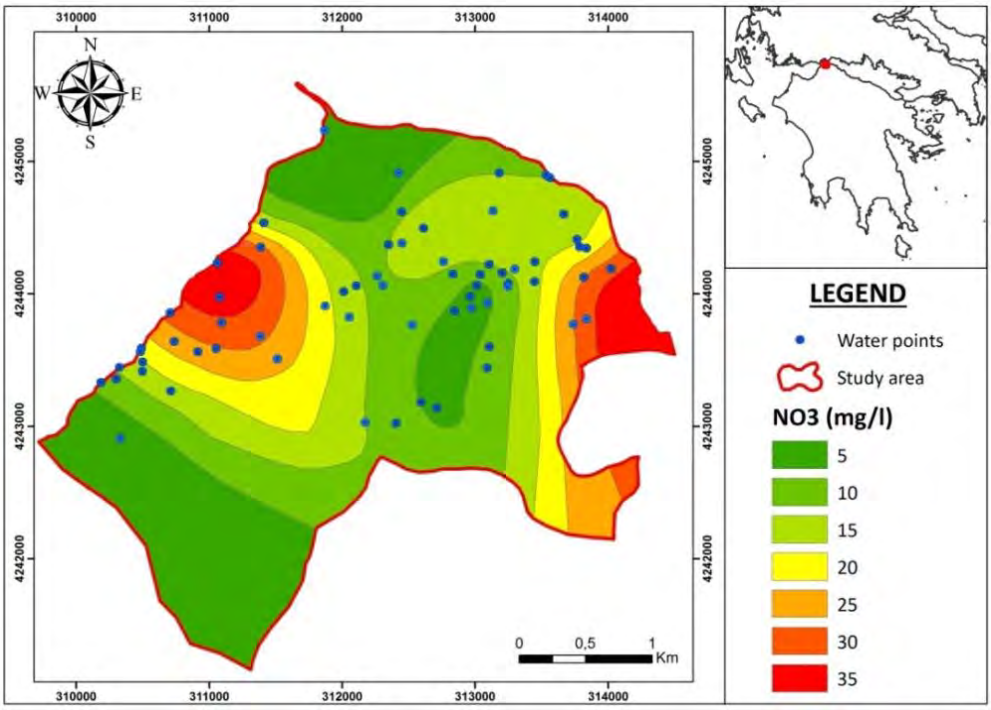

Figure 3 – Map of spatial distribution of nitrate (NO_3^-).

5. Methods of Assessment and Vulnerability Mapping

5.1. Typical DRASTIC Method

In order to apply this method, geological, geomorphological, hydrological, hydrogeological and soil data were used, that originated from fieldwork collected data, combined with information collected from correlation data from 64 boreholes in the study area. In addition, using topography maps from the Hellenic Military Geographical Survey on 1:5.000 and 1:50.000 scales, the Digital Elevation Model (DEM) was created to calculate morphological slope. For each parameter, a thematic layer was created along with the relative calibration values. The final vulnerability index map resulted from the combination of the various thematic layers according to the original DRASTIC method.

5.1.1. Depth to Water (D)

The value of parameter D was obtained using piezometric maps. This parameter defines the vertical distance needed for a contaminant to reach the aquifer. The greater the distance, the better the groundwater is protected from contamination and the lower its value (Table 3).

5.1.2. Recharge (R)

This parameter represents the annual water quantity in mm that infiltrates into the soil surface and reaches the aquifer. The greater the quantity of water infiltrated, the greater the recharge, and consequently, the greater the possibility of contamination (Table 3).

5.1.3. Aquifer Media (A)

Aquifer material plays an important part to the length of the distance and to the pathway through which a contaminant is transported. In general, the greater the size of the grains of the aquifer material, the greater the porosity is and therefore the lower the deterioration capacity of the contaminant. Consequently, the greater the grain size, the higher the value in the evaluation system (Table 3). Data of the aquifer media are from the lithological intersection of 64 boreholes in the study area (Yoxas, 2004).

Table 3 – Ranges and Ratings for each parameter.

Parameter	Range	Rating
Depth to water(m)	0 – 4	9
	4 – 8	8
	8 – 12	7
	> 12	6
Recharge(mm/year)	200 - 300	6
	100 – 200	4
	< 100	2
Aquifer media	Pebble	7
	Pebble – Gravel	6
	Gravel – Sand	4
	Gravel –Sand – Clay	2
Soil cover	Rock	8
	Deep – Shallow	5
	Deep	2
Topography (%)	0 – 2	10
	2 – 6	9
	6 – 12	5
	12 – 18	3
	> 18	1
Impact of vadose zone	Pebble – Gravel	9
	Gravel – Sand	7
	Sand	5
	Clay –Sand	3
Conductivity (m/day)	4 – 10	6
	2 – 4	4
	< 2	2

5.1.4. Soil Cover (S)

The thicker the soil cover, the greater possibility that the contaminant will endure deterioration mechanisms, due to the existing water deposition, that constitutes an important protective mechanism, before it reaches deeper water bodies. Consequently, the thicker the existing soil covers above the formation, the lower the value of the evaluation system (Table 3).

5.1.5. Topography (T)

Low slope values favor infiltration and are associated with greater vulnerability, in opposition to greater slope values, which favor recharge and are associated with low vulnerability. Slopes were set by using the Digital Elevation Model. The lower slope values were graded with a high value in the evaluation system, whereas greater values were graded with a lower value (Table 3).

5.1.6. Impact of Vadose Zone (I)

Vadose zone is the subsoil zone above the aquifer level. It plays an important role lessening the contaminant charge, due to the different existing mechanisms that cause its deterioration. (geochemical, physical, biochemical etc.).

In consequence, the vadose zone material is of crucial importance for the evaluation of this parameter. The greater the grain sizes of the vadose zone material, the greater the value in the evaluation system (Table 3).

5.1.7. Conductivity of the Aquifer (C)

Hydraulic conductivity represents the velocity with which a contaminant is transported through the saturation zone. Its value is dependent on the attributes and characteristics of the aquifer. The greater the hydraulic conductivity is, the faster the place with which contaminants are transported and the greater their vulnerability to contamination. Hydraulic conductivity was allocated by evaluating drills that took place in the study area. Therefore the greater the hydraulic conductivity, the greater the value in the evaluation system (Table 3).

5.1.8. Drastic Index (DI)

According to the criteria taken into account in the original DRASIC method and according to the relative weighted indexes, the creation of the final vulnerability map was feasible. (Figure 4) DI values are divided into four (4) classes and are presented in Table 4.

Table 4– Values of the respective classes.

Drastic Index	Classes
< 79	Very low
80 – 99	Low
100 – 119	Medium
>120	High

As it is concluded by the final vulnerability index map, the higher values (DI>100) are observed in the eastern and western section, covering 19.86% of the study area. The sections with the lower vulnerability index (80<DI<99) cover the greatest area, a percentage of 45.34 %. Finally, areas with the lowest values of the index are located in the central-northwestern section of the study area, while some of them are sparsely observed throughout the southeastern and southwestern area. This covers an area of 33.53 %.

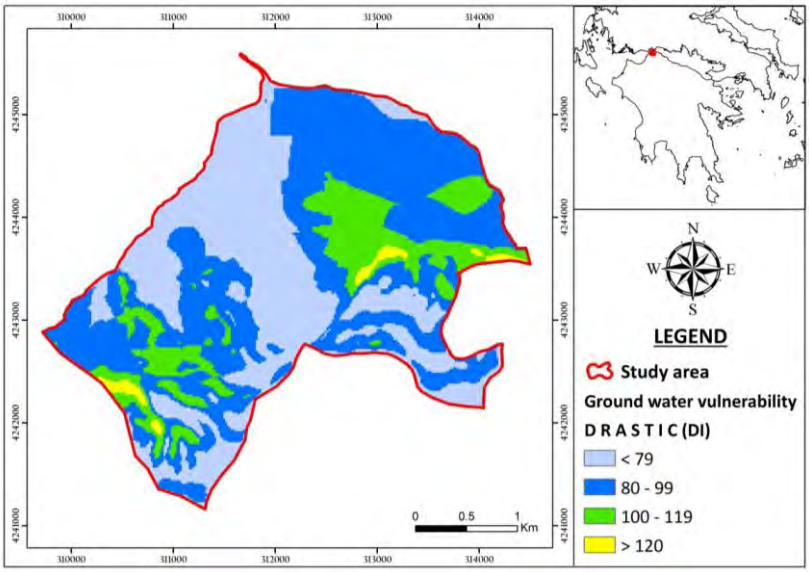

Figure 4 – Distribution map of the Drastic Index (DI).

5.2. Modified DRASTIC-L Method

Taking into consideration the land uses of the study area developed by Corine Land Cover 2004 (US Protection Agency, 1985) and the methodology being applied by Secunda et al. (1998), Al-Adamat et al. (2002), the modified DRASTIC index equation is:

$$\mathrm{MDI} = \sum_{i=1}^{8} r_i \cdot w_i \qquad (2)$$

*where:***MDI = M**odified **D**rastic **I**ndex.

In order to introduce a land use factor into the DRASTIC index, the land use map (Figure 5) was rated according to the weighted values.

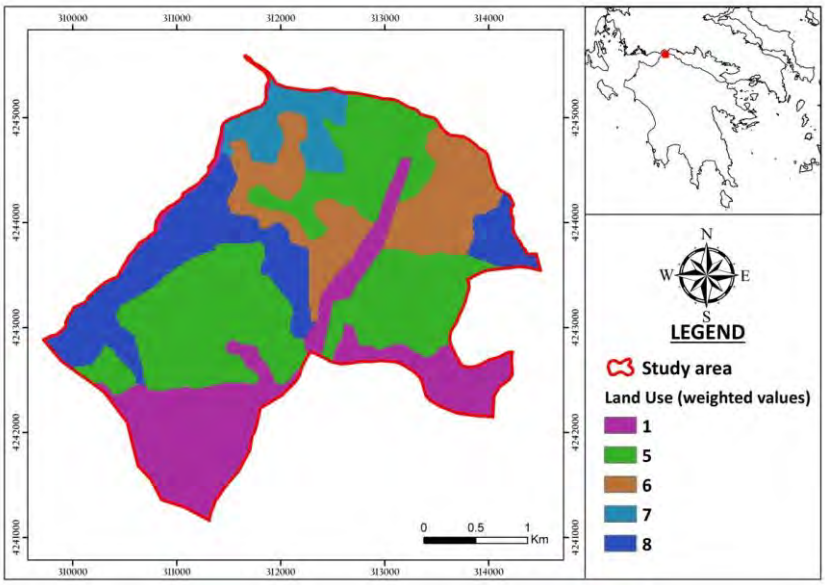

Figure 5 – Land Use criterion with weighted values.

This map was converted into a raster grid and the resultant grid coverage was then added to the DRASTIC index based on equation. 2 (modified from Secunda et al. 1998).

Table 5 – Ranges and Ratings for each parameter.

Parameter	Criteria	D	R	A	S	T	I	C	L	Priority
Depth to water (m)	**D**	1	4	5	2	2	1	5	2	**0.2462**
Recharge (mm/year)	**R**	1/4	1	4	1/2	1/2	1/2	1	1/2	**0.0757**
Aquifer media	**A**	1/5	1/4	1	1/4	1/4	1/3	1	1/4	**0.0375**
Soil cover	**S**	1/2	2	4	1	1/2	2	3	1	**0.1419**
Topography (%)	**T**	1/2	2	4	2	1	3	3	1	**0.1832**
Impact of vadose zone	**I**	1	2	3	1/2	1/3	1	2	1/2	**0.1114**
Conductivity (m/day)	**C**	1/5	1	1	1/3	1/3	1/2	1	1/3	**0.0512**
Land Use	**L**	1/2	2	4	1	1	2	3	1	**0.1529**

Consistency Ratio (CR)=0.0372 <0.1

The preparation of the final map was the result of the combination among the thematic maps with respect to Analytical Hierarchy Process (Saaty 1977, 2003). The AHP parameters as well as its analysis are shown in table 5, indicating the priority vectors of all criteria.

From the combination of the above thematic maps, using the tool Spatial Analyst of ArcGIS, revealed the final map identifying areas of vulnerability, on a scale grading from low to high values respectively (Figure 6).
Using the classification methodology derived from the AHP analysis, the modified DRASTIC-L index was sub – derided into 4 classes, (i) below 79 with very low risk, (ii) 80 – 99 with low risk and (iii) 100 - 119 with medium risk and (iv) above 120 with high risk.
According to AHP analysis, criterion 8 (Land Use), takes high weighted value as well as criterion 1 and criterion 5 respectively. The land use criterion provides a basis for specific assessment in future work.

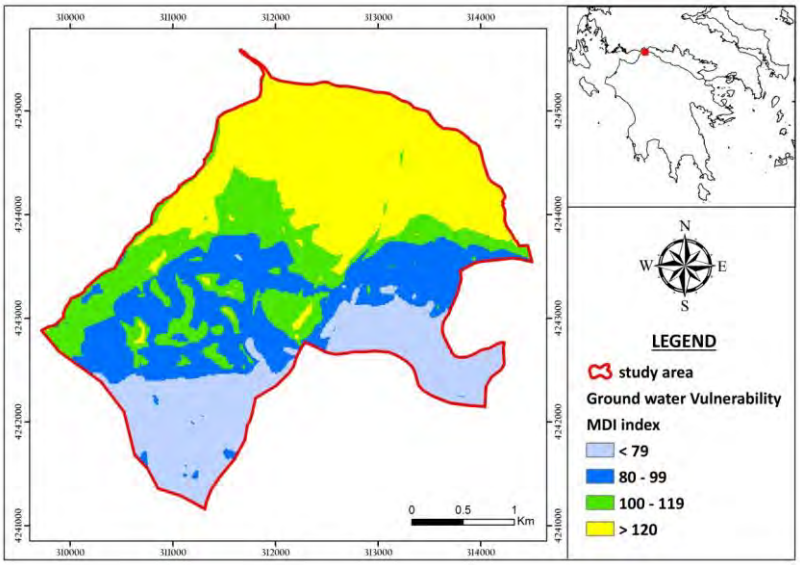

Figure 6 – Distribution map of the Modified Drastic Index (MDI).

The role of land use due to its importance of evaluating the potential effect upon ground water quality resulting from the fact that areas having high values of ground water vulnerability appears to be explained by intense irrigating agricultural zones. As shown in Figure 6, ground water vulnerability increases as the suitability index increases.

6. Groundwater Vulnerability and Nitrate Concentrations in Groundwater

In order to estimate the affection of land use; a correlation between nitrate ions and MDI factor was made. Nitrate contamination has been suggested as an indicator of overall groundwater quality[1] (2006/118/EC). Because drinking water with high nitrate concentrations is a potential health risk, European Union (2006) has set a minimum standard for nitrate in drinking water of 50 mg/L. Identifying areas in the study area where ground water has been impacted by anthropogenic activities (nitrate concentrations at or above 3 mg/L) can help water resource managers protect the water supply by targeting land-use planning and monitoring programs to these vulnerable areas.

According to the distribution map of nitrate composition in groundwater (Figure 3), samples with high values of nitrate composition are seem to be into area with high values of MDI factor. Additionally, low vulnerability zones (low MDI factor) are located into samples with low values of nitrate composition respectively.

By the comparison of concentration of nitrate ions with the results of MDI factor, an interconnection was observed and the correlation factor of cross-plot of these parameters is ordered 70% (Figure 7). Finally, regions with high vulnerability zones were established mainly due to human activities which are intensive in those areas.

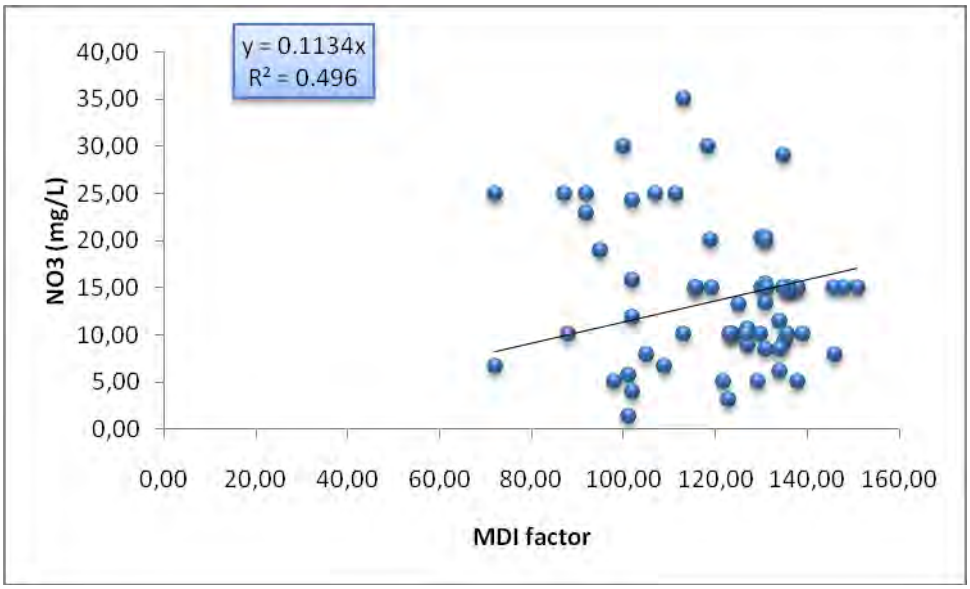

Figure 7 - Cross – plot diagram of nitrate concentration vs MDI factor

7. Conclusion – Discussion

The study area is characterized by several sources of pollutions due to anthropogenic activities. In intensive agricultural areas, continuous recharge of treated effluents and other water used for irrigation can change the configuration of the soil and the subsoil media, leading to higher

[1] European Union (2006) Water Framework Directive 2006/118/EC of the European Parliament and of the Council, Official Journal of the European Union

hydraulic conductivity and therefore higher percolation to groundwater of much kind of pollutants. MDI method indicates these areas where long-term land use activities increase natural potential vulnerability to groundwater pollution, as assessed by original DRASTIC.

Comparing the final MDI value map with the nitrate composition in ground water, it is obvious that areas with high values of MDI factor overlaid to areas with intense anthropogenic activities.

The run of MDI model was derived from AHP analysis which laid to the conclusion that land use factor plays a strong role as it takes high weighted value as well as criterion 1 and criterion 5 respectively.

The final DRASTIC model was tested using hydrochemical data from the aquifer. The analysis of groundwater chemistry was encouraging to find that no sample point with high nitrate levels was found in the areas classified as being of low risk suggesting that the original DRASTIC model for this area provided a conservative estimate of low risk areas.

It is recognized that the approach adopted to produce the DRASTIC index in areas with either intense agricultural activity and coastal aquifer provides important objective information that could be used to inform local decision making.

8. References

Al-Adamat R.N.A. 2002. The use of Geographical Information Systems (GIS) and Remote sensing to investigate Groundwater Quality in the Azraq Basin, Jordan, *Unpublished PhD Thesis*, Coventry University, Coventry UK.

Aller L., Bennett T., Lehr J.H. and Petty R.J. 1987. DRASTIC: A Standardized System for Evaluating Ground water Potential Using Hydrogeological Settings, *Environmental Research Laboratory,US Environmental Protection Agency*. Ada Oklahoma, EPA/600/2–85/018.

European Union (2006) Water Framework Directive 2006/118/EC of the European Parliament and of the Council*, Official Journal of the European Union*

Foster S.S.D. 1987. Fundamental concepts in aquifer vulnerability, pollution risk and protection strategy. In: Van Duijvenbooden W., Weageningh H.G. (eds) TNO Committee on Hydrological Research, The Hague, Vulnerability of soil and groundwater to pollutants, Proc. Inf. 38, 69 – 86.

Koukouvelas I. and Papadopoulos Ch. 1984. Geological study of Argyra – Sela – Ag. Vasileios Dissertation, University of Patras, pp: 27 (in Greek).

Saaty T.L. 2003. Decision making with the AHP: Why is principal eigenvector necessary, *European Journal of Operational Research*, vol. 145, pp: 85 – 91.

Saaty T.L. 1977. A scaling method for priorities in hierarchical structures, *Journal of Mathematical Psychology* 15, 231 – 281

Secunda S., Collin M.L. and Melloul A. J. 1998. Groundwater vulnerability assessment using a composite model combining DRASTIC with extensive agricultural land use in Israel's Sharon region, *Journal of Environmental Management*, vol. 54, pp: 39-57

Tsoflias P. 1971. Geological map of Greece, scale 1:50000*, Nafpactos sheet*, IGME, Athens.

Vrba J. and Zaporozec A. 1994. Guidebook on Mapping Groundwater Vulnerability, *International Contributions to Hydrogeology* (IAH), vol. 16, pp: 131.

US Protection Agency 1985. DRASTIC: a Standard System for Evaluating Groundwater Potential Using Hydrogeological Settings, Ada, Okla., NWWA/EPA Series.163 pp.

Van Stempvoort D., Ewart L. and Wassenaar L. 1993. Aquifer vulnerability index: a GIS-compatible method for groundwater vulnerability mapping*, Canadian Water Resources Journal* vol. 18, pp:25–32

Yoxas G. 2004. Hydrogeological and hydrochemical conditions of alluvial aquifer of Volinaios catchment, NW Peloponnesus*, Dissertation*, University of Patras.

Δελτίο της Ελληνικής Γεωλογικής Εταιρίας, τομ. XLVII , 2013
Πρακτικά 13ου Διεθνούς Συνεδρίου, Χανιά, Σεπτ. 2013

Bulletin of the Geological Society of Greece, vol. XLVII 2013
Proceedings of the 13th International Congress, Chania, Sept. 2013

DEVELOPMENT OF INNOVATIVE ENVIRONMENTAL APPLICATIONS OF ATTAPULGITE CLAY

Zotiadis V.[1] and Argyraki A.[2]

[1] *Edafomichaniki S.A., vzotiad@edafomichaniki.gr*

[2] *National and Kapodistrian University of Athens, Faculty of Geology and Geoenvironment, Department of Economic Geology and Geochemistry, argyraki@geol.uoa.gr*

Abstract

In this paper we present a series of laboratory and field, pilot- scale applications of attapulgite clay as an amendment for the stabilization of metals in contaminated soil and sewage sludge. Attapulgite's structure together with its fine particle size and fibrous habit are responsible for its high specific surface area and sorption properties. A pilot scale application of attapulgite clay as a binder for in situ stabilization of toxic metals in contaminated land showed significant reduction in the water leachable metal fraction (Cu: 17%, Pb: 50%, Zn: 45%, Cd: 41%, Ag: 46%, As: 18%, Mn: 47%, Ba: 45%, Sb: 29%). In a second pilot scale environmental application, an innovative attapulgite "Geosynthetic Reactive Clay - GRC" was designed and developed for "capping" and "stabilization"of toxic metals in contaminated soil. Also, laboratory scale experiments with fresh sewage sludge from a municipal water treatment plant showed that addition of attapulgite clay in sludge, significantly reduced the leachable concentrations of phenol, DOC, Hg, Cu, Mo, Pb, Se, As, Zn and pathogen population over a 4 weeks observation period. The developed soil remediation techniques are promising and cost-effective under present market conditions. Concerning treatment of sewage sludge, attapulgite clay is an effective additive that could enhance the composting procedure creating an environmental added value, final compost product.

Key words: P*alygorskite, soil remediation, sewage sludge treatment, heavy metals.*

Περίληψη

Η εργασία αυτή παρουσιάζει εργαστηριακές και πιλοτικές περιβαλλοντικές εφαρμογές του ορυκτού ατταπουλγίτης για τη σταθεροποίηση μετάλλων σε ρυπασμένα εδάφη και σε ενεργή ιλύ. Η δομή του ατταπουλγίτη σε συνδυασμό με τη λεπτομερή κοκκομετρία του και τον ινόμορφο τύπο κρυστάλλων του δημιουργούν μεγάλη ειδική επιφάνεια για το ορυκτό με σημαντικές προσροφητικές ικανότητες. Αρχικά μία πιλοτική εφαρμογή ατταπουλγιτικής αργίλου ως πρόσθετο σε έργο σταθεροποίησης ρυπασμένου εδάφους από τοξικά μέταλλα είχε ως αποτέλεσμα τη σημαντική μείωση του υδατο-εκχυλίσιμου κλάσματος των μετάλλων (Cu: 17%, Pb: 50%, Zn: 45%, Cd: 41%, Ag: 46%, As: 18%, Mn: 47%, Ba: 45%, Sb: 29%). Μία δεύτερη πιλοτική περιβαλλοντική εφαρμογή της ατταπουλγιτικής αργίλου αναφέρεται στο σχεδιασμό και τη δημιουργία ενός γεωσύνθετου τύπου "Geosynthetic Reactive Clay - GRC" σαν ένα νέο, καινοτόμο εμπορικό προϊόν για την εφαρμογή σε έργα αποκατάστασης ρυπασμένου εδάφους από τοξικά μέταλλα. Τέλος, σε εργαστηριακή κλίμακα εφαρμογής, η προσθήκη ατταπουλγιτι-

κής αργίλου σε ενεργή ιλύ από μονάδα επεξεργασίας λυμάτων, μείωσε τις υδατοεκχυλίσιμες συγκεντρώσεις μία σειράς παραμέτρων, όπως οι φαινόλες, ο διαλυτός οργανικός άνθρακας, τα μέταλλα (Hg, Cu, Mo, Pb, Se, As, Zn), καθώς και το μικροβιολογικό φορτίο παθογόνων οργανισμών σε κλίμακα παρατήρησης τεσσάρων εβδομάδων. Οι παραπάνω εφαρμογές του ατταπουλγίτη σε τεχνικές αποκατάστασης ρυπασμένου εδάφους είναι οικονομοτεχνικά βέλτιστες και ανταγωνιστικές στην υπάρχουσα αγορά περιβαλλοντικών έργων. Σε σχέση με την ενεργή ιλύ, η ατταπουλγιτική άργιλος είναι αποτελεσματικό πρόσθετο, που μπορεί να ευνοήσει την κομποστοποίηση, δημιουργώντας τελικά, ένα αυξημένης περιβαλλοντικής αξίας, εδαφοβελτιωτικό προϊόν .
Λέξεις κλειδιά: *Παλυγορσκίτης, αποκατάσταση, ενεργή ιλύς, βαρέα μέταλλα.*

1. Introduction

The use of mineral-based amendments for remediation of metal and organic contaminants in soils has been widely studied and is gaining broader acceptance as a cost effective remediation technology (O´Day and Vlassopoulos, 2010). The overall aim of in situ amendment technologies is to sequester and stabilize contaminants in soils or biosolids in order to reduce their ability to partition to water or biota, thus decreasing their potential for transport and toxicity. The selection of appropriate amendments is an open field for research on the quest for the most effective mixing proportions at an affordable cost. Environmental applications of attapulgite clay as an effective toxic metal absorbent have previously been described in laboratory scale by many researchers (Álvarez-Ayuso et al., 2003; Shirvani et al., 2006; Potgieter et al., 2006; Veli et al., 2007; Zhang and Pu, 2010) for contaminated land remediation. However, there are not any studies on larger scale experiments involving applications in the field. In this paper we present a series of pilot scale and batch scale applications of attapulgite clay as an amendment for the stabilization of metals in contaminated soil and sewage sludge.

2. Materials and Methods

2.1. Attapulgite Clay

Attapulgite´s (palygorskite) structure consists of modulated 2:1 layers, demonstrating a variable dioctahedral to trioctahedral character expressed by the following general chemical formula Mg5Si8O20(OH)2(OH2)4.4H2O (Gionis et al., 2006). The presence of micropores and channels in attapulgite's structure together with its fine particle size and fibrous habit are responsible for its high specific surface area and its sorption properties (Galan, 1996). The attapulgite clay used in the lab and pilot scale applications presented in this paper are commercial products of Geohellas S.A. selected to fit the design of the specific environmental applications. The raw material is originated from deposits exploited by Geohellas at Grevena, Greece. A typical mineralogical composition of attapulgite clay consists mainly of palygorskite, saponite and quartz with minor amounts of calcite, serpentine, dolomite and occasionally plagioclase and pyroxene. A representative XRD pattern of palygorskite rich attapulgite clay especially selected for the presented applications is given in Figure 1.

2.2. Experimental Design Principles and Concept Application

The tested environmental applications of attapulgite clay as amendment for environmental applications refer to three completed projects that are discussed in the following paragraphs.

2.2.1. Pilot Scale Application of Attapulgite Clay for In Situ Stabilization Toxic Metals in Contaminated Land

The contaminated site for this experiment was located in a public recreational area in Lavrion town, 55 km southeast of Athens, Greece. Field dimensions were 9 m x 12 m and the overburden

material consisted of a mixture of alluvial soil and mining/ metallurgical waste at least to a depth of 30 cm. Detailed description of site history as well as contaminated soil conditions are given in Zotiadis et al. (2012). Preparation of the study area included rotor-tilling to a depth of 30 cm, manual removal of large cobbles and rewetting the soil to amend the initial soil moisture content. Physical properties of contaminated soil were determined by geotechnical laboratory tests. Soil treatment included addition of appropriate amount of attapulgite clay, mixing, homogenization and rewetting to attain saturated conditions. Homogenization of treated soil was repeated on a weekly-basis for a one month period (4 weeks), using a rotor-tiller in parallel with soil rewetting to maintain near-saturation soil conditions. Soil pH was monitored weekly. A final set of samples was collected at the end of the 4 weeks period to study the final geochemical characteristics of the study area while pH monitoring continued for a period of seven (7) months on a monthly basis.

2.2.2. Pilot Scale Application of a "Geosynthetic Reactive Clay - GRC" as an Innovative Product for the Retention of Toxic Elements in Contaminated Land

This case study included the design and application of a "capping" technique for remediation of heavily contaminated soil by toxic metals and is a reference project for the commercial production of GRC product. A new Geosynthetic Clay Composite was developed by substituting impermeable Na-bentonitic clay with permeable attapulgite clay, thus creating an innovative product for the retention of toxic elements in contaminated land (Kollios and Zotiadis, 2012).

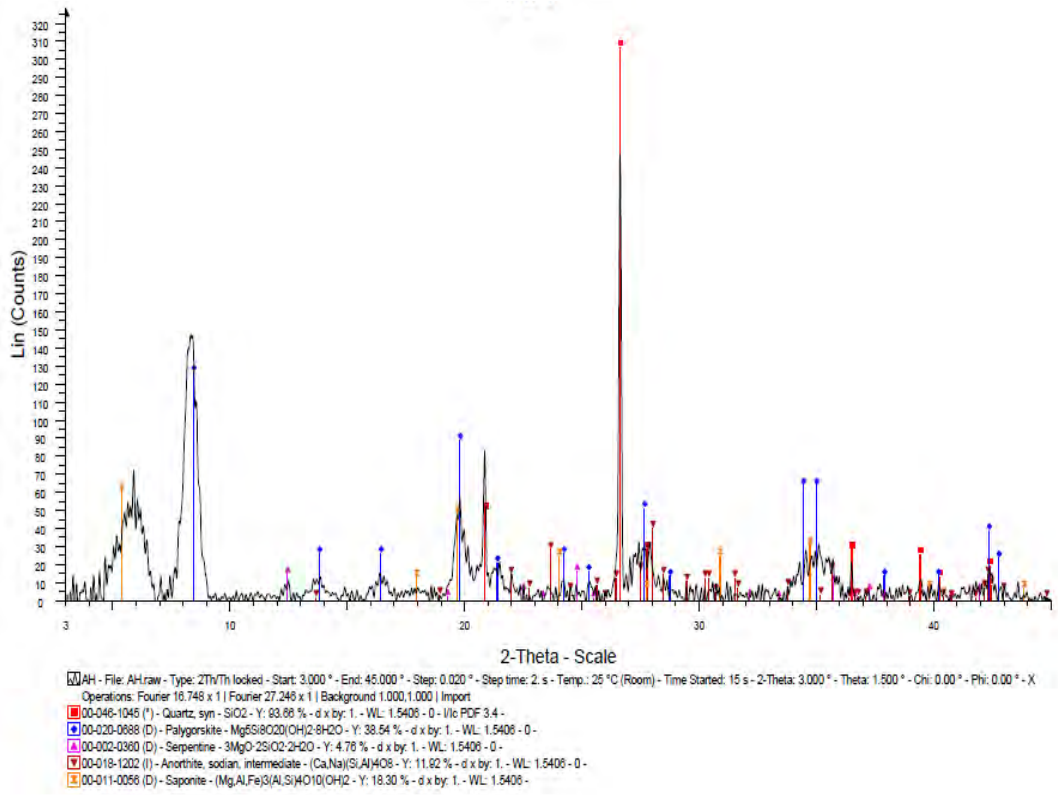

Figure 1 – XRD pattern of a typical palygorskite rich attapulgite clay.

The product was tested in a Primary School yard at Lavrion, Greece. High recorded concentrations of toxic elements in soil and dust of the area are reflected in adverse effects in human health. The aim was to limit the exposure of children to soil containing toxic metals by developing a relatively low cost product with simple construction requirements. The school building was founded in a 4.5 m thick hazardous waste layer consisting of alluvial soil mixed with historical mining and

metallurgical waste (carbonate-rich tailings and slag). Below this depth, Quaternary deposits of alternations of conglomerates and marls continue for 3 to 10 m until they meet the alpine geological basement of metamorphic schist. The contaminated subsoil/soil layer was characterized by determining geotechnical, mineralogical and geochemical parameters prior to the application of attapulgitic GRC. According to the defined geotechnical and geochemical properties, the remediation actions included: a) ex-situ excavation of the contaminated soil/subsoil to the depth of 40 cm, b) placement of a non-woven geotextile over the contaminated subsoil, c) placement of a layer of granular attapulgite clay with thickness of 10 cm, d) covering the attapulgite clay with a second non-woven geo-textile and, e) placement of a layer of clean vegetal soil with a thickness of 30 cm for planting purposes, according to the landscape design.

Leaching experiments were conducted on representative, three fold composite samples of contaminated soil, clean soil and attapulgite clay according to EN 12457-4 (2003) European Standard (one stage batch test at a liquid to solid ratio of 10 L/Kg). Additionally, up flow percolation tests were performed on two (2) subsamples according to the technical specification CEN/TS 14405 (2004). The testing column was designed and packed with the used materials (contaminated soil, geotextile, attapulgite clay, geotextile, vegetal soil) according to the proposed design in order to examine the effectiveness of different thickness of the attapulgite clay layer (i.e. 0 cm, 5 cm, 10 cm, 15 cm).

2.2.3. Laboratory Scale Application of Attapulgite Clay for Treatment of Sewage Sludge from the Municipal Wastewater Treatment Plant of Kamari, Thera

The objectives of this laboratory scale study were to assess the effectiveness of two modified attapulgite clay samples with different grain size distribution, mixed in two different proportions with sludge material (Gidaropoulou et al., 2012). Two types of heat treated material were tested, differing in their grain size distribution; a fine grained sample (F) with particle size distribution (μm) of d10=1.8, d50= 8.9, d90= 24.8 and a coarse grained sample (C) with 90% of grains in the 20/50 mesh size.

Sampling of sewage sludge material was conducted in September 2011 at the Kamari treatment plant. Twenty four hours after collection the sludge was weighted and placed into 5 orthogonal polypropylene flower pots of dimensions 25 x 25 x 50 cm, each containing 12 kg of material. Attapulgite clay was added into four of the sludge containing pots; the material in the fifth pot was left untreated in order to provide a reference sample (SLU). Mixing proportions of each of the fine and coarse grained attapulgite clay samples were 5% and 10% on a dry weight basis. The amended material was homogenized manually and the pots were kept in open air conditions protected from rain and direct sunlight for a period of 4 weeks. Mixing and homogenization of sludge was repeated on a weekly basis during this period and the pH of the material was monitored weekly. A final set of samples was removed from the pots at the end of the 4 weeks period to study the final geochemical and microbiological characteristics of sludge.

Aliquots of untreated and treated sludge samples were subjected to the L/S=10 leaching procedure with deionized water according to EN 12457-4 (2003). Chemical analysis of heavy metals was performed in parallel in the Laboratory of Economic Geology and Geochemistry, University of Athens by using graphite furnace atomic absorption spectroscopy and an accredited external laboratory. Appropriate analytical techniques were used for the determination of the total parameters prescribed by the Council Decision 2003/33/EC. Microbiological analysis was also performed on sludge before and after treatment to determine the following parameters: Coliforms, Fecal coliforms, β-glucuronidase positive E. coli, Enterococci, Salmonella spp, Listeria monocytogenes. This analysis was performed in the external accredited laboratory. Furthermore the sludge samples were studied by X ray diffraction using a Siemens D-5005 diffractometer with Cu *Kα* radiation and scanning electron microscopy (SEM) using a JEOL JSM-5600 system at the Laboratory of Economic Geology and Geochemistry, University of Athens.

3. Results and Discussion

3.1. In Situ Stabilization Toxic Metals in Contaminated Land

The descriptive statistics of water leachable concentrations in untreated and treated soil samples from the pilot scale study in Lavrion are presented in Table 1. Before treatment the determined water leachable metal concentrations exceeded the limit values for inert waste assigned by Directive 2003/33/EC.

Table 1 - Water leachable elemental concentrations (μg/kg) before and after in-situ treatment of Lavrion urban soil with attapulgite clay (n=12).

Element	Mean		Min		Max		Standard Deviation	
	untreated	treated	untreated	treated	untreated	treated	untreated	treated
Cu	544	456	505	329	577	537	34	83
Pb	9198	4609	6491	3146	11109	6267	2325	1179
Zn	12848	7006	9170	4770	15710	9210	3253	1803
Ag	18	9	14	6	20	12	3	2
Mn	2666	1416	1780	780	3330	2220	800	471
As	1455	1190	1312	857	1554	1487	128	224
Cd	40	24	31	20	51	27	8	3
Sb	232	165	203	138	256	169	26	12
Ba	580	312	420	150	710	530	131	186

Consequently the measured water leachable metal concentrations posed significant environmental risk confirming the need for reducing potentially toxic elements' mobility using a stabilization method. Water leachable concentrations after treatment indicated that the performed remediation method reduced significantly the readily bioaccessible water leachable fraction of metals and subsequently the associated exposure risk to humans and biota. The corresponding reduction of water leachable metal fraction of metals in pilot scale application was determined as high as 17% for Cu, 50% for Pb, 45% for Zn, 41% for Cd, 46% for Ag, 18% for As, 47% for Mn, 45% for Ba and 29% for Sb.

3.2. Attapulgite "Geosynthetic Reactive Clay - GRC"

The measured total concentrations of Pb, Zn, As, Cd and Sb in the untreated soil from the school yard in Lavrion greatly exceeded the corresponding intervention values established by the "New Dutch List" (VROM 2009), indicating high poly-metallic soil pollution and presenting high risk of adverse health effects for children exposed to soil contamination (Kollios and Zotiadis, 2012). The mean values of metal concentration determined by water leaching experiments according to EN 12457-4 in the tested samples are presented in Table 2.

The water leachable metal concentrations in contaminated soil were lower than the corresponding limit values for non-hazardous wastes but exceeded the limit values for inert wastes assigned by Directive 2003/33/EC. As a fact the measured water leachable metal values in contaminated soil pose a significant environmental risk confirming the need for reducing potentially toxic elements' mobility using a stabilization binder. On the other hand the water leachable metal values of vegetal soil and attapulgite clay as it was expected are significantly lower than the limit values for inert wastes. The mean values of metals determined by the performed up flow percolation tests are

presented in Table 3. The determined leachable metal values by up flow percolation tests in column without attapulgite clay (blind sample) exceeded the corresponding limit values for inert wastes assigned by Directive 2003/33/EC for arsenic, lead and cadmium. However in the columns with attapulgite clay, a significant reduction of water leachable metal fraction was determined reaching percentages as high as 100% for As, 21% for Ba, 100% for Cd, about 100% for Pb, 100% for Sb and 88% for Zn. Best results were achieved in the percolation test conducted with 10 cm attapulgite clay in the test column. Leachable metal concentration values in all tested columns filled with attapulgite clay were lower than the corresponding limit values for inert wastes assigned by Directive 2003/33/EC.

Table 2 - Water leachable (L/S= 10 L/Kg) metal mean values (mg/ kg) of vegetal soil, contaminated soil, attapulgite clay (EN 12457) and corresponding limit values for inert and non-hazardous wastes according to 33/EC/2003.

Metal	Water leachable (L/S= 10 l/Kg) mean values			Limit Values	
	Vegetal Soil	Contaminated Soil	Attapulgite Clay	Inert Wastes	Non Hazardous Wastes
As	0.012	1.45	nd	0.5	2
Ba	nd	0.74	nd	20	100
Cd	0.0028	0.04	0.0012	0.04	1
Cu	0.08	0.54	0.036	2	50
Hg	nd	nd	nd	0.01	0.2
Mo	nd	0.05	0.011	0.5	10
Ni	0.06	0.02	0.024	0.4	10
Pb	0.01	9.20	nd	0.5	10
Sb	nd	0.035	nd	0.06	0.7
Se	nd	nd	nd	0.1	0.5
Zn	1.4	12.85	1.1	4	50

nd : not detected

3.3. Attapulgite Clay in the Treatment of Sewage Sludge

The effectiveness of attapulgite clay treatment was assessed by comparing the analytical results of leached solutions of treated and untreated sludge (reference sample SLU). The results showed a significant reduction of water leachable fraction for several. Overall the best results were achieved with the 10% mixing proportion of clay. The fine grained material performed better in removing phenol and DOC content in the leachate (100% and 42% reduction respectively in sample SL5F) but the coarse grained material (SL10C) achieved better reduction percentages for metal and metalloid parameters: As (39%), Cu (64%), Hg (100%), Mo (52%), Pb (50%), Zn (38%). The order of metal and metalloid uptake by attapulgite clay was Hg> Cu> Mo> Pb> Se> As> Zn.

With respect to pathogens, results at the end of the experimental period in the untreated and treated samples were compared to pathogen concentrations in the initial sludge sample (Figure 3). A significant reduction in Coliforms, up to 86% was observed for sample SL10C. Samples treated with 10% fine grained attapulgite clay achieved the best reduction in pathogens overall. It is noted that Salmonella spp and Listeria monocytogenes were absent even in the initial sample. Mixing also reduced the moisture content of treated material.

Table 3 - Metal water leachable mean values (mg/ L) of up flow percolation tests (CEN/TS 14405) in the tested GRC.

Metal	Percolation Test *	Percolation Test **	Percolation Test ***	Inert (Co)	Non Hazardous (Co)
As	0.007	nd	nd	0.06	0.3
Ba	0.660	0.580	0.520	4.0	20
Cd	0.021	0.003	0.002	0.02	0.3
Cu	0.011	<0.003	<0.003	0.6	30
Hg	nd	nd	nd	0.002	0.03
Mo	<0.003	<0.003	<0.003	0.2	3.5
Ni	0.002	0.005	0.008	0.12	3
Pb	0.320	<0.003	<0.003	0.15	3
Sb	0.040	nd	nd	0.1	0.15
Se	nd	nd	nd	0.04	0.2
Zn	0.220	0.032	0.027	1.2	15

*, **, ***: Testing column with 0cm*, 5cm **, 10cm *** attapulgite clay.

3.4. Effectiveness of Attapulgite Clay as Contaminated Soil and Biosolids Amendment and Future Research Directions

The effectiveness of metal stabilization techniques on soil depends upon numerous factors besides the type of binder, including physical (i.e. grain size, plasticity, permeability, moisture content, etc.) and geochemical characteristics (type of contaminant, concentration, heterogeneity, leachability, mineralogy, pH, Eh, etc.) of the soil and on other competitive factors (USEPA, 2003). Soil solution pH is an important variable which controls the adsorption of the metal at clay water interfaces. Clays are known to possess a negative surface charge in solution.

The main mechanisms of toxic metals adsorption/ sorption on attapulgite clay have been studied by many researchers. Potgieger et al. (2006) showed that at slightly alkaline conditions more of the positively charged metal ions are adsorbed on the negative clay surface and precipitation of metal hydroxides occurs. Alvarez-Ayuso et al. (2003) suggested reaction of heavy metals with numerous silanol groups. Shirvani et al. (2006) also suggested two mechanisms for adsorption, i.e. replacement of Mg^{2+} in the edges of octahedral layer and inner-sphere complexation on the functional groups on the broken edges of the mineral. Furthermore data of Cai & Xue (2008) confirmed three mechanisms for copper adsorption by palygorskite: (a) onto the surface or in a net-like interstice; (b) forms a Me-complex ion and is trapped in the channel; or (c) into the hexagonal channel of the tetrahedral sites or the unoccupied octahedral sites of the mineral.

Laboratory experimental results indicated that treating sewage sludge with attapulgite clay might have positive effects in reducing the mobility and thus bioavailability of toxic elements in the instance of sludge land application. However, heavy metal content of sewage sludge is variable and hardly comparable (Fuerhacker and Haile, 2011). Furthermore, the fate and transport, mobility, bioavailability and eco-toxicity of potentially harmful elements in sludge-amended soils depends on several factors including pH, cation exchange capacity, organic matter content, soil structure and texture (Basta et al., 2005). All of the above calls for further work in order to explore the speciation of potentially harmful elements in sludge and understand the processes controlling adsorption by attapulgite clay. Besides the stabilization of harmful substances in sewage sludge, attapulgite clay could be used as an amendment for sewage sludge composting. In the initial stage of sludge treatment it reduces the moisture content, improves plasticity, reduces odor and prevents

ammonia losses (Xie et al. 2012). Furthermore it enhances the composting procedure by increasing aerisation and optimizing the required conditions, thus contributing to the production of an organohumus compost which is an added value fertilizer for agricultural applications.

Based on our experimental data as well as the relevant literature it is possible that the effectiveness of the attapulgite clay as a binder for toxic elements stabilization in contaminated soil could be attributed to a combination of factors such as a) direct precipitation as a result of control and time sustention of pH levels to slightly alkaline, b) high adsorption capacity as a result of its high specific surface area, c) sorption capacity derived by the existence of nanopores within the free channels of mineral structure. Further experiments employing advanced techniques utilizing synchrotron light sources such as X-ray absorption fine structure (XAFS) spectroscopy can be used to derive information on the structure and attachment geometry of sorption complexes on mineral surfaces in contact with aqueous solution (Brown and Calas, 2013). Evidence of this type of study combined with further empirical data from laboratory and field scale experiments will shed light into the controlling mechanism of metal sorption by attapulgite clay.

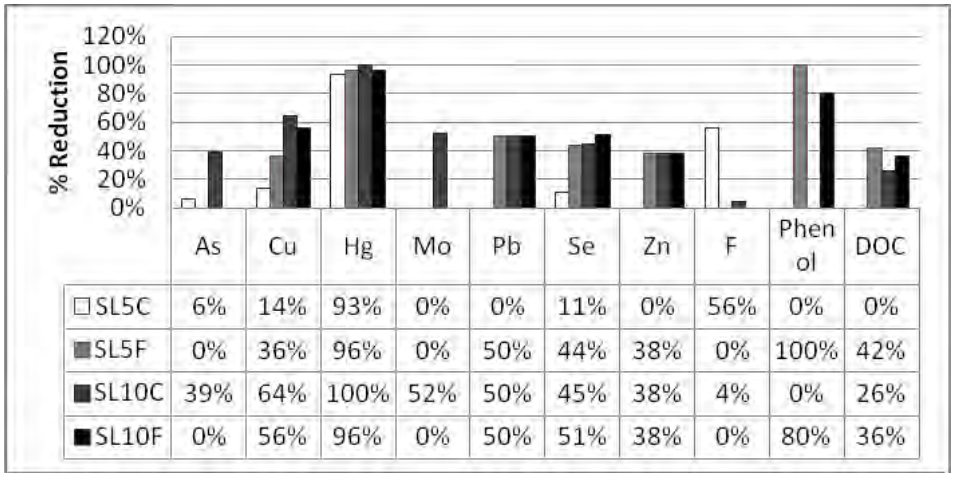

	As	Cu	Hg	Mo	Pb	Se	Zn	F	Phenol	DOC
SL5C	6%	14%	93%	0%	0%	11%	0%	56%	0%	0%
SL5F	0%	36%	96%	0%	50%	44%	38%	0%	100%	42%
SL10C	39%	64%	100%	52%	50%	45%	38%	4%	0%	26%
SL10F	0%	56%	96%	0%	50%	51%	38%	0%	80%	36%

Figure 2 – Reduction (%) in water leachable fraction of selected sludge parameters after treatment with different proportions of coarse (C) and fine (F) attapulgite clay.

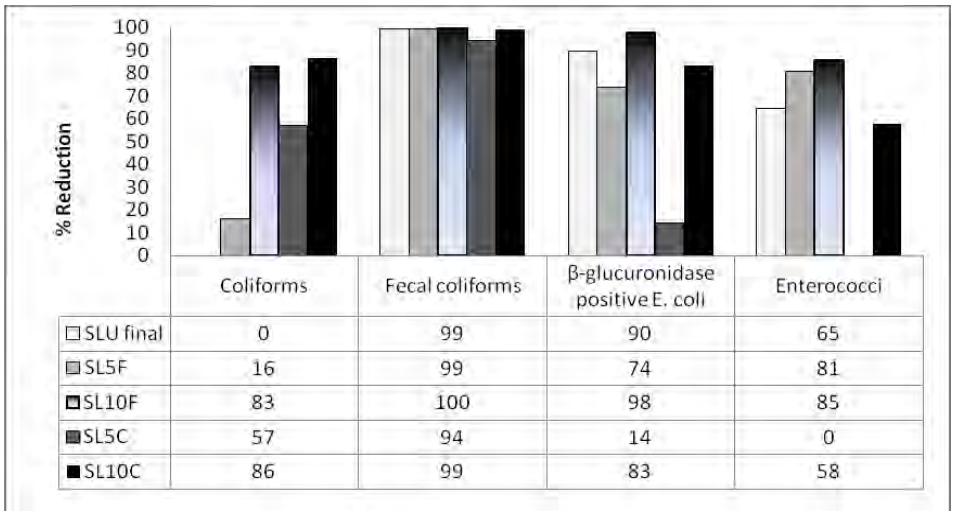

	Coliforms	Fecal coliforms	β-glucuronidase positive E. coli	Enterococci
SLU final	0	99	90	65
SL5F	16	99	74	81
SL10F	83	100	98	85
SL5C	57	94	14	0
SL10C	86	99	83	58

Figure 3 – Reduction (%) in microbiological parameters of sludge after treatment with different proportions of coarse (C) and fine (F) attapulgite clay.

4. Conclusions

A series of batch and pilot scale applications of attapulgite clay have demonstrated the effectiveness of this natural material as an amendment for the stabilization of metals in contaminated soil and sewage sludge. The feasibility of applying attapulgite clay as a binder for in - situ stabilization of toxic metals in contaminated soil was demonstrated in a pilot scale experiment at Lavrion. The reduction of water leachable metal fraction of metals was determined as high as 17% for Cu, 50% for Pb, 45% for Zn, 41% for Cd, 46% for Ag, 18% for As, 47% for Mn, 45% for Ba and 29% for Sb. Results from this study proved that the presence of attapulgite clay reduced significantly the water leachable metal concentrations and subsequently the associated environmental risk to humans and biota. In a different study, attapulgite clay was applied as an amendment sandwiched between two geotextiles by means of a new type of geocomposite material, named "Geosynthetic Reactive Clay - GRC" for toxic metals retention in contaminated land. The effectiveness of this innovative commercial product was assessed in a pilot scale study on a heavily contaminated site.

Also, research results indicated that the use of attapulgite clay has a positive potential in the treatment of sewage sludge. Laboratory scale experiments showed that mixing with 10% attapulgite clay reduces significantly the leachable concentrations of several parameters and that it is mostly effective for removal of phenol, DOC, Hg, Cu, Mo, Pb, Se, As and Zn. Treatment was also effective in the reduction of pathogen concentrations in sludge after the 4 weeks observation period. It is proposed that the method is further tested in a pilot scale field experiment combined with composting in order to further reduce the organic component and pathogens in sludge.

Overall, development and application of attapulgite clay as a binder for immobilizing metals in contaminated soil and biosolids is a promising and cost-effective remediation technique under present market conditions. However, further research is needed in order to explore the mechanism that controls metal sorption by attapulgite clay. Once this is understood many more applications of this natural material will become possible.

5. Acknowledgments

The authors acknowledge the input of various collaborators from the industry and the local authorities in this research, including Edafomichaniki S.A., Thrace Non Wovens & Geosynthetics S.A., Municipality of Lavrion, Municipality and DEYA of Thera Island. Also we thank the postgraduate students E. Theologou and A.E. Gidaropoulou for their contribution in sampling and chemical analysis in two of the discussed projects. Special thanks are due to GEOHELLAS S.A. for supporting technically and financially the research on development of innovative environmental applications for attapulgite clay.

6. References

Álvarez-Ayuso E. and García-Sánchez A. 2003. Palygorskite as a Feasible Amendment to Stabilize Metal Polluted Soils, *Environmental Pollution*, 125, 337-344.

Basta N.T., Ryan J.A. and Chaney R.L. 2005. Trace element chemistry in residual-treated soil: key concepts and metal bioavailability, *Environ Quality,* 34, 49–63.

Brown G. E. Jr. and Calas G. 2013. Mineral-Aqueous Solution Interfaces and Their Impact on the Environment, *Geochemical Perspectives*, 1, (4-5), 483-737.

Cai Y. F. and Xue J. Y. 2008. A study of adsorption and ab-sorption mechanisms of copper in palygorskite, *Clay Minerals*, 43, (2), 195-203.

CEN/TS 14405, 2004. Characterization of waste-Leaching behaviour tests-Up-flow percolation test (under specified conditions).

Council Directive 2003/33/EC Establishing criteria and procedures for the acceptance of waste at landfills pursuant to Article 16 of and Annex II to Directive 1999/31/EC, 19 December 2002, *Official Journal of the European Communities*, L11/27 – 49.

EN 12457-4:2003. *Characterization of waste - Leaching; Compliance test for leaching of granular waste materials and sludges - Part 4: One-stage batch test at a liquid to solids ratio of 10 l/kg for materials with particle size below 10 mm.* European Committee for Standardization.

Fuerhacker M. and Haile T. M. 2011. Treatment and reuse of sludge, in: D.Barcelo and M.Petrovic (eds.) Waste Water Treatment and Reuse in the Mediterranean Region*, Hdb Env Chem*, 14, 63-92.

Galan E. 1996. Properties and applications of palygorskite-sepiolite clays, *Clay Minerals*, 31, 443-453.

Gidaropoulou A.E., Argyraki A., Zotiadis V. and Kacandes G. 2012. A laboratory scale study on sewage sludge treatment by attapulgitic clay, *Proceedings of 4th International Conference EEDSA: Solid Waste Treatment in Crisis* (ISBN: 978-960-6865-54-1). Athens, 30 November – 1 December 2012, 379-386.

Gionis V., Kacandes G.H., Kastritis I.D. and Chryssikos, G.D. 2006. On the structure of palygorskite by mid- and near-infrared spectroscopy, *American Mineralogist*, 91, 1125-1133.

Kollios A. and Zotiadis V. 2012. Design and Application of an Innovative Remediation Technique against Toxic Metals Contaminated Soil in Urban Areas, *Proceedings of 5th European Geosynthetics Congress (EUROGEO 5*), 16-19 September 2012, Valencia, Spain.

O´Day P.A. and Vlassopoulos D., 2010. Mineral-based amendments for remediation, *Elements*, 6, 375-381.

Potgieter J.H., Potgieter-Vermaak S.S. and Kalibantonga P.D. 2006. Heavy metals removal from solution by palygorskite clay, *Minerals Engineering*, 19, 463–470.

Shirvani M., Kalbasi M., Shariatmadari H., Nourbakhsh F. and Najafi B. 2006. Sorption–desorption of cadmium in aqueous palygorskite, sepiolite and calcite suspensions: Isotherm hysteresis, *Chemosphere*, 65, 2178–2184.

US Environment Protection Agency, 2003. Guidance on the use of Stabilisation/Solidification for the Treatment of Contaminated Soil, *R&D Technical Report* P5-064/TR/1.

Veli S. and Alyüz B. 2007. Adsorption of copper and zinc from aqueous solutions by using natural clay, *Journal of Hazardous Materials*, 149, 226–233.

VROM 2009. Soil Remediation Circular 2009, The Ministry of Housing, Spatial Planning and Environment, *Directorate General For Environmental Protection*, Netherlands.

Xie K., Jia X., Xu P., Huang X., Gu W., Zhang F., Yang S., and Tang S. 2012.The addition of modified attapulgite reduces the emission of nitrous oxide and ammonia from aerobically composted chicken manure, *Journal of the Air & Waste Management Association*, 2(10):1174–1181, 2012.

Zhang M. and Pu, J. 2011. Mineral materials as feasible amendments to stabilize heavy metals in polluted urban soils, Journal of Environmental Sciences, 23, 607-615.

Zhen Li, Lin Yin and Kun He. 2006. Iron-rich palygorskite: A potential clay material for contaminated environment remediation, *Chinese Journal of Geochemistry*, 25, Supplement 1/ March, 2006.

Zotiadis V., Argyraki A. and Theologou E. 2012. A Pilot Scale Application of Attapulgitic Clay for Stabilization of Toxic Elements in Contaminated Soil, *Journal of Geotechnical and Geoenvironmental Engineering*, 138, (5), 633-637.

Δελτίο της Ελληνικής Γεωλογικής Εταιρίας, τομ. XLVII , 2013
Πρακτικά 13ου Διεθνούς Συνεδρίου, Χανιά, Σεπτ. 2013

Bulletin of the Geological Society of Greece, vol. XLVII 2013
Proceedings of the 13th International Congress, Chania, Sept. 2013

REVEALING THE GEOHERITAGE OF EASTERN CRETE, THROUGH THE DEVELOPMENT OF SITIA GEOPARK, CRETE, GREECE

Fassoulas C.[1], Staridas S.[1], Perakis V.[2] and Mavrokosta C.[2]

[1] Natural History Museum of Crete, University of Crete, Heraklion 71409, Crete, Greece, fassoulas@nhmc.uoc.gr, staridasgeography@gmail.com

[2] Social & Cultural Development Organization of Sitia Municipality, Sitia 72300, Crete, Greece

Abstract

In the present document we present the main studies, actions, initiatives and infrastructure developed under the project GEOTOPIA aiming to develop a geopark at the easternmost part of Crete, in Sitia area. The developed activities may be considered as model to establish a geopark in a rural area under the provisions of European and Global Geoparks Networks, aiming intimately to a responsible tourist development. Study area includes the eastern coastal zone of Sitia municipality extended westwards to the Sitia mountains. It presents an impressive geological heritage constituted mainly by the landscape variations (including gorges, plateaus and long cave systems), hydrological resources, rock types and abundant mammal fossils. The project resulted in an inventory, mapping and evaluation of geotopes using existing methodologies, in undertaking conservation, educational and geotourisitc activities, among them the development of two educational projects, two local museums, 15 geotrails, outdoor panels and signposts, as well as printed, visual and web material. A management and action plan has been also conducted presenting the goals, the methodologies, the resources and the timetable to manage the area as a real geopark. Furthermore, the plan foresaw the interaction of geopark initiative in respect to other planned investments and activities in the area.
Key words: *Geoparks, Geoheritage, Geotourism, Sustainability, Sitia.*

Περίληψη

Η παρούσα εργασία αναφέρεται στις δράσεις, τις πρωτοβουλίες και τις υποδομές που αναπτύχθηκαν στα πλαίσια του έργου ΓΕΩΤΟΠΙΑ, με στόχο τη δημιουργία ενός γεωπάρκου στην περιοχή της Σητείας, στην Κρήτη. Το σύνολο των δράσεων αυτών μπορεί να θεωρηθεί ως ένα μοντέλο σχεδιασμού ενός γεωπάρκου σε μια αγροτική περιοχή κατά τα πρότυπα της υπεύθυνης και βιώσιμης ανάπτυξης που πρεσβεύουν τα Ευρωπαϊκά και Παγκόσμια Δίκτυα Γεωπάρκων. Η περιοχή μελέτης αφορά στην παράκτια και ορεινή ζώνη στα ανατολικά του Δήμου Σητείας που χαρακτηρίζεται από μια ιδιαίτερη γεωλογική κληρονομία την οποία απαρτίζουν οι ποικίλες μορφές του αναγλύφου, με χαρακτηριστικά φαράγγια, οροπέδια και επιμήκη σπήλαια, οι σημαντικές πηγές, τα ποικιλόμορφα πετρώματα και τα πλούσια απολιθώματα θηλαστικών. Το πρόγραμμα εστιάστηκε στην αναγνώριση, αποτύπωση και αξιολόγηση των γεωτόπων, στην ανάπτυξη δράσεων προστασίας, εκπαίδευσης και γεωτουρισμού, με τη δημιουργία δυο εκπαιδευτικών προγραμμάτων, δυο κέντρων ενημέρωσης, 15

γεω-διαδρομών, πινακίδων ενημέρωσης, καθώς και έντυπου, οπτικού και διαδικτυακού υλικού. Παράλληλα, προχώρησε στη σύνταξη ενός διαχειριστικού σχεδίου δράσης που έθεσε τους στόχους και αναγνώρισε τα μέσα, τις πηγές και το χρονοδιάγραμμα επίτευξής τους, και σχολίασε την αλληλεπίδραση της λειτουργίας του γεωπάρκου με άλλες αναπτυξιακές πρωτοβουλίες και έργα που σχεδιάζονται για την περιοχή.
Λέξεις κλειδιά: *Γεωπάρκα, Γεω-κληρονομιά, γεωτουρισμός, βιωσιμότητα, Σητεία.*

1. Introduction

Geological heritage has been well established as a term many centuries ago by the development of the first geological reserves and the initiatives to recognise and protect it, whereas its value is not only scientific and philosophical as many may argue but extents to economical, educational and touristic too (Ellis et al., 1994; Gray 2004). Accepting this fact, the field for discussing, analysing and considering geoheritage widens a lot, opening new opportunities for study, interpretation and conservation of geological environment.

It is a general trend of all organisations dedicated to the study and conservation of nature to combine development activities together with conservation actions, so that the one can support the other (Milton, 2002). The reason for this new approach is the increasing lack of sufficient funds to support nature conservation. The problem became apparent the last decades but has been magnified due to the economic crisis in Europe. The need to discover resources for study and conservation has been covered in many cases by the adaptation of sustainable development actions because only sustainable development can ensure the prosperity of the present generation and the wellbeing of future ones (Croall 1995; Smith and Rees, 1998). Thus many international organisations have focussed their efforts in identifying actions and means that can support such development activities adapted to the needs of sustainability.

The same has been started in geoheritage management by initiatives aiming, either to identify and promote geological and geomorphological features, or trying to conserve and study their value (Fassoulas and Zouros, 2010; Martini and Pages, 1994). The most successful among the others can be considered the initiative of *geoparks* that has been present in literature for several decades but became active just recently, serving the needs for modern nature management in the form of European geoparks (Zouros, and Martini, 2003). National geoparks or individual geotopes or geosites that have been recognised in many countries, are serving only the needs of conservation and study, with quite a few development activities. Digne Declaration for "the Rights of Mother Earth" established the scientific, philosophical and inherit value of geological heritage and set the basis for the development in 2000 of the European geoparks network (Martini and Pages, 1994).

The European Geoparks not only combine geoconservation and sustainable development as fundamental constituents of their existence, but work and collaborate together at a European scale to maximise the benefits of their actions (Zouros and Martini, 2003). The geoparks thus aim to protect and conserve geological heritage simultaneously with the development of various activities that serve the needs of education and information of visitors, attract tourists through geo-touristic and eco-touristic activities and support in various ways local economy and production. By a sufficient and central management, both geopark and local economy receive benefits to continue implementing actions and ensure the necessary economical resources (Fassoulas and Zouros, 2010). As a general rule, all geoparks have to keep high quality standards in services and products not only for the management structure, but also for the collaborating organisations and stakeholders of the geopark. This is ensured by the unique internal revalidation process that justifies every four years the ability of a geopark to achieve the goals and demands of a European geopark (EGN Charter: http://www.europeangeoparks.org/?page_id=357).

Another very important aspect of European geoparks that discriminates them from other similar or in general, nature protection initiatives, is the fact that they represent bottom up processes that are not governed or manipulated by central or governmental authorities. It is this the main reason that UNESCO has embraced since 2004 European Geoparks and used them as a model to develop the Global Geoparks Network assisted by the organisation. By the Madonie Declaration in 2004, all European Geoparks become automatically Global Geoparks Members.

Following these achievements, an increasing number of territories submit every year applications to become a geopark. Also in Greece, which currently hosts four European Geoparks, namely the Lesvos Petrified Forest, the Psiloritis Natural Park, the Helmos – Vouraikos and the Vikos – Aoos national parks, several territories have expressed their intension to create geoparks. In addition, several years ago a project was implemented by IGME to identify areas of important geological heritage and possibilities to create geoparks in several territories (Theodosiou, 2010).

However, the EGN internal evaluation process has become more strict and formalised in order to cope with the large number of applications and the fact that in several countries like Germany, Great Britain and Spain, a large number of geoparks already exists concentrated in many cases in few regions only. A fundamental question comes thus on the surface; namely, how to create and develop a geopark capable to become a European Geopark in future?

This document presents the basic steps that had been followed, under GEOTOPIA project, in order to create the necessary infrastructure, the facilities and the procedures to develop Sitia Nature Park as a geopark initiative, at the far eastern part of Crete, the Sitia Municipality, and to submit an application for a European Geopark membership in future.

2. Geoheritage Presentation and Analysis

In order to establish a geopark at the area of Sitia a certain strategy has been developed analysed in a series ofs steps, each one resulting in a robust deliverable. The first step was related with the inventory of geological, environmental and cultural features of the area, followed by the analysis and evaluation of geological environment and geotopes. A management plan was then conducted parallel with the development of the geotouristic and geoeducational activities. The final step was focused on the development of an action plan and the establishment of a management structure. The latest two steps are supposed to be completed by the summer of 2013.

2.1. Geological Setting of the Area

The area for the proposed geopark is located at the easternmost part of Crete and at the municipality of Sitia, covering the whole area of former Itanos and parts of the former Sitia and Lefki municipalities (Figure 1). It is characterized by a rich geoheritage which includes impressive rocks and geoformations from both the alpine and post-alpine units, as well as a great variety of landforms. The alpine units comprise the “Plattenkalk unit”, the “Phylites – Quartzites nappe”, the “Tripolitsa nappe” and the “Magassa unit” (Creutzburg et al., 1970; Fytrolakis, 1980). Additionally, the geopark includes large series of post-alpine rocks and especially units from the Miocene, Pliocene and Pleistocene eras (Peters, 1985).

The **Plattenkalk Unit**, is the relatively autochthonous on Crete meaning that it forms the base of the tectonic edifice constructed by the nappes that shape the island (Fassoulas et al., 1999). It includes pelagic, metamorphosed limestone, namely marbles, with very characteristic and distinctive dense bedding planes (Fytrolakis, 1980). Across the bedding planes cherts and other silica material are embedded. The age of these rocks is considered as Upper Jurassic to Oligocene, and their appearance in the area is restricted only at its northeastern part and especially in Cavo Sidero cape. The **Phyllite-Quartzite nappe** consists of pre-alpine and alpine in age, metamorphic rocks of blueschist to greenschist phases metamorphism and is tectonically posed upon plattenkalk rocks (Franz, 1992; Zulauf et al., 2002). Apart from metamorphosed, the rocks of this unit are also very intensely tectonised. Within the area of the geopark the most characteristic rock include purple

phyllites, schists, and quartzites with very impressive outcrops around Karidi, Zakros, at the beaches south of Vai and at the beach Maridati. Additionally, they include meta-conglomerates, and other metamorphosed sedimentary rocks, not to mention the unique red marbles dispersed at the regions between Vai and Toplou Monastery. The **Tripolitsa nappe** consists of a very thick sequence of shallow marine Triassic to Jurassic carbonate rocks including both limestone and dolomites (Creutzburg et al., 1977; Fytrolakis, 1980). In many places these rocks expose a very intense karstic weathering accommodating almost the total of the karstic geoformations of the park, namely the caves, the gorges, the springs and they also shape the most significant aquifers of the territory. These rocks dominate within the park and their outcrops are almost everywhere visible. Over the carbonate series are to be found Eocene flysch deposits comprising conglomerates, sandstone and clay. Tripolitsa rocks normally overlay Phyllites-Quartzites nappe. The **Magassa unit** is the equivalent of the broader Pindos nappe that overlie Tripolitsa rocks elsewhere (Fytrolakis, 1980; Zambetakis, 1977). It includes micro-breccia and oolithic, deep sea, light-colored limestone. These appear mainly around the village of Magassa (also known as Vrisidi), but also in very impressive outcrops at the beach of Agia Eirini, at the region between Ziros and Sitanos, as well as at Plativolo plateau where the Kato Peristeras cave is located. The contacts between these units are in most cases impressive low angle faults.

The **post alpine** sediments occur mainly at the areas along the northern coast and at the area of Zakros, consisting of Middle Miocene sediments (limestone, sandstone, marls and clay) attributed to Skopi, Kastri and Palekastro formations (Peters, 1985). Near the area of Agia Fotia and within the early Miocene Skopi sediments the *Deinotherium giganteum* has been excavated (Poulakakis, et al., 2005). The Pliocene and quaternary rocks occur mainly at the coastal zone in the area between Kato Zakros and Xerokampos, hosting the impressive Pleistocene mammal fauna of the area (Dermitzakis and de Vos, 1987; Kuss, 1980; Reese, 1996).

Landscape of the area is characterized by the presence of the large karstic areas constituted by the Tripolitsa and Magassa limestone. Vertical cliffs exist in many places, bounding the mountainous area from the coastal zone, whereas many gorges form either due to crustal uplift and weathering or due to coastal cave erosion. Various sized plateaus occur everywhere, together with many long, in some cases of several kms scale, caves (Platakis, 1975). Crustal uplift has also created another impressive landform feature in the area of Kato Zakros, that of the coastal terraces, that depict also the Pleistocene glacial sea level changes (Strobl et al., 2009).

2.2. Geotope Inventory and Assessment

Geological field studies and mapping identified more than 88 sites of geological importance in Sitia Nature Park that have been recorded using a template produced for the field inspection. Data collected refer to the geological and geomorphological characteristics of the geotopes, the existence of fossils or other important structures, the geodiversity of the site, the relations and connection to the broader ecological and human environment, aesthetic and visibility characteristics, existing activities and uses, as well as the protection and conservation status. According to the prevailing geological features, the geotopes were after attributed into several categories, like geomorphologic (analysed further into landforms, coastal, karstic, gorges and caves), geological (that are distributed in petrological and stratigraphical), tectonic (categorised further in tectonic, folds, and microtectonic), hydrogeological, fossiliferous, geocultural and geohistorical.

From the 88 geotopes that have been identified, 73 of them were then assessed using the methodology developed by Fassoulas et al., (2012), in order to recognise the touristic, educational, and conservation values (Figure 1). The rest geotopes refer to caves for which we couldn't collect sufficient data. According to this evaluation (Appendix 1) the highest **educational value** share two gorges the Kato Zakros and Moni Toplou, mainly due to their proximity to tourist and other landmark points, followed by the spring of Pano Zakros, the Voila Venetian settlement and the Pindos Tectonic nappe at Xirolimni. Regarding the **touristic value** the geo-archaeological site of

Kastri near Palekastro received the highest rank, closely followed by Maridati beach, the Kato Zakros gorge and the tectonic nappe at Xirolimni, whereas the Voila Venetian settlement and the Moni Toplou gorge got also high value. Due to these two results it becomes apparent that Kato Zakro and Moni Toplou gorges, Voila Venetian castle and settlement, as well as the nappe at Xirolimni appear the most important geotopes of the area in respect to geotourism and education.

Regarding the protection-conservation value (Appendix 1), the majority of the geotopes received values below 5 meaning that quite a few need protection measures and special conservation strategy. The most vulnerable appears the *Deinotherium giganteum* excavation site at Agia Fotia. However, as for the geopark needs, this area is a private land and thus the potential geopark is not allowed by itself to develop any conservation activities without the agreement of the owner. The next most vulnerable site appears the stone path at Magassa-Mitato villages, followed by the coastal caves at Agia Eirini bay and Karidi spring.

Compared to other areas of Crete where the same formula has been applied the results of Sitia geotopes present quite similar touristic and educational values than those of Psiloritis and Lassithi Mountains areas, and much lower compared to protection need values (Fassoulas et al., 2007; Fassoulas et al., 2012). Hence, the concentration of such a large number of impressive geotopes in a small area, and their relation to other geomorphological, environmental and cultural features of the area increase significantly their potential value.

3. Developing Geopark Activities

The next step following the inventory and analysis phases of this project was the design of certain geopark activities to interpret, promote and disseminate the value of geological heritage. These activities in a European geopark are mainly attributed in three basic categories, the interpretation, the educational and the geo-touristic, that in most cases can be combined to each other.

3.1. Interpretation Activities

The interpretation designed for Sitia Natural Park was shared into **insitu** interpretation, and in **printed** material. Insitu interpretation was mainly achieved by the designation and interpretation of certain *geotrails* and the development of outdoor *panels* that refer either to the established trails or to a specific geotope. According to the study and the assessment of geotopes, 15 trails were developed, some of them based on existing road network, some on pre-existing paths and some newly traced. From these trails four of are car or bicycle trails, whereas eleven of are trekking or hiking trails. Many of these trails can be used for various activities and can serve the various needs of a visitor. The trails run over all territory connecting geological, archaeological and touristic places of the area. The *information panels or signposts* are used mainly for the introduction of trails and have been set up at the most important attractions of the area and the places that a big concentration of visitors happens. These have thus been emplaced at the area of Epano and Kato Zakros villages, the Vai Palm Forest, the Moni Touplou Monastery, and the Karidi village. Their dimensions vary in size depending on the number of trails illustrated (Figure 2a). The geotopes' signposts are simpler displays located at the area of the most important geotopes.

Printed material on the other hand was designed for the various needs of visitors as well as the educational processes. The most important item is the *Geotouristic field guide* that has been produced including general and popularised information on the landscape and geology of the area, the natural and cultural environment as well as the main cultural assets in Greek and English language. A series of five bi-lingual *leaflets* has been also produced for the interpretation of the trails distributed in the various geomorphological and geographical areas of the geoparks. In addition, a big geomorphological and *geotouristic map* of a scale of 1:35000 has been produced. The map at its back-side includes again bi-lingual information on the geology of the area as well as on the various geotopes and the developed trails. Finally, a series of 13 small *posters* was also produced in great number for publicity needs.

3.2. Educational Activities

Two educational projects have been developed for Sitia Nature Park that both fit into the special geological, geomorphological and ecological features of the area. One is dedicated to cave and karstic environment, whereas the second explores and interprets the endemic animal and plant species. The educational projects have been designed as museum kits that occur in the form of suitcases, which can be transferred and implemented in many places and not only indoors. Both projects are based on educational pathways approach and on the concepts of inquiry and experiential based learning (Endelson et al., 1999). They include theory and instructions booklets, a number of educational activities that can be performed indoors and outdoors, games, as well as small models and exhibits. The educational projects are indented to be used at the facilities of the two information centres that have been developed in Zakros and Karidi villages, as no other official educational centre exists at the area. Both projects encompass experiential activities along two of the trails around Karidi and Zakros areas, urging children to experience the nature and geology of geopark.

3.3 Geo-Touristic Activities

Activities that are dedicated to support tourism in the area were focused on sustainable and responsible development (Smith and Rees, 1998). Issues of sustainability in tourism have long ago been established aiming to environmental integrity, social justice and maximising local economic benefit (Croall 1995). This philosophy runs across all products that have been designed for tourism in Sitia Nature Park, including the development of trails.

Thus, the main tourist actions developed so far refer to the development of two **information centers** that will act as contact and dissemination points. These have been established at the villages of Pano Zakros in the form of a Local Natural History museum and at the Karidi as a speleological center. *Local Natural History Museum of Zakros* hosts information on the natural environment of the territory, explaining the local geology and geological heritage in the form of posters, six small dioramas of ecosystems and two displays with representative samples of rocks minerals and fossils of the area (Figure 2b). The *Karidi Speleological center* will serve the needs of speleological research and dissemination. It provides all necessary infrastructures for accommodation and hosting of speleological groups and expeditions.

In addition to the developed infrastructure a **video** has been produced to present the values of landscape, geology, environment and culture of the area, contributing also to the dissemination purposes, the visualization of geopark and as a summary of the activities that have been developed. Finally, all information and products of this project have been uploaded in project's **website** that will act as the entrance gate to geopark's visitors, providing in two languages the activities that are developed, the opportunities existing in the area as well as any other tourist and visitor data (www.sitia-geopark.gr). The website hosts a series of interactive google-based maps that presents geotopes and geotrails in pop-up windows, whereas it offer downloadable files for mobile phones or GIS software (Figure 2c).

4. Putting Things Together

One of the most important prerequisites of a territory to be accepted as EGN member is to act already as a real geopark (Fassoulas and Zouros, 2010). It should thus have set all infrastructure and processes in action, should receive visitors and provide information and services to them and manage all activities and materials in a common and sustainable way.

To meet these purposes two further measures have been undertaken, the production of an Action and Management plan, as well as, after a public consultation the establishment of the Management structure that will be responsible for geopark management. The **management plan** is shared in three parts. The first refers to the inventory and recording of all special features of the natural,

cultural and economical environment putting emphasis on the geological heritage of the area. It includes also the evaluation of the geotopes and identifies the value and the strength of the main sites, resulting in a SWOT analysis. The second part deals with the development of a Strategic plan for geopark development presenting the vision for the operation as a geopark. This strategic plan is based on the provisions and consideration of responsible development putting emphasis on education, development of geotourism and conservation. Based on the evaluation of former part it also sets the priorities for the actions and the measures that have to be developed, sets the targets and recognises the means to achieve them. The third part presents the detailed action plan which summarises the goals and the actions to be undertaken, identifies the organisations, stakeholders, economical and human resources to be used for their achievement and sets the time table for their implementation.

The **public consultation** is one of the most important aspects of any development activity and has already started with discussions with the local authorities, the Foundation Panagia Akrotiriani that owns large properties in the area, as well as local trading and tourism associations, organisations dedicated to the conservation of nature (like WWF, Hellenic Speleological Society, etc.), as well as local inhabitants. For these reasons special meetings, public talks and informative events have been developed and also planned. The interest of all engaged organisations appeared considerably high especially due to other development activities that are planned for the area and have caused very serious arguments and objections. This may be identified as the reason that no Management structure has been set yet.

5. Discussion

The development of a geoprak is a challenging issue for many rural areas along Europe that host important geological features and wealthy environment. This effort regardless the money and resources spent is not always successful due the very crucial parameters that normally are not taken into account during the preparation phase. These parameters refer to the establishment of sustainable and responsible tourism and other development actions that will serve also the need for nature conservation and support of local communities. In addition, an issue that is also underestimated is the existence of a strong management structure that should coordinate all activities developed under the umbrella of the geopark, taking into account the will and opinion of local societies, basic constituents of any responsible development action.

The latter is not always considered seriously, and at the level the phrase “geoparks are not only for rocks, but rather for people” (oral expression by Chris Woodley-Stewart-North Pennines Geopark) summarises the philosophy of geoparks, leading to arguments with local societies and finally miss-functioning of geopark that may lead to its rejection during the evaluation phase. Furthermore, a crucial parameter that needs to be considered is that a territory should actively work as an already established geopark which means that education, conservation and geotouristic activities should be in place prior to application.

Considering all the above issues the project to develop the Sitia geopark was undertaken by the Natural History Museum of Crete and the Sitia Municipality Company for Cultural and Economic development. The effort was based on the scientific inventory, recording and mapping of geological heritage of the area and its further evaluation in order to reveal the individual value of each geotope and the capabilities for education and tourism, not excluding their vulnerability in such development activities and the conservation need. It also encompassed all existing information on the environmental, historical and cultural environment. The developed infrastructure, interpretation material and educational activities, were in accordance with a generic action and management plan that was finally delivered with progressive implementation of the project, aiming to sustainable and responsible development of this particular area under the means of a European geopark.

Regardless the important value of geological heritage, several factors point to the high potentiality of developing a geopark in this area. The first and most important is the inhabitants' willingness to develop and support sustainable development activities, respecting and conserving thus their unique environment, which is the base of all tourism activities developed so far. In addition, the area has a high tourism capability as its distance from the big cities of the island and the difficulties in transportation have resulted in a low tourism profile, with minor for the moment infrastructures, and mainly development of eco- and cultural tourism, for which the area is already famous. The third parameter is related to the fantastic cultural heritage which found its outmost expression on the local diet and cousin.

The model proposed under this geopark project is found by many individuals, as well as organisations of the area, as an alternative proposal to the extreme investments that are in progress in the area of easternmost Crete. These investments, although most of them are related to renewable energy -which from a first view appear environmental friendly- if considered under the provision of sustainability and responsible development, one may find significant contrasts especially on the issues that deal with the reduction of negative economic, environmental, and social impacts, the creation of greater economic benefits for local people and enhancement of the well-being of host communities, and their positive contribution to the conservation of natural and cultural heritage. The reasons for these arguments depend on several facts like their incredible size which occupies in many cases several hundreds of hectares on the mountainous area, the feature of these investments that either are water consuming or waste producing and for which both results there is not yet a clear solution, and finally, that are actually implemented in most cases without the positive opinion and acceptance of local communities. Furthermore, these investments due to occupation of large areas, actually lead into fragmentation of natural environment, landscape modification and increase of threats to species and ecosystems.

Considering the management plan developed for geopark and the activities that have been scheduled, the operation of many of these investments, especially at the mountains areas is not consistent with concept developed for the Sitia Nature Park, but also for the geopark initiative itself. Many of the existing trails need to be modified as they cross areas of large investments, the changes of landscape in some areas can be considered as irreversible and tremendous for the scale of the landscape and the operation of these activities can not be in accordance with visitors' attraction needs. During public consultation all aspects and arguments have been exposed, identifying that both initiatives find supports at local societies and authorities. However, only the implementation of the management plan and the operation of the geopark will prove if these various investments can coincide with a geopark and which of the two approaches is more proper of the culture and local characteristics of Sitia.

6. Acknowledgments

Project GEOTOPIA has been co-financed under the INTERREG IIIC Cross border collaboration, Greece – Cyprus 2007 – 2013 program. Two anonymous reviewers are thanked for their critical comments.

7. References

Creutzburg N., Drooger C.W., Meulenkamp J.E., Papastamatiou J., Seidel E. and Tataris A., 1977. Geological map of Crete (1:200.000), IGME, Athens.

Croall, J. 1995. Preserve or Destroy: Tourism and the Environment. London: Calouste Gulbenkian Founation. P. 61.

Dermitzakis M., and de Vos J. 1987. Faunal succession and evolution of mammals in Crete during the Pleistocene. Neues Jahrbuch Geologischer und Palaeontologischer, Abh., 173, 377-408.

Gray M. 2004. Geodiversity: valuing and conserving abiotic nature, J. Wiley &Sons, Ltd, New York, 434pp

Milton K. 2002. *Loving Nature: Towards an Ecology of Emotion*. Routledge, London.
Edelson, D., Gordin, D., & Pea, R., 1999. Addressing the Challenges of Inquiry-Based Learning Through Technology and Curriculum Design, *Journal of the Learning Sciences* 8(3), 391-450.
Ellis N.V. (ed), Bowen D.Q., Campbell S., Knill J.L., McKirdy A.P., Prosser C.D., Vincent M.A. and Wilson, R.C.L, 1996. An introduction to the Geological Heritage Conservation, *Joint Nature Conservation Committee*, 132 p.
Fassoulas C. 1999. The structural evolution of central Crete: Insight into the tectonic evolution of the south Aegean, *J. Geodynamics*, 27, 23-43.
Fassoulas C. and Zouros N. 2010. Evaluating the influence of the Greek geoparks to the local communities, *Bull. Geol. Soc. Greece*, XLIII (2), 896-906.
Fassoulas C., Paragamian K. and Iliopoulos G., 2007. Identification and assessment of Cretan Geotopes, *Bull. Geol. Soc. Greece*, vol. XXXVII, 1780 – 1795.
Fassoulas C., Mouriki D., Dimitriou-Nikolakis P. and Iliopoulos G., 2012. Quantitative assessment of geotopes as an Effective tool for geoheritage management, *Geoheritage*, 4(3), 177-193.
Frantz L., 1992. Die polymetamorphe Entwicklung dew Altkrystaline auf Kreta und Dodekanes (Griechenland): Eine geologische, geochemische und petrologische Bestandsaufnahme. Diss. Enke Verlag, Stuttgart.
Fytrolakis N., 1980. The geological structure of Crete. Problems, observations and conclusions. *Habil. Thesis*, Nat. Techn. Univ. Athens, pp. 143.
Kuss S.E. 1980. Führer Zur Kreta-Exkursion, Des geologisch-paläontologischen Institutes der Universität Freiburg/BR, pp. 51.
Martini G. and Pages J.S. (eds) 1994. Actes du premier symposium international sur la protection du patrimoine geologique, *Memoires de la Societe geologique de France*, 165p.
Peters J.M. 1985. Neogene and quaternary vertical tectonics in the south Hellenic arc and their effect on sedimentation processes, *PhD Thesis*., GUA papers of Geology, Ser. 1, no. 23. Amsterdam.
Platakis E. 1975. Caves and other kartsic forms of Crete, Vols. A'& B', Irakleion, Crete.
Poulakakis N., Lymberakis P., Fassoulas C., 2005. A *Deinotherium giganteum* KAUP, 1829 (Proboscidea, Deinotheriidae) from the middle Miocene of Siteia (East Crete, Greece), *Journal of Vertebrate Paleontology*, 25(3), 732–736.
Reese D.S., 1996. Pleistocene and Holocene Fauna of Crete and its First settlers. Monographs in world Archaeology No. 28., Prehistory Press. Wiscosin.
Smith C. and Rees G. 1998. Economic Development, 2nd edition. Basingstoke: Macmillan. ISBN 0-333-72228-0.
Strobl M., Hetzel R., Ivy-Ochs S., Alfimov V., Kubik P.W., Fassoulas C. and Palumbo L. 2009. A long-term rock uplift rate for eastern Crete from exposure dating of marine terraces, *Geophysical Research Abstracts*, Vol. 11, EGU2009-1953-1.
Theodosiou I. 2010. Designation of Geosites – proposals for geoparks in Greece, *Bull Geol. Soc. Greece*, XLIII (2), 926-938
Zambetakis A., 1977. Stratigraphie et structure de la serie de Mangassa (Crete orientale, Grece). *These* Univ. Curie (Paris), 65pp
Zouros N. and Martini G., 2003. Introduction to the European Geoparks Network, in Zouros N., Martini G. and Frey M.L. (eds) : *Proc 2nd European Geoparks Network Meeting*, Mytilene, Greece, pp17-21
Zulauf G., Kowalczyk G., Krahl J., Petschick R. and Schwanz S., 2002. The tectonometamorphic evolution of high-pressure low-temperature metamorphic rocks of eastern Crete, Greece: constraints from microfabrics, strain, illite crystallinity and paleodifferential stress, *J. Struct. Geol*, 24, 1805-1828.

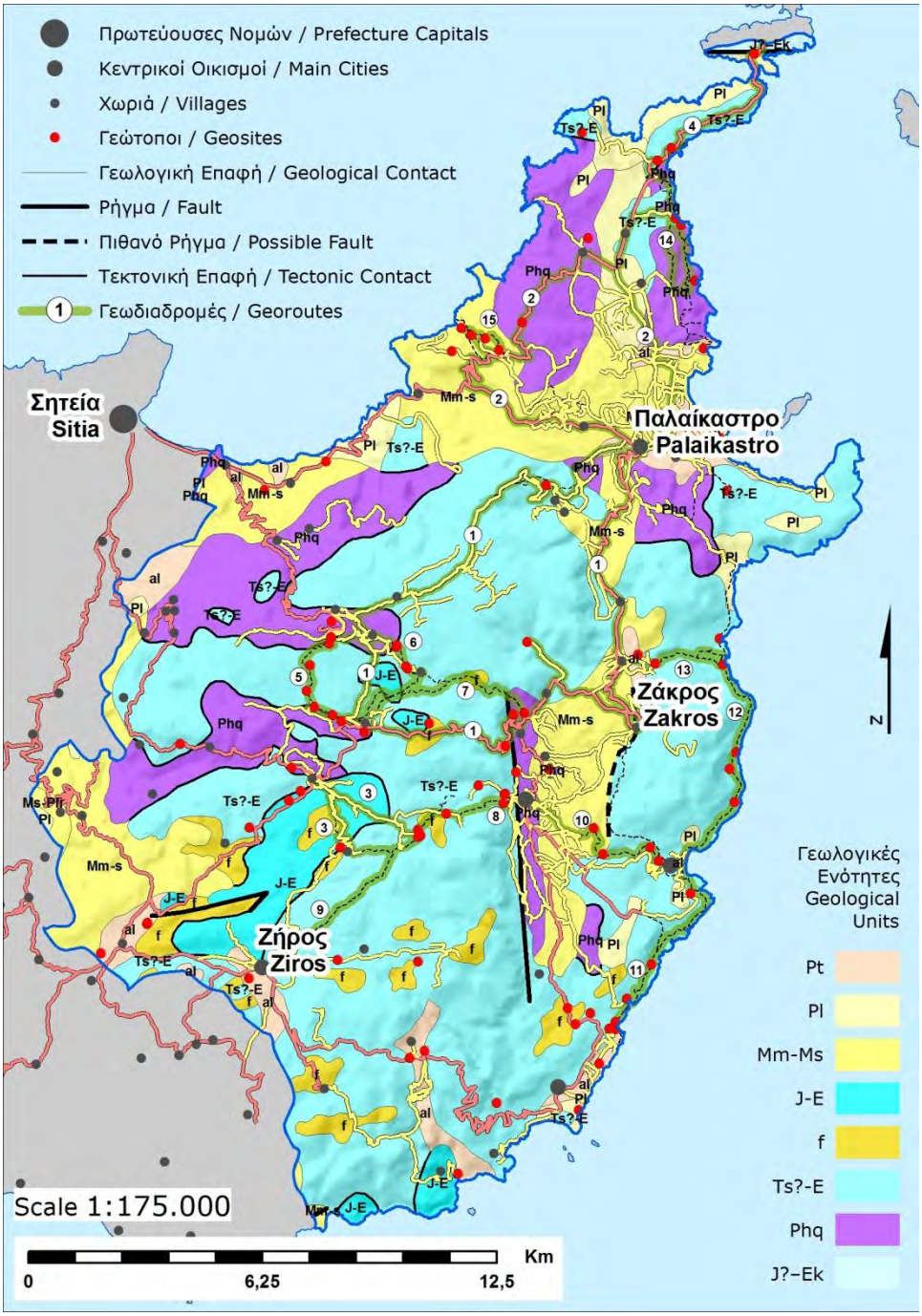

Figure 1 – Simplified geological map of Sitia Nature Park based on Creutzburg et al., 1977 and field studies. Pt, Pleistocene seds.; Pl, Pliocene seds.; Mm-Ms, late Miocene seds.; J-E, Magassa Unit; f, Tripolitsa flysch; Ts?-E, Tripolitsa limestone; Phq, Phyllites-quartzite nappe; J?-Ek, Plattenkalk rocks.

a.

b.

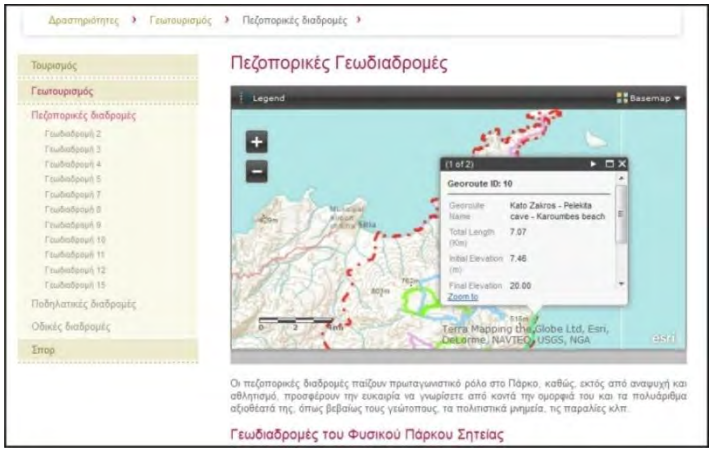

c.

Figure 2 – Images of developed products. a. One of the outdoors panels; b. The Epano Zakros Natural History Museum; c. Capture of project's website with the interactive presentation of geo-trails.

Appendix 1: Sitia Nature Park Geotope assessment

Code	Name	λ	φ	V_{edu}	V_{tour}	V_{prot}
1.1.1	Mavro Mouri Tafoni	26,199143	35,222256	2,88	2,44	2,44
1.1.2	Toplou Monastery Tafoni	26,213046	35,222269	5,23	5,61	3,38
1.1.3	Rock Garden	26,211301	35,112922	4,15	4,31	3,17
1.1.4	Quartzite Walls	26,164487	35,133511	4,26	5,64	2,63
1.1.5	Zakros Boulders	26,279056	35,111859	3,68	4,37	2,9
1.1.6	Kastri Hill	26,277546	35,199825	5,05	6,63	2,88
1.2.1	Katsounaki Sand Dunes	26,242658	35,05778	4,89	3,02	3,41
1.2.2	Psili Ammos Sand Dunes	26,267285	35,251316	4,41	2,68	3,24
1.2.3	Xerokambos Salt Lake	26,237683	35,049575	5,63	3,78	4,42
1.2.4	Hiona Salt Lake	26,277373	35,196582	4,05	3,93	3,56
1.2.5	Coastal Caves Ag Irini bay	26,19557	35,023841	3,7	3,2	4,83
1.3.1	Mavros Kambos	26,19457	35,110634	2,73	3,38	4,17
1.3.2	Zakanthos	26,16324	35,103126	3,53	3,48	4
1.3.3	Handras Plateau	26,092466	35,078751	2,9	4,62	4,5
1.3.4	Ziros Plateau	26,135648	35,0721	2,9	4,62	4,5
1.3.5	Karstic Karrens	26,240842	35,057936	3,31	2,94	1,91
1.4.1	Katsounaki Gorge	26,235495	35,061772	6	4,8	3,83
1.4.2	Kato Zakros Gorge	26,256424	35,098213	7,58	6,48	4,17
1.4.3	Epano Zakros Gorge 1	26,211936	35,115171	3,38	3,11	4,33
1.4.4	Epano Zakros Gorge 2	26,215207	35,120251	4,8	5,17	3
1.4.5	Hohlakies Gorge	26,256821	35,145675	3,88	3,77	3,83
1.4.6	Xerokambos Gorge	26,207515	35,040685	4,25	4,14	2,06
1.4.7	Maza Gorge	26,218053	35,134572	3,73	3,55	2,83
1.4.8	Toplou Monastery Gorge	26,209024	35,225151	6,95	5,68	4,33
2.1.1	Plakoures	26,289982	35,292258	4,6	3,64	2,71
2.1.2	Megali Kefala	26,271085	35,237791	4,6	2,94	2,78
2.1.3	Red Marbles	26,260783	35,267015	4,16	3,7	2,34
2.1.4	Red Metamorphic siltstones	26,214782	35,13417	3,41	5,17	3,8
2.1.5	Maridati	26,273113	35,221557	5,78	6,28	4
2.1.6	Tripolitsa Flysch	26,182183	35,051962	4,45	5,3	3,83
2.1.7	Argilos (Clay)	26,231421	35,038492	4,95	3,83	3,44
2.2.1	Karoumbes Unconformity	26,276656	35,145028	3,43	4,12	2,5
2.2.2	Rousso Spasma	26,246211	35,065047	5,45	3,94	3,28
2.2.3	Agia Fotia Unconformity	26,161591	35,196281	3,8	4,77	3,5
3.1.1	Erimoupoli Detachment Fault	26,264978	35,269997	4	3,4	3,04
3.1.2	Katsidoni Detachment Fault	26,116944	35,128889	2,9	3,4	3,17
3.1.3	Kato Zakros Detachment Fault	26,240173	35,100044	4,1	4,17	3,04
3.1.4	Xirolimni Tectonic Nappe	26,16209	35,157665	6,1	5,83	3,83
3.1.5	Adravastoi Detachment Fault	26,212442	35,126553	4,25	5,2	3,67

Code	Name	λ	φ	V_{edu}	V_{tour}	V_{prot}
3.1.6	Skalia Detachment Fault	26,186143	35,106884	2,68	3,22	2,33
3.1.7	Katsounaki Detachment Fault	26,230936	35,05919	3,85	4,17	2,71
3.2.1	Agrilia Fault Scarp	26,228809	35,063171	4,85	4	4,38
3.2.2	Hamaitoulo Fault Scarp	26,186634	35,053574	3,8	4,07	3,73
3.3.1	Vai Fold	26,265561	35,252968	4,8	3,47	2,88
3.3.2	Profitis Ilias Folds	26,21995	35,228764	4,2	3,87	3,21
3.4.1	Dandoula's Microtectonic Formations	26,180952	35,151134	4,8	4,94	3,67
3.4.2	Magassa Cataclasite	26,184181	35,145828	3,5	3,5	3,67
4.1.1	Karidi Spring	26,171025	35,130679	4,58	5,52	4,67
4.1.2	Epano Zakros Spring	26,211672	35,114971	6,43	5,49	5
4.1.3	Flegas Spring	26,219428	35,151684	5,43	3,14	3,67
4.1.4	Skalia Spring	26,186178	35,105149	3,95	3,08	4
4.1.5	Toplou Monastery Spring	26,202039	35,22779	5,95	3,11	3,61
5.1.1	Epano Zakros Roudists	26,204084	35,117225	3,11	2,33	3,27
5.2.1	Zakros Deinotherium	26,224871	35,120783	1,91	1,96	4,63
5.2.2	Gela's Deinotherium	26,143297	35,189682	3,23	2,22	5,73
5.2.3	Kato Zakros Corals	26,237731	35,106384	2,83	2,81	3,03
5.2.4	Karoumbes Corals	26,27582	35,151409	3,95	3,01	4,17
5.2.5	Toplou Monastery Corals	26,204945	35,226019	3,25	2,34	2,04
5.2.7	Trapeza Urchins and Bivalves	26,238903	35,274174	3,08	2,32	2,73
6.1.1	Petrokopio Ancient Quarry	26,23997	35,248703	3,83	3,94	3,57
6.1.2	Katsounaki Ancient Quarry	26,242744	35,059617	3,73	3,27	2,04
6.1.3	Molivokamino Ancient Quarry	26,253654	35,073189	3,73	3,27	2,04
6.1.4	Pelekita Ancient Quarry	26,279831	35,123928	4,33	3,87	2,28
6.1.5	Petsofas Summit Sanctuary	26,2789	35,187083	3,83	3,94	3,57
6.1.6	Voila Venetian Castle	26,106111	35,08559	6,11	5,81	3,32
6.1.7	Voila Fountain	26,106351	35,085863	2,58	3,18	4,17
6.2.1	Chonos	26,161958	35,153903	3,51	4,1	3,97
6.2.2	Lydia	26,225889	35,189456	3,31	4,1	3,8
6.2.3	Kamares	26,251883	35,147913	3,31	4,1	3,8
6.2.4	Skalia	26,18701	35,105555	2,55	2,9	3,67
6.2.5	Magassa – Mitato Stone Paved Old Path	26,183649	35,146405	4,34	5,23	5,13
6.2.6	Lamnoni Stone Paved Old Path	26,161706	35,075962	3,44	5,08	3,97
6.2.7	Karidi – Agios Ioannis Stone Paved Old Path	26,161859	35,134984	3,51	4,3	3,8

Δελτίο της Ελληνικής Γεωλογικής Εταιρίας, τομ. XLVII , 2013
Πρακτικά 13ου Διεθνούς Συνεδρίου, Χανιά, Σεπτ. 2013

Bulletin of the Geological Society of Greece, vol. XLVII 2013
Proceedings of the 13th International Congress, Chania, Sept. 2013

GIS AS AN EDUCATIONAL TOOL: MAPPING CULTURAL SITES IN GREEK SPACE-TIME

Galani L.[1], Theodorakopoulou K.[2], Skentos A.[2], Kritikos G.[2] and Pavlopoulos K.[2]

[1] National and Kapodistrian University of Athens, Faculty of Primary Education, ligalani@pimedu.uoa.gr,

2 Harokopio University, Department of Geography, ktheodo@hua.gr, thanskentos@hua.gr, gkriti@hua.gr, kpavlop@hua.gr

Abstract

This paper deals with the cartographical presentation of cultural succession in Greek space-time associated with core concepts of geographic and historical education. The pedagogic value of this study is to develop five distinct skills: sense of time-scale, historical and geographic comprehension, spatial analysis and interpretation, ability to perform geo-historical research, and procedure of geo-historical decision-making.

The methodology is based on the calibration of a set of criteria for each cultural site that covers the topics of economy, geomorphology, society, religion, art and science. Further analysis of these data forms a geodatabase. In addition, palaeogeographic and historical maps of the cultural sites derived by the geodatabase provide information about temporal and spatial changes. As result, students will be able to develop a multidimensional and interdisciplinary approach, in order to reconstruct the evolution of the site.

Key words: *geoarchaeology, palaeogeography, data base, education.*

Περίληψη

Το θέμα της παρούσας εργασίας είναι η χαρτογραφική παρουσίαση της πολιτιστικής διαδοχής στον ελληνικό χωρο-χρόνο που σχετίζεται με βασικές έννοιες της γεωγραφικής και ιστορικής εκπαίδευσης. Η παιδαγωγική αξία της μελέτης είναι η ανάπτυξη πέντε διακριτών δεξιότητων: της έννοιας του χρόνου-κλίμακας, της ιστορικής και γεωγραφικής κατανόησης, της χωρικής ανάλυσης και ερμηνείας, της ικανότητας διεξαγωγής γεω-ιστορικής έρευνας, και της γεω-ιστορικής διαδικασίας λήψης αποφάσεων.

Η μεθοδολογία βασίζεται στη βαθμονόμηση μιας σειράς κριτηρίων για κάθε πολιτιστική περιοχή που καλύπτει τα θέματα της οικονομίας, της γεωμορφολογίας, της κοινωνίας των πολιτών, της θρησκείας, της τέχνης και της επιστήμης. Η περαιτέρω ανάλυση αυτών των δεδομένων οδηγεί στη δημιουργία μιας γεω-βάσης. Οι παλαιογεωγραφικοί και ιστορικοί χάρτες των πολιτιστικών χώρων που προέρχονται από την γεωβάση παρέχουν πληροφορίες σχετικά με τις χρονικές και χωρικές μεταβολές. Ως αποτέλεσμα, οι μαθητές θα είναι σε θέση να αναπτύξουν μια πολυδιάστατη και διεπιστημονική προσέγγιση, προκειμένου να ανακατασκευάσουν την εξέλιξη του τόπου.

Λέξεις κλειδιά: *παλαιογεωγραφία, γεωαρχαιολογία, βάση δεδομένων, εκπαίδευση.*

1. Introduction

This paper reports a project taking place in the department of Geography of the Harokopio University, Athens, Greece. The project focuses on Digital Palaeogeography and specifically the cartographical presentation of cultural succession in Greek space and time (Choro-Chronos). What makes the subject of the program particularly important is its association with core concepts of geographic and historical education. The paper is structured in three different parts. The first consists of a review in other similar projects in the fields of Geography, History, Education and GIS. In the second part the authors describe the methodology, the tools they create and how tools are involved to the education. In the end of the paper the implications present authors opinion about the development of the project.

Geography and History in Greek school curriculum are two discrete subjects. Geography is focused on space, with increasingly complex definitions of what space itself is (Lefebvre, 1991). Most individuals define geography as a field of study that deals with maps. This definition is only partially correct. Spatial patterns play a central role in the subject. For the majority of its existence, Geography has used a spatial foundation to understand both the physical and human environment and how natural and human constructed phenomena are related to a spatial dimension.

On the other hand History has, as a central study, the human activity. The aim of the subject is to understand the past and to build a developing picture of how change has happened over time. In part the subject attempts to give a synthetic view of how humans, at a number of time scales, adapt and change.

History and Geography are disciplines which both attempt to understand the world around us through critical analysis of people and their environment. Time and space are inextricably linked, and cannot therefore be divorced and as Massey noticed '…time and space must be thought together... Thinking of time and space together does not mean they are identical (for instance in some undifferentiated four-dimensionality), rather it means that the imagination of one will have repercussions (not always followed through) for the imagination of the other and that space and time are implicated in each other….Thinking about history and temporality necessarily has implications (whether we recognize them or not) for how we imagine the spatial.' (Massey, 2005).

Although at an academic level the approaches of humans and their environment have the potential for the building of a holistic understanding, at the school context (school history and school geography) the barriers of historical and geographical approaches still remain and the two subjects have different content and approaches. A range intersection of History and Geography seems to be Palaeogeography which can be defined as the study of geographical features at periods in the geological past and on the same time the understanding in a variety of contexts such as the study of physical landscapes, but also the study of human or cultural environments.

However, are we able to help students understand that 'time and space must be thought together' developing a learning resource to achieve this more holistic understanding of humans and their environment?

The answer lies in the field of technologies. In order to teach "thinking geographically" many organizations and individuals promote the use of GIS in K-12 geography education (Baker and White 2003; Ludwig et al. 2000; West 2003) According to Baker (2005), the integration of Geographic Information Systems (GIS) in schools could be a solution. GIS, as an instructional technology, has been used not only in the formal but also in informal education all over the world for more than fifteen years as well, in order to be approached significances such as the ecosystems, the demographic characteristics of places, the immigration, the natural destructions, etc. Moreover, through GIS students develop spatial analysis skills, a critic sense on spatial management and encourage them to contact research and to work in groups. GIS make students aware of the importance of geographic information on studding the past and on spatial management.

The development of Historical Geographic Information Systems (HGIS), over the past decade, has been a prospect to use the functionality of GIS systems to interrogate historical spatial data, for example old maps, census data, changing and evolving transport links, or population migrations.

In the U.S.A. there is also an initial attempt to make HGIS style resources open to school-level study. Historical Census Data developed by the University of Illinois at Chicago (Randinsky et al. 2008; GIS for History 2005-20011) was a project which - according to the instructors- make historical census data available to teachers and students in the form of on-line interactive data maps, displaying selected census data for each decade (1790-2000) on US maps at the county level.

2. Methodology - Data Base

2.1 Objectives of the Project

According to Vygotsky (1976) individuals make sense of the world around them by actively creating knowledge and understanding. The main scientific and technical objectives of the project are to:

- Understand that space and time need to be 'thought together', in order students to make use of models of spatial thinking,
- Identify that a GIS style platform would offer a critical medium through which the spatial thinking could be developed,
- Create an interactive platform to present spatio-temporal changes in Greece,
- Encourage generation of deep learning and critical analysis of geography and history through the spatio-temporal lens.

2.2 Defining Criteria for the Geoarchaeological Sites

Our scientific team determined some criteria for the selection of the most suitable archaeological-historical sites. Among the criteria adopted for determining a particular period as a 'learning object' was the duration of its effects, the number of people affected by this, the perceived importance of the event by more people and the different manifestations of social space within the specific period. This will help students to form their own comprehensive mental map.

With this in mind, this research program involves archaeological sites and selected sites. Although it is addressed to the average reader, is seeking the awareness of the public to the basic methods of archeology. This is consistent with the view of Tilden who considers that the interpretation of material culture "should encourage the public to think alone and not telling him what to think".(Tilden, 1977).

Considering all the above theories on the concept of the importance of timing, in the first phase we defined some qualitative criteria for the selection sites:

1) **Palaeogeography-natural geomorphic processes**. The space is a dynamic system that is evolving and adapting continuously to changing influences. Man is part of the space and he intervenes actively in its formulation. Through the study of space and natural processes made at different times, it is possible to explore and highlight: a) the way in which people have adapted their lives to the topography and climate, b) how changes occurring in the natural environment affected the lives of people, c) the possible drastic changes done by people in the environment and ultimately their effects in everyday life.

2) **Economic, social space (architectural, everyday objects):** The study of material remains of the past, helps in the understanding and interpretation of economic, social, political and cultural structure of social groups that created them and the study and research of popular culture

3) **Sacred places-places of worship:** The sacred places are inextricably tied to the organization of human life. Through religion people were expressed: building temples, carving statues, painting pictures, decorating buildings. Religion is not only a belief in a deity, but something deeper setting their lifestyle, the form of the family, the dietary habits, the social relations and the economy. The worship rituals characterize the integral part of life and culture of each period.

4)**Science-technology:** The use of technology by the human race began with the conversion of natural raw materials into simple tools. Both science and technology is a sign of progress and civilization.

5) **Writing:** Writing is a symbolic, visual language system log. Through the writings handed down from generation to generation, the language, the ideas, the habits of communities were transferred.

6) **Networks-communication:** The term of networks is very broad. It includes the necessary infrastructure for the development of cities or villages. We can distinguish from ancient period the transportation networks involving land roads and sea routes. These roads were also routes for trade, communication, economy, exchange of cultures, tastes, knowledge and language.

7) **Residence:** The time in space is reflected in the form of the material remains. The structure of houses, their architecture and the organisation of towns is reflecting the type of everyday life, the civilization and the organisation of societies.

2.3 The Platform: Description and Architecture Design

Further analysis of these data forms a geodatabase. The data base as a product of the process and as an educational tool, gives the ability to create documents, to organize and present the information, to investigate and analyze quantitative data to categorize and classify the information, based on specific criteria. In addition, palaeogeographic and historical maps of the sites derived by the geodatabase provide information about temporal and spatial changes.

The platform will contain spatial/mapped representations of different 'places' through a number of time slices. The maps which form this basic platform have tagged points, behind which exists a 'database' of information and other resources (ex. pictures, sketches, draws, representations, articles, scientific papers, etc.) which can be interrogated by users.

2.4 Analyzing Changes in Conditions Through Time Using Digital Palaeography

A good Geography and History lesson focuses on getting students think geographically and historically. However, how "thinking Geographically" and Historically can be effectuated in the classroom using the "Digital Palaeogeography platform"? Topics related to the geographic understanding of land change and land use change, are: the location of ancient cities and their growth through the time, the location of the temples and of the sacred places, the trade in Aegean Sea, the transportations in the mainland, etc.

The case study cited below presents an application of the project in the classroom. Let's suppose that students according to the curriculum have to study the topic of " Piracy in Aegean Sea".

Possible geographical questions to excite their curiosity are:

- "Do you think that piracy has existed in Greece from ancient time?"
- "If yes, where did pirates live?" (location)
- "How did they choose a place to keep safe their treasure?" (place)
- "What is it like in this place?" (conditions)
- "If you were a pirate, which place in Greece would you choose to settle? (region)
- "How is this place linked to other places?" (connections, links)

- "How are the places you choose similar or different?" (comparison)

All these questions help students identify how the physical geography affected the settlement of islands by the pirates and generally how the geography of Greece influence where people settled and if Braudel's phrase "the islands of the central and eastern Mediterranean, gained a special importance when linked into strategic routes of commerce and defence" has a meaning.

From the movies, piracy is strongly connected to the Caribbean. Using their experiences, students can discuss and set criteria to choose a place where pirates might live.

Exploring the map, they find suitable locations, they write words describing what these places look like and they infer how these descriptions meet the criteria they set before. Data sources availability for each place including features interpreted from diverse data sources ex. historical topographic maps, satellite images, pictures and gravures, in conjunction with historical significance, determines how places that are mapped in the time periods, are connected to the piracy.

Their research using the maps and the database of the project demonstrate that:

1. Pirates using to work in Aegean Sea are faced with a characteristic series of choices, which depend on the character of the islands and the landscape, the volume of traffic, and the wealth of the communities. Piracy began soon after people first used water to carry trade goods from one place to another.
2. Merchant ships of the ancient world usually sailed close to land in going from one destination to another. Pirates chose to live along rocky shores, coves or inlets that provided shelter and kept them hidden from view, therefore it was easy for them to attack their "victims". These safe bases had several things in common: a) Close proximity to strategic - economic value trade routes maritime shipping used, b) Isolated locations that discouraged pursuers from following,
3. Ancient pirate bases in Aegean Sea included islands such Milos, Crete, Andros, Syros, Rodes.

During this "trip" around the islands and the exploration of the piracy world, students may discover that at least one of the ports, Phalasarna, located in the middle of the west coast of Crete, was established far away from the sea. Why pirates choose this place? Did they move their ships to the land to keep them safe? That seems a good problem for them to solve.

Reading all the information from the database, students discover that the city of Phalasarna was already inhabited in the Middle Minoan period, while its development is depicted by the Archaic and Classical tombs discovered in the nearby area. In the middle of the 4th century, the city was at its peak. A port was constructed and city's strategic position in-between the Aegean - Egypt and Western - Eastern Mediterranean Sea crossroads thrust the city to issue coins and to develop naval trade. After the 2nd century B.C. the port was used as a pirate den. The Romans destroyed the city in 67 B.C., most probably because of its turning to piracy.

Using the map and the ability of zoom in, students realise that the port of Phalasarna was established in an existing basin, which was reshaped. Access to the open sea was achieved by building a 100m long canal from the port to the sea that was also functioning as a drainage work and kept it safe. Total annihilation occurred during the 4th century A.D., probably in 365 A.D., when the whole area rose by about 6.6m due to a severe earthquake (figure 1).

Students through that information can explain why Phalasarna is pointed in inland. The buried of the city and the port by tectonic action, shows that landscapes change through time, sometimes slowly, other times violently (transition, change). The study of the geoarchaeology helps them to understand and to explain the strong connection between the landscape and the humans.

Figure 1 - The map of the project. Phalasarna's coastline now and then (zoom in) is presented in the second picture.

2.5 Pedagogic Value of the Platform

The pedagogic value of this project lies in the development of five distinct skills:

a) **Sense of time and scale which is significant to the Chronological thinking**: Students will be able to distinguish between past, present, and future geological and historical time. Time - scale provides the mental map for organizing humans' thought. Having a strong sense of time thought a time line data presentation – ex. of when geological or historical events occurred and in what order- students should be able to examine relationships and to explain the causality among those events. Students should also be able to analyze patterns of succession, for example, the networks of trade and communication in Aegean Sea over the time.

b) **Geographic and Historical Comprehension**: Maps, photographs, paintings, documents and information presented in the geo-historical narrative/information of the database help students to obtain or clarify information on the geographic setting in which a temple or a colony was situated or a historical event occurred. They can also notice the relative and absolute location of the features (places, monuments, temples, etc.) they study, the distances and directions between them, the natural and man-made features of the place, and critical relationships in the spatial distributions of those features and the event occurring there.

c) **Analysis and interpretation of geographic space**: GIS analysis is a process which helps students to see patterns and relationships between features and to interpret the geographical data. They can find out why things are where they are, how things are related and how changes happened through the time and to create new information which helps them to gain a deeper understanding of places. Through the GIS palaeogeographic map, students should be to analyze cause-and-effect relationships bearing in mind multiple causation including the importance of the individual in changes, the influence of ideas and beliefs and the role of chance.

d) **Ability to perform geo-historical research**: Students through digital palaeogeography will be encouraged to develop and implement a research action plan following specific steps such as: to identify the aim/purpose of the investigation, to generate a number of questions to be addressed by the investigation, to collect and use primary and secondary data, to decide which primary and secondary data are needed to answer the questions, to propose individual or team action in response to the research findings.

e) **Analysis interpretation of geo-historical decision-making**: Issue-centered analysis and decision-making activities place students at the center of geo-historical dilemmas and problems faced at critical moments in the past and the near-present. Students evaluate

alternative courses of action, keeping in mind the available information, the interests of those affected by the decision, and the long- and short-term consequences of each.

As result, students will be able to develop multidimensional, evidence driven approach, in order to answer questions and to "rebuild" the historical “Chorochrono” through interdisciplinary and methodological pluralism which characterizes the modern geography, suppressing the barriers between the sciences.

3. Implications

The project will be completed by September 2013. According to the researchers of the project, roaming in Greece with the help of the GIS platform, is an alternative but very important “tool” for the Geography lesson, that allows students to explore the earth at a potential way, and to participate in the learning with an amusing and simultaneously communication way.
Students will be able to develop a multidimensional and interdisciplinary approach, in order to reconstruct the evolution of the site. In this way, historical analysis involves an explicit spatial element, and makes the ‘thinking together’ of space and time concrete.
In the training level, such “tools” as Digital Palaeogeography can improve the process of learning because:

- They can be used to approach scientific and land management questions by analyzing maps for the details they contain
- They help the students to shape more complete intellectual picture of space, strengthening a more catholic approach as they provide the possibility of analysis and composition of space
- They provide the possibility of treatment of each information, with greater occasion of acceptance or rejection that the students develop critical attitude against the knowledge
- They help in the cross-correlation of knowledge
- They contribute in the disengagement from the school book or in the different use of it and
- They promote the spatial thinking through processes and activities that were reported.

4. References

Baker and White 2003. The effects of G.I.S. on students’ attitudes, self-efficacy, and achievement in middle school science classrooms, *Journal of Geography,* 102*,* 243-254.

GIS for History, We the People project, University of Illinois at Chicago, online at http://www.gisforhistory.org/

Lefebvre H. 1991. The production of space, Blackwell, Oxford.

Ludwig S. G. 2000. GIS in Schools, Audet H. R., ESRI.

Massey, D., 2005. For Space, London, Sage.

Radinsky Johnston and Ryan 2008. Bringing Historical Census Data Alive: Historical inquiry with Geographic Information Systems, University of Illinois at Chicago, online article at http://www.uic.edu/educ/bctpi/historyGIS/NEHRadinsky03narrative.pdf .

Tilden 1977. *Interpreting our heritage*, Oxford University Press.

Vygotsky L.S. 1978. *Mind in Society*. Cambridge, MA: Harvard University Press.

West B. 2003. Student attitudes and the impact of GIS on thinking skills and motivation, *Journal of Geography,* 102/(6), 267-274.

Δελτίο της Ελληνικής Γεωλογικής Εταιρίας, τομ. XLVII , 2013
Πρακτικά 13ου Διεθνούς Συνεδρίου, Χανιά, Σεπτ. 2013

Bulletin of the Geological Society of Greece, vol. XLVII 2013
Proceedings of the 13th International Congress, Chania, Sept. 2013

THEORETICAL APPROACH OF TEACHING LITHOSPHERE IN JUNIOR HIGH SCHOOL: A CRITICAL REVIEW OF THE CONTENT AND OBJECTIVES DEFINED BY THE CURRICULUM OF THE MINISTRY OF EDUCATION

Leontakianakos G.[1], Vrachas C.[2], Baziotis G.[3], Baziotis I.[4, 5], Soultati G.[1] and Fermeli G.[1]

[1] Faculty of Geology and Geoenvironment, Department of Hist. Geology and Paleontology, National and Kapodistrian University of Athens, Panepistimiopolis, 15784 Zographou, Athens, Greece, gleontakianakos@yahoo.gr, gfermeli@geol.uoa.gr, gewrgia_soul@hotmail.com

[2]Faculty of Psychology, Pedagogy and Philosophy, Programme of Psychology, National and Kapodistrian University of Athens, Panepistimiopolis, Zographou, Athens, Greece, crisvrach@yahoo.gr

[3]Faculty of Physics, National and Kapodistrian University of Athens, University Campus – Zografou, Athens, Greece, 15784, gbaziotis@synergy.gr

[4]Department of Mineralogy, Petrology and Economic Geology, School of Geology, Aristotle University of Thessaloniki, 54124, Thessaloniki, Greece, baziotis@metal.ntua.gr; ibaziotis@geo.auth.gr

[5]Department of Earth Sciences, University of Perugia, 06100 Perugia, Italy

Abstract

The purpose of this study is an attempt to define the lithosphere concept, as described in the textbook "Geology-Geography" of the 1st Grade of junior high-school. Further we investigate whether the objectives of the corresponding chapter are being implemented according to the curriculum of the Ministry of Education. The main research hypothesis concentrates on the very limited cognitive background of the students regarding the lithosphere. It is based on the absence of a well-organized framework of proportional and gradually increased and specialized flow of knowledge, as suggest the few generalised concepts on the subject of Geography taught on the 5th and 6th grade of the Primary School. According to the Curriculum of the "Geology–Geography" of the Ministry of Education, the lithosphere chapter requires fifteen didactic hours for a sum of nine complexes, mostly cognitive objectives. However, the textbook contains only five didactic hours, an indicator of an asymmetric state of the Curriculum. Our opinion about curriculum content itself, which describes the lithosphere, compared to the strictly scientific definition, is that it represents a simplistic approach and consequently the materialization of the cognitive goals is doubtful.

Key words: *Geoscience education, Curriculum, secondary education*

Περίληψη

Σκοπός της παρούσης εργασίας είναι να μελετηθεί το περιεχόμενο της έννοιας της λιθόσφαιρας όπως περιγράφεται στο σχολικό εγχειρίδιο «Γεωλογία-Γεωγραφία» της

Α΄ Γυμνασίου και να διερευνηθεί εάν υλοποιούνται οι στόχοι της αντίστοιχης διδακτικής ενότητας με βάση το Αναλυτικό Πρόγραμμα Σπουδών του Υπουργείου Παιδείας.
Οι μαθητές της Α΄ Γυμνασίου έρχονται από το Δημοτικό με πολύ περιορισμένο γνωσιολογικό υπόβαθρο για τη λιθόσφαιρα, με ελάχιστες και πολύ γενικές έννοιες που έχουν διδαχθεί στην Ε΄ και Στ΄Δημοτικού στο μάθημα της Γεωγραφίας. Το ερώτημα επομένως που προσπαθούμε να απαντήσουμε με θεωρητικό τρόπο είναι το κατά πόσον οι μαθητές της Α΄ Γυμνασίου με δεδομένο το ενδιαφέρον τους και την ασύμμετρη ανάπτυξή της έννοιας της λιθόσφαιρας στο σχολικό εγχειρίδιο, μπορούν να την κατανοήσουν ικανοποιητικά μέσα από την αναπλαισίωση της επιστημονικής γνώσης και τις κατάλληλες διδακτικές και μεθοδολογικές προσεγγίσεις .
Λέξεις κλειδιά: *Διδακτική γεωεπιστημών, αναλυτικό πρόγραμμα, σχολικά εγχειρίδια, δευτεροβάθμια εκπαίδευση.*

1. Introduction

In the educational practice it is followed a specific didactic guideline, certain aspects of which display a low performance to the optimization of the transmitting and assimilating information process. To that extend, in relation to the first stage of the learning process, directly associated with the main goal of this study, the codification of the cognitive data (e.g. Piaget and Inhelder, 1969; Porpodas, 1996).

In the current study we refer to the content of the geological textbook of the 1st Grade of the Greek junior high-school. We focus on the "lithosphere chapter" and its teaching adequacy. According to the geologists and geophysicists, the term lithosphere is defined as the *"strong outer shell of the earth"* (Anderson, 1995). A more sophisticated definition encloses the concept of lithosphere in the following: *"As lithosphere is defined the rocky outer layer of the Earth of medium thickness approximately 100 km, which overlie the highly viscous asthenosphere; it comprises the solid crust and a portion of the upper lithospheric mantle".*

Research results, in the framework of the European project GEOschools, have clearly shown that a high percentage of students are interested in geosciences. Concepts in reference to the "lithosphere" constitute the 5th in the row subject of interest among the fourteen equivalent proposed by the research, with "Natural disasters" and "Palaeontology" listing first among the preferences of the students (Fermeli et al., 2012).

Geoscience educational publications are reviewed by King (2008) to identify future directions for curriculum and professional development, and research. The review indicates that geoscience education will progress most effectively through: 1) extending geoscience learning to all children, 2) educating teachers in effective implementation of new curriculum initiatives, 3) evaluating the progress of the initiatives and using the results to refine them and 4) researching the whole process to demonstrate its effectiveness and to ensure wide dissemination on the basis of well-founded research findings (Chang, 2001). Furthermore, according to Trend (2007), "*the relationships between children's interest, enjoyment, learning and cognitive processing have received considerable attention in recent years, although the subject focused research has been largely restricted to mathematics, English/literacy (notably understanding texts), physical education and science (but negligible geoscience)*". In the same direction, Chang and Weng (2002) address the importance of using activities as part of geoscience teaching.
The psycho-pedagogical process of knowledge - transmitting in the didactic framework constitutes a complex condition divided into four partial stages: i) the codification of the information within various forms of material means, ii) the de-codification by the teacher, iii) the transmission (transference) of information by the teacher to the student and iv) the primarily hold and throughout the necessary rehearsal procedure consequently the assimilation of information by the student. During

the course of educational evolution, various pedagogical approaches were formulated or implemented in relation to one or more stages of the learning process. A key role to that extend have played the theory of cognitive development of the Swiss psychologist Jean Piaget, the theory of the educational process of the American psychologist Jerome Bruner and the theory of the maximum number of items that the short-term memory can contain by George Miller (e.g. Piaget and Inhelder, 1969; Bruner, 1960; Miller, 1956).
The primary goal of this study is to provide a critical review of the lithosphere concept instructed during the first grade of junior high-school. We attempt to define the concept of lithosphere, as described in the textbook "Geology-Geography" of the 1st Grade of junior high-school (Pavlopoulos & Galani, 2009), and to provide clues whether the objectives of the corresponding chapter are being implemented according to the Curriculum of the Greek Ministry of Education (Governmental Paper: 304 v. B/13-3-2003; 1196 v.B/26-8-2003). After that, we criticized from psycho-pedagogical point of view on which level the students are able to sufficiently comprehend the concept throughout the appropriate didactic and methodological approaches.

2. Methodology

In this stage we present the objectives that settled from the curriculum of the Ministry of Education regarding the Lithosphere subsection of the junior high-school textbook. According to these objectives, we attempt to find the evidences that related with their successiveness Grade. After that, we compared the objectives and specific parts of the textbook related to them. Though, the results of the comparison and recommendations, for those objectives that were not fulfilled, are presented in the table 1.

3. Results and Discussion

3.1. The Comparison Case

A thorough cross-examination of the relation between the standard objectives set by the Curriculum (Governmental Paper: 304v.B/13-3-2003) and the information enclosed in the textbook, with reference point to the three psycho-cognitive theories, came of with the following deductions:

- The first didactic objective (D.O.), according to which the student should be able to identify the position of the lithospheric plates, is insufficiently served in the framework of the textbook (Tab. 1). The identification of each lithospheric plate requires a map with the drawing of the plates in relation to the position of the continents and oceans. Since the standard, set by the curriculum, indicates the efficient completion of a task upon visual/optical graphic means, the successful information imprinting principle presupposes the transmission of the cognitive data in the same manner as it is required to be assimilated by the student. In order for the student to be able to perform in a visual task, which presupposes the acquisition of the information asked through the learning process, that specific kind of information is necessary that it would be transmitted accordingly – that is, via a visually assumed stimulus. The ability of the student to modify-decode the written and verbal information into optical, it could be examined in the framework of a distinctively different objective (an intelligence quota test, a creativity task, assimilation and understanding level of an information taught thoroughly and for a long period of time task, etc.). The novelty of the cognitive data taught to the student and the narrow and specific didactic purpose advocates for the conclusion that the ability measured requires the equivalence between the form of the means through which the information is transmitted and examined throughout a task procedure.
- The second didactic objective aims to enable the student, after the completion of the didactic chapter, to correlate the relative movement of the lithospheric plate with certain

connected phenomena. The textbook includes in two pages a sufficient and adjusted to the cognitive background of the student didactic material. Therefore, as shown to the main section of the discussion, the goal is adequately achieved.

- The third objective is not achieved, in reference to the textbook's organizing of information. Though the curriculum set as standard that the student should be in a position to identify the factors that play a key role to the shaping of the surface of the Earth, not only the textbook is confined to a mere imputation of the concept of those geological factors, but also includes the suggestion that the student should retrieve the relevant information from the previous textbooks of the sixth and fifth Grade of Primary School. This approach reduces the possibility of efficient completion of the curriculum objective, due to two reasons: Firstly, in a practical level, is obliging the student to extract information from a material means that could be as well be damaged or disposed. Secondly, the guideline of the textbook makes the functional assimilation of a certain kind of information considerably difficult, as it does not permit the uninterrupted and ease access to the necessary information and thus constitutes the rehearsal process insufficient. Since the imprinting of data to the long term memory requires the systematic rehearsal of this information. It can be deducted that no such procedure can be adequately completed, unless the curriculum either includes the didactic material of the previous years' textbooks in the current one or restructure and enrich the content of the existing relative chapter.
- The fourth goal, regarding the correlation of the action of geological forces with certain manifestations in the surface of the planet is satisfyingly achieved.
- The recognition of the effects of geological forces, such as the earthquakes and the volcanic eruptions, on people's life presupposes an analysis, followed by examples, case scenarios and photographic material. None of those conditions is filled / accomplished, even though Greece is a country with intense earthquake activity. Therefore, the specific goal cannot be considered adequately accomplished.
- The definition selected to describe basic geological terms (e.g. fossil or lithosphere) demonstrate a high degree of difficulty, due to their immediate reference to strictly scientific terminology. By the term 'difficult' is indicated an inconsistency between the current cognitive status of the student of the 1st degree of junior high-school and the complexity of the information transmitted. In this specific case, there is an abruption of the proportional, gradually increased and specialized flow of cognitive information. The limited, until this certain educational stage, offered and assimilated knowledge – as it was shown on the main part of the discussion – does not constitute an adequate and sufficient cognitive background, in order for the student to correlate the incoming information with the already existing and therefore to proceed to sufficient and functional imprints in the long-term memory.
- The seventh didactic goal, according to which a certain ability to correlate the action of a variety of external forces with specific manifestation of their action should be accomplished, cannot be considered achieved.
- In relation to the identification of the shape of the continents by the student, this specific objective can adequately be achieved as the textbook indicates the necessary visual / optical means. On the contrary, the prerequisite regarding the readiness of the student to describe and to cite basic features of the continents is less possible to be obtained as the information given is limited. In order for the student to become familiarized with the main aspects and characteristics of the surface of the Earth, a suggestion would indicate the offer of audiovisual means attached to the main textbook. In that way the specific educational purpose would be accomplished in a greater extent and the assimilation of the information would be achieved in less time. The combination of audio and visual stimuli would sharpen

the interest of the student for the interaction of various people with and in relation to the environment they inhabit.

- Similarly, the textbook, in reference to the ninth objective, is divided into two distinctive objectives; recognition on the map of basic terrestrial morphological characteristics and additionally, description, by the use of examples, of the impact of those phenomena on man's activities. The textbook does not indicate a relevant map; therefore the first objective is not accomplished. In relation to the second objective, the argumentative form in which the textbook attempts to demonstrate the habitual differences among people living in plain and mountainous areas respectively, aims in sharpening the interest of the student and rendering the cognitive in a more immediate way. That certain approach accomplishes in combining information about the surface elements of the Earth and opinions about living on such places. However, there is no provision for an exercise, which will enable the mnemonic rehearsal and thus help the student to assimilate that information.

Table 1 - Comparison of the objectives that settled from the curriculum of the Ministry of Education regarding the Lithosphere subsection of the junior high-school textbook and recommendations for those targets that were not fulfilled.

Objectives	Attainment	Recommendations
D.O.1	No	Draw a map with the lithospheric plates in relation to the position of the continents and oceans.
D.O.2	Yes	---
D.O.3	No	Give the meaning of the basic terms that influence the shape of the earth`s surface (e.g. erosion) with respective examples.
D.O.4	Yes	---
D.O.5	No	One to two paragraphs of the effects of geological forces on people's life (with examples, case scenarios and photographic material).
D.O.6	No	This objective should be omitted from the textbook of the 1st degree of junior high-school
D.O.7	No	This didactic objective should be merged with D.O.3
D.O.8	No	Incorporation of audiovisual means within the main textbook.
D.O.9	No	Draw a geomorphological map.

3.2. A Criticized Review of the Phycho-Pedagogical Theories

The theoretical psycho-pedagogical approach which is followed based upon the three theories (by Bruner, Piaget, Miller), already addressed in the introduction. According to the first theory, the biological and cognitive development of the person passes through certain pre-defined temporal stages. Those stages are; Sensorimotor (birth – 18/24 months), pre-operational (ages 2 – 6), concrete operational (ages 6 – 12), formal operational (through adolescence to adulthood). During the last stage, which coincides, from an educational point of view, with the 1st Grade of junior high-school, the development of the rational thought is integrated and at the same time is signifying the development of the abstract thought. The contribution of the cognitive developmental theory, despite the various weak points, can be characterized as substantial, as Piaget, by formulating a structural interpretation of human cognitive evolution, has set a more

standard and general ground for the didactic procedure by abridging the theoretical deflections due to intercultural, interracial, inter-social and inter-sex variances (Piaget and Inhelder, 1969).

In the second theory, Bruner (1960, 1986), while having accepted certain parameters of the developmental theory of Piaget (i.e., the cognitive structures of children develop by time, children have a tendency towards learning, children are active participants in the learning process), diversified his approach in several crucial points. According to Bruner's cognitive model, development is a continuous process, rather than a series of predefined stages, while, at the same time, the participation of the adults to that very process constitutes a crucial factor. A major contribution of Bruner's theory is the suggestion that the main objective of education should be the creation of self-reliant, autonomously thinking students, of individuals that would be able to evaluate any given cognitive information and pursue by themselves to upgrade their cognitive capacity. As Bruner underpinned, "*We teach a subject not to produce little living libraries on that subject, but rather….. to take part in the process of knowledge-getting. "Knowledge is a process, not a product"* (Bruner, 1986). Additionally, "*Ideally, interest in the material to be learned is the best stimulus to learning, rather than such external goals as grades or later, competitive advantage*" (Bruner, 1960).

Finally, in the third theory, Miller (1956), after having conducted experiments, (i.e., by asking a person to repeat a set of digits presented), has ascertained that the short-term memory – the function of the immediate and brief storage of data, with a duration between 0-20 seconds (Atkinson & Shiffrin, 1968) before those data are imprinted in the long-term memory - has a capacity limit of 7, minus-plus 2, items. As item is defined every bit of information, which is entrained primarily as acoustic stimulus, such as every particular digit of a number. According to multi-store model and working model a rehearsal process it is required, in order for the new information to be stored in the long-term memory and be available for retrieval at any time. "Working memory is the term used to refer to a system responsible for temporarily storing and manipulating information" (Alloway et al., 2006).

Despite the substantial differences between the above mentioned models regarding the structure and function of the short-term memory, it is suggested that the more systematic and well-organized the procedure of repeating information in short-term scale, the more increased are the possibilities for the student to hold the given cognitive data. Furthermore, the more frequent the rehearsal in long-term scale, the better the chances for the student to absorb the taught information.

4. Conclusions

In this study we address that the following: a) the term "lithosphere" is not covered adequately as described in the textbook of the 1st Grade of junior high-school, b) The majority of the didactic objectives settled by the Curriculum of the Ministry of Education were only partially achieved and c) the considerable knowledge gap in the meaning of the lithosphere between the students of the 1st Grade of junior high-school and previous years' textbooks i. The above conclusions are solely based on a theoretical approach of the topic addressed in the introduction. A more comprehensive study, with analytical questionnaire is ready to be given and the results will be presented in a forthcoming paper. The challenge for the future would be to combine a well balanced structural and conceptual teaching of Earth Sciences with permanent links to attractive interesting topics, i.e. making Earth Sciences something present and related to daily life.

5. Acknowledgments

This work is a part of the international EU Project: GEOschools, supported by the Life Long Learning Programme (EACEA-LLP).

6. References

Alloway T.P., Gathercole S.E., Pickering S.J., 2006. Verbal and Visuospatial Short-Term and Working Memory in Children: Are They Separable?, *Child Development*, 77, 1698–1716.

Anderson D.L. 1995. Lithosphere, asthenosphere, and perisphere, *Reviews of Geophysics*, 33 (1), 125-149.

Atkinson R.C., Shiffrin R.M. 1968. Chapter: Human memory: A proposed system and its control processes, in Spence K.W. and Spence J.T., The psychology of learning and motivation (Volume 2). New York: Academic Press pp. 89–195.

Bruner J. 1960. *The process of education*, Cambridge MA, Harvard University Press. 97 pp.

Bruner J. 1986. *Actual minds, Possible worlds*, Cambridge, MA, Harvard University Press, 202 pp.

Chang C.Y. 2001. Comparing the impacts of problem-based computer-assisted instruction and the direct interactive teaching method on student science achievement, *Journal of Science Education and Technology*, 10, 147-153.

Chang C.Y. and Weng Y.H. 2002. An exploratory study on student`s problem-solving ability in Earth science, *International Journal of Science Education*, 24 (5), 441-451.

Fermeli G., Melendez G., Dermitzakis M., Calonge A., Steininger F. and Makridis G. 2012. Preliminary results from a statistical research on geosciences content and teaching strategies in secondary schools in Greece and Spain, *XVII Simposio sobre Enseñanza de la Geología*, Huelva, 9-14 Julio, Vol. Abstracts 39-47.

Governmental Paper 2003. N. 1196 *v.B'/26-8-2003* (in Greek).

Governmental Paper 2003. N. *304 v B'/* 13-3-2003 (in Greek).

King C. 2008. Geoscience education: an overview, *Studies in Science Education*, 44, 187-222.

Miller G.A. 1956. The magical number seven, *The Psychological Review* 63: 81–97.

Pavlopoulos K. and Galani A. 2009. *Geology & Geography Textbook, A΄ Class of High School*, Athens, OEDB, 175 pp (in Greek).

Piaget J. and Inhelder B. 1969. *The psychology of the child*, New York: Basic Books.

Porpodas K. D. 1996. Cognitive Psychology, Athens. (In Greek).

Trend R. 2007. Individual, situational and topic interest in geoscience among 11 and 12-year old children, *Research Papers in Education*, 20 (3), 271-302.

Δελτίο της Ελληνικής Γεωλογικής Εταιρίας, τομ. XLVII , 2013
Πρακτικά 13ου Διεθνούς Συνεδρίου, Χανιά, Σεπτ. 2013

Bulletin of the Geological Society of Greece, vol. XLVII 2013
Proceedings of the 13th International Congress, Chania, Sept. 2013

DEVELOPING AN INTERACTIVE APPLICATION EMBODIED IN THE GEOSCIENCES EDUCATIONAL PROCEDURE

Tsangaratos P.[1], Perraki M.[1] and Ilia I.[1]

[1] *National Technical University of Athens, School of Mining and Metallurgical Engineering, Department of Geology, ptsag@metal.ntua.gr, maria@metal.ntua.gr, gilia@metal.ntua.gr*

Abstract

The aim of this study is to develop a Geovisual Mineralogical Cognitive Tool (GeMiCo Tool), a digital application that utilizes techniques from the domain of Information and Communication Technology. The application is part of the educational tools used at the Mineralogical Museum of the School of Mining and Metallurgical Engineering, National Technical University of Athens and concerns students of Higher, Primary and Secondary Education. The learning tool developed here embodies Google Earth API (Application Programming Interface), allowing users to interactively display and investigate geological and mineralogical related data. By that, users are able to select and present thematic layers of information related to the geo-exhibits, to create queries and searches and to navigate in 3D environment. The application runs on a large format multi-touch interactive display in the Mineralogical Museum of NTUA that attracts audiences and engages them in interactive collaborative tasks.
Key words: *Virtual Globe, Google Earth API, GeMiCo.*

Περίληψη

Σκοπός της παρούσας μελέτης είναι η παρουσίαση ενός Γεω-οπτικού Ορυκτολογικού Γνωστικού Εργαλείου (GeMiCo Tool), μια ψηφιακή εφαρμογή που χρησιμοποιεί τεχνικές από τον τομέα της Τεχνολογίας των Πληροφοριών και Επικοινωνιών. Η εφαρμογή αποτελεί τμήμα των εκπαιδευτικών εργαλείων που χρησιμοποιούνται στο Ορυκτολογικό Μουσείο "γαιο-ΟΡΑΜΑ" της Σχολής Μηχανικών Μεταλλείων-Μεταλλουργών του Εθνικού Μετσόβιου Πολυτεχνείου και αφορά σε φοιτητές ΑΕΙ καθώς και μαθητές πρωτοβάθμιας και δευτεροβάθμιας εκπαίδευσης. Η εφαρμογή ενσωματώνει το Google Earth API, που επιτρέπει στους χρήστες να διερευνούν και να επεξεργάζονται με διαδραστικό τρόπο γεωλογικά και ορυκτολογικά δεδομένα. Οι χρήστες έχουν τη δυνατότητα να επιλέγουν θεματικά επίπεδα πληροφοριών που σχετίζονται με τα γεω-εκθέματα, να δημιουργούν ερωτήσεις και αναζητήσεις και να πλοηγούνται σε 3D περιβάλλον. Η εφαρμογή είναι εγκαταστημένη σε μια μεγάλου μεγέθους διαδραστική οθόνη (τεχνολογία multi-touch) η οποία προσελκύει το κοινό να συμμετάσχει σε διαδραστικές ατομικές και ομαδικές εργασίες.
Λέξεις κλειδιά: *Virtual Globe, Google Earth API, GeMiCo.*

1. Introduction

The technological enhancement that has been recorded during the last two decades in the Information and Communication Technology domain has changed the way societies appreciate and embrace technology. Technology is becoming the essential component in each of our everyday activities. It's everywhere, in the way we store, recall and report data, in the way we communicate, we travel, we learn. Educational procedures and scientific research practice are primary influenced from such a development. Specifically, web-based information and knowledge systems have revolutionized the traditional lecture-based educational approaches. Currently, there are several education and research initiatives that aim to effectively utilize these technological advances and address the challenges that accompany those by producing powerful educational tools, which could assist in a positive way during the learning process (Manduca & Mogk, 2002, Atkins et al., 2003, Brindisi et al., 2006). According to Blumenfeld et al. (1991), this kind of resource can make difficult or unseen material more accessible, more understandable, and interesting or motivating to students.

The objective of the present paper is to describe such an educational resource addressed for students of Higher Education, the Geo-visual Mineralogical Cognitive (GeMiCo) tool. The tool takes advantage of the power of visualization since it embodies Google Earth's Application Programming Interface (API). The main educational goals of GeMiCo was to allow students to interactively display and investigate geological and mineralogical data on a Virtual Globe and by this support the teaching of geography and geology. Virtual Globes (VG) is similar to desk globes; however they have the additional capability of simultaneous represent many different thematic layers of information. They are capable in showing spatial data and information at multiple scales and in multiple ways, including text, photos, animation, voice recordings and videos (Butler, 2006). The tool is developed as a web-based tool, designed and compiled with Visual Basic 6.0, a third-generation event-driven programming language and integrated development environment (IDE). The application runs on a large format multi-touch interactive horizontal display in the Mineralogical Museum "γαιο-ORAMA" of National Technical University of Athens, which furthermore promotes collaboration among students as it allows small groups of students to gather around the display and become more active participants.

2. Materials and Methods

2.1. Virtual Globes Technology

The core stone of GeMiCo tool is the VG interface. The interface allows data and information that is related to geological and mineralogical concepts to be visualized having a spatial context. The idea that computers could be used to model a Virtual Earth or Globe is as old as the Internet itself. Buckminster Fuller's 1962 concept of a Geoscope and MIT's Aspen Movie Map multimedia project in the 1970s, were both forerunners for the actual development of an interactive, computer-based model of the entire planet (Bailey & Chen, 2011). According to Rakshit & Himmelberger (2008), the advent of VG and online mapping applications, has generated an enormous interest in spatial representations of data among many non-geographic communities, such as educators and researchers, who had previously, very little to no expertise, in geospatial technologies.

VGs are presented as 3D software models, which are capable of modelling the Earth or other environments of the universe, like Moon, Venus and Jupiter. Their main characteristic is the ability to freely move around by changing the viewing angle and position. They allow the representation of different layers of information on the surface of the Earth that may have spatial or non - spatial attributes. VGs are capable of displaying, man - made features such as infrastructure networks and buildings, elevation data or representations of demographic quantities. They can handle spatial data such as geodatabases, shapefiles, KML/KMZ, GPX and raster formats (JPEG, GeoTIFF,

MrSID) and integrate a wide variety of context such as photos, videos, documents, 3D models placing them in a geographic content (De Paor et al., 2008, Tsangaratos, 2011).

There are more than 30 VG available on the Internet but the most popular ones are: Google Earth, NASA World Wind, Marble and ArcGIS Explorer, due to the availability of the data they provide, the ease of use and the advanced functionalities that they include. As already mentioned above, the educational tool developed here embodies a VG and specifically Google Earth's API. The Google Earth API is a free beta service, available for any web site or web–based application. The Plug-in and its JavaScript API allow users to place a version of Google Earth into web pages or web-based applications. The Google Earth API can display placemarks, lines, polygons, overlays and 3D models on the imagery, just as the standalone version of Google Earth can. The plug-in supports several of the Google Earth layers of information, including terrain data, infrastructure network, borders and buildings (Brown, 2006, Tsangaratos, 2011). The Google Earth API as well as Google Earth, uses aerial photos and QuickBird satellite images (less than 1 m resolution) for some areas, Landsat imagery for other areas and Shuttle Radar Topography Mission (SRTM) elevation data for terrain visualization. Since the data come from different sources and the coverage is not uniform, some areas of the globe appear crisp all the way down to street level, whereas other areas are blurry from a great distance. In Google Earth API and Google Earth, no imagery is viewed in real time. According to Google, all of the available terrain and imagery information are less than 3 years old and are continuously updated. The internal coordinate system of Google Earth API and Google Earth is geographic coordinates (latitude/longitude) on the World Geodetic System of 1984 datum. Google Earth API and Google Earth, adopts Keyhole Markup Language (KML) for expressing geographic annotation and visualization. KML is used as the format for describing, organizing and visualizing geographical objects (Wilson et al., 2008). It represents a hierarchical data system where the geographical objects can be populated in a nested tree structure (Wernecke, 2009).

3. Geo-visual Mineralogical Cognitive Tool (GeMiCo)

3.1. General Information

Geo-visual Mineralogical Cognitive (GeMiCo) Tool is a web-based learning tool that takes advantage of the power of visualization. Specifically, the learning tool developed here embodies Google Earth API, allowing students to interactively display and investigate geological and mineralogical data. The GeMiCo tool runs on a large format multi-touch interactive display in the Mineralogical Museum "γαιο-ORAMA" of the School of Mining and Metallurgical Engineering of National Technical University of Athens, Greece (http://www.metal.ntua.gr/index.pl/museum). "γαιο-ORAMA" has a rich mineral collection containing specimens mainly from Greece but also from all over the world, exhibited in a recently (2010) built modern two-floor building of approximately 300 m^2. It is equipped, among others, with interactive multimedia and a set of relative tools and activities, such as the GeMiCo tool, are developed.

Figure 1 shows a screenshot of the tool that presents data and useful information about the area of Lavreotiki (Janikian, 2009). The GeMiCo Tool incorporates advanced information technology, research-quality data sets, and supportive materials in order to facilitate effective inquiry-based science education at all levels. Geological and mineralogical information is often difficult to assimilate by students, since it involves three to four dimensional processes taking place in macro-, micro- and nano- scales. In many cases the students are not able to explore and record large scale geological phenomena in actual conditions. In these cases, research-quality data sets can replace student-collected data, and computer technology can be used to represent the data visually in a friendly-to-use manner.

The GeMiCo Tool is a set of Internet accessible tool that provides much of the functionality of commercial GIS software at no cost. By storing the data in a web environment instead of providing it on CD-ROM or DVD, the tool provides students access to a much larger database. This also

allows the developers to easily update the data sets and system tools without the time consuming and costly process of redistributing them to the end-users.

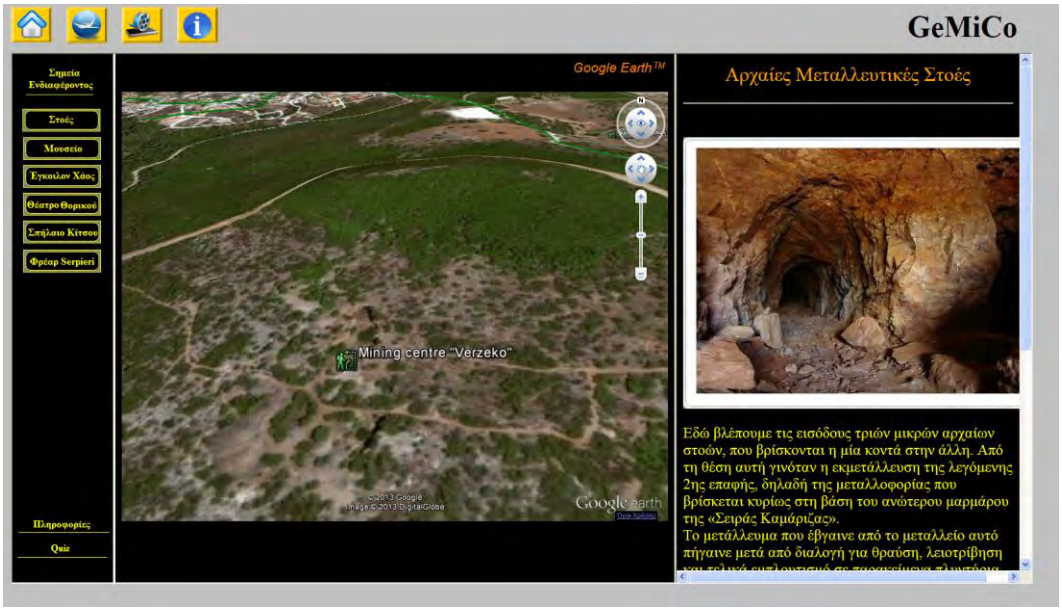

Figure 1 – Geo – visual Mineralogical Cognitive Tool (GeMiCo).

3.2. System Architecture

GeMiCo Tool was designed and compiled using Visual Basic programming language. The main frame consists of a single form, with a split control panel oriented vertically. The left part contains the controls that are used to navigate and explore the available data. The right panel contains a WebBrowser Object, docked into it, specifically a HTML Document. In the case presented, the HTML Document was the Google Earth API. The Google Earth API is a JavaScript library that allows developers to add Earth plug-in objects to their sites. The API also provides programmatic access to the plug-in objects and the features inside of them. Web site developers can use the API to facilitate interaction between standard HTML elements and Earth plug-in instances. A simple javascript code that enables the Google Earth API on a dynamic HTML page and uploads a KML file is shown in Figure 2.

Events that occur in the Google Earth API which is contained in the WebBrowser Object are captured and forwarded to a procedure in the left panel of the main frame. A Visual Basic script, which is embodied in the form's source code, executes specific functions in response to the forwarded events. The same procedure is executed with events and scripts performed in the main frame and forwarded to Google Earth API HTML Object.

The GeMiCo Tool is comprised of three main components:

- Educational web pages designed as user guides and information database.
- An interactive mapping tool, Virtual Globe Frame.
- A set of multiple–choice quizzes and tests designed to perform interactive learning procedures.

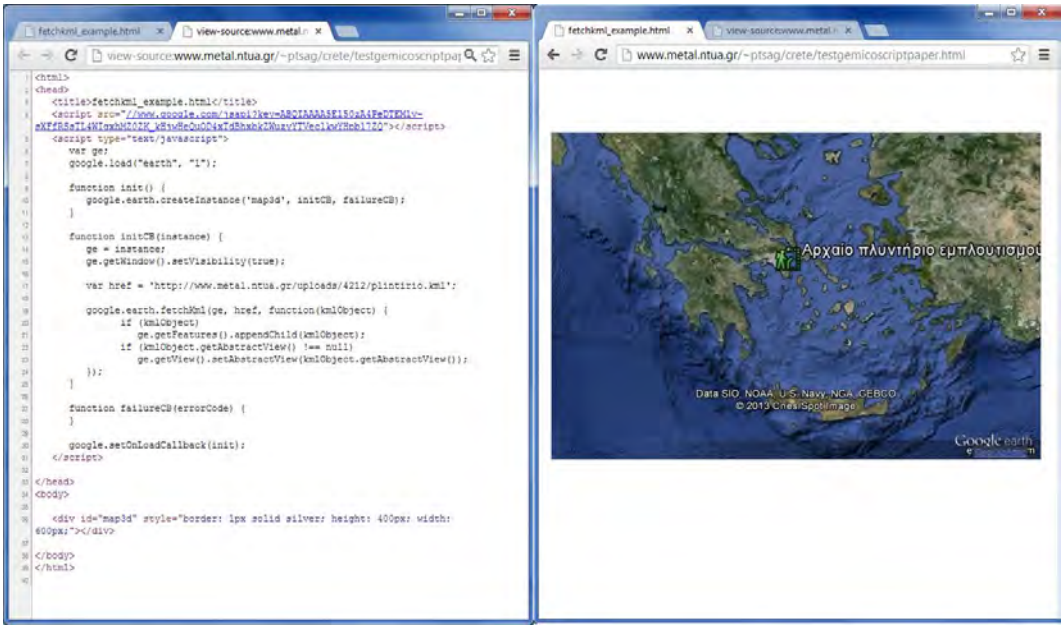

Figure 2 – Javascript Code in HTML.

3.2.1. Educational web pages

The educational web pages embodied in GeMiCo Tool, allow students to work with actual data sets acquired by researchers and provide the ability to manipulate, query and display in their own way the available data. Thus, students are driven by their own curiosity and get more involved in the learning process. The architecture of GeMiCo Tool provides students with the tools to learn about geological processes and mineral formation and occurrence through inquiry and discovery (Figure 3).

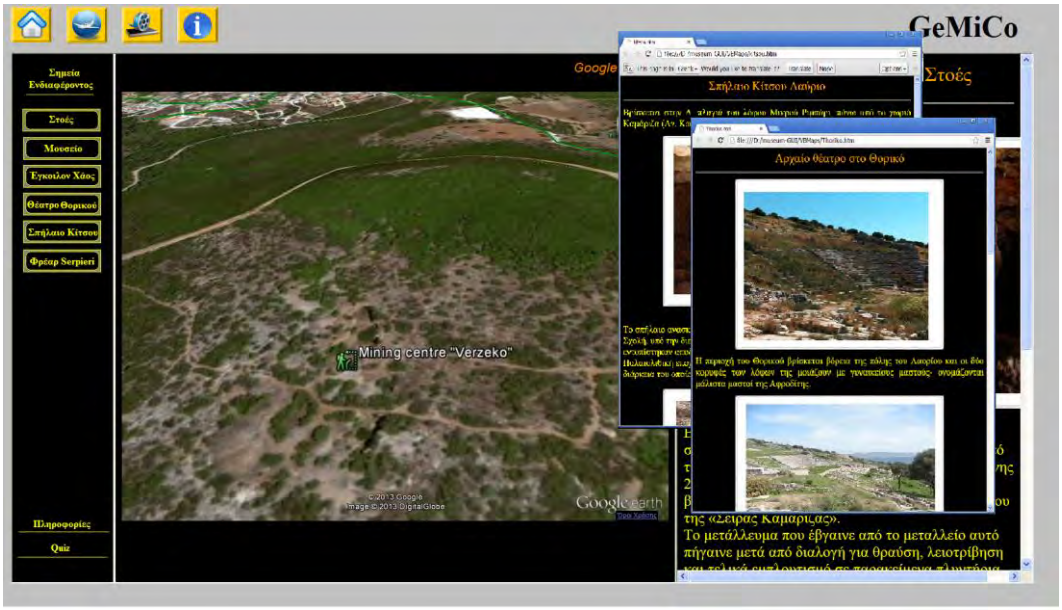

Figure 3 – Educational Web pages.

The web pages are primarily comprised of text and images presented in hypertext markup language (HTML) format. Their main scope is to illustrate information and knowledge concerning geology and mineralogy and to cover topics such as geology, mineral and ore occurrences and topography. These supportive materials include background information, lesson plans, activity outlines, guidelines to activities and assessment suggestions. They are not comprehensive guides to the broad topics; instead, they are designed to provide information and opportunities for discovery on focused topics. The lesson plans, activities, guides and student directions give specific examples of how they can explore each topic using the Google Earth API.

3.2.2. Interactive Mapping Tool

The second component, the Virtual Globe Frame, enables developers to embed Google Earth API, which may be resembled as a mapping and geographical information program, into web pages or web-based applications with the use of JavaScript coding. Since it enables scripting, it provides great potential for the development of educational and other material.

The Google Earth API allows access to spatially referenced data sets within the GIS database. This interactive web mapping tool gives students the ability to create maps and earth views by querying and overlaying geological units, topography data, mineral and ore occurrences etc. (Figure 4). In this section students select the region they want to study and the data sets they wish to view; they can query data to display certain criteria and they can alter the appearance of the display. The Google Earth API mapping tool can be used independently or be paired with the supportive materials provided in the user guides to create meaningful, inquiry-based activities for students.

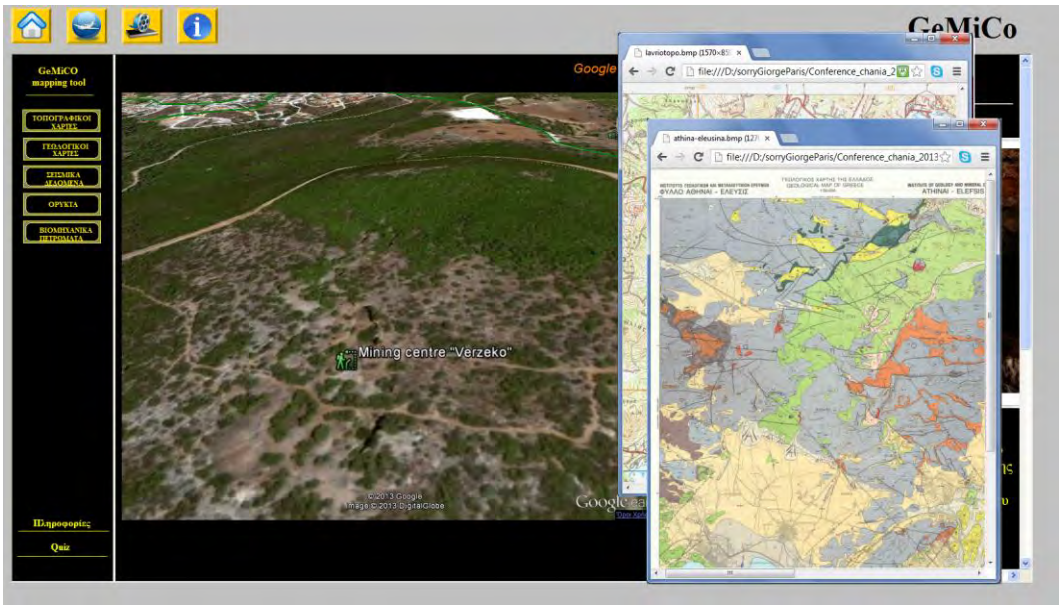

Figure 4 – GeMiCo Interactive mapping tool.

3.2.3. Multiple-choice quizzes and tests

The last component of GeMiCo Tool is the evaluation of the students' learning ability using multiple-choice quizzes and test. According to Crooks (1988), students study having in mind the way they will be tested. If they expect an exam focused on facts, they will memorize details; if they expect a test that will require problem solving or integrating knowledge, they will work toward understanding and applying information. Quizzes and tests are powerful educational tools and by utilizing them the educators achieve four important functions:

- Evaluate students' performance and assess whether they are learning what they are being expected to learn.
- Motivate and assist students to structure their academic efforts.
- Understand how successfully the material is being presented.
- Reinforce and continue the learning process by providing students with indicators of what topics or skills they have not yet mastered and should concentrate on.

The type of test that is most effective in motivating, measuring, and reinforcing learning is the Multiple-Choice Quiz. Zeidner (1987) reported that students prefer the multiple–choice format for examination, a similar result found by Taub & McRury (1990). This type of examination is easier to prepare (the right answer is already written down), questions and answers tend to be less complex than constructed response items, their perceived success rate is higher (some answers may be correct by chance), and incurs less anxiety than the essay type assessment. However, the multiple-choice examination does not seem to invite students to make an in-depth effort to study (Struyven et al., 2004).

In GeMiCo Tool, there is a set 7 multiple-choice quizzes with geological and mineralogical questions of different level of difficulty (Figure 5). The first quiz, Quiz A, is the easiest while the last, Quiz G the most difficult.

Figure 5 – Quiz pages.

4. Evaluating GeMiCo Tool

In order to evaluate the usage and effectiveness of GeMiCo Tool, a set of questionnaires and observations were analyzed. A small group of undergraduate students of the School of Mining and Metallurgical Engineering participated in the evaluation test, in the frames of the 1st semester course "Mineralogy". The main goal was to learn how well the GeMiCO Tool is functioned in a classroom environment and how it is perceived by the students. The evaluation was accomplished using a student questionnaire and observations made by the educators. The distributed questionnaire was based on several evaluating methods of multimedia learning software (Crozat et

al., 2009). Table 1 shows the different evaluation criteria and sub-criteria used. Each sub criteria had a 5-scale rated value, where the lowest indicates higher appreciation by the users. The score of each user achieved during the tests was also analyzed as an indication of the learning power that GeMiCo Tool had. The total number of answered quizzes was 201, performed from a total number of 34 participants during the fall semester of 2012 (Table 2).

Table 1 - Evaluation criteria and sub-criteria.

Criteria	Description	Sub - criteria	
General Feeling	Takes into account the feeling the application gives to the user	Original Simple Active	Standard Complex Passive
Usability	Concerns the ergonomics of the interface of the application	Low level of guidance Low level of workload Low level of user control	High level of guidance High level of workload High level of user control
Multimedia documents	Concerns the quality of text, sound, animation, images, videos, 3D models, etc that are used.	Low quality of media Low level of information	High quality of media High level of information

Table 2 – Performance of students on quizzes .

Quiz (number of participants)	Right answers (%)
A (34)	88.34
B (34)	85.17
C (34)	86.12
D (30)	80.34
E (27)	81.24
F (23)	75.90
G (19)	71.20

5. Discussion and Conclusions

The technical affordances of cloud-based computing, digital textbooks, mobile connectivity, high-quality streaming video and "just-in-time" information gathering, have pushed great amounts of knowledge to the "placeless" Web. This has sparked a robust re-examination of the modern university's mission and its role within networked society (Anderson et al., 2012). As the availability of computers and Internet connections in classrooms increases, the potential of harvesting such resources to advance teaching and learning provides unprecedented opportunities for both researchers and educators (Brindisi et al., 2006). According to Kali & Linn (2008), visualization plays an important role in assisting learning process since it makes, unseen and complex material, visible. By transforming certain content in a more animated format, it allows

users to have a better understanding of the concepts and to gain a more spherical and richer view of the process involving a specific issue. VG have opened the world of satellite images to the general public and allowed entertainment, education and exploration of new findings (Pringle, 2010). To the scientific community, VGs are not only tools that provide huge volumes of freely available images and 3D views of the Earth, but mostly, they are effective channels trying to distribute research findings, data and information. VGs offer researchers a naive alternative to the traditional GIS software, that leads to increased data sharing and facilitating studies at global scale (Yu & Gong, 2012). The presented educational tool assists students to observe satellite, aerial images and terrain models, but also 2-D and 3-D vector data concerning mining site locations, mineral resources, geological and mineralogical data and other related information. The visualization of such multi spatio - temporal data sources helps students to understand geological concepts and to achieve a better learning ability. From the analysis held concerning the distributed questionnaires to the students, the usage and the effectiveness of GeMiCo Tool was rated as valuable. Specifically, most of the students answered that, the general feeling GeMiCo Tool leaves, is that of an original, quite simple and active application. They appreciated the good level of the user control and the high level of the workload, although they ranked the tool with a low level of guidance. As for the level of data quality and information availability, the students ranked the tool with medium to good level. The performance of the students on tests indicated that the learning ability of GeMiCo Tool is thought to be significant high, specifically in low and medium level of difficulty. However, more comprehensive, multiyear and quantitative observations must take place in order to show the progress and learning gains GeMiCo Tool provide to students, with valid statistical indexes. Concluding, the specific features and capabilities of GeMiCo Tool that is appreciated with high value are:

- The ability to play the role of an unlocked gate of knowledge, since it allows user to collect data from the Internet and from user-specified layers of information.
- The ability to assist the learning process and enhance the ability to think spatially.
- The ability to explore dynamic events and (near) real – time data.

6. References

Anderson Q.J., Boyles J.L., and Raine L. 2012. The future impact of the Internet on higher education: Experts expect more-efficient collaborative environments and new grading schemes; they worry about massive online courses, the shift away from on-campus life. Pew Internet & American Life Project, Available online at: http://www.eric.ed.gov/PDFS/ED534048.pdf

Atkins D.E., Droegemeier K.K., Feldman S.I., Garcia Molina H., Klein M.L., Messerschmitt D.G., Messina P., Ostriker J.P. and Wright M.H. 2003. Revolutionizing science and engineering through cyber infrastructure: Report of the National Science Foundation Blue-Ribbon Advisory Panel on cyber infrastructure: Arlington, Virginia, The National Science Foundation, *The Directorate for Computer and Information Science and Engineering*, 84 p., http://www.cise.nsf.gov/sci/reports/atkins.pdf

Bailey J. and Chen A. 2011. The Role of Virtual Globes in Geoscience, *Computers & Geosciences*, Vol. 37, No. 1, pp. 1-2. doi:10.1016/j.cageo.2010.06.001

Blumenfeld P.C., Soloway E., Marx R., Krajcik J.S., Guzdial M. and Palincsar A. 1991. Motivating project-based learning: Sustaining the doing, supporting the learning, *Educational Psychologist*, 26, 369 - 398.

Brindisi C., Seber D., and Moore A. 2006. Evaluating geosciences information systems in the classroom: A case study of Discover Our Earth, *Geosphere*, 2, 1-10.

Brown M. 2006. *Hacking Google® Maps and Google® Earth*, Publisher Wiley, pp 408.

Butler D. 2006. Virtual globes: the web-wide world, *Nature* 439, pp. 776–778.

Crooks T.J. 1988. The Impact of Classroom Evaluation Practices on Students, *Review of Educational Research*, 58(4), 438-481.

Crozat S., Hu O. and Trigano P. 1999. A method for evaluating multimedia learning software, *ICMCS '99 Proceedings of the IEEE International Conference on Multimedia Computing and Systems*, Vol1., 714-719.

De Paor, D.G., Simpson C. and Whitmeyer S. 2008. Deconstructing Classical Geologic Maps Using Google Earth's Keyhole Markup Language, *Geological Society of America Abstracts with Programs*, 40 (6), pp 348.

Janikian Z. 2009. Lavrion and surroundings. Series Geotrails in Greece: Ed. Theodosiou, I., IGME, Publ. Kaleidoskopio. ISBN 978-960-98903-2-8 in English and 978-960-87453-6-0 in greek.

Kali Y. and Linn M.C. 2008. Designing effective visualizations for elementary school science, *The Elementary School Journal*, 109 (2), 181-198.

Manduca C.A. and Mogk D. 2002. Using data in undergraduate science classrooms: Final report on an interdisciplinary workshop at Carleton College, Available at: http://serc.carleton.edu /files/usingdata/usingdata.pdf

Pringle H. 2010. Google Earth shows clandestine worlds, *Science*, 329, 1008–1009.

Rakshit R. and Himmelberger O.Y. 2008. Application of Virtual Globes in Education, *Geography Compass,* 2(6), pp 1995–2010, doi: 10.1111/j.1749-8198.2008.00165.x

Struyven K., Dochy F. and Janssens S. 2004. Student's perceptions about evaluation and assesment in higher education: a review, *Assessment & Evaluation in Higher Education*, 30(4), 331–347.

Traub R.E. and MacRury K. 1990. Multiple-choice vs. free response in the testing of scholastic achievement, in: K. Ingenkamp & R. S. Jager (Eds) *Test und tends 8: jahrbuch der pädagogischen diagnostic* (Weinheim und Base, Beltz Verlag), 128–159.

Tsangaratos P. 2011. Virtual Globes and Geological Modeling, *International Journal of Geosciences*, 2(4), pp. 648-656, doi: 10.4236/ijg.2011.24066.

Wernecke J. 2009. *The KML Handbook: Geographic Visualization for the Web*, Addison-Wesley, Upper Saddle River, p. 368.

Wilson T., Burggraf D., Lake R., Patch S., Martell R., McClendon B., Jones M., Ashbridge M., Hagemark B., Wernecke J. and Reed C. 2008. OGCs KML. Open Geospatial Consortium, Document OGC07-147r2, pp 251. http://www.opengeospatial.org/standards/kmlS.

Yu L. and Gong P. 2012. Google Earth as a virtual globe tool for Earth science applications at the global scale: progress and perspectives, *International Journal of Remote Sensing*, 33:12, 3966-3986.

Zeidner M. 1987. Essay versus multiple-choice type classroom exams: the student's perspective, *Journal of Educational Research*, 80(6), 352–358.